ORTHOPAEDIC BIOMECHANICS

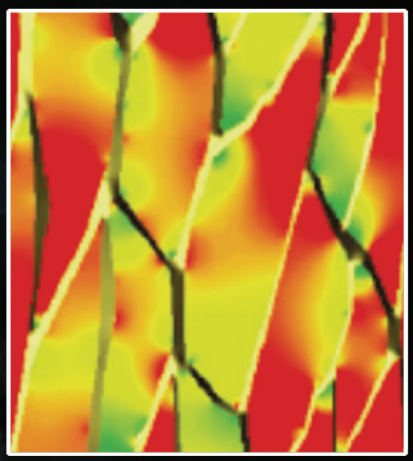

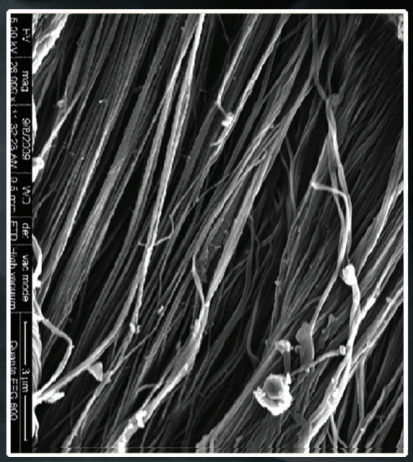

Edited by

Beth A. Winkelstein, PhD

CRC Press
Taylor & Francis Group

ORTHOPAEDIC BIOMECHANICS

ORTHOPAEDIC BIOMECHANICS

Edited by
Beth A. Winkelstein, Ph.D

CRC Press
Taylor & Francis Group
Boca Raton London New York

CRC Press is an imprint of the
Taylor & Francis Group, an **informa** business

CRC Press
Taylor & Francis Group
6000 Broken Sound Parkway NW, Suite 300
Boca Raton, FL 33487-2742

Version Date: 20121016

International Standard Book Number-13: 978-1-4398-6094-6 (eBook - PDF)

Visit the Taylor & Francis Web site at
http://www.taylorandfrancis.com

and the CRC Press Web site at
http://www.crcpress.com

Contents

Section III Biologic Considerations and Clinically Related Orthopaedic Biomechanics

Preface

Orthopaedic biomechanics is the study of the structure and function of the tissues and integrated musculoskeletal system using mechanical and engineering mechanics methods. Indeed, many textbooks and clinical references already focus on biomechanics, or specific anatomical features or perspectives of the musculoskeletal system, like the spine, hand, or surgical management. However, given the strong current attention of orthopaedic, biomechanical, and biomedical engineering research on translational capabilities for the diagnosis, prevention, and treatment of clinical disease states, the need for reviews of the state of the art and current needs in orthopaedics is very timely.

It is the goal of this book to present both foundational engineering and mechanical theories about the biomechanics of orthopaedic tissues and anatomical structures, as well as to address how such approaches are confounded by biological issues that influence and modify biomechanics. It is also the goal of this book to provide a unique perspective related to clinically relevant issues in this field, with particular emphasis on diagnostics, injury, and treatment modalities, all with a biomechanical focus. The contributions for each chapter in this book offer quantitative rigor, biologic approaches, and state-of-the-art presentations of current perspectives of relevant considerations and implications in the field of orthopaedic biomechanics today.

Through its 21 chapters, this book provides an in-depth presentation of updated knowledge about orthopaedic biomechanics across all tissues in the musculoskeletal system, at all length scales, and with direct relevance to engineering and clinical applications. It is divided into three main sections to provide appropriate breadth and depth in reviewing the field. The first section presents basic structure–function relationships for the most major orthopaedic tissue types, including the hard and soft tissue elements of the musculoskeletal system—bone, ligament and tendon, disc, and skeletal muscle. The second section specifically reviews the biomechanics of the most relevant structures of the body—from head to toe. Those sections provide an updated presentation of the quantitative relationships between mechanical loading, structural function, and biological performance and also integrate discussions of relevant clinical perspectives for many of those musculoskeletal structures.

In addition to those discussions, the remaining chapters in the last section of this book specifically address current issues and opportunities facing the orthopaedic biomechanics community today. With advances in technology and improved resolution in experimental techniques, substantial progress has been made in recent years in our understanding of cellular regulation and mechanotransduction as it relates to cellular biomechanics, in the modeling of tissues and mechanics, and in understanding and harnessing the biologic factors that influence and are affected by biomechanics. In particular, chapters provide quantitative perspectives on cellular biomechanics, growth and development, the influence of aging and gender, and the computational modeling of these and other factors. Several chapters focus on trauma and injury, as well as diagnostic techniques such as gait analysis and imaging biomarkers. Lastly, many advances have been made in the fields of tissue engineering and biomaterials for this field, and these are reviewed in the context of current technological and engineering techniques. These engineering approaches, along with traditional prosthetics and orthotics practices, are reviewed to stimulate additional progress in the treatment of orthopaedic diseases.

It is my hope that this book will provide extended utility to readers in that it combines both basic biomechanics presentations and quantitative analyses and models with current practice, technologies, and outlook for the future in this field. Accordingly, I believe it will have a broad appeal to novices trying to learn the basics in this field and researchers who have been working in orthopaedic biomechanics for years. Each chapter provides an outlook for the future, addressing the biggest remaining challenges in each topic that I hope will stimulate further advances and progress in this and related areas.

Thanks to all of the contributors of this book, we have assembled a valuable contemporary resource addressing orthopaedic biomechanics while integrating those concepts with engineering and clinical issues. I hope that its readers also find novel perspectives for the interdisciplinary approaches required to translate orthopaedic biomechanics to today's "real world."

Beth A. Winkelstein, PhD
University of Pennsylvania
Philadelphia, PA

Acknowledgments

This book would not have been possible without the help of many colleagues and friends. It is with deep and sincere thanks that I acknowledge all of the authors for their generous contribution of chapters for this book. Their thoughtful and outstanding reviews, original work, and integration of basic science and clinical perspectives have provided a terrific depth and breadth to the current state of the art in the field of orthopaedic biomechanics. I am also very grateful to Benjamin Guarino for his artistic assistance. In addition, this book would never have been completed without the tireless dedication of Jennifer Leung, who played many critical roles, including ensuring consistency, reviewing chapters, and maintaining quality in all aspects of the work. Lastly, I am thankful for the encouragement, love, and support of my family and friends throughout this process.

Author

Beth A. Winkelstein is a professor of bioengineering and neurosurgery at the University of Pennsylvania, Philadelphia. She received her BSE degree in bioengineering from the University of Pennsylvania (1993) and earned a PhD degree in biomedical engineering from Duke University in 1999. She joined Penn's faculty in 2002 after completing a postdoctoral fellowship in the neuroimmunology of pain at Dartmouth Medical School. Dr. Winkelstein's research focuses on spine biomechanics and defining the mechanisms of painful spine and joint injuries, mechanical and cellular mechanisms of chronic pain, mechanotransduction of pain, and potential diagnostic and therapeutic approaches. She has pioneered several models of painful tissue injuries, which are the first painful neck injury models with clinically relevant pain symptoms. Her group implements rigorous engineering analyses in these *in vivo* systems to define relationships between biomechanical metrics, neuronal plasticity, and cellular mechanisms that drive pain. Her research program also focuses on developing new imaging approaches in ligament tissue biomechanics to understand subfailure microscale and macroscale tissue responses, as well as for the translation to clinical applications for improved diagnostic approaches. Dr. Winkelstein's research has been recognized by awards from the Stapp Car Crash Conference, the International Society for the Study of the Lumbar Spine, and the ASME. She was awarded a Whitaker Young Investigator Award, NIH Career Award, NSF-CAREER, and the 2006 Y.C. Fung Young Investigator Award for the Most Promising Young Bioengineer. She has been funded by the Whitaker Foundation, NSF, NHTSA, CDC, NIH, CSRS, DoD, and industry partners. She serves on the Editorial Board for *Spine* and is the co-editor of the *Journal of Biomechanical Engineering*. She has published more than 80 peer-reviewed manuscripts and is active in the ASME-BED, BMES, CSRS, and World Congress of Biomechanics.

Contributors

Kai-Nan An
Biomechanics Laboratory
Division of Orthopaedic Research
Mayo Clinic
Rochester, Minnesota

Kyriacos A. Athanasiou
Department of Biomedical Engineering
University of California at Davis
Davis, California

Aaron Babb
Biomechanics Laboratory
Division of Orthopaedic Research
Mayo Clinic
Rochester, Minnesota

Richard Baker
School of Health Sciences
University of Salford
Manchester, United Kingdom

Cameron R. Bass
Department of Biomedical Engineering
Duke University
Durham, North Carolina

Michael J. Bey
Henry Ford Hospital
Bone and Joint Center
Detroit, Michigan

Silvia S. Blemker
Department of Mechanical and Aerospace Engineering
Department of Biomedical Engineering
University of Virginia
Charlottesville, Virginia

Danielle R. Bogdanowicz
Biomaterials and Interface Tissue Engineering Laboratory
Department of Biomedical Engineering
Columbia University
New York, New York

Dipan Bose
Center for Applied Biomechanics
University of Virginia
Charlottesville, Virginia

Margaret K. Boushell
Biomaterials and Interface Tissue Engineering Laboratory
Department of Biomedical Engineering
Columbia University
New York, New York

Philip J. Brown
Virginia Tech–Wake Forest University School of Biomedical Engineering and Sciences
and
Virginia Tech–Wake Forest University Center for Injury Biomechanics
Winston-Salem, North Carolina

Li Cao
Department of Biomedical Engineering
Duke University
Durham, North Carolina

Chad Cole
Department of Neurosurgery
Medical College of Wisconsin
Milwaukee, Wisconsin

Jeff Crandall
Center for Applied Biomechanics
University of Virginia
Charlottesville, Virginia

Adam J. Engler
Department of Bioengineering
University of California, San Diego
La Jolla, California

Guy M. Genin
Department of Mechanical Engineering and Materials Science
Washington University in St. Louis
St. Louis, Missouri

Irene Georgakoudi
Department of Biomedical Engineering
Tufts University
Medford, Massachusetts

Christopher L. Gilchrist
Department of Orthopaedic Surgery
Duke University Medical Center
Durham, North Carolina

Michael E. Hahn
Department of Veterans Affairs RR&D
Center of Excellence for Limb Loss Prevention and Prosthetic Engineering
VA Puget Sound Health Care System
and
Department of Orthopaedics and Sports Medicine
University of Washington
Seattle, Washington

Jason J. Hallman
Department of Neurosurgery
Medical College of Wisconsin
and
Clement J. Zablocki Veterans Affairs Medical Center
Milwaukee, Wisconsin

Scott J. Hazelwood
Biomedical Engineering Department
California Polytechnic State University
San Luis Obispo, California

Amira I. Hussein
Orthopaedic and Development Biomechanics Laboratory
Department of Mechanical Engineering
Boston University
Boston, Massachusetts

David Jamison, IV
School of Biomedical Engineering, Science, and Health Systems
Drexel University
Philadelphia, Pennsylvania

Richard Kent
Center for Applied Biomechanics
University of Virginia
Charlottesville, Virginia

Stephen M. Klisch
Mechanical Engineering Department
California Polytechnic State University
San Luis Obispo, California

William R. Ledoux
Department of Veterans Affairs RR&D
Center of Excellence for Limb Loss Prevention and Prosthetic Engineering
VA Puget Sound Health Care System
and
Department of Mechanical Engineering
University of Washington
and
Department of Orthopaedics and Sports Medicine
University of Washington
Seattle, Washington

Winson C. C. Lee
Interdisciplinary Division of Biomedical Engineering
The Hong Kong Polytechnic University
Hung Hom, Kowloon, Hong Kong

Aaron K. L. Leung
Interdisciplinary Division of Biomedical Engineering
The Hong Kong Polytechnic University
Hung Hom, Kowloon, Hong Kong

Andre M. Loyd
Department of Biomedical Engineering
Duke University
Durham, North Carolina

Helen H. Lu
Biomaterials and Interface Tissue Engineering Laboratory
Department of Biomedical Engineering
Columbia University
New York, New York

Regina F. MacBarb
Department of Biomedical Engineering
University of California at Davis
Davis, California

Dennis J. Maiman
Department of Neurosurgery
Medical College of Wisconsin
and
Clement J. Zablocki Veterans Affairs Medical Center
Milwaukee, Wisconsin

Sandeep Mannava
Wake Forest University School of Medicine
Wake Forest Orthopedic Surgery Department
Winston-Salem, North Carolina

Michele A. Marcolongo
Materials Science and Engineering
Drexel University
Philadelphia, Pennsylvania

Elise F. Morgan
Orthopaedic and Development Biomechanics Laboratory
Department of Mechanical Engineering
Boston University
Boston, Massachusetts

Vasilios Moutzouros
Henry Ford Hospital
Department of Orthopaedic Surgery
Detroit, Michigan

Meghan K. Murphy
Department of Biomedical Engineering
University of California at Davis
Davis, California

Barry S. Myers
Department of Biomedical Engineering
Duke University
Durham, North Carolina

David J. Nuckley
Department of Physical Medicine and Rehabilitation
University of Minnesota
Minneapolis, Minnesota

Matthew B. Panzer
Department of Biomedical Engineering
Duke University
Durham, North Carolina

Cathryn D. Peltz
Henry Ford Hospital
Bone and Joint Center
Detroit, Michigan

Frank A. Pintar
Department of Neurosurgery
Medical College of Wisconsin
and
Clement J. Zablocki Veterans Affairs Medical Center
Milwaukee, Wisconsin

Johannes F. Plate
Wake Forest University School of Medicine
and
Wake Forest Orthopedic Surgery Department
Winston-Salem, North Carolina

Kyle P. Quinn
Department of Biomedical Engineering
Tufts University
Medford, Massachusetts

Robert L. Sah
Department of Bioengineering
University of California, San Diego
La Jolla, California

Katherine R. Saul
Department of Biomedical Engineering
Wake Forest School of Medicine and
Virginia Tech–Wake Forest University
School of Biomedical Engineering and
Sciences
Winston-Salem, North Carolina

Lori A. Setton
Department of Biomedical Engineering
Duke University
and
Department of Orthopaedic Surgery
Duke University Medical Center
Durham, North Carolina

Reza Shirazi
Department of Bioengineering
University of California, San Diego
La Jolla, California

Spencer W. Shore
Orthopaedic and Development
Biomechanics Laboratory
Department of Mechanical Engineering
Boston University
Boston, Massachusetts

Brian D. Stemper
Department of Neurosurgery
Medical College of Wisconsin
and
Clement J. Zablocki Veterans Affairs
Medical Center
Milwaukee, Wisconsin

Joel D. Stitzel
Virginia Tech–Wake Forest University
School of Biomedical Engineering and
Sciences
and
Virginia Tech–Wake Forest University
Center for Injury Biomechanics
Winston-Salem, North Carolina

Siddarth D. Subramony
Biomaterials and Interface Tissue
Engineering Laboratory
Department of Biomedical Engineering
Columbia University
New York, New York

Stavros Thomopoulos
Department of Orthopaedic Surgery
Washington University in St. Louis
St. Louis, Missouri

Ginu U. Unnikrishnan
Orthopaedic and Development
Biomechanics Laboratory
Department of Mechanical Engineering
Boston University
Boston, Massachusetts

Chris Van Ee
Design Research Engineering
Novi, Michigan

Shyni Varghese
Department of Bioengineering
University of California, San Diego
La Jolla, California

Beth A. Winkelstein
Departments of Bioengineering and
Neurosurgery
University of Pennsylvania
Philadelphia, Pennsylvania

Christopher Wolfla
Department of Neurosurgery
Medical College of Wisconsin
Milwaukee, Wisconsin

Narayan Yoganandan
Department of Neurosurgery
Medical College of Wisconsin
Milwaukee, Wisconsin

Chunfeng Zhao
Biomechanics Laboratory
Division of Orthopaedic Research
Mayo Clinic
Rochester, Minnesota

Kristin D. Zhao
Biomechanics Laboratory
Division of Orthopaedic Research
Mayo Clinic
Rochester, Minnesota

Section I

Structure and Function of Orthopaedic Tissues

1

Bone Biomechanics

Spencer W. Shore, Ginu U. Unnikrishnan, Amira I. Hussein, and Elise F. Morgan

CONTENTS

1.1 Introduction

The bones in our skeleton must meet a diverse set of functional demands, not all of which are mechanical in nature. Yet, even without detailed consideration of the biological functions of bone as an organ system and of the bone tissues that are the main constituent of whole bones, the biomechanical behavior of bone is a multifaceted, broad subject that is relevant to the study of clinical fractures, bone development, bone adaptation, and bone healing and regeneration. This chapter provides a foundation for all these topics by summarizing the current state of knowledge on the basic mechanical behavior of bone at length scales ranging from hundreds of nanometers to tens of centimeters. However, because the focus of much of the bone mechanics literature is on age-related bone fractures, many of the concepts and data that are presented are most readily connected to the study of how and when bones fail. This chapter is not the first to review bone biomechanics, and our intent is to emphasize the basic concepts and to highlight the recent advances. Some descriptions of methodological approaches and practical considerations are included, but given the scope and depth of the body of research on bone biomechanics, we refer the reader, when possible, to more specialized reviews of these particular concepts. Similarly, this chapter does not review the state of the art in bone mechanobiology or the biomechanics of fracture healing, as specific reviews in these areas have been published recently.[1–5]

This chapter is divided into five sections. The first presents basic concepts that are fundamental to understanding how to study bone as a mechanically functional structure and material. Next, we present a brief summary of the hierarchical structure and composition of bone as they relate to the study of bone mechanics. We then focus sequentially on the mechanical behaviors of bone tissue and whole bones. The final section concludes the chapter with a synthesis of the critical concepts and a list of key areas for future research.

1.2 Basic Concepts

Bone is a complex hierarchical system that undergoes a number of changes at multiple levels of its structural hierarchy as a consequence of aging, disease, and even with changes in physical activity. When considering the mechanical behavior of bone, one can analyze the entirety of a whole bone (e.g., the femur), a large portion of a whole bone (e.g., the proximal femur), or a small portion of the bone tissue that comprises the bone (e.g., a specimen of cortical bone from the femoral neck). The first two examples necessitate treatment of bone as a structure, whereas the third refers to bone as a material. The structural behavior of bone is described by how the bone deforms in response to one or more applied forces, and this behavior depends on the geometry (size and shape) of the bone, as well as on

the direction and magnitude of the applied forces, and the material behavior of the bone tissue. In contrast, the material behavior of bone is independent of its geometric consideration. Studies of the structural behavior of bone typically focus on different questions than those that examine its material behavior. For example, if the goal is to understand the risks of fracture in whole bones, the structural properties should be investigated. However, if one desires to know the changes in the behavior of bone due to mineralization, the material properties are of primary interest.

Experiments that characterize the material behavior of bone perform mechanical tests on specimens of bone tissue that have been machined into standardized shapes of simple geometry, such as parallelepipeds and cylinders. The simple geometric shape allows idealized representation of the applied force(s) and corresponding deformation(s) as geometry-independent quantities known respectively as "stress" and "strain." Stress is the force per unit area acting on a specimen and quantifies the intensity of the force applied. There are two types of stresses: axially applied normal stress ($\sigma_{xx} = F/A_x$), which can be tensile or compressive, and tangentially applied shear stress ($\sigma_{yx} = F/A_y$; Figure 1.1). In general, regions of bone tissue are subjected to both normal and shear stresses during activities of daily living and during trauma. Engineering strain is defined as the deformation of the specimen with respect to its original size and shape. Normal strain is the change in length divided by the original length, whereas shear strain is the change in angle between two lines in the material that were originally perpendicular to each other (Figure 1.1).

The basic descriptions of the material behavior of bone are readily visualized on a stress–strain curve (Figure 1.2). To construct this curve, stress (or strain) is applied at

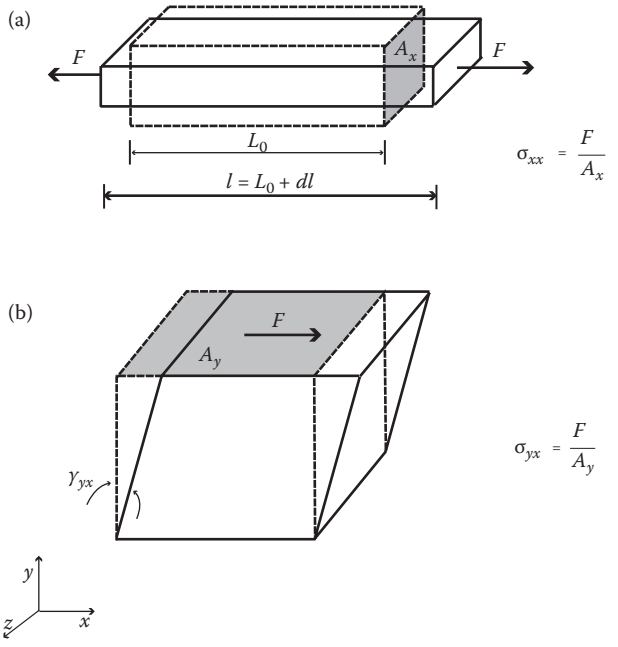

FIGURE 1.1
Schematic representation of normal and shear stresses and strains acting on a specimen. (a) Normal stress (σ_{xx}) is defined as the normal force (F) acting over a unit area (A_x) of the cross section, and (b) shear stress (σ_{yx}) is defined as the ratio of the shear force over a unit area of the cross section (A_y). The dotted lines represent the initial shape of the specimen.

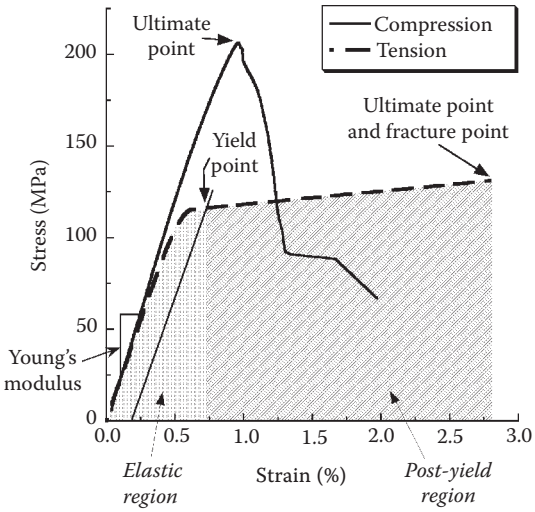

FIGURE 1.2
Stress–strain curves for cortical bone tested in compression and tension along the longitudinal direction (the direction parallel to the diaphyseal axis). Basic material properties that can be defined from the stress–strain curve are illustrated on the plot. The toughness, computed as the area under the stress–strain curve, is illustrated for the tensile curve and is equal to the sum of the two shaded areas. For this material (cortical bone), the ultimate and fracture points are coincident for tensile loading, whereas for compressive loading, the ultimate and yield points are coincident, and the fracture point is difficult to identify. (Data taken from Morgan, E. F. et al., *J. Biomech.Eng.*, 127, 557–562, 2005.)

a constant rate, and the corresponding strain (or stress) is measured in the direction in which the stress (or strain) is applied. This type of mechanical test is known as a uniaxial test. Young's modulus or the elastic modulus is the material property that describes the stiffness of the tissue, and it is defined by the initial slope of the normal stress–normal strain plot obtained from a uniaxial test (Figure 1.2). Similarly, shear modulus is defined as the slope of the initial portion of the shear stress–shear strain curve. The material properties that describe the strength of bone tissues are obtained from the yield and post-yield regions of the stress–strain curve (Figure 1.2). Yielding occurs when the material no longer behaves as an elastic material; that is, if it is loaded past the yield point and then unloaded to zero stress, the specimen exhibits permanent deformation (i.e., the unloading curve will not reach zero strain at zero stress) and/or a reduction in stiffness upon reloading. The stress and strain at the yield point are called the yield stress and yield strain, respectively. The strength of bone tissue is defined either as the yield stress or the ultimate stress, which is defined as the maximum stress the material can sustain before complete fracture. The total strain the specimen can withstand before complete fracture is defined as ductility. Toughness is defined either as the energy that the specimen can absorb before its complete fracture or as the resistance of the tissue to the initiation and propagation of cracks. The former is represented by the area under the stress–strain curve before the fracture point. The latter is known as the "fracture toughness." Quantifying the fracture toughness of a material requires a more specialized type of mechanical test than that typically used to quantify its moduli and strength.

If bone tissue were isotropic, then the stress–strain curve obtained from loading a specimen of tissue along one direction would be the same for any other loading direction. Isotropic materials are those whose material properties are independent of the loading

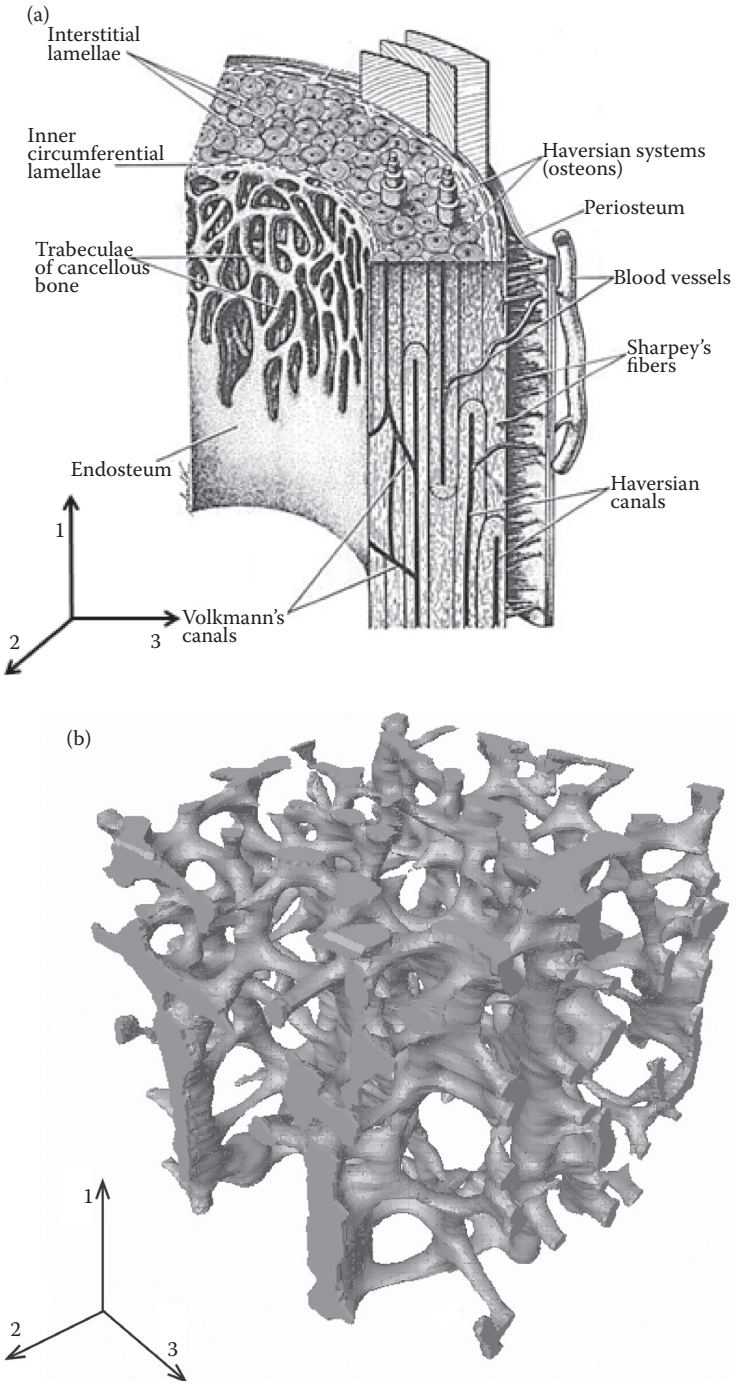

FIGURE 1.3
(a) Microstructure of the cortical wall of a typical diaphysis, with the principal directions of the microstructure indicated by the axes. (b) Three-dimensional rendering of a 5-mm cube of human vertebral trabecular bone with the principal directions indicated by the axes. (Panel (a) from Martin, R. B. et al. *Skeletal Tissue Mechanics*, Springer, New York, 2004. With permission.)

direction. Bone tissue is anisotropic, with direction-dependent material properties. Most types of bone tissue exhibit a class of anisotropy called orthotropy, in which the material properties differ along each of the three mutually perpendicular directions. Some types of bone tissue, such as cortical bone with a secondary osteon structure and trabecular bone from the vertebral body, have distinct material properties in the primary, or "grain," direction and identical properties in all directions perpendicular to the primary direction (Figure 1.3). These materials are known as transversely isotropic materials. Although only two material properties (e.g., Young's and shear moduli) fully describe the elastic behavior of an isotropic material, five elastic constants are required for the complete characterization of a transversely isotropic material, whereas an orthotropic material requires nine elastic constants. For any anisotropic material, the elastic constants can be measured directly if the loads are applied along one or more of the three principal directions of the material. If loads are applied oblique to these axes, then a coordinate transformation is required to compute the elastic constants from the experimentally derived data. Ideally, this transformation is known *a priori*; that is, the relationship between the loading axes and the principal directions is known. When the transformation is not known *a priori*, numerical optimization algorithms have been used with good success to determine elastic constants along the three principal directions of the material.[6–8] The numerical optimization scheme finds the coordinate transformation that gives the best orthotropic representation of the anisotropic stiffness matrix obtained from the obliquely applied experimental data. From the orthotropic stiffness matrix, the material properties along the three principal directions can then be determined.

1.3 Bone Composition and Structure

Bone is a complex tissue consisting of an inorganic phase, an organic phase, and water. It is approximately 60% inorganic, 8% to 10% water, and 30% organic by weight.[9] By volume, the proportions are approximately 40%, 35%, and 25%, respectively. The inorganic phase of bone is composed of an impure form of hydroxyapatite, $Ca_{10}(PO_4)_6(OH)_2$, a naturally occurring calcium phosphate. The impurities are caused by the presence of potassium, magnesium, strontium, and sodium in place of calcium ions, and fluoride in place of hydroxyl ions. The organic phase of bone consists of type I collagen (98% by weight) and a variety of noncollagenous proteins and cells (2% by weight).[10] Type I collagen consists of three polypeptide chains composed of approximately 1000 amino acids each. The collagen molecules are arranged in a parallel fashion and in a quarter-staggered array to form a collagen fibril. Within the collagen fibril, gaps known as "hole zones" (~40 nm) are present between the ends of the molecules. Also, pores exist between the sides of parallel molecules. Mineralization of the matrix starts in the hole zones.[11]

The major cellular components of bones are osteoblasts, bone-lining cells, osteocytes, and osteoclasts. Osteoblasts produce bone by laying down an unmineralized, collagenous matrix called osteoid. Bone-lining cells are a specialized type of osteoblast that cover the surfaces of the bone tissue and regulate the movement of ions across the bone surface. Osteocytes are osteoblasts that escaped apoptosis (programmed cell death) and became embedded in the mineralized tissue. Osteoclasts are multinucleated cells that are responsible for the resorption of bone tissue. A more detailed review of the cellular components of bone can be found elsewhere.[12]

Long bones, such as the tibia, femur, and humerus, can be divided into the epiphysis, metaphysis, and diaphysis (Figure 1.4). The epiphysis is found at each end of the bone and is separated from the rest of the bones by a layer of cartilage called the physis. The central portion of the long bone is called the diaphysis, whereas the metaphysis is the region between the physis and the diaphysis. The outer membrane of the bone is called the periosteum. The periosteum covers the entire length of the bone except on the articulating surface and at tendon and ligament insertion points (Figure 1.4). The endosteum lines the inner surfaces of the long bone and consists of bone-lining cells and other osteoblasts.

Mineralized collagen fibrils are the basic building blocks of bone.[13] In bone, the fibrils are arranged either in a collection of randomly oriented fibrils, as is the case in woven bone, or in parallel arrays within thin sheets called lamellae, as is the case in lamellar bone. Woven bone is mostly found in embryonic and newborn skeletons, in fracture callus, and in some metaphyseal regions of the growing skeleton. Lamellar bone is the more mature form of the bone and is the most common type found in the adult human skeleton. It results from the remodeling of woven bone or from preexisting lamellar tissues. Apart from differences in the arrangement of collagen fibrils, woven and lamellar bone also differ in composition. Woven bone has a smaller average apatite crystal size and higher cell density compared with lamellar bone.[14] Osteocytes are randomly distributed in the woven bone, whereas in the lamellar bone, the osteocytes are closely associated

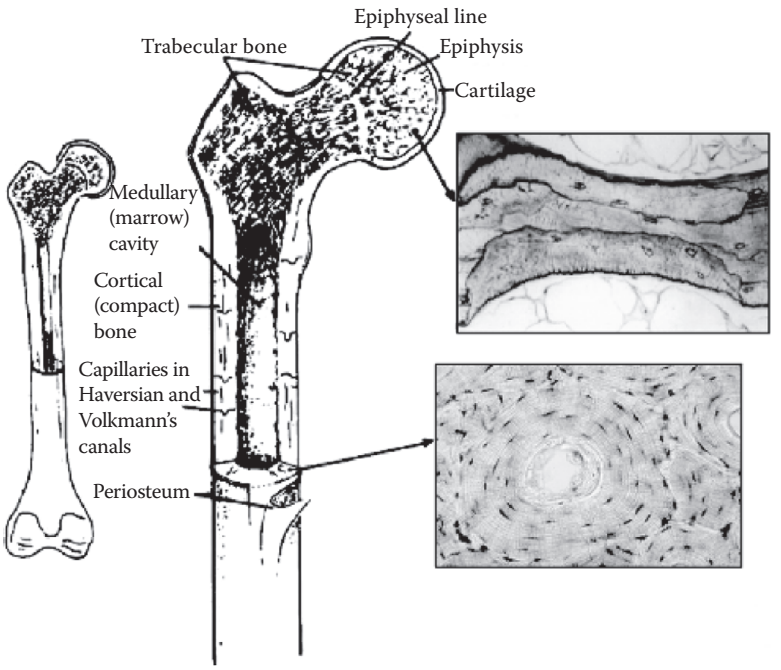

FIGURE 1.4
Structure of the femur, including a detailed view of the trabecular and cortical regions of the bone. (Modified from Hayes, W. C., and Bouxsein, M. L., In *Basic Orthopaedic Biomechanics*, edited by V. C. Mow, and W. C. Hayes, pp. 69–111, Lippincott-Raven, Philadelphia, PA, 1997. Fleisch, H., *Bisphosphonates in Bone Disease: From the Laboratory to the Patient*, p. 212, Parthenon, Nashville, TN, 2000.)

with the mineralized fibril structure.[14,15] The orientation of the collagen fibrils affects the mechanical behavior of the bones. In woven bones, the collagen fibrils are randomly oriented,[16] and, therefore, they exhibit a more isotropic behavior than the oriented lamellar bone. In both woven and lamellar bones, osteocytes are found in small ellipsoidal holes called lacunae. The lacunae are arranged along the interfaces between the lamellae in the lamellar bone. Each osteocyte has dendritic processes that extend through tiny channels called canaliculi and meet at cellular gap junctions with the processes of the surrounding cells.[17,18] The system of lacunae-canaliculi network may play a significant role in bone mechanotransduction.[19]

Lamellar bone can be found as extended parallel arrays of lamellae, called circumferential lamellae, and also as smaller cylindrical structures, known as secondary osteons. These osteons are termed secondary osteons because they are formed through bone remodeling and removal of earlier formed tissue. Each osteon consists of 10 to 30 concentric rings of lamellae that surround a central cavity called the Haversian canal. Another type of canal, called a Volkmann canal, runs transverse to the osteonal axis, providing a radial path for blood flow through the whole bone. The osteons have a typical diameter of approximately 200 μm and lengths of 1 to 3 mm. The outer surface of the osteon is lined with a thin (1–2 μm) layer of calcified mucopolysaccharides with very little collagen, called the cement line. The cement line is thought to form a weak interface between the osteon and the surrounding interstitial lamellae. The presence of the cement line can affect crack growth in cortical bone[20] by serving as a barrier to, or facilitator of, crack propagation, depending on the length of the crack.[21]

At the macrostructure scale of 1 to 10 mm, bone tissue can be categorized into two types: cortical bone (also known as compact bone or dense bone) and trabecular bone (also known as cancellous bone or spongy bone). Cortical bone has a porosity of 5% to 15% due to the presence of Haversian and Volkmann canals, as well as the lacunar-canalicular network. The latter represents approximately 10% of the total porosity in cortical bone.[22] Cortical bone is found in the diaphysis of long bones and also in the form of a thin shell surrounding the trabecular compartment in the metaphyses and epiphyses. In the adult human skeleton, cortical bone is primarily composed of secondary osteons and, to a lesser extent, circumferential lamellae, which line the outer peripheral surface of the bone, and interstitial bone tissue, which are portions of the secondary osteons that have not yet been removed by the remodeling process.

Trabecular bone is much more porous and is primarily found in the axial skeleton and in the metaphyses and epiphyses of long bones. The porosity of trabecular bone varies from 40% in the primary compressive group of the femoral neck to more than 90% in the elderly spine.[23] Trabecular bone consists of a three-dimensional (3D) network of rod-shaped and plate-shaped trabeculae (range of thickness, 50–300 μm) surrounding an interconnected pore space filled with bone marrow. Trabeculae are primarily composed of lamellar bone arranged in packets; however, thicker trabeculae can also contain secondary osteons. Similar to the values of porosity, the spatial arrangement of trabeculae, known as the trabecular architecture, can vary greatly among anatomic sites and with age. Trabecular bone from the vertebral body tends to be predominantly rodlike, whereas that from the proximal femur contains a more balanced mixture of rods and plates.[24] The trabecular architecture also undergoes significant changes with age. The trabeculae become progressively thinner with age, and for certain anatomic sites, such as the vertebral body and proximal tibia, an increase in the anisotropy of the trabecular structure is observed.[25,26]

Several different measures of density are used in biomechanical studies of bone. Ash density is defined as the ratio of ash weight (obtained after subjecting the bone tissue to 500°C) per unit of bone volume. Tissue density, ρ_{tiss}, is defined as the ratio of mass to volume of the mineralized tissue (i.e., the pore space is excluded from the volume calculation). Tissue density is approximately 2.0 g/cm^3 for cortical and trabecular bone and varies very little in the adult skeleton. Apparent density, ρ_{app}, is the ratio of the mass of bone tissue to the total volume of the bone. Volume fraction, V_f (also abbreviated as BV/TV), is the ratio of the volume of the mineralized tissue (BV) to the volume of the specimen (TV), or equivalently, one minus the porosity. The volume fraction, apparent density, and tissue density are related to each other by

$$\rho_{app} = \rho_{tiss} V_f. \tag{1.1}$$

Quantitative measures of trabecular architecture have also become routine to compute as the availability of high-resolution, 3D imaging techniques such as microcomputed tomography (μCT), peripheral quantitative computed tomography (pQCT), and micromagnetic resonance imaging (μMRI) has increased. Particularly with commercial μCT systems, default software algorithms calculate a slate of architectural metrics. These metrics include trabecular thickness (Tb.Th), trabecular spacing (Tb.Sp), trabecular number (Tb.N), connectivity density, structure model index (SMI) (a measure of the "rodlike" versus the "platelike" architecture[27]), and the degree of anisotropy.[28] The latter is a scalar measure of how preferentially the trabecular structure is oriented. Several methods of quantifying the anisotropy of the trabecular structure have been developed, including mean intercept length (MIL),[29] volume orientation distribution,[30] and star volume distribution.[31] In each case, the directional density of the tissue (the amount of tissue in a given direction) can be represented by an ellipsoid, and the ratio of the major and minor axes of this ellipsoid is the degree of anisotropy. The fabric tensor, a positive-definite, second-order tensor that defines three planes of orthotropic symmetry as well as the degree of anisotropy of the structure, can be formulated from the ellipsoid[32,33] (Figure 1.5). In this way, quantitative morphological and anisotropic measures of trabecular architecture can be obtained and used for modeling and analysis.

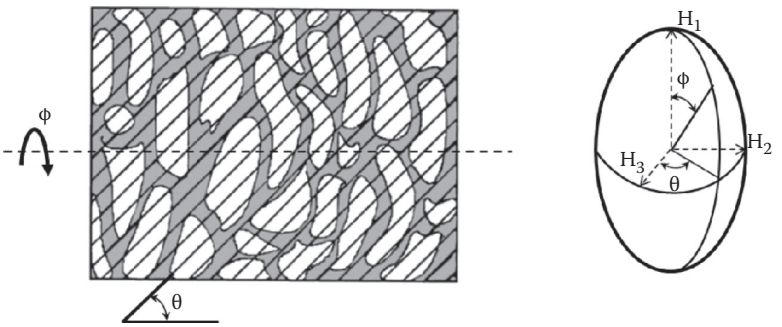

FIGURE 1.5
Fabric representation of two-dimensional trabecular architecture using the mean intercept length (MIL) method. The ellipsoid, constructed from average values of the MIL of 3D trabecular architecture representation, shows the directional density of a tissue structure. (Adapted from Cowin, S. C., and Mehrabadi, M. M., *J. Biomech.* 22, 6–7, 503–515, 1989.)

1.4 Mechanical Properties of Bone Tissue

1.4.1 Cortical Bone

1.4.1.1 Basic Material Properties

As would be expected, based on the ordered osteonal and lamellar structures, cortical bone is anisotropic in its material behavior. The strength and tensile-compressive moduli of cortical bone along the longitudinal direction (the direction aligned with the diaphyseal axis) are greater than the properties along the radial or the circumferential directions (Table 1.1).[34] Comparatively small differences in these properties have been observed in the radial versus circumferential directions, suggesting that cortical bone can be treated as a transversely isotropic material. When loaded in tension along the longitudinal direction, cortical bone exhibits a bilinear stress–strain response consisting of a distinct yield point that separates a linearly elastic region and a region of linear hardening that ends abruptly at a fracture strain of less than 3% (Figure 1.2). The slope of the hardening region is often termed the "post-yield modulus." In contrast, for compressive loading along the longitudinal direction, the bone hardens rapidly after yielding but then exhibits "softening" before reaching failure at approximately 1.5% strain. Cortical bone specimens loaded in the transverse direction, however, fail in a more brittle manner compared with those loaded in the longitudinal direction. Analysis of the ultimate strength of the human femoral bone under various loading modes (Table 1.1) shows that strength is highest under compression in the longitudinal direction and is weakest under tensile loading in the transverse direction. The microstructural mechanisms that give rise to the differences in yield and post-yield behaviors between loading modes and among loading directions have not been well defined.

1.4.1.2 Viscoelasticity

The strength and stiffness of cortical bone are dependent on the rate at which the loads are applied, indicating that this tissue exhibits viscoelasticity. However, the effect of loading rate on strength and modulus is only moderate, as a six-order increase in the strain

TABLE 1.1

Anisotropic and Asymmetric Properties of Human Femoral Cortical Bone

Longitudinal direction	Elastic modulus	17,900 ± 3900 MPa
	Poisson's ratio	0.62 ± 0.26
	Ultimate tensile stress	135 ± 15.6 MPa
	Ultimate compressive stress	205 ± 17.3 MPa
Transverse direction	Elastic modulus	10,100 ± 2400 MPa
	Poisson's ratio	0.62 ± 0.26
	Ultimate tensile stress	53 ± 10.7 MPa
	Ultimate compressive stress	131± 20.7 MPa
Shear	Modulus	3,300 ± 400 MPa
	Ultimate stress	65 ± 4.0 MPa

Source: Reilly, D. T., and Burstein, A. H. *J. Biomech.*, 8, 6, 393–396, IN399–IN311, 397–405, 1975. With permission.

rate only increases the modulus by a factor of two and the strength by a factor of three.[35,36] During normal physiological activities, the bone tissues are subjected to strain rates of 0.1% strain per second to 1.0% strain per second, and the monotonic response of cortical bone can be assumed to have only minor rate dependency. Yet, the stiffening and strengthening effects that have been observed with increasing strain rates are still clinically relevant because strain rates during impact loading can be more than 10-fold greater than the normal physiological range. Bone is more brittle at high strain rates, and the loading rate also has a significant effect on the accumulation of damage within the bone tissue.[37]

1.4.1.3 Damage

When cortical bone is loaded past the yield point, significant degradation of the material properties occurs.[38] As will be discussed later, many of the studies of this mechanical degradation have used fatigue loading and have tracked the progressive loss in stiffness that occurs with increasing duration of loading. Damage in cortical bone has also been studied from the standpoint of deterioration in the tissue microstructure, known as "microdamage." The presence of microdamage in bone was first reported by Frost,[39] and, together with a collection of subsequent studies, that investigation helped to establish microdamage as a normal consequence of physiologic loading.[40]

Microdamage may appear as a debonding of the collagen–hydroxyapatite composite or as slippage of the lamellae along the cement lines.[41] Both of these microstructural events may give rise to the residual strains that are observed upon unloading after the specimen has been loaded past the yield point. Microdamage due to fatigue is fairly uniform in size and randomly distributed in all directions or along the three principal directions.[42] The post-yield behavior of bone is primarily associated with microdamage accumulation and is dependent on the volume fraction, the orientation of the crack relative to the microstructure, and the loading axis.[37,43,44]

Microdamage has been the subject of much attention in the literature as a possible contributor to bone fragility and as a potentially deleterious side effect of antiresorptive drug therapies that are now widely used to treat osteoporosis.[45,46] *In vitro* mechanical tests have found that microdamage is associated with a decrease in modulus,[47] and a weak inverse relationship has also been reported between fracture toughness and microdamage density.[48] Microcrack accumulation increases exponentially with age in cortical bone and is significantly higher in females than in males.[48–50] Although these collective results might suggest a prominent role for microdamage in fracture risk, a definitive link has not yet been established. Evidence that microdamage may be a toughening mechanism for bone tissues in the post-yield region[51] further complicates this picture and underscores the need to better understand the microstructural origins and progression of failure processes in cortical bone.

1.4.1.4 Fracture

Fracture of cortical bone can occur from repetitive, subcritical loads (fatigue failure) or from applied loads that cause local stresses exceeding the strength of the tissue. The fracture toughness of cortical bone has been quantified in terms of the critical stress intensity factor (K_c) and the critical strain energy release rate (G_c). The critical stress intensity factor denotes the local intensity of the stress in the immediate vicinity of a crack tip, whereas the critical strain energy release rate characterizes the fracture toughness in terms of the surface energy of the newly formed surface area that is created in the material as an existing

crack grows. Values of K_{IC}, the fracture toughness for "mode I" loading (tensile loading), range between 2 and 6 MPam$^{1/2}$ and tend to be lower for longitudinal compared with transverse fractures.[52–54] The anisotropic nature of the fracture toughness can be attributed to (1) a crack propagating parallel to the osteon in the longitudinally oriented crack while it propagates perpendicular to the osteons in the transversely oriented crack, and (2) a weak path at the cement lines providing additional energy dissipation mechanisms for the transverse cracks.[55, 56]

The fracture toughness of human cortical bone has been found to increase with crack extension up to crack lengths of approximately 2 mm.[57] This increase in the fracture toughness has been attributed to extrinsic strengthening mechanisms such as crack, bridging by collagen fibers and crack deflection by osteons.[58] These extrinsic toughening mechanisms act away from the crack tip and reduce the stress at the crack tip. The increase in the toughness with the crack extension has been explained using a resistance curve (R-curve) fracture–mechanics approach.[57,59,60] Studies have shown that strain rates as well as aging affect bone's resistance against crack propagation.[61–63]

Using a scratch test with a nanoindentation system, the age-related changes in the toughness of bone at ultrastructural levels were assessed by Wang et al.[64] In these tests, the toughness of cortical bone was found to decrease with age. Using scratch tests, the anisotropic wear resistance of human mandibular cortical bone, along directions parallel and perpendicular to the osteons, was determined by Gao et al.[65] and was found to be greatest in the parallel direction. Even with numerous studies on cortical bone fractures, a complete understanding of the fracture risk associated with aging, disease, or loading modes of the bones is still lacking.

1.4.1.5 Fatigue

Reduction in the mechanical properties due to sustained or cyclic loading over time induces fatigue fracture.[66,67] Fatigue fracture can occur in individuals with increased repetitive physical activities and with the accumulation of unrepaired fatigue-induced microdamage.[68] Fatigue behavior of bone is affected by a number of factors, such as the mode and frequency of the applied load. Cortical bone has greater resistance to fatigue failure in compression than in tension,[66, 69] and substantial reductions in fatigue lifetime have been observed when torsional loading is superimposed on tension–compression loading.[70] Higher loading frequencies have been found to produce longer fatigue lifetimes.[71,72]

Degradation of modulus and Poisson's ratio occur due to fatigue loading.[67,73] This type of reduction in the mechanical properties, termed fatigue-induced damage, has been extensively studied by many researchers.[41,56,68,73,74] Recently, the use of sequential fluorescent stains to label cracks and crack growth[75,76] has enabled more in-depth studies of the relationships between microcracking, microstructure, and macroscale mechanical properties.[77]

1.4.1.6 Multiaxial Loading

Cortical bones can be subjected to multiaxial loading conditions in the body, especially during traumatic events such as a fall. The multiaxial strength of cortical bones cannot be determined from uniaxial material properties alone.[78] Also, isotropic and symmetric failure criteria, such as the von Mises criterion, are not capable of describing the multiaxial strength of cortical bone, which is both anisotropic and stronger in compression than in tension. Therefore, a more generalized failure criterion, the Tsai–Wu criterion, has been

applied to cortical bone.[78] The Tsai–Wu criterion was originally developed for composite materials and can account for differences in tensile and compressive strengths, as well as low shear strength with respect to tensile strength. This failure criterion works well for biaxial stress states but may not be as accurate for triaxial stress states.[79]

1.4.1.7 Influence of Porosity and Mineralization on Mechanical Properties of Cortical Bone

Microstructural parameters such as porosity and mineralization have significant influences on the material properties of cortical bone.[22,80] Porosity increases with age and is negatively correlated with Young's modulus,[22,80] ultimate compressive stress,[81] and fracture toughness.[82] Changes in porosity account for more than 75% of the variability in the strength of the cortical bone.[83] The elastic moduli in the transverse direction are less sensitive to changes in porosity compared with the elastic modulus in the longitudinal direction. Even small changes in the mineralization content can change the modulus and strength of cortical bones and are considered to be the main contributor to bone stiffness.[84] Mineral content does not seem to be related to donor age and does not have a significant effect on the tensile stiffness and strength of aging cortical bone.[83] However, instances of local hypermineralization in cortical tissues can lead to crack formation and propagation.[85]

1.4.1.8 Effects of Aging on Mechanical Properties of Cortical Bone

Age-related changes in the mechanical properties of cortical bone are attributed to an increase in the porosity,[83] hypermineralization,[86] microdamage accumulation,[71] and adverse changes in the collagen network.[87] The strength of cortical bone under tension and compression reduces by approximately 2% per decade after 20 years. Ultimate tensile strain also decreases by approximately 10% per decade, from a high of 5% strain at 20 to 30 years of age to a low of less than 1% strain at more than 80 years of age. Also, fracture toughness decreases significantly with aging,[88,89] most likely due to changes in the collagen network[87] and in the ratio of hardness values between the osteons and the interstitial bone.[69,90] One of the most widely studied age-related changes in the collagen phase of bone is the increase in nonenzymatic glycation,[87,91] which has been shown to stiffen the collagen network[92] and to reduce the fracture toughness of cortical bone.[93]

1.4.1.9 Microscale and Nanoscale Properties of Cortical Tissue

Much of the research on cortical bone described thus far has been conducted on specimens whose dimensions are on the order of several millimeters or centimeters. Cortical bone is hierarchical in nature, and an understanding of the material properties at the microscale is important for defining structure–function relationships in the bone. Early work on the mechanical properties of cortical tissue at length scales of less than several hundred micrometers focused on osteons and interstitial bone using experimental approaches that isolated individual osteons and that machined microbeams (~200 μm length) of cortical tissue for three-point bend tests.[94–99] The mechanical properties of osteons vary with different collagen fiber orientations and also with the mineral density and loading modes; moduli are on the order of 4 GPa for shear loading and 5 to 12 GPa for tensile and compressive loading.[94–97] "Pull-out" and "push-out" tests have been developed to determine the shear strength of osteons[97,100] and the interfacial strength of cement lines.[101,102]

The interfacial strength of the cement line was observed to be significantly lower than the shear strength of the osteonic lamellae.[101,102]

Subsequent work on the small-scale properties of cortical tissue has used nanoindentation testing of osteonal and interstitial lamellae.[103,104] Nanoindentation has the capability to selectively target specific microstructural features on the order of 1 μm, and the results from the indentation tests are relatively independent of specimen size in contrast with the results from microbeam bending tests. The material properties of the cortical tissues derived from nanoindentation depend on the orientation of the indentation[105] and also on the indentation strain rate.[106] Elastic moduli of 22.5 ± 1.3 GPa for the osteonal lamellae and of 25.8 ± 0.7 GPa for interstitial lamellae have been obtained in the longitudinal direction using nanoindentation.[103] The higher elastic modulus of lamellae compared with that of osteons was attributed to the increased mineralization in the lamellae. Most of the studies using nanoindentation were conducted under dry conditions. It should be noted that the properties of cortical bone derived under dry conditions are higher than those obtained under wet conditions.[107] Most recently, focused ion beam and femtosecond lasers have been used to produce microbeam and nanobeam specimens of cortical beams for mechanical testing.[108–110] Focused ion beams, along with atomic force microscopy, are capable of determining anisotropic properties and fracture patterns of cortical tissue.[109]

1.4.1.10 Micromechanical Modeling of Cortical Tissues

As evident from the previous sections, the material properties at the macroscale and microscale are different. The mechanical behavior at any scale is affected by the structural and material properties at the lower level. A number of micromechanical models have been developed to describe the contributions of these small-scale properties to the mechanical behavior of cortical bone and cortical tissue. These models can be broadly divided into ultrastructural models and microstructural models. Ultrastructural models of cortical tissues have focused on the role of minerals and collagen fibers on the behavior of the tissues. Based on the arrangement of microstructural components, the micromechanical model can be further divided into (1) mineral-reinforced collagen matrix model,[111,112] in which the anisotropy is due to the mineral, and (2) collagen-reinforced mineral matrix model,[113,114] in which collagen is treated as the anisotropy-forming material. Microstructural models derive the material properties by assuming the Haversian canal to be embedded in an isotropic extracellular matrix or by assuming the secondary osteonal fibers to be embedded in a matrix of interstitial bone. Hierarchical models that synthesize ultrastructural and microstructural models have also been developed to perform multiscale modeling of cortical bone.[115,116] Determination of the mechanical properties of microstructural components and accurate modeling of microstructural interaction through micromechanical models would certainly improve our understanding of the structure–function–property relationships and damage behavior of cortical bones.

The vast majority of the proposed micromechanical models for cortical bone and cortical tissue have considered only tensile or shear loading and have modeled the cortical material as a fiber-reinforced composite. However, cortical bone exhibits a number of phenomena that are not consistent with that class of composites. These phenomena include higher strength in compression than tension (Table 1.1), marked permanent volumetric strain upon unloading after the yield point has been exceeded,[117,118] and compressive failure patterns consisting of vertical splitting.[117] Evidence that much of the mineral in cortical tissue resides outside the hole zones,[111] essentially resulting

in a ceramic rather than polymeric matrix, may explain these discrepancies. A distinct class of micromechanical models may be needed to describe the compressive behavior of cortical bone and to form a comprehensive picture of the mechanical behavior across the multiple loading modes.

1.4.2 Mechanical Behavior of Trabecular Bone

Trabecular bone—also referred to as cancellous or spongy bone—can be viewed at the apparent level (i.e., the scale at which several trabeculae and intervening pores are simultaneously observable; typically ~5–10 mm) as a highly porous material with anisotropic mechanical properties. Due to its high porosity as compared with cortical bone, the apparent-level mechanical properties of trabecular bone are primarily determined by the volume fraction (or, similarly, the apparent density). More minor, but still important, contributions to the apparent-level behavior come from the architectural arrangement of the trabecular network and the tissue-level properties of the individual trabecula.

1.4.2.1 Basic Material Properties

As with cortical bone, the strength of trabecular bone is greater in compression than in tension and is lowest in shear, although these differences decrease with decreasing apparent density.[119,120] The stress–strain curve for trabecular bone does not exhibit a clear linear region nor a well-defined yield point (Figure 1.6). However, this tissue is nevertheless frequently treated as a linear elastic material, and once the modulus is calculated from a linear or polynomial curve fit[117] to the initial portion of the curve, the yield point is defined by the 0.2% offset method.

1.4.2.2 Density-Dependence and Heterogeneity

Trabecular bone can display substantial spatial heterogeneity in both density and architecture, even within a given anatomic site. For example, in the vertebrae, variations in density

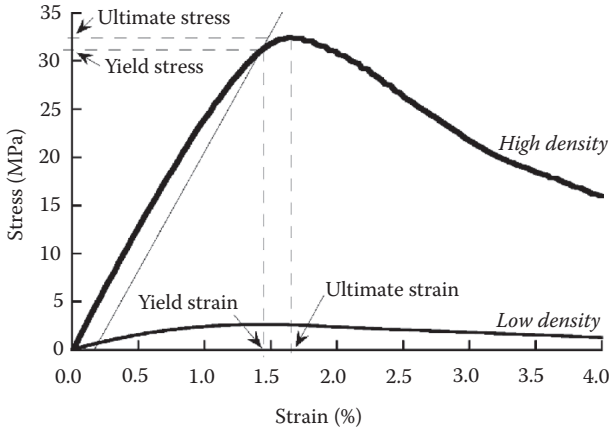

FIGURE 1.6
Stress–strain curves for high- and low-density specimens of trabecular bone loaded in uniaxial compression along the primary direction. Some of the basic material properties are indicated on the figure.

and architecture have been observed along the superior–inferior as well as posterior–anterior directions.[121,122] These variations in density and architecture can then lead to heterogeneity in the apparent-level elastic and strength properties of trabecular bone. Approximately 70% to 90% of the variances in the modulus and strength of trabecular bone can be explained by volume fraction or apparent density.[123–126] These dependencies are typically described using linear or power-law relationships. Numerous studies have indicated that the power-law exponent for human trabecular bone is between 2 and 3 for modulus[124,126] and 2 for compressive strength[23,127] (Figure 1.7). That these exponents are greater than 1 suggests that small decreases in density that occur in the course of the normal aging process have severe consequences for the load-bearing capacity of trabecular bone. However, these power-law relations are often obtained from sets of bone specimens that collectively span a wide range of densities and that are pooled from multiple sites. Within a single anatomic site, the modulus and strength relations seem to be linear because the range of apparent densities is less than an order of magnitude.[23,126,128]

In addition to spatial heterogeneity, the density, architecture, stiffness, and strength of trabecular bone vary with respect to age, disease status, loading direction, and loading mode. Both modulus and strength decrease with age, declining by approximately 10% per decade,[127,129] and pathologies such as osteoporosis, osteoarthritis, and bone cancer have also been shown to affect mechanical properties.[130,131] Variations can also occur within a given anatomic site. For example, Young's modulus can vary by as much as 100-fold within a single epiphysis,[132] and differences in strength of as much as fivefold have been observed within the proximal femur.[133] Typically, the modulus of human trabecular bone ranges between 10 and 3000 MPa, whereas strength, which is linearly and strongly correlated with modulus,[23,132,134] is generally two orders of magnitude smaller, in the range of 0.1 to 30 MPa.

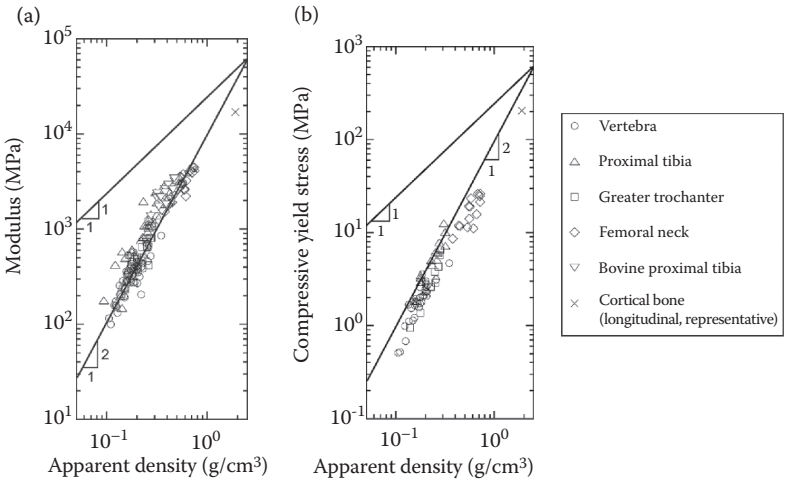

FIGURE 1.7
Log–log plots for (a) Young's modulus and (b) compressive yield strength as functions of apparent density. Lines indicating power-law exponents of 1 and 2 are drawn on the plots. (Data from Morgan, E. F, and Keaveny, T. M., *J. Biomech*., 24, 569–577, 2001; Morgan, E. F. et al., *J. Biomech*. 36, 7, 897–904, 2003.)

1.4.2.3 Anisotropy

The anisotropy that trabecular bone exhibits in microstructure is also present in elastic modulus[127,134,135] and strength.[127,136] Indeed, the principal directions of the mechanical anisotropy of trabecular bone have been found to be very closely aligned with the principal directions of the fabric tensor.[137] As such, trabecular bone typically exhibits orthotropic symmetry,[138,139] although in some cases, such as in the vertebrae, it can display transverse isotropy.[137] The ratios of elastic modulus and strength in the superior–inferior direction to those in the transverse direction in human vertebral bone are 3.4 and 2.8, respectively.[127] Similar ratios for elastic modulus have been found for other anatomic sites.[134,140–142]

The magnitude of the anisotropy in compressive strength seems to increase with age.[127,143] Given that apparent density and volume fraction decrease with age, the age-related increase in anisotropy may be a result of adaptive remodeling. As the total amount of bone tissue declines with age, a greater proportion of the remaining tissue remains oriented in the principal direction, thus mitigating the concomitant decline in stiffness and strength along this direction (Figure 1.8).

1.4.2.4 Yield Strain

Yield strain is a notable exception to the abovementioned mechanical anisotropy and density dependence of trabecular bone. High-density trabecular bone, such as that from the human femoral neck and bovine proximal tibia, tends to have isotropic yield strains.[144,145] The compressive yield strains of human vertebral trabecular bone, which is of much lower density, are higher when the loading direction is 45° oblique to the principal direction as compared with when the loading is "on-axis," but the difference is less than 10%.[145] Ultimate strains in trabecular bone also seem to be isotropic and are in the range of 1.0% to 2.5%,[144,146] whereas yield strains range from 0.70% to 0.77% in compression and from 0.65% to 0.71% in tension.[23]

Yield strains in trabecular bone also exhibit only a weak dependence on apparent density and volume fraction.[23,127,128,147] Compressive yield strains increase slightly with increasing density for human vertebral trabecular bone and are not dependent on density for higher-density trabecular bone. Overall, standard deviations of yield strains within a given anatomic site are on the order of one-tenth of the mean, whereas significant differences in the means occur between sites, indicating that yield strains can be considered relatively constant within sites and heterogeneous across sites.[23] Characterizing yield in trabecular bone in terms of strain rather than stress can, thus, provide a greatly simplified picture of failure in this tissue because a strain-based failure criterion may not need to account for interspecimen differences in apparent density.[148]

1.4.2.5 Viscoelasticity

The viscoelasticity of trabecular bone *in vitro* is minor in that both the compressive modulus and the compressive strength are proportional to the strain rate raised to the power of 0.06.[124,149] Minor, strain-dependent effects in stress-relaxation experiments have been observed,[150] indicating that trabecular bone is technically nonlinearly viscoelastic. Trabecular bone has similar creep characteristics as cortical bone and exhibits an initial rapid increase in strain followed by a steady-state regime with a constant creep rate and, finally, another rapid increase in strain just before creep fracture. Power-law relationships

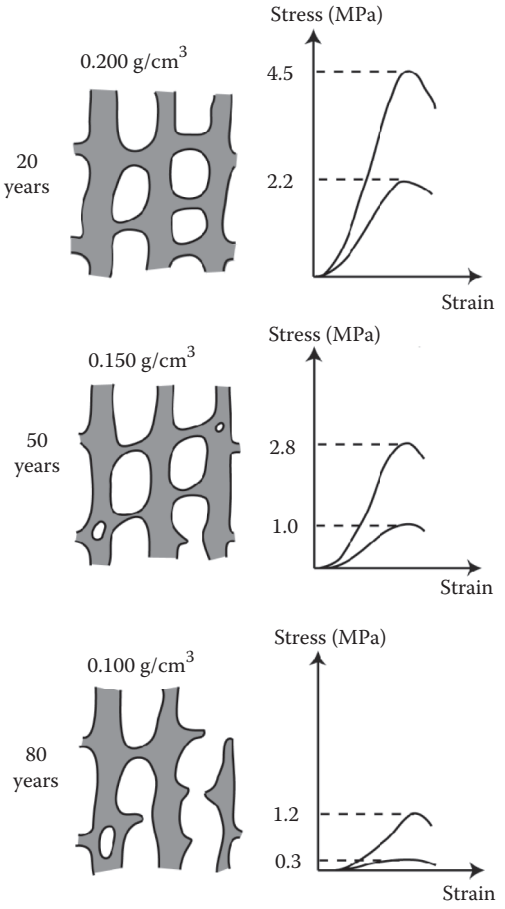

FIGURE 1.8
Two-dimensional schematic of age-related changes in the apparent density and degree of anisotropy of human vertebral trabecular bone. The individual's age is listed on the left. The corresponding stress–strain curves for similarly aged specimens tested in compression in the primary (superior–inferior) direction and in the transverse (medial–lateral or anterior–posterior) direction are shown. In this schematic, the compressive ultimate strength in the primary direction decreases by a little less than fourfold from 20 to 80 years of age, whereas the strength in the transverse direction decreases by more than sevenfold. (From Mosekilde, L., *Technol. Health Care*, 6, 5–6, 287–297, 1998. With permission.)

for creep strain rate and time to failure in creep have been proposed.[151] High strain rates may also affect the contribution of the bone marrow to the mechanical behavior of trabecular bone. Although the stiffening effects of bone marrow are negligible except at high strain rates (10 strain/s), the confining effects of the cortical shell may allow hydraulic stiffening *in vivo* under dynamic loads, such as during burst fracture incidents.[152,153]

1.4.2.6 Post-Yield Behavior and Damage–Reload

Although trabecular bone yields at strains of approximately 0.7% in compression, it can sustain compressive strains of up to 50% while still maintaining a large fraction of its load-bearing capacity. If a specimen is compressed beyond yield (not exceeding 5% strain),

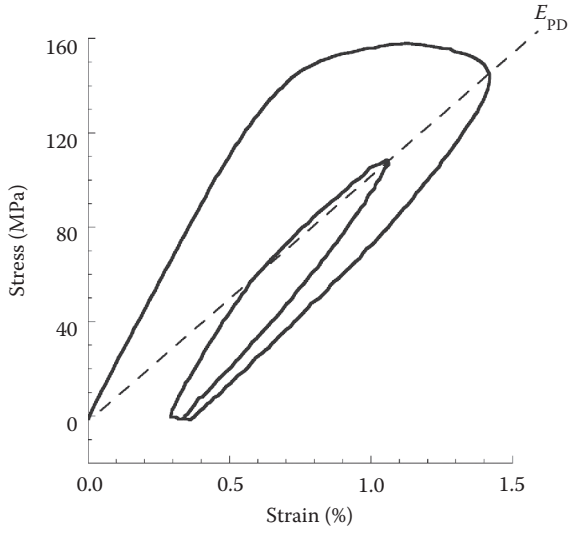

FIGURE 1.9
Post-yield behavior of vertebral trabecular bone for a single load–unload–reload cycle. (From Keaveny, T. M. et al., *J. Orthop. Res.*, 17, 3, 346–353, 1999. With permission.)

unloaded, and reloaded, permanent residual strains and a loss of stiffness (as quantified by a comparison of the slope of the unloading curve with the initial elastic modulus) occur (Figure 1.9).[154] Upon reloading, the initial modulus is initially similar to the original elastic modulus but soon decreases to match the "perfect damage" modulus (a secant modulus from the origin to the point of unloading). The reduced stiffness indicates damage whereas the accumulation of residual strain has the appearance of plasticity, although this residual deformation can result from various mechanisms, such as incomplete crack closure. The magnitudes of this stiffness loss and the amount of residual strain are highly correlated with the value of the applied strain just before unloading (r^2 = 0.94 and 0.96, respectively). Also, modulus is reduced more severely than strength, the loss of which is a function of both applied strain and apparent density.[154] These effects occur in trabecular samples and in the entire vertebral body,[155] indicating that isolated overloads that do not cause overt fracture of the bone may cause subtle but cumulative permanent deformations that could lead to clinical fractures. The qualitative similarity of this damage–reload of trabecular bone to the behavior of cortical bone loaded in tension[38,156] suggests that the dominant physical mechanisms for the damage behavior act at the nanometer scale of the hydroxyapatite and collagen.

1.4.2.7 Microdamage and Fracture

The large reductions in apparent modulus that occur with overloading (Figure 1.9) are the result of damage within the trabeculae, meaning that microscopic cracking occurs as opposed to overt fracture of individual trabecula.[157,158] These cracks can occur at very small scales[159] and seem to be related to the magnitudes of both apparent- and tissue-level strains.[160,161] Measurements of tissue-level deformations via digital image correlation applied to bending tests of single trabeculae indicate that microdamage initiation occurs at tissue-level strains of approximately 1.6% and differs in compression versus tension.[162] It is

important to consider that, due to the porous, irregular structure of trabecular bone, some tissue-level strains can be high enough to induce local yielding and a concomitant decline in whole-specimen properties even for low magnitudes of applied stress,[161,163] consistent with the consensus that the presence of microdamage *in vivo* in trabecular tissue is the norm rather than the exception.

Microdamage within trabecular bone can also be imaged and quantified using radiopaque contrast agents and microcomputed tomography.[161,164] Such methods are able to differentiate and quantify diffuse and linear cracks along the trabecular struts. Diffuse cracks appear more frequently in plate-like trabeculae and are self-limiting in length, whereas linear cracks, which are more common in osteoporotic bone,[165] are more often present in rod-like struts and tend to coalesce and initiate fracture.[166] Under both pre-yield and post-yield loading conditions, microdamage shows significant correlations with microarchitectural parameters and volume fraction, although an increase in the SMI—indicating a predominance of trabecular rods—is the strongest predictor, accounting for 40% of the variance in the amount of microdamage.[167] In general, microdamage has been found to increase with age, similar to the case with cortical bone, and is associated with a low-density and rodlike trabecular architecture.[167–169]

The propagation of damage and yielding in trabecular bone is anisotropic. When loaded in on-axis compression, yielding in rodlike vertebral trabecular bone seems to progress along vertical trabeculae. In contrast, when loaded in the perpendicular direction, local high strains are the result of bending.[170] In a recent study, failure modes were similar for platelike trabeculae in any loading orientation, whereas rodlike trabeculae oriented parallel to the loading axis yielded in compression and rodlike trabeculae oriented perpendicular to loading yielded in bending and tension.[171] Also, on-axis loading can be detrimental to the off-axis mechanical properties due to yielding of the platelike trabeculae in on-axis overloading.

The fracture toughness of trabecular bone has not been studied extensively but may yield insight into fracture etiology. For example, large stress fracture cracks that grow in between struts along the main trabecular direction have been observed in low-trauma fractures.[172] As with many of the mechanical properties of trabecular bone, a strong dependence on density has been found for fracture toughness.[173]

1.4.2.8 Fatigue

The cyclic compressive loading of trabecular bone can cause loss of stiffness and the accumulation of residual strain even for low levels of applied load.[174–176] This type of progressive failure at subcritical loads can lead to the loosening of implants.[177] The rates at which modulus decreases and damage accumulation occurs in fatigue increase with increasing magnitudes of applied strain.[174] The mechanisms of failure in fatigue, however, seem to occur at the ultrastructural level, which means that they are not dependent on site-specific properties such as modulus and yield strain.[178] Interestingly, creep was originally proposed as a dominant mechanism of fatigue failure,[179] but more recent work[180] has contradicted that earlier analysis. Static and cyclic tests on human trabecular specimens under physiologic loads (750–1500 microstrain) indicate that the time required for full recovery of residual deformation is more than 20 times longer than the duration of the applied loads.[175] These results support the notion that nontraumatic fractures may be related to long-term creep effects.

Compressive fatigue life of trabecular bone is also a function of fabric—a measure of the directional density (or, equivalently, anisotropy) of the trabecular structure. A power-law relationship for the number of cycles to failure as a function of volume fraction, fabric, and

applied stress in human vertebral trabecular bone yields an excellent fit to experimental data ($r^2 = 0.95$), and a significant contribution of the degree of anisotropy toward the prediction of fatigue life has been noted.[181] More recently, off-axis fatigue tests have been conducted and have shown that the lifetime decreases drastically as compared with on-axis fatigue loading.[182]

1.4.2.9 Multiaxial Loading

Because complex loading conditions can exist *in vivo,* and nonhabitual events such as falls or accidents can induce off-axis loads, the development of multiaxial failure criteria for trabecular bone is of significant interest. This is particularly important for osteoporotic bone whose structure in whole bones, such as the vertebrae, may be more specifically adapted to habitual loads at the expense of load-bearing capacity in less common loading directions.[183] Early theoretical work on multiaxial failure in trabecular bone proposed fabric-based yield criteria.[184,185] Experimental validation of these criteria was not carried out at the time because some of the necessary data, such as the tensile and compressive strengths of a given specimen, were not obtainable experimentally. This barrier was subsequently overcome using numerical simulation, as discussed later in this chapter. More recent works on multiaxial failure used large sets of data from mechanical tests that used uniaxial, biaxial, and triaxial loading of bovine[186,187] and human[188,189] trabecular bone. The results of these works indicate that the von Mises criterion does not work well for trabecular bone, that the Tsai–Wu criterion is only a reasonable predictor of failure for this tissue when the yield envelope that this criterion predicts is modified to account for interspecimen variations in apparent density, and that fabric-based criteria can also provide moderately accurate predictions of failure under a subset of multiaxial loading conditions. A completely strain-based yield criterion has also been proposed that is independent of density and fabric, although this criterion has not yet been validated against experimental data.[148] The development of these multiaxial criteria represents significant progress in improving constitutive models for numerical simulation of damage accumulation and failure of trabecular bone, whole bones, and bone implant structures.

1.4.2.10 Structure–Composition–Function Relationships

As illustrated in Figure 1.7, density accounts for much, but not all, of the variation in strength and stiffness of trabecular bone. The trabecular architecture also plays a significant role. For example, Ulrich et al.[190] found that the amount of variation in the elastic modulus for a set of specimens from multiple anatomic sites increased from between 37% and 67% when the regression model included only volume fraction to between 82% and 92% if one or several architectural measures were also included. These types of multiple regression analyses often do not yield definitive results regarding the independent role of architecture because many of the architectural parameters are often highly correlated with measures of density. One exception is the degree of anisotropy, which has been found to be highly independent of volume fraction[191] As will be discussed in the next section, the dependence of mechanical properties on the trabecular architecture has led to the formulation of several analytical models for predicting mechanical properties from density and architectural characteristics.

The composition of the trabecular tissue also has a significant effect on apparent-level mechanical properties. Recent work by Chen and McKittrick,[192] in which demineralized,

deproteinized, and untreated samples of bovine femoral trabecular bone and elk antler were tested in compression, showed a strong dependence on density for all three treatments, but noted marked differences among treatments in the failure characteristics. Demineralized samples tended to fail in plastic buckling, whereas deproteinized samples failed by brittle crushing. Also, the elastic modulus and compressive strength of the untreated samples were much larger than the treated samples, indicating a synergistic effect between mineral and protein in trabecular bone tissue.

1.4.2.11 Analytical Modeling

Seminal work in the development of analytical models for the mechanical behavior of trabecular bone arose from treating this porous tissue as a cellular solid.[125,193] Cellular-solid models idealize the microstructure as a periodic array of unit cells, and by accounting for volume fraction, mechanical properties of the material that comprises the cell walls (i.e., tissue-level properties), and the cell geometry, they can mimic the basic modes of failure: buckling, plastic yield, and brittle fracture. Asymmetric, open- and closed-cell models adequately describe the experimental data on trabecular bone; specifically, the dependence of Young's modulus and compressive strength on apparent density raised to the second power[125,192,194] and the dependence of fracture toughness on density raised to a power between one and two.[173,194]

The dependence of modulus on the square of density indicates bending-dominated linear elastic behavior, and the dependence of compressive strength on the square of density indicates failure by buckling.[195] These analytical results are supported by the results of numerical simulations that suggest that bending is the dominant mode of linear elastic deformation in trabecular bone and that maximum tissue-level strains exist in rodlike elements aligned with the compression axis.[196,197] Overall, the cellular-solid models have a substantially advanced mechanistic understanding of the potential modes of deformation and failure in trabecular bone.

A variety of efforts have been undertaken to incorporate less-idealized descriptions of trabecular architecture into analytical models that relate the trabecular structure to the apparent elastic properties. Hodgskinson and Currey[198] correlated apparent density, mineral volume fraction, an alternative, scalar form of fabric, and connectivity to Young's modulus. Apparent density and fabric were identified as the most significant explanatory variables. Cowin[33] developed equations for relating the elastic constants of an orthotropic material to its porosity and fabric. These relations were further developed to uncouple volume fraction from fabric[199] and to ensure positive definiteness of the elasticity tensor *a priori*.[200] Zysset et al.[139] formulated an alternative version of this model based on a different representation of orthotropic elasticity[201], modified to account for the relative extent of anisotropy (akin to the degree of anisotropy) by including the fabric eigenvalues.

A comparison of these models with Gibson's isotropic, cellular-solid model[202] revealed that the anisotropic power models (i.e., orthotropic Boehler and Zysset–Curnier) yielded the best results ($r^2 \leq 0.95$) and reduced the magnitudes of the prediction errors at low volume fractions. Also, recent work has indicated that the fabric–mechanical property relationships may depend on the anatomic site.[191] The development of these analytical models for the prediction of apparent-level elastic properties from the morphological parameters of trabecular bone contributes to the ability to evaluate disease progression and bone stiffness noninvasively in bone in a clinical setting, in addition to providing a foundation for the development of numerical models.

1.4.2.12 Numerical Modeling

The advantages of analytical models in providing closed-form relationships for the mechanical properties of trabecular bone must be balanced against the errors in the model predictions that arise from oversimplifications of the trabecular architecture and tissue-level material properties. For cases in which these errors are too great, numerical models that more closely approximate the irregularity of the trabecular architecture and the inhomogeneity in both architecture and tissue-level properties can be used. For example, Silva and Gibson[203,204] used finite-element modeling to analyze a two-dimensional (2D), nonrepeating, Voronoi honeycomb structure and reported higher strains in cell walls and lower apparent strength as compared with the regular honeycomb structure. Yeh and Keaveny[205] considered 3D, irregularly shaped lattices with varying trabecular rod thicknesses. Their results showed substantial reductions in apparent modulus when the variation in trabecular thickness was increased, even for a constant volume fraction. Although such models do not directly reflect the geometry of trabecular specimens, they have proven useful for examining the effects of trabecular architecture on macroscopic material properties in a controlled manner.

The advent of μCT and ever-increasing amounts of computing power have enabled the creation of finite-element models of trabecular bone that resolve the individual trabeculae with the same, or nearly the same, level of anatomic detail as the μCT images themselves. These "high-resolution finite-element models," or "micromechanical finite-element" (micro-FE) models,[206] capture the complexity of the trabecular architecture implicitly and have become a standard tool in the study of trabecular bone mechanics. The basic strategy in these models is to avoid generating an isoparametric mesh of the trabecular architecture by directly converting voxels from a digital image of a trabecular bone sample into elements of a finite-element mesh. A popular implementation is to directly map image voxels to hexahedral finite elements,[206,207] although marching-tetrahedron methods have also been used. An excellent review of the issues surrounding meshing, convergence, and material property assignments in micro-FE models can be found in the work of Niebur and Keaveny.[208] These micro-FE models have yielded significant progress in determining orthotropic elastic constants, strength characteristics, multiaxial failure criterion, and trabecular tissue properties.

To date, micro-FE analyses of trabecular bone have been used in two general areas of study. The first is in developing structure–function relationships. For this area, the ability to "test" each specimen multiple times, that is, along different loading directions or in different loading modes, is of great benefit. Although quantitative ultrasound (QUS) is a promising experimental approach for this type of nondestructive assessment,[209,210] the accuracy and precision of that method have not yet matched the performance of the micro-FE analyses for the elastic behavior of trabecular bone. Kabel et al.[211] used micro-FE analysis to estimate all nine orthotropic elastic constants of specimens of trabecular bone from multiple anatomic sites and used these data to determine that the fabric–elasticity relationships proposed earlier by Cowin[33] could account for 97% of the variance in the elastic constants. These results confirmed the primary role of both volume fraction and architectural anisotropy in determining apparent elastic properties. Similarly, the use of micro-FE models to simulate destructive (i.e., loading to or past the yield point) tests in different loading modes for any given specimen has aided the development of several promising multiaxial yield criteria.[148,188] Combination of the micro-FE approach with digital topological analysis,[212] a method of classifying the individual trabeculae within a specimen as rods or plates and of quantifying the orientation of each trabecula, has enabled the study of the way in which trabecular architecture modulates loading paths in trabecular bone.

In doing so, this combined approach has provided a direct bridge between the mechanistic approach of cellular-solid modeling and the anatomic fidelity of micro-FE analysis.

Micro-FE modeling has also made substantial contributions in estimating the distributions of stress and strain within trabecular tissue in response to loads applied at the apparent level or applied to the whole bone. Studies have demonstrated that age- and disease-related changes in density and architecture are predicted to have substantial effects on the tissue-level strain distributions, specifically in the spatial variations in these distributions.[183,213] The implications of this spatial heterogeneity in the local mechanical environment of trabecular tissue for microdamage accumulation,[160,168] bone adaptation,[214,215] and bone failure[170,171] have been active areas of recent research.

1.4.2.13 Mechanical Properties of Trabecular Tissue

Trabecular tissue, meaning the bony tissue that comprises individual trabeculae, is similar to cortical bone in both composition and material properties, although subtle differences exist. The difficulty of performing direct mechanical tests on individual trabeculae has prompted the development and application of a variety of techniques such as direct testing of machined microbeams, ultrasound, nanoindentation, and a combined FE–experimental approach. Early tensile and bending tests of individual trabeculae yielded moduli in the range of 1 to 10 GPa,[98,216] as much as an order of magnitude lower than cortical bone. Later studies using ultrasonic,[217,218] nanoindentation,[103,104,219] and scanning acoustic microscopy[220] techniques revealed higher values of approximately 10 to 20 GPa. This discrepancy may be due to mechanical artifacts caused by the small dimensions and nonregular geometry of the trabeculae, in addition to oversimplifying assumptions such as homogeneity, isotropy, and regular geometry.

Elastic and strength properties have also been reported using a combined FE–experimental approach. In these studies, the tissue modulus is determined from a ratio to apparent modulus calibrated against experiments.[221–223] Results from this approach place the elastic modulus of human trabecular tissue at approximately 10% less, tensile yield strain at 15% less, and the tissue strength at 25% greater than cortical bone.[224] More recently, a combined FE–experimental approach has been developed for bending tests of single trabeculae within the trabecular network, and initial results for sheep trabeculae are in the upper range of reported data.[225] As for strength, trabecular tissue is similar to cortical bone in that it exhibits asymmetry in yield strains, with a tensile-compressive strength ratio of 6.2.[224] As for the fatigue characteristics of trabecular tissue, some work has been reported,[226] but much remains to be done. Correctly characterizing the mechanical properties of trabecular tissue can greatly improve the ability of finite-element models and other models to accurately predict apparent-level behavior, as well as the behavior of whole bones.

1.5 Mechanical Behavior of Whole Bones

Our discussion on bone mechanics has thus far been focused on the properties of trabecular and cortical bone as separate tissues and as determined from mechanical tests performed on excised specimens of these tissues. How these two different tissues are combined to form a whole bone, such as the femur, dictates the overall mechanical behavior of that bone. In addition to the respective amounts of cortical and trabecular bone that are

each present, structural and geometric features, such as cortical thickness, the spatial distribution of trabecular bone, cross-sectional area, bone size, and bone shape, all influence the whole-bone mechanical properties and all change with age and disease. The study of the mechanical behavior of whole bones can thus be substantially more complicated than the study of cortical or trabecular bone. However, investigations at the whole-bone level are arguably the ones most directly relevant to understanding the occurrence of fractures, the biomechanics of healing of those fractures, and both the mechanical input for and the outcomes of bone adaptation. Moreover, for rodent models in bone mechanics, whole-bone tests are one of the most practical options for mechanical investigations, given the small size of the skeleton. Indeed, isolation of an apparent-level specimen of trabecular bone is not possible in most cases due to the small amounts of this tissue that are present in any given anatomic site.

1.5.1 Loading of Whole Bones *In Vivo* and *In Vitro*

The principal challenge in the design of laboratory tests that seek to characterize clinically relevant mechanical behavior of a whole bone is to identify loading conditions that are physiologically representative. These loading conditions have been estimated using gait analysis, instrumented prostheses, and, in some cases, direct measurement in tissues. Gait analysis, or more generally, inverse dynamics analysis applied to activities of daily living[227] and to falls,[228,229] can estimate joint contact and muscle forces for a variety of physiological motions. For example, these types of analyses have estimated that the magnitude of the force acting on the femoral head during the stance phase of walking is 234% of the body weight[213,227] and that approximately 85% of the total impact force sustained from a sideways fall to the hip is delivered along a line of action that passes directly through the hip joint.[229] For the spine, intradiscal pressure is a direct indicator of load transferred to the vertebral body via adjacent intervertebral discs. Measurements of intradiscal pressure have been conducted *in vivo* using either an implanted pressure transducer or a pressure transducer that is attached to a needle that is itself inserted in the nucleus pulposus.[230–232] These data have indicated that the pressure at the L4 to L5 disc is 0.1 MPa while standing.[231] However, these pressure responses are just one aspect of vertebral loading *in vivo*, and biomechanical models that account for the complex muscular structure and muscular coactivity in the spine are lacking.[233]

Prostheses instrumented with load sensors that can transmit data remotely have also been designed and implanted in other anatomic sites such as the shoulder, hip, and knee.[234–237] These instrumented implants have the same geometry and function as conventional implants, and the force data that they provide have been invaluable for gauging the accuracy of the force estimates from gait analysis and for optimizing implant design. The data are also advantageous when used by physiotherapists to rehabilitate patients and assess the usefulness of aids such as braces.[234]

Despite many advances in the measurement techniques described above, biological variation and other uncertainties associated with measuring joint contact forces, muscle forces, and impact conditions *in vivo*[238] still hinder accurate and precise estimates of the directions, magnitudes, and locations of the forces and moments that should be applied *in vitro*. Moreover, *in vivo* loading conditions can be sufficiently complex, involving multiple muscle groups and distributed loads across a joint surface, to present major difficulties in recapitulating them *in vitro*. As such, researchers will often use simplified loading conditions, and it is important to note that many such experiments do produce fracture patterns that are commonly observed in the clinical setting. For example, for the proximal

femur, the loading angle is used to represent a fall on the hip rolled forward or backward, or to the side.[239] Common diaphyseal fracture patterns have been categorized according to simple loading modes such as compression, torsion, and bending (Figure 1.10), and one or more of these loading modes are frequently used in laboratory tests in studies of bone adaptation[240] and fracture healing.[241–244] Colles' fractures are simulated by applying compressive forces to the distal radius at an angle that simulates a fall on an outstretched hand.[245] For vertebrae, the common loading modes include compression (Figure 1.11) and compression combined with bending.[155,246] The latter simulates anterior or posterior

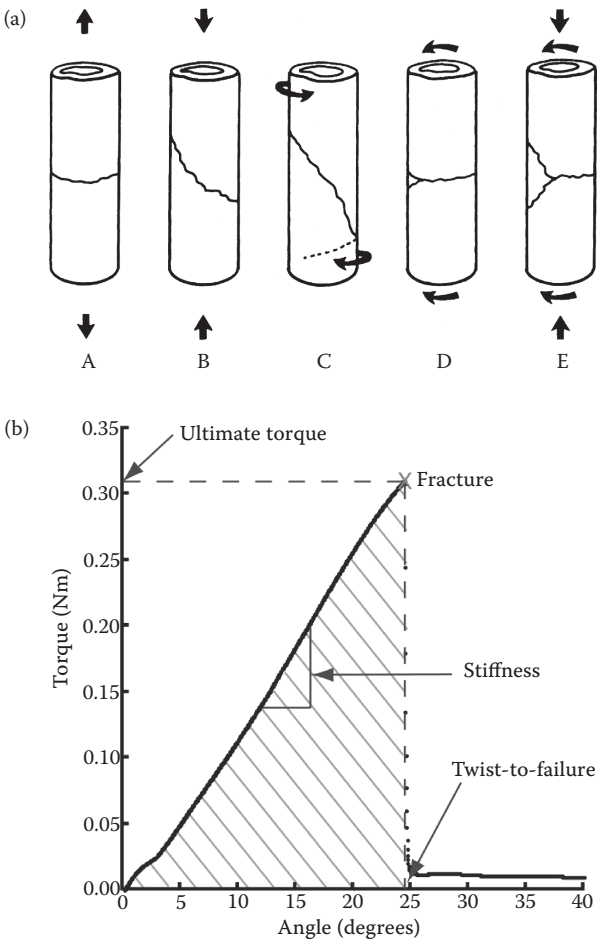

FIGURE 1.10
(a) Fracture patterns in a cylindrical section of bone subjected to different loading configurations. (A) Pure tensile loading produces a transverse fracture. (B) Pure compressive loading produces an oblique fracture. (C) Torsional loading produces a spiral fracture. (D) Bending produces a transverse fracture with a small fragment on the compressive side. (E) Bending superimposed with compression produces a transverse fracture with a larger fragment on the concave side. (From Morgan, E. F. et al., In *Osteoporosis*, edited by R. Marcus, D. Feldman, D. A. Nelson, and C. J. Rosen, pp. 3–25, 2008. With permission.) (b) Torque–twist curve for a rat tibia. The stiffness is defined as the slope of the initial, linear portion of the curve. Ultimate torque, a measure of torsional strength, is defined as the maximum torque sustained by the specimen, and the corresponding amount of deformation is defined as the twist-to-failure. Toughness (area of the shaded region) is the amount of energy required to cause fracture.

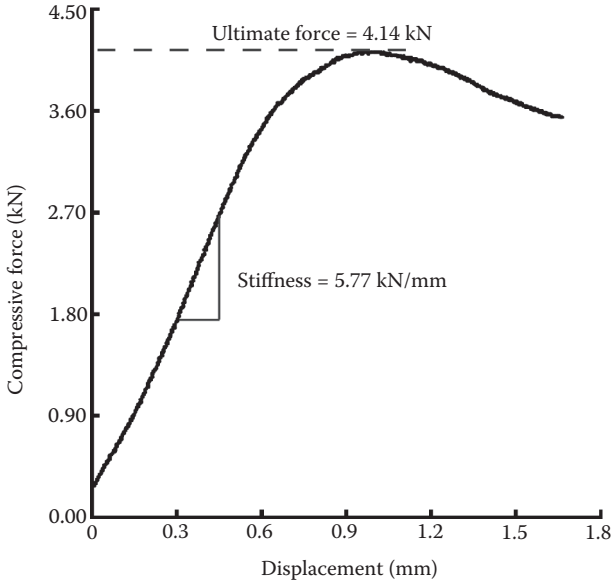

FIGURE 1.11
Representative force–displacement curve for an isolated thoracic vertebra tested in axial compression. The stiffness and ultimate force, a measure of vertebral strength, are marked on the curve.

flexion. Both loading scenarios are simplified representations of the loads to which vertebrae and motion segments are subjected *in vivo*, yet result in clinically observed fracture patterns, including endplate and wedge fractures.

1.5.2 Role of Geometry in Whole-Bone Mechanical Behavior

Principles of engineering mechanics stipulate that the axial stiffness, either in compression or tension, of a structure is proportional to the cross-sectional area, whereas the bending and torsional stiffnesses of beamlike structures (such as diaphyses) depend on how the material (tissue) is distributed around the axis of the bending or the twist (Figure 1.12). Two geometric properties, the areal moment of inertia (also known as the cross-sectional moment of inertia) and the polar moment of inertia, quantify this distribution in manners relevant for bending and torsion, respectively. For example, a cylindrical cross section of a diaphysis with the bone tissue located closer to the diaphyseal axis will have lower bending and torsional stiffnesses compared with another diaphysis with the same amount of bone tissue but with larger inner and outer diameters.

With the widespread availability of digital imaging in both the laboratory and clinical settings, the cross-sectional area and moments of inertia of a cross section of a whole bone can be readily calculated by summing the contribution of individual pixels based on pixel dimension and the relative position of the pixel from the center axis of the bone.[241] Under the assumption of a homogeneous distribution of tissue modulus within that cross section and of equal moduli in the cross sections of different bones that are being compared with one another, these cross-sectional properties represent relative differences among the bones in structural rigidity (axial, flexural, and torsional rigidities). More refined estimates of structural rigidity can be calculated by using the spatial variations in local intensities

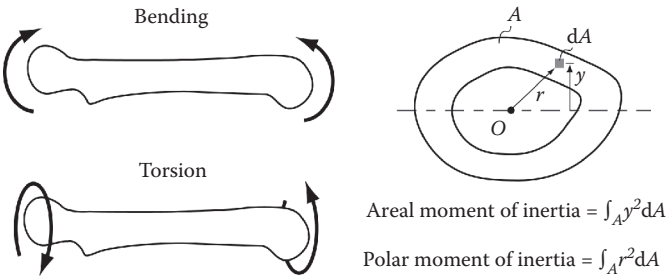

FIGURE 1.12
The bending stiffness of a structure, such as a long bone diaphysis, is proportional to the areal moment of inertia. If the diaphyseal cross section is circular, then the torsional stiffness is proportional to the polar moment of inertia; otherwise, this proportionality is only approximate. These moments of inertia quantify how the tissue is distributed with respect to the axis of bending (shown here as the dotted line on the diaphyseal cross section) or the axis of torsion (the line that passes through point *O* and is directed out of the plane of the figure). (From Morgan, E. F. et al., In *Osteoporosis*, edited by R. Marcus, D. Feldman, D. A. Nelson, and C. J. Rosen, pp. 3–25, 2008. With permission.)

(gray values) within the image of the cross section as estimates of the spatial variations in tissue mineral density, and then using density–modulus relationships to avoid the assumption of a homogeneous modulus distribution.[247,248] This method has been shown to provide estimates of structural rigidity that are significantly correlated to vertebral strength and stiffness.[249]

Conversely, if one has measured the stiffness or rigidity of a whole bone, some estimates of the material properties of the bone tissue can be derived. If the bone is straight, prismatic (the cross-sectional geometry does not change along the length of the structure), and of uniform composition, it is straightforward to calculate the Young's modulus or shear modulus from the value of stiffness obtained from the whole-bone test. However, none of these three descriptors are accurate for vertebral bodies, metaphyses, and diaphyses due to the irregular geometry and spatially heterogeneous composition of these bones. For the latter, one can calculate an effective elastic modulus of the tissue if the true cross-sectional geometry and its variation along the diaphyseal axis are included in the calculations. Without accounting for the true geometry, substantial errors in the calculated modulus could result.[250]

Cross-sectional geometry and other geometric features of whole bones vary greatly among individuals and exhibit marked changes with age. Multiple causes for these variations exist, including genetic differences, patterns of physical activity, gender, and possible compensation for alterations in tissue material properties,[251–253] among a host of other factors. The general pattern of age-related change in the cross-sectional geometry of the diaphysis is continual apposition of bone at the periosteal surface, accompanied by resorption of bone at the endosteal surface. The net result is a thinner cortex and smaller cross-sectional area (despite the increase in periosteal diameter), but not necessarily in any decrease in the moments of inertia.[254,255] The relatively small changes in moment of inertia with age serve to ameliorate the structural consequences of the age-related decline in the amount of bone present, although some controversy exists as to the magnitude of, and gender differences in, this benefit.[253,256,257]

For the vertebrae, an increase in the cross-sectional area with aging has been reported for both men and women,[253] and one study found that this increase was three times

greater in men as compared with women.[258] Thus, in a manner similar to diaphysis but in an anatomic site that has a large fraction of trabecular bone, age-related bone loss in the vertebral centrum is accompanied by an increase in the surface area carrying the load. Given the substantial mechanical importance of the cross-sectional area for the stiffness and strength of the vertebrae, these changes in area are highly noteworthy.

Differences in bone geometry have also been found between individuals with and without fractures. For the proximal femur, features such as neck-shaft angle[259,260] and periosteal and endosteal diameters[257,259,261] are larger in subjects with fractures compared with control subjects. Whether these differences have any causal basis is not clear, although differences in the neck-shaft angle can affect the magnitude of the stresses and strains that the femoral neck experiences under both gait and fall conditions. For the distal radius, Schneider et al.[262] showed that there was significant difference in cortical bone area between fracture and nonfracture cohorts, but that trabecular mass and density provided better indicators of fracture risk. Regarding the axial skeletal, a comparison of fracture versus nonfracture cohorts found that the vertebral cross-sectional area was lower in the former.[258] The role of other geometric features of the vertebrae, such as height and shell curvature, has not been studied extensively.[263]

1.5.3 Relative Roles of Cortical and Trabecular Bone in Mechanical Behavior of Whole Bones

Understanding the biomechanical repercussions of alterations in the material behavior of cortical and trabecular bone requires a study of the respective contributions of these two tissues to whole-bone mechanical behavior. For the vertebrae and proximal femur, the strength of the whole bone is predicted well simply by the density of the trabecular bone and measures of the cross-sectional area of the bone.[264–267] In addition, minor increases in bone density in certain relatively small areas of the proximal femur predicted improved strength, further suggesting the critical role of trabecular bone in whole-bone properties. However, research to date also suggests that the role of the cortical shell in the vertebrae is complex and varies with age. No strong consensus exists as to how much the cortical shell contributes to the stiffness and strength of the vertebrae.[267–270] A micro-FE study estimated that the fraction of the applied compressive load borne by the shell varies from 0.38 to 0.54 across vertebrae.[268] Several finite-element studies have also indicated that the shell load fraction is maximal at the narrowest transverse cross section of the vertebrae[268,271–273] and decreases to only ~15% near the endplates.[268] Furthermore, the shell load fraction was found to increase as the density and modulus of the trabecular bone decrease[271,274] and as disc degeneration advances.[272]

The relative roles of trabecular and cortical bone in the proximal femur seem to vary among subregions. Finite-element analyses have indicated that for both gait and sideways fall-loading conditions, the cortical bone bears approximately 30% of the load in the subcapital region, 50% at the midpoint of the femoral neck, 96% at the base of the femoral neck, and 80% in the intertrochanteric region.[275] Comparisons of stress and strain distributions in healthy versus osteoporotic femora indicate that although the distributions are similar, peak stresses and strains are elevated in the osteoporotic bones.[213,275] Although the locations of the peak stresses and strains are not exclusively in the trabecular compartment, results of other finite-element studies indicate that, for a variety of loading conditions that simulate various types of falls, failure of the trabecular bone begins before or simultaneously with failure of the cortical shell.[276–278] Consistent with these findings, a

more recent investigation used finite-element analysis to explore the mechanisms underlying the decrease in fracture risk in postmenopausal, osteoporotic women who are using anabolic and antiresorptive therapies and found that the estimated benefits to bone strength are largely due to treatment-induced increases in the strength of the trabecular compartment.[279]

1.5.4 *In Vivo* Predictions of Mechanical Behavior of Whole Bones

Many of the whole-bone, finite-element studies already cited in this chapter create the finite-element models from clinically available 3D imaging modalities such as QCT, high-resolution magnetic resonance imaging, and high-resolution pQCT (HR-pQCT). In contrast with micro-FE models, the QCT-based FE models are of coarser resolution such that they do not resolve the individual trabeculae. FE models created from HR-pQCT images can be classified as micro-FE models, but even with the best image resolution that is available currently (~80 μm/voxel), these models represent the trabecular bone as a notably less well-connected structure than exists in reality. However, the advantage of these CT-based FE models is that they can be incorporated into *in vivo* studies, whether retrospective or prospective, to provide estimates of bone strength that can in turn be used to evaluate fracture risk and the effects of various pharmacological treatments on that risk. Several such studies have been published recently, examining fracture load in the distal radius,[280] the effects of glucocorticoid use, alendronate treatment and parathyroid hormone treatment on femoral strength,[279] and the effects of testosterone treatment on bone stiffness in the proximal tibia.[281] However, it should be noted that these studies have not demonstrated a clear predictive advantage to the FE-derived estimates of bone strength over estimates obtained from the average bone mineral density (BMD) at the anatomic site of interest. Thus, although the FE simulations can provide rich insight into biomechanical mechanisms for observed differences in fracture rates among study cohorts, the role of this method for providing predictive capabilities for fracture outcome is not clear. Similarly, estimates of bone stiffness and strength calculated from measurements of bone geometry and of regional bone density that are made using dual-energy X-ray absorptiometry[282]—a 2D X-ray imaging modality that is the standard clinical tool for quantifying (areal) bone density and estimating fracture risk—have provided a wealth of informative, biomechanical data in longitudinal studies of bone growth[283,284] and bone fragility,[285] but have not been identified as superior to BMD as a predictive tool.

1.5.5 Experimental Validation of Finite-Element Predictions of Whole-Bone Mechanical Behavior

In light of the frequent use of finite-element modeling to study the mechanical behavior of whole bones, it is worthwhile to consider the many approaches that have been used to assess the accuracy of the estimates that result from these models. The various assumptions and idealizations regarding bone geometry, loading conditions, and tissue material properties can have severe effects on the results of the model. As a logical first step, the FE-computed values of bone stiffness and bone strength can be compared on a per specimen basis to experimentally measured values. The correlations that result from these comparisons are generally moderate to high (r^2 = 0.82 to 0.86); however, differences between the FE and experimental values can differ by as much as twofold.[286] Another approach is to compare the strains that develop within the trabecular compartment and

on the bone surface. For the latter, strain gauges and digital image correlation have been used as experimental techniques, and the results of the comparisons indicate good agreement in regions of the bone that are of relatively simple geometry (e.g., the diaphysis) and poorer agreement in those with more irregular topology (e.g., the femoral neck). For comparisons of strains in the trabecular compartment, initial studies used only thick cross sections of the bone so that strains could be measured experimentally using standard 2D, noncontact measurement techniques.[287–289] More recently, 3D volumetric methods of digital image correlation have been developed for applications in whole-bone mechanics such that strains within the trabecular compartment can be estimated for intact bones.[290–292] Given the inherent drawbacks of the strain measurements performed on 2D cross sections and the preliminary status of the 3D work, the accuracy of FE predictions of deformation and failure patterns in whole bones has not yet been rigorously validated.

1.6 Conclusions

Bone biomechanics includes the study of the mechanical behavior of whole bones and of bone tissue, as well as a consideration of the bone geometry and the hierarchical structure and composition of bone tissue. Aging, disease, and changes in physical activity can alter a number of these factors, resulting in wide variations in mechanical properties and, oftentimes, in difficulties in identifying the dominant contributors to these variations. Differences among specimens in characteristics such as porosity, mineralization, and trabecular architecture can explain much of the heterogeneity in bone material properties and much of the age-related decline in these properties. However, more subtle changes in the collagenous phase of bone tissue and in bone geometry can also have profound effects on both the load-bearing capacity of bone and on the mechanisms of failure.

The past decade has witnessed tremendous advances in modeling of the elastic and yield behavior of bone tissue and whole bones, in microscale and nanoscale characterization of bone tissue, and in numerical modeling of bone at high levels of anatomic detail. These achievements have enabled significant progress in identifying mechanisms of yielding, damage, and fracture in bone tissue and in obtaining *in vivo* estimates of bone strength. Yet these recent data have also raised new questions. As the literature on microdamage and on *in vivo* modeling of bone strength illustrate, the relevant clinical data do not always match conclusions drawn in the laboratory.

Comprehensive constitutive models for bone tissue—models that account for both the elastic and post-yield behavior—remain elusive. These models now exist for the orthotropic elastic behavior of trabecular bone, but micromechanical models of cortical and trabecular tissues are still limited in scope. Furthermore, the multiaxial yield criteria that have been proposed for cortical and trabecular bones have not yet been validated, and a dearth of both data and models exists for the post-yield behavior of bone tissue under multiaxial stress or strain states. As has been demonstrated for the elastic behavior of bone, using a combination of numerical and analytical modeling with targeted calibration and validation experiments may provide these much needed data on yield and post-yield behavior. Better descriptions of these properties should ultimately lead to improved predictions of the effects of aging, disease, and drug treatments on the biomechanical behavior of bone.

Acknowledgments

This work was supported by grant number 6775754 from the National Science Foundation, Civil, Mechanical and Manufacturing Innovation Division.

References

1. Kelly, D. J., and Jacobs, C. R. 2010. The role of mechanical signals in regulating chondrogenesis and osteogenesis of mesenchymal stem cells. *Birth Defects Research. Part C, Embryo Today* 90(1):75–85.
2. Knothe Tate, M. L., Falls, T. D., McBride, S. H., Atit, R., and Knothe, U. R. 2008. Mechanical modulation of osteochondroprogenitor cell fate. *The International Journal of Biochemistry & Cell Biology* 40(12):2720–2738.
3. Jacobs, C. R., Temiyasathit, S., and Castillo, A. B. 2010. Osteocyte mechanobiology and pericellular mechanics. *Annual Review of Biomedical Engineering* 12:369–400.
4. Ozcivici, E., Luu, Y. K., Adler, B., Qin, Y. X., Rubin, J., Judex, S., and Rubin, C. T. 2010. Mechanical signals as anabolic agents in bone. *Nature Reviews* 6(1):50–59.
5. Morgan, E. F., and Einhorn, T. A. 2009. Biomechanics of fracture healing. In *Primer on the Metabolic Bone Diseases and Disorders of Mineral Metabolism*, edited by C. J. Rosen, 65–69. Hoboken, NJ: John Wiley & Sons, Inc.
6. van Rietbergen, B., Odgaard, A., Kabel, J., and Huiskes, R. 1996. Direct mechanics assessment of elastic symmetries and properties of trabecular bone architecture. *Journal of Biomechanics* 29(12):1653–1657.
7. Odgaard, A. 1997. Three-dimensional methods for quantification of cancellous bone architecture. *Bone* 20(4):315–328.
8. Wang, X., Liu, X., and Niebur, G. L. 2004. Preparation of on-axis cylindrical trabecular bone specimens using micro-CT imaging. *Journal of Biomechanical Engineering* 126(1):122–125.
9. Gong, J. K., Arnold, J. S., and Cohn, S. H. 1964. Composition of trabecular and cortical bone. *The Anatomical Record* 149:325–332.
10. Einhorn, T. A. 1994. Bone metabolism and metabolic bone disease. In *Orthopaedic Knowledge Update 4. Home Study Syllabus*, edited by J. W. Frymoyer, 69–88. The American Academy of Orthopaedic Surgeons, Rosemont, IL.
11. Landis, W. J. 1995. The strength of a calcified tissue depends in part on the molecular structure and organization of its constituent mineral crystals in their organic matrix. *Bone* 16(5):533–544.
12. Morgan, E. F., Barnes, G. L., and Einhorn, T. A. 2008. The bone organ system: form and function. In *Osteoporosis*, edited by R. Marcus, D. Feldman, D. A. Nelson, and C. J. Rosen, 3–25. Elssevier Academic Press, Burlington, MA.
13. Weiner, S., and Wagner, H. D. 1998. The material bone: structure–mechanical function relations. *Annual Review of Materials Science* 28(1):271–298.
14. Su, X., Sun, K., Cui, F. Z., and Landis, W. J. 2003. Organization of apatite crystals in human woven bone. *Bone* 32(2):150–162.
15. Marotti, G. 1979. Osteocyte orientation in human lamellar bone and its relevance to the morphometry of periosteocytic lacunae. *Metabolic Bone Disease and Related Research* 1(4):325–333.
16. Dudley, H. R., and Spiro, D. 1961. The fine structure of bone cells. *The Journal of Biophysical and Biochemical Cytology* 11(3):627–649.
17. Palumbo, C., Palazzini, S., and Marotti, G. 1990. Morphological study of intercellular junctions during osteocyte differentiation. *Bone* 11(6):401–406.

18. Kamioka, H., Honjo, T., and Takano-Yamamoto, T. 2001. A three-dimensional distribution of osteocyte processes revealed by the combination of confocal laser scanning microscopy and differential interference contrast microscopy. *Bone* 28(2):145–149.
19. Cowin, S. C. 2007. The significance of bone microstructure in mechanotransduction. *Journal of Biomechanics* 40(Supplement 1):S105–S109.
20. Burr, D. B., Schaffler, M. B., and Frederickson, R. G. 1988. Composition of the cement line and its possible mechanical role as a local interface in human compact bone. *Journal of Biomechanics* 21(11):939–941, 943–945.
21. O'Brien, F. J., Taylor, D., and Clive Lee, T. 2005. The effect of bone microstructure on the initiation and growth of microcracks. *Journal of Orthopaedic Research* 23(2):475–480.
22. Schaffler, M. B., and Burr, D. B. 1988. Stiffness of compact bone: Effects of porosity and density. *Journal of Biomechanics* 21(1):13–16.
23. Morgan, E. F., and Keaveny, T. M. 2001. Dependence of yield strain of human trabecular bone on anatomic site. *Journal of Biomechanics* 24:569–577.
24. Liu, X. S., Sajda, P., Saha, P. K., Wehrli, F. W., Bevill, G., Keaveny, T. M., and Guo, X. E. 2008. Complete volumetric decomposition of individual trabecular plates and rods and its morphological correlations with anisotropic elastic moduli in human trabecular bone. *Journal of Bone and Mineral Research* 23(2):223–235.
25. Ding, M., Odgaard, A., Linde, F., and Hvid, I. 2002. Age-related variations in the microstructure of human tibial cancellous bone. *Journal of Orthopaedic Research* 20(3):615–621.
26. Mosekilde, L. 1989. Sex differences in age-related loss of vertebral trabecular bone mass and structure–biomechanical consequences. *Bone* 10(6): 425–432.
27. Hildebrand, T., and Ruegsegger, P. 1997. Quantification of bone microarchitecture with the structure model index. *Computer Methods in Biomechanics and Biomedical Engineering* 1(1):15–23.
28. Hildebrand, T., Laib, A., Müller, R., Dequeker, J., and Rüegsegger, P. 1999. Direct three-dimensional morphometric analysis of human cancellous bone: microstructural data from spine, femur, iliac crest, and calcaneus. *Journal of Bone and Mineral Research* 14(7):1167–1174.
29. Whitehouse, W. J. 1974. The quantitative morphology of anisotropic trabecular bone. *Journal of Microscopy* 2:153–168.
30. Odgaard, A., Jensen, E. B., and Gundersen, H. J. 1990. Estimation of structural anisotropy based on volume orientation. A new concept. *Journal of Microscopy* 157 Pt. 2:149–162.
31. Cruz-Orive, L., Karlsson, L., Larsen, S., and Wainschtein, F. 1992. Characterizing structural anisotropy: A new concept. *Micron and Microscopica Acta* 23:75–76.
32. Harrigan, T., and Mann, R. 1984. Characterization of microstructural anisotropy in orthotropic materials using a second rank tensor. *Journal of Material Science* 19:761–767.
33. Cowin, S. C. 1985. The relationship between the elasticity tensor and the fabric tensor. *Mechanics of Materials* 4(2):137–147.
34. Reilly, D. T., and Burstein, A. H. 1975. The elastic and ultimate properties of compact bone tissue. *Journal of Biomechanics* 8(6):393–396, IN399–IN311:397–405.
35. McElhaney, J. H., and Byars, E. F. 1965. Dynamic response of biological materials. *ASME Paper*, No. 65-WA-HUF-9:1–8.
36. McElhaney, J. H. 1966. Dynamic response of bone and muscle tissue. *Journal of Applied Physiology* 21:1231–1236.
37. Zioupos, P., Hansen, U., and Currey, J. D. 2008. Microcracking damage and the fracture process in relation to strain rate in human cortical bone tensile failure. *Journal of Biomechanics* 41(14):2932–2939.
38. Fondrk, M., Bahniuk, E., Davy, D. T., and Michaels, C. 1988. Some viscoplastic characteristics of bovine and human cortical bone. *Journal of Biomechanics* 21(8):623–630.
39. Frost, H. M. 1960. Presence of microscopic cracks in vivo in bone. *Henry Ford Hospital Medical Bulletin* 8:27–35.
40. Martin, R. B. 2003. Fatigue microdamage as an essential element of bone mechanics and biology. *Calcified Tissue International* 73(2):101–107.

41. Varvani-Farahani, A., and Najmi, H. 2010. A damage assessment model for cadaveric cortical bone subjected to fatigue cycles. *International Journal of Fatigue* 32(2):420–427.
42. Nicolella, D. P., Ni, Q., and Chan, K. S. 2011. Non-destructive characterization of microdamage in cortical bone using low field pulsed NMR. *Journal of the Mechanical Behavior of Biomedical Materials* 4(3):383–391.
43. Akkus, O., Knott, D. F., Jepsen, K. J., Davy, D. T., and Rimnac, C. M. 2003. Relationship between damage accumulation and mechanical property degradation in cortical bone: microcrack orientation is important. *Journal of Biomedical Materials Research Part A* 65A(4):482–488.
44. Leng, H., Dong, X. N., and Wang, X. 2009. Progressive post-yield behavior of human cortical bone in compression for middle-aged and elderly groups. *Journal of Biomechanics* 42(4):491–497.
45. Allen, M. R., and Burr, D. B. 2011. Bisphosphonate effects on bone turnover, microdamage, and mechanical properties: What we think we know and what we know that we don't know. *Bone* 49(1): 56–65.
46. Chapurlat, R. D., and Delmas, P. D. 2009. Bone microdamage: a clinical perspective. *Osteoporosis International* 20(8):1299–1308.
47. Burr, D. B., Turner, C. H., Naick, P., Forwood, M. R., Ambrosius, W., Sayeed Hasan, M., and Pidaparti, R. 1998. Does microdamage accumulation affect the mechanical properties of bone? *Journal of Biomechanics* 31(4):337–345.
48. Norman, T. L., Yeni, Y. N., Brown, C. U., and Wang, Z. 1998. Influence of microdamage on fracture toughness of the human femur and tibia. *Bone* 23(3):303–306.
49. Courtney, A. C., Hayes, W. C., and Gibson, L. J. 1996. Age-related differences in post-yield damage in human cortical bone. Experiment and model. *Journal of Biomechanics* 29(11):1463–1471.
50. Schaffler, M. B., Radin, E. L., and Burr, D. B. 1989. Mechanical and morphological effects of strain rate on fatigue of compact bone. *Bone* 10(3):207–214.
51. Vashishth, D., Tanner, K. E., and Bonfield, W. 2000. Contribution, development and morphology of microcracking in cortical bone during crack propagation. *Journal of Biomechanics* 33(9):1169–1174.
52. Bonfield, W., and Datta, P. K. 1976. Fracture toughness of compact bone. *Journal of Biomechanics* 9(3):131–132, IN135:133–134.
53. Norman, T. L., Vashishth, D., and Burr, D. B. 1992. Effect of groove on bone fracture toughness. *Journal of Biomechanics* 25(12):1489–1492.
54. Behiri, J. C., and Bonfield, W. 1984. Fracture mechanics of bone—The effects of density, specimen thickness and crack velocity on longitudinal fracture. *Journal of Biomechanics* 17(1):25–34.
55. Norman, T. L., and Wang, Z. 1997. Microdamage of human cortical bone: incidence and morphology in long bones. *Bone* 20(4):375–379.
56. Schaffler, M. B., Choi, K., and Milgrom, C. 1995. Aging and matrix microdamage accumulation in human compact bone. *Bone* 17(6):521–525.
57. Vashishth, D., Behiri, J. C., and Bonfield, W. 1997. Crack growth resistance in cortical bone: Concept of microcrack toughening. *Journal of Biomechanics* 30(8):763–769.
58. Ritchie, R. O., Kinney, J. H., Kruzic, J. J., and Nalla, R. K. 2006. Cortical bone fracture. In *Wiley Encyclopedia of Biomedical Engineering*. Hoboken, NJ: John Wiley & Sons, Inc.
59. Vashishth, D. 2004. Rising crack-growth-resistance behavior in cortical bone:: implications for toughness measurements. *Journal of Biomechanics* 37(6):943–946.
60. Zimmermann, E. A., Launey, M. E., and Ritchie, R. O. 2010. The significance of crack-resistance curves to the mixed-mode fracture toughness of human cortical bone. *Biomaterials* 31(20): 5297–5305.
61. Kulin, R. M., Jiang, F., and Vecchio, K. S. 2011. Effects of age and loading rate on equine cortical bone failure. *Journal of the Mechanical Behavior of Biomedical Materials* 4(1):57–75.
62. Ural, A., Zioupos, P., Buchanan, D., and Vashishth, D. 2011. The effect of strain rate on fracture toughness of human cortical bone: a finite element study. *Journal of the Mechanical Behavior of Biomedical Materials* 4(7):1021–1032.

63. Koester, K. J., Barth, H. D., and Ritchie, R. O. 2011. Effect of aging on the transverse toughness of human cortical bone: evaluation by R-curves. *Journal of the Mechanical Behavior of Biomedical Materials* 4(7):1504–1513.
64. Wang, X., Yoon, Y. J., and Ji, H. 2007. A novel scratching approach for measuring age-related changes in the in situ toughness of bone. *Journal of Biomechanics* 40(6):1401–1404.
65. Gao, S., Qian, L., and Yu, H. 2009. Anisotropic wear resistance of human mandible cortical bone. *Tribology Letters* 33(1):73–81.
66. Carter, D. R., and Hayes, W. C. 1977. Compact bone fatigue damage—I. Residual strength and stiffness. *Journal of Biomechanics* 10(5–6):325–337.
67. Pidaparti, R. M., Akyuz, U., Naick, P. A., and Burr, D. B. 2000. Fatigue data analysis of canine femurs under four-point bending. *Bio-Medical Materials and Engineering* 10(1):43–50.
68. Zioupos, P., Wang, X. T., and Currey, J. D. 1996. The accumulation of fatigue microdamage in human cortical bone of two different ages in vitro. *Clinical Biomechanics* 11(7):365–375.
69. Zioupos, P., Gresle, M., and Winwood, K. 2008. Fatigue strength of human cortical bone: age, physical, and material heterogeneity effects. *Journal of Biomedical Materials Research Part A* 86A(3):627–636.
70. Vashishth, D., Tanner, K. E., and Bonfield, W. 2001. Fatigue of cortical bone under combined axial-torsional loading. *Journal of Orthopaedic Research* 19(3):414–420.
71. Zioupos, P., Currey, J. D., and Casinos, A. 2001. Tensile fatigue in bone: are cycles-, or time to failure, or both, important? *Journal of Theoretical Biology* 210(3):389–399.
72. Caler, W. E., and Carter, D. R. 1989. Bone creep-fatigue damage accumulation. *Journal of Biomechanics* 22(6–7):625–635.
73. Pattin, C. A., Caler, W. E., and Carter, D. R. 1996. Cyclic mechanical property degradation during fatigue loading of cortical bone. *Journal of Biomechanics* 29(1):69–79.
74. Kruzic, J. J., and Ritchie, R. O. 2008. Fatigue of mineralized tissues: cortical bone and dentin. *Journal of the Mechanical Behavior of Biomedical Materials* 1(1):3–17.
75. Lee, T. C., Arthur, T. L., Gibson, L. J., and Hayes, W. C. 2000. Sequential labelling of microdamage in bone using chelating agents. *Journal of Orthopaedic Research* 18(2):322–325.
76. O'Brien, F. J., Taylor, D., and Lee, T. C. 2002. An improved labelling technique for monitoring microcrack growth in compact bone. *Journal of Biomechanics* 35(4):523–526.
77. O'Brien, F. J., Taylor, D., and Clive Lee, T. 2007. Bone as a composite material: the role of osteons as barriers to crack growth in compact bone. *International Journal of Fatigue* 29(6):1051–1056.
78. Cezayirlioglu, H., Bahniuk, E., Davy, D. T., and Heiple, K. G. 1985. Anisotropic yield behavior of bone under combined axial force and torque. *Journal of Biomechanics* 18(1):61–69.
79. Arramon, Y. P., Mehrabadi, M. M., Martin, D. W., and Cowin, S. C. 2000. A multidimensional anisotropic strength criterion based on Kelvin modes. *International Journal of Solids and Structures* 37(21):2915–2935.
80. Currey, J. D. 1988. The effect of porosity and mineral content on the Young's modulus of elasticity of compact bone. *Journal of Biomechanics* 21(2):131–139.
81. Behrens, J. C., Walker, P. S., and Shoji, H. 1974. Variations in strength and structure of cancellous bone at the knee. *Journal of Biomechanics* 7(3):201–207.
82. Ural, A., and Vashishth, D. 2007. Effects of intracortical porosity on fracture toughness in aging human bone: a microCT-based cohesive finite element study. *Journal of Biomechanical Engineering* 129(5):625–631.
83. McCalden, R. W., McGeough, J. A., Barker, M. B., and Court-Brown, C. M. 1993. Age-related changes in the tensile properties of cortical bone: the relative importance of changes in porosity, mineralization and microstructure. *Journal of Bone and Joint Surgery* 75A:1193–1205.
84. Wang, X., Bank, R. A., TeKoppele, J. M., Hubbard, G. B., Althanasiou, K. A., and Agrawal, C. M. 2000. Effect of collagen denaturation on the toughness of bone. *Clinical Orthopaedics and Related Research* 371:228–239.
85. Boyce, T. M., and Bloebaum, R. D. 1993. Cortical aging differences and fracture implications for the human femoral neck. *Bone* 14(5):769–778.

86. Currey, J. D., Brear, K., and Zioupos, P. 1996. The effects of ageing and changes in mineral content in degrading the toughness of human femora. *Journal of Biomechanics* 29(2):257–260.
87. Wang, X., Shen, X., Li, X., and Mauli Agrawal, C. 2002. Age-related changes in the collagen network and toughness of bone. *Bone* 31(1):1–7.
88. Nalla, R. K., Kruzic, J. J., Kinney, J. H., and Ritchie, R. O. 2004. Effect of aging on the toughness of human cortical bone: evaluation by R-curves. *Bone* 35(6):1240–1246.
89. Burstein, A., Reilly, D., and Martens, M. 1976. Aging of bone tissue: mechanical properties. *The Journal of Bone and Joint Surgery. American Volume* 58(1):82–86.
90. Huja, S., Beck, F., and Thurman, D. 2006. Indentation properties of young and old osteons. *Calcified Tissue International* 78(6):392–397.
91. Nyman, J. S., Roy, A., Acuna, R. L., Gayle, H. J., Reyes, M. J., Tyler, J. H., Dean, D. D., and Wang, X. 2006. Age-related effect on the concentration of collagen crosslinks in human osteonal and interstitial bone tissue. *Bone* 39(6):1210–1217.
92. Vashishth, D., Gibson, G. J., Khoury, J. I., Schaffler, M. B., Kimura, J., and Fyhrie, D. P. 2001. Influence of nonenzymatic glycation on biomechanical properties of cortical bone. *Bone* 28(2): 195–201.
93. Tang, S. Y., and Vashishth, D. 2011. The relative contributions of non-enzymatic glycation and cortical porosity on the fracture toughness of aging bone. *Journal of Biomechanics* 44(2):330–336.
94. Ascenzi, A., Baschieri, P., and Benvenuti, A. 1994. The torsional properties of single selected osteons. *Journal of Biomechanics* 27(7):875–877, 879–884.
95. Ascenzi, A., and Bonucci, E. 1967. The tensile properties of single osteons. *The Anatomical Record* 158(4):375–386.
96. Ascenzi, A., and Bonucci, E. 1968. The compressive properties of single osteons. *The Anatomical Record* 161(3):377–391.
97. Ascenzi, A., and Bonucci, E. 1972. The shearing properties of single osteons. *The Anatomical Record* 172(3):499–510.
98. Choi, K., Kuhn, J. L., Ciarelli, M. J., and Goldstein, S. A. 1990. The elastic moduli of human subchondral, trabecular, and cortical bone tissue and the size-dependency of cortical bone modulus. *Journal of Biomechanics* 23(11):1103–1113.
99. Kuhn, J. L., Goldstein, S. A., Choi, R., London, M., Feldkamp, L. A., and Matthews, L. S. 1989. Comparison of the trabecular and cortical tissue moduli from human iliac crests. *Journal of Orthopaedic Research* 7(6), 876–884.
100. Dong, X. N., and Guo, X. E. 2004. Geometric determinants to cement line debonding and osteonal lamellae failure in osteon pushout tests. *Journal of Biomechanical Engineering* 126(3):387–390.
101. Dong, X. N., Zhang, X., and Guo, X. E. 2005. Interfacial strength of cement lines in human cortical bones. *Mechanics & Chemistry of Biosystems* 2(2):63–68.
102. Bigley, R. F., Griffin, L. V., Christensen, L., and Vandenbosch, R. 2006. Osteon interfacial strength and histomorphometry of equine cortical bone. *Journal of Biomechanics* 39(9):1629–1640.
103. Rho, J.-Y., Tsui, T. Y., and Pharr, G. M. 1997. Elastic properties of human cortical and trabecular lamellar bone measured by nanoindentation. *Biomaterials* 18(20):1325–1330.
104. Zysset, P. K., Edward Guo, X., Edward Hoffler, C., Moore, K. E., and Goldstein, S. A. 1999. Elastic modulus and hardness of cortical and trabecular bone lamellae measured by nanoindentation in the human femur. *Journal of Biomechanics* 32(10):1005–1012.
105. Fan, Z., Swadener, J. G., Rho, J. Y., Roy, M. E., and Pharr, G. M. 2002. Anisotropic properties of human tibial cortical bone as measured by nanoindentation. *Journal of Orthopaedic Research* 20(4):806–810.
106. Fan, Z., and Rho, J.-Y. 2003. Effects of viscoelasticity and time-dependent plasticity on nanoindentation measurements of human cortical bone. *Journal of Biomedical Materials Research Part A* 67A(1):208–214.
107. Hoffler, C. E., Guo, X. E., Zysset, P. K., and Goldstein, S. A. 2005. An application of nanoindentation technique to measure bone tissue lamellae properties. *Journal of Biomechanical Engineering* 127(7):1046–1053.

108. Lim, Y. C., Altman, K. J., Farson, D. F., and Flores, K. M. 2009. Micropillar fabrication on bovine cortical bone by direct-write femtosecond laser ablation. *Journal of Biomedical Optics* 14(6):064021.
109. Chan, Y. L., Ngan, A. H. W., and King, N. M. 2009. Use of focused ion beam milling for investigating the mechanical properties of biological tissues: A study of human primary molars. *Journal of the Mechanical Behavior of Biomedical Materials* 2(4):375–383.
110. Nalla, R. K., Porter, A. E., Daraio, C., Minor, A. M., Radmilovic, V., Stach, E. A., Tomsia, A. P., and Ritchie, R. O. 2005. Ultrastructural examination of dentin using focused ion-beam cross-sectioning and transmission electron microscopy. *Micron* 36(7–8):672–680.
111. Pidaparti, R. M. V., Chandran, A., Takano, Y., and Turner, C. H. 1996. Bone mineral lies mainly outside collagen fibrils: Predictions of a composite model for osternal bone. *Journal of Biomechanics* 29(7):909–916.
112. Katz, J. L. 1980. Anisotropy of Young's modulus of bone. *Nature* 283(5742):106–107.
113. Hellmich, C., and Ulm, F.-J. 2002. A micromechanical model for the ultrastructural stiffness of minearlized tissues. *Journal of Engineering Mechanics* 128:898–908.
114. Hellmich, C., Barthelemy, J., and Dormieux, L. 2004. Mineral–collagen interactions in elasticity of bone ultrastructure—a continuum micromechanics approach. *European Journal of Mechanics - A/Solids* 23:783–810.
115. Sansalone, V., Naili, S., Bousson, V., Bergot, C., Peyrin, F., Zarka, J., Laredo, J. D., and Haïat, G. 2010. Determination of the heterogeneous anisotropic elastic properties of human femoral bone: from nanoscopic to organ scale. *Journal of Biomechanics* 43(10):1857–1863.
116. Martínez-Reina, J., Domínguez, J., and García-Aznar, J. 2010. Effect of porosity and mineral content on the elastic constants of cortical bone: a multiscale approach. *Biomechanics and Modeling in Mechanobiology* 1–14.
117. Morgan, E. F., Yeh, O. C., Chang, W. C., and Keaveny, T. M. 2001. Nonlinear behavior of trabecular bone at small strains. *Journal of Biomechanical Engineering* 123(1):1–9.
118. Fondrk, M. T. 1989. An Experimental and Analytical Investigation into Nonlinear Constitutive Equation of Cortical Bone. Case Western Reserve University.
119. Keaveny, T. M., Wachtel, E. F., Ford, C. M., and Hayes, W. C. 1994. Differences between the tensile and compressive strengths of bovine tibial trabecular bone depends on modulus. *Journal of Biomechanics* 27(9):1137–1146.
120. Keaveny, T. M., Morgan, E. F., and Yeh, O. C. 2003. Bone mechanics. In *Standard Handbook of Biomedical Engineering and Design*, edited by M. Kurtz, 8.1–8.23. New York: McGraw Hill.
121. Banse, X., Deogelaer, J. P., Munting, E., Delloye, C., Cornu, O., and Grynpas, M. 2001. Inhomogeneity of human vertebral cancellous bone: systematic density and structure patterns inside the vertebral body. *Bone* 28(5):563–571.
122. Hulme, P. A., Boyd, S. K., and Ferguson, S. J. 2007. Regional variation in vertebral bone morphology and its contributions to vertebral fracture strength. *Bone* 41(6):946–957.
123. Carter, D. R., and Hayes, W. C. 1976. Bone compressive strength: the influence of density and strain rate. *Science* 194(4270):1174–1176.
124. Carter, D. R., and Hayes, W. C. 1977. The compressive behavior of bone as a two-phase porous structure. *Journal of Bone and Joint Surgery* 59(7):954–962.
125. Gibson, L. J. 1985. The mechanical behaviour of cancellous bone. *Journal of Biomechanics* 18(5):317–328.
126. Morgan, E. F., Bayraktar, H. H., and Keaveny, T. M. 2003. Trabecular bone modulus-density relationships depend on anatomic site. *Journal of Biomechanics* 36(7):897–904.
127. Mosekilde, L., Mosekilde, Le., and Danielsen, C. C. 1987. Biomechanical competence of vertebral trabecular bone in relation to ash density and age in normal individuals. *Bone* 8(2):79–85.
128. Kopperdahl, D. L., and Keaveny, T. M. 1998. Yield strain behavior of trabecular bone. *Journal of Biomechanics* 31(7):601–608.
129. McCalden, R. W., McGeough, J. A., and Court-Brown, C. M. 1997. Age-related changed in the compressive strength of cancellous bone. The relative importance of changes in density and trabecular architecture. *The Journal of Bone and Joint Surgery. American Volume* 79(3):421–427.

130. Pugh, J. W., Radin, E. L., and Rose, R. M. 1974. Quantitative studies of human subchondral cancellous bone. *Journal of Bone and Joint Surgery* 56(2):313–321.
131. Hipp, J. A., Rosenberg, A. E., and Hayes, W. C. 1992. Mechanical properties of trabecular bone within and adjacent to osseous metastases. *Journal of Bone and Mineral Research* 7(10):1165–1171.
132. Goldstein, S. A., Wilson, D. L., and Matthews, L. S. 1983. The mechanical properties of human tibial trabecular bone as a function of metaphyseal location. *Journal of Biomechanics* 16(12):965–969.
133. Brown, T., and Ferguson, A. 1980. Mechanical property distributions in the cancellous bone of the human proximal femur. *Acta Orthopaedica Scandinavica* 51:429–437.
134. Ciarelli, M. J., Goldstein, S. A., Kuhn, J. L., Cody, D. D., and Brown, M. B. 1991. Evaluation of orthogonal mechanical properties and density of human trabecular bone from the major metaphyseal regions with materials testing and computed tomography. *Journal of Orthopaedic Research* 9(5):674–682.
135. Williams, J. L. a. L., J. L. 1982. Preperties and an anisotropic model of cancellous bone from the proximal tibial epiphysis. *Journal of Biomechanical Engineering* 104(1):50–56.
136. Galante, J., Rostoker, W., and Ray, R. D. 1970. Physical properties of trabecular bone. *Calcified Tissue Research* 5:236–246.
137. Odgaard, A., Kabel, J., van Rietbergen, B., Dalstra, M., and Huiskes, R. 1997. Fabric and elastic principal directions of cancellous bone are closely related. *Journal of Biomechanics* 30:487–495.
138. Yang, G., Kabel, J., van Rietbergen, B., Odgaard, A., and Huiskes, R. 1999. The anisotropic Hooke's Law for cancellous bone and wood. *Journal of Elasticity* 53:125–146.
139. Zysset, P. K., Goulet, R. W., and Hollister, S. J. 1998. A global relationship between trabecular bone morphology and homogenized elastic properties. *Journal of Biomechanical Engineering* 120:640–646.
140. Linde, F., Pongsoipetch, B., Frich, L. H., and Hvid, I. 1990. Three-axial strain controlled testing applied to bone specimens from the proximal tibial epiphysis. *Journal of Biomechanics* 23(11):1167–1172.
141. Townsend, P. R., Raux, P., Rose, R. M., Miegel, R. E., and Radin, E. L. 1975. The distribution and anisotropy of the stiffness of cancellous bone in the human patella. *Journal of Biomechanics* 8(6):363–364.
142. Goulet, R. W., Goldstein, S. A., Ciarelli, M. J., Kuhn, J. L., Brown, M. B., and Feldkamp, L. A. 1994. The relationship between the structural and orthogonal compressive properties of trabecular bone. *Journal of Biomechanics* 27(4):375–377.
143. Mosekilde, L. 1998. The effect of modelling and remodelling on human vertebral body architecture. *Technology and Health Care* 6(5–6):287–297.
144. Chang, W. C. W., Christensen, T. M., Pinilla, T. P., and Keaveny, T. M. 1999. Uniaxial yield strains for bovine trabecular bone are isotropic and asymmetric. *Journal of Orthopaedic Research* 17(4):582–585.
145. Bevill, G., Farhamand, F., and Keaveny, T. M. 2009. Heterogeneity of yield strain in low-density versus high-density human trabecular bone. *Journal of Biomechanics* 42:2165–2170.
146. Turner, C. H. 1989. Yield behavior of bovine cancellous bone. *Journal of Biomechanical Engineering* 111(3):256–260.
147. Hvid, I., Bentzen, S. M., Linde, F., Mosekilde, Li. and Pongsoipetch, B. 1989. X-ray quantitative computed tomography: the relations to physical properties of proximal tibial trabecular bone specimens. *Journal of Biomechanics* 22(8–9):837–844.
148. Bayraktar, H. H., Gupta, A., Kwon, R. Y., Papadopoulos, P., and Keaveny, T. M. 2004. The modified super-ellipsoid yield criterion for human trabecular bone. *Journal of Biomechanical Engineering* 126(6):677–684.
149. Linde, F., Norgaard, P., Hvid, Ivan, Odgaard, A., and Soballe, K. 1991. Mechanical properties of trabecular bone. Dependency on strain rate. *Journal of Biomechanics* 24(9):803–809.
150. Burgers, T. A., Lakes, R. S., Garcia-Rodriguez, S., Pill, G. R., and Ploeg, H. L. 2009. Post-yield relaxation behavior of bovine cancellous bone. *Journal of Biomechanics* 42(16):2728–2733.
151. Bowman, S. M., Keaveny, T. M., Gibson, L. J., Hays, W. C., and McMahon, T. A. 1994. Compressive creep behavior of bovine trabecular bone. *Journal of Biomechanics* 27(3):301–305.

152. Ochia, R. S., and Ching, R. P. 2006. Rate dependence of hydraulic resistance in human lumbar vertebral bodies. *Spine* 31(22):2569–2574.
153. Ochoa, J. A., Sanders, A. P., Heck, D. A., and Hillberry, B. M. 1991. Stiffening of the femoral head due to intertrabecular fluid and intraosseous pressure. *Journal of Biomechanical Engineering* 113(3):259–262.
154. Keaveny, T. M., Wachtel, E. F., and Kopperdahl, D. L. 1999. Mechanical behavior of human trabecular bone after overloading. *Journal of Orthopaedic Research* 17(3):346–353.
155. Kopperdahl, D. L., Pearlman, J. L., and Keaveny, T. M. 2000. Biomechanical consequences of an isolated overload on the human vertebral body. *Journal of Orthopaedic Research* 18(5):685–690.
156. Fondrk, M. T., Bahniuk, E. H., and Davy, D. T. 1999. A damage model for nonlinear tensile behavior of cortical bone. *Journal of Biomechanical Engineering* 121(5):533–541.
157. Wachtel, E. F., and Keaveny, T. M. 1997. Dependence of trabecular damage on mechanical strain. *Journal of Orthopaedic Research* 15:781–787.
158. Fyhrie, D. P. a. S., M. B. 1994. Failure mechanisms in human vertebral cancellous bone. *Bone* 15:105–109.
159. Vashishth, D., Koontz, J., Qiu, S. J., Lundin-Cannon, D., Yeni, Y. N., Schaffler, M. B., and Fyhrie, D. P. 2000. In vivo diffuse damage in human vertebral trabecular bone. *Bone* 26:147–152.
160. Nagaraja, S., Couse, T. L., and Guldberg, R. E. 2005. Trabecular bone microdamage and microstructural stresses under uniaxial compression. *Journal of Biomechanics* 38:707–716.
161. Tang, S. Y., and Vashishth, D. 2007. A non-invasive in vitro technique for the three-dimensional quantification of microdamage in trabecular bone. *Bone* 40(5):1259–1264.
162. Jungmann, R., et al. 2011. Local strain and damage mapping in single trabeculae during three-point bending tests. *Journal of the Mechanical Behavior of Biomedical Materials* 4(4):523–534.
163. Morgan, E. F., Yeh, O. C., and Keaveny, T. M. 2005. Damage in trabecular bone at small strains. *European Journal of Morphology* 42:13–21.
164. Wang, X., Masse, D. B., Leng, H., Hess, K. P., Ross, R. D., Roeder, R. K., and Niebur, G. L. 2007. Detection of trabecular bone microdamage by micro-computed tomography. *Journal of Biomechanics* 40(15):3397–3403.
165. Ding, M., and Hvid, I. 2000. Quantification of age-related changes in the structure model type and trabecular thickness of human tibial cancellous bone. *Bone* 26:291–295.
166. Diab, T., and Vashishth D. 2005. Effects of damage morphology on cortical bone fragility. *Bone* 37:96–102.
167. Karim, L., and Vashishth, D. 2011. Role of trabecular microarchitecture in the formation, accumulation, and morphology of microdamage in human cancellous bone. *Journal of Orthopaedic Research* 29(11):1739–1744.
168. Nagaraja, S., Lin, A. S. P., and Guldberg, R. E. 2007. Age-related changes in trabecular bone microdamage initiation. *Bone* 40(4):973–980.
169. Arlot, M. E., Burt-Pichat, B., Rouz, J. P., Vashishth, D., Bouxsein, M. L., and Delmas, P. D. 2008. Microarchitecture influences microdamage accumulation in human vertebral trabecular bone. *Journal of Bone and Mineral Research* 23(10):1613–1618.
170. Shi, X. T., Wang, X., and Niebur, G. L. 2009. Effects of loading orientation on the morphology of the predicted yielded regions in trabecular bone. *Annals of Biomedical Engineering* 37(2):354–362.
171. Shi, X. T., Liu, X. S., Wang, X., Guo, X. E., and Niebur, G. L. 2010. Type and orientation of yielded trabeculae during overloading of trabecular bone along orthogonal directions. *Journal of Biomechanics* 43(13):2460–2466.
172. Boyde, A. 2003. The real response of bone to exercise. *Journal of Anatomy* 203(2):172–189.
173. Cook, R. B., and Zioupos, P. 2009. The fracture toughness of cancellous bone. *Journal of Biomechanics* 42:2054–2060.
174. Moore, T. L. A., and Gibson, L. J. 2003. Fatigue microdamage in bovine trabecular bone. *Journal of Biomechanical Engineering* 125(6):769–776.
175. Yamamoto, E., Crawford, R. P., Chan, D. D., and Keaveny, T. M. 2006. Development of residual strains in human vertebral trabecular bone after prolonged static and cylic loadings at low load levels. *Journal of Biomechanics* 39(10):1812–1818.

176. Burr, D. B., Forwood, M. R., Fyhrie, D. P., Martin, R. B., Schaffler, M. B., and Turner, C. H. 1997. Bone microdamage and skeletal fragility in osteoporotic and stress fractures. *Journal of Bone and Mineral Research* 12(1):6–15.
177. Bauer, T. W., and Schils, J. 1999. The pathology of total joint arthroplasty II. Mechanisms of implant failure. *Skeletal Radiology* 28(9):483–497.
178. Haddock, S. M., Yeh, O. C., Mummaneni, P. V., Rosenberg, W. S., and Keaveny, T. M. 2004. Similarity in the fatigue behavior of trabecular bone across site and species. *Journal of Biomechanics* 37(2):181–187.
179. Bowman, S. M., Cheng, D. W., Keaveny, T. M., Gibson, L. J., Hayes, W. C., and McMahon, T. A. 1998. Creep contributes to the fatigue behavior of bovine trabecular bone. *Journal of Biomechanical Engineering* 120(5):657–654.
180. Moore, T. L. A., O'Brien, F. J., and Gibson, L. J. 2004. Creep does not contribute to fatigue in bovine trabecular bone. *Journal of Biomechanical Engineering* 126:321–329.
181. Rapillard, L., Charlebois, M., and Zysset, P. K. 2006. Compressive fatigue behavior of human vertebral trabecular bone. *Journal of Biomechanics* 39(11):2133–2139.
182. Dendorfer, S., Maier, H. J., Taylor, D., and Hammer, J. 2008. Anisotropy of the fatigue behaviour of cancellous bone. *Journal of Biomechanics* 41(3):636–641.
183. Homminga, J., Van-Rietbergen, B., Lochmuller, E. M., Weinans, H., Eckstein, F., and Huiskes, R. 2004. Osteoporotic vertebral structure is well adapted to the load of daily life, but not to infrequent 'error' loads. *Bone* 34:510–516.
184. Cowin, S. C. 1986. Fabric dependence of an anisotropic strength criterion. *Mechanics of Materials* 5(3):251–260.
185. Pietrusczak S., I. D., and Pande G. N. 1999. A fabric-dependent facture criterion for bone. *Journal of Biomechanics* 32:1071–1079.
186. Fenech, C. M. a. K., T. M. 1999. A cellular solid criterion for predicting the axial-shear failure properties of bovine trabecular bone. *Journal of Biomechanical Engineering* 121(4):414–512.
187. Keaveny, T. M., Wachtel, E. F., Zadesky, S. P., and Arramon, Y. P. 1999. Application of the Tsai–Wu quadratic multiaxial failure criterion to bovine trabecular bone. *Journal of Biomechanical Engineering* 121(1):99–107.
188. Zysset, P. K., and Rincon-Kohli, L. 2006. An alternative fabric-based yield and failure criterion for trabecular bone. In *Mechanics of Biological Tissues*, edited by G. A. a. O. Hozapfel, R. W., 457–470. Berlin: Springer.
189. Rincon-Kohli, L., and Zysset, P. K. 2009. Multi-axial mechanical properties of human trabecular bone. *Biomechanics and Modeling in Mechanobiology* 8:195–208.
190. Ulrich, D., van Rietbergen, B., Laib, A., and Ruegsegger, P. 1999. The ability of three-dimensional structural indices to reflect mechanical aspects of trabecular bone. *Bone* 25(1):55–60.
191. Matsuura, M., Eckstein, F., Lochmuller, E. M., and Zysset, P. K. 2008. The role of fabric in the quasi-static compressive mechanical propreties of human trabecular bone from various anatomical locations. *Biomechanics and Modeling in Mechanobiology* 7(1):27–42.
192. Chen, P., and McKittrick, J. 2011. Compressive mechanical properties of demineralized and deproteinized cancellous bone. *Journal of the Mechanical Behavior of Biomedical Materials* 4(7):961–973.
193. Ashby, M. F., and Medalist, R. F. Mehl, 1983. The mechanical properties of cellular solids. *Metallurgical and Materials Transactions A* 14(9):1755–1769.
194. Gibson, L. J., and Ashby, M. F. 1997. Cancellous bone. In *Cellular Solids: Structure and Properties*, 429–452, Cambridge: Cambridge University Press.
195. Gibson, L. J. 2005. Biomechanics of cellular solids. *Journal of Biomechanics* 38(3):377–399.
196. Muller, R., Gerber, S. C., and Hayes, W. C. 1998. Micro-compression: a novel technique for the nondestructive assessment of local bone failure. *Technology and Health Care* 6(5):433–444.
197. Nazarian, A., and Muller, R. 2004. Time-lapsed microstructural imaging of bone failure behavior. *Journal of Biomechanics* 37(1):55–65.
198. Hodgskinson, R., and Currey, J. D. 1990. The effect of variation in structure on the Young's modulus of cancellous bone: a comparison of human and non-human material. *Proceedings of the Institution of Mechanical Engineers, Part H. Journal of Engineering in Medicine* 204(2):115–121.

199. Turner, C. H., and Cowin, S. C. 1987. Dependence of elastic constants of an anisotropic porous material upon porosity and fabric. *Journal of Materials Science* 22(9):3178–3184.
200. Zysset, P. K., and Curnier, A. 1995. An alternative model for anisotropic elasticity based on fabric tensors. *Mechanics of Materials* 21(4):243–250.
201. Boehler, J. P. 1987. *Applications of Tensor Functions in Solid Mechanics*, Berlin, Heidelberg: Springer.
202. Zysset, P. K. 2003. A review of morphology-elasticity relationships in human trabecular bone: theories and experiments. *Journal of Biomechanics* 36:1469–1485.
203. Silva, M. J., and Gibson, L. J. 1997. The effects of non-periodic microstructure and defects on the compressive strength of two-dimensional cellular solids. *International Journal of Mechanical Sciences* 39(5):549–563.
204. Silva, M. J., and Gibson, L. J. 1997. Modeling the mechanical behavior of vertebral trabecular bone: Effects of age-related changes in microstructure. *Bone* 21(2):191–199.
205. Yeh, O. C., and Keaveny, T. M. 1999. Biomechanical effects of intraspecimen variations in trabecular architecture: a three-dimensional finite element study. *Bone* 25(2):223–228.
206. van Rietbergen, B., Weinans, H., Huiskes, R., and Odgaard, A. 1995. A new method to determine trabecular bone elastic properties and loading using micromechanical finite-element models. *Journal of Biomechanics* 28(1):69–81.
207. Hollister, S. J., Brennan, J. M., and Kikuchi, N. 1994. A homogenization sampling procedure for calculating trabecular bone effective stiffness and tissue level stress. *Journal of Biomechanics* 27(4):433–444.
208. Niebur, G. L., and Keaveny, T. M. 2010. Computational modeling of trabecular bone mechanics. In *Computational Modeling in Biomechanics*, edited by S. De, F. Guilak, and M. R. K. Mofrad, 277–306, Netherlands: Springer.
209. Hakulinen, M. A., Toyras, J., Saaakkala, S., Hirvonen, J., Kroger, H, and Jurvelin, J. S. 2004. Ability of ultrasound backscattering to predict mechanical properties of bovine trabecular bone. *Ultrasound in Medicine & Biology* 30(7):919–927.
210. Hakulinen, M. A., Day, J. S., Toyras, J., Timonen, M., Kroger, H., Weinans, H., Kiviranta, I, and Jurvelin, J. S. 2005. Prediction of density and mechanical properties of human trabecular bone in vitro by using ultrasound transmission and backscattering measurements at 0.2–6.7 MHz frequency range. *Physics in Medicine and Biology* 50(8):1629.
211. Kabel, J., van Rietbergen, B., Odgaard, A., and Huiskes, R. 1999. Constitutive relationships of fabric, density, and elastic properties in cancellous bone architecture. *Bone* 25(4):481–486.
212. Liu, X. S., Sajda, P., Saha, P. K., Wehrli, F. W., and Guo, X. E. 2006. Quantification of the roles of trabecular microarchitecture and trabecular type in determining the elastic modulus of human trabecular bone. *Journal of Bone and Mineral Research* 21(10):1608–1617.
213. Van Rietbergen, B., Huiskes, R., Eckstein, F., and Ruegsegger, P. 2003. Trabecular bone tissue strains in the healthy and osteoporotic human femur. *Journal of Bone and Mineral Research* 18(10):1781–1788.
214. Pauchard, Y., Mattmann, C., Kuhn, A., Gasser, J. A., and Boyd, S. K. 2008. European Society of Biomechanics S.M. Perren Award 2008: using temporal trends of 3D bone micro-architecture to predict bone quality. *Journal of Biomechanics* 41(14):2946–2953.
215. van Rietbergen, B. 2001. Micro-FE analyses of bone: state of the art. *Advances in Experimental Medicine and Biology* 496:21–30.
216. Mente, P. L., and Lewis, J. L. 1989. Experimental method for the measurement of the elastic modulus of trabecular bone tissue. *Journal of Orthopaedic Research* 7(3):456–461.
217. Ashman, R. B., and Rho, J. Y. 1988. Elastic modulus of trabecular bone material. *Journal of Biomechanics* 21(3):177–181.
218. Rho, J. Y., Ashmann, R. B., and Turner, C. H. 1993. Young's modulus of trabecular and cortical bone material: ultrasonic and microtensile measurements. *Journal of Biomechanics* 26(2):111–119.
219. Turner, C. H., Rho, J., Takano, Y., Tsui, T. Y., and Pharr, G. M. 1999. The elastic properties of trabecular and cortical bone tissues are similar: results from two microscopic measurement techniques. *Journal of Biomechanics* 32(4):437–441.

220. Lietniewski, J. 2005. Determination of the elasticity coefficient for a single trabecula of a cancellous bone: scanning acoustic microscopy approach. *Ultrasound in Medicine & Biology* 31(10):1361–1366.
221. Hou, F. J., Lang, S. M., Hoshaw, S. J., Reimann, D. A., and Fyhrie, D. P. 1998. Human vertebral body apparent and hard tissue stiffness. *Journal of Biomechanics* 31(11):1009–1015.
222. Ladd, A. J. C., and Kinney, J. H. 1998. Numerical errors and uncertainties in finite-element modeling of trabecular bone. *Journal of Biomechanics* 31(10):941–945.
223. Niebur, G. L., Feldstein, M. J., Yuen, J. C., Chen, T. J., and Keaveny, T. M. 2000. High-resolution finite element models with tissue strength asymmetry accurately predict failure of trabecular bone. *Journal of Biomechanics* 33(12):1575–1583.
224. Bayraktar, H. H., Morgan, E. F., Niebur, G. L., Morris, G. E., Wong, E. K., and Keaveny, T. M. 2004. Comparison of the elastic and yield properties of human femoral trabecular and cortical bone tissue. *Journal of Biomechanics* 37(1):27–35.
225. Lorenzetti, S., Carretta, R., Muller, R., and Stussi, E. 2011. A new device and method for measuring the elastic modulus of single trabeculae. *Medical Engineering & Physics* 33(8):993–1000.
226. Choi, K., and Goldstein, S. A. 1992. A comparison of the fatigue behavior of human trabecular and cortical bone tissue. *Journal of Biomechanics* 25(12):1371–1381.
227. Bergmann, G., Deuretzbacher, G., Heller, M., Graichen, F., Rohlmann, A., Strauss, J., and Duda, G. N. 2001. Hip contact forces and gait patterns from routine activities. *Journal of Biomechanics* 34(7):859–871.
228. Chiu, J., and Robinovitch, S. N. 1998. Prediction of upper extremity impact forces during falls on the outstretched hand. *Journal of Biomechanics* 31(12):1169–1176.
229. Robinovitch, S., Hayes, W., and McMahon, T. 1991. Prediction of femoral impact forces in falls on the hip. *Journal of Biomechanical Engineering* 113:366.
230. Nachemson, A., and Morris, J. M. 1964. In vivo measurements of intradiscal pressure: Discometry, a method for the determination of pressure in the lower lumbar discs. *The Journal of Bone and Joint Surgery* 46(5):1077.
231. Wilke, H. J., Neef, P., Caimi, M., Hoogland, T., and Claes, L. E. 1999. New in vivo measurements of pressures in the intervertebral disc in daily life. *Spine* 24(8):755.
232. Sato, K., Kikuchi, S., and Yonezawa, T. 1999. In vivo intradiscal pressure measurement in healthy individuals and in patients with ongoing back problems. *Spine* 24(23):2468.
233. Knapik, G. G., and Marras, W. S. 2009. Spine loading at different lumbar levels during pushing and pulling. *Ergonomics* 52(1):60–70.
234. Rohlmann, A., Gabel, U., Graichen, F., Bender, A., and Bergmann, G. 2007. An instrumented implant for vertebral body replacement that measures loads in the anterior spinal column. *Medical Engineering & Physics* 29(5):580–585.
235. Westerhoff, P., Graichen, F., Bender, A., Rohlmann, A., and Bergmann, G. 2009. An instrumented implant for in vivo measurement of contact forces and contact moments in the shoulder joint. *Medical Engineering & Physics* 31(2):207–213.
236. Kim, H. J., Fernandez, J. W., Akbarshahi, M., Walter, J. P., Fregly, B. J., and Pandy, M. G. 2009. Evaluation of predicted knee joint muscle forces during gait using an instrumented knee implant. *Journal of Orthopaedic Research* 27(10):1326–1331.
237. Stansfield, B., Nicol, A., Paul, J., Kelly, I., Graichen, F., and Bergmann, G. 2003. Direct comparison of calculated hip joint contact forces with those measured using instrumented implants. An evaluation of a three-dimensional mathematical model of the lower limb. *Journal of Biomechanics* 36(7):929–936.
238. Cappello, A., Cappozzo, A., Della Croce, U., Leardini, A., Allard, P., Lundberg, A., and Vaughan, C. 1997. *Bone Position and Orientation Reconstruction Using External Markers*, 147–172. Chichester, UK: Wiley.
239. Pinilla, T. P., Boardman, K. C., Bouxsein, M. L., Myers, E. R., and Hayes, W. C. 1996. Impact direction from a fall influences the failure load of the proximal femur as much as age-related bone loss. *Calcified Tissue International* 58:231–235.
240. Turner, C. 1998. Three rules for bone adaptation to mechanical stimuli. *Bone* 23(5):399–407.

241. Cowin, S., ed. 2001. *Bone Mechanics Handbook*, Boca Raton, FL: CRC Press.
242. Akhter, M. P., Iwaniec, U. T., Covey, M. A., Cullen, D. M., Kimmel, D. B., and Recker, R. R. 2000. Genetic variations in bone density, histomorphometry, and strength in mice. *Calcified Tissue International* 67(4):337–344.
243. van der Meulen, M. C., Jepsen, K. J., and Mikic, B. 2001. Understanding bone strength: size isn't everything. *Bone* 29(2):101–104.
244. Wergedal, J. E., Sheng, M. H., Ackert-Bicknell, C. L., Beamer, W. G., and Baylink, D. J. 2005. Genetic variation in femur extrinsic strength in 29 different inbred strains of mice is dependent on variations in femur cross-sectional geometry and bone density. *Bone* 36(1):111–122.
245. Muller, M. E., Webber, C. E., and Bouxsein, M. L. 2003. Predicting the failure load of the distal radius. *Osteoporosis International* 14(4):345–352.
246. Buckley, J. M., Cheng, L., Loo, K., Slyfield, C., and Xu, Z. 2007. Quantitative computed tomography-based predictions of vertebral strength in anterior bending. *Spine* 32(9):1019–1027.
247. Hong, J., Cabe, G. D., Tedrow, J. R., Hipp, J. A., and Snyder, B. D. 2004. Failure of trabecular bone with simulated lytic defects can be predicted non-invasively by structural analysis. *Journal of Orthopaedic Research* 22(3):479–486.
248. Kopperdahl, D. L., Morgan, E. F., and Keaveny, T. M. 2002. Quantitative computed tomography estimates of the mechanical properties of human vertebral trabecular bone. *Journal of Orthopaedic Research* 20(4):801–805.
249. Buckley, J. M., Loo, K., and Motherway, J. 2007. Comparison of quantitative computed tomography-based measures in predicting vertebral compressive strength. *Bone* 40(3):767–774.
250. Levenston, M. E., Beaupre, G. S., and van der Meulen, M. C. 1994. Improved method for analysis of whole bone torsion tests. *Journal of Bone and Mineral Research* 9(9):1459–1465.
251. Beck, T. J., Looker, A. C., Ruff, C. B., Sievanen, H., and Wahner, H. W. 2000. Structural trends in the aging femoral neck and proximal shaft: analysis of the Third National Health and Nutrition Examination Survey dual energy X ray absorptiometry data. *Journal of Bone and Mineral Research* 15(12):2297–2304.
252. Sun, X., Lei, S.-F., Deng, F.-Y., Wu, S., Papacian, C., Hamilton, J., Recker, R., and Deng, H.-W. 2006. Genetic and environmental correlations between bone geometric parameters and body compositions. *Calcified Tissue International* 79(1):43–49.
253. Riggs, B. L., Melton Iii, L. J., 3rd, Robb, R. A., Camp, J. J., Atkinson, E. J., Peterson, J. M., Rouleau, P. A., McCollough, C. H., Bouxsein, M. L., and Khosla, S. 2004. Population-based study of age and sex differences in bone volumetric density, size, geometry, and structure at different skeletal sites. *Journal of Bone and Mineral Research* 19(12):1945–1954.
254. Smith, R. W., Jr., and Walker, R. R. 1980. Femoral expansion in aging women. Implications for osteoporosis and fractures. *Henry Ford Hospital Medical Journal* 28(2–3):168–170.
255. Ruff, C. B., and Hayes, W. C. 1982. Subperiosteal expansion and cortical remodeling of the human femur and tibia with aging. *Science* 217(4563):945–948.
256. Sigurdsson, G., Aspelund, T., Chang, M., Jonsdottir, B., Sigurdsson, S., Eiriksdottir, G., Gudmundsson, A., Harris, T. B., Gudnason, V., and Lang, T. F. 2006. Increasing sex difference in bone strength in old age: The Age, Gene/Environment Susceptibility—Reykjavik study (AGES-REYKJAVIK). *Bone* 39(3):644–651.
257. Szulc, P., Duboeuf, F., Schott, A. M., Dargent-Molina, P., Meunier, P. J., and Delmas, P. D. 2006. Structural determinants of hip fracture in elderly women: re-analysis of the data from the EPIDOS Study. *Osteoporosis International* 17(2):231–236.
258. Duan, Y., Turner, C. H., Kim, B. T., and Seeman, E. 2001. Sexual dimorphism in vertebral fragility is more the result of gender differences in age-related bone gain than bone loss. *Journal of Bone and Mineral Research* 16(12):2267–2275.
259. Kaptoge, S., Beck, T. J., Reeve, J., Stone, K. L., Hillier, T. A., Cauley, J. A., and Cummings, S. R. 2008. Prediction of incident hip fracture risk by femur geometry variables measured by hip structural analysis in the study of osteoporotic fractures. *Journal of Bone and Mineral Research* 23(12):1892–1904.

260. Alonso, C. G., Curiel, M. D., Carranza, F. H., Cano, R. P., and Perez, A. D. 2000. Femoral bone mineral density, neck-shaft angle and mean femoral neck width as predictors of hip fracture in men and women. Multicenter Project for Research in Osteoporosis. *Osteoporosis International* 11(8):714–720.
261. El-Kaissi, S., Pasco, J. A., Henry, M. J., Panahi, S., Nicholson, J. G., Nicholson, G. C., and Kotowicz, M. A. 2005. Femoral neck geometry and hip fracture risk: the Geelong osteoporosis study. *Osteoporosis International* 16(10):1299–1303.
262. Schneider, P., Reiners, C., Cointry, G. R., Capozza, R. F., and Ferretti, J. L. 2001. Bone quality parameters of the distal radius as assessed by pQCT in normal and fractured women. *Osteoporosis International* 12(8):639–646.
263. Bouxsein, M. L., and Karasik, D. 2006. Bone geometry and skeletal fragility. *Current Osteoporosis Reports* 4(2):49–56.
264. Brinckmann, P., Biggemann, M., and Hilweg, D. 1989. Prediction of the compressive strength of human lumbar vertebrae. *Spine* 14(6):606–610.
265. Cody, D. D., Goldstein, S. A., Flynn, M. J., and Brown, E. B. 1991. Correlations between vertebral regional bone mineral density (rBMD) and whole bone fracture load. *Spine* 16:146–154.
266. Lotz, J. C., Gerhart, T. N., and Hayes, W. C. 1990. Mechanical properties of trabecular bone from the proximal femure: a quantitative CT study. *Journal of Computer Assisted Tomography* 14:107–114.
267. McBroom, R. J., Hayes, W. C., Edwards, W. T., Goldberg, R. P., and White, A. A. 1985. Prediction of vertebral body compressive fracture using quantitative computed tomography. *Journal of Bone and Joint Surgery* 67-A(8):1206–1214.
268. Eswaran, S. K., Gupta, A., Adams, M. F., and Keaveny, T. M. 2006. Cortical and trabecular load sharing in the human vertebral body. *Journal of Bone and Mineral Research* 21(2):307–314.
269. Rockoff, S. D., Sweet, E., and Bleustein, J. 1969. The relative contribution of trabecular and cortical bone to the strength of human lumbar vertebrae. *Calcified Tissue Research* 3:163–175.
270. Yodanandan, N., Myklebust, J. B., Cusik, J. F., Wison, C. R., and Sances, A. 1988. Functional biomechanics of the throacolumbar vertebral cortex. *Clinical Biomechanics* 3:11–18.
271. Cao, K. D., Grimm, M. J., and Yang, K. H. 2001. Load sharing within a human lumbar vertebral body using the finite element method. *Spine* 26(12):E253–260.
272. Homminga, J., Weinans, H., Gowin, W., Felsenberg, D., and Huiskes, R. 2001. Osteoporosis changes the amount of vertebral trabecular bone at risk of fracture but not the vertebral load distribution. *Spine* 26(14):1555–1561.
273. Silva, M. J., Keaveny, T. M., and Hayes, W. C. 1997. Load sharing between the shell and centrum in the lumbar vertebral body. *Spine* 22(2):140–150.
274. Faulkner, K. G., Cann, C. E., and Hasegawa, B. H. 1991. Effect of bone distribution on vertebral strength: assessment with a patient-specific nonlinear finite element analysis. *Radiology* 179:669–674.
275. Lotz, J. C., Cheal, E. J., and Hayes, W. C. 1995. Stress distributions within the proximal femur during gait and falls: implications for osteoporotic fracture. *Osteoporosis International* 5(4):252–261.
276. Ford, C. M., Keaveny, T. M., and Hayes, W. C. 1996. The effect of impact direction on the structural capacity of the proximal femur during falls. *Journal of Bone and Mineral Research* 11:377–383.
277. Keyak, J. H., Rossi, S. A., Jones, K. A., and Skinner, H. B. 1998. Prediction of femoral fracture load using automated finite element modeling. *Journal of Biomechanics* 31:125–133.
278. Lotz, J. C., Cheal, E. J., and Hayes, W. C. 1991. Fracture prediction for the proximal femur using finite element models: Part II—Nonlinear analysis. *Journal of Biomechanical Engineering* 113(4):361–365.
279. Keaveny, T. M., Hoffmann, P. F., Singh, M., Palermo, L., Bilezikian, J. P., Greenspan, S. L., and Black, D. M. 2008. Femoral bone strength and its relation to cortical and trabecular changes after treatment with PTH, alendronate, and their combination as assessed by finite element analysis of quantitative CT scans. *Journal of Bone and Mineral Research* 23(12):1974–1982.

280. Boutroy, S., Van Rietbergen, B., Sornay Rendu, E., Munoz, F., Bouxsein, M. L., and Delmas, P. D. 2008. Finite element analysis based on in vivo HR pQCT images of the distal radius is associated with wrist fracture in postmenopausal women. *Journal of Bone and Mineral Research* 23(3):392–399.
281. Zhang, X. H., Liu, X. S., Vasilic, B., Wehrli, F. W., Benito, M., Rajapakse, C. S., Snyder, P. J., and Guo, X. E. 2008. In vivo MRI based finite element and morphological analyses of tibial trabecular bone in eugonadal and hypogonadal men before and after testosterone treatment. *Journal of Bone and Mineral Research* 23(9):1426–1434.
282. Moro, M., Hecker, A., Bouxsein, M., and Myers, E. 1995. Failure load of thoracic vertebrae correlates with lumbar bone mineral density measured by DXA. *Calcified Tissue International* 56(3):206–209.
283. Kontogianni, M. D., Dafni, U. G., Routsias, J. G., and Skopouli, F. N. 2004. Blood leptin and adiponectin as possible mediators of the relation between fat mass and BMD in perimenopausal women. *Journal of Bone and Mineral Research* 19(4):546–551.
284. Black, D. M., Greenspan, S. L., Ensrud, K. E., Palermo, L., McGowan, J. A., Lang, T. F., Garnero, P., Bouxsein, M. L., Bilezikian, J. P., and Rosen, C. J. 2003. The effects of parathyroid hormone and alendronate alone or in combination in postmenopausal osteoporosis. *New England Journal of Medicine* 349(13):1207–1215.
285. Delmas, P. D., and Seeman, E. 2004. Changes in bone mineral density explain little of the reduction in vertebral or nonvertebral fracture risk with anti-resorptive therapy. *Bone* 34(4):599–604.
286. Crawford, R. P., Cann, C. E., and Keaveny, T. M. 2003. Finite element models predict in vitro vertebral body compressive strength better than quantitative computed tomography. *Bone* 33(4):744–750.
287. Bay, B. K., Yerby, S. A., McLain, R. F., and Toh, E. 1999. Measurement of strain distributions within vertebral body sections by texture correlation. *Spine* 24(1):10–17.
288. Silva, M. J., Keaveny, T. M., and Hayes, W. C. 1998. Computed tomography-based finite element analysis predicts failure loads and fracture patterns for vertebral sections. *Journal of Orthopaedic Research* 16(3):300–308.
289. Yerby, S. A., Bay, B. K., Toh, E., McLain, R. F., and Drews, M. J. 1998. The effect of boundary conditions on experimentally measured trabecular strain in the thoracic spine. *Journal of Biomechanics* 31(10):891–897.
290. Hussein, A. I., Unnikrishnan, G. U., and Morgan, E. F. 2011. 3-D experimental measurement of vertebral failure: towards validation of QCT-based finite element models. 57th Annual Meeting of the Orthopaedic Research Society, Long Beach, CA.
291. Hussein, A. I., and Morgan, E. F. 2010. Direct visualization of the initiation and progression of vertebral fractures. *Proceedings of the ASME 2010 Summer Bioengineering Conference,* Naples Beach, FL.
292. Hardisty, M. R., and Whyne, C. M. 2009. Whole bone strain quantification by image registration: a validation study. *Journal of Biomechanical Engineering* 131:064502.
293. Morgan, E. F., Lee, J. J., and Keaveny, T. M. 2005. Sensitivity of multiple damage parameters to compressive overload in cortical bone. *Journal of Biomechanical Engineering* 127:557–562.
294. Martin, R. B., Burr, D., and Sharkey, N. 2004. *Skeletal Tissue Mechanics*, New York: Springer.
295. Hayes, W. C., and Bouxsein, M. L. 1997. Biomechanics of cortical and trabecular bone: implications for assessment of fracture risk. In *Basic Orthopaedic Biomechanics*, edited by V. C. Mow, and W. C. Hayes, 69–111, Philadelphia, PA: Lippincott-Raven.
296. Cowin, S. C., and Mehrabadi, M. M. 1989. Identification of the elastic symmetry of bone and other materials. *Journal of Biomechanics* 22(6–7):503–515.
297. Fleisch, H. 2000. *Bisphosphonates in Bone Disease: From the Laboratory to the Patient*, 212, Nashville, TN: Parthenon.

2

Tendon and Ligament Biomechanics

Stavros Thomopoulos and Guy M. Genin

CONTENTS

2.1 Introduction

Tendons and ligaments are dense regular connective tissues that transmit muscle forces and stabilize joints, respectively. Injuries to these tissues result in significant disability and pain and often require surgical repair for the return of function. Clinical and experimental studies have shown that these tissues heal poorly. Research efforts are therefore under way to enhance healing through rehabilitation, biological, and tissue engineering approaches. In all cases, return of function requires a recapitulation of the biomechanics of the uninjured tendon or ligament. Therefore, an understanding of the mechanical behavior of these tissues is critical. This chapter will review the current understanding of tendon and ligament mechanics. Although strength, toughness, and constitutive response are all important mechanical properties of tendons and ligaments, the primary focus will lie on constitutive descriptions of these tissues. These are divided into two classes. The first class includes phenomenological approaches involving macroscopic frameworks that, when calibrated to tissue-level experiments, provide predictions for the responses of tissues to loading regimes beyond those used in calibration experiments. The second class

includes microstructure-based models that predict constitutive behavior through multiscale structure–function relationships, incorporating nanoscopic and microscopic information such as tissue composition and organization. Features of both classes of models include stress relaxation, energy dissipation, nonlinearity, and the need for careful calibration and validation.

Tendons and ligaments are critical for the biomechanical function of joints. Tendons connect muscles to bones and allow for the transmission of forces between tissues, leading to joint motion. Ligaments connect bones to bones and serve to stabilize joints at the extremes of motion. The mechanical properties of tendons and ligaments derive largely from type I collagen fibers that are arranged in dense, parallel arrays.[1,2] This arrangement results in a resilient tissue with high tensile stiffness in the direction of the fiber orientation.[2] The hierarchical nature of this arrangement leads to toughening mechanisms across the many orders of magnitude of length scale, ranging all the way down to the nanometer level; this design maximizes strength while providing necessary energy dissipation, creating a robust material.[3]

Although these tissues are well suited for their mechanical function, this function also puts them at risk of injury. Some estimates indicate that 50% of sports injuries involve tendons or ligaments (or both).[4] Tendinopathies also affect large portions of the aging population, leading to pain and disability.[5] Many of these disorders lead to ruptures at the tendon/ligament midsubstance, tendon/ligament-to-bone attachment, and tendon/muscle junction. These ruptures can occur after an acute injury (e.g., laceration and sports injury) or after chronic tendon degeneration (e.g., tendinosis and overuse). Disruption of tendon function will result in decreased ability to transmit forces from muscle to bone, reducing motion and debilitating joint function. Disruption of ligament function results in decreased joint stability, predisposing that joint to osteoarthritis in later years.[6]

The response to injury of tendons and ligaments varies widely, and engineered replacements and assistive scaffolds are an important goal in the field. Tendons and ligaments in a synovial environment have a markedly reduced capacity to heal compared to tendons and ligaments in extrasynovial spaces.[2,7,8] For example, lacerations to the intrasynovial tendons of the hand heal poorly due to the low cellularity in the tendon and the propensity of adhesion formation between the tendon's surface and its surrounding sheath.[9–12] The lack of extracellular matrix production at the repair site leads to poor strength or rupture of the repair. The formation of adhesions at the surface of the tendon leads to decreased tendon gliding and lack of digital function. Similarly, anterior cruciate ligament injuries fail to heal, in large part, due to the harsh synovial environment within which they reside.[13–15] In contrast, the extrasynovial Achilles tendon and medial collateral ligament mount a robust, albeit scar-mediated, wound healing response upon being injured.[16–18] The location of the injury also plays a role in the healing of tendons and ligaments. Repairs of midsubstance injuries have better outcomes compared with repairs of tendon/ligament to their bony insertions. This is likely due to the large discrepancy between the mechanical properties of tendon/ligament compared with bone.[19,20] Large stress concentrations arise at bimaterial interfaces with large mismatches in the moduli of the tissues;[21,22] in the case of tendon/ligament and bone, a two-orders-of-magnitude mismatch exists in their moduli.

In all these cases, the desired healing outcome is to restore pain-free mechanical function of the tendon or ligament. Indeed, the primary function of these tissues is to carry, transfer, and respond to load (muscle forces in the case of tendons and joint forces in the case of ligaments). The design of surgical repair strategies and implants thus requires knowledge of the behavior of tendons and ligaments in the settings of normal use, of how

mechanical loads lead to injury, and of how repairs or implanted scaffolds affect the way that these tissues respond to mechanical loads.

This chapter describes models of the constitutive response of the tendon and ligament midsubstance. The goals of such models are twofold. The first is to understand the normal physiologic mechanical response of tendon and ligament as a target for healing and for tissue engineered replacements. The second is as a foundation to understand and adapt the healthy and healing enthesis, the region of complicated material and stress variations that exists at the attachment of tendon and ligament to bone. Such attachments are injured with relative ease, heal poorly, and are not well understood. This chapter begins with a description of the tissues that exist in the midsubstance and then highlights the diversity of tissue that exists as tendon and ligament transition to bone by describing the makeup of the enthesis. The biomechanical response of tendon and ligament midsubstance is then described, followed by microstructural-based mathematical structure–function relationships and phenomenological constitutive frameworks for these tissues. The chapter concludes with descriptions of experimental testing frameworks and of challenges associated with implementing predictive models for tendon and ligament mechanics.

2.2 Structure and Composition

2.2.1 Tendon/Ligament Midsubstance

The organization of tendon and ligament is hierarchical in nature, from the molecular to the tissue scales (Figure 2.1).[1] The widely cited Hodge and Petruska[23] model for the molecular arrangement of collagen describes triple helix type I collagen molecules (300 nm in length, 1.5 nm in diameter) packed together to form microfibrils. Microfibrils are typically defined as five collagen molecules, stacked in a quarter-stagger array. The collagen is stacked with a 36-nm gap between the *N*-terminus of one collagen molecule and the

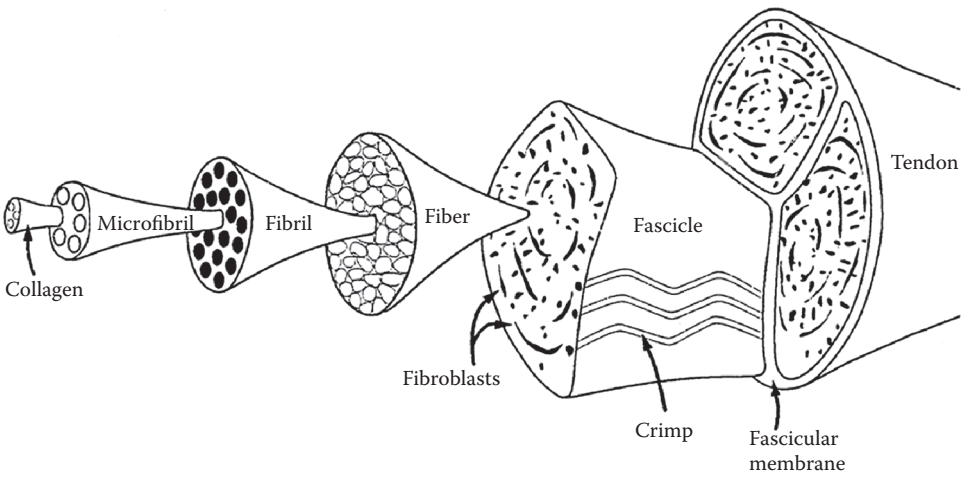

FIGURE 2.1
Organization of tendon is hierarchical in nature, from the molecular (i.e., collagen molecule) to the tissue scale. (From Kastelic, J. et al., *Conn. Tiss. Res.*, 6, 1, 11–23, 1978. With permission.)

C-terminus of the succeeding molecule. The collagen molecules are staggered relative to each other by 67 nm (approximately one-fourth the length of a collagen molecule, hence the common description of "quarter-stagger"). This description of collagen arrangement has recently been modified by Orgel et al.[24,25] X-ray diffraction studies demonstrate that collagen molecules are helically twisted and discontinuous along the length of the microfibrils. Neighboring microfibrils interdigitate, imposing order on a mildly twisted lattice that forms the next-level structure, termed a fibril (50–200 nm in diameter). At the next level of structural hierarchy, fibrils are closely packed into larger structures to form fibers (3–7 μm in diameter). Fibers combine to form fascicles (with diameters on the order of micrometers); at this level, a characteristic "crimp" pattern can be seen histologically.[1,26] Finally, fascicles are bundled together through a fascicular membrane to form tendons (with a diameter on the order of millimeters or centimeters).

Approximately 70% to 80% of the dry weight of tendons and ligaments is composed of type I collagen and nearly 70% of the wet weight is water.[2] The orientation distribution of collagen fibers is highly aligned in the direction of muscle force, with angular deviations on the order of 3°.[19,21]. Between 20% and 30% of the dry weight is made up of proteoglycans, glycosaminoglycans, minor collagens (e.g., type III and type XII), elastin, and cellular material.[27–30] These minor compositional constituents play important roles in the development of the tissue. For example, type V collagen and the proteoglycans biglycan and decorin regulate fibril diameter during collagen fibrillogenesis.[31–34] Mechanical roles for these minor components have also been proposed.[35–37] Many of the fibril-associating collagens and the short-chain proteoglycans form physical cross-bridges between adjacent collagen fibrils. Hypotheses have been proposed that these molecules prevent fiber-fiber sliding and enhance the shear modulus of tendons and ligaments.[38–40] Because proteoglycans and water content have clear roles in the viscoelastic behavior of articular cartilage,[41,42] it has also been proposed that these elements influence the viscoelastic behavior in tendon and ligament as well. Experimental studies testing these hypotheses have produced conflicting results.[35,43,44] Future studies are necessary to elucidate the mechanical role of minor compositional elements in adult tendons and ligaments.

2.2.2 Tendon/Ligament Enthesis (i.e., Bony Attachment)

The mechanical properties of tendon and ligament are dramatically different from those of bone.[45,46] For example, the tensile modulus of tendon is on the order of 200 MPa in the direction of the applied muscle force.[46] Bone, on the other hand, has a modulus of 20 GPa in both tension and compression.[45] Due to this disparity, large stress concentrations will arise at the attachment point of these two materials, and their connection will be at risk for failure. The tendon/ligament-to-bone insertion site overcomes this challenge via a number of strategies:[22] (1) gradations in its composition and structure,[20–22,47,48] (2) a shallow attachment angle at the insertion,[21,22] (3) shaping of tissue morphology of the transitional tissue,[22] and (4) interdigitation of the transitional tissue with bone.[49] The variation in structure and composition along the insertion results in a unique grading of mechanical properties. A shallow angle of attachment prevents stress risers at the interface. Peak stresses are reduced through optimization of the gross shape of the insertion. Interlocking of the tissues through interdigitation increases the toughness of the interface. The four mechanisms described above provide a nanomechanical through macromechanical description of how a robust tendon-to-bone attachment is achieved.[22,47] However, the complex composition, structure, and mechanical behavior

of the tendon/ligament-to-bone insertion results in a particularly difficult challenge for effective response to injury.

2.3 Phenomenology of the Tendon and Ligament Constitutive Response

This section qualitatively describes the responses of a tissue to mechanical loading; the goal of the mathematically constitutive models presented in the next sections is to provide predictions of these responses. A distinction must be made between "material" and "structural" responses. At the level of a mechanical test of a tissue, this is equivalent to the distinction between the stress–strain response of material within a specimen and the load-deformation response of the specimen as a whole. The focus here is on the former: constitutive properties normalized to tissue cross-sectional area (e.g., engineering stress = force / cross-sectional area) and length (e.g., linearized strain = change in length / original length), which describe the qualities of an effective continuum that represents the tissue within a region of a tendon or ligament. In contrast, mechanical properties not normalized to the amount of material present describe a tissue specimen's structural response.

Our objective is to describe the degree to which tendon and ligament at the midsubstance strain in response to stressing for loads ranging up to a critical level beyond which the relationship between stress and strain changes irreversibly due to injury. The distinction between structural and material responses is an important consideration when put in the context of injury and repair. Scar tissue, made up of disorganized, immature, collagen fibers, forms after a tendon tear and has a lower rupture stress and a modulus that is one-tenth that of normal tendon (i.e., the scar tissue is an inferior material for its mechanical role).[17,50–52] However, due to the relatively large volume of scar tissue produced, the maximum force that the scar tissue can withstand before its rupture may reach two-thirds that of normal values. Therefore, whereas the quality of the scar tissue may be an order-of-magnitude lower than the native tendon or ligament, the structural integrity of the tissue as a whole may approach normal values in the long term.

The stress–strain responses of tendon and ligament present two features that complicate their modeling: material nonlinearity and viscoelastic dissipation. Under uniaxial tension, the stress–strain relationship of tendons and ligaments is initially nonlinear (the "toe region"), then enters a linear region, and finally reduces in slope as the tissue yields and fails (Figure 2.2). These features are quantified by the standard measures of modulus (the slope of the linear region of the stress–strain curve), strength (the maximum stress of the stress–strain curve), and toughness (the area under the stress curve, often called "strain energy density") (Figure 2.2). Fiber uncrimping has been proposed as a structural mechanism to explain the nonlinear stiffening of the tissue at low strains.[26,48,53] Initially, collagen fibers are crimped in a wavy configuration, with stretching resisted primarily by the unbending of rope-like collagen fibers. Because the bending resistance of the collagen fibers is relatively small, this deformation mechanism results in low stresses for relatively high imposed strains. As the crimp is removed, more stretched fibers are recruited and become fully engaged against the mechanical load, and the tissue enters the linear portion of the stress–strain curve. At higher strains, fibers begin to break or dissociate, and the tissue enters the yield region of the curve, after which it eventually fails (Figure 2.2).

The second feature of the constitutive response that bears special attention is viscous dissipation. Tendons and ligaments display viscoelastic behavior; namely, the material

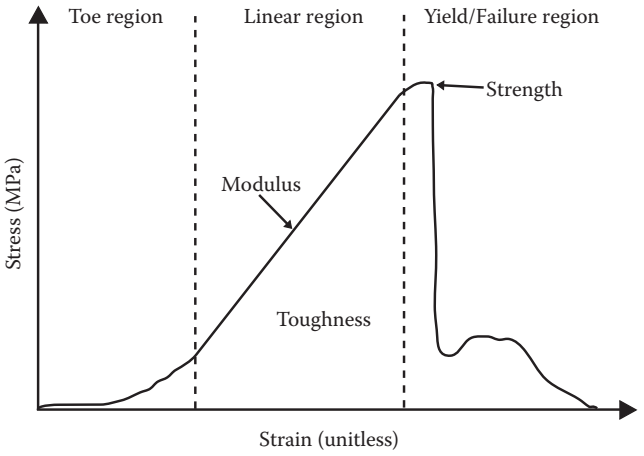

FIGURE 2.2
Under uniaxial tension, the stress–strain relationship of tendons and ligaments is initially nonlinear (the "toe region"), then enters a linear region, and finally reduces in slope as the tissue yields and fails. Based on this behavior, the mechanical properties of modulus (the slope of the linear region of the stress–strain curve), strength (the maximum stress of the stress–strain curve), and toughness (the area under the stress curve, often called "strain energy density") are calculated.

response has characteristics of both elastic solids and viscous fluids. Therefore, the loading history and the time-varying behavior should be considered to fully describe the mechanical properties of these tissues. Typical features of the viscoelastic behavior of tendons and ligaments include hysteresis, stress relaxation, and creep.

Hysteresis is a phenomenon that manifests itself in stress–strain curves for repeated loading cycles. Due to energy dissipation, the loading and unloading curves of tendons/ligaments do not follow the same path. These "hysteresis" curves demonstrate the importance of stress and strain history when characterizing the mechanical properties of viscoelastic materials. Additionally, stress–strain curves associated with subsequent loadings will appear more compliant than the first loading until the tissue has had adequate time to undergo "stress relaxation." Until the material relaxes to its original state, the elastic modulus from the initial loading curve will likely be different than the elastic modulus from the tenth loading curve.[2] To alleviate this concern, experimental protocols should include preconditioning cycles on the tendon or ligament to effectively give each tissue the same loading history and adequate time for relaxation.

To determine the viscoelastic properties of tendons and ligaments, the stress relaxation or creep behavior is typically examined (Figure 2.3). In both cases, the time-varying response of the tissue due to a particular input is determined. In the case of creep, a constant stress is applied, and the change in strain is measured over time. This may be relevant, for example, for anterior cruciate ligament reconstruction; after the graft is tensioned and implanted, creep will lead to loss of tension in the graft over time. In the case of stress relaxation, constant strain is applied, and the change in stress is measured over time. This has relevance to a tendon immediately after muscle activation; the stress in the tendon is initially high and relaxes over time as the force generated by muscle for joint motion is transferred to the bone. As described in the next section, these viscoelastic phenomena can be modeled using simple mechanical analogs (with springs representing the elastic,

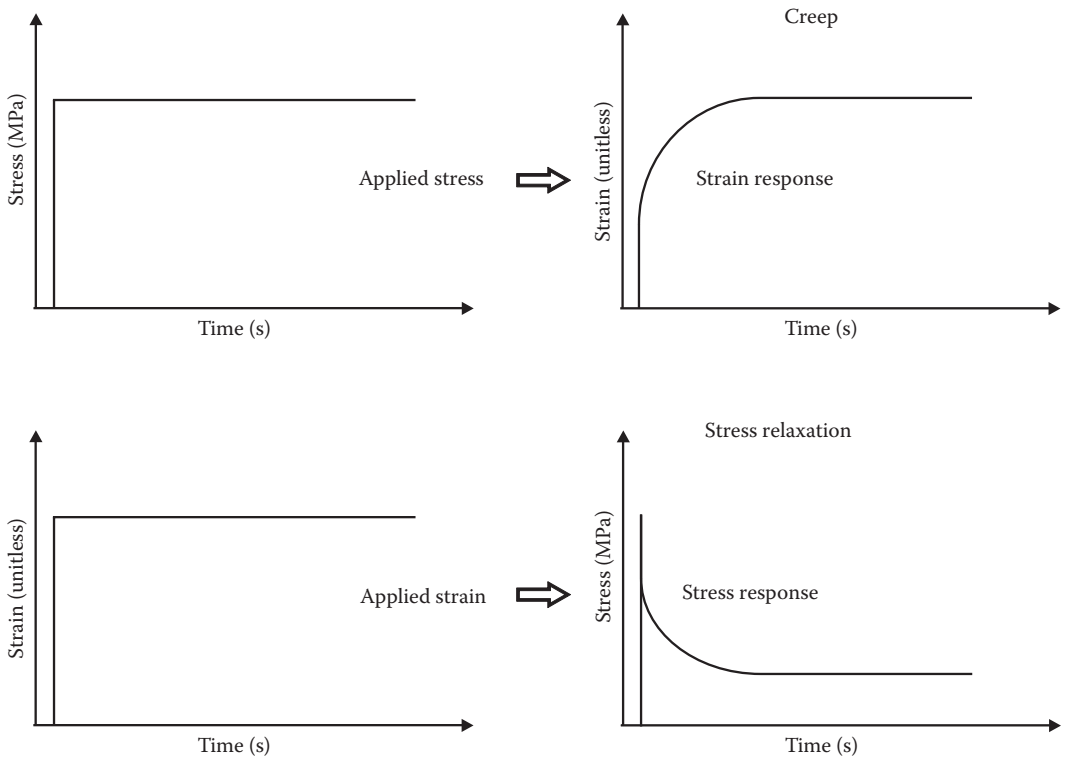

FIGURE 2.3
Stress relaxation and creep behavior can be used to describe the viscoelastic behavior of tendons and ligaments. The time-varying response of the tissue due to a particular input is determined. For creep, a constant stress is applied, and the change in strain is measured over time. For stress relaxation, constant strain is applied, and the change in stress is measured over time.

solid-like behavior and dashpots representing the viscous, fluid-like behavior) as well as more complex theories.

2.4 Biomechanical Modeling

The simplest mechanical models of the rate-dependent behavior associated with tendon mechanics fall under the heading of linear viscoelasticity and involve modifications of the linear theory of elasticity to account for different types of rate dependence. We focus on constitutive relations that are adequate for characterizing the mechanics of tendon and ligament midsubstance, in which the stress state of interest is predominantly uniaxial, and therefore limit the discussion in this chapter primarily to uniaxial relationships. For multiaxial cases, as needed to characterize the relevant mechanics near an insertion site, we refer the reader to the free online solid mechanics text by Bower.[54] We begin with the simplest of these uniaxial models and show why they are often inadequate, and then progress on to models that improve upon linear viscoelasticity in three ways. The first improvement involves nonlinear material behavior, the second involves nonlinear geometry, and

the third involves models that build-up from specific information about tissue structure, rather than reduce down from general principles.

2.4.1 Phenomenological Approaches

2.4.1.1 Springs, Dashpots, and Linear Viscoelasticity

A simple way to represent the rate-dependent behavior of a material in one-dimension involves assembling groups of mechanical springs and dashpots (Figure 2.4). A linear spring can represent the elastic behavior, that is, engineering stress, σ, is linearly related to linearized strain, ϵ according to $\sigma = E\varepsilon$, where Young's modulus E acts as a spring constant. A dashpot can represent the viscous behavior, that is, stress is linearly related to strain rate according to $\sigma(t) = \eta\dot{\varepsilon}(t)$, where η is the viscosity and $\dot{\varepsilon}$ is the time rate of change of strain at a time t.

Throughout this section, we discuss the response of viscoelastic materials to two types of loading that are particularly informative. In both cases, the material is assumed to be stress-free and in its reference configuration at time $t = 0$, and then to be loaded rapidly compared with any timescale over which relaxation occurs. The first test, called a relaxation test (Figure 2.3), involves an instantaneous stretching of the material to a prescribed, infinitesimal, uniaxial strain level, $\varepsilon(t) = \epsilon_o$. In this case, the isometric stress required to hold the material in its deformed configuration will decrease over time from an initial

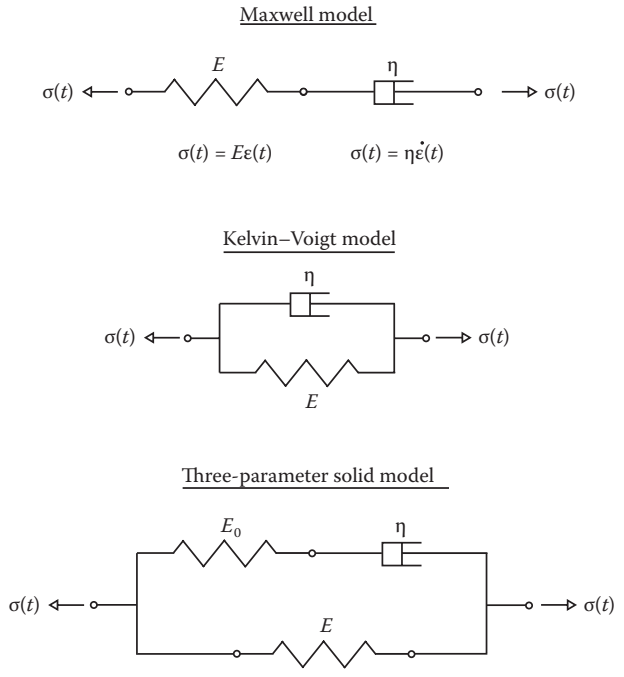

FIGURE 2.4
Rate-dependent behavior of a material in one dimension can be described using assemblages of mechanical springs and dashpots. A linear spring can represent the elastic behavior, and a dashpot can represent the viscous behavior. The Maxwell model involves a spring and a dashpot connected in series and stretched at its end points. The Kelvin–Voigt model is a parallel combination of a spring and dashpot. A commonly used model that alleviates many of the issues with the Maxwell and Kelvin–Voigt models is the three-parameter solid or standard linear viscoelastic model; this model contains a linear spring in parallel with one Maxwell element.

elastic level according to its relaxation function $G(t)$: $\sigma(t) = G(t)\,\epsilon_0$. This function can be used to define more complicated material models. The second test, called a creep test, involves instantaneous application of an applied stress $\sigma(t) = \sigma_0$ In this case, a linear viscoelastic material will stretch elastically and then elongate over time (Figure 2.3).

The first model to be considered is the Maxwell model, involving a spring and a dashpot connected in series and stretched at the end points (Figure 2.4). Simple analysis yields a constitutive relation for such an arrangement:

$$\dot{\varepsilon}(t) = \frac{1}{E}\dot{\sigma}(t) + \frac{1}{\eta}\sigma(t). \tag{2.1}$$

The responses of the model to the two loadings are as follows:

$$\text{creep response:}\quad \sigma(t) = \sigma_0;\ \varepsilon(\sigma_0, t) = \sigma_0 \frac{1}{E}\left(1 + \frac{t}{\tau}\right), \tag{2.2}$$

$$\text{stress relaxation response:}\quad \varepsilon(t) = \varepsilon_0;\ \sigma(\varepsilon_0, t) = \varepsilon_0 G(t);\ G(t) = Ee^{-t/\tau}, \tag{2.3}$$

where $\tau = \eta/E$ is the characteristic time constant of the material. This parameter is indicative of the rate of creep or relaxation for the material and describes its viscoelastic nature (e.g., fluid-like or solid-like). These relaxation and creep behaviors fail to replicate some important mechanical responses of tendons and ligaments. Rather, they are more typical for a fluid: if stretched isometrically for a sufficiently long time interval, they will relax back to a stress-free state; if they are loaded isotonically, they will never stop stretching.

The next obvious choice is the Kelvin–Voigt model, a parallel combination of a spring and dashpot (Figure 2.4). Following a simple analysis of stress and strain, the constitutive equation for this model is

$$\sigma(t) = E\varepsilon(t) + \eta\dot{\varepsilon}(t). \tag{2.4}$$

The creep response and stress relaxation responses in creep and relaxation tests are as follows:

$$\text{creep response:}\quad \sigma(t) = \sigma_0;\ \varepsilon(\sigma_0, t) = \sigma_0 \frac{1}{E}\left(1 - e^{-t/\tau}\right), \tag{2.5}$$

$$\text{stress relaxation response:}\quad \varepsilon(t) = \varepsilon_0;\ \sigma(\epsilon_0, t) = \varepsilon_0(\eta\delta(t) + E), \tag{2.6}$$

where the Dirac delta function, $\delta(t)$, is defined such that $\int_{-a}^{b} \delta(t)\,dt = 1$ for all $\{a,b\} > 0$; $\delta(t) = 0$ for $t \neq 0$ and is unbounded for $t = 0$. Although the Kelvin model captures the fact that tendons and ligaments can sustain and arrest deformation after isotonic stress—necessary because these in fact are pretensioned in physiologic settings—the unbounded stress response to a step strain input makes this model insufficient to describe typical viscoelastic behavior.

A commonly used model that alleviates these issues is the generalized Maxwell model, which contains a linear spring in parallel with any number of Maxwell elements. For

the case of one Maxwell element in parallel with a spring, the model is called the three-parameter solid or standard linear viscoelastic model (Figure 2.4). The constitutive equation for this model is

$$\frac{1}{\eta}\sigma + \frac{1}{E}\dot{\sigma} = \frac{E_0}{\eta}\varepsilon + \left(1 + \frac{E_0}{E}\right)\dot{\varepsilon}. \tag{2.7}$$

The creep and relaxation responses are given by

$$\text{creep response:} \quad \sigma(t) = \sigma_0;\ \varepsilon(\sigma_0, t) = \frac{\sigma_0}{E_0}\left(1 + \left(\frac{E_0}{E + E_0} - 1\right)e^{\frac{E_0}{(E+E_0)}\frac{t}{\tau}}\right), \tag{2.8}$$

$$\text{stress relaxation response:} \quad \varepsilon(t) = \varepsilon_0;\ \sigma(\epsilon_0, t) = \varepsilon_0 G(t);\ G(t) = (E_0 + Ee^{-t/\tau}), \tag{2.9}$$

where the time constant is again $\tau = \frac{\eta}{E}$. These responses can approximate the experimentally observed stress relaxation and creep behaviors of tendons and ligaments over prescribed infinitesimal stretches and over short time intervals because the model overcomes the limitations of fluid-like behavior and infinite stiffness in response to a step stretch. Because relaxation in tendon occurs over multiple timescales, additional time constants can be required. The generalized Maxwell model is easily adapted because the contributions of additional Maxwell elements result in additions to the relaxation function $G(t)$; the observation that the relaxation function in Equation 2.9 is simply that of Equation 2.2 plus a constant E_0 associated with the spring is general, and the relaxation function for a generalized Maxwell solid with N Maxwell elements is $G(t) = E_0 + \sum_{i=1}^{N} E_i e^{-t/\tau_i}$, where E_i is the modulus of Maxwell element i, and $\tau_i = \eta_i/E_i$ is the associated time constant. For a continuous spectrum of time constants, the summation in the relaxation function can be replaced by an integral. For any linear viscoelastic model for which the relaxation function exists, the response to a general, time-varying strain field can be written as a superposition, with the effects of the history of strain represented through the following hereditary integral:

$$\sigma(t) = \int_{-\infty}^{t} G(t - \xi)\frac{\partial \epsilon}{\partial \xi}\, d\xi. \tag{2.10}$$

This convolution integral can handle a very broad range of relaxation functions.

Why, then, are more advanced models needed? The three-parameter and generalized Maxwell models cannot replicate several basic attributes of tendon mechanics under larger stretches or repeated loading. Three problems are immediately obvious. The first is the shape of the stress–strain curve under simple elongation at a constant rate: a tendon or ligament presents a stress–strain curve that is concave up (Figure 2.2), whereas the Maxwell model presents one that is concave down. The closest that the Maxwell model can come to becoming concave up is with $\eta = \infty$, which yields a straight line associated with linear elasticity; the governing equations are linear, and no superposition of these concave-down curves can create a curve that is concave up. The second problem is hysteresis, the tendency of the stress–strain relationship to not follow the loading curve during unloading

due to energy dissipation during loading. The simple models show frequency-dependent hysteresis, but tendons and ligaments show frequency-independent hysteresis and thus show logarithmic relaxation in response to a step loading. Finally, the linear relationships associated with the mechanical elements are themselves invalid at large levels of strain.[55] In the following section, we describe phenomenological and micromechanical approaches to overcoming these limitations.

2.4.1.2 Quasilinear Viscoelasticity

Limitations of the Maxwell, Kelvin–Voigt, and three-parameter models have led investigators to formulate more complex nonlinear viscoelastic constitutive models; although the ability of the generalized Maxwell model to predict the temporal decay of stresses after a stretch is fully adequate, the linear elastic component is not. Fung,[56] therefore, developed a "quasilinear" viscoelasticity (QLV) theory in which the stress relaxation response is assumed to be separable into a linear viscous relaxation portion and a nonlinear elastic response. Mathematically, a QLV model can be defined generally as one that models loading history dependence by a linear convolution integral or a summation of these and which separates elastic nonlinearity from the linear viscous relaxation terms.

Fung's QLV model is quasilinear in the sense that the dependence of response on loading history can be obtained from a linear convolution integral, which preserves the benefits of linearity for calibrating the model and simplifies model predictions. Nonlinearity enters the linear viscoelastic constitutive law by replacing strain with a nonlinear function of strain $\sigma^e(\varepsilon)$, and the resultant model is linear with respect to this function instead of strain itself. The relaxation response of this model following a step strain of ϵ_0, analogous to Equation 2.9, is

$$\sigma(\varepsilon_0, t) = G_R(t)\,\sigma^e(\varepsilon_0), \tag{2.11}$$

where $G_R(t)$ is the "reduced" relaxation function that is normalized by a modulus and is equal to $\sigma(t)/\sigma(0)$ in a relaxation test. $\sigma^e(\varepsilon)$ has the physical meaning of an elastic stress response and is generally nonlinear. Following the same steps needed to derive Equation 2.10 from Equation 2.9 and using the chain rule, the stress response at time t can be obtained for a general strain history through

$$\sigma(t) = \int_0^t G_R(t-\xi)\frac{\partial \sigma^e(\varepsilon)}{\partial \varepsilon}\frac{\partial \varepsilon(\xi)}{\partial \xi}\,d\xi\,. \tag{2.12}$$

To obtain a nominally uniform response over a broad range of time constants, the following reduced relaxation function, $G_R(t)$, is used:

$$G_R(t) = \frac{1 + C\left(E_1\left(\frac{t}{\tau_2}\right) - E_1\left(\frac{t}{\tau_1}\right)\right)}{1 + C\ln\left(\frac{\tau_2}{\tau_1}\right)}, \tag{2.13}$$

where C, τ_1, and τ_2 are material parameters describing the relaxation characteristics of the material, and E_1 is the exponential integral. The combination of the continuous relaxation

spectrum and generalized Maxwell formulation can be visualized as an infinite series of equally weighted Maxwell elements in parallel with a spring.

Fung followed a Kennedi-type exponential nonlinear elastic response for $\sigma^e(\epsilon)$:

$$\sigma^e(\varepsilon) = A(e^{B\varepsilon} - 1), \tag{2.14}$$

where A and B are material coefficients describing the uniaxial elastic characteristics of the material. To solve for the typical experimental testing scenario [the case of an initially stress-free, fully relaxed specimen stretched at (noninfinite) strain rate $\dot{\epsilon}$ over the time interval $0 < t \le t_0$ and then held isometrically], Equation 2.14 is substituted into Equation 2.12:

$$\sigma(t) = \frac{AB\dot{\varepsilon}}{1 + C\ln\left(\frac{\tau_2}{\tau_1}\right)} \int_0^t \left\{1 + C\left[E_1\left(\frac{t-\xi}{\tau_2}\right) - E_1\left(\frac{t-\xi}{\tau_1}\right)\right]\right\} e^{B\dot{\varepsilon}\xi}\, d\xi, \quad 0 < t \le t_0, \tag{2.15}$$

$$\sigma(t) = \frac{AB\dot{\varepsilon}}{1 + C\ln\left(\frac{\tau_2}{\tau_1}\right)} \int_0^{t_0} \left\{1 + C\left[E_1\left(\frac{t-\xi}{\tau_2}\right) - E_1\left(\frac{t-\xi}{\tau_1}\right)\right]\right\} e^{B\dot{\varepsilon}\xi}\, d\xi, \quad t_0 \le t < \infty. \tag{2.16}$$

A least-squares fit with the experimental data can then be used to determine parameters A, B, C, τ_1, and τ_2.[57–59]

This formulation of the QLV model allows for a finite ramp phase, which occurs between $t = 0$ and $t = t_0$. A simplified formulation of the model can be derived, which assumes an instantaneous ramp phase. However, an instantaneous ramp is impossible to achieve experimentally, and the assumption will result in an underestimation of the parameter C.

The effect of variation in the QLV parameters can be observed for stress relaxation (Figure 2.5). Differences in A have a substantial effect on peak and equilibrium stresses. This parameter is found in the elastic stress equation; it is, therefore, expected that it would have a direct and linear effect on the peak and equilibrium stresses of the stress relaxation response. A similar effect, albeit nonlinear, is seen for the effect of B. The parameter C has a profound effect on the relaxation behavior; an increase in C causes an increase in the relaxation rate. The parameters τ_1 and τ_2 influence the early and late relaxation behaviors, respectively. In summary, parameters A and B have the greatest effect on the peak and the equilibrium stresses of the tissue. These parameters describe the elastic behavior of the tissue. Parameter C has the greatest effect on the relaxation rate of the curve and describes the overall viscous nature of the tissue. The two time constants, τ_1 and τ_2, describe the "fast" and "slow" viscous behavior of the tissue, respectively.

Fung's QLV model has been used extensively to determine the properties of a variety of soft tissues, including tendon, ligament, cartilage, vocal cord, muscle, and cardiac tissue.[19,36,50,55,56,58,60–67] However, Fung's QLV cannot always achieve reasonable predictions due to the limitation that all stress relaxation curves must follow a single reduced relaxation function. This has been observed to be inadequate for a range of relevant materials including rat medial collateral ligaments[62] and pure reconstituted collagen.[68] Also, the model is cumbersome to fit because calibrating a QLV model involves calibrating convolved functions unless a perfect instantaneous step stretch relaxation experiment can be performed. In the following, we describe a simplified approach.

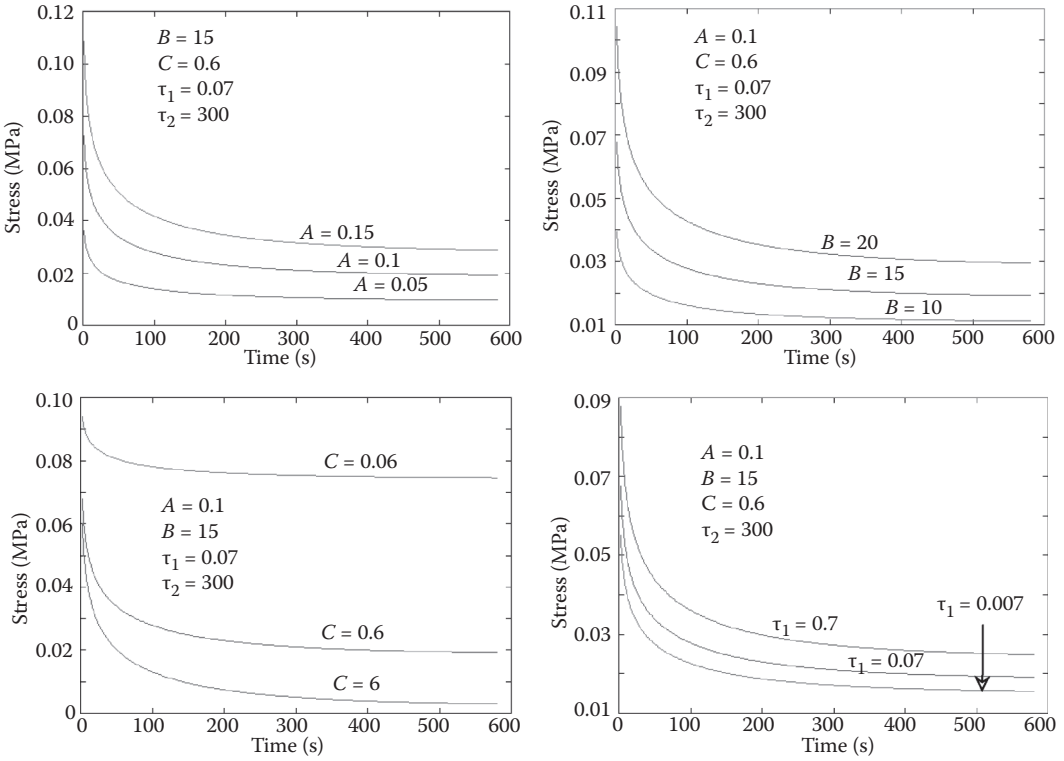

FIGURE 2.5
Effect of variation in the QLV parameters is shown for stress relaxation. Parameters *A* and *B* have the greatest effect on the peak stress and the equilibrium stress of the tissue. These parameters describe the elastic behavior of the tissue. Parameter *C* has the greatest effect on the relaxation rate of the curve and describes the overall viscous nature of the tissue. The two time constants, τ_1 and τ_2, describe the "fast" and "slow" viscous behaviors of the tissue, respectively.

2.4.1.3 Adaptive Quasilinear Viscoelasticty Model

Many extensions to QLV theory exist.[62,68] We focus here on the adaptive QLV model,[69] which overcomes the difficulties described in the previous section by relating stress and strain through the viscoelastic strain function, $V^{(\varepsilon)}(t)$, in a hereditary linear convolution integral that is analogous to Equation 2.9:

$$\begin{aligned} \sigma(t) &= k\left(\varepsilon(t)\right)V^{(\varepsilon)}(t) \\ V^{(\varepsilon)}(t) &= \int_{-\infty}^{t} G_R(t-\xi)\frac{d\varepsilon(\xi)}{d\xi}d\xi \end{aligned} \tag{2.17}$$

where $G_R(t)$ is the Fung reduced relaxation function described above, and $k(\varepsilon)$ is a nonlinear function of strain that converts the viscoelastic strain to a stress by a simple multiplication, outside of the convolution integral. To overcome the Fung QLV limitation of proportional stress relaxations for different amplitudes of instantaneous strain, the model allows different nonlinear behavior for different time constants:

$$\sigma(t) = \sigma_0(\varepsilon(t)) + \sum_i k_i(\varepsilon(t)) V_i^{(\varepsilon)}(t)$$
$$V_i^{(\varepsilon)}(t) = \int_{-\infty}^{t} g_i^R(t-\xi) \frac{d\varepsilon(\xi)}{d\xi} d\xi \qquad i = 1, 2, \ldots, \tag{2.18}$$

Where $\sigma_0(\varepsilon)$ is the fully relaxed elastic response. The reduced, normalized relaxation functions $g_i^R(t)$ are general and need to satisfy only $g^R(0) = 1$ and $g^R(\infty) = 0$. The choice of $g_i^R(t) = e^{-t/\tau_i}$ enables direct analogy to a generalized Maxwell model. We will use this to derive Equation 2.18.

Consider, first, a generalized Maxwell model in which each hypothetical Maxwell element is fully nonlinear and follows

$$\begin{cases} \dot{V}_i + \dfrac{V_i}{\tau_i(\varepsilon)} = \dot{\varepsilon} \\ \sigma_i = k_i\left(\varepsilon(t)\right) V_i(t) \end{cases}, \quad i = 1, 2, \ldots, \tag{2.19}$$

where $\tau_i(\varepsilon) = \dfrac{b_i(\varepsilon)}{k_i(\varepsilon)}$ and the response of the spring in parallel with the hypothetical Maxwell elements is $\sigma_0 = \sigma_0(\varepsilon)$. The constraint of quasilinearity simplifies this model tremendously. Requiring that each hypothetical Maxwell element follow the same arbitrary (nonzero) nonlinear function of strain $\psi_i(\varepsilon)$ requires each time constant τ_i to be *independent* of strain:

$$\left.\begin{array}{l} k_i(\varepsilon) = \eta_i \psi_i(\varepsilon) \\ b_i(\varepsilon) = \beta_i \psi_i(\varepsilon) \\ \tau_i(\varepsilon) = b_i(\varepsilon)/k_i(\varepsilon) \end{array}\right\} \rightarrow \tau_i = \beta_i/\eta_i \,. \tag{2.20}$$

This results in a tremendous mathematical simplification because the nonlinear ordinary differential equation in Equation 2.19 becomes linear:

$$\dot{V}_i + \frac{V_i}{\tau_i} = \dot{\varepsilon} \qquad V_i(t) = \int_{-\infty}^{t} e^{-(t-\xi)/\tau_i} \frac{d\varepsilon(\xi)}{d\xi} d\xi, \quad i = 1, 2, \ldots, \tag{2.21}$$

which is the convolution integral in Equation 2.18 for the case of $g_i(t) = e^{-t/\tau_i}$. Simple, algebraic closed-form solutions exist for the viscoelastic strain $V_i^{(\varepsilon)}(t)$ for many simple loadings, including uniaxial stretching at a constant rate, $\dot{\varepsilon}$, in which case $V_i(t) = \dot{\varepsilon}\tau_i(1 - e^{-t/\tau_i})$, i = 1, 2,…, which can be substituted directly into Equation 2.18. The fitting of the functions $k_i(\varepsilon(t))$ and $\sigma_0(\varepsilon(t))$ is then entirely algebraic and simple, with the result being a framework that is both more flexible and simpler to fit than the Fung QLV model.

2.4.1.4 Extensions to Finite Strain

Both the Fung QLV and adaptive QLV models modify linear viscoelasticity to account for *material* nonlinearity in the behavior of tendons and ligaments. For example, these models permit modeling of a stress–strain curve that, like that of tendon or ligament, is concave up instead of concave down. As written previously, however, they are limited to very small strains because they do not account for the *geometric* nonlinearity that occurs at larger strains. A rule of thumb is that, for strains of below approximately 10%, linear theories provide a reasonable estimate of mechanical response;[70] at this level of strain, the errors associated with applying a linear framework to large strain kinematics begin to become significant compared with uncertainty in material properties for tendon and ligament. The physiologic strain levels measured within tendon and ligament are on the order of 2% to 8%[71,72] and are well within this linear range, meaning that, in general, only material nonlinearity need be considered, and geometric nonlinearity can be ignored.

However, for loading at injurious levels of a tendon or ligament, much higher strains may occur. For this reason, we present here a highly condensed version of finite strain kinematics and a single constitutive law that has proven successful in some situations. The example shown is a full three-dimensional model rather than a one-dimensional model for two reasons. First, the locations within a tendon or ligament at which strains are predicted to be highest are near their bony insertions, and the stress states here are inherently multiaxial.[19,21,22] Second, constitutive models involving finite strain are derived most simply from a general framework involving strain energy, dissipation, and invariants of the strain tensor, and these inherently account for multiaxial stress states.

We refer the reader to the text by Gurtin et al.[73] for a thorough and modern treatment of finite deformation continuum mechanics and present here only a summary of notation to be used in describing one example of a finite strain theory. Measures of strain are based on the deformation gradient tensor, $\mathbf{F}(\mathbf{X},t)$, that maps at time t an infinitesimal vector $\mathbf{dX}$ at a material point $\mathbf{X}$ in the reference configuration (unstressed and undeformed state) of the body of interest to the corresponding infinitesimal vector $\mathbf{dx}$ at the corresponding point $\mathbf{x}$ in the deformed configuration. $\mathbf{F}(\mathbf{X},t)$ is calculated as the spatial gradient in the reference configuration of the function that maps material points $\mathbf{X}$ to deformed state points $\mathbf{x}$. Many valid strain measures can be derived from $\mathbf{F}(\mathbf{X},t)$, all of which can be reduced to engineering strain for very small deformations and rigid body rotations. The deformation measure that we will use here is the left Cauchy–Green deformation tensors, $\mathbf{B} = \mathbf{F}\mathbf{F}^{\mathbf{T}}$, where $\mathbf{F}^{\mathbf{T}}$ is the transpose of $\mathbf{F}$.

The constitutive model presented here is the single integral finite strain model of Johnson et al.,[55] which is an adaptation of the Pipkin–Rogers[74] nonlinear viscoelastic model that reduces to the Fung QLV model at low strain levels. For a body that is initially free of stress and that is fully relaxed, the final form of this constitutive model is, at each point $\mathbf{x}$ in the deformed body at every time t,

$$\begin{aligned}\boldsymbol{T}(t) &= -P(t)\mathbf{1} + C_0\left((1+\mu I_1(t))\mathbf{B}(t) - \mu\mathbf{B}_2(t)\right) \\ &\quad - \left(C_0 - C_\infty\right)\int_0^t G^*(t-\xi)\left(\left(1+\mu I_1(t)\right)\mathbf{B}(t) - \mu\mathbf{B}^*(s,t)\mathbf{B}^{*T}(s,t)\right)d\xi\end{aligned} \tag{2.22}$$

where $P(t) = \text{trace}(\mathbf{T}(t))/3$ is the hydrostatic pressure, $\mathbf{1}$ is the identity tensor, C_0 and C_∞ serve the roles of instantaneous and relaxed elastic moduli, μ is the elastic constitutive

parameter, $I_1(t)$ = trace($\mathbf{B}(t)$), $G^*(t)$ is a time rate of change of a relaxation function, and $\mathbf{B}^*(s,t) = \mathbf{F}(t)\mathbf{F}^T(s)$.

Salient features for the purpose of an introduction to a nonlinear viscoelastic constitutive law follow. First, the form is analogous to that of Equation 2.10. The first line of Equation 2.22, combined with the step response of convolution integral in the second line, represents the elastic response of the material. This elastic response can be shown to be a rewriting of the Mooney–Rivlin constitutive law that is an extension of the neo-Hookean constitutive law. Second, the assumption is made that the material is so much more resistant to volumetric deformation than it is to shear deformation that the former is assumed to be negligible. Third, the hereditary integral in Equation 2.22 is analogous to that of Equation 2.10 in that it includes a reduction over time of the effects of previous strain states of the material. The assumption is further made, as with the Fung QLV model, that this stress relaxation is independent of the degree of straining.

2.4.2 Micromechanical Approaches

The reconstitution of tendon and ligament mechanical properties from the basic structure and organization of the underlying protein and cellular networks represents a broad effort of a large community and is an area of ongoing research effort. The original contributions to this body of work involve the application by Lanir[75–77] of Flory-type averaging to derive tendon and ligament tissue-level mechanical properties from the architecture of collagen fibers. Important contributions to this approach have been made through studies on planar collagenous tissues,[78] the anterior cruciate ligament,[79] the tendon enthesis,[21] and reconstituted collagen matrices.[80–82] To rectify the observation that tendons and ligaments are composed of collagen fibers that, when stretched, exhibit a nominally linear response,[3] this approach assumes that fibers switch gradually from a buckled, non-load-resisting state to a stretched, load-resisting state with increasing levels of tissue strain. The gradual uptake of mechanical load through the recruitment of buckled fibers accounts for the observed increase in mechanical resistance with increasing stretch (i.e., the shift from a nonlinear "toe" region to a linear region; Figure 2.2). Typically, the tissue strain is mapped to the actual strain in a fiber using measured fiber orientation distributions along with the assumption of affine deformation (i.e., strain in each individual fiber is along the direction of the overall tissue strain).[21,78]

A recent model using this approach further explored the origin of nonlinearity in tendon and ligament.[83] The authors developed a microstructural theory for tendon that was based on the viscoelastic properties of collagen fibers and their recruitment. The model applied QLV theory to describe the viscoelastic behavior of each fiber while maintaining the assumption that fibers were wavy and could only bear load when straight. Fibers were recruited with increasing stretch as with previous, simpler models, but behaved as viscoelastic elements. The model was validated using experimental data and theoretical analysis; stress relaxation and creep data under multiple levels of stress and strain were accurately predicted with the theory. Importantly, this and other microstructural models are able to accurately describe tissue-level tendon and ligament mechanical behavior and to connect this behavior to physical processes at the microstructural level. A remarkable feature of this and other Lanir–Sacks type models is that the full complexity of tendon and ligament behavior can often be reconstituted from fundamental principles using fewer parameters than a phenomenological approach would require.

2.5 Experimental Methods

2.5.1 Biomechanical Testing

Experimental determination of the mechanical properties of tendons and ligaments requires far more care than engineering materials. Care must be taken to accurately measure tissue geometry and local strain, to standardize the loading history, and to properly grip the tissue. Most experimental studies use engineering stress, that is, load divided by initial cross-sectional area, when describing stress–strain or stress relaxation behavior. Even the measurement of this elementary property requires care beyond that required for engineering materials: common contact-based methods to determine cross-sectional area measurement are inappropriate for tendons and ligaments, as the tissue will deform with the pressure that is applied during the measurement. Noncontact methods, including laser micrometers and image analysis, are preferred.[84,85]

Measurement of deformation is also a challenge. As tendons and ligaments are anisotropic and have significant regional property variations from bony attachment to midsubstance, it is important to determine strain locally. Recent approaches have focused on image-based techniques for determining local strain on a tendon or ligament surfaces.[2,86,87] Either lines or a texture-rich pattern is applied onto the surface of the tissue, and the deformation is recorded during testing. Deformation is tracked by tracking patterns during the test. Local strain is then calculated from the deformation gradient. Of concern is how "local" is defined in the context of a tendon or ligament. Strain measurement techniques that track fluorescent beads and thereby allow for the measurement of deformation fields with subcellular resolution show that strain fields are heterogeneous even over the surface of an *individual* fibroblast.[88] The question of an appropriate length scale for the application of a continuum theory arises in the modeling of many materials, especially "composite" materials with complicated and heterogeneous microstructures such as tendons and ligaments. The resolution of this issue involves the identification of a length scale sufficiently large that estimated strain fields are not sensitive to the fine details of the placement of measurement markers, and sufficiently small that structural effects can be delineated (e.g., spatial variations of material properties). For a tendon or ligament, the appropriate length scale for local strain fields corresponds to several measurements divided over a length scale associated with the width.

The viscous behavior of tendons and ligaments requires the design and application of specialized testing protocols. As discussed previously, the loading curves for tendons and ligaments do not follow the same path as the unloading curves. Furthermore, sequential loading-unloading curves do not overlap with each other. When determining the mechanical properties of these tissues, careful consideration must be taken to ensure that an accurate and repeatable mechanical test is performed. Fortunately, the hysteresis curves overlap each other after a sufficient number of cycles.[2,89] Therefore, it is critical that tendons and ligaments are preconditioned with multiple loading-unloading cycles before performing a test from which mechanical properties are determined.

Due to the relatively high tensile strength and stiffness of tendons, combined with the low friction and the typically short lengths of ligaments, it is often difficult to grip these tissues effectively for mechanical testing. A number of experimental solutions have been developed to address these concerns. For tendons, specialized clamps are often used to reduce slippage through rough/irregular surfaces or through freezing.[90] When possible, gripping the bone by embedding it in a resin or cement is preferable. Although regional

variation in properties from tendon to bone must be considered in this case, this approach mitigates issues related to slipping of the tissue out of the group.

Numerous studies have shown that tendon and ligament mechanical properties are only marginally strain rate-sensitive.[91–94] In one study, the strain rate was varied from 0.15%/s to 222%/s for uniaxial tensile tests of rabbit medial collateral ligaments.[91] Although the properties changed significantly with strain rate, the changes were small relative to the effects of other factors (e.g., age of the animal). Increasing the strain rate more than 1000-fold, for example, resulted in only a 31% increase in measured strength and an even smaller increase in modulus. Therefore, there exists a wide range of strain rates appropriate for the biomechanical testing of tendons and ligaments.

However, two challenges nevertheless exist relating to timescales. The first is balancing relaxation and preconditioning. All of the constitutive models discussed in this chapter assume that a specimen is in its reference configuration and is free of both stress and strain before the application of load used for calibration of mechanical properties. This requires that a specimen rest in an unstressed state for several times longer than the longest characteristic timescale of the material being tested. If a material's behavior is fit to a generalized Maxwell model, this means allowing the material to relax over an interval that is several times the largest value of the time constant τ_i associated with a significant amplitude (E_i). This can be determined through an initial relaxation test; the longest time constant of the material can be estimated from the time over which a steady baseline isometric force level is reached on a force–time plot. Tendons and ligaments, however, pose additional problems because they exhibit a broad spectrum of time constants, and a log-linear force–time plot will show decrease without end.[62] A log-linear relation of this character is expected for any material that is well modeled by the Fung QLV model.[95,96] Full relaxation of tendons and ligaments is often not possible, and the best strategy is, therefore, to allow for relaxation intervals that are long compared to physiologic loading cycles but short compared to timescales of hours associated with remodeling at the level of tissues,[97–99] cells,[100,101] and cellular cytoskeletons.[102] A reasonable trade-off is to allow a relaxation on the order of 30 minutes.

The second challenge related to timescales involves the characterization of material behavior at high strain rates. Although material properties such as modulus do not change significantly with strain rate in ligaments and tendons, the effects of wave propagation can be dramatic.[91–94,103] Models exist to predict how wave effects appear in relaxation testing, and these are particularly important for testing in the nonlinear regime: here, nonlinearity causes wave fronts to change in nonintuitive ways.[103] In summary, meaningful testing of tendons and ligaments is possible over a very broad range of strain rates, but extra care must be taken when interpreting data from tests performed at very slow and very fast loading rates to avoid unwanted relaxation and wave effects.

2.5.2 Physiologic Considerations

A number of physiologic factors must be considered when determining the mechanical properties of tendons and ligaments. In particular, anatomic location, *in vivo* loading environment, injury/healing status, and age all significantly influence the mechanical properties of the tissue.[2] The properties of tendons and ligaments vary significantly depending on the anatomic location (and, hence, inherent function). For example, the mechanical requirements of hand flexor tendons differ from those of the shoulder rotator cuff tendons.[104,105] Due to the relatively long distances between the forearm muscles and the finger joints, the function of digital flexor tendons depends on gliding of the tendon within a

sheath and around pulleys. Therefore, when determining the properties of digital flexor tendons, the gliding properties are as important as the tensile properties.[106–111] Gliding properties are less important for the function of rotator cuff tendons and the Achilles. In these tissues, the tensile properties are of greatest importance. Similarly, there are significant differences in the properties of the tendon/ligament midsubstance compared with the tendon/ligament-to-bone attachment.[19,48,112] As described previously, a localized measure of strain should be made to localize the properties of each region.

Tendons and ligaments are highly sensitive to their *in vivo* loading environments. Disuse leads to a catabolic environment and a rapid deterioration of the tissue mechanical properties.[113–115] Overuse leads to microdamage and often exacerbates inflammation, resulting in decreased mechanical properties.[116–119] Homeostasis is maintained only under physiologic loading conditions. Therefore, when determining the mechanical properties of these tissues, consideration of the *in vivo* loading environment is critical for proper comparison.

Tendon and ligament healing is a complex process that is beyond the scope of this review chapter. Briefly, the healing process progresses through three phases: inflammation (on the order of days), followed by proliferation (on the order of weeks), followed by remodeling (on the order of months).[8,120] Accrual of mechanical properties is typically not evident until the tendon has reached the remodeling phase of healing. This time course must be considered when determining the mechanical properties of tendons and ligaments in an injury and repair setting.

Fetal development, growth and maturation, and aging significantly influence the properties of tendons and ligaments. During early development, tendons and ligaments are primarily cells with little extracellular matrix.[121] As the tissue develops further, the cell to extracellular matrix ratio decreases, leading to increases in the mechanical properties. Postnatal growth and development result in further remodeling, with consequently increased mechanical properties.[122,123] As the tendon/ligament-to-bone fully mineralizes and the growth plates fuse, the failure mode of the structure shifts from bony avulsion to midsubstance tear.[124] Finally, aging leads to a gradual decrease in the properties of the tissues, as age-related conditions cause degeneration of the tissues.[125] These temporal changes highlight the need for careful control of specimen selection and study design when examining tendon and ligament mechanical properties.

2.6 Conclusions

Tendons and ligaments are necessary for joint function but have a propensity for injury and a poor capacity to heal. To design treatment protocols and tissue engineering replacements, a better understanding of the biomechanics of tendons and ligaments is necessary. This chapter reviewed constitutive descriptions of tendons and ligaments from the phenomenologic and microstructural perspectives. Important features that must be considered in the biomechanical description of tendons and ligaments include stress relaxation, creep, energy dissipation, and nonlinearity. When determining the mechanical properties of tendons and ligaments, a number of experimental (e.g., strain measurement and tissue hydration) and physiologic factors (e.g., anatomic location and age) must be considered. Tissue should be tested in physiologically relevant conditions at the appropriate pH, hydration, and temperature. Strain and geometry should be measured locally using

noncontact methods. Results should be presented in the context of the particular anatomy and the history of the tissue.

Future efforts should continue to explore biomechanical models that can accurately predict constitutive behavior, especially through multiscale descriptions that incorporate the hierarchical nature of the tissues and define their structure–function relationships. Understanding the mechanisms by which tendons and ligaments function will allow engineers and clinicians to synthesize materials and use methods for enhanced healing. Tendon/ligament tissue engineering holds great promise for many applications, including rotator cuff repair and anterior cruciate ligament reconstruction, but only if the biomechanical requirements are recapitulated in the engineered grafts.

Acknowledgment

This work was supported by the National Science Foundation (CAREER 844607).

References

1. Kastelic, J., A. Galeski, and E. Baer. 1978. The multicomposite structure of tendon. *Connective Tissue Research* 6(1):11–23.
2. Woo, S. L., T. Q. Lee, S. D. Abramowitch, and T. W. Gilbert. 2005. Structure and function of ligaments and tendons. In *Basic Orthopaedic Biomechanics and Mechano-Biology*, edited by V. C. Mow and R. Huiskes, 301–342. Philadelphia: Lippincott Williams & Wilkins.
3. Buehler, M. J. 2006. Nature designs tough collagen: explaining the nanostructure of collagen fibrils. *Proceedings of the National Academy of Sciences of the United States of America* 103(33):12285–12290.
4. Kannus, P. 1997. Tendons—a source of major concern in competitive and recreational athletes. *Scandinavian Journal of Medicine andScience in Sports* 7(2):53–54.
5. Praemer, A., S. Furner, and D. Rice. 1992. *Musculoskeletal Conditions in the US*. Park Ridge, IL: American Academy of Orthopaedic Surgeons.
6. Lohmander, L. S., P. M. Englund, L. L. Dahl, and E. M. Roos. 2007. The long-term consequence of anterior cruciate ligament and meniscus injuries: osteoarthritis. *The American Journal of Sports Medicine* 35(10):1756–1769.
7. Woo, S. L., R. H. Gelberman, N. G. Cobb, D. Amiel, K. Lothringer, and W. H. Akeson. 1981. The importance of controlled passive mobilization on flexor tendon healing. A biomechanical study. *Acta Orthopaedica Scandinavica* 52 (6):615–622.
8. Woo, S. L., R. E. Debski, J. Zeminski, S. D. Abramowitch, S. S. Saw, and J. A. Fenwick. 2000. Injury and repair of ligaments and tendons. *Annual Review of Biomedical Engineering* 2:83–118.
9. Gelberman, R. H., S. L. Woo, K. Lothringer, W. H. Akeson, and D. Amiel. 1982. Effects of early intermittent passive mobilization on healing canine flexor tendons. *Journal of Hand Surgery—American Volume* 7(2):170–175.
10. Gelberman, R. H., J. S. Vande Berg, G. N. Lundborg, and W. H. Akeson. 1983. Flexor tendon healing and restoration of the gliding surface. An ultrastructural study in dogs. *Journal of Bone and Joint Surgery. American Volume* 65 (1):70–80.

11. Gelberman, R. H., J. S. Vandeberg, P. R. Manske, and W. H. Akeson. 1985. The early stages of flexor tendon healing: a morphologic study of the first fourteen days. *The Journal of Hand Surgery* 10(6 Pt 1):776–784.
12. Boyer, M. I., C. A. Goldfarb, and R. H. Gelberman. 2005. Recent progress in flexor tendon healing. The modulation of tendon healing with rehabilitation variables. *Journal of Hand Therapy* 18(2):80–85; quiz 86.
13. Fu, F. H., C. H. Bennett, C. Lattermann, and C. B. Ma. 1999. Current trends in anterior cruciate ligament reconstruction. Part I: Biology and biomechanics of reconstruction. *The American Journal of Sports Medicine* 27(6):821–830.
14. Fu, F. H., C. H. Bennett, C. B. Ma, J. Menetrey, and C. Lattermann. 2000. Current trends in anterior cruciate ligament reconstruction. Part II. Operative procedures and clinical correlations. *The American Journal of Sports Medicine* 28(1):124–130.
15. Beynnon, B. D., R. J. Johnson, and B. C. Fleming. 2002. The science of anterior cruciate ligament rehabilitation. *Clinical Orthopaedics and Related Research* (402):9–20.
16. Krueger-Franke, M., C. H. Siebert, and S. Scherzer. 1995. Surgical treatment of ruptures of the Achilles tendon: a review of long-term results. [see comments.]. *British Journal of Sports Medicine* 29(2):121–125.
17. Frank, C., B. MacFarlane, P. Edwards, R. Rangayyan, Z. Q. Liu, S. Walsh, and R. Bray. 1991. A quantitative analysis of matrix alignment in ligament scars: a comparison of movement versus immobilization in an immature rabbit model. *Journal of Orthopaedic Research* 9(2):219–227.
18. Frank, C. B., B. J. Loitz, and N. G. Shrive. 1995. Injury location affects ligament healing. A morphologic and mechanical study of the healing rabbit medial collateral ligament. *Acta Orthopaedica Scandinavica* 66(5):455–462.
19. Thomopoulos, S., G. R. Williams, J. A. Gimbel, M. Favata, and L. J. Soslowsky. 2003. Variation of biomechanical, structural, and compositional properties along the tendon to bone insertion site. *Journal of Orthopaedic Research* 21(3):413–419.
20. Moffat, K. L., W. H. Sun, P. E. Pena, N. O. Chahine, S. B. Doty, G. A. Ateshian, C. T. Hung, and H. H. Lu. 2008. Characterization of the structure–function relationship at the ligament-to-bone interface. *Proceedings of the National Academy of Sciences of the United States of America* 105(23):7947–7952.
21. Thomopoulos, S., J. P. Marquez, B. Weinberger, V. Birman, and G. M. Genin. 2006. Collagen fiber orientation at the tendon to bone insertion and its influence on stress concentrations. *Journal of Biomechanics* 39(10):1842–1851.
22. Liu, Y., V. Birman, C. Chen, S. Thomopoulos, and G. M. Genin. 2011. Mechanisms of bimaterial attachment at the interface of tendon to bone. *Journal of Engineering Materials and Technology* 133(1):011006.
23. Hodge, A. J., and J. A. Petruska. 1963. Recent studies with the electron microscope on ordered aggregates of the tropocollagen molecule. In *Aspects of Protein Structure*, edited by G. N. Ramachandran, 289–300. New York: Academic Press.
24. Orgel, J. P. R. O., A. Miller, T. C. Irving, R. F. Fischetti, A. P. Hammersley, and T. J. Wess. 2001. The in situ supermolecular structure of type I collagen. *Structure* 9(11):1061–1069.
25. Orgel, J. P. R. O., T. C. Irving, A. Miller, and T. J. Wess. 2006. Microfibrillar structure of type I collagen in situ. *Proceedings of the National Academy of Sciences of the United States of America*, 103(24):9001–9005.
26. Kastelic, J. 1980. A structural mechanical model for tendon crimping. *Journal of Biomechanics* 13:887–893.
27. Koob, T. J., and K. G. Vogel. 1987. Site-related variations in glycosaminoglycan content and swelling properties of bovine flexor tendon. *Journal of Orthopaedic Research* 5(3):414–424.
28. Vogel, K. G., J. D. Sandy, G. Pogany, and J. R. Robbins. 1994. Aggrecan in bovine tendon. *Matrix Biology* 14(2):171–179.
29. Bray, D. F., C. B. Frank, and R. C. Bray. 1990. Cytochemical evidence for a proteoglycan-associated filamentous network in ligament extracellular matrix. *Journal of Orthopaedic Research* 8(1):1–12.

30. Vogel, K. G., A. Ordog, G. Pogany, and J. Olah. 1993. Proteoglycans in the compressed region of human tibialis posterior tendon and in ligaments. *Journal of Orthopaedic Research* 11(1):68–77.
31. Wenstrup, R. J., S. M. Smith, J. B. Florer, G. Zhang, D. P. Beason, R. E. Seegmiller, L. J. Soslowsky, and D. E. Birk. 2011. Regulation of collagen fibril nucleation and initial fibril assembly involves coordinate interactions with collagens V and XI in developing tendon. *The Journal of Biological Chemistry* 286(23):20455–20465.
32. Birk, D. E., M. V. Nurminskaya, and E. I. Zycband. 1995. Collagen fibrillogenesis in situ: fibril segments undergo post-depositional modifications resulting in linear and lateral growth during matrix development. *Developmental Dynamics* 202(3):229–343.
33. Reed, C. C., and R. V. Iozzo. 2002. The role of decorin in collagen fibrillogenesis and skin homeostasis. *Glycoconjugate Journal* 19(4–5):249–255.
34. Banos, C. C., A. H. Thomas, and C. K. Kuo. 2008. Collagen fibrillogenesis in tendon development: current models and regulation of fibril assembly. *Birth Defects Research. Part C, Embryo Today* 84(3):228–244.
35. Lujan, T. J., C. J. Underwood, N. T. Jacobs, and J. A. Weiss. 2009. Contribution of glycosaminoglycans to viscoelastic tensile behavior of human ligament. *Journal of Applied Physiology* 106(2):423–431.
36. Elliott, D. M., P. S. Robinson, J. A. Gimbel, J. J. Sarver, J. A. Abboud, R. V. Iozzo, and L. J. Soslowsky. 2003. Effect of altered matrix proteins on quasilinear viscoelastic properties in transgenic mouse tail tendons. *Annals of Biomedical Engineering* 31(5):599–605.
37. Robinson, P. S., T. F. Huang, E. Kazam, R. V. Iozzo, D. E. Birk, and L. J. Soslowsky. 2005. Influence of decorin and biglycan on mechanical properties of multiple tendons in knockout mice. *Journal of Biomechanical Engineering* 127(1):181–185.
38. Redaelli, A., S. Vesentini, M. Soncini, P. Vena, S. Mantero, and F. M. Montevecchi. 2003. Possible role of decorin glycosaminoglycans in fibril to fibril force transfer in relative mature tendons—a computational study from molecular to microstructural level. *Journal of Biomechanics* 36(10):1555–1569.
39. Weiss, J. A., J. C. Gardiner, and C. Bonifasi-Lista. 2002. Ligament material behavior is nonlinear, viscoelastic and rate-independent under shear loading. *Journal of Biomechanics* 35(7):943–950.
40. Bonifasi-Lista, C., S. P. Lake, M. S. Small, and J. A. Weiss. 2005. Viscoelastic properties of the human medial collateral ligament under longitudinal, transverse and shear loading. *Journal of Orthopaedic Research* 23(1):67–76.
41. Mow, V. C., S. C. Kuei, W. M. Lai, and C. G. Armstrong. 1980. Biphasic creep and stress relaxation of articular cartilage in compression: theory and experiments. *Journal of Biomechanical Engineering* 102(1):73–84.
42. Mow, V. C., and A. Ratcliffe. 1997. Structure and function of articular cartilage and meniscus. In *Basic Orthopaedic Biomechanics*, edited by V. C. Mow and W. C. Hayes, 113–177. Philadelphia, PA: Lippincott-Raven.
43. Yin, L., and D. M. Elliott. 2004. A biphasic and transversely isotropic mechanical model for tendon: application to mouse tail fascicles in uniaxial tension. *Journal of Biomechanics* 37(6):907–916.
44. Henninger, H. B., C. J. Underwood, G. A. Ateshian, and J. A. Weiss. 2010. Effect of sulfated glycosaminoglycan digestion on the transverse permeability of medial collateral ligament. *Journal of Biomechanics* 43(13):2567–2573.
45. Bostrom, M.P.G., A. Boskey, J. K. Kauffman, and T. A. Einhorn. 2000. Form and function of bone. In *Orthopaedic Basic Science*, edited by J. A. Buckwalter, T. A. Einhorn and S. R. Simon, 319–369. Rosemont, IL: American Academy of Orthopaedic Surgeons.
46. Woo, S. L., K. An, C.B. Frank, G.A. Livesay, C.B. Ma, J. A. Zeminski, J.S. Wayne, and B. S. Myers. 2000. Anatomy, biology, and biomechanics of tendon and ligament. In *Orthopaedic Basic Science*, edited by J. A. Buckwalter, T. A. Einhorn and S. R. Simon. Rosemont, IL: American Academy of Orthopaedic Surgeons.
47. Genin, G. M., A. Kent, V. Birman, B. Wopenka, J. D. Pasteris, P. J. Marquez, and S. Thomopoulos. 2009. Functional grading of mineral and collagen in the attachment of tendon to bone. *Biophysical Journal* 97(4):976–985.

48. Stouffer, D. C., D. L. Butler, and D. Hosny. 1985. The relationship between crimp pattern and mechanical response of human patellar tendon-bone units. *Journal of Biomechanical Engineering* 107(2):158–165.
49. Milz, S., A. Rufai, A. Buettner, R. Putz, J. R. Ralphs, and M. Benjamin. 2002. Three-dimensional reconstructions of the Achilles tendon insertion in man. *Journal of Anatomy* 200(Pt 2):145–152.
50. Thomopoulos, S., G. R. Williams, and L. J. Soslowsky. 2003. Tendon to bone healing: differences in biomechanical, structural, and compositional properties due to a range of activity levels. *Journal of Biomechanical Engineering* 125(1):106–113.
51. Frank, C., D. McDonald, D. Bray, R. Bray, R. Rangayyan, D. Chimich, and N. Shrive. 1992. Collagen fibril diameters in the healing adult rabbit medial collateral ligament. *Connective Tissue Research* 27(4):251–263.
52. Kamps, B. S., L. H. Linder, C. E. DeCamp, and R. C. Haut. 1994. The influence of immobilization versus exercise on scar formation in the rabbit patellar tendon after excision of the central third. *American Journal of Sports Medicine* 22(6):803–811.
53. Hansen, K. A., J. A. Weiss, and J. K. Barton. 2002. Recruitment of tendon crimp with applied tensile strain. *Journal of Biomechanical Engineering* 124(1):72–77.
54. Bower, A. F. 2010. *Applied Mechanics of Solids*. Boca Raton, FL: CRC Press, Taylor & Francis Group.
55. Johnson, G. A., G. A. Livesay, S. L. Woo, and K. R. Rajagopal. 1996. A single integral finite strain viscoelastic model of ligaments and tendons. *Journal of Biomechanical Engineering* 118(2):221–226.
56. Fung, Y.C. 1972. Ch 7: Stress–strain–history relations of soft tissues in simple elongation. In *Biomechanics: Its Foundations and Objectives*, edited by Y. C. Fung, N. Perrone and M. Anliker, 181–208. San Diego, CA: Prentice-Hall.
57. Nigul, I., and U. Nigul. 1987. On algorithms of evaluation of Fung's relaxation function parameters. *Journal of Biomechanics* 20(4):343–352.
58. Kwan, M. K., T. H. Lin, and S. L. Woo. 1993. On the viscoelastic properties of the anteromedial bundle of the anterior cruciate ligament. *Journal of Biomechanics* 26(4–5):447–452.
59. Gimbel, J. A., J. J. Sarver, and L. J. Soslowsky. 2004. The effect of overshooting the target strain on estimating viscoelastic properties from stress relaxation experiments. *Journal of Biomechanical Engineering* 126(6):844–848.
60. Pradas, M. M., and R. D. Calleja. 1990. Nonlinear viscoelastic behaviour of the flexor tendon of the human hand. *Journal of Biomechanics* 23(8):773–781.
61. Funk, J. R., G. W. Hall, J. R. Crandall, and W. D. Pilkey. 2000. Linear and quasi-linear viscoelastic characterization of ankle ligaments. *Journal of Biomechanical Engineering* 122(1):15–22.
62. Provenzano, P., R. Lakes, T. Keenan, and R. Vanderby, Jr. 2001. Nonlinear ligament viscoelasticity. *Annals of Biomedical Engineering* 29(10):908–914.
63. Woo, S. L. 1982. Mechanical properties of tendons and ligaments. I. Quasi-static and nonlinear viscoelastic properties. *Biorheology* 19(3):385–396.
64. Abramowitch, S. D., and S. L. Woo. 2004. An improved method to analyze the stress relaxation of ligaments following a finite ramp time based on the quasi-linear viscoelastic theory. *Journal of Biomechanical Engineering* 126(1):92–97.
65. Abramowitch, S. D., S. L. Woo, T. D. Clineff, and R. E. Debski. 2004. An evaluation of the quasi-linear viscoelastic properties of the healing medial collateral ligament in a goat model. *Annals of Biomedical Engineering* 32(3):329–335.
66. Doehring, T. C., E. O. Carew, and I. Vesely. 2004. The effect of strain rate on the viscoelastic response of aortic valve tissue: a direct-fit approach. *Annals of Biomedical Engineering* 32(2):223–232.
67. Chan, R. W., and I. R. Titze. 2000. Viscoelastic shear properties of human vocal fold mucosa: theoretical characterization based on constitutive modeling. *Journal of the Acoustical Society of America* 107(1):565–580.
68. Pryse, K. M., A. Nekouzadeh, G. M. Genin, E. L. Elson, and G. I. Zahalak. 2003. Incremental mechanics of collagen gels: new experiments and a new viscoelastic model. *Annals of Biomedical Engineering* 31(10):1287–1296.

69. Nekouzadeh, A., K. M. Pryse, E. L. Elson, and G. M. Genin. 2007. A simplified approach to quasi-linear viscoelastic modeling. *Journal of Biomechanics* 40(14):3070–3078.
70. Ashby, M. F., and D. R. H. Jones. 2012. *Engineering Materials 1*. 4th ed. Oxford, U.K.: Elsevier.
71. Magnusson, S. P., M. V. Narici, C. N. Maganaris, and M. Kjaer. 2008. Human tendon behaviour and adaptation, in vivo. *The Journal of Physiology* 586(1):71–81.
72. Bey, M. J., H. K. Song, F. W. Wehrli, and L. J. Soslowsky. 2002. Intratendinous strain fields of the intact supraspinatus tendon: the effect of glenohumeral joint position and tendon region. *Journal of Orthopaedic Research* 20(4):869–874.
73. Gurtin, M. E., E. Fried, and L. Anand. 2010. *The Mechanics and Thermodynamics of Continua*. Cambridge, MA: Cambridge University Press.
74. Pipkin, A. C., and T. G. Rogers. 1968. A non-linear integral representation for viscoelastic behaviour. *Journal of the Mechanics and Physics of Solids* 16:59–72.
75. Lanir, Y. 1978. Structure–function relations in mammalian tendon: the effect of geometrical non-uniformity. *Journal of Bioengineering* 2(1–2):119–128.
76. Lanir, Y. 1980. A microstructure model for the rheology of mammalian tendon. *Journal of Biomechanical Engineering* 102(4):332–339.
77. Lanir, Y. 1978. Constitutive equations for fibrous connective tissues. *Journal of Biomechanics* 16(1):1–12.
78. Sacks, M. S. 2003. Incorporation of experimentally-derived fiber orientation into a structural constitutive model for planar collagenous tissues. *Journal of Biomechanical Engineering* 125(2):280–287.
79. De Vita, R., and W. S. Slaughter. 2006. A structural constitutive model for the strain rate-dependent behavior of anterior cruciate ligaments. *International Journal of Solids and Structures* 43:1561–1570.
80. Thomopoulos, S., G. M. Fomovsky, P. L. Chandran, and J. W. Holmes. 2007. Collagen fiber alignment does not explain mechanical anisotropy in fibroblast populated collagen gels. *Journal of Biomechanical Engineering* 129(5):642.
81. Marquez, J.P., G.M. Genin, G.I. Zahalak, and E.L. Elson. 2005. Thin bio-artificial tissues in plane stress: the relationship between cell and tissue strain, and an improved constitutive model. *Biophysical Journal* 88:765–777.
82. Marquez, J.P., G.M. Genin, G.I. Zahalak, and E.L. Elson. 2005. The relationship between cell and tissue strain in three-dimensional bio-artificial tissues. *Biophysical Journal* 88:778–789.
83. Einat, R., and L. Yoram. 2009. Recruitment viscoelasticity of the tendon. *Journal of Biomechanical Engineering* 131(11):111008.*
84. Lee, T. Q., and S. L. Woo. 1988. A new method for determining cross-sectional shape and area of soft tissues. *Journal of Biomechanical Engineering* 110(2):110–114.
85. Langelier, E., D. Dupuis, M. Guillot, F. Goulet, and D. Rancourt. 2004. Cross-sectional profiles and volume reconstructions of soft tissues using laser beam measurements. *Journal of Biomechanical Engineering* 126(6):796–802.
86. Li, X., J. Xie, J. Lipner, X. Yuan, S. Thomopoulos, and Y. Xia. 2009. Nanofiber scaffolds with gradations in mineral content for mimicking the tendon-to-bone insertion site. *Nano Letters* 9(7):2763–2768.
87. Derwin, K. A., L. J. Soslowsky, W. D. Green, and S. H. Elder. 1994. A new optical system for the determination of deformations and strains: calibration characteristics and experimental results. *Journal of Biomechanics* 27(10):1277–1285.
88. Legant, W. R., J. S. Miller, B. L. Blakely, D. M. Cohen, G. M. Genin, and C. S. Chen. 2010. Measurement of mechanical tractions exerted by cells in three-dimensional matrices. *Nature Methods* 7(12):969–971.
89. Sverdlik, A., and Y. Lanir. 2002. Time-dependent mechanical behavior of sheep digital tendons, including the effects of preconditioning. *Journal of Biomechanical Engineering* 124(1):78–84.

* The journal incorrectly published the first, rather than the last, names of these authors; the correct last names are Raz and Lanir.

90. Wieloch, P., G. Buchmann, W. Roth, and M. Rickert. 2004. A cryo-jaw designed for in vitro tensile testing of the healing Achilles tendons in rats. *Journal of Biomechanics* 37(11):1719–1722.
91. Peterson, R. H., and S. L. Woo. 1986. A new methodology to determine the mechanical properties of ligaments at high strain rates. *Journal of Biomechanical Engineering* 108(4):365–367.
92. Ng, B. H., S. M. Chou, B. H. Lim, and A. Chong. 2004. Strain rate effect on the failure properties of tendons. *Proceedings of the Institution of Mechanical Engineers. Part H, Journal of Engineering in Medicine* 218(3):203–206.
93. Haut, R. C. 1983. Age-dependent influence of strain rate on the tensile failure of rat-tail tendon. *Journal of Biomechanical Engineering* 105(3):296–299.
94. Crisco, J. J., D. C. Moore, and R. D. McGovern. 2002. Strain-rate sensitivity of the rabbit MCL diminishes at traumatic loading rates. *Journal of Biomechanics* 35(10):1379–1385.
95. Marquez, J. P., G. M. Genin, K. M. Pryse, and E. L. Elson. 2006. Cellular and matrix contributions to tissue construct stiffness increase with cellular concentration. *Annals of Biomedical Engineering* 34(9):1475–1482.
96. Marquez, J. P., E. L. Elson, and G. M. Genin. 2010. Whole cell mechanics of contractile fibroblasts: relations between effective cellular and extracellular matrix moduli. *Philosophical transactions. Series A, Mathematical, Physical, and Engineering Sciences* 368(1912):635–654.
97. Moon, A.G., and R.T. Tranquillo. 1993. The fibroblast-populated collagen microsphere assay of cell traction force: Part1. Continuum model. *AIChE Journal* 39:163–177.
98. Tranquillo, R. T., and J. D. Murray. 1993. Mechanistic model of wound contraction. *Journal of Surgical Research* 55(2):233–247.
99. Barocas, V. H., and R. T. Tranquillo. 1997. An anisotropic biphasic theory of tissue-equivalent mechanics: the interplay among cell traction, fibrillar network deformation, fibril alignment, and cell contact guidance. *Journal of Biomechanical Engineering* 119(2):137–145.
100. Zemel, A., I. B. Bischofs, and S. A. Safran. 2006. Active elasticity of gels with contractile cells. *Physical Review Letters* 97(12):128103.
101. Zemel, A., and S. A. Safran. 2007. Active self-polarization of contractile cells in asymmetrically shaped domains. *Physical Review. E, Statistical, Nonlinear, and Soft Matter Physics* 76(2 Pt 1):021905.
102. Nekouzadeh, A., K. M. Pryse, E. L. Elson, and G. M. Genin. 2008. Stretch-activated force shedding, force recovery, and cytoskeletal remodeling in contractile fibroblasts. *Journal of Biomechanics* 41(14):2964–2971.
103. Nekouzadeh, A., G. M. Genin, P. V. Bayly, and E. L. Elson. 2005. Wave motion in relaxation-testing of nonlinear elastic media. *Proceedings of the Royal Society of London, Series A* 461(2058):1599–1626.
104. Kim, H. M., G. Nelson, S. Thomopoulos, M. J. Silva, R. Das, and R. H. Gelberman. 2010. Technical and biological modifications for enhanced flexor tendon repair. *The Journal of Hand Surgery* 35(6):1031–1037; quiz 1038.
105. Soslowsky, L. J., J. E. Carpenter, J. S. Bucchieri, and E. L. Flatow. 1997. Biomechanics of the rotator cuff. *Orthopedic Clinics of North America* 28(1):17–30.
106. Gelberman, R. H., M. J. Botte, J. J. Spiegelman, and W. H. Akeson. 1986. The excursion and deformation of repaired flexor tendons treated with protected early motion. *The Journal of Hand Surgery* 11(1):106–110.
107. Rothkopf, D. M., S. Webb, R. M. Szabo, R. H. Gelberman, and J. W. May, Jr. 1991. An experimental model for the study of canine flexor tendon adhesions. *The Journal of Hand Surgery* 16(4):694–700.
108. Lieber, R. L., D. Amiel, K. R. Kaufman, J. Whitney, and R. H. Gelberman. 1996. Relationship between joint motion and flexor tendon force in the canine forelimb. *The Journal of Hand Surgery* 21(6):957–962.
109. Uchiyama, S., P. C. Amadio, J. Ishikawa, and K. N. An. 1997. Boundary lubrication between the tendon and the pulley in the finger. *Journal of Bone and Joint Surgery. American Volume* 79(2):213–218.
110. Momose, T., P. C. Amadio, C. Zhao, M. E. Zobitz, and K. N. An. 2000. The effect of knot location, suture material, and suture size on the gliding resistance of flexor tendons. *Journal of Biomedical Materials Research* 53(6):806–811.

111. Zhao, C., P. C. Amadio, M. E. Zobitz, and K. N. An. 2001. Gliding characteristics of tendon repair in canine flexor digitorum profundus tendons. *Journal of Orthopaedic Research*: *Official Publication of the Orthopaedic Research Society* 19(4):580–586.
112. Huang, C. Y., V. M. Wang, R. J. Pawluk, J. S. Bucchieri, W. N. Levine, L. U. Bigliani, V. C. Mow, and E. L. Flatow. 2005. Inhomogeneous mechanical behavior of the human supraspinatus tendon under uniaxial loading. *Journal of Orthopaedic Research* 23(4):924–930.
113. Amiel, D., S. L. Woo, F. L. Harwood, and W. H. Akeson. 1982. The effect of immobilization on collagen turnover in connective tissue: a biochemical–biomechanical correlation. *Acta Orthopaedica Scandinavica* 53(3):325–332.
114. Woo, S. L., M. A. Gomez, Y. K. Woo, and W. H. Akeson. 1982. Mechanical properties of tendons and ligaments. II. The relationships of immobilization and exercise on tissue remodeling. *Biorheology* 19(3):397–408.
115. Woo, S. L., M. A. Gomez, T. J. Sites, P. O. Newton, C. A. Orlando, and W. H. Akeson. 1987. The biomechanical and morphological changes in the medial collateral ligament of the rabbit after immobilization and remobilization. *Journal of Bone and Joint Surgery—American Volume* 69(8):1200–1211.
116. Soslowsky, L. J., S. Thomopoulos, S. Tun, C. L. Flanagan, C. C. Keefer, J. Mastaw, and J. E. Carpenter. 2000. Neer Award 1999. Overuse activity injures the supraspinatus tendon in an animal model: a histologic and biomechanical study. *Journal of Shoulder and Elbow Surgery* 9(2):79–84.
117. Soslowsky, L. J., S. Thomopoulos, A. Esmail, C. L. Flanagan, J. P. Iannotti, J. D. Williamson, 3rd, and J. E. Carpenter. 2002. Rotator cuff tendinosis in an animal model: role of extrinsic and overuse factors. *Annals of Biomedical Engineering* 30(8):1057–1063.
118. Archambault, J., M. Tsuzaki, W. Herzog, and A. J. Banes. 2002. Stretch and interleukin-1beta induce matrix metalloproteinases in rabbit tendon cells in vitro. *Journal of Orthopaedic Research* 20(1):36–39.
119. Riley, G. 2004. The pathogenesis of tendinopathy. A molecular perspective. *Rheumatology (Oxford)* 43(2):131–142.
120. Lin, T. W., L. Cardenas, and L. J. Soslowsky. 2004. Biomechanics of tendon injury and repair. *Journal of Biomechanics* 37(6):865–877.
121. Schweitzer, R., J. H. Chyung, L. C. Murtaugh, A. E. Brent, V. Rosen, E. N. Olson, A. Lassar, and C. J. Tabin. 2001. Analysis of the tendon cell fate using Scleraxis, a specific marker for tendons and ligaments. *Development* 128(19):3855–3866.
122. Ansorge, H. L., S. Adams, D. E. Birk, and L. J. Soslowsky. 2011. Mechanical, compositional, and structural properties of the post-natal mouse Achilles tendon. *Annals of Biomedical Engineering* 39(7):1904–1913.
123. Mikic, B., E. Amadei, K. Rossmeier, and L. Bierwert. 2010. Sex matters in the establishment of murine tendon composition and material properties during growth. *Journal of Orthopaedic Research*: *Official Publication of the Orthopaedic Research Society* 28(5):631–638.
124. Woo, S. L., C. A. Orlando, M. A. Gomez, C. B. Frank, and W. H. Akeson. 1986. Tensile properties of the medial collateral ligament as a function of age. *Journal of Orthopaedic Research*: *Official Publication of the Orthopaedic Research Society* 4(2):133–141.
125. Woo, S. L., J. M. Hollis, D. J. Adams, R. M. Lyon, and S. Takai. 1991. Tensile properties of the human femur–anterior cruciate ligament–tibia complex. The effects of specimen age and orientation. *The American Journal of Sports Medicine* 19(3):217–225.

3

Intervertebral Disc Cell Mechanics and Mechanobiology

Christopher L. Gilchrist, Li Cao, and Lori A. Setton

CONTENTS

3.1 Introduction

The intervertebral disc (IVD) is a complex fibrocartilaginous tissue whose primary function is to resist mechanical loads in the spine. Cells embedded within the IVD extracellular matrix (ECM) are subjected to a variety of physical stimuli under physiologic loading that are known to provide important signals to cells, with the cells' biological responses to their mechanical environment playing potentially critical roles in regulating the development, maintenance, and repair of IVD tissues. Additionally, mechanical factors may play

key roles in the initiation and progression of IVD degeneration, with altered or injurious mechanical loading environments possibly contributing to substantial biological remodeling or breakdown of IVD tissues. Understanding the mechanobiology of IVD cells requires answering several key questions. What is the mechanical environment of IVD cells? What physical stimuli do cells experience under physiologic loading conditions? How do IVD cells sense, interpret, and respond to these mechanical cues in their environment? What changes in mechanical environment and cell responses occur during IVD aging and degeneration, and how do these changes contribute to pathology? Significant progress has been made over the past two decades toward answering these questions, although much remains to be elucidated. This chapter reviews our current knowledge of IVD cell biomechanics, including IVD ECM and cellular mechanics, cell morphology, cell–matrix interactions, and micromechanical stimuli experienced by cells, toward the goal of assessing micromechanical stimuli that are important for regulating the biological responses of IVD cells.

3.2 Background

The IVD is a heterogeneous, fibrocartilaginous tissue that provides load support, energy dissipation, and flexibility in the spine (Figure 3.1a). The IVD is situated between adjacent vertebral bodies and acts as the main joint of the spinal column, occupying approximately one-third of its total height.[1,2] The disc consists of three anatomical zones (Figure 3.1b): the nucleus pulposus (NP), anulus fibrosus (AF), and cartilage endplates. These zones are compositionally, structurally, and mechanically distinct but are highly coupled and work together to meet the complex mechanical demands required of the tissue.

The NP region is a highly hydrated, viscoelastic gel[3–5] that acts mechanically to resist and redistribute spinal compressive loads. The human NP is a dynamic tissue that undergoes significant changes in structure, biochemical composition, and cell population during maturation, during aging, and with degeneration. In the young, healthy human, the NP is composed primarily of water (70%–90% of wet weight), proteoglycans (65% of dry weight), and randomly oriented type II collagen (15%–20% dry weight).[6–8] Proteoglycans found in the NP primarily contain chondroitin and keratan sulfate side chains and are typically freely dispersed, with only ~30% linked to hyaluronan in aggregates.[9] The high concentration of proteoglycans in the NP gives the tissue a high negative fixed-charge density and associated swelling pressure, binding water and giving the tissue its fluid-like behaviors. The NP resists spinal compressive loading through fluid pressurization, with the isotropic, gelatinous nature of the tissue allowing it to uniformly distribute loads radially to the surrounding AF. Other compositionally minor ECM components of the NP include elastin, small proteoglycans, and minor collagens (types III, VI, and IX)[10–12] and laminins.[13–15]

The AF region of the IVD is a fibrocartilaginous structure that is highly organized into distinct lamellae. These lamellae are concentric rings of large, aligned collagen fiber bundles, with 15 to 25 lamellae present in mature human IVDs.[16] Fibers within a given lamella are oriented at approximately 28° to 43° to the transverse plane,[17–20] with adjacent lamella alternating in fiber direction (~120° to each other). Lamellae are thicker anteriorly and thinner posteriorly, inserting into the adjacent vertebral bodies above and below. The highly aligned matrix structure of the AF produces anisotropic material behaviors, with tensile

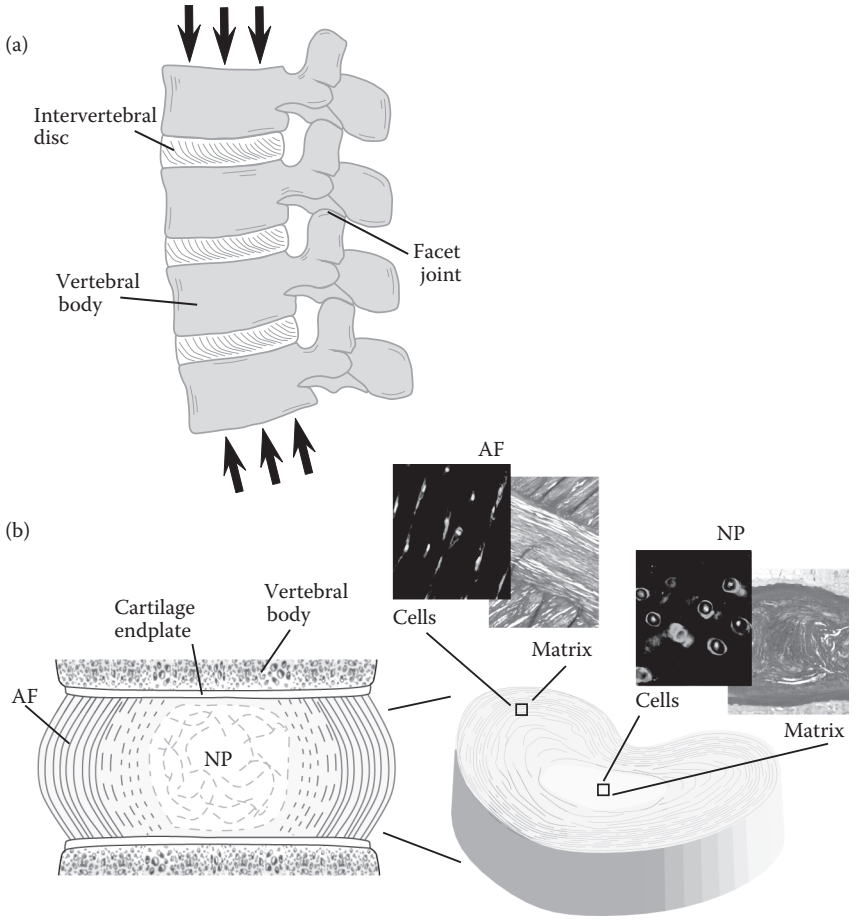

FIGURE 3.1
(See color insert.) (a) Intervertebral disc (IVD) is situated between the vertebral bodies in the spinal column and supports loads, provides flexibility, and dissipates energy in the spine. (b) Disc is composed of distinct anatomic zones: the AF, NP, and cartilage endplates. The AF consists of concentric lamella of highly aligned collagen fibers, with cells typically aligned along the fiber direction. The NP is a gelatinous, highly hydrated tissue, with cells typically exhibiting rounded, unaligned morphologies.

stiffness values that vary by orders of magnitude in the circumferential,[21–24] axial,[25] and radial directions.[26] The AF experiences significant tensile loads under physiologic conditions, acting to constrain the pressurized, fluid-like NP during axial spinal compression,[27] as well as directly resisting spinal torsion.[28] Additionally, compression and outward pressure from the NP give rise to significant annular bulging and outward deformations.[27,29] Compositionally, the ECM of the AF contains a high percentage of collagen (70% of dry weight), primarily type I collagen fibers in the outer AF, with the percentage of type II collagen increasing radially toward the inner AF (with a corresponding decrease of type I collagen).[6] Aggrecan is also present in the AF,[30] acting to maintain tissue hydration and resist compressive loading. Similar to the NP, compositionally minor ECM components include collagen types III, VI, IX, and XI,[11] small proteoglycans (e.g., biglycan and decorin),[10] as well as elastin fibers.[12] Distinct from the adjacent NP, laminin isoforms are rarely distributed throughout either immature or mature AF tissues.

The IVD is separated from the vertebral bodies on the top and the bottom by the cartilage endplates, thin horizontal layers of hyaline cartilage that separate the disc from adjacent vertebral bodies. The endplates affect IVD mechanics by serving as critical regulators of fluid flow, with their permeability and porosity modulating IVD fluid pressurization while simultaneously providing a pathway for nutrient and waste transfer to and from the vascularized vertebral bodies.[1,2] Together, these three components (NP, AF, and cartilage endplates) function as an integral mechanical unit that supports and resists the complex loading demands of the spine.

3.3 Changes with Intervertebral Disc Aging and Degeneration

Aging and degenerative changes in the IVD involve alterations in both ECM biochemical composition and structure. Compositionally, the most dramatic pathologic changes in the disc involve loss of proteoglycan content and changes in proteoglycan structure.[30–32] These changes, in turn, result in decreased negative fixed-charge density, decreased water content, and a loss of swelling pressure,[33,34] impairing the tissue's ability to resist and redistribute compressive loads. Corresponding with these compositional changes are structural alterations including loss of disc height and increased lamellar disorganization in the AF. Changes in ECM composition and structure may result in substantially altered mechanics and kinematics for the entire IVD motion segment, with decreased internal pressurization and disc height resulting in higher compressive loads transferred to the AF, compromising its structure and function (e.g., overload leading to clefts, buckling, or rupture). These changes may also result in nerve compression, spinal canal impingement, and altered spinal loading configurations that can contribute to symptomatic back pain.[35]

The causes of IVD degeneration are complex and remain incompletely understood. Degeneration has been closely associated with inherited genetic factors,[36–38] including defects in ECM genes (e.g., type IX, XI, and II collagens[39–42]) that may predispose the tissue to breakdown or mechanical failure. Additionally, environmental factors such as physical activity and mechanical loading may also play a role in degeneration,[43,44] with mechanical impact, vibration exposure, heavy lifting, and muscle activation, as well as work and lifestyle factors, including gait and posture, being linked to IVD degeneration or damage.[45,46] Thus, aging, predisposing genetic factors, and mechanical factors may (individually or in combination) play key roles in the progression of IVD degeneration through the regulation of biological and biochemical changes. The mechanical factors that may affect cell biological responses in the IVD, and which may be important in both normal and degenerative states, are reviewed in detail in the following sections.

3.4 Intervertebral Disc Cells and Cellular Microenvironment

The cells embedded within the IVD's ECM are responsible for the generation and maintenance of the tissue. Phenotypic behaviors of disc cells are thought to be modulated in part by biophysical stimuli experienced by the cell, with cell responses that may include alterations in gene expression and increases in matrix production and remodeling.[47,48] IVD

cells experience a variety of physical stimuli during physiologic loading, including compressive, tensile, and shear stresses and strains, fluid flows, hydrostatic and osmotic pressures, as well as electrokinetic effects; these stimuli vary regionally within the disc. The IVD contains a heterogeneous cell population, with cell morphology, ECM microenvironment, cell–matrix interactions, and phenotype varying regionally within the disc; each of these cellular and microenvironmental factors may affect how IVD cells experience and respond to mechanical stimuli *in situ*. Additionally, these factors may be altered with aging or degeneration, resulting in cellular responses that may further contribute to IVD pathology through changes in matrix composition, structure, and mechanical function.

3.4.1 Intervertebral Disc Cells

3.4.1.1 Nucleus Pulposus Cells

Cells within the developing and immature NP are derived from the embryonic notochord[49–51] and exhibit morphologic features that reflect this unique embryonic origin: notochordal NP cells have large diameters[14,52,53] containing large intracellular vacuoles, are organized in interconnected cell clusters, and exhibit strong cell–cell interactions characterized by gap junctions,[52,53] cadherins,[54,55] and desmosomal cell–cell adhesions.[56,57] Cells with notochordal-like morphologic features are retained into adulthood or throughout life in some animal species,[58,59] but in the human, many of these morphologic cell features are lost by early adulthood, with only a sparse population of rounded, chondrocyte-like cells remaining in the mature human NP. Mature human NP cells do, however, exhibit phenotypic characteristics distinct from chondrocytes,[60,61] and recent evidence indicates that mature NP cells retain at least some phenotypic features of notochordal cells,[55,62,63] suggesting that the chondrocyte-like cells of the mature human NP may have notochordal origins. NP cell morphology in the mature human IVD has been described as rounded or ellipsoidal, with cell sizes and shapes similar to chondrocytes.[51,64,65] Similarly, quantitative studies of *in situ* NP cell morphology in rat IVDs found NP cell shape to be nearly spheroidal (Figure 3.2a), with cells exhibiting no preferred orientation within the tissue.[66] NP cells may also extend cytoplasm-filled processes of varying length and number away from cell bodies.[67]

NP cells exhibit a well-developed cytoskeleton, with both immature and mature NP cells shown to express F-actin (distributed in a punctuate or cortical arrangement),[68,69] microtubules,[69] and high levels of both vimentin and cytokeratin intermediate filament proteins.[57,59,62,68–71] Quantitative analysis of regional variations in cytoskeletal protein expression in bovine IVDs indicates that NP cells express significantly higher levels of vimentin as compared with AF cells, with these filaments traversing from the NP cell's plasma membrane to the nucleus.[69] The intermediate filament cytoskeletal network is known to support cell shape and resist mechanical loads[72,73] and has been shown to be associated with tissue regions that experience high levels of compressive loading.[74,75] The observed intermediate filament expression patterns in the IVD seem to correspond with this notion.

3.4.1.2 Anulus Fibrosus Cells

Cells of the AF are derived from the axial mesenchyme that surrounds the notochord during development.[76] The AF is formed as cells condense in areas of future IVDs, align in an alternating circumferential pattern, and proceed to lay down the highly aligned collagen

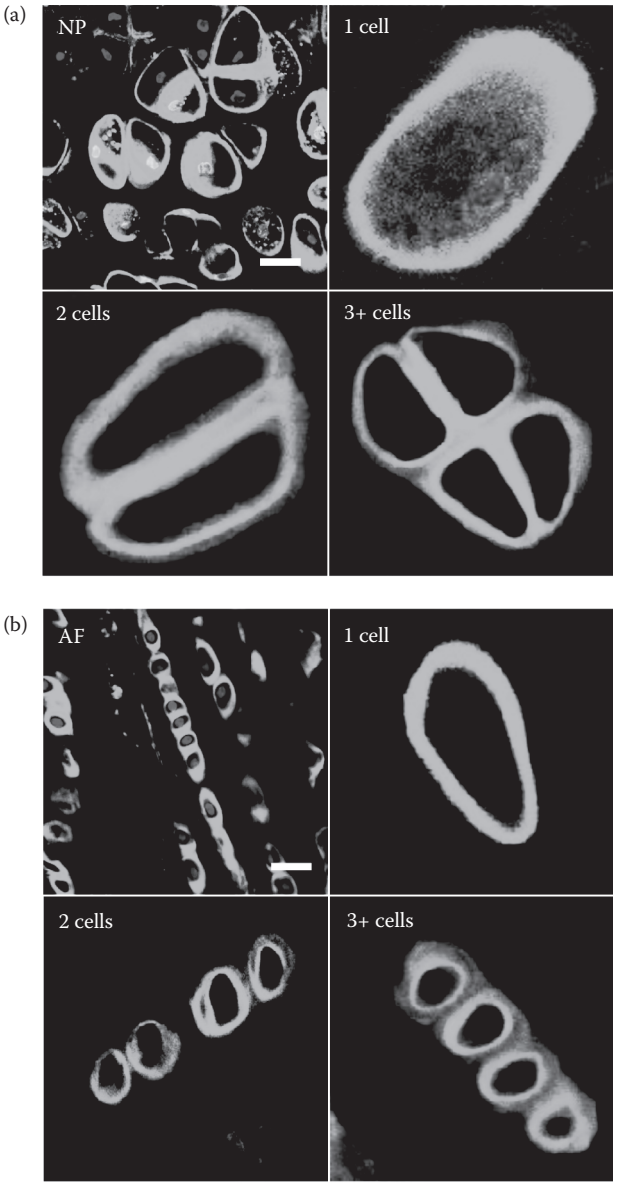

FIGURE 3.2
(See color insert.) (a) NP cell–PCM morphology. In rat IVD tissues, nearly all NP cells are associated with a PCM region that is rich in type VI collagen (green). A majority of cells (>80%) reside in a PCM containing two or more cells in the NP. Scale bar = 20 μm, red = cell nuclei. (b) AF cell–PCM morphology. In rat NP tissues, AF cells are also associated with a PCM region rich in type VI collagen (green). A majority of AF cells are found in the PCM containing one or two cells (>90%) in the inner AF region, whereas more than half of the cells resided in the PCM containing three or more cells in the outer AF region. Scale bar = 20 μm, red = cell nuclei.

fibers that form the lamellar structure of the AF.[56,76] Cells of the AF are generally characterized as fibrochondrocytes because they exhibit phenotypic and morphologic (Figure 3.2b) characteristics of both fibroblasts and chondrocytes, including the expression of both type I and II collagens, as well as aggregating proteoglycans.

AF cell morphology varies with radial position within the tissue, transitioning from elongated, fibroblast-like cells in the outer AF to more rounded or ellipsoidal chondrocyte-like cells in the inner AF. A detailed morphological assessment of AF cells in bovine IVDs using fluorescent cytoskeletal labels[77] identified outer AF cells with elongated, "cord-like" morphologies that were highly aligned along the collagen fiber direction. They further showed evidence of long and interconnected cell processes extending away from the cell body, as well as the expression of the gap junction protein, connexin 43, suggesting some intercellular communication between cells. A separate study of this same cell population in the rat outer AF[66] identified the presence of multiple AF cells sharing a common pericellular matrix (PCM; Figure 3.2b), suggesting that AF cells may interact not only through direct cell–cell communications but also through sharing of a proximal microenvironment. Inner AF cells, in contrast, have been reported to be more spherical or elliptical and share a common PCM with fewer total cells (Figure 3.2b). The complexity of these morphologies alone highlights the challenges in understanding the precise micromechanical stimuli experienced during loading and daily activities.

AF cells exhibit staining for actin, microtubule, and vimentin cytoskeletal networks,[69,77] with both actin and vimentin networks identified within cell processes that extend away from the cell body.[67,70] Outer AF cells in bovine IVD tissues have been shown to express higher levels of β-actin mRNA and protein relative to NP cells.[69] This finding may correspond to the more tensile mechanical environment experienced by cells of the outer AF, in which a more developed contractile actin cytoskeleton may be involved in sensing or resisting tensile loads.

3.4.2 Intervertebral Disc Cell–Matrix Microenvironment

The interface between a cell and its immediate ECM microenvironment may be of particular importance in modulating responses to environmental stimuli, as both physical and chemical cues are transduced to the cell through this interface. The cells of the IVD reside within a PCM, a local matrix microenvironment that surrounds a cell or group of cells and is distinct from the greater ECM. Cellular interactions with the PCM may include receptor–ligand interactions (e.g., integrin-mediated adhesions), transduction of externally applied biophysical stimuli, and active cell sensing of the mechanical stiffness of the PCM, each of which is known to regulate cell behaviors including cell signaling, survival, phenotype, and organization.[78]

3.4.2.1 Pericellular Matrix Constituents

Similar to articular cartilage, the PCM of the IVD can be distinguished from the surrounding matrix by the unique presence of type VI collagen.[11,64,66] In addition to type VI collagen, various other PCM constituents have been identified in the IVD PCM, including collagen types I (mainly AF), II (mainly NP),[11] III, IX, and XI,[11,79] aggrecan,[80,81] and fibronectin.[82,83] Recent evidence also indicates that some PCM constituents may vary regionally within the disc, with the cell-associated presence of several isoforms of the matrix protein laminin identified as being unique to the NP (identified primarily in immature tissues to date). These include the cell-adhesive laminins, LM-511/521[13] and LM-332,[84] as well as cell

surface receptors corresponding to these laminin ligands, which are described in detail below.

3.4.2.2 Pericellular Matrix Morphology

The three-dimensional (3D) morphology of the PCM and enclosed cells is similar to that reported for the chondrocyte that has been termed the "chondron" for articular cartilage. Because of the complexity of IVD cell–PCM units containing multiple cells in a common PCM, we refer to these structures as cell–matrix units (CMUs) for IVD cells. CMU morphology has been quantified in both young (1 month) and old (12 month) rat IVDs using confocal microscopy and fluorescently labeled type VI to identify CMU boundaries,[66] with findings of distinct regional differences in CMU shape, size, and cellular content across IVD regions (Figure 3.3). In the NP, CMUs were found to be spheroidal, with multiple cells encapsulated within one CMU in young rats (average of four cells per CMU), which corresponds with observed cell clustering in NP tissues.[52,53] In older rats, however, the percentage of CMUs with multiple cells in the NP was found to decrease. For cells of the inner AF, CMUs were ellipsoidal with shapes similar to chondrons in articular cartilage,[85] with almost all cells (>90%) present in CMUs that contained only one to two cells. In the outer AF, CMUs also contained multiple cells and were highly aligned along the principal collagen fiber direction (Figure 3.3), corresponding with the elongated, aligned cell morphologies documented in the outer AF. Interestingly, the thickness and volume of the PCM were found to be similar across all IVD regions, suggesting that cells may carefully regulate this feature of the PCM, perhaps in an effort to regulate mechanical loading[86,87] or to limit the maximum diffusive distance.

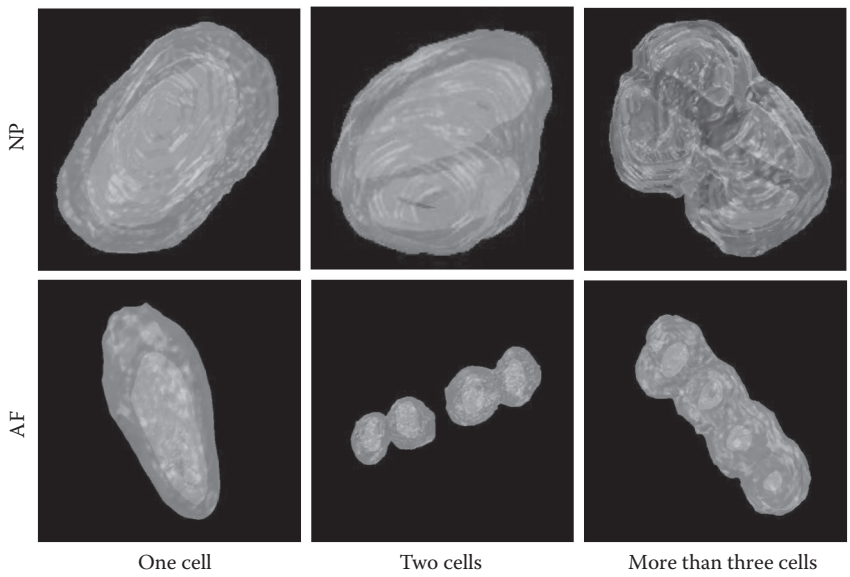

FIGURE 3.3
Three-dimensional *in situ* CMU morphologies for NP and AF cells reconstructed from serial confocal images. CMUs in the NP exhibit a more rounded shape than other regions, with no preferential spatial orientation. CMUs in the AF are often ellipsoidal and in alignment with the local collagen fiber direction of the AF.

3.4.3 Intervertebral Disc Cell–Matrix Interactions

3.4.3.1 Cell Surface Receptors and Adhesion

The receptors that cells use to interact with their surrounding ECM play critical roles in modulating a variety of cell processes including sensing and responding to environmental stimuli, with specific receptor–ligand interactions known to elicit unique downstream cellular responses. Cell surface receptors that modulate cell–matrix interactions have been identified at various stages of IVD development, maturation, and degeneration. These receptors consist primarily of the integrin class of cell–matrix receptors (Figure 3.4), which are known to play critical roles in cell adhesion, signaling, and mechanosensing in a variety of tissues.[88,89] Integrins are heterodimeric proteins consisting of α and β subunits (18 α subunits and 8 β subunits that form 24 known heterodimers), with specific α–β pairings determining ligand-binding specificity. In the developing IVD, both the fibronectin-binding α5β1[82] and the collagen-binding α11β1[90] integrins have been identified in aligned AF cells during anulus formation. These receptors are thought to be key players in cell-directed collagen fibrillogenesis.[91] In immature and mature IVD tissues, integrins that bind collagens (α1, α2, and β1 subunits) and fibronectin (α5, αv, β3, and β5 subunits) continue to be expressed in both AF and NP regions of immature and mature IVD tissues.[15] Corresponding with the unique region-specific expression of laminin identified in the immature NP, NP cells seem to uniquely express a number of laminin-binding integrins (α6 and β4)[14,15,92] and non-integrin (CD239 and CD151)[13] cell surface receptors. Flow cytometric analyses of isolated IVD cells have confirmed this NP-specific expression of laminin receptors in immature NP cells,[13,14] with differential expression between NP and AF cells maintained *in vitro*, suggesting distinctly different roles for AF and NP cells in interacting with laminin proteins.

The involvement of integrins in IVD cell adhesion has been confirmed with *in vitro* experiments utilizing function-inhibiting antibodies to determine the role of individual integrin subunits in attachment to specific matrix proteins. In those studies, both AF and NP cell adhesions to collagens were found to be mediated either entirely (on type II collagen) or in part (on type I collagen) by the α1β1 integrin,[14] with evidence that the α2β1 integrin may also play a role in NP cell adhesion to type II collagen.[93] IVD cell adhesion (both AF and NP cells) to fibronectin, another cell-adhesive ligand found in the disc,[83] was found to be

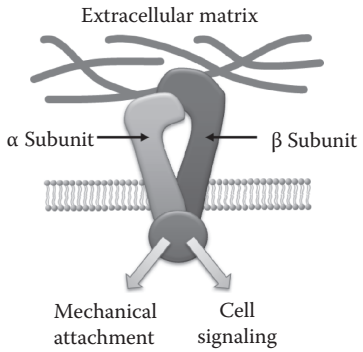

FIGURE 3.4
IVD cell adhesion is mediated through integrin–matrix interactions. Integrin cell surface receptors mediate cell–matrix interactions in the IVD, with specific integrin heterodimers (α–β subunit pairings) determining ligand-binding specificity.

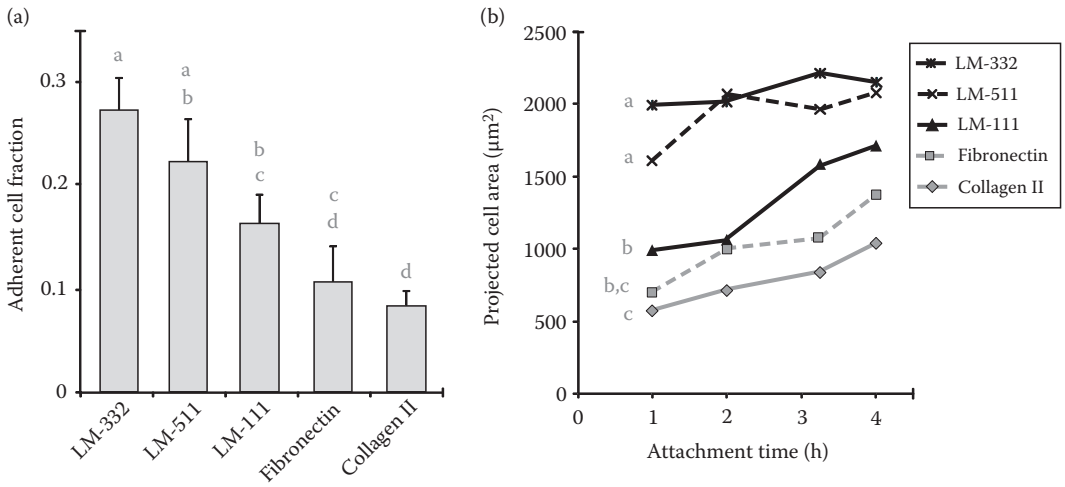

FIGURE 3.5
Adherent fraction of NP cells and cell spreading on ECM substrates. (a) Fraction of adherent cells remaining attached to ECM substrates after application of centrifugal detachment force (200 *g*). Higher numbers of NP cells resist detachment when adherent to laminin ligands (isoforms LM-332, LM-511, and LM-111), as compared with collagen and fibronectin ECM ligands (substrates not labeled with the same letter were statistically different, ANOVA; $p < 0.05$). (b) NP cell spreading dynamics on ECM substrates. NP cells on laminin isoforms LM-332 and LM-511 spread rapidly and to a greater extent as compared with other matrix substrates (error bars omitted for clarity; significant effects of substrate and time were detected via two-way ANOVA, $p < 0.01$). (Adapted from Gilchrist, C. L. et al., *Eur. Cell Mater.*, 21, 523–532, 2011.)

mediated through the α5β1 integrin.[14] Additionally, NP cell adhesion to laminin (isoform LM-111) was found to be mediated in part by the α6 and β1 integrin subunits.[14]

IVD cell adhesion behaviors have been examined on surfaces coated with specific ECM ligands, with results that further highlight the NP cells' preference for laminins. NP cells were found to adhere to two laminin isoforms (LM-511 and LM-332) at twofold or greater numbers than on other ECM ligands (collagen, fibronectin, or LM-111; data not shown) and show significantly higher resistance to detachment forces on laminins as compared with other substrates (Figure 3.5a). NP cells also exhibited significantly higher levels of spreading on these ECM ligands (Figure 3.5b).[14] Additionally, NP cells have been found to attach to these laminin ligands in significantly higher numbers as compared with AF cells,[14,84] supporting the region-specific receptor and ligand expression differences identified between IVD regions.

3.4.4 Intervertebral Disc Cell Changes with Aging and Degeneration

Relatively little is known regarding changes in IVD cell morphologies, the microenvironment, or cell–matrix interactions that may occur with aging or disc degeneration. One of the most dramatic age-related cellular changes in the human IVD is a significant decrease in cell density in both the NP and AF regions.[94–96] Within the first two decades of life, an approximate 10-fold decrease in cell density occurs in both the NP and AF, with no further changes detected with increasing age or degenerative grade. The increased prevalence of cells with cytoplasmic projections and clusters of proliferating cells have also been reported.[70,97,98] Another important cell-related change in the IVD is the increased presence

of other cell types including nerve and Schwann cells, fibroblasts, and endothelial cells associated with increased vasculature.[94,99] In the case of IVD degeneration or herniation, lymphocytes and macrophages increasingly infiltrate the IVD tissues with evidence of many molecular markers of activated monocytes and their related proinflammatory cytokines.[100–102] With regard to IVD cell–matrix interactions, a potentially critical change that correlates with IVD degeneration is the increased presence of fibronectin fragments.[83] These enzymatic degradation products of fibronectin have been shown to stimulate a matrix-degrading signaling pathway in IVD cells[103,104] and initiate degenerative changes in an IVD animal model.[105] This pathway is mediated by the α5β1 integrin and results in the upregulation of matrix metalloproteinases (MMP-9 and MMP-13) and downregulation in the production of matrix molecules including collagens and aggrecan. Similarly, cells within herniated IVD tissue have also been shown to exhibit increased levels of both α5β1 integrin and fibronectin.[106] Further studies are still necessary to evaluate changes in cell shape, cytoskeletal architecture, PCM microenvironment, or cell–matrix interactions, which may regulate or correlate with IVD aging or degeneration.

3.5 Intervertebral Disc Matrix and Cell Mechanics

The physical stimuli experienced by cells embedded within IVD tissue depend directly on the mechanical properties of the ECM, as well as on the properties of the cells themselves. In the IVD, tissue mechanics are extremely complex due to the highly organized lamellar structure, anisotropic and multiphasic material behaviors, and variations in biochemical composition with region and degeneration state. Cellular responses to mechanical loading depend on the physical stimuli, which are transduced to the cell at the microscale, although these microscale stimuli cannot easily be directly measured *in situ*. However, using knowledge of tissue and cell mechanical properties, geometries, and boundary conditions, the microscale stimuli experienced by the cell can be deduced via micromechanical modeling, lending insight into the specific stimuli that may modulate IVD cell biology.

3.5.1 Anulus Fibrosus Tissue Mechanics

Tensile testing of AF tissue in isolated tensile configurations (i.e., uniaxial or biaxial tension) has determined the tissue's equilibrium modulus to be highly dependent on collagen fiber organization, with stiffnesses that are one to two orders of magnitude higher along the principal collagen fiber direction (~10 MPa) as compared with the transverse or radial direction (~0.1 MPa; Table 3.1).[21–24,26,107–110] In contrast, the compressive properties of the AF matrix are significantly lower (~0.3 MPa)[111–116] because the collagen fibers do not contribute significant resistance to compressive loading. AF tissue exhibits significant viscoelastic behaviors in a variety of loading configurations, including tension, compression, and shear. These viscoelastic responses are primarily due to poroelastic effects that result from interstitial fluid flow driven by loading. This flow-dependent viscoelastic behavior is described by the hydraulic permeability of the tissue, which has been found to vary substantially with tissue proteoglycan and water content.[111,112,114–117] AF hydraulic permeability values range from 0.2×10^{-15} to 3.5×10^{-15} $m^4/N\text{-}s$, as determined in direct permeation or compressive loading tests (Table 3.1). These values are approximately one order of magnitude lower than those measured in articular cartilage.

TABLE 3.1

Summary of Material Properties for ECM, PCM, and Cellular Subdomains of IVD

	Young's Modulus (MPa)		Shear Modulus (MPa)	Permeability (m^4/N-s)	Citations
	Circumferential	**Radial**			
ECM					
AF (tension)	0.2–100	0.1–0.4	0.02–0.15	—	21–24, 26, 107–110, 143, 144
AF (compression)	0.2–0.8	0.2–0.8	0.02–0.15	$0.2–3.5 \times 10^{-15}$	111, 112, 115–117
NP (compression)	0.1–1.0	—	0.0001–0.001	9×10^{-16}	121, 122
PCM[a]					
	Young's Modulus (MPa)	**Poisson's Ratio**		**Permeability (m^4/N-s)**	**Citations**
AF/NP	0.03–0.1	0.2	—	7×10^{-17}	126, 127
Cell					
	Young's Modulus (kPa)	**Poisson's Ratio**			**Citations**
AF	0.3–0.6	0.4	—	4×10^{-15}	68, new data for AFM
NP	0.3–0.9	0.4	—	4×10^{-15}	

Sources: From Acaroglu, E. R. et al., *Spine*, 20, 24, 2690–2701, 1995; Ebara, S. et al. *Spine*, 21, 4, 452–461, 1996; Galante, J. O., *Acta Orthop. Scand. Suppl.*, 100, 1–91, 1967; Skaggs, L. et al., *Spine*, 19, 12, 1310–1319, 1994; Wu, H. C. and Yao, R. F., *J. Biomech.*, 9, 1, 1–7, 1976; Iatridis, J. C. et al., *J. Orthop. Res.*, 17, 5, 732–737, 1999; Bass, E. C. et al., *Ann. Biomed. Eng.*, 32, 9, 1231–1242, 2004; Elliott, D. M. and Setton, L. A., *J. Biomech. Eng.*, 123, 3, 256–263, 2001; Fujita, Y. et al., *J. Orthop. Res.*, 15, 6, 814–819, 1997; Fujita, Y. et al., *Med. Eng. Phys.*, 22, 5, 349–357, 2000; O'Connell, G. D. et al., *J. Biomech. Eng.*, 131, 11, 111007, 2009; Best, B. A. et al., *Spine*, 19, 2, 212–221, 1994; Drost, M. R. et al., *J. Biomech. Eng.*, 117, 4, 390–396, 1995; Gu, W. Y. et al., *Spine*, 24, 23, 2449–2455, 1999; Iatridis, J. C. et al., *J. Biomech.*, 31, 6, 535–544, 1998; Yao, H. et al., *Ann. Biomed. Eng.*, 30, 10, 1234–1241, 2002; Iatridis, J. C. et al., *J. Orthop. Res.*, 15, 2, 318–322, 1997; Johannessen, W. and Elliott, D. M., *Spine*, 30, 24, E724–729, 2005; Alexopoulos, L. G. et al., *J. Biomech. Eng.*, 125, 3, 323–333, 2003; Darling, E. M. et al., *Biophys. J.*, 98, 12, 2848–2856, 2010; and Guilak, F. et al., *Spine*, 24, 23, 2475–2483, 1999.

Note: Ranges of values for properties of the ECM of AF and NP are summarized here for application to the modeling of cell–matrix interactions. Property values for the ECM of the AF and NP have been widely studied in directions both along and transverse to the principal fiber direction. Properties given for cell mechanics are obtained from both micropipette and atomic force microscopy (AFM) testing of IVD cells.

[a] No experimental data are available for measurements of the PCM from any region of the IVD. Data given here are for the PCM of articular cartilage based on similarities to the compositional matrix of NP and AF.

Due to the negative charge of proteoglycans within the AF's ECM, there exist a number of electrokinetic effects that modulate ion and water transport within the tissue, as well as affect cell signaling in response to mechanical load.[113,118–120] Electrical (streaming) potentials within AF tissues have been measured in pressure- or deformation-induced fluid flow tests, with values (5–8 mV/MPa) that depend on the strain state of the tissue.[117] Additionally, the AF also exhibits electrical conductivity as a result of the hydrated, charged nature of the matrix, with measured conductivity values of 5 to 10 mS/cm that are dependent on tissue hydration and porosity.[118] Together, these measured mechanical and electrical properties of the AF lend support to the modeling of tissue as a fluid- and electrolyte-filled, collagen fiber–reinforced material that exhibits both anisotropic and viscoelastic behaviors.

Both the mechanical and electrokinetic properties of the AF are known to vary considerably with radial position (outer versus inner), reflecting the differing collagen fiber orientations, hydration states, and proteoglycan content between AF regions. Additionally, these properties may vary significantly with aging or degenerative state. Degenerative changes include increases in shear and compressive moduli,[115] which are likely due to loss of matrix proteoglycans and changes in collagen structure. Permeability may be increased with degeneration in all directions except radially,[117] again likely reflecting decreased proteoglycan content in the tissue. AF tensile properties have not been shown to change dramatically with degeneration,[21] although there is some evidence of stiffening in the radial direction.[109] Finally, degenerative changes in electrokinetic properties (i.e., decreased streaming potentials) have also been documented and may be considerable due to their dependence on negative charge and hydration.[113]

3.5.2 Nucleus Pulposus Tissue Mechanics

The material properties of the NP have been primarily studied with tests of torsional shear because the tissue exhibits viscous, fluid-like behaviors in the healthy state.[4,5] These shear behaviors are highly nonlinear, reflecting the tissue's disperse polymer network that likely stiffens via physical entanglements or chemical interactions in response to applied loads. NP properties have also been measured in confined compression,[121] with an effective aggregate modulus (~1 MPa) that is considerably (approximately twofold to threefold) higher than AF values (Table 3.1). Significant decreases in water and proteoglycan content occur in the nucleus with degeneration and aging, resulting in substantial increases in shear stiffness[122] and permeability[121] and decreases in aggregate modulus (50% decrease) and swelling stress.[121]

3.5.3 Intervertebral Disc Cell Mechanics

The mechanical properties of IVD cells were first studied via micropipette aspiration (Figure 3.6).[68] Isolated cells from immature porcine IVD regions (NP, inner AF, and outer AF) were found to exhibit viscoelastic solid behaviors, with both outer and inner AF cells having properties (average shear modulus of 90 Pa) similar to articular chondrocytes (~130 Pa)[123] but lower than those measured for endothelial cells and fibroblasts.[124,125] In contrast, NP cells were found to be considerably stiffer (550 Pa) than AF cells. This finding may be a result of the more developed, intermediate filament-rich cytoskeleton possessed by notochordal cells from this immature cell population (see Section 3.4.1).

IVD cell mechanical properties have also recently been measured through atomic force microscopy (AFM) indentation (using a 5 μm spherical-tipped indenter), with findings that differ somewhat from micropipette studies. In AFM indentation testing, porcine NP cells were found to have an average elastic modulus of 345 Pa (Figure 3.7), which was significantly lower than that of AF cells (620 Pa). Within the NP cell population, there was a fairly large range of moduli, varying from 49 to 825 Pa. Cell height was also measured via AFM, with NP cells found to be significantly taller (average of ~25 μm) than AF cells (~12 μm), again reflecting the large percentage of notochordal cells present in this cell population. There was a slight but statistically significant negative correlation between NP cell height and stiffness ($p = 0.04$, $R^2 = 0.137$), with taller (i.e., larger) NP cells having lower elastic moduli, whereas there was no correlation detected between AF cell height and stiffness ($p = 0.70$). These findings are in contrast with micropipette experiments, in which porcine NP cells were found to have an instantaneous modulus of ~800 Pa and were stiffer than

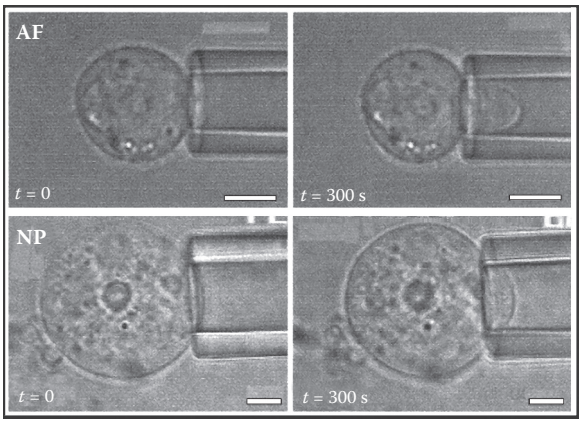

FIGURE 3.6
Micropipette aspiration of AF and NP cells. Initial ($t = 0$) and equilibrium ($t = 300$ s) cell displacements in micropipette aspiration tests of porcine AF and NP cells. NP cells exhibit smaller equilibrium displacements and longer creep times. Tests shown were performed at an aspiration pressure of ~250 Pa. Scale bars = 5 μm. (Adapted from Guilak, F. et al., *Spine*, 24, 23, 2475–2483, 1999.)

AF cells. These discrepancies may be a result of the different testing methods used, with micropipette aspiration and cell indentation applying different types of loading (tensile and compressive, respectively) to the cell. Despite different testing methods, IVD cell stiffness (elastic or instantaneous moduli) in both studies fell in the range between 350 and 800 Pa. These findings indicate that AF cells may be softer than their surrounding ECM

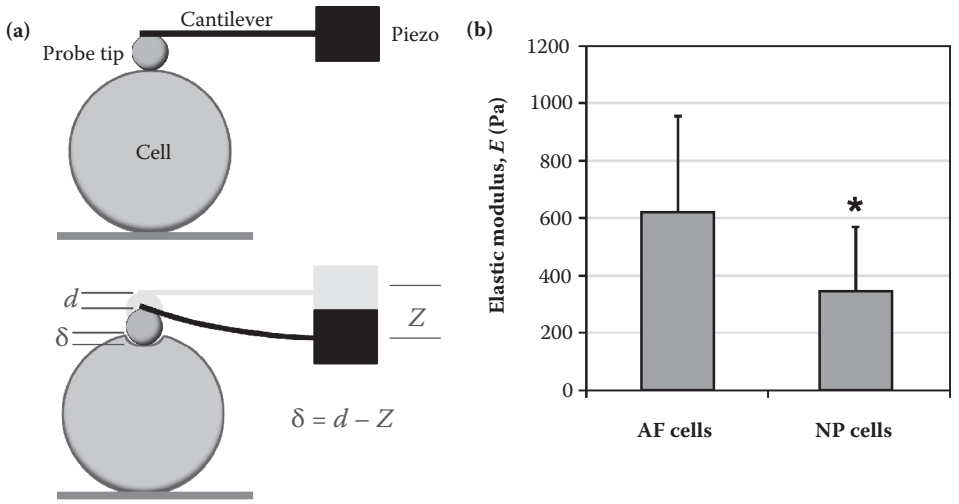

FIGURE 3.7
AFM testing of IVD cells. IVD cell elastic moduli were measured via AFM indentation using a 5 μm diameter spherical probe tip. (a) Schematic illustrating AFM indentation testing configuration. The stiffness of a cell is calculated via the Hertz spherical indentation model using the measured indentation depth (δ). (b) Mean elastic modulus (±standard deviation) for freshly isolated porcine AF ($n = 28$) and NP ($n = 30$) cells. The stiffness of NP cells was found to be significantly less than that of AF cells (*$p < 0.0001$).

environment; however, NP cells may have mechanical properties that more closely match their surroundings. Future work is necessary to determine the properties of mature IVD cell populations and to assess whether changes in cell stiffness occur with maturation or degeneration.

3.5.4 Intervertebral Disc Pericellular Matrix Mechanics

As detailed in Section 3.4.2, both AF and NP cells are surrounded by a PCM that is compositionally and structurally distinct from the surrounding ECM. This pericellular layer may play an important role in modulating the cellular mechanics and physical stimuli experienced by the cell, potentially acting to isolate cells from, or to amplify, gradients in stress, strain, deformation, or flow. In articular cartilage, the stiffness of the PCM has been determined to be considerably greater than that of the cell (~30–100 kPa)[126,127] and may act to either shield or amplify matrix deformations depending on the mechanical properties of the surrounding ECM.[86,87] No direct measurements of PCM material properties have been made in the IVD, although the similarities in PCM constituents (as detailed in Section 3.4.2) between articular cartilage and the IVD imply that they may have similar material properties (Table 3.1). The mechanical implications of this pericellular layer in the IVD have been examined in micromechanical models[128,129] described below.

3.5.5 Modeling of Intervertebral Disc Cell–Pericellular Matrix Micromechanics

Many cell types, including IVD cells, are known to respond biologically to micromechanical factors transduced to the cell during mechanical loading, such as cell deformations and strains, stresses and pressures, fluid flows, and electrokinetic effects.[47,48,130] To understand how these factors affect IVD cell behavior, there is a need to first understand the types and levels of micromechanical stimuli that are experienced by the cell during tissue loading. Direct measurement of these factors within IVD tissues poses significant challenges due to the complex, inhomogeneous, and hierarchical nature of the tissue and the small scale of the cell.

Initial studies of macroscale IVD tissue mechanics measured deformations on the surface of the tissue in response to torsion and compressive loads, with surface strains along the principal collagen fiber direction found to be generally tensile and lower than 5%.[131] Additionally, displacements within the tissue at the macroscale (orders of magnitude greater than the size of a cell) have been measured by using image analysis to track the movement of fiducial markers[132,133] placed within the tissue or noninvasively using tissue image texture patterns to measure intratissue strains.[29,134] These studies indicate that under compressive loading, the inner and outer anulus displace outward and exhibit a characteristic "bulging" behavior, with evidence of high shear strains near the interface between the outer AF and cartilage endplates.[29] Changes in macroscale deformation patterns have also been identified with degeneration, with both compressive axial and tensile radial strains shown to increase. Additionally, the loss of nucleus pressurization (occurring with disc herniation or degeneration) may alter tissue deformation patterns, with the inner AF displacing inward while the outer AF continues to displace outward, potentially disrupting annular structure.[132,133,135]

More recently, studies have also examined deformation behaviors in the AF at scales closer to that of individual cells by tracking fluorescently labeled fiduciary markers and cell nuclei via confocal microscopy.[136–139] These studies have revealed complex microscale deformation patterns, including collagen fiber sliding in response to applied tensile loads,

which result in nonuniform strains at scales similar to individual cells. As a result of collagen fiber sliding, cells positioned along or within fibers potentially experience levels of tensile strains that are lower than overall (macroscale) tissue strains[138] and may expose cells situated between collagen fibers or lamella to high shear environments.[137] Studies of direct strain measurement around cells in other collagen-reinforced connective tissues (meniscus) suggest that despite these local variations in strain magnitudes between cells and lamella, the *principal* strains experienced by cells are very similar to those experienced by the matrix at many distances away from the cells.[140] Overall, these studies highlight the complexity of AF microscale mechanics and indicate that additional studies are needed to determine the magnitudes of strain experienced by cells in the AF.

3.5.5.1 Anulus Fibrosus Cell Microenvironment

Although highly informative, measurements of ECM mechanics at the macroscale or even at the microscale are currently not sufficiently resolved to fully understand the stress, strain, and fluid flow environments at the scale of IVD cells. The mechanical environment at the cellular level may be quite different than that of the adjacent ECM because the cell and its PCM each may have material properties that differ significantly from the surrounding matrix. To better understand the physical stimuli that are present at the scale of the cell, several theoretical models have been developed to predict the detailed mechanical environment of IVD cells under various loading conditions.[128,129,141,142] Axisymmetrical finite-element models (FEM) were initially developed to model single AF cells embedded within a collagen fiber–reinforced lamella, using measured values for cell geometries and the material properties of the cell and ECM. More recently, FEMs have been constructed from the fully 3D morphology of AF cells and their surrounding PCM measured *in situ*[128] to more accurately characterize the mechanical interactions between AF cells, their PCM, and ECM (Figure 3.8a). In these studies, average cellular volumetric strains [tr(ε), where ε is the infinitesimal strain tensor] were found to be significantly amplified relative to the surrounding PCM and ECM (Figure 3.8b), and the PCM was found to significantly attenuate instantaneous fluid pressurization of the cell. That study also examined the influence of multiple cells embedded within one contiguous PCM,[66] with the finding that cells within these multicell units experience higher strains and more sustained pressurization in response to loading. These findings suggest that strain may be a dominant signal regulating many AF biological responses and suggest the need for studies of AF cell responses to well-controlled strain stimuli. Because these multicell units have been documented to decrease with IVD age, age-related alterations in micromechanical stimuli are likely experienced by these cells. Together, the findings of these FEMs identify specific stimuli experienced by AF cells and highlight important roles for cell shape and PCM in modulating physical stimuli at the cellular level.

3.5.5.2 Nucleus Pulposus Cell Microenvironment

Similar 3D FEMs have also been used to investigate the micromechanical environment of NP cells[129] (Figure 3.8a) using *in situ* morphologies of PCM and cells measured from 3D confocal microscopic reconstructions. In such models, behaviors of single, paired, or multiple cells in a contiguous PCM in response to applied compression were examined. Both key differences and similarities were identified between the micromechanical environments of NP and AF cells. NP cells were found to experience complex, temporally varying volumetric strains that were significantly greater than far-field ECM strains, with

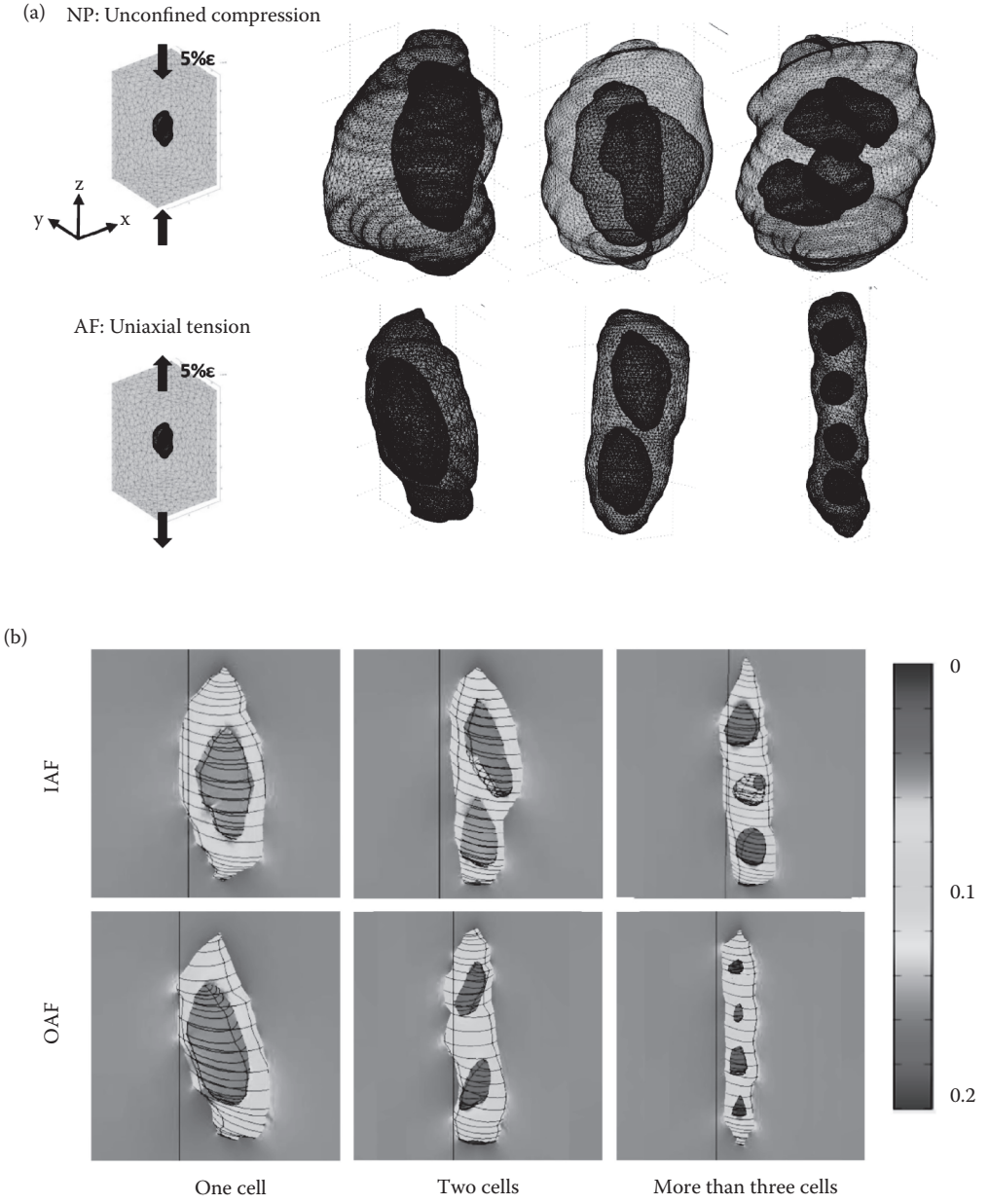

FIGURE 3.8
(See color insert.) (a) Three-dimensional FEM of NP and AF cells in representative CMUs. FEM geometry models of CMUs in tetrahedron element meshes. For clarity, only meshes of the PCM and cell surfaces are shown above (not to scale). CMUs in the NP were subjected to an unconfined compression with 5% compressive strain along the principal axis of the CMU. CMUs in the AF were subjected to a uniaxial tension with 5% tensile strain along the principal axis of the CMU. All surfaces of the ECM are assumed to be free-draining. (b) Model predictions of volumetric strain in the AF cell and surrounding PCM after application of a tensile load. Volumetric strain for AF cells in the inner (IAF) and outer (OAF) regions at equilibrium under uniaxial tension. Strain amplification was seen from the extracellular to the pericellular and cellular scales. The strain amplification ratio was the highest in the CMUs with three or more cells and lowest in the CMUs with just one cell.

strain amplification ratios ranging from ~2 to 4. Similar to findings in the AF, the PCM was found to shield cells from acute increases in fluid pressure, and multiple cells within a continuous PCM (corresponding to cell clustering documented in immature NP tissues) experienced increased strain amplification and greater peak fluid pressures as compared to single cells. In contrast to AF cell micromechanics, deviatoric (shape-altering) strains were attenuated in the cell and PCM relative to the ECM, and significantly longer fluid pressurization periods were predicted after loading. These predictions suggest that fluid pressurization and volume change may be key stimuli involved in NP cell mechanotransduction, whereas AF cells may experience greater overall levels of deformation.

Overall, predictions from these micromechanical models emphasize significant differences between ECM level and cellular level stimuli, with strains and fluid pressures at the cell that were often several-fold higher (or lower) than the immediately adjacent ECM. Such models also illustrate the sensitivity of cell microenvironmental stimuli to cell geometry, cell mechanical properties, and ECM structure, including a potentially critical mechanical role for the PCM in both AF and NP regions. Similar to findings in articular cartilage,[86,126] the PCM has been found to significantly affect transduction of stimuli to the cell, amplifying strains and attenuating peak fluid pressures. Finally, mechanical models highlight possible regional differences in IVD cell microenvironments, with AF cells predicted to experience large kinematic deformations, whereas in the NP, pressure or volume changes may be the dominant stimuli.

3.6 Summary

Significant progress has been made in recent years toward understanding the mechanobiology of the IVD, with studies providing detailed knowledge of disc tissue mechanics at the macroscale and microscale, as well as information on IVD cell morphology, cell mechanics, and microenvironment. This chapter has highlighted a number of key findings from these studies. The IVD is a heterogeneous tissue, with the centrally located NP and the surrounding AF exhibiting distinct differences in ECM composition and structure, and correspondingly unique tissue mechanical behaviors. IVD cells exhibit region-specific characteristics that reflect differences in embryonic origin, tissue structure, ECM composition, and mechanical environment. These include key differences in cell shape, cytoskeletal composition and architecture, cell–matrix interactions, and cell mechanical properties, each of which may affect how cells experience, sense, and respond to mechanical stimuli. IVD cells are surrounded by a PCM that is compositionally and structurally distinct from the surrounding ECM and may play a key role in transducing mechanical stimuli to IVD cells. Multiple cells may reside within a contiguous PCM (or CMU), with PCM geometries varying with tissue region. Lastly, detailed mechanical models of IVD cellular microenvironments (incorporating measured cell and tissue properties) have been developed to better understand mechanical stimuli at the cellular level. These models suggest that the mechanical stimuli experienced by IVD cells are highly sensitive to differences in cell and tissue geometry, as well as mechanical properties. In the AF region, high levels of tissue strain may be a dominant stimuli experienced by cells, whereas cells in the NP may experience fluid pressurization and volume change as primary stimuli.

Despite the detailed information provided by these studies and models, there remain a number of limitations to our current knowledge of IVD cell micromechanics. Most

significantly, there is currently limited information on how micromechanical factors change with IVD aging and degeneration. This information can likely provide key insights into possible pathological changes in IVD mechanobiology. Additionally, how complex cell–matrix interactions may affect mechanical factors at the cell level, including cellular, cytoskeletal, and nuclear strains, also remains to be elucidated. AF cells may possess long cellular processes that extend along, or between, collagen fibers and that have been hypothesized to act as mechanosensors;[67,77] however, how these structures affect micromechanical stimuli experienced by the cell is not understood. Finally, micromechanical models that incorporate osmotic pressure and electrokinetic effects,[118,120] as well as the morphologies and properties of mature human IVD cells, are necessary to assess how degenerative changes in the human may alter the micromechanical environment of IVD cells. Further knowledge in these areas will provide a more complete understanding of how IVD cells experience, sense, and respond to mechanical loading and more completely define the role of mechanical stimuli in normal and pathologic IVD biology.

Acknowledgments

We acknowledge the NIH for funding (AR047442, EB002263, and AR057410) and the contributions of Drs. Eric Darling, Farshid Guilak, and Jun Chen.

References

1. Bogduk, N. 2005. *Clinical Anatomy of the Lumbar Spine and Sacrum.* Edinburgh: Elsevier/Churchill Livingstone.
2. Urban, J. P., and S. Roberts. 2003. Degeneration of the intervertebral disc. *Arthritis Research & Therapy* 5(3):120–130.
3. Cloyd, J. M., N. R. Malhotra, L. Weng, W. Chen, R. L. Mauck, and D. M. Elliott. 2007. Material properties in unconfined compression of human nucleus pulposus, injectable hyaluronic acid-based hydrogels and tissue engineering scaffolds. *European Spine Journal* 16(11):1892–1898.
4. Iatridis, J. C., L. A. Setton, M. Weidenbaum, and V. C. Mow. 1997. The viscoelastic behavior of the non-degenerate human lumbar nucleus pulposus in shear. *Journal of Biomechanics* 30(10):1005–1013.
5. Iatridis, J. C., M. Weidenbaum, L. A. Setton, and V. C. Mow. 1996. Is the nucleus pulposus a solid or a fluid? Mechanical behaviors of the nucleus pulposus of the human intervertebral disc. *Spine* 21(10):1174–1184.
6. Eyre, D. R., and H. Muir. 1977. Quantitative analysis of types I and II collagens in human intervertebral discs at various ages. *Biochimica et Biophysica Acta* 492(1):29–42.
7. Gower, W. E., and V. Pedrini. 1969. Age-related variations in proteinpolysaccharides from human nucleus pulposus, annulus fibrosus, and costal cartilage. *Journal of Bone and Joint Surgery. American Volume* 51(6):1154–1162.
8. Taylor, J. R., and L. T. Twomey. 1988. The development of the human intervertebral disc. In *The Biology of the Intervertebral Disc*, edited by P. Gosh, 39–82. Boca Raton, FL: CRC Press.
9. Jahnke, M. R., and C. A. McDevitt. 1988. Proteoglycans of the human intervertebral disc. Electrophoretic heterogeneity of the aggregating proteoglycans of the nucleus pulposus. *The Biochemical Journal* 251(2):347–356.

10. Melrose, J., P. Ghosh, and T. K. Taylor. 2001. A comparative analysis of the differential spatial and temporal distributions of the large (aggrecan, versican) and small (decorin, biglycan, fibromodulin) proteoglycans of the intervertebral disc. *Journal of Anatomy* 198(Pt 1):3–15.
11. Roberts, S., J. Menage, V. Duance, S. Wotton, and S. Ayad. 1991. 1991 Volvo Award in basic sciences. Collagen types around the cells of the intervertebral disc and cartilage end plate: An immunolocalization study. *Spine* 16(9):1030–1038.
12. Yu, J. 2002. Elastic tissues of the intervertebral disc. *Biochemical Society Transactions* 30(Pt 6):848–852.
13. Chen, J., L. Jing, C. L. Gilchrist, W. J. Richardson, R. D. Fitch, and L. A. Setton. 2009. Expression of laminin isoforms, receptors and binding proteins unique to nucleus pulposus cells of immature intervertebral disc. *Connective Tissue Research* 50(5):294–306.
14. Gilchrist, C. L., J. Chen, W. J. Richardson, R. F. Loeser, and L. A. Setton. 2007. Functional integrin subunits regulating cell–matrix interactions in the intervertebral disc. *Journal of Orthopaedic Research* 25(6):829–840.
15. Nettles, D. L., W. J. Richardson, and L. A. Setton. 2004. Integrin expression in cells of the intervertebral disc. *Journal of Anatomy* 204(6):515–520.
16. Marchand, F., and A. M. Ahmed. 1990. Investigation of the laminate structure of lumbar disc anulus fibrosus. *Spine* 15(5):402–410.
17. Cassidy, J. J., A. Hiltner, and E. Baer. 1989. Hierarchical structure of the intervertebral disc. *Connective Tissue Research* 23(1):75–88.
18. Hickey, D. S., and D. W. Hukins. 1980. X-ray diffraction studies of the arrangement of collagenous fibres in human fetal intervertebral disc. *Journal of Anatomy* 131(Pt 1):81–90.
19. Hickey, D. S., and D. W. Hukins. 1982. Aging changes in the macromolecular organization of the intervertebral disc: An X-ray diffraction and electron microscopic study. *Spine* 7(3):234–242.
20. Horton, W. G. 1958. Further observations on the elastic mechanism of the intervertebral disc. *The Journal of Bone and Joint Surgery. British Volume* 40-B(3):552–557.
21. Acaroglu, E. R., J. C. Iatridis, L. A. Setton, R. J. Foster, V. C. Mow, and M. Weidenbaum. 1995. Degeneration and aging affect the tensile behavior of human lumbar anulus fibrosus. *Spine* 20(24):2690–2701.
22. Ebara, S., J. C. Iatridis, L. A. Setton, R. J. Foster, V. C. Mow, and M. Weidenbaum. 1996. Tensile properties of nondegenerate human lumbar anulus fibrosus. *Spine* 21(4):452–461.
23. Galante, J. O. 1967. Tensile properties of the human lumbar annulus fibrosus. *Acta Orthopaedica Scandinavica. Supplementum* 100:1–91.
24. Wu, H. C., and R. F. Yao. 1976. Mechanical behavior of the human annulus fibrosus. *Journal of Biomechanics* 9(1):1–7.
25. Adams, M. A., and T. P. Green. 1993. Tensile properties of the annulus fibrosus. I. The contribution of fibre–matrix interactions to tensile stiffness and strength. *European Spine Journal* 2(4):203–208.
26. Fujita, Y., N. A. Duncan, and J. C. Lotz. 1997. Radial tensile properties of the lumbar annulus fibrosus are site and degeneration dependent. *Journal of Orthopaedic Research* 15(6):814–819.
27. Nachemson, A. 1960. Lumbar intradiscal pressure. Experimental studies on post-mortem material. *Acta Orthopaedica Scandinavica. Supplementum* 43:1–104.
28. Krismer, M., C. Haid, and W. Rabl. 1996. The contribution of anulus fibers to torque resistance. *Spine* 21(22):2551–2557.
29. O'Connell, G. D., W. Johannessen, E. J. Vresilovic, and D. M. Elliott. 2007. Human internal disc strains in axial compression measured noninvasively using magnetic resonance imaging. *Spine* 32(25):2860–2868.
30. Johnstone, B., and M. T. Bayliss. 1995. The large proteoglycans of the human intervertebral disc. Changes in their biosynthesis and structure with age, topography, and pathology. *Spine* 20(6):674–684.
31. Roughley, P. J. 2004. Biology of intervertebral disc aging and degeneration: Involvement of the extracellular matrix. *Spine* 29(23):2691–2699.

32. Urban, J. P. 2002. The role of the physicochemical environment in determining disc cell behaviour. *Biochemical Society Transactions* 30(Pt 6):858–864.
33. McNally, D.S., and M.A. Adams. 1992. Internal intervertebral disc mechanics as revealed by stress profilometry. *Spine* 17(1):66–73.
34. Nachemson, A. 1992. Lumbar mechanics as revealed by lumbar intradiscal pressure measurements. In *The Lumbar Spine and Back Pain,* edited by M. I. V. Jayson. 4th ed., 157–171. New York: Churchill Livingstone.
35. Hurri, H., and J. Karppinen. 2004. Discogenic pain. *Pain* 112(3):225–228.
36. Battie, M. C., and T. Videman. 2006. Lumbar disc degeneration: Epidemiology and genetics. *Journal of Bone and Joint Surgery. American Volume* 88(Suppl 2):3–9.
37. Sambrook, P. N., A. J. MacGregor, and T. D. Spector. 1999. Genetic influences on cervical and lumbar disc degeneration: A magnetic resonance imaging study in twins. *Arthritis and Rheumatism* 42(2):366–372.
38. Videman, T., J. Saarela, J. Kaprio, A. Nakki, E. Levalahti, K. Gill et al. 2009. Associations of 25 structural, degradative, and inflammatory candidate genes with lumbar disc desiccation, bulging, and height narrowing. *Arthritis and Rheumatism* 60(2):470–481.
39. Annunen, S., P. Paassilta, J. Lohiniva, M. Perala, T. Pihlajamaa, J. Karppinen et al. 1999. An allele of COL9A2 associated with intervertebral disc disease. *Science* 285(5426):409–412.
40. Boyd, L. M., W. J. Richardson, K. D. Allen, C. Flahiff, L. Jing, Y. Li et al. 2008. Early-onset degeneration of the intervertebral disc and vertebral end plate in mice deficient in type IX collagen. *Arthritis and Rheumatism* 58(1):164–171.
41. Matsui, Y., S. K. Mirza, J. J. Wu, B. Carter, C. Bellabarba, C. I. Shaffrey et al. 2004. The association of lumbar spondylolisthesis with collagen IX tryptophan alleles. *The Journal of Bone and Joint Surgery. British Volume* 86(7):1021–1026.
42. Noponen-Hietala, N., E. Kyllonen, M. Mannikko, E. Ilkko, J. Karppinen, J. Ott et al. 2003. Sequence variations in the collagen IX and XI genes are associated with degenerative lumbar spinal stenosis. *Annals of the Rheumatic Diseases* 62(12):1208–1214.
43. Adams, M. A., B. J. Freeman, H. P. Morrison, I. W. Nelson, and P. Dolan. 2000. Mechanical initiation of intervertebral disc degeneration. *Spine* 25(13):1625–1636.
44. Videman, T., M. Nurminen, and J. D. Troup. 1990. 1990 Volvo Award in Clinical Sciences. Lumbar spinal pathology in cadaveric material in relation to history of back pain, occupation, and physical loading. *Spine* 15(8):728–740.
45. Heliövaara, M. 1989. Risk factors for low back pain and sciatica. *Annals of Medicine* 21(4):257–264.
46. Kelsey, J. L. 1975. An epidemiological study of the relationship between occupations and acute herniated lumbar intervertebral discs. *International Journal of Epidemiology* 4(3):197–205.
47. Iatridis, J. C., J. J. MacLean, P. J. Roughley, and M. Alini. 2006. Effects of mechanical loading on intervertebral disc metabolism in vivo. *Journal of Bone and Joint Surgery. American Volume* 88 Suppl 2:41–46.
48. Lotz, J. C., A. H. Hsieh, A. L. Walsh, E. I. Palmer, and J. R. Chin. 2002. Mechanobiology of the intervertebral disc. *Biochemical Society Transactions* 30(Pt 6):853–858.
49. Choi, K. S., M. J. Cohn, and B. D. Harfe. 2008. Identification of nucleus pulposus precursor cells and notochordal remnants in the mouse: Implications for disk degeneration and chordoma formation. *Developmental Dynamics* 237(12):3953–3958.
50. Peacock, A. 1951. Observations on the prenatal development of the intervertebral disc in man. *Journal of Anatomy* 85(3):260–274.
51. Walmsley, R. 1953. The development and growth of the intervertebral disc. *Edinburgh Medical Journal* 60(8):341–364.
52. Hunter, C. J., J. R. Matyas, and N. A. Duncan. 2003. The three-dimensional architecture of the notochordal nucleus pulposus: Novel observations on cell structures in the canine intervertebral disc. *Journal of Anatomy* 202(Pt 3):279–291.
53. Trout, J. J., J. A. Buckwalter, K. C. Moore, and S. K. Landas. 1982. Ultrastructure of the human intervertebral disc. I. Changes in notochordal cells with age. *Tissue & Cell* 14(2):359–369.

54. Gotz, W., M. Kasper, G. Fischer, and R. Herken. 1995. Intermediate filament typing of the human embryonic and fetal notochord. *Cell and Tissue Research* 280(2):455–462.
55. Minogue, B. M., S. M. Richardson, L. A. Zeef, A. J. Freemont, and J. A. Hoyland. 2010. Characterization of the human nucleus pulposus cell phenotype and evaluation of novel marker gene expression to define adult stem cell differentiation. *Arthritis and Rheumatism* 62(12):3695–3705.
56. Hayes, A. J., M. Benjamin, and J. R. Ralphs. 1999. Role of actin stress fibres in the development of the intervertebral disc: Cytoskeletal control of extracellular matrix assembly. *Developmental Dynamics* 215(3):179–189.
57. Lehtonen, E., V. Stefanovic, and M. Saraga-Babic. 1995. Changes in the expression of intermediate filaments and desmoplakins during development of human notochord. *Differentiation* 59(1):43–49.
58. Butler, W. F. 1988. Comparative anatomy and development of the mammalian disc. In *The Biology of the Intervertebral Disc*, edited by P. Gosh, 84–108. Boca Raton, FL: CRC Press.
59. Hunter, C. J., J. R. Matyas, and N. A. Duncan. 2004. Cytomorphology of notochordal and chondrocytic cells from the nucleus pulposus: A species comparison. *Journal of Anatomy* 205(5):357–362.
60. Lee, C. R., D. Sakai, T. Nakai, K. Toyama, J. Mochida, M. Alini, and S. Grad. 2007. A phenotypic comparison of intervertebral disc and articular cartilage cells in the rat. *European Spine Journal* 16(12):2174–2185.
61. Sakai, D., T. Nakai, J. Mochida, M. Alini, and S. Grad. 2009. Differential phenotype of intervertebral disc cells: Microarray and immunohistochemical analysis of canine nucleus pulposus and anulus fibrosus. *Spine* 34(14):1448–1456.
62. Gilson, A., M. Dreger, and J. P. Urban. 2010. Differential expression level of cytokeratin 8 in cells of the bovine nucleus pulposus complicates the search for specific intervertebral disc cell markers. *Arthritis Research & Therapy* 12(1):R24.
63. Risbud, M. V., T. P. Schaer, and I. M. Shapiro. 2010. Toward an understanding of the role of notochordal cells in the adult intervertebral disc: From discord to accord. *Developmental Dynamics* 239(8):2141–2148.
64. Roberts, S., S. Ayad, and P. J. Menage. 1991. Immunolocalisation of type VI collagen in the intervertebral disc. *Annals of the Rheumatic Diseases* 50(11):787–791.
65. Trout, J. J., J. A. Buckwalter, and K. C. Moore. 1982. Ultrastructure of the human intervertebral disc: II. Cells of the nucleus pulposus. *The Anatomical Record* 204(4):307–314.
66. Cao, L., F. Guilak, and L. A. Setton. 2007. Three-dimensional morphology of the pericellular matrix of intervertebral disc cells in the rat. *Journal of Anatomy* 211(4):444–452.
67. Errington, R. J., K. Puustjarvi, I. R. White, S. Roberts, and J. P. Urban. 1998. Characterisation of cytoplasm-filled processes in cells of the intervertebral disc. *Journal of Anatomy* 192(Pt 3):369–378.
68. Guilak, F., H. P. Ting-Beall, A. E. Baer, W. R. Trickey, G. R. Erickson, and L. A. Setton. 1999. Viscoelastic properties of intervertebral disc cells. Identification of two biomechanically distinct cell populations. *Spine* 24(23):2475–2483.
69. Li, S., V. C. Duance, and E. J. Blain. 2008. Zonal variations in cytoskeletal element organization, mRNA and protein expression in the intervertebral disc. *Journal of Anatomy* 213(6):725–732.
70. Johnson, W. E., and S. Roberts. 2003. Human intervertebral disc cell morphology and cytoskeletal composition: A preliminary study of regional variations in health and disease. *Journal of Anatomy* 203(6):605–612.
71. Stosiek, P., M. Kasper, and U. Karsten. 1988. Expression of cytokeratin and vimentin in nucleus pulposus cells. *Differentiation* 39(1):78–81.
72. Brown, M. J., J. A. Hallam, E. Colucci-Guyon, and S. Shaw. 2001. Rigidity of circulating lymphocytes is primarily conferred by vimentin intermediate filaments. *The Journal of Immunology* 166(11):6640–6646.
73. Herrmann, H., H. Bar, L. Kreplak, S. V. Strelkov, and U. Aebi. 2007. Intermediate filaments: From cell architecture to nanomechanics. *Nature Reviews. Molecular Cell Biology* 8(7):562–573.

74. Benjamin, M., C. W. Archer, and J. R. Ralphs. 1994. Cytoskeleton of cartilage cells. *Microscopy Research and Technique* 28(5):372–377.
75. Eggli, P. S., E. B. Hunziker, and R. K. Schenk. 1988. Quantitation of structural features characterizing weight- and less-weight-bearing regions in articular cartilage: A stereological analysis of medial femoral condyles in young adult rabbits. *The Anatomical Record* 222(3):217–227.
76. Rufai, A., M. Benjamin, and J. R. Ralphs. 1995. The development of fibrocartilage in the rat intervertebral disc. *Anatomy and Embryology* 192(1):53–62.
77. Bruehlmann, S. B., J. B. Rattner, J. R. Matyas, and N. A. Duncan. 2002. Regional variations in the cellular matrix of the annulus fibrosus of the intervertebral disc. *Journal of Anatomy* 201(2):159–171.
78. Guilak, F., L. G. Alexopoulos, M. L. Upton, I. Youn, J. B. Choi, L. Cao et al. 2006. The pericellular matrix as a transducer of biomechanical and biochemical signals in articular cartilage. *Annals of the New York Academy of Sciences* 1068:498–512.
79. Eyre, D. R., Y. Matsui, and J. J. Wu. 2002. Collagen polymorphisms of the intervertebral disc. *Biochemical Society Transactions* 30(Pt 6):844–848.
80. Antoniou, J., T. Steffen, F. Nelson, N. Winterbottom, A. P. Hollander, R. A. Poole et al. 1996. The human lumbar intervertebral disc: Evidence for changes in the biosynthesis and denaturation of the extracellular matrix with growth, maturation, ageing, and degeneration. *Journal of Clinical Investigation* 98(4):996–1003.
81. Sztrolovics, R., M. Alini, P. J. Roughley, and J. S. Mort. 1997. Aggrecan degradation in human intervertebral disc and articular cartilage. *The Biochemical Journal* 326(Pt 1):235–241.
82. Hayes, A. J., M. Benjamin, and J. R. Ralphs. 2001. Extracellular matrix in development of the intervertebral disc. *Matrix Biology* 20(2):107–121.
83. Oegema, T. R., Jr., S. L. Johnson, D. J. Aguiar, and J. W. Ogilvie. 2000. Fibronectin and its fragments increase with degeneration in the human intervertebral disc. *Spine* 25(21):2742–2747.
84. Gilchrist, C. L., A. T. Francisco, G. E. Plopper, J. Chen, and L. A. Setton. 2011. Nucleus pulposus cell–matrix interactions with laminins. *European Cells & Materials* 21:523–532.
85. Youn, I., J. B. Choi, L. Cao, L. A. Setton, and F. Guilak. 2006. Zonal variations in the three-dimensional morphology of the chondron measured in situ using confocal microscopy. *Osteoarthritis and Cartilage* 14(9):889–897.
86. Alexopoulos, L. G., L. A. Setton, and F. Guilak. 2005. The biomechanical role of the chondrocyte pericellular matrix in articular cartilage. *Acta Biomaterialia* 1(3):317–325.
87. Choi, J. B., I. Youn, L. Cao, H. A. Leddy, C. L. Gilchrist, L. A. Setton et al. 2007. Zonal changes in the three-dimensional morphology of the chondron under compression: The relationship among cellular, pericellular, and extracellular deformation in articular cartilage. *Journal of Biomechanics* 40(12):2596–2603.
88. Hynes, R. O. 1992. Integrins: Versatility, modulation, and signaling in cell adhesion. *Cell* 69(1):11–25.
89. Schwartz, M. A. 2010. Integrins and extracellular matrix in mechanotransduction. *Cold Spring Harbor Perspectives in Biology* 2(12):a005066.
90. Tiger, C. F., F. Fougerousse, G. Grundstrom, T. Velling, and D. Gullberg. 2001. alpha11beta1 Integrin is a receptor for interstitial collagens involved in cell migration and collagen reorganization on mesenchymal nonmuscle cells. *Developmental Biology* 237(1):116–129.
91. Velling, T., J. Risteli, K. Wennerberg, D. F. Mosher, and S. Johansson. 2002. Polymerization of type I and III collagens is dependent on fibronectin and enhanced by integrins alpha 11beta 1 and alpha 2beta 1. *Journal of Biological Chemistry* 277(40):37377–37381.
92. Chen, J., W. Yan, and L. A. Setton. 2006. Molecular phenotypes of notochordal cells purified from immature nucleus pulposus. *European Spine Journal* 15(Suppl 3):S303–311.
93. Risbud, M. V., A. Guttapalli, T. J. Albert, and I. M. Shapiro. 2005. Hypoxia activates MAPK activity in rat nucleus pulposus cells: Regulation of integrin expression and cell survival. *Spine* 30(22):2503–2509.
94. Boos, N., S. Weissbach, H. Rohrbach, C. Weiler, K. F. Spratt, and A. G. Nerlich. 2002. Classification of age-related changes in lumbar intervertebral discs: 2002 Volvo Award in Basic Science. *Spine* 27(23):2631–2644.

95. Liebscher, T., M. Haefeli, K. Wuertz, A. G. Nerlich, and N. Boos. 2011. Age-related variation in cell density of human lumbar intervertebral disc. *Spine* 36(2):153–159.
96. Roberts, S., H. Evans, J. Trivedi, and J. Menage. 2006. Histology and pathology of the human intervertebral disc. *Journal of Bone and Joint Surgery. American Volume* 88 Suppl 2:10–14.
97. Hastreiter, D., R. M. Ozuna, and M. Spector. 2001. Regional variations in certain cellular characteristics in human lumbar intervertebral discs, including the presence of alpha-smooth muscle actin. *Journal of Orthopaedic Research* 19(4):597–604.
98. Johnson, W. E., S. M. Eisenstein, and S. Roberts. 2001. Cell cluster formation in degenerate lumbar intervertebral discs is associated with increased disc cell proliferation. *Connective Tissue Research* 42(3):197–207.
99. Johnson, W. E., H. Evans, J. Menage, S. M. Eisenstein, A. El Haj, and S. Roberts. 2001. Immunohistochemical detection of Schwann cells in innervated and vascularized human intervertebral discs. *Spine* 26(23):2550–2557.
100. Doita, M., T. Kanatani, T. Harada, and K. Mizuno. 1996. Immunohistologic study of the ruptured intervertebral disc of the lumbar spine. *Spine* 21(2):235–241.
101. Kawaguchi, S., T. Yamashita, K. Yokogushi, T. Murakami, O. Ohwada, and N. Sato. 2001. Immunophenotypic analysis of the inflammatory infiltrates in herniated intervertebral discs. *Spine* 26(11):1209–1214.
102. Nerlich, A. G., C. Weiler, J. Zipperer, M. Narozny, and N. Boos. 2002. Immunolocalization of phagocytic cells in normal and degenerated intervertebral discs. *Spine* 27(22):2484–2490.
103. Anderson, D. G., X. Li, and G. Balian. 2005. A fibronectin fragment alters the metabolism by rabbit intervertebral disc cells in vitro. *Spine* 30(11):1242–1246.
104. Xia, M., and Y. Zhu. 2011. Fibronectin fragment activation of ERK increasing integrin alpha and beta subunit expression to degenerate nucleus pulposus cells. *Journal of Orthopaedic Research* 29(4):556–561.
105. Anderson, D. G., X. Li, T. Tannoury, G. Beck, and G. Balian. 2003. A fibronectin fragment stimulates intervertebral disc degeneration in vivo. *Spine* 28(20):2338–2345.
106. Xia, M., and Y. Zhu. 2008. Expression of integrin subunits in the herniated intervertebral disc. *Connective Tissue Research* 49(6):464–469.
107. Bass, E. C., F. A. Ashford, M. R. Segal, and J. C. Lotz. 2004. Biaxial testing of human annulus fibrosus and its implications for a constitutive formulation. *Annals of Biomedical Engineering* 32(9):1231–1242.
108. Elliott, D. M., and L. A. Setton. 2001. Anisotropic and inhomogeneous tensile behavior of the human anulus fibrosus: Experimental measurement and material model predictions. *Journal of Biomechanical Engineering* 123(3):256–263.
109. O'Connell, G. D., H. L. Guerin, and D. M. Elliott. 2009. Theoretical and uniaxial experimental evaluation of human annulus fibrosus degeneration. *Journal of Biomechanical Engineering* 131(11):111007.
110. Skaggs, D. L., M. Weidenbaum, J. C. Iatridis, A. Ratcliffe, and V. C. Mow. 1994. Regional variation in tensile properties and biochemical composition of the human lumbar anulus fibrosus. *Spine* 19(12):1310–1319.
111. Best, B. A., F. Guilak, L. A. Setton, W. Zhu, F. Saed-Nejad, A. Ratcliffe et al. 1994. Compressive mechanical properties of the human anulus fibrosus and their relationship to biochemical composition. *Spine* 19(2):212–221.
112. Drost, M. R., P. Willems, H. Snijders, J. M. Huyghe, J. D. Janssen, and A. Huson. 1995. Confined compression of canine annulus fibrosus under chemical and mechanical loading. *Journal of Biomechanical Engineering* 117(4):390–396.
113. Gu, W. Y., X. G. Mao, B. A. Rawlins, J. C. Iatridis, R. J. Foster, D. N. Sun et al. 1999. Streaming potential of human lumbar anulus fibrosus is anisotropic and affected by disc degeneration. *Journal of Biomechanics* 32(11):1177–1182.
114. Houben, G. B., M. R. Drost, J. M. Huyghe, J. D. Janssen, and A. Huson. 1997. Nonhomogeneous permeability of canine anulus fibrosus. *Spine* 22(1):7–16.

115. Iatridis, J. C., L. A. Setton, R. J. Foster, B. A. Rawlins, M. Weidenbaum, and V. C. Mow. 1998. Degeneration affects the anisotropic and nonlinear behaviors of human anulus fibrosus in compression. *Journal of Biomechanics* 31(6):535–544.
116. Yao, H., M. A. Justiz, D. Flagler, and W. Y. Gu. 2002. Effects of swelling pressure and hydraulic permeability on dynamic compressive behavior of lumbar annulus fibrosus. *Annals of Biomedical Engineering* 30(10):1234–1241.
117. Gu, W. Y., X. G. Mao, R. J. Foster, M. Weidenbaum, V. C. Mow, and B. A. Rawlins. 1999. The anisotropic hydraulic permeability of human lumbar anulus fibrosus. Influence of age, degeneration, direction, and water content. *Spine* 24(23):2449–2455.
118. Gu, W. Y., and H. Yao. 2003. Effects of hydration and fixed charge density on fluid transport in charged hydrated soft tissues. *Annals of Biomedical Engineering* 31(10):1162–1170.
119. Huyghe, J. M., G. B. Houben, M. R. Drost, and C. C. van Donkelaar. 2003. An ionised/non-ionised dual porosity model of intervertebral disc tissue. *Biomechanics and Modeling in Mechanobiology* 2(1):3–19.
120. Iatridis, J. C., J. P. Laible, and M. H. Krag. 2003. Influence of fixed charge density magnitude and distribution on the intervertebral disc: Applications of a poroelastic and chemical electric (PEACE) model. *Journal of Biomechanical Engineering* 125(1):12–24.
121. Johannessen, W., and D. M. Elliott. 2005. Effects of degeneration on the biphasic material properties of human nucleus pulposus in confined compression. *Spine* 30(24):E724–729.
122. Iatridis, J. C., L. A. Setton, M. Weidenbaum, and V. C. Mow. 1997. Alterations in the mechanical behavior of the human lumbar nucleus pulposus with degeneration and aging. *Journal of Orthopaedic Research* 15(2):318–322.
123. Jones, W. R., H. P. Ting-Beall, G. M. Lee, S. S. Kelley, R. M. Hochmuth, and F. Guilak. 1999. Alterations in the Young's modulus and volumetric properties of chondrocytes isolated from normal and osteoarthritic human cartilage. *Journal of Biomechanics* 32(2):119–127.
124. Sato, M., D. P. Theret, L. T. Wheeler, N. Ohshima, and R. M. Nerem. 1990. Application of the micropipette technique to the measurement of cultured porcine aortic endothelial cell viscoelastic properties. *Journal of Biomechanical Engineering* 112(3):263–268.
125. Thoumine, O., and A. Ott. 1997. Time scale dependent viscoelastic and contractile regimes in fibroblasts probed by microplate manipulation. *Journal of Cell Science* 110(Pt 17):2109–2116.
126. Alexopoulos, L. G., M. A. Haider, T. P. Vail, and F. Guilak. 2003. Alterations in the mechanical properties of the human chondrocyte pericellular matrix with osteoarthritis. *Journal of Biomechanical Engineering* 125(3):323–333.
127. Darling, E. M., R. E. Wilusz, M. P. Bolognesi, S. Zauscher, and F. Guilak. 2010. Spatial mapping of the biomechanical properties of the pericellular matrix of articular cartilage measured in situ via atomic force microscopy. *Biophysical Journal* 98(12):2848–2856.
128. Cao, L., F. Guilak, and L. A. Setton. 2009. Pericellular matrix mechanics in the anulus fibrosus predicted by a three-dimensional finite element model and in situ morphology. *Cellular and Molecular Bioengineering* 2(3):306–319.
129. Cao, L., F. Guilak, and L. A. Setton. 2011. Three-dimensional finite element modeling of pericellular matrix and cell mechanics in the nucleus pulposus of the intervertebral disk based on in situ morphology. *Biomechanics and Modeling in Mechanobiology* 10(1):1–10.
130. Setton, L. A., and J. Chen. 2006. Mechanobiology of the intervertebral disc and relevance to disc degeneration. *Journal of Bone and Joint Surgery. American Volume* 88 Suppl 2:52–57.
131. Stokes, I. A. 1987. Surface strain on human intervertebral discs. *Journal of Orthopaedic Research* 5(3):348–355.
132. Meakin, J. R., and D. W. Hukins. 2000. Effect of removing the nucleus pulposus on the deformation of the annulus fibrosus during compression of the intervertebral disc. *Journal of Biomechanics* 33(5):575–580.
133. Seroussi, R. E., M. H. Krag, D. L. Muller, and M. H. Pope. 1989. Internal deformations of intact and denucleated human lumbar discs subjected to compression, flexion, and extension loads. *Journal of Orthopaedic Research* 7(1):122–131.

134. O'Connell, G. D., E. J. Vresilovic, and D. M. Elliott. 2011. Human intervertebral disc internal strain in compression: The effect of disc region, loading position, and degeneration. *Journal of Orthopaedic Research* 29(4):547–555.
135. O'Connell, G. D., N. R. Malhotra, E. J. Vresilovic, and D. M. Elliott. 2011. The effect of discectomy and the dependence on degeneration of human intervertebral disc strain in axial compression. *Spine* 36(21):1765–1771.
136. Bruehlmann, S. B., P. A. Hulme, and N. A. Duncan. 2004. In situ intercellular mechanics of the bovine outer annulus fibrosus subjected to biaxial strains. *Journal of Biomechanics* 37(2):223–231.
137. Bruehlmann, S. B., J. R. Matyas, and N. A. Duncan. 2004. ISSLS Prize Winner: Collagen fibril sliding governs cell mechanics in the anulus fibrosus: An in situ confocal microscopy study of bovine discs. *Spine* 29(23):2612–2620.
138. Desrochers, J., and N. A. Duncan. 2010. Strain transfer in the annulus fibrosus under applied flexion. *Journal of Biomechanics* 43(11):2141–2148.
139. Michalek, A. J., M. R. Buckley, L. J. Bonassar, I. Cohen, and J. C. Iatridis. 2009. Measurement of local strains in intervertebral disc anulus fibrosus tissue under dynamic shear: Contributions of matrix fiber orientation and elastin content. *Journal of Biomechanics* 42(14):2279–2285.
140. Upton, M. L., C. L. Gilchrist, F. Guilak, and L. A. Setton. 2008. Transfer of macroscale tissue strain to microscale cell regions in the deformed meniscus. *Biophysical Journal* 95(4):2116–2124.
141. Baer, A. E., T. A. Laursen, F. Guilak, and L. A. Setton. 2003. The micromechanical environment of intervertebral disc cells determined by a finite deformation, anisotropic, and biphasic finite element model. *Journal of Biomechanical Engineering* 125(1):1–11.
142. Baer, A. E., and L. A. Setton. 2000. The micromechanical environment of intervertebral disc cells: Effect of matrix anisotropy and cell geometry predicted by a linear model. *Journal of Biomechanical Engineering* 122(3):245–251.
143. Iatridis, J. C., S. Kumar, R. J. Foster, M. Weidenbaum, and V. C. Mow. 1999. Shear mechanical properties of human lumbar annulus fibrosus. *Journal of Orthopaedic Research* 17(5):732–737.
144. Fujita, Y., D. R. Wagner, A. A. Biviji, N. A. Duncan, and J. C. Lotz. 2000. Anisotropic shear behavior of the annulus fibrosus: Effect of harvest site and tissue prestrain. *Medical Engineering & Physics* 22(5):349–357.

4

A Multiscale Perspective on Structure, Mechanics, and Function of Skeletal Muscle

Silvia S. Blemker and Katherine R. Saul

CONTENTS

4.1 Introduction

Skeletal muscles are the motors for all voluntary movements of the body, from walking, to typing, to smiling. Although their functions are highly varied, all skeletal muscles have the same hierarchical structure (Figure 4.1). The fundamental force-generating unit of all skeletal muscles is the sarcomere, which combines the actions of myosin and actin motor proteins. Sarcomeres are arranged in series to form myofibrils. Myofibrils are arranged in parallel to form fibers (or muscle cells). Muscle fibers are encased in connective tissue called endomysium and are arranged in parallel to form fascicles. Muscle fascicles are encased in connective tissue called perimysium to form a whole muscle. Each muscle is encased in connective tissue called an epimysium and is attached to tendon. In the limb/joint systems, tendons transmit forces to bones, and several muscle-tendon units are arranged at each joint to generate torques to rotate joints and produce movement. In nonlimb systems (such as facial, speech, or eye muscles), muscle forces are transmitted via connective tissues and act to deform bodies to the appropriate configuration.

To produce such a variety of movements, each of the more than 650 skeletal muscles in the human body is tuned to perform a specific function. Over the last century, many researchers have observed that this tuning is achieved through structural variations in features at all levels of the above-described hierarchy, and all these variations affect muscle mechanics and function. For example, the molecular structure of the myosin head

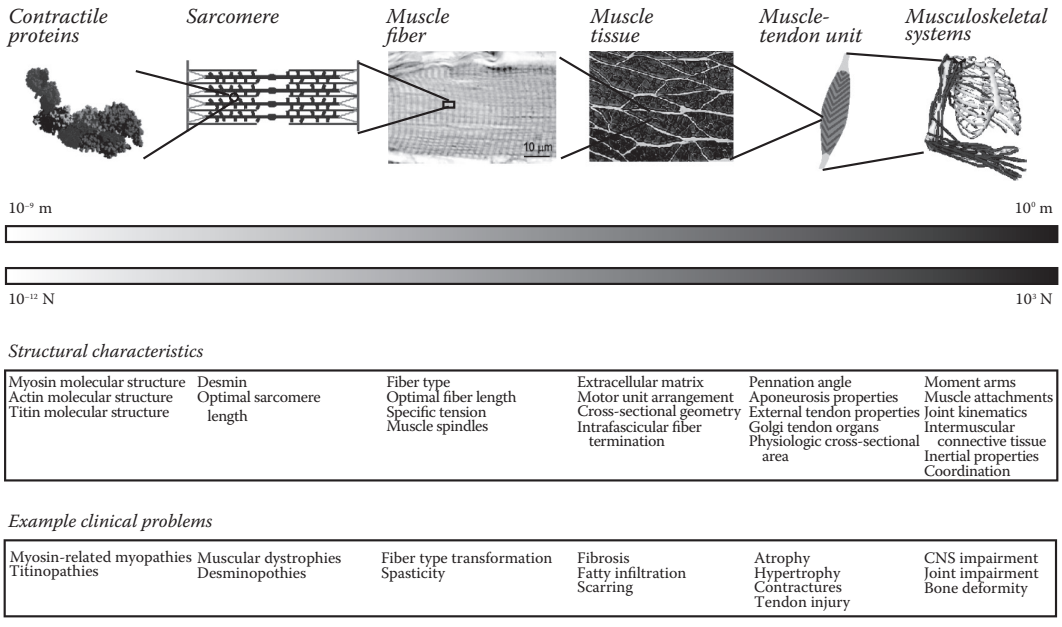

FIGURE 4.1
(See color insert.) Structure and function of muscle across several length scales. Muscle has a unique hierarchical structure that allows the actions of molecular motors that each generate pico-Newtons of force to be coordinated to generate up to 10^3 N of force in a whole muscle. Structural variations at each level of this hierarchy allow muscles to be tuned to their specific shape, size, and function. Similarly, muscle pathologies could arise at any level of this hierarchy and result in muscle dysfunction. ("Contractile proteins" image from Rayment, I., Rypniewski, W. R., Schmidt-Base, K., Smith, R., Tomchick, D. R., Benning, M. M. et al. 1993. Three-dimensional structure of myosin subfragment-1: A molecular motor. *Science* 261(5117):50–58. Reprinted with permission of AAAS. "Muscle tissue" image reprinted from *J. Biomech.*, 43, 16, Sharafi, B. and Blemker, S. S., A micromechanical model of skeletal muscle to explore the effects of fiber and fascicle geometry, 3207–3213, Copyright 2010, with permission from Elsevier. "Musculoskeletal system" image reprinted with kind permission from Springer Science+Business Media: *Ann. Biomed. Eng.*, A model of the upper extremity for simulating musculoskeletal surgery and analyzing neuromuscular control, 33, 6, 2005, 829–840, Holzbaur, K. R., Murray, W. M., Delp, S. L.)

affects the speed at which a sarcomere can contract. The structure of the giant molecule called "titin" affects the passive properties of sarcomeres. The lengths and geometric arrangement of fibers influence the muscle's force-generating capacity. The connective tissues within muscle affect the muscle force transmission to tendons. The morphology and properties of tendons influence the dynamics of muscle behavior during movement. The discoveries of these relationships have aided in the understanding and appreciation of the complex function of muscles, and they have provided scientific underpinnings to the management and treatment of a variety of neuromuscular and musculoskeletal disorders.

The goals of this chapter are to (1) provide an overview of the mechanics and structure of muscle, (2) summarize the most recent understanding on structure–function relationships at all levels of the muscle hierarchy, (3) describe example diseases and clinical problems that are exhibited at each hierarchical level, and (4) point to future research that will help integrate knowledge and discoveries at all hierarchical levels. This chapter is arranged in subsections, each of which corresponds to a hierarchical level in muscle.

4.2 Hierarchical Structure of Muscle

4.2.1 Contractile and Noncontractile Proteins

The fundamental motor that produces muscle contraction is a protein, or "molecular motor," called myosin II (Figure 4.2). Each myosin II molecule has two arms (also called

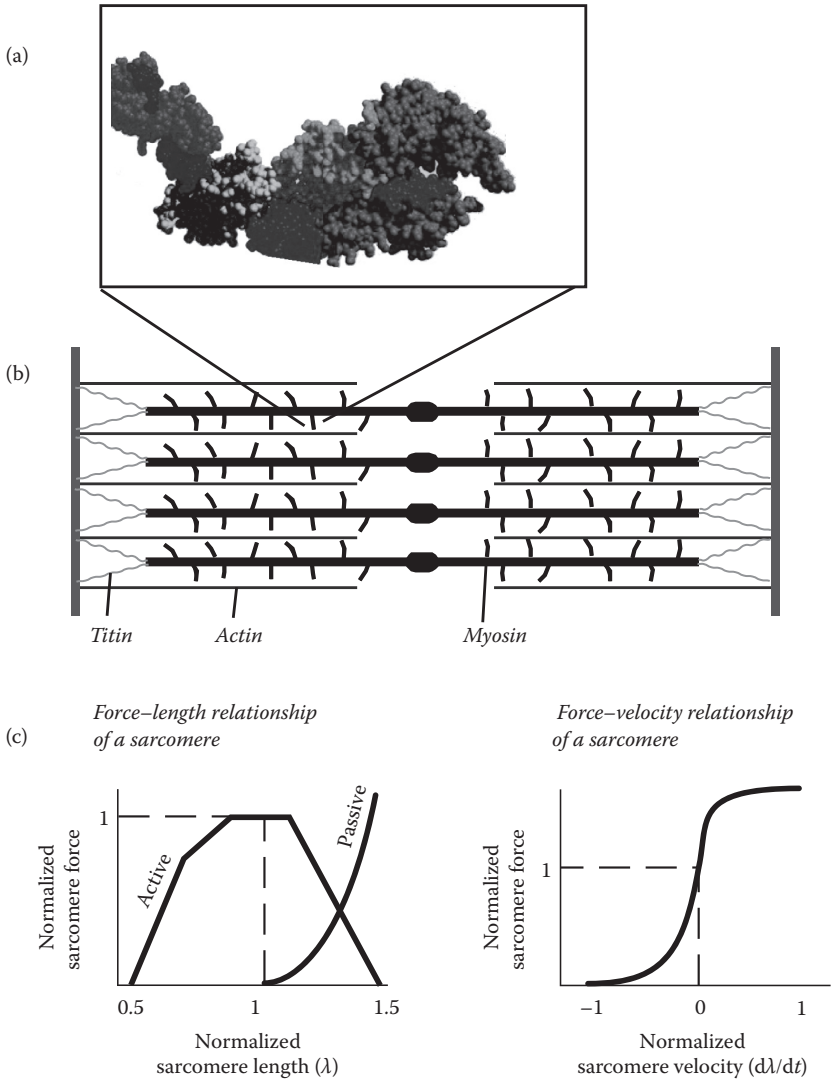

FIGURE 4.2
(See color insert.) Molecular motors and the sarcomere. The action of myosin (a) provides force production within a muscle, and the sarcomere (b) is the fundamental structural unit of a muscle cell. Sarcomeres exhibit a force–length behavior (c) that is a result of changes in overlap between actin and myosin as the proteins slide past each other. Sarcomeres exhibit a force–velocity behavior (c) that is a result of the speed at which myosin motors can attach and reattach to actin. (Part (a) reprinted from Rayment, I., Rypniewski, W. R., Schmidt-Base, K., Smith, R., Tomchick, D. R., Benning, M. M. et al. 1993. Three-dimensional structure of myosin subfragment-1: A molecular motor. *Science* 261(5117):50–58. Reprinted with permission of AAAS.)

"heavy chains"), which are roughly 2000 amino acids long.[1] Each heavy chain consists of two domains: a head and a tail. The head domain is the region of the protein that interacts with actin to produce force, whereas the tail is the region that provides the anchor. The tails have a coiled-coil structure that holds the two heavy chains together, such that each myosin has a strong tail that anchors two heads. Each of the heads also has an intermediate neck domain at the interface between the heads and the tails. This neck domain serves effectively as a "joint" about which the head can rotate and undergo a power stroke to generate force.

Myosin generates force by attaching to the thin filament, undergoing a power stroke, detaching from actin, then reattaching, and so on. Thin filaments are long coiled strands primarily made up of the protein actin. The thin filaments have specific myosin binding sites. When muscles are relaxed, these binding sites are blocked by tropomyosin, but when the muscle contracts, these binding sites are unblocked (regulated by calcium), which opens up this site and allows myosin to bind to actin. A common method to assess the contractile behavior of myosins is an "*in vitro* motility" assay,[2] in which myosin tails are bound to a flat underlying substrate, with their heads pointing upward and allowed to move. When actin filaments are placed in the medium (also in the presence of adenosine triphosphate (ATP) and calcium), the myosins interact with the actin filaments, causing the actin filaments to move around on the substrate. By measuring the displacement and velocity of the actin filaments, one can characterize the contractile properties of myosin.

In vitro motility assays demonstrate that myosin has a characteristic speed, which is determined by the rate at which myosins can attach to actin, hydrolyze ATP, undergo a conformational change, and detach from actin. This means that there is a maximum velocity at which myosin can slide past actin while still generating force. This maximum velocity is determined by the structure of the myosin molecule itself and has a profound effect on the overall function of muscle. This effect is called the muscle force–velocity property, a phenomenon that was first observed by Hill[3] in isolated muscle preparations. Hill observed that the amount of active force generated by a muscle was related to the velocity of muscle shortening, and as shortening velocity increases, force decreases hyperbolically. The velocity of shortening of the muscle when it is resisted by no load is called the "maximum contraction velocity" (V_{max}); this is equivalent to the experiment described above for the *in vitro* motility assay.

There are variations, or isoforms, in the myosin protein structure, which result in differences in the velocity characteristics of the myosin IIs. These isoforms vary in how ATP is hydrolyzed, which ultimately affects the attachment and detachment rate of the myosin molecule. This is functionally significant because it affects a muscle fiber's V_{max}, force, and power production. As an aside, although myosin is perhaps the most conventional or commonly known contractile protein, there are myosins and other molecular motors (other myosins, kinesins, and dyneins) throughout the body, which perform a vast number of functions ranging from vesicle transport to cell division.[4] The commonality of these molecular motors is that they all convert chemical energy into mechanical movement by hydrolyzing ATP, move unidirectionally along tracks of protein polymers (actin or microtubules), and progress in discrete steps along a track.

Although the *in vitro* motility assay provides the ability to measure the speed of contraction, it does not provide a measure of the force generated by myosin molecules; thus, it can measure only V_{max} and not the behavior of myosin when resisted by a load. The need to study myosin forces led muscle biochemists to begin using optical tweezers to study the force-generating behavior of myosin II.[5] Optical tweezers use a highly focused laser beam to provide a force to physically hold and move microscopic dielectric objects.

These systems are capable of applying forces in the pico-Newton (pN) range and measuring displacements in the nanometer range. Based on these measurements, investigators have determined that one double-headed myosin is capable of generating roughly 1.4 pN of force.[6] So, considering that some large muscles generate more than 1000 N of force, this means that there are roughly 10^{15} (a "quadrillion") myosins acting effectively in parallel to generate that maximum level of force. Thus, it seems necessary that muscle would have a specialized hierarchical arrangement such that the actions of all these molecular motors can be coordinated.

There are several other noncontractile proteins that are involved in the regulation of muscle contraction. These will be discussed in the next section on the sarcomere. However, it is important to point out one other major protein called titin.[7,8] This is the largest protein in the body; it is 35,000 amino acid units long, with a molecular weight of more than 3 MDa. Titin's chemical name is also large; it is the longest word in the English language with more than 189,000 letters. Titin is composed of 244 domains connected by peptides, and the unfolding and folding of these domains provide the passive elasticity in skeletal muscle. There are also titin isoforms; different structures of titin are found in different muscles of the body, suggesting that passive elasticity in muscle may be regulated by titin's molecular structure.

4.2.2 The Sarcomere

The fundamental force-producing structure within a skeletal muscle is the sarcomere. Because there are roughly 10,000 myosin molecules in a sarcomere, these proteins need to be arranged in a regular and specialized manner to allow myosin to interact efficiently with actin, direct the force in myosin in a specific direction, allow for shortening and lengthening, and preserve the structural integrity of the system. The sarcomere structure provides all these features (Figure 4.2). The sarcomere arranges thin and thick filaments such that they are able to slide past each other. The thick filament is composed of the myosin molecules, with the tails of all the myosins coiled together to form a thick filament backbone from which the heads emanate. The thin filament is composed of actin, tropomyosin, and troponin, providing binding sites for myosin roughly every 30 nm. The thick and thin filaments form a hexagonal array, allowing each thick filament to interact with six thin filaments. The *z*-disk separates sarcomeres serially. Several important proteins provide the structural integrity of the *z*-disk, including the desmin protein.

The sliding filament theory—first proposed by Gordon et al.[9]—provides an understanding of how the arrangements of actin and myosin filaments influence the length–tension relationship of muscle. As the thick and thin filaments slide past each other, the amount of overlap of myosin heads with actin varies, which influences the force-generating ability of the sarcomere. There is a range of lengths over which maximum overlap between actin and myosin heads within a sarcomere is achieved; this length is often referred to as the "optimal sarcomere" length, which is roughly 2.7 μm in mammalian muscle.[10] This length varies slightly across vertebrates but mostly is within the 2.2 to 2.7 μm range. Based on the sliding filament theory, the optimal sarcomere length can be calculated from the dimensions of the thick and thin filaments.[11] The sarcomere is capable of generating maximum isometric force at this optimal sarcomere length. When the sarcomeres are shorter, active isometric force decreases due to interference and loss of overlap between actin and myosin. At longer lengths, active isometric force also decreases due to less overlap between actin and myosin. Beyond the optimal sarcomere length, passive resistance in the sarcomere increases due to stretching in titin and in other proteins. One note of caution: the

sliding filament theory provides an explanation of the dependence of isometric force on length, but it does not completely capture the force behavior of a sarcomere when it is stretched dynamically.

The specialized structures and arrangements of the sarcomeric proteins allow concerted and effective muscle force generation. As such, disruption of the structure of these proteins through genetic disorders therefore disrupts sarcomere function. Several muscle diseases are a result of genetic mutations or deletions in the genes that encode sarcomeric proteins, including myosin,[11] actin,[12] titin,[13] and desmin proteins.[14] These diseases manifest in major muscle dysfunction, weakness, and progressive wasting.

4.2.3 The Fiber

The fundamental biological unit of muscle is the fiber, which is equivalent to a muscle cell. These are unique cells in that they can be on the order of tens of centimeters long. As such, they are multinucleated cells. The fiber includes all the basic cellular machinery, including the sarcolemma, or the specialized cell membrane of muscle fibers that dips into the interior of the cell to form a t-tubule system of membranous fingers into the cytoplasm. These t-tubule extensions of the sarcolemma extend between myofibrils along the entire length of the fiber. The machinery also includes the sarcoplasmic reticulum (SR), an organelle network of tubules and cisternae, including the terminal cisterna that stores calcium and is located adjacent to the t-tubule system. The muscle cell has important features that provide the ability to receive signals from the central nervous system (CNS) and to quickly react to those signals. Each fiber has a neuromuscular junction, which provides an interface with the CNS. An excitatory signal from the CNS results in a transfer of acetylcholine across the neuromuscular junction, which acts to depolarize the cell. Because the cells are so long, it is important that the depolarization propagates quickly across the entire length; this propagation is made possible by the t-tubule system that extends along the length of the fiber. As the entire cell depolarizes via the t-tubule system, the terminal cisternae release calcium, which initiates the contraction process. Then, as described above, calcium binds to troponin, which changes the conformation of tropomyosin, exposing the binding site on actin and allowing myosin to bind to actin and generate force. When the excitatory signal from the CNS is terminated, the process of reuptake of calcium begins. This process is generally slower than the release process because it requires active ion-pumping channels in the SR to bring the calcium back into the SR.

Fibers are on the order of 50 μm in diameter, and thus, they contain roughly 10^3 myofibrils in parallel. In human limb muscles, each myofibril can have roughly 10^4 sarcomeres in series; thus, each fiber has roughly 10^7 total sarcomeres. It is quite tempting—and thus common practice—to simply scale up the sliding filament theory, along with the force–velocity relation, to predict the force–length–velocity property of a fiber, assuming that all the sarcomeres within a fiber behave uniformly. Impressively, this does work for many situations. However, there are some complexities in sarcomere behavior that should be considered. This is particularly relevant for the descending limb of the length–tension curve, in which the isometric behavior can be considered to be unstable (i.e., a negative slope of the length–tension relationship). When myofibrils lengthen beyond the plateau of the force–length curve, some weak sarcomeres may "pop" to a long length, whereas other sarcomeres shorten.[15] This "popping sarcomere hypothesis" describes behaviors such as force enhancement after stretch and strain injury during lengthening contractions. The study of nonuniform behaviors of sarcomeres remains a current and highly debated topic in the literature.

The concept of "specific tension" is introduced at the fiber level. This value defines the maximum isometric force per unit area of the fiber. Using specific tension as a parameter of interest allows one to compare the force-generating characteristics across fibers that have different diameters and cross-sectional areas. Theoretically, specific tension can be determined from the force generated in each myosin head, the number of myosin heads that are acting within each sarcomere, the number of sarcomeres that are in parallel within the fiber, and the area of the fiber. One might think of this as an intrinsic property of muscle fibers, and so it should be constant across all fibers. However, there are some structural variations that may increase or decrease specific tension, including myosin isoform and sarcomere lattice (i.e., arrangements of myosin and actin filaments). Different lattice arrangements of myosin and actin can result in different densities of contractile proteins. Indeed, specific tension measurements are variable across the literature; however, it is not clear how much of that variability is due to differences in the intrinsic fiber properties and how much is simply due to differences in experimental approach. This issue also comes up when considering the larger scales, because when specific tension is estimated based on measurements at the whole muscle and whole joint levels, the values do not align with those measured at the fiber level.

The number of sarcomeres in series of a given fiber will affect the range over which this muscle can generate force, both in terms of length and velocity. In this regard, it is useful to define something called the "optimal fiber length," which is equal to the number of sarcomeres multiplied by the optimal sarcomere length. The optimal fiber length is the length at which the sarcomeres within that fiber generate maximum force, that is, when the fiber generates maximum force. Another consequence of longer fibers is a larger range of lengths over which the fiber can generate force. Similarly, longer-fibered muscles have higher maximum contraction velocities. As such, when reporting the V_{max} for a particular muscle, this value is commonly defined in terms of optimal fiber lengths per second.

Fibers all have a particular "type" that affects this contraction velocity. The most common ways of referring to the primary fiber types are as "slow twitch" and "fast twitch." Slow twitch fibers have slower myosin isoforms, whereas fast twitch fibers have faster myosin isoforms. The V_{max} of fast fibers is roughly three times greater than that of slow fibers. The speed of the fibers, however, is not the only distinguishing factor among fibers. Another important factor is the manner in which the cell creates ATP—either aerobically or anaerobically. Fibers that create ATP aerobically (i.e., using oxidative metabolism) are more resistant to fatigue, whereas fibers that create ATP anaerobically (i.e., using anaerobic metabolism) fatigue very easily. Generally, fast fibers are "fatigable," whereas slow fibers are more "fatigue resistant," but there are many fibers that exhibit characteristics between these two extremes. The three most commonly found fiber types include "type I" (slow, fatigue resistant), "type IIb" (fast, fatigable), and "type IIa" (moderately fast, moderately fatigue resistant). However, there are a variety of fiber types that are found in human muscle, and more than one characteristic is used to distinguish them.

It is important to note that the fiber membrane (or cell membrane) is an important structure that provides the mechanical connection between the muscle fiber and the surrounding extracellular matrix.[16] The membrane is composed of many important proteins, for example, the dystroglycan complex. Mechanically, this complex links the sarcomeric proteins to the extracellular matrix, which is thought to protect fibers and the membrane from contraction-induced injury.[17–19] The proteins associated with the membrane are also involved in cell signaling and control of the permeability of the membrane. Genetic disorders that involve mutations in these cell membrane proteins—for example, Duchenne muscular dystrophy (which involves mutations in the genes that encode dystrophin)—result in

significant muscle pathology, susceptibility to contraction-induced injury, and progressive muscle wasting.[20]

4.2.4 Muscle Tissue

Individual muscle fibers are organized into bundles, called fascicles (Figure 4.3). Fascicles are composed of muscle fibers, as well as extracellular matrix proteins secreted by the muscle fibers. Extracellular matrix includes proteoglycans, collagens, and glycoproteins, which make up the endomysium and perimysium sheaths that surround the fibers and fascicles, respectively. Collagen types I and III are the predominant types within skeletal muscle and contribute to the tensile integrity of muscle tissue matrix. Proteoglycans are negatively charged compounds formed from a core protein with attached glycosaminoglycans, with several varieties common to muscle extracellular matrix (including chondroitin sulfate, dermatan sulfate, and keratin sulfate).[21] The extracellular matrix plays a role in cell signal transduction, ultimately contributing to the regulation of matrix organization, growth factor activity, and cell growth and differentiation. For example, the degree of collagen cross-linking affects the mechanical properties of muscle in response to tensile loading. Studies in mice have demonstrated that the proteoglycan decorin, which binds to collagen, plays a critical role in the formation and organization of the collagen matrix.[22] Other studies have shown that heparan sulfate proteoglycans are necessary for fibroblast growth factor activity and thus proper skeletal muscle development.[23]

Muscles are innervated by α and γ motor neurons. α motor neurons innervate extrafusal muscle fibers and are primarily responsible for muscle contraction, whereas γ motor neurons innervate the intrafusal muscle fibers found within length-sensitive sensory organs in muscles called muscle spindles. An individual muscle is innervated by many α motor neurons. Each α motor neuron from the ventral horn of the spinal cord innervates multiple

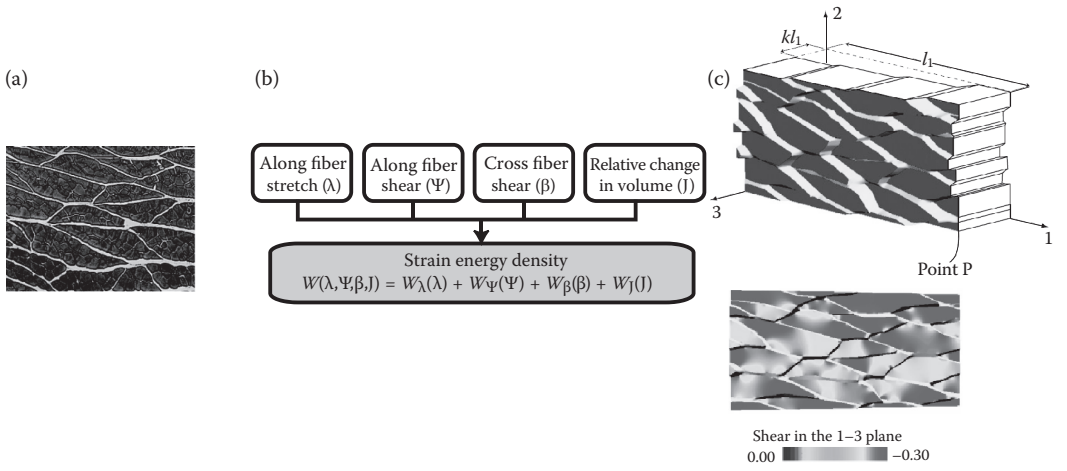

FIGURE 4.3
(See color insert.) Muscle tissue structure. Muscle fibers are arranged within fascicles and surrounded by intramuscular connective tissue (a). Recent advances in micromechanical modeling (b, c) have allowed the exploration of how the morphological properties of fibers and connective tissues affect tissue-level mechanics of muscle. (Parts (a) and (c) reprinted from *J. Biomech*., 43, 16, Sharafi, B. and Blemker, S. S., A micromechanical model of skeletal muscle to explore the effects of fiber and fascicle geometry, 3207–3213, Copyright 2010, with permission from Elsevier.)

muscle fibers distributed throughout the muscle, activating all associated muscle fibers simultaneously. A neuron and its associated muscle fibers are referred to as a "motor unit." Each motor unit is composed of muscle fibers of the same metabolic type (type I, IIa, or IIb). The number of muscle fibers innervated by a single nerve varies according to its function and metabolic type and is referred to as the innervation ratio. This ratio varies from ten to thousands of fibers per motor unit across different types of muscles. In general, small motor units innervating fewer muscle fibers are composed of smaller-diameter, slow twitch (type I) fibers. In contrast, larger motor units may be composed of many larger-diameter, fast twitch (type IIa or IIb) fibers capable of generating high forces.

Modulation of muscle force by the nervous system is primarily achieved by controlling the number of muscle fibers that are activated at once by recruiting the motor units within the muscle. With an orderly recruitment of motor units, force output can be precisely controlled and fatigue can be reduced. Orderly recruitment is also known as Henneman's size principle.[24] Small motor units are recruited first, providing small increments of force control and fatigue resistance. As larger forces are required, larger motor units that provide high forces with reduced fatigue resistance are recruited. In contrast to the physiological recruitment of muscle motor units, externally applied electrical stimulation, which may be used therapeutically, recruits motor units in a manner opposite to orderly recruitment—recruiting large motor units first. Recent experiments have demonstrated that orderly recruitment can be achieved using optical control to activate motor neurons that have had light-activatable proteins inserted, as indicated by several measures of motor unit recruitment.[25]

Muscle composition and function at the tissue level can be altered by injury or disease. Damage to the motor neurons innervating the muscle tissue can affect the organization and composition of the extracellular matrix and muscle motor proteins. Direct injury to the neural system at the spinal cord (e.g., spinal cord injury) or peripheral nerves (e.g., brachial plexus palsy), as well as altered nerve signals due to conditions such as stroke, cerebral palsy, or traumatic brain injury, can result in a loss of motor drive to the muscles.[26] In response to a loss of motor drive, atrophy—or an overall loss of muscle mass—is seen as a result of the catabolism of the fibrils within the muscle fibers. With time, degenerative changes to the muscle fibers and fascicles are seen, with muscle being replaced by fibrous and fatty tissues. This process is variously known as fibrofatty infiltration or fatty atrophy. Degenerative changes at this stage, which may occur over several months or years of denervation, are typically not reversible even if innervation to the muscle is restored.

4.2.5 Muscle-Tendon Unit

Muscle tissue does not produce force in isolation; rather, it transmits force to the skeletal system through a tendon, a connective tissue composed largely of parallel collagen fibers. Tendon is approximately 86% collagen (primarily type I) by dry mass, with the remainder being elastin, proteoglycans, and inorganic compounds. As in muscle, proteoglycans contribute to the formation of links among collagen fibrils and maintain space among fibrils to withstand deformation. The way in which muscle and tendon are arranged in a single muscle-tendon unit plays an important role in the force produced and differs across muscles in the body with different functions. The specific arrangement of muscle fascicles and internal tendons is referred to as muscle architecture (Figure 4.4).

Several parameters can be used to describe the architecture of a muscle-tendon unit. Typically, these include the optimal fiber length of muscle fascicles within the muscle, the physiological cross-sectional area (PCSA) of the whole muscle, the angle of the

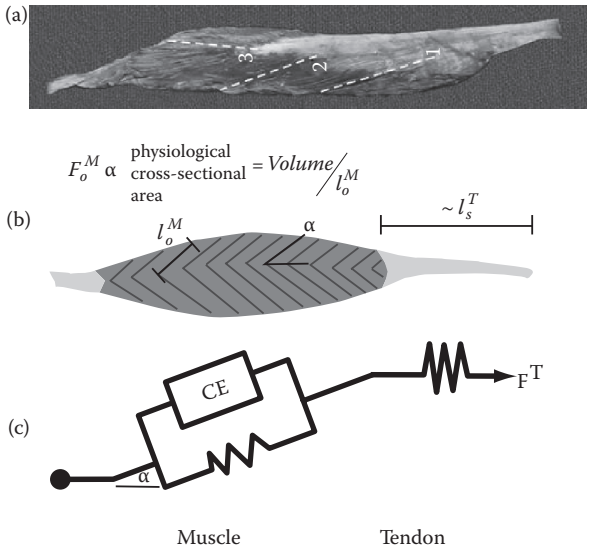

FIGURE 4.4
Muscle-tendon architecture. The arrangements of fascicles and tendons within muscle influence the force-generating capacity of muscles. (a) Architectural measurements on cadaveric muscle provide measurements of pennation angle, muscle length, and muscle volume. (b) Conceptual illustrations of muscle explain how these parameters determine fascicle arrangements. (c) Lumped-parameter models of muscle include elements for the contractile element (CE), the passive muscle properties, and the in-series tendon elasticity. (Part (a) adapted with kind permission from Springer Science+Business Media: *Clin. Orthop. Rel. Res.*, Are current measurements of lower extremity muscle architecture accurate?, 467, 4, 2008, 1074–1082, Ward, S. R., Eng, C. M., Smallwood, L. H., Lieber, R. L.)

muscle fascicles relative to the line of action of the muscle, and the length of the external and internal tendons attached to the muscle tissue. As described previously, the force a muscle produces depends on the length of the sarcomeres and the overlap of the actin and myosin proteins. When expanded to the level of the whole muscle, the force a muscle produces depends, in part, on the length of the fascicles that compose the muscle, specifically, the number of sarcomeres in series within muscle fascicles, and the length of those sarcomeres. Optimal fiber length is the length of the fiber for which the sarcomeres are at optimal sarcomere length. For a given muscle, this value can be determined through fascicle dissection and microscopic or laser diffraction to evaluate sarcomere length.

Force developed by a muscle-tendon unit also depends on the number of muscle fibers that can produce force in parallel. The peak isometric fiber force is related to the PCSA of an individual muscle-tendon unit:

$$F_o^{\text{fiber}} = \text{PCSA} \cdot \sigma_o^{\text{fiber}}. \tag{4.1}$$

PCSA refers to the cross section of muscle taken perpendicularly to the muscle fibers when the fibers are at optimal fiber length. This value can be determined by measuring the volume of a muscle via water displacement, scale, or medical imaging and dividing by the optimal fiber length of a muscle. The peak stress, or specific tension σ_o^{fiber} of muscle, is the isometric force per area produced by muscle fibers at optimal length and

full activation. Specific tension has been measured experimentally using single fibers obtained from animal models as well as calculated based on *in vivo* measurements of muscle cross section and joint torques in humans. Reported values range from ~15 to 60 N/cm^2.[27–32]

Fascicles within a muscle can be arranged in different ways. In some muscles, fascicles are arranged parallel to each other and to the tendon. In others, the fascicles are at an angle to the tendon. The pennation angle α refers to the angle between the muscle fascicles and the line of action of the tendon. Pennate fascicle arrangements can take many different forms. Some muscles have a fanned arrangement of fascicles, whereas others may have a feathered (or bipennate) organization. Pennate muscles typically feature an internal tendon, or aponeurosis, to which the angled fascicles can attach. The angle of pennation alters the force transmitted to the tendon by the muscle fascicles. Only the component of muscle force that is parallel to the line of action of the tendon is considered to be transferred to the tendon. Thus, the force in the tendon may be calculated as

$$F^{\text{tendon}} = F^{\text{fascicle}} \cdot \cos\alpha = \text{PCSA} \cdot \sigma^{\text{fascicle}} \cdot \cos\alpha. \tag{4.2}$$

The length of the tendon or the aponeurosis in a muscle-tendon unit also affects the force that is produced. Consider an isometric contraction of a muscle-tendon unit. When a muscle contracts, the tendon that is in series with the muscle stretches in response to the tension imposed on it, even as the total muscle-tendon length remains constant. The stretch in the tendon will result in an overall shortening of the muscle fascicles. Due to the force–length property of muscle, this change in length of muscle naturally affects the force produced. If this stretch in the tendon is not considered, then the force attributed to muscle at a given length will not be correctly ascertained. For muscles with very short tendons, this effect may be small, but for muscles with very long tendons, the stretch in the tendon may be significant. The length of the tendon at which it just begins to develop force when stretched, known as the tendon slack length, is a common way of representing the amount of tendon in a muscle-tendon unit. Strain is defined relative to tendon slack length. The strain in a tendon for a given force is typically assumed to be 3.3% when the muscle is generating optimal muscle force, with an associated stress of 32 MPa,[33] based on experimental measures of tendon stiffness.[34,35]

Representative muscle architectural parameters have been determined for many human muscle-tendon units. Largely, these parameters have been determined from cadaveric experiments in which lengths and volumes of muscle and tendon are directly measured.[36–39] However, muscles change in size and composition with age,[40,41] fixation of cadaveric muscle can alter muscle volume,[42] and architectural parameters vary among individuals. Thus, there have been efforts to characterize these values *in vivo*. Magnetic resonance imaging is one widely used approach for assessing muscle volumes and lengths noninvasively.[43–45] Ultrasound imaging can be used to characterize pennation angle, muscle length, and volume.[46,47] Although sarcomere length and, ultimately, optimal muscle fascicle length can be difficult to measure *in vivo*, these lengths have been assessed intraoperatively during clinical surgical interventions.[48] In addition, recent advances in optical microendoscopy assessment have demonstrated that sarcomere lengths can be measured during active shortening and lengthening of muscle.[49]

Mathematical models that capture the force-generating implications of different architectural arrangements of muscle fascicles and tendon have been developed. The Hill-type muscle model, based on a collection of seminal works by Hill, captures the force–length and force–velocity properties of muscle via contractile and parallel

elastic components. Modern descriptions of this model approach typically represent the mechanical properties of muscle and tendon using dimensionless curves that are generic to all muscle-tendon units, and then scale them to specific muscle-tendon units using peak isometric force (proportional to PCSA), optimal fiber length, pennation angle, and tendon slack length as scaling parameters.[33] Hill-type models are powerful and capture many of the features of muscle-tendon units that are important to understanding force-generating behavior. However, it does have limitations with regard to some properties that are not included, such as the history-dependent behavior of muscle and interactions among units. In addition, Hill-type models simplify the complex arrangement of fascicles and aponeurosis to pennation angle and tendon slack length. More complex models are needed to understand the role that the three-dimensional arrangements of fascicles and aponeurosis may have on the inhomogeneities of stress and strain within a muscle. To that end, finite-element modeling of muscle-tendon units that seek to represent this complex muscle-tendon architecture has been developed to explore this interplay.[50–52]

The muscle-tendon unit contains proprioceptive sensory receptors that detect the force being generated and participate in the reflex control of the musculoskeletal system. Golgi tendon organs are composed of a collagen network that connects to muscle fibers at one end and terminates in the tendon. Afferent type Ib sensory nerves are integrated into the collagen network and detect force through the compression of the sensory fiber. Golgi tendon organs generate an inhibitory reflex signal to the muscle when high forces are detected. Inhibitory signals are also received by agonists (muscles that have the same action), whereas excitatory signals are received by antagonists (muscles with opposite actions).

There are several clinical concerns that could present themselves at the level of the muscle-tendon unit. Similar to the tissue level, neuromuscular impairment or altered neural signals to the muscle-tendon unit can result in changes to the structure of the muscle. Specifically, disuse or reduced neural excitation can result in atrophy or lessening of muscle volume. In contrast, increased neural signal or increased use, due to exercise for example, can result in hypertrophy or increased muscle volume through the addition of myofibrils. Neuromuscular disorders, such as stroke, spinal cord injury, or cerebral palsy, can also be associated with changes in muscle length. Contractures, or overall shortening of the muscle that prevents the full range of motions in the joints, could be observed, implying a loss of sarcomeres in series and a reduction in optimal fiber length. Also, tearing or complete rupture of the tendon may occur, causing pain and impairing force transmission of the muscle-tendon unit to the bone. Degeneration of the mechanical properties of the tendons is thought to occur with age,[53,54] leading to increased incidence of rupture.[55] Traumatic injuries to the tendons can also occur and result in tears or ruptures. Tendon injuries may be allowed to heal without intervention or could be repaired surgically. Clinical interventions can also occur at the level of the muscle-tendon unit. For example, muscle-tendon contractures may be treated by surgically lengthening the tendon to reduce the passive force of the overall muscle-tendon unit.

4.3 Musculoskeletal Systems

Muscle-tendon units do not act in isolation, but instead act in concert within the musculoskeletal system. The specific configuration of a muscle-tendon unit relative to the

underlying bones and joints plays an important role in the function of the muscle at a joint. The distance of a muscle-tendon unit from the center of rotation of a joint that it crosses contributes to the amount of moment that that unit can generate at that joint. This distance can be characterized by the moment arm of the muscle, which can be quantified in a number of ways. Most simply, the moment arm of a muscle is the perpendicular distance from the line of action of the muscle to the center of rotation of the joint for a given degree of freedom. However, given the complexity of some joint movements and nonlinear muscle paths, a muscle's moment arm can vary with joint posture and can be difficult to assess in such a simple way. Therefore, other methods have been used to characterize muscle moment arms mathematically. A commonly used method is the partial velocity method,[56] derived from the principle of virtual work, in which the moment arm can be calculated for a particular degree of freedom using

$$r = \partial l / \partial \theta \tag{4.3}$$

where r represents the moment arm, l represents the length of the muscle-tendon unit, and θ represents the degree of freedom of interest in radians. This method can be used experimentally to assess the moment arm over the range of a rotational movement by measuring the change in length of a muscle-tendon unit associated with small changes in the rotational position. These types of experiments can be performed in cadaveric specimens with direct measurement of muscle-tendon length over a range of postures. In addition, assessments using this approach have been made *in vivo* using magnetic resonance imaging approaches in which the displacements of voxels within a muscle were tracked and velocities calculated over a range of postures.[57]

The moment arm of a muscle can influence the muscle's moment about a joint in several ways. Moment is a product of moment arm and muscle force. Thus, the moment arm of a muscle has a direct influence on the magnitude of the moment that is produced. In addition, because of the interplay of the change in length of a muscle and moment arm, a larger moment arm results in larger changes in length and higher velocities of a muscle. Of course, the force that a muscle produces depends on its length and shortening velocity. Therefore, the moment arm of a muscle also influences the force produced by the muscle itself, which contributes to the moment produced.

Because muscles produce pulling and not pushing forces, each rotational joint must have at least two muscles actuating it, with one on each side of a joint (agonist and antagonist muscle). Because many joints have more than one degree of freedom associated with them, they may require actuators in several planes of action. Multiple muscles may cross a single joint, and so the moment about a rotational axis produced at a particular joint is the net result of all agonist and antagonist muscles acting at a single joint about that axis. In addition, many muscles do cross more than one joint, so the length and velocities of multiarticular muscles are dependent on the postures and velocities of all the joints they cross. Thus, it is often important to consider multijoint systems as a whole to properly evaluate muscle function.

Movement of a multijoint system (Figure 4.5) depends not only on the mechanical properties of the muscles and musculoskeletal geometry (e.g., moment arms) but also on the coordination of the muscles, the inertial properties of the limb segments, the joint degrees of freedom, additional passive joint moments that may be associated with ligaments or joint capsules, and any external loads that may be present. The coordination of the muscles requires not only the reflex responses that have been previously discussed in this chapter

but also the higher level controls from the motor cortex of the brain. Smooth movement also benefits from sensory information from the proprioceptive receptors, skin and joint free nerve ending receptors, and vestibular and ocular inputs, all of which are integrated by the CNS to allow adjustments to movements in response to all available information. Information regarding motor control of muscle can be assessed using fine-wire or surface electromyographic electrodes that receive electrical signals from motor neurons associated with muscle activation. These signals provide limited information as to which individual muscles are activated during a task and to what degree.

Muscles in a musculoskeletal system may not act independently from one another. There is some evidence that synergies exist whereby certain muscles with complementary functions may be preferentially coactivated during tasks.[58] Additionally, there is evidence that force may be transmitted between adjacent muscles due to the close association of connective tissue in musculoskeletal systems.[59–61,62] These are active areas of current research, and analyses that consider muscles as acting independently neglect some of these potential interactions.

Computational approaches to the analysis of multijoint movement frequently consider muscles as acting independently. The force-generating characteristics of muscle must be considered, whether muscle-tendon units are represented with Hill-type or finite-element representations (or any other approach). Inertial properties of segments and degrees of freedom must be defined to characterize the dynamic properties of the system. Finally, information about the activation of muscles, either from electromyography measurements, computationally derived calculations (e.g., optimization approaches), or experimentally relevant assumptions (e.g., assumed maximal activation), is needed. In combination, these inputs permit the analysis of movement and the roles of muscles in producing movement.

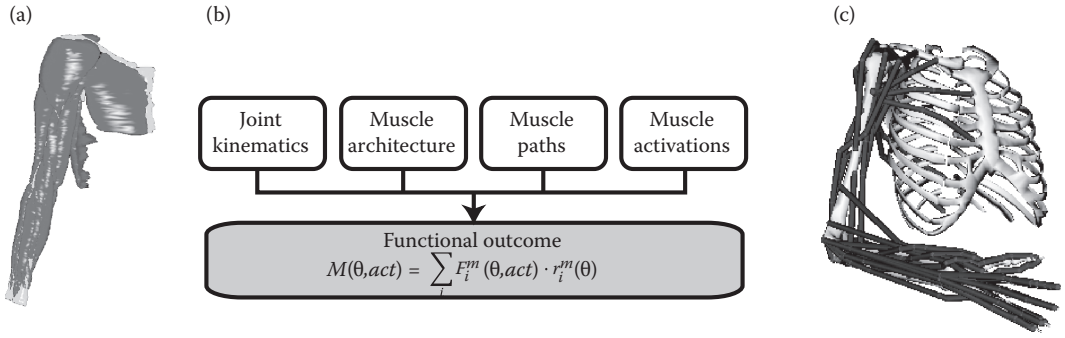

FIGURE 4.5
Multiple muscle systems. Characterization of muscle function necessitates the consideration of how all the muscles are arranged with regard to underlying joints (a) and how these muscles are coordinated to produce movement. Musculoskeletal models (b and c) that characterize joint kinematics, muscle architecture, muscle paths, and muscle activations allow for the prediction and examination of how the structure of muscles influences movement. (Part (a) reprinted from *J. Biomech.*, 40, 4, Holzbaur, K. R., Murray, W. M., Gold, G. E., and Delp S. L. Upper limb muscle volumes in adult subjects, 742–749, 2007, with permission from Elsevier. Part (c) adapted from Springer Science+Business Media: *Ann. Biomed. Eng.*, A model of the upper extremity for simulating musculoskeletal surgery and analyzing neuromuscular control, 33, 6, 2005, 829–840, Holzbaur, K. R., Murray, W. M., Delp, S. L.)

At the level of the musculoskeletal system, there are a number of clinical issues that should be considered. Because bone geometry remodels in response to the forces acting on it, it is clear that abnormal forces generated by injured or diseased muscles will naturally affect the bones as well. Bony deformities associated with spastic, paralyzed, or contracted muscles are common and may require surgical intervention, such as osteotomy, to restore the normal bone geometry. Conversely, because deformities of the skeletal system will alter the paths of the muscles attached to the bones, the moment arms of the muscles will be altered and so too will muscle function be affected. Combined surgical interventions to alter bone and muscle geometries simultaneously are common in these types of clinical cases, for example, in cerebral palsy. Finally, disorders of the CNS may cause abnormal activations of the muscles or abnormal integration of sensory and motor information. In addition to the effects this may have at the tissue level in muscles, abnormal coordination of muscles will directly influence movement production, even in the absence of altered muscle tissue.

4.4 Summary

The complexity of the mechanics of muscle is clear, and the striking ability of the muscles to tune their properties and functions at scales ranging from nanometers to meters is laudable. The discovery of the structure and function of muscle has accelerated tremendously in the last few decades, particularly at the levels of the contractile proteins and sarcomeres. However, the remaining grand challenge in this field is the integration of these discoveries in the context of the larger length scales and overall movement. Without this integration, the relevance of these discoveries to function remains limited. Similarly, the development of a conceptual, mathematical, experimental, computational, or other framework that integrates structure–function discoveries at all length scales would open the doors for many new discoveries and the solution of several important clinical problems. For example, the aging process of muscle manifests itself at all the length scales presented here—from the myosin isoform to motor control of movement. Clearly, muscle impairment with aging cannot be isolated to one particular scale, and the integration of scales would allow for a more holistic perspective on how the aging process affects mobility. Examples like this will hopefully drive the general field of muscle mechanics to integrate knowledge across scales.

References

1. Rayment, I., W. R. Rypniewski, K. Schmidt-Base, R. Smith, D. R. Tomchick, M. M. Benning, et al. 1993. Three-dimensional structure of myosin subfragment-1: A molecular motor. *Science* 261(5117):50–58.
2. Kron, S. J., and J. A. Spudich. 1986. Fluorescent actin filaments move on myosin fixed to a glass surface. *Proceedings of the National Academy of Sciences of the United States of America* 83(17): 6272–6276.

3. Hill, A. V. 1938. Heat of shortening and the dynamic constants of muscle. *Proceedings of the Royal Society of London. Series B. Biological Sciences* 126(843):136–195.
4. Schliwa, M., and G. Woehlke. 2003. Molecular motors. *Nature* 422(6933):759–765.
5. Finer, J. T., R. M. Simmons, and J. A. Spudich. 1994. Single myosin molecule mechanics: Piconewton forces and nanometre steps. *Nature* 368(6467):113–119.
6. Tyska, M. J., D. E. Dupuis, W. H. Guilford, J. B. Patlak, G. S. Waller, K. M. Trybus, D. M. Warshaw, and S. Lowey. 1999. Two heads of myosin are better than one for generating force and motion. *Proceedings of the National Academy of Sciences of the United States of America* 96(8):4402–4407.
7. Granzier, H. L., and S. Labeit. 2004. The giant protein titin: A major player in myocardial mechanics, signaling, and disease. *Circulation Research* 94(3):284–295.
8. Tskhovrebova, L., and J. Trinick. 2003. Titin: Properties and family relationships. *Nat Rev Molecular and Cellular Biology* 4(9):679–689.
9. Gordon, A. M., A. F. Huxley, and F. J. Julian. 1966. Tension development in highly stretched vertebrate muscle fibres. *Journal of Physiology* 184(1):143–169.
10. Woledge, R. C., N. A. Curtin, and E. Homsher. 1985. Energetic aspects of muscle contraction. *Monographs of the Physiological Society* 41:1–357.
11. Oldfors, A. 2007. Hereditary myosin myopathies. *Neuromuscular Disorders* 17(5):355–367.
12. Nowak, K. J., D. Wattanasirichaigoon, H. H. Goebel, M. Wilce, K. Pelin, K. Donner et al. 1999. Mutations in the skeletal muscle alpha-actin gene in patients with actin myopathy and nemaline myopathy. *Nature Genetics* 23(2):208–212.
13. Hackman, P., A. Vihola, H. Haravuori, S. Marchand, J. Sarparanta, J. De Seze et al. 2002. Tibial muscular dystrophy is a titinopathy caused by mutations in TTN, the gene encoding the giant skeletal-muscle protein titin. *American Journal of Human Genetics* 71(3):492–500.
14. Goldfarb, L. G., M. Olive, P. Vicart, and H. H. Goebel. 2008. Intermediate filament diseases: Desminopathy. *Advances in Experimental Medicine and Biology* 642:131–164.
15. Morgan, D. L. 1990. New insights into the behavior of muscle during active lengthening. *Biophysical Journal* 57(2):209–221.
16. Watkins, S. C., E. P. Hoffman, H. S. Slayter, and L. M. Kunkel. 1988. Immunoelectron microscopic localization of dystrophin in myofibres. *Nature* 333(6176):863–866.
17. Consolino, C. M., and S. V. Brooks. 2004. Susceptibility to sarcomere injury induced by single stretches of maximally activated muscles of mdx mice. *Journal of Applied Physiology* 96(2): 633–638.
18. Dellorusso, C., R. W. Crawford, J. S. Chamberlain, and S. V. Brooks. 2001. Tibialis anterior muscles in mdx mice are highly susceptible to contraction-induced injury. *Journal of Muscle Research and Cell Motility* 22(5):467–475.
19. Petrof, B. J., J. B. Shrager, H. H. Stedman, A. M. Kelly, and H. L. Sweeney. 1993. Dystrophin protects the sarcolemma from stresses developed during muscle contraction. *Proceedings of the National Academy of Sciences of the United States of America* 90(8):3710–3714.
20. Wells, D. J., and K. E. Wells. 2002. Gene transfer studies in animals: What do they really tell us about the prospects for gene therapy in DMD? *Neuromuscular Disorders* 12 Suppl 1:S11–S22.
21. Velleman, H. G. 2002. Role of the extracellular matrix in muscle growth and development. *Journal of Animal Science* 80:E8–E13.
22. Danielson, K. G., H. Baribault, D. F. Holmes, H. Graham, K. E. Kadler, and R. V. Iozzo. 1997. Targeted disruption of decorin leads to abnormal collagen fibril morphology and skin fragility. *Journal of Cell Biology* 136(3):729–743.
23. Rapraeger, A. C., A. Krufka, and B. B. Olwin. 1991. Requirement of heparan sulfate for bFGF-mediated fibroblast growth and myoblast differentiation. *Science* 252(5013):1705–1708.
24. Henneman, E., G. Somjen, and D. O. Carpenter. 1965. Functional significance of cell size in spinal motoneurons. *Journal of Neurophysiology* 28:560–580.
25. Llewellyn, M. E., K. R. Thompson, K. Deisseroth, and S. L. Delp. 2010. Orderly recruitment of motor units under optical control in vivo. *Nature Medicine* 16(10):1161–1165.
26. Kandel, E., J. Schwarts, and T. Jessell. 2000. *Principles of Neural Science.* New York: McGraw-Hill Medical.

27. Close, R. I. 1972. Dynamic properties of mammalian skeletal muscles. *Physiological Reviews* 52(1):129–197.
28. Erskine, R. M., D. A. Jones, N. Maffulli, A. G. Williams, C. E. Stewart, and H. Degens. 2011. What causes in vivo muscle specific tension to increase following resistance training? *Experimental Physiology* 96(2):145–155.
29. Lannergren, J., and H. Westerblad. 1987. The temperature dependence of isometric contractions of single, intact fibres dissected from a mouse foot muscle. *Journal of Physiology* 390:285–293.
30. Maganaris, C. N., V. Baltzopoulos, D. Ball, and A. J. Sargeant. 2001. In vivo specific tension of human skeletal muscle. *Journal of Applied Physiology* 90(3):865–872.
31. O'Brien, T. D., N. D. Reeves, V. Baltzopoulos, D. A. Jones, and C. N. Maganaris. 2010. In vivo measurements of muscle specific tension in adults and children. *Experimental Physiology* 95(1): 202–210.
32. Stephenson, D. G., and D. A. Williams. 1981. Calcium-activated force responses in fast- and slow-twitch skinned muscle fibres of the rat at different temperatures. *Journal of Physiology* 317:281–302.
33. Zajac, F. E. 1989. Muscle and tendon: Properties, models, scaling, and application to biomechanics and motor control. *Critical Reviews in Biomedical Engineering* 17(4):359–411.
34. Rack, P. M., and D. R. Westbury. 1984. Elastic properties of the cat soleus tendon and their functional importance. *Journal of Physiology* 347:479–495.
35. Yucesoy, C. A., F. Ates, U. Akgun, and M. Karahan. 2010. Measurement of human gracilis muscle isometric forces as a function of knee angle, intraoperatively. *Journal of Biomechanics* 43(14):2665–2671.
36. Lieber, R. L., B. M. Fazeli, and M. J. Botte. 1990. Architecture of selected wrist flexor and extensor muscles. *The Journal of Hand Surgery* 15(2):244–250.
37. Lieber, R. L., M. D. Jacobson, B. M. Fazeli, R. A. Abrams, and M. J. Botte. 1992. Architecture of selected muscles of the arm and forearm: Anatomy and implications for tendon transfer. *The Journal of Hand Surgery* 17(5):787–798.
38. Murray, W. M., T. S. Buchanan, and S. L. Delp. 2000. The isometric functional capacity of muscles that cross the elbow. *Journal of Biomechanics* 33(8):943–952.
39. Wickiewicz, T. L., R. R. Roy, P. L. Powell, and V. R. Edgerton. 1983. Muscle architecture of the human lower limb. *Clinical Orthopaedics and Related Research*(179):275–283.
40. Dey, D. K., I. Bosaeus, L. Lissner, and B. Steen. 2009. Changes in body composition and its relation to muscle strength in 75-year-old men and women: A 5-year prospective follow-up study of the NORA cohort in Goteborg, Sweden. *Nutrition* 25(6):613–619.
41. Narici, M. V., and N. Maffulli. 2010. Sarcopenia: Characteristics, mechanisms and functional significance. *British Medical Bulletin* 95:139–159.
42. Ward, S. R., and R. L. Lieber. 2005. Density and hydration of fresh and fixed human skeletal muscle. *Journal of Biomechanics* 38(11):2317–2320.
43. Eng, C. M., G. D. Abrams, L. R. Smallwood, R. L. Lieber, and S. R. Ward. 2007. Muscle geometry affects accuracy of forearm volume determination by magnetic resonance imaging (MRI). *Journal of Biomechanics* 40(14):3261–3266.
44. Holzbaur, K. R., W. M. Murray, G. E. Gold, and S. L. Delp. 2007. Upper limb muscle volumes in adult subjects. *Journal of Biomechanics* 40(4):742–749.
45. Tingart, M. J., M. Apreleva, J. T. Lehtinen, B. Capell, W. E. Palmer, and J. J. Warner. 2003. Magnetic resonance imaging in quantitative analysis of rotator cuff muscle volume. *Clinical Orthopaedics and Related Research* (415):104–110.
46. Esformes, J. I., M. V. Narici, and C. N. Maganaris. 2002. Measurement of human muscle volume using ultrasonography. *European Journal of Applied Physiology* 87(1):90–92.
47. O'Brien, T. D., N. D. Reeves, V. Baltzopoulos, D. A. Jones, and C. N. Maganaris. 2010. Muscle-tendon structure and dimensions in adults and children. *Journal of Anatomy* 216(5):631–642.
48. Murray, W. M., V. R. Hentz, J. Friden, and R. L. Lieber. 2006. Variability in surgical technique for brachioradialis tendon transfer. Evidence and implications. *Journal of Bone and Joint Surgery. American Volume* 88(9):2009–2016.

49. Llewellyn, M. E., R. P. Barretto, S. L. Delp, and M. J. Schnitzer. 2008. Minimally invasive high-speed imaging of sarcomere contractile dynamics in mice and humans. *Nature* 454(7205): 784–788.
50. Blemker, S. S., and S. L. Delp. 2005. Three-dimensional representation of complex muscle architectures and geometries. *Annals of Biomedical Engineering* 33(5):661–673.
51. Blemker, S. S., and S. L. Delp. 2006. Rectus femoris and vastus intermedius fiber excursions predicted by three-dimensional muscle models. *Journal of Biomechanics* 39(8):1383–1391.
52. Blemker, S. S., P. M. Pinsky, and S. L. Delp. 2005. A 3D model of muscle reveals the causes of nonuniform strains in the biceps brachii. *Journal of Biomechanics* 38(4):657–665.
53. Carroll, C. C., J. M. Dickinson, J. M. Haus, G. A. Lee, C. J. Hollon, P. Aagaard et al. 2008. Influence of aging on the in vivo properties of human patellar tendon. *Journal of Applied Physiology* 105(6):1907–1915.
54. Wood, L. K., E. M. Arruda, and S. V. Brooks. 2011. Regional stiffening with aging in tibialis anterior tendons of mice occurs independent of changes in collagen fibril morphology. *Journal of Applied Physiology*.
55. Milgrom, C., M. Schaffler, S. Gilbert, and M. van Holsbeeck. 1995. Rotator-cuff changes in asymptomatic adults. The effect of age, hand dominance and gender. *The Journal of Bone and Joint Surgery. British Volume* 77(2):296–298.
56. An, K. N., K. Takahashi, T. P. Harrigan, and E. Y. Chao. 1984. Determination of muscle orientations and moment arms. *Journal of Biomechanical Engineering* 106:280–282.
57. Blemker, S. S., D. S. Asakawa, G. E. Gold, and S. L. Delp. 2007. Image-based musculoskeletal modeling: Applications, advances, and future opportunities. *Journal of Magnetic Resonance Imaging* 25(2):441–451.
58. Safavynia, S. A., G. Torres-Oviedo, and L. H. Ting. 2011. Muscle synergies: Implications for clinical evaluation and rehabilitation of movement. *Topics in Spinal Cord Injury Rehabilitation* 17(1):16–24.
59. Huijing, P. A. 2007. Epimuscular myofascial force transmission between antagonistic and synergistic muscles can explain movement limitation in spastic paresis. *Journal of Electromyography and Kinesiology* 17(6):708–724.
60. Huijing, P. A. 2009. Epimuscular myofascial force transmission: A historical review and implications for new research. International Society of Biomechanics Muybridge Award Lecture, Taipei, 2007. *Journal of Biomechanics* 42(1):9–21.
61. Huijing, P. A., R. W. van de Langenberg, J. J. Meesters, and G. C. Baan. 2007. Extramuscular myofascial force transmission also occurs between synergistic muscles and antagonistic muscles. *Journal of Electromyography and Kinesiology* 17(6):680–689.
62. Yucesoy, C. A., B. H. Koopman, H. J. Grootenboer, and P. A. Huijing. 2007. Finite element modeling of aponeurotomy: Altered intramuscular myofascial force transmission yields complex sarcomere length distributions determining acute effects. *Biomechanics and Modeling in Mechanobiology* 6(4):227–243.
63. Holzbaur, K. R., W. M. Murray, S. L. Delp. 2005. A model of the upper extremity for simulating musculoskeletal surgery and analyzing neuromuscular control. *Annals of Biomedical Engineering* 33(6):829–840.
64. Sharafi, B., S. S. Blemker. 2010. A micromechanical model of skeletal muscle to explore the effects of fiber and fascicle geometry. *Journal of Biomechanics* 43(16):3207–3213.
65. Ward, S. R., C. M. Eng, L. H. Smallwood, R. L. Lieber. 2008. Are current measurements of lower extremity muscle architecture accurate? *Clinical Orthopaedics and Related Research* 467(4): 1074–1082.

Section II

Musculoskeletal Structures

5

Skull Biomechanics

Andre M. Loyd, Chris Van Ee, Matthew B. Panzer, Barry S. Myers, and Cameron R. Bass

CONTENTS

5.1 Introduction

Knowledge of the biomechanics of the skull, the primary structural protector of the brain, is important owing to the severe consequences of brain injury. Traumatic brain injury (TBI) is a common injury in the United States with approximately 1.4 million people receiving medical treatment for TBI each year. Of these 1.4 million cases, 235,000 involved hospitalization of the patient while 50,000 of the cases resulted in patient death.[1] The most common causes of TBI are motor vehicle crashes (20% of cases), blunt impacts from falls (28% of cases), and being

struck by an object (19% of cases).[1] Children are especially vulnerable to head injury involving the skull. Child head injuries are responsible for 2700 deaths per year—30% of all childhood deaths in the United States.[2,3] Furthermore, recent military conflicts have produced numerous cases of TBI owing to high-rate blunt impact with vehicle interiors and deforming helmets under ballistic loading and direct blast shock exposure to the head.[1,4]

This chapter outlines the current understanding of skull biomechanics, including gross and detailed anatomy, local skull material characterization with rate dependency and failure properties, and basic research involving testing of the head including simple skull fracture injury assessment models and injury reference values. This chapter concludes with the state of the art in rapidly developing finite-element (FE) modeling of the skull and future research directions.

5.2 Anatomy

5.2.1 Developmental Gross Anatomy of Skull and Suture

The skull is composed of two major sections: the neurocranium and the viscerocranium.[5] The neurocranium, also called the calvarium or cranial vault, is the superior portion of the head and contains the seven bone plates that protect the brain. These plates from the anterior to the posterior are the left and right frontal bones, the left and right parietal bones, and in the posterior, one occipital bone (Figure 5.1). The temporal bone and the sphenoid bone

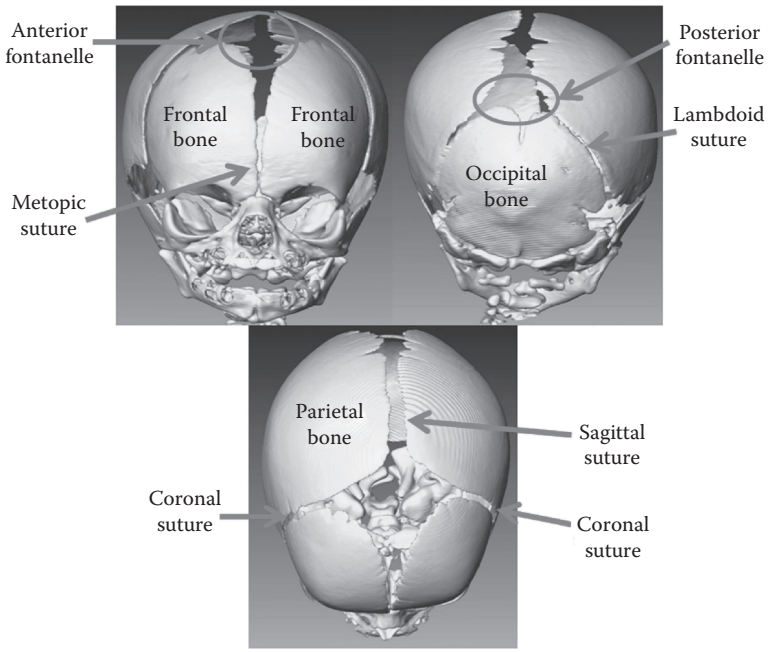

FIGURE 5.1
Views of the newborn skull showing cranial plates, sutures, and fontanelles. The anterior view (top left) and posterior view (top right) are shown, as well as superior view (bottom picture). Circled areas are anterior and posterior fontanelles.

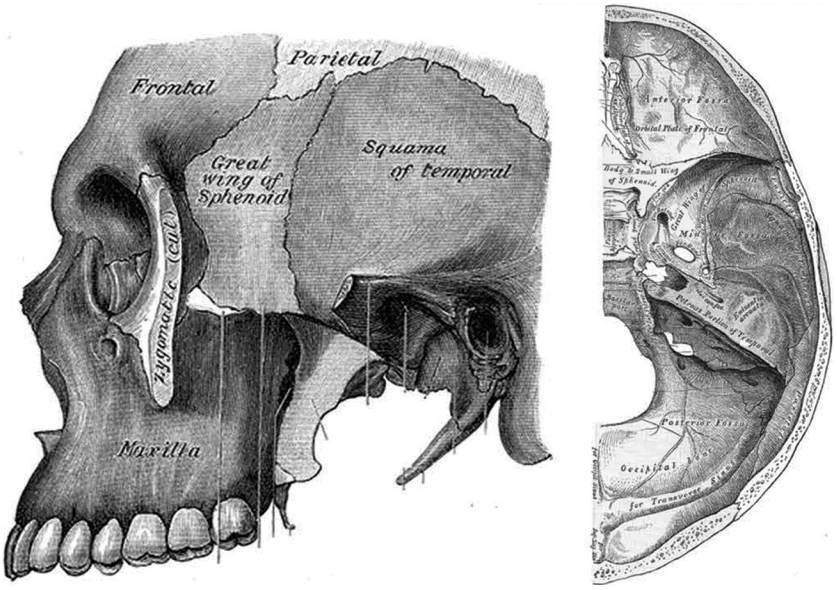

FIGURE 5.2
(See color insert.) Diagram of the skull showing the location of temporal (red) and sphenoid (yellow) bones. Sphenoid and temporal bone form portions of the base of skull (right) and lateral walls (left) of the cranial cap. (From *Gray's Anatomy*, courtesy of Wikimedia Commons.)

form the base of the skull and parts of the lateral walls encapsulating the brain (Figure 5.2).[5] The temporal bone is a "compound structure," meaning that it is composed of multiple sections: the squama temporalis, the mastoid portion, the petrous portion, and the tympanic portion.[5] The viscerocranium refers to the anterior portion of the head and contains the face, the base of the skull, and the mandible.

In the newborn, the plates of the neurocranium are loosely connected by fibrous intersections. These intersections are termed sutures when they join only two bones and are "fontanelles" when they join three or more bones (Figure 5.1).[6] The sutures and fontanelles allow the head to mold and to deform during childbirth and ensure safe passage through the birth canal without damage to the mother. For the adult, the plates are completely fused, and the skull acts like a rigid body that is designed to encase and protect the brain.

5.2.2 Skull Anatomy and Growth

At birth, much of the skull is composed of intramembranous bone with a single layer structure (Figure 5.3a).[7,8] As the brain develops, the periosteal tissues expand and the bones of the cranium move apart, straining the sutures and simultaneously creating space for, and signaling for, the growth of new bone. This is the primary location of bone growth in the pediatric skull and the outer layer of the skull.[9] The bone also transitions from the single layer structure observed in early childhood to the trilayer structure present in adults, which is composed of a cortical table on both the ectocranial (outer table) and endocranial (inner table) surfaces separated by a porous trabecular layer (diploë) with an internal vasculature (Figure 5.3c). This occurs by the simultaneous deposition of new bone on both the ectocranial and the endocranial surfaces and resorption of the inner layer.[9] These two modes of growth, resulting in the nonuniform development of the pediatric skull, may

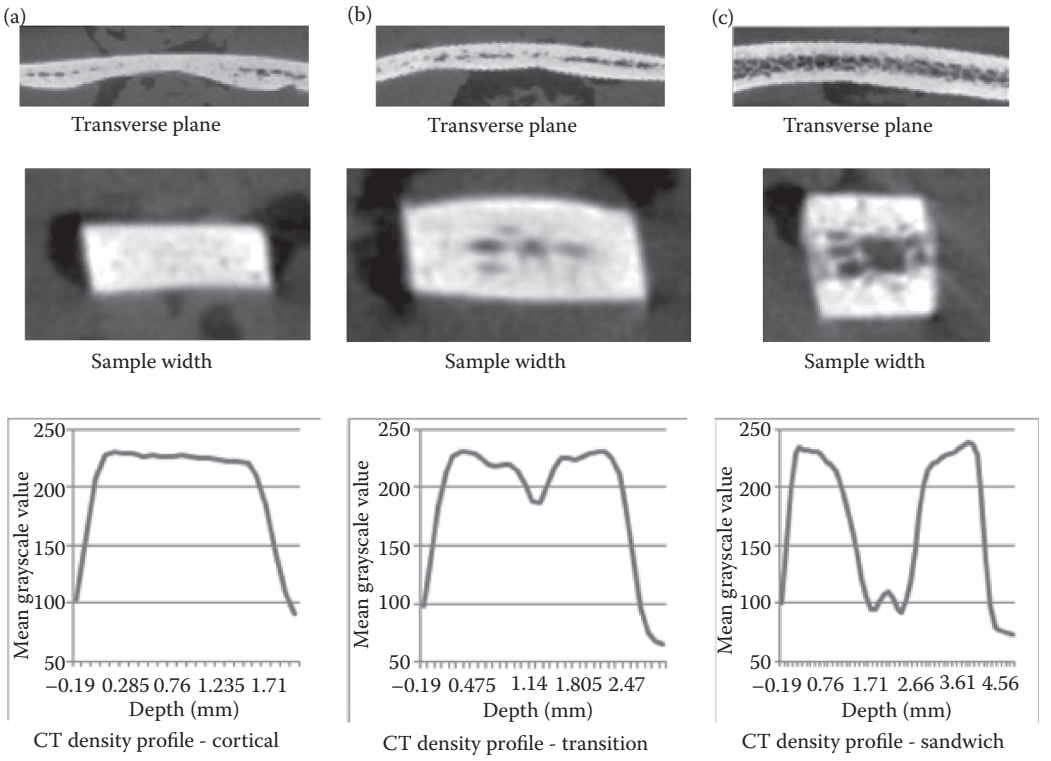

FIGURE 5.3
Axial and cross-sectional CT images of three specimens are shown with the corresponding mean grayscale CT density value of the image plotted as a function of depth. Minimum to maximum grayscale ratio was used to categorize specimens as having either (a) purely cortical, (b) transition, or (c) sandwich structure.

create regional variation in the mechanical properties of the skull. In a 6-year-old, Davis et al. found regional variation in skull structure differentiated into regions of mostly cortical shell (Figure 5.3a), transition (Figure 5.3b), suture (Figure 5.4), and trilayer bone (Figure 5.3c). This trilayer or "diploic" structure is typical of the adult skull; the suture area continues to be a growth region until subsequent bony interdigitation and closing of the sutures by adulthood. Teleologically, this type of structure is well suited for providing rigidity in bending while maintaining a minimal weight.

5.2.2.1 Pediatric Cranial Fontanelles

The largest regions of soft tissue of the neonate skull are the anterior and posterior fontanelles. The anterior fontanelle is located in the anterior of the pediatric head and intersects both anterior corners of the parietal bones and the superior corners of the two frontal bones (Figure 5.1).[11] Additionally, the anterior of the sagittal suture and the top of the two coronal and metopic sutures terminate at the anterior fontanelle. The posterior fontanelle is the junction of the upper apex of the occipital bone and the posterior corners of the parietal bones as well as the lambdoid and sagittal sutures.[11] Additional fontanelles include the posterolateral and anterolateral fontanelles that are present in the lower segments of the pediatric head.[5] The posterior and anterior fontanelles are typically totally fused and

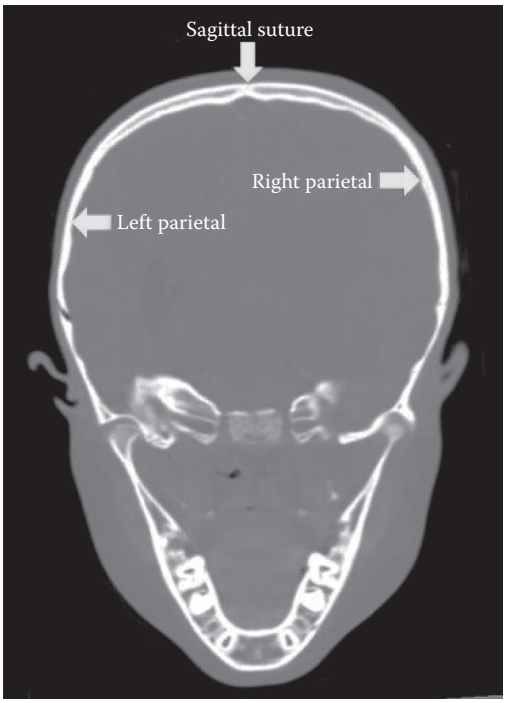

FIGURE 5.4
CT image of the cross section of the intact skull showing the distribution of trilayer and unilayer bone. The oblique coronal view of the left and right parietal regions shown indicates that the bone is thickest and most mature in the area surrounding the sagittal suture. The bone nearer the sides and the apices are composed of only cortical bone.

obliterated by 2 months of age for the posterior fontanelle and by 13.8 months of age for the anterior fontanelle.[9,12]

5.2.2.2 Suture

There are several different anatomical definitions of "suture." Weprin and Rengachary[13] described the suture as "syndesmoses of the cranial vault, in which fibrous tissue is interposed between bony surfaces." Pritchard et al.[14] defined suture as the "entire complex of cellular and fibrous tissues intervening between, and surrounding, the definitive bone edges." Generally, suture is the soft tissue that lies "between two approaching osseous territories, the embryonal dura mater and the pericranial membrane."[15] The suture is separate from the pericranium and the dura mater.[15–20] The suture of the neonate head is in an open or "soft" state, which evolves to a closed state composed of solid bone in the adult. This differentiation is important because the suture's properties, behavior, and age differ greatly from when the suture is open to when the suture is closed.

There are four sutures in the cranial cap: the coronal, lambdoid, metopic, and sagittal sutures. The coronal sutures run vertically between the frontal bone and the parietal bone on both sides of the head. Likewise, the lambdoid suture connects the posterior edges of the parietal bones to the upper edges of the occipital bone on each side of the head.[11] Bones

of these sutures do not meet end-to-end but overlap each other. For this reason, both of these sutures are referred to as overlapping or beveled sutures.[9]

The metopic suture connects the two frontal bones and is located in the center of the forehead. The sagittal suture runs in the sagittal plane at the top of the pediatric head and links the right and left parietal bones. Both the metopic and sagittal sutures are midline sutures and end-to-end sutures, meaning that the bones that they adjoin meet at their ends.[9] Additional sutures include squamosal sutures that are present in the lower segments of the pediatric head.[5]

The detailed morphology of the suture changes with age and affects skull biomechanics. Suture fiber alignment within the coronal suture increases with age in early life. Adamski et al.[21] found that the qualitative and quantitative morphology and fiber structure changes dramatically with age within the first 18 months of life (Figure 5.5). In neonate sutures (Figure 5.6a), the suture mesenchyme is disorderly, with the fibers arranged in a net-like pattern. Only the border regions between the mesenchyme and the dura mater, or pericranium, show substantial alignment in the neonate samples. The suture fibers become more aligned in 9- and 11-month-old specimens from the innermost portion of the mesenchyme, with increasing alignment outward. In the 9-month-old suture (Figure 5.6b), the fibers at the center of the suture are more densely arranged and begin to align as compared with the mesenchyme directly next to the bone interface. The 11-month-old suture (Figure 5.6c) is similar to that of the 9-month-old, with increased alignment in the center of the suture and disorder at the bone front. Finally, in the 18-month-old specimen (Figure 5.6d), the suture contains locally aligned fibers throughout the entire mesenchyme, although the overall orientation varies with respect to the bone. Suture fibers at the bone edge connect at an angle roughly between 45° and 90° to the bone face. In the 18-month-old suture, there are distinct anchor points at which the collagen fibers connect the bone and the suture mesenchyme. The suture is also narrower than at earlier ages due to the encroaching bone fronts, and there is an increase in bony interdigitation. This process of alignment continues until adulthood, at which point sutures are rigidly connected by interdigitated bone (obliterated) or the local suture interfaces are resorbed, leaving no suture paths.[22–24] It has

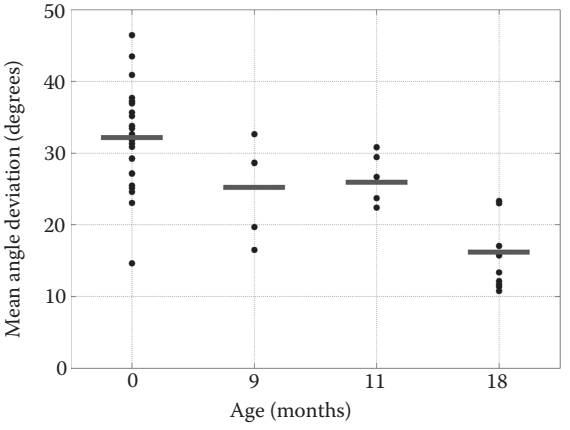

FIGURE 5.5
Average angle of suture fiber deviation decreases with age. Each point represents five samples per coronal suture section. The horizontal bars indicate mean angle deviation from the median comparing all viewing frames within each age group.

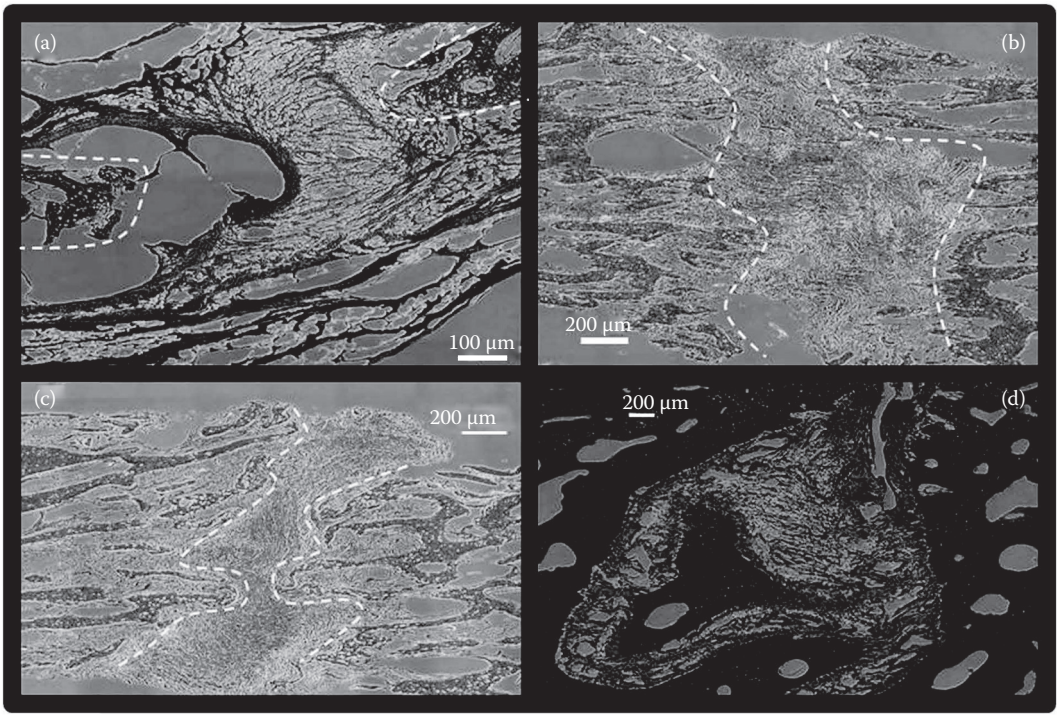

FIGURE 5.6
(See color insert.) Suture samples (Masson's trichrome under transmitted light microscopy). Bone edges are outlined with dashed lines. (a) Neonate, showing the net-like arrangement of fibers in the mesenchyme. (b) The 9-month-old, displaying an increase in arranged fibers although still lacking order at the bone interface. (c) The 11-month-old, similar to the 9-month-old, showing increase in arranged fibers specifically in the bottom portion of the suture. (d) The 18-month-old, suture space narrows and is more clearly defined by bone edge and fibers are more aligned with the bone faces.

been hypothesized that the increased local fiber alignment that develops with age adds strength to the human sutures. Herring[25] hypothesized that the alignment of fibers connecting the two bone faces helps the fibers resist tensile strain,[26] whereas tension within the suture joints has been presumed to induce bone growth and to increase bony interdigitation.[27] Generally, collagen fiber alignment increases the elastic modulus of the bone-suture-bone interface.[28]

5.2.3 Comparative Anatomy of Infants and Adults

The infant skull has approximately 25% the volume of the adult skull,[29] and the infant head mass is ~1 kg, whereas the 50th percentile adult male head mass is ~4.5 kg.[29,30] However, the pediatric skull is not simply an adult skull scaled by body mass; the skulls of adults and infants have substantial morphometric and anatomical differences. The cranial cap, and the brain that it encapsulates, is proportionally larger in the infant head than in the adult head (Figure 5.7). Overall, the head height makes up 25% of the neonate's total body height compared with 14% for the adult.[29,31] Owing to differences in overall size, the bone plates

FIGURE 5.7
Neonate head (left) and the adult head (right) shown on the same scale for comparison.

show more curvature in the infant head.[32,33] These differences in face and basicranial size, along with bone curvature, make the human skull more spherical as an infant, progressing to a more oval shape as an adult.[34] In addition, the temporal and sphenoid bones are more prominent in the cranial cap in the adult head. These two bones comprise a larger percentage area of the calvarium in the adult when compared with the infant head.[5,32]

Anatomically, the pediatric and adult heads differ in the way in which the bones are structured and in the manner by which the bone plates are connected. The infant head has soft spots due to the sutures and fontanelles, making the head pliable as described previously. The sutures between the bones are made of flexible collagen fibers, and the bone itself is just one thin (~1 mm thick) cortical table.[35]

In contrast, the adult head has suture joints that are rigidly connected by interdigitated bone, which makes the skull essentially a solid continuum and not easily deformable.[9,12] The sutures move beyond being simply connected to being highly interdigitated, becoming increasingly interdigitated over time. There are two types of sutural interdigitation: one in which the collagen fibers are perpendicular to the suture and the suture has a capsular space and one in which the collagen fibers are parallel and there is not a capsular space.[9] Interdigitation of the cranial vault sutures stops between the ages of 22 and 26 years.[9] It is currently unknown how the interdigitation stops and what the differences are in the types of sutural interdigitation. It has been hypothesized that the sutures may act as dampers for blunt impact forces, although adult human sutures have not been tested.[25,26,36] The fontanelle is absent with no identifiable trace in the adult.[9,33]

The adult skull bone is also different from the pediatric skull bone. The adult skull bone is thick (>5 mm) with a multilayered structure containing both an inner and an outer table,[37] whereas the pediatric cranial bone ranges from a single layer of cortical bone at early ages to multiple types of bone at later ages. Peterson and Dechow[38] found that the outer table is significantly thicker and denser than the inner table. Furthermore, the diploë is generally homogeneous in young adulthood but may become locally resorbed with

age,[39] leaving only fluid between the inner and outer tables. These properties make the adult head structurally stiffer than the infant's head.[10,29,40–42]

5.3 Material Characterization of the Skull

5.3.1 Pediatric Skull Material Properties and Failure

Although extensive cranial growth occurs between birth and 18 years of age, the details of the effect that this growth has on the mechanical properties of the pediatric skull during this period remain largely unstudied. Despite more recent efforts to investigate pediatric responses, most of the studies focus on neonates and infants.[8,43–45] Coats and Margulies[43] analyzed the properties' dependence on strain rate, region, and age using three-point bending tests for a collection of specimens ranging from 21 weeks of gestation to 13 months old. Baumer et al.[46] reported properties obtained via four-point bending of infant porcine parietal bone to propose a correlation to human tissue. Those studies found that the constitutive properties of cranial bone are age-sensitive but not strain rate–dependent for pediatric specimens under the loading rates considered.

An elastic modulus of 7.1 GPa has been reported for one 6-year-old subject, and a range of moduli spanning from 1.7 GPa for preterm bone to 3.9 GPa for term bone have been reported, although the structures of the bones tested were not presented.[44,45] Margulies and Thibault[47] reported the elastic modulus of a range of pediatric specimens from 19 days to 13 months old in the markedly lower range of 0.3 to 1.3 GPa. Coats and Margulies[43] aggregated results from previous research and reported that, for young pediatric specimens, the ultimate strain varied significantly over a wide range of strain rates from 0.000001 to 100 s^{-1}.

Davis et al.[7] tested samples of a 6-year-old human cranium to failure under four-point bending to study the effects of strain rate and the structure of skull bone on the modulus of elasticity and failure properties for both cranial bone and suture. Loading rate did not have a statistically significant effect on the mechanical properties of the 6-year-old skull over the range of loading rates studied, but these properties were found to depend on the growth patterns and morphology of the skull. The structure of the bone was found to vary with thickness and skull bone type. Davis et al.[7] found the effective modulus of elasticity and strength to failure to vary widely intracranially among cortical bone samples (E = 9.87 GPa, σ_{ult} = 185 MPa). However, the mean elastic modulus from Davis et al. was similar to the adult cortical skull modulus of 12 GPa.[48] The trilayer bone had a statistically significantly lower elastic modulus than did the cortical shell (E = 3.69 GPa, σ_{ult} = 82.9 MPa) and the modulus was even lower in sutures (E = 1.10 GPa, σ_{ult} = 27.18 MPa) in the 6-year-old skull. Yet, ultimate strain was not significantly different among the cortical, sandwich, and suture structures (Figure 5.8).

Davis et al.[7] also showed that skull morphology has a direct and significant effect on the mechanical properties of the skull tissue. The structural rigidity was found to be highest for the trilayer specimens, which is consistent with the teleological intuition that the human cranium grows in such a way that the stiffness of the skull increases as the bone matures. As the bone gets thicker, it also gets stronger, and as the bone morphs from a single layer to a trilayer, it also gets stronger. In addition, the sutures are bounded by trilayer bone that is more than three times as stiff as the suture, but with a similar thickness.[7] This

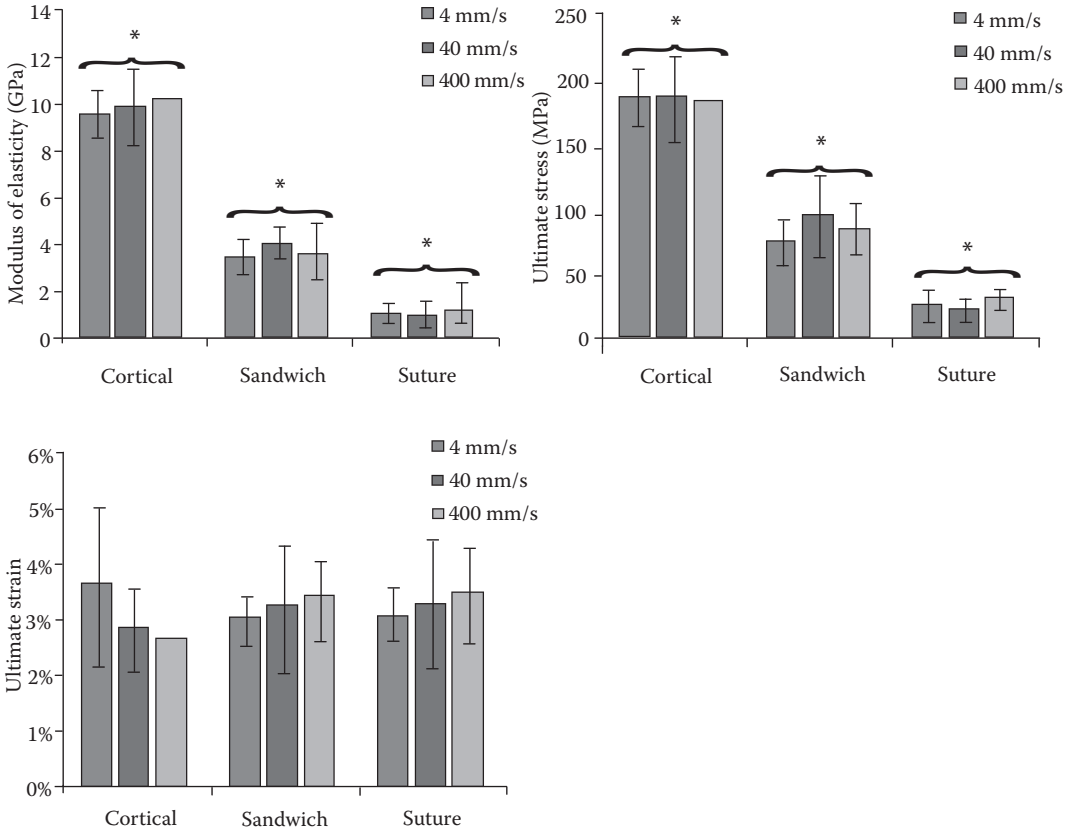

FIGURE 5.8
(See color insert.) Both the modulus of elasticity and ultimate stress differ significantly between cortical, sandwich, and suture skull structures, but the same pattern is not observed for ultimate strain. Varying loading rate from 4 to 400 mm/s has no effect on any of the mechanical properties.

also shows that the differences in morphology and structure directly affect the mechanical properties of the skull bone. Direct comparisons between skull cortical, sandwich, and suture structure types are shown in Figure 5.9 and are compared with pediatric and adult skull elastic moduli.

5.3.2 Adult Skull Material Properties and Failure

The mechanical properties of adult bone have been obtained using a variety of methods.[10,48–50] Estimates of the elastic modulus of the adult sandwich structure range from 5 GPa to more than 12 GPa for the cortical component.[10,48] Several studies have shown that these mechanical properties vary weakly with strain rate for adult bone.[40,48,51] For adults, there is experimental evidence that ultimate stress is rate-dependent and that the modulus of elasticity of adult bone increases with loading rate (Figure 5.10).[40,48,51] Although there are no direct experiments on the strain rate dependence of the adult skull's fracture strength the fracture strength of

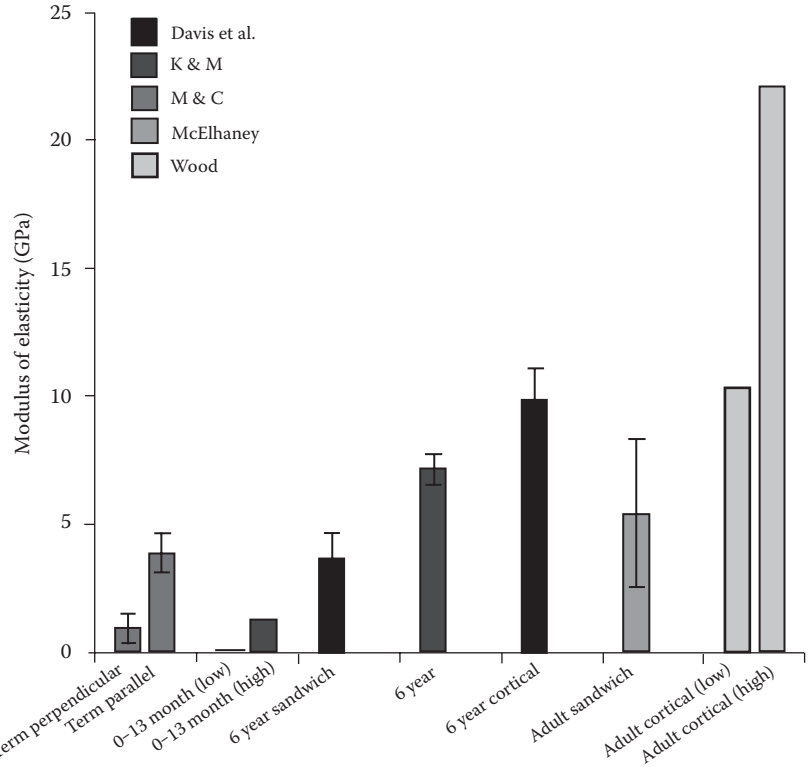

FIGURE 5.9
Comparison of the elastic modulus of the pediatric 6-year-old from several different studies showing upper and lower bounds or error bars where known. (Data from Davis, M. T. et al., *J. Biomech.*, 2012; Kriewall, T. J. et al., *J. Biomech.*, 14, 2, 73–79, 1980; Coats, B. and Margulies, S. S., *J. Neurotrauma*, 23, 8, 1222–1232, 2006; McElhaney, J. H., *J. Appl. Physiol.*, 21, 4, 1231–1236, 1966; Wood, J., *J. Biomech.*, 4, 1, 1–12, 1971.)

cortical bone has been shown to be a function of the loading rate and the apparent density of the bone.[51] The empirical relations determined for these relationships are

$$S = 68\dot{\varepsilon}^{0.06}\rho^2 \tag{5.1}$$

$$E = 3790\dot{\varepsilon}^{0.06}\rho^3, \tag{5.2}$$

where S is the compressive strength (MPa), E is the Young's modulus (MPa), $d\varepsilon/dt$ is the strain rate (s^{-1}), and ρ is the apparent density (g/cm^3). These results correlate well with those of McElhaney.[40] So, the mechanical properties of bone change by only about 4% for the doubling or halving of the strain rate, which is consistent with the measurements of Lakes et al.[52] on the effect of viscoelasticity on the properties of cortical bone over eight decades of strain rate.

The potentially anisotropic material characterization of the isolated adult inner table and outer table of the human parietal and frontal bones has been studied[53–55] based on the observation that the outer table bears direct loading from the nuchal and masticatory musculature.[38,56,57] Peterson and Dechow[57] found that the stiffness of the outer table of the skull was anisotropic in-plane using adult skull samples from the outer table obtained from

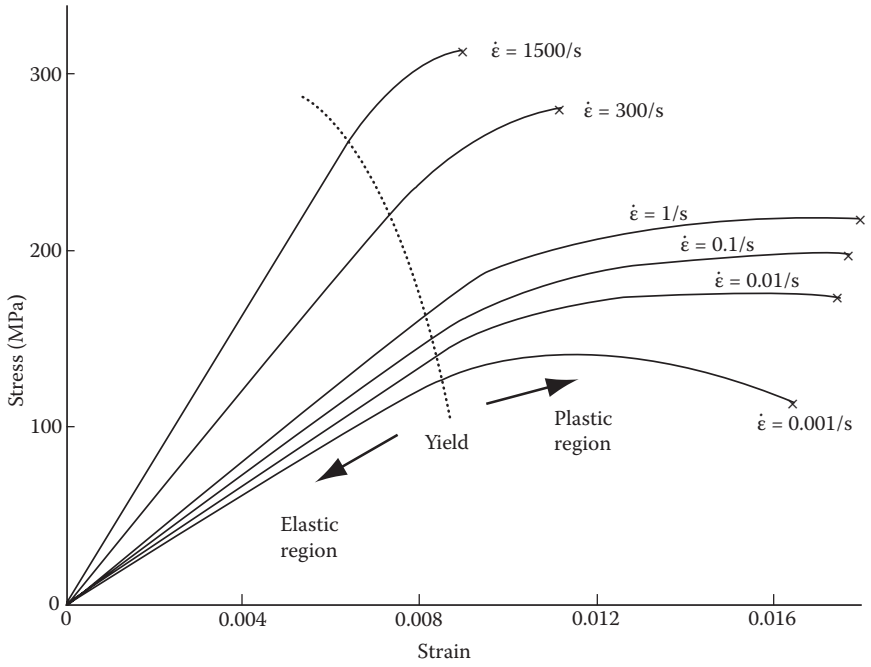

FIGURE 5.10
Stress–strain curves for cortical bone at various strain rates. (Adapted from McElhaney, J. H., *J. Appl. Physiol.*, 21, 4, 1231–1236, 1966.)

multiple sites of the skull including the frontal, occipital, parietal, temporal, and zygomatic bones. They also found that skull thickness and density were not significantly correlated, similar to the findings of Davis et al.[7] in pediatric bone. The values of elastic and shear moduli were both greatest in-plane. The mean elastic modulus in the through-thickness direction was found to vary between 11.7 and 15 GPa, whereas the in-plane minimum moduli varied from 10.5 to 17.7 GPa and from 17.9 to 27.3 GPa for the in-plane minimum and maximum directions. In-plane anisotropy was significantly different between bones and within bones. Peterson and Dechow[57] attributed this to differences between muscle bearing and nonmuscle bearing sites. In-plane anisotropy was found to be 0.66 ± 0.19 for muscle bearing bone and 0.75 ± 0.16 for nonmuscle bearing bone.

5.3.3 Pediatric Suture Material Characterization

Coats and Margulies[43] performed the first experiments to determine the mechanical properties of human pediatric sutures. Their data were limited by small sample size, and they found no direct correlation between age and elastic modulus, although there was a significant interaction between strain rate and age on elastic modulus.[43] Davis et al.[7] found that the Young's modulus in a suture from a 6-year-old was 1.10 ± 0.53 GPa.

It is believed that through development, cranial sutures increase in complexity as they grow and interdigitate.[25,26] Jaslow[58] first presented an interdigitation index measurement (calculated by dividing the jagged suture path by the straight distance) using goat cranial sutures, measuring the value along the skull surface and finding a positive correlation between interdigitation index and energy absorbed, or the total energy sustained by

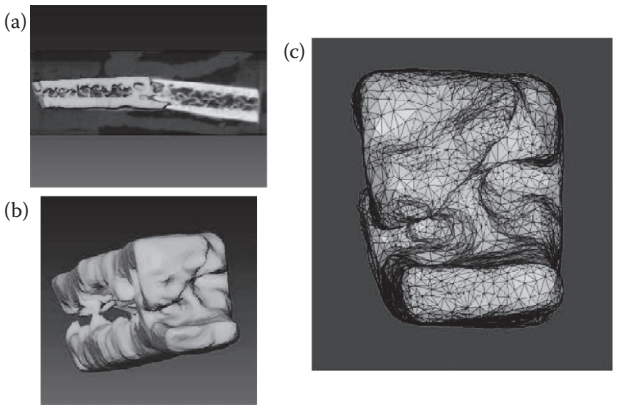

FIGURE 5.11
(See color insert.) Pediatric skull bone images used to measure surface area interdigitation index. (a) Using Avizo 6.0 imaging software, a three-dimensional mesh was created from micro-CT scans of bone–suture–bone strips. (b) Two bones outlining the suture were separated to observe the suture interface. (c) Using LS-DYNA, the surface area was measured from both bone segments and excluded the top, bottom, and sides of the bone strip.

the suture before failure. Jaslow hypothesized that an increase in interdigitation provides an increase in the surface area at the suture interface and, therefore, an increase in possible anchor points for the collagen fibers of the suture, contributing to the strength of the suture. Rafferty and Herring[27] adapted the interdigitation measurement so that it was measured from the ectocranial to the endocranial surface using histological slides of the cross section of porcine sutures. Their work compared suture morphology to *in vivo* strain. Adamski et al.[21] found, however, the interdigitation index as formulated by Jaslow not to be a reliable indicator of three-dimensional (3D) interdigitation. Furthermore, when the 3D structures were included in the calculation of interdigitation, mechanical properties such as the yield stress, yield strain, ultimate stress, Young's modulus, and energy absorbed were not significantly correlated with the interdigitation (Figure 5.11).

5.4 Overall Skull Response to Impact

5.4.1 Skull Fractures

Skull fractures are classified based on the integrity of the overlying scalp, the location of the fracture, and the type of fracture. Open or compound fractures are indicated by a full-thickness laceration of the overlying scalp associated with the fracture. In the absence of a full-thickness laceration associated with the fracture, the fracture is identified as a closed fracture. Fractures can be further classified as vault or basilar skull fractures based on the overall location of the fracture. If the fracture is located in the anterior or posterior skull base, then it is termed a basilar skull fracture. Owing to potentially complicated fracture patterns, there is no existing consensus set of definitions of the skull fracture types in the literature. However, general definitions for skull fracture types are given as follows (Figure 5.12).[59,60]

(1) *Linear fracture:* A single straight fracture that may or may not be restricted to one skull bone (Figure 5.12b). Linear skull fractures are the most common type of skull

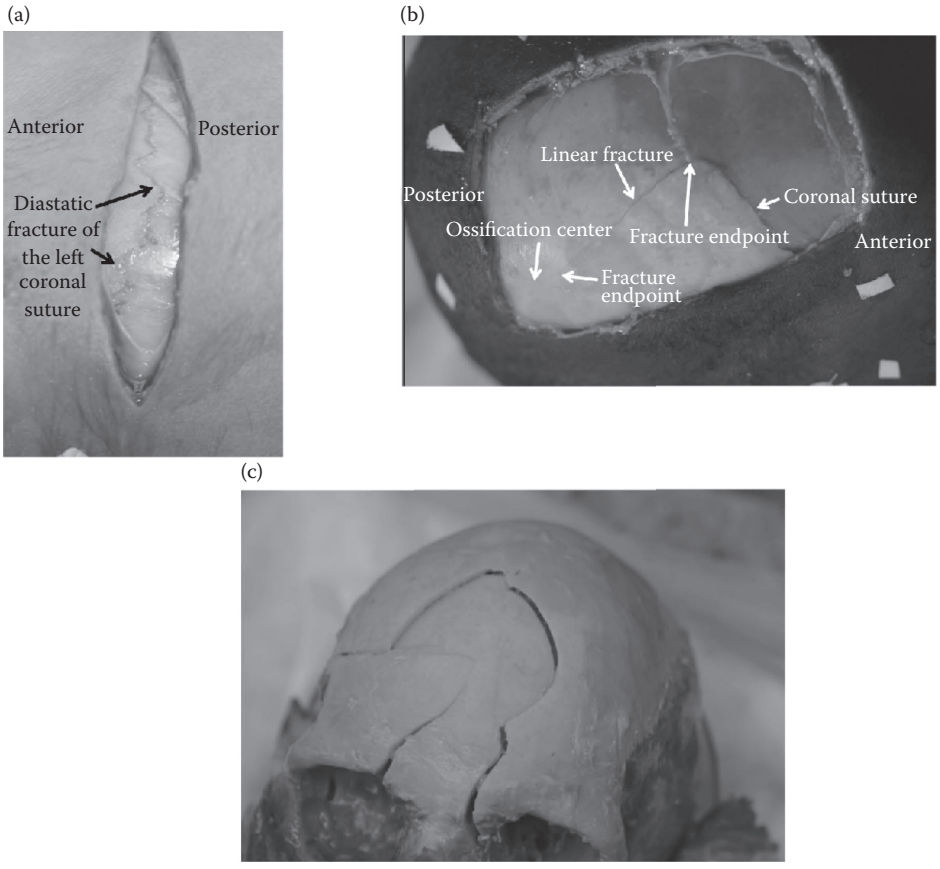

FIGURE 5.12
Different types of skull fractures. (a) Diastatic fracture (arrows) indicated in a pediatric cadaver after blunt impact. (b) Linear fracture indicated in a pediatric cadaver after blunt impact. (c) Large depressed skull fracture in an adult cadaver after blunt impact.

fracture.[61] These fractures generally occur at weaker portions of the bone, away from the point of impact.[62] A linear fracture could have a "straight, zigzagged, or angled configuration."[60] A hairline fracture is a subset of a linear fracture. Linear fractures are also reported with the degree of displacement or movement between the two sides of the fracture.

- *Hairline linear fracture*: A small linear fracture with no displacement
- *Linear fracture with separation*: A fracture wherein the bone separates into two parts with at least 3 mm of separation

(2) *Complex fracture*: A fracture that has "multiple fracture lines and interconnecting fractures."[59] Depressed, multiple linear, comminuted, and stellate fractures are all types of complex fractures.

- *Multiple linear fractures*: Two or more linear fractures that intersect
- *Stellate fracture*: A fracture that has a star shape and wherein the fracture has an indentation from which multiple fractures originate[63]

TABLE 5.1

Example Skull Injuries for Each Code of Abbreviated Injury Scale

AIS Code	Description	Example Skull/Head Injury
1	Minor	Scalp abrasion or contusion
2	Moderate	Simple vault fracture, undisplaced vault fracture (diastatic, linear)
3	Serious	Comminuted vault fracture (open, but intact dura; depressed <2 cm)
4	Severe	Massively depressed vault fracture (large areas >2 cm)
5	Critical	Major skull penetration (>2 cm beneath entrance)
6	Maximum	Massive destruction of both skull and brain
9	Unknown	Used when detailed information is lacking

- *Comminuted fracture*: A fracture in which a portion of the skull bone has broken into fragments
- *Depressed fracture*: A fracture in which the bone caves inward and a section of the skull moves toward the brain or when the outer table of the skull collapses into the inner table of the skull (Figure 5.12c)

(3) *Diastatic fracture:* A fracture that runs along one of the cranial sutures (Figure 5.12a).

The area over which the contact force is applied has been associated with the type of fracture that is produced.[64] A distributed contact produces less injury to the scalp and is more likely to result in linear fractures, some of which could be adjacent to the impact point and others more remote from the site of contact. A contact area of approximately 13 cm^2 represents the transition from distributed loading to localized loading and localized failure for blunt loading at fall and automobile rates. Under more localized loading scenarios, depressed fractures become more common. Focal impacts of surface areas of 5 cm^2 or less can result in punch-through style fractures in which the edges of the fracture match the geometry of the opposing object.

Skull injury data have been classified and correlated using several well-known systems. These include the Abbreviated Injury Scale (AIS) from the Association for the Advancement of Automotive Medicine, which uses a general severity scale ranging from minor injuries at AIS = 1 to untreatable, fatal injuries at AIS = 6 (Table 5.1).[65] AIS levels of 3, 4, and 5 are usually considered significant traumatic injuries. Other descriptive classification systems include the International Classification of Diseases, Ninth Revision (ICD-9), developed by the World Health Organization. ICD-9 codes describing skull fracture range from 800 to 804.[66]

5.4.2 Pediatric Blunt Impact

A large portion of the available literature on the biomechanics of pediatric skull fracture has been necessarily speculative due to limited quantitative data.[56,60,67–69] As a result, much of the impact responses for pediatric heads are estimates from scaling rules.[70–73] One major controversy in pediatric blunt impact biomechanics is the association of skull injury with child abuse, which has been debated in medical literature since Kempe et al.[74] discussed the battered-child syndrome. Because of this dearth of viable information, the association between the two is still largely unresolved.

For the pediatric head, many case reports assert that minor falls (from the height of a bed, chair, or couch) rarely result in serious head injury or skull fracture, and when caretakers suggest that a child has sustained serious injuries from such a fall, abuse should be suspected.[56,60,67] Some of the factors linked to nonaccidental injury are diastatic, branching, depressed, bilateral, or multiple fractures, although there is no consensus as to which of these fracture types suggest that abuse occurred.[56,60,67–69] A recent review of the existing literature determined features that "differentiate fractures resulting from abuse from those sustained from other causes."[74] That review identified two major problems in the existing studies: (1) the difficulty in defining and establishing abuse and (2) the inconsistency in the allegations of which, if any, fracture patterns suggest abuse.

Because the human skull continues to develop into adulthood, with changing structural and material properties, the results of adult skull fracture studies have limited applicability to pediatric head injury.[43,47,63,75–77] One of the few experimental studies using pediatric cadavers to investigate skull fracture patterns was reported by Weber.[78,79] Using 50 postmortem human infant skulls younger than 10 months, Weber analyzed skull fractures from impact heights of 820 mm onto five different types of surfaces: stone, carpet, foam, and camel hair blanket. This height was considered to be a reasonable height for a child to fall from a diaper-changing table. Weber found that all of the skulls fractured for impacts onto stone tile, carpet, and linoleum; 3 of the 15 had fractures that crossed the suture lines.[78] Weber[79] also observed that 1 out of 10 skulls fractured with impacting a 2-cm-thick foam mat and 4 out of 25 fractured when impacting an 8-cm-thick folded camel hair blanket.

In drop tests with 13 pediatric heads, Loyd[8] found that 7 pediatric skulls between 34 weeks of gestation and 24 days did not fracture when dropped from 150 and 300 mm onto a hard flat plate, whereas 5-, 11-, and 22-month-old skulls fractured during 150 or 300 mm drops. Furthermore, 9-month-old, 9-year-old, and 16-year-old cadavers did not sustain any fractures from the 150 to 300 mm drop height, but all fractured during a subsequent 2 m drop test. Three of the four of the specimens in the 5- to 22-month age range experienced diastatic or linear fractures, but the 9- and 16-year-old skulls had no fractures. These results suggest that there may be an age during which fontanelle closure and subsequent bone and suture development without the full bone and suture strength found in adults makes children vulnerable to diastatic and linear skull fractures at drop heights as low as 150 mm.

5.4.3 Adult Blunt Impact

Since the late 1950s, a number of investigators have studied skull fractures to determine the associated bioengineering variables such as force, deformation, stiffness, and energy and to correlate the trauma with these parameters. Allsop[80] gives an overview of the previous studies on skull fracture forces and stiffness. Several different impactors were used to impose the fracture force to the skull, and the energy of the impactors was provided with either gravity (drop tests) or electrohydraulic actuators. These impact tolerance values, based on average impactor pressures, are summarized in Figure 5.13. From these studies, the weakest area of the human cranium was the temporoparietal area, and the strongest was the frontal area. The parietal skull has an impact tolerance that is approximately the average of the frontal and temporoparietal areas.

Christmann et al.[81] conducted static compression tests on 40 human skulls, with the soft tissue intact, to determine the maximum stress upon fracture, strain, elongation, elasticity module, and elasticity coefficient. The compressions were performed at five locations along the medial sagittal part of the calotte. Christmann et al. concluded that the skull, like the cortical bones, is largely elastic.

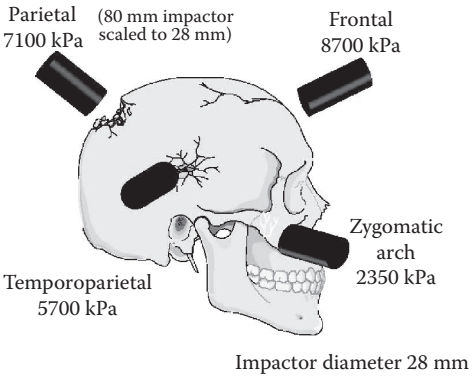

FIGURE 5.13
Approximate average pressure injury tolerances of the adult skull. (Adapted from Springer Science+Business Media: *Accidental Injury: Biomechanics and Prevention*, Skull and facial bone trauma: Experimental aspects, 1993, Allsop, D. L., edited by A. M. Nahum and J. W. Melvin.)

Travis et al.[82] conducted a series of tests examining temporal bone fracture produced in cadavers subjected to realistic automotive impact situations. A portion of that study used piston impacts to the frontal and parietal regions of the skull to impart ipsilateral and contralateral fractures. The impact velocities varied from 7.74 to 10.15 m/s, and the impactor head was a 15.2 cm diameter rigid disc with a total mass of 5.6 and 20.8 kg. They found peak fracture forces of 6650 to 10,700 N for peak accelerations of 340 to 960 *g*.

A recent study performed by Yoganandan and Pintar[83] gives a relatively complete set of biomechanical data on skull fracture (force, deflection, stiffness, and energy) in quasistatic and low-rate dynamic loading conditions. They performed tests, including failure tests, on 12 unembalmed human cadavers using an electrohydraulic testing device. Vertex, parietal, temporal, frontal, and occipital regions were selected as the loading sites. The specimens were isolated at the spine in the Occiput–C_1–C_2 junction, keeping the intracranial contents intact. The tests used a hemispherical anvil with a radius of 48 mm. The overall mean values for failure loads, deflections, stiffness, and energies were 6.4 ± 1.1 kN, 12.0 ± 1.6 mm, 812 ± 139 N/mm, and 33.5 ± 8.5 J for quasistatic loads and 11.9 ± 0.9 kN, 5.8 ± 1.0 mm, 4023 ± 541 N/mm, and 28.0 ± 5.1 J for dynamic loads, respectively. Pathologic alterations were determined by pretest and posttest plane film radiography, close-up computed tomography images, macroscopic evaluation, and defleshing techniques. Although imaging identified the fracture, the precise direction and location of the impact on the skull were not apparent with these techniques. Fracture widths were consistently wider at sites remote from the loading region. In the clinical context, these results emphasize potential difficulties in determining underlying brain injuries from skull fracture imaging alone.[84]

5.4.4 Ballistic Loading

Although much of the historical skull fracture research has concentrated on relatively low-speed impacts with objects of similar or greater mass than the head, these impacts typically result from transportation- and fall-related head injury scenarios. Recently, however, there has been a research thrust to study skull fracture tolerance from impact with high-velocity, low-mass projectiles such as less-lethal kinetic energy munitions[85–87] and behind armor blunt trauma (BABT).[4,88]

Viano et al.[87] reported no skull fractures for direct ballistic impacts on the forehead using 37 mm diameter projectiles ranging from 25 to 35 *g* with impact speeds of 42 ± 10 m/s resulting in peak impact forces of 3.5 ± 0.9 kN. More recently, Crawford et al.[85] reported the results for ballistic forehead impacts using a 38 mm diameter projectile of 103 *g* mass. Skull fractures were produced in four of the tests, and fracture forces ranged from 4413 to 9438 N. Raymond et al.[86] reported peak fracture forces of 5633 ± 2095 N for ballistic impacts to the side of the skull in the temporoparietal region. Fractures from both the studies of Crawford et al. and Raymond et al. ranged from local linear fractures to comminuted/depressed fractures.

Several recent studies have investigated the skull fracture risk from BABT, which is the impact of the backface of a helmet deforming under ballistic impact.[89] Prather et al.[89] recommended a 0.5-inch (1.25-cm) standoff as the threshold for skull fractures with the helmet materials used in their study. The conclusions of that study may be significantly different when considering helmets constructed with modern composite materials with significant backface deformation and yielding behavior that is substantially different than that seen in typical metals.

Bass et al.[4] developed an injury risk assessment for skull fracture owing to high-rate ballistic impact behind ballistic protective helmets using human cadavers based on cadaveric peak impact pressures (Figure 5.14). Helmets were constructed using resin-impregnated enhanced deformation ultrahigh molecular weight polyethylene, with 9 mm incoming projectile velocities between 400 and 460 m/s. For such impacts, the material of protection and the distance between the helmet and the skull were found to be directly related to the levels of injury.[4,88] Using the injury risk function of Bass et al., there is a 50% risk of skull fracture for a peak impact pressure of 51,200 kPa as measured by local force/strain instrumentation. Skull fractures ranged from simple linear fractures to complex combinations of linear fractures and a depressed fracture underneath the helmet impact onto the head (Figure 5.15).

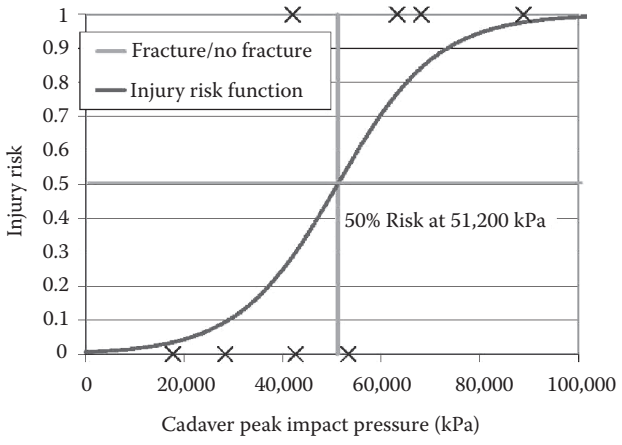

FIGURE 5.14
Injury risk for ballistic behind military helmet impact into the head/skull by 9 mm test bullets from 400 to 460 m/s in terms of local cadaver peak impact pressure. (Reprinted from Bass, C. R. et al., Helmet behind armor blunt trauma. Paper presented at *NATO Specialist Conference on Human Factors in Medicine, Koblenz, Germany*, 2003.)

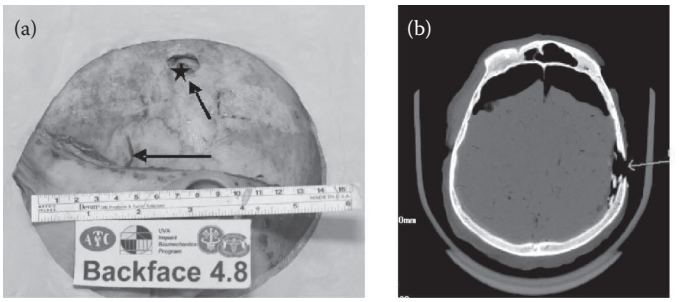

FIGURE 5.15
Ballistic backface skull fracture indicated by arrows. (a) Center of impact is shown with a star. (b) Cross-sectional CT image showing one of the fractures. (Reprinted from Bass, C. R. et al., Helmet behind armor blunt trauma. Paper presented at *NATO Specialist Conference on Human Factors in Medicine, Koblenz, Germany*, 2003.)

5.5 Skull Fracture Injury Reference Values and Risk Assessment Tools

5.5.1 Blunt Impact

The relationships between head kinematics and the occurrence of skull fracture have been the subject of many investigations. Modern sensor technology has recently allowed investigators to accurately measure head dynamics during short-duration injury-producing impacts. An important series of experiments were performed at Wayne State University beginning in the 1940s and into the 1960s.[49,63,90–92] In 1960, Lissner et al.[93] plotted the peak head acceleration versus pulse duration for forehead impacts of six embalmed cadaver tests resulting in linear fracture in an early effort to quantify the relationship between acceleration magnitude, exposure, and the occurrence of fracture. These data points ranged in pulse duration from approximately 1 to 7 ms. Using these data along with additional data from cadaver studies, animal studies, and human volunteer studies, the range of pulse durations was dramatically expanded to include longer pulse durations; the result was the Wayne State Tolerance Curve.[94] To account for different pulse shapes, which may have similar peaks and pulse durations but different injury outcomes, Gadd[95] considered the full impact time history. After plotting the acceleration–impact duration curve on a log–log plot, Gadd approximated a straight-line fit through the data with a slope of –2.5 resulting in the equation for the severity index (SI):

$$\mathrm{SI} = \int_{\Delta t} a^{2.5}\, \mathrm{d}t. \tag{5.3}$$

Gadd also proposed an injury threshold for threat to life of an SI ≥ 1000, based on several sources of data available at that time for analysis. For short-duration events, the SI was an effective discriminator of injury from noninjury cases; however, for long-duration events (such as 1 g for 1000 s), the SI was not useful. Recognizing this limitation, Versace[96] further built on the work of Gadd and proposed weighting the acceleration time pulse by the total length of the effective pulse. The resulting equation, later modified by the National

Highway Traffic Safety Administration, became known as the head injury criterion (HIC) and is given by

$$\mathrm{HIC} = \max\left[\frac{1}{t_2 - t_1}\int_{t_1}^{t_2} a(t)\ \mathrm{d}t\right]^{2.5}\left(t_2 - t_1\right), \tag{5.4}$$

where t_1 and t_2 are time points during the acceleration pulse chosen to produce the maximal HIC value. Today, the HIC is probably the most widely used method to predict head injury, but its use is not without controversy.[30,97,98] In most cases, the calculation of the HIC is limited to a 15-ms time period (HIC15) to avoid the possibility of obtaining high HIC values for pulses of relatively low acceleration with long durations, which have not been shown to result in injury, although a 36-s duration has been used (HIC36).[68,71] Mertz et al.[71] defined injury risk curves for skull fracture within the population with respect to both HIC and peak head acceleration (Figure 5.16). To identify skull fracture injury risk assessment values for other populations, Mertz et al.[68] used scaling techniques based on the relative head size and tissue strengths. The scale factors for acceleration and HIC can be used to scale the skull fracture risk curve shown above (Table 5.2).

More recently, Van Ee et al.[99] analyzed the Weber[78,79] pediatric cadaver drop experiments and reconstructed them using a Child Restraint Air Bag Interaction 6-year-old (CRABI-6) anthropomorphic test device (ATD) to further refine the HIC for the pediatric population. Based on the Van Ee et al. reconstruction, injury risk curves for the prediction of skull fracture using the CRABI-6 ATD were defined. The 5%, 25%, 50%, 75%, and 95% risk for skull fracture correlated with a CRABI-6 peak linear head acceleration of 50, 70, 82, 94, and 114 *g* and a HIC36 of 87, 214, 290, 366, and 493, respectively. These results were in general agreement with Melvin's initially proposed injury assessment reference value (IARV for the CRABI-6 of 390 HIC and a maximum head acceleration of 50 *g* indicating a 5% risk of injury.[70] The results were also similar to the findings of Klinich et al.[100] who suggested provisional CRABI-6 IARV's with their estimated 50% chance of skull fracture at 85 *g* and a 220 HIC based on accident reconstructions of pediatric airbag injuries.

For ballistic impacts, Bass et al.[4] found that the HIC was a poor predictor of cadaveric head/skull injury from the backface deformation of military helmets. Indeed, for all fracture tests, the calculated HIC was well below the HIC injury reference values (Figure 5.17). The HIC values measured in the cadavers for both the fracture and the nonfracture cases were below the typical HIC tolerance values. Owing to the need to stop the projectile before fracturing the skull, skull fracture from ballistic backface deformation of a military helmet is an intrinsically high-rate event. So much of the high-frequency content in the ballistic response signal is filtered using the typical filtering conventions used with HIC. Furthermore, energy is deposited locally, and local skull deformations may be relatively large and may further have limited association with acceleration measurements taken remote from the impact. Use of HIC requires essentially rigid body motion of the head at a relatively low rate compared with ballistic events, so HIC is generally inappropriate for such events.

In addition to acceleration-based injury criteria, other injury criteria have also been proposed. The blunt criterion (BC) is an energy-based design criterion that is defined by the following equation:

$$\mathrm{BC} = \ln\frac{mV^2}{2M^{1/3}TD}, \tag{5.5}$$

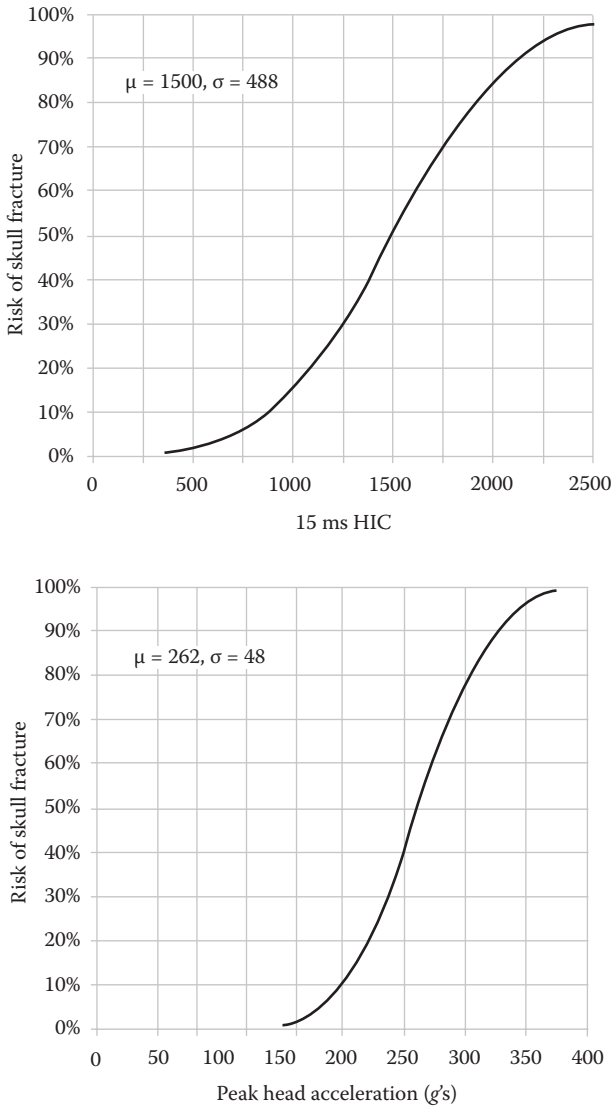

FIGURE 5.16
Adult head injury risk curves for skull fracture as a function of HIC and peak head acceleration.

where m is the mass of the projectile, V is the velocity of the projectile, M is the mass of the struck individual, T is the combined thickness of the soft tissue and skull at the impact location, and D is the diameter of the projectile. Raymond et al.[86] found the BC to be the best predictor of skull fracture occurrence for ballistic impacts to the temporoparietal region of the skull. Interestingly, both Raymond et al. and Crawford et al. reported challenges in accurately quantifying global head acceleration for ballistic tests using skull-mounted accelerometers similar to those used by Bass et al.,[4] indicating that relying on the assumption of head rigid body motion for these short-duration events is likely erroneous due to the excitation of higher modes of skull vibration.

TABLE 5.2

HIC and Acceleration Scaling Factors for Various Anthropometric Sizes

	Scale Factor		Injury Assessment Reference Value	
	Acceleration	**HIC**	**Peak Acceleration (*g*)**	**HIC**
Infant: 6 months	0.865	0.539	156	377
Infant: 12 months	0.887	0.555	154	389
Infant: 18 months	0.889	0.628	160	440
Child: 3 years old	0.970	0.812	175	568
Child: 6 years old	1.505	1.033	189	723
Child: 10 years old	1.053	1.058	190	741
Adult: small female	1.074	1.113	193	779
Adult: mid male	1	1	180	700
Adult: large male	0.971	0.957	175	670

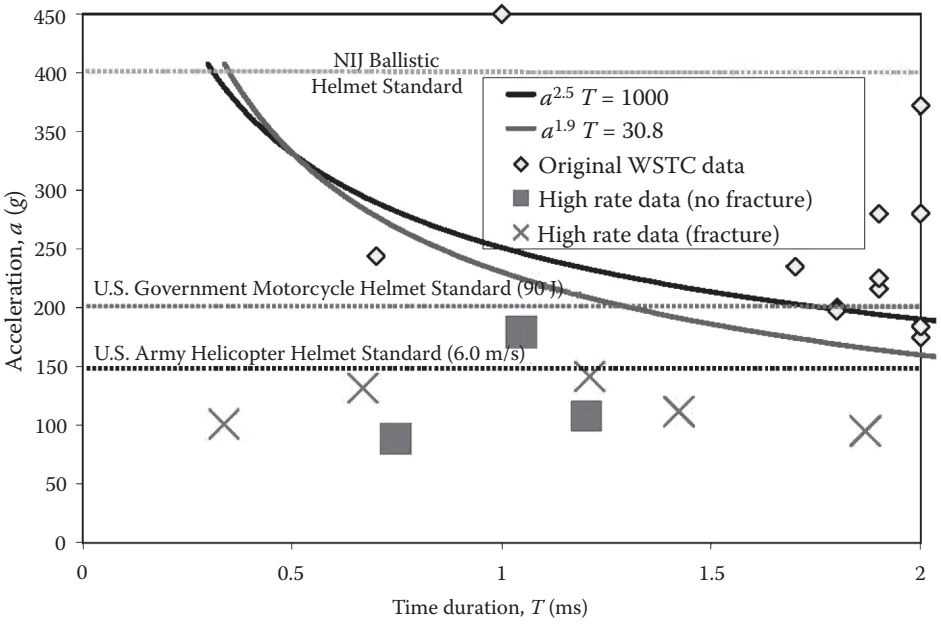

FIGURE 5.17

HIC data from ballistic behind military helmet impact into the head/skull by 9 mm test bullets from 400 to 460 m/s compared with two versions of the Wayne State Tolerance Curve, the current U.S. Army helicopter helmet impact standard and the U.S. government motorcycle helmet impact standard. (Data from Patrick, L. M. et al., Survival by design—Head protection. *Stapp Car Crash Conference Proceedings* SAE Paper 1963-12-0036, 1963; McEntire, B. J., U.S. Army aircrew helmets: Head injury mitigation technology. Presented at the *AGARD AMP Specialists' Meeting on Impact Head Injury: Responses, Mechanisms, Tolerance, Treatment, and Countermeasures, Almagordo, NM*, 1996; U.S. Department of Transportation, 2011, Standard No. 218: Motorcycle Helmets, Code of Federal Regulations, Title 49, Part 571, FMVSS 218. Washington: United States Government Publishing Office.)

5.6 Skull Finite-Element Models

Historically, the development of FE models of the skull has been driven by the development of FE models of head and brain injury. As the complexity of FE head models has increased, so too has the complexity of the corresponding skull models. The skull is particularly important in head models that have focused on the brain's response to blunt impact because the biofidelity of the skull drives the loading and response of the underlying brain tissues. This section outlines the current issues in the development of a biofidelic FE skull model, including skull composition, skull thickness, and material properties.

5.6.1 Skull Composition

The skull is often modeled in a manner similar to engineered sandwich structures as a structural composite of three continuous layers: a layer of cancellous bone (the diploë) sandwiched between two layers of cortical bone (the inner and outer tables). The approach to constructing an FE skull has varied from model to model, in which a two-dimensional shell or three-dimensional solid elements have been used to represent the composition of the skull. Shell elements are computationally cheaper than solid elements, but their accuracy can be limited to thin materials because they are typically based on a plane-stress formulation in which through-thickness stress is not considered.

The simplest skull models have been constructed using a single layer of elements representing the combined properties of the tables and diploë using shell elements[101,102] and solid elements.[103–105] A three-layered shell model based on composite theory has been used to model the skull by representing the three main constituents of the sandwich structure.[102,106] Finally, the three main constituents of the skull have been modeled as separate materials using a solid layer of cancellous bone surrounded by either two shell layers of cortical bone[107,108] or two solid layers of cortical bone.[109,110]

Horgan and Gilchrist[111] compared the brain's response to head impact using skull models with either the three-layered shell, the three-layered solid, or the three-layered shell–solid–shell compositions. Although they found differences in the pressure and stress responses of the brain during impact between the skull composition types, the head mass of each model was not kept constant and likely influenced their results. The limitation of shell elements is particularly important in direct load transmission such as that which occurs with a high-rate blast shock.[112] Being plane-stress elements, dilatational waves (pressure) are not propagated through the surface of the shell material, so the through-thickness bulk properties would only be based on the solid material that the shell elements cover. This becomes a significant issue when the materials that are present have a strong acoustic transmission mismatch across an interface (e.g., bone and soft tissue) or in the skull where acoustic loss is dominated by the diploë layer.[113]

5.6.2 Skull Thickness for Finite-Element Models

The adult human skull varies in thickness within the cranium, with the frontal and occipital regions being thicker than the parietal regions.[114] Although skull thickness may not be an important consideration for simulations when the kinematics of the head imparts the loading to the brain (a rigid skull would likely be adequate), the biofidelity of the skull thickness may have a major effect on the brain during direct impact simulations or in modeling local force transmission or deformations.[115] Ruan and Prasad[116] modified their

original FE head model to create four new models with a constant skull thickness ranging from 4.6 to 9.6 mm, based on their measurements of cadaveric frontal bones. From their cylinder impact simulations, they found that as the skull thickness increased, the skull absorbed less energy during impact and that head impact forces were higher. However, thicker skulls resulted in lower skull deformation, lower impact side pressure, and lower stress in the brain.

5.6.3 Material Properties for Finite-Element Models

Current skull models use material properties that are typically based on isotropic, linear elastic constitutive models.[107,109,110] In models that represent the cortical and cancellous bones as separate skull constituents, cortical bone stiffness ranges between 6 and 15 GPa, whereas cancellous bone stiffness ranges from 0.5 to 4.6 GPa (Table 5.3). For models that have combined the skull into a single material, the stiffness ranges from 1.6 to 8 GPa for the adult skull models and from 0.5 to 4.7 GPa for the pediatric models (Table 5.4).

Bone damage and failure have been introduced into skull models using simplistic elastic–plastic models.[101,102,106–108,117] Failure properties used in various models vary greatly, ranging from 5 to 145 MPa for cortical bone yield stress (yield or ultimate) and from 5 to 30 MPa for cancellous bone (Table 5.5). Material failure or damage in FE analysis is often dependent

TABLE 5.3

Material Properties for Cortical and Cancellous Bone in Skull FE Models

Cortical Bone Properties	Diploë Properties	Reference
G = 5000 MPa	G = 2320 MPa	110
ν = 0.22	ν = 0.24	
ρ = 3000 kg/m^3	ρ = 1750 kg/m^3	
E = 12,200 MPa	E = 1300 MPa	109
ν = 0.22	ν = 0.22	
ρ = 2120 kg/m^3	ρ = 990 kg/m^3	
E = 15,000 MPa	E = 1000 MPa	107,111
ν = 0.22	ν = 0.24	
ρ = 2000 kg/m^3	ρ = 1300 kg/m^3	
E = 6000 MPa	E = 560 MPa	108
ν = 0.25	ν = 0.30	
ρ = 2100 kg/m^3	ρ = 1000 kg/m^3	
E = 15,000 MPa	E = 4600 MPa	106
ν = 0.21	ν = 0.05	
ρ = 1900 kg/m^3	ρ = 1500 kg/m^3	
E = 12,300 MPa	E = 2400 MPa	112
ν = 0.22	ν = 0.19	
ρ = 2000 kg/m^3	ρ = 1300 kg/m^3	

Sources: Ruan, J. S. et al., Finite element modeling of direct head impact. *Stapp Car Crash Conf. Proc.* SAE. Paper 933114, 1993; Al-Bsharat, A. S. et al., *Stapp Car Crash J.*, 43, 321–332, 1999; Horgan, T. J. and Gilchrist, M. D., *Int. J. Crashworthiness*, 84, 353–366, 2003; Kleiven, S. and von Holst, H., Consequences of brain size following impact prediction of subdural hematoma evaluated with numerical techniques. Paper presented at the *International Conference on the Biomechanics of Impacts, Isle of Man, UK*, 2001; Panzer, M. B. et al., Numerical study on the role of helmet protection in blast brain injury, Paper presented at the *Personal Armor Systems Symposium, Quebec City, Canada,* 2010; Willinger, R. et al., *Ann. Biomed. Eng.*, 27, 3, 403–410, 1999; Zhang, L. et al., *Stapp Car Crash J.*, 45, 369–394, 2001.

TABLE 5.4

Material Properties for Combined Skull Bone in Skull FE Models

Combined Skull Bone Properties	Reference
E = 8000 MPa	105
E = 6000 MPa ν = 0.21 ρ = 2100 kg/m^3	102
E = 1600 MPa ν = 0.21	101
E = 4700 MPa* ν = 0.22 ρ = 2150 kg/m^3	103
E = 500 MPa* ν = 0.22 ρ = 2150 kg/m^3	104

Sources: Zhou, C. et al., A new model comparing impact responses of the homogeneous and inhomogeneous human brain. *Stapp Car Crash Conference Proceedings* SAE Paper 952714, 1995; Willinger, R. et al., *Ann. Biomed. Eng.*, 27, 3, 403–410, 1999; Roth, S. et al., *Comput. Methods Programs Biomed.*, 93, 1, 32–45, 2009; Roth, S. et al., *Comput. Methods Programs Biomed.*, 99, 1, 25–33, 2010; Autuori, B. K. et al., *IEEE Trans. Biomed. Eng.*, 53, 7, 1225–1232, 2006.

* Denotes pediatric skull model.

TABLE 5.5

Failure Properties for Skull Bone FE Models

Composite Skull Bone Properties	Reference
Cortical bone: $\sigma_{ultimate}$ = 4.5 MPa Cancellous bone: $\sigma_{ultimate}$ = 4.9 MPa	108
Cortical bone: $\sigma_{ultimate}$ = 90 MPa (tension) Cortical bone: $\sigma_{ultimate}$ = 145 MPa (compression) Cancellous bone: $\sigma_{ultimate}$ = 35 MPa (tension) Cancellous bone: $\sigma_{ultimate}$ = 28 MPa (compression)	102,106
Composite bone: σ_{yield} = 5 MPa Composite bone: E_{tan} = 1400 MPa	101
Cortical bone: σ_{yield} = 90 MPa Cancellous bone: σ_{yield} = 30 MPa	107,117

Sources: Autuori, B. K. et al., *IEEE Trans. Biomed. Eng.*, 53, 7, 1225–1232, 2006; Kleiven, S. and von Holst, H., Consequences of brain size following impact prediction of subdural hematoma evaluated with numerical techniques. Paper presented at the *International Conference on the Biomechanics of Impacts, Isle of Man, UK*, 2001; Kleiven, S., A parametric study of energy absorbing foams for head injury prevention. Paper presented at the *20th Enhanced Safety of Vehicles Conference, Lyons, France*, 2007; Willinger, R. et al., *Ann. Biomed. Eng.*, 27, 3, 403–410, 1999; Willinger, R. and Baumgartner, D., *Int. J. Crashworthiness*, 8, 605–617, 2003; Zhang, L. et al., *Stapp Car Crash J.*, 45, 369–394, 2001.

on mesh size, particularly if failure is being simulated using element removal. Therefore, failure parameters that have been calibrated for one model may not necessarily be accurate for another.

5.7 Conclusions and Gaps in Current Understanding

Because the skull is responsible for containing and protecting the brain, consideration of the biomechanics of the skull will always be important, especially for fundamental injury biomechanics and in assessing potential clinical consequences of head injuries. Information on skull biomechanics feeds the development of biofidelic injury biomechanics models to assess injury; to design automobiles, other vehicles, and equipment; and to assess injury countermeasures. Owing to substantial work on skull biomechanics, including studies considering both children and adults, there is an increasing appreciation of the intricacies of the necessary skull anatomical features, and the material and failure properties.

In a clinical context, there are still several conundrums. For example, skull fractures may be difficult to diagnose during acute clinical presentation, especially in young children. Also, it is uncertain whether the occurrence of skull fractures may protect the brain in some impact scenarios. Improved assessment techniques for such skull fractures may allow inferences on the presence of associated brain injuries and improved treatment.

Of intense interest is the use of clinical or biomechanical data to identify victims of physical abuse, often in young children. Criteria for such identifications in the medical literature are not consistent and have the potential for leading to the misidentification of both abusers and the innocent. It is important to solidify the biomechanical and biomedical understanding of potential abuse scenarios and to provide appropriate and robust guidance for such criminal–medical identifications.

The frontiers of skull biomechanics include age- and region-dependent pediatric skull properties, geriatric properties, and high rate properties. The high rate properties are especially important for blast rate impacts, which may be the source of many mild traumatic brain injuries. These frontiers of skull biomechanics also extend to the incorporation of probabilistic aspects in material models, not solely a mean value nor a mean and a standard deviation. One key gap in skull biomechanics is the lack of postfailure material characterizations. In many injury scenarios, initial failure leads to more serious and potentially life-threatening postfailure behavior. It is not clear if the heuristic models currently used in these situations, such as the assumption of elastic–plastic behavior, or the use of FE model deletion without a theoretical or experimental basis, are appropriate. Such studies represent the far frontiers of human skull biomechanics.

Acknowledgment

The authors gratefully acknowledge support from the National Highway Traffic Safety Administration under cooperative agreement DTNH22-94-Y-07133.

References

1. Summers, C. R., B. Ivans and K. A. Schwab. 2009. Traumatic brain injury in the United States: An epidemiologic overview. *The Mount Sinai Journal of Medicine, New York* 76 (2): 105–110.
2. James, H. E. 1999. Pediatric head injury: What is unique and different? *Acta Neurochirurgica. Supplement* 73:85–88.
3. Kraus, J. F., A. Rock, and P. Hemyari. 1990. Brain injuries among infants, children, adolescents, and young adults. *American Journal of Diseases of Children* 144(6):684–691.
4. Bass C. R., B. Boggess, B. Bush et al. 2003. Helmet behind armor blunt trauma. Paper presented at *NATO Specialist Conference on Human Factors in Medicine, Koblenz, Germany*.
5. Scheuer, L. and S. Black. 2004. *The Juvenile Skeleton.* New York: Academic Press.
6. Sinnatamby, C. S. 2006. Anatomy of the child. In *Last's Anatomy: Regional and Applied*, edited by T. Horne and H. Kenner, 45–51. Edinburgh: Churchill Livingstone.
7. Davis, M. T., A. M. Loyd, H. Shen et al. in press. The mechanical and morphological properties of 6 year-old cranial bone. *Journal of Biomechanics*.
8. Loyd, A. M. 2011. The Structural, Inertial, Geometric and Mechanical Properties of the Pediatric Head. PhD diss., Duke University.
9. Cohen, M. M. 2000. Sutural biology. In *Craniosynostosis: Diagnosis, Evaluation, and Management,* edited by M. M. Cohen and R. E. MacLean, 11–23. New York: Oxford University Press.
10. McElhaney, J. H., J. L. Fogle, J. W. Melvin, R. R. Haynes, V. L. Roberts, and N. M. Alem. 1970. Mechanical properties of cranial bone. *Journal of Biomechanics* 3(5):495–511.
11. Agur, A. M. R. and M. J. Lee 1991. *Grant's Atlas of Anatomy*. Baltimore, MD: Lippincott Williams & Wilkins.
12. Kuffel, C. W. 2004. Orthotic modeling of the developing skull. *Journal of Prosthetics and Orthotics* 16(4S):15–17.
13. Weprin, B. E. and S. S. Rengachary. 1998. Pathogenesis of craniosynostosis and related disorders. calvarial and dural reconstruction. In *Calvarial and Dural Reconstruction*, edited by A. P. Committee, S. S. Rengachary, and E. C. Benzel, 23–34. Park Ridge: The American Association of Neurological Surgeons.
14. Pritchard, J. J., J. H. Scott and F. G. Girgis. 1956. The structure and development of cranial and facial sutures. *Journal of Anatomy* 90(1):73–86.
15. Markens, I. S. 1975. Embryonic development of the coronal suture in man and rat. *Acta Anatomica* 93(2):257–273.
16. Hinton, D., L. Becker, K. F. Muakkassa, and H. J. Hoffman. 1984. Lambdoid synostosis. Part 1: The lambdoid suture: Normal development and pathology of "synostosis." *Journal of Neurosurgery* 61(2):333–339.
17. Markens, I. S. and A. Taverne. 1978. Development of cartilage in transplanted future coronal sutures. *Acta Anatomica* 100(4):428–434.
18. Markens, I. S. and H. Oudhof. 1980. Morphological changes in the coronal suture after replantation. *Acta Anatomica* 107(3):289–296.
19. Ogle, R. C. 2002. Development and growth of the neurocranium. In *Craniofacial Surgery: Science & Surgical Technique,* edited by K. Y. Lin, R. C. Ogle, and J. A. Jane, 64–73. Philadelphia: W.B. Saunders Company.
20. Smith, D. W. and G. Tondury. 1978. Origin of the calvaria and its sutures. *American Journal of Diseases of Children* 132(7):662–666.
21. Adamski, K., A. M. Loyd, K. Smith, A. Samost and C. R. Bass. 2012. Pediatric coronal suture fiber alignment and the effect of interdigitation on suture mechanical properties. Manuscript in preparation.
22. Creutz, U. 1977. Architecture of the human skullcap in the region of the parts bregmatica suturae sagittalis. I. Age dependence. *Gegenbaurs Morphologisches Jahrbuch* 123:666–688.

23. Furuya, Y., M. S. Edwards, C. E. Alpers, B. M. Tress, D. K. Ousterhout, and D. Norman. 1984. Computerized tomography of cranial sutures. Part 1: Comparison of suture anatomy in children and adults. *Journal of Neurosurgery* 61(1):53–58.
24. Retzlaff E. W., J. E. Upledger, F. L. Mitchell and J. Walsh. 1979. Aging of cranial sutures in humans. *The Anatomical Record* 193:663.
25. Herring, S. W. 2000. Sutures and craniosynostosis: A comparative, functional, and evolutionary perspective. In *Craniosynostosis: Diagnosis, Evaluation, and Management*, edited by M. M. Cohen and R. E. MacLean, 3–10. New York: Oxford University Press.
26. Gurdjian, E. S. 1973. Head injury from antiquity to the present with special reference to penetrating head wounds. In *The Beaumont Lecture*. Springfield: Charles C. Thomas.
27. Rafferty, K. L. and S. W. Herring. 1999. Craniofacial sutures: Morphology, growth, and *in vivo* masticatory strains. *Journal of Morphology* 242(2):167–179.
28. Lynch, H. A., W. Johannessen, J. P. Wu, A. Jawa, and D. M. Elliott. 2003. Effect of fiber orientation and strain rate on the nonlinear uniaxial tensile material properties of tendon. *Journal of Biomechanical Engineering* 125(5):726–731.
29. Prange, M. T., J. F. Luck, A. Dibb, C. A. Van Ee, R. W. Nightingale, and B. S. Myers. 2004. Mechanical properties and anthropometry of the human infant head. *Stapp Car Crash Journal* 48:279–299.
30. Prasad, P. and J. W. Melvin. 1985. Review of biomechanical impact response and injury in the automotive environment. Task B Final Report. Ann Arbor: Transportation Research Institute.
31. Burdi, A., D. F. Huelke, R. G. Snyder, and G. H. Lowrey. 1969. Infants and children in the adult world of automobile safety design: Pediatric and anatomical considerations for design of child restraints. *Journal of Biomechanics* 2(3):267–280.
32. Scheuer, L. and S. Black. 2000. *Developmental Juvenile Osteology.* New York: Academic Press.
33. Scheuer, L., S. Black, and M. Schaefer. 2009. *Juvenile Osteology: A Laboratory and Field Manual*. Amsterdam: Elsevier.
34. Silau, A. M., B. Fischer Hansen, and I. Kjaer. 1995. Normal prenatal development of the human parietal bone and interparietal suture. *Journal of Craniofacial Genetics and Developmental Biology* 15(2):81–86.
35. Enlow, D. H. 2000. Normal craniofacial growth. In *Craniosynostosis: Diagnosis, Evaluation, and Management*, edited by M. M. Cohen and R. E. MacLean, 35–50. New York: Oxford University Press.
36. Jaslow, C. and A. Biewener. 1995. Strain patterns in the horncores, cranial bones and sutures of goats *Capra hircus* during impact loading. *Journal of Zoology* 235:193–210.
37. Adeloye, A., K. R. Kattan, and F. N. Silverman. 1975. Thickness of the normal skull in the American blacks and whites. *American Journal of Physical Anthropology* 43(1):23–30.
38. Peterson J. and P. C. Dechow. 2002. Material properties of the inner and outer cortical tables of the human parietal bone. *The Anatomical Record* 268(1):7–15.
39. Skrzat, J., P. Brzegowy, J. Walocha, and W. Wojciechowski. 2004. Age dependent changes of the diploe in the human skull. *Folia Morphologica* 63(1):67–70.
40. McElhaney, J. H. 1966. Dynamic response of bone and muscle tissue. *Journal of Applied Physiology* 21(4):1231–1236.
41. McElhaney, J. H. 1976. Biomechanical aspects of head injury. *Mekhanika Polimerov* 3:465–477.
42. Yoganadan, N., F. Pintar, A. Sances et al. 1996. Biomechanics of skull fracture. In *Traumatic Brain Injury: Bioscience and Mechanics*, edited by F. A. Bandak, R. Eppinger, and A. K. Ommaya, 227–236. New York: Mary Ann Liebert.
43. Coats, B. and S. S. Margulies. 2006. Material properties of human infant skull and suture at high rates. *Journal of Neurotrauma* 23(8):1222–1232.
44. McPherson, G. K. and T. J. Kriewall. 1980. The elastic modulus of fetal cranial bone: A first step towards an understanding of the biomechanics of fetal head molding. *Journal of Biomechanics* 13(1):9–16.
45. McPherson, G. K. and T. J. Kriewall. 1980. Fetal head molding: An investigation utilizing a finite element model of the fetal parietal bone. *Journal of Biomechanics* 13(1):17–26.

46. Margulies, S. S. and K. L. Thibault. 2000. Infant skull and suture properties: Measurements and implications for mechanisms of pediatric brain injury. *Journal of Biomechanical Engineering* 122(4):364–371.
47. Baumer, T. G., B. J. Powell, T. W. Fenton, and R. C. Haut. 2009. Age dependent mechanical properties of the infant porcine parietal bone and a correlation to the human. *Journal of Biomechanical Engineering* 131(11):1100–1106.
48. Wood, J. 1971. Dynamic response of human cranial bone. *Journal of Biomechanics* 4(1):1–12.
49. Evans, F. G., and H. R. Lissner. 1956. Tensile and compressive strength of human parietal bone. *Journal of Applied Physiology* 10(3):493–497.
50. Roberts, V. L. and J. Melvin. 1968. Study of mechanical properties of human calvarium. Presented at the *Symposium on Accident Pathology, Washington, DC*.
51. Carter, D. R. and W. C. Hayes. 1977. The compressive behavior of bone as a two-phase porous structure. *Journal of Bone and Joint Surgery. American Volume* 59(7):954–962.
52. Lakes, R. S., J. L. Katz, and S. S. Sternstein. 1979. Viscoelastic properties of wet cortical bone, I. torsional and biaxial studies. *Journal of Biomechanics* 12(9):657–678.
53. Peterson J. and P. C. Dechow. 1995. Function and variation in elastic properties of the parietal bone. *Journal of Dental Research* 74:SI.
54. Peterson J. and P.C. Dechow. 1996. Function, elastic properties, and microstructure of human circumorbital bone. *Journal of Dental Research* 75:SI.
55. Peterson J., T. Huyen, and P. C. Dechow. 1997. Biomechanics of the human cranial vault: Elastic properties and microarchitecture. *Journal of Dental Research* 76:SI.
56. Behrents R. G., D. S. Carlson, and T. Abdelnour. 1978. In vivo analysis of bone strain about the sagittal suture in *Macaca mulatta* during masticatory movements. *Journal of Dental Research* 57(9–10):904–908.
57. Peterson, J. and P. C. Dechow. 2003. Material properties of the human cranial vault and zygoma. *The Anatomical Record. Part A, Discoveries in Molecular, Cellular, and Evolutionary Biology* 274(1):785–797.
58. Jaslow, C. R. 1990. Mechanical properties of cranial sutures. *Journal of Biomechanics* 23(4):313–321.
59. Bilo, R. A. C., S. G. F. Robben, and R. R. van Rijn. 2010. *Forensic Aspects of Paediatric Fractures: Differentiating Accidental Trauma from Child Abuse.* London: Springer.
60. Hobbs, C. J. 1984. Skull fracture and diagnosis of abuse. *British Medical Journal* 59(3):245–252.
61. Graham, D. I. and T. A. Gennarelli. 2000. Pathology of brain damage after head injury. In *Head Injury*, edited by P. R. Cooper and J. G. Golfinos, 133–153. New York: McGraw Hill.
62. Leestma, J. E. 1988. *Forensic Neuropathology*. New York: Raven Press.
63. Gurdjian, E.S., J. E. Webster and H. R. Lissner. 1950. Biomechanics: Fractures, skull. In *Medical Physics,* edited by O. Glasser, 99–105. Chicago: Year Book Publishers.
64. Melvin, J. W. and F. G. Evans. 1973. Crack propagation in bone. Presented at the *ASME Biomaterials Symposium, New York*.
65. Association for the Advancement of Automotive Medicine. 2008. *Abbreviated Injury Scale, AIS 2005 Update 2008*. Illinois: Association for the Advancement of Automotive Medicine.
66. World Health Organization. 1999. *ICD-9 International Classification of Diseases–ICD9-CM*. Geneva: World Health Organization.
67. Leventhal, J. M., S. A. Thomas, N. S. Rosenfield and R. I. Markowitz. 1993. Fractures in young children: Distinguishing child abuse from unintentional injuries. *American Journal of Diseases of Children* 147(1):87–92.
68. Mertz, H. J., A. Irwin, and P. Prasad. 2003. Biomechanical and scaling bases for frontal and side impact injury assessment reference values. *Stapp Car Crash Journal* 47:155–188.
69. Meservy, C. J., R. Towbin, R. L. McLaurin, P. A. Myers, and W. Ball. 1986. Radiographic characteristics of skull fractures resulting from child abuse. *AJNR, American Journal of Neuroradiology* 149(1):173–175.
70. Melvin, J. W. 1995. Injury assessment reference values for the CRABI 6-month infant dummy in a rear-facing infant restraint with air bag deployment. *Stapp Car Crash Conference Proceedings* SAE Paper 950872.

71. Mertz H. J., P. Prasad, and G. Nusholtz. 1996. Head injury risk assessment for forehead impacts. *Stapp Car Crash Conference Proceedings* SAE Paper 960099.
72. Mertz, H. J., K. Jarrett, S. Moss, M. Salloum, and Y. Zhao. 2001 The Hybrid III 10-year-old dummy. *Stapp Car Crash Journal* 45:319–328.
73. Van Ratingen, M. R., D. Twisk, M. Schrooten, M. C. Beusenberg, A. Barnes, and G. Platten. 1997. Biomechanically based design and performance targets for a 3-year old child crash dummy for frontal and side impact. *Stapp Car Crash Conference Proceedings* SAE Paper 973316.
74. Kempe, C., F. N. Silverman, B. F. Steele, W. Droegemueller, and H. K. Silver. 1962. The battered-child syndrome. *JAMA* 181:17–24.
75. Currey, J. D. and G. Butler. 1975. Mechanical properties of bone tissue in children. *Journal of Bone and Joint Surgery. American Volume* 57(6):810–814.
76. Hodgson, V. R. and L. M. Thomas. 1973. *Breaking Strength of the Human Skull vs. Impact Surface Curvature.* Detroit: Wayne State University School of Medicine.
77. Manzanares, M. C. and D. A. Goret-Nicaise. 1988. Metopic sutural closure in the human skull. *Journal of Anatomy* 161:203–215.
78. Weber, W. 1984. Experimentelle Untersuchungen zu Schädelbruchverletzungen des Säuglings. *Zeitschrift für Rechtsmedizin* 92(2):87–94.
79. Weber, W. 1985. Zur biomechanishen Fragilitat des Sauglingsschadels. *Zeitschrift für Rechtsmedizin* 94(2):93–101.
80. Allsop, D. L. 1993. Skull and facial bone trauma: Experimental aspects. In *Accidental Injury: Biomechanics and Prevention,* edited by A. M. Nahum and J. W. Melvin, 247–267. New York: Springer-Verlag.
81. Christmann, Von C., N. Hung, E. Ehler, and H. G. Wischhusen. 1978. The mechanisms of fracture in the human skull under static loads while still covered by tissue, *Anatomischer Anzeiger* 143(2):192–198.
82. Travis, L. W., R. L. Stalnaker, and J. W. Melvin. 1977. Impact trauma of the human temporal bone. *Journal of Trauma* 17(10):761–766.
83. Yoganandan, N. and F. A. Pintar. 2004. Biomechanics of temporo-parietal skull fracture. *Clinical Biomechanics* 19(3):225–239.
84. Mulroy, M. H., A. M. Loyd, D. Frush, T. Verla, B. S. Myers, and C. R. Bass. 2011. Evaluation of pediatric skull fracture imaging techniques. *Forensic Science International* 214(1–3):167–172.
85. Crawford G., D. Raymond, C. Van Ee, and C. Bir. 2008. Biomechanics of blunt ballistic impacts to the forehead and zygoma. Paper presented at the *American Academy of Forensic Sciences 60th Annual Meeting, Atlanta, GA*.
86. Raymond D., C. Van Ee, G. Crawford, and C. Bir. 2009. Tolerance of the skull to blunt ballistic temporo-parietal impact. *Journal of Biomechanics* 42(15):2479–2485.
87. Viano D. C., C. Bir, T. Walilko, and D. Sherman. 2004. Ballistic impact to the forehead, zygoma, and mandible: Comparison of human and frangible dummy face biomechanics. *Journal of Trauma* 56(6):1305–1311.
88. Sarron, J. C., M. Dannawi, A. Faure, J. P. Caillou, J. Da Cunha, and R. Robert. 2004. Dynamic effects of a 9 mm missile on cadaveric skull protected by aramid, polyethylene or aluminum plate: An experimental study. *Journal of Trauma* 57(2):236–242.
89. Prather, R. 1974. Transient deformation of military helmets and its injury potential, Technical Report EB-TR-74028. Edgewood Arsenal: Department of the Army.
90. Evans F. G., H. R. Lissner, and M. Lebow. 1958. The relation of energy, velocity, and acceleration to skull deformation and fracture. *Surgery, Gynecology & Obstetrics* 107(5):593–601.
91. Gurdjian, E. S. and H. R. Lissner. 1946. Deformations of the skull in head injury studied by the stresscoat technique, quantitative determinations. *Surgery, Gynecology & Obstetrics* 83:219–233.
92. Gurdjian, E. S., J. E. Webster, and H. R. Lissner. 1949. Studies on skull fracture with particular reference to engineering factors. *American Journal of Surgery* 78(5):736–742.
93. Lissner, H. C., M. Lebow, and F. G. Evans. 1960. Experimental studies on the relation between acceleration and intracranial pressure changes in man. *Surgery, Gynecology & Obstetrics* 111:329–338.

94. Gurdjian, E. S., V. L. Roberts, and L. M. Thomas. 1966. Tolerance curves of acceleration and intracranial pressure and protective index in experimental head injury. *Journal of Trauma* 6(5):600–604.
95. Gadd, C. W. 1966. Use of weighted-impulse criterion for establishing injury hazard. *Stapp Car Crash Conference Proceedings* SAE Paper 660793.
96. Versace, J. 1971. A review of the severity index. *Stapp Car Crash Conference Proceedings* SAE Paper 710881.
97. Newman, J. A., N. Shewchenko, and E. Welbourne. 2000. A proposed new biomechanical assessment function—The maximum power index. *Stapp Car Crash Journal* 44:215–247.
98. Prasad, P. 1999. A biomechanical basis for injury criteria used in crashworthiness regulations, Paper presented at the *International Research Conference on the Biomechanics of Impact, Stiges, Spain*.
99. Van Ee, C., B. Moroski-Browne, D. Raymond, K. Thibault, W. Hardy, and J. Plunkett. 2009. Evaluation and refinement of the CRABI-6 anthropomorphic test device injury criteria for skull fracture. Presented at the *ASME International Mechanical Engineering Congress & Exposition, Lake Buena Vista, Florida*.
100. Klinich, K. D., G. M. Hulbert, and L. W. Schneider. 2002. Estimating infant head injury criteria and impact response using crash reconstruction and finite element modeling. *Stapp Car Crash Journal* 46:165–194.
101. Autuori, B., K. Bruyere-Garnier, F. Morriston, M. Brunet, and J. P. Berriest. 2006. Finite element modeling of the head skeleton with a new local quantitative assessment approach. *IEEE Transactions on Bio-Medical Engineering* 53(7):1225–1232.
102. Willinger, R., H. S. Kang, and B. Diaw. 1999. Three-dimensional human head finite-element model validation against two experimental impacts. *Annals of Biomedical Engineering* 27(3):403–410.
103. Roth, S., J. Vappou, J. S. Raul, and R. Willinger. 2009. Child head injury criteria investigation through numerical simulation of real world trauma. *Computer Methods and Programs in Biomedicine* 93(1):32–45.
104. Roth, S., J. S. Raul, and R. Willinger. 2010. Finite element modelling of paediatric head impact: Global Validation against experimental data. *Computer Methods and Programs in Biomedicine* 99(1):25–33.
105. Zhou, C., T. B. Khalil, and A. King. 1995. A new model comparing impact responses of the homogeneous and inhomogeneous human brain. *Stapp Car Crash Conference Proceedings* SAE Paper 952714.
106. Willinger, R. and D. Baumgartner. 2003. Human head tolerance limits to specific injury mechanisms. *International Journal of Crashworthiness* 8:605–617.
107. Kleiven, S. and H. von Holst. 2001. Consequences of brain size following impact prediction of subdural hematoma evaluated with numerical techniques. Paper presented at the *International Conference on the Biomechanics of Impacts, Isle of Man, UK*.
108. Zhang, L., K. H. Yang, R. Dwarampudi et al. 2001. Recent advances in brain injury research: A new human head model development and validation. *Stapp Car Crash Journal* 45:369–394.
109. Al-Bsharat, A. S., W. N. Hardy, K. Yang, T. B. Khalil, A. King, and S. Tashman. 1999. Brain/skull relative displacement magnitude due to blunt head impacts: New experimental data and model. *Stapp Car Crash Journal* 43:321–332.
110. Ruan, J. S., T. B. Khalil, and A. King. 1993. Finite element modeling of direct head impact. *Stapp Car Crash Conference Proceedings* SAE Paper 933114.
111. Horgan, T. J. and M. D. Gilchrist. 2003. The creation of three-dimensional finite element models for simulating head impact biomechanics. *International Journal of Crashworthiness* 84:353–366.
112. Panzer M. B., C. R. Bass, and B. S. Myers. 2010. Numerical study on the role of helmet protection in blast brain injury. Paper presented at the *Personal Armor Systems Symposium, Quebec City, Canada*.
113. Fry, F. J. and J. E. Barger. 1978. Acoustical properties of the human skull. *The Journal of the Acoustical Society of America* 63(5):1576–1590.
114. Lynnerup, N. 2001. Cranial thickness in relation to age, sex and general body build in a Danish forensic sample. *Forensic Science International* 1171(1–2):45–51.

115. Yang, K. H., J. Hu, N. A. White, A. King, C. C. Chou, and P. Prasad. 2006. Development of numerical models for injury biomechanics research: A review of 50 years of publications in the Stapp Car Crash Conference. *Stapp Car Crash Journal* 50:429–490.
116. Ruan, J. S. and P. Prasad. 2001. The effects of skull thickness variations on human head dynamic impact responses. *Stapp Car Crash Journal* 45:395–414.
117. Kleiven, S. 2007. A parametric study of energy absorbing foams for head injury prevention. Paper presented at the *20th Enhanced Safety of Vehicles Conference, Lyons, France*.
118. McEntire, B. J. 1996. U.S. Army aircrew helmets: Head injury mitigation technology. Presented at the *AGARD AMP Specialists' Meeting on Impact Head Injury: Responses, Mechanisms, Tolerance, Treatment, and Countermeasures, Almagordo, NM*.
119. Kriewall, T. J., G. K. McPherson, and A. C. Tsai. 1980. Bending properties and ash content of fetal cranial bone. *Journal of Biomechanics* 14(2):73–79.
120. Billmire, M. E. and P. A. Myers. 1985. Serious head injury in infants: Accident or abuse? *Pediatrics* 75(2):340–342.
121. Patrick, L. M., H. R. Lissner, and E. S. Gurdjian. 1963. Survival by design—Head protection. *Stapp Car Crash Conference Proceedings* SAE Paper 1963-12-0036.
122. U.S. Department of Transportation. 2011. Standard No. 218: Motorcycle Helmets, Code of Federal Regulations, Title 49, Part 571, FMVSS 218. Washington: United States Government Publishing Office.

6

Temporomandibular Joint: Structure, Function, and Current Perspectives

Regina F. MacBarb, Meghan K. Murphy, and Kyriacos A. Athanasiou

CONTENTS

6.1 Introduction

In the particularly active and continually aging society of the United States, injuries and deterioration of the joints are commonplace. Whether they are sports related or result from diseases such as osteoarthritis, the impact on individuals, and on society as a whole, can be overwhelming. Most commonly, injuries or diseases affecting the knee, hip, ankle, and shoulder joints can severely limit an individual's ability to perform daily tasks. Although many methods exist to aid in the recovery of such joints, such as physical therapy, drug treatment, or surgical intervention, little is known about the joints affected by other common activities, such as talking and chewing. These routine actions can become severely

compromised due to the impairment of one of the least understood and under-researched joints of the body: the temporomandibular joint (TMJ). This joint, which is responsible for the hinging motion of the jaw, is essential for properly aligning the upper and lower teeth upon closing of the mouth, known as occlusion.

Proper occlusion is necessary for efficient mastication or chewing. Unfortunately, there are many afflictions that can negatively impact the TMJ, including accidents that disfigure the face as well as a variety of pathologies that all fall under the umbrella of TMJ disorders (TMDs).

Characteristic of intra-articular positional or structural abnormalities, TMD can be broken down into four main categories: pain dysfunction syndrome, internal derangement, arthritis, and traumas.[1] TMD affects 20% to 25% of the population, with only 3% to 4% of patients seeking treatment.[2,3] Although the symptoms associated with TMD may initially be more of a discomfort rather than a hindrance, if left untreated, even the least problematic cases run the risk of becoming severely debilitating. With very few clinically available treatment options for severe TMD, patients have little hope for full recovery once mandibular function has become compromised.

Current clinical interventions for TMD range from physical therapy to highly invasive surgery, depending on the severity of joint damage. In the more nominal cases of TMD, conservative measures are usually taken, including physical therapy, pain management via medication, and occlusal splint therapy.[4–6] When such conservative methods fail to alleviate symptoms associated with TMD, more invasive measures must be taken to counteract the severe pain associated with loss of normal mandibular function. The amount of joint deterioration will indicate the degree of therapeutic invasiveness necessary for mediating the damaged tissue. Less invasive options include arthrocentesis, arthroscopy, or TMJ discectomy.[7–9] In the most severe cases of TMD, wherein both the disc and the articulating surfaces have undergone advanced degenerative changes, a partial or total joint replacement may be the only option. Discal degeneration most commonly presents as deterioration around the outer edge of the disc or as perforations in the disc's center, whereas degeneration of the articulating surfaces is consistent with osteoarthritic changes commonly observed in the knee or hip. Many attempts have been made to create a suitable implant to replace severely damaged features of the TMJ. Only three of such joint replacements are currently approved by the U.S. Food and Drug Administration (FDA): the TMJ concept implant, the Biomet/Lorenz implant, and the TMJ implant total and partial joint replacements.[10]

The lack of suitable FDA-approved clinical options may be correlated with the complex nature of this joint and its associated pathologies. After a discectomy, for example, the articulating surfaces of the joint become highly susceptible to degradation. To address this, many attempts have been made to create replacement discs out of alloplastic or synthetic materials. Unfortunately, these materials lack the ability to withstand the high loads that are characteristic of the TMJ, resulting in breakdown and eventual rejection of the implant.[8] With the main masticatory muscle capable of producing large forces, it is crucial that implant materials be able to withstand such force magnitudes.[11] Increased success has been found with partial and total joint replacements, as exemplified by the three devices currently approved by the FDA; however, they still exhibit a vast array of problems. The most notable issue is that the current joint replacements are unable to withstand the mechanically demanding environment of the jaw for the lifetime of a patient, which can be anywhere from 20 to 60 years, depending on when joint replacement occurs. To date, the longest lifetime of a joint replacement has been found to be in the range of 10 to 15 years, demonstrating that much work needs to be done to make sure such devices can maintain their integrity for the lifetime of patients.[8,10]

A newly explored option for sufferers of severe TMD comes from the promise of engineered replacement tissues. Tissue-engineered replacements offer a unique advantage over metallic or alloplastic implants in that they are created from native materials and therefore can more closely match the mechanical and biochemical properties of the native tissue. Such biological constructs can be engineered to have the appropriate structure–function relationship, which is crucial in that it will allow the tissue-engineered replacements to adapt to and integrate with their environment and, ultimately, become part of the biologically active joint. Regardless of the approach taken to develop effective treatments or therapies for TMD, it is absolutely crucial to first fully understand the design criteria surrounding such an endeavor. This includes not only a thorough understanding of both the biochemical and biomechanical properties of the TMJ and its associated tissues but also how these properties collaborate with one another to maintain the mechanical and biological activity of the joint. Such an understanding will provide clinicians, scientists, and bioengineers with the necessary tools to identify ways to research, prevent, and treat TMD. Currently, much information exists regarding the biochemical makeup of the TMJ tissues, although more characterization is needed to develop consensus in several areas. Standardized information is also lacking with regard to the biomechanical properties of the TMJ as a whole, as well as its individual components. Although many efforts are currently under way to fill this void in our understanding of the TMJ, there is still much to learn. Understanding the biomechanics of healthy, as well as diseased, tissues is key to developing the appropriate therapies for TMD.

6.2 Anatomical Structure–Function Relationships

The efficiency of talking and chewing comes from the jaw's ability to produce fine-tuned and intricate, yet powerful motions. As a result of these motions, the TMJ experiences an extremely complex loading regimen, necessitating its ability to withstand both static and dynamic stress–strain fields on a daily basis. Either static or quasistatic loading conditions can occur during activities such as clenching and grinding. Dynamic loading conditions, on the other hand, occur as the joint undergoes translational, rotational, and slight lateral motion during mastication and speech.[12] Under normal loading conditions, these motions subject the TMJ to a combination of compressive, tensile, and shear stresses, with hydrostatic pressures existing during all positions of occlusion, owing to the extremely complex mechanical environment of the TMJ.

To fully appreciate the mechanical complexity of the TMJ, it is necessary to have a detailed understanding of its anatomical and biochemical makeup, as well as its biomechanical properties, from both macroscopic and microscopic views. Here, the various structures of TMJ are described and their functionality reviewed, culminating in an understanding of how the components of this joint work in unison to meet the functional demands of the jaw.

The anatomical features of the TMJ (Figure 6.1) demonstrate the mechanical complexity of the overall joint. The TMJ connects the lower jaw, or mandible, to the glenoid fossa and articular eminence of the skull. The bilateral condyles of the mandible move in unison as the TMJ functions. This joint can be further characterized as a ginglymo-diarthrodial joint, which reflects the hinging–sliding motion of the TMJ.[1] To protect the major articulating features of the joint from the high loads that occur during hinging–sliding motions, a

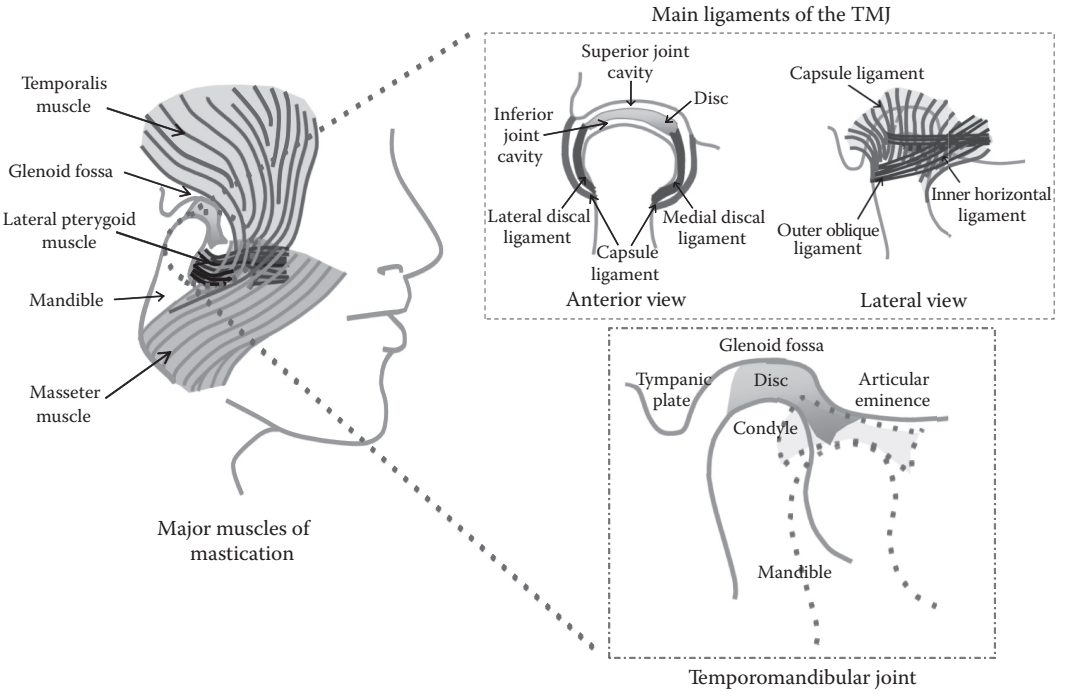

FIGURE 6.1
(See color insert.) Overall anatomy of the TMJ, including the major muscles of mastication, the main ligaments, as well as an enlargement of the joint itself, highlighting its major components. The closed mouth position of the TMJ is shown in solid blue; the open mouth position is shown in dashed red.

thin layer of dense, fibrous, cartilage-like tissue unique to the TMJ covers their surfaces. It is important to note that these cartilage layers are neither vascularized nor innervated, allowing the articulating surfaces to withstand the highly dynamic loading regime found in the TMJ.[13] To further enhance the distribution of the load and to provide shock absorption, a fibrocartilaginous disc separates the superior and inferior articulating surfaces (Figure 6.1). The disc itself is surrounded by a series of ligaments that form the joint capsule, dividing the joint space of the TMJ into superior and inferior compartments. Even from a more macroscopic perspective, it is clear that the TMJ undergoes a complex array of mechanical forces on a daily basis.

6.2.1 Osseous and Articular Features

Looking at the individual components of the TMJ in more detail provides even more insight into the great mechanical demands of this joint. The ability of the TMJ to withstand high loads is attributed to the unique way in which the osseous, or bony, components are situated within the joint. The configuration of the two major osseous features of the TMJ, along with their unique cartilaginous linings, allows them to act as the articulating surfaces of the joint.

The two major articulating surfaces of the TMJ are located in the superior and inferior regions of the joint. The superior articulating surface of the TMJ is composed of the articular eminence and glenoid fossa, both of which are located in the temporal bone of the skull

(Figure 6.1). Bordered posteriorly by the tympanic plate of the temporal bone, the glenoid fossa forms a small, inverted bowl-type structure. Located anterior to the fossa is the convex articular eminence. This structure forms a bony ridge in the anteroposterior direction of the temporal bone.[14] The inferior articulating surface of the TMJ, the condyle, is located at the superior ends of the mandible. Although the fossa and eminence remain stationary because they are part of the skull, the semicylindrical condylar head both rotates and translates with the mandible of the jaw.[15] To distribute loading in the joint, as well as to provide a smooth surface for its articulation, a thin coating of specialized cartilage covers the condyle. This cartilage has been characterized as having four distinct zones, starting as a fibrous cartilage near the articulating surface and then transitioning to a proliferative zone, followed by a mature zone, and, finally, into a hypertrophic zone just above the underlying subchondral bone. Although this general designation applies to the TMJ, there is debate among different researchers about the appropriate names for each zone as well as how to define the different zones.[15–17] The zonal variability in the condylar cartilage, as well as the incongruence between the superior and inferior articulating surfaces, supports the varied mechanical demands and loading patterns placed on the osseous features of the TMJ.

6.2.2 Fibrocartilaginous Disc

To allow the highly incongruent nature of the articulating surfaces of the TMJ to mesh in a physiologically and mechanically efficient manner, a fibrocartilaginous disc is situated between the condylar head and the fossa–eminence unit, segmenting the joint space into inferior and superior regions (Figure 6.1). By adapting and filling the void between the articulating surfaces, the TMJ disc is able to efficiently distribute the high peak forces that would otherwise occur in a discless joint.[12] A consequence of the disc's adaptability is that the forces and loading patterns experienced by this structure constantly change as the joint undergoes various loading regimens.[12] With such mechanical demands, it is necessary for the disc to be held securely in place. Accomplishing this task, an interconnected system of ligaments completely surrounds the disc and attaches it to the condyle and fossa–eminence unit, forming a synovial fluid–filled joint capsule. The synovial fluid in the joint capsule helps the disc fill in the disparities between the articulating surfaces, further attenuating the loads.

The TMJ disc is most commonly viewed as having three distinct zones: an intermediate zone surrounded by a posterior and an anterior band. From a sagittal view, the TMJ disc is thinnest in its intermediate zone with thicker anterior and posterior banding, giving it a biconcave shape. Of the bands, the posterior band is slightly thicker than its anterior counterpart.[1] A more recent view of the TMJ disc is to look at it as a trampoline-type structure composed of two distinct as opposed to three distinct zones (Figure 6.2). In this scheme, the entire periphery is considered one segment of the disc, whereas the center portion is considered a separate segment, reminiscent of a trampoline.[18,19] Viewing the disc in this manner may be more recapitulative of the physiological stress fields, with the outer portion acting as more of a support, load-bearing system and the center region acting as a shock absorber. In this sense, the ligaments attached to the outer region of the disc create tension within its central portion, in particular, in the anteroposterior direction. With this tension in place, the central portion of the disc is able to effectively resist compressive forces; without such tension, the disc would lack the necessary mechanical strength to do so. Considering the TMJ disc as a trampoline may more correctly represent the way forces are sustained and distributed by this very important structure.

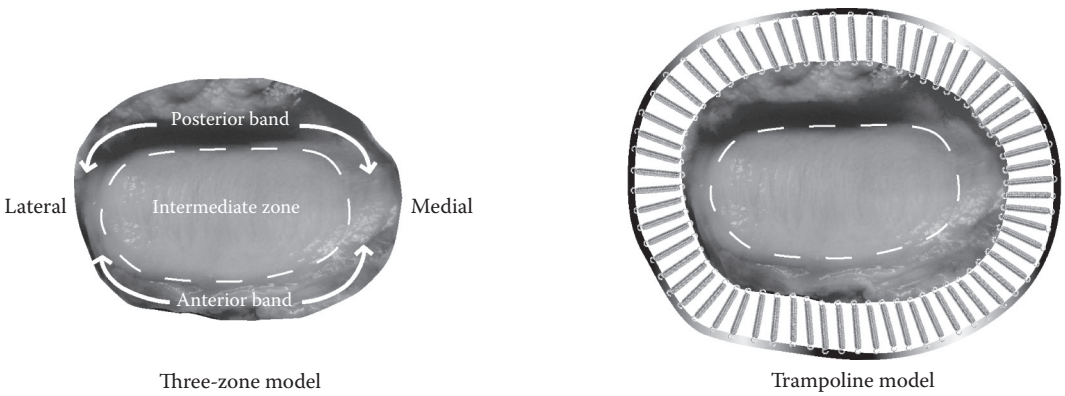

FIGURE 6.2
(See color insert.) Superior view of the three-zone model and the trampoline model representations of the TMJ disc. In the trampoline model, trampoline springs represent the tension-generating function of the ligaments.

6.2.3 Major Temporomandibular Joint Ligaments

Viewing the disc in a trampoline-type configuration may also better fit in with the way it is secured in the joint space. Three main ligaments secure the TMJ: the capsular, collateral, and temporomandibular ligaments (Figure 6.1). The entire periphery of the disc is attached to both the condyle and the fossa–eminence unit of the temporal bone via an array of fibrous connective tissue, creating the joint capsule. This capsule is composed of the capsular ligament, which separates the synovial fluid into two discrete compartments. Unlike the cartilage-like layer covering the articulating surfaces of the TMJ or the fibrocartilage comprising the disc, the joint capsule, which is lined by the synovial membrane, is highly innervated and vascularized. The capsular ligament is fused with the anterior portion of the disc, whereas its posterior portion, known as the bilaminar zone, attaches to the retrodiscal tissue. As the mouth opens and closes, the joint capsule is displaced, causing a redistribution of synovial fluid. As a result, the capsule can be viewed as an important contributor to ensuring proper hydration, nourishment, and lubrication of the TMJ soft tissues.[13]

This joint capsule is connected medially and laterally to the condyle via stiff collagenous connective tissue fibers known as the collateral, or discal, ligaments. These ligaments ensure that the major motion of the joint is in the anteroposterior direction as opposed to the mediolateral direction. Aiding this preferential motion, the disc is more firmly attached to the condyle, allowing it to translate passively with the condyle as the jaw moves.[13,20] The superior portion of the attachments further accommodates this motion by having more slack, allowing the disc to move with the condyle. Furthermore, this configuration allows for rotational motion in the inferior portion of the joint, whereas the superior portion is more prone to translatory motion.[1]

The third major ligament is known as the TMJ ligament. This tough, fibrous ligament helps to support the lateral side of the joint as well as to constrain the rotational opening of the jaw.[20] This ligament is divided into two regions: the outer oblique and the inner horizontal portions. By connecting the articular eminence to the neck of the condyle, the outer oblique component limits the motion of the condyle, therefore controlling how far the mouth can open. The inner horizontal component, on the other hand, connects the articular eminence to the side of the condylar head, limiting the ability of the condyle to translate posteriorly. Overall, the three major ligaments of the TMJ act as taut springs in a

trampoline-like support frame for the disc, providing the disc with the necessary means to function in the mechanically complex environment of the TMJ.

6.2.4 Muscles of Mastication

To facilitate thorough chewing motions, the jaw must be able to move in a variety of directions and produce forces strong enough to break up a food bolus. There are four main muscles that produce the intricate motions necessary for chewing: the masseter, temporalis, medial pterygoid, and lateral pterygoid muscles.[21] The masseter muscle extends from the mandibular angle to the zygomatic arch, or cheekbone, of the temporal bone. It is composed of two parts: the superficial portion, which has vertically aligned fibers, and the deep portion, which has obliquely aligned fibers. The main function of the masseter is to produce the powerful forces required to break apart tough foods. This muscle, which has been found through bite force analysis to produce forces of up to 480 N, is considered the strongest muscle in our body per its weight, giving an idea of the high forces experienced in the TMJ on a daily basis.[22]

Geometrically, the largest muscle found in the TMJ is the temporalis muscle (Figure 6.1). This muscle originates as a tight bundle of fibers in the ramus of the mandible and fans out to form a broad connection with the temporal fossa of the cranium. In the anterior portion of the temporalis muscle, the fibers run vertically, switching to a more oblique orientation in the mid region of the muscle and finally culminating in a horizontal orientation in the posterior region of the muscle. This muscle is capable of directing the jaw to produce many intricate, extremely fine motions, as exemplified by the complexity of the muscle fiber orientation.

Located between the mandibular angle and the pterygoid fossa of the sphenoid, the medial pterygoid muscle follows a similar path as the masseter muscle. Having nearly vertical muscle fibers, the medial pterygoid's main function is to elevate the mandible. The fourth and smallest muscle responsible for controlling motion in the TMJ is the lateral pterygoid muscle. This muscle is composed of both an inferior and superior portion. Although both portions exhibit horizontal muscle fiber alignment, they each have substantially different roles. The inferior portion arises from the lateral pterygoid plate of the sphenoid bone and culminates at the condylar neck. It is mainly associated with protruding and lowering motions of the mandible with respect to the articular eminence as well as lateral movements, making it responsible for translation and rotation of the mandible. Originating from the infratemporal surface of the alisphenoid, or greater sphenoid wing, the superior portion of the pterygoid muscle terminates at the anterior portion of the joint capsule as well as the upper portion of the condylar neck.[20,21] This portion of the pterygoid muscle is responsible for forceful closing and resistance building in the jaw, creating the power stroke motion crucial in generating the forces necessary to chew. A view of the musculature of the TMJ reveals the variety and magnitude of forces generated in this joint as well as the complex array of motions the TMJ must handle daily. With an understanding of the gross structure and function of the ligaments, osseous features, and soft tissues of the joint, we may begin to appreciate the complex loading environment that only results from their cooperative function.

6.3 Biochemical Structure–Function Relationships

Although the overall anatomy can provide much insight into the biomechanical functioning of the TMJ, it is imperative to further consider the biochemical composition of the

joint's load-bearing structures. These biochemical constituents are the microscopic building blocks of the anatomical features of the TMJ, enabling them to withstand the highly dynamic loads of this joint.

6.3.1 Temporomandibular Joint Disc

The TMJ disc has received more attention from researchers than any of the other soft tissues of the TMJ. As a result, the biochemical composition of this tissue is well characterized. The cell density of the TMJ disc has been found to be 681 ± 197 cells/mm^2, of which two distinct cell populations exist. Approximately 70% of the cells are fibroblast-like cells, which are found in greater proportion in the bands of the disc. The non-fibroblast-like cells, having chondrocyte-like characteristics, are found in greater proportion in the disc's intermediate zone.[11] The overall density of these two cell types varies by region in the disc. In the mediolateral direction, more cells are found in the medial and lateral portions compared with the central region, whereas in the anteroposterior direction, the intermediate zone and posterior band have been found to have significantly more cells than the anterior band.[11]

As with all other types of cartilage, the TMJ disc is mainly composed of water, which has been shown to make up 70% to 75% of the disc's weight.[23,24] The remainder of the disc is composed of a dense, fibrous extracellular matrix (ECM) whose main function is to reinforce this tissue so it can function in the mechanically complex environment of the TMJ. Of the various components comprising the disc's ECM, the main constituent is collagen, which has been found in various studies to make up 30% of the wet weight and 83% to 96% of the dry weight of the disc.[25,26] Several types of collagen have been found to comprise the disc, for example, types II, III, VI, IX, and XII; however, the overwhelming majority of the disc's collagen has been established to be collagen type I.[26–30]

Collagen is arguably the most important ECM component for providing and maintaining the mechanical integrity of the TMJ disc. With an average fibril diameter of 44 nm, polarized light microscopy has found collagen to have, on average, thinner fibers in the middle of the disc, whereas the outer ring has been found to have thicker collagen fibers.[31,32] Furthermore, the distribution in diameters has been found to be more uniform in the outer ring than in the middle portion of the disc.[31,32] Although less uniform in terms of diameter, the central region of the disc has been found to exhibit an overall more organized collagen alignment in the anteroposterior direction, compared with fibers running in multiple directions around the periphery of the disc.[23,30,33] This peripheral ring organization is reminiscent of the supporting outer edge of a trampoline, providing further rationale for the trampoline model of the disc (Figure 6.2). This strong outer ring, secured tightly by the surrounding ligaments, provides the necessary support for the center of the disc to act as a shock absorber. The fibers in this outer ring structure have been further characterized as organizing primarily in a transverse orientation, whereas the central region of the disc has been shown to exhibit collagen in sagittal, transverse, and oblique orientations.[30] As can be seen, the collagen fibers exhibit an anisotropic organization within the different regions of the TMJ disc.

Similar to the organization of the collagen, the collagen density also varies by region. The relative distribution of total collagen was measured in several regions of the disc, which showed that, in the anteroposterior direction, the intermediate zone contained higher levels of collagen than the anterior or posterior bands.[34] Greater collagen content was further observed in the medial and central regions in the mediolateral direction of the disc compared with the lateral region. Crimping has also been observed in the collagen of

the TMJ disc. With a mean periodicity of 8 to 23 μm, crimping has been seen most readily in the fibers running anteroposteriorly in the central region of the disc, as well as in those that run between the disc's superior and inferior surfaces.[1,32] Other studies on tendons have found a direct correlation between the periodicity of crimping in collagen fibers and their ability to withstand tensile forces, indicating that the TMJ disc is specifically, but not exclusively, formed to be able to withstand tensile loading regimens.[35] Again, the overall collagen organization and distribution fit in the trampoline-like model described previously, with a ring of collagen existing around the periphery of the disc supporting the fibers aligned in the central region, allowing them to handle anteroposterior tensile loading.

Aside from collagen, elastin has been found to make up 3% to 7% of the dry weight of the disc. Elastin fibers have been found to be distributed throughout the entirety of the porcine disc, with a more dense concentration in the posterior band.[23,36] In a study on the human TMJ disc, 61% of elastin was found in the posterior attachments of the disc comprising the bilaminar zone, 10% was found in the posterior band, and 26% was found in the anterior band.[37] With such a low percentage compared with collagen, elastin most likely aids in discal tissue recovery after a mechanical deformation, making the disc more resilient to peak stresses.[38]

Making up the remainder of the ECM are the proteoglycans, which are composed of a core protein and their associated negatively charged glycosaminoglycan (GAG) side chains. Because of their ability to impede the flow of water throughout the disc, the large proteoglycans, such as aggrecan, are thought to enhance this tissue's compressive properties through a buildup of fluid pressure in the matrix of tissue.[19] The smaller proteoglycans, such as decorin, on the other hand, are thought to promote collagen fibril alignment and orientation.[1,39] The GAG side chains of the proteoglycans have been found to comprise anywhere from 1% to 10% of the dry weight of the disc, although 5% or less of the dry weight is the most common amount reported in the literature.[23,24,26,34,40] Of the many types of GAGs, chondroitin-6-sulfate, chondroitin-4-sulfate, and dermatan and keratin sulfate are the most common forms found in the TMJ disc. Part of the aggrecan proteoglycans, chondroitin sulfate, makes up about 74% of the total GAG concentration, with the remainder being dominated by dermatan over keratin sulfates.[23]

The GAG distribution, like collagen, follows a heterogeneous distribution, with the majority of chondroitin sulfate existing in the intermediate zone, anterior band, and medial side of the porcine TMJ disc.[23] Corroborating this, more GAG has been found in the intermediate zone and anterior band than the posterior band in the anteroposterior direction of the porcine disc.[34] Furthermore, in the mediolateral direction, more GAG was found in the medial as opposed to the central or lateral regions of the disc. In a separate study on the bovine TMJ disc, total GAG was found to exist in higher concentrations in the central region.[24] This was also the result found for the GAG distribution in a study on human TMJ discs.[41] As can be seen, there is little consensus on the distribution of GAG in the TMJ disc. In an attempt to settle this controversy, Kalpakci et al.[40] performed a comparative study on the biochemical properties of the TMJ disc across species. In general, the intermediate zone of the disc was found to have higher levels of GAG than the anterior or posterior bands across all species tested, which included rabbit, goat, human, pig, and cow. The anterior band of the human TMJ disc had significantly less GAG than the other regions tested. GAG levels in the anterior band of the remaining species, however, were comparable across all regions of the disc. As evidenced by this interspecies study, although the GAG distribution follows similar regional patterns between species, the amount of GAG differs, which may reflect the variation in masticatory patterns expressed among species.

6.3.2 Mandibular Condylar Cartilage

Although the TMJ disc is fibrocartilaginous in nature, the cartilage lining the mandibular condyle is more similar to hyaline articular cartilage. As previously mentioned, however, the cartilage of the mandibular condyle is unique to this part of the body. Chondrocytes, the main cell type of this unique cartilage layer, are surrounded by an ECM composed mainly of proteoglycans, GAGs, and several types of collagen. Cell phenotype is specific to each of the four zones of the condylar cartilage. In the fibrous zone, the cells are most similar to the fibroblast-like cells found in the TMJ disc. The proliferative phase is composed of prechondrocyte cells arranged in a heterogeneous manner, whereas mature chondrocytes are arranged within the mature and hypertrophic zones.[15]

Similar to the TMJ disc, the main ECM component of the condylar cartilage is collagen. Total collagen levels have been found to be 2.2 μg/mg wet weight by a hydroxyproline assay.[1] These collagen fibers have been characterized to have a diameter of 30 to 180 nm.[42,43] The main types of collagen in the condylar cartilage are II, IX, and XI.[15,44] Collagen type I, the main collagen of the TMJ disc, has also been found to exist rather extensively in the fibrous zone of this tissue, but only in relatively small amounts in the hypertrophic and mature zones, where the predominant collagen is type II.[43,45,46]

The cartilage lining the condylar head displays an anisotropic alignment of collagen. Within each zone of the condylar cartilage, collagen fibers have been observed to organize in a specific manner. In the fibrous zone, collagen fibers organize in transversely oriented sheet-like structures that run parallel to the surface of the cartilage.[43,47] It has recently been found that collagen fibers are predominantly orientated in the anteroposterior direction throughout the central region of the fibrous zone of the condylar cartilage surface, with a ring-like orientation around the periphery. This finding is extremely similar to the collagen orientation observed in TMJ discs, suggesting that the mechanical properties between these contacting surfaces mesh in a physiologically meaningful way.[48] The prolific, mature, and hypertrophic zones, on the other hand, have been found to exhibit a highly variable collagen network that is perhaps better suited to withstand bulk mechanical changes, such as compressive loads on the condylar head during mastication.[42,43] Crimping has also been established to exist in the collagen of the condylar cartilage, with a mean periodicity of 19.4 μm.[34] This further indicates a role for tensile resistance by this cartilage because collagen crimping periodicity has been correlated with the ability of the tendon to withstand tensile loading.[36]

Data on the other main ECM constituents of the mandibular cartilage are limited. Elastin fibers, having a mean diameter of 350 nm, are observed in all regions of this tissue. Although they have been shown to orient in several directions throughout the layers of this cartilage, regional variations remain uncharacterized.[49] Proteoglycans and GAGs, on the other hand, have been more extensively characterized in the literature. In a study on rat mandibular cartilage, it was found that GAG makes up approximately 6.6 μg/mg of the wet weight.[45] The primary GAG found in the mandibular cartilage is hyaluronic acid, but chondroitin and keratin sulfates have also been identified.[15] The main proteoglycan of mandibular cartilage—aggrecan—has been found to localize in the hypertrophic and mature zones of both rat and porcine tissue. The fibrous and proliferative zones, however, exhibit a greater proportion of other chondroitin sulfate–rich proteoglycans.[44,50,51] In a primate study, on the other hand, chondroitin and keratin sulfate were found to reside mainly in the hypertrophic and mature zones.[29] Compared with the biochemical data available on the TMJ disc, it is clear that a scarcity of information exists for the condylar cartilage. Furthermore, the small amount of information that is available is highly variable between studies, necessitating further characterization of this soft tissue of the TMJ.

6.3.3 Glenoid Fossa–Articular Eminence Cartilage

Biochemical characterization of the superior articulating surface of the TMJ is scarcely found in the literature. In one study, Kim et al.[52] observed the surface of the temporal fossa to be covered in a dense, fibrous tissue, although this tissue has yet to be biochemically described. This dense tissue is most likely composed mainly of collagen, which is supported by the finding of collagen-like crimping in the cartilage layer covering this articulating structure. This crimping has a periodicity of 20.4 μm on average, with larger crimping observed in the cartilage covering the eminence compared with the fossa.[33] The dearth of biochemical characterization of the cartilage lining the fossa–eminence unit is even greater than that for the other TMJ soft tissues. To fully understand the etiology of TMD, a comprehensive description of the anatomical, biochemical, and biomechanical structure–function relationships in all of the tissues comprising the TMJ is required for both healthy and diseased states. Without such knowledge, effective cures for TMD will remain unattainable.

6.4 Biomechanical Properties of the Temporomandibular Joint

Although a thorough understanding of the anatomical and biochemical makeup of the TMJ provides an introduction to the mechanical functionality of this joint, a review of the biomechanical properties of the TMJ is necessary to fully reveal its true mechanical complexity. Fitting the biomechanical properties within the anatomical and biochemical framework will emphasize how the individual structures of the TMJ work together to create a mechanically functional joint. As outlined previously, a major contribution to this mechanical complexity is the incongruence between the articulating surfaces of the TMJ. As a result, the fibrocartilaginous disc is subjected to nonuniform loading during the opening and closing of the mandible.[1] During mastication, these forces are further influenced by the size, consistency, and geometry of the food bolus that is present. This variability means that the duration, magnitude, and location of force application are constantly changing in the TMJ, even within a chewing event.[12,53] To grasp the biomechanical complexity of the TMJ, it is imperative to understand the types of mechanical forces it experiences on a day-to-day basis. Together, consideration of *in vivo* loading patterns, *in vitro* mechanical characterization, and computational modeling can yield a comprehensive understanding of the mechanical functions of the TMJ.

6.4.1 *In Vivo* Loading

Several studies have focused on characterizing the *in vivo* loading of the TMJ to define the full range of forces this tissue is subjected to. Using a monkey model, the articulating surfaces of the TMJ were found to experience a compressive force in response to the masticatory power stroke. It was further observed that during this action, the subcondylar region of the mandible experiences a tensile stress.[54] In a study on the TMJ of miniature pigs, strain gauges placed on the lateral surfaces of the condylar neck and squamosal bone revealed the peak strains on the articulating surfaces of the joint to be mainly compressive, ranging from 223 to 578 με. The tensile strains across the joint, however, were found to be much smaller, ranging from 152 to 364 με. Although the condyle was found to be subjected

to greater compressive forces, this study found the opposite to be true in the lateral region of the articular eminence. Here, greater tensile, rather than compressive, forces were recorded, with an average tensile strain of 212 με.[55] These strains are about an order of magnitude lower than those measured just below the lateral surface of the femoral neck of the hip under physiological loading, which has been recorded at approximately 1500 με.[56] In a separate *in vivo* study, the condyles of baboons were replaced with an instrumented prosthesis to measure the axial compressive loading on this surface during mastication. Loads on the condylar head reached compressive forces of up to 31 N as the baboons ate.[57] It was also shown that more force was exerted on the contralateral rather than the ipsilateral side of the TMJ during mastication.[8] Together, these studies show that the TMJ is subjected to both compressive and tensile forces, the ratio of which changes depending on the location inside the joint. As evidenced by the wide range of stresses and strains during everyday activities, it is clear that the TMJ operates under a highly complex loading environment.

The above studies have revealed the multitude of forces generated nonhomogeneously in the TMJ milieu. These forces also seem to be modulated by opening and closing of the jaw. However, the forces between the articulating surfaces of the TMJ during the translatory motion associated with opening and closing of the mouth have been difficult to quantify. One study examined jaw motion in 20 subjects and found the kinematic center of the condyle–disc complex to be closer to the articular eminence during the opening of the jaw.[58] This study, therefore, suggests that greater force exertion may actually exist during opening, as opposed to closing, of the jaw.

In addition to stresses and strains, significant pressures are also established in the functioning of the TMJ. For example, the intra-articular pressure of the human TMJ was recorded using a needle, transducer, and recording system in patients undergoing arthrocentesis. Pressure levels were found to drop to 53.82 ± 34.40 mmHg (7.18 ± 4.60 kPa) during maximal opening of the mouth.[59] Clenching, however, caused this pressure level to increase to 63.90 ± 52.25 mmHg (8.52 ± 6.97 kPa). Interestingly, these authors noted a significant difference in the pressure forces generated by women during clenching compared with men. On average, females were found to generate pressures of 73.70 ± 61.06 mmHg (9.83 ± 8.14 kPa), whereas males averaged 31.42 ± 11.47 mmHg (4.19 ± 1.53 kPa). This finding may help explain the gender paradox found in TMD, as the ratio of female-to-male patients has been found to be as great as 8:1.[3,60]

Vital information regarding the overall biomechanics of the TMJ has been found through *in vivo* examination of this joint, as exemplified by the results from the studies presented in this section. Unfortunately, such studies have proven quite difficult to carry out and are limited by the fact that it is extremely complicated to perturb the TMJ without causing extensive damage. A biomechanical characterization of the individual joint components has been more readily obtained through *in vitro* testing.

6.4.2 *In Vitro* Testing/Tissue Biomechanics

Several methods to test the *in vitro* biomechanical properties of the TMJ soft tissues can be found throughout the literature, many of which use tissue samples of varying geometry, age, and species. As a result of this discontinuity between studies, there is an abundance of conflicting data describing the biomechanical response and loading environment of the TMJ. Although such inherent differences may exist between studies, one crucial commonality is that they all take the well-established viscoelastic nature of such tissues into consideration.[8,12] Taking on both fluid- and solid-like properties, a viscoelastic material is characteristic of a stress–strain relationship exhibiting time dependency. As a result,

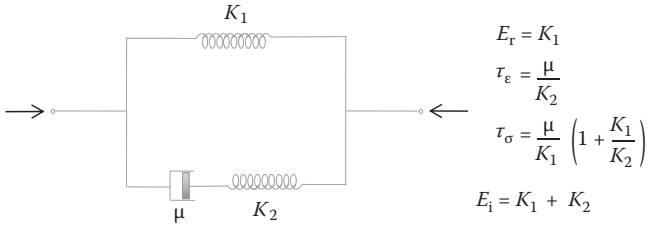

FIGURE 6.3
Kelvin solid represented as a mechanical circuit with accompanying equations to model viscoelastic tissue. The symbols in this figure represent the relaxation modulus (E_r), stress relaxation time constant (τ_ε), and creep time constant (τ_σ), which can be combined to find the instantaneous modulus (E_i) and the coefficient of viscosity (μ).

creep-indentation and stress-relaxation tests are necessary to determine TMJ soft tissue properties.[61] To characterize the viscoelastic response of the TMJ disc under unconfined compression, this tissue has been modeled as a Kelvin solid.[19] Such a model can be viewed as a mechanical circuit that combines a Maxwell viscoelastic element with an elastic element in parallel. The Maxwell element is composed of a spring and a dashpot, representing the elastic nature of a solid and the viscous nature of a fluid. The main parameters that can be obtained from the Kelvin viscoelastic model include the relaxation modulus (E_r), the stress-relaxation time constant (τ_ε), and the creep time constant (τ_σ), which can be combined to find the instantaneous modulus (E_i) and the coefficient of viscosity (μ; Figure 6.3). Such a model has become well established in the field for determining the response of the soft tissues composing the TMJ to various loading regimens.[17,19,40,62–65]

6.4.2.1 Temporomandibular Joint Disc

Of all the soft tissues of the TMJ, the biomechanical properties of the disc are the most thoroughly characterized. The importance of understanding the biomechanics of the disc cannot be overemphasized: most cases of TMD have been highly correlated with a perturbation to the disc, with subsequent breakdown of the surrounding tissues. Therefore, correcting or replacing a damaged disc may help stop the progression of TMD in the many patients whose etiology follows this path. Such an endeavor requires a thorough biomechanical characterization of the TMJ disc.

6.4.2.1.1 Tensile Properties

The tensile properties of the TMJ disc exhibit a distinct anisotropy that correlates with the architecture of the ECM. Beatty et al.[66] tested the tensile stiffness of the porcine TMJ disc using a uniaxial testing machine. In the mediolateral direction, the results showed that the Young's modulus was 3.2 MPa in the central region of the disc, whereas it was found to be 76.4 MPa in the anteroposterior direction. The ultimate tensile strength was found to be 1.6 MPa in the mediolateral direction and 37.4 MPa in the anteroposterior direction of the central portion of the disc. Using a similar testing method, the regional variation of the tensile properties of the TMJ disc was examined, and the Young's moduli of the anterior, intermediate, and posterior bands in the mediolateral direction of the porcine TMJ disc were found to be 9.48, 0.58, and 23.4 MPa, respectively. In the anteroposterior direction, values in the medial, central, and lateral region were found to be 14.3, 18.5, and 10.6 MPa, respectively.[67] Much like the anisotropy defined using biochemical analysis, these two biochemical studies shed light on the anisotropic nature of the tensile properties of the

disc. The direction and location of the highest measured tensile properties were found to correlate with the preferential direction of collagen alignment and the highest amounts of collagen in the disc found via biochemical analysis. Therefore, these studies provide further evidence that tensile properties can be directly correlated to the variation in collagen alignment throughout the disc.

The anisotropy that exists in the tensile properties within the TMJ disc is also species-dependent. In the interspecies study by Kalpakci et al.,[40] the tensile strength of the central portion of the disc in the mediolateral direction was significantly lower than other regions that were tested, regardless of the testing direction; this was true in all species tested, including rabbit, goat, human, pig, and cow. The peak and relaxed Young's modulus of the human TMJ disc was found to be the largest of the five species in the anteroposterior direction with values of 51.7 and 34.4 MPa, respectively. These values were most similar to those measured in the porcine disc, suggesting that the pig model was the closest to mirroring human tissue. The cow, on the other hand, was found to have the lowest TMJ disc tensile properties. These differences, just like those found biochemically, are most likely attributed to the specific masticatory patterns seen in each of the species, implying that the human and pig share the most similar chewing styles.

To understand and characterize disc perforations often observed in TMD, the fracture toughness of the disc was explored.[68] This critical fracture energy analysis was performed by introducing flaws in the anteroposterior direction of the intermediate zone of porcine discs before subjecting them to tensile and shear stresses. Mode I and mode III regimens were used to analyze the resulting crack propagation via tensile and shear stresses, respectively. A mode I regimen causes crack propagation via a tensile stress normal to the plane of the crack, whereas mode III does so through a shear stress parallel to both the plane and front of the crack. By comparing discs receiving an impulsive preload to those not receiving one, the study found discs with damaged collagen networks after preloading to have a 2.3-fold higher fracture toughness under tensile, rather than shear, loading; yet, no such difference was seen in pristine, untouched discs. This finding led to the conclusion that damaged discs require higher energy levels for tensile-induced crack propagation compared with a flawless disc. Although these results seem paradoxical, as a flawed disc would be expected to be more susceptible to stresses, this study found that a damaged collagen network actually stiffens under tensile loading.[68] One possible explanation given in this study was that impulsive loading creates a more permeable ECM. As fluid escapes the network after the impulsive load, the remaining intact collagen accommodates this loss by supporting higher stresses. This result is similar to the response of trabecular bone to compressive loads, in which void spaces within the bone collapse when the bone becomes denser and its capacity to maintain a load increases.[69] Perhaps the collagen fibers actually compact as opposed to breaking apart after an impulsive preload, forming a denser tissue that can withstand higher stresses before failure. Overall, that study highlights how much remains to be defined about the differences in the microenvironment of diseased and healthy discs.[70]

6.4.2.1.2 Compressive Properties

The anisotropy of the tensile properties of the TMJ disc is also observed in its compressive properties, with the disc exhibiting direction-dependent responses to compressive loads. Using an unconfined compression incremental stress relaxation modality, the disc was found to have an overall instantaneous modulus and relaxation modulus of approximately 500 and 80 kPa, respectively. The overall viscosity was also found to be 3.5 MPa/s.[19] A comparison between different regions of the disc, however, revealed the instantaneous modulus to be highest in the anterior and posterior regions of the porcine disc, whereas

the relaxation modulus was found to be largest in the inferior-medial portion of the disc.[18] These results indicated that the regional variability in compressive properties was similar to that seen with the tensile properties of the TMJ disc.

The compressive properties of the TMJ disc, similar to the tensile properties, are species-dependent. Uniaxial confined compression testing was used to measure the viscoelastic properties of the human TMJ disc by determining the aggregate modulus and hydraulic permeability. It was found that the aggregate moduli of the anterior and posterior bands, at 20 and 25 kPa, respectively, were about one-third of the stiffness of the medial, intermediate, and lateral regions of the disc, at 60, 75, and 75 kPa, respectively.[64] The hydraulic permeability in both the anterior and posterior bands was approximately 8.5×10^{-15} m^4/Ns and was approximately 40% more permeable than the mediolateral portions of the disc.[64] These findings suggest that the TMJ disc is subjected to the highest compressive loading regimen in the mediolateral direction, with the anterior and posterior bands being much softer and more permeable. In contrast with these results, a study that used a nanoindentation approach to measure the viscoelastic compressive properties of the porcine disc found it to be approximately 10 times softer in the mediolateral compared with the anteroposterior direction,[65] suggesting the anteroposterior direction to have the highest compressive properties. This discrepancy could be a result of interspecies differences, the use of different testing protocols, or a combination of both.

Testing the differences in compressive properties across species using unconfined compression showed that the cow, goat, and rabbit exhibited significantly higher overall instantaneous and relaxation moduli compared with human and pig.[40] Interestingly, although the cow was found to exhibit the lowest tensile properties in this interspecies study, it demonstrated the highest relaxation modulus (at 120 kPa) in compression. The human and porcine TMJ discs, on the other hand, which were found to have the highest tensile properties, exhibited the lowest compressive properties, with a relaxation modulus between 20 and 30 kPa. This study corroborated the compressive results reported by Yuya et al.,[65] who found that the anteroposterior bands exhibited overall higher compressive stiffness than the mediolateral regions. Therefore, these conflicting results may be due to Yao et al. using a confined compression testing procedure. Although a general consensus has been achieved regarding trends observed in the tensile properties of the TMJ disc regardless of species and testing methods, trends in the compressive properties remain more ambiguous, necessitating additional endeavors to elucidate the compressive properties of the disc.

In addition to clarifying the effects of testing methods and interspecies differences, another area requiring examination relates to how the main biochemical constituents contribute to the compressive properties in the disc. Many studies correlate the compressive properties to proteoglycan levels.[23,26,29,34] The general belief is that more proteoglycans will cause increased resistance to fluid flow in certain regions, causing a local increase in compressive stiffness. Recent studies, however, have been unable to identify such a correlation, finding the anteroposterior regions, which are more often found to have the highest compressive properties, to have lower GAG content than the mediolateral regions. Thus, it has been suggested that the density of the collagen network may be more indicative of compressive properties.[40,67] Future studies on the viscoelastic and biochemical properties of this tissue and their correlation will clarify this issue.

6.4.2.2 Mandibular Condylar Cartilage

The mandibular condylar cartilage has received much attention because it can undergo extensive degradation after disc displacement in TMD. The cartilage covering the condyle

is unlike any other cartilage in the body, necessitating studies to fully explore its mechanical properties.

6.4.2.2.1 Shear/Tensile Properties

The close contact that exists between the TMJ disc and the condylar cartilage suggests that these two tissues experience similar loading regimens and, therefore, will exhibit parallel trends in their tensile properties. Although limited studies have been conducted on the tensile and shear properties of the condylar cartilage, a few recent publications in this area provide insight into how this tissue responds under such loads. Two studies focused on determining the shear behavior of the condylar cartilage. Osteochondral plugs were derived from porcine condylar heads and sheared on a dynamic viscoelastometer. The dynamic shear modulus was found to be 1.5 to 2.0 MPa in the anteroposterior direction, which was 33% higher than the value determined in the mediolateral direction at 0.3 to 0.5 MPa. Comparing these results with those of the TMJ disc, the dynamic shear modulus of condylar cartilage was found to be 1.2 to 1.4 times that of the disc.[71,72]

Porcine osteochondral plugs were tested using a uniaxial testing apparatus to define the condylar cartilage's tensile properties. The Young's modulus was found to be 24.0 MPa in the anteroposterior direction and 10.1 MPa in the mediolateral direction.[48] Supporting these results, a separate study using a similar testing procedure found the Young's modulus of porcine osteochondral plugs to also be higher when tested anteroposteriorly compared with mediolaterally, with values of 9.04 and 6.55 MPa, respectively.[73] Overall, the tensile and shear studies exemplify the anisotropy of the condylar cartilage and suggest the predominant loading direction to be anteroposterior. As the TMJ disc is firmly attached to the condylar head, similar tensile loading regimes in both tissues, as well as similar collagen alignment and organization, further exemplify the mechanical congruence existing between the condyle and TMJ disc.

6.4.2.2.2 Compressive Properties

Similar trends in the compressive properties of the condylar cartilage compared with the TMJ disc should also be expected due to their close proximity and articulation within the joint. As with tensile testing of the condylar cartilage, osteochondral plugs were used in all studies carried out to determine the viscoelastic compressive properties of the condylar cartilage. Two studies have used the porcine model, whereas an additional two studies have used the rabbit model. Kuboki et al.[63] found the condylar cartilage to undergo increased deformation when subjected to constant, as opposed to intermittent, loads. It was further observed that the material became stiffer at higher loads. These results revealed the highly viscoelastic nature of the condylar cartilage, and the authors suggested that this tissue was less stiff than that of the TMJ disc. In a separate study, dynamic nanoindentation via atomic force microscopy was used to measure the elastic modulus and the Poisson's ratio of the condylar cartilage in skeletally mature rabbits. The highest values were found in the anterior portion of the central region of the condyle, with an elastic modulus of 2.34 MPa and a Poisson's ratio of 0.46. Furthermore, it was found that the anterior portion of the condylar cartilage, as a whole, had higher values for these two viscoelastic parameters than the posterior region.[62] In a similar study on neonatal rabbit tissue, similar trends, but decreased values, were measured. This suggested that the viscoelastic heterogeneity of the condylar cartilage varies with age.[74] A more recent study testing porcine samples with a dynamic viscoelastometer found the dynamic complex modulus, storage, and loss modulus to be higher in the anterior region of the central portion of the condylar cartilage, with values of 1.40, 1.36, and 0.34 MPa, respectively. These trends, which are similar to those

of Hu et al.,[62] were found to be linearly proportional to frequency.[75] As seen with the TMJ disc, correlations between GAG distribution and compressive properties were not found. Instead, the highest compressive properties of the condylar cartilage correlate with the regions of highest collagen density, further verifying collagen density to be more indicative of compressive strength than GAG in the soft tissues of the TMJ.

6.4.2.3 Glenoid Fossa Unit

The glenoid fossa is by far the least studied of the soft tissue components of the TMJ. The mechanical properties of the cartilage lining the superior articulating surface of the glenoid fossa still remain largely unknown. Currently, no studies characterizing the tensile properties of this tissue exist; however, one compressive characterization study has been performed. Kim et al.[52] determined the aggregate modulus, the Poisson's ratio, and the permeability of the articular cartilage lining the temporal fossa. It is important to note that the tissue's material properties were found using the linear biphasic theory as opposed to modeling it as a Kelvin solid. This model, which was originally created to model articular cartilage, was developed to take into consideration both the elastic, permeable, porous ECM and the incompressible, synovial fluid.[76,77] Using an indentation apparatus, the aggregate modulus was found to be lowest in the anterior, central, and lateral regions, all at approximately 35 kPa, and highest in the medial and posterior regions, at 42.6 and 58.9 kPa, respectively. The Poisson's ratio was found to be lowest in the anterior and medial regions, both at 0.02, and again highest in the posterior region at 0.13. In terms of permeability, the anterior and medial regions were the lowest at about 9×10^{15} m^4/Ns and highest in the posterior region at 67.3×10^{15} m^4/Ns. The one major conclusion that can be drawn from this study is that like the other soft tissues of the TMJ, the cartilage of the fossa–eminence unit also displays regionally dependent compressive properties.[52] An understanding of how this cartilage fits into the overall functionality of the TMJ cannot be determined until more studies are carried out to further define its mechanical properties.

6.4.3 Modeling of Temporomandibular Joint

Although much information has been gained about the biomechanical nature of the TMJ and its components through *in vivo* and *in vitro* studies, computational modeling offers a unique advantage: modeling allows for the quantification of the forces within tissues during simulated function. Furthermore, a computational model allows select parameters to be isolated so their functionality, alone or in conjunction with other parameters, can be better understood. Such parameters, which can be extremely difficult to alter in biological tissues, can be readily changed in a modeled system. Finally, when the theoretical predictions used to model a system, such as the TMJ, match the experimental and clinical results, modeling can provide an additional means to confirm or validate a hypothesis.

Although several advantages are offered by finite-element analysis, the information achieved through such modeling can be severely limited in poorly characterized tissues. Due to the lack of characterization data on the tissues of the TMJ, most models are currently oversimplified. The information provided by these simplified models, however, can still be quite important. Two-dimensional (2D) finite-element models, developed from magnetic resonance images, provide information on the stress field resulting from 2D motion.[78] To capture the true dimensionality and bilateral nature of the TMJ, however, most modeling studies have focused on creating three-dimensional (3D) models.[53,79–81] In one of the more advanced 3D studies, the bilateral joint was modeled to include the two TMJ discs,

the major ligaments attaching the discs into the joint spaces, as well as the superior and inferior articulating surfaces. Using this model, it was observed that during bruxism, or grinding motions, compressive stresses are higher in the lateral regions of the disc. The authors postulate that during grinding, the two sides of the mandible are subjected to different force fields.[82]

In the study by Tuijt et al.,[83] a biomechanical model of the human masticatory system was used to simulate the forces experienced by the TMJ during opening and closing of the jaw. Their results indicated that the TMJ is subjected to a greater load during opening, rather than closing, of the jaw. This model confirmed the noninvasive clinical study described earlier by Yatabe et al.,[58] which found the kinematic center of the condyle–disc unit to be closer to the articular eminence during opening as opposed to closing, suggesting higher forces during opening. As can be seen from these examples, finite-element modeling of the TMJ provides important information about the biomechanical nature of this joint under realistic loading regimes that cannot be achieved through experimental means alone. A goal for TMJ research should be to continue to characterize the biomechanical nature of the soft tissues of the TMJ through *in vitro* characterization studies and the overall biomechanics of the joint through *in vivo* analysis. Once these characterizations are complete, they can be brought together in computational models to validate findings and provide a working theoretical model for how the whole joint functions under different physiological loading environments. Such models, along with the healthy and diseased tissue characterizations, will provide scientists, engineers, and clinicians with the necessary tools to develop effective treatments for TMD.

6.5 Current Perspectives on Temporomandibular Joint

6.5.1 Tissue Engineering

As previously mentioned, one of the most promising avenues for effective treatment of TMD is engineered replacement tissues. A typical tissue engineering paradigm is shown in Figure 6.4, which illustrates the many approaches that can be taken to engineer tissues to replace those damaged by TMD. The first step in any tissue engineering endeavor is to choose the appropriate cell source. Autologous or allogeneic stem cells, including human embryonic stem cells, mesenchymal stem cells, and induced pluripotent stem cells, are unique in that they provide an undifferentiated, blank slate that, with the appropriate stimuli, can be differentiated into the appropriate cells for creating TMJ tissues with the appropriate stimuli. Unfortunately, we are currently quite far from fully differentiating stem cells that can restore the full TMJ environment. Fully differentiated primary cells, on the other hand, can be isolated from mature tissue.[1,84–86] These cells can either be obtained directly from the source, in this case from the TMJ soft tissues, or from alternative locations, such as the costochondral cells lining the ends of ribs. TMJ disc cells are quite difficult to isolate, resulting in an insufficient cell population for tissue engineering applications.[87] Autologous primary cells from other similar tissues found in the body present a more appropriate option; however, they are associated with donor site morbidity or tissue overgrowth when placed in the TMJ.[88] To avoid these issues, allogeneic or xenogeneic sources may be considered. A major drawback of cells derived from these sources is that they are, in many cases, associated with harmful immunological responses.

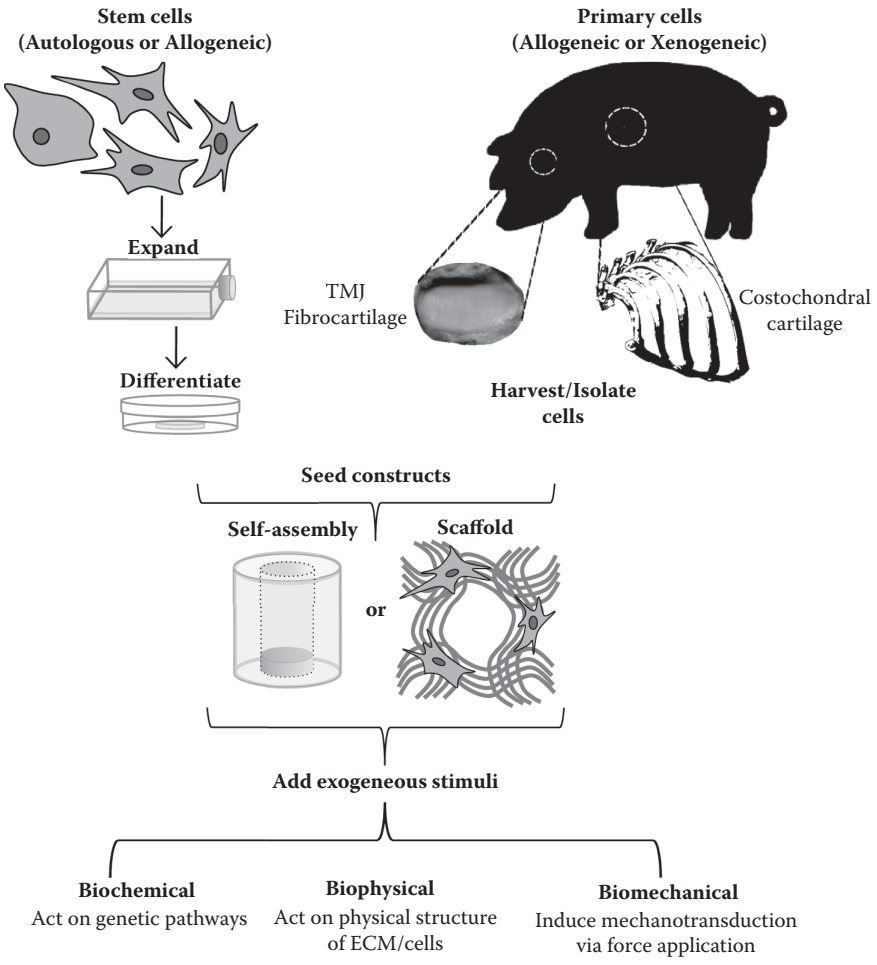

FIGURE 6.4
Typical tissue engineering paradigm for creating tissues recapitulative of native biochemical and biomechanical properties.

Once a cell source is selected and either isolated or differentiated, the cells can be seeded onto a scaffold or self-assembled in a scaffold-free system to promote tissue formation. The benefit of a scaffold-free, self-assembly system is that the issues associated with scaffolding, including biocompatibility, biodegradability, stress shielding, and hindrance of cell-to-cell communication, may be avoided. Once the cells have been seeded in the desired system, the resulting newly formed constructs can be subjected to a vast array of bioactive stimuli with the end goal of forming tissue that is biochemically and mechanically equivalent to the native tissue it is replacing.

Although many aspects of the TMJ soft tissue properties remain to be uncovered, several promising strides have been made toward engineering effective TMJ replacement tissues with mechanical and biochemical properties approaching those of native tissue. In the past decade, most tissue engineering efforts in this area have focused on the TMJ disc, with a more recent interest in the mandibular cartilage and osteochondral components. A

comprehensive overview of the current state of TMJ disc tissue engineering can be found in the textbook by Athanasiou,[1] whereas a review of the advances relevant to mandibular cartilage tissue engineering can be found in the article by Wang and Detamore.[89] Thus far, no efforts have been made on tissue-engineering the cartilage covering the superior articulating surfaces or the discal attachments, demonstrating a major void in this area. Overall, a full comprehension of the structure–function relationships and the loading schemes of both healthy and diseased joints is necessary to create effective replacement tissues to repair or replace pathologic joint components.

6.5.2 Concluding Remarks

By integrating the anatomical, biochemical, and biomechanical properties of the TMJ, we may begin to understand the structure–function relationships among the joint's individual components. Filling the many voids in the current knowledge of the TMJ tissues will elucidate how they unite to form the biologically and mechanically active joint. In terms of biochemical properties, the TMJ disc is well characterized, although some controversy remains on the GAG distribution and whether GAGs play a significant role in the compressive properties of the disc. Recent trends in the literature suggest that compressive properties may be better reflected by the density and organization of the collagen fibrils and not GAGs. More research is needed on the distribution of the different types of collagens as well as on the respective roles of the fibroblast-like and chondrocyte-like cells in the disc. Although the cartilage layer covering the mandibular condyle is also quite well characterized biochemically, similar controversies as with the disc, such as the GAG distribution, the role of GAG, and the role/quantities of the different cells, still remain. This necessitates future studies in these areas. It is also important that efforts to identify the biochemical properties of the cartilage lining the superior articulating surfaces be initiated. As these identified voids are filled, we will be able to use this enhanced understanding of the biochemical makeup of the TMJ soft tissues to begin assembling a complete picture of the changes associated with the disorders of the TMJ and how they lead to a loss of its structure and function.

In terms of biomechanical properties, the most work has again been conducted on the disc, with some literature available on the condylar cartilage; the cartilage lining the fossa–eminence unit, however, is currently lacking such characterization. The most prominent overall drawback in the literature surrounding the biomechanical properties of these tissues is the incongruity among studies. Discontinuities, such as those existing on the relative tensile, shear, and compressive strength of the various tissues, as well as the regional variation associated with each, may only be overcome by standardizing testing methods. This will be a difficult obstacle considering the variations in tissue properties that result from differences in species, age, size, orientation, and location of the tissue source. Most significantly, we must further advance our understanding of the biomechanical nature of the TMJ by developing more physiologically significant testing methods, as this will allow for the measurement of the response of tissues to the stresses and strains they experience in the active joint.

Through carrying out more physiologically relevant *in vitro* and *in vivo* studies, an understanding of the necessary design criteria for replacement tissues and more valid computational models will be achieved. This work must reach beyond the three main TMJ soft tissues described in this chapter because it is imperative that we also reveal the biochemical and biomechanical nature of the discal attachments. Once this information, along with that of the other tissues, has been collected and compiled, finite-element models may be created to truly capture the dynamic nature of this joint, enhancing our abilities to better

understand the TMJ in both the normal and pathologic cases. This will, in turn, aid scientists and clinicians in fully understanding the etiology of TMD and influence the direction taken by tissue engineers to develop biological replacement tissues with the integrity to withstand the dynamic loads of the TMJ for the lifetime of patients. These advances will only be possible if leaders from the clinical, biological, and engineering worlds work hand in hand, which will be greatly aided by continued cross-disciplinary conferences, such as in the TMJ Bioengineering Conference.[90] Having specialists from these three distinct backgrounds working together will put us in the best position to form an understanding of the pathologic mechanisms governing TMD. This will provide us with the necessary tools to reverse-engineer such mechanisms and ultimately identify the most appropriate and effective therapeutic means to bring diseased joints back to a healthy, functional state.

Acknowledgment

This work was supported by grant numbers R01DE015038 and R01DE019666 from NIDCR/NIH.

References

1. Athanasiou, K. A., A. J. Almarza, M. S. Detamore, and K. N. Kalpakci. 2009. Synthesis Lectures on Tissue Engineering, 1(1):1–122.
2. Gray, R. J., S. J. Davies, and A. A. Quayle. 1994. A clinical approach to temporomandibular disorders. 5. A clinical approach to treatment. *British Dental Journal* 177(3):101–106.
3. Solberg, W. K., M. W. Woo, and J. B. Houston. 1979. Prevalence of mandibular dysfunction in young adults. *The Journal of the American Dental Association* 98(1):25–34.
4. Conti, P. C., C. N. dos Santos, E. M. Kogawa, A. C. de Castro Ferreira Conti, and R. de Araujo Cdos. 2006. The treatment of painful temporomandibular joint clicking with oral splints: A randomized clinical trial. *The Journal of the American Dental Association* 137(8):1108–1114.
5. Dao, T. T., and G. J. Lavigne. 2002. Oral splints: The crutches for temporomandibular disorders and bruxism? *Critical Reviews in Oral Biology and Medicine* 9(3):345–361.
6. Nicolakis, P., B. Erdogmus, A. Kopf et al. 2002. Effectiveness of exercise therapy in patients with myofascial pain dysfunction syndrome. *Journal of Oral Rehabilitation* 29(4):362–368.
7. Al-Belasy, F. A., and M. F. Dolwick. 2007. Arthrocentesis for the treatment of temporomandibular joint closed lock: A review article. *International Journal of Oral and Maxillofacial Surgery* 36(9):773–782.
8. Ingawale, S., and T. Goswami. 2009. Temporomandibular joint: Disorders, treatments, and biomechanics. *Annals of Biomedical Engineering* 37(5):976–996.
9. Miloro, M., and B. Henriksen. 2010. Discectomy as the primary surgical option for internal derangement of the temporomandibular joint. *Journal of Oral & Maxillofacial Surgery* 68(4):782–789.
10. Guarda-Nardini, L., D. Manfredini, and G. Ferronato. 2008. Temporomandibular joint total replacement prosthesis: Current knowledge and considerations for the future. *International Journal of Oral and Maxillofacial Surgery* 37(2):103–110.
11. Detamore, M. S., J. N. Hegde, R. R. Wagle et al. 2006. Cell type and distribution in the porcine temporomandibular joint disc. *Journal of Oral and Maxillofacial Surgery* 64(2):243–248.

12. Tanaka, E., and T. van Eijden. 2003. Biomechanical behavior of the temporomandibular joint disc. *Critical Reviews in Oral Biology and Medicine* 14(2):138–150.
13. Bell, W. E. 1982. *Clinical Management of Temporomandibular Disorders*. Chicago: Year Book Medical Publishers.
14. Blaustein, D. I., and L. B. Heffez. 1990. *Arthroscopic Atlas of the Temporomandibular Joint*. Philadelphia: Lea & Febiger.
15. Kuroda, S., K. Tanimoto, T. Izawa et al. 2009. Biomechanical and biochemical characteristics of the mandibular condylar cartilage. *Osteoarthritis Cartilage* 17(11):1408–1415.
16. Luder, H. U., C. P. Leblond, and K. von der Mark. 1988. Cellular stages in cartilage formation as revealed by morphometry, radioautography and type II collagen immunostaining of the mandibular condyle from weanling rats. *The American Journal of Anatomy* 182(3):197–214.
17. Singh, M., and M. S. Detamore. 2009. Biomechanical properties of the mandibular condylar cartilage and their relevance to the TMJ disc. *Journal of Biomechanics* 42(4):405–417.
18. Allen, K. D., and K. A. Athanasiou. 2005. A surface-regional and freeze-thaw characterization of the porcine temporomandibular joint disc. *Annals of Biomedical Engineering* 33(7):951–962.
19. Allen, K. D., and K. A. Athanasiou. 2006. Viscoelastic characterization of the porcine temporomandibular joint disc under unconfined compression. *Journal of Biomechanics* 39(2):312–322.
20. Okeson, J. P. 1985. *Fundamentals of Occlusion and Temporomandibular Disorders*. St. Louis: Mosby.
21. Friedman, M. H., and J. Weisberg. 1985. *Temporomandibular Joint Disorders*: *Diagnosis and Treatment*. Chicago: Quintessence Publishing Co.
22. Bakke, M., L. Michler, K.Han, and E. Moller. 1989. Clinical significance of isometric bite force versus electrical activity in temporal and masseter muscles. *Scandinavian Journal of Dental Research* 97(6):539–551.
23. Detamore, M. S., J. G. Orfanos, A. J. Almarza et al. 2005. Quantitative analysis and comparative regional investigation of the extracellular matrix of the porcine temporomandibular joint disc. *Matrix Biology* 24(1):45–57.
24. Nakano, T., and P. G. Scott. 1996. Changes in the chemical composition of the bovine temporomandibular joint disc with age. *Archives of Oral Biology* 41(8–9):845–853.
25. Gage, J. P., R. M. Shaw, and F. B. Moloney. 1995. Collagen type in dysfunctional temporomandibular joint disks. *The Journal of Prosthetic Dentistry* 74(5):517–520.
26. Nakano, T., and P. G. Scott. 1989. A quantitative chemical study of glycosaminoglycans in the articular disc of the bovine temporomandibular joint. *Archives of Oral Biology* 34(9):749–757.
27. Carvalho, R. S., E. H. Yen, and D. M. Suga. 1993. The effect of growth on collagen and glycosaminoglycans in the articular disc of the rat temporomandibular joint. *Archives of Oral Biology* 38(6):457–466.
28. Landesberg, R., E. Takeuchi, and J. E. Puzas. 1996. Cellular, biochemical and molecular characterization of the bovine temporomandibular joint disc. *Archives of Oral Biology* 41(8–9):761–767.
29. Milam, S. B., R. J. Klebe, R. G. Triplett, and D. Herbert. 1991. Characterization of the extracellular matrix of the primate temporomandibular joint. *Journal of Oral & Maxillofacial Surgery* 49(4):381–391.
30. Minarelli, A. M., and E. A. Liberti. 1997. A microscopic survey of the human temporomandibular joint disc. *Journal of Oral Rehabilitation* 24(11):835–840.
31. Berkovitz, B. K., and J. Pacy. 2002. Ultrastructure of the human intra-articular disc of the temporomandibular joint. *European Journal of Orthodontics* 24(2):151–158.
32. Berkovitz, B. K., and H. Robertshaw. 1993. Ultrastructural quantification of collagen in the articular disc of the temporomandibular joint of the rabbit. *Archives of Oral Biology* 38(1):91–95.
33. Berkovitz, B. K. 2000. Collagen crimping in the intra-articular disc and articular surfaces of the human temporomandibular joint. *Archives of Oral Biology* 45(9):749–756.
34. Almarza, A. J., A. C. Bean, L. S. Baggett, and K. A. Athanasiou. 2006. Biochemical analysis of the porcine temporomandibular joint disc. *The British Journal of Oral & Maxillofacial Surgery* 44(2):124–128.
35. Merrilees, M. J., and M. H. Flint. 1980. Ultrastructural study of tension and pressure zones in a rabbit flexor tendon. *The American Journal of Anatomy* 157(1):87–106.

36. Keith, D. A. 1979. Elastin in the bovine mandibular joint. *Archives of Oral Biology* 24(3):211–215.
37. Gross, A., A. Bumann, and B. Hoffmeister. 1999. Elastic fibers in the human temporo-mandibular joint disc. *International Journal of Oral & Maxillofacial Surgery* 28(6):464–468.
38. Mah, J. 2004. Histochemistry of the foetal human temporomandibular joint articular disc. *European Journal of Orthodontics* 26(4):359–365.
39. Scott, J. E., C. R. Orford, and E. W. Hughes. 1981. Proteoglycan–collagen arrangements in developing rat tail tendon. An electron microscopical and biochemical investigation. *The Biochemical Journal* 195(3):573–581.
40. Kalpakci, K. N., V. P. Willard, M. E. Wong, and K. A. Athanasiou. 2011. An interspecies comparison of the temporomandibular joint disc. *Journal of Dental Research* 90(2):193–198.
41. Kopp, S., G. E. Carlsson, T. Hansson, and T. Oberg. 1976. Degenerative disease in the temporomandibular, metatarsophalangeal and sternoclavicular joints. An autopsy study. *Acta Odontologica Scandinavica* 34(1):23–32.
42. de Bont, L. G., G. Boering, P. Havinga, and R. S. Liem. 1984. Spatial arrangement of collagen fibrils in the articular cartilage of the mandibular condyle: A light microscopic and scanning electron microscopic study. *Journal of Oral and Maxillofacial Surgery* 42(5):306–313.
43. Shibata, S.,O. Baba, M. Ohsako et al. 1991. Ultrastructural observation on matrix fibers in the condylar cartilage of the adult rat mandible. *The Bulletin of Tokyo Medical and Dental University* 38(4):53–61.
44. Teramoto, M., S. Kaneko, S. Shibata et al. 2003. Effect of compressive forces on extracellular matrix in rat mandibular condylar cartilage. *Journal of Bone and Mineral Metabolism* 21(5): 276–286.
45. Delatte, M., J. W. Von den Hoff, R. E. van Rheden, and A. M. Kuijpers-Jagtman. 2004. Primary and secondary cartilages of the neonatal rat: The femoral head and the mandibular condyle. *European Journal of Oral Sciences* 112(2):156–162.
46. Mizoguchi, I., I. Takahashi, M. Nakamura et al. 1996. An immunohistochemical study of regional differences in the distribution of type I and type II collagens in rat mandibular condylar cartilage. *Archives of Oral Biology* 41(8–9):863–869.
47. Luder, H. U., and H. E. Schroeder. 1992. Light and electron microscopic morphology of the temporomandibular joint in growing and mature crab-eating monkeys (*Macaca fascicularis*): The condylar calcified cartilage. *Anatomy and Embryology* 185(2):189–199.
48. Singh, M., and M. S. Detamore. 2008. Tensile properties of the mandibular condylar cartilage. *Journal of Biomechanical Engineering* 130(1):011009.
49. Appleton, J. 1975. The ultrastructure of the articular tissue of the mandibular condyle in the rat. *Archives of Oral Biology* 20(12):823–826.
50. Mao, J. J., F. Rahemtulla, and P. G. Scott. 1998. Proteoglycan expression in the rat temporomandibular joint in response to unilateral bite raise. *Journal of Dental Research* 77(7):1520–1528.
51. Roth, S., K. Muller, D. C. Fischer, and K. H. Dannhauer. 1997. Specific properties of the extracellular chondroitin sulphate proteoglycans in the mandibular condylar growth centre in pigs. *Archives of Oral Biology* 42(1):63–76.
52. Kim, K. W., M. E. Wong, J. F. Helfrick, J. B. Thomas, and K. A. Athanasiou. 2003. Biomechanical tissue characterization of the superior joint space of the porcine temporomandibular joint. *Annals of Biomedical Engineering* 31(8):924–930.
53. Beek, M., J. H. Koolstra, L. J. van Ruijven, and T. M. van Eijden. 2001. Three-dimensional finite element analysis of the cartilaginous structures in the human temporomandibular joint. *Journal of Dental Research* 80(10):1913–1918.
54. Hylander, W. L. 1979. Experimental analysis of temporomandibular joint reaction force in macaques. *American Journal of Physical Anthropology* 51(3):433–456.
55. Herring, S. W., and Z. J. Liu. 2001. Loading of the temporomandibular joint: Anatomical and in vivo evidence from the bones. *Cells Tissues Organs* 169(3):193–200.
56. Cristofolini, L., B. P. McNamara, A. Freddi, and M. Viceconti. 1997. In vitro measured strains in the loaded femur: Quantification of experimental error. *The Journal of Strain Analysis for Engineering Design* 32(3):193–200.

57. Hohl, T. H., and W. H. Tucek. 1982. Measurement of condylar loading forces by instrumented prosthesis in the baboon. *Journal of Maxillofacial Surgery* 10(1):1–7.
58. Yatabe, M., A. Zwijnenburg, C. C. Megens, and M. Naeije. 1997. Movements of the mandibular condyle kinematic center during jaw opening and closing. *Journal of Dental Research* 76(2):714–719.
59. Nitzan, Y., H. M. Wexler, and S. M. Finegold. 1994. Inactivation of anaerobic bacteria by various photosensitized porphyrins or by hemin. *Current Microbiology* 29(3):125–131.
60. Dolwick, M. F., R. W. Katzberg, and C. A. Helms. 1983. Internal derangements of the temporomandibular joint: Fact or fiction? *The Journal of Prosthetic Dentistry* 49(3):415–418.
61. Dogan, F., and M. S. Celebi. 2011. Real-time deformation simulation of non-linear viscoelastic soft tissues. *Simulation* 87:179–187.
62. Hu, K., P. Radhakrishnan, R. V. Patel, and J. J. Mao. 2001. Regional structural and viscoelastic properties of fibrocartilage upon dynamic nanoindentation of the articular condyle. *Journal of Structural Biology* 136(1):46–52.
63. Kuboki, T., M. Shinoda, M. G. Orsini, and A. Yamashita. 1997. Viscoelastic properties of the pig temporomandibular joint articular soft tissues of the condyle and disc. *Journal of Dental Research* 76(11):1760–1767.
64. Yao, H., J. Kuo, L. X. Zhang, and T. Bacroc. 2010. The region-dependent biphasic viscoelastic properties of human temporomandibular joint discs under confined compression. *Journal of Biomechanics* 43(7):1316–1321.
65. Yuya, P. A., E. K. Amborn, M. W. Beatty, and J. A.Turner. 2010. Evaluating anisotropic properties in the porcine temporomandibular joint disc using nanoindentation. *Annals of Biomedical Engineering* 38(7):2428–2437.
66. Beatty, M. W., M. J. Bruno, L. R. Iwasaki, and J. C. Nickel. 2001. Strain rate dependent orthotropic properties of pristine and impulsively loaded porcine temporomandibular joint disk. *Journal of Biomedical Materials Research* 57(1):25–34.
67. Detamore, M. S., and K. A. Athanasiou. 2003. Tensile properties of the porcine temporomandibular joint disc. *Journal of Biomechanical Engineering* 125(4):558–565.
68. Beatty, M. W., J. C. Nickel, L. R.Iwasaki, and M. Leiker. 2003. Mechanical response of the porcine temporomandibular joint disc to an impact event and repeated tensile loading. *Journal of Orofacial Pain* 17(2):160–166.
69. Martin, R. B., D. B. Burr, and N. A. Sharkey. 1998. *Skeletal Tissue Mechanics*. New York: Springer.
70. Beatty, M. W., R. H. Hohl, J. C. Nickel, L. R. Iwasaki, and R. M. Pidaparti. 2008. Mode I and mode III fractures in intermediate zone of full-thickness porcine temporomandibular joint discs. *Annals of Biomedical Engineering* 36(5):801–812.
71. Tanaka, E., Y. Iwabuchi, E. B. Rego et al. 2008. Dynamic shear behavior of mandibular condylar cartilage is dependent on testing direction. *Journal of Biomechanics* 41(5):1119–1123.
72. Tanaka, E., E. B. Rego, Y. Iwabuchi et al. 2000. Biomechanical response of condylar cartilage-on-bone to dynamic shear. *Journal of Biomedical Materials Research Part A* 85(1):127–132.
73. Kang, H., G. Bao, Y. Dong et al. 2000. Tensile mechanics of mandibular condylar cartilage. *Hua Xi Kou Qiang Yi Xue Za Zhi* 18(2):85–87.
74. Patel, R. V., and J. J. Mao. 2003. Microstructural and elastic properties of the extracellular matrices of the superficial zone of neonatal articular cartilage by atomic force microscopy. *Frontiers in Bioscience* 8:18–25.
75. Tanaka, E., Y. Iwabuchi, E. B. Rego et al. 2006. Dynamic compressive properties of the mandibular condylar cartilage. *Journal of Dental Research* 85(6):571–575.
76. Mak, A. F., W. M.Lai, and V. C. Mow. 1987. Biphasic indentation of articular cartilage—I. Theoretical analysis. *Journal of Biomechanics* 20(7):703–714.
77. Mow, V. C., M. C. Gibbs, W. M. Lai, W. B. Zhu, and K. A. Athanasiou. 1989. Biphasic indentation of articular cartilage—II. A numerical algorithm and an experimental study. *Journal of Biomechanics* 22(8–9):853–861.
78. Chen, J., U. Akyuz, L. Xu, and R. M. Pidaparti. 1998. Stress analysis of the human temporomandibular joint. *Medical Engineering & Physics* 20(8):565–572.

79. Mori, H., S. Horiuchi, S. Nishimura et al. 2010. Three-dimensional finite element analysis of cartilaginous tissues in human temporomandibular joint during prolonged clenching. *Archives of Oral Biology* 55(11):879–886.
80. Tanaka, E., R. del Pozo, M. Tanaka et al. 2004. Three-dimensional finite element analysis of human temporomandibular joint with and without disc displacement during jaw opening. *Medical Engineering & Physics* 26(6):503–511.
81. Tanaka, E., D. P. Rodrigo, M. Tanaka et al. 2001. Stress analysis in the TMJ during jaw opening by use of a three-dimensional finite element model based on magnetic resonance images. *International Journal of Oral and Maxillofacial Surgery* 30(5):421–430.
82. Perez Del Palomar, A., and M. Doblare. 2006. Finite element analysis of the temporomandibular joint during lateral excursions of the mandible. *Journal of Biomechanics* 39(12):2153–2163.
83. Tuijt, M., J. H. Koolstra, F.Lobbezoo, and M. Naeije. 2010. Differences in loading of the temporomandibular joint during opening and closing of the jaw. *Journal of Biomechanics* 43(6):1048–1054.
84. Gunja, N. J., D. J. Huey, R. A. James, and K. A. Athanasiou. 2009. Effects of agarose mould compliance and surface roughness on self-assembled meniscus-shaped constructs. *Journal of Tissue Engineering and Regenerative Medicine* 3(7):521–530.
85. Huey, D. J., and K. A. Athanasiou. 2011. Maturational growth of self-assembled, functional menisci as a result of TGF-beta1 and enzymatic chondroitinase-ABC stimulation. *Biomaterials* 32(8):2052–2058.
86. Kalpakci, K. N., E. J. Kim, and K. A. Athanasiou. 2011. Assessment of growth factor treatment on fibrochondrocyte and chondrocyte co-cultures for TMJ fibrocartilage engineering. *Acta Biomaterialia* 7(4):1710–1718.
87. Johns, D. E., M. E.Wong, and K. A. Athanasiou. 2006. Clinically relevant cell sources for TMJ disc engineering. *Journal of Dental Research* 87(6):548–552.
88. Baek, R. M., and Y. T. Song. 2006. Overgrowth of a costochondral graft in reconstruction of the temporomandibular joint. *Scandinavian Journal of Plastic and Reconstructive Surgery and Hand Surgery* 40(3):179–185.
89. Wang, L., and M. S. Detamore. 2007. Tissue engineering the mandibular condyle. *Tissue Engineering* 13(8):1955–1971.
90. Detamore, M. S., K. A. Athanasiou, and J. Mao. 2007. A call to action for bioengineers and dental professionals: Directives for the future of TMJ bioengineering. *Annals of Biomedical Engineering* 35(8):1301–1311.

7

Spine Biomechanics

Chad Cole, Christopher Wolfla, Frank A. Pintar, and Narayan Yoganandan

CONTENTS

7.1 Introduction

The human spinal column is anatomically defined by the vertebrae, intervertebral discs, adjacent muscles and ligaments, and the nervous system that disseminates between and within the spinal tissues.[1] Biomechanically, the spine is defined by posture, load history, disc degeneration, and muscle fatigue. Both the anatomic and biomechanical properties of the spine must be understood at the functional segment level, within the spinal region (i.e., cervical, thoracic, or lumbar), and for the entire spine as a whole. The integration of all these factors allows for the definition of abnormalities and the identification of optimal treatments that ameliorate pain or dysfunction. Here, we review the relevant anatomy and kinematics of the different spinal regions. We then review basic biomechanics as it applies to the spine. Following this foundation, we then present relevant issues in spinal instrumentation for the clinical management of spine conditions.

7.2 Vertebral Column—Anatomy and Kinematics

The human spinal column consists of 33 vertebrae that are interconnected by intervertebral discs, facet capsules, and other ligaments. There are 7 cervical (C1–C7), 12 thoracic (T1–T12), 5 lumbar (L1–L5), 5 fused sacral (S1–S5), and 4 separate coccygeal bones (Figure 7.1). The normal adult vertebral column has four curvatures: the cervical and lumbar regions are lordotic, whereas the thoracic and lumbosacral regions are kyphotic (Figure 7.2). The lordotic curvature is convex ventrally, and the kyphotic curvature is concave ventrally. The thoracic and lumbosacral kyphotic curvatures exist *in utero* and are called the primary curvatures. The cervical and lumbar lordotic curvatures develop with the raising of the head postnatally and the assumption of the erect posture. The cervical curvature is shallow; it begins at the dens of the second cervical vertebra (C2) and terminates at the second thoracic vertebra (T2) (Figure 7.2). The lumbar lordosis develops due to the upright position of the trunk. The sacral curvature is relatively smooth and concave. Variations in the disc and vertebral body dimensions develop to maintain these curvatures, often modified by age-related changes of the vertebra, osteophyte development, trauma, congenital malformations, neurologic disorders, and imbalances of the paraspinal muscles. The center of gravity of the spinal column generally passes from C2 through the vertebra to the promontory of the first sacral vertebra. The center of gravity of the body is located just ventral to the sacral promontory (Figure 7.2). The vertebral column has different types of articulations:

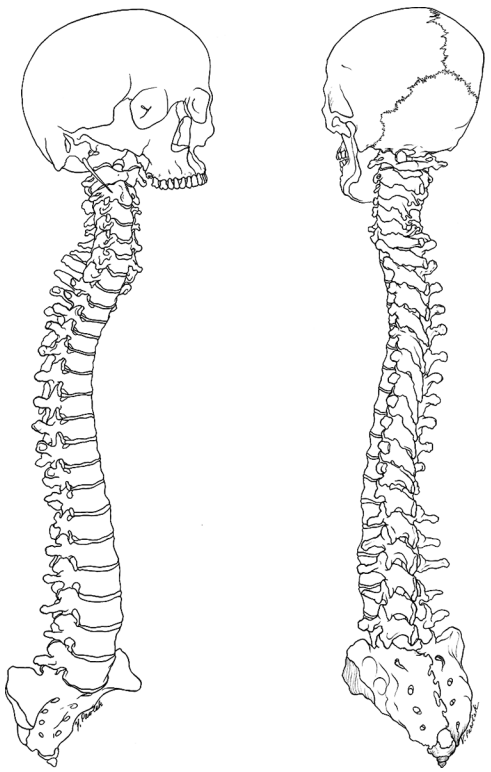

FIGURE 7.1
Schematic of head and spine bone anatomy from antero-oblique and postero-oblique views.

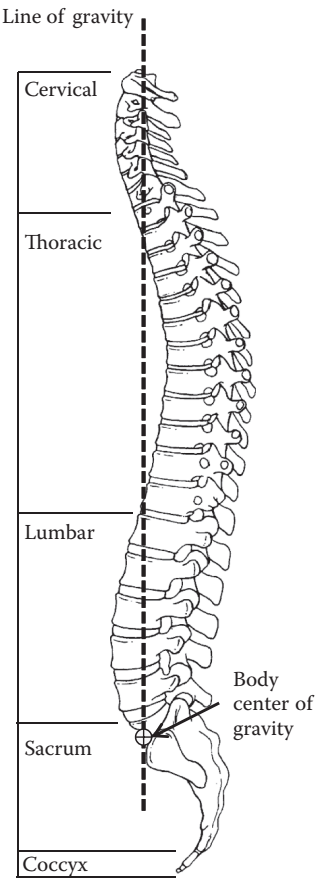

FIGURE 7.2
Lateral view of the spine demonstrating cervical and lumbar lordotic curvature and thoracic kyphotic curvature. The body line of gravity with respect to the spinal axis is also shown.

fibrocartilagenous discs between the vertebral bodies, facet joints between the vertebral arches, and unique articulations such as those found at the craniovertebral junction.

Each vertebra consists of a cylindrically shaped body in the ventral column and a bony arch that comprises the dorsal part, which collectively encase the spinal cord and exiting nerve roots. The outer shell of the vertebral body consists of a thin layer of relatively rigid compact cortical bone. The inner core of each vertebra is made up of soft and porous cancellous bone containing bone marrow. The structure of the cortical bone is aligned in vertical lamellae to resist the compressive forces. The trabeculae of the cancellous bone are ordered like columns, and they resist a variety of loads. The rostral and caudal surfaces of the vertebral body are generally concave and are separated and bound together by the fibrocartilaginous discs. The dorsal arch is composed of the laminae, pedicles, spinous processes, and facet joints. Pedicles are stout bars of bone extending dorsolaterally from the rostral aspect of the vertebral body. The laminae extend dorsally, immediately from the pars interarticularis. They fuse in the midline to form the dorsal wall of the spinal canal. The laminae are oblong plates with a sloping surface. The spinous process arises from the junction of the laminae. The specific orientation of the spinous process varies with the regions of the spine. The cervical transverse processes arise from each side of the vertebral

body near the junction of the pedicle and vertebral body. The thoracic and lumbar transverse processes arise from the junction of the pars interarticularis and pedicle. The transverse and spinous processes serve as attachments for muscles and ligaments. The articular processes arise from the pars interarticularis, interposed between the pedicles, laminae, and facet joints. Generally, superior articular processes project cranially with the articulating surface of the facet on the dorsal surface. Typically, the inferior articular processes project caudally with the articular surface facing ventrally. A thin layer of hyaline cartilage lines the surface of each facet, which is a synovial joint surrounded by a capsule.

7.2.1 Cervical Spine

The craniovertebral junction includes the occipital bone and condyles, the atlas (C1), and the axis (C2). The bony anatomy, joint shapes, and articulations of this region are unique and allow for rotation, flexion, extension, and, to a lesser degree, lateral bending.[2] This not only allows for the complex movements between the head and neck but also establishes stability without compromising the traversing neural and vascular tissues.[3]

The primary movement at the occipital–C1 joint is flexion and extension, often termed more specifically as *capital flexion-extension*.[4] The primary mobility of this joint averages 23° to 24.5°.[4,5] Flexion is limited by contact of the tip of the dens of C2 on the foramen magnum, whereas extension is limited by the tectorial membrane.[4,5] Both lateral bending (average 3.4°–5.5° each side) and axial rotation (2.4°–7.2° each side) are limited by the articulation of the occipital condyle with the lateral mass of the C1, as well as by the alar ligaments.[6,7] There is minimal coronal and sagittal translation of the occiput–C1 joint under normal conditions, which is constrained by the bony anatomy, tectorial membrane, alar ligaments, and apical ligaments.[4,5]

Axial rotation at the atlanto-occipital joint is further limited by the bony anatomy. The paired occipital condyles are proportionally large and in turn articulate with the lateral mass of the atlas, which are also proportionately large.[5] An oblique joint is created as the distance between the condyle tapers from back to front, with mean intracondylar distances of 41.6 and 21.0 mm, respectively, which imposes a further limitation to rotation.[8] This occurs because the superior articular surfaces of the atlas point caudally from lateral to medial (average angle 129.4°), whereas the inferior articular surfaces angle cranially from lateral to medial (average angle 130°–136°).[9]

In contrast with the occipital–C1 joint, the mechanical stability of C1 to C2 is primarily due to ligamentous elements.[5] As such, the atlantoaxial (C1–C2) joint allows for considerable motion to occur in axial rotation, flexion-extension, and lateral bending.[10] Studies using both cadavers and finite-element models demonstrate axial rotation for the atlantoaxial joint to be 23.3° to 38.9° for each side.[11,10] Axial rotation of the atlantoaxial segment is constrained by the joints themselves (capsular ligaments), the ipsilateral transverse ligament, and the contralateral alar ligaments.[2,12] In addition, axial rotation at C1 to C2 is negatively coupled to the axial rotation at the occiput–C1 joint; increasing the axial rotation at C1 to C2 induces axial rotation in the opposite direction (of lesser magnitude) at the occiput–C1.[5]

Flexion and extension at C1 to C2 range from 10.1° to 22.4°, which is comparable to the primary movement at the atlanto-occipital joint (23°–25°).[6,7,13] Of note, C1 to C2 flexion is resisted by the transverse ligament, whereas extension is limited by the tectorial membrane and joint anatomy.[14,15] Lateral bending is limited by the alar ligaments to approximately 6.7°.[7,16] In the normal C1 to C2 joint, translation, distraction, and compression at C1 to C2 are minimal.[4] Anterior translation is primarily limited by the transverse ligament, and secondary stabilizers include the alar and capsular ligaments; translation is usually

restricted to 3 mm or less in adults.[16,17] Posterior translation is limited by the dens on the ventral arch of C1.[5] The tectorial membrane prevents the dens from abutting the ventral spinal cord.[18]

The remaining levels of the cervical spine (C3–C7) consist of cylindrically shaped vertebral bodies ventrally and a vertebral arch dorsally. The vertebral bodies throughout the spine are cylindrically shaped with a wider transverse width than the anteroposterior width. The size gradually increases from C3 to C7, but still remains considerably smaller than in the thoracic and lumbar regions. Paired pedicles, articular facets, laminae, and a spinous process form the posterior arch. Each pars interarticularis, also termed the lateral mass, contains a cephalad and caudal articular facet oriented approximately 45° with respect to the horizontal that aids in limiting anteroposterior stability. The transverse process is unique because it protrudes from the lateral mass and contains a transverse foramen (from C1 to C6) through which the vertebral arteries traverse.

The osseous elements of the cervical spine are connected by a variety of soft tissue structures, which include the intervertebral discs, zygapophysial joints, and ligaments. Intervertebral discs are arranged with an outer collagenous annulus fibrosus that primarily resists tension, shear, and torsion, along with an inner proteoglycan nucleus that primarily withstands compression loads.[19,20] Such compression loading is generated within the C2 to T1 discs during normal physiologic conditions. This is not a pure perpendicular load because the head is approximately three times the weight of the neck and is positioned eccentric to the perpendicular plane midway through the discs.[21] The compressive load is also subject to the nature and magnitude of the loading, extremes of which are found during flexion and extension.[22] As a consequence, the intervertebral discs experience compressive forces with multiple load vectors that are associated with a moment.[23] This creates disproportionate internal load sharing within the disc as well as the annulus. Furthermore, the anatomy of the nucleus pulposus is not central and, as a result, creates disparate anterior and posterior annulus internal load sharing.[20] Thus, during physiologic and traumatic load applications, the cervical intervertebral discs respond to a variety of load vectors, including compression, bending, and tension.[20]

Like the intervertebral disc, the zygapophysial joints respond to a variety of load vectors.[20] As with the intervertebral discs, the contribution to the compressive force resistance by the zygapophysial joints depends on the orientation of the joint and the eccentricity of the external compressive force.[24] The zygapophysial joints provide a complementary role to the discs, but the specific amount changes according to the degeneration of the joint, disc, and vertebral body.[20] The oblique orientation of the facet processes allows the zygapophysial joints to resist both normal and anteroposterior shear forces.[25] Zygapophysial joints also limit the torsion of the disc, although not to the extent as in the thoracolumbar spine.[26] The effectiveness of the zygapophysial joint depends on the integrity of the capsular ligament.[27]

The limitations to lateral bending and axial rotation of the lower cervical spine depend on the resistance of the intervertebral discs along with the obliquely oriented zygapophysial joints. Uncovertebral joints, on the other hand, enable the disc to accommodate to the coupling of lateral bending and axial rotation that is primarily governed by the zygapophysial joints. Uncovertebral joints are located in the vertebral body–disc–vertebral body complex and begin to form late in childhood and develop in size with advancing age.[28] Clefts are formed between the uncinate process of the lower vertebral body and the saddle contour of the caudolateral aspect of the upper vertebral body.[20] Posteriorly, in the region of the uncinate processes, the connection is interrupted where the annulus is disrupted by the transverse cleft, which has traditionally been attributed to the formation of

uncovertebral joints. The uncovertebral joints do not constitute "true" joints incorporating a joint capsule or synovial fluid, but allow for a large degree of axial rotation between the vertebral bodies and through the intervertebral disc, as mentioned previously.[29] This bony formation is met with a limitation because osteophyte formation and projection into the disc space or intervertebral foramina compress nerve roots.

In contrast to the intervertebral discs and zygapophysial joints, ligaments are uniaxial structures that resist only tensile or distractive forces.[23] Ligaments of various types connect vertebral bodies and their posterior elements spanning either one or more levels.[20] For instance, the anterior longitudinal ligament is most effective under an extension bending moment,[30] whereas the interspinous ligaments resist a flexion moment.[31] Internal forces resisted by various ligaments differ depending on the magnitude and application of the load vector and their position relative to the force.[20] From this point of view, the resistance to flexion-extension is greater for the anterior longitudinal ligament and interspinous ligaments than the posterior longitudinal ligament, which lies closer to the center of rotation.[30]

Finally, the range of motion (ROM) for the healthy subaxial cervical spine differs across the segments of the cervical spine. It has been reported that the motion segments from C4 to C7 have the highest amount of flexion-extension ROM.[7] For lateral bending, the motion segments from C2 to C5 tend to have the greatest degrees of motion. In contrast, in axial rotation, the greatest degree of movement tends to exist at C4 to C5. The importance of these motions at specific functional units along the cervical spine can be of significant clinical consequence.[32]

7.2.2 Thoracic Spine

As with other regions and subregions of the spine, the specific anatomy of the thoracic spine dictates its response to mechanical stresses compared with the other more mobile regions of the spine.[33] The thoracic spine is the largest segment of the spine and incorporates a kyphotic curvature. This is in part due to the disparity in heights between the anterior and posterior regions of the vertebral body; the height of the anterior surface is 18 to 22 mm and is normally 1 to 2 mm less than the dorsal surface.[19] In addition, the vertebral bodies are primarily load-bearing, which is facilitated by the gradual increase in the anteroposterior diameter from T1 to T12.[33] The vertebral bodies become the primary load-bearing entity within the thoracic spine, and their compressive strength is directly related to bone density.[34] As such, even minor changes in bone porosity can cause major changes in compressive strength.[19] This is significant clinically as most osseous injuries occur within the thoracic spine due to flexion and axial loading.[35]

The most distinctive anatomic *and* biomechanical characteristic of the thoracic spine is the presence of ribs and their articulations with the transverse processes and vertebrae. The fixed ribs, along with the sternum, add stiffness and limit flexion-extension from T1 to T9. A study of the effects of the biomechanics of the rib cage on spinal motion has revealed that all physiologic movements of the ligamentous spine are decreased by the presence of the rib cage.[36] This finding was most significant for extension, which was reduced by 70%.[36] Additionally, the compression tolerance of the thoracic spine increases by a factor of four in the presence of the rib cage.[36]

Resistance to translation in the thoracic spine depends on and is affected by the orientation of the facets.[31,37] Their coronal orientation between T1 and T8 serves to provide stability primarily against anterior translation.[19] Once the facets transition toward a more sagittal orientation, typically at the level of T9 to T10, a greater degree of anterior translation may occur.[19] This is offset by the ability of facets in the lower thoracic spine to limit

axial rotation.[19] Importantly, attention needs to be paid to the levels of abrupt change in orientation of the facets (T1 and T11) because these levels are more likely susceptible to dislocation.[19]

As in other regions of the spine, thoracic discs mainly function to support bending and to absorb compression loads. Thoracic intervertebral discs carry the majority of the compressive load placed on the trunk.[38] The annulus fibrosus of thoracic discs is thicker than in other spinal regions.[19] Compared with the cervical and lumbar regions, disc height is lower. These two anatomic characteristics may be effective in compensating for the lack of rotation resistance imposed by the coronally oriented upper thoracic facets.[19] Despite this, torsion and bending loads remain the primary cause of disc failure in the thoracic spine.

Similar to the cervical spine, ligaments of the thoracic spine experience only tensile forces during spine motions. The anterior longitudinal ligament functions, therefore, to prevent hyperextension and overdistraction. The posterior longitudinal ligament, although closely adhering to the posterior aspect of the disc annulus, has only a marginal attachment to the vertebral body and primarily limits hyperflexion. The ligamentum flavum allows flexion of the spine and separation of the laminae for eccentric anteriorly applied loads and facilitates the return of the laminae back to their normal position upon the release of load.[19]

Given the biomechanical anatomic properties of the thoracic spine as discussed previously, the full range of flexion and extension approximates 65° to 80° (in the horizontal plane).[19] Although the upper thoracic region (T1–T5) averages 3° per level,[7,39] values increase slightly in the midthoracic region (T5–T10) and reach a maximum in the lower thoracic spine (T11–T12).[23] Axial rotation can be as much as 10° per level in the upper and middle thoracic regions. Maximum bending rotations are from T4 to T9, reflecting the anatomy of the facets in those regions, as discussed earlier.[40] Obviously, in the lower thoracic region, where the facets are more sagittally oriented, axial rotation is dramatically limited.[19]

On the other hand, lateral bending remains fairly consistent at approximately 4° to 5° per level throughout the upper and middle thoracic spine.[19] This increases substantially below the fixed rib cage–sternum complex to 5° to 10° per level.[19] These motions are not completely independent because there is a substantial degree of coupling between lateral bending and axial rotation. During such coupled motion, the spinous process rotates toward the convexity of the curvature of the thoracic spine.[19] The extent of this coupling is variable along the thoracic spine, with the strongest associations occurring in the upper thoracic spine and becoming reversed from T5 to T10.

7.2.3 Lumbar Spine

The kinematics of the lumbar spine, like the subaxial cervical spine, are determined largely by the bony structures, discs, and ligaments. In addition to being the region most commonly affected by symptomatic degenerative processes, it is also commonly injured, particularly at the vulnerable thoracolumbar junction.

The lumbar spine consists of the largest bony and ligamentous elements of the spine. These elements are oriented to create a lordotic posture of 20° to 45°,[41] helping to make this region relatively resistant to failure. The vertebral body diameter increases caudally, whereas the transverse width remains greater than the anterior–posterior width. The fifth lumbar vertebra has a greater height in the ventral aspect than the other lumbar levels, which contributes to the lumbosacral angle and constitutes a transition from the lumbar to the sacral spine.[42] Given the lordotic curve of the lumbar spine, the "compressive force" or force acting perpendicular to the plane midway through the intervertebral disc occurs at the apex of this curve, usually at L3 to L4, when standing upright.[1] In addition, the facets

of the lumbar spine have a progressive sagittal plane orientation that has limited resistance to flexion or translational movements; however, this creates a greater resistance to rotation.[42] In a healthy spine, the limitation to rotation is only 1° to 3° to each side at each lumbar level.[43] In addition to the lordotic posture, prior long-term ("creep") loading[44] and pathologic disc narrowing[45] increase compressive load-bearing of the lumbar spine.

Cadaveric testing has shown that compressive loads within the neutral lumbar spine are mainly carried by the intervertebral discs with little, if any, supported by the neural arch.[46] Sustained compressive loading has been shown to decrease cadaveric disc height by 20%.[1] Such an effect has also been reported during the normal *in vivo* diurnal variation.[47] During this process, the water content of the nucleus pulposus and inner annulus decreases by 20% to 30%; however, an equal degree of water expulsion does not occur at the outer annulus.[1] This differential water loss decreases the hydrostatic resistance to compression within the nucleus but increases the radial, outward pressure at the annulus.[48] This mechanism of water redistribution results in the loss of disc height. The hydration of the nucleus pulposus not only affects the disc height but also the ability of the disc to resist postural loads, as well as herniation. Highly hydrated discs act more like "hydraulic cushions" and are less sensitive to changes in posture.[1] On the other hand, as degenerative discs become more dehydrated, they tend to be more sensitive to small changes with flexion and extension,[1] thereby increasing compressive stresses at the anterior and posterior annuli, respectively.[1,49] Consequently, the annulus is more likely to resist bending when the disc is swollen with water (i.e., early in the morning).[1] Subsequently, when discs are more hydrated, severe bending or acute compressive loading is more likely to cause disc prolapse[1,50] when compared with those discs that have been creep-loaded.[51] This concept is emphasized by the fact that in the laboratory setting, cadaveric degenerated discs with a fibrous nucleus cannot be induced to prolapse.[51] Studies have shown that the highest compressive stress lies within the annulus of dehydrated discs rather than in the nucleus.[1] Degenerated discs have a progressively smaller hydrostatic region when compared with younger (<30 years) highly hydrated discs.[1] The annulus is therefore required to support a larger degree of the compressive stresses creating an increased propensity for disc herniation.

As reviewed previously, the intervertebral disc resists much of the compressive force. As such, discs in the upper lumbar spine tend to resist backward bending more than the wedged discs in the lower spine, but all seem to be well protected by the neural arch[51]; the resistance of the neural arch is then primarily supplemented by the facet joints.[1,51] Similar to the biomechanical behavior of the disc, the compressive stress acting on the zygapophysial joints is similarly affected by changes in posture and disc height.[1,45] Cadaveric studies demonstrate that the flat articular surfaces of the zygapophysial joints resist most of the compressive force.[45] As the zygapophysial joints are inclined at a substantial angle to vertical in the lower lumbar spine, the location of maximum stress on these surfaces varies with posture, particularly with lordotic postures, changing the angle at which adjacent vertebrae are pressed together.[1] The effects of posture become exaggerated when disc height is reduced, either by pathological changes or by sustained loading. Because the vertical spacings of adjacent vertebrae are small compared with their lengths and widths, small angles of flexion or extension lead to large changes in the distribution of stress. Sustained small (2°) angles in extension will load the zygapophysial joints (resist 16% of applied compressive force), whereas flexion by the same amount completely unloads the joints.[1]

Given that the transverse width of the lumbar vertebrae spine is greater than the anterior–posterior width, intervertebral discs have a 50% greater transverse size. Although comparatively little is known about the lumbar spine's resistance to lateral bending, it seems to be primarily a consequence of the increased transverse disc mass.[52] Even more difficult to define has been the role of the disc in resisting axial rotation (torsion). Because

the instantaneous axis of rotation is within the posterior annulus,[43] the anterior annulus becomes stretched with rotation. This movement is limited by the ipsilateral, sagittally oriented facet,[43] though if it is compromised, gross failure occurs at angles between 10° and 20°.[53] Despite the long lever arm of the posterior longitudinal ligament and the strong tensile strength of the ligament flavum, these ligaments provide little resistance against motion given their close proximity to the fulcrum of flexion-extension.[42] Conversely, the short capsular ligaments that are farther away from this fulcrum play a larger role in the maintenance of spinal stability, although somewhat weaker in tensile strength.[54]

7.2.4 Sacrum and Pelvis

Although the structure of the sacrum is somewhat variable, the triangular-shaped sacrum is most commonly formed by the vertical fusion of five vertebrae (Figure 7.1). This creates a rigid structure that consists of two superior articular processes that articulate with the fifth vertebrae: a cornua that articulates inferiorly with the coccyx, and alae that articulate bilaterally with the pelvis. The fifth lumbar vertebra transmits the axial compressive load to the sacrum. The sacrum, in turn, transitions this vertical compressive load into a horizontal trajectory toward the hips through the large surface area of the alae.[55] The sacrum, then, forms the final transition between the axial and appendicular skeletons. This junction is associated with significant stress given its terminal position. The biomechanics of load-bearing, along with the ROM at the L5–S1 junction, depends on its unique structure. The angulation of the L5–S1 junction is highly variable, further complicating the biomechanics of this joint.[55] The degree of angulation at this junction creates a shear force and tendency of L5 to shift anteriorly relative to the sacrum.[56] The propensity for anterior spondylolisthesis needs to be considered when one analyzes the spine in terms of balance and alignment, as this is intimately intertwined with the pelvis and lower extremities.[57]

The anatomy of the lumbosacral junction is further complicated by the high degree of anatomic variability within this region. The lumbosacral junction may be marked by an anatomic transformation of the first sacral segment toward a lumbar configuration (lumbarization) or the fusion between the body of the fifth lumbar vertebra and the sacrum, known as sacralization. Lumbarization occurs in approximately 5% of the population, whereas sacralization is observed in 7.5%.[58] As a result of the biomechanical alterations incurred by sacralization, there is an increased association of disc pathologies.[59] The relative hypermobility reported immediately above the sacralized L5 and probably the altered load distribution at these junctions are attributed to this association.

7.2.5 Muscles of Spine

The superficial musculature of the rostral thoracic region and dorsal neck originates from thoracic spinous processes and inserts laterally on the scapula. They are attached medially to the ligamentum nuchae, which is a fibrous intermuscular septum. The sternocleidomastoid muscles arise from the sternum and the clavicle and insert into the mastoid process of the occipital bone. In the lower thoracic and lumbar spines, several muscles comprise the superficial layer, with the most prominent muscle being the latissimus dorsi. This muscle arises from the spinous process of the lower thoracic vertebrae and extends as a sheet across to the ventral axillae. Both the intercostal muscles and serratus posterior muscles arise from the ribs in different directions. Muscles encircling the abdominal region include the external and internal obliques and the transversus abdominis. The rectus abdominis muscle is located in the ventral abdominal wall.

In the cervical spine, deeper muscles anterior to the vertebral column are less prominent than dorsal or lateral muscles. In this region, the anteriorly located longus coli muscle passes from the atlas to the transverse processes of C3 to C6. Deep lateral muscles include the anterior scalenus, the longus capitis, and the intertransverse muscles. They also attach to the transverse processes. With regard to the deep dorsal musculature, the splenius capitis muscle arises from the lower ligamentum nuchae and the cervical and upper six thoracic transverse processes to attach to the occiput. The narrowest muscle, the splenius cervicis, originates only from the upper six thoracic spinous processes to insert on the posterior tubercles of C1 to C3. The adjacent deeper layer includes the semispinalis capitis and semispinalis cervicis muscles. The more medial semispinalis cervicis arises from the transverse and articular processes of the upper thoracic vertebrae inserting into the spinous process of the cervical spine. The lateral muscle originates from the transverse processes of C3 to C6 and inserts on the occipital bone of the head. The deepest muscles of this group include the iliocostalis and longissimus cervicis, which arise from the upper thoracic ribs and transverse processes, respectively, to end on the transverse processes and facets of C4 to C7. Other deep muscles include the rectus capitis and capitis obliques, which serve as head extensors.

In the thoracic region, the anteriorly located longus coli muscle extends over only a few segments. In the lower thoracic and upper lumbar region, however, the lateral muscle groups are prominent, especially the psoas, intertransverse, and quadratus lumborum muscles. The iliopsoas muscles originate from the lateral aspects of the vertebral bodies and extend to the femur. As in the rest of the spine, the intertransverse muscles extend between the transverse processes. The quadratus lumborum also originates from the transverse processes and runs obliquely to the lateral ileum.

In the deep thoracic and lumbar regions, the dorsally located erector spinae muscle group lies in the vertebrocostal groove directly under the thoracolumbar fascia. This muscle group begins as a tendon attached broadly to the dorsocaudal sacrum and iliac crest and extends the entire length of the spine. Its columns are composed of shorter fascicles. The lateral column represents the iliocostalis muscles, the intermediate column represents the longissimus muscles, and the middle column represents the semispinalis muscles.

The iliocostalis muscles arise from the iliac crest and insert on the angles of each of the ribs (iliocostalis lumborum and thoracis) as well as the cervical transverse processes. The longissimus represents the largest contributing musculature. It arises from the transverse process at the lowest spinal levels and inserts into the transverse processes rostrally with the most rostral fibers inserting onto the mastoid process of the skull. The narrow spinalis muscle arises from the spinous processes of the sacrum and inserts into the spinous processes above it.

Deep to the erector spinae muscle lie the paravertebral or transverse spinal muscles. These muscles, including the semispinalis, have their origins primarily from the vertebral transverse process and insert into the spinous process. The semispinalis group is continuous in the cervical and thoracic regions. The multifidus muscle is different in the cervical and lumbar areas, where the attachments are to the articular joint; however, in the thoracic region, the attachments are to the transverse processes. This muscle is thickest in the lumbar region.

7.2.6 Spinal Cord

The spinal cord and nerve roots traverse the spinal canal. The spinal cord is approximately 40 to 45 cm long in the adult and usually terminates at L1 to L2 (Figure 7.3). The rostral cord at the level of the foramen magnum is continuous with the medulla oblongata. The dura mater, pia

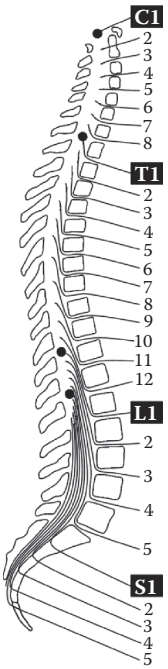

FIGURE 7.3
Schematic of the spinal cord nerve roots, indicating the relationships among spinal segments, nerves, and vertebral bodies.

mater, and arachnoid are the three membranes that cover the spinal cord. The spinal cord is suspended in the spinal canal by dentate ligaments. These arise from the pia and are attached to the dura. The cauda equina consists of the nerve roots below the conus or caudal termination of the spinal cord, and contains the roots that have not yet exited through their neural foramina (Figure 7.3). Spinal nerve roots are composed of a dorsal sensory root and a ventral motor root. With the exception of the C1 and C2 contributions to the spinal accessory nerve, nerve roots leave the spinal canal via the neural foramina. Anatomically, the spinal cord is divided into sections: 8 cervical, 12 thoracic, 5 lumbar, 5 sacral, and 1 coccygeal (Figure 7.3). The tracts within the spinal cord in the cervical and thoracic regions and nerve roots in the lumbar region are somatotopically oriented. The cortical spinal motor tracts are somatotopically arranged so that hand function is located more medially, whereas the foot function is located laterally. The sensory spinothalamic tract is arranged so that hand sensation is located most medially and ventrally, and sacral sensation is located most dorsally and laterally. The sensory posterior columns are similarly arranged in a somatotopic manner. In the lumbar region, the nerve roots are arranged so that the lower sacral segments are located most medially and the exiting upper lumbar regions most laterally (Figure 7.4).

In a normal spine, spinal canal dimensions and hence the subarachnoid space are generous except in the midthoracic region (Figures 7.5 and 7.6). This is important during procedures for spinal instrumentation that might impinge on the neural elements (e.g., sublaminar wire or hook placement). The lumbar spinal canal spacing does not change significantly from the upper to the lower lumbar regions; however, its width increases (Figure 7.5). The lumbar and sacral spinal canal cross-sectional areas are also more generous than in other areas of the spine. These regions contain the cauda equina, which is

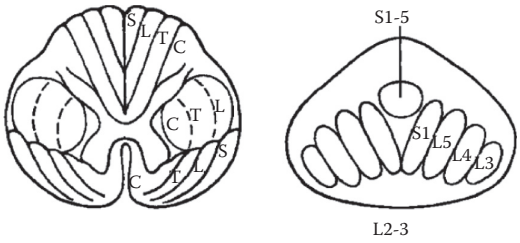

FIGURE 7.4
Nerve roots are arranged so that the lower sacral segments are located most medially and the exiting upper lumbar segments most laterally.

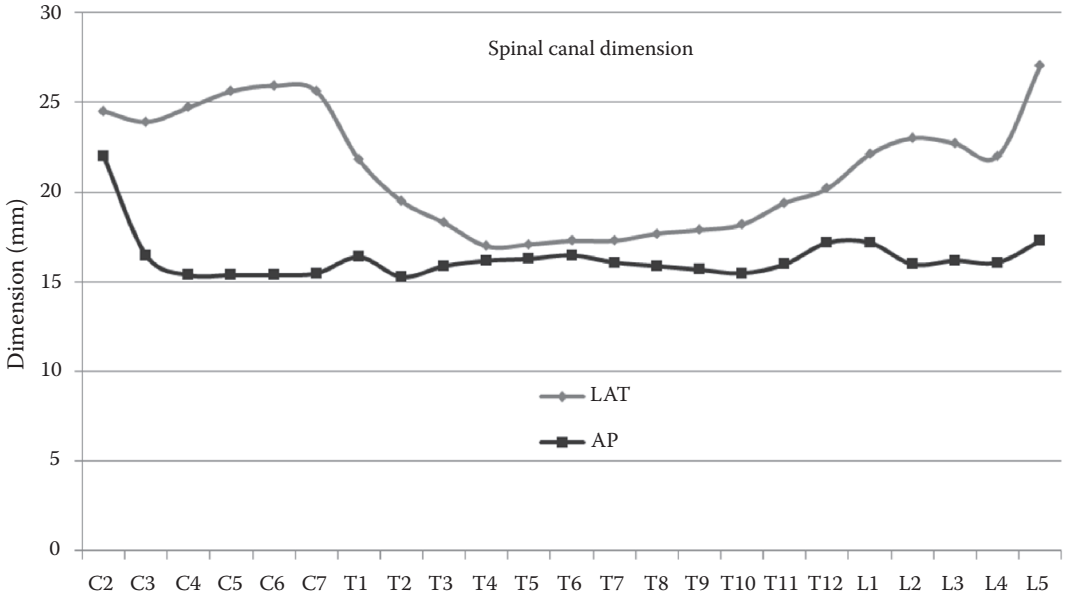

FIGURE 7.5
Lateral and anteroposterior dimensions of the spinal canal as a function of spinal level. (Data from Berry, J. L. et al., *Spine (Philadelphia, Pa)*, 12, 4, 362–367, 1987; Francis, C. C., *Anat. Rec.*, 122, 4, 603–609, 1955; Panjabi, M. M. et al., *J. Orthop. Res.*, 9, 4, 584–593, 1991.)

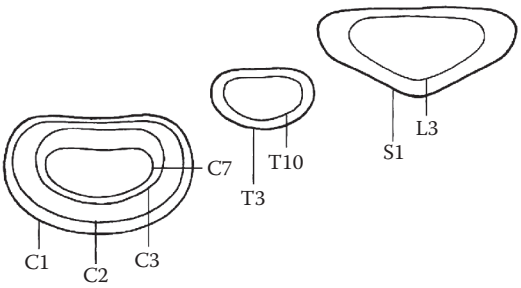

FIGURE 7.6
Typical shapes of the spinal canal.

relatively resistant to traumatic insults. For these reasons, posttraumatic neural element injury in the lumbar region is less severe than that associated with comparable deformation in the other regions of the spinal column, particularly in the midthoracic area.

7.3 Fundamental Biomechanics Concepts for the Spine

Clinical biomechanics of the spine refers to the understanding of the normal and pathologic functions of the human vertebral column due to normal loading or the application of a mechanical insult. The insult could be in the form of traumatic dynamic forces, deformations, or slowly applied loads to the spine.[60] Here, several terms are explained to facilitate a better understanding of clinical spinal biomechanics.

The right-handed Cartesian system of reference is commonly adopted in spine biomechanics (Figure 7.7). The system consists of three axes: *x*, *y*, and *z*. Rotational and translational movements can occur along and about these axes. Translational movements are considered positive if the movements occur along the positive direction of the axis; it is considered negative if the moments are in the negative direction. Similarly, a clockwise

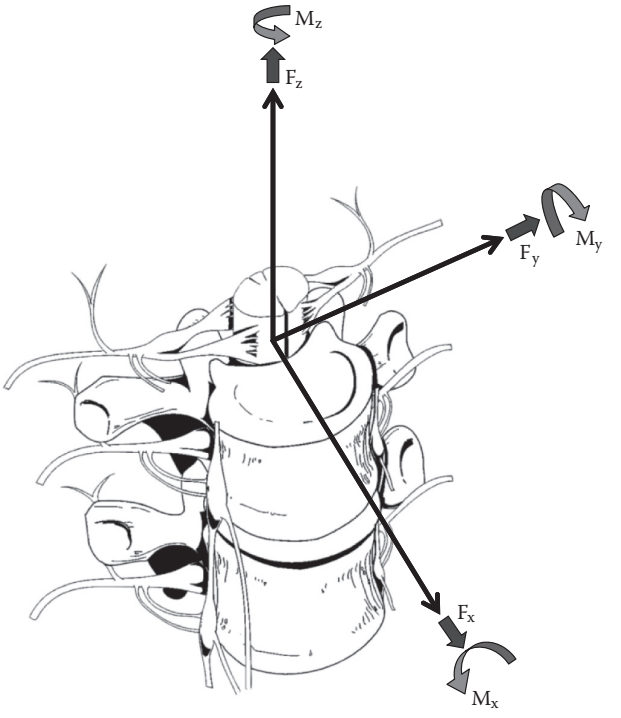

FIGURE 7.7
Right-handed Cartesian coordinate system of reference with the *z* axis oriented along the inferior-to-superior direction, the *x* axis along the dorsal-to-ventral direction, and the *y* axis along the right-to-left direction. For the right-handed system, this results in a positive flexion moment, positive left-to-right lateral bending moment, and positive right-to-left axial twisting moment.

rotation around an axis looking from the origin of the coordinate system toward the positive direction of the axis is termed positive rotation, whereas the counterclockwise rotation is termed negative. The right-handed Cartesian coordinate system of reference is used for the spine with the *z* axis oriented along the caudal-to-rostral direction, the *x* axis along the dorsal-to-ventral direction, and the *y* axis along the right-to-left direction (Figure 7.7). For the right-handed system, this results in a positive flexion moment (extension being negative), positive moment left-to-right lateral bending (right-to-left lateral bending is a negative moment), and positive twisting right axial rotation moment (left axial rotation is a negative moment). This reference system has been adopted by the American Standard for Testing Materials.[61] Once the coordinate system of reference is chosen, the applied force can be divided into its components along or about each axis. Deformation along those axes is translational; it can also be rotational about the axes. Translational deformation results in a change in the length. Rotational deformation results in a change in the angle of the body. Deformations can result in strain, which is defined as the change in unit length (linear) or change in unit angle (shear).

Because of the deformable characteristics of the spine, application of an external force or a load vector results in deformation. Energy is frequently used to relate force and deformation; it represents the amount of work done by a force on a body. It is defined as the area under the force-deformation curve. In contrast, stiffness is defined as the ratio of force to deformation. Because the force-deformation characteristics of a spinal structure are not always linear, the most linear portion of the curve is often selected for obtaining the maximum stiffness of the structure. The typical force-deflection characteristic of a spinal structure (example of a functional unit) is nonlinear; that is, force does not increase linearly with a linear application of deformation. Within the principles of structural mechanics, this biomechanical load-deflection response has been classified into the physiologic loading phase, the traumatic loading phase, and the failure (or posttraumatic) loading phase. The stiffness response of the structure has been used to derive these biomechanical classifications. This system has been used to design a schema to evaluate the onset of spinal injury due to external loads. This may help define the mechanism of spinal disorders.

In the physiologic loading phase, the spinal structure acts as an integral unit, and the stiffness increases gradually to a maximum value. During this phase, the structure obtains its highest stiffness; consequently, its resistance increases with externally applied loads. This region represents the highest mechanical efficiency domain in the structural response. Trauma does not occur during this region of loading. With the increase in the application of load, yielding of the structures of the spine occurs. This is identified biomechanically by the onset of the first decrease in stiffness during the loading process. Previous studies have demonstrated microfailures during this phase of loading.[62] The end of this traumatic range is characterized by changes in the stiffness that correspond to the ultimate load-carrying capacity of the structure. After reaching its peak during the physiologic loading phase, stiffness gradually decreases to zero at the end of the traumatic loading phase, indicating that the structure has reached its ultimate load-carrying capacity. In the subsequent phase (i.e., the posttraumatic loading phase), the structure responds with negative resistance; that is, an increase in the deformation results in a decrease in the load. Trauma has been identified on radiographs when the structure has been loaded to this degree. Based on the simple fundamental force-deformation response and using the stiffness as a mechanics-based criterion, studies have indicated that microtrauma may initiate the loss of a local component before the structure has reached its ultimate load-carrying capacity.[63,64] In other words, even under subfailure loading, the structure may exhibit signs of weakness or microfailure.

7.3.1 Flexibility, Range of Motion, and Coupling

Flexibility is defined as the inverse of stiffness (i.e., ratio of the deformation to an applied load). Flexibility and stiffness are inversely interchangeable in spinal biomechanics. Another quantity, the ROM, is frequently used in spinal biomechanics, referring to the deformation from one extreme to the other extreme under the physiologic range of translation or rotation of an intervertebral joint. Because of the three-dimensional nature of the spinal structure, motions are coupled. Coupling is defined as the capacity of the spine to move in translation or rotation (or both) in association with the principal motion. In other words, it represents obligatory movements of the spine that always accompany a primary motion. Both principal and coupled motions exist in the spine.[65] Principal motion can be defined as the motion associated with the direction or the plane of application of the external force. Any out-of-plane motion therefore is the coupled motion. For example, axial rotation of the upper cervical spine is usually coupled with lateral bending.[66] Similarly, in the lower cervical spine, axial rotation and lateral bending of the vertebra in the opposite direction are usually coupled.[66]

7.3.2 Spinal Instability

The term spinal instability refers to "the loss of the ability of the spine under physiologic loads to maintain relationships between vertebrae in such a way that there is neither damage nor subsequent irritation to the spinal cord or nerve roots and, in addition, there is no development of incapacitating deformity or pain due to structural changes."[23] This oft-quoted definition is entirely clinical.

Flexion-extension radiographs, although occasionally useful, may also be misleading, particularly after acute trauma. If pathology is observed and iatrogenic injury via the act of flexion and extension is not incurred, they are useful.[60] They are, however, not without risk if spinal instability is present. A "normal" flexion-extension radiograph may not always indicate stability. Incomplete patient cooperation and "guarding" against excessive spinal movement due to underlying acute pathology can also disguise an injury that, if not treated properly, may lead to further pathology.

Because of these limitations, numerous authors have attempted to quantify the degree or extent of acute instability by a point system approach incorporating both radiographic and clinical criteria. White and Panjabi[23] themselves described a region-specific point system in which an accumulation of five or more points indicates an unstable spine. The system emphasizes the differences between the cervical, thoracic, and thoracolumbar and lumbar regions. The primary purpose of a stability determination is to delineate the most appropriate management scheme for patient care. Recently, Benzel[60] has presented the quantification of acute instability in subaxial cervical, thoracic, and lumbar regions based on the point system previously suggested by White and Panjabi. In principle, the earlier classification was combined in such a way that regional differences were eliminated, providing a point system that was independent of spinal region.

The definition of stability in clinical practice must address the integrity of each spinal component; each component must be subsequently analyzed to reach a clinical decision. Despite the power of classification systems such as those described above, clinical cases frequently possess characteristics that defy such classification. Examination of a burst fracture, for example, should lend itself to additional questions, such as the nature and extent of vertebral body compression and the number of ligaments in the posterior column that may be stretched beyond their elastic limits or even torn. These questions deal with

component-related problems. Understanding of the biomechanical characteristics and an interrelationship among spinal components is limited. Additional research that relates component attributes to acute and chronic instability is needed. The clinician should have a detailed understanding of the biomechanical properties of the individual components (discs, ligaments, facet joints, and vertebra) and the relationship of their integrity to the overall stability and load-carrying capacity of the spine.

7.3.3 Spinal Soft Tissue Biomechanics

The integrity of the soft tissues is vital to maintaining spinal stability and physiologic function. Physiologic dysfunction in the form of pain or headache occurs due to motor vehicle rear impacts, and these injuries do not often result in osseous damage. These injuries, often, are soft tissue–related.[67] Studies conducted by Yoganandan et al.[68] have helped in delineating some of the mechanisms of headache and neck pain, the two most common complaints of patients with whiplash. Biomechanical tests documented soft tissue injuries in the form of ligament and facet joint compromise secondary to single rear impact acceleration using intact whole-body postmortem human subjects.[68] Cusick and coworkers discussed the formation of a reverse curve of the cervical spine during the earlier stages of the rear impact acceleration wherein the spine attains a nonphysiologic curvature, that is, upper cervical spine flexion associated with lower cervical spine extension.[13,68–74] Using kinematic analysis as a biomechanical basis, these studies indicated that flexion at the upper segment may stretch the posterior suboccipital structures, creating tensile forces, which may affect the related neural structures and be responsible for suboccipital headaches. Local lower cervical spinal extension studies showed that the facet joint slides from the anterior to the posterior direction and the joint stretches ventrally while compressing dorsally, indicating a pinching mechanism.[69,70] The sliding and the pinching mechanism result in a stretching of the joint itself. This local stretching of the lower cervical spine facet joint may be responsible for neck pain in patients with whiplash (Figure 7.8). Differences have been reported between men and women with regard to cervical spine motions during rear impact, in particular, during the time of formation of the nonphysiologic *S* curve.[71,75] Specifically, female intervertebral joints have been shown to undergo a

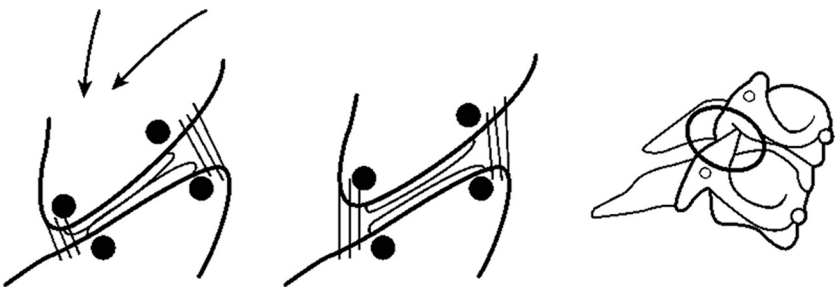

FIGURE 7.8
Diagrammatic representation of the facet joint pinching and sliding mechanisms resulting in a stretch of the facet joint.

higher degree of motion than male joints at the lower cervical spine levels. Those studies seem to support the clinical and epidemiologic finding that females are more susceptible to soft tissue–related injuries than males.[76]

7.4 Additional Gender Effects

The human spine exhibits anatomic and biomechanical differences between genders. It is well known that the rate of maturation process is earlier in women than in men. Men have larger vertebral dimensions than women.[77–79] Lumbar vertebral body heights and cross-sectional areas are greater in men than in women.[80] Additionally, lumbar vertebral body sizes in adult and pediatric women are smaller than in men, after accounting for age, stature, and total body mass.[81–83] Widths of the lumbar vertebrae are also smaller in women.[84] In the adult cervical spine, sizes of vertebrae are also greater in men than in women, and in particular, vertebral bodies are longer along the midsagittal plane, and the canal-to-body ratios are greater.[78,79,81] Lumbar ligaments in women have decreased collagen and increased elastin.[85] In a quantitated computed tomography (QCT) study of 98 adult healthy human volunteers from the North American population between the ages of 18 and 40 years, Yoganandan et al.[86,87] showed that the trabecular bone densities of cervical vertebrae are greater than those of lumbar vertebrae and that the bone density increases caudally in the cervical region. Also, lumbar spine density was the best predictor of cervical vertebral density. Using the same group of 98 volunteers, and size-matching based on sitting height and circumference, several parameters were extracted.[88] Vertebral width (distance between the lateral-most extents of the right and left articular masses), disc-to-facet depth (distance between the anterior-most vertebral body extent and the posterior-most articular mass extent), and segmental support area (triangular area formed by the interfacet width and disc to facet depth) were significantly greater in men than in women.[84]

Regions of cervical vertebrae with specific relevance to posterior surgical procedures were evaluated for gender dependence using the QCT study on 98 human volunteers.[88] Pedicle width, height, length, axis length, and medial and sagittal offsets and transverse and sagittal angulations significantly depended on gender and vertebral level.[89] Although showing gender and level bias, all six linear parameters were larger in men than women. In particular, mean pedicle width and height were 19% and 18% greater in men than in women, respectively; in addition, angular parameters were also gender-dependent.[84] These findings are consistent with the results of a study involving the Japanese population; pedicle width and height data were 5% and 19% greater in men, respectively.[90] Variations in pedicle dimensions and angulations may be important in presurgical planning. Further evaluations of the mean lateral mass width and bicortical screw lengths for two common surgical techniques also indicated greater dimensions in men than in women in the subaxial cervical column, although these parameters showed level dependence.[91] Additionally, using unembalmed human cadaver cervical spinal columns coupled with cryomicrotomy, facet joint width, cartilage thickness, and cartilage gap were extracted from occiput to T1 levels.[92] The cartilage gap in the dorsal region was greater in women than in men, and the overall mean facet cartilage thickness was lower in men than in women. The lack of adequate cartilage in females may expose the underlying adjacent subchondral bone to direct stresses during normal physiologic and traumatic loads.

7.5 Issues Relevant to Spinal Instrumentation

The primary rationale for fusion of many types of human joints is relief from pain, although the correction of a deformity or restoration of normal force transmission (or both) may affect such a decision. In the spine, decompression and protection of neural structures are also of paramount importance. Damage to either the anterior or posterior elements of the spine may result in misalignment, failure to articulate, or a general inability to support axial, torsional, or shear forces.[93] The choice of surgical approach, therefore, involves an understanding of the underlying pathophysiology along with the regional biomechanics. Spinal instrumentation is most frequently used as an adjunct to fusion to provide immediate stability as well as to increase the likelihood of fusion success.

Although a complete discussion of spinal instrumentation techniques is beyond the scope of this chapter, a number of general principles apply. Restoration of normal force transmission in the case of degenerative, traumatic, or iatrogenic instability requires careful preoperative consideration of biomechanical weaknesses in the segments to be instrumented. Theoretically, by increasing the number of fixation points and choosing specific points along a segment, one can increase the segmental distribution of the loads and reduce motion at the kinematically most active motion segments.[32] This includes a global consideration of construct design, which takes into account the forces and moments acting on the instrumented segments and resisted by the applied instrumentation and remaining anatomic structures. Ideally, this strategy would result in decreased intersegmental ROM[32] and promotion of fusion, although the optimal decrease in ROM to promote spinal fusion is not currently known. The choice of fixation points is also a consideration because biomechanical considerations often favor one type over another, whereas anatomic constraints may limit the available options. Finally, the biomechanical properties of the instrumentation systems themselves remain relevant.

7.6 Summary

This chapter focused on spinal biomechanics with an emphasis on clinical concepts for optimizing patient treatment. A summary of the functional anatomy of the spinal column, including the vertebrae, intervertebral discs, ligaments, and muscles, was provided. The importance of protecting the integrity of the spinal cord cannot be overemphasized. Fundamental kinematic and load-bearing differences between the cervical, thoracic, lumbar, and sacral regions demonstrate practical knowledge for the clinical specialist. Newer data demonstrating fundamental differences between genders were also discussed with respect to size, shape, and mineral density of the spine and its tissue components. Clinical biomechanics concepts, including defining the stability of the column and understanding the basics of spinal instrumentation, were briefly discussed to provide context for managing this structure.

Acknowledgment

The authors would like to acknowledge the VA Medical Research Center.

References

1. Dolan, P., and M.A. Adams. 2001. Recent advances in lumbar spinal mechanics and their significance for modelling. *Clinical Biomechanics (Bristol, Avon)* 16(Suppl 1):S8–S16.
2. Martin, M. D., H. J. Bruner, and D. J. Maiman. 2010. Anatomic and biomechanical considerations of the craniovertebral junction. *Neurosurgery* 66(3 Suppl):2–6.
3. White, A. A., 3rd, and M. M. Panjabi. 1978. The clinical biomechanics of the occipitoatlantoaxial complex. *Orthopedic Clinics of North America* 9(4):867–878.
4. Steinmetz, M. P., T. E. Mroz, and E. C. Benzel. 2010. Craniovertebral junction: Biomechanical considerations. *Neurosurgery* 66(3 Suppl):7–12.
5. Wolfla, C. E. 2006. Anatomical, biomechanical, and practical considerations in posterior occipitocervical instrumentation. *The Spine Journal* 6 (6 Suppl):225S–232S.
6. Goel, V. K., C. R. Clark, K. Gallaes, and Y. K. Liu. 1988. Moment–rotation relationships of the ligamentous occipito–atlanto–axial complex. *Journal of Biomechanics* 21(8):673–680.
7. Panjabi, M., J. Dvorak, J. Duranceau et al. 1988. Three-dimensional movements of the upper cervical spine. *Spine (Philadelphia, Pa)* 13(7):726–730.
8. Naderi, S., E. Korman, G. Citak et al. 2005. Morphometric analysis of human occipital condyle. *Clinical Neurology and Neurosurgery* 107(3):191–199.
9. Konig, S. A., A. Goldammer, and H. E. Vitzthum. 2005. Anatomical data on the craniocervical junction and their correlation with degenerative changes in 30 cadaveric specimens. *Journal of Neurosurgery. Spine* 3 (5):379–385.
10. Zhang, H., and J. Bai. 2007. Development and validation of a finite element model of the occipito-atlantoaxial complex under physiologic loads. *Spine (Philadelphia, Pa)* 32(9):968–974.
11. Panjabi, M., J. Dvorak, J. J. Crisco, 3rd, T. Oda, P. Wang, D. Grob. 1991. Effects of alar ligament transection on upper cervical spine rotation. *Journal of Orthopaedic Research* 9(4):584–593.
12. Iai, H., H. Moriya, S. Goto, K. Takahashi, M. Yamagata, and T. Tamaki. 1993. Three-dimensional motion analysis of the upper cervical spine during axial rotation. *Spine (Philadelphia, Pa)* 18(16):2388–2392.
13. Crisco, J. J., 3rd, M. M. Panjabi, T. Oda, D. Grob, and J. Dvorak. 1991. Bone graft translation of four upper cervical spine fixation techniques in a cadaveric model. *Journal of Orthopaedic Research* 9(6):835–846.
14. Dvorak, J., E. Schneider, P. Saldinger, and B. Rahn. 1988. Biomechanics of the craniocervical region: The alar and transverse ligaments. *Journal of Orthopaedic Research* 6(3):452–461.
15. Finn, M. A., D. R. Fassett, T. D. McCall, R. Clark, A. T. Dailey, and D. S. Brodke. 2008. The cervical end of an occipitocervical fusion: A biomechanical evaluation of 3 constructs. Laboratory investigation. *Journal of Neurosurgery. Spine* 9(3):296–300.
16. Dvorak, J., and M. M. Panjabi. 1987. Functional anatomy of the alar ligaments. *Spine (Philadelphia, Pa)* 12(2):183–189.
17. Oda, T., M. M. Panjabi, J. J. Crisco, 3rd, T. R. Oxland, L. Katz, and L. P. Nolte. 1991. Experimental study of atlas injuries. II. Relevance to clinical diagnosis and treatment. *Spine (Philadelphia, Pa)* 16(10 Suppl):S466–473.
18. Tubbs, R. S., D. R. Kelly, E. R. Humphrey et al. 2007. The tectorial membrane: Anatomical, biomechanical, and histological analysis. *Clinical Anatomy* 20(4):382–386.
19. Maiman, D. J., and N. Yoganandan. 1991. Biomechanics of cervical spine trauma. *Clinical Neurosurgery* 37:543–570.
20. Yoganandan, N., S. Kumaresan, and F. A. Pintar. 2001. Biomechanics of the cervical spine. Part 2. Cervical spine soft tissue responses and biomechanical modeling. *Clinical Biomechanics (Bristol, Avon)* 16(1):1–27.
21. Pintar, F. A., N. Yoganandan, M. Pesigan, J. Reinartz, A. Sances, Jr., and J. F. Cusick. 1995. Cervical vertebral strain measurements under axial and eccentric loading. *Journal of Biomechanical Engineering* 117(4):474–478.

22. Kumaresan, S., N. Yoganandan, F. A. Pintar, and D. J. Maiman. 1999. Finite element modeling of the cervical spine: Role of intervertebral disc under axial and eccentric loads. *Medical Engineering & Physics* 21 (10):689–700.
23. White, A. A., and M. M. Panjabi. 1990. *Clinical Biomechanics of the Spine*. 2nd ed. Philadelphia: J. B. Lippincott.
24. Hsu, W. H., E. C. Benzel, T. Y. Chen, and Y. L. Chen. 2008. Axial and coronal orientation of subaxial cervical zygapophysial joints and their effect on axial rotation and lateral bending. *Spine (Philadelphia, Pa)* 33 (22):2409–2414.
25. Onan, O. A., M. H. Heggeness, and J. A. Hipp. 1998. A motion analysis of the cervical facet joint. *Spine (Philadelphia, Pa)* 23 (4):430–439.
26. Ahmed, A. M., N. A. Duncan, and D. L. Burke. 1990. The effect of facet geometry on the axial torque–rotation response of lumbar motion segments. *Spine (Philadelphia, Pa)* 15 (5):391–401.
27. Voo, L. M., S. Kumaresan, N. Yoganandan, F. A. Pintar, and J. F. Cusick. 1997. Finite element analysis of cervical facetectomy. *Spine (Philadelphia, Pa)* 22 (9):964–969.
28. Kumaresan, S., N. Yoganandan, and F. A. Pintar. 1998. Finite element modeling approaches of human cervical spine facet joint capsule. *Journal of Biomechanics* 31 (4):371–376.
29. Boreadis, A. G., and J. Gershon-Cohen. 1956. Luschka joints of the cervical spine. *Radiology* 66 (2):181–187.
30. Myklebust, J. B., F. Pintar, N. Yoganandan et al. 1988. Tensile strength of spinal ligaments. *Spine (Philadelphia, Pa)* 13 (5):526–531.
31. Davis, P. R. 1959. The medial inclination of the human thoracic intervertebral articular facets. *Journal of Anatomy* 93 (Pt 1):68–74.
32. Cheng, B. C., M. A. Hafez, B. Cunningham, H. Serhan, and W. C. Welch. 2008. Biomechanical evaluation of occipitocervicothoracic fusion: Impact of partial or sequential fixation. *The Spine Journal* 8 (5):821–826.
33. el-Khoury, G. Y., and C. G. Whitten. 1993. Trauma to the upper thoracic spine: Anatomy, biomechanics, and unique imaging features. *AJR. American Journal of Roentgenology* 160 (1):95–102.
34. McElhaney, J. H. Dynamic response of bone and muscle tissue. 1966. *Journal of Applied Physiology* 21 (4):1231–1236.
35. Bohlman, H. H. 1985. Treatment of fractures and dislocations of the thoracic and lumbar spine. *Journal of Bone and Joint Surgery. American Volume* 67 (1):165–169.
36. Patrick, L., C. Kroell, and H. Mertz. 1965. Forces on the human body in simulated crashes. *Stapp Car Crash Conference Proceedings* SAE Paper 650961.
37. Panjabi, M. M., J. N. Hausfeld, and A. A. White, 3rd. 1981. A biomechanical study of the ligamentous stability of the thoracic spine in man. *Acta Orthopaedica Scandinavica* 52 (3):315–326.
38. Hirsch, C., and J. Galante. 1967. Laboratory conditions for tensile tests in annulus fibrosus from human intervertebral discs. *Acta Orthopaedica Scandinavica* 38 (2):148–162.
39. Panjabi, M. M., R. A. Brand, Jr., and A. A. White, 3rd. 1976. Three-dimensional flexibility and stiffness properties of the human thoracic spine. *Journal of Biomechanics* 9 (4):185–192.
40. Gregersen, G. G., and D. B. Lucas. 1967. An in vivo study of the axial rotation of the human thoracolumbar spine. *Journal of Bone and Joint Surgery. American Volume* 49 (2):247–262.
41. Lin, R. M., I. M. Jou, C. and Y. Yu. 1992. Lumbar lordosis: Normal adults. *Journal of the Formosan Medical Association* 91 (3):329–333.
42. Benzel, E. C. 2005. *Spine Surgery: Techniques, Complication Avoidance, and Management*. 2nd ed. Philadelphia: Elsevier Churchill Livingstone.
43. Adams, M. A., and W. C. Hutton. 1981. The relevance of torsion to the mechanical derangement of the lumbar spine. *Spine (Philadelphia, Pa)* 6 (3):241–248.
44. Hutton, W.C., and B. M. Cyron. 1978. Spondyloysis. The role of the posterior elements in resisting the intervertebral compressive force. *Acta Orthopaedica Scandinavica* 49 (6):604–609.
45. Dunlop, R. B., M. A. Adams, and W. C. Hutton. 1984. Disc space narrowing and the lumbar facet joints. *The Journal of Bone and Joint Surgery. British Volume* 66 (5):706–710.
46. Nachemson, A. 1963. The influence of spinal movements on the lumbar intradiscal pressure and on the tensile stresses in the annulus fibrosus. *Acta Orthopaedica Scandinavica* 33:183–207.

47. Botsford, D. J., S. I. Esses, and D. J. Ogilvie-Harris. 1994. In vivo diurnal variation in intervertebral disc volume and morphology. *Spine (Philadelphia, Pa)* 19 (8):935–940.
48. Brinckmann, P., and H. Grootenboer. 1991. Change of disc height, radial disc bulge, and intradiscal pressure from discectomy. An in vitro investigation on human lumbar discs. *Spine (Philadelphia, Pa)* 16 (6):641–646.
49. Adams, M. A., P. Dolan, and W. C. Hutton. 1988. The lumbar spine in backward bending. *Spine (Philadelphia, Pa)* 13 (9):1019–1026.
50. McNally, D. S., M. A. Adams, and A. E. Goodship. 1993. Can intervertebral disc prolapse be predicted by disc mechanics? *Spine (Philadelphia, Pa)* 18 (11):1525–1530.
51. Adams, M. A., P. Dolan, and W. C. Hutton. 1987. Diurnal variations in the stresses on the lumbar spine. *Spine (Philadelphia, Pa)*12 (2):130–137.
52. Dolan, K. J., and A. Green. 2006. Lumbar spine reposition sense: The effect of a 'slouched' posture. *Manual Therapy* 11 (3):202–207.
53. Farfan, H. F., J. W. Cossette, G. H. Robertson, R. V. Wells, and H. Kraus. 1970. The effects of torsion on the lumbar intervertebral joints: The role of torsion in the production of disc degeneration. *Journal of Bone and Joint Surgery. American Volume* 52 (3):468–497.
54. Pintar, F. A., N. Yoganandan, T. Myers, A. Elhagediab, and A. Sances, Jr. 1992. Biomechanical properties of human lumbar spine ligaments. *Journal of Biomechanics* 25 (11):1351–1356.
55. Mahato, N. K. 2010. Morphometric analysis and identification of characteristic features in sacra bearing accessory articulations with L5 vertebrae. *The Spine Journal* 10 (7):616–621.
56. Wiltse, L. L. 1962. The etiology of spondylolisthesis. *Journal of Bone and Joint Surgery. American Volume* 44-A:539–560.
57. Schwab, F., V. Lafage, A. Patel, and J. P. Farcy. 2009. Sagittal plane considerations and the pelvis in the adult patient. *Spine (Philadelphia, Pa)* 34 (17):1828–1833.
58. Mahato, N. K. 2010. Complete sacralization of L5 vertebrae: Traits, dimensions, and load bearing in the involved sacra. *The Spine Journal* 10 (7):610–615.
59. Aihara, T., K. Takahashi, A. Ogasawara, E. Itadera, Y. Ono, and H. Moriya. 2005. Intervertebral disc degeneration associated with lumbosacral transitional vertebrae: A clinical and anatomical study. *The Journal of Bone and Joint Surgery. British Volume* 87 (5):687–691.
60. Benzel, E. C. 1995. *Stability and Instability of the Spine*. New York: McGraw-Hill.
61. ASTM F1582-98. 2003. Standard terminology relating to spinal implants. In *ASTM Volume 1301 Medical and Surgical Materials and Devices (i)*. West Conshohocken: ASTM.
62. Yoganandan, N., D. J. Maiman, F. Pintar et al. 1988. Microtrauma in the lumbar spine: A cause of low back pain. *Neurosurgery* 23 (2):162–168.
63. Yoganandan, N., G. Ray, F. A. Pintar, J. B. Myklebust, and A. Sances, Jr. 1989. Stiffness and strain energy criteria to evaluate the threshold of injury to an intervertebral joint. *Journal of Biomechanics* 22 (2):135–142.
64. Yoganandan, N., G. Ray, and A. Sances, Jr. 1985. Assessment of traumatic failure load and microfailure load in an intervertebral disc segment. Paper presented at *ASME Advances in Bioengineering, New York*.
65. Yoganandan, N., F. A. Pintar, B. D. Stemper, C. E. Wolfla, B. S. Shender, and G. Paskoff. 2007. Level-dependent coronal and axial moment-rotation corridors of degeneration-free cervical spines in lateral flexion. *Journal of Bone and Joint Surgery. American Volume* 89 (5):1066–1074.
66. Yoganandan, N., B. D. Stemper, F. A. Pintar, J. L. Baisden, B. S. Shender, and G. Paskoff. 2008. Normative segment-specific axial and coronal angulation corridors of subaxial cervical column in axial rotation. *Spine (Philadelphia, Pa)* 33 (5):490–496.
67. Bogduk, N., and N. Yoganandan. 2001. Biomechanics of the cervical spine. Part 3: Minor injuries. *Clinical Biomechanics (Bristol, Avon)* 16 (4):267–275.
68. Yoganandan, N., J. F. Cusick, F. A. Pintar, and R. D. Rao. 2001. Whiplash injury determination with conventional spine imaging and cryomicrotomy. *Spine (Philadelphia, Pa)* 26 (22):2443–2448.
69. Cusick, J. F., F. A. Pintar, and N. Yoganandan. 2001. Whiplash syndrome: Kinematic factors influencing pain patterns. *Spine (Philadelphia, Pa)* 26 (11):1252–1258.

70. Stemper, B. D., N. Yoganandan, T. A. Gennarelli, and F. A. Pintar. 2005. Localized cervical facet joint kinematics under physiological and whiplash loading. *Journal of Neurosurgery. Spine* 3 (6):471–476.
71. Stemper, B. D., N. Yoganandan, and F. A. Pintar. 2003. Gender dependent cervical spine segmental kinematics during whiplash. *Journal of Biomechanics* 36 (9):1281–1289.
72. Yoganandan, N., F. Pintar, and J. F. Cusick. 1996. Cervical spine kinematics under inertial flexion–extension. In *11th North American Spine Society*, 265–266. Vancouver: North American Spine Society.
73. Yoganandan, N., F. Pintar, and J. F. Cusick. 1998. Head–neck biomechanics in simulated rear impact. In *42nd Association for the Advancement of Automotive Medicine*, 209–231. Charlottesville: Association for the Advancement of Automotive Medicine.
74. Yoganandan, N., F. Pintar, and S. J. Larson. 1998. *Frontiers in Head and Neck Trauma: Clinical and Biomechanical*. Amsterdam: IOS Press.
75. Stemper, B. D., N. Yoganandan, and F. A. Pintar. 2004. Gender- and region-dependent local facet joint kinematics in rear impact: Implications in whiplash injury. *Spine (Philadelphia, Pa)* 29 (16):1764–1771.
76. Cassidy, J. D., L. J. Carroll, P. Cote, M. Lemstra, A. Berglund, and A. Nygren. 2000. Effect of eliminating compensation for pain and suffering on the outcome of insurance claims for whiplash injury. *New England Journal of Medicine* 342 (16):1179–1186.
77. Francis, C. C. 1955. Dimensions of the cervical vertebrae. *The Anatomical Record* 122 (4):603–609.
78. Hukuda, S., and Y. Kojima. 2002. Sex discrepancy in the canal/body ratio of the cervical spine implicating the prevalence of cervical myelopathy in men. *Spine (Philadelphia, Pa)* 27 (3):250–253.
79. Katz, P.R., H. M. Reynolds, D. R. Foust, and J. K. Baum. 1975. Mid-sagittal dimensions of cervical vertebral bodies. *American Journal of Physical Anthropology* 43 (3):319–326.
80. Mosekilde, L. 1990. Sex differences in age-related changes in vertebral body size, density and biomechanical competence in normal individuals. *Bone* 11 (2):67–73.
81. Gilsanz, V., M. I. Boechat, R. Gilsanz, M. L. Loro, T. F. Roe, and W. G. Goodman. 1994. Gender differences in vertebral sizes in adults: Biomechanical implications. *Radiology* 190 (3):678–682.
82. Gilsanz, V., M. I. Boechat, T. F. Roe, M. L. Loro, J. W. Sayre, and W. G. Goodman. 1994. Gender differences in vertebral body sizes in children and adolescents. *Radiology* 190 (3):673–677.
83. Gilsanz, V., A. Kovanlikaya, G. Costin, T. F. Roe, J. Sayre, and F. Kaufman. 1997. Differential effect of gender on the sizes of the bones in the axial and appendicular skeletons. *The Journal of Clinical Endocrinology and Metabolism* 82 (5):1603–1607.
84. Nieves, J. W., C. Formica, J. Ruffing et al. 2005. Males have larger skeletal size and bone mass than females, despite comparable body size. *Journal of Bone and Mineral Research* 20 (3):529–535.
85. Osakabe, T., M. Hayashi, K. Hasegawa et al. 2001. Age- and gender-related changes in ligament components. *Annals of Clinical Biochemistry* 38 (Pt 5):527–532.
86. Yoganandan, N., F. A. Pintar, B. D. Stemper et al. 2006. Trabecular bone density of male human cervical and lumbar vertebrae. *Bone* 39 (2):336–344.
87. Yoganandan, N., F. A. Pintar, B. D. Stemper et al. 2006. Bone mineral density of human female cervical and lumbar spines from quantitative computed tomography. *Spine (Philadelphia, Pa)* 31 (1):73–76.
88. Stemper, B. D., N. Yoganandan, F. A. Pintar et al. 2008. Anatomical gender differences in cervical vertebrae of size-matched volunteers. *Spine (Philadelphia, Pa)* 33 (2):E44–E49.
89. Rao, R. D., S. V. Marawar, B. D. Stemper, N. Yoganandan, and B. S. Shender. 2008. Computerized tomographic morphometric analysis of subaxial cervical spine pedicles in young asymptomatic volunteers. *Journal of Bone and Joint Surgery. American Volume* 90 (9):1914–1921.
90. Chazono, M., S. Soshi, T. Inoue, Y. Kida, and C. Ushiku. 2006. Anatomical considerations for cervical pedicle screw insertion: The use of multiplanar computerized tomography reconstruction measurements. *Journal of Neurosurgery. Spine* 4 (6):472–477.
91. Stemper, B. D., S. V. Marawar, N. Yoganandan, B. S. Shender, and R. D. Rao. 2008. Quantitative anatomy of subaxial cervical lateral mass: An analysis of safe screw lengths for Roy–Camille and Magerl techniques. *Spine (Philadelphia, Pa)* 33 (8):893–897.

92. Yoganandan, N., S. A. Knowles, D. J. Maiman, and F. A. Pintar. 2003. Anatomic study of the morphology of human cervical facet joint. *Spine (Philadelphia, Pa)* 28 (20):2317–2323.
93. Serhan, H. A., G. Varnavas, A. P. Dooris, A. Patwadhan, and M. Tzermiadianos. 2007. Biomechanics of the posterior lumbar articulating elements. *Neurosurgical Focus* 22 (1):E1.
94. Berry, J. L., J. M. Moran, W. S. Berg, and A. D. Steffee. 1987. A morphometric study of human lumbar and selected thoracic vertebrae. *Spine (Philadelphia, Pa)* 12 (4):362–367.
95. Panjabi, M. M., K. Takata, V. Goel, D. Federico, T. Oxland, J. Duranceau et al. 1991. Thoracic human vertebrae: Quantitative three-dimensional anatomy. *Spine (Philadelphia, Pa)* 16 (8): 888–901.

8

Joint Mechanics of the Shoulder

Cathryn D. Peltz, Vasilios Moutzouros, and Michael J. Bey

CONTENTS

8.1 Introduction

The shoulder is one of the human body's most complex joints. Motion of the shoulder girdle occurs through the highly coordinated interaction of four joints, at least ten ligaments, and close to twenty muscles. Our shoulders provide us with the strength and motion necessary to accomplish our activities of daily living, whether that involves throwing a 100-mph fastball or simply placing an item on the top shelf of a refrigerator. When these activities are accomplished with little or no pain, the shoulder can indeed be viewed as being the "perfect compromise between mobility and stability."[1] However, shoulder injuries, such as rotator cuff tears and joint dislocations, are common. These injuries are painful, impair activity levels, and decrease quality of life. Although the etiology of injury is often not well understood, it is generally accepted that many shoulder injuries are associated with altered motion and forces (i.e., the principal variables in the field of engineering mechanics). Altered joint mechanics may contribute to an injury or may occur in response to an injury. The purpose of this chapter is to provide an overview of shoulder biomechanics. The specific objectives are to provide an overview of human shoulder anatomy, review the anatomical structures that contribute to glenohumeral joint stability, describe the joint mechanics of the normal, healthy shoulder, and present the associations between shoulder mechanics and two common shoulder disorders: rotator cuff tears and glenohumeral joint instability.

8.2 Anatomy of the Shoulder

The human shoulder complex consists of three bones (humerus, scapula, and clavicle) and four joints (glenohumeral, scapulothoracic, acromioclavicular, and sternoclavicular joints; Figure 8.1). Shoulder motion occurs primarily at the glenohumeral and scapulothoracic joints. The glenohumeral joint is sometimes referred to as a ball-and-socket joint, although

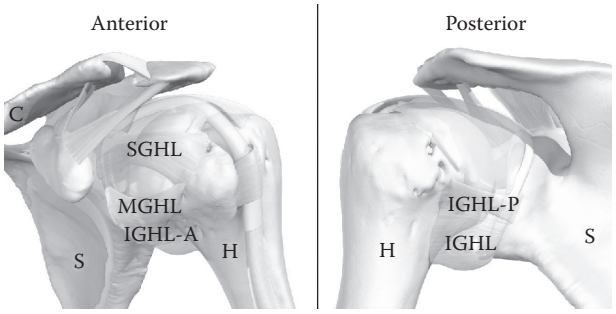

FIGURE 8.1
Bony anatomy of the shoulder includes the humerus (H), scapula (S), and clavicle (C). Glenohumeral joint ligaments consist of the superior glenohumeral ligament (SGHL), middle glenohumeral ligament (MGHL), and the inferior glenohumeral ligament (IGHL). Prominent thickenings of the IGHL complex include the anterior (IGHL-A) and posterior (IGHL-P) bands of the IGHL. (From Copeland, S. et al., *Interactive Shoulder* [Software] 20072011. Available from www.primalpictures.com, 2011. With permission.)

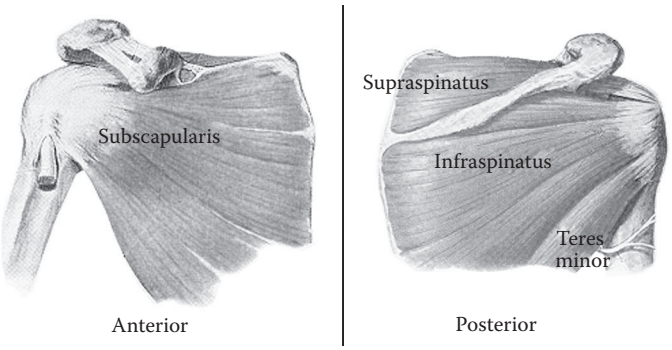

FIGURE 8.2
Rotator cuff muscles include the supraspinatus, infraspinatus, teres minor, and subscapularis. (Reprinted from *Atlas of Human Anatomy*, Netter, F. H., Novartis, East Hanover, NJ, Copyright 1989, with permission from Elsevier.)

the glenoid (i.e., the articulating surface of the scapula) is a particularly shallow socket. The depth of the socket is increased by the labrum, a fibrous ring of connective tissue located along the perimeter of the glenoid. The glenohumeral joint is passively stabilized by four ligaments—the superior glenohumeral ligament (SGHL), the middle glenohumeral ligament (MGHL), the inferior glenohumeral ligament (IGHL), and the coracohumeral ligament (CHL)—and the joint capsule (Figure 8.1). The ligaments are not distinct structures but rather are continuous with the joint capsule tissue. Glenohumeral joint motion and dynamic stability are provided by the rotator cuff (a group of four muscles originating on the scapula and inserting into the lateral aspect of the humeral head; Figure 8.2), the deltoid muscle group, and the biceps long head. Scapulothoracic motion and dynamic stability are provided primarily by the serratus anterior, trapezius, rhomboids, pectoralis minor, levator scapulae, and subclavius muscles.

8.3 Glenohumeral Joint Stability

The mobility of the shoulder is primarily achieved through glenohumeral joint motion, and the stability of the glenohumeral joint is accomplished through a complex interaction of static structures (i.e., articulating geometry, labrum, and ligaments) that passively stabilize the joint and dynamic structures (i.e., muscles) that actively stabilize the joint. The objective of this section is to provide a brief review of the structures involved in providing static and dynamic glenohumeral joint stability.

As a brief aside, the description of shoulder motion can be confusing. For example, previous research has described the elevation of the shoulder in the plane of the scapula as scapular-plane abduction, abduction, elevation, or scaption. Multiple descriptions of the same motion can certainly lead to confusion. The International Society of Biomechanics has promoted an approach for describing glenohumeral joint motion in terms of the plane of elevation, the amount of elevation, and the amount of internal/external rotation of the humerus.[2] This approach can also be used to describe the position of the arm relative to the

torso, and, in the interest of consistency, all shoulder positions and motions in this chapter will be described using this system.

8.3.1 Static Stabilizers

8.3.1.1 Articulating Geometry

It is generally understood that the geometry of the glenoid provides relatively little stability to the glenohumeral joint. One reason for this is because the glenoid is very shallow relative to the size of the humeral head. Specifically, it has been reported that the average depth of the glenoid in the anterior/posterior direction is approximately 2.5 mm.[3] In contrast, the average depth of the glenoid in the superior/inferior direction has been reported to be approximately 9.0 mm.[3,4] With less inherent conformity in the glenoid's anterior/posterior direction, there exists the possibility of greater humeral translation in the anterior/posterior direction than in the superior/inferior direction.[5] Another factor that has been suggested as contributing to the glenohumeral joint's inherent lack of stability is that the glenoid and humeral head do not have equal radii of curvature.[6] However, this finding is based on the geometry of the subchondral bone surfaces. When the radii of curvature are determined from the cartilage surfaces, the glenohumeral joint is reported to be highly congruent.[7] Consequently, Soslowsky et al.[7] conclude that the lack of stability of the glenohumeral joint is not due to the mismatch in the radii of curvature between the humeral head and glenoid, but due to the small surface area of the glenoid that does not fully enclose the humeral head. This theory is supported by cadaveric studies[8] indicating that the articular surface area of the humerus is 21 to 22 cm^2, whereas the glenoid articular surface area is only 8 to 9 cm^2. Moreover, it has been reported[6] that the maximum contact area between the two articular surfaces is only 4 to 5 cm^2. Therefore, only 25% to 30% of the humeral head articular surface area is engaged by the glenoid at any one time.[9]

8.3.1.2 Soft Tissue Structures

The soft tissues surrounding the glenohumeral joint help increase joint stability. For example, the glenoid labrum adds approximately 50% more depth to the glenoid cavity,[3] thereby increasing joint congruity. Injuries to the labrum (i.e., SLAP lesions)[10] have the potential to decrease glenohumeral joint stability by approximately 20%.[11] Thus, the labrum is believed to play an important role in maintaining glenohumeral joint stability.

The glenohumeral ligaments (i.e., SGHL, MGHL, IGHL, and CHL) and the joint capsule provide stability at the end ranges of glenohumeral joint motion.[4,12] Burkart and Debski[12] reported that the SGHL and CHL were important inferior stabilizers (i.e., these ligaments resist inferior translation of the humerus), whereas the MGHL provides anterior stability when the shoulder is elevated in the frontal plane. It was also noted that the IGHL—perhaps the most frequently injured of the glenohumeral ligaments—is an important stabilizer against anterior dislocation when the shoulder is in a position of frontal-plane elevation and external rotation. Although previous research has identified the primary stabilizing function(s) of each ligament (Table 8.1), it is important to recognize that these ligaments are continuous with the joint capsule and are not distinct structures like the anterior cruciate ligament of the knee. Consequently, the mechanical function of these ligaments (or regions of these ligaments) has been shown to be highly complex,[13,14] and passive glenohumeral joint stability occurs through interaction of the various ligaments in a manner that is still not fully understood.

TABLE 8.1

Glenohumeral Ligaments and Their Primary Stabilizing Function

Glenohumeral Ligament	Primary Stabilizing Function
SGHL	Inferior stability with the arm in neutral rotation
MGHL	Anterior stability with the arm at 0°–45° of frontal-plane elevation
IGHL	Anterior band: anteroinferior stability during frontal-plane elevation and external rotation
	Posterior band: posterior stability during sagittal-plane elevation and internal rotation
CHL	Posterior and inferior stability with the arm adducted

Source: Adapted from Lugo, R. et al., *Eur. J. Radiol.*, 68, 1, 16–24, 2008.

8.3.1.3 Passive Muscle Tension

Passive muscle tension also contributes to the static stability of the glenohumeral joint. For example, the passive tension of the subscapularis muscle can function as a barrier to anterior humeral head translation,[15] whereas the passive muscle tension of both the supraspinatus and teres minor increases stability in the posterior direction.[16]

8.3.2 Dynamic Stabilizers

The muscles crossing the glenohumeral joint—in particular, the rotator cuff muscles and the biceps long head—provide dynamic stability in the midranges of motion when glenohumeral ligaments are lax. These muscles direct joint reaction forces into the glenoid, thereby keeping the joint at its most stable configuration. The contribution of individual muscles to joint stability varies with arm position and motion, so it is difficult to precisely characterize the *in vivo* contribution of each muscle to overall glenohumeral stability.[17] This section provides a brief overview of the contribution of individual shoulder muscles to dynamic joint stability.

8.3.2.1 Rotator Cuff

The scapulohumeral muscle group (supraspinatus, infraspinatus, teres minor, subscapularis, and deltoid) plays the most significant role in dynamic stabilization of the glenohumeral joint. In addition to contributing to overall shoulder strength, these muscles actively compress the humeral head into the glenoid cavity. The conventional approach for assessing the role of individual muscles to glenohumeral joint stability has been through cadaver experiments in which individual muscle forces can be systematically varied while quantifying their contribution to joint stability. For example, Blasier et al.[18] investigated the effect of the rotator cuff muscles on posterior stability by measuring the force required to sublux the humeral head in a cadaveric model. Although the subscapularis provided the greatest contribution to posterior stability, it was reported that forces applied to any of the rotator cuff muscles had a significant effect on posterior stability. This finding—that load applied through any of the rotator cuff tendons had a significant contribution to joint stability—was also reported in a similar study on anterior joint stability.[19] Superior translation of the humerus has been reported to be resisted by the supraspinatus, subscapularis, and infraspinatus, depending on the arm's position. These cadaveric experiments strongly suggest

that forces generated by the rotator cuff muscles play a significant role in maintaining dynamic glenohumeral joint stability.

The contribution of the supraspinatus and infraspinatus to glenohumeral joint stability has also been investigated under *in vivo* conditions. Specifically, glenohumeral joint position has been assessed using radiography[20] or magnetic resonance imaging (MRI)[21] after administering a suprascapular nerve block to human volunteers. Howell and Kraft[20] found that paralysis of the supraspinatus and infraspinatus muscles resulted in abnormal anterior translation of the humerus in only 2 of 13 patients tested. Similarly, Werner et al.[21] reported that the humerus always remained centered on the glenoid during frontal-plane elevation after a suprascapular nerve block. Because these nerve block studies assessed glenohumeral joint positioning with static imaging techniques, the extent to which the findings are representative of dynamic muscle function is not clear. However, the findings from these *in vivo* nerve block studies are in stark contrast with the cadaver experiments and suggest that the contribution of individual rotator cuff muscles to glenohumeral joint stability under *in vivo* conditions is still not well understood.

8.3.2.2 Biceps Long Head

Previous research has identified the biceps long head as a significant contributor to dynamic glenohumeral joint stability. For example, Itoi et al.[22] measured the effect of biceps loading on humeral head translations in cadaveric shoulder specimens and reported that the biceps contributed significantly to anterior, inferior, and posterior joint stability. Pagnani et al.[23] reported that the biceps' effectiveness as a stabilizer was most apparent with the shoulder in external, but not internal, rotation. Malicky et al.[19] and Itoi et al.[24] also concluded from cadaveric studies that the biceps was important for anterior stability during frontal-plane elevation. Itoi et al.[24] concluded that, as a stabilizer, the biceps was as efficient as the supraspinatus and infraspinatus, noting that its role becomes more important than that of the cuff muscles with an unstable shoulder.

8.3.2.3 Relationship between Static and Dynamic Stabilizers

It is generally understood that dynamic stabilizers of the glenohumeral joint (e.g., the rotator cuff muscles) are more important in the midranges of motion when the glenohumeral ligaments are lax, whereas the static stabilizers (e.g., glenohumeral ligaments) are most important at the end ranges of motion.[25] However, it is likely that there is significant coordination between the static and dynamic stabilizers throughout the entire range of shoulder motion.[4,25,26] For example, the subscapularis contributes to anterior stability along with the MGHL in the midrange of scapular-plane or frontal-plane elevation.[4,27] Similarly, Labriola et al.[26] demonstrated in a cadaveric model that increases in simulated muscle forces increased glenohumeral joint stability at the end ranges of motion. Thus, static and dynamic stabilizers work synergistically to maintain glenohumeral joint stability throughout the shoulder's entire range of motion.

8.4 Joint Mechanics of the Normal, Healthy Shoulder

Significant research efforts have sought to understand the function of the normal, healthy shoulder through a variety of experimental and computational approaches. Using

examples from representative research studies, the objective of this section is to provide a brief overview of how normal shoulder function has been characterized in terms of joint motions, muscle function, and joint forces.

8.4.1 Resting Posture

The resting posture of the scapula and humerus can vary significantly among individuals, but it is generally accepted that the scapula is orientated approximately 30° anteriorly and 20° forward with respect to the frontal plane and about 3° upward with respect to the sagittal plane (Figure 8.3). There exists approximately 30° of retroversion of the articular surface of the humeral head relative to the shaft of the humerus. This 30° of humeral retroversion complements the 30° of anterior rotation of the scapula relative to the torso.

8.4.2 Glenohumeral Joint Motion

Alterations in glenohumeral joint motion are often associated with pathologic shoulder conditions. Consequently, accurately characterizing glenohumeral joint motion under both normal and pathologic conditions is essential for understanding the etiology and treatment of various shoulder conditions. Previous research has relied on a wide variety of experimental approaches for measuring glenohumeral joint motion, including cadaveric simulations,[28] two-dimensional (2D) imaging,[5] static three-dimensional (3D) imaging,[29] conventional video-based motion measurement systems,[30] bone pins,[31] 2D fluoroscopy combined with shape matching,[32,33] and biplane X-ray imaging.[34] Using these techniques, motions at the glenohumeral joint are typically characterized in terms of both rotations and translations of the humerus with respect to the glenoid.[2] Rotation of the humerus is the predominant motion at the glenohumeral joint, and internal/external rotations of the humerus around its long axis are particularly important for normal shoulder function. For example, Flatow et al.[35] showed that external rotation of the humerus during scapular-plane elevation allows for clearance of the greater tuberosity under the coracoacromial arch.

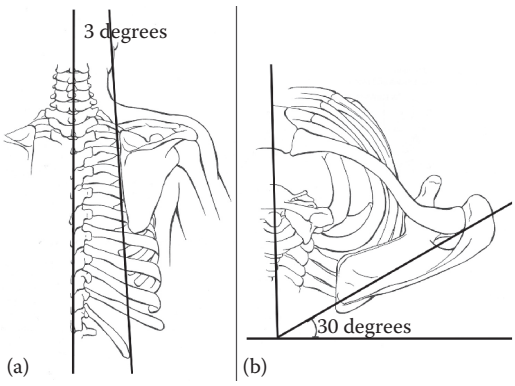

FIGURE 8.3
Normal resting posture of the scapula is approximately (a) 3° upwardly rotated relative to the spine and (b) 30° anterior to the frontal plane. (Adapted from Kuhn, J. E., In *Disorders of the Shoulder: Diagnosis & Management*, edited by J. P. Iannotti and G. R. Williams, Lippincott Williams & Wilkins, Philadelphia, PA, 2006.)

Although humeral rotation is the primary motion at the glenohumeral joint, translations of the humerus do indeed occur during normal shoulder motion. Under normal conditions, glenohumeral joint translations are likely small—typically on the order of several millimeters[5,36]—and therefore may be below the level of *in vivo* accuracy for some measurement techniques. In a radiographic study of 2D glenohumeral joint motion, Poppen and Walker[5] demonstrated that the humerus can translate approximately 3 to 4 mm in the superior/inferior direction during scapular-plane elevation. This range of translation is consistent with the 2 to 3 mm superior/inferior translation range reported by Bey et al.[34] using biplane X-ray analysis and the 1 to 2 mm range reported by Graichen et al.[37,38] using MRI-based techniques. In the anterior/posterior direction, glenohumeral translations are also reported to be in the range of several millimeters. For example, previous studies have reported that the humerus translates approximately 1 to 2 mm in the anterior/posterior direction during external shoulder rotation.[34,39] Howell et al.[36] used radiographic techniques to report approximately 4 mm of posterior translation when the arm is in the cocked position of throwing. In some cases, previous studies have reported glenohumeral translations that are significantly larger than the range of values described here. Although it is certainly conceivable that much larger humeral translations may exist under certain pathologic conditions, it is also important to recognize that not all measurement techniques will have the accuracy necessary to measure the glenohumeral joint motions that occur under *in vivo* conditions.

8.4.3 Scapulothoracic Motion

The motion of the scapula relative to the torso is complex. Extensive research efforts have focused on characterizing scapulothoracic motion in healthy shoulders,[40–42] as well as understanding how scapulothoracic motion is affected by factors such as fatigue,[43] pathology,[44–46] and treatment.[47] Scapulothoracic motion is typically expressed in terms of anterior/posterior tilt, upward/downward rotation, and internal/external rotation (Figure 8.4). Previously reported values for scapulothoracic motion often vary considerably between research studies, but it is generally understood that upward/downward rotation is the scapula's predominant motion, with approximately 50° of upward rotation in healthy shoulders during scapular-plane elevation.[42] McClure et al.[42] have also reported that scapular motion involves approximately 30° of posterior tilt and 24° of external rotation during scapular-plane elevation in healthy subjects.

8.4.4 Relationship between Glenohumeral Joint Motion and Scapulothoracic Motion

Glenohumeral joint motion and scapulothoracic motion are not independent, and their relationship during overall shoulder motion is typically referred to as scapulohumeral rhythm (SHR). It is generally accepted that the SHR—defined as the ratio of glenohumeral joint motion to scapulothoracic motion—in healthy shoulders is approximately 2:1. This ratio indicates that for every 2° of glenohumeral motion, there is 1° of scapulothoracic motion contributing to overall shoulder elevation.[48] However, this SHR of 2:1 should be used as only a general guideline because SHR has been shown to be influenced by factors such as pathology,[44] activity, the resting posture of the scapula, and the method used to measure humeral motion.[42] For example, McClure et al.[42] reported that subjects with healthy shoulders had an SHR of 1.7:1 during scapular-plane elevation and 2:1 during frontal-plane elevation. Values reported in other studies have ranged from 1.25:1 to 3.2:1 under similar conditions.[5,49]

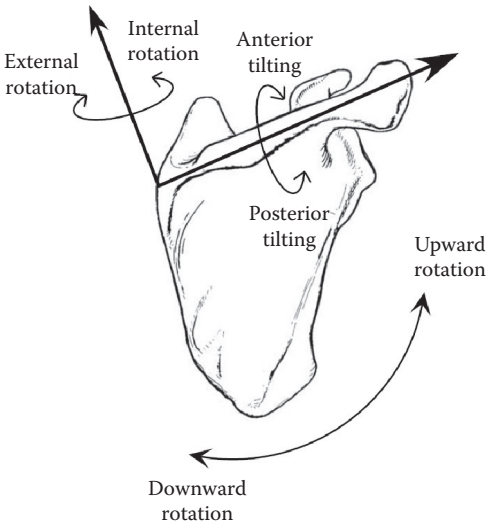

FIGURE 8.4
Three-dimensional motion of the scapula is typically expressed in terms of upward/downward rotation, anterior/posterior tilting, and internal/external rotation relative to the torso. (Reprinted from Karduna, A. R. et al., *J. Shoulder Elbow Surg.*, 14, 4, 393–399, 2005, with permission from Elsevier.)

8.4.5 Muscle Function during Shoulder Motion

As with any joint, the shoulder muscles function synergistically and are highly redundant. Hurov[9] compiled a review of electromyography studies during eight distinct shoulder motions and concluded that the deltoid muscle group was the "true workhorse" of the shoulder. This is not surprising, given that the deltoid muscle has the largest cross-sectional area of all the shoulder muscles.[50] The rotator cuff muscles are important to shoulder function, providing dynamic glenohumeral joint stability and contributing significantly to overall shoulder strength. The posterior rotator cuff muscles (i.e., infraspinatus and teres minor) are the most efficient external rotators of the humerus with the arm at the side.[50,51] Specifically, Gerber et al.[52] reported in a suprascapular nerve block study that the infraspinatus contributes approximately 70% of external rotation strength. The anterior rotator cuff muscle (i.e., subscapularis) contributes significantly to internal rotation of the humerus.[50,51] The supraspinatus muscle is most active during sagittal-plane and frontal-plane elevation,[9,50,51] and it has been reported that the supraspinatus and infraspinatus together contribute approximately 80% of scapular-plane elevation strength.[52]

Previous electromyographic studies have indicated that the long head of the biceps is active during frontal-plane elevation, external rotation, and sagittal-plane elevation.[53,54] Although elbow flexion is likely the primary function of the biceps long head, muscle activity during frontal-plane elevation, rotation, and sagittal-plane elevation suggests that the biceps long head may also play a significant role in maintaining dynamic glenohumeral joint stability. Indeed, cadaveric experiments suggest that simulated biceps forces can have a significant effect on glenohumeral joint motions.[55,56]

The scapulothoracic muscles (e.g., serratus anterior, rhomboidei, and trapezius) are important contributors to shoulder motion and strength. The serratus anterior and rhomboidei are believed to stabilize the scapula against the torso, thus providing a stable base of support necessary for facilitating glenohumeral joint motion and generating large

shoulder forces.[1] In addition, the serratus anterior is the main torque generator during scapular-plane elevation[57] and contributes substantially to posterior tilting of the scapula during elevation. The trapezius is primarily responsible for upward rotation of the scapula.[58] However, the upper trapezius also attaches to the clavicle and has been shown to be involved in elevation and retraction of the clavicle as well.[59] The lower trapezius is attached only to the scapula (in particular, the scapular spine) and is therefore more effective in upward rotation of the scapula.

8.4.6 Glenohumeral Joint Forces

It is generally accepted that glenohumeral joint forces vary with arm position and the magnitude of muscle forces, but there are relatively little data available on actual glenohumeral joint forces that occur under *in vivo* conditions. Computational models of the shoulder have estimated that glenohumeral joint contact forces range from 130% to 240% of body weight.[60] In recent years, several studies have directly measured glenohumeral joint forces through the use of custom-instrumented implants in patients undergoing total shoulder arthroplasty (Table 8.2).[61–63] Westerhoff et al.[63] reported that activities such as lifting a coffee pot or a 2 kg weight from a board to head height resulted in forces of approximately 100% to 150% of the body weight. The force while passively holding a 10 kg weight with the arm at the side was only 12% of the body weight, but increased to 92% of the body weight as the weight was raised to belt height. A follow-up study in the same patient population measured forces during sagittal-plane and frontal-plane elevation of the straight

TABLE 8.2

In Vivo Glenohumeral Joint Forces during Various Activities of Daily Living

Activity	Peak Force (% Body Weight)
Wheelchair propulsion, 1% incline (3 km/h)[144]	45
Wheelchair propulsion, 2% incline (3 km/h)[144]	50
Forward flexion to 90° without weight, fast speed[62]	59
Wheelchair propulsion, 3% incline (3 km/h)[144]	61
Wheelchair propulsion, 4% incline (3 km/h)[144]	62
Coronal-plane abduction to 90° without weight, fast speed[62]	65
Steering with two hands[63]	74 (range, 40–89)
Forward flexion to 90° without weight, slow speed[62]	73 (range, 55–87)
Combing[63]	76 (range, 59–105)
Coronal-plane abduction to 90° without weight, slow speed[62]	81 (range, 46–115)
Lifting a 2 kg weight onto table at belt height[63]	87 (range, 54–133)
Lifting a 2 kg weight onto table at head height[63]	98 (range, 93–104)
Nailing[63]	98 (range, 80–117)
Forward flexion to 90° with 2 kg weight, fast speed[62]	101
Coronal-plane abduction to 90° with 2 kg weight, fast speed[62]	101
Lifting a 1.5 kg coffee pot[63]	105 (range, 90–125)
Forward flexion to 90° with 2 kg weight, slow speed[62]	122
Steering with one hand[63]	122 (range, 106–137)
Setting down a 1.5 kg coffee pot[63]	123 (range, 105–153)
Coronal-plane abduction to 90° with 2 kg weight, slow speed[62]	129

Source: Data from Bergmann, G. et al. *J. Biomech.*, 44, 8, 1543–1552, 2011; Westerhoff, P. et al., *J. Biomech.*, 42, 12, 1840–1849, 2009; Westerhoff, P. et al., *Clin. Biomech. (Bristol, Avon)*, 2011.

Note: The activities are listed in order of ascending joint force.

arm holding a 2 kg weight.[62] Joint forces ranged from 70% to 238% of the body weight and increased with elevation angle.[62] It is not known if the forces recorded in patients who have undergone total shoulder arthroplasty are representative of healthy shoulders. Nonetheless, these data clearly demonstrate that high joint forces concentrated over a relatively small load-bearing area (i.e., the articulating area of the glenoid) could contribute to the development of pathologic conditions (e.g., labral tears, glenohumeral joint arthritis) as a result of a subtle change in glenohumeral joint motion.

8.5 Rotator Cuff Pathology

8.5.1 Clinical Presentation and Examination

Rotator cuff pathology is a common condition that occurs most often in individuals older than 40 years and includes the diagnoses of subacromial impingement and rotator cuff tears.[64] Patients with rotator cuff pathology will present to their clinician with complaints of pain, weakness, and oftentimes stiffness. Proper questioning can lead to valuable information that can distinguish isolated subacromial impingement from full-thickness rotator cuff tears. Pain can be present in both conditions and is localized over the deltoid region or posterior acromial area. Pain with activity, as well as at times of rest, can also be apparent. Individuals with full-thickness rotator cuff tears will complain of significant shoulder weakness, which is not typically associated with subacromial impingement.

The physical examination begins with an inspection of the shoulder, with particular focus on the bony anatomy and muscular definition of the posterior shoulder. Patients with a chronic rotator cuff tear often demonstrate significant posterior shoulder atrophy. Active and passive ranges of motion are next examined and can be limited in patients with both rotator cuff tears and isolated subacromial impingement. The Neer exam is a specific subacromial impingement test that involves passively elevating the shoulder in the sagittal plane while stabilizing the scapula.[65] A positive Neer test, indicating impingement, is one in which the patient experiences pain at the end range of shoulder elevation. The Hawkins test is a provocative test for isolated subacromial impingement and is performed by internally rotating the humerus with the shoulder positioned at 90° of the sagittal-plane elevation and 90° of elbow flexion.[66,67] Pain during this maneuver indicates subacromial impingement. When a rotator cuff tear is suspected, the degree of active motion restriction reported by the patient can predict the size of the tear. Patients with shoulder weakness, but well-maintained active motion, typically have a smaller single-tendon tear, whereas patients with weakness and a lack of active motion are more likely to have a multitendon tear.

Manual shoulder strength testing is often performed as part of the physical exam to assess the condition of the individual rotator cuff muscle–tendon units. The Jobe test, which is believed to isolate the supraspinatus, is performed by first positioning the shoulder at a 90° sagittal-plane elevation, 30° frontal-plane elevation, and full internal rotation.[68] With the shoulder in this position, strength is qualitatively assessed as the patient resists a downward force applied to the shoulder. Patients with a supraspinatus cuff tear will have considerable weakness when comparing this test between their involved and uninvolved shoulders. The infraspinatus can be tested by having patients externally rotate against resistance with their arm and elbow at their side. The subscapularis can be assessed with

a belly-press test or lift-off test. The belly-press test is a simple maneuver in which patients place their hand on their abdomen and attempt to push inward without rotating their shoulder. Similarly, the lift-off test is a maneuver in which the patients internally rotate their shoulder behind their back and attempt to lift their hand off the lower lumbar area. Patients who are unable to stabilize their elbow or shoulder during the belly-press test, or who are unable to perform the lift-off test, likely have a subscapularis tear. For all the aforementioned tests, it is important to compare the findings from the involved shoulder with, ideally, the uninvolved contralateral shoulder.

Medical imaging is frequently used in the diagnosis of rotator cuff pathology. Conventional radiographs allow for the assessment of bony pathology, such as a curved or hooked acromion.[69] Advanced imaging (i.e., ultrasound imaging or MRI) can also aid in the diagnosis when a rotator cuff tear is suspected. The benefits of ultrasound imaging are its lower cost and dynamic examination potential, although results are generally believed to be operator dependent. MRI is beneficial in identifying tear size, tear location, tendon retraction, and the extent to which muscular atrophy or fatty degeneration has occurred in conjunction with the rotator cuff pathology.

8.5.2 Rotator Cuff Pathology and Glenohumeral Joint Motion

Glenohumeral joint motion has been shown to be altered in the presence of a rotator cuff tear. Perhaps the most common approach to assess the effects of a rotator cuff tear on glenohumeral joint motion has been through cadaveric experiments in which joint motion can be accurately measured while imposing individual muscle forces and tendon conditions (e.g., intact versus simulated tear). Although many cadaver studies follow qualitatively similar testing protocols, these cadaver studies have sometimes shown contradictory findings regarding the effects of simulated rotator cuff tears on glenohumeral joint motion. For example, Yu et al.[70] used cadaveric shoulder specimens to study the effect of preexisting rotator cuff tears, simulated complete tears, and simulated surgical repair on humeral translations. They reported that the humerus translated inferiorly relative to the scapula with a simulated tear when compared with the repaired state at 60° of frontal-plane elevation. In addition, this study reported an inferior shift in humeral head position with the simulated complete tear when compared with the pathologic condition (i.e., an existing small tear) at all joint positions tested.[70] Kedgley et al.[71] performed a similar cadaveric experiment in which glenohumeral joint motion was measured in response to three increasingly larger cuts to the rotator cuff tendons. However, this study failed to detect any differences in superior/inferior humeral translation after any of the rotator cuff tendon cuts. In contrast to these studies by Yu et al. and Kedgley et al., a cadaveric study by Mura et al.[72] reported that simulated rotator cuff tears resulted in superior translation of the humerus. Moreover, the authors reported that not only did superior translation increase with the number of tendons torn but also that superior translation increased significantly and progressively with each incremental cut in the infraspinatus tendon. These contradictory findings—which may be explained due to experimental differences in experimental protocol (e.g., magnitude and direction of applied forces, joint positions/motions tested), sample sizes, or measurement technique accuracy—also highlight challenges associated with performing cadaveric experiments. Specifically, cadaveric studies are unable to accurately replicate *in vivo* conditions because the muscle forces and joint forces that occur *in vivo* are largely unknown.

It has been hypothesized that glenohumeral joint motion is also influenced by the integrity of the transverse force couple formed by the anterior (subscapularis) and posterior

(infraspinatus) rotator cuff muscles. According to this theory, the glenohumeral joint is able to maintain normal joint mechanics when this force couple is intact (Figure 8.5).[73] The specific clinical implication of this theory is that isolated tears of the supraspinatus tendon may not necessarily lead to altered glenohumeral joint mechanics if the remaining rotator cuff muscles are able to adequately stabilize the joint.[74] If the rotator cuff tear involved the infraspinatus or subscapularis tendons in addition to the supraspinatus tendon, then this force couple would be disrupted and abnormal joint mechanics would result. Despite a recent anatomical study indicating that "small" rotator cuff tears that were traditionally believed to involve only the supraspinatus tendon may actually involve both the supraspinatus and infraspinatus tendons,[75] the force couple concept has been supported by several cadaveric experiments.[72,74] For example, Parsons et al.[74] reported that the direction of joint reaction forces was not altered with an incomplete or complete supraspinatus tear compared with the intact condition, but that direction did change with the involvement of the infraspinatus or subscapularis.[74] Other cadaveric experiments have shown that superior humeral translation does not necessarily occur with an isolated supraspinatus tear, but that extending the tear to include the infraspinatus does indeed result in superior humeral translation.[72]

Human *in vivo* studies have demonstrated that rotator cuff tears are often associated with superior translation of the humerus. For example, Keener et al.[76] used radiographic analysis to estimate the static position of the humerus relative to the glenoid and reported that superior migration of the humerus was positively correlated with tear size. Similarly, Ludewig and Cook[44] have reported increased superior translation of the humerus in patients diagnosed with subacromial impingement. These *in vivo* studies, along with cadaveric studies such as the one reported by Mura et al., all tend to suggest that rotator cuff pathology is associated with superior translation of the humerus. More specifically, clinical reports have supported the notion that superior migration of the humerus is an important factor in the development of rotator cuff pathology.[65,77] However, it is important to recognize that it is still unclear if abnormal glenohumeral joint motion contributes to the development of rotator cuff pathology, if rotator cuff pathology leads to abnormal glenohumeral joint motion, or if both scenarios may exist.

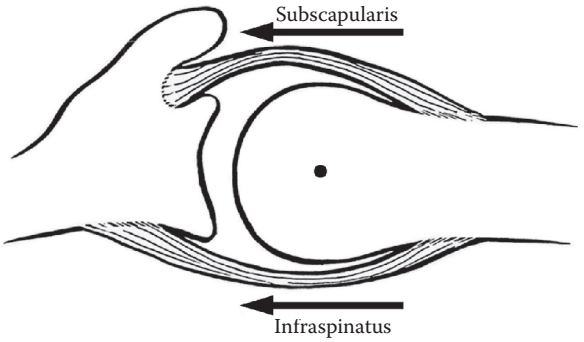

FIGURE 8.5
Transverse force couple is formed by anterior (subscapularis) and posterior (infraspinatus, teres minor) muscle groups. It has been hypothesized that this force couple may be sufficient to maintain normal glenohumeral joint mechanics by overcoming the superiorly directed forces imparted by the deltoid muscle group, even if the supraspinatus muscle–tendon complex has been compromised by a rotator cuff tear. (Adapted from Burkhart, S. S., *Clin. Orthop.*, 267, 45–56, 1991.)

8.5.3 Rotator Cuff Pathology and Scapulothoracic Motion

Abnormal scapulothoracic motion has been shown to exist in patients diagnosed with subacromial impingement. Specifically, human *in vivo* studies have shown that patients diagnosed with subacromial impingement have less posterior tilting, more upward rotation, and greater internal rotation of the scapula relative to the thorax than subjects with normal, healthy shoulder function.[44,78] It has been hypothesized that these alterations in scapulothoracic motion decrease the subacromial space and increase the likelihood of impingement, but this is speculative because studies that rely on skin-mounted markers or sensors are currently unable to accurately measure the distance between the humerus and coracoacromial arch.

Scapulothoracic motion has also been shown to be altered in the presence of rotator cuff tears. For example, a study by Mell et al.[79] measured scapulothoracic motion with electromagnetic sensors during sagittal-plane elevation and scapular-plane elevation in three groups of subjects: (1) patients with a rotator cuff tear, (2) patients with a rotator cuff tendinopathy, and (3) healthy control subjects. That study found that the scapula of patients with a rotator cuff tear was more upwardly rotated in the initial two-thirds of elevation than in patients with tendinopathy and control subjects. McCully et al.[80] measured scapulothoracic motion in subjects after a suprascapular nerve block, used as a model for dysfunction of the supraspinatus and infraspinatus. They found no changes in posterior tilting of the scapula but did report increases in scapular external rotation and upward rotation. Although the supraspinatus and infraspinatus muscles are not believed to be directly involved in controlling scapular motion, the authors suggested that dysfunction of these muscles does seem to result in compensatory changes in scapulothoracic motion.

Pain may also contribute to alterations in scapulothoracic motion. Scibek et al.[81] measured scapulothoracic motion during shoulder elevation in patients with rotator cuff tears before and after injecting the subacromial space with lidocaine to alleviate pain. The study reported changes in SHR, with glenohumeral rotation increasing while upward/downward rotation of the scapula decreased. As a follow-up study, that same research team reported that pain and tear size were associated with increased reliance on scapular motion during shoulder elevation, but that pain was the primary predictor of SHR.[82] Taken together, these studies lend support to the notion that alterations in scapulothoracic motion may be in response to pain associated with rotator cuff tears or impingement.

8.5.4 Rotator Cuff Pathology and Joint Forces

Previous research has demonstrated that the magnitude and direction of glenohumeral joint forces can also be modified in the presence of rotator cuff pathology. For example, Yu et al.[70] demonstrated with a cadaver study that a simulated complete rotator cuff tear was associated with a more inferiorly directed joint reaction force, suggesting that increased inferior force could contribute to joint instability. Parsons et al.[74] performed a similar cadaveric experiment by investigating the effects of five different rotator cuff conditions (from an intact rotator cuff to a three-tendon rotator cuff tear) on glenohumeral joint reaction forces. The study reported that significant changes in glenohumeral joint forces occurred only when the simulated rotator cuff tear extended into the infraspinatus tendon, lending further support to the concept that an intact force couple may be sufficient to maintain glenohumeral joint mechanics.

8.5.5 Nonoperative Treatment of Rotator Cuff Pathology

Nonoperative treatment for rotator cuff pathology focuses primarily on improving flexibility and strengthening the rotator cuff muscles. Flexibility exercises often include anterior shoulder stretching and posterior shoulder stretching through cross-body adduction.[83] Rotator cuff strengthening exercises are frequently performed using an elastic band and include internal and external rotation with the arm at the patient's side and scapular-plane elevation if there is no pain.[83] Other important factors that are often addressed during nonoperative treatment include the function of the scapular-stabilizing muscles,[84,85] tightness of the posterior capsule or posterior rotator cuff, and posture of the spine.[47] Kibler et al.[85] advocate that the muscles responsible for stabilizing the scapula are often weak in patients with rotator cuff pathology, and, therefore, strengthening scapular-stabilizing muscles should be an important component of any physical therapy protocol.

Research aimed at assessing the effectiveness of nonoperative treatments for rotator cuff pathology has largely relied on outcome measures such as pain, range of motion, and subjective patient-based assessments of function. Although it is difficult to make direct comparisons between previously published studies due to significant differences in physical therapy protocols, pain relief is commonly reported in response to physical therapy. However, there are conflicting findings regarding shoulder function after physical therapy. For example, Baydar et al.[86] report that range of motion, pain, and shoulder strength were significantly improved in patients with full-thickness rotator cuff tears after six months of physical therapy. In contrast, it has been reported that even though patients often report less pain and improved shoulder function after physical therapy, deficits in range of motion and strength frequently persist,[83] and most patients do not return to healthy levels of shoulder function.[47]

It is possible that physical therapy relieves pain by restoring normal glenohumeral joint motion and increasing the subacromial space, but accurately measuring the subacromial space under *in vivo* conditions is difficult. The subacromial space is approximately 2 to 7 mm wide, depending on the position of the arm,[87] so a 1-mm superior translation of the humerus (corresponding to a 14%–50% decrease in the subacromial space) may be clinically significant. However, few studies have investigated the effects of physical therapy on 3D joint motion before and after therapy using techniques that are sufficiently accurate to detect these subtle changes in joint motion. Consequently, the effects of physical therapy on both altered glenohumeral joint motion and scapulothoracic motion are not yet fully understood.

8.5.6 Operative Treatment of Rotator Cuff Pathology

The effects of human rotator cuff repair on shoulder function have been investigated extensively through clinical studies. Clinical assessments of shoulder function are typically reported with objective measures of strength and motion (i.e., range of motion and stability) or subjective measures of pain and function (i.e., pain scores and standardized questionnaires). Previous research indicates that rotator cuff repair may provide short-term to medium-term pain relief and patient satisfaction, but that long-term shoulder function may be poor. For example, normal shoulder strength is rarely restored after rotator cuff repair.[88–94] In a study of long-term (16–25 years) outcomes after rotator cuff repair, Borgmastars et al.[95] found that only 37% of patients had relief of persistent pain and 43% had impaired activities of daily living due to shoulder complaints. The authors recommended that patients be warned "to expect less than permanent relief" after surgical

rotator cuff repair.[95] Furthermore, despite improvements in the understanding of rotator cuff pathology, and advances in surgical treatment options, repairs of large, chronic rotator cuff tears have been reported to fail to heal in 20% to 95% of cases.[96–98]

Cadaveric studies have been used extensively to investigate specific aspects of rotator cuff repair. Previous studies have focused on specific surgical techniques—single-row repair versus double-row repair[99] or the extent of subacromial decompression[100,101]—and have quantified outcomes in terms of glenohumeral joint kinematics, glenohumeral joint contact forces and pressures, glenohumeral joint contact area, tendon–bone interface contact pressure, and rotator cuff pressure.[55,70,99–101] The primary benefits of cadaveric experiments are the ability to precisely and systematically evaluate factors that may be difficult to control under *in vivo* conditions (e.g., rotator cuff tear size) and report highly accurate measurements that may be difficult (or currently impossible) to acquire under *in vivo* conditions. Unfortunately, the extent to which cadaveric experiments simulate *in vivo* conditions is not known because the complex forces and motions that occur under *in vivo* conditions are largely unknown. Furthermore, cadaveric studies are unable to model the long-term biological events that are associated with the development or treatment of rotator cuff pathology.

Recently, biplane X-ray and dual-fluoroscopy systems have been developed and used to evaluate *in vivo* shoulder motion.[32,34,87,102–104] For example, Bey et al. used biplane X-ray imaging to study dynamic 3D glenohumeral joint motion after rotator cuff repair. Their study reported that pain decreased significantly after surgery, but that abnormal glenohumeral joint motion and deficits in shoulder strength persisted two years post-surgery.[105] These *in vivo* data suggest that current rotator cuff repair techniques may not adequately restore normal glenohumeral joint biomechanics. However, additional research is needed to fully understand the effects of rotator cuff pathology, nonoperative treatment, and surgical repair on glenohumeral joint mechanics and long-term shoulder function.

8.6 Glenohumeral Joint Instability

8.6.1 Clinical Presentation, Examination and Management

The glenohumeral joint is stabilized by a number of anatomical structures that prevent subluxation or dislocation of the humeral head (i.e., labrum, joint capsule, and ligaments). Injury to any of these structures can lead to an increased risk of dislocation or subluxation; shoulder instability is commonly classified by the direction of subluxation or dislocation. Anterior instability is by far the most common type of instability, and the mechanism of injury typically involves a large force applied to the anterior capsulolabral complex with the shoulder in a vulnerable position (e.g., 90° of frontal-plane elevation and external rotation). This causes the humeral head to translate anteriorly relative to the glenoid. Posterior instability can result from a large posteriorly directed force with the shoulder in various positions such as 90° of sagittal-plane elevation (i.e., as would occur during falling on an outstretched arm) or adduction with internal rotation. Traumatic posterior dislocation can also occur from a violent muscle contracture, electrical shock, or seizure.[106–108] Posterior dislocations are difficult to diagnose and have been reported to be missed in almost 80% of cases.[109] Inferior dislocations are extremely rare and are believed to occur as a result of a hyperabduction force. The humeral head is often locked below the glenoid, a condition termed "luxatio erecta."

Traumatic instability typically presents in one of two ways. First, a patient can sustain an injury in which the humeral head shifts slightly out of the glenoid socket but is relocated to its proper anatomical position with relatively little effort. This is termed a "subluxation event." Second, the patient can present with an injury in which the humeral head is displaced outside of the glenoid socket. This dislocation event requires a formal reduction of the humeral head back to its articulation with the glenoid. Both groups of patients will present with a reduced glenohumeral joint when examined clinically, will complain of pain and looseness, and will report difficulties in reaching. Patients who have had a frank dislocation that has been reduced tend to have a stiffer and more painful shoulder compared with patients who have had a subluxation event. The shoulder position in which the patient reports feelings of giving way can often predict both the type and the severity of instability. The number of reported episodes of dislocation/subluxation can also lend insight into the patient's baseline level of joint laxity.

In contrast to the instability that occurs in response to a traumatic event, multidirectional instability is a condition that is apparent without any obvious trauma. The patient presents with capsular laxity that allows for the humeral head to subluxate or dislocate with relatively little effort. The traditional approach to managing multidirectional instability involves exercises designed to strengthen the secondary stabilizers (i.e., rotator cuff and other surrounding muscles). If episodes of dislocation/subluxation persist after nonoperative therapies, then surgical repair is indicated. However, surgical solutions are difficult because there is typically no single lesion in patients diagnosed with multidirectional instability.

Physical examination of the patient with complaints of instability should begin with inspection and palpation of the shoulder. Next, active range of motion is measured and, if possible, compared with the uninvolved shoulder. If limitations in active range of motion are observed, then passive range of motion should be gently evaluated in sagittal-plane elevation, frontal-plane elevation, external rotation, and internal rotation. Provocative testing for instability begins with the apprehension test, with the patient lying supine and his or her shoulder elevated to 90° in the frontal plane. The clinician progressively externally rotates the patient's shoulder, and a positive exam is indicated if the patient feels anxiety with this maneuver.[110] The Jobe relocation test can also be performed in conjunction with the apprehension test. The examiner places his or her hand on the anterior shoulder and manually applies a posteriorly directed force while externally rotating the shoulder. Patients with anterior instability report that their anxiety level is relieved with the placement of this posteriorly directed force.[111] Translational tests can also be performed to assess for anterior, posterior, or multidirectional instability. Anterior and posterior drawer tests allow the examiner to subjectively assess the amount of humeral translation that results from anteriorly directed or posteriorly directed forces.[112] Load-shift testing can be performed with the patient in the seated position, with the scapula stabilized by one hand and the opposite hand used to translate the humeral head.[113] For example, applying an inferiorly directed force to the patient's adducted arm can cause the humerus to translate inferiorly and produce a sulcus sign, that is, subacromial dimpling indicating inferior or multidirectional instability.[114]

Imaging for glenohumeral joint instability primarily involves radiographs, with scapular "Y" and axillary views being particularly important (Figure 8.6). The axillary view can clearly show the direction of instability if the shoulder is dislocated, as well as any bony deformity to the glenoid or humeral head when the joint is reduced. If further imaging is needed to assess for soft tissue injuries (e.g., labral tear), a computed tomography arthrogram, MRI, or MRI arthrogram can all be helpful in identifying soft tissue injuries.

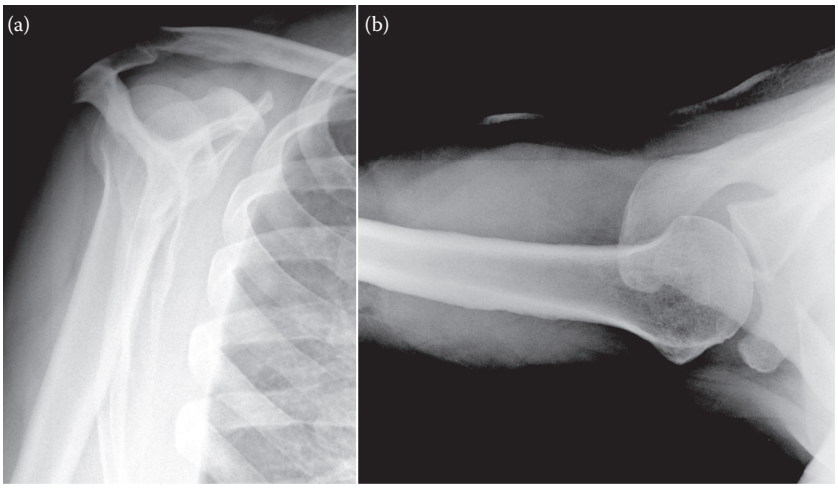

FIGURE 8.6
Radiographic imaging is often used for diagnosing glenohumeral joint instability. Scapular "Y" views (a) and axillary views (b) of the humerus and scapula are particularly important.

8.6.2 Joint Instability and Glenohumeral Joint Motion

Previous research has reported glenohumeral joint translations in patients diagnosed with joint instability using a variety of measurement techniques. For example, Hawkins et al.[115] used conventional radiography to measure 2D glenohumeral joint translations in subjects under anesthesia. The study demonstrated that patients with instability had greater glenohumeral joint translations than control subjects, with anterior translations reported to be 17%, 29%, and 28% of glenoid width in healthy control subjects, patients with anterior instability, and patients with multidirectional instability, respectively. Glenoid width has previously been reported to be approximately 29 mm,[116] so these reported translations are estimated to range from approximately 5 to 8 mm. More recently, Graichen et al.[29,37,38,117] quantified 3D glenohumeral joint motion using advanced MRI-based techniques, with von Eisenhart-Rothe et al.[39] reporting glenohumeral translations of the involved shoulder in patients with traumatic instability to be 1 to 2 mm greater than those of the contralateral shoulder.

Although imaging-based techniques (like those mentioned previously) are perhaps the most common approaches to quantify glenohumeral joint translations under *in vivo* conditions, other measurement techniques have been used. For example, Jorgensen and Bak[118] used a knee laxity testing device to measure anterior/posterior translations in response to an applied load. The data were reported in terms of side-to-side differences, and patients with unilateral shoulder instability were found to have significantly greater translations in the affected shoulder. Ogston and Ludewig[46] used an electromagnetic tracking system to assess glenohumeral and scapulothoracic motion during frontal-plane and scapular-plane elevation in control subjects with normal shoulder function and patients diagnosed with multidirectional instability. No significant differences in glenohumeral joint translations were reported. However, those results may have been influenced by the testing of activities that did not directly load the glenohumeral joint in a manner similar to a clinical examination of shoulder instability. Magit et al.[119] also used an electromagnetic tracking system to measure the total anterior/posterior translation while manually applying anterior and

posterior forces to the shoulder of patients diagnosed with anterior instability. In contrast to the relatively small translations in the aforementioned studies,[39,46,115] that study reported that the total anterior/posterior translation averaged 30 mm across all patients and ranged from 22 to 52 mm.[119] The wide discrepancy in glenohumeral translations that is reported in patients diagnosed with shoulder instability likely reflects differences in measurement technique, experimental protocol (i.e., shoulder positions tested, magnitude and direction of applied forces), and subject populations. Consequently, there remains considerable uncertainty regarding the magnitude and direction of *in vivo* glenohumeral translations in patients diagnosed with joint instability.

8.6.3 Joint Instability and Scapulothoracic Motion

Although the clinical examination of patients with shoulder instability focuses primarily on the glenohumeral joint, previous research has provided some evidence that scapulothoracic motion may also be altered in patients with instability. Paletta et al.[120] used radiographic imaging to assess SHR in patients diagnosed with anterior instability prior to surgery and two years after anterior stabilization surgery. This study reported that SHR in patients with instability was significantly different than in control subjects with normal shoulder function, and that these differences in SHR persisted after surgery. More recently, Ogston and Ludewig[46] have measured scapular motion in patients diagnosed with multidirectional instability and reported that these patients had less upward rotation and more internal rotation of the scapula than asymptomatic control subjects. Matias and Pascoal[121] performed a similar study and found that patients with glenohumeral instability had greater protraction and anterior tilting of the scapula. Given the limited number of studies focusing on this topic, there is still little consensus regarding the clinical implications of altered scapulothoracic motion in patients diagnosed with glenohumeral instability. Specifically, it is unknown if altered scapulothoracic motion represents a compensatory mechanism in response to glenohumeral pathology or if it contributes in some way to the underlying pathology in patients with atraumatic instability. However, the findings from these studies suggest that abnormal scapulothoracic motion may indeed be associated with glenohumeral instability and that additional research in this area is warranted.

8.6.4 Nonoperative Treatment of Joint Instability

Physical therapy exercises are often prescribed as the initial treatment course for patients diagnosed with shoulder instability. Physical therapy protocols implicitly seek to restore normal glenohumeral joint mechanics and focus specifically on restoring the shoulders' range of motion while protecting the static stabilizers and strengthening the dynamic glenohumeral joint stabilizers. Finnoff et al.[122] emphasize the importance of strengthening the rotator cuff muscles, and computational models of the shoulder have suggested that rotator cuff strengthening may reduce the risk of recurrent anterior instability.[26] Exercises that strengthen scapular stabilizing muscles (e.g., serratus anterior, upper and lower trapezius) are also recommended, based on the hypothesis that patients with shoulder instability may also have abnormal scapulothoracic motion.[46,122,123]

Nonoperative treatment for glenohumeral instability is not always successful, with previous research suggesting that nonoperative treatments fail to result in a satisfactory clinical outcome in 44% to 94% of patients.[26,124] Patients who have a single traumatic episode that results in glenohumeral joint dislocation are particularly at risk for recurrent joint instability. For example, Burkhead and Rockwood[125] assessed the effects of nonoperative

therapy on shoulder instability, reporting that 80% of patients with atraumatic instability reported "good" or "excellent" results. In contrast, only 12% of patients whose instability results from a traumatic event reported good or excellent results.[125] Robinson et al.[126] documented the effects of physical therapy on shoulder function after anterior dislocation and reported that recurrent instability occurred in 56% of the patients within two years of the primary dislocation. Furthermore, persistent functional deficits (e.g., limited range of motion) were also reported in patients who did not report any episodes of recurrent instability and whose clinical outcome was considered "satisfactory."[126] Hovelius and Saeboe[124] reported on the long-term (25 years) outcomes of 223 shoulders that had sustained a first-time anterior dislocation. The study found that 57% had recurrent instability after the primary dislocation and that 28% of the shoulders eventually required a surgical stabilization procedure. In contrast to the majority of studies that used conventional clinical outcomes to assess the effects of physical therapy on patients with instability, Nyiri et al.[127] measured glenohumeral and scapulothoracic motions in healthy control subjects and in patients diagnosed with multidirectional instability who were treated nonoperatively. Physical therapy was reported to be successful for increasing shoulder strength, but abnormal joint mechanics persisted after conservative treatment. Taken together, previous research indicates that many patients diagnosed with instability may benefit from nonoperative treatment, but that a significant percentage of those patients—particularly those whose instabilities are due to traumatic joint dislocation—may eventually require surgical repair.

8.6.5 Operative Treatment of Joint Instability

The operative treatment of joint instability has been studied extensively through cadaveric experiments.[128–136] In very general terms, the typical experimental approach for these studies involves testing the specimen in its native condition, creating a simulated injury, testing the specimen in its injured condition, repairing the injury, and then testing the specimen in its repaired condition. Variables that are commonly manipulated include arm position, applied loads (e.g., muscle forces or joint forces), injury severity, and surgical repair technique. Outcomes are typically quantified in terms of joint motion (i.e., translations, rotations, range of motion), forces, joint contact pressures, or joint contact area. The findings from these cadaveric studies will often demonstrate that the injured condition is significantly different than the native condition, thus supporting the claim of a valid injury model. Furthermore, the surgical repair condition is often shown to closely approximate the native condition, which supports claims regarding the efficacy of a particular surgical repair technique.

Cadaveric studies have contributed significantly to the body of knowledge regarding shoulder function, but interpreting the clinical significance of findings from cadaveric experiments can be problematic for several reasons. First, the findings represent only the immediate postoperative (e.g., "time zero") condition, and the relationship between "time zero" outcomes and the long-term outcomes is not particularly well understood. Factors affecting long-term outcomes (e.g., postoperative activity levels and biological processes associated with healing) cannot be studied in cadaveric experiments. Second, clinical interpretation of cadaver studies can be difficult because the biomechanical outcome measures that are most commonly reported (e.g., measures of forces or motions) are rarely used in *in vivo* patient-based studies. Instead, patient-based studies typically evaluate subjective assessments of pain and function, physical measurements (e.g., strength, active range of motion), and the presence or absence of recurrent instability. Consequently, with little overlap in these outcome measures, it is difficult to make direct comparisons between

cadaver studies and *in vivo* patient-based studies. For example, osteoarthritis and range of motion deficits after surgical treatment for instability have been previously reported in clinical studies,[137–143] but the factors that lead to this condition have not been adequately explained by cadaveric experiments. It is plausible that altered joint mechanics after surgery could lead to abnormal cartilage contact patterns and the development of arthritis over time, but this mechanism cannot be adequately tested in cadaveric studies. Recent technological advancements that now provide the ability to make accurate measures of *in vivo* joint motion[102,105] and *in vivo* joint forces[61,62] may provide a means for reconciling the findings from cadaveric experiments with the long-term clinical outcomes. Additional research on the long-term *in vivo* sequelae after surgical treatment of joint instability is clearly needed.

8.7 Summary

This chapter has provided an overview of shoulder biomechanics under normal and pathologic conditions. This review has attempted to highlight some of the research efforts that have contributed to our understanding of shoulder mechanics. In addition, this chapter has discussed two of the most common pathologic conditions that affect the shoulder: rotator cuff tears and glenohumeral joint instability. Clearly, there are many opportunities for additional research. For example, the mechanical role of individual muscles, tendons, and ligaments and their complex interaction under *in vivo* conditions are still not particularly well understood. Research efforts aimed at predicting and objectively validating *in vivo* muscle forces, tendon/ligament forces, and joint forces through a combination of *in vivo*, *in vitro*, and computational approaches are of great need and are highly encouraged. Similarly, the interaction between glenohumeral joint motion and scapulothoracic motion under *in vivo* conditions is also not fully understood. In particular, the effects of pathologic conditions and approaches to their treatment (both operative and nonoperative) on glenohumeral joint motion, scapulothoracic motion, and their interaction, as well as the relationship between measures of joint motion and conventional clinical outcomes (e.g., subjective assessments of pain and function), are certainly areas in which additional research is warranted. Given the rapid advancements in imaging, computational modeling, and *in vivo* sensing, we anticipate that future research efforts will continue to reveal the complexities of *in vivo* shoulder function. Future efforts aimed at understanding the etiology, diagnosis, and treatment of shoulder injuries will be critical to allow individuals with shoulder injuries the opportunity to remain active and maintain a high quality of life.

References

1. Veeger, H. E., and F. C. van der Helm. 2007. Shoulder function: The perfect compromise between mobility and stability. *Journal of Biomechanics* 40(10):2119–2129.
2. Wu, G., F. C. van der Helm, H. E. Veeger, M. Makhsous, P. Van Roy, C. Anglin, J. Nagels, A. R. Karduna, K. McQuade, X. Wang, F. W. Werner, and B. Buchholz. 2005. ISB recommendation on definitions of joint coordinate systems of various joints for the reporting of human joint motion—Part II: Shoulder, elbow, wrist and hand. *Journal of Biomechanics* 38(5):981–992.

3. Howell, S. M., and B. J. Galinat. 1989. The glenoid-labral socket. A constrained articular surface. *Clinical Orthopaedics* (243):122–125.
4. Lugo, R., P. Kung, and C. B. Ma. 2008. Shoulder biomechanics. *European Journal of Radiology* 68(1):16–24.
5. Poppen, N. K., and P. S. Walker. 1976. Normal and abnormal motion of the shoulder. *Journal of Bone and Joint Surgery American Volume* 58(2):195–201.
6. McPherson, E. J., R. J. Friedman, Y. H. An, R. Chokesi, and R. L. Dooley. 1997. Anthropometric study of normal glenohumeral relationships. *Journal of Shoulder and Elbow Surgery* 6(2): 105–112.
7. Soslowsky, L. J., E. L. Flatow, L. U. Bigliani, and V. C. Mow. 1992. Articular geometry of the glenohumeral joint. *Clinical Orthopaedics* (285):181–190.
8. Warner, J. J., M. K. Bowen, X. H. Deng, J. A. Hannafin, S. P. Arnoczky, and R. F. Warren. 1998. Articular contact patterns of the normal glenohumeral joint. *Journal of Shoulder and Elbow Surgery* 7(4):381–388.
9. Hurov, J. 2009. Anatomy and mechanics of the shoulder: Review of current concepts. *Journal of Hand Therapy* 22(4):328–342; quiz 343.
10. Snyder, S. J., R. P. Karzel, W. Del Pizzo, R. D. Ferkel, and M. J. Friedman. 1990. SLAP lesions of the shoulder. *Arthroscopy* 6(4):274–279.
11. Lippitt, S., and F. Matsen. 1993. Mechanisms of glenohumeral joint stability. *Clinical Orthopaedics* (291):20–28.
12. Burkart, A. C., and R. E. Debski. 2002. Anatomy and function of the glenohumeral ligaments in anterior shoulder instability. *Clinical Orthopaedics and Related Research* (400):32–39.
13. Malicky, D. M., L. J. Soslowsky, J. E. Kuhn, M. J. Bey, C. M. Mouro, J. A. Raz, and C. A. Liu. 2001. Total strain fields of the antero-inferior shoulder capsule under subluxation: A stereoradiogrammetric study. *Journal of Biomechanical Engineering* 123(5):425–431.
14. Moore, S. M., B. Ellis, J. A. Weiss, P. J. McMahon, and R. E. Debski. 2010. The glenohumeral capsule should be evaluated as a sheet of fibrous tissue: A validated finite element model. *Annals of Biomedical Engineering* 38(1):66–76.
15. DePalma, A. F., A. J. Cooke, and M. Prabhakar. 1967. The role of the subscapularis in recurrent anterior dislocations of the shoulder. *Clinical Orthopaedics and Related Research* 54:35–49.
16. Ovesen, J., and S. Nielsen. 1986. Anterior and posterior shoulder instability. A cadaver study. *Acta Orthopaedica Scandinavica* 57(4):324–327.
17. Itoi, E., H. C. Hsu, and K. N. An. 1996. Biomechanical investigation of the glenohumeral joint. *Journal of Shoulder and Elbow Surgery* 5(5):407–424.
18. Blasier, R. B., L. J. Soslowsky, D. M. Malicky, and M. L. Palmer. 1997. Posterior glenohumeral subluxation: Active and passive stabilization in a biomechanical model. *Journal of Bone and Joint Surgery American Volume* 79(3):433–440.
19. Malicky, D. M., L. J. Soslowsky, R. B. Blasier, and Y. Shyr. 1996. Anterior glenohumeral stabilization factors: Progressive effects in a biomechanical model. *Journal of Orthopaedic Research* 14(2):282–288.
20. Howell, S. M., and T. A. Kraft. 1991. The role of the supraspinatus and infraspinatus muscles in glenohumeral kinematics of anterior shoulder instability. *Clinical Orthopaedics* 263:128–134.
21. Werner, C. M., D. Weishaupt, S. Blumenthal, A. Curt, P. Favre, and C. Gerber. 2006. Effect of experimental suprascapular nerve block on active glenohumeral translations in vivo. *Journal of Orthopaedic Research* 24(3):491–500.
22. Itoi, E., S. R. Newman, D. K. Kuechle, B. F. Morrey, and K. N. An. 1994. Dynamic anterior stabilisers of the shoulder with the arm in abduction. *The Journal of Bone and Joint Surgery British Volume* 76(5):834–836.
23. Pagnani, M. J., X. H. Deng, R. F. Warren, P. A. Torzilli, and D. W. Altchek. 1995. Effect of lesions of the superior portion of the glenoid labrum on glenohumeral translation. *Journal of Bone and Joint Surgery American Volume* 77(7):1003–1010.

24. Itoi, E., D. K. Kuechle, S. R. Newman, B. F. Morrey, and K. N. An. 1993. Stabilising function of the biceps in stable and unstable shoulders. *The Journal of Bone and Joint Surgery British Volume* 75(4):546–550.
25. Abboud, J. A., and L. J. Soslowsky. 2002. Interplay of the static and dynamic restraints in glenohumeral instability. *Clinical Orthopaedics* (400):48–57.
26. Labriola, J. E., T. Q. Lee, R. E. Debski, and P. J. McMahon. 2005. Stability and instability of the glenohumeral joint: The role of shoulder muscles. *Journal of Shoulder and Elbow Surgery* 14 (1 Suppl S):32S–38S.
27. Turkel, S. J., M. W. Panio, J. L. Marshall, and F. G. Girgis. 1981. Stabilizing mechanisms preventing anterior dislocation of the glenohumeral joint. *Journal of Bone and Joint Surgery American Volume* 63(8):1208–1217.
28. Debski, R. E., P. J. McMahon, W. O. Thompson, S. L. Woo, J. J. Warner, and F. H. Fu. 1995. A new dynamic testing apparatus to study glenohumeral joint motion. *Journal of Biomechanics* 28(7):869–874.
29. Graichen, H., H. Bonel, T. Stammberger, A. Heuck, K. H. Englmeier, M. Reiser, and F. Eckstein. 1998. A technique for determining the spatial relationship between the rotator cuff and the subacromial space in arm abduction using MRI and 3D image processing. *Magnetic Resonance in Medicine* 40(4):640–643.
30. Fleisig, G. S., J. R. Andrews, C. J. Dillman, and R. F. Escamilla. 1995. Kinetics of baseball pitching with implications about injury mechanisms. *The American Journal of Sports Medicine* 23(2):233–239.
31. Yanagawa, T., C. J. Goodwin, K. B. Shelburne, J. E. Giphart, M. R. Torry, and M. G. Pandy. 2008. Contributions of the individual muscles of the shoulder to glenohumeral joint stability during abduction. *Journal of Biomechanical Engineering* 130(2):021024.
32. Boyer, P. J., D. F. Massimini, T. J. Gill, R. Papannagari, S. L. Stewart, J. P. Warner, and G. Li. 2008. In vivo articular cartilage contact at the glenohumeral joint: Preliminary report. *Journal of Orthopaedic Science* 13(4):359–365.
33. Nishinaka, N., H. Tsutsui, K. Mihara, K. Suzuki, D. Makiuchi, Y. Kon, T. W. Wright, M. W. Moser, K. Gamada, H. Sugimoto, and S. A. Banks. 2008. Determination of in vivo glenohumeral translation using fluoroscopy and shape-matching techniques. *Journal of Shoulder and Elbow Surgery* 17(2):319–322.
34. Bey, M. J., S. K. Kline, R. Zauel, T. R. Lock, and P. A. Kolowich. 2008. Measuring dynamic in-vivo glenohumeral joint kinematics: Technique and preliminary results. *Journal of Biomechanics* 41(3):711–714.
35. Flatow, E. L., L. J. Soslowsky, J. B. Ticker, R. J. Pawluk, M. Hepler, J. Ark, V. C. Mow, and L. U. Bigliani. 1994. Excursion of the rotator cuff under the acromion. Patterns of subacromial contact. *The American Journal of Sports Medicine* 22(6):779–788.
36. Howell, S. M., B. J. Galinat, A. J. Renzi, and P. J. Marone. 1988. Normal and abnormal mechanics of the glenohumeral joint in the horizontal plane. *Journal of Bone and Joint Surgery American Volume* 70(2):227–232.
37. Graichen, H., S. Hinterwimmer, R. von Eisenhart-Rothe, T. Vogl, K. H. Englmeier, and F. Eckstein. 2005. Effect of abducting and adducting muscle activity on glenohumeral translation, scapular kinematics and subacromial space width in vivo. *Journal of Biomechanics* 38(4):755–760.
38. Graichen, H., T. Stammberger, H. Bonel, M. Haubner, K. H. Englmeier, M. Reiser, and F. Eckstein. 2000. Magnetic resonance-based motion analysis of the shoulder during elevation. *Clinical Orthopaedics* (370):154–163.
39. von Eisenhart-Rothe, R. M., A. Jager, K. H. Englmeier, T. J. Vogl, and H. Graichen. 2002. Relevance of arm position and muscle activity on three-dimensional glenohumeral translation in patients with traumatic and atraumatic shoulder instability. *The American Journal of Sports Medicine* 30(4):514–522.
40. Amasay, T., and A. R. Karduna. 2009. Scapular kinematics in constrained and functional upper extremity movements. *The Journal of Orthopaedic and Sports Physical Therapy* 39(8):618–627.

41. Braman, J. P., S. C. Engel, R. F. Laprade, and P. M. Ludewig. 2009. In vivo assessment of scapulohumeral rhythm during unconstrained overhead reaching in asymptomatic subjects. *Journal of Shoulder and Elbow Surgery* 18(6):960–967.
42. McClure, P. W., L. A. Michener, B. J. Sennett, and A. R. Karduna. 2001. Direct 3-dimensional measurement of scapular kinematics during dynamic movements in vivo. *Journal of Shoulder and Elbow Surgery* 10(3):269–277.
43. Ebaugh, D. D., P. W. McClure, and A. R. Karduna. 2006. Scapulothoracic and glenohumeral kinematics following an external rotation fatigue protocol. *The Journal of Orthopaedic and Sports Physical Therapy* 36(8):557–571.
44. Ludewig, P. M., and T. M. Cook. 2000. Alterations in shoulder kinematics and associated muscle activity in people with symptoms of shoulder impingement. *Physical Therapy* 80(3):276–291.
45. McClure, P. W., L. A. Michener, and A. R. Karduna. 2006. Shoulder function and 3-dimensional scapular kinematics in people with and without shoulder impingement syndrome. *Physical Therapy* 86(8):1075–1090.
46. Ogston, J. B., and P. M. Ludewig. 2007. Differences in 3-dimensional shoulder kinematics between persons with multidirectional instability and asymptomatic controls. *The American Journal of Sports Medicine* 35(8):1361–1370.
47. Ludewig, P. M., and J. P. Braman. 2011. Shoulder impingement: Biomechanical considerations in rehabilitation. *Manual Therapy* 16(1):33–39.
48. Inman, V. T., J. B. Saunders, and L. C. Abbott. 1996. Observations of the function of the shoulder joint. 1944. *Clinical Orthopaedics* (330):3–12.
49. Ludewig, P. M., T. M. Cook, and D. A. Nawoczenski. 1996. Three-dimensional scapular orientation and muscle activity at selected positions of humeral elevation. *The Journal of Orthopaedic and Sports Physical Therapy* 24(2):57–65.
50. Bassett, R. W., A. O. Browne, B. F. Morrey, and K. N. An. 1990. Glenohumeral muscle force and moment mechanics in a position of shoulder instability. *Journal of Biomechanics* 23(5):405–415.
51. Kronberg, M., G. Nemeth, and L. A. Brostrom. 1990. Muscle activity and coordination in the normal shoulder. An electromyographic study. *Clinical Orthopaedics* (257):76–85.
52. Gerber, C., S. Blumenthal, A. Curt, and C. M. Werner. 2007. Effect of selective experimental suprascapular nerve block on abduction and external rotation strength of the shoulder. *Journal of Shoulder and Elbow Surgery* 16(6):815–820.
53. Basmajian, J. V., and A. Latif. 1957. Integrated actions and functions of the chief flexors of the elbow: A detailed electromyographic analysis. *Journal of Bone and Joint Surgery American Volume* 39-A(5):1106–1118.
54. Furlani, J. 1976. Electromyographic study of the m. biceps brachii in movements at the glenohumeral joint. *Acta Anatomica* 96(2):270–284.
55. Su, W. R., J. E. Budoff, and Z. P. Luo. 2010. The effect of posterosuperior rotator cuff tears and biceps loading on glenohumeral translation. *Arthroscopy* 26(5):578–586.
56. Youm, T., N. S. ElAttrache, J. E. Tibone, M. H. McGarry, and T. Q. Lee. 2009. The effect of the long head of the biceps on glenohumeral kinematics. *Journal of Shoulder and Elbow Surgery* 18(1):122–129.
57. Phadke, V., P. Camargo, and P. Ludewig. 2009. Scapular and rotator cuff muscle activity during arm elevation: A review of normal function and alterations with shoulder impingement. *Revista Brasileira de Fisioterapia* 13(1):1–9.
58. Ludewig, P. M., and J. F. Reynolds. 2009. The association of scapular kinematics and glenohumeral joint pathologies. *The Journal of Orthopaedic and Sports Physical Therapy* 39(2):90–104.
59. Johnson, G. R., D. Spalding, A. Nowitzke, and N. Bogduk. 1996. Modelling the muscles of the scapula morphometric and coordinate data and functional implications. *Journal of Biomechanics* 29(8):1039–1051.
60. Anglin, C., U. P. Wyss, and D. R. Pichora. 2000. Glenohumeral contact forces. *Proceedings of the Institution of Mechanical Engineers. Part H* 214(6):637–644.
61. Bergmann, G., F. Graichen, A. Bender, M. Kaab, A. Rohlmann, and P. Westerhoff. 2007. In vivo glenohumeral contact forces—measurements in the first patient 7 months postoperatively. *Journal of Biomechanics* 40(10):2139–2149.

62. Bergmann, G., F. Graichen, A. Bender, A. Rohlmann, A. Halder, A. Beier, and P. Westerhoff. 2011. In vivo gleno-humeral joint loads during forward flexion and abduction. *Journal of Biomechanics* 44(8):1543–1552.
63. Westerhoff, P., F. Graichen, A. Bender, A. Halder, A. Beier, A. Rohlmann, and G. Bergmann. 2009. In vivo measurement of shoulder joint loads during activities of daily living. *Journal of Biomechanics* 42(12):1840–1849.
64. Sher, J. S., J. W. Uribe, A. Posada, B. J. Murphy, and M. B. Zlatkin. 1995. Abnormal findings on magnetic resonance images of asymptomatic shoulders. *Journal of Bone and Joint Surgery American Volume* 77(1):10–15.
65. Neer, C. S., 2nd. 1972. Anterior acromioplasty for the chronic impingement syndrome in the shoulder: A preliminary report. *Journal of Bone and Joint Surgery American Volume* 54(1):41–50.
66. Hawkins, R. J., and J. C. Kennedy. 1980. Impingement syndrome in athletes. *The American Journal of Sports Medicine* 8(3):151–158.
67. Valadie, A. L., 3rd, C. M. Jobe, M. M. Pink, E. F. Ekman, and F. W. Jobe. 2000. Anatomy of provocative tests for impingement syndrome of the shoulder. *Journal of Shoulder and Elbow Surgery* 9(1):36–46.
68. Jobe, F. W., and D. R. Moynes. 1982. Delineation of diagnostic criteria and a rehabilitation program for rotator cuff injuries. *The American Journal of Sports Medicine* 10(6):336–339.
69. Nicholson, G. P., D. A. Goodman, E. L. Flatow, and L. U. Bigliani. 1996. The acromion: Morphologic condition and age-related changes. A study of 420 scapulas. *Journal of Shoulder and Elbow Surgery* 5(1):1–11.
70. Yu, J., M. H. McGarry, Y. S. Lee, L. V. Duong, and T. Q. Lee. 2005. Biomechanical effects of supraspinatus repair on the glenohumeral joint. *Journal of Shoulder and Elbow Surgery* 14(1 Suppl S):65S–71S.
71. Kedgley, A. E., G. A. Mackenzie, L. M. Ferreira, J. A. Johnson, and K. J. Faber. 2007. In vitro kinematics of the shoulder following rotator cuff injury. *Clinical Biomechanics (Bristol, Avon)* 22(10):1068–1073.
72. Mura, N., S. W. O'Driscoll, M. E. Zobitz, G. Heers, T. R. Jenkyn, S. M. Chou, A. M. Halder, and K. N. An. 2003. The effect of infraspinatus disruption on glenohumeral torque and superior migration of the humeral head: A biomechanical study. *Journal of Shoulder and Elbow Surgery* 12(2):179–184.
73. Payne, L. Z., X. H. Deng, E. V. Craig, P. A. Torzilli, and R. F. Warren. 1997. The combined dynamic and static contributions to subacromial impingement. A biomechanical analysis. *The American Journal of Sports Medicine* 25(6):801–808.
74. Parsons, I. M., M. Apreleva, F. H. Fu, and S. L. Woo. 2002. The effect of rotator cuff tears on reaction forces at the glenohumeral joint. *Journal of Orthopaedic Research* 20(3):439–446.
75. Mochizuki, T., H. Sugaya, M. Uomizu, K. Maeda, K. Matsuki, I. Sekiya, T. Muneta, and K. Akita. 2008. Humeral insertion of the supraspinatus and infraspinatus. New anatomical findings regarding the footprint of the rotator cuff. *Journal of Bone and Joint Surgery. American Volume* 90(5):962–969.
76. Keener, J. D., A. S. Wei, H. M. Kim, K. Steger-May, and K. Yamaguchi. 2009. Proximal humeral migration in shoulders with symptomatic and asymptomatic rotator cuff tears. *Journal of Bone and Joint Surgery American Volume* 91(6):1405–1413.
77. Neer, C. S., 2nd. 1983. Impingement lesions. *Clinical Orthopaedics* (173):70–77.
78. Lukasiewicz, A. C., P. McClure, L. Michener, N. Pratt, and B. Sennett. 1999. Comparison of 3-dimensional scapular position and orientation between subjects with and without shoulder impingement. *The Journal of Orthopaedic and Sports Physical Therapy* 29(10):574–583; discussion 584–586.
79. Mell, A. G., S. LaScalza, P. Guffey, J. Ray, M. Maciejewski, J. E. Carpenter, and R. E. Hughes. 2005. Effect of rotator cuff pathology on shoulder rhythm. *Journal of Shoulder and Elbow Surgery* 14(1 Suppl S):58S–64S.
80. McCully, S. P., D. N. Suprak, P. Kosek, and A. R. Karduna. 2006. Suprascapular nerve block disrupts the normal pattern of scapular kinematics. *Clinical Biomechanics (Bristol, Avon)* 21(6): 545–553.

81. Scibek, J. S., A. G. Mell, B. K. Downie, J. E. Carpenter, and R. E. Hughes. 2008. Shoulder kinematics in patients with full-thickness rotator cuff tears after a subacromial injection. *Journal of Shoulder and Elbow Surgery* 17(1):172–181.
82. Scibek, J. S., J. E. Carpenter, and R. E. Hughes. 2009. Rotator cuff tear pain and tear size and scapulohumeral rhythm. *Journal of Athletic Training* 44(2):148–159.
83. Kuhn, J. E. 2009. Exercise in the treatment of rotator cuff impingement: A systematic review and a synthesized evidence-based rehabilitation protocol. *Journal of Shoulder and Elbow Surgery* 18(1):138–160.
84. Kibler, W. B. 2006. Scapular involvement in impingement: Signs and symptoms. *Instructional Course Lectures* 55:35–43.
85. Kibler, W. B., J. McMullen, and T. Uhl. 2001. Shoulder rehabilitation strategies, guidelines, and practice. *Orthopedic Clinics of North America* 32(3):527–538.
86. Baydar, M., E. Akalin, O. El, S. Gulbahar, C. Bircan, O. Akgul, M. Manisali, B. Torun Orhan, and R. Kizil. 2009. The efficacy of conservative treatment in patients with full-thickness rotator cuff tears. *Rheumatology International* 29(6):623–628.
87. Bey, M. J., S. K. Brock, W. N. Beierwaltes, R. Zauel, P. A. Kolowich, and T. R. Lock. 2007. In vivo measurement of subacromial space width during shoulder elevation: Technique and preliminary results in patients following unilateral rotator cuff repair. *Clinical Biomechanics (Bristol, Avon)* 22(7):767–773.
88. Bigoni, M., M. Gorla, S. Guerrasio, A. Brignoli, A. Cossio, P. Grillo, and E. C. Marinoni. 2009. Shoulder evaluation with isokinetic strength testing after arthroscopic rotator cuff repairs. *Journal of Shoulder and Elbow Surgery* 18(2):178–183.
89. Cole, B. J., L. P. McCarty, 3rd, R. W. Kang, W. Alford, P. B. Lewis, and J. K. Hayden. 2007. Arthroscopic rotator cuff repair: Prospective functional outcome and repair integrity at minimum 2-year follow-up. *Journal of Shoulder and Elbow Surgery* 16(5):579–585.
90. Kirschenbaum, D., M. P. Coyle, Jr., J. P. Leddy, P. Katsaros, F. Tan, Jr., and R. P. Cody. 1993. Shoulder strength with rotator cuff tears. Pre- and postoperative analysis. *Clinical Orthopaedics* (288):174–178.
91. Nho, S. J., B. S. Brown, S. Lyman, R. S. Adler, D. W. Altchek, and J. D. MacGillivray. 2009. Prospective analysis of arthroscopic rotator cuff repair: Prognostic factors affecting clinical and ultrasound outcome. *Journal of Shoulder and Elbow Surgery* 18(1):13–20.
92. Park, J. Y., S. H. Lhee, J. H. Choi, H. K. Park, J. W. Yu, and J. B. Seo. 2008. Comparison of the clinical outcomes of single- and double-row repairs in rotator cuff tears. *The American Journal of Sports Medicine* 36(7):1310–1316.
93. Rokito, A. S., J. D. Zuckerman, M. A. Gallagher, and F. Cuomo. 1996. Strength after surgical repair of the rotator cuff. *Journal of Shoulder and Elbow Surgery* 5(1):12–17.
94. Walker, S. W., W. H. Couch, G. A. Boester, and D. W. Sprowl. 1987. Isokinetic strength of the shoulder after repair of a torn rotator cuff. *Journal of Bone and Joint Surgery. American Volume* 69(7):1041–1044.
95. Borgmastars, N., M. Paavola, V. Remes, M. Lohman, and M. Vastamaki. 2010. Pain relief, motion, and function after rotator cuff repair or reconstruction may not persist after 16 years. *Clinical Orthopaedics and Related Research* 468(10):2678–2689.
96. Galatz, L. M., C. M. Ball, S. A. Teefey, W. D. Middleton, and K. Yamaguchi. 2004. The outcome and repair integrity of completely arthroscopically repaired large and massive rotator cuff tears. *Journal of Bone and Joint Surgery. American Volume* 86-A(2):219–224.
97. Gazielly, D. F., P. Gleyze, and C. Montagnon. 1994. Functional and anatomical results after rotator cuff repair. *Clinical Orthopaedics and Related Research* (304):43–53.
98. Harryman, D. T., 2nd, L. A. Mack, K. Y. Wang, S. E. Jackins, M. L. Richardson, and F. A. Matsen, 3rd. 1991. Repairs of the rotator cuff. Correlation of functional results with integrity of the cuff. *Journal of Bone and Joint Surgery. American Volume* 73(7):982–989.
99. Grimberg, J., A. Diop, K. Kalra, C. Charousset, L. D. Duranthon, and N. Maurel. 2010. In vitro biomechanical comparison of three different types of single- and double-row arthroscopic

rotator cuff repairs: Analysis of continuous bone-tendon contact pressure and surface during different simulated joint positions. *Journal of Shoulder and Elbow Surgery* 19(2):236–243.
100. Denard, P. J., T. J. Bahney, S. B. Kirby, and R. M. Orfaly. 2010. Contact pressure and glenohumeral translation following subacromial decompression: How much is enough? *Orthopedics* 33(11):805.
101. Fagelman, M., M. Sartori, K. B. Freedman, A. G. Patwardhan, G. Carandang, and G. Marra. 2007. Biomechanics of coracoacromial arch modification. *Journal of Shoulder and Elbow Surgery* 16(1):101–106.
102. Bey, M. J., R. Zauel, S. K. Brock, and S. Tashman. 2006. Validation of a new model-based tracking technique for measuring three-dimensional, in vivo glenohumeral joint kinematics. *Journal of Biomechanical Engineering* 128(4):604–609.
103. Braun, S., P. J. Millett, C. Yongpravat, J. D. Pault, T. Anstett, M. R. Torry, and J. E. Giphart. 2010. Biomechanical evaluation of shear force vectors leading to injury of the biceps reflection pulley: A biplane fluoroscopy study on cadaveric shoulders. *The American Journal of Sports Medicine* 38(5):1015–1024.
104. Massimini, D. F., G. Li, and J. P. Warner. 2010. Glenohumeral contact kinematics in patients after total shoulder arthroplasty. *Journal of Bone and Joint Surgery. American Volume* 92(4):916–926.
105. Bey, M. J., C. D. Peltz, K. Ciarelli, S. K. Kline, G. Divine, M. van Holsbeeck, S. Muh, P. A. Kolowich, T. R. Lock, and V. Moutzouros. 2012. In vivo shoulder function after surgical repair of a torn rotator cuff: Glenohumeral joint mechanics, shoulder strength, clinical outcomes, and their interaction. *The American Journal of Sports Medicine* 39(10):2117–2129.
106. Carew-McColl, M. 1980. Bilateral shoulder dislocations caused by electric shock. *The British Journal of Clinical Practice* 34(8–9):251–254.
107. Lindholm, T. S., and E. Elmstedt. 1980. Bilateral posterior dislocation of the shoulder combined with fracture of the proximal humerus. A case report. *Acta Orthopaedica Scandinavica* 51(3):485–488.
108. Mills, K. L. 1974. Simultaneous bilateral posterior fracture-dislocation of the shoulder. *Injury* 6(1):39–41.
109. McLaughlin, Hl. 1952. Posterior dislocation of the shoulder. *Journal of Bone and Joint Surgery. American Volume* 24-A-3:584–590.
110. Rowe, C. R., and B. Zarins. 1981. Recurrent transient subluxation of the shoulder. *Journal of Bone and Joint Surgery American Volume* 63(6):863–872.
111. Jobe, F. W., R. S. Kvitne, and C. E. Giangarra. 1989. Shoulder pain in the overhand or throwing athlete. The relationship of anterior instability and rotator cuff impingement. *Orthopedic Reviews* 18(9):963–975.
112. Gerber, C., and R. Ganz. 1984. Clinical assessment of instability of the shoulder. With special reference to anterior and posterior drawer tests. *The Journal of Bone and Joint Surgery. British Volume* 66(4):551–556.
113. Silliman, J. F., and R. J. Hawkins. 1993. Classification and physical diagnosis of instability of the shoulder. *Clinical Orthopaedics and Related Research* (291):7–19.
114. Neer, C. S., 2nd, and C. R. Foster. 1980. Inferior capsular shift for involuntary inferior and multidirectional instability of the shoulder. A preliminary report. *Journal of Bone and Joint Surgery. American Volume* 62(6):897–908.
115. Hawkins, R. J., J. P. Schutte, D. H. Janda, and G. H. Huckell. 1996. Translation of the glenohumeral joint with the patient under anesthesia. *Journal of Shoulder and Elbow Surgery* 5(4): 286–292.
116. Iannotti, J. P., J. P. Gabriel, S. L. Schneck, B. G. Evans, and S. Misra. 1992. The normal glenohumeral relationships. An anatomical study of one hundred and forty shoulders. *Journal of Bone and Joint Surgery. American Volume* 74(4):491–500.
117. Graichen, H., T. Stammberger, H. Bonel, Englmeier Karl-Hans, M. Reiser, and F. Eckstein. 2000. Glenohumeral translation during active and passive elevation of the shoulder—a 3D open-MRI study. *Journal of Biomechanics* 33(5):609–613.

118. Jorgensen, U., and K. Bak. 1995. Shoulder instability. Assessment of anterior-posterior translation with a knee laxity tester. *Acta Orthopaedica Scandinavica* 66(5):398–400.
119. Magit, D. P., J. E. Tibone, and T. Q. Lee. 2008. In vivo comparison of changes in glenohumeral translation after arthroscopic capsulolabral reconstructions. *The American Journal of Sports Medicine* 36(7):1389–1396.
120. Paletta, G. A., Jr., J. J. Warner, R. F. Warren, A. Deutsch, and D. W. Altchek. 1997. Shoulder kinematics with two-plane x-ray evaluation in patients with anterior instability or rotator cuff tearing. *Journal of Shoulder and Elbow Surgery* 6(6):516–527.
121. Matias, R., and A. G. Pascoal. 2006. The unstable shoulder in arm elevation: A three-dimensional and electromyographic study in subjects with glenohumeral instability. *Clinical Biomechanics (Bristol, Avon)* 21 Suppl 1:S52–S58.
122. Finnoff, J. T., S. Doucette, and G. Hicken. 2004. Glenohumeral instability and dislocation. *Physical Medicine and Rehabilitation Clinics of North America* 15(3):v–vi, 575–605.
123. Ludewig, P. M., and J. F. Reynolds. 2009. The association of scapular kinematics and glenohumeral joint pathologies. *The Journal of Orthopaedic and Sports Physical Therapy* 39(2):90–104.
124. Hovelius, L., and M. Saeboe. 2009. Neer Award 2008: Arthropathy after primary anterior shoulder dislocation—223 shoulders prospectively followed up for twenty-five years. *Journal of Shoulder and Elbow Surgery* 18(3):339–347.
125. Burkhead, W. Z., Jr., and C. A. Rockwood, Jr. 1992. Treatment of instability of the shoulder with an exercise program. *Journal of Bone and Joint Surgery. American Volume* 74(6):890–896.
126. Robinson, C. M., J. Howes, H. Murdoch, E. Will, and C. Graham. 2006. Functional outcome and risk of recurrent instability after primary traumatic anterior shoulder dislocation in young patients. *Journal of Bone and Joint Surgery. American Volume* 88(11):2326–2336.
127. Nyiri, P., A. Illyes, R. Kiss, and J. Kiss. 2010. Intermediate biomechanical analysis of the effect of physiotherapy only compared with capsular shift and physiotherapy in multidirectional shoulder instability. *Journal of Shoulder and Elbow Surgery* 19(6):802–813.
128. Alberta, F. G., N. S. Elattrache, T. Mihata, M. H. McGarry, J. E. Tibone, and T. Q. Lee. 2006. Arthroscopic anteroinferior suture application resulting in decreased glenohumeral translation and external rotation. Study of a cadaver model. *Journal of Bone and Joint Surgery American Volume* 88(1):179–187.
129. Wang, V. M., M. T. Sugalski, W. N. Levine, R. J. Pawluk, V. C. Mow, and L. U. Bigliani. 2005. Comparison of glenohumeral mechanics following a capsular shift and anterior tightening. *Journal of Bone and Joint Surgery American Volume* 87(6):1312–1322.
130. Bohnsack, M., B. Bartels, S. Ostermeier, O. Ruhmann, M. Wellmann, F. Mansouri, and C. Hurschler. 2009. Biomechanical stability of an arthroscopic anterior capsular shift and suture anchor repair in anterior shoulder instability: A human cadaveric shoulder model. *Knee Surgery, Sports Traumatology, Arthroscopy* 17(12):1493–1499.
131. Farber, A. J., N. S. ElAttrache, J. E. Tibone, M. H. McGarry, and T. Q. Lee. 2009. Biomechanical analysis comparing a traditional superior-inferior arthroscopic rotator interval closure with a novel medial-lateral technique in a cadaveric multidirectional instability model. *The American Journal of Sports Medicine* 37(6):1178–1185.
132. Ghodadra, N., A. Gupta, A. A. Romeo, B. R. Bach, Jr., N. Verma, E. Shewman, J. Goldstein, and M. T. Provencher. 2010. Normalization of glenohumeral articular contact pressures after Latarjet or iliac crest bone-grafting. *Journal of Bone and Joint Surgery. American Volume* 92(6):1478–1489.
133. Kaar, S. G., S. D. Fening, M. H. Jones, R. W. Colbrunn, and A. Miniaci. 2010. Effect of humeral head defect size on glenohumeral stability: A cadaveric study of simulated Hill–Sachs defects. *The American Journal of Sports Medicine* 38(3):594–599.
134. Marquardt, B., C. Hurschler, J. Schneppendahl, K. A. Witt, W. Potzl, and J. Steinbeck. 2006. Quantitative assessment of glenohumeral translation after anterior shoulder dislocation and subsequent arthroscopic bankart repair. *The American Journal of Sports Medicine* 34(11):1756–1762.
135. Sekiya, J. K., A. C. Wickwire, J. H. Stehle, and R. E. Debski. 2009. Hill–Sachs defects and repair using osteoarticular allograft transplantation: Biomechanical analysis using a joint compression model. *The American Journal of Sports Medicine* 37(12):2459–2466.

136. Wellmann, M., W. Petersen, T. Zantop, M. Herbort, P. Kobbe, M. J. Raschke, and C. Hurschler. 2009. Open shoulder repair of osseous glenoid defects: Biomechanical effectiveness of the Latarjet procedure versus a contoured structural bone graft. *The American Journal of Sports Medicine* 37(1):87–94.
137. Bigliani, L. U., D. M. Weinstein, M. T. Glasgow, R. G. Pollock, and E. L. Flatow. 1995. Glenohumeral arthroplasty for arthritis after instability surgery. *Journal of Shoulder and Elbow Surgery* 4(2):87–94.
138. Fabre, T., M. L. Abi-Chahla, A. Billaud, M. Geneste, and A. Durandeau. 2010. Long-term results with Bankart procedure: A 26-year follow-up study of 50 cases. *Journal of Shoulder and Elbow Surgery* 19(2):318–323.
139. Lusardi, D. A., M. A. Wirth, D. Wurtz, and C. A. Rockwood, Jr. 1993. Loss of external rotation following anterior capsulorrhaphy of the shoulder. *Journal of Bone and Joint Surgery. American Volume* 75(8):1185–1192.
140. Rosenberg, B. N., J. C. Richmond, and W. N. Levine. 1995. Long-term followup of Bankart reconstruction. Incidence of late degenerative glenohumeral arthrosis. *The American Journal of Sports Medicine* 23(5):538–544.
141. Brophy, R. H., and R. G. Marx. 2005. Osteoarthritis following shoulder instability. *Clinics in Sports Medicine* 24(1):47–56.
142. Green, A., and T. R. Norris. 2001. Shoulder arthroplasty for advanced glenohumeral arthritis after anterior instability repair. *Journal of Shoulder and Elbow Surgery* 10(6):539–545.
143. Pelet, S., B. M. Jolles, and A. Farron. 2006. Bankart repair for recurrent anterior glenohumeral instability: Results at twenty-nine years' follow-up. *Journal of Shoulder and Elbow Surgery* 15(2):203–207.
144. Westerhoff, P., F. Graichen, A. Bender, A. Halder, A. Beier, A. Rohlmann, and G. Bergmann. 2011. Measurement of shoulder joint loads during wheelchair propulsion measured in vivo. *Clinical Biomechanics* 26(10):982–989.
145. Copeland, S., L. U. Bigliani, R. J. Emery, and A. A. Amis. 2011. *Interactive Shoulder* [Software] 20072011. Available from www.primalpictures.com. (Access June 2011).
146. Netter, F. H. 1989. *Atlas of Human Anatomy*. East Hanover, NJ: Novartis.
147. Kuhn, J. E. 2006. The scapulothoracic articulation: Anatomy, biomechanics, pathophysiology, and management. In *Disorders of the Shoulder: Diagnosis & Management*, edited by J. P. Iannotti and G. R. Williams, 1057–1086. Philadelphia, PA: Lippincott Williams & Wilkins.
148. Karduna, A. R., P. J. Kerner, and M. D. Lazarus. 2005. Contact forces in the subacromial space: Effects of scapular orientation. *Journal of Shoulder and Elbow Surgery* 14(4):393–399.
149. Burkhart, S. S. 1991. Arthroscopic treatment of massive rotator cuff tears. Clinical results and biomechanical rationale. *Clinical Orthopaedics* (267):45–56.

9

Biomechanics of the Wrist and Hand

Chunfeng Zhao, Kristin D. Zhao, Aaron Babb, and Kai-Nan An

CONTENTS

The hand, including the wrist, is complex in its anatomy, structure, and function. It is an integral part of most daily activities; therefore, it is predisposed to a high incidence of injury as compared with other components of the musculoskeletal system. Wrist and hand injuries are recognized as the most common occupational disorders, including pathologies such as carpal tunnel syndrome (CTS), trigger finger, and tendonitis.[1,2] Furthermore, wrist fractures are the most prevalent fractures occurring in the human body.[3] Due to the complexity of the hand and wrist, as well as its predisposition to injury, the field of hand surgery evolved as the first specialized surgical field.[4,5] Biomechanics encompasses the relationship between the anatomy, structure, and function of the human body and is fundamental to understanding modern hand surgery.

9.1 Anatomy

9.1.1 Bone and Joints in the Hand and Wrist

The human hand is composed of the wrist, palm, and the five digits (Figure 9.1). The wrist is a very complex joint in the hand consisting of eight carpal bones arranged in two rows that are stabilized by a complex ligament system. The proximal row of four bones from lateral to medial are the scaphoid, lunate, triquetrum, and pisiform bones. The four bones of the distal row from lateral to medial are the trapezium, trapezoid, capitate, and hamate bones. There are a total of 15 bones that form the wrist articulation with the forearm and also articulate with each other in multiple subjoints. At the distal end of the forearm, the radius and ulna articulate at the distal radioulnar joint (DRUJ), which is formed by the head of the ulna and the ulnar notch of the radius (Figure 9.1). The next joint distally is the radiocarpal joint, which is formed by the distal radius and proximal row of the carpal bones. This joint is separated from the DRUJ by an articular disk lying between the radius and the styloid process of the ulna. The joint between the proximal and distal rows of the carpal bones is the midcarpal joint. The distal joint in the wrist is the carpometacarpal joint, which is formed by the distal row of carpal bones and the proximal head of the metacarpal bones. The hand palm is made up of five metacarpal bones that provide the base for the five individual digits. The fingers contain a total of 14 phalanges: two in the thumb and three in each of the 4 fingers. There are five proximal phalanges, four middle phalanges (excluding the thumb), and five distal phalanges (Figure 9.1). Even if the wrist is considered as a single joint, there are a total of 15 joints in the hand, including the wrist, five metacarpophalangeal (MCP) joints, four proximal interphalangeal (PIP) joints, and five distal interphalangeal (DIP) joints.

Anatomically, the carpal tunnel is a narrow (1–1.5 cm diameter) space at the base of the palm, bounded dorsally, medially, and laterally by the carpal bones and palmarly by the flexor retinaculum, a thick ligament.[6] Within the carpal tunnel are the flexor digitorum profundus (FDP) and flexor digitorum superficialis (FDS) tendons to each finger, the flexor

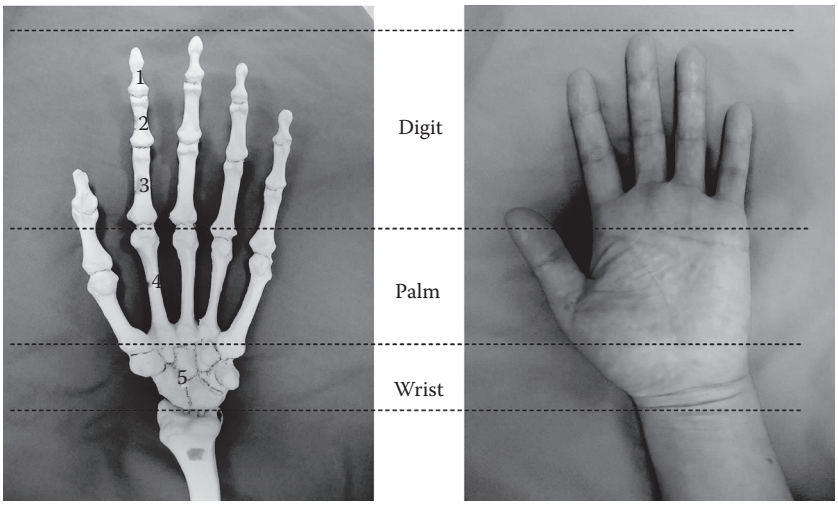

FIGURE 9.1
(See color insert.) Human hand bony structure and functional components including wrist, palm, and digits. 1, distal phalanx; 2, middle phalanx; 3, proximal phalanx; 4, metacarpal bone; 5, carpal bones.

pollicis longus (FPL) tendon, the tenosynovium associated with these tendons, two bursae (the radial one for the FPL and the ulnar one for the other tendons), and the median nerve.

9.1.2 Muscles and Their Innervation

The muscles that enable hand motion can be classified into extrinsic and intrinsic muscle groups. The majority of hand muscles are located in the forearm and are called extrinsic muscles because the muscle origins are located proximal to the hand. The extrinsic muscles can be subdivided into flexor and extensor muscle groups. Flexor muscles are located on the front (volar or palmar) side of the forearm including four FDS and FDP muscles. There are two extrinsic muscles that control thumb flexion: the FPL and the flexor pollicis brevis muscles. All five finger flexor muscles are innervated by the median nerve, except for the little and ring finger FDP muscles, which are innervated by the ulnar nerve. The hand extensor muscles are in the dorsal forearm and include a total of eight extensor muscles to move the five fingers. Four extensor digitorum muscles control the extension of the index, middle, ring, and little fingers. There are two additional extensors in the hand: one for the index finger, the extensor indicis, and one for the little finger, the extensor digitorum minimi. The thumb has two extrinsic extensor muscles: the extensor pollicis longus and the extensor pollicis brevis. All extrinsic extensor muscles are innervated by the radial nerve.

Intrinsic muscles of the hand include four groups of muscles that are located within the hand. They are the thenar (thumb), hypothenar (little finger), interossei muscles, and lumbrical muscles. Although the intrinsic muscles are not as powerful as the extrinsic muscles, they play an important role in regulating extrinsic muscle motion, stabilizing the hand joints, and performing precise activities. The thenar eminence contains three muscles: the abductor pollicis brevis, flexor pollicis brevis, and the opponens pollicis. The bellies of these muscles form a thick, fleshy area directly proximal to the thumb. These are all supplied by the recurrent branch of the median nerve, and together, their synergistic actions lead chiefly to opposition of the thumb, which is a very critical function. The hypothenar also contains three muscles: abductor digiti minimi, flexor digiti minimi, and opponens digiti minimi, which are all supplied by the ulnar nerve. There are four dorsal interossei muscles and three volar interossei muscles that lie between metacarpal bones. All interossei muscles are supported by the deep branch of the ulnar nerve. There are four lumbrical muscles that originate from the FDP tendons and are innervated by the median and ulnar nerves. The median nerve innervates the two radial lumbricals, and the deep branch of the ulnar nerve innervates the two ulnar lumbricals.

The functional performance of the wrist including its kinetics, kinematics, and stabilization is mainly related to six wrist control muscles. These include the extensor carpi radialis brevis, extensor carpi radialis longus, extensor carpi ulnaris, flexor carpi radialis, flexor carpi ulnaris, and the abductor pollicis longus muscles. The extrinsic hand muscles also play a role in hand motion secondary to their long tendons crossing the wrist joint. The three wrist extensor muscles and abductor pollicis longus are innervated by the radial nerve. The flexor carpi radialis muscle is controlled by the median nerve, and the flexor carpi ulnaris muscle is innervated by the ulnar nerve.

9.1.3 Tendons in the Hand

Tendons are essentially connective tissues that connect the muscles at their proximal end and insert on bones at the distal end. When muscles contract, the forces are transmitted

to bone through the tendons, which then moves the joints. Although the muscles introduced above have their own tendons (named similar to their associated muscles), the critical tendons are the long tendons that cross multiple joints, such as the FDP tendon. The tendons in the hand are anatomically divided into five zones (Figure 9.2). Zone I is the most distal portion, whereas zone II is the tendon portion that is located within the flexor sheath. Zone II is also the critical zone in which two of the flexor tendons (FDP and FDS) are frequently injured. Zone III is the tendon portion from the proximal flexor sheath to the distal carpal tunnel, zone IV is the tendon within the carpal tunnel area, and zone V is the most proximal portion of the tendon from the muscle origin to the proximal wrist (Figure 9.2).

Tendons in the hand can also be classified into intrasynovial and extrasynovial based on their surrounding environment.[7–9] Intrasynovial tendons are those tendons that are located in the zone II area enclosed by a synovial sheath and surrounded by synovial fluid. In the intrasynovial tendon region, the tendon surface is covered by a thin visceral synovial membrane called the "epitenon," which includes several layers of epitenon cells seeded on the surface (Figure 9.3a). These cells have a similar function to synovial cells in secreting synovial substances that serve as lubricants to decrease friction during tendon motion. This unique structure effectively decreases friction, reduces abrasion, and eliminates wear.[10] Extensor tendons in the dorsal wrist area are also intrasynovial tendons. In contrast, the tendons located within the subcutaneous soft tissues are extrasynovial tendons. These tendons are regularly covered by the loose connective tissue paratenon (Figure 9.3b). The portion of flexor tendons in zone IV is located within the carpal tunnel region, which is across the wrist area. The tendons in this area are unique and are a hybrid type of tendon. Ettema et al.[11] reported that flexor tendons in zone IV are covered by subsynovial connective tissue (SSCT), paratenon-like tissue that is similar to that of extrasynovial tendons. The entire SSCT within the carpal tunnel is covered by enclosed bursas, which are sacs that are filled with synovial fluid. Therefore, the flexor tendons in this region exhibit both intrasynovial and extrasynovial gliding mechanisms (Figure 9.3c).

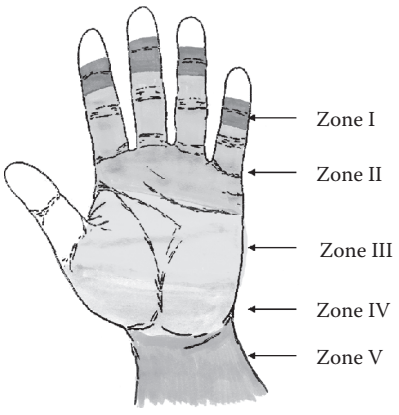

FIGURE 9.2
(See color insert.) Flexor tendons are divided into five zones in the hand, wrist, and forearm. Zone I is the most distal portion. Zone II is the tendon portion that is located within the flexor sheath. Zone II is the critical zone in which two of the flexor tendons (FDP and FDS) are frequently injured. Zone III is the tendon portion from the proximal flexor sheath to the distal carpal tunnel. Zone IV is the tendon within the carpal tunnel area. Zone V is the most proximal portion of the tendon from the muscle origin to the proximal wrist.

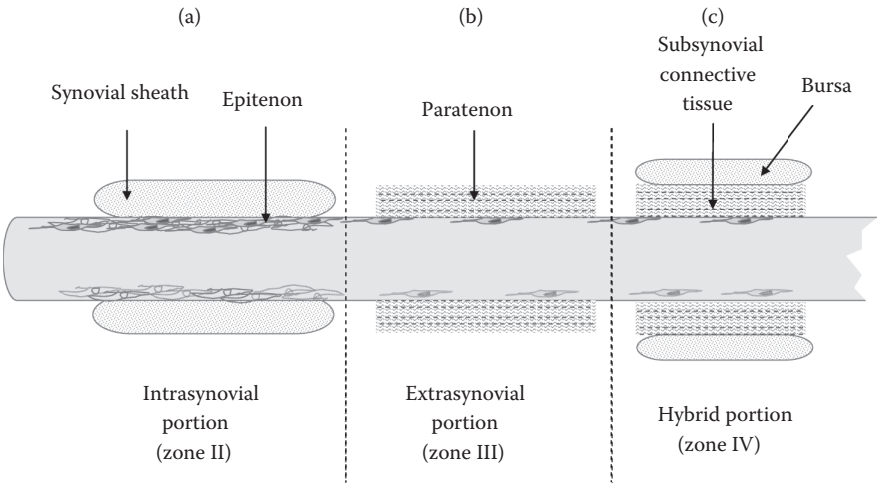

FIGURE 9.3
In zone II, the intrasynovial tendon surface is covered by epitenon, which includes several layers of epitenon cells seeding on the surface (a). In zone III, the extrasynovial tendon is wrapped by loose connective tissue or paratenon (b). In zone IV, the flexor tendons indicate a hybrid region of the tendon that is wrapped by paratenon and synovial sheath bursa (c).

The flexor tendons in zone V of the hand originate from the flexor muscles in the forearm and end at the proximal entrance of the carpal tunnel. The tendons in zone V are typically extrasynovial tendons.

9.2 Function

The human hand is used for crucial functions such as physically manipulating objects, sensing the environment, and communicating through gestures. The biomechanical structure of the hand can be considered as linkage systems in the digits and intercalated bony segments in the wrist that are stabilized by ligaments, balanced by muscle forces, mobilized by tendon translations, and constrained by geometry. Therefore, to ensure normal hand function, there must be a normal bony structure, healthy joints stabilized by normal ligaments, appropriate muscle forces, and suitable tendon excursions.

9.2.1 Kinematics of Wrist and Hand

Because the wrist is the base of the hand and links the hand and forearm together, the function of the wrist is essential for functional performance of the hand. Although the hand has multiple degree-of-freedom motions, the wrist only allows motion in two directions, flexion–extension and radial–ulnar deviation, which is perpendicular to the flexion–extension plane. Axial rotation or pronation/supination of the hand relies on the radius and ulna rotating about each other (Figure 9.4). At the proximal radioulnar joint (PRUJ), the ulna rotates around the radial head; at the DRUJ, the radius rotates around

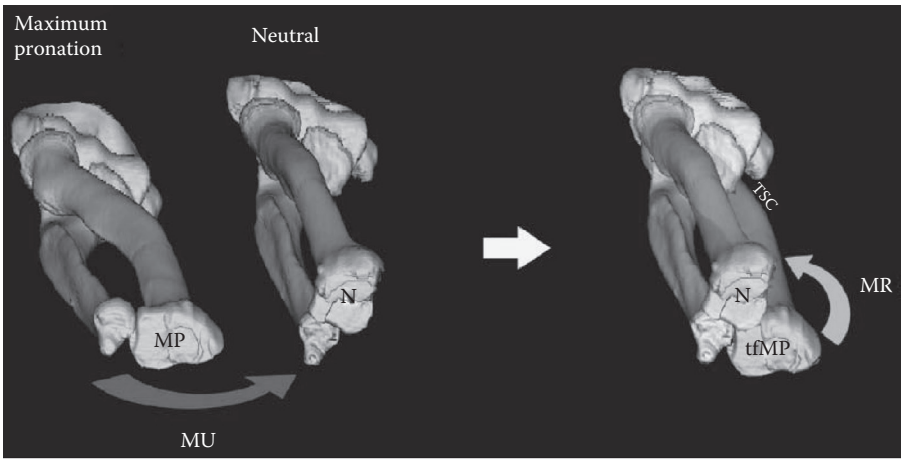

FIGURE 9.4
Illustration of how various registration matrices are generated, using the right forearm in a subject. The ulna bone from the test condition, in this case maximum pronation (MP), was registered to the ulna bone of the neutral condition. The matrix from this transformation is designated as MU. This transformation aligns the forearm of the test condition to the neutral condition as shown by the registered image on the right. The radius bone of the properly aligned forearm of the test condition (tfMP), when registered to the radius of the neutral condition, generates the transformation matrix (MR), which is then used to calculate the finite helical axis parameters. (Reprinted from *Journal of Biomechanics*, 41(1), Tay, S. C. et al, A method for *in-vivo* kinematic analysis of the forearm, 56–62, Copyright 2008, with permission from Elsevier.)

the ulnar head to pronate and supinate the hand. Therefore, both the PRUJ in the elbow joint and the DRUJ in the wrist directly affect hand functional performance in axial rotation. A normal range of motion for the wrist consists of 70° of extension, 60° of flexion, 30° of radial deviation, 50° of ulnar deviation, 70° of pronation, and 75° of supination.[12] However, wrist kinematics between carpal bones is highly complicated due to the irregular size and shape of the bones, their small articulating surfaces, and the complex forces that act across the wrist. There is still some debate regarding the direction of rotation and contribution of each individual carpal bone to global wrist motion.[13,14] The complexity of wrist kinematics contributes to the challenge of measuring and diagnosing wrist joint dynamic instability. It is generally believed that the wrist joint moves as two rows. However, the scaphoid bone, as a member of the proximal row, has been considered as a link between the two rows.[15,16] Craigen and Stanley[17] and others have proposed that the wrist joint may behave kinematically as columns defined as the vertical carpal bone motion, rows defined as transverse (proximal row and distal row) carpal bone motion, or both. Many techniques have been used to study the three-dimensional (3D) wrist kinematics in cadavers including biplanar radiographic techniques, electromagnetic tracking, and video-based systems.[18–21] However, the applicability of these techniques is limited by the difficulty in simulating normal wrist loading conditions, the invasiveness of implanting radiopaque markers, and the mechanical obstruction of motion that can occur from protruding marker pins.[22] Recently, advanced imaging techniques such as spiral computed tomography (CT) scanning or magnetic resonance imaging (MRI) have been used to study carpal kinematics *in vivo*.[13,23–27] These investigations use markerless registration techniques that allow carpal kinematics to be acquired noninvasively *in*

vivo, thus allowing researchers to make comparisons between healthy individuals and subjects with wrist joint instabilities and ligamentous injuries. Four-dimensional (three dimensions + time) CT imaging techniques[28] that enable investigators to analyze carpal kinematics *in vivo* during *dynamic motion* have recently emerged. These methods will widen the pathologies that can be investigated and diagnosed clinically using noninvasive modalities.

The interphalangeal joints are considered to be hinge joints because the collateral ligaments limit the abduction–adduction and axial rotation of the PIP and DIP joints. The volar ligaments (volar plate) at the finger joints prevent finger overextension. The range of motion (from extension to flexion) of the fingers is 0° to 90° for the MCP, 0° to 100° for the PIP, and 0° to 80° for the DIP joints.[29] However, the MCP joints are also able to perform 20° to 30° of abduction–adduction. The thumb metacarpal is based on the trapezium to form the thumb basal joint (trapeziometacarpal, TMC), which has a complex range of motions including abduction–adduction, flexion–extension, and circumduction. This complex joint system makes the human hand more delicate and capable of operating a wide variety of tools and devices and able to perform gestures, which distinguishes the human species from others. The majority of hand activities and motion tasks can be accomplished with 70% of the maximum range of wrist and hand motion.[30] However, some activities may exceed the maximum range of motion, such as dart throwing in wrist ulnar deviation, and may cause clinical problems, such as wrist ligament injuries that lead to an unstable wrist.[26,31]

9.2.2 Kinetics of Wrist and Hand

Because the hand is frequently used to physically manipulate the environment, force generation is an important function. When the hand is used for a forceful motion, a tremendous amount of force is encountered at the wrist and finger joints (Tables 9.1 through 9.4).[32,33] The force distribution among the wrist and finger joints has great potential for injury to the associated bone and soft tissue. For example, Kienböck's disease, the disorder of avascular necrosis of the lunate bone, is thought to result from cumulative trauma with compression of the lunate bone leading to ischemia and eventual necrosis.[34] On average,

TABLE 9.1

DIP Joint Constraint Forces in Units of Applied Force of Index Finger under Isometric Hand Function

Function	Compressive Force (CX2)	Dorsal Shear Force (CY2)	Radial Shear Force (CZ2)
Tip pinch	2.4–2.7	0.2–0.3	−0.1–−0.1
Key pinch	2.9–12.5	0.7–3.2	0.7–0.9
Pulp pinch	3.0–4.6	0.0–−0.2	−0.1–−0.2
Grasp	2.8–3.4	0.5–0.7	−0.2–−0.2
Briefcase grip	0.0–0.0	0.0–0.0	0.0–0.0
Holding glass	2.5–2.9	0.2–0.3	−0.2–−0.2
Opening big jar	5.2–9.5	1.7–3.3	0.3–0.5

Source: An, K. N. et al., Forces in the normal and abnormal hand. *J. Orthop. Res.* 1985. 3. 202–211. Copyright Wiley-VCH Verlag GmbH & Co. KGaA. Reproduced with permission.

TABLE 9.2

PIP Joint Constraint Forces in Units of Applied Force of Index Finger under Isometric Hand Function

Function	Compressive Force (CX4)	Dorsal Shear Force (CY4)	Radial Shear Force (CZ4)
Tip pinch	4.4–4.9	0.9–1.1	0.0–0.0
Key pinch	4.9–19.4	1.1–4.5	0.3–1.1
Pulp pinch	4.8–5.8	1.1–1.4	0.0–0.0
Grasp	4.5–5.3	1.0–1.3	0.0–−0.1
Briefcase grip	1.7–1.9	0.0–0.2	0.0–0.0
Holding glass	4.3–4.4	1.1–1.1	0.0–−0.1
Opening big jar	7.2–14.2	2.4–4.9	0.2–0.8

Source: An, K. N. et al., Forces in the normal and abnormal hand. *J. Orthop. Res.* 1985. 3. 202–211. Copyright Wiley-VCH Verlag GmbH & Co. KGaA. Reproduced with permission.

TABLE 9.3

MCP Joint Constraint Forces in Units of Applied Force of Index Finger under Isometric Hand Function

Function	Compressive Force (CX6)	Dorsal Shear Force (CY6)	Radial Shear Force (CZ6)
Tip pinch	3.5–3.9	2.1–2.3	0.1–0.2
Key pinch	14.7–27.1	3.9–5.7	0.0–0.1
Pulp pinch	4.0–4.6	2.2–2.4	0.1–0.1
Grasp	3.2–3.7	2.9–3.1	0.3–0.4
Briefcase grip	1.0–1.3	0.6–0.7	0.0–0.0
Holding glass	4.0–4.1	0.9–0.9	0.2–0.2
Opening big jar	14.8–24.3	6.5–9.9	0.2–0.3

Source: An, K. N. et al., Forces in the normal and abnormal hand. *J. Orthop. Res.* 1985. 3. 202–211. Copyright Wiley-VCH Verlag GmbH & Co. KGaA. Reproduced with permission.

approximately 20% of axial wrist joint force is transmitted by the distal end of the ulna, and 80% is transmitted through the radius in the neutral position.[12] The midcarpal joint is made up of articulations between the proximal row (scaphoid, lunate, triquetrum, pisiform bones) and the distal row (trapezium, trapezoid, capitate, hamate bones). At the midcarpal joint, approximately 30% of force is transmitted across the scaphotrapezial joint in the proximal row of carpal bones, 20% through the scaphocapitate joint, 30% through the lunocapitate joint, and 20% through the triquetrohamate joint with the wrist in the neutral position. However, the percentage of force transmission through the wrist is greatly affected by the wrist joint position (Figure 9.5).[35] The force transmitted through the finger joints is also considerably higher during hand activities. During a fingertip pinch, for example, the joint forces in the DIP, PIP, and MCP are 2.7, 5, and 4 times the pinch force, respectively.[35] In addition, shear forces applied dorsally will result in forces at the proximal ends of each

TABLE 9.4

Changes in Total Force Transmission (Newtons) at Intercarpal Joint after Simulation Procedures Used to Treat Kienböck's Disease

Joint	Intact	STT-Fusion	SC-Fusion	CH-Fusion	Capit. Short.	4 mm Leveling
Radio-ulnocarpal						
Ulno-triquetral	12 ± 3	11 ± 2[a]	11 ± 2 NS	8 ± 2[b]	26 ± 10[c]	21 ± 4[c]
Ulno-lunate	23 ± 8	22 ± 8 NS	22 ± 7 NS	25 ± 7 NS	23 ± 10 NS	35 ± 10[c]
Radio-lunate	52 ± 8	49 ± 8 NS	46 ± 10[b]	55 ± 8 NS	18 ± 8[c]	25 ± 6[c]
Radio scaphoid	74 ± 13	77 ± 14[a]	80 ± 16[a]	72 ± 12 NS	93 ± 11[c]	78 ± 12[b]
Midcarpal						
Triquetral-hamate	36 ± 6	35 ± 6 NS	34 ± 6[a]	20 ± 8[c]	90 ± 15[c]	38 ± 5 NS
Lunocapitate	51 ± 6	48 ± 6 NS	45 ± 9[a]	60 ± 8[a]	—	44 ± 5[c]
Scaphocapitate	32 ± 4	40 ± 9[a]	—	38 ± 4[b]	16 ± 8[c]	39 ± 7[c]
Scaphotrapezial	51 ± 8	—	53 ± 7 NS	46 ± 7[b]	87 ± 9[c]	51 ± 7 NS

Source: Reprinted from *J. Hand Surg. Am.*, 15(3), Horii, E. et al., Effect on force transmission across the carpus in procedures used to treat Kienbock's disease, 393–400, Copyright 1990, with permission from Elsevier.

Note: STT, scapho trapezial-trapezoidal; SC, scapho capitate; CH, capitate-hamate; Capit. Short., capitate shortening plus capitate-hamate fusion; 4 mm Leveling, radial shortening/ulnar lengthening (4 mm). Mean ± SD, $n = 6$.

[a] $p < 0.05$; [b] $p < 0.005$; [c] $p < 0.001$; NS, not significant compared with intact (Tukey's test).

phalanx of the three joints amounting to 33% of pinch force at the DIP, 100% at the PIP, and 200% at the MCP joint (Figure 9.6).

The most common hand motion is a gripping motion. In general, there are two patterns of grip: the power grip and the precision grip. The power grip (crush grip) occurs in actions such as holding onto a baseball bat. The precision grip (pinch grip) occurs in actions such as picking up a key, which is distinguished by the relative thumb position and palm involvement. In the power grip, the flexed fingers hold the object against the palm with the thumb adducted. A well-developed hypothenar fat pad and a more robust fifth metacarpal diameter help stabilize the object against the palm, tightly secured by the strong thumb.[36] The precision grip holds the object away from the palm using the volar aspect of the fingers and the opposed thumb. Grip strength can be quantitatively measured by a hand dynamometer. Many factors affect the magnitude of the grip strength, including the measurement device used and the specific protocol, body and arm position, repetitive grip, time of day, and training.[37,38] Grip strength is increased with the wrist in supination but decreases in pronation.[39] Mathiowetz et al.[40] reported higher grip strength to be obtained with the elbow in 90° of flexion. However, Su et al.[41] found significantly higher grip strength with the elbow fully extended rather than flexed. Shoulder position also affects grip strength. The highest grip strength was found with the shoulder in 180° of flexion, and the lowest was found with the shoulder in 0° of flexion.[41] The effects of joint posture on grip are due to the length–tension relationship of the muscles as well as the changes in moment arms with joint position. Bao and Silverstein[37] measured 120 subjects within a range of ages from 20 to 60 years. The average strength was 470 N for a power grip

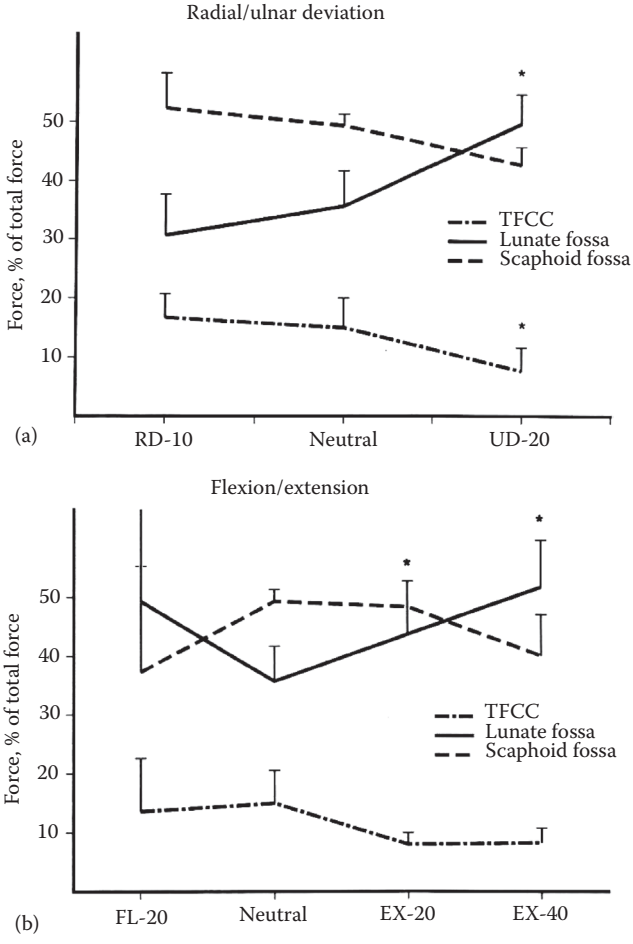

FIGURE 9.5
Proportional changes of force transmission during radial/ulnar deviation and flexion/extension motion. (*, $p < 0.05$, significantly different from neutral position). (a) Force transmission changes in radial/ulnar deviation. (b) Force transmission changes in flexion/extension motion. (Reprinted from *Journal of hand Surgery*, 17(2), Hara, T. et al., Force distribution across wrist joint: Application of pressure-sensitive conductive rubber, 339–347, Copyright 1992, with permission from Elsevier.)

and 125 N for a pinch grip in males. Both were significantly higher than values for females, with 294 N for a power grip and 89 N for a pinch grip. They also found the strength of power and pinch grip to decrease with increasing age. This decreased grip strength was significant in females.[37,42]

9.2.3 Stability and Joint Constraints

Normal hand function relies on a healthy and stable joint. Joint stability and constraints are provided by the joint articular surfaces, joint capsule, surrounding ligaments, and active musculotendinous units. Primary joint stability relies on the muscle and tendon response to sustained pinch and grip forces (Figures 9.7 and 9.8).[43,44] In contrast, the

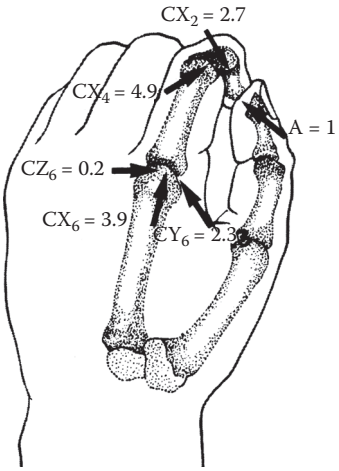

FIGURE 9.6
Resultant finger joint force during tip pinch function of one unit force, that is, $A = 1$. (Reprinted from *Joint Replacement Arthroplasty*, An, K. N. and Cooney, W. P. I., Biomechanics, edited by B. F. Morrey, 137–146, Copyright 1991, with permission from Elsevier.)

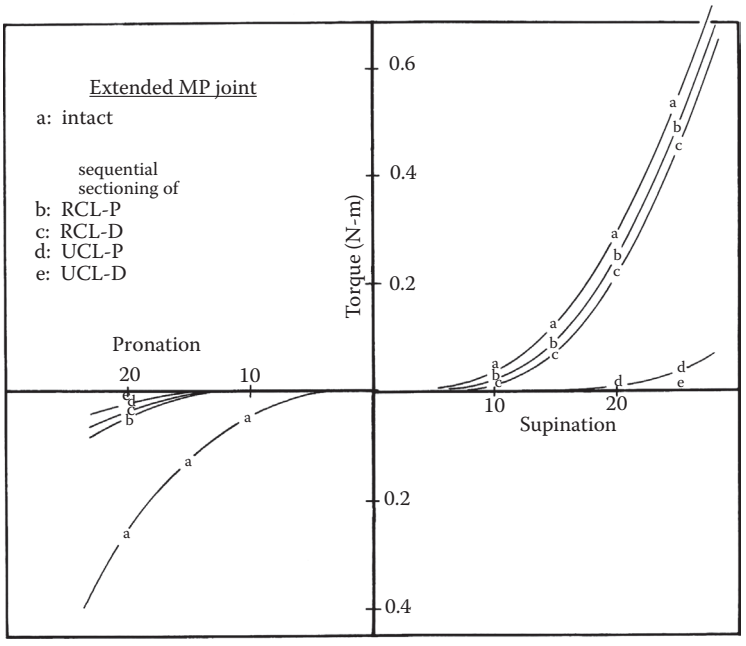

FIGURE 9.7
Load-displacement curves obtained by measuring the restraining torques with joints in supination and pronation. Curves *a* and *e* represent the restraining torques when the palmar and dorsal portions of the UCL were sectioned, respectively. The differences in load between each curve at a given displacement indicate the contribution of that particular sectioned element. For example, the difference in load between curves *a* and *b* represents the contribution of the palmar portion of the RCL. (Reprinted from *J. Hand Surg. Am.*, 10, Minami, A. et al., Ligament stability of the metacarpophalangeal joint: A biomechanical study, 255–260, Copyright 1985, with permission from Elsevier.)

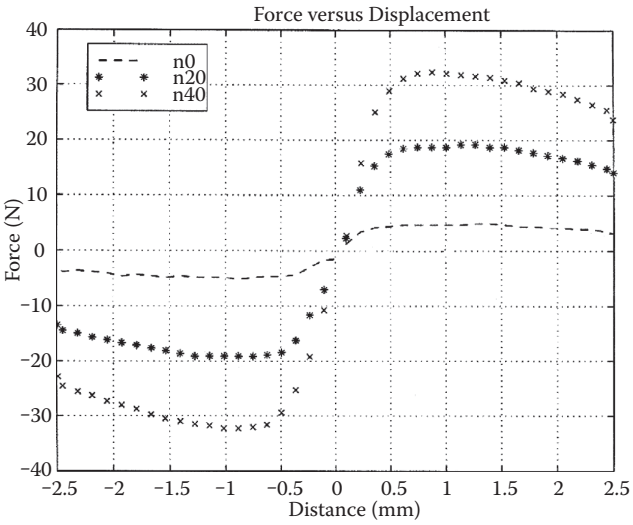

FIGURE 9.8
Sample graph of force versus displacement. Force is in the direction of motion and is measured by the load cell. In this particular graph, the positive displacement represents movement of the proximal phalanx of the implant in the radial direction. The negative displacement represents movement in the ulnar direction, both with three different axial loads. (Reprinted from *Clin. Biomech.*, 18, Kung, P. L. et al., Intrinsic stability of an unconstrained metacarpophalangeal joint implant, 119–125, Copyright 2003, with permission from Elsevier.)

ligaments and capsules seem to play the role of initial stabilizer against instantaneous joint load and provide a secondary contribution to maintaining joint stability. Because many joints in the wrist and hand have large ranges of motion in three dimensions, bony geometry does not contribute much to joint stability.[34] Because of these anatomic characteristics, the stabilizing ligamentous constraints are of great importance. Joint stabilization is accomplished by the combined and simultaneous action of tension forces in the retaining ligaments and compression forces between the articulating surfaces. In the wrist joint, this intrinsic ligamentous stability is provided mainly by the horizontal triangular fibrocartilage complex (TFCC) or distal radioulnar ligament (Figure 9.9), which plays an important role not only in stabilizing the DRUJ but also in mediating normal function to the radiocarpal and ulnocarpal joints.[44,45] The TFCC ligament is divided into two zones. The central zone is thin and mechanically weak. The peripheral zone is strong and divided into the palmar and dorsal distal radioulnar ligaments. The longitudinally oriented collagen fibers, which are structurally adapted to bear tensile loads, dictate the mechanical properties.[46] The roles of the palmar and dorsal portions of TFCC ligaments in resisting the dorsal and volar subluxation of DRUJ depend on the forearm pronation and supination (Figure 9.10).[47–49]

In the finger joints, the collateral ligament stabilizers are important. Orientation of the fibers in various portions of the ligaments determines the restrictive direction of bony or joint motion. In a series of anatomic studies in which different areas of the collateral ligaments were sectioned,[43,50–52] the role of each portion of the collateral ligament to joint stability was identified. Each part of the ligament, thus, has its own characteristic contribution to resist forces and moments under various loading and displacement conditions. The locations of the bony insertion and the fiber orientations of the collateral ligaments around the finger and thumb joints have been extensively studied and reported in the literature.[43,50–52]

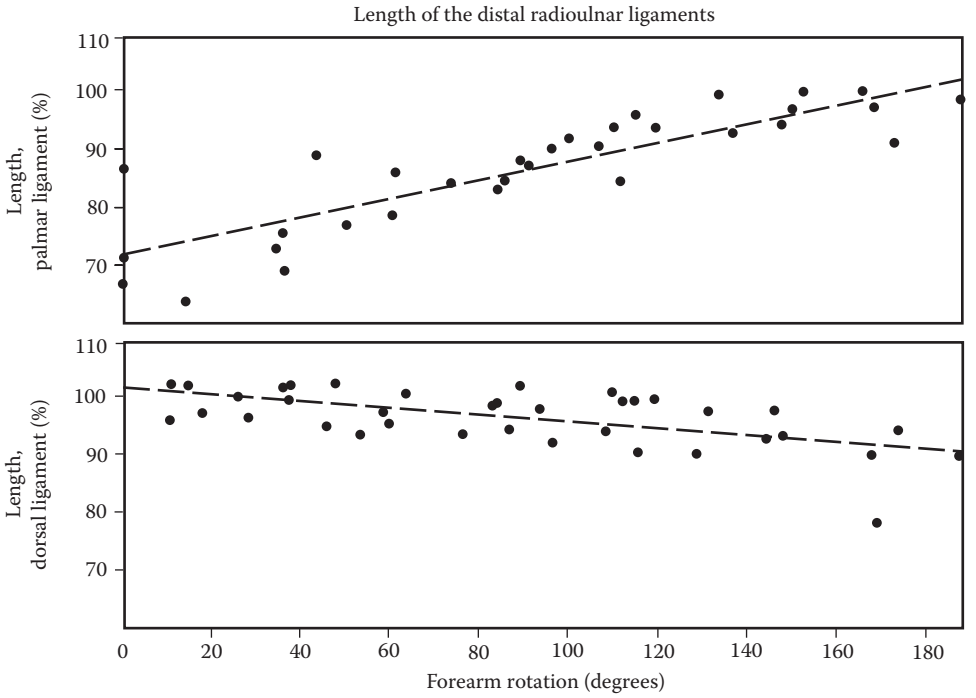

FIGURE 9.9
Change in lengths of the palmar (top) and dorsal (bottom) distal radioulnar ligaments with forearm rotation; the lengths of the ligaments are expressed as a percentage of their length in maximal tension; the 0° of forearm rotation is the full pronation position. Each marker shows a different specimen. (Reprinted from *J. Hand Surg. Am*., 16, Schuind, F. et al., The distal radioulnar ligaments: A biomechanical study, 1106–1114, Copyright 1991, with permission from Elsevier.)

This information is essential in understanding the mechanism of finger joint stability. From the anteroposterior view, the insertions of the radial collateral ligament (RCL) are closer to the center line of the metacarpal than those of the ulnar collateral ligament (UCL) (Figure 9.11). The dorsal fibers originating from the metacarpal head are more distal than those of the volar portion.

9.2.4 Tendon Excursion and Gliding

Healthy bony structure, normal joint kinematics, and appropriate muscle force are all essential for hand function. However, tendon gliding and excursion are also important for normal hand biomechanics. The majority of hand extrinsic muscles have long tendons that connect the muscles and bones together. These tendons also cross over multiple joints including the wrist, MCP, PIP, and DIP joints. Therefore, a large gliding excursion is needed to achieve full joint motion. Because tendons transmit force from muscle to bone to produce joint motion, tendon excursion is directly proportional to muscle shortening and is also affected by the joint's range of motion. If tendon excursion is hindered, the muscle and joint function is also affected. With time, disused muscle will hypotrophy and joint contracture will develop, leading to a destruction of the muscle–tendon–bone unit.[53] The understanding of tendon motion biomechanics, therefore, is essential.

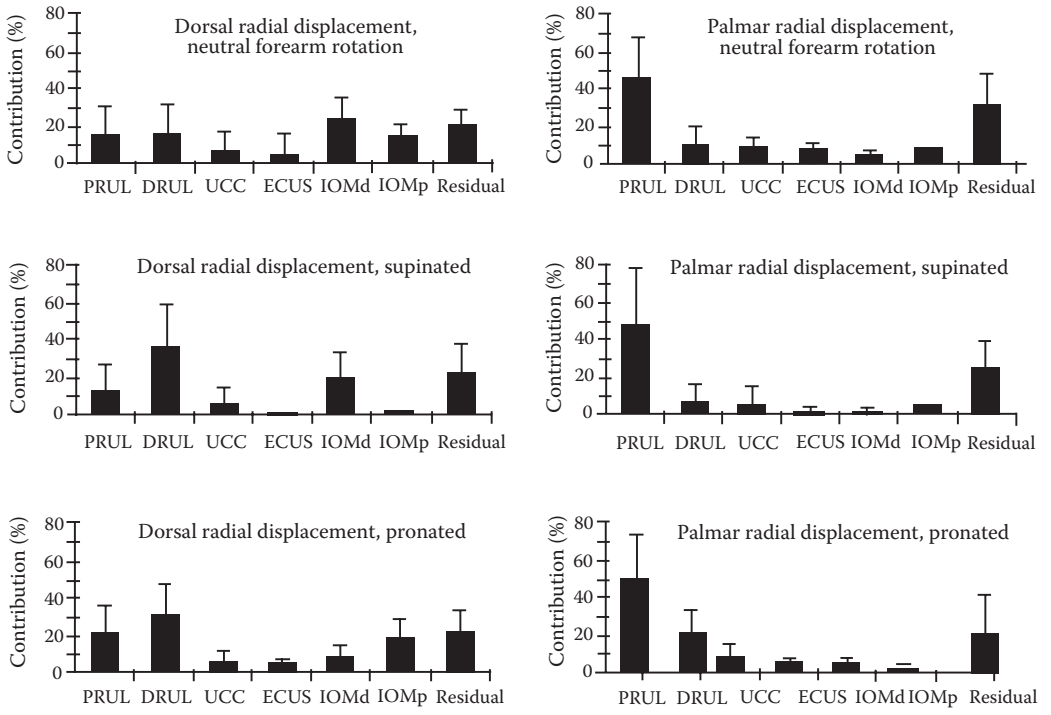

FIGURE 9.10
Histograms of the percentage contribution to constraint in each position of forearm rotation. Because no difference was detected based on varying wrist position, all histograms reflect the wrist in neutral extension. (Reprinted from *Journal of Hand Surgery*, 25(4), Stuart, P.R. et al., The Dorsopalmar Stability of the Distal Radioulnar Joint, 689–699, Copyright 2000, with permission from Elsevier.)

Tendon function is regularly estimated using tendon excursion during hand and finger motion. Tendon excursion measurements vary at different levels and accumulate proximally, for example, the flexor tendon excursion measured at the wrist level is longer than that measured at the MCP level.[54] In pathological conditions, tendon motion can be affected by many factors, including intrinsic factors, such as tendon adhesion and contracture, and extrinsic factors, such as muscle problems, joint contracture, bone shortening, or pulley resections.[55,56] The motion of the tendon in the hand is also affected by the position of the wrist. Wehbe et al.[57] measured 36 cadaveric hands with buried metallic sutures using radiograph confirmation. The average excursion was 32 mm for the FDP tendon and 24 mm for the FDS tendon with the wrist in a neutral position. With increased wrist range of motion, the amplitude of the profundus tendon excursion increased to 50 mm and the superficialis tendon reached 49 mm. The relationship of tendon excursion to joint motion has been well studied both experimentally and mathematically.[58] For single joint motion, the ratio of joint motion and tendon excursion can be determined by the joint moment arm. In general, the larger the tendon moment arm at the joint, the greater the tendon excursion. Horibe et al.[59] measured the FDP tendon excursion as a function of finger joint motion using cadaveric specimens. The experiments revealed that every 10° increase in motion of the DIP joint (small moment arm) is associated with a 1.2 mm FDP tendon excursion, but every 10° of the metacarpal joint (large moment arm) is associated with 2.2 mm

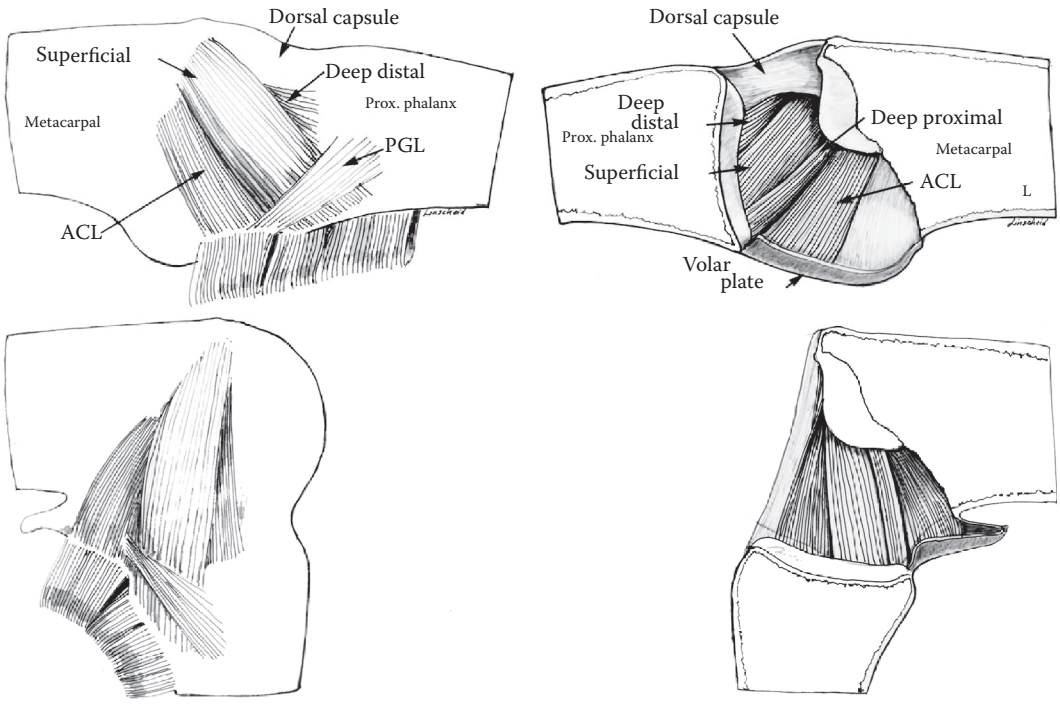

FIGURE 9.11
Structure of the collateral ligament in MCP joint. External view: the collateral ligament was separated into two components, the superficial and the deep. The deep distal component is hidden beneath the superficial portion when the joint is in extension (top) but becomes increasingly taut and visible as the joint is flexed (bottom). Internal view (view from the joint): the deep layer of the collateral ligament is separated into two portions, the deep distal and deep proximal. The deep proximal component lengthens in extension (top) and shortens in flexion (bottom). These fibers bulge laterally during joint flexion. (Reprinted from *Joint Replacement Arthroplasty*, An, K. N. and Cooney, W. P. I., Biomechanics, edited by B. F. Morrey, 137–146, Copyright 1991, with permission from Elsevier.)

of FDP tendon excursion. With this concept, the tendon excursion can be mathematically calculated based on the joint moment arm.[58,60] The moment arm is defined as the perpendicular distance between the joint center of rotation and the central longitudinal axis of the tendon (Figure 9.12). To best understand the relationship between tendon excursion, joint angular motion, and moment arm, the geometric concept of the radian has been used

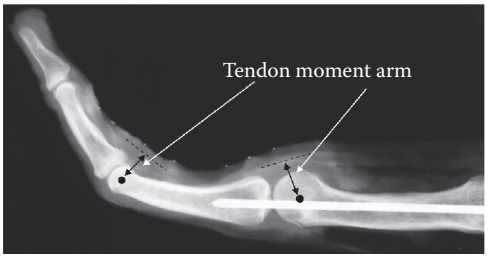

FIGURE 9.12
The tendon moment arm is defined by the perpendicular distance between the joint center rotation to the midline of the tendon longitudinal axis.

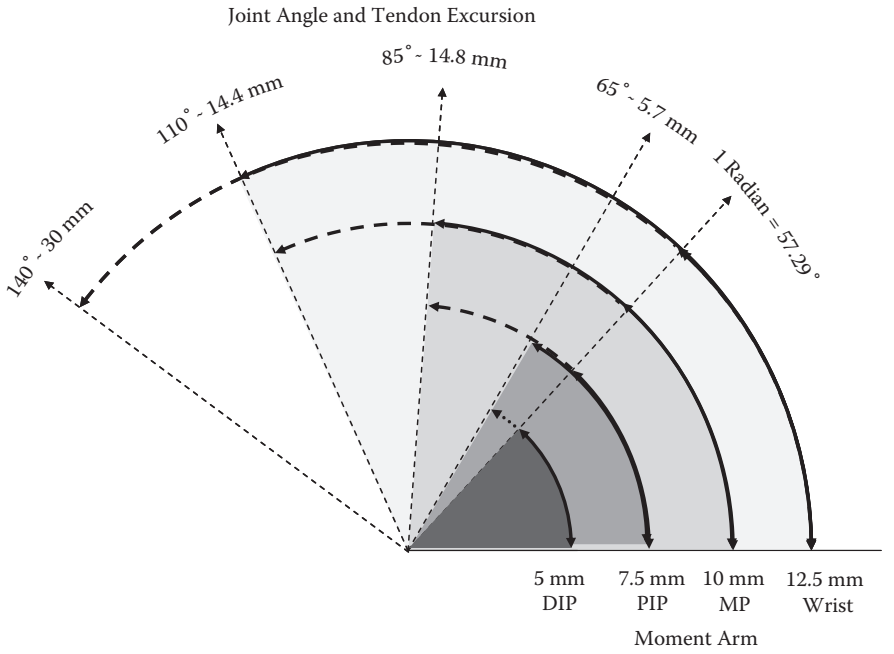

FIGURE 9.13
Based on the theory that tendon excursion is equal to moment arm when the joint moves 1 radian (57.29°), the FDP tendon excursion can be calculated.

(Figure 9.13).[58] The radian is a unit of angular measure that is described as the plane angle subtended by a circular arc as the length of the arc divided by the radius of the arc. One radian is equal to 57.29°, which means that when a joint moves 57.29°, the tendon excursion is equal to this joint moment arm. The moment arms of the hand joints have been reported as 12.5 mm at the wrist, 10 mm at the MCP, 7.5 mm at the PIP, and 5 mm at the DIP joints.[58,61] Based on the angular motion of the finger joints (MCP: 85°, PIP: 110°, and DIP: 65°), the excursion is calculated as 14.8 mm in MCP, 14.4 mm in PIP, and 5.7 mm in DIP joint (Figure 9.13). These results, indeed, were similar to excursion that was experimentally measured using human fingers.[57,59] This mathematical calculation model provides a useful tool for the validation of *in vivo* measurement of tendon excursion.[62–64]

The force applied to tendons during hand and finger motion also affects tendon excursion due to its deformation and overcoming of friction. Excursion with active motion is longer than the excursion with passive motion due to the difference in the force applied to the tendon.[65–67] Although passive joint motion can induce a pushing force from the distal to the proximal direction, which can create tendon motion, this passive tendon excursion is limited by tendon buckling, especially with the wrist in a flexed position (Figure 9.14).[46,67] In contrast, active motion not only eliminates this tendon buckling effect but also elongates the tendon to create more tendon excursion even without joint motion. In addition, the active force on the tendon drives the tendons toward the volar direction, creating a bowstring effect, especially when the joint is in a flexed position. In the normal condition, the pulley system within the finger restricts the tendon bowstring to maintain the tendon close to the phalanges during flexion. However, a pulley defect due to tendon injury or repair leads to the tendon bowstring, which will increase the tendon-joint moment arm leading to more tendon excursion. As the moment arm increases, less force and longer

FIGURE 9.14
(See color insert.) Passive DIP and PIP joint motion result in buckling of the FDP tendon when the wrist is placed in flexion position, in which the force applied to the tendon was diminished. (Adapted from *J. Hand Surg. Am.*, 17, Horii, E. et al., Comparative flexor tendon excursion after passive mobilization: An in vitro study, 559–566, Copyright 1992, with permission from Elsevier.)

excursion are required to move the joint. Anatomic pulley structures within the flexor sheath balance the force generation and tendon movement.[61] Because the moment arms in different joints are different, tendon tension can be varied by manipulating joint motion. Using this concept, many postoperative rehabilitation protocols have been developed.[68–71]

Tendon excursion in the hand, especially flexor tendons in zone II, can be affected by tendon friction within the flexor sheath. Although this effect is not obvious in the physiological condition because the normal frictional force is very small, tendon excursion can be hindered in some pathological conditions that cause the tendon friction to be increased, such as trigger finger or repaired flexor tendon after injuries.[1,72] For flexor tendon injuries and surgical repairs, understanding the force applied to the tendon with different therapies, tendon friction after trauma and tendon repair, and the repair strength with different surgical techniques are important issues that have been extensively studied.[73–76] Tendon friction is composed of external and internal sources of resistance. The external resistance comes from joint stiffness, surrounding soft tissue resistance, mass of the digit requiring lift, and resistance of antagonist muscles. The internal resistance consists of surface friction between tendon and sheath, the bulk friction due to the fit of the tendon within the flexor sheath, and biological adhesions. The energy expended by internal resistance is approximately 10% of the total energy required to flex the digit.[77] However, after tendon repair, the internal resistance increases by 274% for low frictional repair techniques and increases by 599% for high frictional repair techniques, which make up 24% and 31% of the total work of flexion, respectively.[77] External resistance can also dramatically increase after trauma and surgical procedures due to the presence of soft tissue edema, joint swelling, and pain-induced antagonist muscle contraction.[77] As the total resistance increases, more tendon force is needed to move the finger during active motion. Therefore, the frictional force of the repaired tendon becomes an important issue especially when a passive rehabilitation program is chosen, in which a low force is applied to the tendon. In this case, a low frictional repair technique should be considered to decrease the repaired tendon frictional force to achieve the maximum tendon excursion during therapy. In an animal *in vivo* experimental model, low frictional suture techniques have been shown to produce

less adhesion formation and smooth surface remodeling within 6 weeks compared with a high frictional suture.[67,78]

Tendon gliding excursion is determined by three extrinsic factors: (1) the relative joint motions, (2) the integrity of the pulley system, and (3) the force applied to the tendon. Pathological changes, such as joint contracture, pulley injuries, or muscle dysfunction, affect normal tendon gliding. Tendon gliding is also directly affected by an intrinsic factor, that is, adhesions, which often occur after tendon injury, hindering tendon gliding. Clinicians must clearly understand the causes that hinder tendon gliding and treat them accordingly. For example, a joint contracture must be solved before treating the tendon adhesions (tenolysis). Otherwise, even if the tendon is freed, it is still unable to glide due to an immobilized joint, which can once again lead to tendon adhesion. Therefore, it is important for clinicians to understand the tendon gliding mechanism.

9.3 Pathomechanics of Hand and Wrist—Current Concepts

Numerous hand disorders can impair hand function and affect daily activities. Forceful hand motion with high repetitive frequency has been generally accepted as a high risk for work-related musculoskeletal problems of the distal upper extremities. CTS and tendinopathy are common overuse injuries in the hand and wrist that affect soft tissue structures. However, joint instability is a common pathology that affects the bony motion and often leads to cartilage and bone involvement in osteoarthritis (OA). Here, we provide a brief description of these pathologies in the context of structure and function.

9.3.1 Abnormal Joint Motion and Instability

9.3.1.1 TMC Joint Instability as a Precursor to Osteoarthritis

The TMC joint of the thumb base has a complex geometry with distinctive kinematics and joint ligamentous constraints. Therefore, with subtle changes in ligamentous soft tissue stabilizers due to a variety of intrinsic factors, hypermobility can ensue. Quantifying joint kinematics can provide insight into the normal range of motion (workspace) of the thumb,[79–82] as well as establish normative data from which to compare specific populations of individuals, including age- and gender-specific groups. The metacarpal and trapezium joint surfaces are characterized by a unique saddle shape that dictates unique kinematic patterns in the various directions of movement. Joint kinematics have been quantified *in vitro* using an electromagnetic system to quantify the movement of the trapezium and metacarpal.[18] Points residing on the proximal and distal metacarpal were tracked dynamically and expressed relative to the trapezial coordinate system throughout the movements. During flexion–extension, the center of rotation of the metacarpal is located within the trapezium; in abduction–adduction, it is located within the base of the metacarpal. This alteration in the center of rotation throughout the complex TMC motion contributes to the difficulty in the overall understanding of thumb pathology.

Subtle changes in kinematics can alter joint contact patterns and lead to articular cartilage changes and OA. Observation of the TMC joint *in vitro* as well as in individuals with TMC osteoarthritis has provided information about the degenerative process. Researchers have loaded muscles *in vitro* in various thumb positions and noted the contact area relative

to the joint positions (e.g., flexion of the thumb resulted in contact areas in the volar regions of the trapezium relative to extension).[79] Furthermore, after harvesting surgical specimens during basal joint arthroplasty, investigators used direct inspection and methylene blue staining to investigate wear in the articular cartilage.[83–85] Eburnation, or hardening of subchondral bone, was found over a greater articular surface area on the trapezium than on the metacarpal. The authors concluded that translation of the metacarpal on the trapezium is involved in the production of arthritic surface lesions, supporting the hypothesis of pathological joint instability as the cause of TMC osteoarthritis.[85]

9.3.1.2 Scapholunate Dissociation

The scapholunate joint is an important carpal joint for providing wrist movement. Similar to the anterior cruciate ligament in the knee, the scapholunate interosseous ligament (SLIL) can be considered as the primary stabilizer of the scapholunate joint.[86] Injuries to the SLIL are the most frequent cause of carpal instability and account for a considerable degree of wrist dysfunction. Patients with SLIL injuries may experience wrist pain or a snapping sensation with motion,[87,88] without any abnormalities in the relationship between the scaphoid and lunate position on static or stress radiographs.[89,90] The concept of dynamic scapholunate instability has been proposed to describe undiagnosed subtle changes in the wrist joint, which precede static instability.[91]

Scapholunate instability is the most common form of carpal dysfunction and encompasses a spectrum of disease that is both difficult to diagnose and to treat. Oftentimes, the acute wrist injury is called a "sprain" after static radiography fails to reveal an abnormality. The continued rotatory subluxation of the scaphoid goes on to produce chronic pain and degenerative changes of the wrist. The incidence of scapholunate injury associated with acute wrist injury has been cited at roughly 5%; however, the incidence is likely much higher.[92] In addition, the association of scapholunate injuries with distal radius fractures has been estimated to be as high as 85% with intra-articular fractures.[93] The scaphoid is considered the bridge between the proximal and distal carpal rows and is attached to the lunate through the SLIL. Once this linkage is disrupted, abnormal carpal motion occurs and can lead to progressive degenerative changes to the wrist. Destot[94] first recognized the scapholunate dissociation in 1926 as a radiographic finding, but these injuries were not truly investigated until 1972 when Dobyns et al.[95] detailed traumatic instabilities of the wrist. The pathophysiology of progressive degenerative changes in scapholunate instability has been delineated. The scaphoid is responsible for flexion of the proximal carpal row during radial deviation as it flexes during this motion. The force necessary for this motion is transmitted through the SLIL and is offset by the extension force on the lunate by the triquetrum through the lunotriquetral interosseous ligament. When the linkage between the scaphoid and lunate is disrupted, the scaphoid is unable to bridge the midcarpal kinematics and dorsal intercalated segment instability ensues, leading to abnormal motion and eventual collapse of the carpal architecture.

The SLIL is the major stabilizer of the scapholunate joint and is made up of three divisions: dorsal, proximal or membranous, and palmar.[96] The dorsal portion is roughly three times thicker and resists torsion better than the palmar and proximal portions.[96] Although the SLIL is the major stabilizer, isolated sectioning of the ligament may not produce abnormalities on static radiographs. There are also secondary stabilizers, volar carpal ligaments and the dorsal capsule, which are important in the stability of motion. The volar carpal ligaments include the radioscaphocapitate ligament, the long radiolunate ligament, the scaphotrapezial ligament, and the scaphocapitate ligament. The

radioscaphocapitate ligament has specifically been shown to be an important secondary stabilizer of the scapholunate joint.[97] The dorsal stabilizers include the dorsal intercarpal ligament and dorsal radiocarpal ligament.[98] Even if the secondary stabilizers are not initially injured, the abnormal carpal motion produced from SLIL injury will eventually lead to the chronic degeneration of these secondary structures. As time elapses, the wrist will progress through stages of ligamentous disruption and instability. The initial stage is referred to as "predynamic instability" and occurs when the scapholunate membrane is attenuated, producing abnormal motion between the scaphoid and lunate that causes wrist pain without any evidence of pathology on static or stress radiography. With continued abnormal motion, the patient moves onto dynamic instability. Further ligamentous injury to the palmar or dorsal portions of the SLIL occurs and may be detected in dynamic studies such as stress radiography.[98] Static instability occurs next and can be seen as a widening of the scapholunate gap on plain film radiographs. Static instability may or may not be associated with DISI, depending on how dorsally rotated the lunate has become. The final stage is the development of arthritic changes known as scapholunate advanced collapse (SLAC) wrist. The pattern of arthritic changes begins at the radial styloid and progresses to the radioscaphoid fossa and then to the lunocapitate joint. There is likely significant injury to the secondary ligamentous stabilizers of the wrist once arthritic changes consistent with SLAC wrist are present.[98]

The diagnosis of scapholunate instability is often missed in the initial stages of injury because initial diagnosis relies on plain radiography. Sometimes, the scapholunate injury is overshadowed by a more extensive injury such as an intra-articular distal radius fracture. Scapholunate instability may also be present in the setting of a chronic inflammatory disease such as rheumatoid arthritis. There are various modalities currently used to diagnose scapholunate pathology including radiography, fluoroscopy, arthroscopy, CT, and MRI. Radiographs are initially taken and include at least two views: a lateral view with the wrist in neutral flexion–extension and an anteroposterior projection with the forearm and hand in full supination. Additional radiographs are often used if the initial static views are normal and clinical suspicion is still high. Such additional images include stress views in ulnar and radial deviation and longitudinal compression when the patient makes a tight fist. Fluoroscopy has been used as a dynamic examination of the wrist; however, the images are two-dimensional projections of 3D objects. The complex architecture and overlapping of carpal articulations cause difficulty in delineating subtleties of motion in fluoroscopic images. MRI has been shown to be helpful in diagnosing ligamentous injuries in many joints; however, it has been concluded that MRI cannot reliably exclude tears of the intrinsic carpal ligaments.[98] Arthroscopy has become the gold standard for identifying scapholunate injuries when noninvasive testing is inconclusive. Therefore, a reliable noninvasive modality is needed to diagnose scapholunate instability early in the disease process, and a new technique involving four-dimensional CT imaging may provide a method to quantify the subtle abnormal motion seen in these injuries.

The treatment of scapholunate instability depends on the timing of intervention after the injury. There has been no standardized window to determine between acute, subacute, and chronic injuries. The majority of investigators agree that in acute injury, when the SLIL is still viable for repair, the ideal surgical intervention is primary repair of the SLIL with percutaneous pinning of the scapholunate joint.[98] However, the treatment of subacute and chronic states continues to be a topic of debate in the literature. One model of treatment that most authors agree on is surgical intervention performed as soon as the diagnosis can be confirmed.[98] Intrinsic ligaments tend to undergo rapid degeneration as early as 2 to 6 weeks after the initial injury, and many patients are not adequately diagnosed within

this timeframe. If the SLIL is irreparable at the time of surgery, another surgical option is needed to reconstruct the scapholunate articulation. There have been many procedures described, from different ligament reconstructions to the use of bone anchors to various fusions. The goal of these surgical interventions is to restore the normal mechanics of the wrist, to relieve pain, and to restore function. If there is associated arthritis at the time of surgery, some form of intercarpal arthrodesis is usually advocated. The most controversial situation arises when there is an irreparable SLIL without associated osteoarthritis.[99] There have been many procedures advocated, but no optimal reconstruction has been identified to date.

9.3.2 Repetitive Soft Tissue Injury in the Hand and Wrist

9.3.2.1 Carpal Tunnel Syndrome

CTS is the most common compressive neuropathy of the wrist, with an estimated lifetime risk of 10%[100] and a prevalence of approximately 3%.[101,102] The prevalence can vary between 0.6% and 61% depending on occupation.[103–106] The precise etiology of CTS has remained elusive, but contributing factors include repetitive manual activities,[107–109] anatomic anomalies,[110,111] autoimmune or hematologic disorders, arthritis, trauma, and neoplasms.[112–114] However, the most commonly assigned etiology is idiopathic.[115–117]

The carpal tunnel is a narrow tunnel at the base of the palm and contains nine tendons (four tendons of the FDP, four tendons of the FDS, and the flexor pollicis) and the median nerve. The carpal tunnel also includes the tenosynovium associated with each tendon and two bursae: the radial one for the FPL and the ulnar one for the other tendons. With its three bony walls and thick ligamentous roof, the carpal tunnel behaves like a closed compartment.[6] Increasing pressures result in ischemia of the median nerve, which, in turn, produces the clinical symptoms of CTS and hand disability.[118–120] Indeed, although the specific etiology inducing the pressure elevation is idiopathic in most cases, there is a strong consensus that pressure elevation within the carpal tunnel is the immediate and direct cause of the neuropathy.[121–124] Pressure is typically minimal with the wrist in the neutral position, maximal in wrist flexion, and intermediate in wrist extension.[124,125]

The most common histologic finding in CTS is noninflammatory synovial fibrosis associated with edema.[126–128] Fibrosis seems to be critical for the development of CTS.[129] Marked synovial thickening and fibrosis around the flexor tendons and fluid in the tendon sheath are clearly shown on MRI in patients with CTS.[130–133] Synovial sheath hypertrophy can be seen on CT imaging.[134] The tendons and synovium within the carpal tunnel are unique. Tendons can be classified into extrasynovial or intrasynovial tendons. Intrasynovial tendons, such as flexor tendons in zone II, have a parietal and visceral synovial sheath that forms a closed compartment containing fluid for lubrication. Extrasynovial tendons, like the Achilles tendon, are surrounded by loose fibrillar paratenon, which functions as a sleeve, permitting free tendon movement against the surrounding tissue.[135,136] Tendons within the carpal tunnel are a hybrid of both tendon types. Parallel sheets of fibrous tissue lie between the visceral synovium (VS) of the carpal tunnel bursae and the epitenon of the digital flexors. When a tendon moves within the carpal tunnel, the fibrils connected to the tendon are stretched first, followed by fibrils connected to the paratenon layers. In this way, the lengthening propagates layer by layer until finally the VS moves (Figure 9.3c). This intervening tissue is referred to as the SSCT. Patients with CTS have an increased diameter of collagen fibers and increased phagocytosis of elastin within the SSCT.[137–140] In addition, there is a marked increase in fibroblastic density, vascular

proliferation, and collagen type III and type VI, with associated transforming growth factor-beta (TGF-β) activity.[11] TGF-β is a protein that controls many cell functions and is upregulated in numerous disease states. These histopathological findings are consistent with the presence of a chronic injury and its associated ischemia. The permeability of the SSCT is so low that extra water within SSCT due to edema is not easy to flush away, leading to increased hydrostatic pressure and eventual ischemia.[141] The SSCT in patients with CTS is stiffer and possesses a higher Young's modulus than the SSCT of unaffected individuals.[142,143] The altered stiffness and strength of the SSCT leads to pathological kinematics of the tendon and SSCT. The ratio between tendon and SSCT motion was studied using a fluoro-technique with metallic markers embedded within the flexor tendons and SSCT in normal human cadavers.[143,144] If the SSCT motion is decreased with the tendon's motion (i.e., the ratio increases), the fibers within the SSCT are overstretched and may cause the SSCT to tear. Similarly, if the SSCT's motion is increased with the tendon's motion, it suggests that SSCT becomes stiffer leading to synchronization of SSCT and tendon motion. The "shear index" has been proposed as an equation to indicate the possible injury of the SSCT that potentially initiates the SSCT healing process. Shear index = TE – SE / TE × 100%, where TE is the tendon excursion and SE is the SSCT excursion. If repeated injuries surpass the healing tolerance, the SSCT may develop fibrosis, which has been commonly observed in patients with CTS. Ettema et al.[145,146] used this concept and found that the relative SSCT and tendon motion in patients with CTS presented two different motion patterns compared with the normal cadavers. One common pattern was that the SSCT excursion related to tendon motion increases (shear index increases), which indicated a dissociation between the SSCT and the tendon. The other pattern was that this ratio of SSCT excursion and tendon motion decreased (shear index decreases), denoting an adherence between the SSCT and the tendon. Although these studies revealed the abnormal kinematics of the SSCT in patients with CTS, the measurement technique has to be performed during an open CTS surgical procedure to directly identify the SSCT and tendon motion. More recently, a high-resolution ultrasound technique has been used as a noninvasive method to quantify the SSCT motion.[147–149] This technique provides a potential breakthrough to assess the kinematics of SSCT and may become a novel clinical tool for CTS screening, diagnosis, and prognosis.

9.3.2.2 Tendinopathy of Wrist and Hand

The most common tendinopathy in the hand is "trigger finger," although its etiology has not been identified. Flexor tendons, including FDP and FDS tendons in zone II, are enclosed by a narrow synovial sheath, which is reinforced by a pulley system. The function of this pulley system is to prevent the tendon from bowstringing when the fingers flex. The trigger finger is observed to have pathological changes in both the tendon and the first pulley at the flexor sheath entrance (A1 pulley).

Either a narrowed A1 pulley, an enlarged flexor tendon, or a combination of both disturbs the excursion of the tendon through the pulley. It has been speculated that repetitive forceful use of a digit leads to narrowing of the fibrous digital sheath. However, the relationship of trigger finger to work activities is debated. Gorsche et al.[150] investigated the prevalence of the trigger finger in a meat-packing plant with 665 subjects. The point prevalence of trigger finger was 14%. The person-year incidence rate for tool use workers was significantly higher than the non-tool users. They concluded that trigger finger might be associated with powerful hand use. In contrast, Kasdan et al.[151] studied 516 patients with trigger finger and found that there was no relationship between employed patients and

nonemployed patients. The great challenge for these studies is the difficulty in quantitatively assessing the magnitude, frequency, and pattern of the hand use in different patient populations. Moore[1] suggested that repetitive activity somehow causes a noninflammatory degeneration in the tendon or pulley (or both) leading to a trigger finger. Drossos et al.[152] reported that the histologic features of the A1 pulley of trigger digits were correlated with the severity of clinical symptoms. With more severe disease, the gliding surface begins to wear and is gradually replaced by a secondary invasive hyperplasia from the outer layer. Another hypothesized mechanism is that the triggering finger might be developed from tendon ischemia because the tendon node is often observed at the zone II and zone III conjunction, in which the tendon nutrition transitions from an extrinsic blood supply to an intrinsic synovial diffusion.[153] More recently, Tung et al.[154] investigated the mechanical properties of the A1 pulley in all five fingers using human cadaveric hands. Because the ring finger has been clinically reported as the most common affected digit for trigger finger,[155–158] that group suspected that the A1 pulley of the ring finger had the least compliance. However, their results demonstrated that the A1 pulley in the middle finger exhibits the highest stiffness among the five fingers, which did not support the hypothesis (Figure 9.15).[154] Nevertheless, the trigger finger is a clinical orthopaedic disorder initiated by biomechanical factors. The vicious cycle of biomechanics and pathology needs further investigation for this and other disorders of the wrist and hand.

The other common tendinopathy in the upper extremity is de Quervain's disease, which was named after Swiss physician, Fritz de Quervain (1895).[159] It is a painful and debilitating disorder that has also been described as stenosing tenosynovitis, similar to trigger finger but occurs at the first dorsal compartment of the wrist. This compartment consists of the abductor pollicis longus and extensor pollicis brevis tendons enclosed within a synovial sheath passing through a narrow osseofibrous tunnel, which is also similar to the trigger finger. Although de Quervain's disease was initially described as an inflammatory condition, investigations confirmed that inflammatory cells are absent in de Quervain's disease and degeneration of the tendon is present.[160–162] The most common histological findings were tendon sheath fibrotic thickening, an increase in vascularity,

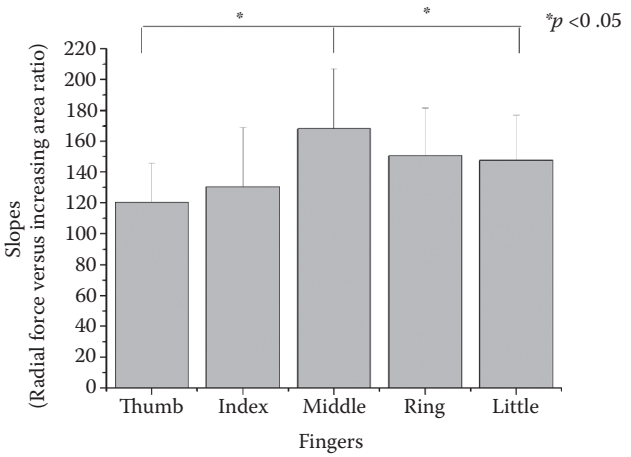

FIGURE 9.15
Mechanical testing of the A1 pulley showed the stiffness of the A1 pulley in the middle finger to be significantly higher (*) than the thumb and small finger A1 pulley. (Reprinted from *Clin. Biomech.*, 25, Tung, W.-L. et al., A comparative study of A1 pulley compliance, 530–534, Copyright 2010, with permission from Elsevier.)

and tendon degeneration.[160,162] However, the etiology of this noninflammatory fibrosis is also unknown. What is known is that forceful and repetitive hand motion is a risk factor for de Quervain's disease. Some studies have demonstrated that the repeated use of a firm grasp, together with ulnar deviation of the wrist, could predispose an individual to de Quervain's disease.[163,164] However, others have reported an association with wrist radial deviation.[165,166] Anatomic factors may play a role in de Quervain's disease, such as a septation between extensor pollicis brevis and abductor pollicis longus tendons in the first dorsal compartment, which has been reported in 24% to 77% of the cases.[167,168] This anatomical feature was observed in every case during surgical treatment,[169–172] which indicated that the septum between two tendons might be associated with the etiology of the de Quervain's disease. Kutsumi et al.[173] investigated the gliding characteristic of the extensor pollicis brevis and abductor pollicis longus tendons within the first dorsal compartment with varied wrist positions using human cadavers. They found that septation within the compartment as well as wrist position combine to affect the gliding resistance of the extensor pollicis brevis. They speculated that a frictionally induced tenosynovitis of the extensor pollicis brevis might be the primary source of pathology in de Quervain's disease.

9.4 Summary

The hand is a useful organ for physical activities, sensitive feedback, and social communications. It is also the first organ that protects the body from injury. Hand traumas and overuse injuries are important clinical problems, including fracture, tendon laceration, and tendonitis. Therefore, understanding hand biomechanics, anatomic structure, and functional kinematics is essential. The carpal bones contain a complex bony geometry, structure, and ligamentous linkages. The intrinsic and extrinsic stability of the hand is still not fully understood. Research into carpal kinematics plays an important role in obtaining the optimal outcomes for carpal instability treatments, either surgical or nonsurgical approaches. Advanced dynamic imaging techniques may provide an important diagnostic approach for this field.

Flexor tendon injuries are common and still present a surgical challenge. Improved outcomes after tendon injury are still a relevant topic for research, requiring strategies developed using multidisciplinary approaches. Hand surgeons must be familiar with several repair techniques that can be used in different conditions and justified in individuals based on each circumstance. Also, hand therapists need to fully understand the injury status, repair techniques, and magnitude of different rehabilitation protocols to balance the relative benefits and risks required to achieve optimal outcomes. Tissue engineering approaches, such as cell or growth factor–based interventions, biological enhancement, and chemical surface modification, provide potentials to improve the clinical outcomes.

The etiology of chronic tendonitis in the hand, including trigger finger and de Quervain's disease, is still unknown. It is generally accepted that mechanical factors are the initiators. However, what the mechanisms are from overuse or repetitive motion to a final pathological change is still not understood. This unknown factor also applies to the CTS, the most common neuropathy in humans. Recent research on SSCT may help define the etiology of CTS and hopefully help find the missing link between repetitive motion or overuse injuries and CTS.

References

1. Moore, J.S. 2000. Flexor tendon entrapment of the digits (trigger finger and trigger thumb). *Journal of Occupational and Environmental Medicine* 42:526–545.
2. Patijn, J., R. Vallejo, M. Janssen et al. 2011. Carpal tunnel syndrome. *Pain Practice* 11:297–301.
3. Roidis, N.T., S.A. Papadakis, N. Rigopoulos et al. 2006. Current concepts and controversies in the management of radial head fractures. *Orthopedics* 29(10): 904–916; quiz 917–918.
4. Manske, P.R. 2005. History of flexor tendon repair. *Hand Clinics* 21:123–127.
5. Glickel, S.Z. 2004. A history of hand surgery in New York City. *Journal of Hand Surgery* 29:774–784.
6. Cobb, T.K., B.K. Dalley, R.H. Posteraro et al. 1992. The carpal tunnel as a compartment. An anatomic perspective. *Orthopaedic Review* 21:451–453.
7. Duffy, F.J., J.G. Seiler, C.A. Hergrueter et al. 1992. Intrinsic mitogenic potential of canine flexor tendons. *Journal of Hand Surgery (Edinburgh, Scotland)* 17:275–277.
8. Landi, A.P., F.P. Altman, J. Pringel et al. 1980. Oxidative enzyme metabolism in rabbit intrasynovial flexor tendons. I. Changes in enzyme activity of the tenocytes with age. *Journal of Surgical Research* 29:276–280.
9. Lundborg, G. 1976. Experimental flexor tendon healing without adhesion formation—a new concept of tendon nutrition and intrinsic healing mechanisms. A preliminary report. *Hand* 8:235–238.
10. Uchiyama, S., P.C. Amadio, J.H. Coert et al. 1997. Gliding resistance of extrasynovial and intrasynovial tendons through the A2 pulley. *Journal of Bone and Joint Surgery. American Volume* 79:219–224.
11. Ettema, A.M., P.C. Amadio, C. Zhao et al. 2004. A histological and immunohistochemical study of the subsynovial connective tissue in idiopathic carpal tunnel syndrome. *Journal of Bone and Joint Surgery. American Volume* 86-A:1458–1466.
12. An, K.-N., R.A. Berger, and W.P. Cooney III, eds. 1991. *Biomechanics of the Wrist*. New York: Springer-Verlag.
13. Crisco, J.J., J.C. Coburn, D.C. Moore et al. 2005. In vivo radiocarpal kinematics and the dart thrower's motion. *Journal of Bone and Joint Surgery. American Volume* 87:2729–2740.
14. Kobayashi, M., R.A. Berger, L. Nagy et al. 1997. Normal kinematics of carpal bones: A three-dimensional analysis of carpal bone motion relative to the radius. *Journal of Biomechanics* 30:787–793.
15. Amadio, P. C., T.H. Berquist, D.K. Smith et al. 1989. Scaphoid malunion. *Journal of Hand Surgery* 14:679–687.
16. Keir, P.J., and R.P. Wells. 1999. Changes in geometry of the finger flexor tendons in the carpal tunnel with wrist posture and tendon load: An MRI study on normal wrists. *Clinical Biomechanics* 14:635–645.
17. Craigen, M.A., and J.K. Stanley. 1995. Wrist kinematics. Row, column or both? *Journal of Hand Surgery (Edinburgh, Scotland)* 20:165–170.
18. Imaeda, T., G. Niebur, W.P. Cooney, 3rd et al. 1994. Kinematics of the normal trapeziometacarpal joint. *Journal of Orthopaedic Research* 12:197–204.
19. Ishikawa, J., W.P. Cooney 3rd, G. Niebur et al. 1999. The effects of wrist distraction on carpal kinematics. *The Journal of Hand Surgery* 24:113–120.
20. Jantea, C., K. An, R. Linscheid et al. eds., 1994. *The Role of the Scapho-Trapezial-Trapezoidal Ligament Complex on Scaphoid Kinematics.* New York: Plenum.
21. Park, M.J., W.P. Cooney, 3rd, M.E. Hahn et al. 2002. The effects of dorsally angulated distal radius fractures on carpal kinematics. *Journal of Hand Surgery* 27:223–232.
22. Wolfe, S.W., and J.J. Crisco. 1994. Mechanical evaluation of the scaphoid shift test. *The Journal of Hand Surgery* 19:762–768.
23. Feipel, V., and M. Rooze. 1999. Three-dimensional motion patterns of the carpal bones: An in vivo study using three-dimensional computed tomography and clinical applications. *Surgical and Radiologic Anatomy* 21:125–131.

24. Goto, A., H. Moritomo, T. Murase et al. 2005. In vivo three-dimensional wrist motion analysis using magnetic resonance imaging and volume-based registration. *Journal of Orthopaedic Research* 23:750–756.
25. Moojen, T.M., J.G. Snel, M.J. Ritt et al. 2002. Three-dimensional carpal kinematics in vivo. *Clinical Biomechanics* 17:506–514.
26. Moritomo, H., T. Murase, A. Goto et al. 2006. In vivo three-dimensional kinematics of the midcarpal joint of the wrist. *Journal of Bone and Joint Surgery. American Volume* 88:611–621.
27. Wolfe, S.W., J.J. Crisco, and L.D. Katz. 1997. A non-invasive method for studying in vivo carpal kinematics. *Journal of Hand Surgery (Edinburgh, Scotland)* 22:147–152.
28. Leng, S., K.D. Zhao, M. Qu et al. 2011. Dynamic CT technique for assessment of wrist joint instabilities. *Medical Physics* 38:1–7.
29. Kokmen, E., R.W. Bossemeyer, Jr., W.J. Williams. 1977. Quantitation of motion perception in the digits: A psychophysical study in normal human subjects. *Annals of Neurology* 2:279–284.
30. Arnauw, G., R. Verdonk, A. Harth et al. 1991. Prosthetic versus tendon allograft replacement of ACL-deficient knees. *Acta Orthopaedica Belgica* 57 Suppl 2:67–74.
31. Wolfe, S.W., J.J. Crisco, C.M. Orr et al. 2006. The dart-throwing motion of the wrist: Is it unique to humans? *Journal of Hand Surgery* 31:1429–1437.
32. An, K.N., E.Y. Chao, W.P. Cooney et al. 1985. Forces in the normal and abnormal hand. *Journal of Orthopaedic Research* 3:202–211.
33. Horii, E. M. Garcia-Elias, K. N. An, A. T. Bishop, W. P. Cooney, R. L. Linscheid, E. Y. S. Chao. 1990. Effect on force transmission across the carpus in procedures used to treat Kienbock's disease. *Journal of Hand Surgery* 15(3): 393–400.
34. Schuind, F., S. Eslami, and P. Ledoux. 2008. Kienbock's disease. *Journal of Bone and Joint Surgery. British Volume* 90:133–139.
35. An, K-N., and W. P. I. Cooney. 1991. Biomechanics. In *Joint Replacement Arthroplasty*, edited by B. F. Morrey, 137–146. New York: Churchill Livingstone.
36. Marzke, M.W., K.L. Wullstein. and S.F. Viegas. 1992. Evolution of the power ("squeeze") grip and its morphological correlates in hominids. *American Journal of Physical Anthropology* 89:283–298.
37. Bao, S., and B. Silverstein. 2005. Estimation of hand force in ergonomic job evaluations. *Ergonomics* 48:288–301.
38. Roberts, H.C., H.J. Denison, H.J. Martin et al. 2011. A review of the measurement of grip strength in clinical and epidemiological studies: Towards a standardised approach. *Age and Ageing* 40:423–424.
39. Richards, L.G., B. Olson, and P. Palmiter-Thomas. 1996. How forearm position affects grip strength. *American Journal of Occupational Therapy* 50:133–138.
40. Mathiowetz, V., C. Rennells, and L. Donahoe. 1985. Effect of elbow position on grip and key pinch strength. *Journal of Hand Surgery* 10:694–697.
41. Su, C.Y., J.H. Lin, T.H. Chien et al. 1994. Grip strength in different positions of elbow and shoulder. *Archives of Physical Medicine and Rehabilitation* 75:812–815.
42. Kung, P.L., P. Chou, R.L. Linscheid et al. 2003. Intrinsic stability of an unconstrained metacarpophalangeal joint implant. *Clinical Biomechanics* 18:119–125.
43. Minami, A., K.N. An, W.P. Cooney, 3rd et al. 1985. Ligament stability of the metacarpophalangeal joint: A biomechanical study. *Journal of Hand Surgery* 10:255–260.
44. Kauer, J.M. 1992. The distal radioulnar joint. Anatomic and functional considerations. *Clinical Orthopaedics and Related Research* 37–45.
45. Palmer, A.K. 1981. Trapezial ridge fractures. *Journal of Hand Surgery* 6:561–564.
46. Horii, E., G.T. Lin, W.P. Cooney et al. 1992. Comparative flexor tendon excursion after passive mobilization: An in vitro study. *Journal of Hand Surgery* 17:559–566.
47. Acosta, R., W. Hnat, and L. R. Scheker. 1993. Distal radio-ulnar ligament motion during supination and pronation. *Journal of Hand Surgery (Edinburgh, Scotland)* 18:502–505.
48. af Ekenstam, F., and C. G. Hagert. 1985. Anatomical studies on the geometry and stability of the distal radio ulnar joint. *Scandinavian Journal of Plastic and Reconstructive Surgery* 19:17–25.

49. Schuind, F., K.N. An, L. Berglund et al. 1991. The distal radioulnar ligaments: A biomechanical study. *Journal of Hand Surgery* 16:1106–1114.
50. Baskies, M.A., and S. K. Lee. 2009. Evaluation and treatment of injuries of the ulnar collateral ligament of the thumb metacarpophalangeal joint. *Bulletin of the NYU Hospital for Joint Diseases* 67:68–74.
51. Fessler, J.F. 1989. Hoof injuries. *Veterinary Clinics of North America. Equine Practice* 5:643–664.
52. Werner, D., S.H. Kozin, M. Brozovich et al. 2003. The biomechanical properties of the finger metacarpophalangeal joints to varus and valgus stress. *Journal of Hand Surgery* 28:1044–1051.
53. Carroll, L.L., A.H. Tzamaloukas, A.E. Scremin et al. 1993. Hand dysfunction in patients on chronic hemodialysis. *International Journal of Artificial Organs* 16:694–699.
54. Gelberman, R.H., S.L. Woo, D. Amiel et al. 1990. Influences of flexor sheath continuity and early motion on tendon healing in dogs [see comment]. *Journal of Hand Surgery* 15:69–77.
55. Benson, M.D., A.S. Cohen, K.D. Brandt et al. 1975. Neuropathy, M components, and amyloid. *Lancet* 1:10–12.
56. Tang, J.B., J. Ryu, and V. Kish. 1997. Scapholunate interosseous ligament sectioning adversely affects excursions of radial wrist extensor and flexor tendons. *Journal of Hand Surgery* 22:720–725.
57. Wehbe, M.A., and J.M. Hunter. 1985. Flexor tendon gliding in the hand. Part I. In vivo excursions. *Journal of Hand Surgery* 10:570–574.
58. Doyle, J.R. 2001. Palmar and digital flexor tendon pulleys. *Clinical Orthopaedics and Related Research* 84–96.
59. Horibe, S., S.L. Woo, J.J. Spiegelman et al. 1990. Excursion of the flexor digitorum profundus tendon: A kinematic study of the human and canine digits. *Journal of Orthopaedic Research* 8:167–174.
60. Brand, P.W., K.C. Cranor, and J.C. Ellis. 1975. Tendon and pulleys at the metacarpophalangeal joint of a finger. *Journal of Bone and Joint Surgery. American Volume* 57:779–784.
61. Goodman, H.J., and J. Choueka. 2005. Biomechanics of the flexor tendons. *Hand Clinics* 21:129–149.
62. Maganaris, C.N. 2000. In vivo measurement-based estimations of the moment arm in the human tibialis anterior muscle-tendon unit. *Journal of Biomechanics* 33:375–379.
63. Manal, K., J.D. Cowder, and T.S. Buchanan. 2010. A hybrid method for computing achilles tendon moment arm using ultrasound and motion analysis. *Journal of Applied Biomechanics* 26:224–228.
64. Yoshii, Y., H.R. Villarraga, J. Henderson et al. 2009. Speckle tracking ultrasound for assessment of the relative motion of flexor tendon and subsynovial connective tissue in the human carpal tunnel. *Ultrasound in Medicine and Biology* 35:1973–1981.
65. Lieber, R., M. Silva, D. Amiel et al. 1999. Wrist and digital joint motion produce unique flexor tendon force and excursion in the canine forelimb. *Journal of Biomechanics* 32:175–181.
66. Panchal, J., S. Mehdi, J.O. Donoghue et al. 1997. The range of excursion of flexor tendons in Zone V: A comparison of active vs passive flexion mobilisation regimes. *British Journal of Plastic Surgery* 50:517–522.
67. Zhao, C., P.C. Amadio, T. Momose et al. 2002. Remodeling of the gliding surface after flexor tendon repair in a canine model in vivo. *Journal of Orthopaedic Research* 20:857–862.
68. Cooney, W.P., K. Weidman, D. Malo et al. 1985. Management of acute flexor tendon injury in the hand. *Instructional Course Lectures* 34:373–381.
69. Lin, G.T., P.C. Amadio, K.N. An et al. 1989. Functional anatomy of the human digital flexor pulley system. *Journal of Hand Surgery* 14:949–956.
70. Silfverskiold, K.L., and E.J. May. 1993. Gap formation after flexor tendon repair in zone II. Results with a new controlled motion programme. *Scandinavian Journal of Plastic and Reconstructive Surgery and Hand Surgery* 27:263–268.
71. Tanaka, T., P.C. Amadio, C. Zhao et al. 2005. Flexor digitorum profundus tendon tension during finger manipulation. *Journal of Hand Therapy* 18(3): 330–338; quiz 338.
72. Zhao, C., P.C. Amadio, M.E. Zobitz et al. 2002. Effect of synergistic motion on flexor digitorum profundus tendon excursion. *Clinical Orthopaedics and Related Research* 223–230.

73. Lin, G.T., K.N. An, P.C. Amadio et al. 1989. Effects of synergistic wrist motion on flexor tendon excursion in the hand. *Journal of Biomechanics* 22:1048.
74. Tanaka, T., P.C. Amadio, C. Zhao et al. 2004. Gliding characteristics and gap formation for locking and grasping tendon repairs: A biomechanical study in a human cadaver model. *Journal of Hand Surgery* 29:6–14.
75. Zhao, C., P.C. Amadio, P. Paillard et al. 2004. Digital resistance and tendon strength during the first week after flexor digitorum profundus tendon repair in a canine model in vivo. *Journal of Bone and Joint Surgery. American Volume* 86-A:320–327.
76. Zhao, C., P.C. Amadio, T. Tanaka et al. 2005. Short-term assessment of optimal timing for postoperative rehabilitation after flexor digitorum profundus tendon repair in a canine model. *Journal of Hand Therapy* 18(3): 322–329; quiz 329.
77. Zhao, C., P.C. Amadio, L. Berglund et al. 2003. A new testing device for measuring gliding resistance and work of flexion in a digit. *Journal of Biomechanics* 36:295–299.
78. Zhao, C., P.C. Amadio, T. Momose et al. 2001. The effect of suture technique on adhesion formation after flexor tendon repair for partial lacerations in a canine model. *Journal of Trauma* 51:917–921.
79. Koff, M.F., K.D. Zhao, C.M. Mierisch et al. 2007. Joint kinematics after thumb carpometacarpal joint reconstruction: An in vitro comparison of various constructs. *The Journal of Hand Surgery* 32:688–696.
80. Kuo, L.C., W.P. Cooney, 3rd, K.N. An et al. 2009. Effects of age and gender on the movement workspace of the trapeziometacarpal joint. *Proceedings of the Institution of Mechanical Engineers. Part H - Journal of Engineering in Medicine* 223:133–142.
81. Kuo, L.C., W.P. Cooney, 3rd, K.R. Kaufman et al. 2004. A quantitative method to measure maximal workspace of the trapeziometacarpal joint—normal model development. *Journal of Orthopaedic Research* 22:600–606.
82. Kuo, L.C., W.P. Cooney, Q.S. Chen et al. 2004. A kinematic method to calculate the workspace of the trapeziometacarpal joint. *Proceedings of the Institution of Mechanical Engineers. Part H–Journal of Engineering in Medicine* 218:143–149.
83. Ateshian, G. A., S.D. Kwak, L. J. Soslowsky et al. 1994. A stereophotogrammetric method for determining in situ contact areas in diarthrodial joints, and a comparison with other methods. *Journal of Biomechanics* 27:111–124.
84. Pellegrini, V.D., Jr. 1991. Osteoarthritis of the trapeziometacarpal joint: The pathophysiology of articular cartilage degeneration. I. Anatomy and pathology of the aging joint. *Journal of Hand Surgery* 16:967–974.
85. Pelligrini, V.D., Jr. 1991. Osteoarthritis of the trapeziometacarpal joint: The pathophysiology of articular cartilage degeneration. II. Articular wear patterns in the osteoarthritic joint. *Journal of Hand Surgery* 16:975–982.
86. Berger, R.A. 1997. The ligaments of the wrist. A current overview of anatomy with considerations of their potential functions. *Hand Clinics* 13:63–82.
87. Howard, F.M., T. Fahey, and E. Wojcik. 1974. Rotatory subluxation of the navicular. *Clinical Orthopaedics and Related Research* 134–139.
88. Jackson, W.T., and J. M. Protas. 1981. Snapping scapholunate subluxation. *The Journal of Hand Surgery* 6:590–594.
89. Adams, B.D., and R. A. Berger. 2002. An anatomic reconstruction of the distal radioulnar ligaments for posttraumatic distal radioulnar joint instability. *Journal of Hand Surgery* 27:243–251.
90. Bickert, B., M. Sauerbier, and G. Germann. 2000. Scapholunate ligament repair using the Mitek bone anchor. *Journal of Hand Surgery (Edinburgh, Scotland)* 25:188–192.
91. Berdia, S., W.H. Short, F.W. Werner et al. 2006. The hysteresis effect in carpal kinematics. *Journal of Hand Surgery* 31:594–600.
92. Jones, W.A. 1988. Beware the sprained wrist. The incidence and diagnosis of scapholunate instability. *Journal of Bone and Joint Surgery. British Volume* 70:293–297.
93. Mehta, J.A., G.I. Bain, and R.J. Heptinstall. 2000. Anatomical reduction of intra-articular fractures of the distal radius. An arthroscopically-assisted approach. *Journal of Bone and Joint Surgery. British Volume* 82:79–86.

94. Destot, E. ed., 1926. *Injuries of the Wrist: A Radiological Study.* New York: FRB.
95. Dobyns, J.H., R.L. Linscheid, E.Y. Chao et al. 1975. Traumatic instability of the wrist. *Instructional Course Lectures* 24:189–199.
96. Berger, R.A. 1996. The gross and histologic anatomy of the scapholunate interosseous ligament. *Journal of Hand Surgery* 21:170–178.
97. Pollock, P.J., R.N. Sieg, M.F. Baechler et al. 2010. Radiographic evaluation of the modified Brunelli technique versus the Blatt capsulodesis for scapholunate dissociation in a cadaver model. *Journal of Hand Surgery* 35:1589–1598.
98. Manuel, J., and S.L. Moran. 2007. The diagnosis and treatment of scapholunate instability. *Orthopedic Clinics of North America* 38:261–277, vii.
99. Moran, S.L., W.P. Cooney, R.A. Berger et al. 2005. Capsulodesis for the treatment of chronic scapholunate instability. *Journal of Hand Surgery* 30:16–23.
100. Stevens, J.C., S. Sun, C.M. Beard et al. 1988. Carpal tunnel syndrome in Rochester, Minnesota, 1961 to 1980. *Neurology* 38:134–138.
101. Atroshi, I. 1999. Results of revision carpal tunnel release. *Journal of Hand Surgery* 24:199–200.
102. Papanicolaou, G.D., S.J. McCabe, and J. Firrell. 2001. The prevalence and characteristics of nerve compression symptoms in the general population. *Journal of Hand Surgery* 26:460–466.
103. Abbas, M.F., R.H. Faris, P.I. Harber et al. 2001. Worksite and personal factors associated with carpal tunnel syndrome in an Egyptian electronics assembly factory. *International Journal of Occupational and Environmental Health* 7:31–36.
104. Atisook, R., M. Benjapibal, P. Sunsaneevithayakul et al. 1995. Carpal tunnel syndrome during pregnancy: Prevalence and blood level of pyridoxine. *Journal of the Medical Association of Thailand* 78:410–414.
105. de Krom, M.C., P.G. Knipschild, A.D. Kester et al. 1992. Carpal tunnel syndrome: Prevalence in the general population. *Journal of Clinical Epidemiology* 45:373–376.
106. Tanaka, S., D.K. Wild, P.J. Seligman et al. 1994. The US prevalence of self-reported carpal tunnel syndrome: 1988 National Health Interview Survey data. *American Journal of Public Health* 84:1846–1848.
107. Armstrong, T.J., W.A. Castelli, F.G. Evans et al. 1984. Some histological changes in carpal tunnel contents and their biomechanical implications. *Journal of Occupational Medicine* 26:197–201.
108. Blanc, P.D., J. Faucett, J.J. Kennedy et al. 1996. Self-reported carpal tunnel syndrome: Predictors of work disability from the National Health Interview Survey Occupational Health Supplement. *American Journal of Industrial Medicine* 30:362–368.
109. Kutluhan, S., G. Akhan, S. Demirci et al. 2001. Carpal tunnel syndrome in carpet workers. *International Archives of Occupational and Environmental Health* 74:454–457.
110. Amadio, P. C. 1987. Carpal tunnel syndrome, pyridoxine, and the work place. *Journal of Hand Surgery* 12:875–880.
111. Levy, M., and M. Pauker. 1978. Carpal tunnel syndrome due to thrombosed persisting median artery. A case report. *Hand* 10:65–68.
112. Amadio, P. C. 1988. Certification in hand surgery: Another view. *Plastic and Reconstructive Surgery* 82:556–558.
113. Barfred, T., and T. Ipsen. 1985. Congenital carpal tunnel syndrome. *Journal of Hand Surgery* 10:246–248.
114. Imran, D., and L.C. Bainbridge. 1999. Carpal tunnel syndrome after distal release of the flexor digitorum profundus and subsequent retraction of the lumbrical muscle into the carpal tunnel. *Journal of Hand Surgery (Edinburgh, Scotland)* 24:303–304.
115. Nakamichi, K., and S. Tachibana. 1998. Histology of the transverse carpal ligament and flexor tenosynovium in idiopathic carpal tunnel syndrome. *Journal of Hand Surgery* 23:1015–1024.
116. Stewart, J.D., and A. Eisen. 1978. Tinel's sign and the carpal tunnel syndrome. *BMJ* 2:1125–1126.
117. Szabo, R.M. 1998. Carpal tunnel syndrome as a repetitive motion disorder. *Clinical Orthopaedics and Related Research* 78–89.
118. Gelberman, R.H., P.T. Hergenroeder, A.R. Hargens et al. 1981. The carpal tunnel syndrome. A study of carpal canal pressures. *Journal of Bone and Joint Surgery* 63:380–383.

119. Lundborg, G., R.H. Gelberman, M. Minteer-Convery et al. 1982. Median nerve compression in the carpal tunnel—functional response to experimentally induced controlled pressure. *Journal of Hand Surgery* 7:252–259.
120. Szabo, R.M., and L. K. Chidgey. 1989. Stress carpal tunnel pressures in patients with carpal tunnel syndrome and normal patients. *Journal of Hand Surgery* 14:624–627.
121. Luchetti, R., R. Schoenhuber, M. Alfarano et al. 1990. Carpal tunnel syndrome: Correlations between pressure measurement and intraoperative electrophysiological nerve study. *Muscle and Nerve* 13:1164–1168.
122. Rojviroj, S., W. Sirichativapee, W. Kowsuwon et al. 1990. Pressures in the carpal tunnel. A comparison between patients with carpal tunnel syndrome and normal subjects. *Journal of Bone and Joint Surgery. British Volume* 72:516–518.
123. Werner, C.O., D. Elmqvist, and P. Ohlin. 1983. Pressure and nerve lesion in the carpal tunnel. *Acta Orthopaedica Scandinavica* 54:312–316.
124. Rempel, D., P.J. Keir, W.P. Smutz et al. 1997. Effects of static fingertip loading on carpal tunnel pressure. *Journal of Orthopaedic Research* 15:422–426.
125. Rempel, D., R. Manojlovic, D.G. Levinsohn et al. 1994. The effect of wearing a flexible wrist splint on carpal tunnel pressure during repetitive hand activity. *Journal of Hand Surgery* 19:106–110.
126. Chell, J., A. Stevens, and T.R. Davis. 1999. Work practices and histopathological changes in the tenosynovium and flexor retinaculum in carpal tunnel syndrome in women. *Journal of Bone and Joint Surgery. British Volume* 81:868–870.
127. Lluch, A.L. 1992. Thickening of the synovium of the digital flexor tendons: Cause or consequence of the carpal tunnel syndrome? *Journal of Hand Surgery (Edinburgh, Scotland)* 17:209–212.
128. Neal, N.C., J. McManners, and G.A. Stirling. 1987. Pathology of the flexor tendon sheath in the spontaneous carpal tunnel syndrome. *Journal of Hand Surgery (Edinburgh, Scotland)* 12:229–232.
129. Scelsi, R., M. Zanlungo, and P. Tenti. 1989. Carpal tunnel syndrome. Anatomical and clinical correlations and morphological and ultrastructural aspects of the tenosynovial sheath. *Italian Journal of Orthopaedics and Traumatology* 15:75–80.
130. Bak, L., S. Bak, P. Gaster et al. 1997. MR imaging of the wrist in carpal tunnel syndrome. *Acta Radiologica* 38:1050–1052.
131. Howe, F.A., D.E. Saunders, A.G. Filler et al. 1994. Magnetic resonance neurography of the median nerve. *British Journal of Radiology* 67:1169–1172.
132. Keberle, M., M. Jenett, W. Kenn et al. 2000. Technical advances in ultrasound and MR imaging of carpal tunnel syndrome. *European Radiology* 10:1043–1050.
133. Maurer, J., A. Bleschkowski, A. Tempka et al. 2000. High-resolution MR imaging of the carpal tunnel and the wrist. Application of a 5-cm surface coil. *Acta Radiologica* 41:78–83.
134. John, V., H.E. Nau, H.C. Nahser et al. 1983. CT of carpal tunnel syndrome. *AJNR: American Journal of Neuroradiology* 4:770–772.
135. Cohen, M.J., and L. Kaplan. 1987. Histology and ultrastructure of the human flexor tendon sheath. *Journal of Hand Surgery* 12:25–29.
136. Kannus, P. 2000. Structure of the tendon connective tissue. *Scandinavian Journal of Medicine and Science in Sports* 10:312–320.
137. Jinrok, O., C. Zhao, P.C. Amadio et al. 2004. Vascular pathologic changes in the flexor tenosynovium (subsynovial connective tissue) in idiopathic carpal tunnel syndrome. *Journal of Orthopaedic Research* 22:1310–1315.
138. Oh, J., C. Zhao, P.C. Amadio et al. 2004. Vascular pathologic changes in the flexor tenosynovium (subsynovial connective tissue) in idiopathic carpal tunnel syndrome. *Journal of Orthopaedic Research* 22:1310–1315.
139. Oh, J., C. Zhao, P.C. Amadio et al. 2005. Immunolocalization of collagen types in the subsynovial connective tissue within the carpal tunnel in humans. *Journal of Orthopaedic Research* 23:1226–1231.

140. Oh, J., C. Zhao, M.E. Zobitz et al. 2006. Morphological changes of collagen fibrils in the subsynovial connective tissue in carpal tunnel syndrome. *Journal of Bone and Joint Surgery. American Volume* 88:824–831.
141. Osamura, N., C. Zhao, M.E. Zobitz et al. 2007. Permeability of the subsynovial connective tissue in the human carpal tunnel: A cadaver study. *Clinical Biomechanics* 22:524–528.
142. Osamura, N., C. Zhao, M.E. Zobitz et al. 2007. Evaluation of the material properties of the subsynovial connective tissue in carpal tunnel syndrome. *Clinical Biomechanics* 22:999–1003.
143. Yamaguchi, T., N. Osamura, C. Zhao et al. 2008. Relative longitudinal motion of the finger flexors, subsynovial connective tissue, and median nerve before and after carpal tunnel release in a human cadaver model. *Journal of Hand Surgery* 33:888–892.
144. Yoshii, Y., C. Zhao, J. Henderson et al. 2008. Effects of carpal tunnel release on the relative motion of tendon, nerve, and subsynovial connective tissue in a human cadaver model. *Clinical Biomechanics* 23:1121–1127.
145. Ettema, A.M., K.N., An, C., Zhao et al. 2008. Flexor tendon and synovial gliding during simultaneous and single digit flexion in idiopathic carpal tunnel syndrome. *Journal of Biomechanics* 41:292–298.
146. Ettema, A.M., C. Zhao, P.C. Amadio et al. Gliding characteristics of flexor tendon and tenosynovium in carpal tunnel syndrome: A pilot study. *Clinical Anatomy* 2007;20:292–299.
147. Ettema, A.M., M. Belohlavek, C. Zhao et al. 2006. High-resolution ultrasound analysis of subsynovial connective tissue in human cadaver carpal tunnel. *Journal of Orthopaedic Research* 24:2011–2020.
148. Oh, S., M. Belohlavek, C. Zhao et al. 2007. Detection of differential gliding characteristics of the flexor digitorum superficialis tendon and subsynovial connective tissue using color Doppler sonographic imaging. *Journal of Ultrasound in Medicine* 26:149–155.
149. Yoshii, Y., H.R. Villarraga, J. Henderson et al. 2009. Ultrasound assessment of the displacement and deformation of the median nerve in the human carpal tunnel with active finger motion. *Journal of Bone and Joint Surgery. American Volume* 91:2922–2930.
150. Gorsche, R., J.P. Wiley, R. Renger et al. 1998. Prevalence and incidence of stenosing flexor tenosynovitis (trigger finger) in a meat-packing plant. *Journal of Occupational and Environmental Medicine* 40:556–560.
151. Kasdan, M.L., V.M. Leis, K. Lewis et al. 1996. Trigger finger: Not always work related. *Journal of the Kentucky Medical Association* 94:498–499.
152. Drossos, K., M. Remmelink, N. Nagy et al. 2009. Correlations between clinical presentations of adult trigger digits and histologic aspects of the A1 pulley. *Journal of Hand Surgery* 34:1429–1435.
153. Amadio, P. C., P. Frasca, and J. M. Hunter. 1982. Histology and scanning electron microscopy of flexor tendons in trigger finders. *Transactions of the Annual Meeting of the Orthopaedic Research Society* 345.
154. Tung, W-L., C. Zhao, Y. Yoshii et al. 2010. A comparative study of A1 pulley compliance. *Clinical Biomechanics* 25:530–534.
155. Al-Qattan, M.M. 2007. Trigger fingers requiring simultaneous division of the A1 pulley and the proximal part of the A2 pulley. *Journal of Hand Surgery: European Volume* 32:521–523.
156. Bonnici, A.V., and J. D. Spencer. 1988. A survey of 'trigger finger' in adults. *Journal of Hand Surgery (Edinburgh, Scotland)* 13:202–203.
157. Newport, M.L., W.F. Blair, and C.M. Steyers, Jr. 1990. Long-term results of extensor tendon repair. *Journal of Hand Surgery* 15:961–966.
158. Nimigan, A.S., D.C. Ross, B.S. Gan. 2006. Steroid injections in the management of trigger fingers. *American Journal of Physical Medicine and Rehabilitation* 85:36–43.
159. Ilyas, A.M., M. Ast, A.A. Schaffer et al. 2007. de Quervain tenosynovitis of the wrist. *Journal of the American Academy of Orthopaedic Surgeons* 15:757–764.
160. Clarke, M.T., H.A. Lyall, J.W. Grant et al. 1998. The histopathology of de Quervain's disease. *Journal of Hand Surgery (Edinburgh, Scotland)* 23:732–734.

161. Meachim, G., and C. Roberts. 1969. The histopathology of stenosing tendovaginitis. *Journal of Pathology* 98:187–192.
162. Read, H.S., G. Hooper, and R. Davie. 2000. Histological appearances in post-partum de Quervain's disease. *Journal of Hand Surgery (Edinburgh, Scotland)* 25:70–72.
163. Lipscomb, P.R. 1951. Stenosing tenosynovitis at the radial styloid process (de Quervain's disease). *Annals of Surgery* 134:110–115.
164. Wood, M.B., and J.H. Dobyns. 1986. Sports-related extraarticular wrist syndromes. *Clinical Orthopaedics and Related Research* 93–102.
165. Bums, B.H., and V. H. Ellis. 1936. Stenosing tendovaginitis at the radial styloid process. *Lancet* 1:717.
166. Muckart, R.D. 1964. Stenosing tendovaginitis of abductor pollicis longus and extensor pollicis brevis at the radial styloid (de Quervain's disease). *Clinical Orthopaedics and Related Research* 33:201–208.
167. Leao, L. 1958. de Quervain's disease—a clinical and anatomical study. *Journal of Bone and Joint Surgery. American Volume* 40:1063–1070.
168. Mahakkanukrauh, P., and C. Mahakkanukrauh. 2000. Incidence of a septum in the first dorsal compartment and its effects on therapy of de Quervain's disease. *Clinical Anatomy* 13:195–198.
169. Jackson, W.T., S.F. Viegas, T.M. Coon et al. 1986. Anatomical variations in the first extensor compartment of the wrist. A clinical and anatomical study. *Journal of Bone and Joint Surgery. American Volume* 68:923–926.
170. Keon-Cohen, B. 1951. de Quervain's disease. *Journal of Bone and Joint Surgery. British Volume* 33:96–99.
171. Loomis, L.K. 1951. Variations of stenosing tenosynovitis at the radial styloid process. *Journal of Bone and Joint Surgery. American Volume* 33-A:340–346.
172. Witt, J., G. Pess, and R.H. Gelberman. 1991. Treatment of de Quervain tenosynovitis. A prospective study of the results of injection of steroids and immobilization in a splint. *Journal of Bone and Joint Surgery. American Volume* 73:219–222.
173. Kutsumi, K., P.C. Amadio, C. Zhao et al. 2005. Gliding resistance of the extensor pollicis brevis tendon and abductor pollicis longus tendon within the first dorsal compartment in fixed wrist positions. *Journal of Orthopaedic Research* 23:243–248.

10

Lower Limb Structure, Function, and Locomotion Biomechanics

William R. Ledoux and Michael E. Hahn

CONTENTS

10.1 Introduction

The lower extremities, each composed of a thigh, leg, and foot for the purposes of this chapter, are the primary mechanisms by which humans maintain upright posture and move their bodies. During quiet stance, they support the body with subtle anterior/posterior and medial-lateral movements, whereas during locomotion, they guide the body through a complex mechanism of weight transfer, ground impact, and propulsion. Within

each lower extremity are three major joints, namely, the hip, knee, and ankle, as well as numerous smaller joints, most of which are in the foot. In this chapter, we review the lower extremities by first summarizing the relevant anatomy, then describing the structure and function of the lower limb, and then providing more details of locomotion biomechanics.

10.2 Anatomy of Lower Limb

This section is a brief overview of the relevant anatomical structures of the lower limb. It is not intended to be all-encompassing, and we invite the reader to examine other more detailed references.[1–3]

10.2.1 Hip

The hip joint is formed by an articulation between the acetabulum of the pelvis and the head of the femur (Figure 10.1). The acetabulum is a concave structure generally oriented anteriorly, laterally, and inferiorly with respect to the main body of the pelvis. The femoral head is essentially spherical in shape, located superior, medial, and anterior to the main body of the femur due to the oblique orientation of the femoral neck. The joint is cushioned by a relatively thick articular cartilage on the superior aspect of the acetabulum, but has a conversely thinner articular cartilage on the femoral head. The acetabular labrum is a fibrocartilage ring, stabilizing and surrounding all but the inferior rim of the acetabulum. Superficial to the labrum is the hip joint capsule, consisting of two unique layers of collagen fibers. One layer forms a tube running longitudinally from the bone tissue surrounding the acetabular labrum distally and laterally to the intertrochanteric crest and line. The other layer is more annular in structure, forming a set of bands running circumferentially about the femoral neck. The multilayered joint capsule of the hip provides a robust system to limit excessive ranges of motion. There are three major ligaments superficial to the joint capsule (Figure 10.1). The iliofemoral and pubofemoral ligaments span the anterior aspect of the joint primarily, limiting the extent of abduction, adduction, and extension. The ischiofemoral ligament spans the posterior and superior aspects of the joint, limiting adduction and extension. The ischiofemoral ligament has a unique design, with fibers arranged in both a linear and spiral configuration. The spiral configuration provides a natural spring tension when the joint is taken into extension, thus providing a form of passive energy storage, which helps return the joint to its neutral orientation. Lastly, the ligamentum teres lies within the joint capsule, spanning the gap between the fovea of the femoral head and the inferior aspect of the acetabulum. The ligamentum teres does not provide much structural support to the joint, but rather serves as a protective sheath for the acetabular branch of the obturator artery.

The variety of muscular functions necessary for complex hip movement and whole body support during locomotion requires substantial muscular redundancy and diversity of function. The musculature of the hip may be grouped into six functional categories, with several muscles providing secondary support in more than one plane of motion. For sagittal plane control, there are hip flexors and extensors. The flexor group includes the iliopsoas, sartorius, rectus femoris, and the tensor fascia latae (a minor contributor). The extensor group includes the gluteus maximus as well as the hamstrings, which consist of the biceps femoris, semitendinosus, and semimembranosus. For coronal plane control, there are abductors and adductors. The abductor group consists of the gluteus medius and

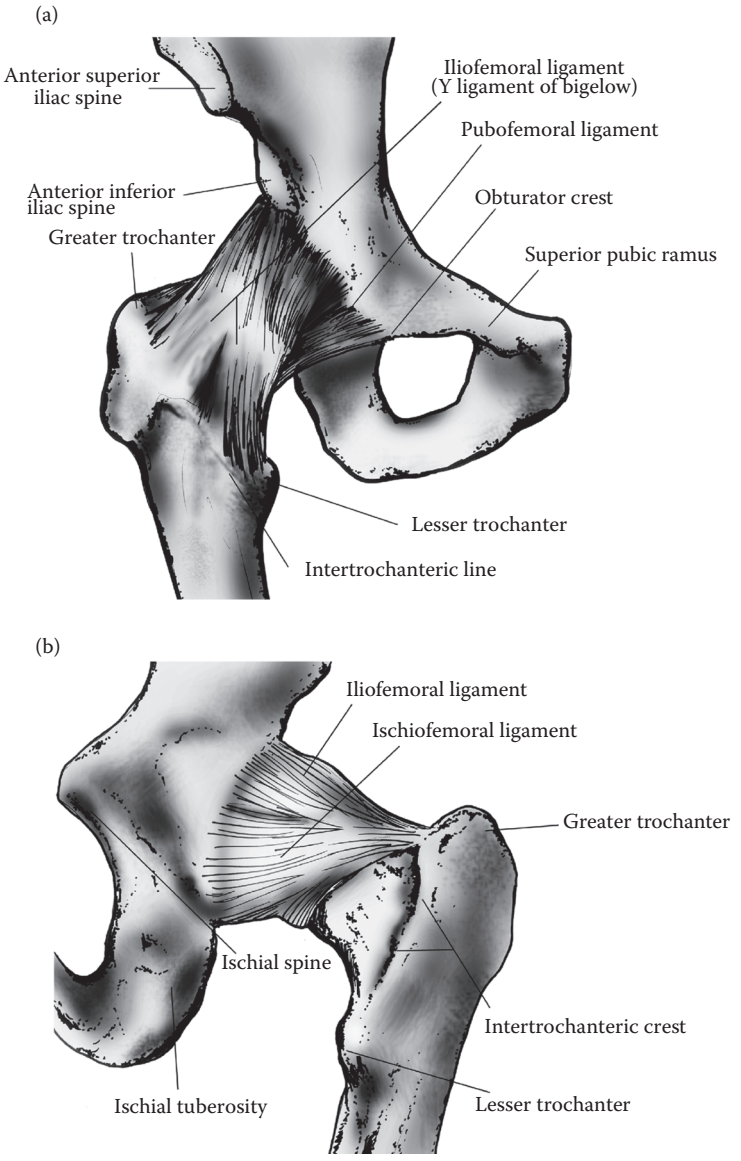

FIGURE 10.1
Sketch of the hip joint, including anterior (a) and posterior (b) views of the primary bony and ligamentous structures.

minimus, as well as the tensor fascia latae, whereas the sartorius provides a minor contribution. The adductor group includes the adductor brevis, longus, and magnus, as well as the pectineus and gracilis. For transverse plane control, there are internal and external rotators. The internal rotator group consists of the gracilis, semitendinosus, and semimembranosus, and minor position-specific contributions come from the gluteus medius, minimus, and the tensor fascia latae. Lastly, the external rotator group includes six muscles solely dedicated to providing external rotator function, including the piriformis, gemellus superior and inferior, obturator internus and externus, and the quadratus femoris.

10.2.2 Knee

The knee joint is formed by the articulation between the femur, tibia, and patella (Figure 10.2). The femoral articular surface consists of discrete features—a medial and lateral condyle, as well as an anterior patellar groove. The articular features of the tibia are also termed the medial and lateral condyle and are separated by the intercondylar eminence (a double ridge of nonarticular bone, the significance of which is discussed later). The articular surface of the patella is simply its posterior face, with two distinct facets that articulate with the surfaces of the patellar groove on the femur. Articular cartilage covers all aspects of the articular surfaces. Additional cushion, support, and stability are provided by a medial and lateral set of menisci attached to the tibial condyles. The menisci form a higher profile supporting the ring around the outer edge of each tibial condyle, leaving the center area clear for articular cartilage loading. The knee joint capsule surrounding the tibiofemoral articulation is not as fibrous as the hip capsule, providing more mobility at the expense of intrinsic stability. The anterior cruciate connects the posterior–medial aspect of the lateral femoral condyle to the anterior portion of the intercondylar eminence. The posterior cruciate connects the anterior–lateral aspect of the medial femoral condyle to the posterior aspect of the tibia, approximately 1 cm distal to the joint line (generally known as the popliteal fossa). The anterior and posterior cruciate ligaments provide passive resistance

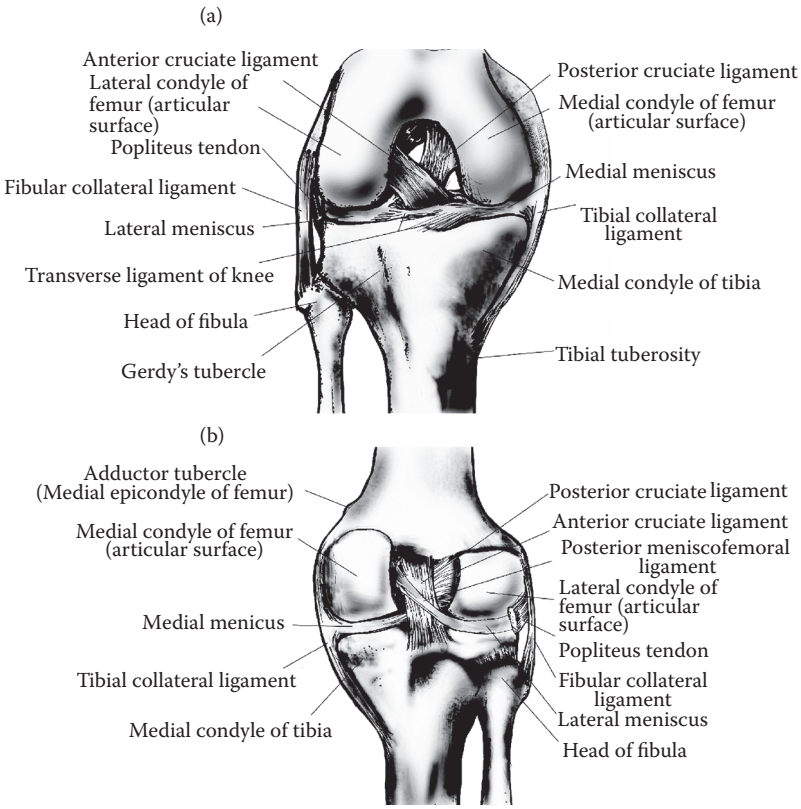

FIGURE 10.2
Sketch of the knee joint, including anterior (a) and posterior (b) views of the femoral, tibial, and ligamentous structures. The patella was removed to allow a full anterior view.

to anterior and posterior translation as well as to internal-external rotation. The medial collateral (or tibial collateral) connects the medial femoral condyle, slightly superior and posterior to the adductor tubercle, to the medial aspect of the tibia, approximately 4 to 5 cm distal to the joint line. The lateral (or fibular collateral) collateral connects the lateral femoral epicondyle, just anterior to the origin of the lateral head of the gastrocnemius, to the head of the fibula, sharing a common insertion with the biceps femoris tendon. The medial and lateral collateral ligaments primarily provide passive resistance to valgus and varus motion, respectively. They may also provide some support to the resistance of internal-external rotation. The last major component of the knee joint system is the patellar tendon, which connects the inferior pole of the patella to the tibial tuberosity. It transfers the quadriceps muscle tension to the anterior surface of the tibia, generating an extensor moment.

There are two major muscle groups that affect the knee: the extensors and the flexors. The extensors are commonly referred to as the quadriceps muscle group, consisting of the rectus femoris and the vastus lateralis, medialis, and intermedius. The flexor group includes the hamstrings (biceps femoris, semitendinosus, and semimembranosus) as the primary movers and the sartorious, gracilis, and popliteus as secondary, assisting muscles. The gastrocnemius can act as a flexor as well, when the limb is not supporting the body's weight.

10.2.3 Foot and Ankle

Excluding the tibia and fibula, there are 28 bones in the foot (Figure 10.3); together, both feet make up more than one quarter of all the bones in the human body. These bones are divided into three groups: tarsals, metatarsals, and phalanges. The tarsal bones include the calcaneus, talus, navicular, cuboid, and the three cuneiforms (medial, intermediate, and lateral). The hindfoot consists of the calcaneus and talus, whereas the navicular, cuboid, and cuneiforms make up the midfoot (Figure 10.3). There are 5 metatarsals and 14 phalanges, which together are known as the forefoot, as well as 2 sesamoids beneath the head of the first metatarsal in the tendon of the flexor hallucis brevis.

The talus, arguably the central and most important bone of the foot, interfaces directly with the lower leg (via the tibia and fibula) and the midfoot (via the navicular) and indirectly with the ground (via the calcaneus); it is a major component of three critical foot joints (talocrural, talocalcaneal, and talonavicular, discussed below) and, as such, is integral to motion in all three cardinal planes. The calcaneus, or heel bone, normally strikes the ground first during walking; its position during weight-bearing often dictates how the remainder of the foot functions throughout the stance phase. The navicular is a major component of the medial longitudinal arch and is considered the "keystone" of the foot. Finally, the first ray consists of the first metatarsal and the hallux (proximal and distal first phalanges); the body is propelled forward each step by these bones. All the bones of the foot work in conjunction to arrest the impact of walking and to serve as a propulsive platform during late contact gait (discussed below).

There are more than 50 cartilaginous articulations in the foot, ranging from major joints with wide surface areas and large ranges of angular motion to relatively narrow joints that allow for small gliding motions between bones. Because a detailed review is beyond the scope of this chapter, only the major joints will be reviewed.

The talocrural (or ankle) joint is the articulation between the tibia, fibula, and talus (Figure 10.4a and b); the dome of the talus fits into the tibial plafond and is held in place by the medial and lateral malleoli. The primary motion of the ankle joint is dorsiflexion and plantar flexion, with the axis of rotation running approximately from the medial malleolus to the lateral malleolus, declinated approximately 8^{o}[4] and externally rotated approximately

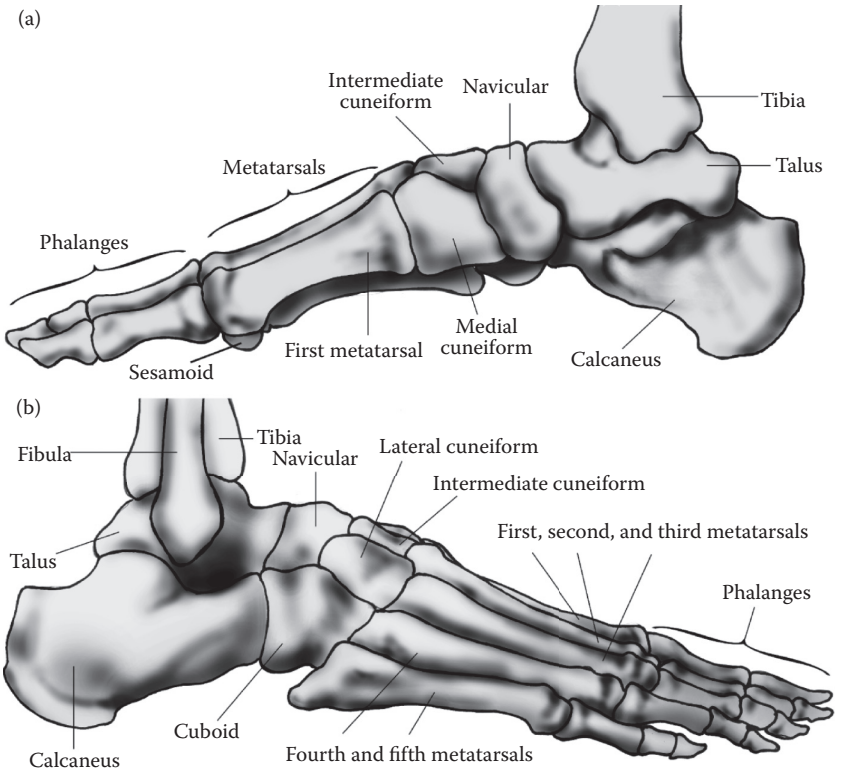

FIGURE 10.3
Medial (a) and lateral (b) views of the bones of the foot and ankle.

20° to 25°.[5] Because the dome of the talus is wider anteriorly, the ankle is most stable when the foot is dorsiflexed. Laterally, the ankle joint is supported by the lateral ligamentous complex, which consists of three ligaments: the anterior talofibular, the posterior talofibular, and the calcaneofibular ligament (Figure 10.5). These ligaments are often injured when a person has an inverting ankle sprain (i.e., inversion of the foot and external rotation of the tibia, as can occur when landing on uneven terrain).[6] Medially, support is provided by the deltoid ligament, which is a broad sheet of ligamentous tissue that has substantial anatomical variation[1] and generally consists of four ligaments: the anterior and posterior tibiotalars, the tibiocalcaneal, and the tibionavicular (Figure 10.5). Finally, the syndesmosis of the tibiofibular joint, or "high ankle" as in a high ankle sprain, is fibrous and not capsular. Very little motion is possible at this joint. The fibula is held to the tibia with three ligaments: the interosseous ligament, the anterior inferior tibiofibular ligament, and the posterior inferior tibiofibular ligament (Figure 10.5).

The talocalcaneal (or subtalar) joint is the complex articulation between the talus and the calcaneus (Figure 10.4b). The calcaneus has several articulations with the talus: the posterior facet, middle facet, and anterior facet. The posterior facet is oval and has its own joint capsule, whereas the middle and anterior facets, which are long and narrow, share a joint capsule with the talonavicular joint. The motion of the talocalcaneal joint ranges from external rotation, dorsiflexion, and eversion to internal rotation, plantar flexion, and

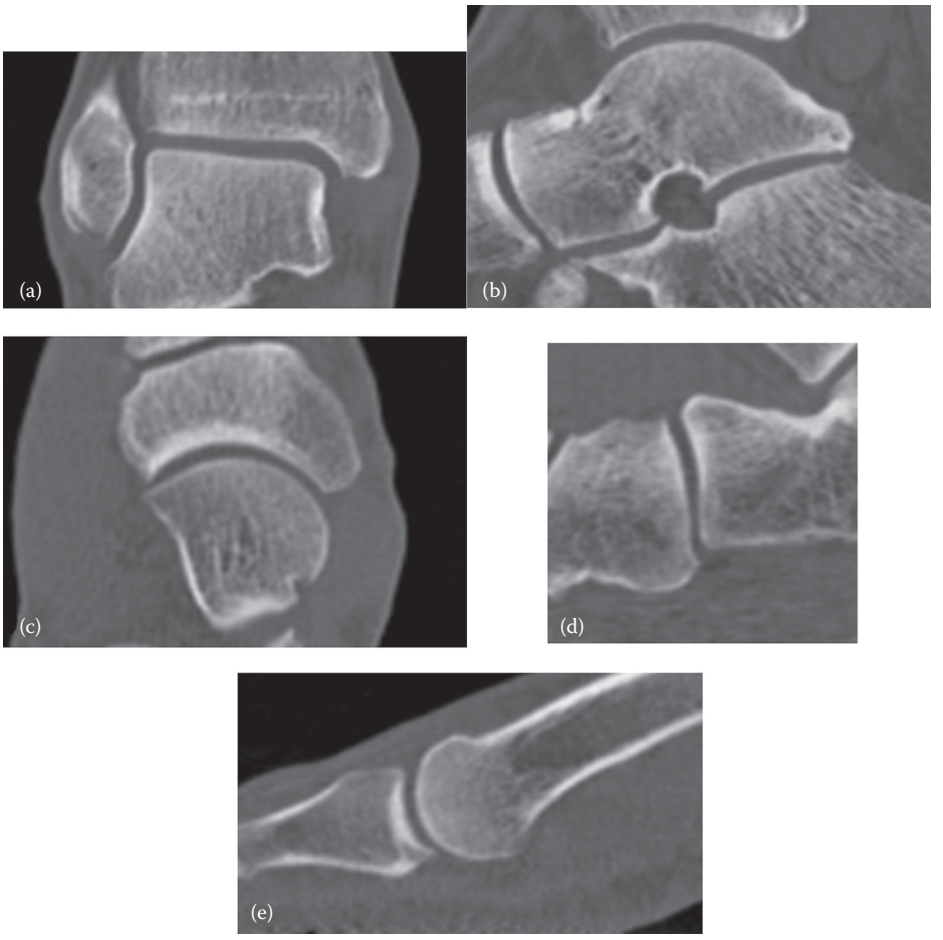

FIGURE 10.4
(a) Anterior view of a coronal plane slice of a computed tomography (CT) scan of the talocrural joint. (b) Medial view of a sagittal plane slice of a CT scan of the talocalcaneal, talocrural, and talonavicular joint. (c) Superior view of a transverse plane slice of a CT scan of the talonavicular joint. (d) Medial view of a sagittal plane slice of a CT scan of the calcaneocuboid joint. (e) Medial view of a sagittal plane slice of a CT scan of the first metatarsophalangeal joint.

inversion. The axes of rotation are elevated 42° and internally rotated 23°.[4] The major ligaments that guide the motion of the talus and calcaneus include the extracapsular cervical and interosseous ligaments, as well as the lateral, posterior, and medial talocalcaneal ligaments (Figure 10.5), which are all part of the capsule of the posterior facet.

The talonavicular joint shares a common joint space with the middle and anterior facets of the talocalcaneal joint (Figure 10.4b and c); this combined joint is sometimes referred to as the talocalcaneonavicular joint. The head of the talus is supported by the ovoid surface of the posterior navicular and the plantar calcaneonavicular (spring) ligament (Figure 10.5). The axis of rotation of this joint has been estimated as being elevated 38.5° in the sagittal plane and internally rotated 14.1°;[7] as these axes are similar to the subtalar joint, the motion of these two joints is similar. This is expected, given that both joints provide motion relative to the talus. This joint also includes the dorsal talonavicular ligament and the calcaneonavicular portion of the bifurcate ligament, in addition to the aforementioned

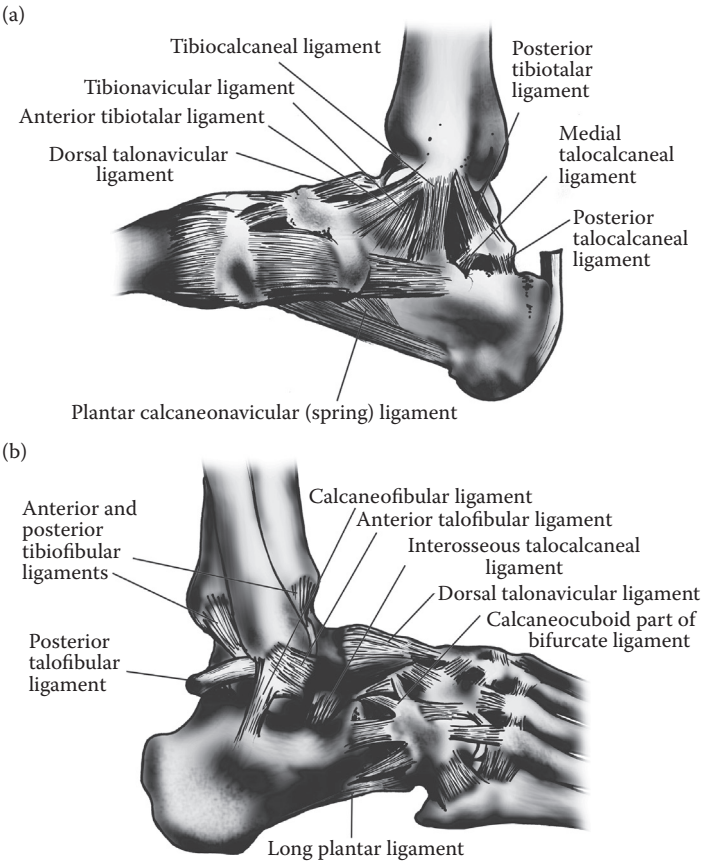

FIGURE 10.5
Medial (a) and lateral (b) views of the ligaments of the foot and ankle.

plantar calcaneonavicular ligament (Figure 10.5). The spring ligament consists of two components, namely, the superomedial and inferior calcaneonavicular ligament, the former of which has a fibrocartilagenous surface that supports the head of the talus.

Without going into the anatomy of ligaments, other joints of note are the calcaneocuboid joint (Figure 10.4d), which is an integral part of the lateral longitudinal arch. Together with the talonavicular joint, this joint makes up the transverse tarsal (midtarsal or Chopart) joint. The tarsometatarsal (or Lisfranc) joint is the articulation between the tarsal bones (the cuneiforms and cuboid) and the five metatarsals. The last joint of interest is the first metatarsophalangeal joint (MTPJ or great toe joint), which is the articulation between the first metatarsal and the first proximal phalanx (Figure 10.4e).

There are 12 extrinsic muscles that originate in the lower limb and insert in the foot. These muscles can be divided into an anterior group (tibialis anterior, extensor hallucis longus, and extensor digitorum longus), a peroneal group (peronius longus, peronius brevis, and peronius tertius), and a posterior group [soleus, gastrocnemius (medial and lateral heads), plantaris, flexor hallucis longus, flexor digitorum longus, and tibialis posterior]. There are too many complex muscle interactions to discuss in this chapter, and thus, only a few of interest will be highlighted here. The gastrocsoleal complex, which is active during late stance, by way of the Achilles tendon, is the primary muscle for plantar flexion. The

tibialis anterior, which is active earlier in the stance to prevent rapid plantar flexion ("foot slap"), is the main dorsiflexor of the foot. The tibialis posterior is the primary inverter of the foot, whereas the peronius brevis is the main evertor; they are both active later in the stance, providing support to the foot via co-contraction. In general, the foot and ankle extrinsic musculature is redundant, especially across the joints of the hindfoot, with multiple muscles having similar functions.

There are two dorsal intrinsic muscles (extensor hallucis brevis and extensor digitorum brevis) that help extend the first through the fourth MTPJs and four layers of plantar intrinsic musculature in the foot that, in general, help support the arch of the foot, but also are able to move specific toes. The first plantar layer consists of the abductor hallucis, flexor digitorum brevis, and abductor digiti minimi; the second layer includes the flexor digitorum accessorius and the lumbricals. The third plantar layer consists of the flexor hallucis brevis, the adductor hallucis, and the flexor digiti minimi brevis, and the fourth layer includes the dorsal and plantar interossei.

In addition to the bones, ligaments, and muscles described previously, there are a few additional specialized anatomical structures in the foot. These include the plantar aponeurosis or fascia, the long plantar ligament, and the plantar soft tissue. The plantar aponeurosis is a ligament-like structure that originates at the plantar surface of the calcaneus, splitting into three components (medial, central, and lateral). The central portion then subdivides into five branches (for each of the metatarsal heads). The insertion is complex, with each portion further subdividing into deep and superficial fibers. The long plantar ligament originates from the plantar surface of the calcaneus deep to the plantar aponeurosis and extends to the cuboid and the bases of the second, third, and fourth metatarsals. This ligament, together with the plantar fascia, helps maintain the longitudinal arch of the foot. The plantar soft tissue covers most of the plantar surface of the foot and is often referred to as the heel pad beneath the calcaneus where it is thickest. It consists of elastic septae that form close-celled chambers of adipose tissue and is integral in distributing loads during ground contact.

10.3 Structure and Function of Lower Limb

Having provided an overview of the anatomy of the lower extremity, we can now expand on this base to discuss various aspects of the structure and function of the major joints.

10.3.1 Hip

Due to the spherical shape of the femoral head and the highly congruent fit of the acetabulum, the hip system is generally thought to act as a ball-in-socket joint, providing three rotational degrees of freedom (DOFs): flexion-extension in the sagittal plane, abduction-adduction in the coronal plane, and internal-external rotation in the transverse plane. Minimal superior translation can occur during full weight-bearing conditions as the articular cartilage is compressed. Translation in other directions is restricted in normal function due to the stiff joint capsule and complex orientation of ligaments crossing the joint. The primary functions of the hip during locomotion can be grouped into three main areas: (1) support of upper body in static and dynamic posture, (2) transmission of force between the pelvis and lower extremities, and (3) position control of the distal leg components during the swing phase of gait.

The shape and positioning of the acetabulum are unique structural features that enable the hip to support the upper body. The acetabulum is oriented to face inferiorly, with the inferior rim positioned more medially and the superior rim more laterally. With respect to a vertical reference line, the acetabular orientation forms an angle of approximately 35° to 40° (Figure 10.6). The angle tends to increase with age. A lower angle results in a greater risk of superior subluxation. Due to the high vertical loads that the hip encounters with every weight-bearing step, this structure is critical to ensure stability. Another bony geometry that provides stability is a natural acetabular anteversion, in which the acetabulum faces anteriorly. With respect to the coronal plane, this angle is approximately 20° to 30°. As the angle decreases, there is an increased risk of anterior subluxation. Additional stability is provided by the acetabular labrum, a stiff cuff of fibrocartilage material that serves to deepen the socket, increasing contact with the femoral head and augmenting the overall stability of the hip joint system.

From the femoral head to the main longitudinal shaft of the femur, the femoral neck is oriented in a manner suited to an ideal balance between force transfer and dissipation. The femoral neck forms an angle of approximately 125° with respect to the long axis of the femur, positioning the femoral head in a position and orientation to efficiently articulate with the acetabulum (Figure 10.6). A larger angle (making a more vertical system overall) would transmit too much vertical force, and a smaller angle (closer to a right angle system) would dissipate too much force, causing excessive bending moments in the femoral neck.

In combination with the angulation of the femoral neck, the bones of the pelvis and femur have a unique alignment of internal trabecular structures that help transfer weight-bearing forces from the femoral shaft, through the femoral neck, across the acetabular

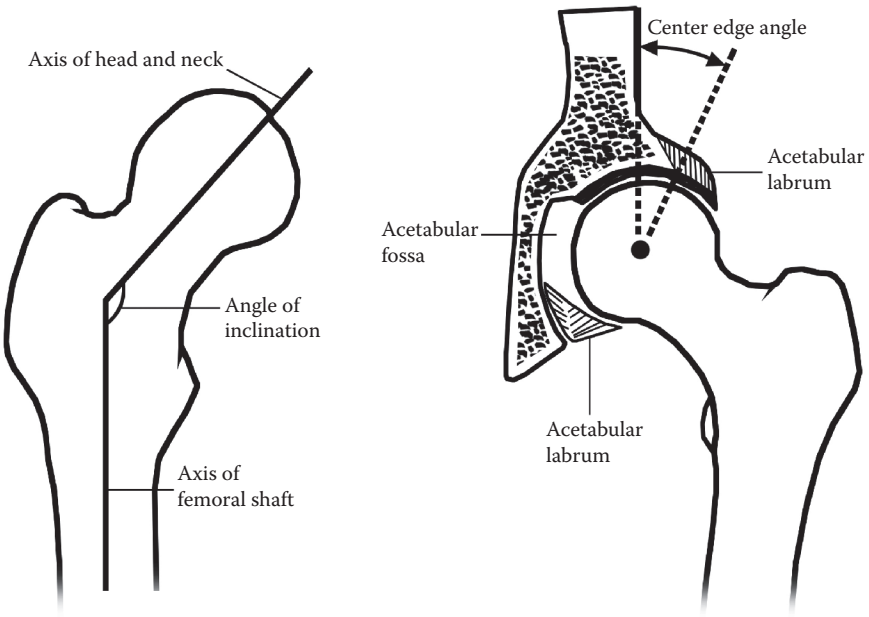

FIGURE 10.6
Sketch of two structurally important coronal plane angles formed by the geometry of the pelvis and femur; the femoral neck orientation angle (angle of inclination) on the left, and the acetabulum orientation (center edge) angle on the right.

articulation, and then through the pelvic rami to finally articulate with the sacrum. The unique structures of the femur and pelvis allow for an ideal scenario in which forces much larger than body weight can pass through critical bony tissue and be dissipated in a manner that reduces potentially injurious stress.[8,9]

The hip joint functions to position the lower limb in a manner appropriate for maintaining forward progression during gait, providing the base of support necessary for the limb to provide overall stability and stance phase control. To do this, the hip muscles produce a substantial flexor moment during the last stage of stance phase, generating enough power to move the thigh anteriorly into swing phase. The hip power generated during this push-off stage is augmented by a large ankle plantar flexor moment and power generation. Together, these two joints serve to raise the lower extremity and move it to a more anterior position. Through the last stage of swing phase, the hip must perform a braking task, decelerating the swinging limb in preparation for a foot strike, leading into the next stance phase. This is performed by an eccentric contraction by the extensor muscle group (hamstrings), generating a substantial extensor moment and subsequent power absorption phase. The ability of the hip musculature to modulate hip flexion during the swing phase is one of the hallmarks of able-bodied gait. Many of the asymmetries visually observed in clinical populations can be explained by an imbalance between the hip flexor and extensor muscle groups and the timing of their respective contractions.

10.3.2 Knee

The knee joint is often thought to have only 2 DOFs: flexion-extension in the sagittal plane and internal-external rotation in the transverse plane. However, due to the shape of the femoral condyles and the forces exerted by the knee flexors and extensors, there is also a translational DOF (anterior/posterior) as the knee moves through the full range of flexion and extension. The combination of anterior/posterior translation and flexion-extension is commonly termed the "roll back" phenomenon. Associated with this phenomenon is the observation that the knee joint axis is not a fixed pin system but rather an instantaneous center of rotation. The motion of this axis has been calculated using a finite helical axis (FHA) during passive joint motion[10] and during running.[11] Position of the instantaneous center of rotation during running has been reported to move by as much as 20 mm posteriorly, 10 mm distally during the flexion phase of stance, and 10 to 20 mm in the posterior and proximal directions after peak knee flexion.[11]

Another combined motion that is unique to the knee system is often termed the "screw home" mechanism. This motion is defined by a transverse plane rotation between the tibia and femur that occurs automatically between full extension and approximately 20° of knee flexion. Due to the different radii of curvature and the size difference between the two femoral condyles, when the knee is flexed, the tibia internally rotates slightly, and when the knee is extended, the tibia externally rotates back into what is considered the "home" position. This motion occurs most easily in an open kinetic chain system (i.e., no ground contact) but can also be observed during cyclic flexion-extension motions like those experienced during gait and the pedaling motion of cycling. The primary functions of the knee joint during locomotion can be grouped broadly into body weight support during dynamic posture and swing limb control to facilitate safe walking and gait cycle initiation.

The articular surfaces of the femur and tibia are not fully congruent. In the sagittal plane, the femoral condyles have variable radii of curvature, increasing in radius from the anterior edge to the posterior edge of the articular surface. In the coronal plane, the medial and lateral condyles have a more uniform, singular radius of curvature. The concave structure

of each tibial condyle has a much larger radius of curvature than the femoral condyles, creating inadequate congruency between the two articulating structures. This incongruence can decrease the stability of the joint system. The medial and lateral menisci provide a greater articulating surface to enhance joint congruency and thus stability. Further enhancement of stability is achieved by the menisci's attachment to a variety of structures in the knee system. The menisci share some attachment sites, such as the intercondylar tubercles of the tibia, the tibial condyles via the coronary ligaments (posterior aspect of the tibia), the patella via the patellomeniscal ligaments, and the transverse ligament (anterior aspect of the tibia). Additionally, each meniscus also has a unique set of attachment sites. The medial meniscus attaches to the medial collateral ligament and the semimembranosus tendon. The lateral meniscus attaches to the posterior meniscofemoral ligament, the posterior cruciate ligament, the popliteus tendon, and occasionally, the anterior cruciate ligament. All these attachments allow the meniscal tissue to serve as a unique hub, or anchor, to assist in maintaining the stability of the knee.

The menisci are believed to absorb approximately 40% to 60% of the load crossing the knee joint during locomotion.[12–14] Depending on the intensity of locomotion, the loads across the knee can reach up to six times the body weight (e.g., during running). Based on the amount of articular surface available and the geometry of the articular structures, laboratory observations have estimated that the stresses on the tibiofemoral articulation would increase by three to five times if the menisci are removed.[12–14] The increased local stress on the articular cartilage substantially increases the probability of early onset osteoarthrosis and subsequent progression of osteoarthritis in the knee system.

One of the major functions of the knee is to provide sufficient extensor moment to sustain standing posture and stability during locomotion. If the quadriceps tendon were to insert at the tibial tuberosity without first crossing the patella, the angle of insertion would be quite low, and the perpendicular distance between its line of action and the knee joint center would be greatly reduced. By inserting the patella into the system, the quadriceps tendon must traverse this bone, which increases the angle of insertion and subsequently increases the moment arm of the system. Thus, the knee system can produce a greater extensor moment without having to increase the contractile tension of the quadriceps muscle group. This patellofemoral tendon insertion angle-moment arm relationship is not fixed but is a dynamic system. As the knee becomes more flexed, the patellar groove deepens, allowing the patella to reduce slightly to the posterior. This minor change in position reduces the functional moment arm of the quadriceps tendon, thereby reducing the resulting extensor moment.

10.3.3 Foot and Ankle

The foot and ankle provide a basis of support for the body during posture and locomotion. In quiet stance, approximately one-half of the body weight is distributed through each foot, but due to the acceleration of the center of mass (COM) of the body, forces greater than body weight are borne beneath the foot with each step during walking.[15] Due to muscle co-contraction, ankle joint forces can be nearly five times the body weight after heel off.[16] With its complex structure of bones, joints, muscles, tendons, ligaments, and fat pads, the foot is able to achieve a wide variety of functions over the large ranges of forces that it bears. For instance, the energy of initial impact followed by weight acceptance is attenuated by the structures of the foot; the heel pad serves as a mechanical filter for the high frequency of impact, whereas the motion of the joints of the foot helps provide a smooth landing when body weight is applied to each limb. Even still, later in the stance phase during push off, the multiple bones and soft tissue structures of the foot are able to maintain a firm structural platform for support.

10.3.3.1 Motion of the Joints of Foot and Ankle

The joints of the foot allow motion in the three cardinal planes, although rotations in the sagittal and coronal planes are larger than the transverse. When nonweight-bearing, the foot can move from maximal plantar flexion, inversion, and internal rotation to maximal dorsiflexion, eversion, and external rotation (Figure 10.7).[17] Of course, the foot's primary function is to interface with the ground while standing and walking. Therefore, its behavior during weight-bearing motion is of greater interest. From the instant the heel contacts the ground, through midstance when both the hindfoot and the forefoot are weight-bearing, to toe-off when just the great toe is touching, the foot joints move through an intricate set of motions. Although numerous technologies are now available for motion analysis (see Section 10.4), we focus here on bone pin studies that have been conducted on cadavers[18] and living subjects.[19]

Before heel strike, to allow for foot clearance during swing phase, the talocrural joint is dorsiflexed with the anterior extrinsic muscle group firing. Immediately after heel strike, the talocrural joint plantar flexes rapidly, but the eccentric contraction of the anterior muscles prevents the forefoot from rapidly hitting the ground. At the same time, the talocalcaneal and talonavicular joints, and to a lesser extent, the calcaneocuboid joint, are everting. These motions allow for the relatively gentle interaction between the foot and ground by partially absorbing the energy of heel strike. Once the forefoot comes in contact with the ground, body weight is distributed more anteriorly. The talocrural joint dorsiflexes as the tibia rotates anteriorly, whereas the foot in general dorsiflexes (i.e., the arch is getting lower), as seen at the talonavicular and first metatarsal–medial cuneiform joints and from the first metatarsal relative to the calcaneus and talus. Later in midstance, the gastrocsoleal complex becomes active. Once heel off occurs, most of the foot begins to plantar flex at the talocrural, talocalcaneal, talonavicular, and calcaneocuboid joints, whereas the first MTPJ continues to dorsiflex. At the same time, the talocalcaneal, talonavicular, and calcaneocuboid joints all begin to invert. Furthermore, most of the transverse plane motion

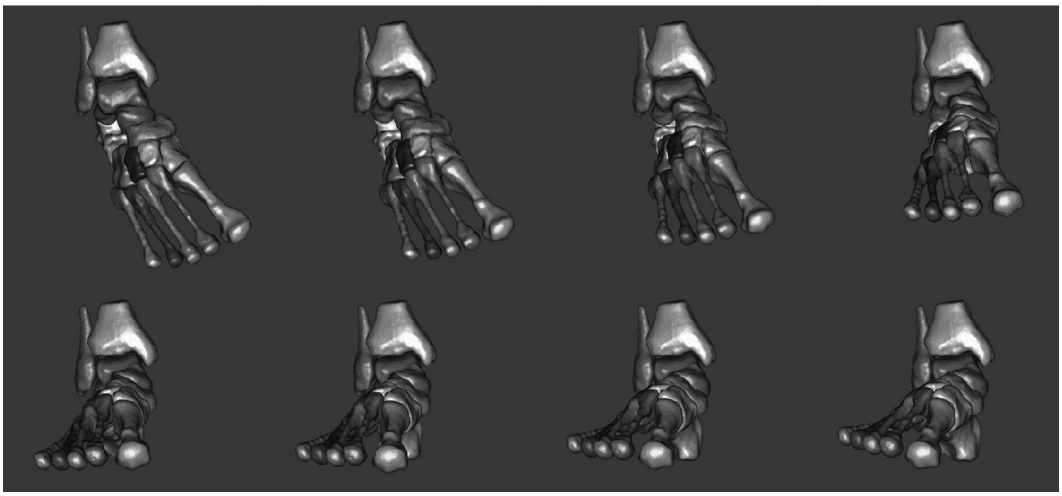

FIGURE 10.7
(See color insert.) Neutrally aligned foot in eight positions.[17] From top left to bottom right: from maximal plantar flexion, inversion, and internal rotation to maximal dorsiflexion, eversion, and external rotation. Neutral position is the bottom left position. (Reprinted with permission from the American Society of Mechanical Engineers.)

of the foot takes place in the last 20% of the stance when most of the joints, including the talocalcaneal, talonavicular, and first metatarsophalangeal, as well as the first metatarsal relative to the talus and calcaneus, are adducting. This complex series of motions is then repeated with each step.

10.3.3.2 Arch of the Foot: Windlass Mechanism and Midtarsal Joint Locking

Beginning at the calcaneus and extending through the talus, navicular, and to the metatarsals, the bones of the foot form an arch that is held upright by passive soft tissue structures (including the plantar aponeurosis, the long plantar ligament, and numerous other plantar ligaments) and active musculature (the tibialis posterior and intrinsic musculature). As two examples of foot arch function, we will discuss the windlass mechanism and the concept of midtarsal joint locking.

The windlass mechanism was first described by Hicks,[20] who noted that when the great toe was extended, the effect was a pull on the plantar pad that lies inferior to the head of the first metatarsal. This, in turn, pulled on the plantar aponeurosis, which effectively shortened the distance between the head of the first metatarsal and the calcaneus, leading to an increased arch height. The windlass mechanism can easily be observed by putting your foot flat against the floor and looking at the medial longitudinal arch while manually extending the great toe. The arch of the foot will get higher. Hicks also noted that this mechanism functions with every step as the great toe is extended during push off. He speculated that the increased arch height seen during push off is not the result of any musculature, but rather the passive generation of tension in the plantar aponeurosis. The windlass mechanism has been further studied; using a cadaver model, Thordarson et al.[21] demonstrated that sequentially cutting the plantar fascia decreased the ability of great toe dorsiflexion to shorten the arch. *In vivo* studies have also quantified that passive great toe dorsiflexion does raise arch height,[22] and that diabetic subjects have thicker plantar fascia, which leads to an early windlass mechanism (i.e., increased tension).[23] More recently, Wilken et al.[24] have found evidence of the windlass mechanism using a five-segment kinematic foot model in living subjects; when first metatarsophalangeal dorsiflexion occurred in late stance, there was also calcaneal inversion as well as forefoot plantar flexion and adduction. Interestingly, although not as explicitly discussed as the windlass mechanism, these exact motions were also seen in a recent cadaveric foot motion analysis study.[18]

Midtarsal joint locking is a second functional aspect of the foot arch. This was first presented by Elftman[25] in the context of describing the changing axes of rotation of the calcaneocuboid and talonavicular joints. Midtarsal joint unlocking occurs when the foot is dorsiflexed, everted, and externally rotated (e.g., at heel strike), causing the axes of rotation of the midtarsal joint to align and allowing the foot to become more flexible. Later in the stance phase, when the heel is off the ground and the foot is plantar flexed, inverted, and internally rotated, the axes of rotation of the midtarsal joint are less aligned and the foot is stiffer. As such, the foot is able to adapt to uneven surfaces at weight acceptance, yet functions as a stiff platform during propulsion. In a nonweight-bearing study that investigated midtarsal joint locking, Blackwood et al.[26] quantified the effect of hindfoot coronal plane position on the motion of the forefoot in the sagittal plane. When the calcaneus was everted, the range of motion of the metatarsals from peak dorsiflexion to peak plantar flexion was significantly greater than when the calcaneus was inverted. Although the effects of the foot musculature and the weight of the body were not accounted for, this study provides insight into the effect of the passive midtarsal joint characteristics on the allowable motion of the forefoot. A final note on this concept is that perhaps "locking" is

not the best choice of words because the midtarsal joint does not literally lock but rather becomes stiffer.

10.3.3.3 Foot Type

Any discussion of foot structure and function would be incomplete without mentioning the concept of foot type. Although feet come in varying lengths and widths, they can, for the most part, be classified into one of three categories: pes cavus (high arched), neutrally aligned, or pes planus (low arched or flatfoot; Figure 10.8). Cavus feet often have an inverted hindfoot and an adducted forefoot in addition to a high arch; planus feet often have an everted hindfoot and an abducted forefoot, although in neither case are these rotations absolute. Neutrally aligned feet, as the name implies, have a neutrally positioned hindfoot and forefoot. This is not to say that neutrally aligned feet are "normal" and the others are not because there are many feet that have increased or decreased arch height and still function normally and are asymptomatic. Of course, in extreme cases, the function of cavus and planus feet breaks down. Specifically, severely deformed feet are not able to achieve the normal ranges and patterns of motion necessary to attenuate forces during weight acceptance and to properly provide a basis of support during push off. Cavus feet are often stiff, and the arch is not able to relax when loaded; thus, the forces experienced

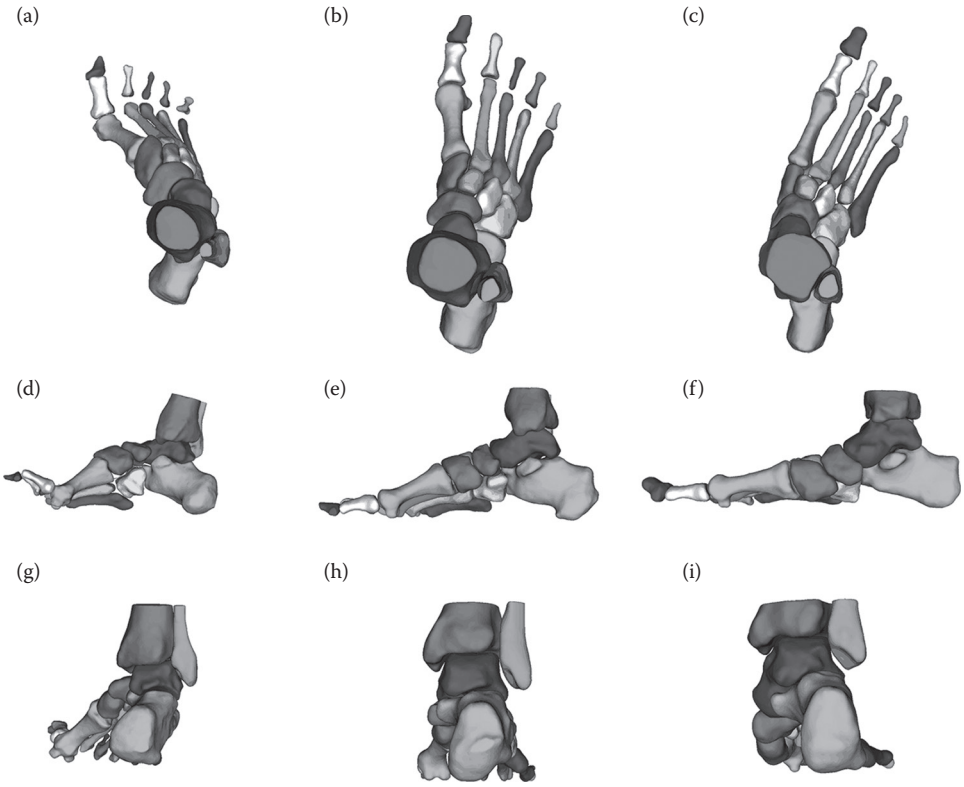

FIGURE 10.8
(See color insert.) Pes cavus (a, d, and g), neutrally aligned (b, e, and h), and pes planus (c, f, and i) foot types. Right foot, transverse plane superior view (a, b, and c), sagittal plane medial view (d, e, and f), and coronal plane posterior view (g, h, and i).

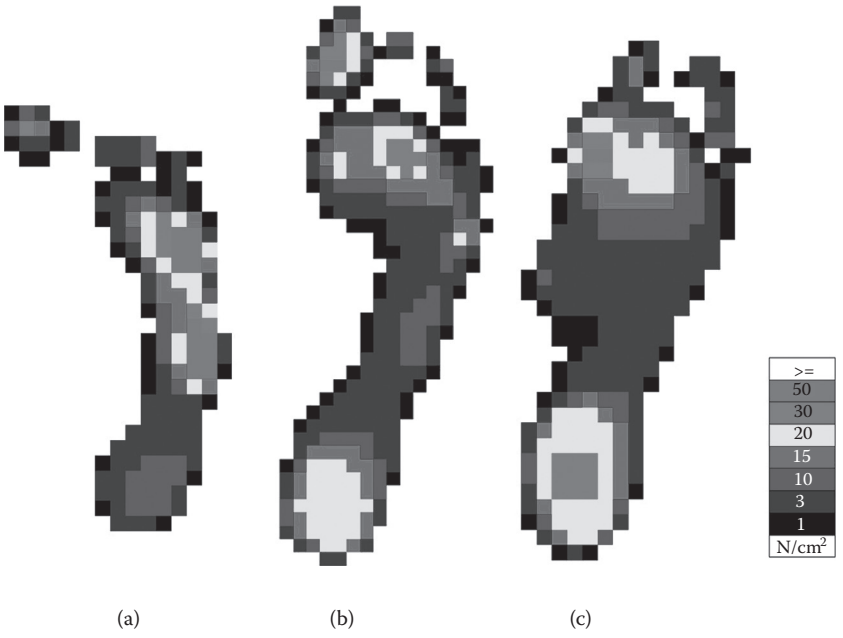

FIGURE 10.9
(See color insert.) Distribution of plantar pressure for pes cavus (a), neutrally aligned (b), and pes planus (c) subjects. The cavus subject bears load on the lateral side of the foot, specifically on the base and head of the fifth metatarsal. The neutrally aligned subject bears load through the second metatarsal and the great toe. The planus subject bears load through the first metatarsal head.

at heel strike are not dissipated properly. Planus feet are often too relaxed when loaded, particularly in push off, leading to aberrant motion in which some joints are forced to function at their extreme end range of motion. Additionally, cavus feet have a more lateral load distribution, whereas planus feet have a more medial load distribution (Figure 10.9). All these aberrant loading conditions can potentially lead to the development of arthritis because joints are loaded at nonphysiological forces and moments.

10.4 Locomotion Biomechanics

We have reviewed the anatomy of the lower extremity and detailed some important aspects of the structure and function of the hip, knee, and foot and ankle. In this section, we review various facets of locomotion biomechanics. This is a very broad topic, which we have addressed by highlighting some important considerations, but the reader is cautioned that this is not meant to be a comprehensive review. We begin with an overview of human locomotion before reviewing link-segment gait analysis and describing how joint kinetics are calculated. We also discuss joint-specific models, multisegment foot models, and sequential models. We next review various techniques for tracking foot bone motion other than retroreflective motion analysis and describe the use of biplane fluoroscopy. Finally, we review computational foot modeling and cadaveric gait simulation.

10.4.1 Overview of Human Locomotion

During healthy, able-bodied locomotion, humans use a well-coordinated pattern of joint movements to sustain forward motion. Traditionally, human gait is described as occurring in a cyclic fashion with each cycle beginning with initial contact of a single limb. Therefore, a full right limb gait cycle would begin at right heel strike and continue until the next right heel strike. During walking, therefore, this cycle accounts for two periods of double support and two periods of single support, with each limb experiencing one stance phase (approximately 60% of the gait cycle) and one swing phase (approximately 40% of the gait cycle). This section gives a brief introduction to the sagittal plane patterns of human gait. A more detailed description of these patterns may be found in Chapter 15 and elsewhere.[15]

At initial foot contact (or heel strike), the hip is typically somewhat flexed, the knee is extended, and the ankle is in a neutral or slightly dorsiflexed orientation. Immediately after heel strike, the ankle will plantar flex to an orientation that is termed "foot flat." The rate of plantar flexion is controlled by eccentric activity of the ankle dorsiflexors. Body weight is then transferred from the opposite limb, requiring the knee to flex slightly as it decelerates the additional mass using eccentric activity of the knee extensors. After weight acceptance, the knee extends actively as the leg moves into midstance and single limb support. Following midstance, the knee begins to flex and the ankle begins to dorsiflex as the body mass progresses anteriorly toward the opposite limb's forthcoming heel strike. During this stage of weight transition to a period of double support, ankle plantar flexors eccentrically control the rate of tibial progression, and knee flexion occurs passively. After weight transfer, the ankle plantar flexors actively initiate push off, whereby the foot leaves the ground and the limb enters a swing phase. From initial heel strike to just before push off, the hip moves smoothly from a flexed to an extended position. During push off, the knee continues to flex and the hip begins to flex, lifting the limb as the plantar flexors propel the foot off the ground. During the swing phase, the ankle returns to a slightly dorsiflexed position, the knee actively flexes to its maximal level, and the hip continues to flex. From midswing until the next heel strike, the hip continues to flex, the knee actively extends, and the ankle maintains a slightly dorsiflexed position. As the heel strikes, one gait cycle has been completed, and a new cycle begins again.

10.4.2 Link-Segment Gait Analysis

Inverse dynamic calculations are among the most commonly performed in the quantitative analysis of human gait and are considered the standard approach for estimating joint kinetics. These calculations require the following steps:

1. Selection of an appropriate model, often referred to as the link-segment model
2. Input of kinematic and external force data
3. Input of anthropometric and inertial characteristics, often referred to as body segment parameters (BSPs)

The link-segment model is representative of the subject's skeletal structure, whereby each anatomical segment of the subject is represented by a rigid body in the model that has a single point COM (Figure 10.10). In applying inverse dynamics calculations to link-segment models, several assumptions are often made to simplify the required calculations. These assumptions are described by Winter[27] as follows:

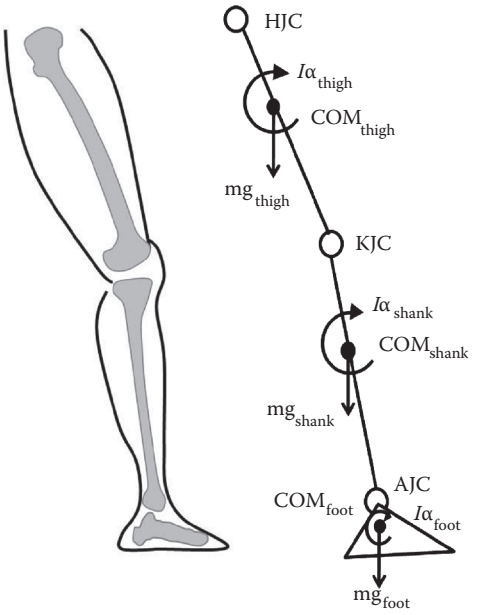

FIGURE 10.10
Sagittal plane stylized sketch of the anatomical leg, with an example of the traditional link-segment model used to represent three segments of the lower limb system. Each segment of the anatomical leg is represented by a rigid body segment whose mass is represented by a fixed-point mass (COM). These point masses are acted on by gravity (g). Each segment has an associated mass moment of inertia (I) and an angular acceleration (α). HJC, hip joint center; KJC, knee joint center; AJC, ankle joint center.

1. Each segment's mass is located as a point mass at its COM.
2. The location of each segment's COM remains fixed during the movement.
3. The joints are considered to be fixed hinge (or ball and socket) joints.
4. The mass moment of inertia of each segment about its COM (or about either proximal or distal joints) is constant during movement.
5. The length of each segment remains constant during the movement.

Despite widespread use, inputs into the inverse dynamic calculations may be prone to error and lead to erroneous solutions. These errors stem from inaccuracies in BSPs,[28–30] reflective marker tracking,[31] ground reaction force measurement,[32] joint center locations,[33–36] estimated center of pressure locations,[37] rigid body assumptions,[38] and skin movement artifacts.[39] For a comprehensive review of the interaction of many of these potential sources of error and their impact on the estimation of lower limb joint kinetics in general, see Riemer et al.[40]

10.4.3 Joint-Specific Models

To enhance the anatomical accuracy of link-segment modeling, several groups have developed techniques to estimate either the position of the centers of rotation or the primary axes of the joints. For the hip, anthropometric proportional regression models to locate the hip joint center (represented by the center of the femoral head)[41,42] have been used widely for many years and are, in fact, the standard representation of the hip joint center in gait

analysis software packages provided by motion analysis companies. These models rely on assumptions of proportionality between the dimensions of the pelvis, functional leg length, and the relative position of the femoral head. For the knee and ankle, other techniques have been developed that use a least squares optimization approach to estimate the functional joint axis.[43] This method requires the collection of relative segmental motion controlled through specific ranges. For the ankle, this entails full dorsiflexion/plantar flexion range of motion in a standing trial. For the knee, full flexion-extension is measured in a trial wherein the limb is unweighted.

Other joint-specific models have been developed that use an FHA calculation technique to define joint centers and primary axes of motion in complex joint systems (i.e., multiple articulations). The FHA describes the motion between two objects as a rotation about, and a translation along, an axis that can change its position and orientation.[10,44] This method is advantageous because of its ability to quantify changes in position of an axis over the course of a movement that is too complex to be accurately identified as a stationary axis. Two examples in which these techniques have been most effective are in the definition of subtalar joint motion and in the definition of segment end point locations in prosthetic foot systems. Motion of the subtalar joint may be described as occurring about a nonorthogonal axis, involving two primary components of motion. As the foot inverts with respect to the lower leg, it also plantar flexes slightly; similarly, when the foot everts with respect to the lower leg, it also dorsiflexes slightly. The orientation of the subtalar joint axis may be visualized as passing from the inferior and posterior aspects of the calcaneus through the head of the talus; this orientation, is approximately 42° above horizontal and approximately 23° medial to the sagittal plane of the foot coordinate system.[25]

Description of relative segmental motion can be challenging in cases in which there is no clearly defined joint axis or segment end point. Such a scenario exists when trying to define segment motion in lower limb amputees walking on commonly prescribed prosthetic components. Today's commonly prescribed prosthetic feet are nonarticulated energy storage and return (NA-ESR) systems. They are typically constructed from carbon fiber composites, have a "J"-shaped design, and lack a clearly defined axis of rotation. To facilitate comparison with the natural foot-ankle complex and to simplify the required calculations, typical assessments of NA-ESR prosthetic foot performance have used constrained link-segment models that assume that the ankle's axis of rotation is approximated by the lateral malleolus position[45–50] and behaves as a fixed hinge. In NA-ESR prosthetic feet, this assumption is problematic as no true "ankle" articulation exists. The extent to which the joint center remains fixed is unknown, and its approximation by the lateral malleolus has been questioned.[51] Recently, a technique has been reported for determining the instantaneous center of rotation of NA-ESR prosthetic feet in the sagittal plane during overground walking conditions.[52] An FHA approach was used to determine the position of the center of rotation in the sagittal plane for a series of NA-ESR prosthetic feet. It was determined that over the course of the stance phase, the sagittal FHA position diverged markedly from the typically assumed fixed axis location. Specifically, in all NA-ESR feet tested, the FHA was at its peak anterior position 45 to 74 mm forward of the assumed fixed axis position after the first 5° of tibial rotation. Throughout the initial 40% to 45% of the stance phase, the FHA shifted posteriorly by 35% to 82 mm, moving toward the assumed fixed axis location (equivalent to the anatomical location of the lateral malleolus) and reaching its peak posterior position. Throughout the remaining 55% to 60% of the stance phase, the FHA shifted anteriorly by 32 to 50 mm, finishing 22 to 55 mm anterior to the assumed fixed position. Similarly, the vertical FHA position was found to diverge from the assumed fixed axis location. In all feet tested, the FHA began stance phase at its peak superior position, ranging from 22 mm superior to 4 mm inferior to

the assumed fixed axis location. Throughout the initial 30% to 35% of the stance, the FHA shifted inferiorly by 12 to 33 mm, moving below the assumed fixed axis position. The FHA then briefly shifted superiorly, remaining below the assumed fixed axis location in all but one of the feet. This was followed by a second inferior shift of 10 to 16 mm throughout the remaining 40% of the stance, resulting in a peak inferior position of 13 to 26 mm below the assumed fixed axis location.

Use of the FHA technique in this case revealed inadequacies in the current approach to link-segment models as they are applied to biomechanical analysis of prosthetic foot components. Furthermore, that study provided reference data for the range of center of rotation displacements that can occur in today's prosthetic feet. From these data, many inferences may be drawn by prosthetic designers and clinicians who may better estimate the utility of each prosthetic foot component based on the mechanical needs of their patient.

10.4.4 Multisegment Foot Models

Although full-body motion analysis studies have been widely accepted for more than two decades, these techniques tend to simplify the foot and ankle.[53,54] Since the late 1990s, there has been an increased effort in developing more sophisticated, multisegment rigid body foot models. For a thorough and comprehensive review of these models, the reader is encouraged to review the recent article by Deschamps et al.[55] These authors performed an extensive literature search, placing no restrictions on the sex or age that was observed, and included studies that (1) had at least three segments (not including the tibia), (2) collected kinematic data with motion capture systems using markers affixed to the subjects, (3) placed markers on the surface of living subjects (no bone pins or cadavers), and (4) conducted weight-bearing activities. They also performed a systematic evaluation of the scientific evidence of each study. From an initial group of 161 citations, 41 were included in the detailed review. Those 41 were then narrowed down to include 15 multisegment foot models; of those, only two (the Oxford Foot Model[56] and the Milwaukee Foot Model[57–59]) are widely used in clinical studies. The authors reviewed the study procedures as well as the reproducibility and experimental errors of the various models. They noted that the models lacked uniformity in both technical and terminological aspects, and they suggested that rigorous repeatability studies, before appreciating the full clinical utility of multisegment foot models, must be undertaken.

10.4.5 Sequential Modeling

It has been recommended that joint models should limit the number of DOFs necessary to fully describe the motions and forces resolved.[60] The primary benefits in reducing a model's DOF are enhanced communication between engineers and clinicians and the application of modeling outcomes in clinical practice, especially in the design and implementation of joint replacement systems. In recent years, a group of researchers have been developing novel modeling techniques for the ankle and knee joints that are reduced to a single DOF.[61–66] That group has moved from a more traditional "simultaneous" solution focus to a "sequential" solution focus.[64] A simultaneous approach in this case refers to the inclusion of all possible biological structures (e.g., ligaments, muscles, and articular surfaces), a full 6 DOF description of motion, and all force and motion equations being solved together.[67–72] Models requiring simultaneous solutions are dependent on external forces being applied and on the assigned elastic and damping characteristics of the connecting elements (i.e., ligaments and muscles). The sequential approach begins with foundational

knowledge of joint kinematics under passive conditions. It is based on the assumptions that a few anatomical structures are enough to guide passive joint motion, and that relatively complex motion can be expressed as just 1 DOF.[64,65,73–75] After initial passive motion modeling to understand the basic role of the fundamental anatomical structures in guiding passive motion, the other anatomical structures and external force components are added into the model in sequential fashion, thus completing the model's description of the mechanical system.

Several studies have used the sequential modeling approach to better understand the mechanical system of the knee. Considering the posterior cruciate ligament, the medial collateral ligament, and portions of the anterior cruciate ligament to be isometric,[76,77] and assuming the articular structures to be rigid, several studies have demonstrated that spatial and planar equivalent mechanisms can be used to replicate the motion of the femur with respect to the tibia using 1 DOF.[61,63,65,74,75,78] From these various studies, it has been concluded that 1 DOF models provide good replication of experimental motion. When efforts were made to model more complex representations of the articular surfaces, Ottoboni et al.[78] determined that a limit exists beyond which model accuracy is not improved. Increasing the complexity of the articular structure representations from spherical and planar surfaces for the femoral condyles and tibial plateaus, respectively,[75] to spherical surfaces for both surfaces,[63] model outcomes were improved. However, when complexity was increased still further with optimal B-spline approximation of femoral and tibial articular surfaces,[61] model outcome parameters did not improve, the model suffered from singularity problems, and its estimated motion did not match experimental data as well as the simpler spherical approximations of articular structures.[78]

A similar approach has been applied to the ankle joint. Several reports have shown that the ankle joint complex can be represented as a single DOF system in unloaded conditions.[79–81] A two-dimensional model published by Leardini et al.[79] revealed a complementary interaction between the articular surfaces and the ligaments of the ankle joint complex. The 1 DOF modeling approach was developed further to investigate whether similar results could be obtained in a spatial model of the ankle joint complex.[82] They tested two different simplified representations of the articular structures:

(1) Three articulating contact points between the tibia-fibula complex and the talus-calcaneus complex (modeled by spheres contacting a planar surface, two at the distal surface of the mortise and one on the lateral aspect of the talus).

(2) A single articulating contact point between the tibia-fibula complex and the talus-calcaneus complex (modeled by a sphere contacting a planar surface, at a point on the mortise that was centered between the two original points of approach 1).

The first approach was based on findings from least squares approximation of the digitized points that were closest during motion to their neutral position. The second approach was determined from a simplified equivalent mechanism.

Findings from Di Gregorio et al.'s work[82] indicate that the current 1 DOF approaches to ankle modeling do not adequately predict experimental measurements of ankle joint complex motion. However, their efforts represent the first 1 DOF models able to reproduce at least some of the complex three-dimensional (3D) motions of the ankle system.

Working from the previous efforts by Di Gregorio et al.,[82] the same group further improved the 1 DOF approach to modeling ankle motion.[83] In particular, major improvements were made to the representation of articular surfaces. Specifically, the newer model

included three sphere-to-sphere contact points to represent the medial and lateral aspects of the articulation between the tibial mortise and the trochlea tali, as well as the lateral talofibular articulation. These modifications allowed the model to estimate ankle joint complex motion to within 2.5 mm of displacement and within 1° of rotation. Furthermore, these models were made to be specimen-specific, using a refined optimization approach that was able to determine optimal geometric parameters within 14 hours for each specimen. It is possible that current and future efforts will produce models that represent more accurate descriptions of the articular structures of the ankle joint complex, likely resulting in 1 DOF models that more closely match model estimations with experimental measurements.

From this brief review of knee and ankle modeling papers, it seems that a 1 DOF approach can provide reasonable replication of experimental motion of the ankle joint complex. Furthermore, these models provide a minimized parameter set with moderate computational cost to arrive at a model solution. Because one of the overall objectives of the knee and ankle 1 DOF models is to provide a robust platform for designing new endoprosthetic components for joint arthroplasty, these results seem quite promising for the provision of simplified, yet robust models of the complex knee and ankle joint systems.

10.4.6 Tracking Foot Bone Motion

As discussed above, many groups have used computerized infrared camera systems with retroreflective or active surface markers to track foot bone motion.[55] However, skin motion artifact is a difficult problem to overcome, and the foot bones are small, which necessitates grouping bones together (e.g., the cuneiforms, cuboid, and navicular as a "midfoot" segment). As such, the position of most of the foot bones is not easily determined with surface markers. Lundberg et al.[84–86] used X-ray stereophotogrammetry to evaluate the orientations of the bones of the foot in several static positions using a specialized jig; they implanted tantalum balls into the foot bones and moved the foot incrementally in prescribed angular offsets. van Langelaan[7] conducted a similar study to measure tarsal bone motion. These works contributed to our understanding of the axes of motion possible in the foot, but due to technical constraints, no dynamic foot motions were included. Other groups have also evaluated the orientations of the bones of the foot using time-sequence magnetic resonance imaging (MRI)[87–92] or computed tomography (CT).[93] These techniques improved visualization of the bony orientations during dynamic ranges of motion, but still required static positioning of the feet in a jig. The static positions could be animated to represent bone motion, but this may not represent actual dynamic bone motion during gait. More recently, retroreflective markers attached to bone pins have been used to quantify foot bone motion.[19,94,95] These studies represent the gold standard of *in vivo* foot bone motion data; however, the invasiveness of this methodology limits its utility to the research laboratory and consequently is not useful for larger clinical studies. None of the current technologies of surface marker motion capture, X-ray stereophotogrammetry, time-sequence MRI or CT, or bone pin motion capture are ideal for accurately and precisely tracking dynamic individual foot bone motion in clinical populations.

10.4.7 Descriptions of Joint Motion Using Biplane Fluoroscopy

Although modern imaging techniques such as MRI and CT can acquire 3D bone positions accurately and avoid the inherent errors of marker placement and skin motion artifacts present in retroreflective motion analysis systems, the time required to collect the data makes it unwieldy to study the dynamics of gait. Therefore, a few groups have begun to

use single and biplane fluoroscopy to quantify lower extremity dynamic bone motion. Single plane fluoroscopy has been used to study both knee[96,97] and hindfoot kinematics.[98] Although the flexibility and utility of using a single fluoroscope are obvious and attractive, the complex anatomy of the foot, with many small, occluding bones, may require the use of a biplane system to fully study its motion. Tashman et al.[99–104] have been at the forefront of developing high-speed, biplane fluoroscopic systems using both radiographic stereophotogrammetric analysis and model-based approaches. They have described the relevant methods in great detail,[99] explored anterior cruciate ligament deficiency in canines,[100] studied running motion after anterior cruciate ligament reconstruction,[101] and reported the validity of model-based tracking for both the knee and shoulder.[102–104] Additionally, Li et al.[105–107] have used dual C-arms to study both knee and ankle motion;[108–110] a similar setup has been used elsewhere.[111] However, in both cases, the setup of the biplane system required quasi-dynamic data collection because subjects were not able to walk unfettered through the field of view. Despite the great progress made in the development of this field, the use of a biplane fluoroscopy system to study foot bone motion remains incompletely explored to date.

10.4.8 Computational Modeling of the Foot

In the last 30 years, many foot models of varying degrees of mathematical and anatomical complexity have been developed.[112–119] For the purposes of this chapter, we will limit our discussion to more recent finite-element (FE) foot models. Chen et al.[120,121] developed an FE foot model to predict the efficiency of custom total contact insoles at reducing peak plantar pressures. Although individual bones were segmented, the foot was simplified into seven components; the tarsal and metatarsal bones were grouped into medial and lateral columns, and the bones of each phalange were lumped together. All materials were considered homogeneous and linear elastic. Their simulation consisted of moving the ground toward the foot to mimic midstance. Reduction in peak normal stress from the flat to custom insoles ranged from 19.8% to 56.8%. Gefen[122,123] generated a model of the foot of similar complexity and anatomical detail that was aimed at examining the effect of diabetes on the mechanics of the foot during stance phase. That model was based on five planar sagittal cross sections of the foot; bones and cartilage were linear elastic and isotropic, whereas the ligaments, fascia, and fat were nonlinear. To simulate diabetic plantar soft tissue, Gefen et al.[124] used earlier work from his group that applied an indentor during an MRI scan. Simulations generated increased stress concentrations beneath the metatarsal heads of the diabetic tissue. Recently, an FE foot model developed by Cheng et al.[125] has been used to study the plantar aponeurosis, Achilles tendon, and the windlass mechanism. Each bone in the foot was modeled separately, including cartilage elements between each bone, 67 foot ligaments, and a complex fan-like structure to represent the plantar aponeurosis; all materials except the plantar fascia were linear elastic, homogeneous, and isotropic. They found that stress concentrations occurred at the medial calcaneal tubercle, and the medial plantar aponeurosis bore more stress than the lateral.

One of the most comprehensive efforts on FE foot modeling is the work of Cheung et al., who have modeled the effects of plantar fascia release,[126,127] insole design,[128,129] stiffer plantar soft tissue,[130] Achilles tendon loading,[131] sock friction,[132] and high heels.[133] The model anatomy was generated from 2-mm MRI slices of a normal male subject; they included 28 bones, 72 ligaments, and the plantar fascia, which were all linear elastic, homogeneous, and isotropic. The more recent versions of that model included some of the extrinsic musculature as well.[129] As a representative finding of one of their studies, the use of an arch

support was found to be more effective than insole thickness or stiffness at reducing plantar pressure during simulations of midstance.[129]

Cavanagh et al. have made extensive progress on their FE foot modeling efforts since the mid-1990s. Their earlier work involved a plane strain model of the second metatarsal to explore the effect of insole and tissue thickness on plantar pressure.[134] More recently, they used ultrasound and inverse FE modeling to determine the material properties of the plantar soft tissue[135] and developed a library of foam material parameters for use with FE models.[136] They have used a plane strain FE model to conduct a parametric analysis that explored insole conformity (flat, half conforming, and full confirming), insole thickness (6.3, 9.5, and 12.7 mm), and insole material (Poron Cushioning, Microcel Puff Lite, and Microcel Puff), determining that conformity was the most important variable.[137] A 3D FE model of the first ray was also developed and used to explore the effect of material properties, to study hallux limitus, and to investigate the effects of the hallux varus angle after surgery for arthrodesis of the first ray.[138] Finally, they developed a 3D subject-specific FE foot model that was used to explore the peak stresses within the tissues beneath the metatarsal heads, demonstrating that peak internal stresses were not located in the same region as the peak plantar pressure.[139]

Over the last few decades, the field of computational foot modeling has made great strides in both model complexity and validation and in using these models to address clinically relevant issues. The more sophisticated models are able to conduct detailed parametric analyses and explore complex parameters that cannot be easily or ethically studied on human subjects or cadaveric specimens.

10.4.9 Cadaveric Gait Simulation

Cadaveric gait simulators are an alternative way to investigate foot structure and function. The first and most widely published dynamic cadaveric gait simulator was developed by Sharkey et al.[140] and has been used to address many biomechanical questions.[141–146] The most recent version of the simulator consists of the foot and surrogate tibia, the ground (force plate and pedobarograph in series), an aluminum housing frame, and a carriage attached to the proximal tibia. To simulate gait, the carriage is pulled anteriorly on a linear bearing, while two additional motors adjust the superior/inferior translation and the tibial sagittal plane angle. Linear stepper motors connected to tendons via freeze clamps supply respective muscle forces. During gait simulation, the foot is completely unconstrained. Transverse plane tibial motion could be unconstrained but is typically fixed through the use of a locking mechanism. Coronal plane rotation of the tibia is not allowed. Control of the vertical ground reaction force (vGRF) is performed though repeated trial and error adjustments; between simulations, the tibia can shift superiorly or inferiorly, or muscle forces can be adjusted to alter the ground reaction force. The velocity of simulation is scaled to 1/20th that of physiological gait.

The universal musculoskeletal simulator (UMS), developed at the Cleveland Clinic, is unique from other gait simulators in that it was designed as a general purpose tool with the ability to simulate the kinematics and kinetics of a variety of joints. The UMS consists of a force plate articulated by a 6 DOF parallel robot and five tendon actuators. Relative tibial kinematics were prescribed by mounting the tibia in a device and registering it to the UMS with a microscribe 3D digitizer, and then moving a mobile force plate to recreate the tibia to ground kinematics. The programmability of the robot allows the tibia kinematics to vary between simulation trials and studies. The vGRF is controlled with a manual iterative optimization routine using a manual vGRF feedback control method. This group has reported the design of the system, provided component and system-level validated results,

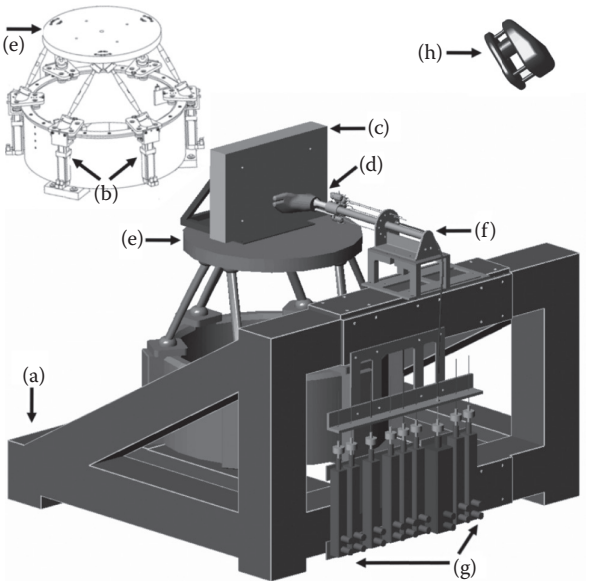

FIGURE 10.11
RGS schematic with (a) surrounding frame, (b, inset) parallel robot motors, (c) force plate, (d) cadaveric foot, (e, main image and inset) mobile platform, (f) tibia mounting frame, (g) tendon actuation system, and (h) motion analysis system.

and demonstrated the system's ability to study the knee and ankle joint.[147] Gait simulations have been performed in 3.2 seconds at 66.7% body weight with eight control and eight diabetic cadaveric specimens to study the effects of diabetes on midfoot joint pressures.[148] The UMS has also been used as a simple mechanical testing device to characterize the mechanical response of the foot to aid in the development of computation foot models.[149]

Gait simulators have also been developed by several other research teams.[150–153] Most recently, the robotic gait simulator (RGS) has been developed by researchers at the VA Puget Sound and the University of Washington (Figure 10.11). The RGS consists of a 6 DOF parallel robot mounted with a force plate and a pressure plate, nine tendon actuators in series with nine load cells, a retroreflective motion analysis system, and a real-time PXI controller. The RGS is unique in its automated fuzzy logic vGRF controller,[154] and it has been used to study prosthetic feet,[155] flatfeet,[156] the effect of great toe fusion angle,[157] and foot bone kinematics.[18]

For certain applications, such as, simulating variations of a surgical procedure on the same foot, human test subjects are impractical or unethical, and computational models are difficult to evaluate. As such, cadaveric gait simulators are excellent tools for studying these problems, provided their kinetics and kinematics are sufficiently validated.

10.5 Summary and Future Perspectives

This chapter has reviewed the relevant anatomy of the three major joints of the lower extremity (hip, knee, and ankle) and included some of the smaller (i.e., foot) joints as well. The relevant osseous structures have been reviewed, and the important muscles and

ligaments have been highlighted. In addition, some of the highly specialized anatomy has also been described. An overview of the structure and function of the lower extremity has also been provided, again emphasizing the hip, knee, and ankle, while also going into greater detail at the foot. Lastly, we have reviewed a broad scope of topics related to locomotion biomechanics, beginning with a description of how humans walk and then including many specialized topics, such as joint-specific modeling or methods for tracking foot bone motion. Moving forward, there are numerous topics that could have been discussed in this chapter and will likely gain importance in the field over time. These include the following areas (in no particular order): markerless motion capture, patient (and joint-specific) forward and inverse dynamic analyses, multiscale modeling, greatly improved accuracy and efficiency for computational modeling, dynamic imaging, better understanding of neural control mechanisms, and lower extremity prosthetic research.

Acknowledgments

This work was partially supported by the Department of Veterans Affairs, Rehabilitation Research and Development grant A4843C. The authors would like to thank Chris Pacheco, Andrew B. Sawers, and Yangqiu Hu for original artwork, Patrick M. Aubin for the gait simulator summary, as well as Joseph M. Iaquinto and Eric C. Whittaker for their editorial suggestions.

References

1. Sarrafian, S. K. 1993. *Anatomy of the Foot and Ankle: Descriptive, Topographic, Functional*. Philadelphia, PA: J.B. Lippincott.
2. Williams, P.W., R. Warwick, M. Dyson, L.H. Bannister, eds. 1989. *Gray's Anatomy*. 37th ed. New York: Churchill Livingstone.
3. Netter, F.H. 1989. *Atlas of Human Anatomy*. Summit, NJ: Ciba-Geigy Corporation.
4. Inman, V.T. 1976. *The Joints of the Ankle*. Baltimore, MD: Williams & Wilkins.
5. Hicks, J.H. 1953. The mechanics of the foot I. *The Joints* 78:345–357.
6. Safran, M.R., R.S. Benedetti, A.R. Bartolozzi, 3rd, and B.R. Mandelbaum. 1999. Lateral ankle sprains: A comprehensive review: Part 1: Etiology, pathoanatomy, histopathogenesis, and diagnosis. *Medicine and Science in Sports and Exercise* 31:S429–437.
7. van Langelaan, E.J. 1983. A kinematic analysis of the tarsal joints, an X-ray photogrammetric study. *Acta Orthopaedica Scandinavica Supplement* 204:1–269.
8. Frankel, V.H. 1960. *The Femoral Neck: Function, Fracture Mechanisms, Internal Fixation*. Springfield, IL: Charles C. Thomas.
9. Inman, V.T. 1947. Functional aspects of the abductor muscles of the hip. *Journal of Bone and Joint Surgery. American Volume* 29:607–619.
10. Blankevoort, L., R. Huiskes, and A. de Lange. 1990. Helical axes of passive knee joint motions. *Journal of Biomechanics* 23:1219–1229.
11. van den Bogert, A.J., C. Reinschmidt, and A. Lundberg. 2008. Helical axes of skeletal knee joint motion during running. *Journal of Biomechanics* 41:1632–1638.
12. Fukuda, Y., S. Takai, N. Yoshino, K. Murase, S. Tsutsumi, K. Ikeuchi, and Y. Hirasawa. 2000. Impact load transmission of the knee joint-influence of leg alignment and the role of meniscus and articular cartilage. *Clinical Biomechanics (Bristol, Avon)* 15:516–521.

13. Seedhom, B.B. 1976. Loadbearing function of the menisci. *Physiotherapy* 62:223.
14. Seedhom, B.B., D. Dowson, and V. Wright. 1974. Proceedings: Functions of the menisci. A preliminary study. *Annals of the Rheumatic Diseases* 33:111.
15. Perry, J. 1992. *Gait Analysis: Normal and Pathological Function*. Thorofare, NJ, SLACK Incorporated.
16. Stauffer, R.N., E.Y. Chao, and R.C. Brewster. 1977. Force and motion analysis of the normal, diseased, and prosthetic ankle joint. *Clinical Orthopaedics and Related Research* 189–196.
17. Hu, Y., W.R. Ledoux, M. Fassbind, E.S. Rohr, B.J. Sangeorzan, and D. Haynor. 2011. Multi-rigid image segmentation and registration for the analysis of joint motion from three-dimensional magnetic resonance imaging. *Journal of Biomechanical Engineering* 133:101005.
18. Whittaker, E.C., P.M. Aubin, and W.R. Ledoux. 2011. Foot bone kinematics as measured in a cadaveric robotic gait simulator. *Gait & Posture* 33:645–650.
19. Lundgren, P., C. Nester, A. Liu, A. Arndt, R. Jones, A. Stacoff, P. Wolf, and A. Lundberg. 2008. Invasive in vivo measurement of rear-, mid- and forefoot motion during walking. *Gait & Posture* 28:93–100.
20. Hicks, J.H. 1954. The mechanics of the foot II. The plantar aponeurosis and the arch. *Journal of Anatomy* 88:25–31.
21. Thordarson, D.B., P.J. Kumar, T.P. Hedman, and E. Ebramzadeh. 1997. Effect of partial versus complete plantar fasciotomy on the windlass mechanism. *Foot & Ankle International* 18:16–20.
22. Kappel-Bargas, A., R.D. Woolf, M.W. Cornwall, and T.G. McPoil. 1998. The windlass mechanism during normal walking and passive first metatarsalphalangeal joint extension. *Clinical Biomechanics (Bristol, Avon)* 13:190–194.
23. D'Ambrogi, E., C. Giacomozzi, V. Macellari, and L. Uccioli. 2005. Abnormal foot function in diabetic patients: The altered onset of Windlass mechanism. *Diabetic Medicine* 22:1713–1719.
24. Wilken, J., S. Rao, C. Saltzman, and H.J. Yack. 2011. The effect of arch height on kinematic coupling during walking. *Clinical Biomechanics (Bristol, Avon)* 26:318–323.
25. Elftman, H. 1960. The transverse tarsal joint and its control. *Clinical Orthopedics* 16:41–45.
26. Blackwood, C.B., T.J. Yuen, B.J. Sangeorzan, and W.R. Ledoux. 2005. The midtarsal joint locking mechanism. *Foot & Ankle International* 26:1074–1080.
27. Winter, D.A. 2009. *Biomechanics and Motor Control of Human Movement*, 4th ed. Hoboken, NJ: John Wiley & Sons, Inc.
28. Ganley, K.J., and C.M. Powers. 2004. Determination of lower extremity anthropometric parameters using dual energy X-ray absorptiometry: The influence on net joint moments during gait. *Clinical Biomechanics (Bristol, Avon)* 19:50–56.
29. Rao, G., D. Amarantini, E. Berton, and D. Favier. 2006. Influence of body segments' parameters estimation models on inverse dynamics solutions during gait. *Journal of Biomechanics* 39:1531–1536.
30. Reinbolt, J.A., R.T. Haftka, T.L. Chmielewski, and B.J. Fregly. 2007. Are patient-specific joint and inertial parameters necessary for accurate inverse dynamics analyses of gait? *IEEE Transactions on Bio-Medical Engineering* 54:782–793.
31. Richards, J.G. 1999. The measurement of human motion: A comparison of commercially available systems. *Human Movement Science* 18:589–602.
32. Kuo, A.D. 1998. A least-squares estimation approach to improving the precision of inverse dynamics computations. *Journal of Biomechanical Engineering*. 120:148–159.
33. Challis, J.H. and D.G. Kerwin. 1996. Quantification of the uncertainties in resultant joint moments computed in a dynamic activity. *Journal of Sports Sciences* 14:219–231.
34. Delp, S.L., and W. Maloney. 1993. Effects of hip center location on the moment-generating capacity of the muscles. *Journal of Biomechanics* 26:485–499.
35. Holden, J.P., and S.J. Stanhope. 1998. The effect of variation in knee center location estimates on net knee joint moments. *Gait & Posture* 7:1–6.
36. Stagni, R., A. Leardini, A. Cappozzo, M. Grazia Benedetti, and A. Cappello. 2000. Effects of hip joint centre mislocation on gait analysis results. *Journal of Biomechanics* 33:1479–1487.

37. McCaw, S.T., P. DeVita. 1995. Errors in alignment of center of pressure and foot coordinates affect predicted lower extremity torques. *Journal of Biomechanics* 28:985–988.
38. Zhang, X.D., S.W. Lee, and P. Braido. 2004. Towards an integrated high-fidelity linkage representation of the human skeletal system based on surface measurement. *International Journal of Industrial Ergonomics* 33:215–227.
39. Taylor, W.R., R.M. Ehrig, G.N. Duda, H. Schell, P. Seebeck, and M.O. Heller. 2005. On the influence of soft tissue coverage in the determination of bone kinematics using skin markers. *Journal of Orthopaedic Research* 23:726–734.
40. Riemer, R., E.T. Hsiao-Wecksler, and X. Zhang. 2008. Uncertainties in inverse dynamics solutions: A comprehensive analysis and an application to gait. *Gait & Posture* 27:578–588.
41. Bell, A.L., D.R. Pedersen, and R.A. Brand. 1990. A comparison of the accuracy of several hip center location prediction methods. *Journal of Biomechanics* 23:617–621.
42. Tylkowski, C.M., S.R. Simon, and J.M. Mansour. 1982. The Frank Stinchfield Award Paper. Internal rotation gait in spastic cerebral palsy. *Hip* 89–125.
43. Schwartz, M.H., and A. Rozumalski. 2005. A new method for estimating joint parameters from motion data. *Journal of Biomechanics* 38:107–116.
44. Woltring, H.J., R. Huiskes, A. de Lange, and F.E. Veldpaus. 1985. Finite centroid and helical axis estimation from noisy landmark measurements in the study of human joint kinematics. *Journal of Biomechanics* 18:379–389.
45. Barr, A.E., K.L. Siegel, J.V. Danoff, C.L. McGarvey, 3rd, A. Tomasko, I. Sable, and S.J. Stanhope. 1992. Biomechanical comparison of the energy-storing capabilities of SACH and Carbon Copy II prosthetic feet during the stance phase of gait in a person with below-knee amputation. *Physical Therapy* 72:344–354.
46. Gitter, A., J.M. Czerniecki, and D.M. DeGroot. 1991. Biomechanical analysis of the influence of prosthetic feet on below-knee amputee walking. *American Journal of Physical Medicine & Rehabilitation* 70:142–148.
47. Powers, C.M., S. Rao, and J. Perry. 1998. Knee kinetics in trans-tibial amputee gait. *Gait & Posture* 8:1–7.
48. Su, P.F., S.A. Gard, R.D. Lipschutz, and T.A. Kuiken. 2008. Differences in gait characteristics between persons with bilateral transtibial amputations, due to peripheral vascular disease and trauma, and able-bodied ambulators. *Archives of Physical Medicine and Rehabilitation* 89:1386–1394.
49. Supan, T., M. Lebiedowska, R. Dodson, S. Verhulst, and M. Dufour. 2010. The effect of a Talux® prosthetic foot on gait parameters and limb loading of nonvascular transtibial amputees. *Journal of Prosthetics and Orthotics* 22:43–52.
50. Underwood, H.A., C.D. Tokuno, and J.J. Eng. 2004. A comparison of two prosthetic feet on the multi-joint and multi-plane kinetic gait compensations in individuals with a unilateral transtibial amputation. *Clinical Biomechanics (Bristol, Avon)* 19:609–616.
51. Rusaw, D., and N. Ramstrand. 2010. Sagittal plane position of the functional joint centre of prosthetic foot/ankle mechanisms. *Clinical Biomechanics (Bristol, Avon)* 25:713–720.
52. Sawers, A.B., and M.E. Hahn. 2011. Trajectory of the center of rotation in non-articulated energy storage and return prosthetic feet. *Journal of Biomechanics* 44:1673–1677.
53. Kadaba, M.P., H.K. Ramakrishnan, and M.E. Wootten. 1990. Measurement of lower extremity kinematics during level walking. *Journal of Orthopaedic Research* 8:383–392.
54. Apkarian, J., S. Naumann, and B. Cairns. 1989. A three-dimensional kinematic and dynamic model of the lower limb. *Journal of Biomechanics* 22:143–155.
55. Deschamps, K., F. Staes, P. Roosen, F. Nobels, K. Desloovere, H. Bruyninckx, and G.A. Matricali. 2011. Body of evidence supporting the clinical use of 3D multisegment foot models: A systematic review. *Gait & Posture* 33:338–349.
56. Carson, M.C., M.E. Harrington, N. Thompson, J.J. O'Connor, and T.N. Theologis. 2001 Kinematic analysis of a multi-segment foot model for research and clinical applications: A repeatability analysis. *Journal of Biomechanics* 34:1299–1307.

57. Kidder, S.M., G.F. Harris, F.S. Abuzzahab, and J.E. Johnson. 1996. A biomechanical model for foot and ankle motion analysis. In: *Human Motion Analysis: Current Applications and Future Directions*, edited by Harris, G. F. and P. A. Smith, 133–151. New York: Institute of Electrical and Electronics Engineers.
58. Myers, K.A., M. Wang, R.M. Marks, and G.F. Harris. 2004. Validation of a multisegment foot and ankle kinematic model for pediatric gait. *IEEE Transactions on Neural Systems and Rehabilitation Engineering* 12:122–130.
59. Long, J.T., D.C. Eastwood, A.R. Graf, P.A. Smith, and G.F. Harris. 2010. Repeatability and sources of variability in multi-center assessment of segmental foot kinematics in normal adults. *Gait & Posture* 31:32–36.
60. Bull, A.M.J., and A.A. Amis. 1998. Knee joint motion: Description and measurement. *Proceedings of the Institution of Mechanical Engineers. Part H* 212:357–372.
61. Di Gregorio, R., and V. Parenti-Castelli. 2003. A spatial mechanism with higher pairs for modelling the human knee joint. *Journal of Biomechanical Engineering* 125:232–237.
62. Feikes, J.D., J.J. O'Connor, and A.B. Zavatsky. 2003. A constraint-based approach to modelling the mobility of the human knee joint. *Journal of Biomechanics* 36:125–129.
63. Parenti-Castelli, V., and R. Di Gregorio. 2000. Parallel mechanisms applied to the human knee passive motion simulation. In *Advances in Robot Kinematics*. Dordrecht: Kluwer.
64. Parenti-Castelli, V., A. Leardini, R. Di Gregorio, and J.J. O'Connor. 2004. On the modeling of passive motion of the human knee joint by means of equivalent planar and spatial parallel mechanisms. *Autonomous Robots* 16:219–232.
65. Wilson, D.R., J.D. Feikes, J.J. O'Connor. 1998. Ligaments and articular contact guide passive knee flexion. *Journal of Biomechanics* 31:1127–1136.
66. Wilson, D.R., J.D. Feikes, A.B. Zavatsky, and J.J. O'Connor. 2000. The components of passive knee movement are coupled to flexion angle. *Journal of Biomechanics* 33:465–473.
67. Abdel-Rahman, E., and M.S. Hefzy. 1993. A two-dimensional dynamic anatomical model of the human knee joint. *Journal of Biomechanical Engineering* 115:357–365.
68. Andriacchi, T.P., R.P. Mikosz, S.J. Hampton, and J.O. Galante. 1983. Model studies of the stiffness characteristics of the human knee joint. *Journal of Biomechanics* 16:23–29.
69. Blankevoort, L., R. Huiskes, and A. de Lange. 1988. The envelope of passive knee joint motion. *Journal of Biomechanics* 21:705–720.
70. Blankevoort, L., J.H. Kuiper, R. Huiskes, and H.J. Grootenboer. 1991. Articular contact in a three-dimensional model of the knee. *Journal of Biomechanics* 24:1019–1031.
71. Tumer, S.T., and A.E. Engin. 1993. Three-body segment dynamic model of the human knee. *Journal of Biomechanical Engineering* 115:350–356.
72. Wismans, J., F. Veldpaus, J. Janssen, A. Huson, and P. Struben. 1980. A three-dimensional mathematical model of the knee-joint. *Journal of Biomechanics* 13:677–685.
73. O'Connor, J.J., T.W. Lu, D.R. Wilson, J. Feikes, and A. Leardini. 1998. Review: Diarthrodial joints–kinematic pairs, mechanisms or flexible structures? *Computer Methods in Biomechanics and Biomedical Engineering* 1:123–150.
74. O'Connor, J.J., T.L. Shercliff, E. Biden, J.W. Goodfellow. 1989. The geometry of the knee in the sagittal plane. *Proceedings of the Institution of Mechanical Engineers. Part H* 203:223–233.
75. Wilson, D.R., and J.J. O'Connor. 1997. A three-dimensional geometric model of the knee for the study of joint forces in gait. *Gait & Posture* 5:108–115.
76. Fuss, F.K. 1989. Anatomy of the cruciate ligaments and their function in extension and flexion of the human knee joint. *The American Journal of Anatomy* 184:165–176.
77. Rovick, J.S., J.D. Reuben, R.J. Schrager, and P.S. Walker. 1991. Relation between knee motion and ligament length patterns. *Clinical Biomechanics* 6:213–220.
78. Ottoboni, A., V. Parenti-Castelli, N. Sancisi, C. Belvedere, and A. Leardini. 2010. Articular surface approximation in equivalent spatial parallel mechanism models of the human knee joint: An experiment-based assessment. *Proceedings of the Institution of Mechanical Engineers. Part H* 224:1121–1132.

79. Leardini, A., J.J. O'Connor, F. Catani, and S. Giannini. 1999. A geometric model of the human ankle joint. *Journal of Biomechanics* 32:585–591.
80. Leardini, A., R. Stagni, and J.J. O'Connor. 2001. Mobility of the subtalar joint in the intact ankle complex. *Journal of Biomechanics* 34:805–809.
81. Stagni, R., A. Leardini, J.J. O'Connor, and S. Giannini. 2003. Role of passive structures in the mobility and stability of the human subtalar joint: A literature review. *Foot & Ankle International* 24:402–409.
82. Di Gregorio, R., V. Parenti-Castelli, J.J. O'Connor, and A. Leardini. 2007. Mathematical models of passive motion at the human ankle joint by equivalent spatial parallel mechanisms. *Medical & Biological Engineering & Computing* 45:305–313.
83. Franci, R., V. Parenti-Castelli, C. Belvedere, and A. Leardini. 2009. A new one-DOF fully parallel mechanism for modelling passive motion at the human tibiotalar joint. *Journal of Biomechanics* 42:1403–1408.
84. Lundberg, A., I. Goldie, B., Kalin, and G. Selvik. 1989. Kinematics of the ankle/foot complex: Plantarflexion and dorsiflexion. *Foot and Ankle* 9:194–200.
85. Lundberg, A., O.K. Svensson, C. Bylund, I. Goldie, and G. Selvik. 1989. Kinematics of the ankle/foot-Part 2: Pronation and supination. *Foot and Ankle* 9:248–253.
86. Lundberg, A., O.K. Svensson, C. Bylund, and G. Selvik. 1989. Kinematics of the ankle/foot complex-Part 3: Influence of leg rotation. *Foot and Ankle* 9:304–309.
87. Udupa, J.K., B.E. Hirsch, H.J. Hillstrom, G.R. Bauer, and J.B. Kneeland. 1998. Analysis of in vivo 3-D internal kinematics of the joints of the foot. *IEEE Transactions on Bio-Medical Engineering* 45:1387–1396.
88. Stindel, E., J.K. Udupa, B.E. Hirsch, D. Odhner, and C. Couture. 1999. 3D MR image analysis of the morphology of the rear foot: Application to classification of bones. *Computerized Medical Imaging and Graphic* 23:75–83.
89. Stindel, E., J.K. Udupa, B.E. Hirsch, and D. Odhner. 1999. A characterization of the geometric architecture of the peritalar joint complex via MRI: An aid to the classification of foot type. *IEEE Transactions on Medical Imaging* 18:753–763.
90. Stindel, E., J.K. Udupa, B.E. Hirsch, and D. Odhner. 2001. An in vivo analysis of the motion of the peri-talar joint complex based on MR imaging. *IEEE Transactions on Bio-Medical Engineering* 48:236–247.
91. Siegler, S., J.K. Udupa, S.I. Ringleb, C.W. Imhauser, B.E. Hirsch, D. Odhner, P.K. Saha E. Okereke, and N. Roach. 2005. Mechanics of the ankle and subtalar joints revealed through a 3D quasi-static stress MRI technique. *Journal of Biomechanics* 38:567–578.
92. Wolf, P., R. Luechinger, P. Boesiger, E. Stuessi, and A. Stacoff. 2007. A MR imaging procedure to measure tarsal bone rotations. *Journal of Biomechanical Engineering* 129:931–936.
93. Beimers, L., G.J. Maria Tuijthof, L. Blankevoort, R. Jonges, M. Maas, and C.N. van Dijk. 2008. In-vivo range of motion of the subtalar joint using computed tomography. *Journal of Biomechanics* 41:1390–1397.
94. Arndt, A., P. Wolf, A. Liu, C. Nester, A. Stacoff, R. Jones, P. Lundgren, and A. Lundberg. 2007. Intrinsic foot kinematics measured in vivo during the stance phase of slow running. *Journal of Biomechanics* 40:2672–2678.
95. Nester, C., R.K. Jones, A. Liu, D. Howard, A. Lundberg, A. Arndt, P. Lundgren, A. Stacoff, and P. Wolf. 2007. Foot kinematics during walking measured using bone and surface mounted markers. *Journal of Biomechanics* 40:3412–3423.
96. Fregly, B.J., H.A. Rahman, and S.A. Banks. 2005. Theoretical accuracy of model-based shape matching for measuring natural knee kinematics with single-plane fluoroscopy. *Journal of Biomechanical Engineering* 127:692–699.
97. Yamaguchi, S., K. Gamada, T. Sasho, H. Kato, M. Sonoda, and S.A. Banks. 2009. In vivo kinematics of anterior cruciate ligament deficient knees during pivot and squat activities. *Clinical Biomechanics (Bristol, Avon)* 24:71–76.
98. Yamaguchi, S., T. Sasho, H. Kato, Y. Kuroyanagi, and S.A. Banks. 2009. Ankle and subtalar kinematics during dorsiflexion-plantarflexion activities. *Foot & Ankle International* 30:361–366.

99. You, B.M., P. Siy, W. Anderst, and S. Tashman. 2001. In vivo measurement of 3-D skeletal kinematics from sequences of biplane radiographs: Application to knee kinematics. *IEEE Transactions on Medical Imaging* 20:514–525.
100. Tashman, S., and W. Anderst. 2003. In-vivo measurement of dynamic joint motion using high speed biplane radiography and CT: Application to canine ACL deficiency. *Journal of Biomechanical Engineering* 125:238–245.
101. Tashman, S., D. Collon, K. Anderson, P. Kolowich, and W. Anderst. 2004. Abnormal rotational knee motion during running after anterior cruciate ligament reconstruction. *The American Journal of Sports Medicine* 32:975–983.
102. Bey, M.J., R. Zauel, S.K. Brock, and S. Tashman. 2006. Validation of a new model-based tracking technique for measuring three-dimensional, in vivo glenohumeral joint kinematics. *Journal of Biomechanical Engineering* 128:604–609.
103. Bey, M.J., S.K. Kline, S. Tashman, and R. Zauel. 2008. Accuracy of biplane x-ray imaging combined with model-based tracking for measuring in-vivo patellofemoral joint motion. *Journal of Orthopaedic Surgery and Research* 3:38.
104. Anderst, W., R. Zauel, J. Bishop, E. Demps, and S. Tashman. 2009. Validation of three-dimensional model–based tibio-femoral tracking during running. *Medical Engineering & Physics* 31:10–16.
105. Li, G., L.E. DeFrate, S.E. Park, T.J. Gill, and H.E. Rubash. 2005. In vivo articular cartilage contact kinematics of the knee: An investigation using dual-orthogonal fluoroscopy and magnetic resonance image–based computer models. *The American Journal of Sports Medicine* 33:102–107.
106. Li, G., L.E. Defrate, H.E. Rubash, and T.J. Gill. 2005. In vivo kinematics of the ACL during weight-bearing knee flexion. *Journal of Orthopaedic Research* 23:340–344.
107. Li, G., S.K. Van de Velde, and J.T. Bingham. 2008. Validation of a non-invasive fluoroscopic imaging technique for the measurement of dynamic knee joint motion. *Journal of Biomechanics* 41:1616–1622.
108. de Asla, R.J., L. Wan, H.E. Rubash, and G. Li. 2006. Six DOF in vivo kinematics of the ankle joint complex: Application of a combined dual-orthogonal fluoroscopic and magnetic resonance imaging technique. *Journal of Orthopaedic Research* 24:1019–1027.
109. Li, G., L. Wan, and M. Kozanek. 2008. Determination of real-time in-vivo cartilage contact deformation in the ankle joint. *Journal of Biomechanics* 41:128–136.
110. Wan, L., R.J. de Asla, H.E. Rubash, and G. Li. 2008. In vivo cartilage contact deformation of human ankle joints under full body weight. *Journal of Orthopaedic Research* 26:1081–1089.
111. Caputo, A.M., J.Y. Lee, C.E. Spritzer, M.E. Easley, J.K. DeOrio, J.A. Nunley, 2nd, and L.E. DeFrate. 2009. In vivo kinematics of the tibiotalar joint after lateral ankle instability. *The American Journal of Sports Medicine* 37:2241–2248.
112. Nakamura, S., R.D. Crowninshield, and R.R. Cooper. 1981. An analysis of soft tissue loading in the foot—a preliminary report. *Bulletin of Prosthetics Research* 18 (BPR 10-35):27–34.
113. Simkin, A. 1982. Structural Analysis of the Human Foot in Standing Posture. PhD. Tel-Aviv University.
114. Meglan, D. 1991. Enhanced Analysis of Human Locomotion. PhD. The Ohio State University.
115. Scott, S.H., and D.A. Winter. 1993. Biomechanical model of the human foot: Kinematics and kinetics during the stance phase of walking. *Journal of Biomechanics* 26:1091–1104.
116. Gilchrist, L.A., and D.A. Winter. 1996. A 2-part, viscoelastic foot model for use in gait simulations. *Journal of Biomechanics* 29:795–798.
117. Patil, K.M., L.H. Braak, and A. Huson. 1996. Analysis of stresses in two-dimensional models of normal and neuropathic feet. *Medical & Biological Engineering & Computing* 34:280–284.
118. Ledoux, W.R. 1999. A Biomechanical Model of the Human Foot with Emphasis on the Plantar Soft Tissue. PhD. University of Pennsylvania.
119. Gefen, A., M. Megido-Ravid, Y. Itzchak, and M. Arcan. 2000. Biomechanical analysis of the three-dimensional foot structure during gait: A basic tool for clinical applications. *Journal of Biomechanical Engineering* 122:630–639.

120. Chen, W.P., F.T. Tang, and C.W. Ju. 2001. Stress distribution of the foot during mid-stance to push-off in barefoot gait: A 3-D finite element analysis. *Clinical Biomechanics (Bristol, Avon)* 16:614–620.
121. Chen, W.P., C.W. Ju, and F.T. Tang. 2003. Effects of total contact insoles on the plantar stress redistribution: A finite element analysis. *Clinical Biomechanics (Bristol, Avon)* 18:S17–24.
122. Gefen, A. 2002. Stress analysis of the standing foot following surgical plantar fascia release. *Journal of Biomechanics* 35:629–637.
123. Gefen, A. 2003. Plantar soft tissue loading under the medial metatarsals in the standing diabetic foot. *Medical Engineering & Physics* 25:491–499.
124. Gefen, A., M. Megido-Ravid, M. Azariah, Y. Itzchak, and M. Arcan. 2001. Integration of plantar soft tissue stiffness measurements in routine MRI of the diabetic foot. *Clinical Biomechanics (Bristol, Avon)* 16:921–925.
125. Cheng, H.Y., C.L. Lin, H.W. Wang, and S.W. Chou. 2008. Finite element analysis of plantar fascia under stretch—the relative contribution of windlass mechanism and Achilles tendon force. *Journal of Biomechanics* 41:1937–1944.
126. Cheung, J.T., M. Zhang, and K.N. An. 2004. Effects of plantar fascia stiffness on the biomechanical responses of the ankle–foot complex. *Clinical Biomechanics (Bristol, Avon)* 19:839–846.
127. Cheung, J.T., K.N. An, and M. Zhang. 2006. Consequences of partial and total plantar fascia release: A finite element study. *Foot & Ankle International* 27:125–132.
128. Cheung, J.T., and M. Zhang. 2005. A 3-dimensional finite element model of the human foot and ankle for insole design. *Archives of Physical Medicine and Rehabilitation* 86:353–358.
129. Cheung, J.T., and M. Zhang. 2008. Parametric design of pressure-relieving foot orthosis using statistics-based finite element method. *Medical Engineering & Physics* 30:269–277.
130. Cheung, J.T., M. Zhang, A.K. Leung, and Y.B. Fan. 2005. Three-dimensional finite element analysis of the foot during standing—a material sensitivity study. *Journal of Biomechanics* 38:1045–1054.
131. Cheung, J.T., M. Zhang, and K.N. An. 2006. Effect of Achilles tendon loading on plantar fascia tension in the standing foot. *Clinical Biomechanics (Bristol, Avon)* 21:194–203.
132. Dai, X.Q., Y. Li, M. Zhang, and J.T. Cheung. 2006. Effect of sock on biomechanical responses of foot during walking. *Clinical Biomechanics (Bristol, Avon)* 21:314–321.
133. Yu, J., J.T. Cheung, Y. Fan, Y. Zhang, A.K. Leung, and M. Zhang. 2008. Development of a finite element model of female foot for high-heeled shoe design. *Clinical Biomechanics (Bristol, Avon)* 23 (Suppl 1):S31–38.
134. Lemmon, D.R., T.Y. Shiang, A. Hashmi, J.S. Ulbrecht, and P.R. Cavanagh. 1997. The effect of insoles in therapeutic footwear: A finite-element approach. *Journal of Biomechanics* 30:615–620.
135. Erdemir, A., M.L. Viveiros, J.S. Ulbrecht, and P.R. Cavanagh. 2006. An inverse finite-element model of heel-pad indentation. *Journal of Biomechanics* 39:1279–1286.
136. Petre, M.T., A. Erdemir, and P.R. Cavanagh. 2006. Determination of elastomeric foam parameters for simulations of complex loading. *Computer Methods in Biomechanics and Biomedical Engineering* 9:231–242.
137. Goske, S., A. Erdemir, M. Petre, S. Budhabhatti, and P.R. Cavanagh. 2006. Reduction of plantar heel pressures: Insole design using finite element analysis. *Journal of Biomechanics* 39:2363–2370.
138. Budhabhatti, S.P., A. Erdemir, M. Petre, J. Sferra, B. Donley, and P.R. Cavanagh. 2007. Finite element modeling of the first ray of the foot: A tool for the design of interventions. *Journal of Biomechanical Engineering* 129:750–756.
139. Cavanagh, P.R., A. Erdemir, and M. Petre. 2008. A finite element approach to examine the relationship between plantar pressure and internal stress in the foot. *54th Annual Meeting of the Orthopaedic Research Society*. San Francisco, CA.
140. Sharkey, N.A., and A.J. Hamel. 1998. A dynamic cadaver model of the stance phase of gait: Performance characteristics and kinetic validation. *Clinical Biomechanics (Bristol, Avon)* 13:420–433.
141. Donahue, S.W., and N.A. Sharkey. 1999. Strains in the metatarsals during the stance phase of gait: Implications for stress fractures. *Journal of Bone and Joint Surgery. American Volume* 81A:1236–1244.

142. Michelson, J.D., A.J. Hamel, F.L. Buczek, and N.A. Sharkey. 2002. Kinematic behavior of the ankle following malleolar fracture repair in a high-fidelity cadaver model. *Journal of Bone and Joint Surgery. American Volume* 84-A:2029–2038.
143. Hamel, A.J., N.A. Sharkey, F.L. Buczek, and J. Michelson. 2004. Relative motions of the tibia, talus, and calcaneus during the stance phase of gait: A cadaver study. *Gait & Posture* 20:147–153.
144. Kirane, Y.M., J.D. Michelson, and N.A. Sharkey. 2008. Evidence of isometric function of the flexor hallucis longus muscle in normal gait. *Journal of Biomechanics* 41:1919–1928.
145. Kirane, Y.M., J.D. Michelson, and N.A. Sharkey. 2008. Contribution of the flexor hallucis longus to loading of the first metatarsal and first metatarsophalangeal joint. *Foot & Ankle International* 29:367–377.
146. Okita, N., S.A. Meyers, J.H. Challis, and N.A. Sharkey. 2009. An objective evaluation of a segmented foot model. *Gait & Posture* 30:27–34.
147. Noble, L.D., Jr., R.W. Colbrunn, D.G. Lee, A.J. van den Bogert, and B.L. Davis. 2010. Design and validation of a general purpose robotic testing system for musculoskeletal applications. *Journal of Biomechanical Engineering* 132:025001.
148. Lee, D.G., and B.L. Davis. 2009. Assessment of the effects of diabetes on midfoot joint pressures using a robotic gait simulator. *Foot & Ankle International* 30:767–772.
149. Erdemir, A., P.A. Sirimamilla, J.P. Halloran, and A.J. van den Bogert. 2009. An elaborate data set characterizing the mechanical response of the foot. *Journal of Biomechanical Engineering* 131:094502.
150. Hurschler, C., J. Emmerich, and N. Wulker. 2003. In vitro simulation of stance phase gait part I: Model verification. *Foot & Ankle International* 24:614–622.
151. Wulker, N., C. Hurschler, and J. Emmerich. 2003. In vitro simulation of stance phase gait part II: Simulated anterior tibial tendon dysfunction and potential compensation. *Foot & Ankle International* 24:623–629.
152. Nester, C.J., A.M. Liu, E. Ward, D. Howard, J. Cocheba, T. Derrick, and P. Patterson. 2007. In vitro study of foot kinematics using a dynamic walking cadaver model. *Journal of Biomechanics* 40:1927–1937.
153. Kim, K.J., H.B. Kitaoka, Z.P. Luo, S. Ozeki, L.J. Berglund, K.R. Kaufman, and K.N. An. 2001. In vitro simulation of the stance phase of gait. *Journal of Musculoskeletal Research* 5:113–121.
154. Aubin, P.M., E.C. Whittaker, and W.R. Ledoux. 2012. A robotic cadaveric gait simulator with fuzzy logic vertical ground reaction force control. *IEEE Transactions on Robotics* 28:246–255.
155. Aubin, P.M., M.S. Cowley, and W.R. Ledoux. 2008. Gait simulation via a 6-DOF parallel robot with iterative learning control. *IEEE Transactions on Bio-Medical Engineering* 55:1237–1240.
156. Jackson, L.T., P.M. Aubin, M.S. Cowley, B.J. Sangeorzan, and W.R. Ledoux. 2011. A robotic cadaveric flatfoot analysis of stance phase. *Journal of Biomechanical Engineering* 133:051005.
157. Bayomy, A.F., P.M. Aubin, B.J. Sangeorzan, and W.R. Ledoux. 2010. Arthrodesis of the first metatarsophalangeal joint: A robotic cadaver study of the dorsiflexion angle. *Journal of Bone and Joint Surgery. American Volume* 92:1754–1764.

Section III

Biologic Considerations and Clinically Related Orthopaedic Biomechanics

11

Musculoskeletal Cell Mechanics

Shyni Varghese and Adam J. Engler

CONTENTS

11.1 Introduction

Musculoskeletal mechanics occur over many length scales, from macroscopic muscle extension and weight-bearing bone compression to microscopic muscle fibers, down to the cytoskeleton that supports the bone cell structure and facilitates muscle cell contraction. At each length scale, the surrounding environment can play a critical role in modulating the mechanical behavior; this is especially true at the cellular and the subcellular length scales wherein the intrinsic properties of the environment, that is, composition, structure, and elasticity of adjacent extracellular proteins, can modulate cell behavior and the transduction of their signals. Passive properties "felt" by cells via actomyosin contractions occur using many varied mechanisms and invoke a wide range of cell responses, that is, the induction of gene expression through calcification. This area has been a significant focus of research in musculoskeletal cell mechanics over the past decade. However, the inverse case in which solid and shear stresses are actively applied to these systems has also been a source of much enthusiasm. To appreciate the breadth of the understanding of musculoskeletal cell mechanics as well as the open questions in the field, this chapter provides an introductory review of musculoskeletal structures, followed by a presentation of the recent literature on mechanotransduction, for both bone and muscle.

11.2 Bone Structure and Composition

Bone is a highly vascularized, dynamic, and responsive tissue with functions ranging from structural support to the protection of vital organs and even serving as a reservoir of minerals in the body. The adult human skeleton contains 206 bones that are generally divided into five categories based on their shape, which is roughly determined by their anatomical location(s).[1] These categories are broken down into long bones, short bones, flat bones, irregular bones, and sesamoid bones. Long and short bones are associated with movement; femur and cuneiform bones are examples of long and short bones, respectively. Flat bones typically function to protect vital organs (i.e., scapula, ribs), whereas sesamoid bones are embedded in tendons and ligaments (i.e., the patella).

From a structural perspective, bone is a biphasic composite structure containing organic and inorganic phases. The organic phase (also referred to as osteoid) is composed primarily of type I collagen, noncollagenous proteins (such as osteocalcin and bone sialoprotein), proteoglycans, and other organic structural components.[2] The mineralized phase is composed of calcium phosphate that has been described as poorly to semicrystalline. Although bone mineral has several similarities to hydroxyapatite,[3] Raman analyses suggest that there are several compositional differences between bone mineral and hydroxyapatite, as evidenced by the replacement of hydroxyl groups with carbonate groups.[4] Bone mineral is present in the form of mineralized fibrils of collagen within the osteoid. The composite structure provides bone with its strength and load-bearing capacity, with Young's moduli ranging from approximately 10 to 15 GPa for trabecular bone and 19 to 21 GPa for cortical bone.[5] The mineralized phase provides stiffness, whereas the protein phase allows bone to resist tension while reducing brittleness to some extent.[2]

Osteoblasts and osteoclasts are involved in the formation, maintenance, and turnover of bone. Osteoblasts are mononuclear cells of mesenchymal origin, whereas osteoclasts are multinucleated cells of hematopoietic origin.[6] Osteoblasts are formed through the differentiation of pre-osteoblasts, which are, in turn, formed by the differentiation of multipotent mesenchymal progenitors. These cells have limited mitotic activity and are chiefly responsible for the production of bone matrix and deposition. In doing so, they contribute to osteoid formation, which subsequently undergoes mineralization. When osteoblasts become trapped in a matrix, they terminally differentiate into mature bone cells, known as osteocytes. Osteocytes reside in empty spaces within bone called lacunae and are characterized by the presence of cytoplasmic extensions that reside in canals known as canaliculi. They are also capable of bone resorption to a limited degree, in what is known as osteocytic osteolysis.[7] However, the main contributors to bone resorption are osteoclasts. They are characterized by their large size (~40 μm) and the presence of vacuoles containing tartrate-resistant acid phosphatases. The osteoclast-mediated bone resorption releases calcium and phosphate ions into extracellular fluid. Osteoclast-mediated bone resorption and osteoblast-mediated bone formation form the basis of bone remodeling, a factor contributing to skeletal homeostasis.[8,9] Frostian modeling and remodeling concepts proposed by Frost described the distinct mechanisms by which osteoblasts and osteoclasts contribute to the development of skeletal tissue and how physiological changes such as aging contribute to this process. A detailed description of how mechanical stresses contribute to bone remodeling/bone homeostasis is discussed later in this chapter.

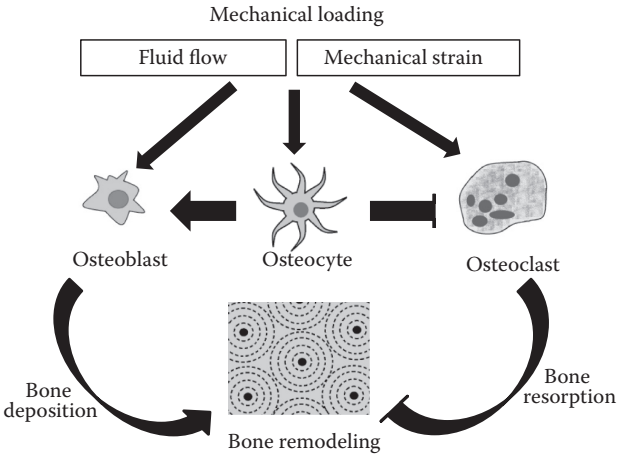

FIGURE 11.1
Schematic showing the various types of bone cells and their role in mechanosensing and bone remodeling.

Bone is a highly complex tissue with various levels of hierarchical organization ranging from the nanoscale to the macroscale. The first level of hierarchy involves molecular components of bone tissue such as collagen molecules, inorganic minerals, and water. The higher levels of organization involve multiple components and the macroscopic architecture of bone. The hierarchical structure of bone gives it repetitive load-bearing ability, heterogeneous and anisotropic mechanical properties, viscoelasticity, resistance to crack propagation, nutritional supply and fluid flow, and functional properties such as functional adaptation with respect to the mechanical environment. Mechanical loading is vitally important to bone formation, normal growth, architecture, tissue homeostasis, and fracture healing. Bone formation and remodeling are well known to be influenced by a highly active mechanical environment (Figure 11.1). Physiological loading such as interstitial fluid flow, hydrostatic pressure, compression, and strains associated with bending and stretching provides various types of mechanical cues to bone tissues (Figure 11.1).[10–12]

11.3 Mechanical Environment and Bone Architecture

The profound influence of the mechanical and physiological environment on bone tissue was speculated for centuries based on observations made by Galileo and da Vinci. Galileo's observations suggest a relationship between bone architecture and the size and shape of the species (Figure 11.2), whereas da Vinci's observations indicate a relationship between mechanical properties and their volume.[13]

The complex structure of bone is optimized to withstand active mechanical loading. The ability of bone tissues to change their shape, microstructure, and bulk density in response to the local mechanical and physical environment has led to various types of bone tissues depending on their anatomic locations and functional demands. The ability

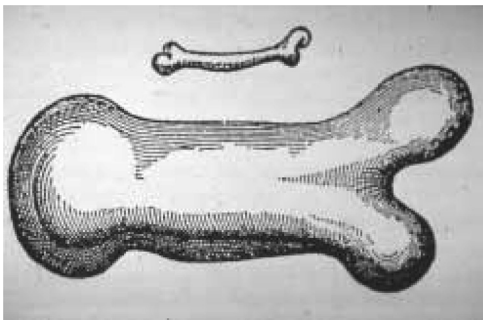

FIGURE 11.2
Galileo's illustration, depicting a pattern between bone structure and anatomical shape. (Reproduced from Martin, R.B., *J. Musculoskelet. Neuronal. Interact.*, 7(1), 48, 2007.)

of bone tissue to respond to mechanical stresses and change their morphology accordingly was expressed qualitatively by Roux in 1881 and mathematically by Julius Wolff in 1892.[14] These theories state that when bone is placed under increased mechanical loading, it undergoes remodeling to improve its strength to resist that loading. Wolff's law further states that trabecular bone is the first to respond to mechanical stress by rearrangement of the trabeculae, followed by changes in cortical bone. The concept of load-induced bone remodeling provides a mechanistic insight into why bone tissues have different architectures and densities depending on their anatomic locations. The ability of bones to adapt to changes in mechanical loading is evident from several real-world observations, such as the different bone densities between the throwing arm and racquet-holding arm of tennis players.[15] Just as an active mechanical environment can contribute to the strengthening of bone, the disuse of bone tissue, such as in microgravity or during inactivity, leads to the loss of bone mass.[16] Although the ability of bone to adapt to the mechanical environment is well established, the mathematical expression of Wolff's law is not sufficient to represent the complex changes in bone tissue with altered mechanical loading. Recently, the more general term of "bone functional adaptation" has gained popularity for describing the architectural and functional changes in bone due to mechanical stresses.[14] According to this new terminology, increased strains and loading lead to increased bone matrix deposition. The premise of "bone functional adaptation" is that the tissue strives to maintain an equilibrium level of strain. Increased strain on the bone promotes bone deposition, which, in turn, makes the tissue stronger and decreases the perceived strain to the equilibrium level. Decreased application of strain conversely leads to increased bone resorption and thereby weakens the bone, increasing the perceived strain to the equilibrium level.[14]

The mechanical loading-induced architectural changes in bone ensure that the bone tissues placed at each location throughout the mammalian skeleton have the optimal structure and mechanics to withstand location-specific functional load bearing without damage. This means that higher bone formation is achieved where the mechanical stress on the bone tissue is greatest. Such stress-sensitive strengthening of bone tissue reduces stress hotspots within bones that could lead to their structural failure. Thus, bone tissues also follow the principles of optimum structural design, that is, they are mechanically efficient in terms of strength-to-weight ratio.

In a matured skeleton, the process by which bone tissue adapts is termed "remodeling" and is governed mainly through specific biomechanical cues. Bone remodeling, which involves the antagonistic and sequential activities of bone resorption and bone formation, is fundamental to bone homeostasis. It is also a self-repairing process that is used to repair the microfractures and damaged/old bone layers. According to Weibull's theory, bone remodeling–mediated changes in bone volume reduce the structural flaw–mediated failure of bone tissues.[13] In this way, bone remodeling controls both bone density and fatigue damage that occurs routinely because of the high strains experienced by bone in stress-prone regions.[13,17] As discussed previously, the cell populations involved in this process are osteoblasts and osteoclasts. These cell types work as a synchronized team called the basic multicellular unit.[18] Studies have indicated that during remodeling, the new bone is aligned along the dominant local loading direction, suggesting the role of local mechanical stress on bone modeling.[19] The relationship between bone modeling, remodeling, and the mechanical environment is postulated by Frost[20] in his mechanostat theory. Beyond demonstrating the role of mechanical stresses on bone modeling and remodeling, Frostian theory describes the window of physiological mechanical stress that is palatable for maintaining bone homeostasis. It is also important to note that the adaptive response of bone differs for static and dynamic mechanical cues. Lanyon and Rubin[21] demonstrated that an avian ulna subjected to static mechanical loading did not undergo any changes in bone remodeling, whereas an avian ulna subjected to intermittent loading showed substantial changes in remodeling, despite the fact that both static and mechanical loads were deemed sufficient to produce strains in the functional dynamic strain range.

The various factors affecting bone remodeling can be briefly stated through three rules, as summarized by Turner:[22] (1) bone remodeling is dependent on dynamic cues, more so than static cues; (2) adaptation of bone can be achieved with even brief mechanical stimulation; and (3) bone cells, which are responsible for translating mechanical cues into an adaptive tissue response, become accustomed to loading environments and thereby are less responsive to routine loading.

The mechanical environment of the site of healing plays an important role in the repair of bone fractures. A number of mechanical factors ranging from the fracture geometry to the gap to fixation play an important role in bone repair. It is well known that fractures with smaller gaps heal faster compared with fractures with larger gaps.[23] Fixation of the injured site also has a significant effect on the healing process. For instance, rigid fixation limits callus formation due to minimized interfragmentary motion of the impaired tissue, whereas a flexible fixation, which permits interfragmentary movement of the tissues, improves the healing process by enhancing the callus formation.[24] It is also important to note that an unstable fixation can prevent healing. Larsson et al.[25] have shown that both the amount and direction of local interfragmentary movement affect the healing process, with moderate axial interfragmentary movement enhancing the rate of healing and fracture repair.

Although most of the early work on bone mechanobiology concentrated on organ-level analysis,[26] modern mechanobiology has elucidated the various cellular and molecular mechanisms that explain how differences in the mechanical loading on bone can be translated at the tissue level into the subsequent remodeling of bone (Figure 11.3). Insights into this field have substantially improved our understanding of mechanotransduction in bone, especially on the contributions of the various cell types in bone, and are discussed in the subsequent sections of this chapter.

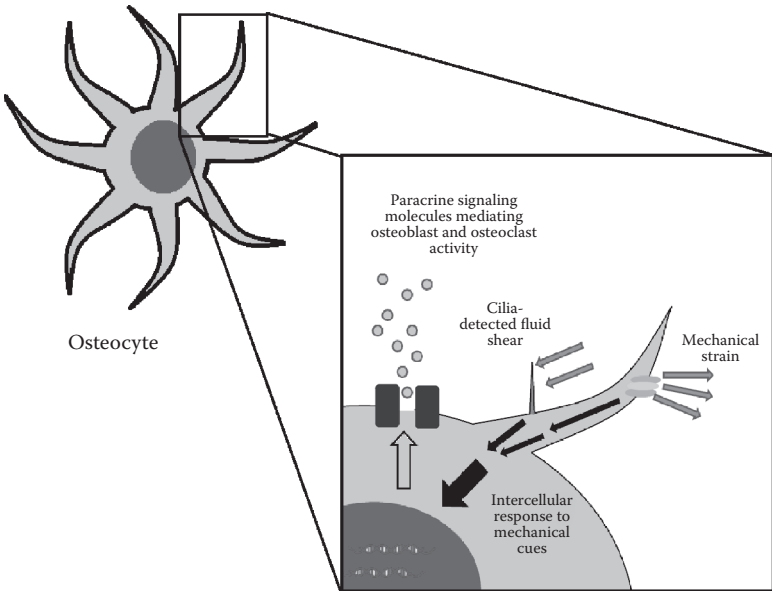

FIGURE 11.3
Schematic showing the various mechanisms through which osteocytes and osteoblasts function as the chief mechanosensors in bone tissue.

11.4 Bone Mechanotransduction at the Cellular Level

Unlike soft tissues such as cartilage and tendon, the matrix stiffness (i.e., elastic modulus) of bone tissue is much higher, making the strain generated in bone tissue far less. For instance, even during substantial load bearing, values of mechanical strain in bone are often in the range of 0.1% to 0.5%;[27] the remarkable effect of such small strains on bone tissue suggests the central role that cells play on mechanosensing-mediated changes of bone tissue. Although the ability of different types of bone cells to respond to mechanical stimuli has been very well established, it is hard to identify the critical cell type that is responsible for orchestrating the response of mechanical signals.

The role of osteocytes on mechanosensing has been established over the years. Osteocytes, having long cytoplasmic extensions, form the majority of the cells in bone and play a major role in mechanotransduction.[28] Application of mechanical strain has been shown to change cell shape as well as the orientation and distribution of actin and paxillin in mouse tibial and calvarial osteocytes, indicating the ability of osteocytes to respond to both loading and strain.[29,30] Mechanical strain has been found to increase the activity of glucose-6 phosphate dehydrogenase and leads to earlier expression of c-*fos* in osteocytes *in vivo*.[31] Interestingly, c-*fos* has been implicated as a key regulator of osteoclastogenesis;[32] although this may suggest the somewhat counterintuitive statement that increases in loading could support bone resorption through increased osteoclast activity, there is direct evidence showing that mechanical loading inhibits osteoclastogenesis by osteocytes.[33]

Several studies have elucidated a number of methods in which bone cells may sense and transmit mechanical cues. One such mechanical response is the influx of Ca^{2+} via mechanically stimulated ion channels in bone cells.[34] The role of calcium is particularly important

because higher intracellular calcium is vital for nitrous oxide synthase, which is required to synthesize nitrous oxide, an important signaling molecule in bone.

Previous studies have demonstrated that the application of loading to bone stimulates fluid flow through lacunae containing osteocytes and through canaliculi away from the loaded region. This is due to a slight decrease in lacunae size in the loaded region, forcing fluid through the Haversian network; this fluid flow could stimulate synthetic activity and inhibits resorptive activity in bone. Indeed, Klein-Nulend et al.[35] found evidence that, *in vitro*, only osteocytes (and not osteoblasts) responded to pulsatile fluid flow through the release of prostaglandin E_2 and suggested that osteocytes played a major role in sensing mechanical cues. Osteocytes have also been reported to distinguish between mechanical strain and fluid flow in response to pulsating fluid flow, primary human bone cells produced both nitrous oxide and prostaglandin E_2, whereas cyclic strain was found to only increase nitrous oxide (NO) production.[36] The vital role of osteocytes in mechanosensing has also been underscored through the demonstrated lack of unloading-stimulated bone loss due to specific osteocyte ablation in a transgenic mouse model.[37]

There are several potential mechanisms as to how osteocytes could detect this fluid shear. One such mechanism, outlined by Cowin and Weinbaum,[27] is shear-induced strain on the osteocyte glycocalyx. Fluid flow induced by loading is expected to apply strain to the osteocyte membrane, which could be translated to intracellular responses via integrin–cytoskeleton complexes in the osteocyte glycocalyx. Further evidence that fluid flow plays a major role in mechanotransduction in bone is provided by the fact that higher expressions of osteopontin were induced in osteoblasts (MC3T3-E1 cells) by fluid shear but not by mechanical strain, suggesting that fluid shear promotes higher osteogenic activity.[38] Recently, Burra et al.[39] have demonstrated the role of cell–cell interactions in osteocyte-mediated mechanotransduction. Their study demonstrated the opening of hemichannels (specifically, 43 connexin) in response to mechanical loading. Interestingly, it showed that disruption of the glycocalyx was sufficient to affect hemichannel opening on the cell body in response to mechanical cues. In this way, this study underscored the importance of the glycocalyx of the cytoplasmic extension in mechanotransduction, as well as the role of integrins located on the glycocalyx in transmitting mechanical cues from bone. Further emphasizing the role of cytoplasmic extensions in mechanosensing, mechanical stimulation of both the cell body as well as the cytoplasmic extensions was found to stimulate intracellular NO production in single osteocytes.[40] Single osteocytes were also found to communicate with other osteocytes independent of these cytoplasmic extensions. Instead, it is likely that the osteocytes communicated through cell-secreted soluble factors. This suggests that the primary function of these extensions may be mechanosensing rather than cell–cell communication.

Recently, the role of primary cilia in sensing load-induced shear flow in bone cells has been elucidated. The role of primary cilia in mechanotransduction in bone cells has recently been probed, specifically in MC3T3-E1 osteoblasts and MLO-Y4 osteocytes.[41] The authors found that these cells possessed primary cilia that projected above the cell, and that these cilia were deflected when the cells were exposed to fluid flow. Additionally, the authors also noted that in contrast with previous theories regarding mechanotransduction in bone cells, the cilia-mediated intracellular responses were independent of Ca^{2+} flux and stretch-activated ion channels (Figure 11.4).

It has been proposed that in response to fluid flow, osteocytes regulate bone synthesis and resorption via the stimulation of osteoblasts and osteoclasts, respectively. When subjected to pulsatile fluid flow, osteocytes have been demonstrated to promote the differentiation of osteoblasts while inhibiting their proliferation via soluble cues, such as nitrous

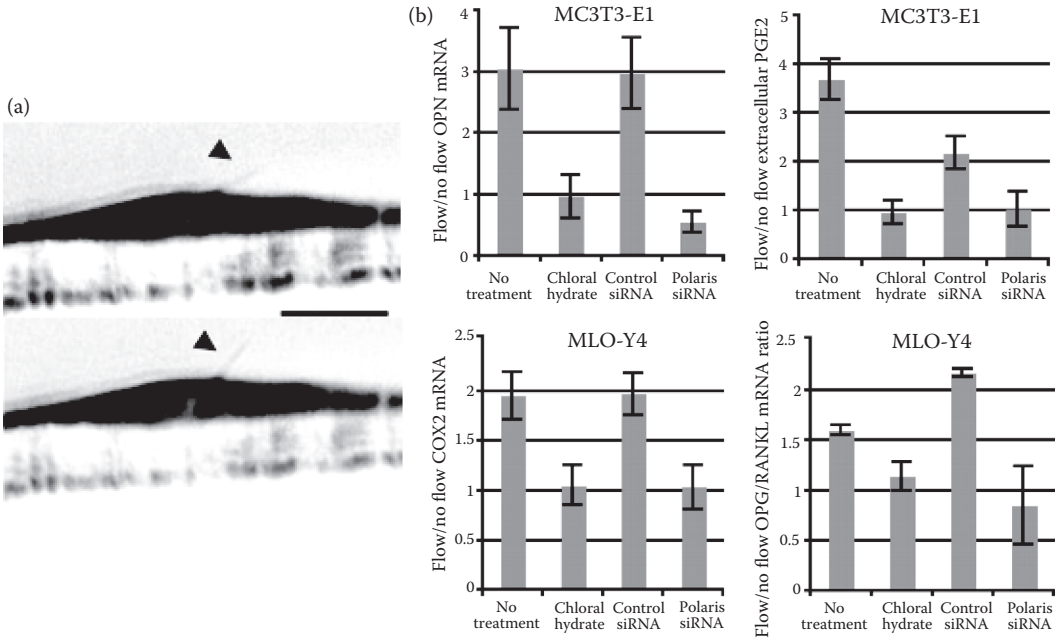

FIGURE 11.4
Role of primary cilia in mechanosensing. (a) Movement of cilia in response to fluid flow (arrow indicates cilia). (b) Effects of various treatments designed to knock out the cilia-mediated response to fluid flow, on gene expression in MC3T3-E1 osteoblasts and MLO-Y4 osteocytes. Chloral hydrate treatment or deletion of the protein Polaris via small interfering RNA can be used to dissemble primary cilia. Osteopontin (OPN), cyclooxygenase-2, and prostaglandin E_2 are all mature, mechanosensitive proteins, and their primary cilia-dependent upregulation with flow is shown here. (Adapted from Malone, A.M.D. et al., *Proc. Natl. Acad. Sci. U.S.A.*, 104(33), 13325–13330, 2007.)

oxide.[42] A study by Taylor et al.[43] suggests that gap junctions also play a major role in the translation of mechanical signals perceived by osteocytes into an osteoblastic response using an osteocyte–osteoblast coculture system. This study showed that osteocytes subjected to shear flow were able to induce an increase in alkaline phosphatase activity in osteoblasts shielded from the shear flow, and that physical contact between osteoblasts and osteocytes was required for this response. It must be noted that these are *in vitro* studies using different osteocyte and osteoblast cell lines, and that the interaction between these cells *in vivo* is likely a combination of soluble cues and gap junctions.

Two important signaling molecules related to the regulation of bone remodeling by osteocytes and osteoblasts are the receptor activator of nuclear factor-κB ligand (RANKL) and osteoprogenerin (OPG), which promote and inhibit osteoclastogenesis, respectively, and have been implicated in the response of bone stromal cells to shear flow (Figure 11.3).[44] You et al.[33] have reported the ability of osteocytes to induce osteoclast formation in the absence of loading and to inhibit osteoclastogenesis in response to mechanical loading through a RANKL/OPG-mediated mechanism. MLO-Y4 osteocytes promoted the formation of osteoclasts from RAW264.7 osteoclast precursors in an *in vitro* coculture system. However, when the osteocytes were subjected to oscillatory fluid flow, their ability to support osteoclast formation was significantly diminished. Application of fluid flow was found to decrease the expression of RANKL in relation to OPG; because RANKL can

promote the formation of osteoclasts, this is a potential mechanism through which osteocytes could indirectly regulate bone resorption in response to fluid shear. Additionally, conditioned medium obtained from osteocytes subjected to fluid shear was found to inhibit osteoclast formation, even in conditions known to support it. Indeed, conditioned medium from flow-subjected osteocytes was found to contain increased levels of OPG (an inhibitor of osteoclastogenesis) and decreased levels of RANKL (a promoter of osteoclastogenesis); this demonstrated the ability of osteocytes subjected to fluid flow to inhibit osteoclast activity. Mechanical loading has also been shown to reduce RANKL expression in bone stromal cells, which could thereby decrease osteoclast activity.[45] This study also showed that application of strain led to the activation of extracellular receptor kinase 1/2 and N-terminal Jun kinase; given the important role of these kinases in cellular mechanoregulation, it is clear that the application of strain plays a key role in mechanoregulation.

Osteoclasts are large, multinucleated cells and are chiefly responsible for resorption of bone matrix through the secretion of enzymes such as tartrate-resistance acid phosphatase (TRAP).[46] Interestingly, in a study by Kurata et al.,[47] osteoclasts have also been shown to respond directly to mechanical stimulus. Their study showed that isolated rabbit osteoclasts subjected to mechanical strain had upregulated osteoclast marker enzymes, TRAP, and cathepsin K, which are all major markers of osteoclast activity. Mechanically strained osteoclasts also showed increased resorptive activity on their ivory substrate; this suggests that mechanical strain promotes increased resorption of osteoclasts in the absence of signals from osteoblasts. Although increased resorption in response to mechanical strain may seem somewhat counterintuitive, it is important to note that osteoblasts and osteocytes have been shown to inhibit osteoclast maturation in response to mechanical stress, as previously mentioned. Moreover, stretching of isolated chicken osteoclasts has been reported to lead to increases in intracellular Ca^{2+} levels via a calcium-conducting ion channel.[48] The authors of this study speculate that this could be a pathway through which mechanical cues regulate osteoclastic activities, as increases in Ca^{2+} have been shown to lead to a decrease in adhesion molecules and resorptive activity of osteoclasts.[49,50]

An argument against the proposed mode of mechanosensing by osteocytes, however, is that strains predicted in bone are believed to be too small to produce a significant intracellular response in osteocytes. To this end, several studies have investigated strain amplification mechanisms in these cells. A model developed by Han et al.[51] suggests that flexural rigidity of molecules responsible for tethering the cytoplasmic extensions to the canalicular wall transmits hoop tension to the core actin bundle and plays a role in strain amplification in osteocytes. More recently, models have also been developed to study the flow-induced response. Wang et al.[52] have developed a theoretical model of osteocyte mechanosensing; according to their model, cytoplasmic extensions serve to amplify mechanical signals as a result of flow through canaliculi via activity of $\alpha_v\beta_3$ integrin, suggesting that cell–extracellular matrix (ECM) interaction could also play a role in the sensing of mechanical cues by these cells. These various models have provided valuable insights into the abilities of osteocytes to sense even the minute strains within bone.

11.5 Muscle Origin, Classification, Composition, and Architecture

Like bone, muscle is a highly dynamic, vascularized tissue with extremely complex macromolecular and micromolecular organization. Derived from the mesodermal germ layer,

muscle is most commonly recognized as being responsible for vertebrate locomotion. Actually, muscle is a tissue that takes many forms, that is, skeletal, cardiac, and smooth. The first two muscle types are well known, whereas smooth muscle forms a contractile layer within many smaller blood vessels. Each muscle type has unique functions, but a more common denominator for muscle is that, regardless of its specialization, all muscle types undergo contraction. Muscle is also not strictly the domain of vertebrates either; many invertebrates, most notably *Drosophila* and *C. elegans*, lack a calcified skeletal structure but still have muscle to move body segments, wings, legs, etc.[53] For all of its differences, as a basic feature of all muscle regardless of origin, muscle cells contain actin and myosin arranged in register with one another. This is the first part of a highly organized cytoskeletal architecture, which differs greatly from bone and the previous discussion. In this section, muscle cell architecture and composition are discussed and then related to mechanotransduction in the next section.

Muscle actin and myosin form thin and thick filaments, respectively, so that the head domains on myosin can bind to actin filaments, produce a conformational change on adenosine triphosphate (ATP) hydrolysis, and propel the protein forward relative to actin. The actomyosin structure is stabilized by several key proteins (Figure 11.5a, top): tropomyosin

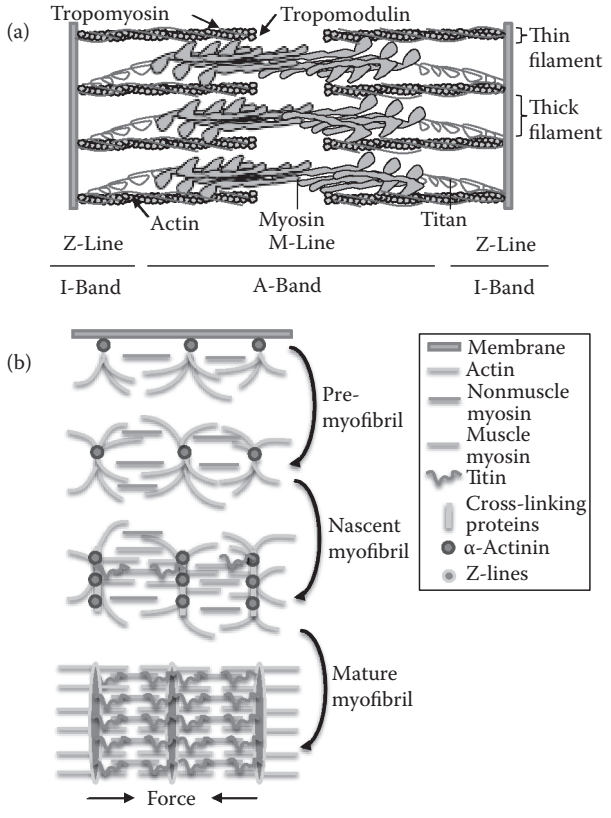

FIGURE 11.5
(See color insert.) Sarcomere: the contractile "force" behind muscle. (a) Sarcomere is complex structure composed of repeating units of actin- and myosin-containing filaments (thin and thick, respectively) that are bound by Z-lines. Actin and myosin slide against one another to generate contractions. (b) Sarcomere assembly model.

regulates where the myosin head binds on thin filaments, tropomodulin caps these thin filaments, and titin sets the length between and anchors thick filaments to Z-lines, which are a collection of aligned cross-linking proteins that link thin and thick filaments together. Together, these proteins make up a repeating unit known as the sarcomere. Sarcomeres have been classically observed in electron micrographs as having electron dense and light regions that correspond to Z-lines and myosin tail regions (M-line), respectively. Regional differences in density have been given names including A-bands and I-bands. Sarcomeric structure is maintained in both skeletal and cardiac muscle, although smooth muscle lacks the highly ordered nature of sarcomeres, opting for a more diffusely arranged actomyosin contractile apparatus.[54]

During development, dramatic changes occur as the sarcomere assembles (see Figure 11.5b). Initially actomyosin structures are exceedingly small, less organized, localized at perimembranous regions, and referred to as "premyofibrils".[55,56] They are composed of nonmuscle myosin type II (NMMII), which pulls on actin filaments to form these initial contractile elements, which are held together by a small amount of α-actinin termed "Z-bodies." As contraction begins, elongated muscle cell shape and polarized forces align adjacent fibrils[57–60] and cells as they "feel" each other.[61] This allows room for thin and thick filament elongation, that is, the addition of actin monomers to the ends of thin filaments permits its extension. Myofibrils with longer thin filaments can generate more force and thus are recruited to the central axis of the cell, becoming part of nascent myofibrils. At the same time, nascent myofibrils begin to recruit proteins such as muscle myosin type II (MMII), titin to thick filaments and zeugmatin, muscle LIM protein (MLP), α-actinin–associated LIM protein, cypher, myopodin, and additional α-actinin to the ends of filaments.[55,62] During this process, titin and actin capture muscle myosin type II and substitute thick filaments containing MMII for those that contain immature NMMII, which may then be recycled back to perimembranous regions of the muscle cell. Proteins associated with filament ends (i.e., those listed above and others) also begin to coalesce to form Z-lines from the immature Z-bodies. However, the transition to fully matured fibrils occurs only after two key changes are made: (1) cross-linking proteins fuse Z-lines, forming laterally clustered structures up to ~160 nm,[63] and (2) titin sets the sarcomere length and positions thick filaments by aligning its C-terminus with M-lines.[64] The reason for setting sarcomere length so late in assembly is twofold: first, titin expression is highly regulated due to its large size and the amount of processing it undergoes.[55,60,65] Second, it ensures that the thin and thick filaments are fully assembled and in place before adjusting their relative locations to one another.[55,65] Sarcomere spacing thus becomes another hallmark of this process with a gradual transition from fibers with short periodicity of less than 1 μm to fibers with 2-μm spacing.[55,56,58,60] Maximum actomyosin binding and peak contractile velocity occur at this sarcomere length and can be determined by measuring contractile velocity for a range of externally applied forces and isometric muscle lengths[66]; this is the essence of the Frank–Starling law,[67] which essentially states that myocardial stretch increases its contractility (up to optimal spacing at which point velocity decreases). The sarcomere is attached to the extracellular space, and so can transduce contractions, via the intermediate filament (IF) protein desmin and costameres, a complex, muscle-specific adhesion system that primarily links muscle to laminin and collagen.[62] Although much of the biological organization of this linkage is beyond the scope of this chapter, we will revisit this structure to some degree when discussing muscle mechanotransduction in the next section.

As with bone, muscle is extremely dynamic. One need only to have had their arm in a cast for several weeks to appreciate that muscle disuse can lead to atrophy. This analogy is

perhaps useful when applied to sarcomere structure as well. Although they may seem to be very static and well defined in this myofibrillogenesis model, recent data suggest that sarcomeres are much more dynamic than previously thought.[62] For example, titin has been shown to have largely unrestricted movement within and between sarcomeres unless there is sufficient calcium load and force to sequester it within a given sarcomere.[68] Moreover, assembly duration can be influenced by the surrounding environment; for example, as the matrix stiffens with time, it is matched by increasing force generation, permitting labile structures to fuse or even generate, as is the case with precardiac mesoderm.[69] Muscle remodeling and stiffening continue in cardiomyocytes through neonatal stages, likely affecting myofibrillogenesis.[70] Higher muscle stiffness in digital flexor tendons has even been associated with precise muscle control.[71]

Muscle organization above the length of the sarcomere is extremely hierarchical, well established, and dependent on muscle type. For skeletal muscle, cells fuse together to form muscle fibers, which are bundled into fascicles, and ultimately arranged into the muscle itself. At this larger length scale, there are still appreciable molecular connections. Fibers are labeled as "slow" (type I) or "fast" (type II) depending on their myoglobin content, ATP source (oxidative metabolism or glycolysis, respectively), and the specific isoform of myosin heavy chain that they use.[72] Cardiac muscle fibers are much like slow skeletal muscle fibers because cardiac fibers have significant myoglobin and use aerobic respiration. On the other hand, these cells do not fuse into long, multinucleated fibers but rather are connected together by a class of adhesive structures called intercalated discs. These structures electrically connect the myocytes into a syncytium by allowing the spread of action potentials (gap junctions) and are responsible for transducing forces during myocardial contraction (desmosomes).[73] Although the molecular details of these structures are not the focus here, the discussion of their role in force transduction will be pursued in the following section.

11.6 Mechanisms to Transduce Mechanically Induced Muscle Signals

Because myocytes use these elaborate sarcomeres to contract, they must send both biochemical and mechanical signals to their nuclei and surroundings to indicate what the contractile state of the sarcomere is. Although both sets of signals originate from essentially the same structures, myocytes have evolved a unique and completely separate set of protein cascades to accomplish these tasks. The former involves a series of phosphoproteins and enzymes that translocate to inform the cell of contraction or to regulate it, whereas the latter, mechanical transduction of force, involves even more complex cytoskeletal structures called costameres, the dystroglycan complex (DGC), and the ECM. Cells have both mechanisms in place with disparate functions, but both contain redundant signaling pathways ubiquitous to all adherent cells. Here, the transduction signaling systems are detailed, and we provide an interpretation of the mechanism(s) behind them.

11.6.1 Intracellular Biochemical Signaling

Many sarcomere-based biochemical signals originate at highly cross-linked regions, that is, the M-line, Z-line, etc., via translocation or phosphorylation of sarcomeric-associated proteins, although other less cross-linked sarcomeric regions certainly provide some

exceptions to this rule.[62] In fact, several widely studied human myopathies (e.g., familial hypertrophic cardiomyopathy) are caused by sarcomeric-associated protein mutations,[74] which can impair the propagation of relevant biochemical signals, indicating contraction. Yet, even understanding normal protein function has given significant mechanistic insight into these diseases. MLP is an excellent example of a stretch-induced biochemical signaling protein at the Z-line[75] where its absence causes a dilated cardiomyopathy.[76,77] It binds at the α-actinin–actin interface,[78] which enables it to span adjacent thin filaments, but more importantly, it also contains a series of binding sites that may act to initiate signaling cascades.[62,79] Its absence normally causes cardiomyocytes to have assembly defects in costameres and intercalated discs, which impairs force transduction,[80] while also causing muscle to have higher passive stiffness.[81] As a signaling molecule itself, stretch from chronic pressure overload causes nuclear translocation,[82,83] preventing it from signaling to nebulin-related anchoring protein, zyxin, and others and encouraging sarcomere instability[79,80] while promoting a yet to be determined nuclear function. On the other hand, some sarcomere-based signaling proteins altered in myopathies cannot be examined in such a manner. For example, forms of limb-girdle muscular dystrophy have a missense mutation in the immunoglobulin repeat protein myotilin, a protein that stabilizes Z-lines.[84] Mechanistic study of this protein, however, has shown that its deletion does not significantly alter development or sarcomere function, suggesting that its signaling role during contraction may be accomplished by other proteins in its absence.[85]

The M-line is another well-studied biochemical signaling region that can be influenced by mechanics. Unlike the Z-line, in which signaling proteins often also have structural roles, M-line signaling proteins are more evenly mixed between myosin-associated proteins and metabolic enzymes. For instance, a small percentage of muscle creatine kinase (MCK) binds to the M-line to replenish the local ATP concentration by transferring the N-phosphoryl group from the phosphocreatine to adenosine diphosphate (ADP).[86] MCK activity has been reported to be significantly greater in stiff muscle compared with compliant muscle,[87] but for our discussion here, it is most important to note that MCK-null diaphragm myocytes produce 16% less contractile force,[88] although due to cycling, complete loss of contraction only occurs when all creatine kinases are oblated.[89] Other glycolytic enzymes, including β-enolase,[90] also bind to the M-line, but perhaps one of the clearest examples of force-induced activation at the M-line is the C-terminal, titin kinase region of titin. This domain interacts with Next to BRCA1 gene 1 protein (NBR1) when it is exposed to force,[91] which subsequently recruits muscle-specific RING finger 2 (MuRF2) from the nucleus to activate a serum response factor signal.[92] Similar with these other cascades, titin kinase mutation disrupts this pathway and causes myopathies.[92]

11.6.2 Transducing Forces in Muscle Cells

Direct force transduction is the other principal mechanism by which muscle can provide mechanical signals to itself and its neighbors. Unlike bone, muscle does not undergo a substantial amount of fluid shear but rather feels and generates significant uniaxial tension and solid shear from contracting sarcomeres. Because muscle actively generates these forces, it has evolved several specific molecular transduction mechanisms, which will be reviewed here.

As indicated earlier, sarcomeres generate forces that are physically transduced in muscle via a pathway that connects costameres to integral membrane structures to the ECM and, ultimately, to an adjacent muscle cell (Figure 11.6). During force transduction, each of these structures contains proteins that are compliant and can undergo a conformational change

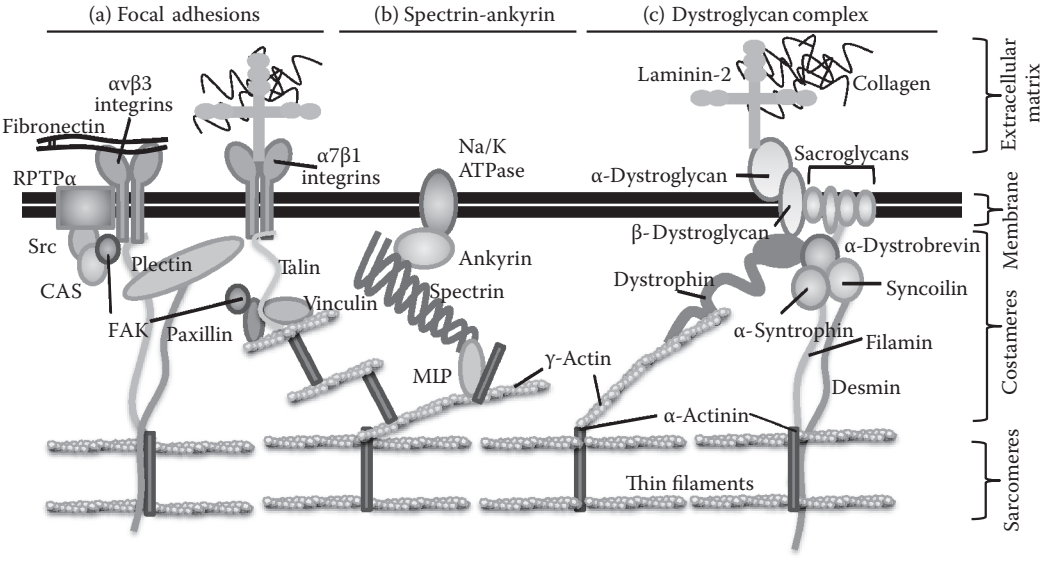

FIGURE 11.6
(See color insert.) Schematic of three costameric connective structures: (a) focal adhesions, (b) spectrin-ankyrin, and (c) DGC between sarcomeres and the ECM as indicated. Although vastly incomplete and omitting all of the biochemical signaling pathways, the sheer complexity of the diagram and multiple transductive pathways for force is apparent.

when force is applied, that is, force-induced unfolding.[93] This new folded structure may then reveal a cryptic binding site, initiating intracellular and intercellular signaling that would not otherwise occur. Although all proteins may be subject to this phenomenon to a degree, only a subset will actually reveal a binding site. Although we focus on muscle-specific occurrences, it is important to note that nonmuscle cells also generate and transduce forces using nonmuscle myosins, that is, stem cells,[94,95] and this results in a cellular "pre-stress" that is globally balanced so that the cell is in static equilibrium.[96] Locally, however, force transduction and imbalances are common and, for most cell types, can be sensed by proteins that undergo force-induced unfolding. Common examples of this are the vinculin-talin complex[97,98] and receptor-like tyrosine phosphatases (RPTPs),[99] both of which are akin to components of the DGC in muscle. With vinculin-talin, forces stretch open talin rod domains, exposing docking sites for vinculin, which separates its head and tail domains to expose a cryptic binding site.[97] Force-dependent focal complexes require RPTP-α activation to induce translocation of Src family kinases.[99] Further downstream, RhoA is required for mechanosensing and tension generation via phosphorylation of myosin light chains,[95,100] and this signal is then further propagated by Rho effectors such as Rho-associated protein kinase[95] and mammalian Diaphanous-related formins.[94] Expression of these effectors has been shown to be cell type-specific, with the latter having higher expression in muscle.[94,101]

For muscle-specific mechanisms, this discussion begins by describing the connection between sarcomere Z-lines and costameres, which, depending on the costameric complex, is generally mediated by IFs (Figure 11.6). Desmin, a muscle-specific IF, links these large structures[62] and has been used as a marker for differentiation because it is only expressed in myocytes maturing toward myotubes.[94,102] Because desmin is extremely compliant, it has also been shown to be mechanosensitive. Several specific missense mutations can impair

desmin function, limit myofibril assembly, and lead to desminopathies that adversely affect skeletal and cardiac muscle function.[103–105] Eight of these fourteen mutations impair filament assembly and might cause local forces to be improperly transduced from sarcomere to costamere.[106] However, evidence shows that some disease-causing mutations, that is, DesA360P, DesQ389P, and DesD399Y, are assembly-competent. Despite this, it is not certain whether each mutation will give rise to impaired transduction. For example, DesA360P has similar tensile properties to normal desmin, but DesQ389P and DesD399Y do not have consistent transductive properties.[107] Such differences imply that broadly categorizing mutations by disease phenotype may not be reflective of similar mechanotransductive mechanisms.

Costameres can broadly be described in muscle as all extracellular adhesive mechanisms.[62,98,108] Because some ubiquitous focal adhesion proteins were mentioned earlier in this section, we again turn to muscle-specific costamere protein complexes, with key exceptions such as vinculin.[98] These structures are linked to Z-lines, and, as such, they repeat the typical sarcomere striation pattern. Vinculin, being a costamere hallmark, was first observed in muscle to also repeat this pattern at the plasma membrane.[109] More importantly, for our discussion, costameres are classically known not just as physical linkers between desmin and the DGC within the plasma membrane but also as force transducers,[110] as has been shown using classic silicone substrates.[111] Currently, costameres contain at least 23 distinct proteins in two connective complexes outside of the previously mentioned vinculin-talin complex, namely, the spectrin-ankyrin and dystrophin complexes.[108,112] In the former complex, spectrin filaments are anchored to the membrane through ankyrin (Figure 11.6b).[62,108] Both spectrin[113,114] and ankyrin[115] have been shown to be very extensible and would serve as good force-transducing candidates. They are linked to sarcomeres via MLP, which as in Z-lines binds the α-actinin–actin interface.[78] Surprisingly enough, ankyrins bind to Na^+K^+ ATPases linking the complex to the plasma membrane, and as such, they cannot transmit force to the ECM and adjacent cells.

The third, most well-studied, and perhaps strongest costameric connection is the dystrophin-associated protein complex (DAPC).[116,117] Dominating the DAPC is the protein dystrophin, which connects Z-line α-actinin–bound γ-actin to the DGC and α-syntrophin (Figure 11.6c). DAPC shows the same banding patterns and often the same expression intensity as all other costameric complexes.[118] Frame-shift mutations cause premature truncation before the actin-binding regions in dystrophin, and this type of mutation is responsible for Becker and Duchenne muscular dystrophies, two of the most common dystrophies.[62,119–121] A difference in severity between the two dystrophies has to do with where the frame-shift and deletion occur, either preserving partial binding or no binding at all, respectively; this directly correlates with mechanical function and force transduction versus healthy muscle.[121] Thus, the partial truncation of Becker muscular dystrophy is characterized by slow progressive muscle weakening, particularly of the muscles in the legs and pelvis due to insufficient production of functional dystrophin. On the other hand, Duchenne muscular dystrophy, in which functional dystrophin is produced due to mutation, is far more severe with muscle degeneration and eventually death. In the latter case, partial rescue exceeding 20% protein restoration seems to be sufficient to restore force transmission, whereas lower expression maintains Becker-like symptoms in a patient.[122] Given its large size, micro-dystrophins containing the actin-binding regions have been used and seem to be an effective strategy for restoring the force-transducing capacity of the DAPC.[123] Aside from dystrophin, syncoilin binds to the desmin IF network to form a second linkage in the DAPC.[108,116,124] Little is known about this connection other than that it is highly upregulated in regenerating muscle,[124] suggesting that it might be one of the

initial force transducers in muscle. However, it is required neither for force transduction nor costamere formation, but to generate maximal isometric force, the desmin-syncoilin connectin is required.[125]

Transduction of these signals to the ECM and adjacent cells terminates with the extracellular connections at the base of costameres, be it integrins or the DGC. There are several muscle-specific integrin isoforms, but the most well-studied is the α7β1 heterodimer.[126] This transmembrane structure binds to laminin on the extracellular side to link the cell to adjacent cells via ECM. Further interactions between laminin and other ECM proteins, including collagen, have been well documented.[127] α7 and β1 have two and four isoforms, respectively, and their expression and localization within myofibers seem to be developmentally and functionally regulated.[128] β1 integrin is a promiscuous binder and is lethal when deleted.[127] However, muscle cells will attempt to compensate for α7 deficiencies with α5 integrin. This results in a shift to fibronectin binding, as α5 is the primary fibronectin matrix binding integrin, and also impairment of force transduction. Due to this, a dystrophic-like phenotype develops in α7-deficient muscle.[128] Although the specific amount of transduction is not clear in normal myocytes, α7β1 overexpression is observed in both Duchenne and limb-girdle muscular dystrophy and may partially rescue force transduction.[126,129] Together, these data implicate α7β1 integrins as important but not critical transducers given the multiple, redundant pathways present in myocytes. On the other hand, the DGC is an exceedingly complex structure consisting of α- and β-dystroglycans, which are integral membrane glycoproteins. The former binds to laminin-α2 (merosin) to form extracellular connections, whereas the latter associates with dystrophin and sarcoglycans, another transmembrane protein complex with α, β, γ, and δ subunits (with the γ subunit directly interacting with dystrophin). Sarcoglycans, in turn, bind to sarcospan to complete the complex.[116] A common feature of proteins in this complex is their heavy glycosylated state, which changes between different muscles depending on the binding partners within their ECM[130] and has been implicated as another possible source of dystrophic-like symptoms.[131,132] As with α7β1 integrins, disrupting the DPC link causes a dystrophic-like phenotype. Disruption of the direct transductive link from sarcomere to ECM by serving the laminin-dystroglycan connection is another congenital dystrophy,[133] but interestingly enough, deletion of a sarcoglycan can actually increase myocyte contractility.[134] Unique links between the sarcoglycan and other costameric proteins, including filamin,[134,135] give rise to significant debates as to what really is the force transducer or the set of transducers, which mechanisms are indispensible, and most importantly, from the perspective provided here, how we can accurately determine the biomechanics of this transduction.

11.6.3 Biochemical Signaling Meets Force Transduction in the Nucleus

Despite such a forward-looking discussion surrounding the connections from sarcomere to costameres to integral protein complexes, and ultimately, the ECM, the mechanical initiation of biochemical signals need not only move toward the extracellular space. Although it was not previously introduced, two different families of proteins, the LINK and SUN superfamilies,[136] have been implicated in providing a physical link between the actin cytoskeleton (i.e., sarcomeres) and the nucleus. This may, in part, explain the reason why nuclear deformation has been observed in skeletal myoblasts during fusion and maturation.[137] Transduction via these proteins is then linked to a lamin-rich nuclear skeleton. Mutations in lamin A/C cause a variety of muscle diseases including Emery–Dreifuss muscular dystrophy, dilated cardiomyopathy, and Hutchinson–Gilford progeria

syndrome.[138] The genetic problems associated with these diseases likely limit the degree of nucleocytoskeletal assembly and linkage with the cytoplasmic cytoskeleton, leading to increased nuclear deformation and a lack of nuclear factor κB–regulated transcription.[139] Thus, it would seem that the effect of the interaction between the cytoskeleton and nucleus on muscle force transduction is still very much an open-ended discussion.

11.7 Unanswered Questions and Conclusions

Much of the literature cited here contains minimal descriptions of how the force is distributed among cells *in situ*. Whole muscle fiber models or bone explant cultures present significant findings, but it is difficult to extrapolate continuum details down to the single cell. *In vitro* culture assays present very well-refined techniques to explore myofibril formation and measure contractile forces against a substrate. Yet, both approaches do not completely satisfy the need for a complete mechanical description of cells at their length scale but in an *in situ* model. With the growing complexity of the structural components of bone and muscle, this problem only seems to become further exacerbated. New engineering techniques dealing with biological structures *in vivo* are clearly needed to move the field from simply examining how specific proteins alter global transduction and phenotype to demonstrating how cellular mechanics change in the *in vivo* context.

Acknowledgments

The authors acknowledge funding support from the National Institutes of Health (OD00-6460, EB011727, and HL106529 to A. J. Engler) and the California Institute of Regenerative Medicine (RN2-00945 to S. Varghese).

References

1. Martini, F.H. 2005. *Anatomy & Physiology*. Singapore: Prentice Hall.
2. Weiner S., and H.D. Wagner. 1998. The material bone: Structure–mechanical function relations. *Annual Review of Materials Science* 28:271–298.
3. Posner, A.S. 1969. Crystal chemistry of bone mineral. *Physiological Reviews* 49(4):760–792.
4. Gamsjäger, S., M. Kazanci, E. Paschalis, and P. Fratzl. 2008. Raman application in bone imaging. *Raman Spectroscopy for Soft Matter Applications*, edited by M. Amer., 227–269. Hoboken: John Wiley & Sons.
5. Rho, J.Y., R.B. Ashman, and C.H. Turner. 1993. Young's modulus of trabecular and cortical bone material: Ultrasonic and microtensile measurements. *Journal of Biomechanics* 26(2):111–119.
6. Boyle, W.J., W.S. Simonet, and D.L. Lacey. 2003. Osteoclast differentiation and activation. *Nature* 423(6937):337–342.
7. Aarden, E.M., P.J. Nijweide, and E.H. Burger. 1994. Function of osteocytes in bone. *Journal of Cellular Biochemistry* 55(3):287–299.

8. Frost, H.M. 1963. *Bone Remodelling Dynamics*. Springfield: Charles C. Thomas.
9. Robling, A.G., A.B. Castillo, and C.H. Turner. 2006. Biomechanical and molecular regulation of bone remodeling. *Annual Reviews in Biomedical Engineering* 8:455–498.
10. Chen, J.C., and D.R. Carter. 2005. Important concepts of mechanical regulation of bone formation and growth. *Current Opinion in Orthopaedics* 16:338–345.
11. Hillsley, M.V., and J.A. Frangos. 1994. Review: Bone tissue engineering: The role of interstitial fluid flow. *Biotechnology and Bioengineering* 43(7):573–581.
12. Ehrlich, P.J., and L.E. Lanyon. 2002. Mechanical strain and bone cell function: A review. *Osteoporosis International* 13(9):688–700.
13. Martin, R.B. 2007. The importance of mechanical loading in bone biology and medicine. *Journal of Musculoskeletal and Neuronal Interactions* 7(1):48.
14. Ruff, C., B. Holt, and E. Trinkaus. 2006. Who's afraid of the big bad Wolff? "Wolff's law" and bone functional adaptation. *American Journal of Physical Anthropology* 129(4):484–498.
15. Jones, H., J. Priest, C. Tichenor, and D. Nagel. 1977. Humeral hypertrophy in response to exercise. *Journal of Bone and Joint Surgery* 59:204–208.
16. Vico, L. et al. 2000. Effects of long-term microgravity exposure on cancellous and cortical weight-bearing bones of cosmonauts. *The Lancet* 355(9215):1607–1611.
17. Bigley, R.F. et al. 2007. Volume effects on fatigue life of equine cortical bone. *Journal of Biomechanics* 40(16):3548–3554.
18. Taylor, D., J.G. Hazenberg, and T.C. Lee. 2007. Living with cracks: Damage and repair in human bone. *Nature Materials* 6(4):263–268.
19. Petrtýl, M., J. Hert, and P. Fiala. 1996. Spatial organization of the haversian bone in man. *Journal of Biomechanics* 29(2):161–167.
20. Frost, H.M. 1987. Bone "mass" and the "mechanostat": A proposal. *The Anatomical Record* 219(1):1–9.
21. Lanyon, L.E., and C.T. Rubin. 1984. Static vs dynamic loads as an influence on bone remodeling. *Journal of Biomechanics* 17(12):897–905.
22. Turner, C.H. 1998. Three rules for bone adaptation to mechanical stimuli. *Bone* 23(5):399–407.
23. Claes, L., P. Augat, G. Suger, and H.J. Wilke. 1997. Influence of size and stability of the osteotomy gap on the success of fracture healing. (Translated from Eng) *Journal of Orthopaedic Research* 15(4):577–584 (in Eng).
24. Augat, P. et al. 1998. Local tissue properties in bone healing: Influence of size and stability of the osteotomy gap. *Journal of Orthopaedic Research* 16(4):475–481.
25. Larsson, S. et al. 2001. Effect of early axial dynamization on tibial bone healing: A study in dogs. *Clinical Orthopaedics and Related Research* 388:240–251.
26. Mullender, M.G., R. Huiskes, and H. Weinans. 1994. A physiological approach to the simulation of bone remodeling as a self-organizational control process. *Journal of Biomechanics* 27(11):1389–1394.
27. Cowin, S.C., and S. Weinbaum. 1998. Strain amplification in the bone mechanosensory system. *American Journal of the Medical Sciences* 316(3):184–188.
28. Santos, A., A. Bakker, and J. Klein-Nulend. 2009. The role of osteocytes in bone mechanotransduction. *Osteoporosis International* 20(6):1027–1031.
29. Vatsa, A. et al. 2008. Osteocyte morphology in fibula and calvaria—Is there a role for mechanosensing? *Bone* 43(3):452–458.
30. Vatsa, A., C.M. Semeins, T.H. Smit, and J. Klein-Nulend. 2008. Paxillin localisation in osteocytes—Is it determined by the direction of loading? *Biochemical and Biophysical Research Communications* 377(4):1019–1024.
31. Skerry, T.M., L.E. Lanyon, L. Bitensky, and J. Chayen. 1989. Early strain-related changes in enzyme activity in osteocytes following bone loading in vivo. *Journal of Bone and Mineral Research* 4(5):783–788.
32. Grigoriadis, A.E. et al. 1994. c-Fos: A key regulator of osteoclast-macrophage lineage determination and bone remodeling. *Science* 266(5184):443–448.

33. You, L. et al. 2008. Osteocytes as mechanosensors in the inhibition of bone resorption due to mechanical loading. *Bone* 42(1):172–179.
34. Mikuni-Takagaki, Y. 1999. Mechanical responses and signal transduction pathways in stretched osteocytes. *Journal of Bone and Mineral Metabolism* 17(1):57–60.
35. Klein-Nulend, J. et al. 1995. Sensitivity of osteocytes to biomechanical stress in vitro. *The FASEB Journal* 9(5):441–445.
36. Mullender, M. et al. 2004. Mechanotransduction of bone cells *in vitro*: Mechanobiology of bone tissue. *Medical and Biological Engineering and Computing* 42(1):14–21.
37. Tatsumi, S. et al. 2007. Targeted ablation of osteocytes induces osteoporosis with defective mechanotransduction. *Cell Metabolism* 5(6):464–475.
38. Owan, I. et al. 1997. Mechanotransduction in bone: Osteoblasts are more responsive to fluid forces than mechanical strain. (Translated from Eng) *American Journal of Physiology* 273(3 Pt 1):C810–C815 (in Eng).
39. Burra S. et al. 2010. Dendritic processes of osteocytes are mechanotransducers that induce the opening of hemichannels. *Proceedings of the National Academy of Sciences of the United States of America* 107(31):13648–13653.
40. Vatsa, A. et al. 2006. Bioimaging of intracellular NO production in single bone cells after mechanical stimulation. *Journal of Bone and Mineral Research* 21(11):1722–1728.
41. Malone, A.M.D. et al. 2007. Primary cilia mediate mechanosensing in bone cells by a calcium-independent mechanism. *Proceedings of the National Academy of Sciences of the United States of America* 104(33):13325–13330.
42. Vezeridis, P.S., C.M. Semeins, Q. Chen, and J. Klein-Nulend. 2006. Osteocytes subjected to pulsating fluid flow regulate osteoblast proliferation and differentiation. *Biochemical and Biophysical Research Communications* 348(3):1082–1088.
43. Taylor, A.F. et al. 2007. Mechanically stimulated osteocytes regulate osteoblastic activity via gap junctions. *American Journal of Physiology—Cell Physiology* 292(1):C545–C552.
44. Kim, C.H., L. You, C.E. Yellowley, and C.R. Jacobs. 2006. Oscillatory fluid flow-induced shear stress decreases osteoclastogenesis through RANKL and OPG signaling. *Bone* 39(5):1043–1047.
45. Rubin, J., T.C. Murphy, X. Fan, M. Goldschmidt, and W.R. Taylor. 2002. Activation of extracellular signal–regulated kinase is involved in mechanical strain inhibition of RANKL expression in bone stromal cells. *Journal of Bone and Mineral Research* 17(8):1452–1460.
46. Teitelbaum, S.L. 2000. Bone resorption by osteoclasts. *Science* 289(5484):1504–1508.
47. Kurata, K. et al. 2001. Mechanical strain effect on bone-resorbing activity and messenger RNA expressions of marker enzymes in isolated osteoclast culture. *Journal of Bone and Mineral Research* 16(4):722–730.
48. Wiltink, A., P.J. Nijweide, W.J.J.M. Scheenen, D.L. Ypey, and B. Duijn. 1995. Cell membrane stretch in osteoclasts triggers a self-reinforcing Ca2+ entry pathway. *Pflügers Archiv European Journal of Physiology* 429(5):663–671.
49. Tsuzuki, T., K. Okabe, H. Kajiya, and T. Habu. 2000. Osmotic membrane stretch increased cytosolic Ca^{2+} and inhibits bone resorption activity in rat osteoclasts. *Japanese Journal of Physiology* 50(1):67–76.
50. Zaidi, M., B.S. Moonga, and O.A. Adebanjo. 1999. Novel mechanisms of calcium handling by the osteoclast: A review–hypothesis. *Proceedings of the Association of American Physicians* 111(4):319–327.
51. Han, Y., S.C. Cowin, M.B. Schaffler, and S. Weinbaum. 2004. Mechanotransduction and strain amplification in osteocyte cell processes. *Proceedings of the National Academy of Sciences of the United States of America* 101(47):16689–16694.
52. Wang, Y., L.M. McNamara, M.B. Schaffler, and S. Weinbaum. 2007. A model for the role of integrins in flow induced mechanotransduction in osteocytes. *Proceedings of the National Academy of Sciences of the United States of America* 104(40):15941–15946.
53. Hooper, S.L., and J.B. Thuma. 2005. Invertebrate muscles: Muscle specific genes and proteins. *Physiological Reviews* 85(3):1001–1060.

54. Murphy, R.A. 1976. Structural proteins in the myofilaments and regulation of contraction in vertebrate smooth muscle. *Federation Proceedings* 35(6):1302–1306.
55. Sanger, J.W. et al. 2005. How to build a myofibril. *Journal of Muscle Research and Cell Motility* 26(6–8):343–354.
56. Rhee, D., J.M. Sanger, and J.W. Sanger. 1994. The premyofibril: Evidence for its role in myofibrillogenesis. *Cell Motility and the Cytoskeleton* 28(1):1–24.
57. Zemel, A., F. Rehfeldt, A.E. Brown, D.E. Discher, and S.A. Safran. 2010. Optimal matrix rigidity for stress fiber polarization in stem cells. *Nature Physics* 6(6):468–473.
58. Du, A., J.M. Sanger, K.K. Linask, and J.W. Sanger. 2003. Myofibrillogenesis in the first cardiomyocytes formed from isolated quail precardiac mesoderm. *Developmental Biology* 257(2):382–394.
59. Engler, A.J. et al. 2008. Embryonic cardiomyocytes beat best on a matrix with heart-like elasticity: Scar-like rigidity inhibits beating. *Journal of Cell Science* (121):3794–3802.
60. Sanger, J.W. et al. 2002. Myofibrillogenesis in skeletal muscle cells. *Clinical Orthopaedics and Related Research* (403 Suppl):S153–S162.
61. Engler, A.J. et al. 2004. Myotubes differentiate optimally on substrates with tissue-like stiffness: Pathological implications for soft or stiff microenvironments. *Journal of Cell Biology* 166(6):877–887.
62. Clark, K.A., A.S. McElhinny, M.C. Beckerle, and C.C. Gregorio. 2002. Striated muscle cytoarchitecture: An intricate web of form and function. *Annual Review of Cell and Developmental Biology* 18:637–706.
63. Franzini-Armstrong, C. 1973. The structure of a simple Z line. *Journal of Cell Biology* 58(3):630–642.
64. Horowits, R., and R.J. Podolsky. 1988. Thick filament movement and isometric tension in activated skeletal muscle. *Biophysical Journal* 54(1):165–171.
65. Ehler, E., B.M. Rothen, S.P. Hammerle, M. Komiyama, and J.C. Perriard. 1999. Myofibrillogenesis in the developing chicken heart: Assembly of Z-disk, M-line and the thick filaments. *Journal of Cell Science* 112 (Pt 10):1529–1539.
66. Oba, T., R.J. Baskin, and R.L. Lieber. 1981. Light diffraction studies of active muscles fibres as a function of sarcomere length. *Journal of Muscle Research and Cell Motility* 2(2):215–224.
67. Patterson, S.W., and E.H. Starling. 1914. On the mechanical factors which determine the output of the ventricles. *Journal of Physiology* 48(5):357–379.
68. da Silva Lopes, K., A. Pietas, M.H. Radke, and M. Gotthardt. 2011. Titin visualization in real time reveals an unexpected level of mobility within and between sarcomeres. *Journal of Cell Biology* 193(4):785–798.
69. Young, J.L., and A.J. Engler. 2011. Hydrogels with time-dependent material properties enhance cardiomyocyte differentiation in vitro. *Biomaterials* 32(4):1002–1009.
70. Jacot, J.G., A.D. McCulloch, and J.H. Omens. 2008. Substrate stiffness affects the functional maturation of neonatal rat ventricular myocytes. *Biophysical Journal* 95(7):3479–3487.
71. Ward, S.R., G.J. Loren, S. Lundberg, and R.L. Lieber. 2006. High stiffness of human digital flexor tendons is suited for precise finger positional control. *Journal of Neurophysiology* 96(5):2815–2818.
72. Schiaffino, S., V. Hanzlikova, and S. Pierobon. 1970. Relations between structure and function in rat skeletal muscle fibers. *Journal of Cell Biology* 47(1):107–119.
73. Holthofer, B., R. Windoffer, S. Troyanovsky, and R.E. Leube. 2007. Structure and function of desmosomes. *International Review of Cytology* 264:65–163.
74. Thierfelder, L. et al. 1994. Alpha-tropomyosin and cardiac troponin T mutations cause familial hypertrophic cardiomyopathy: A disease of the sarcomere. *Cell* 77(5):701–712.
75. Schallus, T., K. Feher, A.S. Ulrich, G. Stier, and C. Muhle-Goll. 2009. Structure and dynamics of the human muscle LIM protein. *FEBS Letters* 583(6):1017–1022.
76. Geier, C. et al. 2008. Beyond the sarcomere: CSRP3 mutations cause hypertrophic cardiomyopathy. *Human Molecular Genetics*. 17(18):2753–2765.
77. Zolk, O., P. Caroni, and M. Bohm. 2000. Decreased expression of the cardiac LIM domain protein MLP in chronic human heart failure. *Circulation* 101(23):2674–2677.
78. Harper, B.D., M.C. Beckerle, and P. Pomies. 2000. Fine mapping of the alpha-actinin binding site within cysteine-rich protein. *The Biochemical Journal* 350 Pt 1:269–274.

79. Knoll, R. et al. 2002. The cardiac mechanical stretch sensor machinery involves a Z disc complex that is defective in a subset of human dilated cardiomyopathy. *Cell* 111(7):943–955.
80. Ehler, E. et al. 2001. Alterations at the intercalated disk associated with the absence of muscle LIM protein. *Journal of Cell Biology* 153(4):763–772.
81. Clark, K.A., H. Lesage-Horton, C. Zhao, M.C. Beckerle, and D.M. Swank. 2011. Deletion of Drosophila muscle LIM protein decreases flight muscle stiffness and power generation. *American Journal of Physiology. Cell Physiology* 301(2):C373–C382.
82. Boateng, S.Y., S.E. Senyo, L. Qi, P.H. Goldspink, and B. Russell. 2009. Myocyte remodeling in response to hypertrophic stimuli requires nucleocytoplasmic shuttling of muscle LIM protein. *Journal of Molecular and Cellular Cardiology* 47(4):426–435.
83. Ecarnot-Laubriet, A. et al. 2000. Downregulation and nuclear relocation of MLP during the progression of right ventricular hypertrophy induced by chronic pressure overload. *Journal of Molecular and Cellular Cardiology* 32(12):2385–2395.
84. Salmikangas, P. et al. 2003. Myotilin, the limb-girdle muscular dystrophy 1A (LGMD1A) protein, cross-links actin filaments and controls sarcomere assembly. *Human Molecular Genetics* 12(2):189–203.
85. Moza, M. et al. 2007. Targeted deletion of the muscular dystrophy gene myotilin does not perturb muscle structure or function in mice. *Molecular and Cellular Biology* 27(1):244–252.
86. Wallimann, T., and H.M. Eppenberger. 1985. Localization and function of M-line-bound creatine kinase. M-band model and creatine phosphate shuttle. *Cell and Muscle Motility* 6:239–285.
87. McHugh, M.P. et al. 1999. The role of passive muscle stiffness in symptoms of exercise-induced muscle damage. *The American Journal of Sports Medicine* 27(5):594–599.
88. LaBella, J.J. et al. 1998. Absence of myofibrillar creatine kinase and diaphragm isometric function during repetitive activation. *Journal of Applied Physiology* 84(4):1166–1173.
89. Watchko, J.F., M.J. Daood, B. Wieringa, and A.P. Koretsky. 2000. Myofibrillar or mitochondrial creatine kinase deficiency alone does not impair mouse diaphragm isotonic function. *Journal of Applied Physiology* 88(3):973–980.
90. Foucault, G., M. Vacher, T. Merkulova, A. Keller, and M. Arrio-Dupont. 1999. Presence of enolase in the M-band of skeletal muscle and possible indirect interaction with the cytosolic muscle isoform of creatine kinase. *The Biochemical Journal* 338(Pt 1):115–121.
91. Grater, F., J. Shen, H. Jiang, M. Gautel, and H. Grubmuller. 2005. Mechanically induced titin kinase activation studied by force-probe molecular dynamics simulations. *Biophysical Journal* 88(2):790–804.
92. Lange, S. et al. 2005. The kinase domain of titin controls muscle gene expression and protein turnover. *Science* 308(5728):1599–1603.
93. Holle, A.W., and A.J. Engler. 2011. More than a feeling: Discovering, understanding, and influencing mechanosensing pathways. *Current Opinion in Biotechnology* (22):648–654.
94. Engler, A.J., S. Sen, H.L. Sweeney, and D.E. Discher. 2006. Matrix elasticity directs stem cell lineage specification. *Cell* 126(4):677–689.
95. McBeath, R., D.M. Pirone, C.M. Nelson, K. Bhadriraju, and C.S. Chen. 2004. Cell shape, cytoskeletal tension, and RhoA regulate stem cell lineage commitment. *Developmental Cell* 6(4):483–495.
96. Wang, N. et al. 2002. Cell prestress. I. Stiffness and prestress are closely associated in adherent contractile cells. *American Journal of Physiology. Cell Physiology* 282(3):C606–C616.
97. del Rio, A. et al. 2009. Stretching single talin rod molecules activates vinculin binding. *Science* 323(5914):638–641.
98. Anastasi, G. et al. 2009. Dystrophin–glycoprotein complex and vinculin–talin–integrin system in human adult cardiac muscle. *International Journal of Molecular Medicine* 23(2):149–159.
99. von Wichert, G. et al. 2003. RPTP-alpha acts as a transducer of mechanical force on alphav/beta3-integrin-cytoskeleton linkages. *Journal of Cell Biology* 161(1):143–153.
100. Peyton, S.R., and A.J. Putnam. 2005. Extracellular matrix rigidity governs smooth muscle cell motility in a biphasic fashion. *Journal of Cellular Physiology* 204(1):198–209.
101. Chan, M.W., F. Chaudary, W. Lee, J.W. Copeland, and C.A. McCulloch. 2010. Force-induced myofibroblast differentiation through collagen receptors is dependent on mammalian diaphanous (mDia). *Journal of Biological Chemistry* 285(12):9273–9281.

102. Stewart, N.T., K.M. Byrne, C.A. Ragle, J.L. Vierck, and M.V. Dodson. 2001. Patterns of expression of muscle-specific markers of differentiation in satellite cell cultures: Determination by enzyme-linked immunoculture assay and confocal immunofluorescent assay. *Cell Biology International* 25(9):873–884.
103. Dalakas, M.C. et al. 2000. Desmin myopathy, a skeletal myopathy with cardiomyopathy caused by mutations in the desmin gene. *New England Journal of Medicine* 342(11):770–780.
104. Goldfarb, L.G., and M.C. Dalakas. 2009. Tragedy in a heartbeat: Malfunctioning desmin causes skeletal and cardiac muscle disease. *Journal of Clinical Investigation* 119(7):1806–1813.
105. Goldfarb, L.G. et al. 1998. Missense mutations in desmin associated with familial cardiac and skeletal myopathy. *Nature Genetics* 19(4):402–403.
106. Bar, H. et al. 2005. Severe muscle disease–causing desmin mutations interfere with in vitro filament assembly at distinct stages. *Proceedings of the National Academy of Sciences of the United States of America* 102(42):15099–15104.
107. Kreplak, L., and H. Bar. 2009. Severe myopathy mutations modify the nanomechanics of desmin intermediate filaments. *Journal of Molecular Biology* 385(4):1043–1051.
108. Ervasti, J.M. 2003. Costameres: The Achilles' heel of Herculean muscle. *Journal of Biological Chemistry* 278(16):13591–13594.
109. Pardo, J.V., J.D. Siliciano, and S.W. Craig. 1983. Vinculin is a component of an extensive network of myofibril-sarcolemma attachment regions in cardiac muscle fibers. *Journal of Cell Biology* 97(4):1081–1088.
110. Danowski, B.A., K. Imanaka-Yoshida, J.M. Sanger, and J.W. Sanger. 1992. Costameres are sites of force transmission to the substratum in adult rat cardiomyocytes. *Journal of Cell Biology* 118(6):1411–1420.
111. Harris, A.K., P. Wild, and D. Stopak. 1980. Silicone rubber substrata: A new wrinkle in the study of cell locomotion. *Science* 208(4440):177–179.
112. Kee, A.J., P.W. Gunning, and E.C. Hardeman. 2009. Diverse roles of the actin cytoskeleton in striated muscle. *Journal of Muscle Research and Cell Motility* 30(5–6):187–197.
113. Johnson, C.P., H.Y. Tang, C. Carag, D.W. Speicher, and D.E. Discher. 2007. Forced unfolding of proteins within cells. *Science* 317(5838):663–666.
114. Krieger, C.C. et al. 2011. Cysteine shotgun-mass spectrometry (CS-MS) reveals dynamic sequence of protein structure changes within mutant and stressed cells. *Proceedings of the National Academy of Sciences of the United States of America* 108(20):8269–8274.
115. Lee, G. et al. 2006. Nanospring behaviour of ankyrin repeats. *Nature* 440(7081):246–249.
116. Ehmsen, J., E. Poon, and K. Davies. 2002. The dystrophin-associated protein complex. *Journal of Cell Science* 115(Pt 14):2801–2803.
117. Rybakova, I.N., J.R. Patel, and J.M. Ervasti. 2000. The dystrophin complex forms a mechanically strong link between the sarcolemma and costameric actin. *Journal of Cell Biology* 150(5):1209–1214.
118. Porter, G.A., G.M. Dmytrenko, J.C. Winkelmann, and R.J. Bloch. 1992. Dystrophin colocalizes with beta-spectrin in distinct subsarcolemmal domains in mammalian skeletal muscle. *Journal of Cell Biology* 117(5):997–1005.
119. Bushby, K. et al. 2009. Diagnosis and management of Duchenne muscular dystrophy. Part 1: Diagnosis and pharmacological and psychosocial management. *Lancet Neurology* 9(1):77–93.
120. Merrick, D., L.K. Stadler, D. Larner, and J. Smith. 2009. Muscular dystrophy begins early in embryonic development deriving from stem cell loss and disrupted skeletal muscle formation. *Disease Models & Mechanisms* 2(7–8):374–388.
121. Stedman, H.H. et al. 1991. The mdx mouse diaphragm reproduces the degenerative changes of Duchenne muscular dystrophy. *Nature* 352(6335):536–539.
122. Li, D., Y. Yue, and D. Duan. 2008. Preservation of muscle force in Mdx3cv mice correlates with low-level expression of a near full-length dystrophin protein. *The American Journal of Pathology* 172(5):1332–1341.
123. Banks, G.B., P. Gregorevic, J.M. Allen, E.E. Finn, and J.S. Chamberlain. 2007. Functional capacity of dystrophins carrying deletions in the N-terminal actin-binding domain. *Human Molecular Genetics* 16(17):2105–2113.

124. Moorwood, C. 2008. Syncoilin, an intermediate filament-like protein linked to the dystrophin associated protein complex in skeletal muscle. *Cellular and Molecular Life Sciences* 65(19):2957–2963.
125. Zhang, J. et al. 2008. Syncoilin is required for generating maximum isometric stress in skeletal muscle but dispensable for muscle cytoarchitecture. *American Journal of Physiology. Cell Physiology* 294(5):C1175–1182.
126. Burkin, D.J., and S.J. Kaufman. 1999. The alpha7beta1 integrin in muscle development and disease. *Cell and Tissue Research* 296(1):183–190.
127. Hay, E.D. 1991. *Cell Biology of Extracellular Matrix.* 2nd ed., 468. New York: Plenum Press.
128. Nawrotzki, R., M. Willem, N. Miosge, H. Brinkmeier, and U. Mayer. 2003. Defective integrin switch and matrix composition at alpha 7-deficient myotendinous junctions precede the onset of muscular dystrophy in mice. *Human Molecular Genetics* 12(5):483–495.
129. Milner, D.J., and S.J. Kaufman. 2007. Alpha7beta1 integrin does not alleviate disease in a mouse model of limb girdle muscular dystrophy type 2F. *The American Journal of Pathology* 170(2):609–619.
130. Winder, S.J. 2001. The complexities of dystroglycan. *Trends in Biochemical Sciences* 26(2):118–124.
131. Grewal, P.K., and J.E. Hewitt. 2003. Glycosylation defects: A new mechanism for muscular dystrophy? *Human Molecular Genetics* 12(Spec No 2):R259–R264.
132. Hewitt, J.E., and P.K. Grewal. 2003. Glycosylation defects in inherited muscle disease. *Cellular and Molecular Life Sciences* 60(2):251–258.
133. Grewal, P.K., P.J. Holzfeind, R.E. Bittner, and J.E. Hewitt. 2001. Mutant glycosyltransferase and altered glycosylation of alpha-dystroglycan in the myodystrophy mouse. *Nature Genetics* 28(2):151–154.
134. Griffin, M.A. et al. 2005. gamma-Sarcoglycan deficiency increases cell contractility, apoptosis and MAPK pathway activation but does not affect adhesion. *Journal of Cell Science* 118(Pt 7):1405–1416.
135. Thompson, T.G. et al. 2000. Filamin 2 (FLN2): A muscle-specific sarcoglycan interacting protein. *Journal of Cell Biology* 148(1):115–126.
136. Dahl, K.N., A.J. Ribeiro, and J. Lammerding. 2008. Nuclear shape, mechanics, and mechanotransduction. *Circulation Research* 102(11):1307–1318.
137. Abe, T. et al. 2004. Myocyte differentiation generates nuclear invaginations traversed by myofibrils associating with sarcomeric protein mRNAs. *Journal of Cell Science* 117(Pt 26):6523–6534.
138. Dahl, K.N. et al. 2006. Distinct structural and mechanical properties of the nuclear lamina in Hutchinson–Gilford progeria syndrome. *Proceedings of the National Academy of Sciences of the United States of America* 103(27):10271–10276.
139. Lammerding, J. et al. 2004. Lamin A/C deficiency causes defective nuclear mechanics and mechanotransduction. *Journal of Clinical Investigation* 113(3):370–378.

12

Biomechanics of Musculoskeletal System Growth and Development

David J. Nuckley

CONTENTS

The growth and development of the musculoskeletal system is a complex process mediated by biological and mechanical factors that produce isolated tissues with differential properties. Together, the tissues of the musculoskeletal system join to produce the body's form and structure while providing stability and movement capabilities. During maturation, genetics, nutrition, hormones, and mechanical forces drive the tissues of the musculoskeletal system to transform with temporal specificity. These factors individually and collectively produce changes that alter the constituent makeup of the tissue, its morphology, and its biomechanical response. This chapter aims to detail the biomechanical effects of growth and development both on isolated musculoskeletal tissues and on the system as a whole. This review chiefly focuses on typical development and its effects on orthopaedic biomechanics. Bone, ligament, tendon, intervertebral disc, cartilage, and skeletal muscle ontogeny are individually discussed as well as their integration into the complete musculoskeletal system. Basic maturation biology and biochemistry are presented to contextualize the changes in tissue morphology, size, and biomechanics. The effects of growth and development are discussed because they pertain to the integrated musculoskeletal system

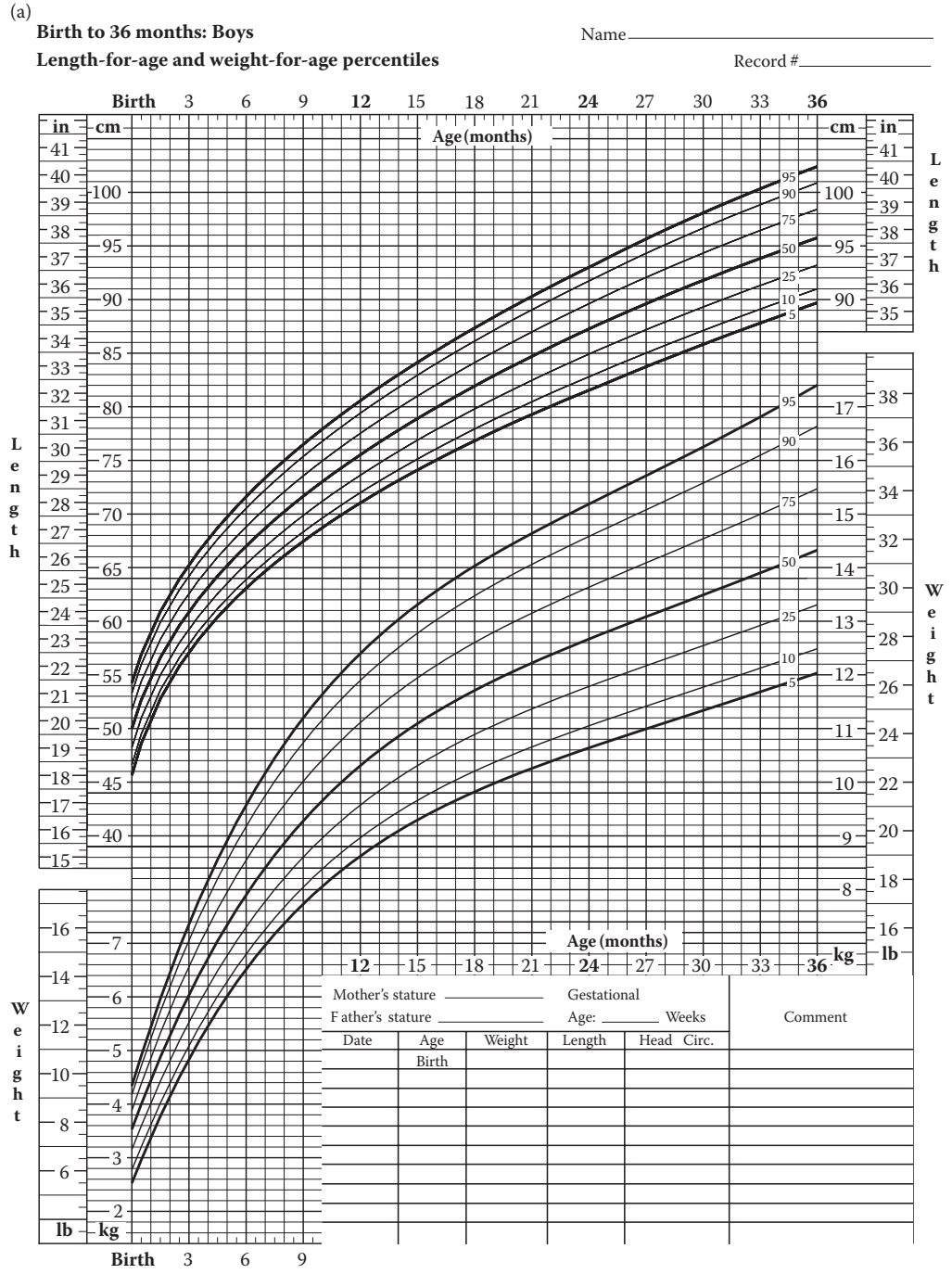

FIGURE 12.1
Growth charts for early development (from birth to 36 months) for boys (a) and girls (b). The National Center for Health Statistics and the National Center for Chronic Disease Prevention and Health Promotion have sponsored the accumulation of data to support these growth curves. (Reprinted from http://www.cdc.gov/growthcharts/. Published May 30, 2000; modified April 20, 2001.)

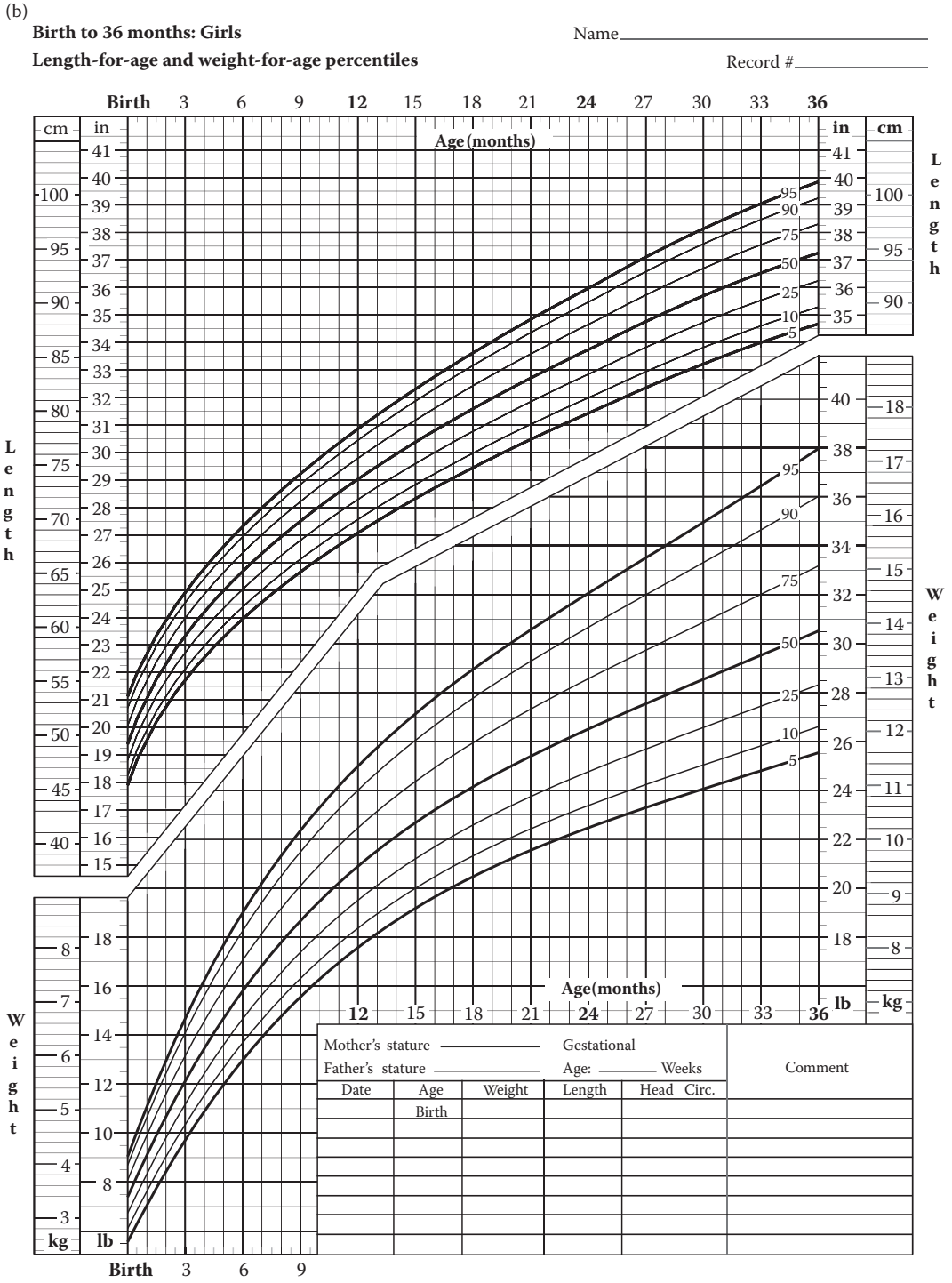

FIGURE 12.1 (Continued)

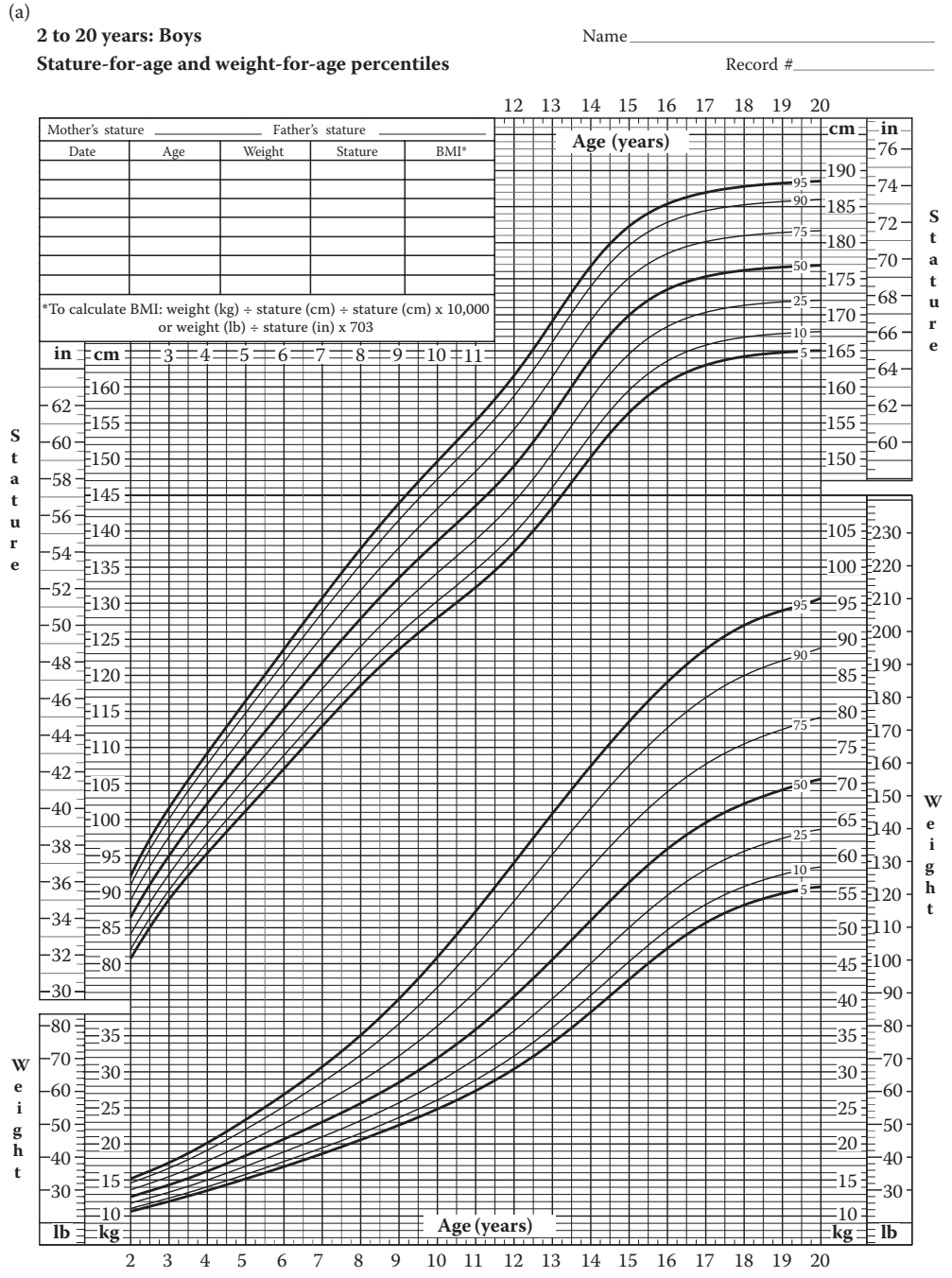

FIGURE 12.2
Growth charts detailing stature and weight changes from childhood through adulthood in boys (a) and girls (b). The National Center for Health Statistics and the National Center for Chronic Disease Prevention and Health Promotion have sponsored the accumulation of data to support these growth curves. (Reprinted from http://www.cdc.gov/growthcharts/. Published May 30, 2000; modified November 21, 2000.)

(b)

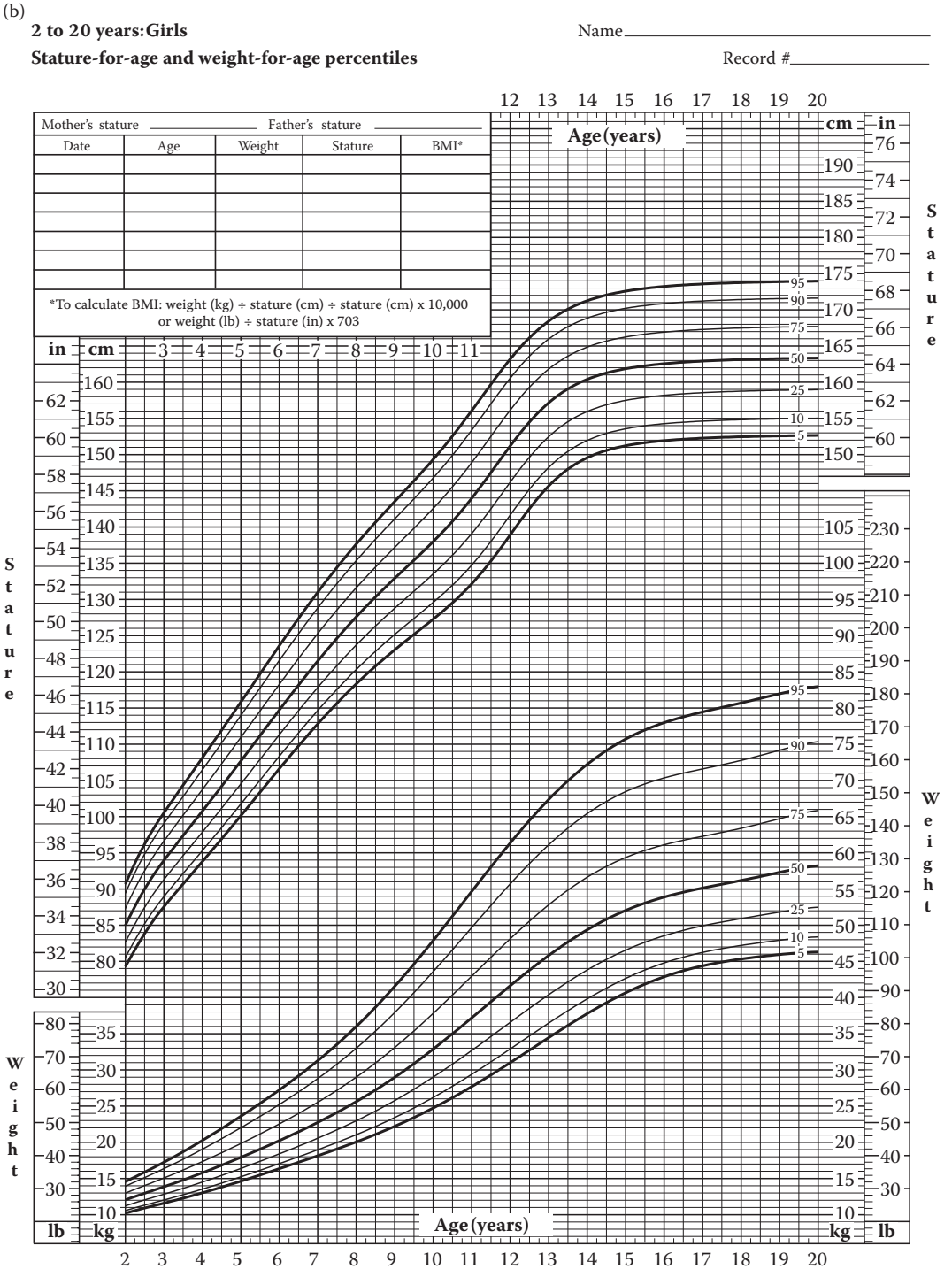

FIGURE 12.2 (Continued)

at various joints. The final section-includes the modeling of biomechanical systems with immature properties and the scaling of biomechanical models for the prediction of musculoskeletal/orthopaedic outcomes.

Human development and growth involve significant changes that include cellular proliferation from a single zygocyte to approximately 100 trillion cells in adulthood. The musculoskeletal system not only participates in this cellular explosion but also produces and organizes the structural extracellular matrix that supports the body. To contextualize these changes, the structural and motion-granting system for the body must maintain its function while also increasing in height by approximately 3.5-fold and increasing in weight by approximately 17-fold from birth to adulthood. Growth charts describing the mean and distribution (confidence intervals) of changes in human stature and weight reveal the musculoskeletal system's size and its developmental rate of change (Figures 12.1 and 12.2). Musculoskeletal system "development" may be defined as the cellular proliferation, synthesis of extracellular matrix proteins, and matrix organization, whereas "growth" is the increase in size of the tissue as a result of development. Although these terms are often used synonymously, stature and weight charts display growth that may not always be concomitant with highly organized and structured tissues. Growth charts have historically been used to predict the biomechanical properties of the musculoskeletal system; however, there may be a lag in the mechanical properties of the tissue while its newly increased size becomes more organized to provide structural support. This review aims to detail the development and growth processes of musculoskeletal tissues, their biomechanical properties, and their applications in computational models to describe maturation phenomena.

12.1 Biological Review of Musculoskeletal System Growth and Development

The musculoskeletal system develops largely through the differentiation of cells into specialized lines capable of synthesizing, mediating, or organizing extracellular matrix and cell–cell interactions. This cellular and extracellular matrix morphogenesis leads to individual specialized tissues designed for the support, stability, and motion of the body. Growth of the musculoskeletal system involves an increase in cell proliferation, organization, and extracellular matrix deposition such that the tissues increase in size. Much of the understanding of human development and growth is based on studies of animal models. Therefore, although many of these tissues may be ubiquitous, caution should be used in directly applying patterns from animal models to the human. Finally, because these tissues have been described in detail elsewhere in this book, only their maturation and growth processes will be described as it pertains to the tissues' pathway from embryologic mesenchymal cells to their eventual mature structural morphology.

This section reviews the embryologic, fetal, postnatal, child, adolescent, and adult stages of human development. Embryologic development—mechanistically biologic—involves cellular proliferation, condensation, and extracellular matrix synthesis, which results in skeletal, muscular, ligament, and tendon elements at approximately seven weeks. This is the origin of skeletal ossification and involuntary muscle fiber contractions that mechanistically integrate mechanical stresses into tissue development.[1] Thus, although the first seven weeks of development are primarily biologically driven, the remainder of growth and

development involves both biological and mechanical stimuli. Skeletal development and remodeling, as well as articular cartilage development, are modulated by these mechanical stresses on the fetus. These mechanical forces of basic movements persist until birth and through postnatal growth, causing a complex interdependence of skeletogenesis, soft tissue development, and muscular development.[2] Despite dealing with these tissues independently in this chapter, it is critical to recognize that the musculoskeletal system development and growth are an integrated biological-mechanical mediated program wherein the tissues interact with and support each other.

12.1.1 Bone

Axial skeletogenesis and growth occur through stages of tissue differentiation, chondrification, and ossification. They are presented here as discrete steps, but, in reality, they represent a continuum of activity. Embryonic mesenchymal cells differentiate, condense, and transform into chondrocytes, which form cartilage at primary centers of chondrification. These centers of chondrification spread and fuse with other centers to produce a cartilaginous model of the future skeleton typically by the eighth week of development *in utero*.[3,4] *De novo* mineralization of the skeleton occurs as bone replaces this cartilaginous tissue and thus initiates a process of continued lifelong remodeling. Initial bone (hydroxyapatite crystal) deposition begins at the inner membrane of chondrocyte-produced matrix vesicles.[5] The binding of calcium with phosphate-metabolizing enzymes creates a calcium hydroxyapatite crystal that grows until it ruptures the vesicle and seeds the extracellular matrix. These hydroxyapatite crystals propagate in the hospitable environment provided by the collagen extracellular matrix. This process is initiated in one of two forms, as either intramembranous or endochondral ossification. Intramembranous ossification is the direct mineralization of plate-like bones, which are highly vascular. The clavicle is the first bone to form, followed by the skull, facial bones, and mandible.[5] Endochondral ossification, which describes the bone formation in the long bones and spine, is chondrocyte-mediated about the primary ossification centers typically located near the centroid of the bone. These chondrocytes aggregate and enlarge, and the cytoplasm becomes vacuolated. As the cells degenerate, their residual intracellular matrix becomes the substrate for mineralization.[5] This mineralized primary center of ossification results in the diaphysis of the bone. Ossified cartilage is seeded with osteoprogenitor cells, which then transform the tissue into woven bone. These new bone structures are continually remodeled with osteoblast/osteoclast activity to moderately increase bone size and substantially enhance the organization of the bone into its trabecular and cortical morphologies.

Skeletogenesis continues with the development of secondary ossification centers from infancy to adolescence; these foci mature via endochondral ossification and typically appear at the ends of long bones and superior-inferior margins of vertebral bodies. These epiphyses connect to the bone diaphysis via the physis, or growth plate, which is responsible for the rapid increase in the length of bones. The physis synchronizes longitudinal and lateral chondrogenesis with osteogenesis (interstitial cartilage growth with appositional bone growth), while bearing load and responding to local and systemic forces and factors.[6–9] Although functionally ubiquitous, the physis mediates bone growth throughout childhood and adolescence in bones as diverse as vertebrae and femurs. This growth involves the synthesis and subsequent replacement of cartilage in the growth plate by bony tissue through temporally and spatially chondrocyte-coordinated differentiation, growth, and remodeling events.

Morphologically, the physis is an avascular, aneural tissue that maintains a distinct cellular and matrix organization throughout its development.[7,10,11] The role of the physis

is the chondrocyte production of an extracellular matrix and the subsequent calcification of that matrix in a balanced function.[12] Collagen types I, II, IX, X, and XI have been implicated as primary matrix components within the physis.[13,14] Type X collagen is unique to the physis and may ensure the normal distribution of matrix vesicles and proteoglycans within the physis matrix, impacting the supporting properties of the physis and the mineralization process.[14] The purpose of the physis is supported by a complex cellular organization, which is subdivided into zones that are morphologically distinct and functionally identified.[15] At the border between the epiphysis and the physis lies a reserve zone of cartilaginous tissue; this is followed by the proliferative zone and hypertrophic zone, which finally gives rise to the metaphysis. The reserve zone contains spherically shaped cells that actively synthesize protein and an extracellular matrix rich in hydroxyproline but with randomly distributed and oriented collagen fibrils. This zone is thought to be responsible for matrix production and storage of the nutritional elements required for use in subsequent zones. The next proximal zone is the proliferative zone, which contains flattened chondrocytes aligned in vertical columns perpendicular to the physis surface.[7,11] The rate of long bone longitudinal growth is equal to the rate of production of new chondrocytes at the top of the proliferative zone multiplied by the size of exiting chondrocytes.[7] Each column of chondrocytes has been discovered to produce approximately five cells per day, leading to a growth rate of approximately 150 μm per day. The hypertrophic zone is morphologically distinct because the size of the chondrocytes increases as the matrix is prepared for calcification. It is also in this zone that provisional calcification takes place and cellular apoptosis occurs.[7,11]

The metaphysis is morphologically new bone prepared for remodeling at the physeal border. Metaphyseal functions include the resorption of the transverse septa (cellular columns) through vascular ingrowth, bone formation, and bone remodeling. The calcified matrix created in the hypertrophic zone is replaced by primary spongiosa and then is subsequently remodeled by osteoblast/osteoclast function into secondary spongiosa in the metaphysis.[7,11] The cessation of bone growth (which is hormonally mediated) involves the physeal union or growth plate closure wherein the dense parallel plates of the metaphyseal and epiphyseal surfaces both ossify. This epiphyseal line may be present radiographically long into adulthood. Although growth plate closure is often referred to as the transition to skeletal maturity, bone continually remodels in the presence of biological and mechanical stimuli. Throughout adulthood, an estimated 5% of cortical bone and 25% of trabecular bone are renewed annually, and typically, these are associated with very little growth in the skeleton.[16]

12.1.2 Soft Connective Tissue

The soft connective tissues with the greatest effect on orthopaedic function and musculoskeletal biomechanics include ligaments, tendons, articular cartilage, and intervertebral discs. Here, these tissues are individually discussed with regard to their embryonic and postnatal development. The biological development and growth of these connective tissues are as unique in their spatial and temporal tissue organization as the resulting biomechanical functions they provide.

Tendon and ligament development has not received the attention from developmental biologists that other soft connective tissues have. Tendons originate from the mesodermal layers, which are different from the origins of skeletal muscle despite their anatomic juxtaposition.[17] Also, trunk tendons have been shown to develop differently from limb tendons. The trunk tendons originate from the dorsal region of the sclerotome adjacent to

the dermomyotome from which the myogenic cells that form muscles develop.[18] The presence of this myotome is necessary for tendon progenitor cell development.[18] Embryonic development of limb tendons is more distinct from muscle development and has been shown to occur without the presence of muscle progenitors.[19] Late limb tendon development does require the presence of muscles for the organization of the cells. Ligament developmental embryology has not been well defined because of a lack of biomarkers, but it has been speculated that ligament progenitor cells are colocalized with tendon cells during embryonic development. From embryologic origins to tissue, the cells of both the ligaments and tendons condense and differentiate into fibroblasts. These fibroblasts align in rows within both tissues and begin fibrillogenesis. The control of the orientation of these rows is unknown, but it is clear that the orientation of the extracellular matrix and the subsequent fibrillar tissue are dependent on fibroblast arrangement.[20] Fibrillogenesis involves the fibroblast-mediated assembly of extracellular collagen molecules to form fibrils. Next, the fibrils are aligned end-to-end and then bundled cross-sectionally to form collagen fibers. This primarily type I collagen fiber is the principal structural unit of both ligaments and tendons; however, the elastin component is present in both tissues in varying concentrations. Elastic fibrillogenesis involves the development of fibrillin microfibrils upon which elastin can be deposited and organized within the tissue. The temporal relationship between collagen and elastin fibrillogenesis is not known, but tissue sampling has demonstrated that both are present throughout maturation.[21] Ligament and tendon growth has been observed to include increases in collagen fibril diameter and tissue length up to adulthood.[22]

Articular cartilage maturation begins in embryogenesis as differentiation from the mesoderm germ layer colocalized with the cartilage production of the skeletal system. As the cells of the mesenchyme condense and differentiate into chondroblasts, they begin synthesizing extracellular matrix proteins to develop the skeleton anlage.[23] During this embryologic formation, synovial joints develop via interzone formation, cavitation, and morphogenesis.[24,25] Chondrogenesis, or articular cartilage development, becomes morphologically distinct from bone growth in fetal development as the articular chondrocytes at the interzone condense and flatten.[26,27] These chondrocytes have been found to distribute across the layers of the articular cartilage and express different proteins based on their location; signaling is thought to originate from the synovium of the joint.[23,27] Postnatal extracellular matrix production and organization by these articular cartilage chondrocytes develop a tissue morphologically different than epiphyseal cartilage, and this tissue in early childhood adopts the adult morphology.[28,29] This includes the calcified zone of the articular cartilage, which interfaces with the subchondral bone.[23,24,27] Although the growth plate chondrocytes erode after adolescent growth in humans, the articular cartilage chondrocyte number, phenotype, and expression persist through adulthood. This maintenance is thought to be regulated through interactions with the synovium.[24] Load bearing and skeletal growth affect articular cartilage growth in terms of thickness and bone surface coverage; this has not, however, been well documented in humans.

Embryonic development of the intervertebral disc involves the mesenchymal peripheral regions of the disc, replete with dense cells, aligning in a multilaminar appearance.[3] The cells of this perichordal tissue differentiate and produce extracellular matrix proteins (hyaline-like cartilage), which will comprise the annulus fibrosus.[30–32] The synthesis, condensation, and organization of the matrix of the annulus fibrosus typically occur in the presence of high vascularity and cellularity. Each of these diminishes with postnatal development. The nucleus pulposus embryonic development also occurs in a vascular-rich environment wherein notochordal cells differentiate to produce the proteins of the nucleus pulposus. The nucleus pulposus cells synthesize collagen type I, type II (A and B),

and a chondroitin sulfate proteoglycan.[31,32] These notochordal cells are subsequently replaced by chondrocyte-like nucleus pulposus cells in postnatal development. Before spinal longitudinal growth, the intervertebral discs maintain a high degree of cellularity and increase their height throughout adolescence.[3] As skeletal maturity approaches, annulus fibrosus and nucleus pulposus extracellular matrix protein synthesis diminishes, and cellular apoptosis decreases the number of prechondrocyte and fibroblast cells.

12.1.3 Skeletal Muscle

The growth and development of skeletal muscle involve a series of highly controlled and concerted pathways that include molecular, cellular, and mechanical mechanisms. Skeletal myogenesis is described herein based on healthy human *in vivo* mechanisms; however, significant literature has been devoted to mediating and affecting the development of skeletal muscle.[33–35] Much can be gained from that literature, but for our purposes, the natural progression of skeletal muscle development and growth will be reviewed.[36]

The paraxial mesoderm is the origin for most embryonic skeletal muscles through progressive differentiation and clustering into somites. The cells of the dorsal region of the somites form the dermomyotome—the predecessor of the dermis and the musculature.[37] The muscle progenitor cells of the dermomyotome delaminate and differentiate into myoblasts in the presence of myogenic regulatory factors.[38] The myoblasts, in turn, differentiate into myocytes and fuse to form multinucleated muscle fibers in a single layer or myotome.[39] This embryonic development results in two types of skeletal muscle fibers: temporally, (1) embryonic or primary fibers arise initially, which are then (2) followed by secondary or fetal fibers. These fibers are morphologically distinct and are the precursors to slow-twitch and fast-twitch fibers.[40] At this point in fetal development, the muscles have been fully partitioned into anatomic bundles representing the adult muscle forms.[41]

The maturation of muscles from postnatal to adulthood is characterized by the development of vascular beds, the lengthening of the muscles, and the bundling of greater and greater numbers of myofibers in cross section. As the axial skeleton increases in size, the muscles increase in length, which is accomplished through the addition of sarcomeres in series at the musculotendinous junction.[42] This increasing muscle length associated with bone length growth has been shown to be at the expense of muscle cross-sectional area.[43] The maximum muscle cross-sectional area was found to peak one year after the maximum bone dimensions were identified in a lower extremity study of maturation in girls.[43] In general, the cross-sectional area of muscles increases throughout childhood and adolescent development, and this growth is primarily attributed to an increase in the mean fiber size.[44] Fiber diameters increase in childhood through adolescence by increased sarcomere addition *in parallel*.[42,45] Furthermore, longitudinal data on the vastus lateralis (the largest and lateral-most part of the quadriceps femoris of the upper leg) exhibit a change in fiber-type predominance from type I at five years to type II in adulthood.[44] Thus, the length, cross-sectional packing, and fiber types all change with postnatal growth and development of muscles.

12.2 Developmental Biomechanics of Musculoskeletal Tissues

The growth and development of tissues and their mechanical environments are intrinsically entwined such that the progression (or modification) begets clear changes in the

other. This section focuses on the effects of growth and development on the mechanics of musculoskeletal tissues. Many studies have, however, evaluated the effects of altered mechanics on the growth and development of tissues.[2,15,46–52] These studies provide significant insight into the mechanisms of maturation, but for the purposes of this review, we will focus on the biomechanical changes that result from natural healthy development and growth. There exist a dearth of longitudinal data tracking the changes in mechanics of tissues, and, by its brevity, this review underscores the need for greater research efforts to characterize musculoskeletal tissues across the maturation spectrum.

Musculoskeletal tissue properties have been measured with human subjects, cadaver tissues, and postmortem animal tissues. Each of these models offers insight into the ontogenic curves describing a tissue's biomechanical response, but they also carry limitations. Few experiments can be done on isolated tissues in human subjects, and with children, the experimental challenges abound. Cadaver tissues offer the greatest promise in the mechanical characterization of musculoskeletal tissues, but these are difficult to acquire. The inability to use injured tissues (the leading cause of death for children) and the emotional sensitivity of the loss of a child lead to fewer tissue bequests. Finally, animal models can provide insight into the relationships between biomechanical properties and maturation; but, unfortunately, they do not provide accurate human property data due to genetic and rate-of-development discrepancies. This section reviews the literature from a human tissue perspective and provides mechanical property data based on tissue type, loading modality, tissue orientation, and loading rate.

12.2.1 Bone

Immature bone and growth plates have very different biomechanical responses than their adult counterparts. Unfortunately, few studies have documented longitudinal data on bone biomechanics to uncover the functions that describe the biomechanical properties of bone throughout maturation. Pediatric cortical bone exhibits a lower bending strength and modulus of elasticity compared with adult cortical bone. Furthermore, developing cortical bone absorbs more energy and has greater deformation at failure than its adult counterpart.[53,54] Currey[54] compared pediatric and adult femoral cortical bone and found that the modulus of elasticity and the strength were lower for children, whereas the energy absorption and deformation prior to failure were greater. The biomechanics are driven by tissue changes that include an initial cortical thickness increase throughout childhood, which gives way to greater cancellous bone growth in adolescence.[55] This has been measured in vertebral bone samples; vertebral cortical bone density and strength increase in childhood and reach a plateau in early adolescence, whereas the cancellous bone density increases in late puberty and seems to be dependent on mechanical stresses on the spine.[56] The compressive stress of a vertebral lumbar bone (L3) has been shown to increase from 2.4 MPa in a 10.5-year-old, to 3.1 MPa in a 15-year-old, to 3.7 MPa in a 17.5-year-old.[57] The compressive stiffness and size-normalized stiffness of isolated vertebral bodies both exhibit increases with age in a baboon model (Figure 12.3). This demonstrates that the structural organization of the vertebral body changes with age, as does the dimensional growth of the vertebrae.[58] Finally, skull failure stress in adult samples exhibits a resistance to fracture, which is approximately 11-fold greater than neonatal skull tissues.[59] The neonatal skull tissues also exhibit large dependence on the loading rate with respect to both stiffness and fracture loads.[60]

Maturation has distinct effects on the mineral density of the axial skeleton and consequently its mechanical response. The mineral density and hydroxyapatite crystal size both

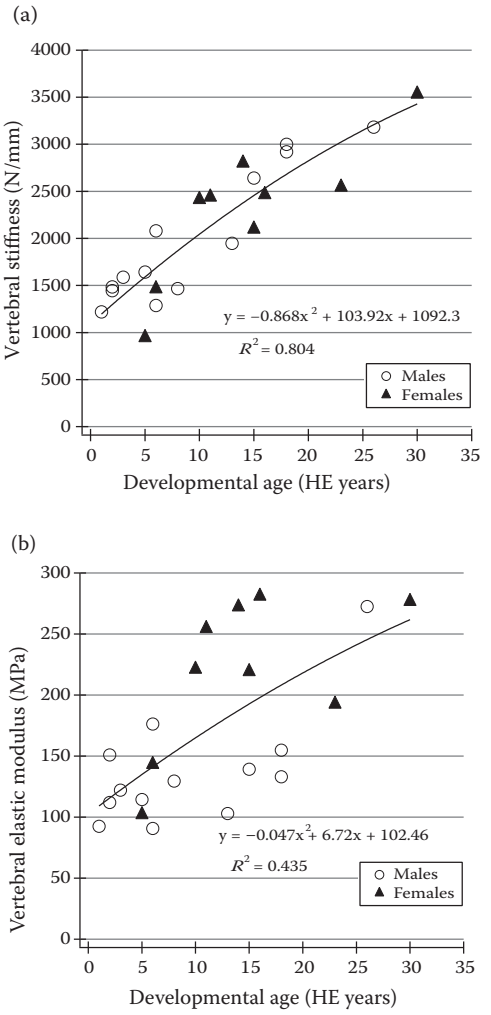

FIGURE 12.3
Compressive stiffness and elastic modulus of isolated vertebral bodies across the developmental spectrum. (a) Compressive stiffness, and (b) modulus of elasticity both increase with development and growth in baboon T9 thoracic vertebrae. These relationships are shown with a second-order polynomial fit to the data because of the relevance of this fit for other growth-related measures. Sex differences are not apparent in stiffness but seem to be present when these data are normalized by cross-sectional area for elastic modulus. HE = human equivalent. (Reprinted from *Bone*, 35(3), Nuckley, W. et al., Spinal maturation affects vertebral compressive mechanics and vBMD with sex dependence, 720–728, Copyright 2004, with permission from Elsevier.)

exhibit increases with advancing skeletal maturity.[61,62] Changes in the volumetric bone mineral density not only occur in early growth and ossification but also persist throughout puberty when large increases in bone density have been observed.[63] Bone mineral density has also been found to be directly related to the compressive yield strength of the bone in vertebral samples undergoing growth and development (Figure 12.4).[58] This relationship between compressive strength of bone and its density has been well characterized in an adult sample demonstrating increasing compressive strength with increased density.[64–66] A distinct difference between these adult and immature samples is the mechanism of

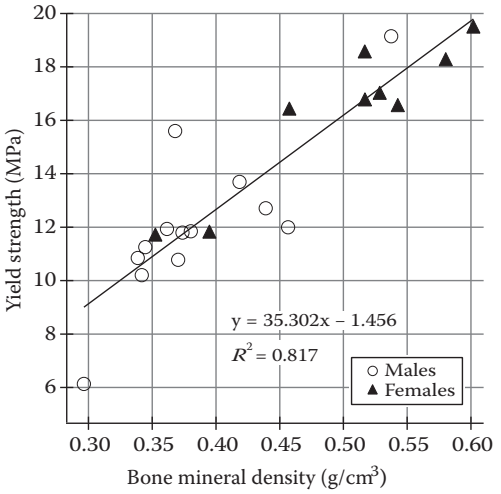

FIGURE 12.4
Relationship between yield strength and bone mineral density in maturing vertebrae. Baboon T9 thoracic vertebrae demonstrate an increase in compressive yield strength, which is concomitant with increasing bone density. (Reprinted from *Bone*, 35(3), Nuckley, W. et al., Spinal maturation affects vertebral compressive mechanics and vBMD with sex dependence, 720–728, Copyright 2004, with permission from Elsevier.)

failure; the tissues undergoing growth and development all failed at the cartilaginous physis or growth plate.

The cartilaginous physis is an anisotropic tissue with unique biomechanical responses related to its morphology that vary with development and applied load.[67] The pressure epiphysis is a secondary ossification center at the articular ends of long bones, and the traction epiphysis is a secondary center of ossification at the site of a tendon attachment. Axial bone loads and muscular forces at these sites produce differential growth rates that are thought to be responsible for the curvatures of long bones and the morphology of cancellous bone. The stresses that develop with the application of load to the physis are dependent on both the strain and the strain rate, clearly defining the physis as a viscoelastic material.[68] The growth plate is more compliant (10-fold) in the axial versus the radial direction and exhibits a similar permeability in each plane.[69–71] Furthermore, the mechanical properties vary by region or depth in the physis as well as throughout maturation to adulthood.[70] The tensile moduli and ultimate stress of the growth plates have been shown to increase with development.[71,72] This viscoelastic tissue maintains the lowest elastic modulus and hardness measurements compared with its surrounding tissues, the primary spongiosa and the epiphyseal trabecular bone and cartilage.[73] Not surprisingly, there is greater collagen content in regions of the physis that have been found to be the stiffest and strongest, indicating regional variations in the growth plate mechanics.[74] The failure mechanics of the physis have been shown to be positively correlated with the number of contours on the plate surface.[75] These undulations are seen on the physis-metaphysis boundary, and they dictate local and gross mechanical properties (shear resistance) to the growth plate complex.[74] Low levels of tension increase the synthetic activity of physeal cartilage, and small compressive forces tend to decrease its osteogenic activity.[76] As the physis develops, its tensile mechanical properties (modulus and

ultimate failure load) increase, although not merely due to size changes in the tissue.[72,77] The tensile load required for physis failure increases with age, whereas the displacement decreases. This suggests a reduced ductility of the developing physis with increasing age.[68] The aforementioned research includes long bone and vertebral specimens, but the physis is a ubiquitous tissue throughout growth and development, so these results should apply to all physes in the musculoskeletal system.

12.2.2 Soft Connective Tissue

General ligament mechanical properties have been evaluated as a function of development and have elucidated ligament stiffness, and modulus of elasticity increases with skeletal maturity. These increases in ligament mechanical properties have been well documented from postnatal growth through adulthood.[22,78–80] The ligament tensile failure mechanism is bony avulsion in younger ligaments and midsubstance failure in skeletally mature ligaments.[81] Clinically, it is commonly regarded that pediatric ligaments are stronger than their bony insertion. Other experiments have evaluated the changes in ligament mechanics from maturity to a degenerative state and have found that the modulus, ultimate stress, and strain energy decrease with age. Furthermore, there is a reversal in the failure mechanism, in which older ligaments tend to avulse bone at failure.[81,82] Tendons are similar structures that follow a maturation biomechanics pattern akin to the ligament. Increasing stiffness and cross-sectional area normalized stiffness (Young's modulus) have been observed in animal tendons across the developmental spectrum.[78,83–85] Similar results were found in an *in vivo* human study of the patellar tendon in which the stiffness and Young's modulus increased significantly from young children to adults.[86] These mechanical changes may be due to microstructural increases in fibril diameter, fibril packing, or collagen cross-linking.[86] Specifically, that research identified a significant increase in the cross-sectional area of the tendon in females, which leads to increased mechanical properties.

The healthy growth and development of articular cartilage have not been investigated in depth from a biomechanical perspective. Articular cartilage has been shown to thin and become more organized in postnatal development.[87,88] These changes are associated with an increase in the modulus of elasticity with advancing age.[88] Stress relaxation experiments identified that the equilibrium modulus was positively correlated with collagen cross-linking and growth and maturation of the articular cartilage.[88] Together, these studies point toward an increase in the organization, and subsequent mechanical properties, of articular cartilage, but the temporal sequence has yet to be fully described.

Intervertebral disc mechanical properties have been primarily evaluated from the degeneration perspective.[31,89–91] Consequently, little data exist on the biomechanics of intervertebral disc development. Collagen content in the annulus fibrosus and nucleus pulposus has been demonstrated to increase with age, indicating an ability to carry greater load in adulthood.[92] The degree of collagen cross-linking in the annulus affects the tissues' resilience, and this cross-linking has also been shown to be age related.[93] Using an animal model, intervertebral disc samples have been measured to increase threefold in their stiffness from birth to adulthood (Figure 12.5).[77] These samples exhibit a significant increase in compressive stiffness and cross-sectional area normalized stiffness, demonstrating that both the size of the tissue as well as its material properties are changing (tissue organization).

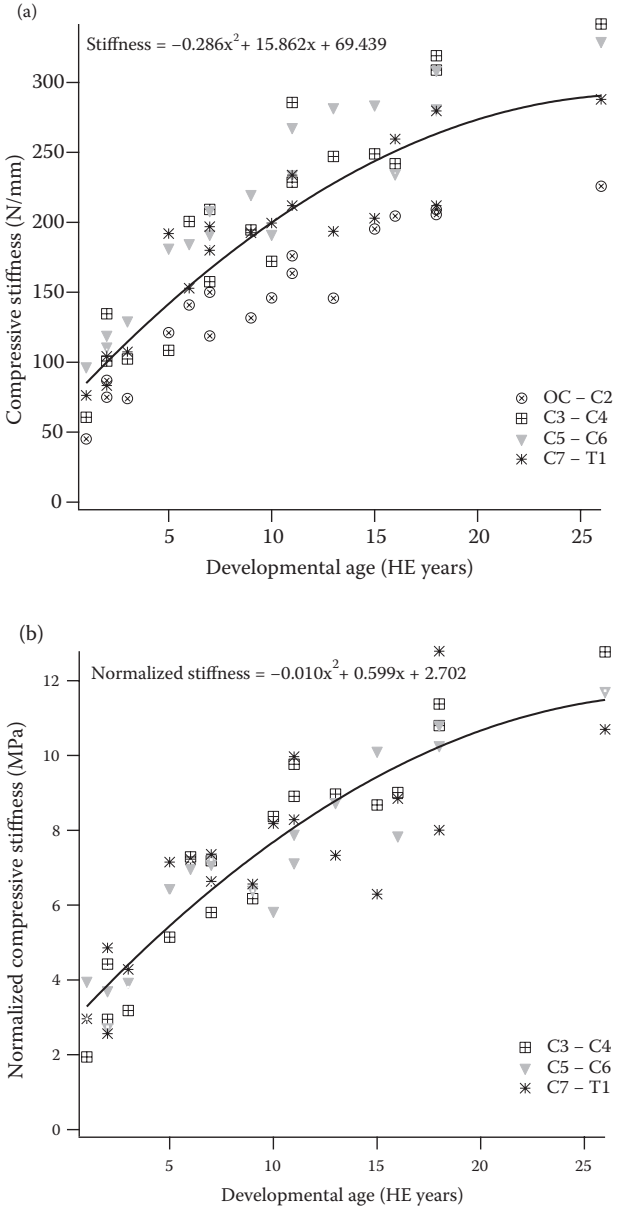

FIGURE 12.5
Compressive stiffness and normalized compressive stiffness as a function of growth and development. (a) Growth curves (HE is human equivalent) for cervical spine compressive stiffness separated by spinal level and fit with a second-order polynomial ($r^2 = 0.7477$, $n = 72$); (b) disc cross-sectional area normalized compressive stiffness exhibits a similar growth course exemplified by a 4× increase in the compressive material properties of the spine throughout maturation from infancy to adulthood ($r^2 = 0.8176$, $n = 54$). (Reprinted from *J. Biomech.*, 39(16), Nuckley, D. J. and Ching, R. P., Developmental biomechanics of the cervical spine: tension and compression, 3045–3054, Copyright 2006, with permission from Elsevier.)

12.2.3 Skeletal Muscle

Several studies have investigated muscle strength and activation in children compared with adults in the upper and lower extremities,[94–99] as well as the trunk.[100,101] These studies measured lower muscle force or joint torque values in children compared with adults. When the muscle force values were normalized by the muscle physiologic cross-sectional area, the differences between children and adults diminished. The remaining differences were suggested to be related to the inability of children to fully recruit the higher threshold motor units.[98,99] The muscle fiber composition has been shown to be similar between adults and children, indicating that composition does not change with growth and development.[102,103] Maximum isometric muscle force values have been measured by Beenakker et al.[104] in 270 healthy children and adolescents for 11 muscle groups, and identified advancing muscle strength with age as a function of muscle and sex (Figure 12.6). These data provide ontogenic curves describing typical muscle force production capabilities and

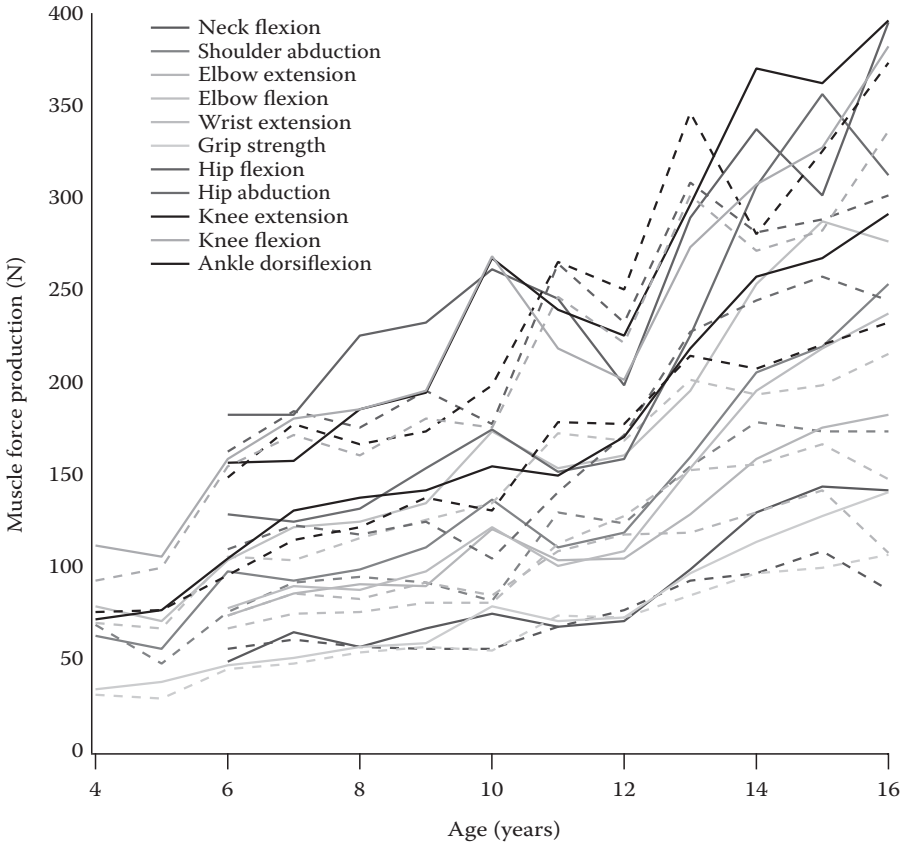

FIGURE 12.6
(See color insert.) Maximum isometric muscle force production for different muscle groups throughout growth and development. Although each curve advances with subject age, the shape and slope of the curves are muscle group-dependent. These functional data reveal up to a 4-fold increase in muscle force production from 4 to 16 years of age. (Data from *Neuromuscul. Disord.*, 11(5), Beenakker, E. A. et al., Reference values of maximum isometric muscle force obtained in 270 children aged 4–16 years by hand-held dynamometry, 441–446, Copyright 2001.)

also exhibit a direct relationship with a child's weight.[104] Neck isometric voluntary contraction forces have also been measured in children, adolescents, and adults for bending in flexion, extension, and lateral bending. These human muscle growth trajectories exhibited significant increases in force production as a function of age and have been modeled as a second-order polynomial (Figure 12.7). In an effort to describe the maximum voluntary contraction of the neck muscles as a function of anthropometry, the data were regressed by the neck circumference. Although neck circumference is not a good predictor of neck muscle strength in adults, in children and adolescents, neck circumference explained 61% of the maximum voluntary contraction variance (Figure 12.8). This provides a good predictive value of neck muscle maximum voluntary contraction, but to understand the maturation mechanics of skeletal muscles, the change in the tendon slack length (TSL) with maturation must also be studied.

TSL represents the shortest length at which the tendon carries a load. This length plays a key role in determining the force–length properties of a muscle. Due to the developing nature of pediatric musculature, TSL in children is longer relative to muscle length compared with adults.[105] Muscle lengthening lags behind bone lengthening throughout development, and it is the tendon length that increases to enable force production throughout the musculoskeletal maturation process.[106] Despite changes in tendon and muscle length, the pennation angle remains the same for both developing and mature musculoskeletal systems.[105]

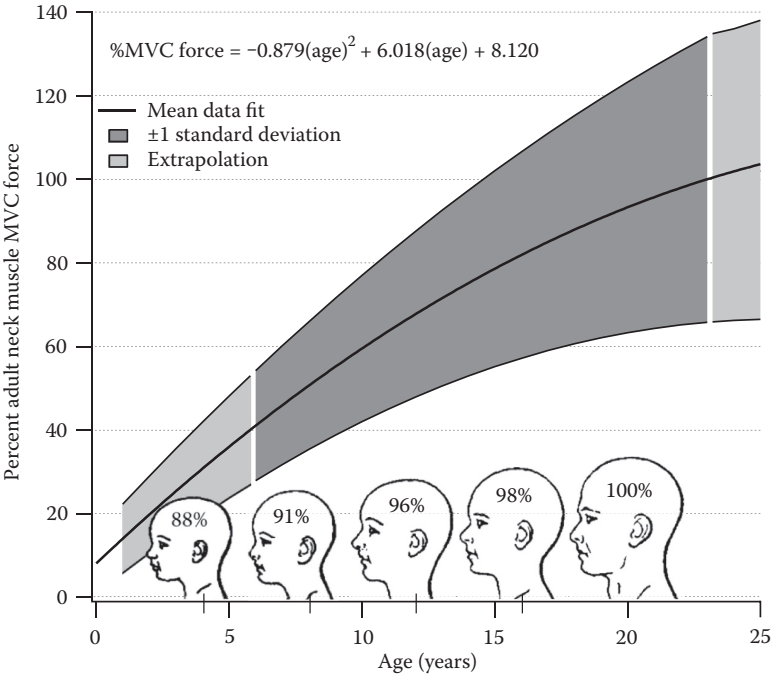

FIGURE 12.7
Percentage of neck muscle maximum voluntary contraction (MVC) force as a function of age. Maximum voluntary contraction force data for 120 children in each direction of flexion, extension, and lateral bending were normalized to the adult data (18–23 years) and fit with a second-order polynomial. The mean and standard deviation of neck muscle strength throughout growth and development are shown with head circumference data for comparison. Note that an 8-year-old has an average head circumference of 91% of the adult, whereas their neck strength is approximately 50% of the adult.

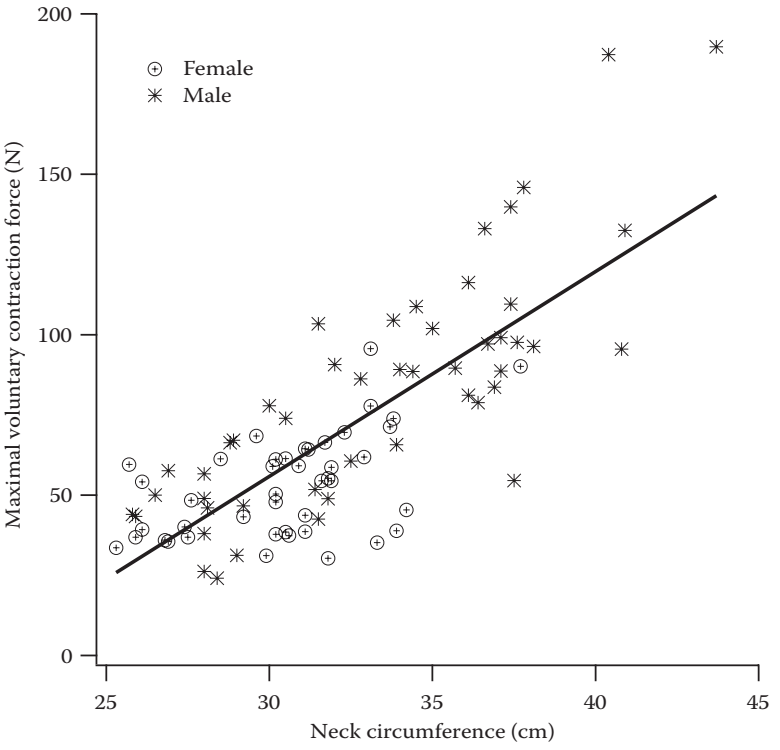

FIGURE 12.8
Neck muscle maximum voluntary contraction force as a function of neck circumference in developing children (4–18 years of age). A linear relationship describes the predictive ability of neck circumference such that 61% of the forward-flexion maximum voluntary contraction force variance is explained by neck circumference.

12.3 Developmental Biomechanics of the Musculoskeletal Structures

The mechanics of bone, articular cartilage, ligaments, tendons, and muscles have been suggested to develop and grow in an integrated and codependent fashion, which is based on a common genetic or mechanical mechanism (or both). The multifactorial nature of development and growth results in individual musculoskeletal systems that respond to mechanical stimuli with a high degree of variability. This is due to genetic differences and environmental influences that are temporally unique for each person. As a result of this variability and the scarcity of tissue property data in the literature, an integrated understanding of the effects of maturation on systemic orthopaedic biomechanics is imprecise at best. Children of similar chronological age may not necessarily have the same "biological age" or "biomechanical age." This section details orthopaedic structures and joint systems that have been studied due to their incidence in pathologic and injury orthopaedics; as such, the developing spine and extremities will be specifically examined here. Finally, the role of other literature, such as those regarding injuries, obesity, and child abuse, will be discussed to further contextualize the role of growth and development on human orthopaedic biomechanics.

12.3.1 Biomechanics of the Developing Spine

Spinal maturation involves substantial increases in the size of osteoligamentous tissues while concurrently and continually protecting the neural elements within the spine and allowing for tremendous range of motion. The osteoligamentous spine is in continual flux because its tissue material properties are increasing with age, as are the structural mechanical properties (due to increases in size and amount of tissue). These changes manifest as increased stiffness, decreased range of motion, and increased tolerance to loading as an infant advances to adulthood. Furthermore, the shape of the neonatal spine is anteriorly concave and progresses to develop cervical and lumbar lordotic curves only after birth and the advent of head-up posture and walking, respectively.[107] These multifarious tissue and anatomic changes with maturation create a spinal column that has mechanical responses that are difficult to predict throughout the maturation process.

Spinal flexibility experiments for the immature cervical spine revealed increasing stiffness and decreasing range of motion with advancing age. The compressive stiffness of individual spinal segments exhibits a greater than twofold increase in stiffness from 2 years to adulthood (Figure 12.9). Similarly, Luck et al.[108] measured the tensile stiffness of 18 cadaveric cervical spines ranging in age from 20 weeks of gestation to 14 years old. That study measured an approximately threefold increase in spinal segment tensile stiffness from the very young to the oldest tissues evaluated. These changing structural and material properties of the cervical spine with development have been found to vary by spinal level as well. The tolerance of the infant and pediatric cervical spine has also been

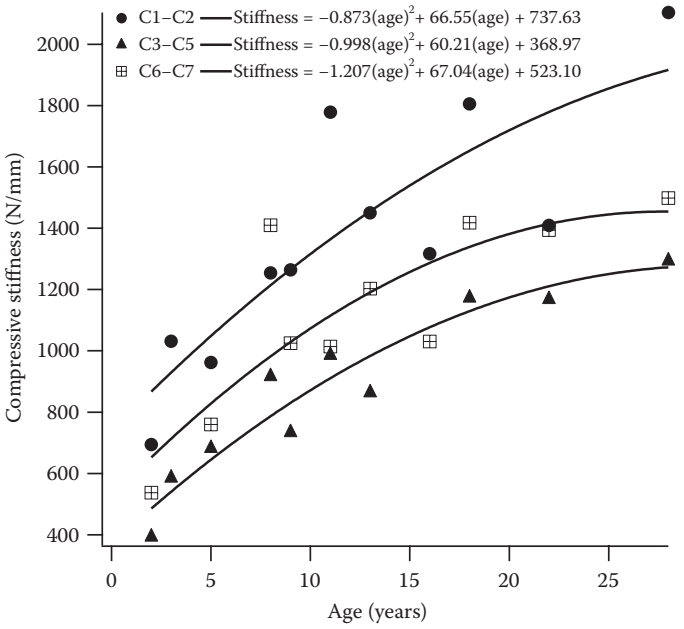

FIGURE 12.9
Compressive stiffness of human cervical spine segments across the developmental spectrum. These spinal segments in the upper (C1–C2), middle (C3–C5), and lower (C6–C7) cervical spine demonstrate increasing compressive stiffness with growth and development and follow a second-order polynomial with regard to age, until adulthood. These data demonstrate human spinal segment nondestructive biomechanics throughout maturation and display spinal level specificity.

investigated and found to be significantly greater (three-fold) in adults than in younger tissues. Our own results have been used to generate biomechanical growth curves describing the changing tolerance of these spinal segments throughout growth and development (Figure 12.10). Duncan[109] measured newborn infant spinal column tensile failure loads to be, on average, 467 N and 2-week-old child failure loads to be 654 N. These data align with our series of isolated human C1–C2 tensile failure experiments; our polynomial fit of the experimental data approaches a failure load of 479 N at birth. The tensile tolerance reported by Luck et al.[108] for dynamic failure follows a similar curve but provides critical data at the younger end of the developmental spectrum. That group further identified that differences between spinal levels were not present in the perinatal/neonatal samples but were evident as development progressed to childhood. The tensile failure mechanics of the cervical spine have also been measured in full-length osteoligamentous cervical spines and were found to increase with age in a study by Ouyang et al.[110] The tensile tolerance was measured to be maturation dependent, wherein young child spines (ages 2–4 years) failed at an average of 595 N, whereas older children (ages 6–12 years) succumbed to injury at an average of 868 N.[110] These data reflect a quasistatic loading of the cervical spine (5 mm/s) to failure while our data were collected dynamically at 1 m/s. This increase in tensile failure load with advancing age and increasing loading rate has been previously reported[111] and indicates yet another variable to consider in evaluating the biomechanics of the developing spine.

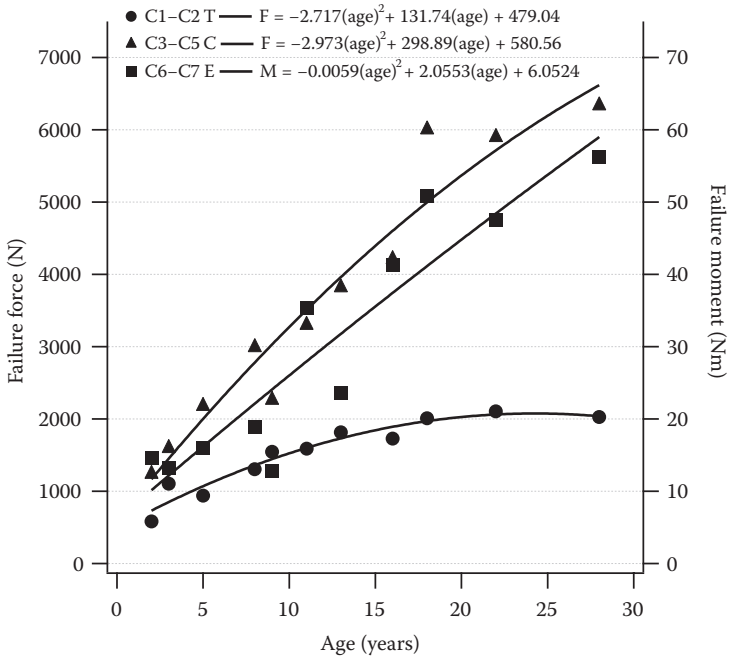

FIGURE 12.10
Growth and development changes the tolerance of spinal segments. The tensile, compressive, and bending tolerances of different spinal segments (C1–C2, C3–C5, and C6–C7) were measured using immature human cadaver samples. Maturation significantly increases the tolerance of the spine in each loading mode with different coefficients describing the "biomechanical growth" function.

12.3.2 Biomechanics of the Developing Extremities

The long bones of the extremities continue to grow in length from the proximal and distal epiphyseal plates. The muscles in turn lengthen to accommodate the longitudinal growth and increase their cross-sectional area to increase their force production capabilities. Wells et al.[112] measured limb dimensional properties in infants to 18-month-olds in an effort to describe the anthropometric growth progression of extremity biomechanics. This section reviews the few studies that evaluate extremity biomechanics on isolated orthopaedic tissues and then highlights research that details the functional extremity kinetics and kinematics throughout growth and development.

Orthopaedic tissue biomechanical properties for the extremities have been evaluated only in those critical areas in which pediatric injuries predominate. The effects of maturation on the femur and humerus are the most reported isolated musculoskeletal tissues of the extremities. Femur bending strength has been shown to increase with growth and development wherein values for a child were 176.9 MPa and for the adult were 208.7 MPa.[53] The femurs of children also exhibited a lower elastic modulus and ash content and absorbed more energy per unit area than the adult femurs. The quadriceps tendon force and the physiologic cross-sectional area of the quadriceps in children (5.7 kN and 101 cm^2) were measured to significantly increase with maturation to adulthood (10.1 kN and 183 cm^2).[113] Franklyn et al.[107] performed an excellent review of femur biomechanics in the maturing lower extremity. Few other studies have examined the effects of maturation on the osteoligamentous extremities.[57,114,115] The fetal humerus, for example, has been shown to have similar compressive strength as the fetal femur (35.28 versus 35.87 MPa, respectively).[115] Furthermore, as these bones mature to adolescence, their strength increases but is not significantly different between the humerus and the femur.[116] Finally, a number of studies have measured functional muscle mechanics in children, adolescents, and adults and may provide additional understanding of the biomechanical response of the extremities.[43,44,98,99,104,113]

Kinematic and kinetic experiments of human motion typically follow sports or task analyses, but these too can provide insight into the changes with growth and development that affect the biomechanics of the extremities. Gait studies examining typically developing children have identified the kinematics and kinetics of gait for the purposes of comparison with pathologic gait.[117–122] Chester et al.[118] determined differences between young children and adolescents using principal component analysis. They found that growth and development produced increased plantarflexion moments, larger knee flexor and extensor moments, decreased hip extensor moments at heel-strike, and increased hip flexor moments leading up to toe-off. Similar results were measured by Cupp et al.[119] when they compared young children with adult gait kinetics. Contrary to this finding, Ounpuu et al.[120] measured pediatric gait in 31 typically developing children (ages 5–16 years) and reported no difference in gait mechanics compared with adults. They suggest that gait kinematic and kinetic patterns are established as early as 5 years of age, which, if correct, would mean that the musculoskeletal mechanics of gait are conserved throughout a process of leg lengthening and growth. Schwartz et al.[122] collected kinetic, kinematic, and electromyographic (EMG) data on 83 children and adolescents (4–17 years old) walking at a self-selected speed. These data, although not explicitly compared with adult gait data, represent a repository of gait features that can inform how the lower extremities biomechanically mature. The pediatric gait data of Schwartz et al.[122] were comparable with the pediatric results of Bovi et al.[117] who also collected adult gait data. Bovi et al.[117] demonstrated differential kinematics and kinetics for children and adults across a number of gait tasks. A comprehensive review of

these gait mechanics studies may provide insight into growth and developmental changes that act to either alter biomechanics or preserve biomechanical function. Finally, an upper extremity study was performed to track three-dimensional (3D) kinematics in children (5–18 years old).[123] This research by Petuskey et al.[123] identified age-specific differences in shoulder and elbow kinematics for activities of daily living. Together, these studies suggest that growth and maturation affect both the musculoskeletal system's individual tissue properties and the integrated use of the extremities in functional activities.

12.3.3 Developmental Biomechanics Insight Gained from Study of Injury, Child Abuse, and Obesity

There exists unconventional data sets that may be drawn upon to change our understanding of the orthopaedic biomechanics of the developing human. Although these data sets include pathology, injury, child abuse, and obesity, this chapter will examine those data sets in which either the input loads (car crashes and falls) or additional loads (obesity) on the musculoskeletal system may be known. Thus, knowing the energy of a car crash and the position of the child, the mechanics of the injury scenario may be modeled to provide insight into the mechanics of the child's musculoskeletal system. Likewise, a rapid increase or decrease in a child's body weight would load their orthopaedic structures differently and may provide a glimpse into the maturation of these tissues.

Orthopaedic injuries to infants, children, and adolescents can provide data on the mechanisms of tissue failure, tolerance of tissues, and the influence tissues have on the failure mechanics of other tissues throughout maturation. There are numerous studies examining the epidemiology, presentation, and mechanisms of injuries to the immature musculoskeletal system.[59,124–136] Generally, children are less susceptible to injury than adults given a similar impact energy to the body; these child injuries are also less likely to result in permanent disability.[137,138] The flexibility of the thorax, for example, enables greater deformation before rib fracture, which reduces the risk for associated internal injuries in children. Specifically, automotive crash testing and evaluation have led to the prediction of the biomechanical response of children and adolescents for the development of safety guidelines based on the tolerance of immature orthopaedic tissues[135,139–143] Sports injuries have followed a similar course in which patterns and mechanisms of injury have been well documented; for a review of sports injuries, see the volume edited by Micheli.[144] Differential patterns of injury occur in children and adolescents, compared with adults, which require specialized treatments. Unfortunately, although the injury patterns are well described, the biomechanical mechanisms of these injuries are not completely known, creating difficulty in diagnosis and treatment of these injuries.

The study of child abuse has produced biomechanical insight and models to establish the relationship between injuries and loads being applied to the developing body. Pierce and Bertocci[145] performed a review of the use of biomechanics in differentiating accidents from child abuse, but that work also provides evidence to support the biomechanical measurements of orthopaedic tissue maturation. Head injury mechanisms and biomechanics were modeled in young children to evaluate the probability of severe injuries, and these "real-world" analyses may be used to validate the data describing the mechanical properties of the skull.[146,147] Similarly, long bone material properties are used to predict the fracture patterns of immature bone, and these have been shown to support different loading patterns in children.[148]

Another factor that affects orthopaedic biomechanics during development is obesity. Although the loads that obese children are applying to their musculoskeletal system are

known, the response of individual orthopaedic tissues to this increased body mass has not been measured. Furthermore, adiposity in children affects the mechanical factors associated with growth and development modulation. Specifically, bone mass has been shown to be diminished in obese children compared with their age-matched counterparts with healthy body mass indices (BMIs); these decrements were improved when weight-bearing exercise was performed.[149] Obesity has been associated with increased (twice higher) risk of fractures in children, but the hypothesized mechanism of decreased bone density has not been experimentally investigated.[150,151] Obesity has also been linked to abnormal skeletal alignment, which affects healthy bone and cartilage development.[152] For example, the measurement of gait kinetics in obese children identified significant differences compared with their counterparts with healthy BMIs.[153,154] In sum, there are little data describing the specific modifications to growth and development that obesity produces, but by studying obesity longitudinally, we may learn more about the biomechanics of the musculoskeletal system.

12.4 Biomechanics Modeling of Growth and Development

In an effort to describe the growth and development of biomechanical systems, computer modeling and scaling efforts have attempted to describe the musculoskeletal system. These efforts use existing tissue material property, morphology, and anthropometry data to describe the spectrum of maturation effects on the biomechanical response of the musculoskeletal system. This section reviews the general principles of scaling relationships and computational modeling and specifically includes examples of orthopaedic structures.

Analytically, scaling relationships have been identified to follow many functions, and typical growth patterns have been suggested to provide a basis for musculoskeletal biomechanics modeling. Scaling ratios have been developed to relate biomechanical parameters between two specific ages; this scalar approach provides very specific values for a single age of a child. Dimensionless scaling ratios have been used to scale musculoskeletal tissue properties by size, mass density, and Young's modulus, but these methods have yet to be validated.[155] Linear scaling approaches have been used to scale pediatric anatomic geometry and material properties from calcaneal tendon and other well-characterized tissues to obtain first-order estimates of pediatric spinal mechanics.[139,156,157] Based on observations of human growth (i.e., the stature and weight growth charts), it seems most likely that changes in anatomic geometry and tissue material properties follow a nonlinear course. In the human population, height, weight, inverse pulse rate, and metacarpal cortical bone area, for example, all demonstrate second-order polynomial functions with development (Figure 12.11).[158–162] These second-order polynomials fit growth characteristics by age (through 30 years) and may help elucidate the relationship between musculoskeletal biomechanical parameters and development. The biomechanical data presented herein are also best fit using a second-order polynomial. Because the second-order polynomial has a biological basis in development, the maturation of the biomechanical response of individual joints or systems will likely follow a similar pattern.

Experimental and theoretical modeling of human orthopaedic biomechanics has been approached using human subjects, anthropomorphic test devices, cadavers, and computational (rigid body and finite-element deformable) models. Human subject and cadaveric models have been largely used to describe the current state of biomechanics for developing

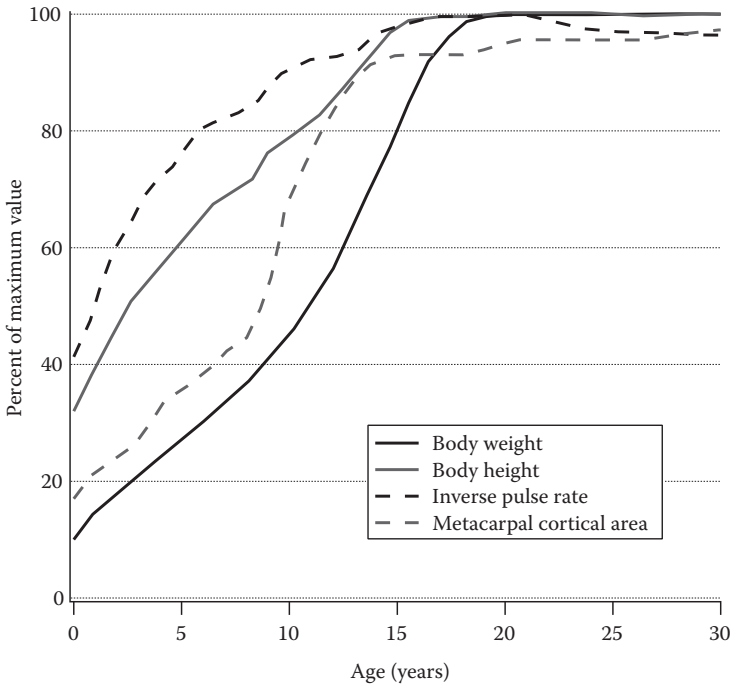

FIGURE 12.11
Growth curves describing function for scaling. Body height and weight, as well as metacarpal cortical area and inverse pulse rate, all exhibit the smallest least-squares error when fit with a second-order polynomial. These representative growth curves demonstrate the utility of fitting a second-order polynomial to growth and maturation data sets including biomechanical parameters. (Data from Iliff, A. and Lee, V. A., *Child Dev.*, 23, 4, 237–245, 1952; Prichett, J. W., *Pratical Bone Growth*, 1st ed., Seattle, WA: James W. Prichett, MD, 1993; Rosenfield, R. L. and Cara, J. F. Somatic growth and maturation, in *Endocrinology*, edited by L. J. DeGroot, pp. 2554–2568, Philadelphia, PA: W.B. Saunders Co., 1995; Rossman, I., Aging changes, in *Clinical Geriatrics*, edited by I. Rossman, pp. 9–15, Philidelphia: J. B. Lippincott, 1986; West, G. B. et al., *Nature*, 413, 6856, 628–631, 2001.)

orthopaedic tissues. The limitations of cadaveric tissue experimentation, including tissue availability, interspecimen variability, and technically difficult experimental preparations, may be overcome through the use of physical anthropomorphic test devices and computational models. Regardless of model and simulation development, it is critical that the parameters of any model are experimentally based and that the response of the model is validated. Because this is not always practical, the development of pediatric computational models should include a robust discussion of the assumptions, scaling, and other factors that defined the model and simulation environment.

Since the early 1970s, anthropomorphic test devices have been used in automotive crash simulations to determine protection reference values in an effort to minimize human injuries. These adult test dummies currently include biofidelic structure, mass, stiffness, energy dissipation, as well as transducers to measure the biomechanical environment experienced by the dummy. Child anthropomorphic test devices have recently been developed based on the 50th percentile male Hybrid III; 10-year-old, 6-year-old, 3-year-old, and 12-month-old anthropomorphic test devices exist with scaled biofidelic properties and measurement instrumentation. These dummies derive their biofidelic responses from a scaling of the Hybrid III 50th percentile "tensed" adult male.[163,164] Aside from automotive

crash scenarios, test dummies can also be used in fall and sports biomechanics investigations. For example, a toddler head anthropomorphic test device was developed to assess falls and was validated with skull fracture data.[165] Unfortunately, the kinematic and kinetic response of the "child" anthropomorphic test devices has not been validated. Despite this and their need for biofidelity enhancement, these devices provide unique insight into whole body kinetics and kinematics.

Computational models have been used increasingly to understand musculoskeletal system biomechanics (see Chapter 14). Computer modeling and simulation are important tools in predicting biomechanical outcomes with the benefits of easily altering parameters and evaluating their sensitivity and importance to a problem. These models can be defined and exercised with deformable or rigid body solutions, two-dimensional or 3D complexity, and quasistatic or dynamic mechanics algorithms. A computational model's ability to provide useful biomechanical insights into orthopaedic tissue or system behavior strongly depends on the availability of accurate experimental data to define the model's geometry, material properties, failure mechanics, kinematics, kinetics, or muscle activation. Once defined, the model's response should also be validated against other data to describe its functional domain and limitations. Musculoskeletal modeling using rigid bodies and defining joint mechanics and muscle mechanics has provided system-level approaches to orthopaedic problems. The deformable finite-element method has also been used to model the same systems but to evaluate the biomechanics at a tissue level.

Computational modeling of the developing musculoskeletal system adds the variable of age to the equation, but as has been presented, that does not equate to the application of a simple scalar to an adult model. Computational models of the immature head and neck have been developed and exercised in an attempt to prevent injuries to children. These cervical spine models have included age-specific head size/mass, ligament elasticity, muscle strength, as well as the orientation of the facets and vertebral bone density.[166,167] Such studies suggest that the child head and neck cannot be treated simply as a linear scaled-down version of an adult, but rather that the material properties and developmental anatomy need to be age-specific.[167,168] Finite-element models of the immature skull and brain have also been developed in an attempt to understand injuries to children.[169] A full mesh of the skull and brain was developed using the data by Franklyn et al.[106] and human cadaver skull data (n = 23).[170] Unfortunately, there is a lack of pediatric skull property data, and thus many of the parameters were estimated. Another modeling effort included the development of an ergonomic model to predict the biomechanical responses of children of various ages for certain lifting tasks.[171] That model utilizes child stature to scale many parameters and employs limited muscle force data in a linear extrapolation to cover age and joint angle differences; because this rigid body kinetic model is not validated, its effectiveness cannot be determined. Finally, we have embarked on musculoskeletal modeling of the child (6 years old) head and neck using the OpenSim (Simtk.org) platform. Musculoskeletal multibody modeling uses correctly defined anatomic geometry, mass, and moment of inertia properties coupled with joint flexibility and range of motion data to limit the model and muscle activation, strength, and length–tension data to drive the model. Although many of these parameters have been defined using the literature, this model has yet to be validated with any loading other than quasistatic planar neck bending. The modeling efforts discussed herein demonstrate the state of modeling for developing and growing orthopaedic tissues. Although many of these computational efforts provide insight into the biomechanical response of the body throughout growth and development, the reliability of their predictions critically relies on their validation with age-specific biomechanical responses. Thus, greater biomechanics research is needed to more completely

and accurately model and describe the growth and maturation of the musculoskeletal system.

12.5 Future Directions in Developmental Biomechanics

Growth and development have been shown to alter tissue constituents, size, and organization by means of biological initiators and modulation due to biological and mechanical stimuli. These changes in isolated musculoskeletal/orthopaedic tissues convey altered mechanical properties to the tissues, their joint systems, and the body. Characterization of these changes is critical for addressing the biomechanical response of the musculoskeletal system to loading under pathologic or potentially injurious situations. Unfortunately, the characterization of the development and growth of the musculoskeletal system is far from complete with regard to its biomechanical response. In sum, research efforts have identified ontogenetic curves describing the biomechanical response of individual tissues and some joint systems using human subject, cadaver, and postmortem animal models. These data have been used in scaling algorithms and computational models to assist in predicting the biomechanical response of a joint system across the maturation spectrum.

Specifically, research on the development and growth of orthopaedic tissues has resulted in rich insight into the biomechanics of these tissues and joint systems as well as an improved generalized understanding of maturation processes. Experiments on isolated musculoskeletal system tissues have exhibited increases in mechanical properties like tissue stiffness, energy absorption, and failure strength; these properties have been found to follow a second-order polynomial increase with aging. Both the material properties of the tissues and their structure (i.e., size) contribute to these increases in tissue mechanics. Bones, connective tissues, and muscles all develop and mature in concert but have differences in their temporal ontogeny with regard to increased tissue size, structural organization, and mechanical competence. Moreover, these patterns of growth and development are heterogeneous across joints, sexes, and in the face of pathology or external factors. The modeling of musculoskeletal system growth and development has enabled the generalization of tissue and joint system changes and the associated biomechanical responses.

Because the biology and mechanics of growth and development are inextricably linked, greater insight into the mechanistic underpinnings of this relationship is essential for improvements in musculoskeletal health and injury prevention. Future research efforts in developmental biomechanics are critical in describing the relative roles of a tissue's increase in constituent concentration, increase in size, and degree of organization. Furthermore, the link between musculoskeletal system tissues throughout maturation is currently poorly understood; for example, we are unable to predict the effects of increasing muscle mass in adolescence on the health and biomechanical competence of cartilage growth and maturation. The study of tissues undergoing maturation processes can provide insight not only into the growth of tissues but also into their potential regenerative stimuli and biological and mechanical responses. The engineering of orthopaedic tissues may also be enhanced through the understanding of a tissue's native growth and organization. An improved understanding of the way our adult musculoskeletal system is constructed may have far-reaching outcomes in orthopaedic health care for all individuals; there is currently a great need for improved research in this area.

Acknowledgments

The author would like to thank the following for their support and motivation of biomechanical investigations into the growth and development of musculoskeletal tissues: Dr. Randal Ching, Amy Lavallee, Jarrod Carter, Susanne Booma, Hitesh Mehta, and Richard Harrington. Support for the biomechanics research herein was provided by a grant from the Eunice Kennedy Shriver National Institute of Child Health and Human Development, National Institutes of Health.

References

1. Trueta, J. 1968. *Studies of the Development and Decay of the Human Frame*. Philadelphia, PA: W.B. Saunders.
2. Carter, D. R., M. C. Van Der Meulen, and G. S. Beaupre. 1996. Mechanical factors in bone growth and development. *Bone* 18(1 Suppl):5S–10S.
3. Ogden, J. A., T. M. Ganey, J. Sasse, P. J. Neame, and D. R. Hilbelink. 1994. Development and maturation of the axial skeleton. In *The Pediatric Spine: Principles and Practice*, edited by S. L. Weinstein, 3–69. New York: Raven Press.
4. Trelstad, R. L. 1977. Mesenchymal cell polarity and morphogenesis of chick cartilage. *Developmental Biology* 59(2):153–163.
5. Scheuer, L., and S. Black. 2000. *Developmental Juvenile Osteology*. San Diego: Academic Press.
6. Bick, E. M., and J. W. Copel. 1951. The ring apophysis of the human vertebra. *Journal of Bone and Joint Surgery. American Volume* 33-A (3):783–787.
7. Brighton, C. T. 1987. Morphology and biochemistry of the growth plate. *Rheumatic Diseases Clinics of North America* 13(1):75–100.
8. Doskocil, M., P. Valouch, and V. Pazderka. 1993. On vertebral body growth. *Functional and Developmental Morphology* 3(3):149–155.
9. Lawson, J. P., J. A. Ogden, R. W. Bucholz, and S. A. Hughes. 1987. Physeal injuries of the cervical spine. *Journal of Pediatric Orthopedics* 7(4):428–435.
10. Hunziker, E. B. 1988. Growth plate structure and function. *Pathology and Immunopathology Research* 7(1–2):9–13.
11. Hunziker, E. B. 1994. Mechanism of longitudinal bone growth and its regulation by growth plate chondrocytes. *Microscopy Research and Technique* 28(6):505–519.
12. Brighton, C. T. 1978. Structure and function of the growth plate. *Clinical Orthopaedics and Related Research* (136):22–32.
13. Linsenmayer, T. F., R. D. Eavey, and T. M. Schmid. 1988. Type X collagen: a hypertrophic cartilage-specific molecule. *Pathology and Immunopathology Research* 7(1–2):14–19.
14. Kwan, K. M., M. K. Pang, S. Zhou, S. K. Cowan, R. Y. Kong, T. Pfordte et al. 1997. Abnormal compartmentalization of cartilage matrix components in mice lacking collagen X: implications for function. *Journal of Cell Biology* 136(2):459–471.
15. Villemure, I., and I. A. Stokes. 2009. Growth plate mechanics and mechanobiology. A survey of present understanding. *Journal of Biomechanics* 42(12):1793–1803.
16. Martin, R. B., D. B. Burr, and N. A. Sharkey. 1998. *Skeletal Tissue Mechanics*. New York: Springer.
17. Tozer, S., and D. Duprez. 2005. Tendon and ligament: development, repair and disease. *Birth Defects Research. Part C, Embryo Today* 75(3):226–236.
18. Brent, A. E., R. Schweitzer, and C. J. Tabin. 2003. A somitic compartment of tendon progenitors. *Cell* 113(2):235–248.

19. Brent, A. E., T. Braun, and C. J. Tabin. 2005. Genetic analysis of interactions between the somitic muscle, cartilage and tendon cell lineages during mouse development. *Development* 132(3):515–528.
20. Benjamin, M., and J. R. Ralphs. 2000. The cell and developmental biology of tendons and ligaments. *International Review of Cytology* 196:85–130.
21. Penner, A. S., M. J. Rock, C. M. Kielty, and J. M. Shipley. 2002. Microfibril-associated glycoprotein-2 interacts with fibrillin-1 and fibrillin-2 suggesting a role for MAGP-2 in elastic fiber assembly. *Journal of Biological Chemistry* 277(38):35044–35049.
22. Haut, R. C. 1983. Age-dependent influence of strain rate on the tensile failure of rat-tail tendon. *Journal of Biomechanical Engineering* 105(3):296–299.
23. Zuscik, M. J., M. J. Hilton, X. Zhang, D. Chen, and R. J. O'Keefe. 2008. Regulation of chondrogenesis and chondrocyte differentiation by stress. *Journal of Clinical Investigation* 118(2):429–438.
24. Archer, C. W., G. P. Dowthwaite, and P. Francis-West. 2003. Development of synovial joints. *Birth Defects Research. Part C, Embryo Today* 69(2):144–155.
25. Pacifici, M., E. Koyama, and M. Iwamoto. 2005. Mechanisms of synovial joint and articular cartilage formation: recent advances, but many lingering mysteries. *Birth Defects Research. Part C, Embryo Today* 75(3):237–248.
26. Archer, C. W., H. Morrison, and A. A. Pitsillides. 1994. Cellular aspects of the development of diarthrodial joints and articular cartilage. *Journal of Anatomy* 184(Pt 3):447–456.
27. Cancedda, R., P. Castagnola, F. D. Cancedda, B. Dozin, and R. Quarto. 2000. Developmental control of chondrogenesis and osteogenesis. *International Journal of Developmental Biology* 44(6):707–714.
28. Buckwalter, J. A., and H. J. Mankin. 1998. Articular cartilage: tissue design and chondrocyte–matrix interactions. *Instructional Course Lectures* 47:477–486.
29. Guilak, F. 2000. The deformation behavior and viscoelastic properties of chondrocytes in articular cartilage. *Biorheology* 37(1–2):27–44.
30. Theiler, K. 1988. Vertebral malformations. *Advances in Anatomy, Embryology, and Cell Biology* 112:1–99.
31. Urban, J. P., S. Roberts, and J. R. Ralphs. 2000. The nucleus of the intervertebral disc from development to degeneration. *American Zoologist* 40(1):53–61.
32. Urban, J. P., and S. Roberts. 1995. Development and degeneration of the intervertebral discs. *Molecular Medicine Today* 1(7):329–335.
33. Bismuth, K., and F. Relaix. 2010. Genetic regulation of skeletal muscle development. *Experimental Cell Research* 316(18):3081–3086.
34. Kramer, H. F., and L. J. Goodyear. 2007. Exercise, MAPK, and NF-kappaB signaling in skeletal muscle. *Journal of Applied Physiology* 103(1):388–395.
35. Mok, G. F., and D. Sweetman. 2011. Many routes to the same destination: lessons from skeletal muscle development. *Reproduction* 141(3):301–312.
36. Grefte, S., A. M. Kuijpers-Jagtman, R. Torensma, and J. W. Von den Hoff. 2007. Skeletal muscle development and regeneration. *Stem Cells and Development* 16(5):857–868.
37. Christ, B., and C. P. Ordahl. 1995. Early stages of chick somite development. *Anatomy and Embryology* 191(5):381–396.
38. Gros, J., M. Scaal, and C. Marcelle. 2004. A two-step mechanism for myotome formation in chick. *Developmental Cell* 6(6):875–882.
39. Tajbakhsh, S., and M. Buckingham. 2000. The birth of muscle progenitor cells in the mouse: spatiotemporal considerations. *Current Topics in Developmental Biology* 48:225–268.
40. Van Swearingen, J., and C. Lance-Jones. 1995. Slow and fast muscle fibers are preferentially derived from myoblasts migrating into the chick limb bud at different developmental times. *Developmental Biology* 170(2):321–337.
41. Haushka, S. D. 1994. The embryonic origin of muscle. In *Myology*, edited by A.G. Engel and C. Franzini-Armstrong, 3–73. New York: McGraw Hill.
42. Goldspink, G. 1972. Postembryonic growth and differentiation of striated muscle. In *The Structure and Function of Muscle*, edited by G. H. Bourne, 179–236. New York: Academic Press.

43. Xu, L., P. Nicholson, Q. Wang, M. Alen, and S. Cheng. 2009. Bone and muscle development during puberty in girls: a seven-year longitudinal study. *Journal of Bone and Mineral Research* 24(10):1693–1698.
44. Lexell, J., M. Sjostrom, A. S. Nordlund, and C. C. Taylor. 1992. Growth and development of human muscle: a quantitative morphological study of whole vastus lateralis from childhood to adult age. *Muscle Nerve* 15(3):404–409.
45. Taber, LA. 1995. Biomechanics of growth, remodeling, and morphogenesis. *Applied Mechanics Reviews* 48(8):488–545.
46. Beaupre, G. S., S. S. Stevens, and D. R. Carter. 2000. Mechanobiology in the development, maintenance, and degeneration of articular cartilage. *Journal of Rehabilitation Research and Development* 37(2):145–151.
47. LeVeau, B. F., and D. B. Bernhardt. 1984. Developmental biomechanics. Effect of forces on the growth, development, and maintenance of the human body. *Physical Therapy* 64(12):1874–1882.
48. Li, K. W., A. K. Williamson, A. S. Wang, and R. L. Sah. 2001. Growth responses of cartilage to static and dynamic compression. *Clinical Orthopaedics and Related Research* (391 Suppl):S34–48.
49. Stokes, I. A. 2008. Mechanical modulation of spinal growth and progression of adolescent scoliosis. *Studies in Health Technology and Informatics* 135:75–83.
50. Turner, C. H., and F. M. Pavalko. 1998. Mechanotransduction and functional response of the skeleton to physical stress: the mechanisms and mechanics of bone adaptation. *Journal of Orthopaedic Science* 3(6):346–355.
51. Wren, T. A., G. S. Beaupre, and D. R. Carter. 2000. Mechanobiology of tendon adaptation to compressive loading through fibrocartilaginous metaplasia. *Journal of Rehabilitation Research and Development* 37(2):135–143.
52. Amini, S., D. Veilleux, and I. Villemure. 2010. Tissue and cellular morphological changes in growth plate explants under compression. *Journal of Biomechanics* 43(13):2582–2588.
53. Currey, J. D., and G. Butler. 1975. The mechanical properties of bone tissue in children. *Journal of Bone and Joint Surgery. American Volume* 57(6):810–814.
54. Currey, J. D. 1979. Changes in the impact energy absorption of bone with age. *Journal of Biomechanics* 12(6):459–469.
55. Staheli, L. T. 1992. *Fundamentals of Pediatric Orthopaedics*. New York: Raven Press.
56. Mora, S., W. G. Goodman, M. L. Loro, T. F. Roe, J. Sayre, and V. Gilsanz. 1994. Age-related changes in cortical and cancellous vertebral bone density in girls: assessment with quantitative CT. *AJR. American Journal of Roentgenology* 162(2):405–409.
57. Weaver, J. K., and J. Chalmers. 1966. Cancellous bone: its strength and changes with aging and an evaluation of some methods for measuring its mineral content. *Journal of Bone and Joint Surgery. American Volume* 48(2):289–298.
58. Nuckley, D. J., M. P. Eck, J. W. Carter, and R. P. Ching. 2004. Spinal maturation affects vertebral compressive mechanics and vBMD with sex dependence. *Bone* 35(3):720–728.
59. Ommaya, A. K., W. Goldsmith, and L. Thibault. 2002. Biomechanics and neuropathology of adult and paediatric head injury. *British Journal of Neurosurgery* 16(3):220–242.
60. Runge, C.F., A. Youssef, K. L. Thibault, S. M. Kurtz, G. Magram, and L. E. Thibault. 1998. Material Properties of Human Infant Skull and Suture: Experiments and Numerical Analysis. Paper read at 9th Injury Prevention through Biomechanics Symposium, Detroit, MI.
61. Lu, P. W., C. T. Cowell, S. A. Loyd-Jones, J. N. Briody, and R. Howman-Giles. 1996. Volumetric bone mineral density in normal subjects, aged 5–27 years. *The Journal of Clinical Endocrinology and Metabolism* 81(4):1586–1590.
62. Nuzzo, S., C. Meneghini, P. Braillon, R. Bouvier, S. Mobilio, and F. Peyrin. 2003. Microarchitectural and physical changes during fetal growth in human vertebral bone. *Journal of Bone and Mineral Research* 18(4):760–768.
63. Gilsanz, V., D. Gibbens, T. Roe, M. Carlson, M. Senac, M. Boechat et al. 1988. Vertebral bone density in children: effect of puberty. *Radiology* 166(3):847–850.
64. Carter, D. R., and W. C. Hayes. 1976. Bone compressive strength: the influence of density and strain rate. *Science* 194(4270):1174–1176.

65. Edmondston, S. J., K. P. Singer, R. E. Day, R. I. Price, and P. D. Breidahl. 1997. Ex vivo estimation of thoracolumbar vertebral body compressive strength: the relative contributions of bone densitometry and vertebral morphometry. *Osteoporosis International* 7(2):142–148.
66. Keller, T. S. 1994. Predicting the compressive mechanical behavior of bone. *Journal of Biomechanics* 27(9):1159–1168.
67. Canale, S. T. 1998. Physeal injuries. In *Skeletal Trauma in Children*, edited by N. E. Green and M. F. Swiontkowski, 17–58. Philadelphia, PA: W.B. Saunders Co.
68. Bright, R. W. 1991. Physeal injuries. In *Fractures in Children*, edited by C. A. Rockwood, K. E. Wilkins, and R. E. King, 87–186. Philadelphia, PA: J.B. Lippincott Co.
69. Cohen, B., W. M. Lai, and V. C. Mow. 1998. A transversely isotropic biphasic model for unconfined compression of growth plate and chondroepiphysis. *Journal of Biomechanical Engineering* 120(4):491–496.
70. Sergerie, K., M. O. Lacoursiere, M. Levesque, and I. Villemure. 2009. Mechanical properties of the porcine growth plate and its three zones from unconfined compression tests. *Journal of Biomechanics* 42(4):510–516.
71. Williams, J. L., P. D. Do, J. D. Eick, and T. L. Schmidt. 2001. Tensile properties of the physis vary with anatomic location, thickness, strain rate and age. *Journal of Orthopaedic Research* 19(6):1043–1048.
72. Guse, R. J., J. F. Connolly, R. Alberts, and L. Lippiello. 1989. Effect of aging on tensile mechanical properties of the rabbit distal femoral growth plate. *Journal of Orthopaedic Research* 7(5):667–673.
73. Lee, F. Y., J. Y. Rho, R. Harten, Jr., J. R. Parsons, and F. F. Behrens. 1998. Micromechanical properties of epiphyseal trabecular bone and primary spongiosa around the physis: an in situ nanoindentation study. *Journal of Pediatric Orthopedics* 18(5):582–585.
74. Cohen, B., G. S. Chorney, D. P. Phillips, H. M. Dick, J. A. Buckwalter, A. Ratcliffe et al. 1992. The microstructural tensile properties and biochemical composition of the bovine distal femoral growth plate. *Journal of Orthopaedic Research* 10(2):263–275.
75. Greco, F., L. de Palma, N. Specchia, and M. Mannarini. 1989. Growth-plate cartilage metabolic response to mechanical stress. *Journal of Pediatric Orthopedics* 9(5):520–524.
76. Mankin, K. P., and D. J. Zaleske. 1998. Response of physeal cartilage to low-level compression and tension in organ culture. *Journal of Pediatric Orthopedics* 18(2):145–148.
77. Nuckley, D. J., and R. P. Ching. 2006. Developmental biomechanics of the cervical spine: tension and compression. *Journal of Biomechanics* 39(16):3045–3054.
78. Nakagawa, Y., K. Hayashi, N. Yamamoto, and K. Nagashima. 1996. Age-related changes in biomechanical properties of the Achilles tendon in rabbits. *European Journal of Applied Physiology and Occupational Physiology* 73(1–2):7–10.
79. Torp, S., R. G. C. Arridge, C. D. Armeniades, and E. Baer. 1975. Structure–property relationships in tendon as a function of age. In *Structure of Fibrous Biopolymers*, edited by E. D. T. Atkins and A. Keller, 197–221. London: Butterworths.
80. Woo, S. L., J. A. Weiss, M. A. Gomez, and D. A. Hawkins. 1990. Measurement of changes in ligament tension with knee motion and skeletal maturation. *Journal of Biomechanical Engineering* 112(1):46–51.
81. Woo, S. L., C. A. Orlando, M. A. Gomez, C. B. Frank, and W. H. Akeson. 1986. Tensile properties of the medial collateral ligament as a function of age. *Journal of Orthopaedic Research* 4(2):133–141.
82. Noyes, F. R., and E.S. Grood. 1976. The strength of the anterior cruciate ligament in humans and rhesus monkeys: age-related and species-related changes. *Journal of Bone and Joint Surgery. American Volume* 58(8):1074–1082.
83. Danielsen, C. C., and T. T. Andreassen. 1988. Mechanical properties of rat tail tendon in relation to proximal–distal sampling position and age. *Journal of Biomechanics* 21(3):207–212.
84. Silver, F. H., Y. P. Kato, M. Ohno, and A. J. Wasserman. 1992. Analysis of mammalian connective tissue: relationship between hierarchical structures and mechanical properties. *Journal of Long-Term Effects of Medical Implants* 2(2–3):165–198.
85. Silver, F. H., J. W. Freeman, and G. P. Seehra. 2003. Collagen self-assembly and the development of tendon mechanical properties. *Journal of Biomechanics* 36(10):1529–1553

86. O'Brien, T. D., N. D. Reeves, V. Baltzopoulos, D. A. Jones, and C. N. Maganaris. 2010. Mechanical properties of the patellar tendon in adults and children. *Journal of Biomechanics* 43(6):1190–1195.
87. Bank, R. A., M. T. Bayliss, F. P. Lafeber, A. Maroudas, and J. M. Tekoppele. 1998. Ageing and zonal variation in post-translational modification of collagen in normal human articular cartilage. The age-related increase in non-enzymatic glycation affects biomechanical properties of cartilage. *The Biochemical Journal* 330(Pt 1):345–351.
88. Julkunen, P., T. Harjula, J. Iivarinen, J. Marjanen, K. Seppanen, T. Narhi et al. 2009. Biomechanical, biochemical and structural correlations in immature and mature rabbit articular cartilage. *Osteoarthritis Cartilage* 17(12):1628–1638.
89. Koeller, G. M., S. Muehlhaus, W. Meier, and F. Hartmann. 1986. Biomechanical properties of human intervertebral discs subjected to axial dynamic compression— influence of age and degeneration. *Journal of Biomechanics* 19:807–816.
90. White, A. A., and M. M. Panjabi. 1990. *Clinical Biomechanics of the Spine*. 2nd ed. New York: Lippincott.
91. Yamada, H. 1973. Ratios for age changes in the mechanical properties of human organs and tissues. In *Strength of Biological Materials*, edited by F. G. Evans, 255–271. Huntington, NY: Robert E. Krieger Publishing Co.
92. Scott, J. E., T. R. Bosworth, A. M. Cribb, and J. R. Taylor. 1994. The chemical morphology of age-related changes in human intervertebral disc glycosaminoglycans from cervical, thoracic and lumbar nucleus pulposus and annulus fibrosus. *Journal of Anatomy* 184(Pt 1):73–82.
93. Pokharna, H. K., and F. M. Phillips. 1998. Collagen crosslinks in human lumbar intervertebral disc aging. *Spine* 23(15):1645–1648.
94. De Ste Croix, M., M. Deighan, and N. Armstrong. 2003. Assessment and interpretation of isokinetic muscle strength during growth and maturation. *Sports Medicine* 33(10):727–743.
95. Neu, C. M., F. Rauch, J. Rittweger, F. Manz, and E. Schoenau. 2002. Influence of puberty on muscle development at the forearm. *American Journal of Physiology-Endocrinology and Metabolism* 283(1):E103–107.
96. Rauch, F., D. A. Bailey, A. Baxter-Jones, R. Mirwald, and R. Faulkner. 2004. The 'muscle-bone unit' during the pubertal growth spurt. *Bone* 34(5):771–775.
97. Grosset, J. F., I. Mora, D. Lambertz, and C. Perot. 2008. Voluntary activation of the triceps surae in prepubertal children. *Journal of Electromyography and Kinesiology* 18(3):455–465.
98. Falk, B., C. Usselman, R. Dotan, L. Brunton, P. Klentrou, J. Shaw et al. 2009. Child–adult differences in muscle strength and activation pattern during isometric elbow flexion and extension. *Applied Physiology, Nutrition, and Metabolism* 34(4):609–615.
99. Asai, H., and J. Aoki. 1996. Force development of dynamic and static contractions in children and adults. *International Journal of Sports Medicine* 17(3):170–174.
100. Carron, A. V., and D. A. Bailey. 1974. Strength development in boys from 10 through 16 years. *Monographs of the Society for Research in Child Development* 39(4):1–37.
101. Lefkof, M. B. 1986. Trunk flexion in healthy children aged 3 to 7 years. *Physical Therapy* 66(1):39–44.
102. Dubowitz, V. 1965. Enzyme histochemistry of skeletal muscle. *Journal of Neurology, Neurosurgery and Psychiatry* 28(6):516–524.
103. Paasuke, M., J. Ereline, and H. Gapeyeva. 2000. Twitch contraction properties of plantar flexor muscles in pre- and post-pubertal boys and men. *European Journal of Applied Physiology* 82(5–6):459–464.
104. Beenakker, E. A., J. H. van der Hoeven, J. M. Fock, and N. M. Maurits. 2001. Reference values of maximum isometric muscle force obtained in 270 children aged 4–16 years by hand-held dynamometry. *Neuromuscular Disorders* 11(5):441–446.
105. O'Brien, T. D., N. D. Reeves, V. Baltzopoulos, D. A. Jones, and C. N. Maganaris. 2010. Muscle–tendon structure and dimensions in adults and children. *Journal of Anatomy* 216(5):631–642.
106. Wren, T. A. 2003. A computational model for the adaptation of muscle and tendon length to average muscle length and minimum tendon strain. *Journal of Biomechanics* 36(8):1117–1124.

107. Franklyn, M., S. Peiris, C. Huber, and K. H. Yang. 2007. Pediatric material properties: a review of human child and animal surrogates. *Critical Reviews in Biomedical Engineering* 35(3–4):197–342.
108. Luck, J. F., R. W. Nightingale, A. M. Loyd, M. T. Prange, A. T. Dibb, Y. Song et al. 2008. Tensile mechanical properties of the perinatal and pediatric PMHS osteoligamentous cervical spine. *Stapp Car Crash Journal* 52:107–134.
109. Duncan, J. M. 1874. Laboratory note: on the tensile strength of the fresh adult foetus. *British Medical Journal* 2(729):763–764.
110. Ouyang, J., Q. Zhu, W. Zhao, Y. Xu, W. Chen, and S. Zhong. 2005. Biomechanical assessment of the pediatric cervical spine under bending and tensile loading. *Spine* 30(24):E716–723.
111. Nuckley, D. J., S. M. Hertsted, M. P. Eck, and R. P. Ching. 2005. Effect of displacement rate on the tensile mechanics of pediatric cervical functional spinal units. *Journal of Biomechanics* 38(11):2266–2275.
112. Wells, J. P., D. L. Hyler-Both, T. D. Danley, and G. H. Wallace. 2002. Biomechanics of growth and development in the healthy human infant: a pilot study. *Journal of the American Osteopathic Association* 102(6):313–319.
113. O'Brien, T. D., N. D. Reeves, V. Baltzopoulos, D. A. Jones, and C. N. Maganaris. 2010. In vivo measurements of muscle specific tension in adults and children. *Experimental Physiology* 95(1):202–210.
114. Asang, E., G. Wittmann, H. Hopp, and P. Watzinger. 1973. [Experimental and practical biomechanics of the human leg]. *Die Medizinische Welt* 24(15):576–581.
115. Yamada, H. 1970. *Strength of Biological Materials*. Baltimore: Williams and Wilkins.
116. Lindahl, O., and A. G. Lindgren. 1967. Cortical bone in man. II. Variation in tensile strength with age and sex. *Acta Orthopaedica Scandinavica* 38(2):141–147.
117. Bovi, G., M. Rabuffetti, P. Mazzoleni, and M. Ferrarin. 2011. A multiple-task gait analysis approach: kinematic, kinetic and EMG reference data for healthy young and adult subjects. *Gait & Posture* 33(1):6–13.
118. Chester, V. L., and A. T. Wrigley. 2008. The identification of age-related differences in kinetic gait parameters using principal component analysis. *Clinical Biomechanics (Bristol, Avon)* 23(2):212–220.
119. Cupp, T., D. Oeffinger, C. Tylkowski, and S. Augsburger. 1999. Age-related kinetic changes in normal pediatrics. *Journal of Pediatric Orthopedics* 19(4):475–478.
120. Ounpuu, S., J. R. Gage, and R. B. Davis. 1991. Three-dimensional lower extremity joint kinetics in normal pediatric gait. *Journal of Pediatric Orthopedics* 11(3):341–349.
121. Rosengren, K. S., F. J. Deconinck, L. A. Diberardino, 3rd, J. D. Polk, J. Spencer-Smith, D. De Clercq et al. 2009. Differences in gait complexity and variability between children with and without developmental coordination disorder. *Gait & Posture* 29(2):225–229.
122. Schwartz, M. H., A. Rozumalski, and J. P. Trost. 2008. The effect of walking speed on the gait of typically developing children. *Journal of Biomechanics* 41(8):1639–1650.
123. Petuskey, K., A. Bagley, E. Abdala, M. A. James, and G. Rab. 2007. Upper extremity kinematics during functional activities: three-dimensional studies in a normal pediatric population. *Gait & Posture* 25(4):573–579.
124. Bruns, W., and N. Maffulli. 2000. Lower limb injuries in children in sports. *Clinics in Sports Medicine* 19(4):637–662.
125. Damore, D. T., J. D. Metzl, M. Ramundo, S. Pan, and R. Van Amerongen. 2003. Patterns in childhood sports injury. *Pediatric Emergency Care* 19(2):65–67.
126. Grady, M. F., and A. Goodman. 2010. Common lower extremity injuries in the skeletally immature athlete. *Current Problems in Pediatric and Adolescent Health Care* 40(7):170–183.
127. Lallier, M., S. Bouchard, D. St-Vil, J. Dupont, and M. Tucci. 1999. Falls from heights among children: a retrospective review. *Journal of Pediatric Surgery* 34(7):1060–1063.
128. Le, T. B., and V. R. Hentz. 2000. Hand and wrist injuries in young athletes. *Hand Clinics* 16(4):597–607.
129. Anderson, J. M., and A. H. Schutt. 1980. Spinal injury in children: a review of 156 cases seen from 1950 through 1978. *Mayo Clinic Proceedings* 55(8):499–504.

130. Apple, D. F., Jr., C. A. Anson, J. D. Hunter, and R. B. Bell. 1995. Spinal cord injury in youth. *Clinical Pediatrics* 34(2):90–95.
131. Baker, C., H. Kadish, and J. E. Schunk. 1999. Evaluation of pediatric cervical spine injuries. *The American Journal of Emergency Medicine* 17(3):230–234.
132. Birney, T. J., and E. N. Hanley, Jr. 1989. Traumatic cervical spine injuries in childhood and adolescence. *Spine* 14(12):1277–1282.
133. Eleraky, M. A., N. Theodore, M. Adams, H. L. Rekate, and V. K. Sonntag. 2000. Pediatric cervical spine injuries: report of 102 cases and review of the literature. *Journal of Neurosurgery* 92(1 Suppl):12–7.
134. Kewalramani, L. S., and J. A. Tori. 1980. Spinal cord trauma in children. Neurologic patterns, radiologic features, and pathomechanics of injury. *Spine* 5(1):11–18.
135. Myers, B. S., and B. A. Winkelstein. 1995. Epidemiology, classification, mechanism, and tolerance of human cervical spine injuries. *Critical Reviews in Biomedical Engineering* 23(5–6):307–409.
136. Ogden, J. A. 1990. *Skeletal Injury in the Child*. 2nd ed. Philadelphia, PA: W.B. Saunders.
137. Dejeammes, M., C. Tarriere, C. Thomas, and D. Kallieris. 1984. Exploration of biomechanical data towards a better evaluation of tolerance for children involved in automotive accidents. In *Advances in Belt Restraint Systems*, 427–440. Warrendale, PA: Society of Automotive Engineers, Inc.
138. Weber, K. 1993. Child passenger protection. In *Accidental Injury: Biomechanics and Prevention*, edited by A. M. Nahum and J. W. Melvin, 493–511. New York: Springer-Verlag.
139. Eppinger, R., E. Sun, F. Bandak, M. Haffner, N. Khaewpong, and M. Maltese. 1999. *Development of Improved Injury Criteria for the Assessment of Advanced Automotive Restraint Systems-II*. Washington DC: National Highway Traffic Safety Administration.
140. Kleinberger, M., and L. Summers. 1997. Mechanisms of Injuries for Adults and Children Resulting from Airbag Interactions. Paper read at the Association for the Advancement of Automotive Medicine, Orlando, FL.
141. Mertz, H. J., P. Prasad, and A. L. Irwin. 1997. Injury Risk Curves for Children and Adults in Frontal and Rear Collisions. Proceedings of STAPP 41st Annual Meeting (973318):13–19.
142. Yoganandan, N., and F. Pintar. 1989. Epidemiology and Injury biomechanics of motor vehicle related trauma to the human spine. *Stapp Car Crash Conference* no. 33.
143. Mertz, H. J. 1994. Injury assessment values used to evaluate Hybrid III response measurements. In *Hybrid III: The First Human-Like Crash Test Dummy*, edited by S. H. Backaitis and H. J. Mertz, 407–422. Warrendale, PA: Society of Automotive Engineers, Inc.
144. Micheli, L. J. (ed.). 2000. Issue devoted to the pediatric and adolescent athlete. *Clinics in Sports Medicine* vol. 19.
145. Pierce, M. C., and G. Bertocci. 2008. Injury biomechanics and child abuse. *Annual Review of Biomedical Engineering* 10:85–106.
146. Thompson, A. K., G. Bertocci, W. Rice, and M. C. Pierce. 2011. Pediatric short-distance household falls: biomechanics and associated injury severity. *Accident; Analysis and Prevention* 43(1):143–150.
147. Coats, B., and S. S. Margulies. 2008. Potential for head injuries in infants from low-height falls. *Journal of Neurosurgery. Pediatrics* 2(5):321–330.
148. Pierce, M. C., G. E. Bertocci, E. Vogeley, and M. S. Moreland. 2004. Evaluating long bone fractures in children: a biomechanical approach with illustrative cases. *Child Abuse & Neglect* 28(5):505–524.
149. Mughal, M. Z., and A. V. Khadilkar. 2011. The accrual of bone mass during childhood and puberty. *Current Opinion in Endocrinology, Diabetes, and Obesity* 18(1):28–32.
150. Shultz, S. P., J. Anner, and A. P. Hills. 2009. Paediatric obesity, physical activity and the musculoskeletal system. *Obesity Reviews* 10(5):576–582.
151. Wearing, S. C., E. M. Hennig, N. M. Byrne, J. R. Steele, and A. P. Hills. 2006. Musculoskeletal disorders associated with obesity: a biomechanical perspective. *Obesity Reviews* 7(3):239–250.
152. Wearing, S. C., E. M. Hennig, N. M. Byrne, J. R. Steele, and A. P. Hills. 2006. The impact of childhood obesity on musculoskeletal form. *Obesity Reviews* 7(2):209–218.

153. Shultz, S. P., M. R. Sitler, R. T. Tierney, H. J. Hillstrom, and J. Song. 2009. Effects of pediatric obesity on joint kinematics and kinetics during 2 walking cadences. *Archives of Physical Medicine and Rehabilitation* 90(12):2146–2154.
154. Nantel, J., M. Brochu, and F. Prince. 2006. Locomotor strategies in obese and non-obese children. *Obesity (Silver Spring, Md.)* 14(10):1789–1794.
155. Yoganandan, N., S. Kumaresan, F. Pintar, and T. A. Gennarelli. 2002. Pediatric biomechanics. In *Accidental Injury: Biomechanics and Prevention,* 2nd ed., edited by A.M. Nahum and J.W. Melvin, 493–511. New York: Springer-Verlag.
156. Melvin, J. W. 1995. Injury Assessment Reference Values for the CRABI 6-month Infant Dummy in a Rear-Facing Infant Restraint with Air Bag Deployment. SAE International Congress and Exposition Paper #950872.
157. Mertz, H. J., and D. A. Weber. 1982. Interpretations of the Impact Responses of a Three-Year-Old Child Dummy Relative to Child Injury Potential. SAE Transactions Paper #826048.
158. Iliff, A., and V. A. Lee. 1952. Pulse rate, respiratory rate, and body temperature of children between two months and eighteen years of age. *Child Development* 23(4):237–245.
159. Prichett, J. W. 1993. *Pratical Bone Growth*. 1st ed. Seattle, WA: James W. Prichett, MD.
160. Rosenfield, R. L., and J. F. Cara. 1995. Somatic growth and maturation. In *Endocrinology*, edited by L. J. DeGroot, 2554–2568. Philadelphia, PA: W.B. Saunders Co.
161. Rossman, I. 1986. Aging changes. In *Clinical Geriatrics*, edited by I. Rossman, 9–15. Philidelphia: J. B. Lippincott.
162. West, G. B., J. H. Brown, and B. J. Enquist. 2001. A general model for ontogenetic growth. *Nature* 413(6856):628–631.
163. Backaitis, S. H., and H. J. Mertz. 1994. *Hybrid III: The First Human-Like Crash Test Dummy*. Warrendale, PA: Society of Automotive Engineers, Inc.
164. DeSantis Klinich, K., R. A. Saul, G. Auguste, S. Backaitis, and M. Kleinberger. 1996. *Techniques for Developing Child Dummy Protection Reference Values*. NHTSA Event Report: Child Injury Protection Team.
165. Ibrahim, N. G., and S. S. Margulies. 2010. Biomechanics of the toddler head during low-height falls: an anthropomorphic dummy analysis. *Journal of Neurosurgery. Pediatrics* 6(1):57–68.
166. Cazon, A., and A. Suescun. 2009. A head–neck biomechanical model of a 6-year-old child for frontal crash studies. *International Journal of Vehicle Safety* 4(4):257–270.
167. Kumaresan, S., N. Yoganandan, F. A. Pintar, D. J. Maiman, and S. Kuppa. 2000. Biomechanical study of pediatric human cervical spine: a finite element approach. *Journal of Biomechanical Engineering* 122(1):60–71.
168. Kumaresan, S., N. Yoganandan, and F. A. Pintar. 1997. Age-Specific Pediatric Cervical Spine Biomechanical Responses: Three-Dimensional Nonlinear Finite Element Models. Proceedings of STAPP 41st Annual Meeting (973319):31–61.
169. Klinich, K. D., G. M. Hulbert, and L. W. Schneider. 2002. Estimating infant head injury criteria and impact response using crash reconstruction and finite element modelling. *Stapp Car Crash Journal* 46:165–194.
170. Coats, B., and S. S. Margulies. 2006. Material properties of human infant skull and suture at high rates. *Journal of Neurotrauma* 23(8):1222–1232.
171. Waters, T. R., and A. Garg. 2010. Two-dimensional biomechanical model for estimating strength of youth and adolescents for manual material handling tasks. *Applied Ergonomics* 41(1):1–7.

13

Gender and Aging: Considerations for Orthopaedics

Brian D. Stemper, Jason J. Hallman, Frank A. Pintar, and Dennis J. Maiman

CONTENTS

Biomechanics, as a science, refers to the study of the mechanics of biological systems. As such, the biomechanical response of the human body is dependent on several factors including geometry, material properties, boundary conditions, and loading. Whereas boundary conditions and loading describe the external environment, geometry and material properties are inherent characteristics of the biological system. The biological system can be composed of a single tissue (e.g., ligament) or a composite of multiple tissues acting in concert to achieve a specific response. For example, on a segmental level, opposing vertebrae of the spine are interconnected by the intervertebral discs, facet joints, ligaments, and muscles. These tissues act together to provide stability to the body and limit motions within the physiologic realm. Likewise, the response of the human knee joint is governed by opposing long bones, ligaments, tendons, menisci, and cartilage. The overall response of a multitissue system depends on the intrinsic and coupled responses of the individual tissues.

Regional variations exist for specific systems within the body. For example, the biomechanical response of the lumbar spine is known to be quite different from the cervical spine due to structural and material differences.[1] However, experimental research has generally demonstrated relative consistency from person to person for a given system. The level of consistency increases when accounting for specific factors that are known to affect the biomechanical response of human tissues and structures. Two of the factors that most influence human biomechanics are gender and age. This chapter will serve as a review of existing literature on gender- and age-related biomechanical differences. It is not intended to be comprehensive. Rather, it will discuss primarily experimental studies that have endeavored to quantify the effects of gender and age on the physiologic and traumatic biomechanics of human tissues.

13.1 Biomechanical Effects of Gender

Although the scientific study of human mechanics and movement has advanced across hundreds of years, quantification of biomechanical differences between men and women beyond the abdominal region is a relatively new phenomenon. An understanding of fundamental biomechanical gender differences has come to light over the past 20 years, wherein females are no longer thought of as scaled-down males. Rather, distinct anatomical and material differences exist that change the method by which tissues respond to loads and the mechanics of movement in such a way that gender-dependent clinical guidelines, tolerance thresholds, and safety enhancements may be required. This section discusses some of the relevant areas of research in which these differences have been identified, quantified, and advanced.

13.1.1 Intrinsic Gender Differences in the Spine

The spinal column consists of 24 bony vertebrae separated by intervertebral discs anteriorly and facet joints posteriorly. Spinal ligaments span between vertebrae, and muscles attach to add active stabilizing support. The cervical spine can be thought of as a column that supports the mass of the head (Figure 13.1a). *Stability* is a mechanical concept associated with

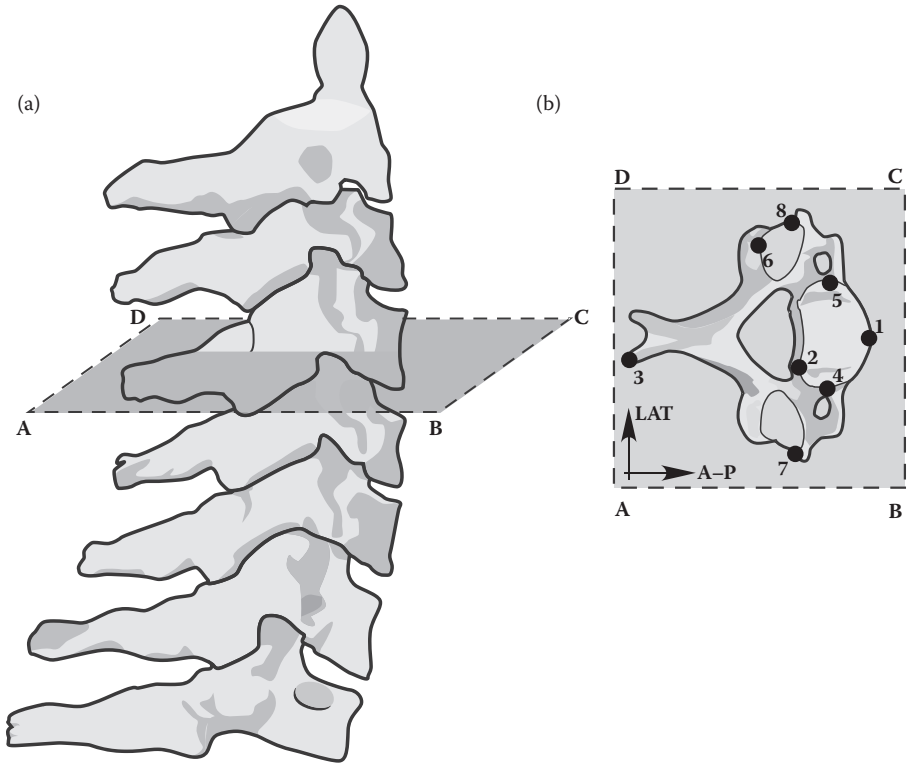

FIGURE 13.1
(a) Lateral view of the cervical spine from C2 to T1 and (b) axial view of the C4 vertebra. Biomechanically relevant metrics include vertebral depth as the anterior–posterior (A–P) distance from point 1 to point 3, vertebral body depth (A–P distance from 1 to 2), vertebral body width (lateral (LAT) distance from 4 to 5), vertebral width (LAT distance from 7 to 8), and disc-facet depth (A–P distance from 1 to 6).

columns that describes their ability to bear loads without buckling. The stability of a column depends on its length, cross-sectional dimensions, and material properties. Although the length of the cervical spine is a fairly uncomplicated metric that encompasses the axial distance from the base of the cranium to the cervicothoracic junction, the cross-sectional dimensions are less clear due to anatomical inhomogeneity within the transverse plane. One method of estimating the cross-sectional dimensions of the spine in relation to stability is through the quantity of area moment of inertia. This metric quantifies the bending resistance of a column and is computed similar to the cross-sectional area with shape and the plane of loading taken into account. For example, in the case of spinal flexion–extension bending, the metric places more emphasis on the anterior–posterior cervical spine dimension (e.g., in the plane of loading) than the medial–lateral dimension (e.g., out of the plane of loading). In general, columns of shorter length and with greater cross-sectional dimensions are more stable and, therefore, more capable of resisting static or dynamic loads.

Anatomically based studies have identified significant differences in cervical spine cross-sectional geometry between men and women that may contribute to decreased head–neck and spinal stability in females. Direct comparisons of vertebral and vertebral body depth and width (Figure 13.1b) between males and females have identified greater dimensions in males.[2–4] However, given the larger overall body size of the average male compared with the average female, a smaller female cervical spine is to be expected. A more appropriate comparison for the determination of true gender differences would be based on males and females of similar size. In that regard, Stemper et al.[5,6] reported significant cervical spine anatomical differences for a population of males and females size-matched based on head circumference or sitting height. Their study focused on biomechanically relevant metrics such as disc-facet depth, defined as the distance from the anterior of the vertebral body to the posterior aspect of the facet joints, as well as more traditional metrics including vertebral and vertebral body width and depth (Figure 13.1). Vertebral and vertebral body width and depth, as well as disc-facet depth, were found to significantly vary by spinal level and between genders.[6] Females had smaller vertebral dimensions in all cases for this size-matched population. Similar findings were reported by Vasavada et al.[7] for a population of 14 pairs of height- and neck-length–matched men and women. Specifically, female cervical vertebral bodies were significantly smaller in the anterior–posterior dimension, and the overall vertebral depth (e.g., vertebral body to spinous process) was significantly smaller in females at lower cervical levels (C5–C7). Although the medial–lateral vertebral body width was smaller in females, differences did not attain statistical significance. Perhaps the most relevant finding of that study was that gender differences were more pronounced for the neck (9%–16% different) rather than the head (3%–6%) metrics, indicating that a more slender neck in females was responsible for maintaining stability of a relatively more massive head. These anatomically based studies clearly identify a more slender cervical column in females, even when size-matched to males. These differences are likely to be accentuated in the general population, wherein females are smaller than males. These anatomically based differences likely result in a less stable female cervical column that is less capable of resisting the types of inertial loading experienced during automotive collisions and other traumas to the neck.

In addition to biomechanical relevance, gender differences in spinal anatomy may also have clinical implications. With regard to cervical spine pedicle geometry, important for the placement of pedicle screws, Rao et al.[8] reported significantly smaller pedicle dimensions in females along with significant gender differences for initial screw placement location and orientation. Other studies have reported similar findings with regard

to pedicle anatomy.[9,10] Incorrect placement and orientation or screw diameter increases the risk of injuring the spinal cord, nerve root, or vertebral arteries during screw insertion.[11,12] Cervical spine lateral mass dimensions were also quantified for the placement of lateral mass screws using Roy–Camille or Magerl techniques.[13] Significant differences in lateral mass width and both screw lengths were identified between genders, with females demonstrating smaller dimensions for each metric and at all cervical spinal levels that were investigated. Excessively long or misdirected lateral mass screws can result in damage to the spinal nerve root, vertebral artery, or caudal facet joint using either technique.[14–17] Malik et al.[18] investigated anatomical characteristics in the cervical spine relevant for intervertebral disc and uncovertebral joint resection in the context of placement of artificial discs. Resection of those structures requires a thorough understanding of anatomical variation due to the close proximity of the transverse foramen and vertebral artery lateral to the uncovertebral joint. That study reported interforaminal distances for the transverse foramina and distances from the uncus tip and ridge to the medial aspect of the foramen. All those dimensions were significantly smaller in females. The studies highlighted in this section clearly demonstrate a clinically relevant gender dependence in cervical spine anatomy that should be accounted for during surgical planning for instrumentation to stabilize the spine after disease or trauma.

Anatomical gender differences have also been identified in the thoracic and lumbar spinal regions. The lordotic curvature of the lumbar spine in humans, which is an important characteristic not present in other anthropoids, permits greater flexibility of the torso and reduces the axial load on the intervertebral discs, while also minimizing posterior–anterior shear forces during lifting due to the dorsal orientation of the interspinous and supraspinous ligaments.[19] Gender differences have been identified with regard to the overall magnitude of lumbar lordosis, commonly measured as the sagittal plane angle between upper and lower lumbar segments (e.g., L1–L2 disc versus L5–S1 disc).[20] Fernand and Fox[21] found that females had a significantly larger mean lordotic angle than males. Farfan et al.[20] and Stagnara et al.[22] had previously hypothesized, but were not able to statistically prove, that a gender difference existed. A number of other studies reported similar findings with females demonstrating an average of 40% greater lumbar lordotic curvature than males.[23–27] The accentuated lordotic curvature in females is thought to be an evolutionary trait designed to compensate for the anterior augmentation of the female abdomen during pregnancy by moving the center of mass posteriorly to remain in-line with the pelvis.[28]

Other anthropometric differences have been identified in thoracic and lumbar vertebrae. For example, differences in lumbar spinal facet joint shape and orientation may have biomechanical implications due to the role of these structures in facilitating controlled movement, resisting shear forces, and preventing excessive flexion and axial rotation.[29] Facet sizes were generally found to be larger in males compared with females at most levels of the thoracic and lumbar spines.[30] Smaller facet sizes could contribute to decreased shear stiffness in female lumbar spinal motion segments that may lead to accelerated posterior column degeneration and the eventual development of degenerative spondylolisthesis. Consistent clinical findings of a female preponderance for this condition would tend to support this assertion.[31–34] Mosekilde[35] identified significantly greater lumbar spine vertebral body cross-sectional areas in males that would tend to increase the axial load-carrying capacity in that population.

Soft tissue material differences between genders have also been identified in the spine. Static measurements of segmental flexibility have identified gender differences in cervical, thoracic, and lumbar spinal regions. In the cervical region, Nightingale et al.[36] reported

flexion strength and stiffness of the cadaveric upper cervical spine to be significantly greater in male than in female spinal segments. A similar finding was reported in the lumbar spine, wherein measurement of segmental axial stiffness in 298 patients revealed significantly increased stiffness magnitudes in males compared with females.[37] Also, Stemper et al.[38] investigated axial mechanical properties in the thoracic spine. Their study reported similar findings to the studies highlighted above, in that male segments had a significantly increased stiffness than female segments. However, the study also identified significantly increased intervertebral disc cross-sectional area in male cadaveric specimens, although disc height was not gender dependent. When accounting for greater cross-sectional areas, the authors reported that the elastic modulus for female specimens was greater than that for male specimens. This finding highlights the complex effect of the gender factor in spinal biomechanics because biomechanical differences attributed to gender may actually be manifesting the effect of size differences because the average female is considerably smaller than the average male.[39] However, continued investigation of these differences is warranted given the significant differences identified in some of the studies highlighted in this section when also accounting for subject size. Additionally, significant gender differences in spinal ligamentous components[40] indicate that biomechanical differences are likely the result of material, in addition to structural, differences between the sexes.

13.1.2 Extrinsic Gender Differences in the Spine

In the physiologic environment, the neck muscles provide support for the head–neck complex, maintain an upright head–neck orientation, and generate movements of the head and cervical spine. They are also important for dynamic stabilization during inertial loading scenarios, such as automotive rear impacts, wherein differential motion between the head and thorax may lead to injury of the cervical spine soft tissues.[41–45] The ability of the neck muscles to stabilize the head–neck complex is dependent on their moment-generating capacity, which, in turn, is dependent on the maximum contractile force of the muscle and its distance from the center of rotation (i.e., the moment arm). Experimental studies have investigated the maximum isometric moment-generating capacity of men and women using resistance gauges.[46–50] These testing protocols typically involve a seated subject that places their head in an initial position and statically applies force with the forehead (flexion) or occiput (extension) to a fixed resistance gauge. In 1999, Jordan et al.[49] reported that maximum isometric strength from 100 volunteers was 20% to 25% greater in males during flexion and extension. A subsequent study by Vasavada et al.[50] of 11 males and 5 females revealed that maximum moments in females were actually lower at 40% to 50% of males. An anatomical study of gender differences in neck muscle size and position using upright magnetic resonance imaging (MRI) identified significantly smaller muscle areas in females and muscles positioned closer to the cervical spine, which may explain the moment-generating differences.[51] These studies have clearly identified significantly greater moment-generating capacity in males. Coupled with approximately equal head size (only 3%–6% greater in males), these findings indicate a much greater ability of the neck muscles in males to stabilize the head–neck complex under inertial loading scenarios. Greater dynamic stability of the head–neck complex would decrease spinal motions and the associated likelihood of injury.

Gender differences in muscle geometry have also been identified in trunk muscles. These muscles are important for maintaining body posture due to the limited intrinsic stability of the spine. Investigations of trunk muscle geometry have focused on anatomical

cross-sectional areas and moment arms as measured in axial MRI scans. Greater cross-sectional areas are associated with increased contractile forces. As stated previously, greater moment arms are associated with greater moment-generating capacities. Two studies using 92 patients with lower back pain and 30 normal volunteers reported significantly greater cross-sectional areas of the trunk muscles in males.[52,53] Gender differences in trunk muscle areas exceeded those predicted by body mass extrapolations,[52] indicating that the decrease in trunk muscle size for females was greater than body mass scaling would have predicted. Another study by Jorgensen et al.[54] reported significant gender differences in moment arms from the coronal and sagittal planes. Their study reported that males exhibited significantly larger moments for a majority of muscles and at a majority of spinal levels. Male muscle moment arms were approximately 14% greater in the coronal plane and 18% greater in the sagittal plane. Together, these studies have clearly demonstrated significant gender differences in skeletal muscles associated with the cervical, thoracic, and lumbar spines. Relative to body size, smaller muscles in females indicate a decreased ability to stabilize the trunk or head–neck complex, which may directly or indirectly lead to an increased risk of injury during dynamic loading.

Range-of-motion assessment forms a basic component for the clinical evaluation of the cervical spine and has been used to diagnose disability.[55–58] A number of studies have investigated the cervical spine range of motion under different bending modes using human volunteers and incorporating either active or passive muscle activation protocols. Active range of motion involves the patient moving their head in flexion–extension, lateral bending, and axial rotation to a self-determined maximum level, whereas a motion analyzer or cervical range-of-motion device is used to measure the gross head movements. Passive range-of-motion testing involves using a device to induce pure moments of the head and measuring the force/resistance in addition to the head movements.

Large-scale studies investigating active range of motion for 58 to 337 volunteers aged between 11 and 97 years have reported mixed results regarding gender differences in the maximum range of motion.[59–64] Three studies reported no significant gender differences for flexion–extension, lateral bending, or axial rotation.[61,62,64] However, the largest study of 337 volunteers found significant gender differences for extension, lateral bending, and axial rotation.[59] Two other studies reported similar results for extension,[60,63] axial rotation,[63] and coupled lateral bending during axial rotation.[63] In all cases, females had greater cervical spine ranges of motion than males. Studies incorporating a passive range-of-motion protocol have unanimously reported significant gender differences.[65–67] Specifically, in addition to reporting gender differences in total range of motion, passive motion studies have also reported greater flexibility of the female neck/cervical spine compared with males.

As discussed above, a majority of studies investigating cervical spine range of motion have focused on angular motions (e.g., flexion–extension, lateral bending, and axial rotation). However, studies investigating linear motion of the head–neck complex (e.g., protraction/retraction) have also reported gender differences. Contrary to angular measures, it was found that females have lower protraction/retraction range of motion than males.[68,69] Greater angular range of motion for extension and other bending modes indicates that female gender is a factor that should be accounted for by clinicians in the assessment of cervical spine pathology, trauma, and degeneration. However, decreased protraction/retraction motion in females has other biomechanical implications. Decreased anterior–posterior translation range of motion for females may lead to increased injury risk for dynamic scenarios incorporating that mode of loading, such as automotive rear impacts.[70]

In fact, an area of trauma research that has generated a large amount of gender-based research is in the study of cervical spine soft tissue injuries sustained during automotive rear impacts. These injuries are commonly referred to as "whiplash" injuries, with the clinical diagnosis as whiplash associated disorders (WADs). Epidemiological and clinical investigations have typically reported that females sustain a greater number of whiplash injuries than males.[71–75] Experimental studies designed to delineate an explanation for this gender bias have incorporated human volunteers and postmortem human subject (PMHS) specimens. Investigations subjecting human volunteers to subinjury accelerations in automotive seats have reported greater head-to-torso retraction motions[76] and greater head accelerations[77–79] in females. Although head motions are not directly related to the injury mechanism for WADs, these motions would imply more severe cervical spine segmental displacements that contribute to greater soft tissue distortions and an increased injury risk. Intact head–neck complexes have been studied experimentally to better understand the isolated cervical spine motions that lead to soft tissue distortions. Specifically, two experimental studies by Stemper et al.[80] reported significantly increased cervical spine segmental angulations and facet joint linear motions[81] in female PMHS specimens compared with males. Localized facet joint motions were significantly different from physiologic extension motions[82] and contribute to increased ligamentous distortions that increase the injury potential. A more recent study by that same group proposed gender-specific injury tolerance thresholds based on these findings.[70] These human volunteer- and PMHS-based studies have demonstrated differences in the dynamic biomechanics of the cervical spine between males and females that may contribute to greater injury risk in women. Explanations for these differing biomechanics likely include a combination of the structural, material, and neck muscle differences highlighted above.

13.1.3 Intrinsic Gender Differences in the Hip and Lower Extremities

The hip represents the articulation between the lateral pelvis and the proximal femur. This spherical joint allows flexion and extension in the sagittal plane, abduction and adduction in the coronal plane, and internal and external rotation in the transverse plane. To permit these motions, the proximal femur anatomy consists of the ball-like protrusion of the femoral head, which swivels and rotates within the acetabulum. The joint forces are transmitted primarily by direct compression between the acetabulum and the femoral head. These bone components are held in contact by overlying soft tissue of the joint capsule, which is composed, namely, of the iliofemoral, ischiofemoral, and the pubofemoral ligaments.

Gender differences in skeletal anatomy contribute to differences in the compressive mechanical loading of both the acetabulum and the femur. The pelvis represents the structure with the most notable gender difference in the skeletal anatomy. In females, the iliac wings are broader and shallower, and the pelvic outlet is considerably wider. These anatomical variations compared with the male pelvis enable females to complete childbirth.[83] However, a secondary result of the broader pelvis is an altered acetabular placement in females. Specifically, radiological assessment and anatomical dissection studies have noted that the acetabular locations in females are wider apart and located more anteriorly.[84–88] In these studies, the acetabulum was located at the center of a sphere approximated by the acetabular surface. One study analyzed computed tomography images and located each acetabulum with respect to the anterior pelvic plane, that is, the plane defined by each anterior–superior iliac spine and the pubic symphysis. In females, the acetabulum locations were found to be significantly more anterior compared with males. This placement

of the hip joint is of interest particularly for knee orthopaedics considerations, as discussed later in this chapter.[87] In addition to the wider placement and anterior location with respect to the anterior pelvic plane, the female acetabulum orientation is angled more anteriorly. This angulation, that is, anteversion, is defined by the angle formed between the coronal plane and a line drawn between the anterior and posterior brims of the acetabulum (Figure 13.2). Quantified within the transverse plane, anteversion was significantly greater in females.[84,87] Yet, when imaged in the coronal plane, another radiographic study found that the female acetabulum contact area in the standing posture was significantly less compared with the male contact area.[89] This suggests that the female acetabulum may be subject to greater wear stresses due to higher contact pressures over a reduced area. In fact, that same study used subject body mass to estimate contact pressures within the hip joint. Accounting for subject-specific body mass, acetabular contact pressures were estimated to be an average of 20% greater in females compared with males. As a consequence, the female hip may be subjected to increased wear over a person's lifetime. This interpretation has not been corroborated by epidemiology; risk of overuse-related osteoarthritis was not significantly higher for females compared with males.[90]

In conjunction with acetabular differences, the wider female pelvis is also associated with anatomical differences in the proximal femur. Because of their smaller stature, females generally possess smaller femurs than males. In particular, the femoral head, cantilevered on the medial aspect of the proximal femur by the femoral neck, is on average 5 mm smaller in females.[84,88] This smaller head is attached to the shorter and thinner femoral neck, which is angled anteriorly, that is, with greater anteversion. The magnitude of anteversion of the femoral neck was quantified to be 25.2 ± 9.8° in females and 20.3 ± 9.9° in males.[88] The cross-sectional area of the femoral neck is also reduced in females.[91] Therefore, estimated stress in the femoral neck during

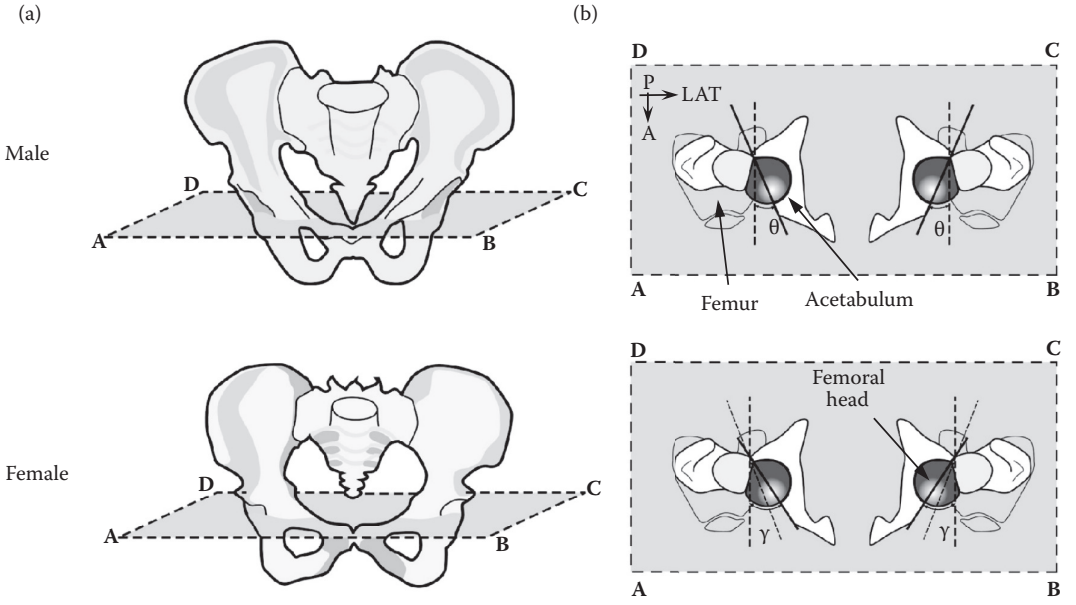

FIGURE 13.2
(a) Frontal and (b) cross-sectional views of the male and female pelvis. In females, the acetabulum is oriented with greater anteversion (angle γ) compared with males (angle θ).

normal ambulation was also higher in females than in males, even after accounting for a reduced female body mass.

These gender-specific anatomical variations such as femoral neck anteversion and head diameter are particularly relevant when surgical orthopaedics interventions are under consideration for degenerative joint diseases such as osteoarthritis. For example, normal joint alignment must be restored during total joint arthroplasty, and a femoral neck anteversion angle appropriate for males would be inappropriate for females. Because the hip axially loads the femur at the femoral head, femoral neck orientation is also an important parameter for biomechanical tolerances at the joint. Therefore, the femur is often characterized both by the load-bearing "mechanical axis," that is, the line defined by the center of the femoral head to the center of the distal femur, and by the noncoincident "anatomical axis" along the femoral diaphysis.[92] These axes play an important role during biomechanical experiments to define tolerance as well as clinical reference lines for reconstruction. Specifically, the noncoincident anatomical axis induces bending moments within the femoral diaphysis even when compressive loads are directed along the mechanical axis.[93,94] For joint reconstruction, both axes must be considered when anatomical joint lines are established by the surgeon.

The knee also exhibits gender-dependent characteristics and represents the articulation between the distal femur and the proximal tibia. Because its primary anatomical movement is flexion and extension in the sagittal plane, this joint is considered a hinge. Although the terminology implies a pinned rotation within the joint, both rotation and sliding between the surfaces represent normal motions. Compressive forces are transmitted between the two bone segments, that is, the femur and the tibia, through three subjoints: the medial tibiofemoral articulation (the half of the knee on the inside of the leg), the lateral tibiofemoral articulation (the half of the knee on the outside of the leg), and the patellofemoral articulation (between the femur and the patella). The medial and lateral tibiofemoral components form the weight-bearing structures, which transmit forces axially by means of intermediary cartilages known as menisci; the patellofemoral articulation redirects tension generated by the quadriceps muscle group in the thigh around the anterior of the knee through the quadriceps tendon to the proximal tibia. These joints are held in contact by four primary knee ligaments: (1) the medial collateral ligament, (2) the lateral collateral ligament, (3) the anterior cruciate ligament (ACL), and (4) the posterior cruciate ligament.

As with the hip joint, gender-based anatomical differences between female and male anatomy can alter knee biomechanics. Because the female pelvis is wider, the female femur approaches the knee from locations more lateral with respect to the midsagittal plane. Consequently, the axis of rotation of the female knee is typically oriented more valgus, or angled inward, than the axis of the male knee.[92,95] For example, a series of 120 normal subjects were radiographed from the frontal view to quantify biomechanical alignment in the stance posture. Significant differences were found between genders for the knee axis, defined by the angle between the articular surfaces of the knee and the horizontal; the female axis was 0.4 ± 1.3° (valgus), whereas the male axis was –1.0 ± 1.4° (varus) (Figure 13.3).[95] In addition to having a valgus orientation for the joint, the force produced by the quadriceps through the patella was directed more laterally in females than in males. This was quantified as the angle between the femoral mechanical axis and the line defined between the center of the tibial plateau and the center of the patella. Using planar radiography during subject stance, this angle measured 10.4 ± 5.1° in females but was 6.1 ± 5.6° in males.[95] A more recent study using biplanar fluoroscopy reported similar results: 10.0° versus 4.5° for females and males, respectively.[96]

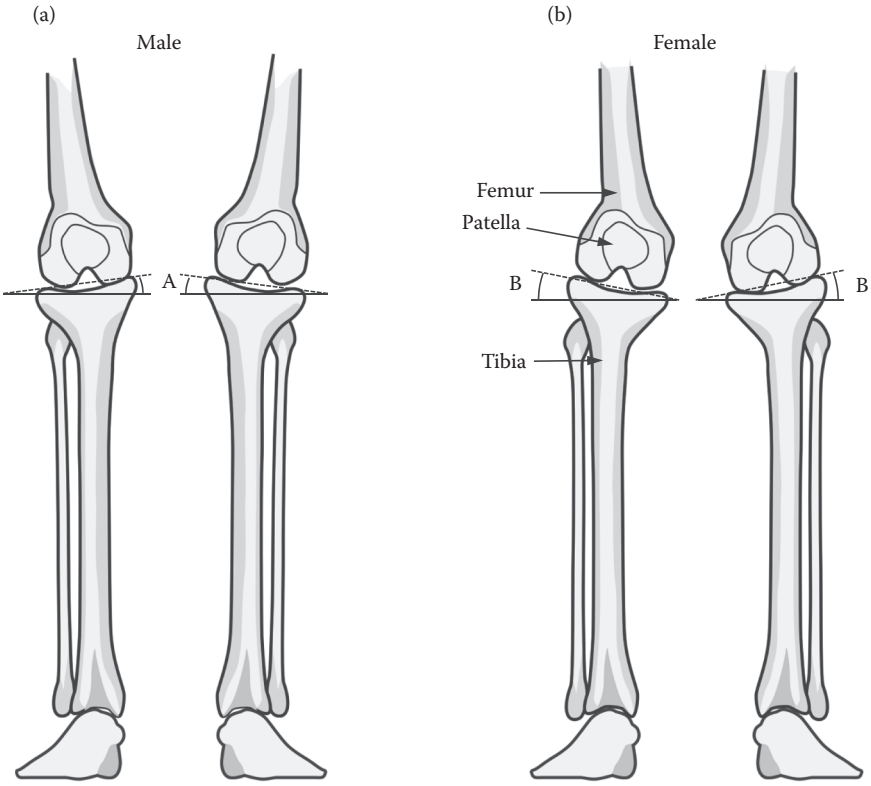

FIGURE 13.3
Frontal view of the knee axis angle in males (a) and females (b). Angles are exaggerated to demonstrate the outward male knee axis angle (A) compared with the inward female knee axis angle (B).

13.1.4 Extrinsic Gender Differences in the Hip and Lower Extremities

The previous section demonstrated that the bony anatomy of the lower extremities predisposes males and females to variations in biomechanical loading scenarios that require unique considerations. As with the vertebral column, there are also extrinsic gender-specific characteristics relating to hip and knee function that also must be considered. Because the primary function of the lower extremities is ambulation, the next section addresses these extrinsic factors with an emphasis on lower extremity function. When warranted, biomechanical tolerance factors are also addressed.

Gender differences in acetabulum orientation at the hip may play a role in pelvic fracture risk. As discussed, the female acetabulum is oriented with greater anteversion, that is, anterior rotation. Because the acetabulum orientation is not associated with any change to the acetabular wall thickness between genders,[84,87] this orientation may have an effect on the acetabular fracture risk for females compared with males in traumatic axial loading of the femur in a seated posture, such as that which occurs during motor vehicle crashes. For example, in a frontal impact automotive crash, the occupant translates forward until restraints resist this motion. Often, this restraint loading includes knee contact with the knee bolster beneath the instrument panel in the car. The impact force from knee bolster contact is axially transmitted by the femur, and, therefore, the femoral head loads the posterior acetabular wall. Biomechanical experiments have demonstrated that this

loading mechanism produces acetabular fractures with peak loads ranging from 4.4 to 8.1 kN.[93,94] Because the female acetabulum is more exposed to this loading through acetabular orientation without associated thickening of the acetabular wall, fracture risk may be greater for that population.[84] Yet, insufficient data exist currently to provide a quantitative comparison.

Gender differences in the lower extremities have also been noted through investigations of passive and active joint tissue responses. Such studies have used both isolated human tissue as well as living volunteer subjects. For example, a volunteer study incorporating 24 collegiate athletes examined the passive (ligamentous) and active (tensed musculature) laxity of the knee at 30° and 60° of flexion.[97] Laxity was quantified as the amount of internal rotation during an 80 N dynamic load applied medially at the forefoot; limb reaction force was also measured. During passive and active muscle states, forced rotations were 16% and 27% greater, respectively, in females. This indicated that the passive ligamentous joint provides less restraint, and that the active stabilizing musculature is weaker in females compared with males. This difference was reported to be even greater during external rotation of the ankle.[98] Knee laxity may be directly related to the mechanical properties of knee ligaments. Twenty unpaired isolated cadaveric ACLs were loaded dynamically at 100% per second until failure, and statistical models were developed for stress, strain, and strain energy density at failure as well as the modulus of elasticity.[99] In an attempt to account for as many confounding parameters as possible, covariates of gender, age, body mass, height, body mass index, ligament length, ligament volume, and minimum cross-sectional area were considered. Based on multivariate linear regression models, ligament properties of stress, strain, and strain energy density were significantly dependent on gender; the modulus of elasticity was not significantly dependent on gender.

In addition to single-cycle loads, volunteer experiments have suggested that the female knee ligaments may be more vulnerable to repeated loading. Specifically, mild cyclic loading (150 N) of the ACL was performed on male and female volunteers.[100] Anterior displacement of the tibia, used as a measure of ACL stretch, was measured before and after 10 min of loading at 0.1 Hz with the knee oriented at 35° and 90° of flexion. Tibial displacement increased by more than 20% after cyclic loading in females and was significantly greater than in males. Muscle reflex guarding of the knee was also shown to be less responsive in females compared with males. At 0° (no flexion), the knees of 24 volunteers were subjected to sudden ligament distractions in both the varus and valgus directions using a 7° ramp-and-hold loading function.[101] Muscle reflex response was observed using surface electromyography (EMG) for males and females. Females demonstrated reduced reflex intensity (e.g., EMG magnitude) compared with males, suggesting reduced stretch-induced muscle guarding of the knee joint in females.

The previously described *in vivo* and *ex vivo* quantitative mechanical studies may explain the increased knee valgus and internal rotation demonstrated by females compared with males in athletics-related tasks. Those differences were highlighted by a study wherein females and males performed a 60 cm vertical drop task.[102] The motions of the volunteer subjects were tracked using retroreflective targets and recorded using three-dimensional (3D) motion capture. Comparing lower limb landing kinematics, females were found to land in a more erect posture compared with males, with 22.8 ± 8.0° of knee flexion compared with 30.0 ± 7.7° at foot contact. This limb orientation was suggested to result from weaker muscle groups in females and may place greater demands on the stabilizing ligaments of the knee.[103] Other studies using vertical drop and vertical jump tasks have found significantly greater knee valgus in females than in males.[104–109] For example, motion capture was performed while male and female volunteers performed vertical drop and step-down

tasks.[106] Comparing both tasks, females demonstrated significantly greater knee valgus than males. In that study, the average female knee valgus during the vertical drop was 6°, whereas the average male valgus during the step-down task was –1.2° (varus). In similar tasks, females also demonstrated greater knee internal rotation. Recorded during a single limb vertical drop task using 3D motion capture, knee kinematics were quantified in male (n = 18) and female (n = 19) athletes.[110] Females demonstrated significantly greater internal rotation during landing compared with males: 12.6 ± 1.2° versus 9.4 ± 0.9°.

Quantitatively, these studies have demonstrated the extrinsic gender differences at the hip and knee. Compared with male anatomical characteristics, female pelvis and lower extremities are characterized by increased acetabular exposure to femur loading while seated, increased passive and active joint laxity of the knee in abduction–adduction and internal–external rotation loads, and increased knee valgus in active ambulatory tasks. The extrinsic gender differences demonstrated by these studies and others may guide the clinician with decisions of diagnosis and treatment for orthopaedics pathologies of the hip and knee.

13.2 Biomechanical Effect of Aging and Degeneration

Aging refers to progressive changes within the tissues of the body that are associated with the passage of time. Spinal degeneration describes the deterioration of biological tissues that occurs with aging due to repeated loading. However, aging and degeneration are not synonymous because degeneration is a mechanical and chemical process that is not dependent exclusively on the passage of time. The rate of degeneration within specific tissues is a function of loading history, genetics, and a number of other factors. Degeneration of the spine and other tissues has many health and biomechanical effects. A considerable body of clinical and experimental literature exists on different degenerative conditions affecting a majority of tissues within the human body. Rather than summarize the entire body of literature, this section will highlight some of the biomechanical changes associated with degeneration from the tissue level to the body segment level.

13.2.1 Aging and Degeneration Differences in the Spine

The biomechanical effects of aging and degeneration on spinal tissues have been investigated on the tissue, segmental, and spinal levels. From an isolated tissue standpoint, the mechanical response of spinal ligaments has been quantified for different age groups. Because ligaments provide resistance only under tension, experimentation has focused on defining the tensile response of isolated ligaments and on the ligamentum flavum, anterior and posterior longitudinal ligaments, and the supraspinous and interspinous ligaments in the cervical and lumbar spinal regions. For the intact ligamentum flava, Nachemson and Evans[111] demonstrated that the resting stress decreased approximately linearly with age. Resting stress was defined as the latent ligamentous stress remaining after separation of the vertebral arches from the bodies, which decreased by approximately 50% between 20 and 65 years of age. That study also reported that stress at rupture and modulus of elasticity, a measure of normalized stiffness, decreased approximately linearly with age. Rupture stress and modulus of elasticity decreased more rapidly, maintaining only 50% of their values from 20 years of age at 50 and 55 years, respectively. A later study by Chazal et al.[112] reported similar findings for the posterior longitudinal ligament, wherein the mean stress

was 25% lower for the 70- to 80-year age group compared with the overall sample (50–80 years old). Another study corroborated those findings by demonstrating a significant negative correlation between mechanical properties of the lumbar anterior longitudinal ligament and specimen age.[113] That study also reported a significant positive correlation between anterior longitudinal ligament mechanical properties and vertebral bone density, although it remains to be proven whether the relationship was causative or simply associated with the two concurrent degenerative processes. These findings clearly demonstrate that ligament mechanical properties deteriorate with age. The types of mechanical changes outlined here would create greater segmental laxity due to a lower elastic modulus and greater injury potential owing to a decreased rupture stress with age.

The degenerative process of the intervertebral discs has been well documented in the literature due to the likely association with altered lumbar spine mechanics and lower back pain. Clinical studies of disc degeneration have documented tears and fissures of the annulus fibrosus, nucleus dehydration and herniation, and loss of disc height and related those signs to clinical symptoms in patients.[114–123] Although the primary loading mode for the lumbar spine is compression due to its support of the body weight, the annular fibers experience tension due to Pascal's Law, which indicates that pressure applied to a confined incompressible fluid is distributed equally in all directions. As such, the tensile properties of the annulus fibrosus have been experimentally investigated. Studies have typically demonstrated a deterioration of physiologic and ultimate properties of the annulus of the disc with aging. For example, Galante[124] reported decreasing elongation and energy dissipation at tensile failure for annulus samples obtained from older specimens. Likewise, Acaroglu et al.[125] reported decreased ultimate stress and strain energy density in aged compared with nondegenerated discs. A more recent study reported stronger correlations between annulus tensile properties and intervertebral disc degeneration grade than with age.[126] This finding highlights the fact that deterioration in the spinal mechanical response is more dependent on the degeneration of its components rather than the passage of time. In addition to tensile loading of the annulus fibrosus, it sustains compressive loads during bending. Umehara et al.[127] experimentally demonstrated an increasing compressive modulus with degeneration in lumbar intervertebral discs, with greater regional irregularity than for normal specimens. These findings demonstrate a decrease in the mechanical properties of the intervertebral disc with degeneration.

Effects of degeneration on isolated spinal tissues, as highlighted in the previous paragraphs, contribute to changes on a segmental level. In general, the bending response of lumbar spine motion segments has demonstrated degeneration grade–dependent changes. Nachemson et al.[128] and Mimura et al.[129] have reported decreasing range of motion (i.e., decreased flexibility) in flexion–extension and lateral bending for grossly degenerated specimens. Similarly, Fujiwara et al.[130] reported decreasing range of motion in flexion–extension, lateral bending, and axial rotation for specimens with the highest levels of disc degeneration. Interestingly, their study identified increasing segmental flexibility with degeneration up to the penultimate level of degeneration before the decrease in flexibility for the highest level of degeneration for flexion–extension and axial rotation.

In addition to degeneration of the intervertebral disc, facet joints could sustain osteoarthritic changes including subchondral sclerosis, cartilage degeneration, and osteophyte formation. Fujiwara et al.[130] also investigated the mechanical effects of facet joint degeneration. Decreasing motion segment flexibility was reported for increasing levels of subchondral sclerosis under all loading modalities. Likewise, decreasing motion segment flexibility was reported with increasing levels of cartilage degeneration and osteophyte formation for all loading modes except axial rotation and extension (due to cartilage degeneration) or axial

rotation alone (due to osteophyte formation). That study was the first to identify the differing biomechanical effects of intervertebral disc and facet joint degeneration in the lumbar spine. Findings on the mechanical effects of disc degeneration agree with the three stages of spinal degeneration: dysfunction, instability, and stabilization,[131] whereas mechanical effects of facet joint degeneration demonstrated a progressive restriction to segmental motion.

The biomechanical effects of degeneration have also been quantified in the cervical spine. However, those studies have demonstrated considerably less consistency with regard to the biomechanical effects of degeneration than in the lumbar spine. For example, Lysell[132] and Moroney et al.[133] reported no remarkable differences in the response of the cervical spine for degenerated segments. However, Ball and Meijers[134] reported that disc narrowing and osteophyte formation resulted in reduced angular mobility. Likewise, in an experimental study incorporating younger cervical spines, coupled with a comparative literature review, Board et al.[135] reported that younger spines demonstrated greater segmental ranges of motion at all loading levels compared with older spines from previously reported studies. Decreased mobility in degenerated spines as reported in those studies[132,133] mirrors the experimental findings for the most severely degenerated lumbar spine specimens. However, the lack of consistency among the studies highlights a need for continued and more in-depth investigations of the effects of spinal degeneration on cervical spine biomechanics.

The effect of aging on active cervical spine range of motion has been investigated in a number of studies, with almost unanimous consensus in the literature that older volunteers have decreased ranges of motion in flexion–extension, lateral bending, and axial rotation.[59,61–65,136–139] Malmstrom et al.[63] reported that the range of motion in extension decreased by 5.9% per decade. Similarly, Lansade et al.[64] demonstrated a decrease of approximately 7.0° per decade across all six primary motions. Although the primary motions exhibited significant decreases, coupled spinal motions generally did not change with aging. Malmstrom et al.[63] reported that coupled lateral bending during axial rotation changed direction from ipsilateral to contralateral for only the 70- to 79-year age group. No other age-specific differences in coupled motions were identified. Other studies reported no significant changes in coupled motions with age, although Trott et al.[61] identified considerably decreased coupling motion magnitude beyond the 20- to 29-year age group.

This section has highlighted experimental studies investigating biomechanical changes associated with the degeneration of spinal tissues. On the tissue level, degeneration was shown to decrease elastic modulus and rupture stress for spinal ligaments and annulus fibrosus. However, studies investigating the effects of degeneration on segmental mechanics have demonstrated conflicting results that may be attributed to increasing flexibility for mild and moderate levels of degeneration followed by decreased flexibility for severely degenerated segments. Therefore, continued biomechanical studies are required to outline the continuous process of degeneration.

13.2.2 Aging and Gender Differences in the Hip and Lower Extremities

The most common age-induced biomechanical considerations at the hip include increased risk of hip fracture and osteoarthritis. Although females do not experience an increased risk of osteoarthritis at the hip compared with males, there is an increased risk with increasing age.[85,90] On the other hand, hip fracture risk in elderly females is significantly higher than in age-matched males, a consequence of multiple interacting factors.[91,140,141] Hip fractures are characterized by a fracture of the proximal femur occurring at the femoral neck or within the trochanters.[142] Such fractures are generally associated with falls in which direct impact to the hip occurs.[143] Females at 50 years of age are estimated to have

a lifetime fragility fracture risk of 40%, a risk more than three times greater than that of males.[140] Biomechanically, this increased fracture risk is attributed to osteoporosis as well as gender-specific anatomical characteristics of the hip that have been presented earlier.[91,144,145] Osteoporosis, a loss of bone density and bone trabeculae, is a common contributory factor and is associated with advancing age.[91,146] With insufficient bone density, the force and energy tolerance of the joint to impact loading can be substantially reduced. For example, 17 cadaveric femurs were tested to failure to compare age effects on mechanical tolerance.[147] Specimens were grouped by age into younger and older groups with average ages of 33 and 74 years, respectively. In the medial–lateral direction, older specimens sustained half as much force to fracture (3.4 versus 7.2 kN) and absorbed only 31% of the energy (5.5 versus 18.0 J). Also, femur ultimate strength was correlated with bone mineral density ($r = 0.92$), a common diagnostic indicator for osteoporosis.[147] Another biomechanical study found that increased femoral anteversion may lead to decreased fracture strength.[148] Thirty-three femurs were oriented with femoral neck angles ranging from 0° to 30° and loaded until failure. Force at fracture averaged 4.1 ± 0.9, 3.8 ± 0.9, and 3.1 ± 0.9 kN for anteversion angles of 0°, 15°, and 30°, respectively. A decreasing trend in fracture load was observed with increasing angle, and force was reduced a statistically significant 24% with 30° of anteversion. Thus, the increased risk of hip fracture due to osteoporosis experienced by females may be augmented by the anteverted female femur anatomy.[88]

Clinically, degeneration-related knee injuries include both acute ligamentous trauma and progressive age-related osteoarthritis. A 13-year review of injuries in collegiate athletics in the United States found that between 6% and 22% of female athletes sustained noncontact ACL injuries annually between 1990 and 2002.[149] Compared with male athletes in identical sports, females were 2.5 to 5.8 times more likely to sustain a noncontact ACL injury. The relationship between injury risk and lower extremity biomechanics was prospectively assessed in an exclusively female population.[150] For that study, the lower limb kinematics of 205 female athletes was quantified prior to competition. Nine subjects sustained a confirmed ACL rupture during the study period. From 3D motion capture analysis, injured subjects demonstrated significantly greater valgus knee angles during a vertical drop task than did the uninjured subjects. A meta-analysis of epidemiological studies found that females older than 55 years are significantly more likely to suffer from osteoarthritis of the knee.[90] Furthermore, knee osteoarthritis was significantly more severe in females. Epidemiological studies have found that knee alignment, in particular, was associated with increased risk of knee osteoarthritis and the progression of degeneration.[151–153] For example, the influence of knee alignment was examined in a prospective osteoarthritis study.[151] Patients with mild knee arthritis (males = 57, females = 173) were reexamined after 18 months to assess disease progression. Valgus knee alignment (>2°) was associated with a nearly fivefold increase in risk of osteoarthritis progression in the lateral tibiofemoral joint and a decreased risk of progression in the medial tibiofemoral joint. Therefore, females are at greater risk of age-related and activity-related knee injuries and disorders.

13.3 Summary

This chapter has highlighted the biomechanical differences in the response of the human body based on gender and aging/degeneration. In both cases, significant differences were

identified in the intrinsic response of isolated tissues and components, as well as the gross extrinsic response of body segments. With regard to gender, anatomically based studies have identified a more slender cervical column, enhanced lumbar lordosis, smaller facet sizes, a broader and more shallow pelvis with a wider pelvic outlet, and more laterally oriented knee joints in females. Gender differences in clinically relevant anatomy of the cervical spine were also reported. Other studies have identified significant gender differences in spinal segment flexibility, overall head–neck flexibility, dynamic cervical spine kinematics, and neck/trunk muscle locations and moment-generating capacity. Many of these gender-based differences are more complex and are not based solely on anthropometric size differences alone, and may contribute to higher dynamic injury potential and rates of mechanically based disease in women. For example, differing injury rates between men and women have come to light in some loading scenarios, and it has long been accepted that women sustain higher rates of degenerative spondylolisthesis.

With regard to aging and degeneration, considerable research efforts have been expended toward understanding the process of degradation of orthopaedics tissues over time and due to repeated use/overuse. In the spine, material degeneration has been quantified for spinal ligaments and the annulus fibrosus component of the intervertebral disc, younger spinal segments are more flexible than older, degenerated spinal segments, and intervertebral disc and facet joint degeneration affect spinal segmental biomechanics differently. Although coupling motions do not change over time, cervical spine range of motion for flexion–extension, lateral bending, and axial rotation consistently and progressively decreases with age. In the hip and lower extremities, age-related changes include a higher potential for osteoarthritis-related hip fractures and osteoporosis-related long bone fractures. Additionally, differing knee anatomy in females leads to differing wear patterns and a higher risk of osteoarthritis in that population.

Although this brief review is by no means comprehensive, it does highlight the biomechanical effects of gender and aging/degeneration in the spine and lower extremities. Whereas aging and degeneration have been consistent and established areas of biomechanical research, it is clear that the effect of gender requires further investigation on the tissue, component, and system levels. Nonetheless, the studies identified in this chapter have highlighted the fundamental differences in biomechanics between men and women that cannot simply be explained by differences in body size.

Acknowledgments

This work was supported in part by the Office of Naval Research through Naval Air Warfare Center Aircraft Division Contract N00421-10-C-0049 and the Department of Veterans Affairs Medical Research.

References

1. White, A. A., and M. M. Panjabi. 1978. *Clinical Biomechanics of the Spine*. Philadelphia, PA: J.B. Lippincott & Co.

2. Francis, C. C. 1955. Dimensions of the cervical vertebrae. *The Anatomical Record* 122(4):603–609.
3. Katz, P. R., H. M. Reynolds, D. R. Foust et al. 1975. Mid-sagittal dimensions of cervical vertebral bodies. *American Journal of Physical Anthropology* 43(3):319–326.
4. Hukuda, S., and Y. Kojima. 2002. Sex discrepancy in the canal/body ratio of the cervical spine implicating the prevalence of cervical myelopathy in men. *Spine* 27(3):250–253.
5. Stemper, B. D., N. Yoganandan, F. A. Pintar et al. 2008. Anatomical gender differences in cervical vertebrae of size-matched volunteers. *Spine* 33(2):E44–49.
6. Stemper, B. D., J. J. Derosia, N. Yogananan et al. 2009. Gender dependent cervical spine anatomical differences in size-matched volunteers. *Biomedical Sciences Instrumentation* 45:149–154.
7. Vasavada, A. N., J. Danaraj, and G. P. Siegmund. 2008. Head and neck anthropometry, vertebral geometry and neck strength in height-matched men and women. *Journal of Biomechanics* 41(1):114–121.
8. Rao, R. D., S. V. Marawar, B. D. Stemper et al. 2008. Computerized tomographic morphometric analysis of subaxial cervical spine pedicles in young asymptomatic volunteers. *Journal of Bone and Joint Surgery. American Volume* 90(9):1914–1921.
9. Ebraheim, N. A., R. Xu, T. Knight et al. 1997. Morphometric evaluation of lower cervical pedicle and its projection. *Spine* 22(1):1–6.
10. Ludwig, S. C., J. M. Kowalski, C. C. Edwards, 2nd et al. 2000. Cervical pedicle screws: Comparative accuracy of two insertion techniques. *Spine* 25(20):2675–2681.
11. Abumi, K., Y. Shono, M. Ito et al. 2000. Complications of pedicle screw fixation in reconstructive surgery of the cervical spine. *Spine* 25(8):962–969.
12. Neo, M., T. Sakamoto, S. Fujibayashi et al. 2005. The clinical risk of vertebral artery injury from cervical pedicle screws inserted in degenerative vertebrae. *Spine* 30(24):2800–2805.
13. Stemper, B. D., S. V. Marawar, N. Yoganandan et al. 2008. Quantitative anatomy of subaxial cervical lateral mass: An analysis of safe screw lengths for Roy-Camille and Magerl techniques. *Spine* 33(8):893–897.
14. Levine, A. M., C. Mazel, and R. Roy-Camille. 1992. Management of fracture separations of the articular mass using posterior cervical plating. *Spine* 17(10 Suppl): S447–454.
15. Heller, J. G., D. H. Silcox, 3rd, and C. E. Sutterlin, 3rd. 1995. Complications of posterior cervical plating. *Spine* 20(22):2442–2448.
16. Graham, A. W., M. L. Swank, R. E. Kinard et al. 1996. Posterior cervical arthrodesis and stabilization with a lateral mass plate. Clinical and computed tomographic evaluation of lateral mass screw placement and associated complications. *Spine* 21(3):323–328; discussion 329.
17. Deen, H. G., E. W. Nottmeier, and R. Reimer. 2006. Early complications of posterior rod-screw fixation of the cervical and upper thoracic spine. *Neurosurgery* 59(5):1062–1067; discussion 1067–1068.
18. Malik, S. W., B. D. Stemper, U. Metkar et al. 2010. Location of the transverse foramen in the subaxial cervical spine in a young asymptomatic population. *Spine* 35(12):E514–519.
19. Farfan, H. F. 1978. The biomechanical advantage of lordosis and hip extension for upright activity. Man as compared with other anthropoids. *Spine* 3(4):336–342.
20. Farfan, H. F., R. M. Huberdeau, and H. I. Dubow. 1972. Lumbar intervertebral disc degeneration: The influence of geometrical features on the pattern of disc degeneration—a post mortem study. *Journal of Bone and Joint Surgery. American Volume* 54(3):492–510.
21. Fernand, R., and D. E. Fox. 1985. Evaluation of lumbar lordosis. A prospective and retrospective study. *Spine* 10(9):799–803.
22. Stagnara, P., J. C. De Mauroy, G. Dran et al. 1982. Reciprocal angulation of vertebral bodies in a sagittal plane: Approach to references for the evaluation of kyphosis and lordosis. *Spine* 7(4):335–342.
23. Bergenudd, H., B. Nilsson, A. Uden et al. 1989. Bone mineral content, gender, body posture, and build in relation to back pain in middle age. *Spine* 14(6):577–579.
24. Youdas, J. W., T. R. Garrett, S. Harmsen et al. 1996. Lumbar lordosis and pelvic inclination of asymptomatic adults. *Physical Therapy* 76(10):1066–1081.

25. Youdas, J. W., T. R. Garrett, K. S. Egan et al. 2000. Lumbar lordosis and pelvic inclination in adults with chronic low back pain. *Physical Therapy* 80(3):261–275.
26. Norton, B. J., S. A. Sahrmann, and F. L. Van Dillen. 2004. Differences in measurements of lumbar curvature related to gender and low back pain. *The Journal of Orthopaedic and Sports Physical Therapy* 34(9):524–534.
27. Janssen, M. M., X. Drevelle, L. Humbert et al. 2009. Differences in male and female spino-pelvic alignment in asymptomatic young adults: A three-dimensional analysis using upright low-dose digital biplanar X-rays. *Spine* 34(23):E826–832.
28. Whitcome, K. K., L. J. Shapiro, and D. E. Lieberman. 2007. Fetal load and the evolution of lumbar lordosis in bipedal hominins. *Nature* 450(7172):1075–1078.
29. Adams, M. A., and W. C. Hutton. 1983. The mechanical function of the lumbar apophyseal joints. *Spine* 8(3):327–330.
30. Masharawi, Y., B. Rothschild, K. Salame et al. 2005. Facet tropism and interfacet shape in the thoracolumbar vertebrae: Characterization and biomechanical interpretation. *Spine* 30(11):E281–292.
31. Macnab, I. 1950. Spondylolisthesis with an intact neural arch; the so-called pseudo-spondylolisthesis. *The Journal of Bone and Joint Surgery. British Volume* 32-B(3):325–333.
32. Rosenberg, N. J. 1975. Degenerative spondylolisthesis. Predisposing factors. *Journal of Bone and Joint Surgery. American Volume* 57(4):467–474.
33. Postacchini, F., and D. Perugia. 1991. Degenerative lumbar spondylolisthesis. Part I: Etiology, pathogenesis, pathomorphology, and clinical features. *Italian Journal of Orthopaedics and Traumatology* 17(2):165–173.
34. Matsunaga, S., K. Ijiri, and K. Hayashi. 2000. Nonsurgically managed patients with degenerative spondylolisthesis: A 10- to 18-year follow-up study. *Journal of Neurosurgery* 93(2 Suppl):194–198.
35. Mosekilde, L. 1990. Sex differences in age-related changes in vertebral body size, density and biomechanical competence in normal individuals. *Bone* 11(2):67–73.
36. Nightingale, R. W., V. Carol Chancey, D. Ottaviano et al. 2007. Flexion and extension structural properties and strengths for male cervical spine segments. *Journal of Biomechanics* 40(3):535–542.
37. Brown, M. D., D. C. Holmes, A. D. Heiner et al. 2002. Intraoperative measurement of lumbar spine motion segment stiffness. *Spine* 27(9):954–958.
38. Stemper, B. D., D. Board, N. Yoganandan et al. 2010. Biomechanical properties of human thoracic spine disc segments. *Journal of Craniovertebral Junction and Spine* 1(1):18–22.
39. Tilley, A. R. 2002. *The Measure of Man and Woman*. New York, John Wiley & Sons.
40. Osakabe, T., M. Hayashi, K. Hasegawa et al. 2001. Age- and gender-related changes in ligament components. *Annals of Clinical Biochemistry* 38(Pt 5):527–532.
41. Sturzenegger, M., G. DiStefano, B. P. Radanov et al. 1994. Presenting symptoms and signs after whiplash injury: The influence of accident mechanisms. *Neurology* 44(4):688–693.
42. Ono, K., and M. Kanno. 1996. Influences of the physical parameters on the risk to neck injuries in low impact speed rear-end collisions. *Accident; Analysis and Prevention* 28(4):493–499.
43. Siegmund, G. P., D. J. Sanderson, B. S. Myers et al. 2003. Awareness affects the response of human subjects exposed to a single whiplash-like perturbation. *Spine* 28(7):671–679.
44. Hendriks, E. J., G. G. Scholten-Peeters, D. A. van der Windt et al. 2005. Prognostic factors for poor recovery in acute whiplash patients. *Pain* 114(3):408–416.
45. Stemper, B. D., N. Yoganandan, J. F. Cusick et al. 2006. Stabilizing effect of precontracted neck musculature in whiplash. *Spine* 31(20):E733–738.
46. Moroney, S. P., A. B. Schultz, and J. A. Miller. 1988. Analysis and measurement of neck loads. *Journal of Orthopaedic Research* 6(5):713–720.
47. Leggett, S. H., J. E. Graves, M. L. Pollock et al. 1991. Quantitative assessment and training of isometric cervical extension strength. *The American Journal of Sports Medicine* 19(6):653–659.
48. Mayoux-Benhamou, M. A., and M. Revel. 1993. Influence of head position on dorsal neck muscle efficiency. *Electromyography and Clinical Neurophysiology* 33(3):161–166.
49. Jordan, A., J. Mehlsen, P. M. Bulow et al. 1999. Maximal isometric strength of the cervical musculature in 100 healthy volunteers. *Spine* 24(13):1343–1348.

50. Vasavada, A. N., S. Li, and S. L. Delp. 2001. Three-dimensional isometric strength of neck muscles in humans. *Spine* 26(17):1904–1909.
51. Stemper, B. D., N. Yoganandan, J. L. Baisden et al. 2008. Biomechanical Implications of Gender-Dependent Muscle Locations. *2008 ASME Summer Bioengineering Conference. Marco Island, FL*: SBC2008-192339.
52. Cooper, R. G., S. Hollis, and M. I. V. Jayson. 1992. Gender variation of human spinal and paraspinal structures. *Clinical Biomechanics (Bristol, Avon)* 7:120–124.
53. Marras, W. S., M. J. Jorgensen, K. P. Granata et al. 2001. Female and male trunk geometry: Size and prediction of the spine loading trunk muscles derived from MRI. *Clinical Biomechanics (Bristol, Avon)* 16(1):38–46.
54. Jorgensen, M. J., W. S. Marras, K. P. Granata et al. 2001. MRI-derived moment-arms of the female and male spine loading muscles. *Clinical Biomechanics (Bristol, Avon)* 16(3):182–193.
55. Mealy, K., H. Brennan, and G. C. Fenelon. 1986. Early mobilization of acute whiplash injuries. *British Medical Journal (Clinical Research Ed.)* 292(6521):656–657.
56. Hildingsson, C., and G. Toolanen. 1990. Outcome after soft-tissue injury of the cervical spine. A prospective study of 93 car-accident victims. *Acta Orthopaedica Scandinavica* 61(4):357–359.
57. Borchgrevink, G. E., A. Kaasa, D. McDonagh et al. 1998. Acute treatment of whiplash neck sprain injuries. A randomized trial of treatment during the first 14 days after a car accident. *Spine* 23(1):25–31.
58. Dall'Alba, P. T., M. M. Sterling, J. M. Treleaven et al. 2001. Cervical range of motion discriminates between asymptomatic persons and those with whiplash. *Spine* 26(19):2090–2094.
59. Youdas, J. W., T. R. Garrett, V. J. Suman et al. 1992. Normal range of motion of the cervical spine: An initial goniometric study. *Physical Therapy* 72(11):770–780.
60. Mayer, T., S. Brady, E. Bovasso et al. 1993. Noninvasive measurement of cervical tri-planar motion in normal subjects. *Spine* 18(15):2191–2195.
61. Trott, P. H., M. J. Pearcy, S. A. Ruston et al. 1996. Three-dimensional analysis of active cervical motion: The effect of age and gender. *Clinical Biomechanics (Bristol, Avon)* 11(4):201–206.
62. Castro, W. H., A. Sautmann, M. Schilgen et al. 2000. Noninvasive three-dimensional analysis of cervical spine motion in normal subjects in relation to age and sex. An experimental examination. *Spine* 25(4):443–449.
63. Malmstrom, E. M., M. Karlberg, P. A. Fransson et al. 2006. Primary and coupled cervical movements: The effect of age, gender, and body mass index. A 3-dimensional movement analysis of a population without symptoms of neck disorders. *Spine* 31(2):E44–50.
64. Lansade, C., S. Laporte, P. Thoreux et al. 2009. Three-dimensional analysis of the cervical spine kinematics: Effect of age and gender in healthy subjects. *Spine* 34(26):2900–2906.
65. Dvorak, J., J. A. Antinnes, M. Panjabi et al. 1992. Age and gender related normal motion of the cervical spine. *Spine* 17(10 Suppl):S393-398.
66. McGill, S., J. Seguin, and G. Bennett. 1994. Passive stiffness of the lumbar torso in flexion, extension, lateral bending, and axial rotation. Effect of belt wearing and breath holding. *Spine* 19(6):696–704.
67. McClure, P., S. Siegler, and R. Nobilini. 1998. Three-dimensional flexibility characteristics of the human cervical spine in vivo. *Spine* 23(2):216–223.
68. Hanten, W. P., R. M. Lucio, J. L. Russell et al. 1991. Assessment of total head excursion and resting head posture. *Archives of Physical Medicine and Rehabilitation* 72(11):877–880.
69. Hanten, W. P., S. L. Olson, J. L. Russell et al. 2000. Total head excursion and resting head posture: Normal and patient comparisons. *Archives of Physical Medicine and Rehabilitation* 81(1):62–66.
70. Stemper, B. D., N. Yoganandan, F. A. Pintar et al. 2011. The relationship between lower neck shear force and facet joint kinematics during automotive rear impacts. *Clinical Anatomy* 24(3):319–326.
71. Spitzer, W. O., M. L. Skovron, L. R. Salmi et al. 1995. Scientific monograph of the Quebec Task Force on Whiplash-Associated Disorders: Redefining "whiplash" and its management. *Spine* 20(8 Suppl):1S-73S.

72. Chapline, J. F., S. A. Ferguson, R. P. Lillis et al. 2000. Neck pain and head restraint position relative to the driver's head in rear-end collisions. *Accident; Analysis and Prevention* 32(2):287–297.
73. Krafft, M., A. Kullgren, A. Lie et al. 2003. The risk of whiplash injury in the rear seat compared to the front seat in rear impacts. *Traffic Injury Prevention* 4(2):136–140.
74. Jakobsson, L., H. Norin, and M. Y. Svensson. 2004. Parameters influencing AIS 1 neck injury outcome in frontal impacts. *Traffic Injury Prevention* 5(2):156–163.
75. Storvik, S. G., B. D. Stemper, N. Yoganandan et al. 2009. Population-based estimates of whiplash injury using NASS CDS data. *Biomedical Sciences Instrumentation* 45:244–249.
76. Siegmund, G. P., D. J. King, J. M. Lawrence et al. 1997. Head/Neck Kinematic Response of Human Subjects in Low-Speed Rear-End Collisions. *41st Stapp Car Crash Conference, Lake Buena Vista, FL*.
77. van den Kroonenberg, A., M. Philippens, H. Cappon et al. 1998. Human Head-Neck Response during Low-Speed Rear End Impacts. *42nd Stapp Car Crash Conference, Tempe, AZ*.
78. Dehner, C., M. Elbel, S. Schick et al. 2007. Risk of injury of the cervical spine in sled tests in female volunteers. *Clinical Biomechanics (Bristol, Avon)* 22(6):615–622.
79. Linder, A., A. Carlsson, M. Y. Svensson et al. 2008. Dynamic responses of female and male volunteers in rear impacts. *Traffic Injury Prevention* 9(6):592–599.
80. Stemper, B. D., N. Yoganandan, and F. A. Pintar. 2003. Gender dependent cervical spine segmental kinematics during whiplash. *Journal of Biomechanics* 36(9):1281–1289.
81. Stemper, B. D., N. Yoganandan, and F. A. Pintar. 2004. Gender- and region-dependent local facet joint kinematics in rear impact: Implications in whiplash injury. *Spine* 29(16):1764–1771.
82. Stemper, B. D., N. Yoganandan, T. A. Gennarelli et al. 2005. Localized cervical facet joint kinematics under physiological and whiplash loading. *Journal of Neurosurgery. Spine* 3(6):471–476.
83. Milne, N. 1990. Sexing of human hip bones. *Journal of Anatomy* 172:221–226.
84. Wang, S. C., C. Brede, D. Lange et al. 2004. Gender differences in hip anatomy: Possible implications for injury tolerance in frontal collisions. *Annual Proceedings. Association for the Advancement of Automotive Medicine* 48:287–301.
85. O'Connor, M. I. 2006. Osteoarthritis of the hip and knee: Sex and gender differences. *Orthopedic Clinics of North America* 37(4):559–568.
86. Traina, F., M. De Clerico, F. Biondi et al. 2009. Sex differences in hip morphology: Is stem modularity effective for total hip replacement? *Journal of Bone and Joint Surgery. American Volume* 91 Suppl 6:121–128.
87. Tohtz, S. W., D. Sassy, G. Matziolis et al. 2010. CT evaluation of native acetabular orientation and localization: Sex-specific data comparison on 336 hip joints. *Technology and Health Care* 18(2):129–136.
88. Nakahara, I., M. Takao, T. Sakai et al. 2011. Gender differences in 3D morphology and bony impingement of human hips. *Journal of Orthopaedic Research* 29(3):333–339.
89. Genda, E., N. Iwasaki, G. Li et al. 2001. Normal hip joint contact pressure distribution in single-leg standing—effect of gender and anatomic parameters. *Journal of Biomechanics* 34(7):895–905.
90. Srikanth, V. K., J. L. Fryer, G. Zhai et al. 2005. A meta-analysis of sex differences prevalence, incidence and severity of osteoarthritis. *Osteoarthritis Cartilage* 13(9):769–781.
91. Crabtree, N. J., H. Kroger, A. Martin et al. 2002. Improving risk assessment: Hip geometry, bone mineral distribution and bone strength in hip fracture cases and controls. The EPOS study. European Prospective Osteoporosis Study. *Osteoporosis International* 13(1):48–54.
92. Chao, E. Y., E. V. Neluheni, R. W. Hsu et al. 1994. Biomechanics of malalignment. *Orthopedic Clinics of North America* 25(3):379–386.
93. Yoganandan, N., F. A. Pintar, T. A. Gennarelli et al. 2001. Mechanisms and factors involved in hip injuries during frontal crashes. *Stapp Car Crash Journal* 45:437–448.
94. Rupp, J. D., M. P. Reed, T. A. Jeffreys et al. 2003. Effects of hip posture on the frontal impact tolerance of the human hip joint. *Stapp Car Crash Journal* 47:21–33.
95. Hsu, R. W., S. Himeno, M. B. Coventry et al. 1990. Normal axial alignment of the lower extremity and load-bearing distribution at the knee. *Clinical Orthopaedics and Related Research* (255):215–227.

96. Varadarajan, K. M., T. J. Gill, A. A. Freiberg et al. 2009. Gender differences in trochlear groove orientation and rotational kinematics of human knees. *Journal of Orthopaedic Research* 27(7):871–878.
97. Wojtys, E. M., L. J. Huston, H. J. Schock et al. 2003. Gender differences in muscular protection of the knee in torsion in size-matched athletes. *Journal of Bone and Joint Surgery. American Volume* 85-A(5):782–789.
98. Park, H. S., N. A. Wilson, and L. Q. Zhang. 2008. Gender differences in passive knee biomechanical properties in tibial rotation. *Journal of Orthopaedic Research* 26(7):937–944.
99. Chandrashekar, N., H. Mansouri, J. Slauterbeck et al. 2006. Sex-based differences in the tensile properties of the human anterior cruciate ligament. *Journal of Biomechanics* 39(16):2943–2950.
100. Sbriccoli, P., M. Solomonow, B. H. Zhou et al. 2005. Neuromuscular response to cyclic loading of the anterior cruciate ligament. *The American Journal of Sports Medicine* 33(4):543–551.
101. Cammarata, M. L., and Y. Y. Dhaher. 2010. Evidence of gender-specific motor templates to resist valgus loading at the knee. *Muscle Nerve* 41(5):614–623.
102. Decker, M. J., M. R. Torry, D. J. Wyland et al. 2003. Gender differences in lower extremity kinematics, kinetics and energy absorption during landing. *Clinical Biomechanics (Bristol, Avon)* 18(7):662–669.
103. Gehring, D., M. Melnyk, and A. Gollhofer. 2009. Gender and fatigue have influence on knee joint control strategies during landing. *Clinical Biomechanics (Bristol, Avon)* 24(1):82–87.
104. Ford, K. R., G. D. Myer, and T. E. Hewett. 2003. Valgus knee motion during landing in high school female and male basketball players. *Medicine and Science in Sports and Exercise* 35(10):1745–1750.
105. Kernozek, T. W., M. R. Torry, V. A. N. H. H et al. 2005. Gender differences in frontal and sagittal plane biomechanics during drop landings. *Medicine and Science in Sports and Exercise* 37(6):1003–1012; discussion 1013.
106. Earl, J. E., S. K. Monteiro, and K. R. Snyder. 2007. Differences in lower extremity kinematics between a bilateral drop-vertical jump and a single-leg step-down. *The Journal of Orthopaedic and Sports Physical Therapy* 37(5):245–252.
107. Hughes, G., J. Watkins, and N. Owen. 2008. Gender differences in lower limb frontal plane kinematics during landing. *Sports Biomechanics* 7(3):333–341.
108. Hughes, G., J. Watkins, and N. Owen. 2010. The effects of opposition and gender on knee kinematics and ground reaction force during landing from volleyball block jumps. *Research Quarterly for Exercise and Sport* 81(4):384–391.
109. Yamazaki, J., T. Muneta, Y. J. Ju et al. 2010. Differences in kinematics of single leg squatting between anterior cruciate ligament-injured patients and healthy controls. *Knee Surgery, Sports Traumatology, Arthroscopy* 18(1):56–63.
110. Nagano, Y., H. Ida, M. Akai et al. 2007. Gender differences in knee kinematics and muscle activity during single limb drop landing. *Knee* 14(3):218–223.
111. Nachemson, A. L., and J. H. Evans. 1968. Some mechanical properties of the third human lumbar interlaminar ligament (ligamentum flavum). *Journal of Biomechanics* 1(3):211–220.
112. Chazal, J., A. Tanguy, M. Bourges et al. 1985. Biomechanical properties of spinal ligaments and a histological study of the supraspinal ligament in traction. *Journal of Biomechanics* 18(3):167–176.
113. Neumann, P., T. Keller, L. Ekstrom et al. 1993. Structural properties of the anterior longitudinal ligament. Correlation with lumbar bone mineral content. *Spine* 18(5):637–645.
114. Coventry, M. B., R. K. Ghormley, and J. W. Kernohan. 1945. The intervertebral disc: Its microscopic anatomy and pathology. Part II. Changes in the intervertebral disc concomitant with age. *Journal of Bone and Joint Surgery. American Volume* 27:233–247.
115. Friberg, S., and C. Hirsch. 1949. Anatomical and clinical studies on lumbar disc degeneration. *Acta Orthopaedica Scandinavica* 19(2):222–242, illust.
116. Hirsch, C., and F. Schajowicz. 1953. Studies on structural changes in the lumbar annulus fibrosus. *Acta Orthopaedica Scandinavica* 22(3):184–231.
117. Walker, A. E. 1964. Anatomical factors related to pathogenesis of acute spine injuries. The neurosurgeon's viewpoint. *Journal of Bone and Joint Surgery. American Volume* 46:1806–1810.

118. Lawrence, J. S. 1969. Disc degeneration. Its frequency and relationship to symptoms. *Annals of the Rheumatic Diseases* 28(2):121–138.
119. Kirkaldy-Willis, W. H., J. H. Wedge, K. Yong-Hing et al. 1978. Pathology and pathogenesis of lumbar spondylosis and stenosis. *Spine* 3(4):319–328.
120. Frymoyer, J. W., A. Newberg, M. H. Pope et al. 1984. Spine radiographs in patients with low-back pain. An epidemiological study in men. *Journal of Bone and Joint Surgery. American Volume* 66(7):1048–1055.
121. Modic, M. T., W. Pavlicek, M. A. Weinstein et al. 1984. Magnetic resonance imaging of intervertebral disk disease. Clinical and pulse sequence considerations. *Radiology* 152(1):103–111.
122. Isherwood, I., D. J. Prendergast, D. S. Hickey et al. 1986. Quantitative analysis of intervertebral disc structure. *Acta Radiologica. Supplementum* 369:492–495.
123. Pearce, R. H., B. J. Grimmer, and M. E. Adams. 1987. Degeneration and the chemical composition of the human lumbar intervertebral disc. *Journal of Orthopaedic Research* 5(2):198–205.
124. Galante, J. O. 1967. Tensile properties of the human lumbar annulus fibrosus. *Acta Orthopaedica Scandinavica. Supplementum* 100:101–191.
125. Acaroglu, E. R., J. C. Iatridis, L. A. Setton et al. 1995. Degeneration and aging affect the tensile behavior of human lumbar anulus fibrosus. *Spine* 20(24):2690–2701.
126. Ebara, S., J. C. Iatridis, L. A. Setton et al. 1996. Tensile properties of nondegenerate human lumbar anulus fibrosus. *Spine* 21(4):452–461.
127. Umehara, S., S. Tadano, K. Abumi et al. 1996. Effects of degeneration on the elastic modulus distribution in the lumbar intervertebral disc. *Spine* 21(7):811–819; discussion 820.
128. Nachemson, A. L., A. B. Schultz, and M. H. Berkson. 1979. Mechanical properties of human lumbar spine motion segments. Influence of age, sex, disc level, and degeneration. *Spine* 4(1):1–8.
129. Mimura, M., M. M. Panjabi, T. R. Oxland et al. 1994. Disc degeneration affects the multidirectional flexibility of the lumbar spine. *Spine* 19(12):1371–1380.
130. Fujiwara, A., T. H. Lim, H. S. An et al. 2000. The effect of disc degeneration and facet joint osteoarthritis on the segmental flexibility of the lumbar spine. *Spine* 25(23):3036–3044.
131. Kirkaldy-Willis, W. H., and H. F. Farfan. 1982. Instability of the lumbar spine. *Clinical Orthopaedics and Related Research* (165):110–123.
132. Lysell, E. 1969. Motion in the cervical spine. An experimental study on autopsy specimens. *Acta Orthopaedica Scandinavica. Supplementum* 123:121+.
133. Moroney, S. P., A. B. Schultz, J. A. Miller et al. 1988. Load-displacement properties of lower cervical spine motion segments. *Journal of Biomechanics* 21(9):769–779.
134. Ball, J., and K. A. Meijers. 1964. On cervical mobility. *Annals of the Rheumatic Diseases* 23:429–438.
135. Board, D., B. D. Stemper, N. Yoganandan et al. 2006. Biomechanics of the aging spine. *Biomedical Sciences Instrumentation* 42:1–6.
136. Walmsley, R. P., P. Kimber, and E. Culham. 1996. The effect of initial head position on active cervical axial rotation range of motion in two age populations. *Spine* 21(21):2435–2442.
137. Feipel, V., B. Rondelet, J. Le Pallec et al. 1999. Normal global motion of the cervical spine: An electrogoniometric study. *Clinical Biomechanics (Bristol, Avon)* 14(7):462–470.
138. Sforza, C., G. Grassi, N. Fragnito et al. 2002. Three-dimensional analysis of active head and cervical spine range of motion: Effect of age in healthy male subjects. *Clinical Biomechanics (Bristol, Avon)* 17(8):611–614.
139. Demaille-Wlodyka, S., C. Chiquet, J. F. Lavaste et al. 2007. Cervical range of motion and cephalic kinesthesis: Ultrasonographic analysis by age and sex. *Spine* 32(8):E254–261.
140. Pietschmann, P., M. Rauner, W. Sipos et al. 2009. Osteoporosis: An age-related and gender-specific disease—a mini-review. *Gerontology* 55(1):3–12.
141. Ito, M., T. Nakata, A. Nishida et al. 2011. Age-related changes in bone density, geometry and biomechanical properties of the proximal femur: CT-based 3D hip structure analysis in normal postmenopausal women. *Bone* 48(3):627–630.
142. Im, G. I., and M. J. Lim. 2011. Proximal hip geometry and hip fracture risk assessment in a Korean population. *Osteoporosis International* 22(3):803–807.

143. Hayes, W. C., E. R. Myers, J. N. Morris et al. 1993. Impact near the hip dominates fracture risk in elderly nursing home residents who fall. *Calcified Tissue International* 52(3):192–198.
144. Brownbill, R. A., and J. Z. Ilich. 2003. Hip geometry and its role in fracture: What do we know so far? *Current Osteoporosis Reports* 1(1):25–31.
145. Silva, M. J. 2007. Biomechanics of osteoporotic fractures. *Injury* 38 Suppl 3: S69–76.
146. Keaveny, T. M., and O. C. Yeh. 2002. Architecture and trabecular bone—toward an improved understanding of the biomechanical effects of age, sex and osteoporosis. *Journal of Musculoskeletal & Neuronal Interactions* 2(3):205–208.
147. Courtney, A. C., E. F. Wachtel, E. R. Myers et al. 1995. Age-related reductions in the strength of the femur tested in a fall-loading configuration. *Journal of Bone and Joint Surgery. American Volume* 77(3):387–395.
148. Pinilla, T. P., K. C. Boardman, M. L. Bouxsein et al. 1996. Impact direction from a fall influences the failure load of the proximal femur as much as age-related bone loss. *Calcified Tissue International* 58(4):231–235.
149. Agel, J., E. A. Arendt, and B. Bershadsky. 2005. Anterior cruciate ligament injury in national collegiate athletic association basketball and soccer: A 13-year review. *The American Journal of Sports Medicine* 33(4):524–530.
150. Hewett, T. E., G. D. Myer, K. R. Ford et al. 2005. Biomechanical measures of neuromuscular control and valgus loading of the knee predict anterior cruciate ligament injury risk in female athletes: A prospective study. *The American Journal of Sports Medicine* 33(4):492–501.
151. Sharma, L., J. Song, D. T. Felson et al. 2001. The role of knee alignment in disease progression and functional decline in knee osteoarthritis. *JAMA* 286(2):188–195.
152. Sharma, L., F. Eckstein, J. Song et al. 2008. Relationship of meniscal damage, meniscal extrusion, malalignment, and joint laxity to subsequent cartilage loss in osteoarthritic knees. *Arthritis and Rheumatism* 58(6):1716–1726.
153. Moisio, K., A. Chang, F. Eckstein et al. 2011. Varus–valgus alignment: Reduced risk of subsequent cartilage loss in the less loaded compartment. *Arthritis and Rheumatism* 63(4):1002–1009.

14

Computational Approaches to Studying Normal and Pathological Mechanobiology of Whole Joints and Their Tissues

Reza Shirazi, Scott J. Hazelwood, Robert L. Sah, and Stephen M. Klisch

CONTENTS

14.1 Introduction

Practical difficulties and ethical considerations in experimental methods motivate the use of computational models as an indispensable complementary tool for the assessment of biological tissues and joints under both normal and pathological conditions. For example, in the knee joint, different components such as articular cartilage (AC), meniscus, bone, ligament, and muscle tissues provide distinct and complementary roles to facilitate a smooth transition of load between the thigh and the shank. Perturbation of any single component can disrupt the interactions between, and affect the functionality of, all component tissues. Accurate assessment of the biomechanical function of whole joints and the manner in which that function evolves during development and growth, degeneration, and surgical intervention is a challenging task due to complexities in tissue properties, geometry, and loading conditions.

To model the biomechanics of biological tissue and whole joints, boundary-value problems (BVPs) must be carefully specified before the development of solution strategies. The BVP statement typically includes the identification of a tissue material model (i.e., elastic, poroelastic, viscoelastic), the geometry of the structure (i.e., cylindrical discs tested *in vitro* or complex native joint geometries present *in vivo*), and equations that define boundary conditions on the external surfaces of the structure (i.e., applied displacements for confined compression stress relaxation experiments or applied time-dependent force distributions for intact joints). Before the development of computational approaches using computers, both exact and approximate analytical solutions were obtained that solve BVPs; for example, see Timoshenko and Goodier[1] for a rich catalogue of classic BVP solutions using linear elastic material models.

Computational solutions, often based on finite-element analysis (FEA), have a long history of being used to solve BVPs with classic engineering stress equations (i.e., linear isotropic elasticity) that become intractable by complex geometries and loading conditions. Examples of complex geometries include the AC geometries of intact joints.[2–5] Also, modeling complex heterogeneities or experimental loading conditions may lead to intractable BVPs even for standard geometries (i.e., cylindrical discs) and loading conditions (i.e., compression); examples include modeling AC with depth-dependent properties[6–10] or those subjected to dynamic compression.[11–13]

There are advantages and disadvantages for using computational approaches as opposed to experimental measurements when studying the biomechanics of tissues and joints. Computational modeling uses simplifying assumptions for material properties and boundary conditions, but can predict multiple variables such as force, displacement, strain, stress, volume/area changes, and contact pressure/area, some of which are difficult, currently, to measure experimentally. Experimental approaches, however, provide potentially more accurate results but offer less flexibility in the number of variables that can be measured simultaneously. Validated computational models can alternatively and more efficiently predict the relative importance of design parameters that govern tissue and joint behavior and, consequently, facilitate design changes in experimental and surgical approaches. To provide the best benefit, it is emphasized that computational models should be carefully validated, an objective that is normally accomplished by ensuring that predicted variables are within a range of experimental measurements. Variables used for validation often include displacements, strains, contact pressures, and forces; the variables chosen for validation depend on the study being conducted. As such, care should be taken

so that the predictions of computational models are used only in the range and type of tests for which they are validated.

In this chapter, we provide an overview of computational modeling, mostly through the use of FEA, of the tissues of diarthrodial joints and of whole joint models, both for normal and pathological conditions. In-depth overviews of several computational studies are provided for bone tissue and whole bones (with an emphasis on remodeling), AC (at both the explant and whole tissue levels), and the whole knee joint. In general, we discuss computational solutions for modeling tissue and joint biomechanics with emphasis on (1) normal versus abnormal function *in vivo*, (2) improving our understanding of structure–function relations that govern physiological and pathological biomechanical behavior, and (3) tissue growth and remodeling (G&R). Although the focus here is on bone and AC tissues, many of the computational approaches discussed have also been used for a variety of other tissues such as intervertebral disc, arterial, skin, and brain tissues.

14.2 Computational Approaches to Bone Remodeling

Bone remodeling is a dynamic cellular process regulated by the mechanical environment of bone and metabolic factors. Through the coordinated actions of cell teams collectively known as basic multicellular units (BMUs), resorption of bone by osteoclasts is followed by bone formation within the resorption cavity by osteoblasts. Resorption at a specific bone location takes approximately one month to complete, whereas formation follows over the next two to three months, resulting in temporary porosity during the process, which is known as "remodeling space." Through remodeling, the skeleton renews bone tissue, adapts to mechanical loads, and provides a supply of essential minerals. In addition, remodeling is the only mechanism able to remove fatigue damage in bone, preventing eventual failure under normal conditions.[14]

The concept of bone remodeling regulation by mechanical factors, popularized by the premises of Wolff, has been established by many experimental studies, although the specific mechanisms of the regulatory process are still not known. It is believed that bone contains mechanosensors (thought to be the osteocytes within the bone matrix) that regionally monitor the mechanical environment of bone. These sensors are thought to activate biological processes to increase or decrease active BMUs to maintain the mechanical environment within genetically predetermined limits.[15] Evidence of this phenomenon is supported by experiments demonstrating the response of bone under various states of mechanical loading. Bone tissue insufficiently loaded (commonly referred to as "disuse") is removed by bone remodeling,[16] possibly due to an increase in osteocyte apoptosis,[17] which may result from disuse-induced hypoxia.[18] Theories suggest that osteocytes may also directly sense and respond to fluid movement, or lack thereof, within the lacunar-canalicular network resulting from cyclic loads on bone. It has been hypothesized in these cases that osteocytes may be stimulated by streaming potentials (through ionic currents resulting from fluid movement)[19] or fluid shear stresses acting on the cell.[20] More recently, fluid flow across cilia extending from the osteocyte surface has been postulated as another possible mechanism for osteocytes to sense mechanical signals and regulate remodeling.[21] Fatigue microdamage from physiological and supraphysiological loading of bone also has been found experimentally to initiate remodeling,[22] possibly through osteocyte apoptosis resulting from microcrack formation in loaded bone.[23]

14.2.1 Computational Models of the Bone Remodeling Process

Mathematical models of bone remodeling are useful in synthesizing known information on the various biological processes associated with remodeling and developing or exploring hypotheses concerning mechanisms of the remodeling process. Several investigators have developed computational models that mimic the phenomenological processes associated with BMU-based bone remodeling. A few of these simulations are presented here. The model by Hart and Davy[24] related the rate of remodeling to the strain history of bone. Bone geometry and material properties were updated in their model in response to resorption or formation by BMUs, which allowed for the prediction of the bone structure over time as the model proceeded in an iterative fashion. Reeve[25] and Thomsen et al.[26] developed stochastic models from histomorphometric data to examine remodeling on trabecular surfaces and used their models to investigate possible mechanisms of bone loss or gain associated with osteoporosis and its treatment.

Mullender and Huiskes[27] incorporated mechanosensors into their computational remodeling algorithm by modeling the ability of osteocytes to sense the surrounding mechanical environment and then to signal osteoclasts and osteoblasts to alter bone mass accordingly. Trabecular architecture was predicted by their model in a small region of bone. More recently, signaling factors responsible for the coupling actions of osteoclasts and osteoblasts within BMUs have been incorporated into mathematical models of bone remodeling to investigate the effects of cytokines and growth factors on remodeling responses.[28–30]

14.2.2 Incorporating the Bone Remodeling Process with Finite-Element Analysis

Although the previously described mathematical models of the bone remodeling process may include simplified loading conditions on basic bone geometries, other methods are needed to investigate the realistic loading conditions on whole bone structures. FEA is one method that may be used to investigate the influence of the mechanical environment on the regulatory processes of bone remodeling.

14.2.2.1 Using Finite-Element Analysis to Model Whole Bone Adaptation

Huiskes et al.[31] and Weinans et al.[32] developed models in which remodeling was regulated by sensors that strived to bring the strain energy per unit bone mass throughout the structure to a preset value. The stimulus (S) for remodeling was determined from n different loading conditions:

$$S = \frac{1}{n}\sum_{i=1}^{n}\frac{U_i}{\rho} \tag{14.1}$$

where U_i is the strain energy density of the ith loading condition, and ρ is the local tissue density. Changes in density over time were related to the stimulus S by

$$\begin{aligned} \Delta\rho &= A\Delta t\{S - k(1+s)\}^2 \text{ for } S \geq k(1+s) \\ \Delta\rho &= A\Delta t\{S - k(1-s)\}^2 \text{ for } S \leq k(1-s) \\ \Delta\rho &= 0 \text{ for } k(1-s) < S < k(1+s) \end{aligned} \tag{14.2}$$

where A is a time constant, Δt is the time period, k is the target equilibrium stimulus, and s is a parameter that defines the "dead zone" region where no net formation or resorption occurs. By incorporating this algorithm with finite-element models of the femur, the effects of the material properties of hip replacements on stress shielding around implant stems were examined.

Using a daily stress stimulus, Ψ, to determine the rates of bone resorption and formation, Beaupré et al.[33] used a finite-element model of the femur to investigate normal and abnormal loading effects on the functional adaptation of the internal structure of bone. In their study, the average stimulus for k different activities was defined as

$$\Psi = \left\{ \sum_{i=1}^{k} n_i \sigma_{\text{energy } i}^{m} \right\}^{\frac{1}{m}} \tag{14.3}$$

where n_i is the number of cycles of the ith activity, and m is an empirical constant. For this simulation, the stress term was defined as

$$\sigma_{\text{energy}} = \sqrt{2EU} \tag{14.4}$$

where E is the elastic modulus, and U is the strain energy density. Representing each activity by a set of loading conditions, Ψ was used to determine the bone resorption and formation rates and, subsequently, the density changes in the bone structure over time.

Remodeling to remove fatigue microdamage accumulation in the bone matrix was incorporated into a finite-element model of the femur by Doblaré and García.[34] In their study, damage was not considered in terms of microcrack density or crack length, but rather was related to porosity and the directional distribution of bone mass. Taking a similar approach to that proposed by Beaupré et al.,[33] and subsequent models from the same research group, a daily stress stimulus approach was used to stimulate remodeling. In their algorithm, damage accumulation was correlated to bone resorption (increased porosity and therefore increased defects in the material), whereas damage removal was associated with bone formation (increased bone mass and therefore fewer bone defects). The algorithm was then incorporated into a finite-element model of the femur to examine the effects of remodeling around total hip replacements. This model was further modified to include cellular activity (remodeling rates and densities of osteoclasts to resorb bone and osteoblasts to form bone) associated with remodeling and to take into account the degrading effects of damage on bone material properties to better predict stress fractures for various loading conditions.[35]

14.2.2.2 Merging the Concepts of the Bone Remodeling Process with Finite-Element Models of Bone Adaptation

Although the above models are excellent examples of using FEA to investigate whole bone adaptation under various conditions, each assumes that bone mass can be added as easily as it can be removed, which is not consistent with the physiological process of remodeling in which it is difficult to add substantial bone mass. In this sense, they are not necessarily solely models of bone remodeling but combine not only the coordinated actions of the bone cells (remodeling) but also the independent actions of the cells that alter the size and shape of bone associated with modeling. One algorithm that attempts to faithfully reproduce the

physiological processes of BMU-based bone remodeling (resorption by osteoclasts preceding formation by osteoblasts) is presented in the work of Hazelwood et al.[36] In their study, the local mechanical stimulus for remodeling (Φ) is assumed to be a function of the principal strain component with the maximum magnitude (ε) from n different daily activities performed R_L cycles per day:

$$\Phi = \sum_{i=1}^{n} \varepsilon_i^q R_{Li} \tag{14.5}$$

where the value for the exponent q was set to 4 based on studies that determined the number of cycles and strain levels needed to maintain bone mass.[37] With the mechanical stimulus in this form, it is reasonable to assume that the rate at which damage forms in bone (dD_F/dt) is proportional to Φ multiplied by a damage constant k_D (1.85×10^5 mm/mm;[2] determined by the equilibrium state when the bone formation and resorption rates are equal):

$$\frac{dD_F}{dt} = k_D \Phi. \tag{14.6}$$

Here, damage is defined as microcracks in the bone matrix in terms of total crack length per section area of bone.

Offsetting damage formation is damage removal by remodeling. Assuming that the BMU activation frequency for remodeling (f_a) is initiated by damage (D) and the area removed by each resorbing BMU is A (0.0284 mm^2), then the rate of damage removal is given by

$$\frac{dD_R}{dt} = Df_a AF_s \tag{14.7}$$

where F_s (set to 5) is a damage removal specificity factor to spatially associate BMU remodeling with damage in the bone matrix.[38] The rate of damage accumulation is then the difference of the damage formation (Equation 14.6) and removal (Equation 14.7) rates:

$$\frac{dD}{dt} = \frac{dD_F}{dt} - \frac{dD_R}{dt}. \tag{14.8}$$

In this model, BMUs are activated to begin remodeling by damage present in the bone matrix. As is typical of pharmacological dose–response curves, the relationship between BMU activation frequency and damage ($f_{a(damage)}$) was assumed to be sigmoidal with coefficients selected to fit the curve within known ranges of experimental data:[39]

$$f_{a(damage)} = \frac{(f_{a0})(f_{a(max)})}{f_{a0} + (f_{a(max)} - f_{a0})e^{[k_r(f_{a(max)})(D-D_0)/D_0]}}. \tag{14.9}$$

The initial equilibrium activation frequency f_{a0} (0.00670 BMUs/mm^2/day), the maximum activation frequency $f_{a\,(max)}$ (0.50 BMUs/mm^2/day), and the initial equilibrium amount of

damage D_0 (0.0366 mm/mm^2) were determined from numerous experimental studies;[36] and k_r (–1.6) defined the shape of the curve. It was also assumed that BMUs were activated to begin remodeling when bone tissue is insufficiently loaded (in a state of disuse) based on the stimulus Φ. Again, the relationship between BMU activation frequency and Φ ($f_{a\,(disuse)}$) was assumed to be sigmoidal:

$$f_{a(disuse)} = \frac{(f_{a(max)})}{1 + e^{k_b(\Phi - k_c)}} \text{ for } \Phi < \Phi_0 \tag{14.10}$$

where k_b (6.5 × 10^{10} cycles per day^{-1}) and k_c (9.4 × 10^{-11} cycles per day) are coefficients that define the shape of the curve, and the equilibrium value for the mechanical stimulus (Φ_0 = 1.875 × 10^{-10} cycles per day) was determined from the calculations of Beaupré et al.[33] on the strain necessary to maintain cortical bone mass (roughly 500 με applied 3000 times per day).

At any given time, the densities of resorbing (N_R) and forming (N_F) BMUs can be calculated from the activation frequency history and the remodeling period [assumed to be 25 days for resorption (T_R), 5 days for reversal (T_I), and 64 days for formation (T_F)]:

$$N_R = \int_{T_R} f_a \, dt \tag{14.11}$$

$$N_F = \int_{T_F} f_a \, dt. \tag{14.12}$$

The rate of change of porosity (dp/dt) is calculated from N_R and N_F and the rates at which bone is resorbed ($Q_R = A/T_R$) and formed ($Q_F = (A - A_H)/T_F$) for each BMU, where A_H (0.00126 mm^2) is the area of a Haversian canal:

$$\frac{dp}{dt} = Q_R N_R - Q_F N_F. \tag{14.13}$$

Bone porosity is then related to modulus by the relationships

$$E = 23{,}400(1 - p)^{5.74} \text{ (MPa) for } p < 0.097 \tag{14.14}$$

$$E = 14{,}927(1 - p)^{1.33} \text{ (MPa) for } p \geq 0.097, \tag{14.15}$$

which were obtained from the data of Currey[40] for cortical bone ($p < 0.097$) and Rho et al.,[41] as modified by Turner et al.,[42] for trabecular bone ($p \geq 0.097$).

This remodeling algorithm was combined with a finite-element model of the femur to investigate the effects of bone's mechanical environment on the remodeling process. A three-dimensional (3D) finite-element mesh of the femur consisting of second-order tetrahedral elements was created in Abaqus (Simulia, Providence, RI) from a computed tomography (CT) scan of a representative cadaveric femur. Convergence studies were performed to select the appropriate mesh density. The bone remodeling algorithm was incorporated into the finite-element model through a user material (UMAT) subroutine, with the strain

results from the FEA supplied to the algorithm to predict the appropriate remodeling response.

Hip joint and muscle forces representing three different load cases during single leg stance of walking (heel strike and toe-off) and stair climbing were applied to the model. A total of 5000 daily load cycles were assumed for walking representative of normal activity, and an additional 20 daily load cycles were assumed for stair climbing. The magnitudes and directions of the hip joint and muscle forces were consistent with *in vivo* measurements.[43–45] The model was constrained rigidly in the distal region of the femur above the femoral condyles and was allowed to evolve under loading from its initial homogeneous state until the remodeling parameters reached steady state.

The FEA model was validated by comparing the bone density predicted by the model to the morphological features of a femur. Results from the model were similar to femoral architecture in that dense cortical bone developed, forming the diaphysis and the calcar region in the neck, and trabecular bone of varying densities was observed in the femoral head and trochanter. The model was further validated with agreement in the predicted cortical strain values with levels measured *in vivo*.[46–48]

14.2.3 Computational Assessment of the Effects of Bisphosphonate Treatment on Bone Mechanics

Bisphosphonates are drugs developed to treat bone diseases involving elevated bone remodeling, such as postmenopausal osteoporosis. They act to reduce remodeling by suppressing osteoclast function, including inhibiting the activation of new BMUs, shortening the osteoclast life span, and disrupting the efficiency with which osteoclasts resorb bone.[49,50] Because they act on cells that resorb bone, the result of treatment is typically increased bone volume and reduced fracture risk; however, suppression of remodeling after treatment also leads to significant microdamage accumulation[51] and concern that the fracture risk for these patients may increase in the long term.

The remodeling algorithm described in Section 14.2.2.2 was used to evaluate the effects of long-term bisphosphonate treatment after postmenopausal osteoporosis on bone mechanics. A 1 cm^3 representative volume of trabecular bone under uniaxial cyclic loading of a 1 MPa stress was modeled.[52] Estrogen loss during menopause was assumed to increase the strain threshold of the cells that regulate remodeling[53] and was modeled as an increase in the equilibrium value for the mechanical stimulus (Φ_0), which was set to simulate the 11% bone loss observed in the lumbar spines of women five years after menopause.[54] Bisphosphonate treatment was simulated by incorporating a drug potency variable (P_o) into the algorithm and reducing the BMU activation frequency by $1 - P_o$, where

$$P_o = P_{max}(1 - e^{-\tau_s N_R}) \tag{14.16}$$

and P_{max} and τ_s are coefficients reflecting the dosage and chemical structure of the bisphosphonate. Model parameters were selected to provide drug potencies simulating the reductions in activation frequency found *in vivo* after alendronate (a bisphosphonate) treatment at low (5 mg/day) and clinical (10 mg/day) doses.[52] In addition, the effects of bisphosphonates also were simulated by reducing the area resorbed by each BMU.[51]

Simulation results paralleled the bone volume increases in osteoporotic patients observed by Tonino et al.[55] using alendronate doses of 5 or 10 mg/day. Due to the reduction in remodeling and, therefore, the related decline in the damage removal rate, initial gains in microdamage were observed (Figure 14.1).[52] Within three years, damage had reached its

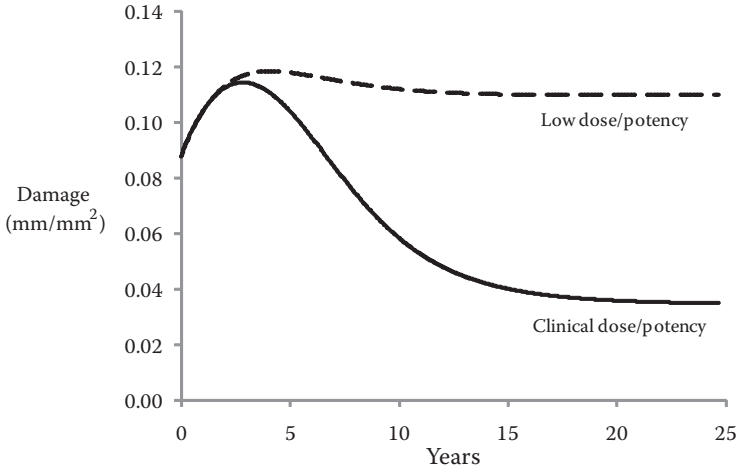

FIGURE 14.1
Predicted damage accumulation (mm crack length/mm^2 bone area) by the remodeling algorithm in a representative volume of trabecular bone under cyclic loading after bisphosphonate treatment for low and clinical dosages. Damage was predicted to increase in the first few years (as is observed clinically), but the added bone mass as a result of treatment eventually controlled the rate at which damage formed, such that damage accumulation reached an equilibrium level at the low dose and decreased below the pretreatment level for the clinical dose.

maximum value and then trended downward at varying rates depending on drug potency and dosage as the damage removal rate surpassed the diminishing damage formation rate. The model results suggest that while damage accumulation is of concern in the short term, increasing bone volume with long-term bisphosphonate treatment may sufficiently reduce strain and damage formation rates to control (and possibly reduce) damage accumulation in the long term.

14.2.4 Computational Study of Hip Implant the Effects on Femoral Bone Mechanics

The FEA model described in Section 14.2.2.2 was also used to investigate the effects of hip replacement surgery on femoral remodeling and bone mechanics. To simulate pain and loss of function due to osteoarthritis (OA), the model was later subjected to reduced loading conditions[56] for one year prior to surgery. The resulting model after one year of reduced loads represented the preoperative state of the femur.

The implants modeled were an 11 × 142 mm conventional tapered stem implant and a 49 mm resurfacing component. Although conventional implants have proven very successful, bone loss due to stress shielding is still evident in the proximal femur.[57] The clinical consequences of stress shielding are debatable,[58] but it is advantageous to maintain as much bone as possible in the proximal femur in case revision surgery is necessary. Hip resurfacing arthroplasty has recently proven to be a popular alternative to conventional hip arthroplasty due to the preservation of proximal bone in the femur resulting from a more natural loading state. Still, femoral neck fractures remain a complication with resurfacing components.[59]

In this FEA model, each of the implants (Figure 14.2) was inserted, and analyses were run to simulate two years of postoperative use, with the reduced loading conditions preoperatively returning to normal levels at three months postoperatively. Insertion of the tapered stem led to reductions in bone volume fraction along the stem, in particular, in

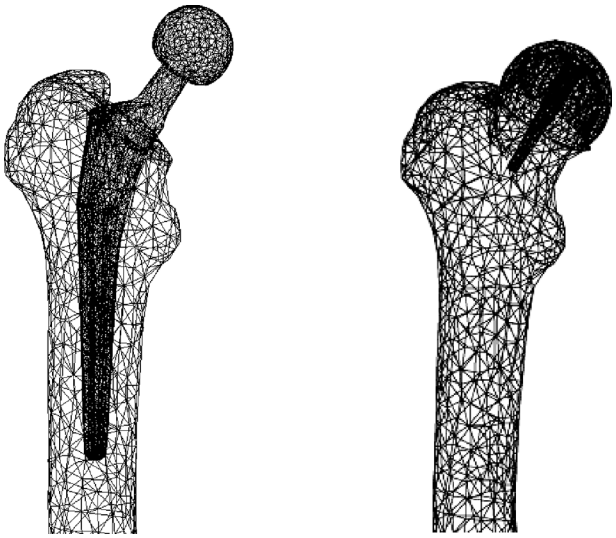

FIGURE 14.2
Finite-element meshes of the femur with an 11 × 142 mm conventional tapered stem implant (left) and a 49 mm resurfacing implant (right). The mesh with the conventional implant consists of 46,907 second-order tetrahedral elements (70,169 nodes), and the mesh with the resurfacing implant contains 28,864 elements (44,224 nodes).

the proximal medial region where a 24% loss of bone occurred at two years (Figure 14.3a). Damage levels in the bone were slightly elevated at the distal–medial end of the stem. Transient bone loss of less than 10% was observed in the femoral head and neck after implantation of the resurfacing component (Figure 14.3b). Damage levels in the femoral neck and in the head adjacent to the rim of the implant were elevated (Figure 14.3c) and were still increasing over the 2-year period. Although bone loss after hip resurfacing arthroplasty was minimal compared with that after conventional hip arthroplasty in similar regions of the femur, the consequences of bone loss and damage accumulation in the femoral head and neck, with subsequent increases in fracture risk, after hip resurfacing still need further investigation.

14.3 Computational Approaches to Articular Cartilage Mechanics

The extracellular solid matrix of AC contains glycosaminoglycans (GAGs) and a cross-linked collagen (COL) network. The GAGs are negatively charged molecules that primarily resist compressive loads,[60,61] whereas the COL network primarily resists tensile and shear loads.[62,63] Due in part to its complex molecular structure, AC typically behaves as an anisotropic material with substantial tension–compression asymmetry (e.g., tension modulus ~1–2 orders of magnitude greater than compressive modulus)[64–77] and likely experiences finite, multidimensional strains when subject to typical loads (e.g., maximum compressive strains of ~20% to 30%).[4,7,78] Furthermore, AC tissue is highly heterogeneous; the GAG content,[79] compression modulus,[80] and COL fibril orientation[81,82] all vary markedly with depth

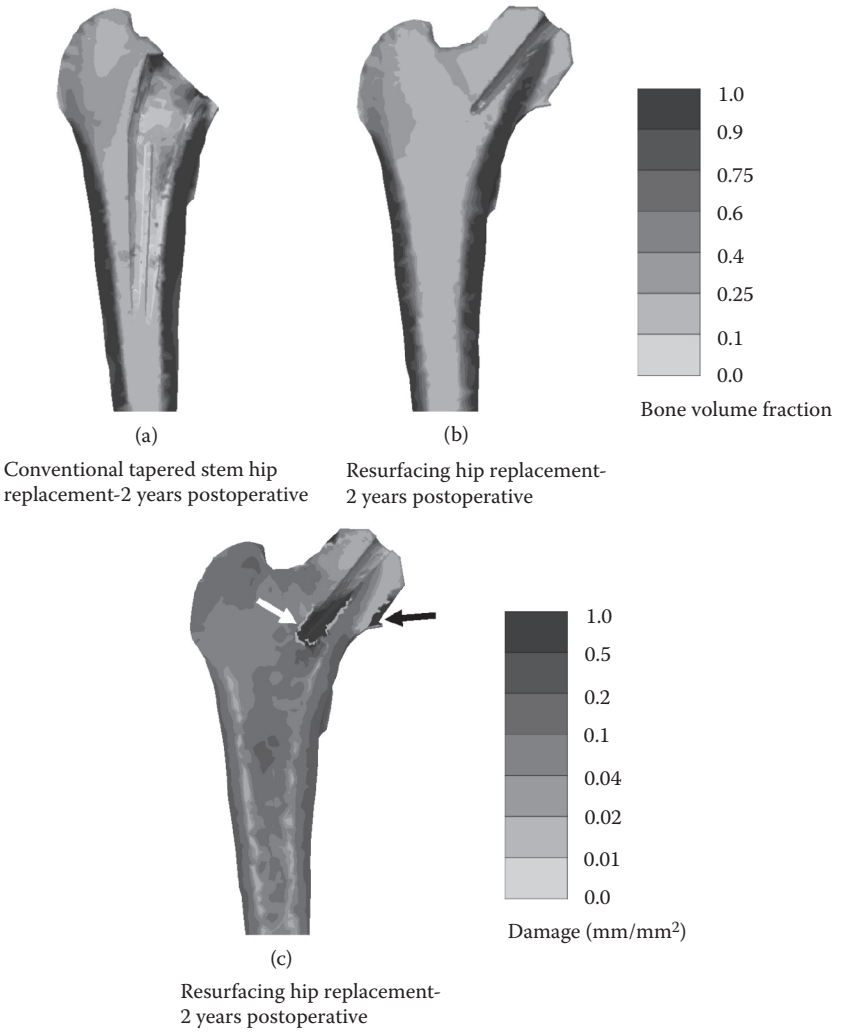

FIGURE 14.3
Predicted femoral bone volume fraction after implantation of (a) conventional tapered stem implant (not shown) and (b) the resurfacing implant at 2 years after surgery (implants not shown). For the conventional stem, bone loss was predicted along the length of the implant stem, with the highest amount of loss observed in the proximal medial region of the femur. For the resurfacing implant, bone loss of less than 10% was observed in the femoral head and neck at 2 years after insertion of the implant. Damage (c) was predicted to be highest over the 2-year period at the tip of the resurfacing component stem (white arrow) and in the femoral head adjacent to the implant rim (black arrow).

from the articular surface. At the superficial zone, fibrils are horizontally oriented pharallel to the articular surface,[82] whereas they become rather random in the transitional zone,[83] and are perpendicular to the articular surface in the deep zone[81,82,84] to anchor the tissue firmly to the subchondral bone.[85,86] Consequently, the development and implementation of accurate material models that may be used for delineating structure–function relations for this tissue are challenging tasks.

14.3.1 Nonlinear Fibril-Reinforced Tissue Models

In earlier attempts in which AC was modeled as a poroelastic material composed of an isotropic homogeneous porous medium filled with permeating fluid, the measured global load-displacement behavior of AC specimens in confined compression tests was adequately predicted by analytical solutions.[87–90] Classic anisotropic approaches using strain tensor invariants derived from material symmetry concepts[91] have given way to models that are more descriptive of tissue structure–function relations. One popular structural approach that models tissue as a matrix reinforced with a discrete number of reinforcing fiber families has been widely implemented in tissue continuum mechanics[92–97] and structural FEA[6,98–100] approaches. An alternative continuum mechanics approach that models the fiber-reinforced matrix using continuous COL fibril distribution functions has become increasingly popular in recent years.[101–114]

14.3.1.1 Fibril-Reinforced Structural FEA of Full-Thickness AC Tissue

In the structural FEA approach, COL fibrils are simulated as a material distinct from a porous isotropic solid matrix filled with water. Such fibril-reinforced structural FEA has been successfully applied to both confined and unconfined tests yielding satisfactory results in agreement with measurements[99] and has extensively been used in recent studies of AC mechanics.[115–118]

Using a validated structural FEA model as the foundation,[99,119] a recent study[10] showed the importance of depth-dependent COL fibril structure on mechanical function by using an axisymmetric nonlinear fibril-reinforced poroelastic FEA model of AC incorporating the tissue fibril network as three distinct groups: horizontal at the superficial region, random in the transitional region, and vertical in the deep zone.[10] Vertical fibrils significantly

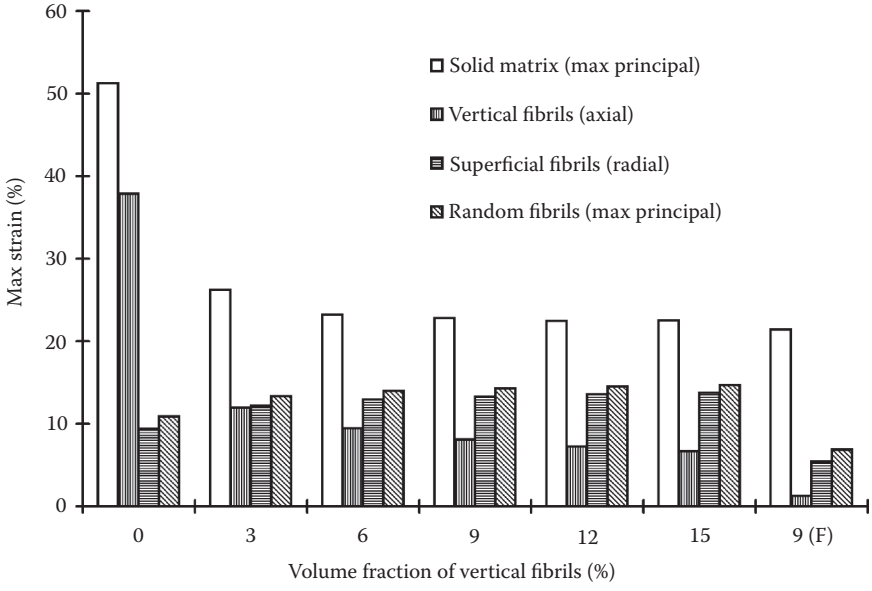

FIGURE 14.4
Maximum strains in the solid matrix and collagen fibril networks of AC at transient (t = 0.5 s) in the relaxation model given for various vertical volume fraction values and the case with free sliding at the base. (From Shirazi, R. and Shirazi-Adl, A., *J. Orthop. Res.*, 26 (5), 608–615, 2008. With permission.)

increased the transient stiffness of the AC in the relaxation model, an effect that completely disappeared at equilibrium. This stiffening effect was associated with changes in the pore pressure that dramatically increased at the center of the tissue. Despite the considerable increase in the axial reaction forces and pore pressure when vertical fibrils are present, the maximum principal strain in the solid matrix and the maximum tensile strain in the vertical fibrils themselves dropped markedly as higher volume fractions were considered (Figure 14.4). The foregoing dramatic role of vertical fibrils on the transient mechanics of AC was highly sensitive to the strain rate in the relaxation model. The deformation pattern of vertical fibrils predicted in this study was in agreement with the reported observations on posttransient microdeformation of AC in creep despite differences in indenter profile, load magnitude, and tissue geometry.[120–123]

14.3.1.2 Continuous Collagen Fibril Distribution Model Predictions of True COL Fibril Modulus Changes due to In Vitro Growth Hormone Treatment

In this section, the focus is on how a continuous fibril distribution model may be implemented using the commercial FEA solver Abaqus to better understand how tissue structure–function relations evolve during select *in vitro* growth protocols. To model the COL constituent using a continuous fibril distribution function, a local spherical coordinate system was used to parameterize a unit sphere at each tissue material point.[114] At each material point, the solid matrix deformation gradient tensor **F** defines the deformation relative to a reference configuration; consequently, the Lagrangian strain tensor is $\mathbf{E} = (1/2)(\mathbf{F}^T\mathbf{F} - \mathbf{I})$ (where T is the transpose operator and **I** is the identity tensor). The unit sphere is divided into a discrete number of pyramidal volume elements, dV, each oriented in a different direction **n**. The true fibril strain energy, Ψ (per fibril volume dV^f), is a function of the scalar fibril strain $E_n = \boldsymbol{n} \cdot \mathbf{E}\boldsymbol{n}$ (where $\cdot$ is the dot product). The total COL strain energy, W^{COL} (per sphere volume), is obtained by integrating the apparent fibril strain energy, $\phi_n^f\Psi$ (per pyramidal volume dV), over the unit sphere volume, V^{tot}, while only including those fibrils that are in tension:

$$W^{\mathrm{COL}} = \left(\frac{1}{V^{\mathrm{tot}}}\right)\int \phi_n^f H\Psi \,\mathrm{d}V \tag{14.17}$$

where $\phi_n^f = \mathrm{d}V^f/\mathrm{d}V$ is the directional fibril volume fraction, and H is the Heaviside step function of E_n. Consequently, COL second Piola–Kirchhoff stress ($\mathbf{S}^{\mathrm{COL}}$) and elasticity ($\mathbb{C}^{\mathrm{COL}}$) tensors are derived using standard formulae as $\mathbf{S}^{\mathrm{COL}} = \partial W^{\mathrm{COL}}/\partial\mathbf{E}$ and $\mathbb{C}^{\mathrm{COL}} = \partial^2 W^{\mathrm{COL}}/\partial\mathbf{E}\partial\mathbf{E}$, respectively.

To implement these equations in an FEA model of AC tissue, the COL constituent is combined with a GAG constituent to form the solid matrix. GAG second Piola–Kirchhoff stress ($\mathbf{S}^{\mathrm{GAG}}$) and elasticity $\mathbb{C}^{\mathrm{GAG}}$ tensors must be proposed; then, total solid matrix second Piola–Kirchhoff stress (**S**) and elasticity ($\mathbb{C}$) tensors are obtained from $\mathbf{S} = \mathbf{S}^{\mathrm{COL}} + \mathbf{S}^{\mathrm{GAG}}$ and $\mathbb{C} = \mathbb{C}^{\mathrm{COL}} + \mathbb{C}^{\mathrm{GAG}}$, respectively. For implementation with the UMAT feature of Abaqus, all components of the total solid matrix Cauchy stress tensor **T** and the Jacobian stiffness matrix $\bar{\mathbb{C}}^{\mathrm{COL}}$ are derived and coded directly in the UMAT. The Cauchy stress is derived from $\mathbf{S}^{\mathrm{COL}}$ using the relation $\mathbf{T} = (1/J)\mathbf{F}\mathbf{S}\mathbf{F}^T$, where J is the determinant of **F**. Using indicial notation and summation convention rules, the Jacobian stiffness matrix $\bar{\mathbb{C}}^{\mathrm{COL}}$ that is preferred by Abaqus is derived ("Abaqus Theory Manual" version 6.10, Section 1.5.3, Stress Rates).

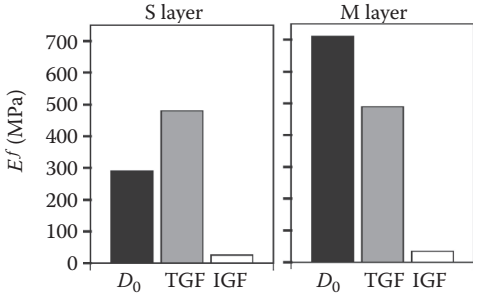

FIGURE 14.5
True collagen fibril modulus predictions for the S and M layers of bovine calf AC before (D_0) and after (D_{12}) *in vitro* growth (IGF and TGF). The effect of TGF-β1 treatment was to increase and decrease for the S and M layers, respectively, toward a homeostatic value of 480 to 490 MPa. Conversely, the effect of IGF-1 treatment was to decrease for the S and M layers toward a homeostatic value of 26 to 34 MPa. (Data from Stender, M. et al. Differential Regulation of Articular Cartilage Tensile Properties by IGF-1 and TGF-B1 during In vitro Growth. Paper read at *International Conference on the Mechanics of Biomaterials and Tissues*, Hawaii, 2011.)

Experimental data were available for studies of bovine calf articular explants.[76,124] Briefly, explants were harvested and ~0.5-mm-thick specimens were obtained from adjacent superficial (S) and middle (M) layers and either mechanically tested immediately (D_0; day 0) or cultured *in vitro* for 12 days (D_{12}; day 12) in medium supplemented with TGF-β1 or IGF-1. Samples were tested either in confined compression (CC), unconfined compression (UCC), or uniaxial tension (UT), and equilibrium mechanical properties were measured (CC modulus H_A, UCC modulus E^-, UCC Poisson's ratio ν, and tensile modulus E^+). After mechanical testing, biochemical measures (COL, GAG, and water contents) were obtained.

Immature bovine AC exhibits an approximately linear stress–strain curve in UT.[72,125] Therefore, a quadratic true COL strain energy density function is used, $\Psi = \Psi(E_n) = (1/2)E^f(E_n)^2$, where E^f is the true COL fibril modulus. An isotropic fibril distribution was used for both S and M layers.[126–128] The GAG stress equation (not presented here) has two material constants; these are chosen to depend on experimental measurements of GAG density to match theoretical predictions of swelling pressure–density relations using a Poisson–Boltzmann model.[129] Consequently, the FEA model is used to predict E^f by providing the best fit to the experimental UT experiments. FEA employed static analysis to model equilibrium and applied appropriate load and displacement boundary conditions to simulate CC, UCC, and UT experiments.

True COL fibril modulus predictions for all experimental groups are shown in Figure 14.5. For untreated specimens, predicted E^f values were 290 and 710 MPa for the S and M layers, respectively. TGF-β1 treatment increased and decreased E^f for the superficial and middle layers, respectively, toward a homeostatic value of 480 to 490 MPa. IGF-1 treatment decreased E^f for both layers toward a homeostatic value of 26 to 34 MPa (results not published). Thus, the novel findings of this FEA study are that COL fiber moduli for immature AC tissue may vary substantially in the depth direction yet may be regulated toward homeostatic values via treatment with either TGF-β1 or IGF-1. In addition, FEA predictions of total tissue mechanical properties in compression and UT (results not shown) fall within a standard deviation of experimental results, highlighting the ability of the model to capture substantial tension–compression asymmetry typical of COL fibril-reinforced tissues.

14.3.2 Nonlinear Viscoelastic Tissue Models

AC generally exhibits both fluid flow–dependent and –independent (i.e., intrinsic) viscoelastic (VE) behavior.[116,130–134] Intrinsic VE is perhaps best summarized with regard to a tissue's stress relaxation response to a step change in strain, for which the relaxation function described by a time constant, τ, and relaxation ratio, R, governs the transient stress response, whereas an equilibrium elastic function both modulates the transient response and governs the equilibrium stress response. AC tissue has been modeled using linear,[116,135,136] quasilinear,[130,132] and nonlinear[134,137,138] VE models; the distinction between these types of VE models can be characterized by the forms of the relaxation and elastic response functions.[138] Here, focus is on how a constituent-based nonlinear VE model may be implemented in MATLAB® (Version 7, Mathworks Inc., Natick, MA) to obtain computational solutions to UT stress relaxation experiments to better understand how tissue structure–function relations change due to GAG depletion.

14.3.2.1 Collagen Viscoelastic Parameter Changes due to GAG Depletion

Previous studies have suggested that VE parameters may change after GAG depletion of AC[139–144] and other biological tissues.[145–148] Although most GAG depletion studies with AC have involved the use of mature tissue, a recent study[144] suggested that GAG interactions regulate tissue VE properties in a manner dependent on the tissue's maturational stage.

As described in the previous section, the AC solid matrix is modeled as a mixture of COL and GAG constituents [see Thomas et al.[138] for more details]. For analysis of UT experiments, flow-dependent VE and intrinsic GAG VE are neglected.[137,149–152] Consequently, the time-dependent total solid matrix second Piola–Kirchhoff stress is modeled using constituent-based VE as

$$\mathbf{S}(t) = {}^{e}\mathbf{S}^{\mathrm{GAG}}(t) + {}^{e}\mathbf{S}^{\mathrm{COL}}(0) + \int_0^t G^{\mathrm{COL}}(t-\tau)\frac{d\,{}^{e}\mathbf{S}^{\mathrm{COL}}(t)}{d\tau}\,\mathrm{d}\tau \tag{14.18}$$

where ${}^{e}\mathbf{S}^{\mathrm{GAG}}(t)$ is the time-dependent elastic GAG stress, ${}^{e}\mathbf{S}^{\mathrm{COL}}(0)$ is the elastic COL stress in the reference configuration, the convolution integral represents the time-dependent COL stress, ${}^{e}\mathbf{S}^{\mathrm{COL}}$ is the elastic COL stress, and G^{COL} is the COL relaxation function that is represented as the Prony series:

$$G^{\mathrm{COL}}(t) = 1 + \sum_{i=1}^{n} g_i^{\mathrm{COL}} \exp\left(\frac{-t}{\tau_i^{\mathrm{COL}}}\right) \tag{14.19}$$

where g_i^{COL} and τ_i^{COL} are COL amplification coefficients and time constants, respectively. The relaxation ratio, R, is defined as equilibrium stress divided by peak stress, and the time constant, τ, is defined as the amount of time t it takes for the tissue stress to relax by 63.2% from its peak value after a step increase in strain; when more than one term is used in the Prony series, then an aggregate COL relaxation ratio, R_A^{COL}, and an aggregate COL time constant, τ_A^{COL}, can be defined as functions of g_i^{COL} and τ_i^{COL}.[138]

To implement this nonlinear VE model in computational analyses, a time discretization procedure can be used to calculate $\mathbf{S}^{\mathrm{COL}}(t + \Delta t)$ after a time increment Δt.[138] Computational solutions were obtained in MATLAB. Briefly, at each time increment, the increment in

applied normal strain (two directions) is calculated based on the testing protocol. At each time point, $t + \Delta t$, the VE stress is calculated using an iterative computational solution coded in MATLAB, iterating on assumed values of normal strains in the transverse directions until the calculated normal stresses in the transverse directions are approximately zero (using a specified error tolerance) as required by traction-free boundary conditions on the lateral surfaces of the test specimen. Then, this solution procedure is repeated for subsequent time increments until the final time step is reached. In this approach, using MATLAB to ensure that the stress equations satisfy the boundary conditions, the stiffness matrix is not needed because, due to the assumed homogeneous stress state for UT, the equilibrium equations are satisfied *a priori*.

Experimental data are available from Asanbaeva.[153] Briefly, bovine calf AC explants were harvested and ~0.25-mm-thick specimens were obtained from ~0.6 mm below the surface. The control group (no GAG depletion; GD-0) did not receive enzyme treatment. Other explants were treated with guanidine HCl (Gnd) to remove ~55% (GD-55) or ~85% (GD-85) of GAG mass. After treatment, samples were tested in UT, and the stresses were measured during a stress relaxation period. After mechanical testing, biochemical measures (GAG, COL, and water contents) were obtained.

Either the biochemical data or results from previous studies were used to specify all material constants except for a COL elastic modulus parameter, γ_1, and COL relaxation parameters. For each specimen, γ_1 was calculated so that the model matched the equilibrium stress measured at the end of the relaxation period. For G^{COL}, two terms were used for the GD-0 and GD-55 groups, whereas one term was used for the GD-85 group based on the criterion that the computational solution does not depend on initial guesses of the relaxation parameters. Then, the iterative optimization procedure was implemented to determine COL VE parameters that produced a best fit to experimental stresses. After optimization, the aggregate relaxation ratio R_A^{COL} and aggregate time constant τ_A^{COL} were calculated. Correlations between model parameters $\left(\gamma_1, \tau_A^{\mathrm{COL}}, R_A^{COL}\right)$ with biochemical contents were investigated.

The model parameters $\left(\gamma_1, R_A^{\mathrm{COL}}\right)$ were significantly correlated with GAG content ($p < 0.01$ and 0.001, respectively; Figure 14.6). None of these parameters were significantly correlated with COL content or water content. The increase in γ_1 that was evident with GAG

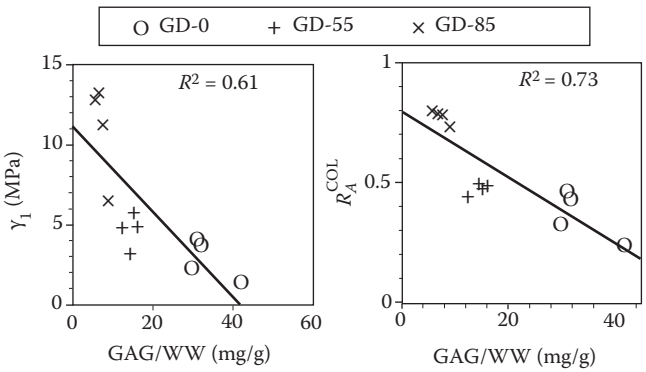

FIGURE 14.6
Model parameters $\left(\gamma_1, R_A^{\mathrm{COL}}\right)$ versus GAG content. GD-0 = control group. GD-55 and GD-85 = experimental groups with ~55% and 85% GAG depletion, respectively. Linear regression results only shown for significant correlations (*t*-test analysis of regression slope, $p < 0.05$). (Modified from Thomas, G. C. et al., *J. Biomech. Eng.*, 131, 101002, 2009. With permission.)

depletion indicates that GAG–COL interactions produce a more compliant tissue, which may be a key property that underlies a mechanism for rapid volumetric expansion during developmental growth. Furthermore, the increase in R_A^{COL} that occurs with GAG depletion indicates that GAG–COL interactions provide a lower relaxation ratio and enhanced COL viscous properties, which may be a mechanism that protects cells against excessive matrix strains during repeated loading. Upon considering results from other studies using more mature tissue,[139–142,144] it seems that GAG–COL interactions on tissue VE parameters as predicted here may diminish as the tissue matures, indicative of a remodeling response during development and growth.

14.3.3 Computational Approaches to Articular Cartilage Growth and Remodeling

Tissue G&R depends on biological factors that may be regulated by local mechanical conditions such as stress, strain, or fluid velocities.[154] Continuum mechanics G&R models attempt to quantify the mechanobiological "feedback loop" via modeling the temporal evolution of tissue composition and, consequently, biomechanical properties that filter an external stimulus before signaling the cell nucleus to initiate mRNA production. Since the early pioneering bone remodeling studies,[33,155–157] many authors have developed and implemented G&R models for both hard and soft tissue; see the reviews in the works of Cowin[158] and Ambrosi et al.[159] Here, focus is on our own implementation of AC G&R algorithms with the commercial FEA program Abaqus.[160,161] Other recent studies have also integrated soft tissue G&R algorithms with Abaqus.[162–167]

14.3.3.1 Modeling In Vitro Growth and Remodeling of Articular Cartilage Tissue

The computational G&R algorithm separates the solution of the G&R BVP into two parts: one that describes the actual mechanical loading with a time scale (i.e., increment) on the order of seconds, and another that describes the resulting G&R of the tissue with a time scale of 1 day. This approach is similar to the concept of using a daily G&R stimulus parameter from earlier studies with bone and AC tissue.[157,168] For the first time increment, poroelastic FEA (Abaqus) determines time-averaged values of mechanical variables (i.e., relative fluid velocity or maximum shear stress) used to determine incremental growth laws for each finite element (Figure 14.7). Then, the incremental growth BVP[169] is solved using an "elemental growth routine" (in MATLAB) to determine new values of the finite-element geometry, composition, and stress equations in a compatible configuration (Figure 14.7) [see Ficklin et al.[161] for full details]. However, for heterogeneous G&R, the new compatible tissue configuration will not be in equilibrium, so Abaqus is used to calculate a global equilibrium state. This incremental G&R solution proceeds in an iterative manner for the entire growth process.

This G&R FEA approach has been used to simulate *in vitro* growth of AC explants subjected to dynamic CC,[160] dynamic UCC,[170] and steady-state permeation.[161] For example, we simulated[161] *in vitro* growth of bovine calf AC explants in a steady-state permeation bioreactor using growth laws triggered by maximum shear stress.[171] Cylindrical disc specimens were modeled using 7812 poroelastic brick elements (C3D8P) with strain-dependent permeability defined in the UMAT. Analysis steps include an initial compression to prevent separation of the tissue from the porous platens during permeation, coupled steady-state permeation loading using Abaqus and the G&R algorithm, CC of the disc after G&R, release of the disc from the permeation chamber after CC testing, and slicing of the disc for heterogeneous biochemical testing.

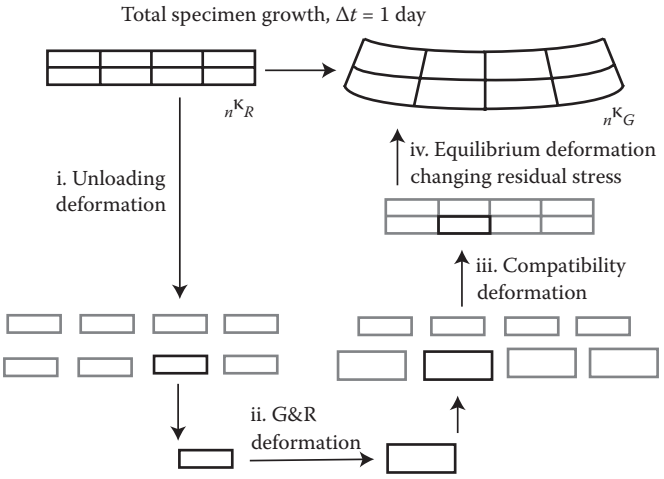

FIGURE 14.7
Total specimen growth BVP for one increment (n) in the G&R FEA. Each solid matrix finite element is (i) unloaded from its configuration before growth ($_n\kappa_R$) by relieving residual stress, (ii) grown to a new volume, (iii) mechanically deformed back into its pregrowth compatible configuration, and (iv) loaded via residual stress to an equilibrium configuration ($_n\kappa_G$) of the total specimen FEA after growth. Steps i. to iii. were solved using MATLAB and step iv. was solved using Abaqus.

The results illustrate that the G&R FEA model can predict the evolution of nonuniform tissue composition (Figure 14.8), pore pressure gradients, residual stress, and mechanical properties due to differential and nonuniform growth.[161] In this example, G&R FEA was used to develop a better understanding of the mechanobiological response of AC tissue explants grown in a steady-state permeation bioreactor. In our own experiments with tissue harvested from bovine calf knees, we found that cell viability was compromised during 12 days of growth in the steady-state permeation bioreactor (unpublished data), and the FEA results may explain this phenomenon. As the tissue matures via G&R, the FEA model predicts that steep pore pressure gradients develop near the drain side, where fluid that flows out of the tissue is accompanied by compressive matrix strains that become higher than reported values for causing cell death.[123] Consequently, the FEA results suggest that as tissue-engineered constructs cultivated in permeation bioreactors become

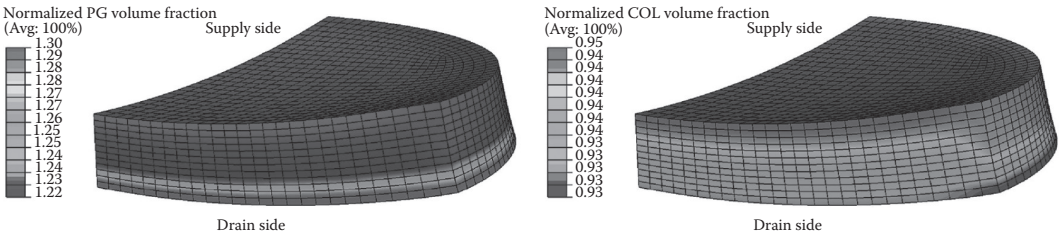

FIGURE 14.8
(See color insert.) FEA specimens released from a permeation chamber after growth: contours of the final proteoglycan (PG) and collagen (COL) volume fractions for a shear growth trigger normalized. This configuration corresponds to release from the permeation chamber. The average dimension of the elements are 25.33 × 63.85 μm. The curvature deformation is scaled by a factor of 5 to highlight the nonuniform geometry that results from growth.

more mature, the magnitudes of compressive strains may increase to levels that actually threaten cell viability, suggesting that loading paradigms must be carefully monitored and possibly altered during *in vitro* tissue engineering protocols.

14.4 Computational Approaches to Whole Knee Joint Mechanics

Throughout adult life, the AC of diarthrodial joints such as the knee experiences a high level of biomechanical stress.[172] In many individuals and at most anatomical sites, AC is able to maintain a relatively normal structure with little change in compressive properties over decades. However, trauma and, in some individuals, age may cause local damage and onset and progression of OA. After even minor injuries, adult AC as a tissue has a poor intrinsic capacity for repair.[173] Effective preventive and treatment strategies may be aided by a thorough understanding of knee joint biomechanics during physiological *in vivo* loading arising from daily activities.

In addition to AC that covers the ends of long bones in the knee joint, the menisci and ligaments contribute to the load-bearing and stability functions in the joint. Malfunction or perturbation of any of these tissues may affect the other tissues by altering the load-bearing pathways and, consequently, mechanical variables such as stress and strain in a manner that induces degeneration or damage. For example, if the anterior cruciate ligament (ACL) is torn or damaged, or a meniscus is torn or the joint is (partially) meniscectomized during treatment, AC tissue may be required to bear pathological levels of stress and strain.

The menisci of the knee have microstructural properties similar to AC, and, consequently, accurate modeling of their biomechanics is challenging. On the other hand, although major ligaments in the knee joint have different bundles and are not entirely straight, they can be accurately simulated by one-dimensional elements such as "truss" or "spring" elements. Here, we focus on the FEA models of the tibio femoral joint that have been used to predict stress and strain changes due to pathological or treatment-induced changes to the ligament, meniscal, and bone tissues of that joint.

14.4.1 Passive versus Active FEA Models of the Knee Joint

Bendjaballah et al.[174] initiated a paradigm shift in developing complex FEA models of the knee joint that has now become widely adopted. Their work used imaging techniques (CT scans) to construct complex 3D geometries of cartilages and menisci. In that model, isotropic and anisotropic material properties for, respectively, AC and meniscus were assumed, with the latter composed of isotropic nonfibrillar solid matrix reinforced by COL fibril elements. Nonlinear stress–strain curves with different initial pre-strains were used to model the anterior cruciate, posterior cruciate, medial collateral, and lateral collateral ligaments.

Since then, other researchers have developed FEA models of the knee joint with 3D geometries constructed similarly using imaging. The loading conditions in those models differ and include axial compression,[4,175,176] drawer shear, flexion–extension,[177] internal–external rotation,[178] varus–valgus rotation,[179] or combinations thereof.[180,181] Some studies modeled bone, which is much stiffer than cartilage, as a rigid material,[174] whereas other studies[5,175] modeled bone tissue as a deformable elastic material; the latter studies have

shown that modeling bone as rigid or elastic changes the predictions of contact variables by only 2%.

In a recent study,[4] both AC and menisci were modeled as anisotropic composites with isotropic hyperelastic solid matrices reinforced by fibrillar COL networks with different orientations at different depths (Figure 14.9). Also, elastic material properties of the nonfibrillar AC solid matrix were assumed to vary along the depth from the articular surface in accordance with experimental data.[80] Homogeneous in-plane distribution of COL fibrils with random orientations were modeled (Figure 14.9) in superficial zones of femoral and tibial cartilage layers,[82] as well as bounding surfaces of menisci.[182] COL type I in menisci[183,184] and COL type II in AC were used, with the latter assumed as 70% of the former.[185] In the transitional zone and deep zone of AC, however, random[83] and vertical[82] fibrils were modeled (Figure 14.9), respectively.

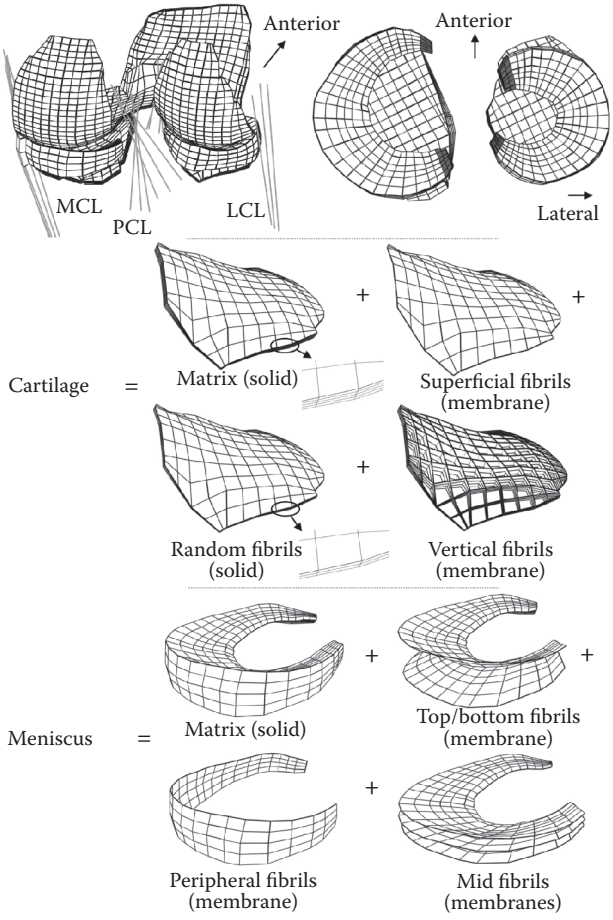

FIGURE 14.9
Finite-element mesh of the knee. Top left: posterior view of the knee joint with tibial and femoral cartilage layers, menisci, and major ligaments. Top right: top view of menisci and tibial AC. Middle and bottom: tibial lateral cartilage and medial meniscus, respectively, showing distinct elements representing solid matrix along with collagen fibril networks at different zones. Tibial medial plateau, femoral cartilage, and lateral meniscus have similar structures, although they are not shown here. Random fibrils in cartilage are distributed on the two upper layers of cartilage. (From Shirazi, R. et al., *J. Biomech.*, 41 (16), 3340–3348, 2008. With permission.)

In the bulk region of each meniscus in between peripheral surfaces, COL fibrils were assumed to be dominant in the circumferential direction.[4,182] For details on the implementation of fibril orientations in the AC and meniscus, see the work of Shirazi et al.[4] Predictions of key mechanical variables, such as deflections and contact pressures, were compared with, and were in the range of, measurements from several independent studies [see Table 1 in Shirazi et al.].[4]

Other researchers[186–188] also developed FEA models of the whole knee joint that, in addition to the tissues mentioned above, included the patellar cartilage, muscles such as quadriceps and hamstrings, medial and lateral patellofemoral ligaments, and the patellar tendon. Such models have implications for the study of rehabilitation strategies. Each rehabilitation exercise recruits specific muscles to different extents, and the simulation of such exercises may aid in the development of therapeutic strategies that optimize the recovery of a reconstructed ligament. As an example, a recent study investigated the biomechanics of the entire joint in open kinetic chain extension exercises,[189] which are commonly performed during physical therapies or after joint reconstruction. In that study, the effect of the weight of the leg and the foot, with and without a moderate resistive force of 30 N acting at the ankle perpendicular to the tibia, on different tissues in and around the knee joint was studied at different flexion angles from 0° to 90°. It was predicted that the resistive load substantially increased the required cruciate ligaments, patellar tendon, and quadriceps forces, especially at near 90° angles. It was also suggested that in the joint with ACL injury or after ACL reconstruction, exercise should preferably be avoided at near full extension positions under large resistant forces.

14.4.2 Ligament-Meniscal Injuries and Their Adverse Effects

Axial compressive and anterior–posterior shear forces, commonly occurring in daily activities such as running, jumping, and ascending/descending stairs, arise directly due to gravity- and acceleration-induced inertial loads and indirectly due to activation of muscles crossing the knee joint. The drawer forces, directed in the anterior–posterior direction, at higher magnitudes can cause excessive strains in the ACL, which is known as a primary restraint to anterior translation of the tibia relative to the femur.

Injuries or alterations to the ACL and menisci influence the overall joint response as well as the mechanical role of the remaining components, with the likelihood of exacerbating the joint condition causing recurrent injuries and further damage. Existing ACL reconstruction techniques use different ligament pre-tension/pre-strain levels and replacement materials such as bone–patellar tendon–bone and hamstring grafts with much stiffer material properties.[190] The pre-tension level and type of graft material have been recognized as primary variables that influence the outcome of reconstruction attempts. Meniscal tears are also commonly observed along with ACL ruptures[191] as the risk of meniscus failure increases in ACL-deficient knees.[192] Due to the dramatic adverse effect of total meniscectomy on load distribution and development of joint OA, partial meniscectomies are performed with the resection of the torn tissues. Concurrent ACL and meniscus ruptures are treated by ACL reconstruction and partial meniscectomy. The incidence of OA in mid- and long-term outcome studies of ACL reconstruction[193] and partial meniscectomy[194] has nevertheless persisted. Here, we focus on how FEA may be used to predict the effect of various loads and joint perturbations on joint contact loads, AC strains/stresses, and ACL forces with the goal of improving our understanding of likely short-term effects of foregoing ACL and meniscal treatment modalities on whole joint biomechanics.

To examine the effects of changes in ACL tissue properties or pre-strain levels, ACL material properties were replaced by patellar tendon properties,[190] or pre-strain levels in both anteromedial and posterolateral bundles of the ACL were changed by +4% or −4% strains; in other words, the initial values of 1% and 8%, respectively, were modified to either 5% and 12% (tauter case) or −3% and 4% (slacker case). Moreover, to examine the effects of partial meniscectomy, an internal portion of either lateral or medial meniscus at posterior–central regions was resected [see the location of resection in Figure 14.1 in Shirazi and Shirazi-Adl].[181] Finally, concurrent ACL perturbations and lateral meniscectomy was studied. In

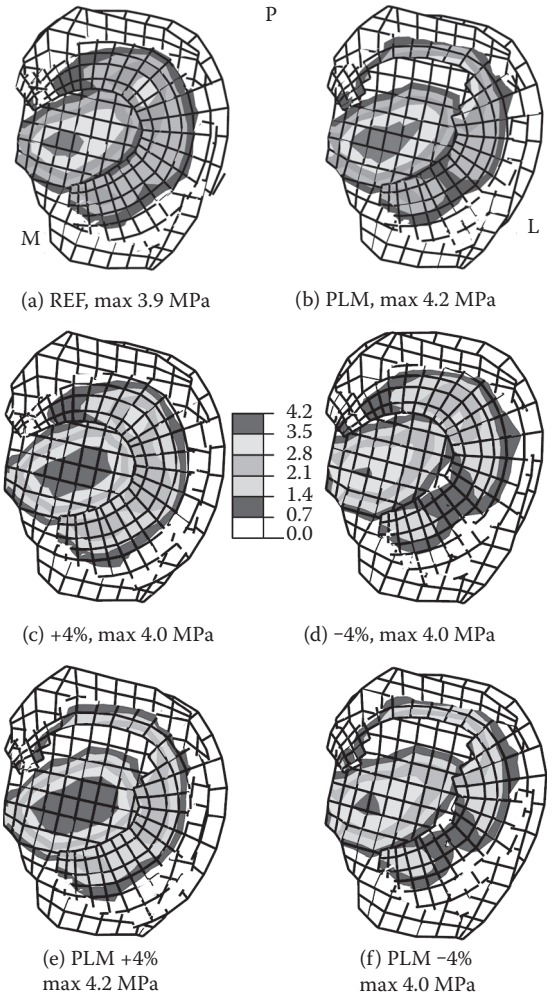

FIGURE 14.10
(See color insert.) Contact stress distribution on the lateral tibial plateau under 200 N drawer and 1500 N compression preload. (a) REF, reference intact; (b) PLM, partial lateral meniscectomy; (c) +4%, plus 4% strain in ACL pre-strain; (d) −4%, minus 4% strain in ACL pre-strain; (e) PLM +4%, combined PLM with 4% strain increase in ACL pre-strain; (f) PLM −4%: combined PLM with 4% decrease in ACL pre-strain. Note that the maximum pressure is given for each case with a common legend for ease in comparisons. L, M, and P label the lateral, medial, and posterior directions, respectively. (From Shirazi, R., and Shirazi-Adl, A., *Clin. Biomech. (Bristol, Avon)*, 24 (9), 755–761, 2009. With permission.)

the reference intact case, large ACL forces were predicted under the anterior drawer alone, which further increased by 30% with a compression preload. Increasing ACL pre-strain by 4% strain or replacing it with the stiffer patellar tendon increased the total joint contact load, particularly the portion transferred via the uncovered cartilage areas (Figure 14.10). In contrast, decreasing ACL pre-strain by 4% strain markedly decreased joint contact loads on both the covered and uncovered areas of the lateral plateau and unloaded an articular area at the anterior–central region of the lateral meniscus (Figure 14.10).

Partial lateral meniscectomy altered the load distribution patterns on the tibial plateaus and the femoral condyles by shifting the applied compression away from the menisci (covered regions) onto the cartilage at uncovered regions, in particular, on the sides of the resection (Figure 14.10). Concurrent changes in ACL pre-strain and meniscectomy further influenced contact stresses. A more slack ACL in the joint with partial lateral meniscectomy substantially decreased the load on the covered area of the lateral plateau to its minimum among all cases considered and resulted in a second unloaded area below the lateral meniscus on the anterior–central region away from the resected area (Figure 14.10). On the other hand, a more tense ACL increased the load transferred via the uncovered areas at cartilage–cartilage contact on both plateaus (Figure 14.10). Foregoing alterations further intensify in the event of greater external forces, larger meniscal resections, full ACL deficiency, and damage to the COL fibril networks.

Such studies on meniscectomy[174–176] and ACL reconstruction[180,181,187] predict substantial changes to tissue stress and strain across the joint that may cause further degenerative changes and indicate that these types of models may be used to improve or refine surgical techniques and guide postoperative therapeutic techniques. Adequate considerations of the new mechanical environment of the joint are crucial for an improved assessment of the likelihood of success in treatment attempts to avert further joint disorders.

14.4.3 Cartilage Biomechanics and Underlying Bone Injuries

Onset and progression of AC degeneration have been hypothesized to be associated with perturbations in underlying bone tissue[195] through acute injuries and chronic changes. Local alterations in the subchondral bone stiffness are expected to influence stresses and deformations in the adjacent AC, if not the entire knee joint. Overgrowth of the subchondral plate, known as bone boss,[196] as well as softening after either bone bruises[197] or degeneration[198] are commonly detected in knee joints especially after ACL injury. In trauma or repetitive impact loading, local detachments of the AC from its underlying calcified cartilage or deep COL fibrillation have been observed preceding early bone changes.[199,200] Despite extensive experimental studies on the interactions between AC and its underlying bony support,[201] the relative importance of subchondral injuries and their likely effects on the mechanical environments of both AC and bone remain poorly quantified.

Due to difficulties in controlled experimental studies of such injuries in the subchondral region as well as their detection by joint imaging, computational FEA modeling is recognized as an invaluable method to simulate perturbed conditions and to determine their effects on the joint. Although bony elements do not noticeably affect contact predictions in the intact knee joint,[175] their incorporation is essential if subchondral injuries are to be investigated. Here, we focus on a study that quantified the influence of osteochondral bone tissue defects on AC and whole joint mechanics.

An existing knee joint FEA model[4] was extended to incorporate the proximal tibial bone. The transient response of the joint was subsequently investigated under axial compressive

forces up to six times the body weight. The tibial AC was further refined, whereas the calcified cartilage, as well as the bony structure of the proximal tibia (i.e., subchondral, trabecular, and cortical bones), were added to a depth of 16 mm (Figure 14.11). Due to the stated objective, loading conditions, and the large number of finite elements in the model, the joint lateral compartment alone was simulated while neglecting the medial compartment and joint ligaments.[4] Calcified cartilage thickness was assumed constant at 0.2 mm, whereas the subchondral and cortical bone thicknesses were assumed to be 0.4 mm. Trabecular bone was simulated by six layers of brick elements with the thickness varying from 0.5 mm at the top layer to 5.0 mm at the bottom (Figure 14.11). To study the effect of tibial bone fracture, and in accordance with the literature on the size of defects,[196,202] a local region of the tibial bone and its calcified cartilage under the loaded area of the cartilage (i.e., 15% or 116 mm^2 of the lateral compartmental surface and to 7.1 mm depth; Figure 14.11)

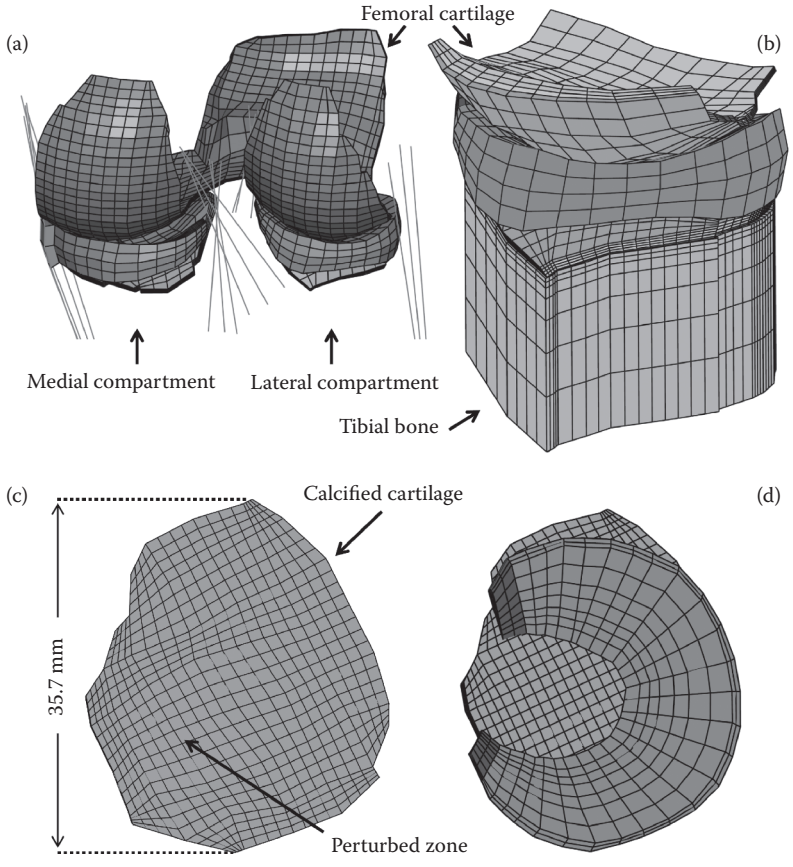

FIGURE 14.11
(See color insert.) Finite-element model. (a) Posterior view of the tibiofemoral joint (also used to extract the lateral compartment to study the effect of bone injuries on overlying AC and knee joint biomechanics). (b) Lateral compartment of the joint with the calcified cartilage and tibial bony elements (subchondral, cancellous, and cortical) incorporated. (c) Top view of the tibial lateral cartilage at the calcified region depicting the localized area for various osteochondral defect models used in this study. (d) Top view of menisci (horns in blue) and tibial AC. (From Shirazi, R. and Shirazi-Adl, A., *J. Biomech.*, 42 (15), 2458–2465, 2009. With permission.)

was weakened by reducing its elastic modulus either to $E = 20$ MPa or further to $E = 5$ MPa with Poisson's ratio of 0.0 in both cases.

The effect of a local tibial bone boss at this region was also investigated by increasing the stiffness of solid matrix brick elements at the deep one (quarter AC thickness) or two (half AC thickness) AC layers to that of the calcified cartilage ($E = 300$ MPa) or subchondral bone ($E = 3000$ MPa). In additional cases, horizontal splitting at the cartilage–bone interface was simulated by detaching the AC from the calcified cartilage at the same localized defect, thus resulting in free sliding (separation with no penetration). Moreover, the local absence of vertical COL fibrils was evaluated by removing vertical membrane elements at the deep zone in the same region. The combined effects of base split and absence of vertical fibrils with or without an underlying bone defect were also modeled in separate cases. Finally, the effect of the deformability of bony elements on the joint response was studied in the case with rigid elements for all tibial bony structures.

Briefly, localized tibial bone damage increased overall joint compliance and substantially altered both the pattern and magnitude of contact pressures and AC strains in both the tibia and the femur. These alterations were further exacerbated when bone damage was combined with base AC split and the absence of deep vertical COL fibrils. Local bone boss markedly changed contact pressures and strain patterns in neighboring AC. Bone bruise/fracture and overgrowth adversely perturbed the homeostatic balance in the mechanical environment of AC surrounding and opposing the lesion as well as the joint compliance. As such, they potentially contribute to the initiation and development of posttraumatic OA.

14.5 Summary

This chapter provides a broad introduction on the use of computational approaches, often based on FEA modeling, to study the biomechanics and mechanobiology of whole joints and their constituent tissues under normal and pathological conditions. Specifically, examples range from hard and soft tissue mechanics to G&R, effects of clinical treatments of pathological conditions including prosthetic, pharmacological, and surgical interventions, and whole joint mechanics under both intact and postsurgical conditions. The examples illustrate the broad applications of computational models and span several hierarchical levels, from individual tissue constituents (collagen, hydroxyapatite, and GAGs), to intact tissues (bone, cartilage, and meniscus), and to whole organs (femur) and joints. The benefits of such applications hinge on the accuracy and validation of the computational models.

Some recent analyses suggest that contemporary microstructural models still continue to have their shortcomings when rigorously validated against experimental data[203] and must be continually improved upon. One likely avenue for improvement is more in-depth microstructural and nanomechanical analyses. For example, recent findings on estimates of collagen elastic modulus indicate that it likely varies between the molecular, fibril, and fiber scales (by as much as one order of magnitude).[204,205] Bridging those scales, that is, from nano to micro to macro or continuum, will be a great challenge in the future that will likely improve the accuracy and value of computational models.

Experimental and computational studies work synergistically to improve each other. Accurate measurements of material properties and geometrical data by experimental

approaches provide accurate input to, and consequently improved predictions of, FEA models. Future work should include more extensive validation of computational models, especially with the development of new technologies for conducting the desired experimental studies aimed at measuring data for validation. On the other hand, computational methods such as FEA may also more effectively guide experimental protocols by providing predictive strategies to address pathological conditions such as *in vitro* tissue engineering protocols or *in vivo* surgical treatments, and thereby improve tissue and joint repair strategies.

Acknowledgments

This work was supported by grants from the National Institutes of Health (S. J. Hazelwood, R. L. Sah, and S. M. Klisch), Fonds Québécois de la Recherche sur la Nature et les Technologies (R. Shirazi), and the Donald E. Bently Center for Engineering Innovation (S. M. Klisch).

References

1. Timoshenko, S., and N. Goodier. 1951. *Theory of Elasticity*. 2nd ed. New York: McGraw Hill.
2. Ferguson, S.J., J.T. Bryant, R. Ganz, and K. Ito. 2000. The influence of the acetabular labrum on hip joint cartilage consolidation: A poroelastic finite element model. *Journal of Biomechanics* 33 (8):953–960.
3. Anderson, A.E., B.J. Ellis, S.A. Maas, C.L. Peters, and J.A. Weiss. 2008. Validation of finite element predictions of cartilage contact pressure in the human hip joint. *Journal of Biomechanical Engineering* 130 (5):051008.
4. Shirazi, R., A. Shirazi-Adl, and M. Hurtig. 2008. Role of cartilage collagen fibrils networks in knee joint biomechanics under compression. *Journal of Biomechanics* 41 (16):3340–3348.
5. Shirazi, R., and A. Shirazi-Adl. 2009. Computational biomechanics of articular cartilage of human knee joint: Effect of osteochondral defects. *Journal of Biomechanics* 42 (15):2458–2465.
6. Li, L.P., M.D. Buschmann, and A. Shirazi-Adl. 2000. A fibril reinforced nonhomogeneous poroelastic model for articular cartilage: Inhomogeneous response in unconfined compression. *Journal of Biomechanics* 33 (12):1533–1541.
7. Krishnan, R., S. Park, F. Eckstein, and G.A. Ateshian. 2003. Inhomogeneous cartilage properties enhance superficial insterstitial fluid support and frictional properties, but do not provide a homogeneous state of stress. *Journal of Biomechanical Engineering* 125 (3):569–577.
8. Wilson, W., J.M. Huyghe, and C.C. van Donkelaar. 2007. Depth-dependent compressive equilibrium properties of articular cartilage explained by its composition. *Biomechanics and Modeling in Mechanobiology* 6:43–53.
9. Julkunen, P., W. Wilson, J.S. Jurvelin, J. Rieppo, C.J. Qu, M.J. Lammi, and R.K. Korhonen. 2008. Stress–relaxation of human patellar articular cartilage in unconfined compression: Prediction of mechanical response by tissue composition and structure. *Journal of Biomechanics* 41 (9):1978–1986.
10. Shirazi, R., and A. Shirazi-Adl. 2008. Deep vertical collagen fibrils play a significant role in mechanics of articular cartilage. *Journal of Orthopaedic Research* 26 (5):608–615.
11. Suh, J.K., Z. Li, and S.L.-Y. Woo. 1995. Dynamic behavior of a biphasic cartilage model under cyclic compressive loading. *Journal of Biomechanics* 28:357–364.

12. Buschmann, M.D., Y.J. Kim, M. Wong, E. Frank, E.B. Hunziker, and A.J. Grodzinsky. 1999. Stimulation of aggrecan synthesis in cartilage explants by cyclic loading is localized to regions of high interstitial fluid flow. *Archives of Biochemistry and Biophysics* 366:1–7.
13. Yao, H., and W.Y. Gu. 2004. Physical signals and solute transport in cartilage under dynamic unconfined compression: Finite element analysis. *Annals of Biomedical Engineering* 32 (3): 380–390.
14. Parfitt, A.M. 1993. Bone age, mineral density, and fatigue damage. *Calcified Tissue International* 53 Suppl 1:S82–85; discussion S85–86.
15. Lanyon, L.E. 1987. Functional strain in bone tissue as an objective and controlling stimulus for adaptive bone remodelling. *Journal of Biomechanics* 20:1083–1093.
16. Li, X.J., W.S. Jee, S.Y. Chow, and D.M. Woodbury. 1990. Adaptation of cancellous bone to aging and immobilization in the rat: A single photon absorptiometry and histomorphometry study. *The Anatomical Record* 227 (1):12–24.
17. Aguirre, J.I., L.I. Plotkin, S.A. Stewart, R.S. Weinstein, A.M. Parfitt, S.C. Manolagas, and T. Bellido. 2006. Osteocyte apoptosis is induced by weightlessness in mice and precedes osteoclast recruitment and bone loss. *Journal of Bone and Mineral Research* 21 (4):605–615.
18. Dodd, J.S., J.A. Raleigh, and T.S. Gross. 1999. Osteocyte hypoxia: A novel mechanotransduction pathway. *American Journal of Physiology* 277 (3 Pt 1):C598–602.
19. Weinbaum, S., S.C. Cowin, and Y. Zeng. 1994. A model for the excitation of osteocytes by mechanical loading-induced bone fluid shear stresses. *Journal of Biomechanics* 27:339–360.
20. Reich, K.A., C.V. Gay, and J.A. Frangos. 1990. Fluid shear stress as a mediator of osteoblast cyclic adenosine monophosphate production. *Journal of Cellular Physiology* 143:100–104.
21. Temiyasathit, S., and C.R. Jacobs. 2010. Osteocyte primary cilium and its role in bone mechanotransduction. *Annals of the New York Academy of Sciences* 1192:422–428.
22. Mori, S., and D.B. Burr. 1993. Increased intracortical remodeling following fatigue damage. *Bone* 14 (2):103–109.
23. Verborgt, O., G.J. Gibson, and M.B. Schaffler. 2000. Loss of osteocyte integrity in association with microdamage and bone remodeling after fatigue in vivo. *Journal of Bone and Mineral Research* 15 (1):60–67.
24. Hart, R.T., and D.T. Davy. 1989. Theories of bone modeling and remodeling. In *Bone Mechanics*, edited by S.C. Cowin, 253–277. Boca Raton: CRC Press.
25. Reeve, J. 1986. A stochastic analysis of iliac trabecular bone dynamics. *Clinical Orthopaedics and Related Research* (213):264–278.
26. Thomsen, J.S., L. Mosekilde, R.W. Boyce, and E. Mosekilde. 1994. Stochastic simulation of vertebral trabecular bone remodeling. *Bone* 15 (6):655–666.
27. Mullender, M.G., and R. Huiskes. 1995. Proposal for the regulatory mechanism of Wolff's law. *Journal of Orthopaedic Research* 13 (4):503–512.
28. Lemaire, V., F.L. Tobin, L.D. Greller, C.R. Cho, and L.J. Suva. 2004. Modeling the interactions between osteoblast and osteoclast activities in bone remodeling. *Journal of Theoretical Biology* 229 (3):293–309.
29. Pivonka, P., J. Zimak, D.W. Smith, B.S. Gardiner, C.R. Dunstan, N.A. Sims, T.J. Martin, and G.R. Mundy. 2008. Model structure and control of bone remodeling: A theoretical study. *Bone* 43 (2):249–263.
30. Ryser, M.D., N. Nigam, and S.V. Komarova. 2009. Mathematical modeling of spatio-temporal dynamics of a single bone multicellular unit. *Journal of Bone and Mineral Research* 24 (5):860–870.
31. Huiskes, R., H. Weinans, and B. van Rietbergen. 1992. The relationship between stress shielding and bone resorption around total hip stems and the effects of flexible materials. *Clinical Orthopaedics and Related Research* (274):124–134.
32. Weinans, H., R. Huiskes, and H.J. Grootenboer. 1992. Effects of material properties of femoral hip components on bone remodeling. *Journal of Orthopaedic Research* 10:845–853.
33. Beaupré, G.S., T.E. Orr, and D.R. Carter. 1990. An approach for time-dependent bone modeling and remodeling-application: A preliminary remodeling simulation. *Journal of Orthopaedic Research* 8 (5):662–670.

34. Doblaré, M., and J.M. García. 2001. Application of an anisotropic bone-remodelling model based on a damage-repair theory to the analysis of the proximal femur before and after total hip replacement. *Journal of Biomechanics* 34 (9):1157–1170.
35. García-Aznar, J.M., T. Rueberg, and M. Doblaré. 2005. A bone remodelling model coupling microdamage growth and repair by 3D BMU-activity. *Biomechanics and Modeling in Mechanobiology* 4 (2–3):147–167.
36. Hazelwood, S.J., R.B. Martin, M.M. Rashid, and J.J. Rodrigo. 2001. A mechanistic model for internal bone remodeling exhibits different dynamic responses in disuse and overload. *Journal of Biomechanics* 34 (3):299–308.
37. Whalen, R.T., D.R. Carter, and C.R. Steele. 1988. Influence of physical activity on the regulation of bone density. *Journal of Biomechanics* 21 (10):825–837.
38. Burr, D.B., and R.B. Martin. 1993. Calculating the probability that microcracks initiate resorption spaces. *Journal of Biomechanics* 26 (4–5):613–616.
39. Martin, B. 1995. Mathematical model for repair of fatigue damage and stress fracture in osteonal bone. *Journal of Orthopaedic Research* 13 (3):309–316.
40. Currey, J.D. 1988. The effect of porosity and mineral content on the Young's modulus of elasticity of compact bone. *Journal of Biomechanics* 21 (2):131–139.
41. Rho, J.Y., R.B. Ashman, and C.H. Turner. 1993. Young's modulus of trabecular and cortical bone material: Ultrasonic and microtensile measurements. *Journal of Biomechanics* 26:111–119.
42. Turner, C.H., V. Anne, and R.M. Pidaparti. 1997. A uniform strain criterion for trabecular bone adaptation: Do continuum-level strain gradients drive adaptation? *Journal of Biomechanics* 30 (6):555–563.
43. Brand, R.A., D.R. Pedersen, and J.A. Friederich. 1986. The sensitivity of muscle force predictions to changes in physiologic cross-sectional area. *Journal of Biomechanics* 19 (8):589–596.
44. Heller, M.O., G. Bergmann, J.P. Kassi, L. Claes, N.P. Haas, and G.N. Duda. 2005. Determination of muscle loading at the hip joint for use in pre-clinical testing. *Journal of Biomechanics* 38 (5):1155–1163.
45. McLeish, R.D., and J. Charnley. 1970. Abduction forces in the one-legged stance. *Journal of Biomechanics* 3 (2):191–209.
46. Aamodt, A., J. Lund-Larsen, J. Eine, E. Andersen, P. Benum, and O.S. Husby. 1997. In vivo measurements show tensile axial strain in the proximal lateral aspect of the human femur. *Journal of Orthopaedic Research* 15 (6):927–931.
47. Carter, D.R. 1978. Anisotropic analysis of strain rosette information from cortical bone. *Journal of Biomechanics* 11 (4):199–202.
48. Lanyon, L.E., W.G. Hampson, A.E. Goodship, and J.S. Shah. 1975. Bone deformation recorded in vivo from strain gauges attached to the human tibial shaft. *Acta Orthopaedica Scandinavica* 46 (2):256–268.
49. Rodan, G.A. 1998. Mechanisms of action of bisphosphonates. *Annual Review of Pharmacology and Toxicology* 38:375–388.
50. Rodan, G.A., and H.A. Fleisch. 1996. Bisphosphonates: Mechanisms of action. *Journal of Clinical Investigation* 97 (12):2692–2696.
51. Mashiba, T., C.H. Turner, T. Hirano, M.R. Forwood, C.C. Johnston, and D.B. Burr. 2001. Effects of suppressed bone turnover by bisphosphonates on microdamage accumulation and biomechanical properties in clinically relevant skeletal sites in beagles. *Bone* 28 (5):524–531.
52. Nyman, J.S., O.C. Yeh, S.J. Hazelwood, and R.B. Martin. 2004. A theoretical analysis of long-term bisphosphonate effects on trabecular bone volume and microdamage. *Bone* 35 (1): 296–305.
53. Frost, H.M. 1998. On rho, a marrow mediator, and estrogen: Their roles in bone strength and "mass" in human females, osteopenias, and osteoporoses—insights from a new paradigm. *Journal of Bone and Mineral Metabolism* 16 (2):113–123.
54. Recker, R., J. Lappe, K. Davies, and R. Heaney. 2000. Characterization of perimenopausal bone loss: A prospective study. *Journal of Bone and Mineral Research* 15 (10):1965–1973.

55. Tonino, R.P., P.J. Meunier, R. Emkey, J.A. Rodriguez-Portales, C.J. Menkes, R.D. Wasnich, H.G. Bone, A.C. Santora, M. Wu, R. Desai, and P.D. Ross. 2000. Skeletal benefits of alendronate: 7-year treatment of postmenopausal osteoporotic women. Phase III Osteoporosis Treatment Study Group. *The Journal of Clinical Endocrinology and Metabolism* 85 (9):3109–3115.
56. Hurwitz, D.E., C.H. Hulet, T.P. Andriacchi, A.G. Rosenberg, and J.O. Galante. 1997. Gait compensations in patients with osteoarthritis of the hip and their relationship to pain and passive hip motion. *Journal of Orthopaedic Research* 15 (4):629–635.
57. Schmidt, R., T.E. Nowak, L. Mueller, and R.P. Pitto. 2004. Osteodensitometry after total hip replacement with uncemented taper-design stem. *International Orthopaedics* 28 (2):74–77.
58. Engh, C.A., Jr., A.M. Young, C.A. Engh, Sr., and R.H. Hopper, Jr. 2003. Clinical consequences of stress shielding after porous-coated total hip arthroplasty. *Clinical Orthopaedics and Related Research* (417):157–163.
59. Cossey, A.J., D.L. Back, A. Shimmin, D. Young, and A.J. Spriggins. 2005. The nonoperative management of periprosthetic fractures associated with the Birmingham hip resurfacing procedure. *Journal of Arthroplasty* 20 (3):358–361.
60. Lai, W.M., J.S. Hou, and V.C. Mow. 1991. A triphasic theory for the swelling and deformation behaviors of articular cartilage. *Journal of Biomechanical Engineering* 113:245–258.
61. Basser, P.J., R. Schneiderman, R.A. Bank, E. Wachtel, and A. Maroudas. 1998. Mechanical properties of the collagen network in human articular cartilage as measured by osmotic stress technique. *Archives of Biochemistry and Biophysics* 351:207–219.
62. Venn, M., and A. Maroudas. 1977. Chemical composition and swelling of normal and osteoarthrotic femoral head cartilage. I. Chemical composition. *Annals of the Rheumatic Diseases* 36 (2):121–129.
63. Mow, V.C., and A. Ratcliffe. 1997. Structure and function of articular cartilage and meniscus. In *Basic Orthopaedic Biomechanics*, edited by V.C. Mow and W.C. Hayes, 113–177. New York: Raven Press.
64. Woo, S.L-Y., P. Lubock, M.A. Gomez, G.F. Jemmott, S.C. Kuei, and W.H. Akeson. 1979. Large deformation nonhomogeneous and directional properties of articular cartilage in uniaxial tension. *Journal of Biomechanics* 12:437–446.
65. Akizuki, S., V.C. Mow, F. Muller, J.C. Pita, D.S. Howell, and D.H. Manicourt. 1986. Tensile properties of human knee joint cartilage: I. Influence of ionic conditions, weight bearing, and fibrillation on the tensile modulus. *Journal of Orthopaedic Research* 4:379–392.
66. Chang, D.G., L.M. Lottman, A.C. Chen, R.M. Schinagl, D.R. Albrecht, R.A. Pedowitz, J. Brossman, L.R. Frank, and R.L. Sah. 1999. The Depth-Dependent, Multi-Axial Properties of Aged Human Patellar Cartilage in Tension. Paper read at *Transactions of the Orthopaedic Research Society*.
67. Soltz, M.A., and G.A. Ateshian. 2000. A conewise linear elasticity mixture model for the analysis of tension-compression nonlinearity in articular cartilage. *Journal of Biomechanical Engineering* 122:576–586.
68. Korhonen, R.K., J. Toyras, M.T. Nieminen, J. Rieppo, J. Hirvonen, H.J. Helminen, and J.S. Jurvelin. 2001. Effect of Ionic Environment on the Compression-Tension Nonlinearity of Articular Cartilage in the Direction Perpendicular to Articular Surface. Paper read at *Transactions of the Orthopaedic Research Society*.
69. Elliott, D.M., D.A. Narmoneva, and L.A. Setton. 2002. Direct measurement of the Poisson's ratio of human patella cartilage in tension. *Journal of Biomechanical Engineering* 124:223–228.
70. Laasanen, M., J. Toyras, R. Korhonen, J. Rieppo, S. Saarakkala, M. Nieminen, J. Hirvonen, and J.S. Jurvelin. 2003. Biomechanical properties of knee articular cartilage. *Biorheology* 40:133–140.
71. Wang, C.C., N.O. Chahine, C.T. Hung, and G.A. Ateshian. 2003. Optical determination of anisotropic material properties of bovine articular cartilage in compression. *Journal of Biomechanics* 36 (3):339–353.
72. Charlebois, M., M.D. McKee, and M.D. Buschmann. 2004. Nonlinear tensile properties of bovine articular cartilage and their variation with age and depth. *Journal of Biomechanical Engineering* 126:129–137.

73. Chahine, N.O., C.C. Wang, C.T. Hung, and G.A. Ateshian. 2004. Anisotropic strain-dependent material properties of bovine articular cartilage in the transitional range from tension to compression. *Journal of Biomechanics* 37:1251–1261.
74. Huang, C.Y., A. Stankiewicz, G.A. Ateshian, and V.C. Mow. 2005. Anisotropy, inhomogeneity, and tension-compression nonlinearity of human glenohumeral cartilage in finite deformation. *Journal of Biomechanics* 38 (4):799–809.
75. Ficklin, T., G. Thomas, J.C. Barthel, A. Asanbaeva, E.J.-M.A. Thonar, K. Masuda, A.C. Chen, R.L. Sah, A. Davol, and S.M. Klisch. 2007. Articular cartilage mechanical and biochemical property relations before and after in vivo growth. *Journal of Biomechanics* 40:3607–3614.
76. Williams, G.M., K.J. Dills, C.R. Flores, M.E. Stender, K.M. Stewart, L.M. Nelson, A.C. Chen, K. Masuda, S.J. Hazelwood, S.M. Klisch, and R.L. Sah. 2010. Differential regulation of immature articular cartilage compressive moduli and Poisson's ratios by in vitro stimulation with IGF-1 and TGF-beta1. *Journal of Biomechanics* 43 (13):2501–2507.
77. Temple, M.M., W.C. Bae, M.Q. Chen, M. Lotz, D. Amiel, R.D. Coutts, and R.L. Sah. 2007. Age- and site-associated biomechanical weakening of human articular cartilage of the femoral condyle. *Osteoarthritis Cartilage* 15:1042–1052.
78. Donzelli, P.S., R.L. Spilker, G.A. Ateshian, and V.C. Mow. 1999. Contact analysis of biphasic transversely isotropic cartilage layers and correlations with tissue failure. *Journal of Biomechanics* 32 (10):1037–1047.
79. Maroudas, A., and M. Venn. 1977. Chemical composition and swelling of normal and osteoarthrotic femoral head cartilage. II. Swelling. *Annals of the Rheumatic Diseases* 36 (5):399–406.
80. Schinagl, R.M., D. Gurskis, A.C. Chen, and R.L. Sah. 1997. Depth-dependent confined compression modulus of full-thickness bovine articular cartilage. *Journal of Orthopaedic Research* 15:499–506.
81. Benninghoff, A. 1925. Form und Bau der Gelenkknorpel in ihren Beziehungen zur Funktion. *Zeitschrift für Zellforschung* 2:783–862.
82. Minns, R.J., and F.S. Steven. 1977. The collagen fibril organization in human articular cartilage. *Journal of Anatomy* 123 (Pt 2):437–457.
83. Broom, N.D., and D.L. Marra. 1986. Ultrastructural evidence for fibril-to-fibril associations in articular cartilage and their functional implication. *Journal of Anatomy* 146:185–200.
84. Lane, J.M., and C. Weiss. 1975. Review of articular cartilage collagen research. *Arthritis and Rheumatism* 18:553–562.
85. Redler, I., V.C. Mow, M.L. Zimny, and J. Mansell. 1975. The ultrastructure and biomechanical significance of the tidemark of articular cartilage. *Clinical Orthopaedics and Related Research* 112:357–362.
86. Broom, N.D., and C.A. Poole. 1982. A functional-morphological study of the tidemark region of articular cartilage maintained in a non-viable physiological condition. *Journal of Anatomy* 135:65–82.
87. Mow, V.C., S.C. Kuei, W.M. Lai, and C.G. Armstrong. 1980. Biphasic creep and stress relaxation of articular cartilage in compression: Theory and experiment. *Journal of Biomechanical Engineering* 102:73–84.
88. Frank, E.H., and A.J. Grodzinsky. 1987. Cartilage electromechanics—II. A continuum model of cartilage electrokinetics and correlation with experiments. *Journal of Biomechanics* 20 (6):629–639.
89. Buschmann, M.D., J. Soulhat, A. Shirazi-Adl, J.S. Jurvelin, and E.B. Hunziker. 1998. Confined compression of articular cartilage: Linearity in ramp and sinusoidal tests and the importance of interdigitation and incomplete confinement. *Journal of Biomechanics* 31:171–178.
90. Chen, A.C., W.C. Bae, R.M. Schinagl, and R.L. Sah. 2001. Depth- and strain-dependent mechanical and electromechanical properties of full-thickness bovine articular cartilage in confined compression. *Journal of Biomechanics* 34:1–12.
91. Almeida, E.S., and R.L. Spilker. 1997. Mixed and penalty finite element models for the nonlinear behavior of biphasic soft tissues in finite deformation. Part I—alternative formulations. *Computer Methods in Biomechanics and Biomedical Engineering* 1:25–46.
92. Wu, H.C., and R.F. Yao. 1976. Mechanical behavior of the human annulus fibrosus. *Journal of Biomechanics* 9 (1):1–7.

93. Weiss, J.A., B.N. Maker, and S. Govindjee. 1996. Computer methods in applied mechanics and engineering. *Computer Methods in Applied Mechanics and Engineering* 135:107–128.
94. Klisch, S.M., and J.C. Lotz. 1999. Application of a fiber-reinforced continuum theory to multiple deformations of the annulus fibrosus. *Journal of Biomechanics* 32 (10):1027–1036.
95. Eberlein, R., G.A. Holzapfel, and C.A. Schulze-Bauer. 2001. An anisotropic constitutive model for annulus tissue and enhanced finite element analyses of intact lumbar disc bodies. *Computer Methods in Biomechanics and Biomedical Engineering* 4:209–230.
96. Elliott, D.M., and L.A. Setton. 2000. A linear material model for fiber-induced anisotropy of the anulus fibrosus. *Journal of Biomechanical Engineering* 122:173–179.
97. Wagner, D.R., and J.C. Lotz. 2004. Theoretical model and experimental results for the nonlinear elastic behavior of human annulus fibrosus. *Journal of Orthopaedic Research* 22 (4):901–909.
98. Li, L.P., J. Soulhat, M.D. Buschmann, and A. Shirazi-Adl. 1999. Nonlinear analysis of cartilage in unconfined ramp compression using a fibril reinforced poroelastic model. *Clinical Biomechanics* 14 (9):673–682.
99. Soulhat, J., M.D. Buschmann, and A. Shirazi-Adl. 1999. A fibril-network-reinforced biphasic model of cartilage in unconfined compression. *Journal of Biomechanical Engineering* 121:340–347.
100. Holzapfel, G.A., T.C. Gasser, and R.W. Ogden. 2004. Comparison of a multi-layer structural model for arterial walls with a fung-type model, and issues of material stability. *Journal of Biomechanical Engineering* 126 (2):264–275.
101. Lanir, Y. 1978. Structure-strength relations in mammalian tendon. *Biophysical Journal* 24:541–554.
102. Lanir, Y. 1983. Constitutive equations for fibrous connective tissues. *Journal of Biomechanics* 16:1–12.
103. Aspden, R.M. 1994. Fibre reinforcing by collagen in cartilage and soft connective tissues. *Proceedings of the Royal Society of London. Series B* 258:195–200.
104. Schwartz, M.H., P.H. Leo, and J.L. Lewis. 1994. A microscructural model for the elastic response of articular cartilage. *Journal of Biomechanics* 27 (7):865–873.
105. Hurschler, C., B. Loitz-Ramage, and J.R. Vanderby. 1997. A structurally based stress–stretch relationship for tendon and ligament. *Journal of Biomechanical Engineering* 119:392–399.
106. Sacks, M.S. 2003. Incorporation of experimentally-derived fiber orientation into a structural constitutive model for planar collagenous tissues. *Journal of Biomechanical Engineering* 125 (2):280–287.
107. Driessen, N.J., C.V. Bouten, and F.P. Baaijens. 2005. A structural constitutive model for collagenous cardiovascular tissues incorporating the angular fiber distribution. *Journal of Biomechanical Engineering* 127 (3):494–503.
108. Gasser, T.C., R.W. Ogden, and G.A. Holzapfel. 2006. Hyperelastic modelling of arterial layers with distributed collagen fibre orientations. *Journal of the Royal Society Interface* 3:15–35.
109. Lei, F., and Z.S. Andras. 2006. The influence of fibril organization on the mechanical behaviour of articular cartilage. *Proceedings of the Royal Society A* 462:3301–3322.
110. Ateshian, G.A. 2007. Anisotropy of fibrous tissues in relation to the distribution of tensed and buckled fibers. *Journal of Biomechanical Engineering* 129 (2):240–249.
111. Quinn, T.M., and V. Morel. 2007. Microstructural modeling of collagen network mechanics and interactions with the proteoglycan gel in articular cartilage. *Biomechanics and Modeling in Mechanobiology* 6 (1–2):73–82.
112. Federico, S., and W. Herzog. 2008. Towards an analytical model of soft biological tissues. *Journal of Biomechanics* 41:3309–3313.
113. Kroon, M. 2010. A continuum mechanics framework and a constitutive model for remodelling of collagen gels and collagenous tissues. *Journal of the Mechanics and Physics of Solids* 58 (6):918–933.
114. Shirazi, R., P. Vena, R.L. Sah, and S.M. Klisch. 2011. Modeling the collagen fibril network of biological tissues as a nonlinearly elastic material using a continuous volume fraction distribution function. *Mathematics and Mechanics of Solids* 16 (7):707–716.
115. Laasanen, M.S., J. Toyras, R.K. Korhonen, J. Rieppo, S. Saarakkala, M.T. Nieminen, J. Hirvonen, and J.S. Jurvelin. 2003. Biomechanical properties of knee articular cartilage. *Biorheology* 40 (1–3):133–140.

116. Wilson, W., C.C. van Donkelaar, B. van Rietbergen, K. Ito, and R. Huiskes. 2004. Stresses in the local collagen network of articular cartilage: A poroviscoelastic fibril-reinforced finite element study. *Journal of Biomechanics* 37:357–366.
117. Wilson, W., C. van Burken, C. van Donkelaar, P. Buma, B. van Rietbergen, and R. Huiskes. 2006. Causes of mechanically induced collagen damage in articular cartilage. *Journal of Orthopaedic Research* 24 (2):220–228.
118. Julkunen, P., P. Kiviranta, W. Wilson, J.S. Jurvelin, and R.K. Korhonen. 2007. Characterization of articular cartilage by combining microscopic analysis with a fibril-reinforced finite-element model. *Journal of Biomechanics* 40 (8):1862–1870.
119. Shirazi, R., and A. Shirazi-Adl. 2005. Analysis of articular cartilage as a composite using nonlinear membrane elements for collagen fibrils. *Medical Engineering & Physics* 27 (10):827–835.
120. Thambyah, A., and N. Broom. 2006. Micro-anatomical response of cartilage-on-bone to compression: Mechanisms of deformation within and beyond the directly loaded matrix. *Journal of Anatomy* 209 (5):611–622.
121. Kaab, M.J., K. Ito, J.M. Clark, and H.P. Notzli. 1998. Deformation of articular cartilage collagen structure under static and cyclic loading. *Journal of Orthopaedic Research* 16:743–751.
122. Notzli, H., and J. Clark. 1997. Deformation of loaded articular cartilage prepared for scanning electron microscopy with rapid freezing and freeze-substitution fixation. *Journal of Orthopaedic Research* 15:76–86.
123. Bae, W.C., C.W. Lewis, M.E. Levenston, and R.L. Sah. 2006. Indentation testing of human articular cartilage: Effects of probe tip geometry and indentation depth on intra-tissue strain. *Journal of Biomechanics* 39:1039–1047.
124. Stender, M., N. Balcom, B. Berg-Johansen, K. Dills, D. Dyk, S. Hazelwood, R. Sah, and S. Klisch. 2011. Differential Regulation of Articular Cartilage Tensile Properties by IGF-1and TGF-B1 during In vitro Growth. Paper read at *International Conference on the Mechanics of Biomaterials and Tissues*, Hawaii.
125. Asanbaeva, A., K. Masuda, E.J.-M.A. Thonar, S.M. Klisch, and R.L. Sah. 2008. Cartilage growth and remodeling: Modulation of balance between proteoglycan and collagen in vitro with beta-aminopropionitrile. *Osteoarthritis Cartilage* 16:1–11.
126. Rieppo, J., M.M. Hyttinen, E. Halmesmaki, H. Ruotsalainen, A. Vasara, I. Kiviranta, J.S. Jurvelin, and H.J. Helminen. 2009. Changes in spatial collagen content and collagen network architecture in porcine articular cartilage during growth and maturation. *Osteoarthritis Cartilage* 17 (4):448–455.
127. Julkunen, P., J. Iivarinen, P.A. Brama, J. Arokoski, J.S. Jurvelin, and H.J. Helminen. 2010. Maturation of collagen fibril network structure in tibial and femoral cartilage of rabbits. *Osteoarthritis Cartilage* 18 (3):406–415.
128. van Turnhout, M.C., H. Schipper, B. Engel, W. Buist, S. Kranenbarg, and J.L. van Leeuwen. 2010. Postnatal development of collagen structure in ovine articular cartilage. *BMC Developmental Biology* 10:62.
129. Buschmann, M.D., and A.J. Grodzinsky. 1995. A molecular model of proteoglycan-associated electrostatic forces in cartilage mechanics. *Journal of Biomechanical Engineering* 117:179–192.
130. Mak, A.F. 1986. The apparent viscoelastic behavior of articular cartilage—the contributions from the intrinsic matrix viscoelasticity and interstitial fluid flows. *Journal of Biomechanical Engineering* 108:123–130.
131. Suh, J.-K., and M.R. DiSilvestro. 1999. Biphasic poroviscoelastic behavior of hydrated biological soft tissue. *Journal of Applied Mechanics* 66:528–535.
132. Huang, C.Y., V.C. Mow, and G.A. Ateshian. 2001. The role of flow-independent viscoelasticity in the biphasic tensile and compressive responses of articular cartilage. *Journal of Biomechanical Engineering* 123 (5):410–417.
133. Korhonen, R.K., M.S. Laasanen, J. Toyras, R. Lappalainen, H.J. Helminen, and J.S. Jurvelin. 2003. Fibril reinforced poroelastic model predicts specifically mechanical behavior of normal, proteoglycan depleted and collagen degraded articular cartilage. *Journal of Biomechanics* 36 (9):1373–1379.

134. García, J.J., and D.H. Cortes. 2006. A nonlinear biphasic viscohyperelastic model for articular cartilage. *Journal of Biomechanics* 39 (16):2991–2998.
135. Suh, J.K., and S. Bai. 1998. Finite element formulation of biphasic poroviscoelastic model for articular cartilage. *Journal of Biomechanical Engineering* 120:195–201.
136. DiSilvestro, M.R., and J.K. Suh. 2001. A cross-validation of the biphasic poroviscoelastic model of articular cartilage in unconfined compression, indentation, and confined compression. *Journal of Biomechanics* 34 (4):519–525.
137. Park, S., and G.A. Ateshian. 2006. Dynamic response of immature bovine articular cartilage in tension and compression, and nonlinear viscoelastic modeling of the tensile response. *Journal of Biomechanical Engineering* 128 (4):623–630.
138. Thomas, G.C., A. Asanbaeva, P. Vena, R.L. Sah, and S.M. Klisch. 2009. A nonlinear constituent based viscoelastic model for articular cartilage and analysis of tissue remodeling due to altered glycosaminoglycan–collagen interactions. *Journal of Biomechanical Engineering* 131:101002.
139. Kempson, G.E., H. Muir, C. Pollard, and M. Tuke. 1973. The tensile properties of the cartilage of human femoral condyles related to the content of collagen and glycosaminoglycans. *Biochimica et Biophysica Acta* 297:456–472.
140. Kempson, G.E., M.A. Tuke, J.T. Dingle, A.J. Barrett, and P.H. Horsfield. 1976. The effects of proteolytic enzymes on the mechanical properties of adult human articular cartilage. *Biochimica et Biophysica Acta* 428:741–760.
141. Schmidt, M.B., V.C. Mow, L.E. Chun, and D.R. Eyre. 1990. Effects of proteoglycan extraction on the tensile behavior of articular cartilage. *Journal of Orthopaedic Research* 8:353–363.
142. DiSilvestro, M.R., and J.K. Suh. 2002. Biphasic poroviscoelastic characteristics of proteoglycan-depleted articular cartilage: Simulation of degeneration. *Annals of Biomedical Engineering* 30 (6):792–800.
143. Asanbaeva, A., K. Masuda, E.J. Thonar, S.M. Klisch, and R.L. Sah. 2007. Mechanisms of cartilage growth: Modulation of balance between proteoglycan and collagen in vitro using chondroitinase ABC. *Arthritis and Rheumatism* 56:188–198.
144. Asanbaeva, A., J. Tam, B.L. Schumacher, S.M. Klisch, K. Masuda, and R.L. Sah. 2008. Articular cartilage tensile integrity: Modulation by matrix depletion is maturation-dependent. *Archives of Biochemistry and Biophysics* 474:175–182.
145. Al Jamal, R., P.J. Roughley, and M.S. Ludwig. 2001. Effect of glycosaminoglycan degradation on lung tissue viscoelasticity. *American Journal of Physiology. Lung Cellular and Molecular Physiology* 280 (2):L306–315.
146. Tanaka, E., J. Aoyama, M. Tanaka, T. Van Eijden, M. Sugiyama, K. Hanaoka, M. Watanabe, and K. Tanne. 2003. The proteoglycan contents of the temporomandibular joint disc influence its dynamic viscoelastic properties. *Journal of Biomedical Materials Research Part A* 65 (3):386–392.
147. Elliott, D.M., P.S. Robinson, J.A. Gimbel, J.J. Sarver, J.A. Abboud, R.V. Iozzo, and L.J. Soslowsky. 2003. Effect of altered matrix proteins on quasilinear viscoelastic properties in transgenic mouse tail tendons. *Annals of Biomedical Engineering* 31 (5):599–605.
148. Liao, J., and I. Vesely. 2004. Relationship between collagen fibrils, glycosaminoglycans, and stress relaxation in mitral valve chordae tendineae. *Annals of Biomedical Engineering* 32 (7):977–983.
149. Li, L.P., and W. Herzog. 2004. The role of viscoelasticity of collagen fibers in articular cartilage: Theory and numerical formulation. *Biorheology* 41 (3–4):181–194.
150. Li, L.P., W. Herzog, R.K. Korhonen, and J.S. Jurvelin. 2005. The role of viscoelasticity of collagen fibers in articular cartilage: Axial tension versus compression. *Medical Engineering & Physics* 27 (1):51–57.
151. Wilson, W., C.C. van Donkelaar, B. van Rietbergen, and R. Huiskes. 2005. A fibril-reinforced poroviscoelastic swelling model for articular cartilage. *Journal of Biomechanics* 38 (6):1195–1204.
152. Taylor, W.R., R.M. Ehrig, M.O. Heller, H. Schell, P. Seebeck, and G.N. Duda. 2006. Tibio-femoral joint contact forces in sheep. *Journal of Biomechanics* 39 (5):791–798.
153. Asanbaeva, A. 2006. Cartilage Growth and Remodeling: Modulation of Growth Phenotype and Tensile Integrity. PhD, Bioengineering, University of California, San Diego, La Jolla.

154. Guilak, F., R.L. Sah, and L.A. Setton. 1997. Physical regulation of cartilage metabolism. In *Basic Orthopaedic Biomechanics*, edited by V. C. Mow and W. C. Hayes, 179–207. New York: Raven Press.
155. Cowin, S.C., and D.M. Hegedus. 1976. Bone remodeling I: A theory of adaptive elasticity. *Journal of Elasticity* 6:313–325.
156. Cowin, S.C. 1993. Bone stress adaptation models. *Journal of Biomechanical Engineering* 115:528–533.
157. Carter, D.R., and M. Wong. 1988. Mechanical stresses and endochondral ossification in the chondroepiphysis. *Journal of Orthopaedic Research* 6 (1):148–154.
158. Cowin, S.C. 2004. Tissue growth and remodeling. *Annual Review of Biomedical Engineering* 6:77–107.
159. Ambrosi, D., G.A. Ateshian, E. Arruda, S. Cowin, J. Dumais, A. Goriely, G. Holzapfel, J.D. Humphrey, R. Kemkemer, E. Kuhl, J. Olberding, L.A. Taber, and K. Garikipati. 2011. Perspectives on biological growth and remodeling. *Journal of the Mechanics and Physics of Solids* 59:863–883.
160. Davol, A., M.S. Bingham, R.L. Sah, and S.M. Klisch. 2008. A nonlinear finite element model of cartilage growth. *Biomechanics and Modeling in Mechanobiology* 7 (4):295–307.
161. Ficklin, T.P., A. Davol, and S.M. Klisch. 2009. Simulating the growth of articular cartilage explants in a permeation bioreactor to aid in experimental protocol design. *Journal of Biomechanical Engineering* 131:041008:1–11.
162. Wilson, W., N.J. Driessen, C.C. van Donkelaar, and K. Ito. 2006. Prediction of collagen orientation in articular cartilage by a collagen remodeling algorithm. *Osteoarthritis Cartilage* 14 (11):1196–1202.
163. Kuhl, E., R. Maas, G. Himpel, and A. Menzel. 2007. Computational modeling of arterial wall growth. Attempts towards patient-specific simulations based on computer tomography. *Biomechanics and Modeling in Mechanobiology* 6 (5):321–331.
164. Socci, L., G. Pennati, F. Gervaso, and P. Vena. 2007. An axisymmetric computational model of skin expansion and growth. *Biomechanics and Modeling in Mechanobiology* 6 (3):177–188.
165. Socci, L., G. Pennati, D. Gastaldi, and P. Vena. 2008. Modeling and mechanobiology of cerebral aneurysms. *Journal of Applied Biomaterials & Biomechanics* 6 (2):63–71.
166. Ramasubramanian, A., and L.A. Taber. 2008. Computational modeling of morphogenesis regulated by mechanical feedback. *Biomechanics and Modeling in Mechanobiology* 7 (2):77–91.
167. Young, J.M., J. Yao, A. Ramasubramanian, L.A. Taber, and R. Perucchio. 2010. Automatic generation of user material subroutines for biomechanical growth analysis. *Journal of Biomechanical Engineering* 132 (10):104505.
168. Carter, D.R., and M. Wong. 2003. Modelling cartilage mechanobiology. *Philosophical Transactions of the Royal Society of London. Series B, Biological Sciences* 358 (1437):1461–1471.
169. Klisch, S.M. 2006. Continuum models of growth with special emphasis on articular cartilage. In *Mechanics of Biological Tissue*, edited by G.A. Holzapfel and R.W. Ogden, 119–133. Berlin, Heidelberg: Springer-Verlag.
170. Davol, A., R.L. Sah, and S.M. Klisch. 2005. A Cartilage Growth Finite Element Model for Simulation of In vitro Unconfined Compression. Paper read at *International Conference on the Mechanics of Biological Tissue*.
171. Jin, M., E.H. Frank, T.M. Quinn, E.B. Hunziker, and A.J. Grodzinsky. 2001. Tissue shear deformation stimulates proteoglycan and protein biosynthesis in bovine cartilage explants. *Archives of Biochemistry and Biophysics* 395 (1):41–48.
172. Hodge, W.A., R.S. Fijan, K.L. Carlson, R.G. Burgess, W.H. Harris, and R.W. Mann. 1986. Contact pressures in the human hip joint measured in vivo. *Proceedings of the National Academy of Sciences of the United States of America* 83:2879–2883.
173. Buckwalter, J.A., and H.J. Mankin. 1998. Articular cartilage: Degeneration and osteoarthritis, repair, regeneration, and transplantation. *Instructional Course Lectures* 47:487–504.
174. Bendjaballah, M.Z., A. Shirazi-Adl, and D.J. Zukor. 1995. Biomechanics of the human knee joint in compression: Reconstruction, mesh generation and finite element analysis. *The Knee* 2 (2):69–79.

175. Donahue, T.L., M.L. Hull, M.M. Rashid, and C.R. Jacobs. 2002. A finite element model of the human knee joint for the study of tibio-femoral contact. *Journal of Biomechanical Engineering* 124 (3):273–280.
176. Pena, E., B. Calvo, M.A. Martinez, D. Palanca, and M. Doblaré. 2005. Finite element analysis of the effect of meniscal tears and meniscectomies on human knee biomechanics. *Clinical Biomechanics (Bristol, Avon)* 20 (5):498–507.
177. Moglo, K.E., and A. Shirazi-Adl. 2005. Cruciate coupling and screw-home mechanism in passive knee joint during extension—flexion. *Journal of Biomechanics* 38 (5):1075–1083.
178. Jilani, A., A. Shirazi-Adl, and M.Z. Bendjaballah. 1997. Biomechanics of human tibio-femoral joint in axial rotation. *The Knee* 4 (4):203–213.
179. Bendjaballah, M.Z., A. Shirazi-Adl, and D.J. Zukor. 1997. Finite element analysis of human knee joint in varus–valgus. *Clinical Biomechanics (Bristol, Avon)* 12 (3):139–148.
180. Moglo, K.E., and A. Shirazi-Adl. 2003. On the coupling between anterior and posterior cruciate ligaments, and knee joint response under anterior femoral drawer in flexion: A finite element study. *Clinical Biomechanics (Bristol, Avon)* 18 (8):751–759.
181. Shirazi, R., and A. Shirazi-Adl. 2009. Analysis of partial meniscectomy and ACL reconstruction in knee joint biomechanics under a combined loading. *Clinical Biomechanics (Bristol, Avon)* 24 (9):755–761.
182. Aspden, R.M., Y.E. Yarker, and D.W. Hukins. 1985. Collagen orientations in the meniscus of the knee joint. *Journal of Anatomy* 140 (Pt 3):371–380.
183. Haut, R.C., and R.W. Little. 1972. A constitutive equation for collagen fibers. *Journal of Biomechanics* 5 (5):423–430.
184. Morgan, F.R. 1960. Mechanical properties of collagen and leather fibres. *American Leather Chemists Association Journal* 55 (1):4–23.
185. Shirazi-Adl, S.A., S.C. Shrivastava, and A.M. Ahmed. 1984. Stress analysis of the lumbar disc-body unit in compression. A three-dimensional nonlinear finite element study. *Spine* 9 (2):120–134.
186. Mesfar, W., and A. Shirazi-Adl. 2006. Knee joint mechanics under quadriceps—hamstrings muscle forces are influenced by tibial restraint. *Clinical Biomechanics (Bristol, Avon)* 21 (8):841–848.
187. Mesfar, W., and A. Shirazi-Adl. 2006. Biomechanics of changes in ACL and PCL material properties or prestrains in flexion under muscle force-implications in ligament reconstruction. *Computer Methods in Biomechanics and Biomedical Engineering* 9 (4):201–209.
188. Besier, T.F., G.E. Gold, G.S. Beaupré, and S.L. Delp. 2005. A modeling framework to estimate patellofemoral joint cartilage stress in vivo. *Medicine and Science in Sports and Exercise* 37 (11):1924–1930.
189. Mesfar, W., and A. Shirazi-Adl. 2008. Computational biomechanics of knee joint in open kinetic chain extension exercises. *Computer Methods in Biomechanics and Biomedical Engineering* 11 (1):55–61.
190. Butler, D.L., M.D. Kay, and D.C. Stouffer. 1986. Comparison of material properties in fascicle-bone units from human patellar tendon and knee ligaments. *Journal of Biomechanics* 19 (6): 425–432.
191. Indelicato, P.A., and E.S. Bittar. 1985. A perspective of lesions associated with ACL insufficiency of the knee. A review of 100 cases. *Clinical Orthopaedics and Related Research* (198):77–80.
192. Noyes, F.R., R.W. Bassett, E.S. Grood, and D.L. Butler. 1980. Arthroscopy in acute traumatic hemarthrosis of the knee. Incidence of anterior cruciate tears and other injuries. *Journal of Bone and Joint Surgery. American Volume* 62 (5):687–695, 757.
193. van der Hart, C.P., M.P. van den Bekerom, and T.W. Patt. 2008. The occurrence of osteoarthritis at a minimum of ten years after reconstruction of the anterior cruciate ligament. *Journal of Orthopaedic Surgery and Research* 3:24.
194. Rangger, C., T. Klestil, W. Gloetzer, G. Kemmler, and K.P. Benedetto. 1995. Osteoarthritis after arthroscopic partial meniscectomy. *The American Journal of Sports Medicine* 23 (2):240–244.
195. Radin, E.L., and R.M. Rose. 1986. Role of subchondral bone in the initiation and progression of cartilage damage. *Clinical Orthopaedics and Related Research* (213):34–40.

196. Henderson, I.J., and D.P. La Valette. 2005. Subchondral bone overgrowth in the presence of full-thickness cartilage defects in the knee. *Knee* 12 (6):435–440.
197. Meyer, E.G., T.G. Baumer, J.M. Slade, W.E. Smith, and R.C. Haut. 2008. Tibiofemoral contact pressures and osteochondral microtrauma during anterior cruciate ligament rupture due to excessive compressive loading and internal torque of the human knee. *The American Journal of Sports Medicine* 36 (10):1966–1977.
198. Boyd, S.K., R. Muller, and R.F. Zernicke. 2002. Mechanical and architectural bone adaptation in early stage experimental osteoarthritis. *Journal of Bone and Mineral Research* 17 (4):687–694.
199. Meachim, G., and G. Bentley. 1978. Horizontal splitting in patellar articular cartilage. *Arthritis and Rheumatism* 21 (6):669–674.
200. Radin, E.L., R.B. Martin, D.B. Burr, B. Caterson, R.D. Boyd, and C. Goodwin. 1984. Effects of mechanical loading on the tissues of the rabbit knee. *Journal of Orthopaedic Research* 2:221–234.
201. Karsdal, M.A., D.J. Leeming, E.B. Dam, K. Henriksen, P. Alexandersen, P. Pastoureau, R.D. Altman, and C. Christiansen. 2008. Should subchondral bone turnover be targeted when treating osteoarthritis? *Osteoarthritis Cartilage* 16 (6):638–646.
202. Karataglis, D., M.A. Green, and D.J. Learmonth. 2006. Autologous osteochondral transplantation for the treatment of chondral defects of the knee. *Knee* 13 (1):32–35.
203. Thomopoulos, S., G.M. Fomovsky, P.L. Chandran, and J.W. Holmes. 2007. Collagen fiber alignment does not explain mechanical anisotropy in fibroblast populated collagen gels. *Journal of Biomechanical Engineering* 129 (5):642–650.
204. Gautieri, A., S. Vesentini, A. Redaelli, and M.J. Buehler. 2010. Hierarchical nanomechanics of collagen microfibrils. *Nature Precedings*: hdl:10101/npre.2010.4995.1: Posted 11 Oct 2010.
205. Gautieri, A., S. Vesentini, A. Redaelli, and M.J. Buehler. 2011. Hierarchical structure and nanomechanics of collagen microfibrils from the atomistic scale up. *Nano Letters* 11 (2):757–766.

15

Clinical Gait Analysis

Richard Baker

CONTENTS

15.1 Introduction

More than 10% of the adult population has some difficulty walking 400 m, and in the elderly, this figure increases to more than 50%.[1,2] Many professionals, including physiotherapists, prosthetists, orthotists, podiatrists, and specialists in orthopedic rehabilitation and neurological medicine, devote a considerable part of their working lives to helping such people walk more easily. Many of the interventions that these professionals administer are based on an assessment of how the individual walks, and this is largely based on direct observation. In this sense, "clinical gait analysis" is as old as the above professions. Pioneers such as the neurologist Guillaume Duschenne (1806–1875) and the orthopedic surgeon Freiderich Trendelenberg (1844–1924) made considerable use of their observational skills to inform their clinical practice. Over the last 30 years, however, technologies have been developed to measure various aspects of walking and have been incorporated into clinical services to make this information available to health professionals. It is clinical gait analysis, in this sense, that is the focus of this chapter.

Walking in the community is an immensely complex and variable activity. Walking in a straight line at consistent speed constitutes a very small part of our normal physical activity. Starting, stopping, turning, maneuvering around obstacles and other people, adapting to different terrain, accelerating and decelerating, and ascending and descending a variety of inclines and stairs are all important aspects of functional walking. More than 40% of walking is in bouts of less than 13 steps and 75% of walking is in bouts of less than 41 steps.[3] Clinical gait analysis focuses on straight-line walking in an idealized environment, not because of the belief that this represents "normal walking" but because this is a well-defined stereotypical activity that provides a window into the general function of the human locomotor system. It is generally assumed that basing clinical interventions on this insight will lead to improved capability and performance for the much broader range of walking activities.

Clinical gait analysis has two elements that are of interest to the biomechanist. The first is the measurement process and the second is the interpretation placed on the measurements taken. Making measurements is, in principle, an objective process. Here, the use of the phrase "in principle" is important. The validation of technology to measure movements of the human body is extremely challenging. There are no irrefutable gold standards for making measurements, and all of the current techniques have considerable inherent limitations. Even the conceptual biomechanical basis is challenging because it requires imposing a degree of mathematical regularity and uniformity on body structures and functions that are far from regular or uniform. The interpretive process is more transparently subjective. There is, as yet, no general unified theory of why we walk the way we do, and the clinical interpretation of data still varies considerably from one facility to another. A substantial amount of work is still required to develop an understanding of the biomechanics of walking to a level where clinical decision making can be deemed as objective- and evidence-based. There is thus still a crucially important role for biomechanical engineers within clinical gait analysis to address the challenges of both making measurements *and* interpreting the meaning of those measurements. The aim of this chapter is to outline those challenges.

15.2 Biomechanical Concepts

15.2.1 Gait Cycle and Temporal Spatial Parameters

Clinical gait analysis is based on the assumption that straight-line walking in an idealized environment is a stereotypical and repetitious activity. The unit of repetition is the *gait cycle*, which, from the perspective of either leg, comprises a *stance phase* (when the foot is in contact with the ground) and a *swing phase* (when the leg is moving freely above the ground). By convention, the gait cycle starts at the instant that the swing foot makes contact with the floor (*foot contact*) and continues until the same foot once again makes contact with the floor at the next foot contact. The historical term *heel strike* is seldom used because it may not be the heel that makes contact with the ground, and, in most people, the foot is better considered as being placed on the ground rather than striking it. Similarly, *foot off* is preferred to *toe off* to describe the division between the stance and swing phases. Natural subdivisions of stance arise when considering the other limb. Both feet are in contact with the ground in early stance (until *opposite foot off*), and this is described as *first*

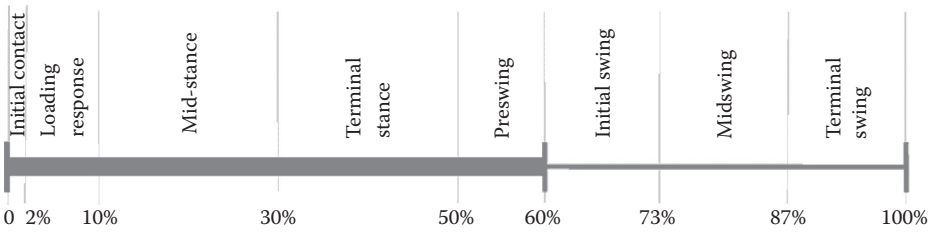

FIGURE 15.1
Subdivisions of gait cycle. Percentages refer to approximate timings as a proportion of the gait cycle for healthy adults.

TABLE 15.1

Temporal–Spatial Parameters Describing Walking

Parameter	Definition
Stride length	Distance between any point on the foot between one initial contact and the next for the same limb in the direction of walking
Step length	Distance by which a point on the foot is in front of the same point on the other foot at initial contact in the direction of walking
Stride time	Time between one initial contact and the next for the same limb
Cadence	Number of steps or strides per unit time; most often quoted as "steps per minute"
Walking speed	Average speed of movement over a gait cycle (equivalent to stride length divided by stride time)
Step/stride width	The distance between the feet at initial contact perpendicular to the direction of walking
Stance/swing/single support/ double support time	Time spent in a specific phase often described as a percentage of stride time

double support. After this, there is a period of *single support* until *opposite foot contact*, after which *second double support* lasts until foot off. Further subdivisions of the gait cycle are largely arbitrary. Despite having several deficiencies, Perry's subdivisions are the most widely accepted (Figure 15.1).

With the general gait cycle defined, a number of interrelated temporal spatial parameters can be used to give a general impression of how walking is achieved (Table 15.1). A particular distinction is between a *step*, which is the act of moving one foot in front of the other, and a *stride*, which is the combination of consecutive steps of opposite limbs. Modified definitions have been proposed for walking that is not constrained to a straight line.[4]

15.2.2 Gait Graphs

Most clinical gait analysis focuses on the variation of a number of continuous variables across the gait cycle. Kinematic variables describe movement generally in terms of joint angles. Kinetic variables describe loads such as the applied ground reaction or joint moments. All these are plotted on *gait graphs*, which have a consistent format (Figure 15.2). Data from different sides are most easily compared by the use of different colors (not illustrated).

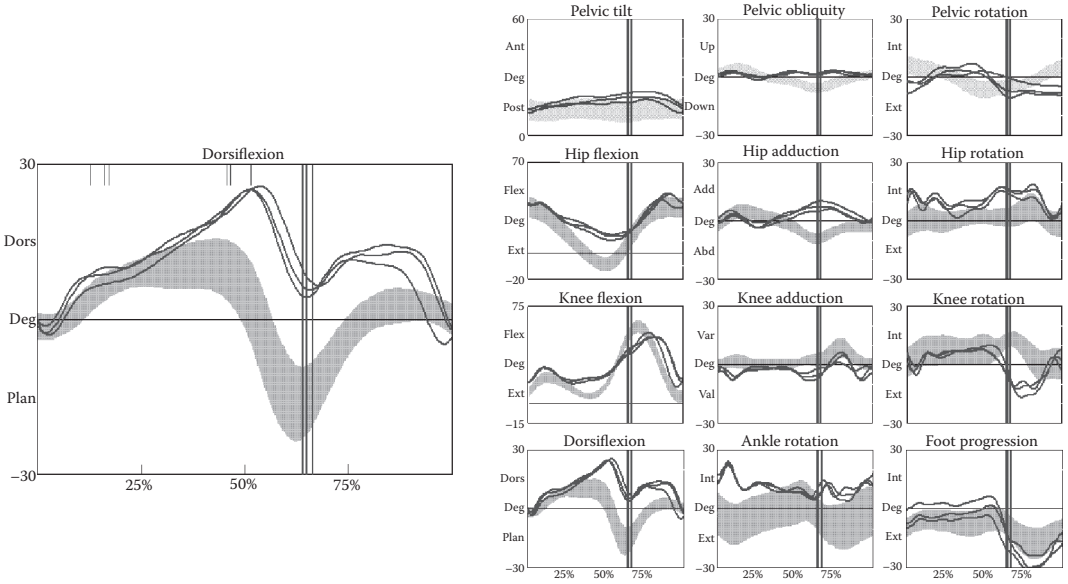

FIGURE 15.2
Standard layout of an individual gait graph and an array of gait graphs. Data from each gait cycle are time-normalized to fit across the horizontal axis, which is labeled as a percentage of the gait cycle. The timing of toe off is indicated by a vertical line across the entire height of the graph and that of opposite foot off and foot contact by tick marks at the top of the graph. It is common to find normative data plotted in the background as a bar representing the ±1 SD range. There is always some degree of variability between data from different gait cycles, and this variability can be an important characteristic of the gait pattern. It can be represented graphically by overplotting data from several cycles on the same axes.

Different related variables are often plotted on adjacent graphs in an array. In Figure 15.2, data for three-dimensional (3D) joint angles are plotted, with each row representing a different joint and each column representing a different plane. Consistent plotting of such arrays can greatly aid in their interpretation. Data can look very different when plotted using different scales or aspect ratios, and it is generally considered to be best practice to keep these consistent for any particular gait analysis service.

15.2.3 Kinematics

Kinematic analysis is based on the assumption that the skeleton can be modeled as a number of rigid bodies corresponding to bones or groups of bones. An orthogonal coordinate system (CS) is defined as being embedded in each segment (Figure 15.3). Although there is general agreement that these systems are aligned with the major anatomical planes (sagittal, coronal, and transverse), the precise definition of these segments is open to some interpretation. Attempts have been made to standardize conventions across biomechanics,[5,6] but those used in clinical gait analysis do not always conform. It is almost universal, for example, for the proximal–distal axis of the tibia to pass from the ankle joint axis to the knee joint axis in clinical gait analysis.[7] Even with consistent definitions, the identification of landmarks can be difficult. This has led to a recent shift in the use of functional definitions of CSs.[8]

A variety of different assumptions can be made about how these rigid bodies are linked. Models with six degrees of freedom, which make no assumptions about joint constraints, have recently achieved some popularity.[9,10] Most models, however, assume some

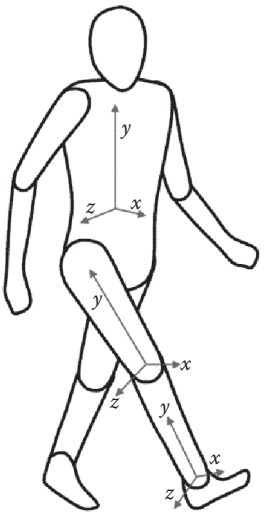

FIGURE 15.3
Orthogonal CSs for the right tibia, femur, and the trunk segments. The International Society of Biomechanics convention labels *x* as anterior, *y* as proximal, and *z* as lateral.

constraints. The hip is generally assumed to be a ball-and-socket joint described by three rotational degrees of freedom. There is less consensus for the knee. The earliest models used in clinical gait analysis assumed a ball joint,[11,12] but more recent approaches have included both a simple hinge joint and a hinge joint with constrained joint translations,[13] among others. There is even less agreement at the ankle and within the foot. Most clinical gait analyses assume that the foot is a single segment linked to the tibia by a joint of either two or three degrees of rotational freedom. Over the last few years, however, there has been interest in a variety of models and methods describing the foot as a number of different segments.[14–18]

3D joint angles are the primary kinematic output used in clinical gait analysis. Joint angles are not vector quantities, and, although most gait analysts understand the general meaning of the terms, precise definitions are less well understood. Three broad systems have been used: Cardan/Euler angles,[19] the joint CS,[20] and globographic angles.[21] Although these are often regarded as different, the mathematical equivalence of the three systems has recently been established.[22] All three require choices to be made that can be referred to as sequence, configuration, or orientation dependence, which affect the calculated angles. Globographic representation is the oldest, and perhaps the least ambiguous, method to visualize with the orientation of the principal axis of the distal segment being represented on a spherical grid (Figure 15.4). For the hip, flexion is analogous to longitude (the angular distance around the bipolar axis), abduction is analogous to latitude (movement out of the equatorial plane), and internal–external rotation is the movement around the principal axis (which is actually equivalent to surface bearing, the measurement on a compass). There has been an assumption that the same convention can be used to describe all joints,[5,6] but Baker[7] has argued that, for the biomechanically defined angles to correspond with conventional clinical terms, the convention must reflect the anatomical characteristics of each joint. Pelvic coronal plane obliquity, for example, will not accurately reflect the relative height of the hip joint centers if the convention adopted for the hip and knee is applied to the pelvis.[23]

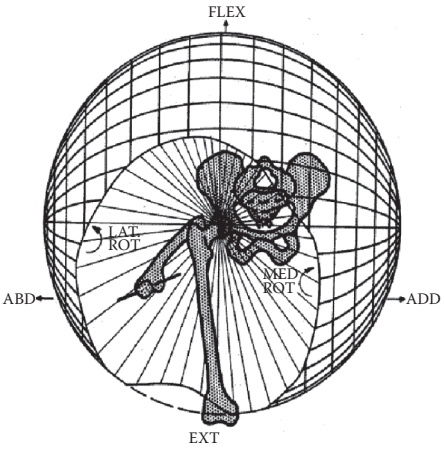

FIGURE 15.4
Globographic representation of hip joint angles. FLEX, flexion; EXT, extension; ABD, abduction; ADD, adduction; LAT ROT, lateral rotation; MED ROT, medial rotation. (Adapted from Dempster, W. T. *Space Requirements of the Seated Operator (WADC Technical Report:55–159).* Ohio: Wright-Patterson Airforce Base, 1956. With kind permission from Springer Science+Business Media: *Lehrbuch Der Muskel Und Gelenkmechanik*, 1917, Strasser, H.)

Although joint angles are the focus of kinematic analysis in clinical gait analysis, other outputs from more complex analyses are becoming more common. The most important of these are the calculations of musculotendinous unit lengths (often referred to as *muscle lengths*). In these analyses, the distance between a tendon's origin on one bone and the corresponding insertion on another is calculated. This is often calculated as a straight line distance but, via points or wrapping surfaces,[24] can be incorporated in more advanced modeling packages. These can be extremely useful in assessing whether biarticular muscles are functioning concentrically or eccentrically (shortening or being stretched), which cannot be easily deduced by considering the joint angles separately.

15.2.4 Kinetics

Kinetic measures in clinical gait analysis originate from measurements of the ground reaction. Despite this, it is fairly common to find clinical services ignoring direct representation of the ground reaction and focusing on how this is reflected in measurements of joint moments and powers. Joint moments represent the net moment exerted by the ground reaction on a joint once the effects of gravity and inertia on segments distal to the joint have been accounted for by an inverse dynamic analysis; in this way, it is possible for joint moments to be recorded during the swing as well as stance phases. Moments calculated in this way must be opposed by equal and opposite moments exerted by internal structures. It is often assumed that these are exerted by muscles, but ligaments and other soft tissues crossing the joints may also be involved. It is also important to note that the muscles generally act in agonist–antagonist pairs to exert moments. The agonist acts to cause the movement of the joint in one direction, and the antagonist, on the opposing side of the joint, acts to cause movement in the opposite direction. Moments required by the agonist muscles may be considerably greater than the net external moment if there is antagonistic activity in the muscles crossing a joint. Joint moments are a vector quantity,

and there is no ambiguity in how they should be calculated. They are almost always presented as orthogonal components about the principal axes of the CS of either the proximal or distal segment. It has been suggested that presenting components about the three axes of the joint CS may be more clinically insightful.[25] In this case, the moment will represent the net activity in the muscle groups with a specific anatomical arrangement (e.g., the hip abductors/adductors). Joint power calculations are also common, being the scalar product of joint angular velocity and joint moment.[26] These represent the power that would have to be exerted at individual joints if each joint were independently actuated. Considerable care is required in interpreting power data, however, because many important muscles act across multiple joints, violating this assumption.

Forward dynamics, in which the muscle activations required to drive the body to match a specific pattern of movement are calculated, has become an important part of contemporary biomechanics.[27–29] Given that there are many more muscles than there are joint degrees of freedom in the lower limbs, this is a redundant problem, and some form of optimization is required to choose a particular set of muscle activations. This also requires a model of how the ground reaction responds to changes in muscle activation, which is not straightforward. In principle, such techniques allow the specific function of different muscles to be identified[30–32] and should allow the modeling of the effect of interventions that might influence muscle activations or the geometry of the musculoskeletal system.[33,34] In the past, the time taken to format data for these techniques prohibited routine clinical use, but recent advances have largely overcome this. They are, however, known to be sensitive to modeling assumptions such as how to scale anatomical data to fit individuals. This can be a particular issue in clinical gait analysis, in which the person being analyzed often has an abnormal musculoskeletal anatomy.[35] Nowadays, such models offer broad general insights but will only be of limited clinical applicability until these sensitivity issues are more fully understood. The cumulative effect of these results is very poorly understood, and these data are rarely used in clinical gait analyses.

15.2.5 Electromyography

Electromyography (EMG) uses measurements of the electrical activity arising from muscles as an indicator of which muscles are acting at different times in the gait cycle. The raw signal comprises many superimposed high-frequency pulses (action potentials) arising from the firing of different motor units within the muscles. The magnitude of the signal is influenced by a number of factors such as the impedance of the muscle itself, of any subcutaneous tissues, and of the skin–electrode interface. Accordingly, the emphasis in clinical practice is generally on the phasing and timing of muscle activity. The different stages of signal processing are illustrated in Figure 15.5. The raw signal is first half-wave rectified. A range of filters can then be used to detect the overall pattern or "envelope" of activity. Some evaluation centers go even further and determine whether a muscle is active or inactive depending on whether the value of this envelope is greater than a certain threshold level. Raw signals often seem to show rapid onset or ending of muscle activity, however, and these can be masked by envelope filtering. Many analysts feel that any processing of the data reduces the information content and prefer to review the raw signal. EMG signals tend to exhibit more cycle-to-cycle variability than kinematics or kinetics, and, because of inherent difficulties in overplotting the raw signals, data from several cycles are often plotted side by side. EMG is most useful in conditions that affect the central nervous system, such as in cerebral palsy (CP) or stroke, when excessive antagonistic activity might be expected at joints, and joint moments may be inappropriate as indicators of muscle group function.

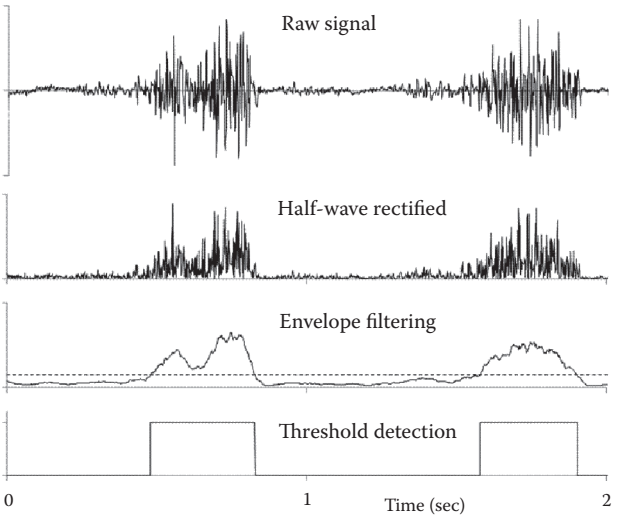

FIGURE 15.5
Different stages of signal processing for clinical EMG from the gastrocnemius muscle over two gait cycles.

15.2.6 Other Biomechanical Data

Kinematics, kinetics, and EMG form the core measurements of most clinical gait analysis systems. Other data can be useful. Perhaps the most obvious is simple digital video. This can provide additional information that is not incorporated in standard kinematic or kinetic models. The alignment of different segments of a deformed foot, for example, is not specified by many widely used kinematic models but is generally apparent from good quality video recordings. Digital video is also extremely useful as a quality assurance tool. It is also useful to orient the analyst to the person being analyzed. It may not be obvious from the kinematic data, for example, what combination of walking aids a person was using or that markers could only be placed on clothing, an action that might affect data quality.

The force per unit area applied under the foot during the stance phase is generally referred to as "foot pressure" and can also provide valuable information either independently or in association with kinematic and kinetic data, particularly in pathologies that make skin on the foot susceptible to breaking down. Oxygen consumption measurements have also been proposed as general measures of the efficiency of walking.[36] Collecting high-quality kinematic, kinetic, and EMG data, however, takes considerable time. This is a particular issue in persons with disability who are often either young or elderly and who may struggle to cooperate physically or mentally for extended periods. In most centers, therefore, the focus of clinical gait analysis is on kinematics, kinetics, and EMG.

15.3 Measurement Technology

15.3.1 Kinematic Measurement Systems

Most commercially available clinical gait analysis systems are essentially kinematic measurement systems. Passive marker-based systems are, by far, the most common. In these

systems, retroreflective spherical markers are placed on a person's skin using hypoallergenic double-sided sticky tape. Light in the visible or infrared spectrum is emitted from an annular source around a camera lens, reflects off the markers, and is detected on the charge-coupled device sensor of a video camera. Stroboscopic pulsing of high-intensity light over very short durations makes such systems relatively insensitive to ambient light conditions (the latest generation of analysis systems are capable of capturing data outdoors in full sunlight) and reduces blurring of the moving markers. As with other forms of digital video, the sensor resolution has improved markedly in recent years, with 16 megapixel cameras operating at up to 120 frames per second at full resolution being commercially available now. Perhaps even more importantly, digital image processing using full grayscale bandwidth has dramatically increased the effective resolution of modern cameras. Modern systems use multiple cameras to ensure that the markers can be seen anywhere on the person. A state-of-the-art clinical facility might now use 10 cameras allowing up to 50 markers of 5 mm diameter to be tracked to a resolution of less than 1 mm. As digital imaging technology has improved, the real cost of entry-level systems has dropped consistently over the years at the same time as the effective resolution has improved. Systems from the leading manufacturers are still a considerable expense. Within the last year, new suppliers have entered the market, offering products at as little as 10% of the price of standard systems. Neither the quality of these systems nor the potential impact on the market of these new products has yet been properly assessed.

A small number of systems use active markers, powered light sources placed on the person's skin. The requirement for a power source often also requires bigger markers or that the markers to be linked by cables, but the use of color or other coding schemes can greatly simplify marker tracking. The number of systems that use inertial sensors (often incorporating gyroscopes, accelerometers, and magnetometers) is increasing as sophisticated processing technologies are allowing the inherent problems of drift (in integrating inertial signals) and magnetic field variability (for magnetometers) to be minimized.

An important, but essentially mundane, role for biomechanists in the past has been to operate, analyze data from, and maintain complex kinematic measurement systems. Despite systems becoming more reliable and more automated, this role has not yet disappeared entirely. Although almost all stages of the data capture workflow could be automated (and indeed have been) in different products, the manufacturers have generally been extremely slow to produce reliable, fully automated data capture systems. They still also tend to sell complex systems with considerable flexibility for a range of different applications, which makes them over complex for the limited technical demands of clinical gait analysis. In many centers, there is still a belief that professional biomechanists are required to oversee this type of measurement equipment, but the key professional role for biomechanists in clinical gait analysis is undoubtedly in ensuring the appropriate interpretation of data once captured.

15.3.2 Kinematic Modeling

Marker-based systems, by definition, record the position of markers, and some sort of processing is required to obtain the joint angles, or *pose*, from these positional data. Most clinical gait analyses use the conventional gait model (CGM), also known as the Davis or Newington,[11] Helen Hayes,[12,37] or Vicon Clinical Manager or Plug-in Gait model (Vicon, Oxford, UK). This approach calculates segment axes from markers that are placed over specific anatomical landmarks. Another early method was the calibrated anatomical systems technique (CAST),[38,39] which proposed that clusters of markers on a rigid plate should

be attached to each segment to define a *technical* CS while the person was walking. The orientation of the *anatomical* CS relative to the technical CS is then determined in a separate calibration process during which the person stands still and relevant anatomical landmarks are identified either using some pointing device with markers attached or by placing additional markers on the skin. Comparison of the CGM and CAST techniques[10] shows considerable differences between them, particularly in the transverse plane, suggesting that they are influenced in different ways by the movement of the soft tissues.

There are shortcomings with both approaches, making repeatable measurement difficult. Even in centers of clinical excellence, measurement variability is often of a similar magnitude to changes that are considered to indicate pathology.[40] The main reason for this is the difficulty in accurately placing markers in relation to anatomical landmarks. These landmarks are generally features of the bony anatomy (e.g., lateral malleolus, anterior superior iliac spine), which can be felt through the skin; they are used to guide marker placement but also serve to define the CS for each segment. They are often broad and poorly defined, vary between individuals, and may be particularly difficult to identify in people with a high body mass index. The accuracy, as well as the repeatability, of both approaches is also limited. The predominant factor in this is the movement of markers, or clusters of markers, with respect to the underlying bone as a consequence of the movement of the underlying soft tissues as the person walks. This is now widely known as *soft-tissue artifact* (STA).[41] This motion can be considerable,[42–45] even in relatively slim people, and is assumed to increase with body mass. Neither the CGM nor CAST is based on an explicit underlying model (despite the name of the CGM). The assumptions on which they are based are thus implicit, poorly understood, and often incompatible with the kinetic or advanced kinematic models for which their outputs serve as inputs. To address these limitations, research has focused on *kinematic fitting* and *functional calibration*, and these techniques are starting to become implemented in software written for the clinical gait analysis market.

Kinematic fitting techniques[46–48] assume a linked rigid segment model of the body with the position of markers specified with respect to the different segments. The pose of the model is obtained by an optimization process to obtain a least squares fit between the measured marker positions and the modeled marker positions. This technique has several advantages. The explicit definition of the underlying model allows a clear definition of joint angles and other parameters. Most implementations assume rigid segments of joints with only rotational degrees of freedom, which lead to kinetic models that are consistent with kinematic data (variable length segments in the CGM and translational degrees of freedom in the CAST mean that this is not generally the case for these two approaches). Although kinematic fitting does not remove STA, it offers potential to minimize its effect. Incorporating information about known joint constraints and fixed segment lengths may reduce susceptibility to STA. Such models also lend themselves to the incorporation of statistical or biomechanical models of STA, which also have the potential to improve results.

Kinematic fitting also lends itself to functional model calibration. This step became necessary because of the difficulty in palpating many anatomical landmarks and placing markers consistently. Functional calibration assumes that the properties of the model, principally, the location of joint centers and the orientation of joint axes (for one or two degrees of freedom of joints), are more reliably determined from the movement data themselves than from the palpated landmarks. Thus, if the hip is assumed to be a ball-and-socket joint, then its location with respect to both the pelvis and femur segments can be determined by optimizing the location of the joint center to minimize the least squares distance between the measured and modeled markers. Early attempts to do this from walking data

alone[46–48] were limited by the small range of movements exhibited by several joints. It is now assumed that separate calibration trials, in which the person moves the joint through a wider range of motions, are required.[8,49–51]

15.3.3 Kinetics

Most active or passive marker-based kinematic measurement systems for gait analysis allow data from force plates to be integrated. However, systems based on inertial sensors generally detect the relative movements of the segments rather than their absolute positions in space and so are less suited to combining with such measurements. The earliest electrical force plates derived measurements from strain gauges attached to columns supporting a plate.[52] About 20 years later, an alternative design was introduced that replaced the strain gauges with piezoelectric transducers. Until fairly recently, there have been few advances in the basic principles of force plate design, although the associated signal conditioning has benefitted from developments in general electronics. Such force plates are susceptible to vibrations and require attachment to substantial foundations to ensure that the lowest resonant frequencies are above those of interest in biomechanics. Over the last few years, new plate designs have been developed that are less dependent on such foundations and can be used much more flexibly.

15.3.4 Electromyography

The principles of EMG have remained relatively unchanged for many years. The essential requirement is for a pair of electrodes to pick up the electrical potentials generated by electrochemical reactions occurring in muscle cells. Surface EMG is most commonly used in clinical practice. Two electrodes are placed a short distance apart on the skin along the length of a muscle, and they detect a potential difference as an action potential travels along it. The magnitude of the action potential is approximately 90 mV and is attenuated through the muscle, fascia, subcutaneous tissues, and skin, and thus it can be as low as 50 μV at the skin surface. Dry electrodes (a simple metal plate typically 10–15 mm in diameter pressing on the skin) can be used, but disposable, self-adhesive Ag/AgCl electrode pairs (~10 mm in diameter and spaced 20 mm apart) are most common. It is now generally accepted that shaving and abrading the skin under the electrode are not generally required (but may be used for particular individuals).

Attenuation of the EMG signal by the soft tissues restricts the use of surface electrodes to muscles within approximately 25 mm of the skin. It can also be difficult to isolate a signal arising from smaller muscles from signals arising from neighboring muscles (known as "cross-talk"). Fine-wire electrodes are required if reliable data from small or deep muscles are desired. In clinical gait analysis, the most common application is for the tibialis posterior, which lies deep in the leg. Typical fine-wire electrodes are 50 μm in diameter with an insulating coating of nylon. Approximately 2 mm of the coating is removed from the ends of two wires, which are passed down the center of a hypodermic needle. The wires are bent over to form barbs of different lengths so that when the needle is inserted and withdrawn, the wires are left in the muscles with the uninsulated portions separated by a few millimeters. The electrodes are only sensitive to signals in the immediate vicinity of the muscles and are thus highly dependent on their accurate placement. This requires a detailed knowledge of musculoskeletal anatomy (which can be altered in different medical conditions) and considerable skill in the insertion of the needles. A muscle stimulator can be used to check that the electrode is in the correct muscle.

Such small signals are susceptible to electromagnetic interference from a variety of sources that can be picked up by connecting wires. Accordingly, high-impedance differential amplifiers are placed close to the electrodes (which are somewhat misleadingly sometimes referred to as *active* electrodes). Older systems required such preamplifiers to be connected to a central data collector or transmitter often worn in a backpack. More modern preamplifiers incorporate wireless transmitters to communicate directly with a base unit. Even given state-of-the-art electrodes and amplifiers, some low-frequency "movement artifact" is often present in the signal. Information of interest in the gait analysis signal is lower than 10 Hz,[53] however, and this artifact can easily be removed using a high-pass filter with a cut-off of around 20Hz.

15.4 Clinical Applications

Clinical gait analysis only gives information about how someone walks. That person only benefits from the experience if the information can be used by clinicians to select from a number of treatment options (including the possibility of not treating). The clinical application of gait analysis depends then on a partnership between the gait analyst and the treating clinician. It might be argued that in a perfect world, the clinician would be trained to interpret gait analysis data and implement the conclusions drawn from them; but, in reality, this is very rarely the case. In many centers, the clinical gait analyst comes from a clinical background, such as physiotherapy, and may not have a particularly strong background in biomechanics. Most clinical gait analysis services would benefit from having health professionals with a biomechanics background taking on a more central role in physical assessment, capture of gait data, and interpretation of results. Current attitudes toward professional roles, both within biomechanics and the other health professions, are probably the biggest barrier to this, but training and accreditation issues are also considerable. Currently, the United Kingdom is one of the few countries to have a professional structure to allow biomechanists to be acknowledged as health care professionals.

Gait analysis can be useful clinically in four contexts: diagnosis, assessment, monitoring, and prediction.[54,55] Diagnosis is the identification of the disease or condition affecting a person. Although gait analysis might have such a role, it is much more generally the case that the condition is known when the person is referred and what is required is an assessment of the severity, extent, or nature of the condition. It may also be useful to monitor how the person's condition is progressing over time. If the time period has included some intervention, then the monitoring process is essentially an evaluation of the outcome of that treatment. One of the great hopes for instrumented gait analysis is that it might allow the prediction of results, particularly through simulating surgery,[33] but reliable systems for doing so are still in the considerably distant future.

There are 11 criteria for any biomechanical measure to be clinically useful (Table 15.2). One criterion is cost effectiveness, which is a particular issue for gait analysis because it is heavily dependent on space, staff time, and complex instrumentation, making it a particularly expensive procedure. In some institutions, a single gait analysis costs as much as several magnetic resonance imaging (MRI) scans. To justify this cost, the clinical benefits must be clear. This is a particular challenge in rehabilitation medicine in which gait analysis would seem to be most appropriate, because treatment costs in that field tend to be fairly low. Even for a relatively expensive drug, such as botulinum toxin, the cost of using

TABLE 15.2

Criteria for Clinically Useful Biomechanical Measures

1.	Reproducible
2.	Stable (independent of mood, motivation, and pain)
3.	Accurate
4.	Appropriately validated
5.	Capable of distinguishing between normal and abnormal
6.	Must not alter the function it is measuring
7.	Reported in form analogous to accepted clinical concepts
8.	Cost effective
9.	Not observable by the skilled clinician
10.	Influential for clinical decision making
11.	Absence of pain as a major factor

Sources: Data adapted from Baker, R., *J. Neuroeng. Rehab.*, 3, 4, 2006; Brand, R. A., *Iowa Orthop. J.*, 9, 61–64, 1987.

gait analysis to assess whether the injections are appropriate for the individual may be greater than the treatment costs themselves. It may well be cheaper to simply try the intervention and see if it works than it is to perform a gait analysis to predict its effectiveness.

Another issue for clinical gait analysis is the ability to detect abnormal from normal walking. There are three issues here: (1) the reproducibility of the measurements themselves, (2) the stability of the measure for an individual person, and (3) the range of variability in the healthy population. As outlined above, the measurement systems themselves have improved to a level in which submillimeter accuracy is possible in detecting marker locations. The accuracy of the process is now limited by the accuracy with which an orthogonal CS can be defined within an irregularly shaped body segment and the ability of clinical gait analysts to place markers (or conduct function calibration procedures) to determine these. A recent systematic review[56] suggests that best practice results in measurement reliability (reproducibility) of between 2° and 5° for major joint angles. Most studies of reliability have focused on multiple assessments on a single day, often in healthy people. It is assumed that the stability of measures for an individual over days and weeks is not a particular problem, but there is little evidence to support this. Levels of variability within the healthy population are also substantial with the standard deviation (SD) varying between 2° and 7°, depending on the joint angle (although this includes any measurement error, which can account for up to half of the recorded variability). Gait graphs (Figure 15.2) tend to plot the normal range as represented by ±1 SD, and gait analysts need to remember that, by the definition of standard deviation, more than 30% of healthy individuals will have gait traces falling outside this range. In summary, clinical gait analysis is likely to be most useful in people with quite considerable gait abnormalities. As a rule of thumb, gait analysis is unlikely to detect abnormalities in joint angles that are not apparent from direct observation or video recordings, but it does have the capacity to quantify these. Kinetic data and EMG are subject to similar factors but also have the advantage that they measure quantities that are not apparent from visual observation.

The last two criteria in Table 15.2, *influential for clinical decision making* and *absence of pain as a major factor,* also affect the applicability of clinical gait analysis. In many conditions, gait analysis can characterize a person's gait pattern, but treatment decisions may not be based on this. This may be because no treatment is available or because there is a generic

treatment that is delivered to all patients regardless of the specific characteristics of their gait. The presence of pain can also complicate the interpretation of gait data considerably. People often walk differently when they experience pain, but it is extremely difficult to distinguish whether the pain is a consequence of the abnormal gait pattern or is the cause of it.

For these reasons, gait analysis has only found wide acceptance in clinical practice in a few specific areas of medicine, and there is considerable debate about just how useful it is even in these fields.[57,58] Its most common application is in assessing children who have CP for complex orthopedic surgery. In relation to other conditions, clinical gait analysis is perhaps better considered as a clinical research tool to understand how walking is affected by those conditions and how various interventions can improve this. Gait analyses for clinical service provision (mainly in CP and similar conditions) and for clinical research are both extremely important. They generally use the same measurement technologies and procedures, but the way data are analyzed and interpreted is quite different. Doing either well requires an understanding of these differences.

15.4.1 Gait Analysis for Clinical Service Provision

This section will focus on service provision for people with CP and related conditions (particularly children). CP is a consequence of brain damage that occurs before, during, or shortly after birth.[59] It results in the impaired coordination of movement and muscle weakness, and a range of other disturbances of sensation, perception, cognition, communication, and behavior, and in epilepsy. Spasticity, in which the reflexes are poorly inhibited and which leads to muscles activating inappropriately when movement is attempted, is very common. Although the brain damage does not get any worse, the growth of the musculoskeletal system is affected by abnormal movement and loading during activity and results particularly in muscle contracture (muscles are too short) and weakness, joint contracture (ligaments restrict the available range of movement), and bony deformities (particularly abnormal twists along the femur and tibia). These factors further restrict walking ability, and, by middle-to-late childhood, significant problems with walking and other motor functions are common.

Orthopedic surgeons can do nothing about the brain damage. They are, however, able to correct many of the musculoskeletal abnormalities or impairments[60] using a combination of muscle lengthening procedures and skeletal realignments. Each child is affected differently by the condition and has a different combination of impairments that requires correction. Identifying these is difficult, and, in the past, surgeons would operate on different impairments at different times over a number of years. However, many modern centers now aim to combine these procedures into a single operation (single-event multilevel surgery) conducted in late childhood when both the walking pattern and musculoskeletal anatomy have matured. Most of those centers consider clinical gait analysis as *essential* to decide which combination of impairments is affecting a particular child.[61]

In this context, clinical gait analysis combines video recording and instrumented measures of walking (as described previously) with a standardized physical assessment of joint range of movement, bony alignment, and muscle strength. It is commonly assumed that the findings of the physical assessment should correlate directly with gait analysis data, and several studies have presented a general lack of correlation as disappointing.[62,63] If gait analysis gave the same information as a physical examination, however, then decision making could be based on the physical examination alone. Rather, it is the lack of a simple relationship between impairments and walking ability that requires the use of

complex techniques such as gait analysis. Children with CP often use walking aids and wear a variety of different orthoses or splints. Clinical gait analysis is often conducted with the child barefoot and using a minimum of walking aids to assess his or her underlying capacity to walk unassisted, and then repeated using that person's usual orthoses and walking aids to see the typical walking on a day-to-day basis. In this way, a clinical gait analysis session is quite time-consuming with many services allocating between 2 and 4 h per child. Ensuring that the child maintains concentration and compliance with procedures over this period is a considerable challenge and is an important part of the clinical gait analyst's role. In the past, measurement technology was more difficult to use on younger and hence smaller individuals, but now the major limitation in this assessment is the maturity to cooperate with and complete the measurement protocol.

Modern gait analysis systems perform most data analysis and modeling in real time or very quickly after capture. Some postprocessing is required, but this can generally be achieved before the end of the gait analysis session. This is important to allow quality assurance processes to be completed before the child leaves. Data interpretation can take considerable time (some centers allocate as much as one person-day for this), and there is only a slowly emerging consensus on how this interpretation should be approached. One approach is to identify significant *gait features* from the graphs. Features are aspects of the graphs that differ from the reference data of healthy individuals and may include offsets throughout the gait cycle, local maximum or minimum values, or inappropriate timing of events. Once the features have been identified, these can be grouped according to which underlying impairment they are considered to be related. Thus, a child with CP might have gait features of reduced hip extension and increased anterior pelvic tilt, which are often both associated with tight hip flexors. These can then be related to the findings of the physical examination. Hip flexor tightness, for example, can be related to an impairment of hip flexor contracture or spasticity, and the physical examination is important to determine this. Once the impairment has been established, then treatment decisions are often clear-cut. Hip flexor contracture requires surgical lengthening, for example, whereas hip flexor spasticity might respond to injections of botulinum toxin. The result of this process is the association of all features of the gait data with a specific impairment. Sometimes, the association will be a direct consequence of the impairment—excessive knee flexion in the stance phase may be associated with the impairment of weak knee extensors. Alternatively, the association may represent a compensatory mechanism—excessive knee flexion in the swing phase might be a compensation for calf spasticity to achieve clearance in swing. The final report is then a listing of the impairments. Supplementary sections can list the evidence (gait features and aspects of the physical examination) for each impairment.

In most major centers, the results are presented to the surgeon and discussed in person because there is generally some subjectivity in the identification of the impairments. This approach also allows for treatment options to be discussed. It is important to note that the preferred option depends on a range of factors beyond gait analysis, including the clinician's preference and expertise, local facilities, results from medical imaging and other tests, and the assessment of the psychosocial status of the individual. In most situations, the final decision rests with the person being analyzed (and, if children, their parents) in direct consultation with the treating clinician.

Clinical gait analysis is delivered as a clinical service and is subject to clinical governance, which is "a system through which (healthcare) organisations are accountable for continuously improving the quality of their services and safeguarding high standards of care by creating an environment in which excellence in clinical care will flourish."[64] One of the key principles in modern clinical governance is that all procedures are conducted in

adherence with written protocols based on an appropriate evidence base (criterion 4; Table 15.2). This can appear stifling and conservative to biomechanists who have often been educated in environments that nurture innovation and experimentation, but it is an essential safeguard to ensure the safety of patient services. Considerable validation is required before any change in procedures or processes is introduced. Another aspect of clinical governance is in ensuring the competence of staff to perform particular aspects of the gait analysis. A particular issue is in clinical decision making. Most countries restrict clinical decision making to specific health professionals. Gait analysis reports should be restricted to an analysis of the gait data and should not include treatment recommendations unless they are made by someone with such a qualification.

15.4.2 Gait Analysis for Clinical Research

Gait analysis for clinical research uses the same measurement techniques as does gait analysis for clinical service provision, but the purpose, as well as the context, analytical techniques, and interpretation, is quite different. Perhaps the most important difference is that the focus of the analysis is almost always on a group of participants rather than on one individual. This relaxes some of the limitations on the applicability of gait analysis, particularly those related to the repeatability of measurements. As long as measurement variability is randomly distributed, then the sample mean can be defined to arbitrary precision by increasing the sample size.

Research applications will generally fall into two categories: (1) descriptive studies categorizing a particular population or (2) intervention studies assessing outcomes. In relation to growth and development or aging, descriptive studies categorizing changes with age are particularly important. Longitudinal studies follow individuals over a period, whereas cross-sectional studies study a range of people of different ages at the same time. Fully describing the methodologies for intervention studies is beyond the scope of this chapter, but randomized clinical trials in which participants are randomized to receive one of two interventions (one is often either the current standard treatment for a condition or even no treatment) are the most common.[65,66]

Clinical gait analysis generates a huge amount of data, which also raises particular statistical issues. Modern inferential statistics is based on calculating the probability that a particular variable would have its measured value (or greater) by chance. A probability of less than 1 in 20 ($p < 0.05$) is generally assumed to indicate a statistically significant finding. If multiple tests are performed, however, a false positive or type I error should be expected to occur, for every 20 tests conducted (on average). Given the number of variables generated during gait analysis, it is virtually certain that at least one will give a false positive. There are two ways of protecting against such errors. The first is through experimental design and by nominating a small number of variables to be analyzed *before* conducting the trial. The second is by correcting the p value in light of the total number of tests corrected (Bonferroni correction).[67]

Although the multivariate nature of gait analysis data gives them a richness and complexity that is one of their strengths, it does mean that assessing the overall quality of the gait pattern requires some thought. The Gillette gait index (originally called the normalcy index),[68] was based on a principal component analysis of 16 kinematic and temporal spatial parameters but has recently been superseded by two alternatives: the gait deviation index (GDI)[69] and the gait profile score (GPS).[70,71] These are both based on the root mean square difference of kinematic data from the mean trace for people without any neuromusculoskeletal pathology. The GDI emerges out of a particularly efficient process for compressing

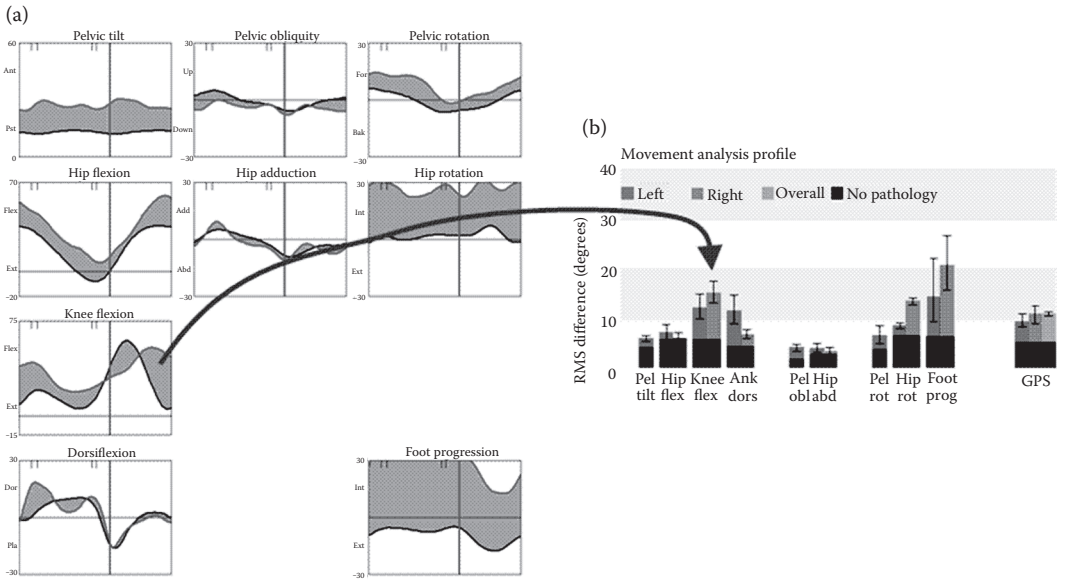

FIGURE 15.6
(See color insert.) Movement analysis profile (MAP). (a) Data from the person being assessed and the average values for healthy adults plotted on the same graphs with the area between these traces shaded. This is a good visual representation of the root mean square difference between the traces that are the values plotted in the MAP histogram on (b). Values for (a) are in red and those in b are in blue. The gait profile score (GPS) is the root mean square average of the values for all the data and can be taken as an overall score of gait abnormality. It can be defined for (a) (red), (b) (blue), or both (green). (Reprinted from *Gait Posture*, 30, 3, Baker, R., et al., 265–269, Copyright 2009, with permission from Elsevier.)

gait analysis data but can only be calculated for the combined data set. The GPS offers none of the potential to compress data but can be presented for individual kinematic variables (termed *the movement analysis profile* when presented as a histogram; Figure 15.6).

15.5 Biomechanical Interpretation of Gait Analysis Data

The interpretation process for gait analysis data in a clinical service context is largely a pattern recognition process that only requires a fairly superficial knowledge of what the data actually represent. Most clinical research projects focus primarily on statistical interpretation, which, again, often overshadows any biomechanical analysis. It is somewhat disappointing that rigorous and detailed biomechanical analysis of gait analysis data is comparatively rare. This is largely a consequence of there being no overarching theory of why we walk the way we do, which could be used to frame such an analysis.

Perhaps the first comprehensive biomechanical description of human walking was that of Gaston Carlet[72] based on his collaboration with Jules Marey in Paris in the 1860s. It was not until the work of Saunders et al.,[73] immediately after World War II, that anyone attempted a description of walking in terms that aimed to be useful clinically. For many years, their *determinants of gait* formed the basis of clinical education in walking, but over the last decade, a series of papers[74–78] have shown that the ideas do not stand up to detailed

scientific scrutiny. Inman also defined two *prerequisites of walking*. These were expanded by Perry[79] and popularized by Gage[80] as the *prerequisites of normal gait*; these are stability during stance, clearance in swing, adequate step length, prepositioning of the foot in late swing, and energy efficiency. Although popular with clinicians, these criteria have been largely ignored by biomechanists, possibly because they seem to offer a series of aspects of walking rather than a generalized theory.

Over the last decade, a number of researchers calling themselves the "Dynamic Walking Group" have endeavored to understand walking through very simple models based on an inverted pendulum model of walking.[78] They have sometimes pushed the analysis to extreme limits for such simple models. Their work has tended to focus on the modeling of the kinematics and energetics of walking, particularly through defining the rate of biomechanical work as the dot product of the ground reaction and velocity of the center of mass. This has led to a particular focus on energy consumed during step-to-step transitions, which is assumed to be a collision in which energy is lost.[81,82] There have been few attempts to apply such methods to pathological walking, and, indeed, it is unclear how common impairments could be incorporated into such simple models of walking.

At the other end of the spectrum, there is considerable interest in extremely complex models of the musculoskeletal system. These typically model the musculoskeletal system as 10 to 15 rigid segments linked with up to 24 degrees of freedom.[33,34,83] The coordinates in the segment CS of the origins and insertions of around 25 muscles in each limb allow the line of action of muscles to be calculated as straight line paths (or as wrapping around simple 3D surfaces).[24] The activation dynamics of musculotendinous units can also be modeled to determine the force generated as a function of muscle physiological cross-sectional area, pennation angle, fiber length, and tendon slack length.[84] Such models can be used as the basis for a variety of advanced analytical techniques[28] and also for forward dynamic simulations.[29] Anderson and Pandy[83] used such a simulation to demonstrate that walking, to optimize the total energy requirement, results in kinematic, kinetic, and muscle activation patterns that are similar to those measured in healthy people. More recently, such simulations have been driven to track data from individuals captured with gait analysis systems.[27,85] Such simulations present the possibility of different analytical techniques including induced acceleration analysis[30,32,40] and power flow analysis.

Despite considerable excitement over these techniques in the biomechanics community, they have had little impact on clinical service provision and only slightly more on clinical research. All the forward models require a model of how the ground reaction arises from the foot's contact with the floor. How this is achieved is still a subject of some debate, with perhaps the most widely adopted approach using a number of nonlinear springs between the foot and the ground.[86] Few of the approaches have a strong anatomical basis, and so it is largely unclear how different pathologies might affect the models. Another limitation is that complex models are described by a large number of parameters, many of which are taken from a rather limited number of studies on cadavers of the elderly.[87] It is unclear just how accurate the original data are or how they should be scaled to match individuals. Some studies suggest that results are sensitive to the measured levels of variability in such parameters,[88–90] but a recent study has suggested that qualitative conclusions may still be valid.[35]

A series of papers have modeled muscle function in CP gait using advanced computational models.[91–100] The major achievements of that work have been a series of qualitative conclusions, most of which, with the benefit of hindsight, seem quite straightforward. This is deceptive, however, because the modeling process has often been an essential driver for formulating the problem in such a way as to create this transparency. Because such little work has been done assessing the sensitivity and stability of models, the validity of

quantitative results is less convincing. Yet, considering how the variation of parameters affects results within a particular model probably does give useful information.

All current avenues of biomechanical interpretation for clinical gait analysis data are somewhat limited. Clinical gait analysis is largely based on rather superficial pattern recognition. The Dynamic Walking Group has focused on models that are probably too simple to be clinically insightful. The computational biomechanists, by contrast, generally work with overcomplex models. Clinicians themselves, when they have engaged with biomechanics, have tended to adopt a compartmentalized rather than integrative approach that few biomechanists have chosen to pursue. Seeking to develop biomechanical models of appropriate complexity to inform future clinical progress remains a considerable and important challenge for contemporary biomechanics.

15.6 Potential for Future Work

The measurements upon which clinical gait analyses are made are still difficult, and measurement variability is still probably the major barrier toward the increased use of these techniques. Published studies suggest that acceptable levels of measurement variability are possible,[101] but these have generally been conducted in tightly controlled research conditions. Maintaining such levels of performance in the routine clinical environment is still a challenge. The introduction of kinematic fitting and functional calibration techniques into clinical practice should bring considerable improvement. Further research into how STA and ambiguous definition of anatomical landmarks affect data is required to support the next generation of measurement technology. There are inherent limitations to the accuracy of measurement systems based on skin-mounted markers, and measurement procedures are extremely time-consuming. Research into markerless 3D data capture has moved forward considerably over the last decade,[102,103] and at least one system is now commercially available. Additional work is required to confirm that these are capable of delivering the levels of accuracy and reliability required for clinical implementation. A relatively simple development would be that of fully automated data capture that could save considerable time and thus reduce costs.

A new generation of sensors and software designed for controlling video games (such as the Kinect for Xbox from Microsoft) offers potential for motion capture, but the accuracy and repeatability of such systems also need to be defined. For high-accuracy measurements, alternative imaging methodologies are almost certainly required. Uniplanar[44,45,104,105] and biplanar fluoroscopic[106–108] and dynamic MRI[109–111] technologies have established proof of concept and need to be researched further. These are all limited in the capture volume that is possible (for different reasons), and widespread clinical implementation is only a prospect for the distant future.

There is also a need to develop our understanding of gait data themselves. There is considerable variability across different clinical centers as to how gait analysis data are interpreted and reported. Most clinical interpretation is essentially a subjective pattern recognition process with little incorporation of any true biomechanics. As explained above, this can be partly attributed to the lack of any general theory of why we walk the way we do. Biomechanists currently working in this area tend to divide into two camps depending on whether they focus on extremely simple models or on extremely complex models. Both have their limitations, and it is possible that a focus on the middle ground of

what might be referred to as "appropriately complex models" might be productive. There are also very few biomechanists who are immersed in the clinical environment and who are able to incorporate their own clinical insight into this process. This leaves poor communication between clinicians and biomechanists as an inhibitor to progress and results in contemporary biomechanics being of little relevance to the clinical community in this area. Engaging biomechanists more centrally in clinical processes and using their understanding to derive biomechanical modeling projects could lead to rapid and much more clinically relevant improvements of our understanding of human walking.

Part of the communication barrier between biomechanists and clinicians has been the insistence over the years that data can only be represented on gait graphs, and that, if clinicians want to use clinical gait analysis techniques, they must learn to interpret data presented in this format. This format does not reflect the paradigm in which most clinicians have been educated, and many simply refuse to engage with the potential that clinical gait analysis offers. Modern computer graphics offer considerable opportunities to consider presenting clinical gait analysis in a variety of ways. Presenting data in terms of computer-enhanced representations of a person walking fits much more closely with the existing worldview of most clinicians than does a gait graph. Exploring the potential to use such tools to develop a more user-friendly clinical gait analysis for the future is an important task that has, thus far, received very little attention from biomechanists.

References

1. Gardener, E. A., F. A. Huppert, J. M. Guralnik, and D. Melzer. 2006. Middle-aged and mobility-limited: Prevalence of disability and symptom attributions in a national survey. *Journal of General Internal Medicine* 21(10):1091–1096.
2. Iezzoni, L. I., E. P. McCarthy, R. B. Davis, and H. Siebens. 2001. Mobility difficulties are not only a problem of old age. *Journal of General Internal Medicine* 16(4):235–243.
3. Orendurff, M. S., J. A. Schoen, G. C. Bernatz, A. D. Segal, and G. K. Klute. 2008. How humans walk: Bout duration, steps per bout, and rest duration. *Journal of Rehabilitation Research and Development* 45(7):1077–1089.
4. Huxham, F., J. Gong, R. Baker, M. Morris, and R. Iansek. 2006. Defining spatial parameters for non-linear walking. *Gait & Posture* 23(2):159–163.
5. Wu, G., S. Siegler, P. Allard, C. Kirtley, A. Leardini, D. Rosenbaum, et al. 2002. ISB recommendation on definitions of joint coordinate system of various joints for the reporting of human joint motion—Part I: Ankle, hip, and spine. International Society of Biomechanics. *Journal of Biomechanics* 35(4):543–548.
6. Wu, G., and P. R. Cavanagh. 1995. ISB recommendations for standardization in the reporting of kinematic data. *Journal of Biomechanics* 28(10):1257–1261.
7. Baker, R. 2003. ISB recommendation on definition of joint coordinate systems for the reporting of human joint motion—Part I: Ankle, hip and spine. *Journal of Biomechanics* 36(2):300–302.
8. Schwartz, M. H., and A. Rozumalski. 2005. A new method for estimating joint parameters from motion data. *Journal of Biomechanics* 38(1):107–116.
9. Buczek, F. L., M. J. Rainbow, K. M. Cooney, M. R. Walker, and J. O. Sanders. 2009. Implications of using hierarchical and six degree-of-freedom models for normal gait analyses. *Gait & Posture* 31(1):57–63.
10. Collins, T. D., S. N. Ghoussayni, D. J. Ewins, and J. A. Kent. 2009. A six degrees-of-freedom marker set for gait analysis: Repeatability and comparison with a modified Helen Hayes set. *Gait & Posture* 30(2):173–180.

11. Davis, R. B., S. Ounpuu, D. Tyburski, and J. R. Gage. 1991. A gait analysis data collection and reduction technique. *Human Movement Science* 10(5):575–587.
12. Kadaba, M. P., H. K. Ramakrishnan, and M. E. Wootten. 1990. Measurement of lower extremity kinematics during level walking. *Journal of Orthopaedic Research* 8(3):383–392.
13. Yamaguchi, G. T., and F. E. Zajac. 1989. A planar model of the knee joint to characterize the knee extensor mechanism. *Journal of Biomechanics* 22(1):1–10.
14. Carson, M. C., M. E. Harrington, N. Thompson, J. J. O'Connor, and T. N. Theologis. 2001. Kinematic analysis of a multi-segment foot model for research and clinical applications: A repeatability analysis. *Journal of Biomechanics* 34(10):1299–1307.
15. Leardini, A., M. G. Benedetti, F. Catani, L. Simoncini, and S. Giannini. 1999. An anatomically based protocol for the description of foot segment kinematics during gait. *Clinical Biomechanics (Bristol, Avon)* 14(8):528–536.
16. Saraswat, P., M. S. Andersen, and B. A. Macwilliams. 2010. A musculoskeletal foot model for clinical gait analysis. *Journal of Biomechanics* 43(9):1645–1652.
17. Simon, J., L. Doederlein, A. S. McIntosh, D. Metaxiotis, H. G. Bock, and S. I. Wolf. 2006. The Heidelberg foot measurement method: Development, description and assessment. *Gait & Posture* 23(4):411–424.
18. Stebbins, J., M. Harrington, N. Thompson, A. Zavatsky, and T. Theologis. 2006. Repeatability of a model for measuring multi-segment foot kinematics in children. *Gait & Posture* 23(4):401–410.
19. Tupling, S. J., and M. R. Pierrynowski. 1987. Use of Cardan angles to locate rigid bodies in three-dimensional space. *Medical & Biological Engineering & Computing* 25(5):527–532.
20. Grood, E. S., and W. J. Suntay. 1983. A joint coordinate system for the clinical description of three-dimensional motions: Application to the knee. *Journal of Biomechanical Engineering* 105(2): 136–144.
21. Strasser, H. 1917. *Lehrbuch Der Muskel Und Gelenkmechanik*. Berlin: Springer.
22. Baker, R. 2011. Globographic visualisation of three dimensional joint angles. *Journal of Biomechanics* 44(10):1885–1891.
23. Baker, R. 2001. Pelvic angles: A mathematically rigorous definition which is consistent with a conventional clinical understanding of the terms. *Gait & Posture* 13(1):1–6.
24. Charlton, I. W., and G. R. Johnson. 2001. Application of spherical and cylindrical wrapping algorithms in a musculoskeletal model of the upper limb. *Journal of Biomechanics* 34(9):1209–1216.
25. Schache, A. G., and R. Baker. 2007. On the expression of joint moments during gait. *Gait & Posture* 25(3):440–452.
26. Winter, D. A., and D. G. E. Robertson. 1978. Joint torque and energy patterns in normal gait. *Biological Cybernetics* 29(3):137–142.
27. Thelen, D. G., and F. C. Anderson. 2006. Using computed muscle control to generate forward dynamic simulations of human walking from experimental data. *Journal of Biomechanics* 39(6):1107–1115.
28. Zajac, F. E., R. R. Neptune, and S. A. Kautz. 2002. Biomechanics and muscle coordination of human walking. Part I: Introduction to concepts, power transfer, dynamics and simulations. *Gait & Posture* 16(3):215–232.
29. Zajac, F. E., R. R. Neptune, and S. A. Kautz. 2003. Biomechanics and muscle coordination of human walking: Part II: Lessons from dynamical simulations and clinical implications. *Gait & Posture* 17(1):1–17.
30. Anderson, F. C., and M. G. Pandy. 2003. Individual muscle contributions to support in normal walking. *Gait & Posture* 17(2):159–169.
31. Kepple, T. M., K. L. Siegel, and S. J. Stanhope. 1997. Relative contributions of the lower extremity joint moments to forward progression and support during gait. *Gait & Posture* 6:1–8.
32. Siegel, K. L., T. M. Kepple, and S. J. Stanhope. 2006. Using induced accelerations to understand knee stability during gait of individuals with muscle weakness. *Gait & Posture* 23(4): 435–440.
33. Delp, S. L. 1990. Surgery Simulation: A Computer Graphics System to Analyze and Design Musculoskeletal Reconstructions of the Lower Extremity. PhD diss., Stanford University.

34. Delp, S. L., F. C. Anderson, A. S. Arnold, P. Loan, A. Habib, C. T. John, et al. 2007. Opensim: Open-source software to create and analyze dynamic simulations of movement. *IEEE Transactions on Bio-Medical Engineering* 54(11):1940–1950.
35. Correa, T. A., R. Baker, H. Kerr Graham, and M. G. Pandy. 2011. Accuracy of generic musculoskeletal models in predicting the functional roles of muscles in human gait. *Journal of Biomechanics* 44(11):2096–2105.
36. Schwartz, M. H., S. E. Koop, J. L. Bourke, and R. Baker. 2006. A nondimensional normalization scheme for oxygen utilization data. *Gait & Posture* 24(1):14–22.
37. Kadaba, M. P., H. K. Ramakrishnan, M. E. Wootten, J. Gainey, G. Gorton, and G. V. Cochran. 1989. Repeatability of kinematic, kinetic, and electromyographic data in normal adult gait. *Journal of Orthopaedic Research* 7(6):849–860.
38. Benedetti, M. G., F. Catani, A. Leardini, E. Pignotti, and S. Giannini. 1998. Data management in gait analysis for clinical applications. *Clinical Biomechanics (Bristol, Avon)* 13(3):204–215.
39. Cappozzo, A., F. Catani, U. D. Croce, and A. Leardini. 1995. Position and orientation in space of bones during movement: Anatomical frame definition and determination. *Clinical Biomechanics (Bristol, Avon)* 10(4):171–178.
40. Neptune, R. R., S. A. Kautz, and F. E. Zajac. 2001. Contributions of the individual ankle plantar flexors to support, forward progression and swing initiation during walking. *Journal of Biomechanics* 34(11):1387–1398.
41. Leardini, A., L. Chiari, U. Della Croce, and A. Cappozzo. 2005. Human movement analysis using stereophotogrammetry. Part 3. Soft tissue artifact assessment and compensation. *Gait & Posture* 21(2):212–225.
42. Akbarshahi, M., A. G. Schache, J. W. Fernandez, R. Baker, S. Banks, and M. G. Pandy. 2010. Non-invasive assessment of soft-tissue artifact and its effect on knee joint kinematics during functional activity. *Journal of Biomechanics* 43(7):1292–1301.
43. Benoit, D. L., D. K. Ramsey, M. Lamontagne, L. Xu, P. Wretenberg, and P. Renstrom. 2006. Effect of skin movement artifact on knee kinematics during gait and cutting motions measured in vivo. *Gait & Posture* 24(2):152–164.
44. Cappozzo, A., F. Catani, A. Leardini, M. G. Benedetti, and U. D. Croce. 1996. Position and orientation in space of bones during movement: Experimental artefacts. *Clinical Biomechanics (Bristol, Avon)* 11(2):90–100.
45. Tsai, T.-Y., T.-W. Lu, M.-Y. Kuo, and H.-C. Hsu. 2009. Quantification of three-dimensional movement of skin markers relative to the underlying bones during functional activities. *Biomedical Engineering - Applications Basis Communications* 21:223–232.
46. Charlton, I. W., P. Tate, P. Smyth, and L. Roren. 2004. Repeatability of an optimised lower body model. *Gait & Posture* 20(2):213–221.
47. Lu, T.-W., and J. J. O'Connor. 1999. Bone position estimation from skin marker co-ordinates using global optimisation with joint constraints. *Journal of Biomechanics* 32(2):129–134.
48. Reinbolt, J. A., J. F. Schutte, B. J. Fregly, B. I. Koh, R. T. Haftka, A. D. George, et al. 2005. Determination of patient-specific multi-joint kinematic models through two-level optimization. *Journal of Biomechanics* 38(3):621–626.
49. Ehrig, R. M., W. R. Taylor, G. N. Duda, and M. O. Heller. 2007. A survey of formal methods for determining functional joint axes. *Journal of Biomechanics* 40(10): 2150–2157.
50. Ehrig, R. M., W. R. Taylor, G. N. Duda, and M. O. Heller. 2006. A survey of formal methods for determining the centre of rotation of ball joints. *Journal of Biomechanics* 39(15):2798–2809.
51. Leardini, A., A. Cappozzo, F. Catani, S. Toksvig-Larsen, A. Petitto, V. Sforza, et al. 1999. Validation of a functional method for the estimation of hip joint centre location. *Journal of Biomechanics* 32(1):99–103.
52. Cunningham, D. M., and G. W. Brown. 1952. Two devices for measuring the forces acting on the human body during walking. *Proceedings of the Society for Experimental Stress Analysis* 2:75–90.
53. Antonsson, E. K., and R. W. Mann. 1985. The frequency content of gait. *Journal of Biomechanics* 18(1):39–47.

54. Baker, R. 2006. Gait analysis methods in rehabilitation. *Journal of Neuroengineering and Rehabilitation* 3:4.
55. Brand, R. A. 1987. Can biomechanics contribute to clinical orthopaedic assessments. *Iowa Orthopaedic Journal* 9:61–64.
56. McGinley, J. L., R. Baker, R. Wolfe, and M. E. Morris. 2009. The reliability of three-dimensional kinematic gait measurements: A systematic review. *Gait & Posture* 29(3):360–369.
57. Gage, J. R. 2003. Con: Interobserver variability of gait analysis. *Journal of Pediatric Orthopedics* 23(3):290–291.
58. Wright, J. G. 2003. Pro: Interobserver variability of gait analysis. *Journal of Pediatric Orthopedics* 23(3):288–289.
59. Rosenbaum, P., N. Paneth, A. Leviton, M. Goldstein, and M. Bax. 2007. A report: The definition and classification of cerebral palsy. April 2006. *Developmental Medicine and Child Neurology. Supplement* (109):8–14.
60. Bache, C. E., P. Selber, and H. K. Graham. 2003. The management of spastic diplegia. *Current Orthopaedics* 17(2):88–104.
61. Gage, J. R., M. H. Schwartz, S. E. Koop, and T. F. Novacheck. 2009. *The Identification and Treatment of Gait Problems in Cerebral Palsy*. *Clinics in Developmental Medicine*. London: Mac Keith Press.
62. Desloovere, K., G. Molenaers, H. Feys, C. Huenaerts, B. Callewaert, and P. Van de Walle. 2006. Do dynamic and static clinical measurements correlate with gait analysis parameters in children with cerebral palsy? *Gait & Posture* 24(3):302–313.
63. Thompson, N. S., R. J. Baker, A. P. Cosgrove, J. L. Saunders, and T. C. Taylor. 2001. Relevance of the popliteal angle to hamstring length in cerebral palsy crouch gait. *Journal of Pediatric Orthopedics* 21(3):383–387.
64. Scally, G., and L. J. Donaldson. 1998. Clinical governance and the drive for quality improvement in the new NHS in England. *British Medical Journal* 317(7150):61–65.
65. Baker, R., M. Jasinski, I. Maciag-Tymecka, J. Michalowska-Mrozek, M. Bonikowski, L. Carr, et al. 2002. Botulinum toxin treatment of spasticity in diplegic cerebral palsy: A randomized, double-blind, placebo-controlled, dose-ranging study. *Developmental Medicine and Child Neurology* 44(10):666–675.
66. Thomason, P., R. Baker, K. Dodd, N. Taylor, P. Selber, R. Wolfe, and H. K. Graham. 2011. Single-event multilevel surgery in children with spastic diplegia: A pilot randomized controlled trial. *Journal of Bone and Joint Surgery. American Volume* 93(5):451–460.
67. Bland, M. 2000. *An Introduction to Medical Statistics.* 3rd ed. Oxford: Oxford University Press.
68. Schutte, L. M., U. Narayanan, J. L. Stout, P. Selber, J. R. Gage, and M. H. Schwartz. 2000. An index for quantifying deviations from normal gait. *Gait & Posture* 11(1):25–31.
69. Schwartz, M. H., and A. Rozumalski. 2008. The gait deviation index: A new comprehensive index of gait pathology. *Gait & Posture* 28(3):351–357.
70. Baker, R., J. L. McGinley, M. H. Schwartz, S. Beynon, A. Rozumalski, H. K. Graham, et al. 2009. The gait profile score and movement analysis profile. *Gait & Posture* 30(3):265–269.
71. Beynon, S., J. L. McGinley, F. Dobson, and R. Baker. 2010. Correlations of the gait profile score and the movement analysis profile relative to clinical judgments. *Gait & Posture* 32(1):129–132.
72. Carlet, G. 1872. Essai experimental sur la locomotion humaine, etude de la marche. *Annales des Sciences Naturelles: Zoologie* 15.
73. Saunders, J. B., V. T. Inman, and H. D. Eberhart. 1953. The major determinants in normal and pathological gait. *Journal of Bone and Joint Surgery. American Volume* 35A(3):543–558.
74. Gard, S. A., and D. S. Childress. 2001. What determines the vertical displacement of the body during normal walking? *Journal of Prosthetics and Orthotics* 13(3):64–67.
75. Gordon, K. E., D. P. Ferris, and A. D. Kuo. 2009. Metabolic and mechanical energy costs of reducing vertical center of mass movement during gait. *Archives of Physical Medicine and Rehabilitation* 90(1):136–144.
76. Kerrigan, D. C., U. Della Croce, M. Marciello, and P. O. Riley. 2000. A refined view of the determinants of gait: Significance of heel rise. *Archives of Physical Medicine and Rehabilitation* 81(8):1077–1080.

77. Kerrigan, D. C., P. O. Riley, J. Lelas, and U. Della Croce. 2001. Quantification of pelvic rotation as a determinant of gait. *Archives of Physical Medicine and Rehabilitation* 82(2):217–220.
78. Kuo, A. D. 2007. The six determinants of gait and the inverted pendulum analogy: A dynamic walking perspective. *Human Movement Science* 26(4):617–656.
79. Perry, J. 1992. *Gait Analysis*. Thorofare, NJ: SLACK, Inc.
80. Gage, J. R., ed. 2004. *The Treatment of Gait Problems in Cerebral Palsy*. London: MacKeith Press.
81. Donelan, J. M., R. Kram, and A. D. Kuo. 2002. Mechanical work for step-to-step transitions is a major determinant of the metabolic cost of human walking. *The Journal of Experimental Biology* 205(Pt 23):3717–3727.
82. Kuo, A. D., J. M. Donelan, and A. Ruina. 2005. Energetic consequences of walking like an inverted pendulum: Step-to-step transitions. *Exercise and Sport Sciences Reviews* 33(2):88–97.
83. Anderson, F. C., and M. G. Pandy. 2001. Dynamic optimization of human walking. *Journal of Biomechanical Engineering* 123(5):381–390.
84. Zajac, F. E. 1989. Muscle and tendon: Properties, models, scaling, and application to biomechanics and motor control. *Critical Reviews in Biomedical Engineering* 17(4):359–411.
85. Thelen, D. G., F. C. Anderson, and S. L. Delp. 2003. Generating dynamic simulations of movement using computed muscle control. *Journal of Biomechanics* 36(3):321–328.
86. Anderson, F., and M. Pandy. 1999. A dynamic optimization solution for vertical jumping in three dimensions. *Computer Methods in Biomechanics and Biomedical Engineering* 2(3):201–231.
87. Delp, S. L., and J. P. Loan. 1995. A graphics-based software system to develop and analyze models of musculoskeletal structures. *Computers in Biology and Medicine* 25(1):21–34.
88. Arnold, A. S., S. Salinas, D. J. Asakawa, and S. L. Delp. 2000. Accuracy of muscle moment arms estimated from MRI-based musculoskeletal models of the lower extremity. *Computer Aided Surgery* 5(2):108–119.
89. Scheys, L., K. Desloovere, P. Suetens, and I. Jonkers. 2011. Level of subject-specific detail in musculoskeletal models affects hip moment arm length calculation during gait in pediatric subjects with increased femoral anteversion. *Journal of Biomechanics* 44(7):1346–1353.
90. Scheys, L., A. Spaepen, P. Suetens, and I. Jonkers. 2008. Calculated moment-arm and muscle-tendon lengths during gait differ substantially using MR based versus rescaled generic lower-limb musculoskeletal models. *Gait & Posture* 28(4):640–648.
91. Arnold, A. S., D. J. Asakawa, and S. L. Delp. 2000. Do the hamstrings and adductors contribute to excessive internal rotation of the hip in persons with cerebral palsy? *Gait & Posture* 11(3):181–190.
92. Arnold, A. S., M. Q. Liu, M. H. Schwartz, S. Ounpuu, and S. L. Delp. 2006. The role of estimating muscle-tendon lengths and velocities of the hamstrings in the evaluation and treatment of crouch gait. *Gait & Posture* 23(3):273–281.
93. Fox, M. D., J. A. Reinbolt, S. Ounpuu, and S. L. Delp. 2009. Mechanisms of improved knee flexion after rectus femoris transfer surgery. *Journal of Biomechanics* 42(5):614–619.
94. Goldberg, S. R., F. C. Anderson, M. G. Pandy, and S. L. Delp. 2004. Muscles that influence knee flexion velocity in double support: Implications for stiff-knee gait. *Journal of Biomechanics* 37(8):1189–1196.
95. Hicks, J., A. Arnold, F. Anderson, M. Schwartz, and S. Delp. 2007. The effect of excessive tibial torsion on the capacity of muscles to extend the hip and knee during single-limb stance. *Gait & Posture* 26(4):546–552.
96. Hicks, J. L., M. H. Schwartz, A. S. Arnold, and S. L. Delp. 2008. Crouched postures reduce the capacity of muscles to extend the hip and knee during the single-limb stance phase of gait. *Journal of Biomechanics* 41(5):960–967.
97. Higginson, J. S., F. E. Zajac, R. R. Neptune, S. A. Kautz, C. G. Burgar, and S. L. Delp. 2006. Effect of equinus foot placement and intrinsic muscle response on knee extension during stance. *Gait & Posture* 23(1):32–36.
98. Higginson, J. S., F. E. Zajac, R. R. Neptune, S. A. Kautz, and S. L. Delp. 2006. Muscle contributions to support during gait in an individual with post-stroke hemiparesis. *Journal of Biomechanics* 39(10):1769–1777.

99. Reinbolt, J. A., M. D. Fox, A. S. Arnold, S. Ounpuu, and S. L. Delp. 2008. Importance of preswing rectus femoris activity in stiff-knee gait. *Journal of Biomechanics* 41(11):2362–2369.
100. Thelen, D. D., S. A. Riewald, D. S. Asakawa, T. D. Sanger, and S. L. Delp. 2003. Abnormal coupling of knee and hip moments during maximal exertions in persons with cerebral palsy. *Muscle Nerve* 27(4):486–493.
101. McGinley, J. L., R. Baker, and R. Wolfe. 2006. Quantification of kinematic measurement variability in gait analysis. *Gait & Posture* 24:S55–S56.
102. Corazza, S., L. Mundermann, A. M. Chaudhari, T. Demattio, C. Cobelli, and T. P. Andriacchi. 2006. A markerless motion capture system to study musculoskeletal biomechanics: Visual hull and simulated annealing approach. *Annals of Biomedical Engineering* 34(6):1019–1029.
103. Mundermann, L., S. Corazza, and T. P. Andriacchi. 2006. The evolution of methods for the capture of human movement leading to markerless motion capture for biomechanical applications. *Journal of Neuroengineering and Rehabilitation* 3:6.
104. Stagni, R., S. Fantozzi, A. Cappello, and A. Leardini. 2005. Quantification of soft tissue artefact in motion analysis by combining 3D fluoroscopy and stereophotogrammetry: A study on two subjects. *Clinical Biomechanics (Bristol, Avon)* 20(3):320–329.
105. Fantozzi, S., M. G. Benedetti, A. Leardini, S. A. Banks, A. Cappello, D. Assirelli, et al. 2003. Fluoroscopic and gait analysis of the functional performance in stair ascent of two total knee replacement designs. *Gait & Posture* 17(3):225–234.
106. Li, G., M. Kozanek, A. Hosseini, F. Liu, S. K. Van de Velde, et al. 2009. New fluoroscopic imaging technique for investigation of 6dof knee kinematics during treadmill gait. *Journal of Orthopaedic Surgery and Research* 4:6.
107. Torry, M. R., K. B. Shelburne, D. S. Peterson, J. E. Giphart, J. P. Krong, C. Myers, et al. 2011. Knee kinematic profiles during drop landings: A biplane fluoroscopy study. *Medicine and Science in Sports and Exercise* 43(3):533–541.
108. Van de Velde, S. K., A. Hosseini, M. Kozanek, T. J. Gill, H. E. Rubash, and G. Li. 2010. Application guidelines for dynamic knee joint analysis with a dual fluoroscopic imaging system. *Acta Orthopaedica Belgica* 76(1):107–113.
109. Powers, C. M., F. G. Shellock, and M. Pfaff. 1998. Quantification of patellar tracking using kinematic MRI. *Journal of Magnetic Resonance Imaging* 8(3):724–732.
110. Rebmann, A. J., and F. T. Sheehan. 2003. Precise 3D skeletal kinematics using fast phase contrast magnetic resonance imaging. *Journal of Magnetic Resonance Imaging* 17(2):206–213.
111. Ward, S. R., F. G. Shellock, M. R. Terk, G. B. Salsich, and C. M. Powers. 2002. Assessment of patellofemoral relationships using kinematic MRI: Comparison between qualitative and quantitative methods. *Journal of Magnetic Resonance Imaging* 16(1):69–74.

16

Injury Biomechanics

Richard Kent, Jeff Crandall, and Dipan Bose

CONTENTS

16.1 Introduction

Injury results from intentional or unintentional damage to the body from acute exposure to different forms of energy. If the source of energy is mechanical in nature, injury results when stresses and strains or forces and deformations cause physical or functional failure of tissues. Injury is considered one of the most serious and under-recognized health problems affecting society today. The advent of mechanized modes of transportation in the nineteenth and twentieth centuries exposed humans to speeds that put them at risk of injury in the event of a vehicle collision. Worldwide, the World Health Organization estimates that 1.2 million people die each year in road crashes, and as many as 50 million are injured or disabled.[1] Transportation-related injuries are the leading cause of deaths for Americans aged 1 to 44 and are the most common cause of physician contacts and hospitalization for all Americans.[2] The rapid motorization of developing countries similarly will lead to unparalleled morbidity and mortality in the upcoming decades. In addition to the staggering human costs, the economic consequences for lost productivity, legal and medical costs, and insurance expenses are enormous. Despite the prevalence and expense, injury is not the result of an unavoidable accident but rather a problem that can be addressed with adequate attention and support. As part of a larger injury control program that includes addressing exposure, behavior modification, and postinjury management, injury prevention strategies must be based on knowledge of the mechanisms of injury as well as the body's response and tolerance. Furthermore, such strategies must be imposed in conjunction with tools and techniques for assessing the effectiveness of injury

countermeasures. Injury biomechanics uses the principles of mechanics to characterize the physiological and physical response of tissues to impact that can result in injury and forms the cornerstone of effective injury programs based on countermeasure design.

Simply stated, the ultimate objective of injury biomechanics is the prevention of trauma through environmental modifications. To develop effective injury countermeasures, it is necessary to have a clear understanding of what the mechanisms of injury are, to describe the mechanical response of the tissues involved, to have a basic understanding of human tolerance to impact, and to have tools that can be used as human surrogates. Viano et al.[3] identified five specific objectives for the field of injury biomechanics:

(1) Identify and define the mechanisms of injury
(2) Quantify the responses of the human body tissues and systems to a range of input conditions
(3) Determine the level of response at which tissues or systems will fail to recover
(4) Develop protective materials and structures that reduce the levels of energy and force delivered to the body
(5) Develop test devices and computer models that respond to input in a human-like manner so that protective systems can be accurately evaluated

Although the objectives of injury biomechanics are easily delineated, the complexities of the human body make them quite challenging to achieve. Biological materials are inherently hierarchical in structure with a temporal component to their development, proliferation, damage, and death. Thus, injury biomechanics must potentially bridge length and time scales of several orders of magnitude to characterize the response and failure of tissues. Unlike traditional engineering materials, biological tissues are complicated by the fact that the human body has the ability to grow, adapt, and repair itself in response to its environment. In loading situations in which microdamage occurs but no catastrophic failure of the tissue results, tissue trauma may heal if given sufficient time between loading exposures. With insufficient time for healing, accumulated damage can result in the failure of the material or a reduction in its mechanical tolerance to an acute loading event. The body's tolerance to injury and its resilience is dependent on both physiologic and mechanical conditions. Although little research has characterized the effect of biomechanical and biochemical parameters of the physiologic condition on the tolerance of tissues, preexisting medical conditions have been shown as general risk factors for injury, including arterial occlusive disease, heart disease, hepatitis/liver cirrhosis, carcinoma/malignant disease, coagulation disorder, obesity, cardiopulmonary disease, and diabetes.[4,5] Similarly, the presence of alcohol, drugs, and pharmacologic agents in the body at the time of loading can influence the potential for injury. Mackay[6] notes that even daily variations in the state of organs (e.g., stomach contents and bladder volume) will have an influence on the response and tolerance of soft tissues.

Although injury biomechanics helps in our understanding of the physical parameters and underlying mechanisms responsible for injury causation, it is equally important to be able to quantify the likelihood of injury sustainability under applied loading conditions and related parameters. Mathematical expressions estimating the likelihood of injury at different severities are an essential part of injury evaluation and development of injury control measures. The mathematical expressions, also known as injury risk functions, are based on statistical methods applied to experimentally determined biomechanics data. As with any other analytical procedure, it is imperative that the raw

biomechanics data are of sound quality to ensure accurate evaluation of injury using the risk functions. Details and statistical background about injury risk functions are presented in the next section.

16.2 Injury Risk Functions

A major objective of injury biomechanics research is the development of mathematical expressions that relate engineering parameters to the risk of tissue or structural injury. The injury risk functions can be classified in many different ways based on the underlying statistical method. Each method has its own merits and assumptions, which need to be appropriated before its selection in the development of an injury risk function. Primarily, an injury risk function can assume that the distribution of the injury data follows one of the standard models (e.g., normal, Poisson, logarithmic), which would make the injury risk function a parametric model. In contrast, no inherent distribution may be assumed for the underlying injury data in the case of a nonparametric model (Table 16.1). An assumption about the distribution of the data potentially provides more efficiency and statistical power for the analysis of multivariate injury data. When no justifiable choice for the assumption of the injury distribution can be made, the nonparametric models offer a viable approach to interpret the characteristics of the underlying data with a minimum set of assumptions (Table 16.1).

Another distinction between the injury risk functions is the defined relationship between the explanatory variables or predictors (i.e., the applied load/stimulus and other

TABLE 16.1

Summary of Relative Advantages and Disadvantages of Parametric and Nonparametric Injury Risk Models

	Parametric Methods	Nonparametric Methods
Advantages	1. Easy to compare two populations quantitatively. 2. The risk curve is defined by few (two or three) distributional parameters. 3. Good for small sample sizes. 4. Standardized, well-developed, and easy-to-implement techniques. 5. Injury risk can be extrapolated if distributional assumptions are valid. 6. Multivariate analysis can be easily performed.	1. Makes less stringent assumptions about the data. 2. No distribution is assumed. 3. Can be used for small sample sizes. 4. Can be used for benchmarking the parametric models.
Disadvantages	1. Distributional assumptions are forced on the injury data. 2. Certain underlying conditions or assumptions must be met, particularly for smaller sample sizes. For very small sample sizes (i.e., $n<6$), distribution must be known *a priori*. 3. Risk is extrapolated based on the assumed distribution in regions that lack experimental data points.	1. Difficult to compare two populations due to lack of parameters. 2. The injury risk is represented in a stepwise incremental function and is not continuous. 3. The risk between two consecutive injury data points is assumed to be constant. 4. Difficult to measure quantities like hazard rates. 5. Less statistical power for the lack of parameterization.

relevant parameters) and the outcome of interest (i.e., risk of injury). Typically, regression-based methods can be expressed with the outcome written as a linear combination of the predictor variables. The outcome and the predictor variables can be directly combined as in the case of a linear regression model or can be combined using a link function such as a "logit" function. The alternate approach is to use "survival methods" in which the likelihood of outcome is estimated by the probability of success or failure up to the point of the applied load/stimulus. Parametric and nonparametric assumptions are equally valid in the case of survival methods as well, and the selection of model depends on the underlying data distribution.

16.2.1 Nonparametric Injury Risk Models

The product-limit method (also commonly known as the Kaplan–Meier method) of estimating the survival function is one of the most standard nonparametric injury risk models.[7] In this method, both injury and noninjury data are binned in separate intervals, and the proportion of samples surviving (not failing or being injured) is estimated to a particular value of the stimulus. The survival function may be inverted to produce the probability of failure injury risk curve. No distributional assumptions are made in this method, and the shape of the injury risk curve is completely controlled by the data points. Mathematically speaking, the survival function $S(t)$ or the probability of surviving to the stimulus = t is defined by Equation 16.1:

$$S(t) = \prod_i \left(1 - \frac{\delta i}{n + 1 - i}\right), \tag{16.1}$$

where

$$\delta_i = \begin{cases} 1 & \text{if failure at } t_i \\ 0 & \text{if censored at } t_i \end{cases},$$

t_i is the time of the ith event, and n is the number of samples.

A typical example of a Kaplan–Meier probability of injury risk curve is shown in Figure 16.1. Please note that the probability of failure is numerically equal to $F(t) = 1 - S(t)$ (Figure 16.1).

16.2.2 Parametric Binary Regression Models

Parametric injury criteria, which assume an underlying form of the injury distribution, can be either a regression-based model or a survival analysis model. The underlying form of the distribution (i.e., logistic, normal, Weibull, etc.) in this case is chosen *a priori*, and the development of the injury criteria model involves estimating the parameters of the distribution using different optimizing techniques. Binary regression models are the most common forms of parametric injury criteria that are used when the exact injury data are available. The binary regression models are applicable when the outcome (typically injury) is expressed dichotomously: injured or not injured. It should be noted that while the injury data in the binary regression models are treated as exact data points (the exact amount of stimulus required to cause an injury is known), the noninjury data points will always be censored. In particular, they will be right-censored because the additional amount of

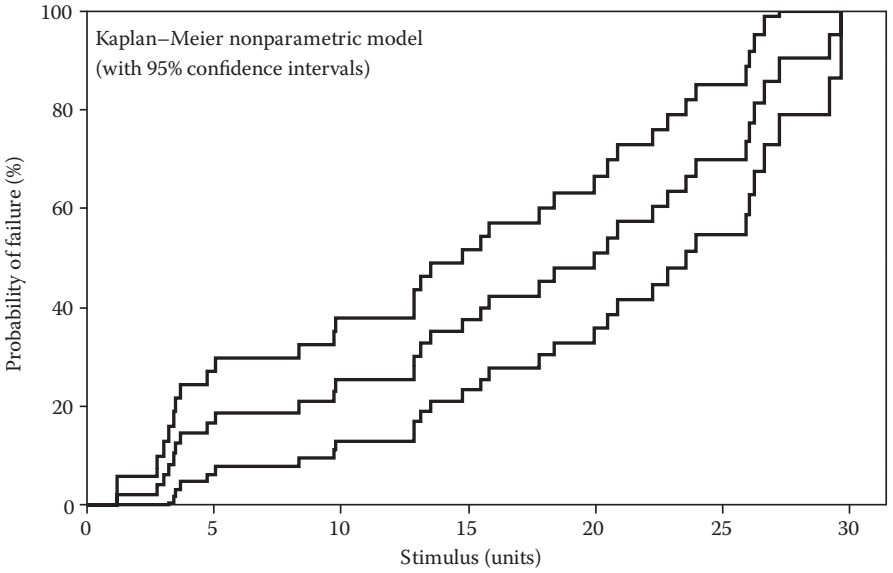

FIGURE 16.1
Kaplan–Meier nonparametric survival model based on hypothetical injury and noninjury data points. In the underlying data, it is assumed that the failure points are exact data points while the nonfailure points are right-censored.

stimulus required to cause an injury is never known. Among the binary regression models, logistic regression, which assumes a logistic distribution, and probit regression, which assumes a normal distribution, are the most popularly used for representing injury criteria using results from biomechanical data.

Binary regression models allow for analyzing the relationship between multiple covariates or explanatory variables and a single outcome or dependent variable; these are referred to as multivariate models. The explanatory variables must include the stimulus variable that is responsible for the injury causation such as displacement, force, or acceleration. Additional explanatory variables or covariates may include the demographic characteristics of the subject (e.g., sex, age, and anthropometry) and the test conditions, among other parameters that may affect the risk of injury along the stimulus variable. Specifically, a regression model estimates how the dependent outcome changes as an individual independent variable is varied while controlling for the other covariates in the model. In a regression model, the error associated with each variable is assumed to be random, and thus, the underlying data should be such that the regression error is uncorrelated across the observations. Furthermore, the independent covariates must be linearly independent and not multicollinear. The form of any binary regression model may be expressed as shown in Equation 16.2, where Y is the dependent outcome variable (typically injury outcome in an injury risk function), x_i is one of the independent explanatory variables, and β_i is the corresponding regression coefficient parameter:

$$Y \approx f(x_i, \beta_i). \tag{16.2}$$

The development of the regression model involves estimating the regression coefficients of the model using curve-fitting techniques such as maximum likelihood estimation or least-squares error estimation based on the sampled data. As the model is determined with appropriate values of the regression coefficients (β_i), the output of the model may be expressed either in terms of an odds ratio for each covariate or as a predictive model in which the risk of injury is expressed for a chosen set of covariate values. The odds ratio for the covariate x_i is expressed in terms of β_i, indicating the risk change in the outcome variable, Y, for a unit change in the covariate variable, x_i, while controlling for the remaining covariates. Similarly, in the prediction model, fixed values are assigned to all covariates except for the covariate of interest, say, x_i, and then for a range of x_i, the probability of outcome Y may be plotted as a function of x_i using the functional form of Equation 16.2.

The form of the function f, as shown in Equation 16.3, depends on the chosen binary regression model. The function f for the logistic regression model is described as

$$Y = \frac{1}{1+e^{-z}}, \text{ where } z = \beta_0 + \beta_1 x_1 + \ldots + \beta_i x_i. \tag{16.3}$$

In Equation 16.3, the outcome variable Y typically ranges between 0 and 1 and expresses the probability of injury in that range. Among the regression coefficients, β_0 is also known as the intercept or the baseline risk. It expresses the risk when all covariates (x_i) have a null value. The adjusted odds ratio for variable x_i in this case would be $e\beta^i$. An example of injury criteria based on biomechanical data and using logistic regression model is shown in Figure 16.2.

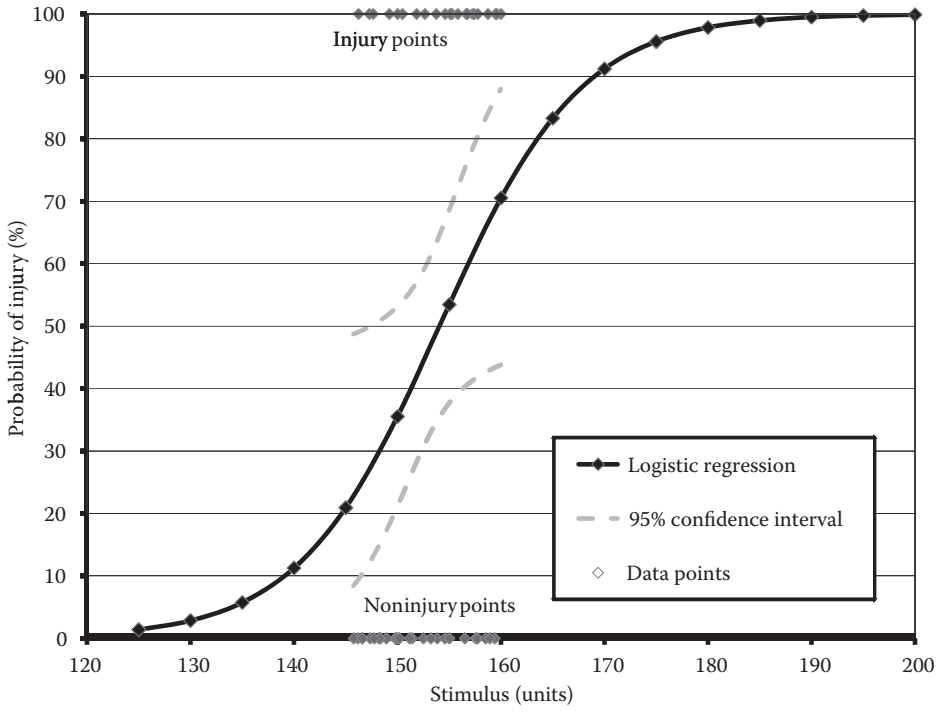

FIGURE 16.2
Logistic regression model based on hypothetical injury and noninjury data points.

16.2.3 Parametric and Semiparametric Survival Models

Survival analysis is a branch of statistics that involves modeling of time to event data; typically in the field of medicine and health, death or failure is considered the "event" in the survival analysis. Adapting this to our objective of developing an injury risk function, survival analysis allows for modeling any engineering parameter such as force or displacement (analogous to time) required to injure (analogous to failure or death) a tissue specimen. In essence, an injury risk function developed based on survival analysis attempts to answer questions such as, what is the probability (or fraction) for a long-bone specimen to survive (i.e., not fracture) when the applied axial force exceeds a threshold value of force? With the goal of defining injury risk, the same model can also be represented as a probability of injury function in which each point on the curve defines the probability of injury for that value of the stimulus and lower. An important feature of survival analysis is that the data points can be censored in nature. Although in the regression models, an exact value of the stimulus is assigned for each of the injury and noninjury data points, the survival model allows the data points to be entered as a range of stimuli. For instance, the stimulus value for a left-censored data point may be entered as (0, 40), meaning that the injury happens in this range between 0 and 40 units of stimulus but the exact injury stimulus is not known. This feature to handle censored data type is particularly useful to represent experimental biomechanics data.

To understand the survival analysis model, it is necessary to first present some of the standard definitions of a survival model. Typically, the survival function, also referred to as the "survivorship function" or "cumulative survival rate," denoted by $S(t)$, is defined as the probability that a specimen will survive a stimulus value higher than t, as expressed in Equation 16.4:

$$S(t) = P(T > t). \tag{16.4}$$

As discussed above, the injury risk is represented by the probability of injury function, also the cumulative distribution function, denoted by $F(t)$ which, by definition, is the probability that a specimen will fail for stimulus value t and lower:

$$F(t) = 1 - S(t). \tag{16.5}$$

The continuous variable survival time, t, has a probability density function defined as the limit of the probability that a specimen fails in a very small stimulus interval per unit of the stimulus:

$$f(t) = \frac{\lim_{\Delta t \to 0} P[\text{specimen } t \text{ fails in the interval } (t, t + \Delta t)]}{\Delta t}. \tag{16.6}$$

Similar to the probability density function, the hazard function $h(t)$ expresses the conditional failure rate. The conditional failure rate, also known as the hazard rate, is defined as the limit of the probability that a specimen fails in a very small stimulus interval, $(t, t + \Delta t)$, assuming that the specimen survived to stimulus t:

$$h(t) = \frac{\lim_{\Delta t \to 0} P[\text{specimen } t \text{ fails in the interval } (t, t + \Delta t) \text{ given that it survived until } t]}{\Delta t}. \tag{16.7}$$

The hazard function is related to the probability density function, $f(t)$, cumulative distribution function, $F(t)$, and the survival function, $S(t)$, according to

$$h(t) = \frac{f(t)}{1 - F(t)} = -\frac{d}{dt}\log S(t). \tag{16.8}$$

Based on this foundation for survival analysis, injury risk models may be developed that are either nonparametric or parametric in nature. The application of survival analysis to develop a nonparametric injury criterion has been discussed in a previous section. As we see in Equations 16.4 through 16.8, the survival analysis model can also be used to fit the injury data to a curve while assuming a certain distribution of the underlying failure data. In that case, the functional form of $F(t)$ and $f(t)$ will be a two-parameter or three-parameter model, depending on the assumed distribution, which may be optimized using standard statistical methods.

As discussed in the beginning of this section, the choice of the assumed distribution may have implications for the risk representation. For instance, the hazard function as described in Equations 16.7 and 16.8 may have restrictions based on the assumed distribution. Although the exponential distribution is associated with a constant hazard function, the hazard function in the case of a Weibull distribution may be monotonically increasing, decreasing, or constant. Similarly, the assumed distribution may have different flexibilities to accommodate the different shapes of the injury risk curve. The Weibull distribution may either be a two-parameter or a three-parameter distribution, in which case, the latter provides more flexibility for curve fitting. Another important consideration is that the logistic and the normal probability density functions extend from $-\infty$ to $+\infty$, and therefore, the integrated cumulative probability distribution shows a nonzero risk at zero stimulus. This is typically substantial when the mean failure stimulus is close to the zero value. The choice of Weibull distribution function, which starts from zero, eliminates the artifact of nonzero risk at zero stimulus.

Although parametric survival analysis models are powerful when an assumption of the underlying distribution can be made, most biomechanical data do not conform to a particular distribution.[8–10] A commonly used survival model when the underlying distribution is not known is the Cox proportional hazards model.[8] The hazard function in this case can take any shape not dictated by a distribution; however, the hazard functions of different individuals are assumed to be proportional and independent of the stimulus value. The hazard function, or the proportion of specimens failing per unit value of the stimulus, for the Cox proportional hazards model is described by

$$h(t, x) = h_0(t)\exp(\beta_i x_i), \tag{16.9}$$

where $h_0(t)$ is the baseline hazard for the stimulus t, x's are the covariate values, and β's are the regression coefficients for the covariates. This model is described as a semiparametric model in which the stimulus variable does not follow any distributional assumptions, but the covariates are assumed to have a known distribution.

Although there are multiple ways of expressing an injury risk function, the selection of the appropriate model is determined based on limitations of the statistical model, if any, associated with the underlying assumptions, and the goodness-of-fit of the data points to the assumed model. A decision-making flowchart can be used as a rough guideline for the selection of the type of injury risk function (Figure 16.3).

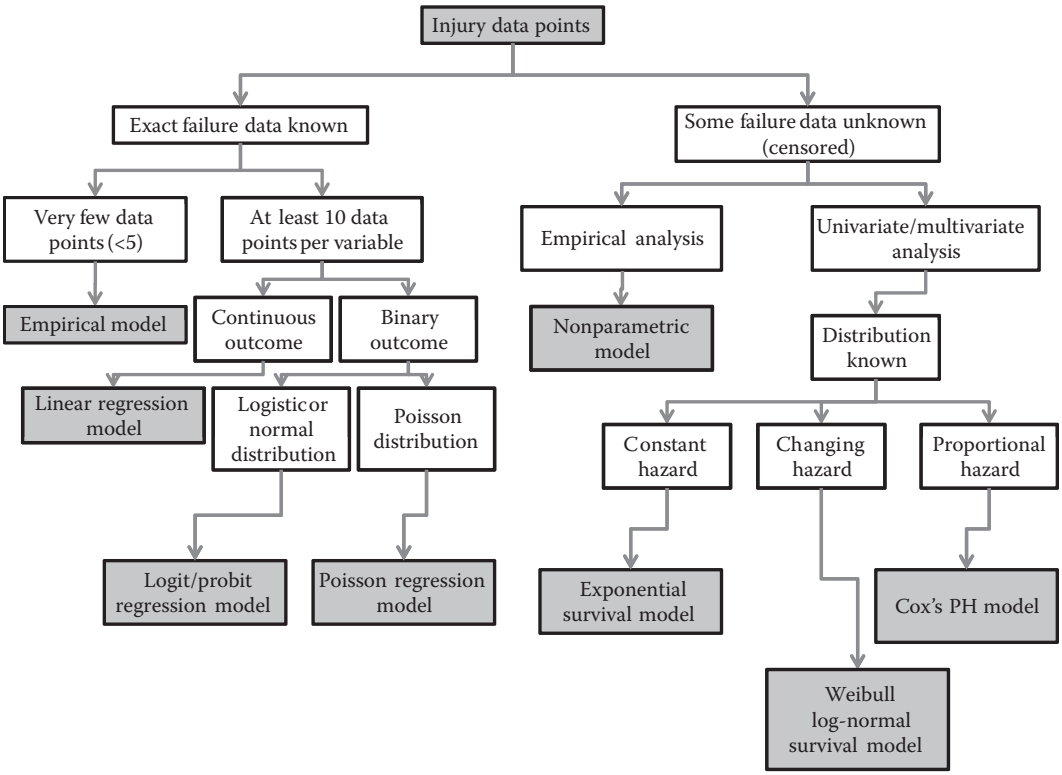

FIGURE 16.3
Decision flow chart for selecting the appropriate injury criteria model based on the method of data collection (censored and noncensored data), sample size, and distribution of the injury data.

16.3 Injury Mechanisms and Risk Functions for Relevant Orthopaedic Body Regions

16.3.1 Head

The head can sustain a range of injuries, and the mechanisms of those injuries encompass a range of mechanical loads and deformation mechanisms, including contact forces and noncontact inertial loading from rotational and linear motions imparted through the neck. Injuries associated with contact forces include skull fractures, contusions, and most forms of hematoma. In contrast, direct contact is not necessary for motions of sufficient magnitude to be generated to induce concussive injuries, including diffuse axonal injury or subdural hematoma. Gennarelli and Meaney[11] categorized several injuries as mechanistically related either to contact (direct blow necessary, head motion unnecessary) or to motion (direct blow unnecessary, motion necessary) (Table 16.2).[2] Most clinical presentations include injuries caused by both types of loading (contact and inertial) because real-world loading modes rarely generate either type of loading in isolation.

Historical injury criteria for the head have not adequately described the relationships between mechanical loading and injury risk over the range of possible mechanisms.[12] Improving the robustness and specificity of injury criteria for the head is a major driver of

TABLE 16.2

Head Injury Mechanisms

Contact Injuries	Motion Injuries
Skull deformation injuries	Skull–brain relative motions
Local skull fractures (linear, depressed)	Subdural hematoma
Extradural/Epidural hematoma	Contrecoup contusions
Coup contusions	Intermediate coup contusions
Remote vault and basilar skull fractures	
Contrecoup contusions	Brain deformations
Shockwave injuries	Concussion syndromes
Intracerebral hematoma	Diffuse axonal injury
	Intracerebral and tissue tear hemorrhage

Source: Adapted from Gennarelli, T. and Meaney, D., Mechanisms of primary head injury. In *Neurosurgery,* edited by R. H. Wilkins and S. S. Rengachary, vol. 2, 2nd ed., 2611–2621, New York: McGraw Hill, 1996.

contemporary injury biomechanics research. The head injury criterion (HIC) is based on the translational acceleration of the head's center of gravity and is perhaps the most widely used injury criterion for the head.[13] Its veracity in a range of loading situations has been questioned, however, and alternative criteria have been proposed, including those considering rotational motion,[14–16] directionality,[17] and the rate of change of the head's kinetic energy.[12] Combined experimental and computational injury-predicting algorithms have also been proposed and have been shown to discriminate injurious loading from noninjurious loading more robustly compared with the HIC.[18] This approach may also allow for greater resolution in the prediction of specific injuries by considering multiple aspects of the head/brain mechanics (i.e., hemorrhages caused by relative motion between skull and brain in contrast to brain contusions caused by large hydrostatic stresses).

16.3.2 Cervical Spine

Understanding the injury mechanisms and tolerances of the cervical spine is hampered by the complexity of the mechanical interactions of its components and, historically, by the frequent misinterpretation of the segmental mechanics that can occur if cervical spine mechanics are inferred only from gross head motion.[19,20] The cervical spine is composed of seven vertebrae but can be classified morphologically and mechanistically into distinct upper and lower multisegment regions. The upper cervical spine includes the base of the skull and the first two vertebrae, the axis and the atlas, and the function of the intervening joints is distinct from those of the distal vertebrae of the lower cervical spine. The occipital-atlantal joint allows substantial flexion-extension rotation, and the atlantoaxial joint enables substantial axial rotation. The lower cervical vertebrae are similar to each other but increase in size inferiorly. The kinematic behaviors of the lower cervical intervertebral joints are dictated by their morphology, which differs from the upper vertebrae.[21] The mobility of the cervical spine allows the existence of injury mechanisms that are not apparent from the gross head motions. Myers and Winkelstein[19] summarized key injury mechanisms for selected injuries of the cervical spine (Table 16.3), but stressed that the mechanisms refer to the loads applied to the spine at the site of injury, not necessarily to the loads applied to, or the gross movements of, the head. It is apparent from this summary that the nature of the observed trauma does not necessarily uniquely define the loading mode that generated it. For example, teardrop fractures and clay shoveler's fractures can be sustained from multiple loading modes.

TABLE 16.3

Cervical Spine Injury Mechanisms

Compression	Tension–extension
Jefferson fracture	Hangman's fracture
Multipart atlas fracture	Anterior longitudinal ligamentous damage
Vertebral body compression fracture	Disc rupture
Teardrop fracture	Horizontal fracture of vertebral body
	Teardrop fracture
Compression–flexion	
Teardrop fracture	Tension–flexion
Burst fracture	Bilateral facet dislocation
Wedge compression fracture	Unilateral facet dislocation
Hyperflexion sprain	
Bilateral facet dislocation	Torsion
Unilateral facet dislocation	Atlantoaxial rotary dislocation
	Unilateral atlantoaxial facet dislocation
Compression-extension	
Hangman's fracture	Shear
Clayshoveler's fracture	Odontoid fracture
Posterior element fractures	Transverse ligament rupture
Anterior longitudinal ligamentous rupture	
Anterior disc rupture	Lateral bending (in combined loading)
Horizontal vertebral body fracture	Asymmetric injury
Teardrop fracture	Nerve root avulsion
	Peripheral nerve injury
Tension	
Occipito-atlantal dislocation	

Source: Adapted from Myers, B. and Winkelstein, B., *Crit. Rev. Biomed. Eng.*, 23 (5–6), 307–409, 1995.

The tolerance of the cervical spine to the loading modes listed in Table 16.3 is sensitive to the position of the spine, the boundary conditions, the inertia of the head, and the eccentricity of loading, among other factors.[19] Defining the tolerance levels from these is also hampered by the lack of pure spinal loading in real-world injurious situations. Experimental studies quantifying tolerance values for several loading modes have been summarized by Myers and Winkelstein[19] and McElhaney et al.[22]

16.3.3 Thorax

The torso contains many anatomical structures, and the specific injury mechanisms and tolerances applicable to this region are numerous. In the thorax, rib fractures are the most common serious skeletal thoracic injury.[23] These injuries can be life-threatening, particularly for those with preexisting pulmonary pathology or in the elderly. As more ribs are fractured, there is a progression of pathophysiological findings, including ventilation–perfusion abnormalities, increased respiratory work, hypoxemia, and decreased functional residual capacity.[24] If a sufficient number of fractures occur on adjacent ribs, the intervening rib segments may lose continuity with the rest of the thorax resulting in flail chest. Flail chest occurs when a segment of the anterior or lateral chest wall (or both) is freely movable because of multiple rib fractures. This allows the segment to move paradoxically with changes in intrathoracic pressure (i.e., inward on inspiration and outward on expiration), impairs ventilation, and thereby affects oxygenation of the blood. The predominant mechanism of rib fracture is the deformation of the thorax.[25] Complex deformation

patterns can be generated in actual injurious loading situations, such as impingement of a seatbelt during a car crash, and the development of robust injury predictors for a range of deformation profiles is an area of active research.[26–28]

The thorax also contains a variety of joints and ligaments, muscles, lymphatics, fascia, nerves, viscera, and blood vessels. The organs of the thorax include the heart and lungs, both of which may sustain blunt trauma. Injuries to these structures occur from a variety of load paths, including direct compression due to thoracic deformation from an external impact and contacts between other structures within the thoracic cavity. Trauma may also occur, particularly at attachment sites, when the thorax is accelerated.[29] Unlike rib fractures, this soft tissue injury is sensitive to the rate at which the chest is loaded. The lungs can also be lacerated by broken ribs or by direct impact.[30] Hemothorax and pneumothorax occur when blood or air, respectively, appears in the pleural cavity between the visceral and parietal pleura. Hemothorax and pneumothorax are typically caused by punctures or lacerations of the lung tissue, blood vessels, parietal pleura, or visceral pleura caused by broken ribs. The presence of blood or air in this cavity compresses the lungs and impedes respiration. Severe cases can be fatal. During thoracic impact, the heart can be subject to contusion, laceration, arrhythmia, cardiac tamponade (which occurs when blood accumulates in the pericardial cavity, resulting in compression of the heart and great vessels; it is conceptually similar to a hemothorax in the pleural cavity), or cardiac arrest. Side impacts of automobiles produce a large proportion of cardiovascular injury, although it is not clear whether this is primarily due to differences in the dynamics of different types of vehicle crashes; side impacts generally produce higher levels of deformation rate compared with restrained frontal impacts. However, it is also possible that differences in the human tolerance to anterior versus lateral loading may be responsible for the different injury risks associated with crash directions. High-speed blunt impacts (> 15–20 m/s) seem to interrupt the electromechanical transduction of the heart wall and may result in commotio cordis, cardiac fibrillation, or arrest.[31] Several mechanisms of aortic injury have been proposed, depending on the type, mechanism, and site of the injury. Although the mechanism of aortic rupture remains incompletely described, it does appear that deformation of the thoracic cage is required. Internal pressure or whole-thorax acceleration does not seem to generate clinically relevant injuries.[29,32–34]

16.3.4 Abdomen, Pelvis, and Extremities

The abdomen, like the thorax, is heterogeneous; it is filled with organs and other structures having a range of inertial and material properties and body attachments.[35] This characteristic plays an important role in the mechanisms and tolerances of abdominal injury. For example, in the case of steering wheel rim impacts (as occurs in vehicle impacts), it has been observed that the organs displace in a direction normal to the applied penetration during impact; the liver moves toward the head and can be displaced such that an injury does not occur.[36] In tests simulating a lower rate of impact, the organ effectively slides out of the path of the impactor and sustains no injury. In a higher-rate test, the organ did not have time to displace, and as a result, it experienced more loading and an associated increase in tissue deformation. This phenomenon could be manifest in a rate-sensitive injury risk if the impact is aligned in such a manner as to induce organ motion. In simple terms, an internal organ is able to slip out of the way in a low-speed test and is not able to in a high-speed test due to its inertia. This motility may explain the occasional observation that the abdomen's tolerance to deformation is modulated by the rate of its deforma-

tion,[37,38] although additional research is required to fully elucidate the roles of deformation, location of deformation, rate of deformation, and rate of loading.

The injury tolerance of the pelvis is strongly dependent on the direction of loading, the particular structures engaged, and the position of the femur in some cases. Recent research in this area has focused on loading through the knee–thigh–hip complex, such as that from impact with the knee bolster in a frontal car crash.[39] In that case, the acetabulum has the lowest fracture tolerance (i.e., is the "weak link") for a neutral (seated) femur position. Flexion and adduction of the hip joint decrease this tolerance by approximately 1% per degree of flexion and 2% per degree of adduction; abduction increases the tolerance by approximately 1% per degree.[39] The injury pattern can also change with femur orientation, with acetabular or femoral neck fractures being more common with hip extension or abduction and acetabular dislocations being more common with hip flexion and adduction.[40] In lateral loading, the fracture tolerance of the pelvis depends on the particular anatomical structures that are engaged, primarily whether the loading surface engages the greater trochanter and proximal femur, the iliac wing, and, to a lesser extent, the ischium.[41]

Injury tolerances of the long bones and some joints of the upper extremities have been summarized by Duma et al.[42] for small females in a variety of loading modes. Loading along the axis of the tibia is reported to be a prevalent mechanism of below-knee injury in car crashes[43] and is a contributing factor in nearly 82% of all lower extremity injuries.[44] The consensus among investigators is that the most severe injuries, such as calcaneus and tibia pilon fractures, are caused primarily or solely by axial loading because the calcaneus and tibia are situated along the axial loading path of the lower extremity.[45–47] A substantial sagittal plane bending moment may develop in the axially loaded tibial shaft because it naturally has significant anterior convex curvature.[48] In fact, axial loads to the curved tibia can result in such high bending moments, a currently utilized injury criterion for the tibia, referred to as the tibia index, which uses the curved-beam theory to combine axial and bending loads.[49]

Excessive ankle rotation can produce malleolar fractures, fibula fractures, or ligament tears.[50–52] One study in particular confirmed that malleolar fractures could be generated by pure blunt axial loading, dorsiflexion (induced by forefoot impact loading), dorsiflexion combined with axial loading (induced by midfoot impact loading), and pure eversion.[53] The authors also showed that retrospective analyses of malleolar fracture mechanisms are not reliable indicators of the injury mechanism responsible for any particular injury. From a biomechanical perspective, malleolar fractures produced by dorsiflexion can be explained by the fact that the anterior talus is wider than the posterior talus. During dorsiflexion, the wider portion is forced between the malleoli generated by outward forces on the bones. Confirmation of this hypothesized injury mechanism was provided in experimental studies by Rudd et al.[54] and Portier et al.,[55] who reported malleolar fractures with forced dorsiflexion of the ankle.

16.4 Summary

Injury biomechanics provides the scientific foundation and tools for the development of countermeasures and is a key part of injury prevention efforts. This chapter presented

a broad overview of the methodological approaches used in the generation of quantitative risk functions from biomechanical injury data and summarized some of the specific considerations for key body regions. Apparent from this overview, our knowledge of injury mechanisms and tolerances has expanded substantially since becoming the subject of rigorous study in the years after the Second World War, but key aspects of injury mechanics remain unknown. Future research in this area should focus on increasing the resolution of models relating mechanical loads to the generation of trauma. In the head, for example, this increased resolution will include greater understanding of the relationship between strain and strain rate in the brain tissue and the initiation of cell death. In the thorax, it will include enhanced understanding of how changing load distribution patterns, both spatially and temporally, can be used to restrain a vehicle occupant without causing injury.

In a more general sense, it is imperative that the drivers of individual tolerance variability throughout the entire body be better understood. Factors such as aging at both ends of the life spectrum, gender, obesity and body habits, and genetic make-up are thought to influence injury mechanics, yet the relationships remain essentially unknown, even directionally in many instances.

References

1. Peden, M., R. Scurfield, D. Sleet, D. Mohan, A. Hyder, E. Jarawan et al. 2004. World report on road traffic injury prevention. Geneva: World Health Organization.
2. Committee on Trauma Research, Commission on Life Sciences, National Research Council and Institute of Medicine. 1985. *Injury in America: A Continuing Public Health Problem*. Washington, D.C.: National Academic Press.
3. Viano, D. C., A. I. King, J. W. Melvin, and K. Weber. 1989. Injury biomechanics research: An essential element in the prevention of trauma. *Journal of Biomechanics* 22(5):403–417.
4. Broos, P. L., A. D'Hoore, P. Vanderschot, P. M. Rommens, and K. H. Stappaerts. 1993. Multiple trauma in patients of 65 and over. Injury patterns. Factors influencing outcome. The importance of an aggressive care. *Acta Chirurgica Belgica* 93(3):126–130.
5. Wutzler, S., M. Maegele, I. Marzi, T. Spanholtz, A. Wafaisade, and R. Lefering. 2009. Association of preexisting medical conditions with in-hospital mortality in multiple-trauma patients. *Journal of the American College of Surgeons* 209(1):75–81.
6. Mackay, M. 2007. The increasing importance of the biomechanics of impact trauma. *Sadhana* 32(4):397–408.
7. Kaplan, E. L., P. Meier. 1958. Nonparametric estimation from incomplete observations. *Journal of the American Statistical Association* 53(282):457–481.
8. Cox, D. 1972. Regression models and life tables. *Journal of the Royal Statistical Society. Series B, Statistical Methodology* 34(2):187–220.
9. Di Domenico, L. and G. Nusholtz. 2003. Comparison of parametric and non-parametric methods for determining injury risk. *SAE World Congress & Exhibition* Paper 2003-01-1362.
10. Kent, R. W. and J. R. Funk. 2004. Data censoring and parametric distribution assignment in the development of injury risk functions from biomechanical data. *SAE World Congress & Exhibition* Paper 2004-01-0317.
11. Gennarelli, T. and D. Meaney. 1996. Mechanisms of primary head injury. In *Neurosurgery,* edited by R. H. Wilkins, and S. S. Rengachary, 2611–2621, vol. 2, 2nd ed. New York: McGraw Hill.

12. Newman, J. A., N. Shewchenko, and E. Welbourne. 2000. A proposed new biomechanical head injury assessment function—the maximum power index. *Stapp Car Crash Journal* 44:215–247.
13. Kleinberger, M., E. Sun, R. Eppinger, S. Kuppa, and R. Saul, 1998. Development of improved injury criteria for the assessment of advanced automotive restraint systems. Final Report. Washington, D.C.: U.S. Department of Transportation.
14. Hirsch, A. E., and A. K. Ommaya. 1970. Protection from brain injury: The relative significance of translational and rotational motions of the head after impact. *Stapp Car Crash Conference Proceedings* SAE Paper 700899.
15. Newman, J. 1986. A Generalized Model for Brain Injury Threshold (GAMBIT). Paper presented at the *IRCOBI Conference on the Biomechanics of Impact, Zurich, Switzerland*.
16. Thibault, L., and T. Gennarelli. 1990. Brain injury: an analysis of neural and neurovascular trauma in the nonhuman primate. *Annual Proceedings. Association for the Advancement of Automotive Medicine* 34:331–351.
17. Kleiven, S. 2003. Influence of impact direction on the human head in prediction of subdural hematoma. *Journal of Neurotrauma* 20(4):365–379.
18. Takhounts, E., R. Eppinger, J. Q. Campbell, R. Tannous, E. Power, and L. Shook. 2003. On the development of the Simon finite element head model. *Stapp Car Crash Journal* 47:107–133.
19. Myers, B., and B. Winkelstein. 1995. Epidemiology, classification, mechanism, and tolerance of human cervical spine injuries. *Critical Reviews in Biomedical Engineering* 23(5–6):307–409.
20. Nightingale, R., J. McElhaney, W. Richardson, T. Best, and B. Myers. 1996. Experimental cervical spine impact injury: Head motion, injury classification, and injury mechanism. *Journal of Bone and Joint Surgery. American Volume* 78(3):412–421.
21. White, A., and M. Panjabi. 1990. *Clinical Biomechanics of the Spine*. 2nd ed. Philadelphia, PA: J. B. Lippincott Company.
22. McElhaney, J., R. Nightingale, B. Winkelstein, V. Chancey, B. Myers. 2002. Biomechanical aspects of cervical trauma. In *Accidental Injury: Biomechanics and Prevention*, edited by A. Nahum, and J. Melvin, 324–373. New York: Springer.
23. Pattimore, D., P. Thomas, and S. Dave. 1992. Torso injury patterns and mechanisms in car crashes: An additional diagnostic tool. *Injury* 23(2):123–126.
24. Cogbill, T. H., J. Landercasper. 1996. Injury to the chest wall. In: *Trauma*, 3rd ed., edited by D. V. Feliciano, E. E. Moore, K. L. Mattox, 355–374, Stamford, CT: Appleton & Lange.
25. Kent, R., and J. Patrie. 2004. Chest deflection tolerance to blunt anterior loading is sensitive to age but not to load distribution. *Forensic Science International* 149(2–3):121–128.
26. Kent, R., J. Patrie, and, N. Benson. 2003. The Hybrid III dummy as a discriminator of injurious and non-injurious restraint loading. *Annual Proceedings. Association for the Advancement of Automotive Medicine* 47:51–75.
27. Petitjean, A. M. Lebarbe, P. Potier, X. Trosseille, and J. Lassau. 2002. Laboratory reconstructions of real world frontal crash configurations using the Hybrid III and THOR dummies and PMHS. *Stapp Car Crash Journal* 46:27–54.
28. Shaw, G., D. Parent, S. Purtsezov, D. Lessley, J. Crandall, R. Kent et al. 2009. Impact response of restrained PMHS in frontal sled tests: Skeletal deformation patterns under seatbelt loading. *Stapp Car Crash Journal* 53:1–48.
29. Forman, J., S. Stacey, J. Evans, and R. Kent. 2008. Posterior acceleration as a mechanism for blunt traumatic injury of the aorta. *Journal of Biomechanics* 41(6):1359–1364.
30. Stitzel, J. D., F. S. Gayzik, J. J. Hoth, J. Mercier, H. D. Gage, K. A. Morton, S. M. Duma et al. 2005. Development of a finite element-based injury metric for pulmonary contusion. Part I: Model development and validation. *Stapp Car Crash Journal* 49:271–289.
31. Cooper, G. J., B. P. Pearce, M. C. Stainer, and R. L. Maynard. 1982. The biomechanical response of the thorax to nonpenetrating impact with particular reference to cardiac injuries. *Journal of Trauma* 22(12):994–1008.

32. Hardy, W. N., C. S. Shah, J. M. Kopacz, K. H. Yang, C. A. Van Ee, R. Morgan et al. 2006. Study of potential mechanisms of traumatic rupture of the aorta using in situ experiments. *Stapp Car Crash Journal* 50:247–266.
33. Hardy, W. N., C. S. Shah, M. J. Mason, J. M. Kopacz, K. H. Yang, A. I. King et al. 2008. Mechanisms of traumatic rupture of the aorta and associated peri-isthmic motion and deformation. *Stapp Car Crash Journal* 52:233–265.
34. Lee, S. and Kent, R. 2007. Blood flow and fluid–structure interactions in the human aorta during traumatic rupture conditions. *Stapp Car Crash Journal* 51:211–233.
35. Rouhana, S. 2002. Biomechanics of abdominal trauma. In *Accidental Injury: Biomechanics and Prevention*, edited by A. Nahum, and J. Melvin, 405–453. New York: Springer.
36. Shaw, C.G., D. Lessley, J. Bolton, and J. Crandall. 2004. Assessment of the THOR and Hybrid III crash dummies: Steering wheel rim impacts to the upper abdomen. *SAE World Congress & Exhibition* Paper 2004-01-0310.
37. Kent, R., S. Stacey, M. Kindig, W. Woods, J. Evans, S. Rouhana et al. 2008. Biomechanical response of the pediatric abdomen. Part 2: Injuries and their correlation with engineering parameters. *Stapp Car Crash Journal* 52:135–166.
38. Rouhana, S., R. El-Jawahri, and T. Laituri. 2010. Biomechanical considerations for abdominal loading by seat belt pretensioners. *Stapp Car Crash Journal* 54:381–406.
39. Rupp, J. 2006. Biomechanics of Hip Injuries in Frontal Motor-Vehicle Crashes. PhD diss., University of Michigan.
40. Salzar, R., C. Bass, R. Kent, S. Millington, M. Davis, S. Lucas et al. 2006. Development of injury criteria for pelvic fracture in frontal crashes. *Traffic Injury Prevention* 7(3):299–305.
41. King, A. 2002. Injury to the thoracolumbar spine and pelvis. In *Accidental Injury: Biomechanics and Prevention*, edited by A. Nahum, and J. Melvin, 454–490. New York: Springer.
42. Duma, S. M., J. R. Crandall, R. W. Rudd, R. W. Kent. 2003. Small female head and neck interaction with a deploying side air bag. *Accident; Analysis and Prevention* 35(5):811–816.
43. Crandall, J. R., E. Dekel, G. W. Hall, P. Schreiber, and W. D. Pilkey. 1995. The Effects of Lower Extremity Boundary Conditions on Ankle Response during Joint Rotation Tests. *Proceedings of the 23rd International Workshop on Human Subjects for Biomechanical Research, San Diego, CA*.
44. Fildes, B., J. Lenard, J. C. Lane, P. Vulcan, and K. Seyer. 1995. Lower Limb Injuries to Passenger Car Occupants. Paper presented at the *IRCOBI Conference on the Biomechanics of Impact, Brunnen, Switzerland*.
45. Morris, A., P. Thomas, A. Taylor, and W. Wallace. 1997. Mechanisms of fractures in ankle and hind-foot injuries to front seat car occupants—an in-depth accident data analysis. *Stapp Car Crash Conference Proceedings* SAE Paper 973328.
46. Pilkey, W. D., E. Sieveka, J. R. Crandall, and G. S. Klopp. 1994. The influence of vehicular intrusion and rotation on occupant protection in full frontal and frontal offset crashes. *Proceedings of the 14th ESV Conference* Paper 4-S4-W-31.
47. Sherwood, C., B. O'Neill, and S. Hurwitz. 1999. Lower Extremity Causation in Frontal Crashes. Paper presented at the *IRCOBI Conference on the Biomechanics of Impact, Sitges, Spain*.
48. Funk, J. R., J. R. Kerrigan, and J. R. Crandall. 2004. Dynamic bending tolerance and elastic-plastic material properties of the human femur. *Annual Proceedings. Association for the Advancement of Automotive Medicine* 48:215–233.
49. Mertz, H. J. 1984. Injury assessment values used to evaluate Hybrid III response measurements. NHTSA Docket 74-14, Notice 32. Enclosure 2 of Attachment 1 of Part III. General Motors Submission USG 2284, March 22, 1984.
50. Begeman, P., P. Balakrishnan, R. Levine, and A. King. 1993. Dynamic human ankle response to inversion and eversion. *Stapp Car Crash Conference Proceedings* SAE Paper 933115.
51. Begeman, P., and P. Prasad. 1990. Human ankle impact response in dorsiflexion. *Stapp Car Crash Conference Proceedings* SAE Paper 902308.

52. Petit, P., L. Portier, J. Y. Foret-Bruno, X. Trosseille, C. Parenteau, J. C. Coltat et al. 1996. Quasistatic Characterization of the Human Foot–Ankle Joints in a Simulated Tensed State and Updated Accidentological Data. Paper presented at the *IRCOBI Conference on the Biomechanics of Impact, Dublin, Ireland*.
53. Srinivasan, S., C. P. Sherwood, J. R. Funk, and J. R. Crandall. 2001. Retrospective assessment of malleolar fracture mechanism in impact environment. *Annual Proceedings. Association for the Advancement of Automotive Medicine* 45:405–407.
54. Rudd, R., J. Crandall, S. Millington, and S. Hurwitz. 2004. Injury tolerance and response of the ankle joint in dynamic dorsiflexion. *Stapp Car Crash Journal* 48:1–26.
55. Portier, L., P. Petit, A. Domont, X. Trosseille, J. Le Coz, C. Tarriere et al. 1997. Dynamic biomechanical dorsiflexion responses and tolerances of the ankle joint complex. *Stapp Car Crash Conference Proceedings* SAE Paper 973330.

17

Injury Mechanisms of Several Common Sports-Related Orthopaedic Injuries

Philip J. Brown, Sandeep Mannava, Johannes F. Plate, and Joel D. Stitzel

CONTENTS

17.1 Introduction

Athletic injuries sustained during sporting activities are the most common injuries in the modern Western societies of the world.[1] The risk of acute injury greatly varies depending on the sport played. Endurance sports tend to have a higher risk of overuse, fatigue, and stress-related injuries. Team sports and many newer sports such as snowboarding, cycling, and power sports include elements of high speed and acceleration, as well as contact between players, putting the athletes at higher risk of acute injury.[1]

The incidence of sports and recreation injuries treated in hospital emergency departments between July 2000 and June 2001 in the United States was 15.4 per 1000 individuals of the general population.[2] The National Collegiate Athletic Association (NCAA) created an Injury Surveillance System (ISS) in 1982 and has been collecting injury and exposure data from 17 sports considered at high risk for injury. Hootman et al.[3] analyzed the ISS database for injury data from 15 sports between 1988 and 2004, including men's baseball, men's basketball, women's basketball, women's field hockey, men's fall football, men's spring football, women's gymnastics, men's ice hockey, men's lacrosse, women's lacrosse, men's soccer, women's soccer, women's softball, women's volleyball, and men's wrestling. This data sample contains 5,244,088 athlete exposures and 72,316 injuries (1.37%).

Injury rates were found to be fairly constant throughout the time of the Hootman study. Across all divisions (I, II, and III) and seasons, the injury rate for in-game play was 13.8 per 1000 athlete exposures (A-E), which is considered to be a single athlete participating in one game or practice. This is 3.5 times that of the practice injury rate, which was 4.0 per 1000 A-E. When injuries were stratified according to body region, more than 50% of all injuries were those to the lower extremity in both the practice and in-game settings.[3] Upper extremity is the second most common body region injured during athletic competition, with

injury rates at 18% in games and 21% in practice. Ankle sprains are the most common injuries in all levels of collegiate sports, accounting for 14.8% of all injuries related in the ISS. Anterior cruciate ligament (ACL) injuries and concussions were also common, but less prevalent.[3]

In this chapter, five common sports-related injuries to the lower and upper extremity are presented and analyzed. Specifically, the orthopaedic biomechanics of ACL ruptures, lateral ankle ligament sprains, partial and complete rotator cuff tears, meniscal tears, and proximal fifth metatarsal fractures are reviewed in detail. This chapter addresses the relevant clinical and biomechanical injury mechanisms and biomechanical tissue properties of the structures involved.

17.2 Anterior Cruciate Ligament Tears

The ACL is commonly torn during athletic activities, potentially resulting in lasting decline in activity level.[4] It has been estimated that approximately 175,000 primary ACL surgeries are performed annually in the United States with an estimated cost of more than $2 billion.[5] Hootman et al.[3] estimated that between the years of 1988 and 2004, more than 2000 ACL injuries occurred in NCAA competitions annually. Of all sports, ACL injuries most commonly occurred during football, comprising 53% of the total injuries sustained during competition. ACL injury rates are also common in women's gymnastics, women's basketball, and women's soccer.[3]

The ACL is one of the four major knee ligaments, which function to constrain the distal femur and proximal tibia to form the joint. The knee joint has six degrees of freedom, including three translational and three rotational. Because the primary axis of rotation has a much greater range of motion compared with the other axes, the knee is often simplified to a single axis of flexion and extension.[6] The other ligaments of the knee include the medial collateral ligament (MCL), lateral collateral ligament, and the posterior cruciate ligament (PCL). The ACL and PCL are primarily responsible for respectively restraining the relative anterior and posterior translational motion of the femoral condyles and the tibial plateau. Anatomically, the ACL originates from the lateral wall of the femoral intercondylar notch and inserts on the anterior portion of the tibial plateau.[7] Noncontact ACL tears are common during athletic competition and are typically seen when an athlete suddenly decelerates, lands, or pivots about a planted foot.[4] The ACL acts against anterior displacement of the tibial plateau relative to the distal femur and also prevents hyperextension of the knee joint.[7]

The primary mechanism of ACL failure occurs when there is a joint shear load on the knee (Figure 17.1). This shear force acts on the tibia, forcing it anteriorly while the femur is forced posteriorly. The shear force starts as a posteriorly directed ground reaction force on the foot, which creates a flexion moment about the knee.[4] The flexion moment is counteracted by a quadriceps muscle force, which creates an opposing extension moment. The quadriceps force is transmitted through the patella, which is a sesamoid bone that sits on the patellar surface between the femoral condyles. The patella slides along the patellar surface and effectively increases the moment arm of the quadriceps on the knee joint. Force passes through the patellar tendon to the anterior tibia, thereby pulling the tibia both anteriorly and superiorly. The superiorly directed component of the force from the patellar tendon creates an extension moment about the joint. The anteriorly directed component of the force from the patellar ligament creates a shear load on the joint. This shear force is counteracted by tension force from the ACL.[4]

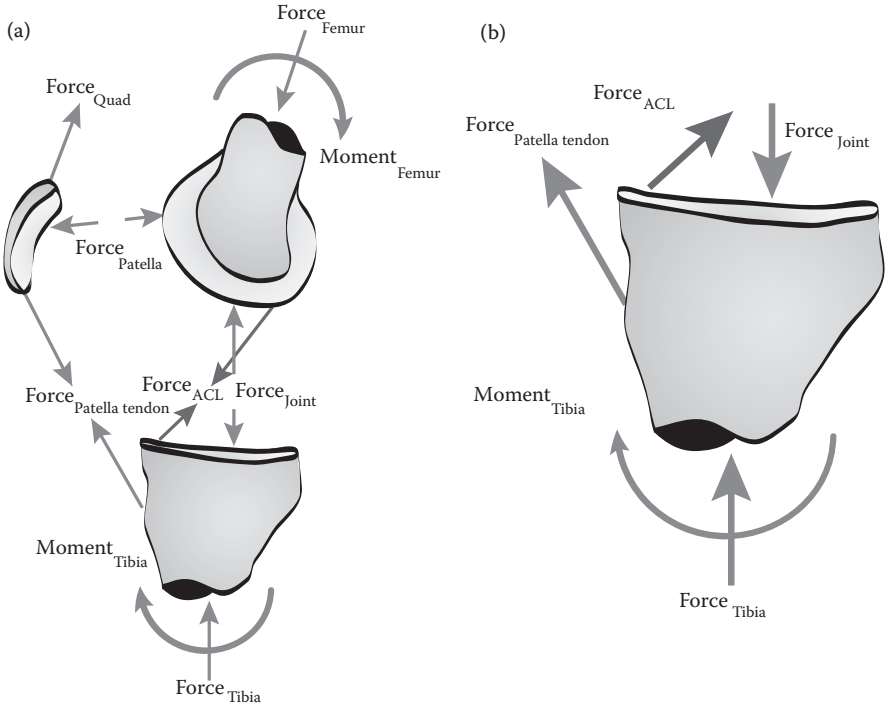

FIGURE 17.1
Simplified two-dimensional free body diagram of the forces involved in the knee joint during a quadriceps contraction, which occurs in a sudden deceleration. (a) Free body diagram of the distal femur, proximal tibia, and patella. (b) Distal tibia free body diagram highlighting the role of the ACL force in knee joint mechanics.

Clinically, differences in gender seem to influence ACL injury rates that are treated by orthopedists. Biomechanically, there seem to be structural differences that may explain these clinical observations. Chandrashekar et al.[8] studied the differences in mechanical properties between the male and female ACL. They found that the male ACL has a greater yield strain, yield stress, ultimate load, stiffness, modulus of elasticity, and energy absorption at failure than the female ACL in tensile loading. These values are summarized in Table 17.1, along with the combined average properties and the percentages of difference between the sexes. For that study, stress was calculated using the minimum cross-sectional area of the ACL, and a strain rate of 100% strain per second was used.[8]

The difference in structural properties, such as ultimate load and extension at failure, of the ACL between sexes has been attributed to the size difference that exists between male and female ACLs. The average cross-sectional area of a male and female athlete ACL is 48.9 and 36.1 mm^2, respectively.[9] However, in addition to the difference in size, the mechanical properties differ significantly between the sexes as well, demonstrated by multivariate regression modeling.[8] Because the female ACL has both a smaller minimum cross section and ultimate stress, females are at a higher risk for injury during competitive athletics.[10] When comparing various athletic competitions of similar skill level, females have a higher rate of ACL injury than males. For example, it has been reported that females have an injury rate of 4.1 and 2.4 times that of males in basketball and soccer, respectively.[9]

TABLE 17.1

Sex-Based Differences in Mechanical Properties of the Human ACL

Sex	Elongation at Failure (mm)	Strain at Failure	Load at Failure (N)	Stress at Failure (MPa)	Stiffness (N/mm)	Modulus of Elasticity (MPa)	Energy at Failure (N/mm)
Male (n = 8)	8.95 ± 2.12	0.30 ± 0.06	1818 ± 699	26.35 ± 10.08	308 ± 89	128 ± 35	7280 ± 3624
Female (n = 9)	7.48 ± 2.56	0.27 ± 0.08	1266 ± 527	22.58 ± 8.92	199 ± 88	99 ± 50	4691 ± 3623
Combined (n = 17)	8.17 ± 2.41	0.28 ± 0.07	1526 ± 658	24.36 ± 9.38	250 ± 102	113 ± 45	5909 ± 3753
Difference (%)	16.40	8.36	30.36	14.29	35.30	22.49	35.56

Source: Chandrashekar, N. et al., *J. Biomech.* 39(16), 2943–2950, 2006. With permission.
Note: Mean ± SD.

When isolating the shear force generated in the knee joint, the tension force in the ACL can be expressed as a function of the joint flexion angle. When the flexion angle of the joint is small, the elevation angle of the ACL relative to the tibial plateau is large. The elevation angle of the ACL decreases from 40° at full extension to 0° at 120° of knee flexion.[11] The resultant ACL tension is a function of the cosine of the elevation angle and the magnitude of the shear force. The greater the elevation angle, the greater the force generated in the ACL required to maintain equilibrium. Thus, the tension experienced by the ACL is greater at a low knee flexion angle and lower at a high knee flexion angle. Equilibrium can be found by analyzing the free body diagram of the force and moment vectors on the tibial plateau (Figure 17.2).

The force on the ACL can be found by simultaneously solving three equations of dynamic equilibrium. These include equations for the force vector equilibrium on the tibia in the inferior–superior (y) direction (Equation 17.1) and in the anterior–posterior (x) direction (Equation 17.2), and an equation for the equilibrium of moments about the joint center (JC; Equation 17.3).

$$\sum F_{\text{tibia}_y} = F_{\text{GRF}} + F_{\text{patella}} \sin\beta + F_{\text{ACL}} \sin\alpha - F_{\text{joint}} = m_{\text{leg}} * a_{\text{leg}_y}, \tag{17.1}$$

$$\sum F_{\text{tibia}_x} = F_{\text{ACL}} \cos\alpha + F_{\text{patella}} \cos\beta = m_{\text{leg}} * a_{\text{leg}_x}, \tag{17.2}$$

$$\sum M_{\text{tibia}_{\text{JC}}} = M_{\text{GRF}} - F_{\text{patella}} * b + F_{\text{ACL}} * a = I_{\text{leg}_{\text{JC}}} * \alpha_{\text{leg}_{\text{JC}}}, \tag{17.3}$$

where F_{tibia_x} and F_{tibia_y} are the resultant force on the tibia in the x and y directions, respectively; F_{GRF} and M_{GRF} are the ground reaction force and moment, respectively; F_{patella} is the patella tendon force; F_{ACL} is the ACL force; F_{joint} is the joint space force; a is the perpendicular distance from F_{ACL} to JC; b is the perpendicular distance from F_{patella} to JC; α is the angle of ACL from tibial plateau; β is the angle of patella tendon from tibial plateau; $\alpha_{\text{leg}_{\text{JC}}}$ is the angular acceleration of the leg about the JC; a_{leg_x} and a_{leg_y} are the linear acceleration of the

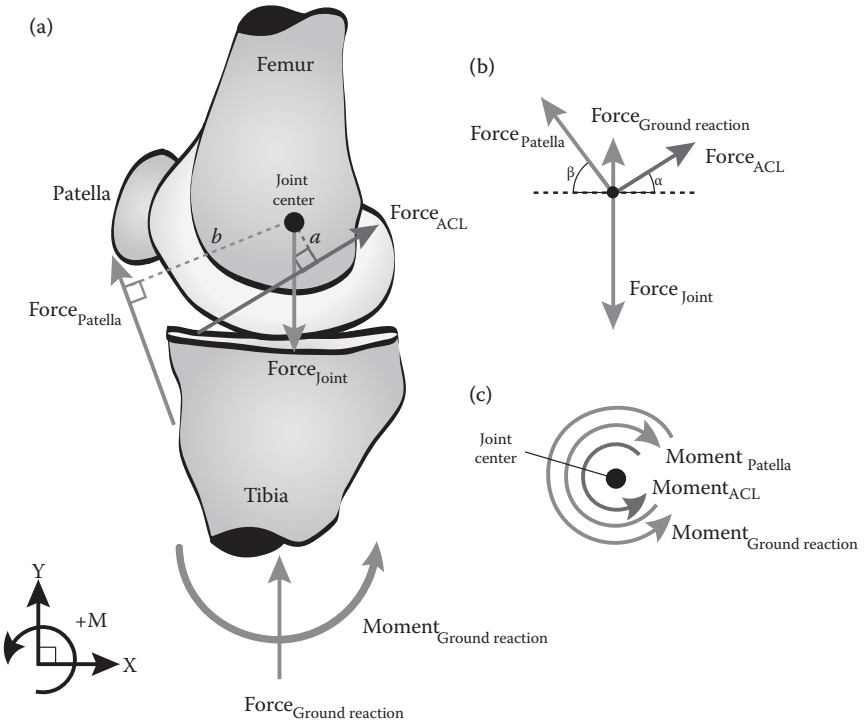

FIGURE 17.2
(a) Vector addition of the free body diagram for the tibial plateau. (b) Simplified two-dimensional dynamic equilibrium of forces; (c) moments on the tibia about the JC. β is the angle of the patella tendon force on the *xy* plane with respect to the tibial *x* axis. α is the angle of the ACL force on the *xy* plane with respect to the tibial *x* axis. The perpendicular distance between the JC and the patella force vector is *b,* and the ACL force vector is *a*.

lower leg in the *x* and *y* directions, respectively; m_{leg} is the mass of lower leg; $M_{tibia_{JC}}$ is the moment of the tibia about the JC; and $I_{leg_{JC}}$ is the moment of inertia of the leg about the JC.

In addition to isolated shear loading of the knee joint, the knee can be loaded by an internal–external rotational moment or a valgus–varus moment. Shear loading has been found to be the primary mode of ACL tensioning, whereas internal–external moment and valgus–varus moment do not produce significant tension in the ACL in isolation.[12] However, during physical activity, the knee is typically loaded in a combined loading state, in which shear and moment loads act simultaneously. Depending on the knee flexion angle, the combined loading states modulate the tension in the ACL, either increasing or decreasing the force compared with pure shear loading.[13] Studies show that the ACL is most vulnerable to failure at low knee flexion angles while under shear loading, coupled with internal rotation moment and valgus moment of the knee (Figure 17.3). In this vulnerable position, the ACL wraps around the PCL, thereby increasing tension.[13,14]

Ten female athletes who sustained ACL injuries were studied using video analysis by Koga et al.[14] The ACL injury was found to have occurred within 40 ms after contact of the injured leg with the ground. During this 40 ms period, there was a mean knee flexion angle change from 23° to 24° and a mean valgus angle change from neutral 0° to 12°, and the knee moved from 5° of external rotation to 8° of internal rotation. The mean peak ground reaction force was 3.2 times the body weight at the time of injury.[14] These findings

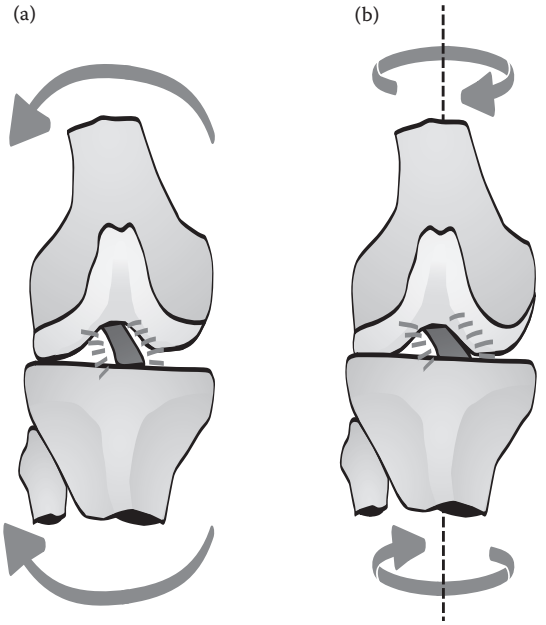

FIGURE 17.3
Additional moments applied to the right knee that will tension the ACL. (a) Valgus moment; (b) internal rotation.

support the current understanding of the ACL injury mechanism of sudden deceleration caused by cutting or landing on one foot while also subjecting the knee to additional internal and valgus moments.

The injury mechanism of ACL tears is well studied, and many investigators feel that an improved biomechanical understanding of the mechanism may help prevent these debilitating injuries in both the athletic and general populations. Current investigations have also examined the clinical and biomechanical results of varying reconstruction techniques to improve the functionality of injured patients. Other research efforts have focused on the consequences of ACL rupture to the knee with respect to knee joint stability and degeneration of cartilage or the meniscus. The majority of patients with ACL tears range from the teens to 30 years old. These patients often experience early-onset osteoarthritis (OA) that presents 10 to 20 years later.[15–17] In patients with repaired or removed ACLs, there are negative impacts to somatosensation, muscle activation, muscle strength, balance, and biomechanical loading of the joint, which are all thought to contribute to early-onset OA.[18]

17.3 Lateral Ankle Ligament Sprain

Among athletic injuries, ankle ligament sprains are the most frequent injury.[19] Most commonly, ankle sprains are caused by injury to the lateral ligaments of the ankle joint.[20] These ligamentous injuries account for an estimated 27,000 injuries *per day* in the United States, occurring at a rate of 1 injury per 10,000 people per day.[21,22] Ankle sprains from sports and

recreation tend to occur commonly in court games and team sports such as soccer, volleyball, handball, and basketball.[19]

The ankle is composed of three primary joints, which include the talocrural joint, the subtalar joint, and the distal tibiofibular syndesmosis.[23] The talocrural joint is responsible for the hinge motion of plantarflexion and dorsiflexion of the foot and consists of the superior dome of the talus, the tibial plafond, the medial malleolus, and the lateral malleolus as part of the fibula.[19] The talocrural joint is constrained by a medial and a lateral group of supporting ligaments. The medial side is supported by the deltoid ligament consisting of five components. The superficial portion of the deltoid ligament contains the tibiocalcaneal component and the tibiotalar component. The deep portion contains the anterior, posterior, and deep tibiotalar components.[7] The lateral side is supported by the anterior talofibular ligament (ATFL), the calcaneofibular ligament (CFL), and the posterior talofibular ligament (PTFL).[7] The subtalar joint is composed of the calcaneus and talus bones and allows for inversion and eversion or pronation and supination.[19] The subtalar joint is supported by several other ligaments as well as partially being supported by the ATFL.

The ATFL is the weakest ligament on the lateral side. It connects the anterior–inferior border of the distal fibula to the neck of the talus.[24] It is approximately 20 to 25 mm long, 7 to 10 mm wide, and 2 mm thick.[19,25,26] In quasistatic tensile testing, the ATFL has been reported to have a failure load of 138.9 ± 24 and 231 ± 129 N.[27,28] In the same set of tests, the CFL was reported to have failure loads of 346 ± 55 and 307 ± 142 N.[27,28] The PTFL and CFL are roughly two to three times as strong as the ATFL.[27] However, when looking at ligament mechanics with respect to sports injury, dynamic properties of the tissue must be taken into account due to the nature and duration of the injury event.

Funk et al.[29] tested the viscoelastic properties of the medial and lateral ligaments of the ankle. The ligaments were harvested from three 50th percentile male cadaver ankles, tested in uniaxial tension, and the response was fitted to a quasilinear viscoelasticity model. The fresh cadaveric ligaments were also tested to failure at 280 mm/s. The average failure loads of the ATFL, PTFL, and CFL were 297, 554, and 598 N, respectively.[29] These values are higher than those reported previously[27,28] partially due to the viscoelastic effects of dynamic loading and because the specimens were middle-aged males, as opposed to older or female specimens tested in other studies.[27–29]

The principal function of the ATFL is to prevent the relative anterior displacement and internal rotation of the talus with respect to the tibia and fibula.[19,30–32] Due to its anatomical location, function, and relative weakness with respect to the other ankle joint ligaments, the ATFL is most prone to injury.[19] It has been reported that 73% of all ankle sprains involve the isolated partial or complete tear of the ATFL.[19,20,33] It is also estimated that between 20% and 25% of ankle sprains have both AFTL and CFL ruptures.[34,35]

Analysis of the mechanism of injury of lateral ankle sprains revealed dynamic ankle inversion-supination, in addition to internal rotation of the foot with respect to the leg as the cause of injury.[19,25] Lateral ankle sprains have also been found when plantarflexion of the ankle joint with subtalar joint inversion occurs.[19,36] When the ankle is plantarflexed and internally rotated, the bony stability of the joint is diminished, resulting in the supporting ligaments carrying a larger portion of the load from weight-bearing or inertial loading.[34] Because the injury is caused by a sudden dramatic twisting of the foot, it has been suggested that the duration of time for the injury to occur is 40 ms, which is the typical time of peak force for a landing from a jump.[19,37]

Most studies assessing the internal forces of the lateral ankle ligaments during weight-bearing within a complete ankle joint have estimated the forces from other measureable parameters such as strain.[38–40] However, within ligament tissue, strain does not correlate

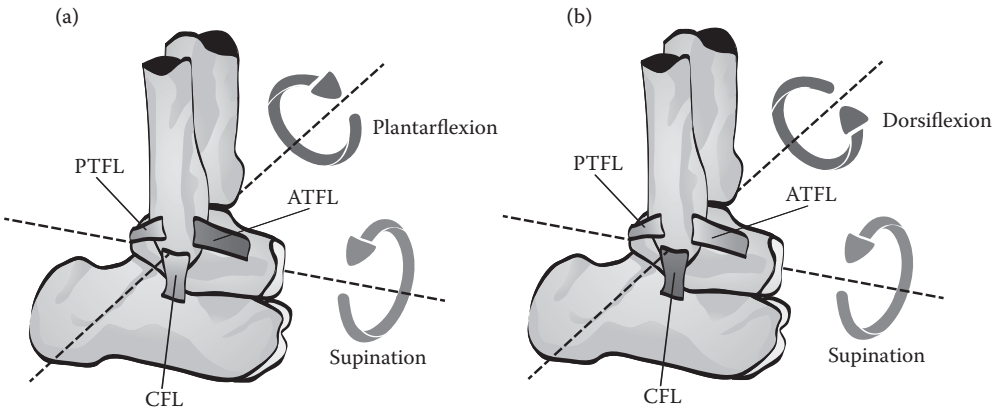

FIGURE 17.4
(a) Injury mechanism for ATFL tears, which includes plantarflexion and supination of the foot. (b) Injury mechanism for CFL tears, which includes the dorsiflexion and supination of the foot.

linearly to load; therefore, this technique may produce inaccurate results. A study by Bahr et al.[32] was able to directly measure the forces in the ATFL and CFL under both non-weight-bearing and weight-bearing scenarios at different joint angles by using calibrated buckle load transducers. The ligament tensions were measured at varying positions of plantarflexion-dorsiflexion and pronation-supination. The weight-bearing scenario was tested with a 375 N axial load applied to the tibia. The ATFL peak tension force was found to be 76 ± 23 N in supination at 20° plantarflexion (the largest angle of supination tested) within the weight-bearing configuration. There was a trend for increasing force in the ATFL by increasing plantarflexion, supination, and weight-bearing. The CFL force was highest (109 ± 28 N) in supination and 10° of dorsiflexion (the largest angle of dorsiflexion tested). A similar trend was seen in the CFL, in which force increased with increasing supination and dorsiflexion. Weight-bearing seemed to have relatively no effect on CFL force.[32] The injury mechanism trends found in ATFL and CFL tears with regard to plantarflexion-dorsiflexion and pronation-supination of the foot can be seen in Figure 17.4.

Ankle sprains are among the most common sports-related injuries and have been well studied for this reason. Many efforts have been made to analyze the skeletal muscular biomechanics of this injury. Further studies have been conducted to determine the stability of the ankle after a single sprain, as well as after repetitive sprains.

17.4 Rotator Cuff Tears

Degenerative, chronic rotator cuff injuries are common in the elderly population with a prevalence of 50% in patients older than 80 years.[41] Traumatic rotator cuff tears are often observed in athletes who compete in overhead sports such as baseball, racquet sports, swimming, volleyball, and golf. Traumatic rotator cuff tears are also seen in contact sports such as football, rugby, hockey, and lacrosse.

The shoulder joint is a ball-and-socket joint comparable to the hip joint. The shoulder is composed of the proximal humerus known as the head of the humerus, which is in contact

with the glenoid fossa of the scapula and is referred to as the glenohumeral joint. Whereas the hip is constrained by the large bony socket of the acetabulum, which provides passive stabilization, the shoulder has a small socket compared with the diameter of the humerus head. This allows the shoulder a greater range of motion but at the sacrifice of its passive stabilization. The stability of this joint is maintained by active stabilization provided by the rotator cuff muscles and the surrounding ligaments. The rotator cuff is a group of four intrinsic muscle tendon units (subscapularis, supraspinatus, infraspinatus, and teres minor) that act as dynamic stabilizers of the glenohumeral joint and help provide joint torque.[7]

Shoulder joint stabilization is maintained through two mechanisms. First, the rotator cuff supplies a counteracting force on the humerus opposing the primary force vector of the deltoid. This force couple maintains the articular alignment of the humeral head in the center of the glenoid cavity while allowing for joint torque to be generated about the JC, thereby producing stable pain-free motion.[42] The rotator cuff also provides a compressive force on the humerus against the glenoid and labrum, which is known as a concavity compression, to further stabilize the joint against dislocation.[43]

Factors resulting in tears of the rotator cuff can be classified into three categories: intrinsic, extrinsic, and traumatic. Intrinsic factors relate to reduced vascularity and may be attributed to the aging process resulting in degenerative tears.[44] Extrinsic factors can include impingement caused by a coracoacromial arch abnormality or coracoacromial arch narrowing, leading to compression and increased friction during upper extremity motion (Figure 17.5). This friction leads to irritation of the subacromial bursa and is thought to be involved in rotator cuff tears. Traumatic factors include tensile overload due to a single event such as a collision or the accumulation of microtrauma from repetitive actions.[44,45] Rotator cuff tears are often multifactorial; for instance, repetitive microtrauma may lead to extrinsic irritation, swelling, and impingement. This may also be coupled with an intrinsic decrease in vascularity and altered biomechanical properties, which, in turn, may lead to impingement and subsequent partial-thickness and full-thickness tears.[44]

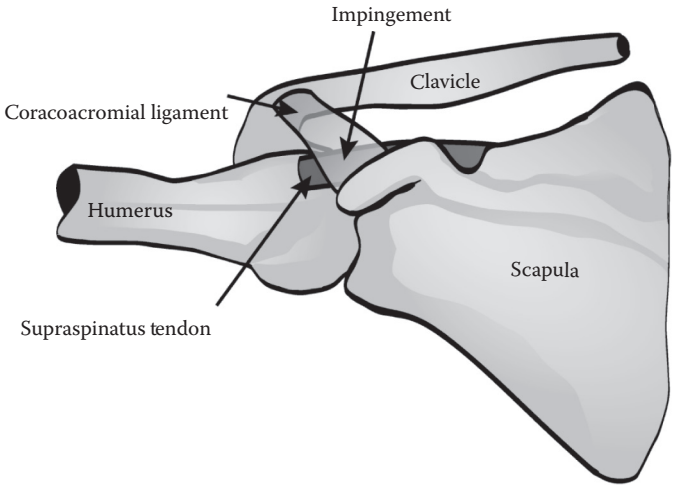

FIGURE 17.5
(See color insert.) Impingement of the supraspinatus occurs whenever the arm is positioned above the horizontal plane. The coracoacromial ligament (blue) compresses the bursa and supraspinatus tendon (red) against the humerus.

Trauma to the rotator cuff can result from a single dynamic impact or repetitive overhead arm swinging muscle fatigue, both of which result in unbalanced forces about the glenohumeral joint and eventual full-thickness or partial rotator cuff tears.[42] Full-thickness tears occur as a result of mechanical weakening, often due to a combination of several factors including age, major trauma, multiple episodes of minor trauma or fatigue, steroids, subacromial impingement, or decreased capillary density.[46] In contact sports, a partial or complete tear of the rotator cuff is usually the result of a single high-energy impact to the humerus, sometimes resulting in dislocation.[44] However, noncontact athletes that participate in sports that involve an overhead motion of the arm are also susceptible to rotator cuff tears.[42] These athletes experience degeneration of the rotator cuff, resulting from the formation of multiple microtraumas that accumulate over time.[44] The rotator cuff tears when the strength of the tendon is less than the stress experienced through the tendon and insertion. The tear will initiate at the structurally weakest point and propagate through a path of stress concentration.[46]

The supraspinatus tendon is the most commonly torn rotator cuff tendon.[47] Eleven tendons from five males and six females with an average age of 64 years were mechanically tested by Itoi et al.[46] to determine their structural and mechanical properties. The tendons were cut into three even strips (anterior, middle, and posterior) and tested in a position that simulated 140° of abduction. The thickness of each strip of tendon was found to be significantly different (Table 17.2). The anterior and middle strips were 3.5 ± 0.5 and 3.6 ± 0.7 mm in thickness. The posterior strip was thinner at 2.9 ± 0.5 mm. The anterior strip withstood an ultimate load of 411 N, which was 2.5 times that of the middle strip at 152 N and 4.5 times that of the posterior strip at 88 N. The ultimate stresses followed a similar trend (anterior, 16.5 ± 7.1 MPa; middle, 6.0 ± 2.6 MPa; posterior, 4.1 ± 1.3 MPa).[46] These findings indicate that under a distributed load, tears will occur in the weakest location, which is the posterior portion of the supraspinatus tendon. This may also mean that tears occurring in another portion of the supraspinatus tendon will progress in the posterior direction.

Patients who experience recurring posterior dislocations after the age of 40 often have tears in the infraspinatus and teres minor tendons in the posterior portion of the rotator cuff.[48] Posterior dislocation of the shoulder may result in rupture of the posterior joint capsule and teres minor, which are often accompanied by lesions in the infraspinatus; however, posterior dislocations are rare.[49] Halder et al.[50] tested the mechanical properties of the infraspinatus tendon in four evenly divided sections and full-thickness teres minor tendons. Twenty-two fresh cadaver shoulders with a mean age of 74 years were tested in the neutral 0° abduction hanging arm position and 60° abduction until failure.

The mid-superior and inferior strips of the infraspinatus have a higher ultimate load, stiffness, ultimate stress, and elastic modulus than the superior strip and mid-inferior

TABLE 17.2

Geometric and Tensile Properties of the Supraspinatus Tendon

	Width (mm)	Thickness (mm)	Area (mm^2)	Failure Load (N)	Ultimate Stress (MPa)
Anterior strip	7.4 ± 0.7	3.5 ± 0.5	25.5 ± 4.3	411.1 ± 158.8	16.5 ± 7.1
Middle strip	7.0 ± 1.2	3.6 ± 0.7	24.7 ± 5.8	152.6 ± 87.5	6.0 ± 2.6
Posterior strip	7.5 ± 1.2	2.9 ± 0.5	21.9 ± 5.3	88.1 ± 32.1	4.1 ± 1.3
p value	0.48	0.0355	0.27	<0.0001	<0.0001

Source: Itoi, E. et al., *J. Orthop. Res.*, 13(4), 578–584, 1995. With permission.
Note: Mean ± SD.

TABLE 17.3

Geometric and Tensile Properties of the Infraspinatus Tendon

	Thickness (mm)	Area (mm^2)	Failure Load (N)	Ultimate Stress (MPa)	Stiffness (N/mm)	Elastic Modulus (MPa)
Superior strip	3.4 ± 0.8	29.0 ± 9.4	501	15	109	94
Mid-superior strip	3.2 ± 0.9	26.3 ± 7.8	662	25	143	130
Mid-inferior strip	2.7 ± 1.1	20.8 ± 8.9	331	13	85	84
Inferior strip	2.2 ± 0.9	26.2 ± 8.5	717	30	169	146
Teres minor	3.6 ± 1.1	49.0 ± 17.0	75	2	29	17

Source: Halder, A. et al., *Clin. Biomech. (Bristol, Avon)*, 15(6), 456–462, 2000.
Note: Mean age, 74.8 years (mean ± SD).

strip. The majority (72.7%) of the mid-superior and superior strips failed at the insertion site. The majority (63.6%) of the mid-inferior and inferior strips failed at the midsubstance of the tendon. The teres minor failed most often (59.1%) in the midsubstance.[50] It was much weaker than the infraspinatus, which can be attributed to the fact that it remains muscular near the insertion site on the humerus. The structural weakness of the superior portion of the infraspinatus tendon may dictate where whole or partial tears originate.[50] The resultant strength of the infraspinatus tendon was 2058 ± 688 N, which is much higher than the estimated peak external rotation force transmitted through the muscle tendon unit (909 N).[50,51] The geometric, structural, and mechanical properties of the hanging arm tests are presented in Table 17.3.

Partial tears of the rotator cuff can take place on the articular surface or the bursal surface. Bursal surface tears of the suprascapularis may be an indicator of abrasive degeneration against the acromion (Figure 17.5).[44] It is also thought that the narrowing of the coracoacromial arch may lead to partial tears on the articular surface of the rotator cuff as well.[52] This may be due to the generation of shear stresses between the layers of the tendon.[44] Partial tears due to trauma are often seen on the articular surface.[53] Degenerative tears are often found on the articular side with lamination causing intratendinous tears and are attributed to vascular deficiencies.[44]

The mechanisms for rotator cuff injury are not as well understood as many other common sports injuries such as ACL tears or ankle sprains. Many investigators continue to study the mechanical and physiological changes that occur before, during, and after a rotator cuff tear. Many current investigations study the effectiveness of rotator cuff repair techniques with regard to both mechanical strength and clinical outcome.

17.5 Meniscus Tears

Knee injuries account for approximately 3% to 5% of all physician visits. The peak rate of meniscal tears in males occurs between the ages of 21 and 30 years and, in females, between 11 and 20 years.[54] Males also sustain meniscal tears more often than females at a rate of 9.0/10,000 individuals to 4.2/10,000 individuals, which is a ratio of 2.1:1.[55] Meniscal tears in younger patients are often the result of trauma and are typically associated with twisting on a loaded and flexed knee.[56]

The menisci are two distinct structures that help distribute the joint load across the articular surfaces of the tibial plateau and the femoral condyles.[57] They act to fill the joint space by compensating for the incongruity between the shape of the femoral condyles and tibial articulating surface.[7] The menisci lubricate the joint and create additional contact surface area between the two articulating surfaces.[7,54,55,57–59] They also absorb shock during movement and stabilize the joint.[7,58] When observed in the cross section, the menisci are wedge-shaped with a flat surface in contact with the tibia and a concave surface in contact with the femur.[58] The thick peripheral border of the meniscus is attached to the inside of the joint capsule. The inner free border of each meniscus tapers to a thin free edge.[60]

The lateral meniscus is semicircular and covers a larger area than the medial meniscus.[60] The anterior horn is attached to the tibia behind the ACL. The posterior horn attaches behind the intercondylar eminence and in front of the PCL. The lateral meniscus is also loosely attached to the peripheral joint capsule.[60] It is also constrained by the posterior meniscofemoral ligament, which extends from the posterior horn of the lateral meniscus to the medial femoral condyle.[57] The lateral meniscus is 10.6 mm wide at the posterior horn, 11.6 mm wide at its midpoint, and 10.2 mm wide at its anterior horn.[57,61] It has been found to translate an average of 11.2 mm anteriorly/posteriorly during flexion/extension of the knee.[62]

The medial meniscus is semi-lunar-shaped. The anterior horn of the medial meniscus attaches to the tibial plateau anterior to the ACL's attachment on the tibial plateau. This attachment merges with the transverse ligament that connects the anterior horns of the medial and lateral menisci.[60] The posterior horn is securely attached to the posterior intercondylar fossa of the tibia. The periphery of the medial meniscus is attached to the joint capsule all along its length, and at its midpoint, it is firmly attached to the deep MCL.[60] The widest point of the medial meniscus is 10.6 mm, the midpoint is, on average, 9.6 mm, and the anterior horn is 7.7 mm wide.[57] Through the range of flexion and extension of the knee, the medial meniscus translates an average of 5.1 mm, which is about half as much as the excursion of the lateral meniscus.[57]

The menisci are structurally composed of a strong collagen matrix.[59] The majority of these fibers are oriented circumferentially, whereas a small portion of the fibers are oriented radially.[59,60,63] The primary functions of the menisci are load transmission and shock absorption. The distributed joint force is applied normal to the surface of the menisci. Due to the wedge shape of the meniscus, this normal force can be divided into an axially oriented compressive force component and a radially oriented force component. The semicircular shape of the menisci resists this radial force through the circumferentially oriented fiber bundles. This force is transmitted through the meniscus and into the ligament attachments on the tibia (Figure 17.6).[59,63] The circumferentially oriented fiber bundles are stiff and resist the radially directed force from the femur with tension force that travels circumferentially through the meniscus and into the attaching ligaments. The circumferential force in the meniscus produces hoop strain and hoop stress.[59,63] The lateral meniscus has been shown to transmit 50% of the joint compressive load in extension and 85% in flexion.[60] The radially oriented fibers tie the circumferential fibers together. The surface of the menisci is composed of randomly oriented collagen fibers that provide a smooth gliding surface.[60] This arrangement allows each meniscus to slide along the articular surfaces of both the femoral condyles and tibial plateau, while optimally distributing load across these surfaces, which diminishes stress concentrations.

The meniscus acts as a biphasic composite material with nonisotropic elastic material properties in addition to fluid viscous properties. This is due to the different collagen fiber orientations and the interstitial fluid that permeates the collagen matrix.[60] Several

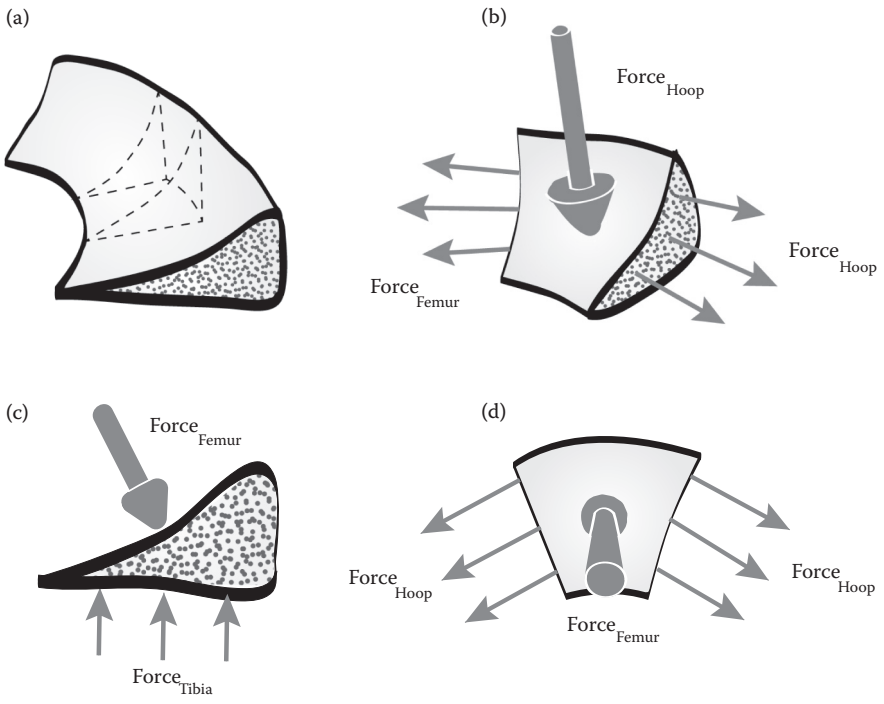

FIGURE 17.6
Section of meniscus showing how compressive stress between the tibia and femur presents itself as hoop stress in the meniscus. (a) Section of meniscus; (b) three-dimensional view of free body diagram; (c) circumferential cross-sectional view; (d) top-down view.

studies have been conducted to measure the mechanical properties of the menisci both in the radial and circumferential directions (Table 17.4). Tissakht and Ahmed[64] measured the ultimate stress, strain, and elastic modulus of the menisci for the anterior, central, and posterior sections in the medial, middle, and distal layers of each section (Tables 17.4 and 17.5). Chia et al.[65] studied the effects of strain rate on the compressive modulus in the medial

TABLE 17.4
Elastic Modulus of the Meniscus Comparing Recent Studies

	Radial Direction			Circumferential Direction		
Elastic Modulus (MPa)	**Anterior**	**Central**	**Posterior**	**Anterior**	**Central**	**Posterior**
Whipple et al. 1984	—	26.26	—	—	132.76	—
Farinaccio 1989	—	—	—	167.54	115.11	146.8
Fithian et al. 1990	—	—	—	159.32	160.98	158.57
Skaggs and Mow 1990	10.84	32.68	42.28	—	—	—
Tissakht and Ahmed 1995	7.82	11.49	13.04	99.75	90.22	102.12

Source: Whipple, T. L. et al., *Clin. Orthop. Rel. Res.*, 183(105–114), 1984; Farinaccio, R., An Experimental and Numerical Study of the Mechanical Response of the Knee Menisci. Masters Thesis. McGill Univeristy, 1989; Fithian, D. C. et al., *Clin. Orthop. Rel. Res.*, 252(19–31), 1990; Skaggs, D. L. and Mow, V. C., *Trans. Orthop. Res. Soc.*, 15(248), 1990; Tissakht, M. and Ahmed, A. M., *J. Biomech.*, 28(4), 411–422, 1995.
Note: Modulus measured in MPa.

TABLE 17.5

Average Tensile Properties of the Lateral and Medial Meniscus by Layer

		Radial Direction		Circumferential Direction	
		Maximum Stress (MPa)	**Maximum Strain (%)**	**Maximum Stress (MPa)**	**Maximum Strain (%)**
Lateral meniscus	Proximal	3.75 ± 1.85	41.4 ± 20.75	17.27 ± 5.75	20.6 ± 7.06
	Middle	2.52 ± 1.73	55.24 ± 18.15	15.95 ± 4.07	26.37 ± 7.38
	Distal	3.53 ± 1.99	38.97 ± 23.64	18.22 ± 5.48	21.97 ± 10.97
Medial meniscus	Proximal	3.04 ± 1.00	42.35 ± 20.40	16.32 ± 3.81	27.53 ± 13.70
	Middle	1.57 ± 0.90	53.51 ± 18.35	15.1 ± 2.98	31.05 ± 9.98
	Distal	3.38 ± 1.46	33.47 ± 18.32	17.21 ± 4.31	27.17 ± 10.53

Source: Tissakht, M. and Ahmed, A. M., *J. Biomech.*, 28(4), 411–422, 1995. With permission.
Note: Mean ± SD (n = 31).

meniscus of ten fresh cadaver knees with a mean age of 40.4 years. At equilibrium, the axial and radial compressive moduli were found to be 83.4 and 76.1 kPa, and at a strain rate of 32%/s, which is comparable to what is seen in walking, the axial and radial compressive moduli were 718 and 605 kPa, respectively. These data suggest that the rate of strain on the meniscus plays an important role in the mechanical response of the tissue.[65]

Meniscus tears are heterogeneous injuries that include vertical longitudinal, oblique, complex, transverse, and horizontal tear structural disruptions.[66] The majority (81%) of tears occur in the oblique and vertical longitudinal classifications.[66] Vertical longitudinal tears are also known as "bucket handle tears"; this injury is commonly associated with ACL injury. Bucket handle tears are more common on the medial meniscus and typically start in the posterior horn and extend anteriorly.[54] It is thought that the medial meniscus is more commonly affected because it has a more firm attachment to the posterior tibia than the lateral meniscus.[54] Tears in the medial meniscus may also occur more often because of its firm attachment to the MCL, which can increase the tension in the meniscus when strained. The injury mechanism for meniscal tears is similar to that of ACL tears in that an acute varus or valgus moment is applied with an internal or external moment to the weight-bearing knee joint.[67]

17.6 Proximal Fifth Metatarsal Fractures

Fractures of the fifth metatarsal are the most common foot fracture.[68] Fractures of the proximal base of the fifth metatarsal can occur in a variety of ways, each of which gives clues as to how the injury was caused. This section will discuss three distinct fractures of the proximal fifth metatarsal and the injury mechanisms attributed to each.

The fifth metatarsal consists of a base, tuberosity, shaft, and head (Figure 17.6).[69] The tuberosity is a prominence that extends laterally off of the base of the metatarsal and is an attachment point for the peroneus brevis tendon and peroneus tertius tendon. The lateral band of the plantar ligament also attaches to the inferior aspect of the base. The base of the fifth metatarsal contacts the cuboid to form the cuboid–fifth metatarsal articulation and contacts the fourth metatarsal to create the fourth and fifth intermetatarsal articulation.[69]

The base of the fifth metatarsal is also constrained by the plantar and dorsal metatarsal ligaments and the plantar and dorsal tarsometatarsal ligaments.

The proximal end of the fifth metatarsal has been divided into three zones to classify fracture type (Figure 17.7).[70–75] The first zone is the most proximal area of the tuberosity of the metatarsal; this includes the insertion of the peroneus brevis tendon and the calcaneometatarsal ligamentous.[70] The second zone covers the area around where the fourth and fifth metatarsals articulate. The third zone is distal to the ligament insertions and extends to the shaft of the metatarsal.[70]

Each of the proximal zones of the fifth metatarsal classifies a particular fracture type (Figure 17.7). Typically, fractures in the first zone are classified as avulsion fractures, where the tendon pulls the bone away at the site of its insertion. In fractures of zone I, the peroneus brevis tendon is pulled out of the metatarsal tuberosity.[76] This occurs at the very tip of the tuberosity where the peroneus brevis attaches. Avulsion fractures are the most common among proximal fifth metatarsal fractures.[76] It is believed that this fracture is the result of inversion and plantarflexion of the foot.[76] This type of fracture is reported to have sufficient healing from nonoperative means.[70,77–80]

Fractures in zone II occur more distal on the tuberosity and extend obliquely from the lateral cortex into the space where the fourth and fifth metatarsals articulate.[81] Fractures of this kind are referred to as Jones fractures after the physician who originally identified it in 1902. Jones fractures are the result of an acute flexion of the metatarsal medially while the foot is in supination.[82]

The Jones fracture is caused by the firm restriction of the fourth and fifth metatarsal base in the transverse plane. The adductor moment of the peroneus brevis, coupled with lateral load on an inverted distal foot about a fulcrum load from the fourth metatarsal, creates a bending moment on the fifth metatarsal in the area between the peroneus brevis and tertius tendons (Figure 17.7).[76] In this case, the fifth metatarsal may be analyzed as a beam in bending (Figure 17.8). This bending stress peaks at a point opposite the fourth metatarsal fulcrum on the lateral side of the distal tuberosity. The peak tension and compression stress appear on the outside of the cortex at the point of maximum bending stress. The peak compressive stress is on the medial side in contact with the fourth metatarsal, and the peak tensile stress is opposite on the lateral side.

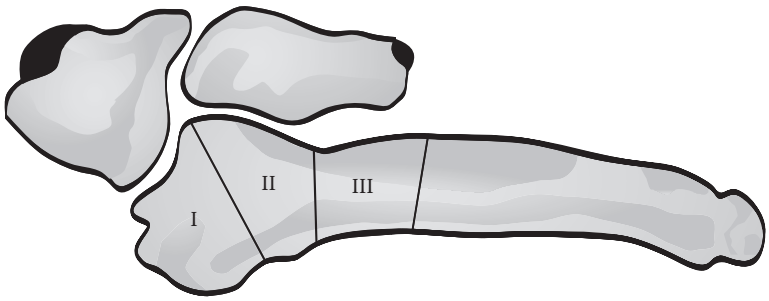

FIGURE 17.7
Schematic of the three fracture zones of the proximal fifth metatarsal. Zone I depicts the area where tuberosity avulsion fractures occur. Zone II depicts the area where Jones fractures occur. Zone III depicts where diaphyseal stress fractures occur. (Adapted from Quill, G. E., Jr., *Orthop. Clin. North Am.*, 26(2), 353–361, 1995.)

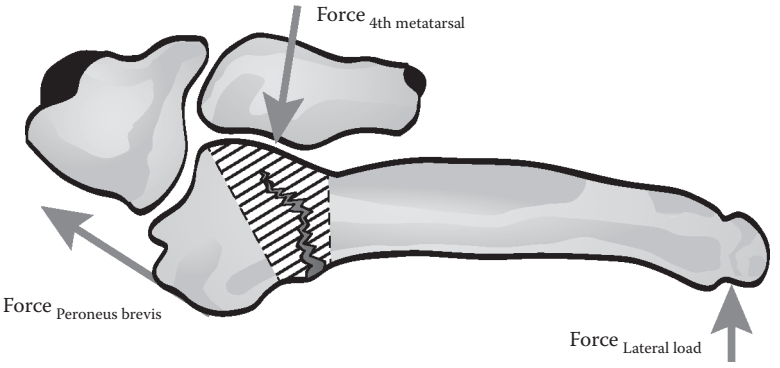

FIGURE 17.8
Free body diagram representative of the loading experienced in a Jones fracture of the fifth metatarsal.

Fractures in zone III, which is the proximal diaphyseal region of the fifth metatarsal, occur as a result of fatigue stress accumulation, also known as a "stress fracture." The mechanism of a stress fracture includes repetitive cycles of stress on the affected area.[82] Each cycle of stress is below the yield stress of the bone, meaning any one of these cycles would be noninjurious by itself.[76] However, the accumulation of these multiple stresses in the bone, over time, creates microcracks and can lead to yielding. These fractures are more common in athletes that have to change directions quickly; for example, these injuries commonly occur in sports such as soccer, football, baseball, and basketball.[83]

The fifth metatarsal stress fractures are thought to be due to poor load distribution across the bottom of the foot. This may be attributed to a lack of support of the diaphysis of the metatarsal, which can be due to improper cleat/shoe fit or design.[82] The third, fourth, and fifth metatarsals have considerably larger second moments of area in the vertical direction as compared with the horizontal direction with regard to bending. This predisposes these bones to fracture as a result of repetitive horizontal loading.[84] In physiologic loading, the metatarsal bones are subjected to much higher normal stresses due to bending than shear stresses. Neglecting the shear stress in the metatarsal does not produce significant error and therefore can be ignored to simplify calculations.[84]

By using the mechanics of material beam theory on the fifth metatarsal, Arangio et al.[46] were able to estimate the maximum principal stress in any transverse cross section of the bone. In the first case, a 1 N load was applied to the head of the fifth metatarsal in the superior direction while the base of the metatarsal was constrained. It was found that the peak stress of –1.05 MPa occurred on the lateral aspect of the metatarsal on a plane 4.05 cm from the proximal tip of the tuberosity. The second case tested was a 1 N load applied to the head in a medial direction. The peak tensile stress of 0.95 MPa occurred on the lateral aspect of the cross section, 3.38 cm from the proximal tip of the tuberosity.[85] Both of these peak stresses were estimated in zone III, in which stress fractures are thought to occur.

This model did not take into account the fulcrum three-point bending effect of the fifth metatarsal bending about the fourth metatarsal in medial loading. Adding in that constraint may shift the point of maximum principal stress back into zone II, where Jones fractures occur. It is estimated that during normal walking, the fifth metatarsal experiences loads of up to 50 N.[86] By using a common average yield strength of cortical bone, Arangio et al.[85] estimate that the failure load of the fifth metatarsal is ~100 N, giving the bone a safety factor of II during normal physiological loading.

The interosseous blood supply to the fifth metatarsal tuberosity comes from multiple metaphyseal vessels that enter through the nonarticulating surface.[74,75] The blood supply to the proximal diaphysis comes from the nutrient artery that divides into intramedullary branches. The area where the branches of the nutrient artery join with the blood supply to tuberosity has the worst outcome for fracture healing.[69] The underlying tenuous blood supply to the "watershed" area of the proximal metaphyseal and diaphyseal regions impairs the healing of fractures and makes it difficult to recreate a union between the fracture pieces.[74,75]

In practice, it is common to use compression screws for stress fractures and Jones fractures of the proximal base. For active patients and athletes, Jones fractures and stress fractures are commonly treated surgically by using a modulated intramedullary compression screw. The screw acts much like rebar in a concrete structure. The intramedullary screw provides a preload of compression to the metatarsal and takes advantage of the cortical bones' ability to withstand higher compressive loads than tensile loads. When the metatarsal is bent, the lateral side of the metatarsal will experience less tensile stress. The screw itself also provides resistance against bending stress.

17.7 Summary

Athletic injuries are the most common injuries found in the modern world. More than half of all sports injuries occur in the lower extremity followed by injuries to the upper extremity. Endurance sports tend to have a greater occurrence of overuse, fatigue, degenerative, and stress-related injuries. Team sports and sports involving high speed, acceleration, or player contact have higher rates of acute traumatic injury.

Traumatic injury in athletic competition can be classified as noncontact injury, in which the injury is self-induced or from contact with another athlete or obstacle. Acute injuries discussed in this chapter include ACL tears, ankle sprains, meniscal tears, impact-related rotator cuff tears, Jones fractures, and avulsions of the fifth metatarsal. Ankle ligament sprains are the most common athletic injury. A majority of ankle sprains are caused by injury to the lateral ligaments of that joint. ACL and meniscus tears often occur as a result of dynamic moments and shear forces to the weight-bearing knee. Jones fractures and avulsions are caused by a lateral force applied to a plantarflexed and inverted foot. Acute trauma to the rotator cuff is typically associated with a dislocated shoulder from an impact.

Overuse injuries are the result of an accumulation of microtrauma at a rate higher than the body's rate of healing. Two such injuries were discussed in this chapter, including rotator cuff tears and stress fractures of the fifth metatarsal. Fatigue-related rotator cuff tears are common in overhead arm-swinging sports such as tennis or baseball. Stress fractures of the fifth metatarsal are the result of cyclic vertical or lateral loading (or both) to the foot.

Future research for these injuries should continue to investigate the musculoskeletal biomechanics surrounding the injury event. This will focus on better understanding the dynamic forces and moments about the relevant joints in addition to the joint angles with respect to the time of injury. Research on the short-term and long-term symptoms after an injury, as well as the outcome of the orthopaedic repair, is also very important. New methods and techniques of injury repair, injury prevention, and rehabilitation are needed to improve clinical practice and patient care.

References

1. Parkkari, J., U. M. Kujala, and P. Kannus. 2001. Is it possible to prevent sports injuries? Review of controlled clinical trials and recommendations for future work. *Sports Medicine* 31(14):985–995.
2. Gotsch, K., J. L. Annest, P. Holmgreen, and J. Gilchrist. 2002. Nonfatal sports- and recreation-related injuries treated in emergency departements—United States, July 2000–2001. *Morbidity and Mortality Weekly Report 2002* 51(33):736–740.
3. Hootman, J. M., R. Dick, and J. Agel. 2007. Epidemiology of collegiate injuries for 15 sports: Summary and recommendations for injury prevention initiatives. *Journal of Athletic Training* 42(2):311–319.
4. Yu, B., and W. E. Garrett. 2007. Mechanisms of non-contact ACL injuries. *British Journal of Sports Medicine* 41 (Suppl 1):i47–i51.
5. Gottlob, C. A., C. L. Baker, Jr., J. M. Pellissier, and L. Colvin. 1999. Cost effectiveness of anterior cruciate ligament reconstruction in young adults. *Clinical Orthopaedics and Related Research* (367):272–282.
6. Kibler, W. B. 1996. *ACSM's Handbook for the Team Physician*. Baltimore, MD: Williams & Wilkins.
7. Canale, S. T., and J. H. Beaty. 2007. *Campbell's Operative Orthopaedics*, 11th ed., Philadelphia, PA: Mosby Elsevier.
8. Chandrashekar, N., H. Mansouri, J. Slauterbeck, and J. Hashemi, eds. 2006. Sex-based differences in the tensile properties of the human anterior cruciate ligament. *Journal of Biomechanics* 39(16):2943–2950.
9. Anderson, A. F., D. C. Dome, S. Gautam, M. H. Awh, and G. W. Rennirt. 2001. Correlation of anthropometric measurements, strength, anterior cruciate ligament size, and intercondylar notch characteristics to sex differences in anterior cruciate ligament tear rates. *The American Journal of Sports Medicine* 29(1):58–66.
10. Dugan, S. A. 2005. Sports-related knee injuries in female athletes: What gives? *American Journal of Physical Medicine & Rehabilitation* 84(2):122–130.
11. Herzog, W., and L. J. Read. 1993. Lines of action and moment arms of the major force-carrying structures crossing the human knee joint. *Journal of Anatomy* 182(Pt 2):213–230.
12. Berns, G. S., M. L. Hull, and H. A. Patterson. 1992. Strain in the anteromedial bundle of the anterior cruciate ligament under combination loading. *Journal of Orthopaedic Research* 10(2):167–176.
13. Markolf, K. L., D. M. Burchfield, M. M. Shapiro, M. F. Shepard, G. A. Finerman, and J. L. Slauterbeck. 1995. Combined knee loading states that generate high anterior cruciate ligament forces. *Journal of Orthopaedic Research* 13(6):930–935.
14. Koga, H., A. Nakamae, Y. Shima, J. Iwasa, G. Myklebust, L. Engebretsen et al. 2010. Mechanisms for noncontact anterior cruciate ligament injuries: Knee joint kinematics in 10 injury situations from female team handball and basketball. *The American Journal of Sports Medicine* 38(11):2218–2225.
15. Lohmander, L. S., P. M. Englund, L. L. Dahl, and E. M. Roos. 2007. The long-term consequence of anterior cruciate ligament and meniscus injuries: osteoarthritis. *The American Journal of Sports Medicine* 35(10):1756–1769.
16. Lohmander, L. S., A. Ostenberg, M. Englund, and H. Roos. 2004. High prevalence of knee osteoarthritis, pain, and functional limitations in female soccer players twelve years after anterior cruciate ligament injury. *Arthritis and Rheumatism* 50(10):3145–3152.
17. von Porat, A., E. M. Roos, and H. Roos. 2004. High prevalence of osteoarthritis 14 years after an anterior cruciate ligament tear in male soccer players: A study of radiographic and patient relevant outcomes. *Annals of the Rheumatic Diseases* 63(3):269–273.
18. Ingersoll, C. D., T. L. Grindstaff, B. G. Pietrosimone, and J. M. Hart. 2008. Neuromuscular consequences of anterior cruciate ligament injury. *Clinics in Sports Medicine* 27(3):383–404, vii.
19. Fong, D. T., Y. Y. Chan, K. M. Mok, P. Yung, and K. M. Chan. 2009. Understanding acute ankle ligamentous sprain injury in sports. *Sports Medicine, Arthroscopy, Rehabilitation, Therapy & Technology* 1(1):1–14.

20. Renstrom, P. A., and L. Konradsen. 1997. Ankle ligament injuries. *British Journal of Sports Medicine* 31(1):11–20.
21. Makhani, J. S. 1962. Diagnosis and treatment of acute ruptures of the various components of the lateral ligaments of the ankle. *American Journal of Orthopedics* 4:224–228.
22. McCulloch, P. G., P. Holden, D. J. Robson, D. I. Rowley, and S. H. Norris. 1985. The value of mobilisation and non-steroidal anti-inflammatory analgesia in the management of inversion injuries of the ankle. *The British Journal of Clinical Practice* 39(2):69–72.
23. Hertel, J. 2000. Functional instability following lateral ankle sprain. *Sports Medicine* 29(5):361–371.
24. Ferran, N. A., and N. Maffulli. 2006. Epidemiology of sprains of the lateral ankle ligament complex. *Foot and Ankle Clinics* 11(3):659–662.
25. Safran, M. R., J. E. Zachazewski, R. S. Benedetti, A. R. Bartolozzi, 3rd, and R. Mandelbaum. 1999. Lateral ankle sprains: A comprehensive review. Part 2: Treatment and rehabilitation with an emphasis on the athlete. *Medicine and Science in Sports and Exercise* 31(7 Suppl):S438–S447.
26. Burks, R. T., and J. Morgan. 1994. Anatomy of the lateral ankle ligaments. *The American Journal of Sports Medicine* 22(1):72–77.
27. Attarian, D. E., H. J. McCrackin, D. P. DeVito, J. H. McElhaney, and W. E. Garrett, Jr. 1985. Biomechanical characteristics of human ankle ligaments. *Foot and Ankle* 6(2):54–58.
28. Siegler, S., J. Block, and C. D. Schneck. 1988. The mechanical characteristics of the collateral ligaments of the human ankle joint. *Foot and Ankle* 8(5):234–242.
29. Funk, J. R., G. W. Hall, J. R. Crandall, and W. D. Pilkey. 2000. Linear and quasi-linear viscoelastic characterization of ankle ligaments. *Journal of Biomechanical Engineering* 122(1):15–22.
30. Stephens, M. M., and G. J. Sammarco. 1992. The stabilizing role of the lateral ligament complex around the ankle and subtalar joints. *Foot and Ankle* 13(3):130–136.
31. Nigg, B. M., G. Skarvan, C. B. Frank, and M. R. Yeadon. 1990. Elongation and forces of ankle ligaments in a physiological range of motion. *Foot and Ankle* 11(1):30–40.
32. Bahr, R., F. Pena, J. Shine, W. D. Lew, and L. Engebretsen. 1998. Ligament force and joint motion in the intact ankle: A cadaveric study. *Knee Surgery, Sports Traumatology, Arthroscopy* 6(2):115–121.
33. Woods, C., R. Hawkins, M. Hulse, and A. Hodson. 2003. The Football Association Medical Research Programme: An audit of injuries in professional football. An analysis of ankle sprains. *British Journal of Sports Medicine* 37(3):233–238.
34. Liu, S. H., and T. M. Nguyen. 1999. Ankle sprains and other soft tissue injuries. *Current Opinion in Rheumatology* 11(2):132–137.
35. Brostrom, L. 1967. Ankle sprains. *Lakartidningen* 64(16):1629–1644.
36. Vitale, T. D., and L. M. Fallat. 1988. Lateral ankle sprains: evaluation and treatment. *The Journal of Foot Surgery* 27(3):248–258.
37. Tyler, T. F., M. P. McHugh, M. R. Mirabella, M. J. Mullaney, and S. J. Nicholas. 2006. Risk factors for noncontact ankle sprains in high school football players: The role of previous ankle sprains and body mass index. *The American Journal of Sports Medicine* 34(3):471–475.
38. Cawley, P. W., and E. P. France. 1991. Biomechanics of the lateral ligaments of the ankle: An evaluation of the effects of axial load and single plane motions on ligament strain patterns. *Foot and Ankle* 12(2):92–99.
39. Colville, M. R., R. A. Marder, J. J. Boyle, and B. Zarins. 1990. Strain measurement in lateral ankle ligaments. *The American Journal of Sports Medicine* 18(2):196–200.
40. Renstrom, P., M. Wertz, S. Incavo, M. Pope, H. C. Ostgaard, S. Arms, and L. Haugh. 1988. Strain in the lateral ligaments of the ankle. *Foot and Ankle* 9(2):59–63.
41. Yamamoto, A., K. Takagishi, T. Osawa, T. Yanagawa, D. Nakajima, H. Shitara, and T. Kobayashi. 2010. Prevalence and risk factors of a rotator cuff tear in the general population. *Journal of Shoulder and Elbow Surgery* 19(1):116–120.
42. Hudson, V. J. 2010. Evaluation, diagnosis, and treatment of shoulder injuries in athletes. *Clinics in Sports Medicine* 29(1):19–32, table of contents.
43. Ecklund, K. J., T. Q. Lee, J. Tibone, and R. Gupta. 2007. Rotator cuff tear arthropathy. *Journal of the American Academy of Orthopaedic Surgeons* 15(6):340–349.

44. McConville, O. R., and J. P. Iannotti. 1999. Partial-thickness tears of the rotator cuff: Evaluation and management. *Journal of the American Academy of Orthopaedic Surgeons* 7(1):32–43.
45. Blevins, F. T., W. M. Hayes, and R. F. Warren. 1996. Rotator cuff injury in contact athletes. *The American Journal of Sports Medicine* 24(3):263–267.
46. Itoi, E., L. J. Berglund, J. J. Grabowski, F. M. Schultz, E. S. Growney, B. F. Morrey, and K. N. An. 1995. Tensile properties of the supraspinatus tendon. *Journal of Orthopaedic Research* 13(4):578–584.
47. Gschwend, N., D. Ivosevic-Radovanovic, and D. Patte. 1988. Rotator cuff tear—relationship between clinical and anatomopathological findings. *Arch Orthop Trauma Surg* 107(1):7–15.
48. Neviaser, R. J., T. J. Neviaser, and J. S. Neviaser. 1988. Concurrent rupture of the rotator cuff and anterior dislocation of the shoulder in the older patient. *Journal of Bone and Joint Surgery. American Volume* 70(9):1308–1311.
49. Ovesen, J., and S. Nielsen. 1986. Posterior instability of the shoulder. A cadaver study. *Acta Orthopaedica Scandinavica* 57(5):436–439.
50. Halder, A., M. E. Zobitz, F. Schultz, and K. N. An. 2000. Mechanical properties of the posterior rotator cuff. *Clinical Biomechanics (Bristol, Avon)* 15(6):456–462.
51. Hughes, R. E., and K. N. An. 1996. Force analysis of rotator cuff muscles. *Clinical Orthopaedics and Related Research* (330):75–83.
52. Gartsman, G. M., and J. C. Milne. 1995. Articular surface partial-thickness rotator cuff tears. *Journal of Shoulder and Elbow Surgery* 4(6):409–415.
53. Itoi, E., and S. Tabata. 1992. Incomplete rotator cuff tears. Results of operative treatment. *Clinical Orthopaedics and Related Research* (284):128–135.
54. Greis, P. E., D. D. Bardana, M. C. Holmstrom, and R. T. Burks. 2002. Meniscal injury: I. Basic science and evaluation. *Journal of the American Academy of Orthopaedic Surgeons* 10(3):168–176.
55. Cox, C. L., J. P. Deangelis, R. A. Magnussen, R. W. Fitch, and K. P. Spindler. 2009. Meniscal tears in athletes. *Journal of Surgical Orthopaedic Advances* 18(1):2–8.
56. McDermott, I. 2011. Meniscal tears, repairs and replacement: Their relevance to osteoarthritis of the knee. British Journal of Sports Medicine 45(4):292–297.
57. Allen, A. A., G. L. Caldwell, Jr., and F. H. Fu. 1995. Anatomy and biomechanics of the meniscus. *Operative Techniques in Orthopaedics* 5(1):2–9.
58. Aagaard, H., and R. Verdonk. 1999. Function of the normal meniscus and consequences of meniscal resection. *Scandinavian Journal of Medicine & Science in Sports* 9(3):134–140.
59. Jones, R. S., G. C. Keene, D. J. Learmonth, D. Bickerstaff, N. S. Nawana, J. J. Costi, and M. J. Pearcy. 1996. Direct measurement of hoop strains in the intact and torn human medial meniscus. *Clinical Biomechanics (Bristol, Avon)* 11(5):295–300.
60. Arnoczky, S. P., and C. A. McDevitt. 2000. The Meniscus: Structure, Function, Repair, and Replacement. In *Orthopaedic Basic Science: Biology and Biomechanics of the Musculoskeletal System*, edited by J. A. Buckwalter, T. A. Einhorn and S. R. Simon, 2nd ed., 532–545. American Academy of Orthopaedic Surgeons: American Academy of Orthopaedic Surgeons.
61. Ferrer-Roca, O., and C. Vilalta. 1980. Lesions of the meniscus. Part I: Macroscopic and histologic findings. *Clinical Orthopaedics and Related Research* 146:289–300.
62. Thompson, W. O., F. L. Thaete, F. H. Fu, and S. F. Dye. 1991. Tibial meniscal dynamics using three-dimensional reconstruction of magnetic resonance images. *The American Journal of Sports Medicine* 19(3):210–215; discussion 215–216.
63. Arangio, G. A. 1983. Proximal diaphyseal fractures of the fifth metatarsal (Jones' fracture): two cases treated by cross-pinning with review of 106 cases. *Foot and Ankle* 3(5):293–296.
64. Tissakht, M., and A. M. Ahmed. 1995. Tensile stress-strain characteristics of the human meniscal material. *Journal of Biomechanics* 28(4):411–422.
65. Chia, H. N., and M. L. Hull. 2008. Compressive moduli of the human medial meniscus in the axial and radial directions at equilibrium and at a physiological strain rate. *Journal of Orthopaedic Research* 26(7):951–956.

66. Metcalf, R. W., R. T. Burks, M. S. Metcalf, and J. B. McGinty. 1996. Arthroscopic meniscectomy. In *Operative Arthroscopy,* edited by J. McGinty, R. Caspari, R. Jackson, and G. Poehling, 2nd ed., 263–297, Philadelphia, PA: Lippincott-Raven.
67. Poulsen, M. R., and D. L. Johnson. 2011. Meniscal injuries in the young, athletically active patient. *The Physician and Sports Medicine* 39(1):123–130.
68. Zwitser, E. W., and R. S. Breederveld. 2010. Fractures of the fifth metatarsal; diagnosis and treatment. *Injury* 41(6):555–562.
69. Nunley, J. A. 2001. Fractures of the base of the fifth metatarsal: The Jones fracture. *Orthopedic Clinics of North America* 32(1):171–180.
70. Dameron, T. B., Jr. 1995. Fractures of the proximal fifth metatarsal: Selecting the best treatment option. *Journal of the American Academy of Orthopaedic Surgeons* 3(2):110–114.
71. Lawrence, S. J., and M. J. Botte. 1993. Jones' fractures and related fractures of the proximal fifth metatarsal. *Foot and Ankle* 14(6):358–365.
72. DeLee, J. C., J. P. Evans, and J. Julian. 1983. Stress fracture of the fifth metatarsal. *The American Journal of Sports Medicine* 11(5):349–353.
73. Clapper, M. F., T. J. O'Brien, and P. M. Lyons. 1995. Fractures of the fifth metatarsal. Analysis of a fracture registry. *Clinical Orthopaedics and Related Research* (315):238–241.
74. Shereff, M. J., Q. M. Yang, F. J. Kummer, C. C. Frey, and N. Greenidge. 1991. Vascular anatomy of the fifth metatarsal. *Foot and Ankle* 11(6):350–353.
75. Smith, J. W., S. P. Arnoczky, and A. Hersh. 1992. The intraosseous blood supply of the fifth metatarsal: implications for proximal fracture healing. *Foot and Ankle* 13(3):143–152.
76. Quill, G. E., Jr. 1995. Fractures of the proximal fifth metatarsal. *Orthopedic Clinics of North America* 26(2):353–361.
77. Dameron, T. B., Jr. 1975. Fractures and anatomical variations of the proximal portion of the fifth metatarsal. *Journal of Bone and Joint Surgery. American Volume* 57(6):788–792.
78. DeLee, J. C. 1986. Fractures and dislocations of the foot. In *Surgery of the Foot and Ankle,* edited by R. A. Mann. 2:1627–1640, 6th ed. St. Louis: C.V. Mosby.
79. Josefsson, P. O., M. Karlsson, I. Redlund-Johnell, and B. Wendeberg. 1994. Closed treatment of Jones fracture. Good results in 40 cases after 11–26 years. *Acta Orthopaedica Scandinavica* 65(5):545–547.
80. Rettig, A. C., K. D. Shelbourne, and J. Wilckens. 1992. The surgical treatment of symptomatic nonunions of the proximal (metaphyseal) fifth metatarsal in athletes. *The American Journal of Sports Medicine* 20(1):50–54.
81. Dameron, T. B., Jr. 1992. Jones fracture. *Southern Medical Journal* 85(12):1264–1265.
82. Viladot, A., and A. Viladot, Jr. 1998. Stress fractures in the foot. *Foot and Ankle Surgery* 4(1):3–11.
83. Johnson, D. L., and R. A. Pedowitz. 2007. *Practical Orthopaedic Sports Medicine & Arthroscopy*, 1st ed. Philadelphia, PA: Lippincott, Williams & Wilkins.
84. Arangio, G. A., H. Beam, G. Kowalczyk, and E. P. Salathe. 1998. Analysis of stress in the metatarsals. *Foot and Ankle Surgery* 4(3):123–128.
85. Arangio, G. A., D. Xiao, and E. P. Salathe. 1997. Biomechanical study of stress in the fifth metatarsal. *Clinical Biomechanics (Bristol, Avon)* 12(3):160–164.
86. Stokes, I. A., W. C. Hutton, and J. R. Stott. 1979. Forces acting on the metatarsals during normal walking. *Journal of Anatomy* 129(Pt 3):579–590.
87. Farinaccio, R. 1989. An Experimental and Numerical Study of the Mechanical Response of the Knee Menisci. Masters Thesis. McGill University.
88. Fithian, D. C., M. A. Kelly, and V. C. Mow. 1990. Material properties and structure–function relationships in the menisci. *Clinical Orthopaedics and Related Research* 252(19–31).
89. Skaggs, D. L., and V. C. Mow. 1990. Function of radial fibers in the meniscus. *Transaction of the Orthopaedics Research Society* 15:(248).
90. Whipple, T. L., R. B. Caspari, J. F. Meyers. 1984. Arthroscopic meniscectomy. An interim report at three to four years after operation. *Clinical Orthopaedics and Related Research* 183(105–114).

18

Imaging Approaches to Quantify Tissue Structure and Function from the Microscale to the Macroscale

Kyle P. Quinn, Irene Georgakoudi, and Beth A. Winkelstein

CONTENTS

18.1 Introduction

Clinical and laboratory assessments of musculoskeletal tissue pathology often rely on imaging techniques to provide quantitative information on the functional, structural, or mechanical properties of the tissue. A wide variety of imaging approaches have been developed to characterize the structural and functional properties of musculoskeletal tissues at different scales. In this chapter, a brief overview of the current and emerging diagnostic

imaging modalities is provided, with a focus on those that are specifically related to orthopaedic applications and the relevant hard and soft tissues. Specific applications to quantify musculoskeletal structure and function at the macroscale in the clinic and at the microscale in the laboratory are highlighted. Finally, quantitative imaging approaches that characterize the kinematic responses of tissues to provide insight into mechanical function and tolerance are described.

18.2 Image Modalities for Obtaining Structural Data

A wide range of imaging modalities have been developed with varied methodologies, associated resolutions, risks, and functionality (Table 18.1). As such, these modalities also have different utilities in both the clinical and research settings, lending themselves to certain tissue types, clinical applications, and length scales. Here, we provide a brief review of the major imaging modalities used clinically for orthopaedic applications or those that have specific advantages for defining structure and function in biomechanical research. Where possible, we provide context for the clinical use and specific application to the tissues of the musculoskeletal system.

18.2.1 Radiography

Diagnostic radiography is the standard imaging technology used to assess the structural properties of bone tissue. Transmission images are produced using very-short wavelength (0.01–1 nm) electromagnetic waves (X-rays). X-rays are more likely to be absorbed by denser tissues enabling substantial contrast between bone and the soft

TABLE 18.1

Summary of Image Modalities Used to Quantify Tissue Structure at Different Length Scales

Image Modality	Source of Contrast	Spatial Resolution	Depth Penetration	Notes
CT	Absorption of X-rays	0.5–1 mm	>50 cm	Excellent hard tissue contrast through use of ionizing radiation
MRI	Hydrogen proton spin	0.1–1 mm	>50 cm	Different soft tissues detectable through a range of specialized scans
Sonography	Ultrasound backscatter	0.1–1 mm	1–50 cm	Muscle injury detectable
OCT	Backscattering of visible-NIR light	10 μm	1–2 mm	Soft tissue microstructure can be quantified with handheld probe
Optical microscopy	Stains, birefringence, endogenous scattering, and/or fluorescence	0.2–20 μm	3–1000 μm	Variety of endogenous and exogenous probes enables contrast for a wide range of biological components; potential for nondestructive, depth-resolved imaging
Electron microscopy	Electron beam interaction with sample	0.05–10 nm	<100 nm	Destructive technique can provide surface topology information

tissues that surround it. Through an inverse radon transform, computed tomography (CT) X-ray systems can recreate two-dimensional (2D) image slices based on the attenuation of X-rays at various angles, which allows the three-dimensional (3D) reconstruction of biological tissues. The use of CT enables the quantification of intricate joint geometries and the diagnosis of complex fractures that would otherwise be undetectable. The spatial resolution of CT is typically limited to 0.1 to 1 mm, and image scans typically can be acquired in 5 to 10 minutes.[1] Although CT possesses excellent diagnostic value for assessing mineralized tissues, the cost of this technology and the use of ionizing radiation both limit its more widespread use. Furthermore, many soft tissues are similar in density, and so this imaging modality is less likely to produce contrast of significant diagnostic value.

18.2.2 Magnetic Resonance Imaging

Magnetic resonance imaging (MRI) processes image data in a similar manner as CT does, which allows for 3D reconstruction; however, the image contrast is derived from the concentration of hydrogen protons. A strong magnetic field (typically ranging from 1.5 to 3 T) is applied, causing the protons to align in one direction. A radiofrequency transmitter also modifies the electromagnetic field and causes some protons to change alignment. As the RF transmitter is turned on and off, some protons will resonate a detectable radio signal. Excellent soft tissue contrast can be produced using standard T1-weighted, T2-weighted, or proton density-weighted scans.[2] T1-weighted images are sensitive to the time it takes for the longitudinal magnetization to return to its original state after an RF pulse, and these images are typically used to highlight fat deposition. T2-weighted images, on the other hand, measure how long the transverse magnetization lasts, which highlights water content and so can be used to identify edema. Although T1- and T2-weighted scans provide good resolution for soft tissue assessment, a variety of specialized MRI scans have also been developed to target different tissue characteristics; these are described in more detail in Section 18.3 as they apply to specific clinical applications and tissue types. Due to the tomographic reconstruction techniques used, 3D models of any anatomical location can be produced. However, spatial resolution is generally limited to 0.1 to 1 mm.[1] Although MRI is capable of providing detailed 3D images of tissue structure at the macroscopic level, the long acquisition times, high device costs, and the inability to bring ferromagnetic materials near the device limit its use in many clinical musculoskeletal applications.

18.2.3 Diagnostic Sonography

Sonography provides a noninvasive approach to quantify tissue structure using ultrasound waves and a piezoelectric transducer. Ultrasound frequencies, typically on the order of 2 to 20 MHz, are directed toward the tissue of interest and reflect back where there is a change in acoustic impedance. Diagnostic sonography can be used for penetration depths of up to 20 cm, while still providing excellent spatial resolution on the order of 1 mm^3 (Table 18.1). Improved resolution can be achieved using higher frequencies, but the penetration depth will suffer due to increased scattering. Due to its resolution, modest cost, and lack of ionizing radiation, sonography is currently used for a variety of clinical assessments. For orthopaedic applications, sonography offers excellent diagnostic value in detecting muscle injuries and even bone erosion that can develop in rheumatoid arthritis.[3–5]

18.2.4 Optical Coherence Tomography

The development and expanded use of optical coherence tomography (OCT) over the last 20 years have provided a means to quantify soft tissue structure with higher resolution (approximately 10 μm) compared with that of traditional clinical diagnostic techniques. Analogous to ultrasound imaging, OCT measures the amount of light that is backscattered to a probe. Using a low-coherence light source, the relatively small amount of backscattered light can be detected through interferometry. By combining light reflected back from the sample and a reference mirror and measuring the interference pattern, the backscattered signal at specific depths can be isolated. Although its spatial resolution enables the quantification of smaller structural elements than the macroscopic organ, such as collagen organization, the penetration depth of OCT is limited to 1 to 2 mm (Table 18.1). This limitation in depth has constrained the clinical applicability of OCT to studies of macular diseases or epithelial pathology.[6–8] However, more recent experimental studies related to orthopaedic biomechanics have quantified collagen fiber organization and kinematics in both isolated tendon and intervertebral disc tissue.[9–10]

18.2.5 Optical Microscopy

The standard clinical mode of imaging used to assess tissue structure and function at the microscale is light microscopy. A range of histological techniques have been developed to quantify tissue structure and function and to define pathologies. Traditional histological protocols require chemical fixation and processing of the tissue, embedding, and sectioning at thicknesses of less than 20 μm. A variety of staining techniques have been developed to differentiate muscle, ligament, cartilage, bone, and other musculoskeletal tissue components; immunohistochemistry enables the detection of specific carbohydrates, lipids, or proteins as well. However, due to the destructive nature of these protocols, invasive biopsies are a prerequisite for histological analysis in the clinic, and large sample sizes are required to characterize temporal changes in biomedical research. Optical resolution (d), according to the Raleigh criterion, is defined by the diffraction limit:

$$d = \frac{0.61\lambda}{n \sin \theta}, \tag{18.1}$$

where λ is the wavelength of light, n is the index of refraction of the medium in which the objective is being used, and θ is the half-angle over which the objective lens can gather light. Using a high-numerical aperture oil immersion objective, the diffraction-limited resolution can reach approximately 200 nm (Table 18.1). Imaging at different depths within a tissue sample can be achieved with confocal microscopes in which a pinhole rejects out-of-focus light. However, absorption, light scattering, and the potential for photodamage outside of the focal region generally limit the depth penetration of that modality to the outer 500 μm of tissues.

Although fluorescent or absorptive dyes can be used to identify tissue microstructure, nonlinear optical microscopy techniques provide a means to quantify cell and matrix organization through endogenous sources of contrast. Two-photon excited fluorescence (TPEF) microscopy has been used to identify microstructural organization based on the principle that two longer wavelength photons can be simultaneously absorbed and used to excite a molecule that will normally emit a single, shorter wavelength fluorescent photon on relaxation to the initial state.[11–12] This relatively rare occurrence of

multiphoton absorption can be realized in a manner that is efficient enough to yield detectable fluorescence signal through the use of femtosecond-pulsed mode-locked titanium/sapphire laser sources that emit light of high peak, but relatively low average, intensity. In this way, the potential for phototoxicity is minimized. Furthermore, multiphoton absorption only occurs within the focal volume of the beam where photon density is highest, providing intrinsic 3D sectioning ability. The use of near-infrared (NIR) light to excite fluorophores improves depth penetration due to a reduction in light scattering. Although many standard fluorescent dyes that are excited in the 350 to 450 nm range can be used in TPEF microscopy, endogenous cellular fluorophores can also be excited to provide quantitative information about cellular biochemical status. Collagen and elastin organization can also be detected through TPEF. However, collagen and myosin fiber orientation can typically be detected and isolated from cellular fluorescence through second harmonic generation (SHG) imaging. Using the same equipment as TPEF imaging, SHG is a nonlinear process with the same advantages (e.g., intrinsic 3D sectioning, near-infrared light source, etc.). In SHG imaging, noncentrosymmetric materials (i.e., lacking symmetry about a point), such as collagen, cause a frequency doubling phenomenon as the light travels through the material.[13–14] The SHG signal at exactly half of the initial wavelength can be detected in either the forward or backward direction. The application of SHG imaging to orthopaedic research has largely been limited to the quantification of fiber structure and organization in muscle, tendon, and engineered constructs.[14–16]

18.2.6 Electron Microscopy

Electron microscopy uses an electron beam with a much shorter wavelength than visible light to identify the ultrastructure of a specimen. As a result, resolutions of less than 0.05 nm can be achieved.[17] Transmission electron microscopy (TEM) images can be produced from very thin tissue sections; however, scanning electron microscopy (SEM) is more amenable for defining ultrastructure in biomedical applications without the need for ultramicrotomy. SEM, unlike TEM, is based on secondary electron emission as the beam interacts with the surface of the sample. Scattering electrons may produce additional secondary electron emissions, which can blur the image, and, as a result, SEM typically has a slightly lower resolution than TEM. Although electron microscopy can provide unparalleled resolution, the complex tissue processing that is required to produce a conductive sample surface and the need to work in a vacuum eliminate the possibility of live cell microscopy. Although SEM is rarely used for clinical orthopaedic applications, experimental biomechanical studies have frequently used SEM to assess the fiber diameters, fiber orientations, and crimp patterns in ligaments and tendons.[18–21]

18.3 Quantification of Musculoskeletal Structure and Function by Clinical Imaging

Musculoskeletal tissue structure and physiology are traditionally assessed in the clinical setting using noninvasive techniques such as radiography, MRI, or sonography. Unlike radiography and sonography, magnetic resonance (MR) approaches offer a great degree of flexibility in sources of image contrast and an ability to obtain 3D image volumes of

particular anatomic features in any orientation. In this section, we focus on advanced MR image acquisition and processing techniques to quantify musculoskeletal structure and function. Image processing approaches to define 3D joint anatomy and kinematics are reviewed, and specialized spin-locked MR scans to assess articular cartilage and intervertebral disc degeneration are also described. Recently, both functional and diffusion MRI approaches, which were originally developed for neuroimaging applications, have been implemented to characterize muscle physiology and microstructural organization and to detect pathology related to disease or trauma. These are also briefly summarized in this section.

18.3.1 Image Analysis of Joint Biomechanics

The 3D imaging approaches are particularly useful in defining joint anatomy and kinematics for the very complicated joints—such as the ankle, shoulder, and spine—which undergo complex motions with many articulations during even the simplest normal activities. For example, the ankle has many articulations, and the joint itself experiences complicated multiaxial and coupled 3D motions. On the other hand, the shoulder has fewer articulations, but has an extensive range of motions. Furthermore, both of these joints and others throughout the musculoskeletal system are difficult to image using planar techniques due to their orientations and the close proximity of the bones in the joint. These issues present even greater challenges when measuring changes in motion compared with normal responses of the joints. Recently, several approaches have been developed that use MRI and CT to capture the full 3D motion of bones.[22–25] These approaches have utility for providing diagnostic information about joint disease and pathology. They also provide data to help in image-guided orthopaedic surgery, in which the bony structures need to be identified in preoperative images for optimal surgical planning.[26–28] These image data can also help with surgical management and follow-up by registering postoperative images with those of the preoperative images for progressive comparisons.

The segmentation and separation of the bones in MRI and CT images of a joint are key to defining normal anatomy and biomechanics, as well as abnormal motions. However, such processes also present a variety of challenges.[29] Bones are situated very close to each other, which can exacerbate the inherent challenges in segmentation; measuring the joint space between bones often depends on the orientation with which the slice planes are taken with respect to the articulating bone surfaces. Because there are multiple bones at a joint and their surfaces are usually curved, it is even harder to select a slice plane that is optimal for a specific application. Both MRI and CT pose hurdles for differentiating the edges of bones and distinguishing them from surrounding soft tissues; this problem is amplified where the bones or soft tissue (i.e., ligaments and tendons) come together to form a joint. Although methods have been developed to segment bones in 3D using MR, they are few in number and have focused largely on nonarticulating bones, such as the skull.[30,31] More complicated methods have been developed for use with articulating joints, but many of them use slice-by-slice strategies, which require a considerable amount of user time.

To use such image segmentation approaches to define joint kinematics, it is necessary to not only classify image voxels as part of a specific bone but to also describe the shape, location, and relative motions of the bone. The demand for motion analysis also introduces the need for sensitive and specific object registration between different time points or positions. Typically, image registration assumes that each of the bones of the joint complex is a rigid body, but that the spatial arrangements of the bones may change between image

volumes captured in different positions.[29] Owing to the difficulties presented above, a live-wire method for segmenting bones can be used in which a user provides assistance to help direct the segmentation process; an algorithm performs the delineation in a slice-by-slice manner. This approach is more reproducible and efficient than manual boundary tracing and has become popular for clinical applications.[29,32]

Although the live-wire method is manageable for small subject numbers, it becomes impractical for obtaining kinematic data from large groups or image sets with hundreds of slices. A solution can be obtained by segmenting of the bones of a given joint in one 3D image volume and then using that as a rigid model to automatically delineate the bones in the other 3D images of the same joint.[29] Several other strategies for segmentation of the same bone in different positions, such as oriented active shape models and live-wire active shape models, have also been developed.[29,33] Long bones, such as the tibia and fibula at the ankle joint and the glenoid and the humerus at the shoulder joint, pose challenges in kinematic analysis because different aspects of those bones appear in different images taken for different positions of the joints. Using a method in which the same articulating parts of these bones are automatically identified and trimmed in all images facilitates consistent motion analysis.[34] Analysis of the motion of a bone (translation and rotation) with respect to a reference position is carried out by tracking the surface of the bone between images. This registration of images can be done by using the image intensity pattern in the immediate exterior and in the interior of the surfaces and by maximizing the normalized mutual information criterion.[35]

Broadly, these techniques have been used for a variety of clinical orthopaedic applications in the ankle and shoulder. Specifically, the set of architectural parameters derived from measurements in images of the foot and ankle has been used to pinpoint the kinematic parameters that most effectively characterized deviations from normalcy in a variety of pathologic conditions.[36–38] Those studies also led to the development of quantitative diagnostic techniques for ankle ligament injuries and the quantification of the support characteristics of external stabilizers such as ankle braces. Those techniques were combined with what Siegler et al.[39,40] called "stressed MRI," in which the joint was placed in an additional position via an ankle-loading device and imaged again to define the internal flexibility of the ankle and subtalar joints in normal patients and in patients with ligament injuries. Their work identified the architectural parameters that carry the most specific information about the health of a joint. Rhoad et al.[41] used the same approaches to study the biomechanics of the gleno humeral joint. In their work, they demonstrated in nine asymptomatic joints that it is possible to accurately quantify the translation and rotation of the humerus relative to the glenoid through MR images taken in 10° increments of actively achieved internal and external rotations.

Stressed MRI or CT has also been used to define the 3D relationships between bones in the cervical spine. Flexibility studies were applied to investigate the effect of age, gender, and posture on cervical spine mechanics and to quantify the effects of cervical spine fusions on the postsurgical mechanical properties of the cervical spine.[42,43] Stressed CT has the ability to leverage the multislice approach to image regions of the spine that are otherwise obstructed by other joints using conventional planar imaging. For example, the anatomical locations of the clavicle and shoulder obscure the cervicothoracic junction (CTJ) during planar imaging, making it difficult to measure CTJ anatomy or biomechanical responses to even simple loading scenarios in the spine. Stressed CT was coupled with mechanical loading in a cadaver model to segment vertebral surfaces and reconstruct them for clinically relevant loading scenarios.[44] That approach produced small errors in translations (0.1 mm) and vertebral rotations (<0.9°, for primary and coupled rotations). Although stressed

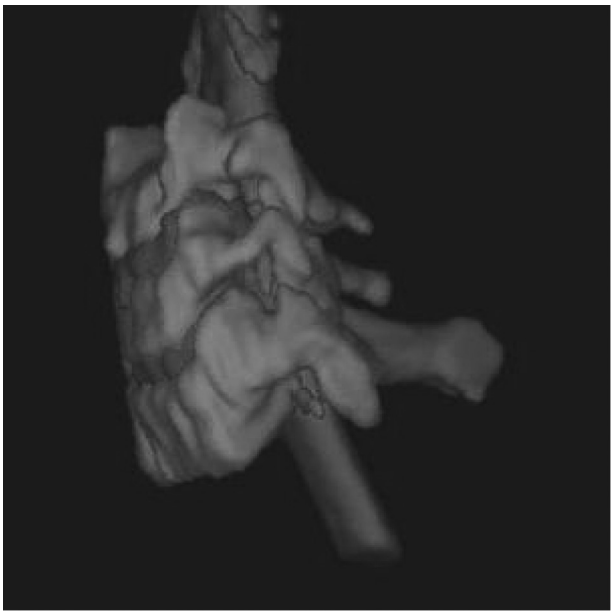

FIGURE 18.1
(See color insert.) 3D reconstruction of three cervical vertebrae (yellow) and their intervertebral discs (orange), as well as the spinal cord (purple) and nerve roots (cyan). The architectures of these musculoskeletal and neural tissues were produced using segmentation of sagittal (bone) and axial (neural) MR images.

CT was adequate for defining the bony kinematics of the CTJ, it is not pragmatic for clinical applications due to the use of ionizing radiation. Recent work using the image analysis methods described above has demonstrated that 3D MR images can provide similar utility for defining spinal biomechanics.[45] In fact, combining sagittal and axial MR image scans that are optimized for bone and neural elements, respectively, has provided a means to simultaneously define architectural relationships between the bone *and* neural elements in the spine (Figure 18.1). That technique has also shown promise in providing a novel imaging diagnostic approach to localize neural tissue impingement during spinal positioning that evokes pain but is not detectable on conventional clinical MRI.[46]

18.3.2 Quantitative Evaluation of Osteoarthritis and Degeneration Using T1-rho MRI

Traditionally, T2-weighted images have been used to qualitatively evaluate intervertebral disc degeneration based on morphology and T2 signal intensity. However, T1-rho imaging has emerged as a potential quantitative biomarker for early disc and articular cartilage degeneration.[47–50] The application of a low-power spin-lock pulse, and the measurement of the subsequent spin-lattice (T1-rho) relaxation, enables high sensitivity to interactions between water and macromolecules. T1-rho contrast has been shown to correlate with the proteoglycan content of bovine articular cartilage tissue.[48] In addition, histological comparisons of fresh osteoarthritic cartilage from the tibial and femoral condyles demonstrate that T1-rho imaging enables a quantitative determination of degeneration that is correlated with a loss of proteoglycan content.[51] Correlations between T1-rho and sulfated glycosaminoglycan content have also been established in research studies using human cadaveric intervertebral disc.[49] In the intervertebral disc, an early hallmark of degeneration is the

breakdown of glycosaminoglycans in the nucleus pulposus, which ultimately leads to a reduced nucleus pulposus pressure and a reduced disc height that is observed in the later stages of degeneration. By detecting lower levels of proteoglycan content, T1-rho imaging may enable an earlier detection of degeneration.[49] Indeed, T1-rho outcomes seem to be more strongly associated with clinical symptoms of degeneration than those from traditional T2-based assessments.[50] The application of T1-rho imaging shows promise for the early detection of osteoarthritis and disc degeneration, but may also have applicability to the evaluation of tissue fibrosis or other disease states that involve extracellular matrix pathology.

18.3.3 Functional MRI to Assess Metabolic and Hemodynamic Changes in Muscle

Functional MRI (fMRI) has been used extensively to assess temporal and spatial patterns in brain activity.[52–54] More recently, fMRI techniques have been applied to assess normal muscle function during exercise or abnormalities in function in diseased states.[55–59] Muscle fMRI often uses the rapid acquisition of T2-weighted images to identify metabolic changes during exercise. The change in T2 signal intensity has been attributed to increases in intracellular osmolytes; however, hemodynamic changes may also contribute to the change in T2 signal intensity.[55] Blood oxygen level dependence (BOLD) contrast fMRI is sensitive to oxyhemoglobin content in microvasculature, and this technique has traditionally been used in neuroimaging studies.[57] Detectable changes in BOLD imaging have also been observed after exercise and ischemia in muscle tissue.[55,56,58] Differences in patient age, weight, and physical fitness can produce challenges in evaluating disease states in muscle studies using BOLD imaging.[59] Although the sensitivity and specificity of this technique for muscle-related studies may not be fully defined, it likely has diagnostic value to noninvasively monitor the effectiveness of therapy approaches and the muscle healing processes over time.

18.3.4 Diffusion MRI to Study Muscle Physiology, Structure, and Injury

Diffusion-weighted imaging has been used extensively to define the structure of a wide variety of anatomical tissues, including brain, spinal cord, kidneys, heart, prostate, and the intervertebral disc.[60–71] Application of this technique and its utility has recently been expanded to include skeletal muscle. The normal diffusion of water is altered by the presence and orientation of physical barriers such as cell membranes, myelin, lipids, and proteins; the measure of how water diffusion changes provides a quantitative value for an apparent diffusion.[72] Therefore, if there are abnormalities in the tissue that change the fat or water content, the signals on T1- and T2-weighted sequences are also changed.[73] The fast and slow components of the signal are thought to reflect the movements in the extracellular and intracellular spaces, respectively.[74] Because the enlargement of the extracellular space is believed to be associated with markers of tissue injury in muscle, such as atrophy, quantification of changes in the fast apparent diffusion coefficient has been hypothesized as providing a sensitive imaging marker of muscle tissue responses.[60,73,75,76] Indeed, diffusion-weighted imaging has been used to define the structure and diffusive properties of muscles of the lower extremities and lower back in healthy and injured humans, providing responses with normal aging, exercise, and different degrees of injury producing muscle denervation.[77–79]

Because muscular degeneration is associated with fatty infiltration that results in a change of the signal detected with diffusion-weighted MRI, this imaging approach has

begun to receive more attention for its utility as a clinical diagnostic of predicting injury progression, symptom resolution, and treatment effectiveness. In particular, the degree of fatty infiltration (quantified by the normalized ratio of fat to muscle) has been quantified in subjects with traumatic neck pain, such as whiplash-associated disorders (WAD).[60,75,76] A higher amount of fat was detected in the posterior extensor muscles of subjects who had been exposed to a motor vehicle crash producing WAD II symptoms (i.e., whiplash) than in those from healthy asymptomatic subjects.[75] Although the fatty infiltration varied throughout the cervical levels, for subjects who were evaluated between three months and three years after the trauma, the differences were independent of age, pain symptoms, and disability sores.[75] The anterior neck muscles were also found to exhibit greater fatty infiltrate in the anterior muscles, along with the cross-sectional area, especially for the deeper muscle groups.[76] Furthermore, those subjects with neck pain from whiplash exhibit greater fatty infiltration than those subjects with neck pain not due to trauma, who were not different from controls.[73] More recently, these imaging techniques and analyses have been used to follow the temporal responses of patients with whiplash and show the potential for delineating those individuals in whom symptoms may resolve from those in which chronic pain develops.[80]

In addition to measuring differences in diffusion rate with diffusion-weighted MRI approaches, the direction of diffusion can be quantified through diffusion tensor imaging (DTI). Anisotropy in diffusion arises from the microstructural organization of a tissue, and tissues with strong fiber orientations, such as white matter and a variety of muscles types, have been characterized with this technique.[81–87] Defining fiber orientation is key to understanding structure–function relationships for muscle tissues and detecting the onset of disease. The fiber direction in muscle tissue is acquired through the application of at least six gradients in different directions that are used to derive a gradient tensor.[82,83] Through fiber tracking, the muscle fiber orientations of different subcompartments in the soleus muscle have been quantified in neutral and plantarflexion configurations.[82] The reduced anisotropy observed in patients with calf muscle injuries demonstrates that DTI also has utility in detecting and evaluating muscle injuries.[87] Collectively, both diffusion-tensor and diffusion-weighted MR techniques offer a variety of metrics to evaluate both the structure and function of muscle tissue at the macroscale.

18.4 Quantification of Tissue Structure and Function at the Microscale

Several different imaging approaches have been developed and exploited to provide quantitative metrics of the structure and function of orthopaedic tissues. To date, the collagen fiber organization in soft tissues and mineral density in bone have been studied most extensively. Approaches to quantifying the structural organizations of both of these tissues are reviewed in this section, with a focus on the engineering approaches, specific analysis techniques, and relative trade-offs among imaging modalities. More recently, molecular imaging using clinical imaging modalities and nonlinear optical microscopy have enabled methods that evaluate the biochemical status and define the metabolic activity in tissues and cells. These approaches are also highlighted as they can be integrated with other imaging outcomes and provide promise for future discovery in orthopaedic biomechanics.

18.4.1 Collagen Fiber Organization

Changes in tissue microstructure and overall mechanical function have been used to quantify engineered tissue development and to detect mechanical injury and disease states.[20,88–95] To measure these structural and functional changes in musculoskeletal tissues, the quantification of the load-bearing collagen fibers is often required. In addition to diffusion-tensor MRI, optical imaging approaches can provide information about the average fiber orientation for tissue without directly visualizing the collagen fibers. Small angle light scattering (SALS) has been used to quantify the collagen fiber organization of tendon, cardiac tissue, and engineered scaffolds through the scattering patterns produced by visible light transmission.[96–99] When light with a wavelength similar to that of the collagen fibers is transmitted through a tissue, it scatters preferentially in a direction perpendicular to the fiber orientation. Angular sampling of this scattering pattern can provide a measure of the fiber orientation distribution of the tissue within the beam profile. By quantifying the fiber alignment patterns at different magnitudes of tissue deformation, SALS has been used to characterize fiber alignment patterns in aortic valve leaflets.[96] In particular, that work has demonstrated that changes in collagen fiber orientation during loading do not directly follow the local deformation in some tissues. However, because fiber alignment can only be measured using SALS at a single point in the tissue at a time, raster scanning by moving the beam or tissue sample is required to reconstruct a fiber alignment map of whole tissues. As a result, image acquisition is typically limited to use with specimens in a static configuration, and this approach is used mainly to define the general structural organization or the *changes* in such organization associated with a specific applied deformation or load.

Collagen fiber orientation in a tissue can also be investigated through the use of polarized light.[21,88,89,100–106] This technique exploits the natural linear birefringence of collagen to define collagen fiber organization. Birefringence causes light to travel through the tissue at a speed that is dependent on the orientation of its fibers.[103,107] Both the average fiber direction and the magnitude that the light speed is retarded can be quantified from a series of images taken with polarizers oriented in different directions. In studies in which polarized light passes through a tissue sample that has multiple layers of fibers, the measured light retardation can be used to estimate the strength of fiber alignment through the thickness of the tissue.[91] Typically, a set of orthogonal polarizers are placed before and after the sample and incrementally rotated to determine a transmission extinction angle that corresponds to the fiber orientation in the sample.[108,109] However, a quantitative determination of the fiber orientation cannot be made through this approach because it is unknown which of the two orthogonal polarizer orientations corresponds to the collagen fiber orientation. The use of a single rotating linear polarizer and a fixed circular analyzer in quantitative polarized light imaging (QPLI) eliminates any ambiguity in the absolute fiber orientation.[91,110] However, QPLI measurement techniques assume that linear birefringence is the dominant optical property of the tissue. If the tissue also exhibits diattenuation (e.g., it acts as a partial polarizer), fiber angle measurements will systematically deviate from the true fiber orientation. In engineered collagen gels and *ex vivo* human cadaveric capsular ligament tissue, the unique ability of QPLI to acquire data with high temporal resolution and adjustable spatial resolution has enabled nondestructive measures of collagen fiber kinematics *during* continuous loading.[91,111,112] The fiber kinematic measurements inferred through changes in light retardation using QPLI have enabled the detection and localization of microstructural damage[90] and the development of image-based multiscale models characterizing the tissue's mechanical properties.[113]

However, QPLI requires light transmission through the tissue to determine fiber alignment, and so this work is limited by the variability in alignment through the thickness of the tissue.

Imaging modalities such as confocal microscopy, SEM, SHG, and atomic force microscopy have been used for applications in which the visualization of the collagen fibers at the microscale is needed.[12,15,18–20,114–118] Because the exact fiber orientation is not directly measured during image acquisition using these microscopy techniques, image processing is required to elucidate quantitative measurements of fiber alignment and organization. Techniques using a 2D Fourier transform have often been used to assess fiber orientation in collagenous tissues.[16,117,119] Typically, power spectral density (PSD) maps are produced from the square of the magnitude of the Fourier-transformed images (Figure 18.2). By angularly sampling the PSD, a distribution of the collagen fiber orientations can be produced (Figure 18.2). This image analysis technique has been used in SHG imaging studies to identify microstructural damage in both fatigue-loaded rat patellar tendon and collagenase-injected equine superficial digital flexor tendon.[120,121] In addition, these Fourier-based methods also have been used to assess the structure of engineered constructs and to guide tissue engineering protocols.[16,117,119]

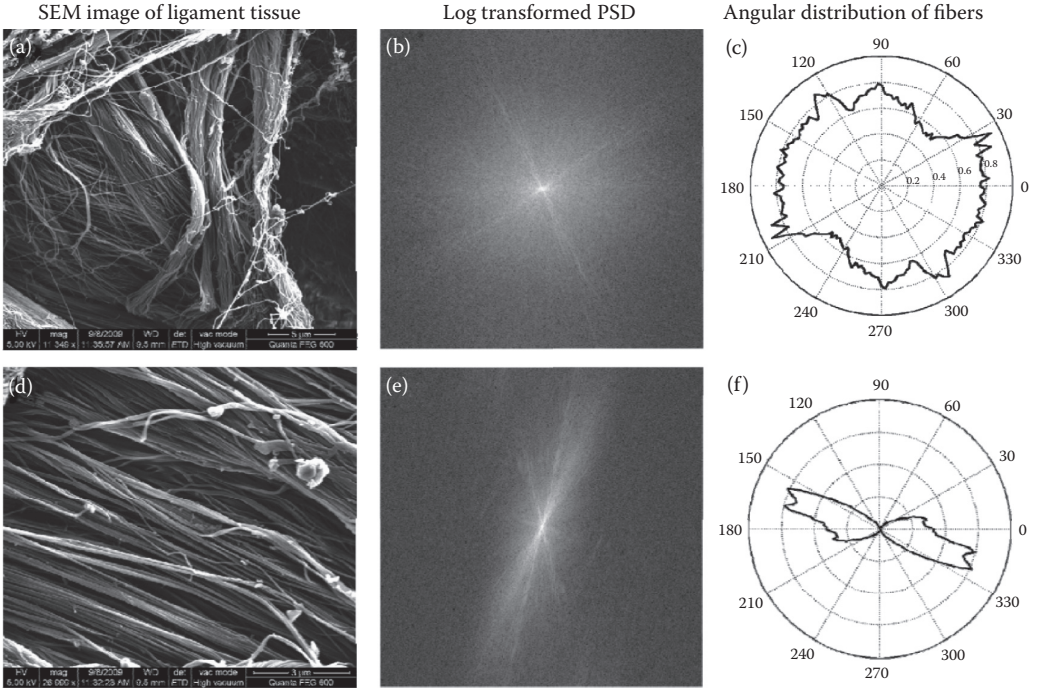

FIGURE 18.2
Fourier-derived collagen fiber orientation distributions from SEM images of cadaveric human facet capsular ligament tissue. SEM images (a, d) were transformed into PSD maps (b, e), and the fiber distribution (c, f) was determined through angular sampling of the PSD. The increased fiber alignment that is visually apparent in (d) translates to the increased power in the orthogonal direction in (e) and the higher fiber alignment detected between 160° and 170°, which is evident in (f).

To quantify regional differences in fiber organization, Fourier-based analyses can be performed on smaller tissue subregions. However, the size of the PSD image and the range of spatial frequencies will decrease when applied over smaller areas, which limits the resolution at which unique data can be sampled at different angles in the frequency domain. Additional techniques applied within the spatial domain, such as the Hough transform, can be used to identify fiber orientation information by characterizing the polar coordinates of specific image locations.[122] By making cumulative measurements of the polar coordinates associated with weighted pixel locations, the Hough transform has been used to determine collagen fiber orientations within 32 × 32 pixel subregions in SHG images.[16] This image processing technique has also been applied to identify muscle fiber orientation from ultrasound images[123] and is amenable to any imaging modality with sufficient contrast and resolution to visualize discrete fiber bundles.

18.4.2 Bone Organization

Dual-emission X-ray absorptiometry (DEXA) uses two X-ray beams with different energy levels to produce a sensitive measure of bone mineral density that has proven helpful in assessing osteoporosis and the potential for bone fracture.[124] However, DEXA does not provide a complete understanding of the mechanical strength of bone because, although it does provide a quantitative measure of bone mineral density, it lacks information on the structural organization of the tissue.[125] Furthermore, the ionizing radiation source that is required for this approach also limits how frequently DEXA or quantitative CT imaging can be used to clinically evaluate osteoporosis. Images of trabecular bone can also be obtained through MRI, and the microstructural organization of bone can be quantified by texture analysis techniques and correlated with the overall mechanical properties of the tissue.[1] In addition to morphological measurements, such as trabecular thickness and the ratio of bone volume to total volume, the fractal organization of trabecular bone has been quantified from MR images as a means of assessing the structural properties of the tissue in diseased states.[126] For textural analysis, CT or MR images are transformed into a binary image based on a pixel intensity threshold that isolates trabecular bone from bone marrow. Frequently, a box-counting method is then used to determine the fractal dimension of these binarized images. The number of boxes needed to cover the binarized image is determined for different box sizes, and the slope of the inverse power law relationship between box size and number of boxes corresponds to the fractal dimension.[1,126] A higher fractal dimension measured through box-counting has been correlated with greater elastic modulus.[1] Additionally, the inverse power law decay of the 2D PSD of radiographic images can provide insights into the fractal organization through analysis by Fourier-based algorithms. Similar to the box-counting method, the slope of a log-transformed radially sampled PSD function over log-transformed spatial frequency is related to the fractal dimension.[127] Fourier-based textural analysis demonstrates the ability to identify patients with hip fractures and is independent of age or bone mineral density.[128]

18.4.3 Noninvasive Assessments of Tissue Biochemical Status

Most clinical imaging modalities, such as CT or MRI, are sensitive to endogenous sources of contrast that reveal anatomical information. Molecular imaging techniques use these imaging modalities to quantify specific biochemical differences in the tissue without the

need for tissue biopsy and histological analysis. Specific techniques, such as single photon emission computed tomography or positron emission tomography, are capable of 3D localization of gamma-emitting isotopes to reveal cellular metabolic activity or specific gene or protein expression. These techniques have been used to detect and localize mesenchymal stem cell (MSC) differentiation and osteoblast activity in studies of bone formation.[129] Optical imaging approaches, such as bioluminescence imaging, have also been used in molecular imaging and do not suffer from the safety concerns associated with other modalities. *In vivo* animal studies have identified joint inflammation in a murine model of arthritis using a firefly luciferase reporter gene controlled by the protein complex nuclear factor-κB.[130] However, the spatial resolution limits of these techniques present challenges in discriminating differences between cell numbers and the level of metabolic activity or gene expression.

Establishing a mechanistic understanding of the relationship between cellular biochemical processes and extracellular deposition and remodeling requires measurements at the microscale. TPEF microscopy can be used to determine the metabolic activity of individual cells.[12,131] Relationships between metabolism and the differentiation status of MSCs have been established through TPEF to help guide the development of engineered musculoskeletal tissues *in vitro*.[12] This imaging approach uses the intrinsic fluorescence of two coenzymes involved in oxidative phosphorylation: the reduced form of nicotinamide adenine dinucleotide and the oxidized form of flavin adenine dinucleotide, which can be isolated from each other during image acquisition through different excitation and emission wavelengths.[12,132] The pixelwise quantification of a cellular redox ratio of these two fluorophores can be computed and is proportional to the ratio of energy consumption to energy storage (Figure 18.3). The intrinsic 3D sectioning ability of TPEF and use of near-infrared excitation wavelengths can enable future work to provide quantitative information on the *in vivo* biochemical status of musculoskeletal tissues during repair and regeneration.

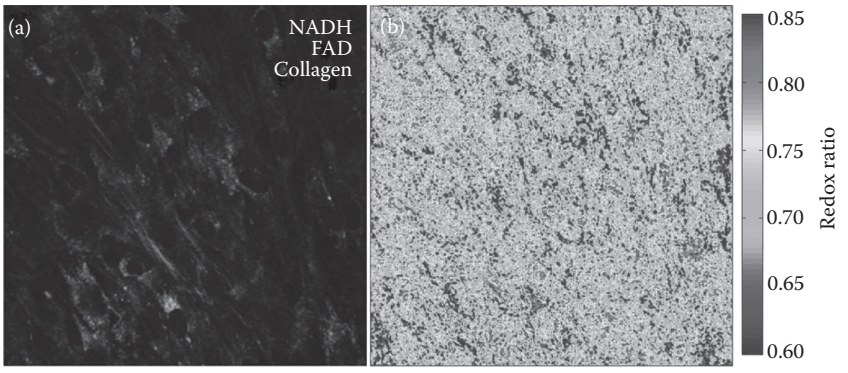

FIGURE 18.3
(See color insert.) Nonlinear optical image of a mesenchymal stem cell culture undergoing osteoblastic differentiation. (a) False-color image highlights nicotinamide adenine dinucleotide (NADH; green) and flavin adenine dinucleotide (FAD; blue) fluorescence in cell mitochondria detected through TPEF imaging and collagen deposition (red) detected through SHG imaging. (b) Map of the cellular redox ratio FAD/(NADH+FAD) can be determined from the TPEF images, indicating higher redox ratios to be in regions with collagen fiber deposition.

18.5 Dynamic Measurements of Structural Kinematics

As imaging techniques become more sophisticated, it has become practical to use them to define the kinematics of bones and soft tissues during normal physiological motions, during injurious loading, and throughout tissue repair and regeneration processes. In particular, with current technological advances, it is now possible to define complicated joint motions in 3D with sufficiently high temporal resolution to define the dynamic response of joints. Furthermore, it is also possible to quantify dynamic subfailure, microstructural responses of ligaments during loading using markerless tracking techniques. These are reviewed briefly in this section, along with elastographic techniques using clinical image modalities, to measure the mechanical properties of tissues *in vivo*.

18.5.1 Measuring Bony Kinematics through High-Speed Radiography

Clinical and experimental assessments of joint kinematics are required to understand a variety of musculoskeletal injuries and disorders. Although a variety of motion capture systems have been used in studies of gait analysis[133,134] and cadaveric injury simulations,[135,136] radiography is often needed to overcome soft tissue artifacts to make noninvasive measurements of complex joint kinematics. Bony motions from high-speed radiography are typically quantified by tracking distinct morphological features or radiopaque beads.[137,138] Through a combination of high-speed biplane radiography and static CT measurements, *in vivo* measurements of the canine anterior cruciate ligament (ACL) were quantified during treadmill walking.[139] Similarly, an orthogonal radiographic system was used to assess joint laxity in patients after ACL reconstruction.[140] High-speed radiographic imaging has also been used in studies of human volunteers to determine the cervical spine kinematics during low-speed rear-end impacts.[137] Facet joint capsule deformation has been inferred from the bony kinematics of the posterior elements in the cervical spine during whole-cadaver whiplash simulations to assess the potential for ligament injury.[141,142] Collectively, these radiographic techniques enable a noninvasive understanding of the macroscale joint kinematics, which can aid in clinical diagnostic evaluations and experimental studies to understand injury potential.

18.5.2 Quantifying Collagen Fiber Kinematics through Vector Correlation

The kinematics of load-bearing collagen fibers have been described during soft tissue deformation using OCT, QPLI, and traditional light microscopy.[9,89,91,107] The extinction of fiber undulation and a rotation of fiber alignment toward the direction of loading have been described during tensile loading in a variety of studies initially dating back to the work of Viidik in the late 1960s.[9,91,107] These descriptions of the overall fiber kinematics of soft tissue have provided a foundation for understanding the microstructural organization of tissues and have enabled the development of a number of microstructural models describing mechanical behavior.[113,116,143–145] However, quantitative measurements of local fiber kinematics have remained challenging due to the small scale and high density of collagen fibers. Furthermore, the complex fiber kinematic response of a tissue to applied loads differs among tissue regions and between samples, which creates challenges in developing a mechanistic understanding of the microstructural organization and its relationship to mechanical function. However, the recent establishment of a vector correlation technique to quantify localized changes in fiber alignment has enabled a sensitive

image-based detection of microstructural damage.[90,146] By correlating QPLI-based fiber alignment in consecutive alignment maps during loading, rapid asynchronous changes in the pixelwise fiber alignment measurements have been identified. In this method, both the mean fiber direction (α) and the strength of alignment (δ) in that mean direction (i.e., retardation) acquired during QPLI are used to construct a fiber alignment vector for each pixel.[147] For each pixel location in each fiber alignment map, two groups (z and w) of alignment vectors are created from a 5 × 5 window centered at that pixel in the preceding and following alignment maps (Figure 18.4). The variances and covariance (σ_z^2, σ_w^2, σ_{zw}) of the two sets of alignment vectors (z and w) are computed as

$$\sigma_z^2 = \frac{1}{24}\sum_{j=1}^{24}\left(z_j - \bar{z}\right)^*\left(z_j - \bar{z}\right), \tag{18.2}$$

$$\sigma_w^2 = \frac{1}{24}\sum_{j=1}^{24}\left(w_j - \bar{w}\right)^*\left(w_j - \bar{w}\right), \tag{18.3}$$

$$\sigma_{zw} = \frac{1}{24}\sum_{j=1}^{24}\left(z_j - \bar{z}\right)^*\left(w_j - \bar{w}\right), \tag{18.4}$$

where the Cartesian coordinates of the alignment vectors in z and w are represented in complex form, and $\bar{z}$ and $\bar{w}$ represent the mean vectors of the group in each map.[147] The vector correlation coefficient (ρ_{zw}) between alignment maps in a given pixel window is then defined as

$$\rho_{zw} = \frac{\sigma_{zw}}{\sigma_z \sigma_w}. \tag{18.5}$$

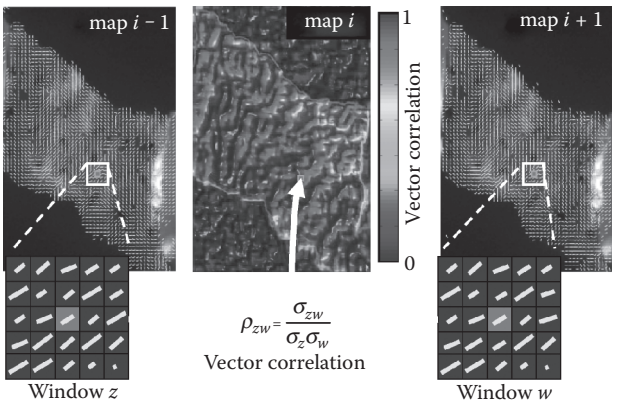

FIGURE 18.4
(See color insert.) Schematic of a pixelwise vector correlation calculation to assess changes in collagen fiber alignment. The vector correlation for each pixel in a given map (i) is calculated from the alignment surrounding the pixel in the maps immediately preceding (i − 1) and following (i + 1) it. Normal realignment patterns throughout the ligament tissue are demonstrated by correlation values near 1.

The magnitude of this complex correlation measurement is computed to produce a single measure of fiber realignment surrounding the pixel and ranges from 0 to 1, with 1 representing synchronized fiber realignment between maps. Decreases in the vector correlation coefficient that are detected at a given location in the tissue during loading have been associated with transient decreases in the tissue's overall stiffness, suggesting sensitivity to a loss of structural integrity (i.e., damage) at the microscale.[90,146] In addition to damage detection, this vector correlation metric has been used to track tissue deformation during loading by identifying the tissue locations that maximize the correlation value between maps.[148] The incorporation of vector correlation tracking has enabled measurements of both unrecovered laxity in ligament tissue and altered fiber alignment after preconditioning loading protocols.[149] In addition, altered fiber alignment and unrecovered strain have been reported to be colocalized in the cervical facet capsular ligament after loading, simulating the joint kinematics during whiplash simulations.[150]

18.5.3 Quantitative Elastography Using Clinical Imaging Modalities

In most experimental studies that quantify the mechanical properties of biological tissues, specimens are excised from their *in vivo* environment and deformed in a material testing machine, while force and displacement responses are recorded using transducers. However, this traditional approach to material testing is not feasible during *in vivo* experiments or in a clinical setting. As a result, elastographic imaging techniques have been developed to provide noninvasive measures of the mechanical properties for living tissues. Typically, a quasistatic or dynamic mechanical input is applied, and tissue displacement is quantified through sonography or MRI. Correlation techniques have been used with sonography to provide a measure of ACL deformation[151] and, together with assumptions of an isotropic linear elastic material, enable the stiffness measurements. Commercial sonoelastography systems have been used to differentiate reduced plantar fascia stiffness in patients with fasciitis.[152] MR elastography uses a mechanical vibration and phase-contrast imaging to enable noninvasive measures of muscle tissue tension.[153] At the microscale, OCT elastography has been used to characterize stiffness in engineered collagen constructs.[154] Although the majority of these techniques provide qualitative or semiquantitative information about tissue stiffness, the development of quantitative measures that account for the anisotropy and nonlinear elastic responses at larger strains is needed.

18.6 Clinical Considerations and Implications

Substantial advances have been made in developing specialized scans using existing clinical imaging modalities over the last 20 years. Specifically, various MRI scans have been developed with sensitivity to tissues with different molecular compositions or kinematics. Techniques such as T1-rho MRI and diffusion MRI may offer improved sensitivity to the early stages of disease or subtle tissue injuries. The continued development of these specialized scans offers the potential for providing a more immediate impact on clinical diagnoses. Additional progress in developing and commercializing molecular imaging probes for MR, radiographic, and optical imaging technologies may further enhance the quantification of specific biological processes. However, a mechanistic understanding of

the development of clinical problems such as osteoarthritis, acute injuries, or chronic joint pain will likely require imaging and biomechanical evaluation at both the macroscale and microscale due to the hierarchical organization of musculoskeletal tissues.

Although the direct implementation of optical techniques to noninvasive diagnostic imaging is severely limited by light penetration, optical technologies, such as OCT or nonlinear microscopy, have the potential to advance basic orthopaedic research by providing 3D information related to tissue microstructure and cellular function. OCT has been used in clinical applications and certainly offers improved spatial resolution relative to MRI, CT, and sonography. However, its source of contrast is limited to light reflectance or retardance. Nonlinear optical microscopy, on the other hand, offers a wide range of potential intrinsic sources of contrast through techniques such as multiphoton excited fluorescence, SHG, and coherent anti-Stokes Raman spectroscopy. The ability of nonlinear microscopy and OCT to acquire depth-resolved images can enable the evaluation of *in vivo* and *in vitro* models without sample excision and sectioning. Furthermore, because these imaging techniques are nondestructive and rely on endogenous sources for contrast, tissues can be continuously monitored longitudinally over the course of a study. By combining the microstructural information available through TPEF and SHG with biochemical measurements such as cellular redox ratios, nonlinear microscopy can enable a more complete understanding of dynamic processes such as tissue development, injury, and repair.

Due to the depth penetration limitations of OCT (1–2 mm) and nonlinear optical microscopy (0.5–1 mm), noninvasive assessments of musculoskeletal tissues are limited in the clinical setting. Although optical imaging applications for orthopaedic research will primarily be limited to experimental settings, the development of minimally invasive probes may enable some degree of clinical translation. Needle-like optical probes have been developed for brain imaging and demonstrate the ability to acquire multiphoton microscopy images that are centimeters from the surface.[155,156] Photoacoustic tomography, which achieves contrast through optical absorption by hemoglobin and improved depth penetration by measuring isothermal expansion with ultrasonic detectors, may also bridge the gap between the depth penetration of optical techniques and traditional diagnostic imaging.[157,158] Although many new optical approaches may provide advanced clinical diagnostic capabilities, it remains unknown whether any of these specialized techniques can overcome the challenges associated with commercializing biomedical optical technologies for widespread clinical use. Nonetheless, continued research using multimodal optical imaging technologies at the microscale is likely to provide a more complete mechanistic understanding of musculoskeletal problems, such as osteoarthritis or whiplash-associated disorders, which are frequently reported in the clinic but lack a sensitive clinical diagnostic imaging modality.

Acknowledgments

This work was supported by grant no. R01EB007542 from NIBIB/NIH (I. Georgakoudi), grant no. F32AR061933 from NIAMS/NIH (K.P. Quinn), and the Catharine D. Sharpe Foundation (B.A. Winkelstein). This material is also based on work supported by the National Science Foundation under grant no. 0547451 (B.A. Winkelstein).

References

1. Link, T. M., Majumdar, S., Lin, J. C., Newitt, D., Augat, P., Ouyang, X., Mathur, A., and Genant, H. K. 1998. A comparative study of trabecular bone properties in the spine and femur using high-resolution MRI and CT. *Journal of Bone and Mineral Research* 13(1):122–132.
2. Bencardino, J. T., Beltran, J., Feldman, M. I., and Rose, D. J. 2009. MR imaging of complications of anterior cruciate ligament graft reconstruction. *Radiographics* 29(7):2115–2126.
3. Wakefield, R. J., Gibbon, W. W., Conaghan, P. G., O'Connor, P., McGonagle, D., Pease, C., Green, M. J., Veale, D. J., Isaacs, J. D., and Emery, P. 2000. The value of sonography in the detection of bone erosions in patients with rheumatoid arthritis: A comparison with conventional radiography. *Arthritis and Rheumatism* 43(12):2762–2770.
4. Woodhouse, J. B., and McNally, E. G. 2011. Ultrasound of skeletal muscle injury: An update. *Seminars in Ultrasound, CT, and MR* 32(2):91–100.
5. Harcke, H. T., Grissom, L. E., and Finkelstein, M. S. 1988. Evaluation of the musculoskeletal system with sonography. *AJR. American Journal of Roentgenology* 150(6):1253–1261.
6. Figurska, M., Robaszkiewicz, J., and Wierzbowska, J. 2010. Optical coherence tomography in imaging of macular diseases. *Klinika Oczna* 112(4–6):138–146.
7. Huang, P., Hunter, M., and Georgakoudi, I. 2009. Confocal light scattering spectroscopic imaging system for in situ tissue characterization. *Applied Optics* 48(13):2595–2599.
8. Puliafito, C. A., Hee, M. R., Lin, C. P., Reichel, E., Schuman, J. S., Duker, J. S., Izatt, J. A., Swanson, E. A., and Fujimoto, J. G. 1995. Imaging of macular diseases with optical coherence tomography. *Ophthalmology* 102(2):217–229.
9. Hansen, K. A., Weiss, J. A., and Barton, J. K. 2002. Recruitment of tendon crimp with applied tensile strain. *Journal of Biomechanical Engineering* 124(1):72–77.
10. Matcher, S. J., Winlove, C. P., and Gangnus, S. V. 2004. The collagen structure of bovine intervertebral disc studied using polarization-sensitive optical coherence tomography. *Physics in Medicine and Biology* 49(7):1295–1306.
11. Georgakoudi, I., Rice, W. L., Hronik-Tupaj, M., and Kaplan, D. L. 2008. Optical spectroscopy and imaging for the noninvasive evaluation of engineered tissues. *Tissue Engineering. Part B, Reviews* 14(4):321–340.
12. Rice, W. L., Kaplan, D. L., and Georgakoudi, I. 2010. Two-photon microscopy for non-invasive, quantitative monitoring of stem cell differentiation. *PLoS One* 5(4):e10075.
13. Campagnola, P. J., and Loew, L. M. 2003. Second-harmonic imaging microscopy for visualizing biomolecular arrays in cells, tissues and organisms. *Nature Biotechnology* 21(11):1356–1360.
14. Williams, R. M., Zipfel, W. R., and Webb, W. W. 2005. Interpreting second-harmonic generation images of collagen I fibrils. *Biophysical Journal* 88(2):1377–1386.
15. Psilodimitrakopoulos, S., Santos, S. I., Amat-Roldan, I., Thayil, A. K., Artigas, D., and Loza-Alvarez, P. 2009. In vivo, pixel-resolution mapping of thick filaments' orientation in nonfibrilar muscle using polarization-sensitive second harmonic generation microscopy. *Journal of Biomedical Optics* 14(1):014001.
16. Bayan, C., Levitt, J. M., Miller, E., Kaplan, D., and Georgakoudi, I. 2009. Fully automated, quantitative, noninvasive assessment of collagen fiber content and organization in thick collagen gels. *Journal of Applied Physics* 105(110):102042.
17. Erni, R., Rossell, M. D., Kisielowski, C., and Dahmen, U. 2009. Atomic-resolution imaging with a sub-50-pm electron probe. *Physical Review Letters* 102(9):096101.
18. Yahia, L., Brunet, J., Labelle, S., and Rivard, C. H. 1990. A scanning electron microscopic study of rabbit ligaments under strain. *Matrix* 10(1):58–64.
19. Hurschler, C., Provenzano, P. P., and Vanderby, R. 2003. Scanning electron microscopic characterization of healing and normal rat ligament microstructure under slack and loaded conditions. *Connective Tissue Research* 44(2):59–68.

20. Provenzano, P. P., and Vanderby, R., Jr. 2006. Collagen fibril morphology and organization: Implications for force transmission in ligament and tendon. *Matrix Biology* 25(2):71–84.
21. Jarvinen, T. A., Jarvinen, T. L., Kannus, P., Jozsa, L., and Jarvinen, M. 2004. Collagen fibres of the spontaneously ruptured human tendons display decreased thickness and crimp angle. *Journal of Orthopaedic Research* 22(6):1303–1309.
22. Hirsch, B. E., Udupa, J. K., and Samarasekera, S. 1996. New method of studying joint kinematics from three-dimensional reconstructions of MRI data. *Journal of the American Podiatric Medical Association* 86(1):4–15.
23. Van Sint Jan, S., Giurintano, D. J., Thompson, D. E., and Rooze, M. 1997. Joint kinematics simulation from medical imaging data. *IEEE Transactions on Bio-Medical Engineering* 44(12):1175–1184.
24. Feipel, V., and Rooze, M. 1999. Three-dimensional motion patterns of the carpal bones: an in vivo study using three-dimensional computed tomography and clinical applications. *Surgical and Radiologic Anatomy* 21(2):125–131.
25. You, B. M., Siy, P., Anderst, W., and Tashman, S. 2001. In vivo measurement of 3-D skeletal kinematics from sequences of biplane radiographs: Application to knee kinematics. *IEEE Transactions on Medical Imaging* 20(6):514–525.
26. Hoad, C. L., and Martel, A. L. 2002. Segmentation of MR images for computer-assisted surgery of the lumbar spine. *Physics in Medicine and Biology* 47(19):3503–3517.
27. de la Fuente, M., Ohnsorge, J. A., Schkommodau, E., Jetzki, S., Wirtz, D. C., and Radermacher, K. 2005. Fluoroscopy-based 3-D reconstruction of femoral bone cement: A new approach for revision total hip replacement. *IEEE Transactions on Bio-Medical Engineering* 52(4):664–675.
28. Chen, J. X., Wechsler, H., Pullen, J. M., Zhu, Y., and MacMahon, E. B. 2001. Knee surgery assistance: Patient model construction, motion simulation, and biomechanical visualization. *IEEE Transactions on Bio-Medical Engineering* 48(9):1042–1052.
29. Liu, J., Udupa, J. K., Saha, P. K., Odhner, D., Hirsch, B. E., Siegler, S., Simon, S., and Winkelstein, B. A. 2008. Rigid model–based 3D segmentation of the bones of joints in MR and CT images for motion analysis. *Medical Physics* 35(8):3637–3649.
30. Bomans, M., Hohne, K. H., Tiede, U., and Riemer, M. 1990. 3-D segmentation of MR images of the head for 3-D display. *IEEE Transactions on Medical Imaging* 9(2):177–183.
31. Heinonen, T., Eskola, H., Dastidar, P., Laarne, P., and Malmivuo, J. 1997. Segmentation of T1 MR scans for reconstruction of resistive head models. *Computer Methods and Programs in Biomedicine* 54(3):173–181.
32. Falcao, A. X., Udupa, J. K., and Miyazawa, F. K. 2000. An ultra-fast user-steered image segmentation paradigm: Live wire on the fly. *IEEE Transactions on Medical Imaging* 19(1):55–62.
33. Liu, J., and Udupa, J. K. 2009. Oriented active shape models. *IEEE Transactions on Medical Imaging* 28(4):571–584.
34. Saha, P. K., Udupa, J. K., Falcao, A. X., Hirsch, B. E., and Siegler, S. 2004. Iso-shaping rigid bodies for estimating their motion from image sequences. *IEEE Transactions on Medical Imaging* 23(1):63–72.
35. Wells, W. M., 3rd, Viola, P., Atsumi, H., Nakajima, S., and Kikinis, R. 1996. Multi-modal volume registration by maximization of mutual information. *Medical Image Analysis* 1(1):35–51.
36. Stindel, E., Udupa, J. K., Hirsch, B. E., and Odhner, D. 1999. A characterization of the geometric architecture of the peritalar joint complex via MRI: An aid to the classification of foot type. *IEEE Transactions on Medical Imaging* 18(9):753–763.
37. Stindel, E., Udupa, J. K., Hirsch, B. E., and Odhner, D. 2001. An in vivo analysis of the motion of the peri-talar joint complex based on MR imaging *IEEE Transactions on Bio-Medical Engineering* 48(2):236–247.
38. Stindel, E., Udupa, J. K., Hirsch, B. E., Odhner, D., and Couture, C. 1999. 3D MR image analysis of the morphology of the rear foot: Application to classification of bones. *Computerized Medical Imaging and Graphic* 23(2):75–83.
39. Siegler, S., Lapointe, S., Nobilini, R., and Berman, A. T. 1996. A six-degrees-of-freedom instrumented linkage for measuring the flexibility characteristics of the ankle joint complex. *Journal of Biomechanics* 29(7):943–947.

40. Siegler, S., Wang, D., Plasha, E., and Berman, A. T. 1994. Technique for in vivo measurement of the three-dimensional kinematics and laxity characteristics of the ankle joint complex. *Journal of Orthopaedic Research* 12(3):421–431.
41. Rhoad, R. C., Klimkiewicz, J. J., Williams, G. R., Kesmodel, S. B., Udupa, J. K., Kneeland, J. B., and Iannotti, J. P. 1998. A new in vivo technique for three-dimensional shoulder kinematics analysis. *Skeletal Radiology* 27(2):92–97.
42. McClure, P., Siegler, S., and Nobilini, R. 1998. Three-dimensional flexibility characteristics of the human cervical spine in vivo. *Spine* 23(2):216–223.
43. Hilibrand, A. S., Balasubramanian, K., Eichenbaum, M., Thinnes, J. H., Daffner, S., Berta, S., Albert, T. J., Vaccaro, A. R., and Siegler, S. 2006. The effect of anterior cervical fusion on neck motion. *Spine* 31(15):1688–1692.
44. Simon, S., Davis, M., Odhner, D., Udupa, J., and Winkelstein, B. 2006. CT imaging techniques for describing motions of the cervicothoracic junction and cervical spine during flexion, extension, and cervical traction. *Spine* 31(1):44–50.
45. Winkelstein, B. A., Udupa, J. K., Hilibrand, A. S., Schuster, J. M., Siegler, S., Hirsch, B. E., Borthakur, A., and Melhem, E. R. 2009. A novel 3D stress MR imaging approach to detect altered biomechanics in neck pain patients. Cervical Spine Research Society Annual Meeting, Salt Lake, UT, Paper no. 17.
46. Winkelstein, B. A., Hilibrand, A. S., Schuster J. M., Siegler S., Hirsch B. E., Borthakur A., and Udupa J. K. Novel 3D stress MR imaging approach to detect altered neck biomechanics in radiculopathy patients, *Journal of Medical Hypotheses* submitted.
47. Auerbach, J. D., Johannessen, W., Borthakur, A., Wheaton, A. J., Dolinskas, C. A., Balderston, R. A., Reddy, R., and Elliott, D. M. 2006. In vivo quantification of human lumbar disc degeneration using T(1rho)-weighted magnetic resonance imaging. *European Spine Journal* 15 Suppl 3:S338–344.
48. Duvvuri, U., Reddy, R., Patel, S. D., Kaufman, J. H., Kneeland, J. B., and Leigh, J. S. 1997. T1rho-relaxation in articular cartilage: Effects of enzymatic degradation. *Magnetic Resonance in Medicine* 38(6):863–867.
49. Johannessen, W., Auerbach, J. D., Wheaton, A. J., Kurji, A., Borthakur, A., Reddy, R., and Elliott, D. M. 2006. Assessment of human disc degeneration and proteoglycan content using T1rho-weighted magnetic resonance imaging. *Spine* 31(11):1253–1257.
50. Blumenkrantz, G., Zuo, J., Li, X., Kornak, J., Link, T. M., and Majumdar, S. 2010. In vivo 3.0-tesla magnetic resonance T1rho and T2 relaxation mapping in subjects with intervertebral disc degeneration and clinical symptoms. *Magnetic Resonance in Medicine* 63(5):1193–1200.
51. Li, X., Cheng, J., Lin, K., Saadat, E., Bolbos, R. I., Jobke, B., Ries, M. D., Horvai, A., Link, T. M., and Majumdar, S. 2011. Quantitative MRI using T1rho and T2 in human osteoarthritic cartilage specimens: Correlation with biochemical measurements and histology. *Magnetic Resonance Imaging* 29(3):324–334.
52. Buccino, G., Binkofski, F., Fink, G. R., Fadiga, L., Fogassi, L., Gallese, V., Seitz, R. J., Zilles, K., Rizzolatti, G., and Freund, H. J. 2001. Action observation activates premotor and parietal areas in a somatotopic manner: An fMRI study. *European Journal of Neuroscience* 13(2):400–404.
53. Logothetis, N. K., Pauls, J., Augath, M., Trinath, T., and Oeltermann, A. 2001. Neurophysiological investigation of the basis of the fMRI signal. *Nature* 412(6843):150–157.
54. Phan, K. L., Wager, T., Taylor, S. F., and Liberzon, I. 2002. Functional neuroanatomy of emotion: A meta-analysis of emotion activation studies in PET and fMRI. *NeuroImage* 16(2):331–348.
55. Damon, B. M., Wadington, M. C., Hornberger, J. L., and Lansdown, D. A. 2007. Absolute and relative contributions of BOLD effects to the muscle functional MRI signal intensity time course: Effect of exercise intensity. *Magnetic Resonance in Medicine* 58(2):335–345.
56. Donahue, K. M., Van Kylen, J., Guven, S., El-Bershawi, A., Luh, W. M., Bandettini, P. A., Cox, R. W., Hyde, J. S., and Kissebah, A. H. 1998. Simultaneous gradient-echo/spin-echo EPI of graded ischemia in human skeletal muscle. *Journal of Magnetic Resonance Imaging* 8(5):1106–1113.

57. Ledermann, H. P., Schulte, A. C., Heidecker, H. G., Aschwanden, M., Jager, K. A., Scheffler, K., Steinbrich, W., and Bilecen, D. 2006. Blood oxygenation level–dependent magnetic resonance imaging of the skeletal muscle in patients with peripheral arterial occlusive disease. *Circulation* 113(25):2929–2935.
58. Meyer, R. A., Towse, T. F., Reid, R. W., Jayaraman, R. C., Wiseman, R. W., and McCully, K. K. 2004. BOLD MRI mapping of transient hyperemia in skeletal muscle after single contractions. *NMR in Biomedicine* 17(6):392–398.
59. Slade, J. M., Towse, T. F., Gossain, V., and Meyer, R. A. 2011. Peripheral microvascular response to muscle contraction is unaltered by early diabetes, but decreases with age. *Journal of Applied Physiology* 11(5):1361–1371.
60. Elliott, J., Pedler, A., Beattie, P., and McMahon, K. 2010. Diffusion-weighted magnetic resonance imaging for the healthy cervical multifidus: A potential method for studying neck muscle physiology following spinal trauma. *The Journal of Orthopaedic and Sports Physical Therapy* 40(11):722–728.
61. Basser, P. J., Mattiello, J., and LeBihan, D. 1994. MR diffusion tensor spectroscopy and imaging. *Biophysical Journal* 66(1):259–267.
62. Basser, P. J., and Pierpaoli, C. 1996. Microstructural and physiological features of tissues elucidated by quantitative-diffusion-tensor MRI. *Journal of Magnetic Resonance. Series B* 111(3):209–219.
63. Frindel, C., Robini, M., Croisille, P., and Zhu, Y. M. 2009. Comparison of regularization methods for human cardiac diffusion tensor MRI. *Medical Image Analysis* 13(3):405–418.
64. Hoischen, A., Landwehr, C., Kabisch, S., Ding, X. Q., Trost, D., Stropahl, G., Wigger, M., Radlwimmer, B., Weber, R. G., and Haffner, D. 2009. Array-CGH in unclear syndromic nephropathies identifies a microdeletion in Xq22.3-q23. *Pediatric Nephrology* 24(9):1673–1681.
65. Hsieh, T. J., Chang, J. M., Chuang, H. Y., Ko, C. H., Hsieh, M. L., Liu, G. C., and Hsu, J. S. 2009. End-stage renal disease: In vivo diffusion-tensor imaging of silent white matter damage. *Radiology* 252(2):518–525.
66. Jones, D. K., Simmons, A., Williams, S. C., and Horsfield, M. A. 1999. Non-invasive assessment of axonal fiber connectivity in the human brain via diffusion tensor MRI. *Magnetic Resonance in Medicine* 42(1):37–41.
67. Kataoka, M., Kido, A., Yamamoto, A., Nakamoto, Y., Koyama, T., Isoda, H., Maetani, Y., Umeoka, S., Tamai, K., Saga, T., Morisawa, N., Mori, S., and Togashi, K. 2009. Diffusion tensor imaging of kidneys with respiratory triggering: Optimization of parameters to demonstrate anisotropic structures on fraction anisotropy maps. *Journal of Magnetic Resonance Imaging* 29(3):736–744.
68. Notohamiprodjo, M., Glaser, C., Herrmann, K. A., Dietrich, O., Attenberger, U. I., Reiser, M. F., Schoenberg, S. O., and Michaely, H. J. 2008. Diffusion tensor imaging of the kidney with parallel imaging: Initial clinical experience. *Investigative Radiology* 43(10):677–685.
69. Ries, M., Jones, R. A., Basseau, F., Moonen, C. T., and Grenier, N. 2001. Diffusion tensor MRI of the human kidney. *Journal of Magnetic Resonance Imaging* 14(1):42–49.
70. Sosnovik, D. E., Wang, R., Dai, G., Reese, T. G., and Wedeen, V. J. 2009. Diffusion MR tractography of the heart. *Journal of Cardiovascular Magnetic Resonance* 11, 47.
71. Virta, A., Barnett, A., and Pierpaoli, C. 1999. Visualizing and characterizing white matter fiber structure and architecture in the human pyramidal tract using diffusion tensor MRI. *Magnetic Resonance Imaging* 17(8):1121–1133.
72. Hagmann, P., Jonasson, L., Maeder, P., Thiran, J. P., Wedeen, V. J., and Meuli, R. 2006. Understanding diffusion MR imaging techniques: From scalar diffusion-weighted imaging to diffusion tensor imaging and beyond. *Radiographics* 26 Suppl 1, S205–223.
73. Elliott, J., Sterling, M., Noteboom, J. T., Darnell, R., Galloway, G., and Jull, G. 2008. Fatty infiltrate in the cervical extensor muscles is not a feature of chronic, insidious-onset neck pain. *Clinical Radiology* 63(6):681–687.
74. Sehy, J. V., Ackerman, J. J., and Neil, J. J. 2002. Evidence that both fast and slow water ADC components arise from intracellular space. *Magnetic Resonance in Medicine* 48(5):765–770.

75. Elliott, J., Jull, G., Noteboom, J. T., Darnell, R., Galloway, G., and Gibbon, W. W. 2006. Fatty infiltration in the cervical extensor muscles in persistent whiplash-associated disorders: A magnetic resonance imaging analysis. *Spine* 31(22):E847–855.
76. Elliott, J. M., O'Leary, S., Sterling, M., Hendrikz, J., Pedler, A., and Jull, G. 2010. Magnetic resonance imaging findings of fatty infiltrate in the cervical flexors in chronic whiplash. *Spine* 35(9):948–954.
77. Yanagisawa, O., Shimao, D., Maruyama, K., and Nielsen, M. 2009. Evaluation of exercised or cooled skeletal muscle on the basis of diffusion-weighted magnetic resonance imaging. *European Journal of Applied Physiology* 105(5):723–729.
78. Yanagisawa, O., Shimao, D., Maruyama, K., Nielsen, M., Irie, T., and Niitsu, M. 2009. Diffusion-weighted magnetic resonance imaging of human skeletal muscles: Gender-, age- and muscle-related differences in apparent diffusion coefficient. *Magnetic Resonance Imaging* 27(1):69–78.
79. Holl, N., Echaniz-Laguna, A., Bierry, G., Mohr, M., Loeffler, J. P., Moser, T., Dietemann, J. L., and Kremer, S. 2008. Diffusion-weighted MRI of denervated muscle: A clinical and experimental study. *Skeletal Radiology* 37(12):1111–1117.
80. Elliott, J., Pedler, A., Kenardy, J., Galloway, G., Jull, G., and Sterling, M. 2011. The temporal development of Fatty infiltrates in the neck muscles following whiplash injury: An association with pain and posttraumatic stress. *PLoS One* 6(6):e21194.
81. Sinha, S., Sinha, U., and Edgerton, V. R. 2006. In vivo diffusion tensor imaging of the human calf muscle. *Journal of Magnetic Resonance Imaging* 24(1):182–190.
82. Sinha, U., Sinha, S., Hodgson, J. A., and Edgerton, R. V. 2011. Human soleus muscle architecture at different ankle joint angles from magnetic resonance diffusion tensor imaging. *Journal of Applied Physiology* 110(3):807–819.
83. Sinha, U., and Yao, L. 2002. In vivo diffusion tensor imaging of human calf muscle. *Journal of Magnetic Resonance Imaging* 15(1):87–95.
84. Stieltjes, B., Kaufmann, W. E., van Zijl, P. C., Fredericksen, K., Pearlson, G. D., Solaiyappan, M., and Mori, S. 2001. Diffusion tensor imaging and axonal tracking in the human brainstem. *NeuroImage* 14(3):723–735.
85. Wedeen, V. J., Reese, T. G., Napadow, V. J., and Gilbert, R. J. 2001. Demonstration of primary and secondary muscle fiber architecture of the bovine tongue by diffusion tensor magnetic resonance imaging. *Biophysical Journal* 80(2):1024–1028.
86. Xue, R., van Zijl, P. C., Crain, B. J., Solaiyappan, M., and Mori, S. 1999. In vivo three-dimensional reconstruction of rat brain axonal projections by diffusion tensor imaging. *Magnetic Resonance in Medicine* 42(6):1123–1127.
87. Zaraiskaya, T., Kumbhare, D., and Noseworthy, M. D. 2006. Diffusion tensor imaging in evaluation of human skeletal muscle injury. *Journal of Magnetic Resonance Imaging* 24(2):402–408.
88. Gimbel, J. A., Van Kleunen, J. P., Mehta, S., Perry, S. M., Williams, G. R., and Soslowsky, L. J. 2004. Supraspinatus tendon organizational and mechanical properties in a chronic rotator cuff tear animal model. *Journal of Biomechanics* 37(5):739–749.
89. Quinn, K. P., and Winkelstein, B. A. 2008. Altered collagen fiber kinematics define the onset of localized ligament damage during loading. *Journal of Applied Physiology* 105(6):1881–1888.
90. Quinn, K. P., and Winkelstein, B. A. 2009. Vector correlation technique for pixel-wise detection of collagen fiber realignment during injurious tensile loading. *Journal of Biomedical Optics* 14(5):054010.
91. Tower, T. T., Neidert, M. R., and Tranquillo, R. T. 2002. Fiber alignment imaging during mechanical testing of soft tissues. *Annals of Biomedical Engineering* 30(10):1221–1233.
92. Ghole, S. A., Ivancic, P. C., Tominaga, Y., Gimenez, S. E., and Panjabi, M. M. 2004. Incremental and single trauma produce equivalent subfailure soft tissue injury of the cervical spine. *Clinical Biomechanics (Bristol, Avon)* 19(8):784–789.
93. Pollock, R. G., Wang, V. M., Bucchieri, J. S., Cohen, N. P., Huang, C. Y., Pawluk, R. J., Flatow, E. L., Bigliani, L. U., and Mow, V. C. 2000. Effects of repetitive subfailure strains on the mechanical behavior of the inferior glenohumeral ligament. *Journal of Shoulder and Elbow Surgery* 9(5):427–435.

94. Provenzano, P. P., Alejandro-Osorio, A. L., Valhmu, W. B., Jensen, K. T., and Vanderby, R., Jr. 2005. Intrinsic fibroblast-mediated remodeling of damaged collagenous matrices in vivo. *Matrix Biology* 23(8):543–555.
95. Provenzano, P. P., Heisey, D., Hayashi, K., Lakes, R., and Vanderby, R., Jr. 2002. Subfailure damage in ligament: A structural and cellular evaluation. *Journal of Applied Physiology* 92(1):362–371.
96. Billiar, K. L., and Sacks, M. S. 1997. A method to quantify the fiber kinematics of planar tissues under biaxial stretch. *Journal of Biomechanics* 30(7):753–756.
97. Hiester, E. D., and Sacks, M. S. 1998. Optimal bovine pericardial tissue selection sites. I. Fiber architecture and tissue thickness measurements. *Journal of Biomedical Materials Research* 39(2):207–214.
98. Nguyen, T. D., Liang, R., Woo, S. L., Burton, S. D., Wu, C., Almarza, A., Sacks, M. S., and Abramowitch, S. 2009. Effects of cell seeding and cyclic stretch on the fiber remodeling in an extracellular matrix-derived bioscaffold. *Tissue Engineering Part A* 15(4):957–963.
99. Sacks, M. S., and Chuong, C. J. 1992. Characterization of collagen fiber architecture in the canine diaphragmatic central tendon. *Journal of Biomechanical Engineering* 114(2):183–190.
100. Thomopoulos, S., Williams, G. R., and Soslowsky, L. J. 2003. Tendon to bone healing: Differences in biomechanical, structural, and compositional properties due to a range of activity levels. *Journal of Biomechanical Engineering* 125(1):106–113.
101. Quinn, K. P., Lee, K. E., Ahaghotu, C. C., and Winkelstein, B. A. 2007. Structural changes in the cervical facet capsular ligament: Potential contributions to pain following subfailure loading. *Stapp Car Crash Journal* 51, 169–187.
102. Diamant, J., Keller, A., Baer, E., Litt, M., and Arridge, R. G. 1972. Collagen; ultrastructure and its relation to mechanical properties as a function of ageing. *Proceedings of the Royal Society of London. Series B. Biological Sciences* 180(60):293–315.
103. Dickey, J. P., Hewlett, B. R., Dumas, G. A., and Bednar, D. A. 1998. Measuring collagen fiber orientation: A two-dimensional quantitative macroscopic technique. *Journal of Biomechanical Engineering* 120(4):537–540.
104. Gathercole, L. J., and Keller, A. 1991. Crimp morphology in the fibre-forming collagens. *Matrix* 11(3):214–234.
105. Whittaker, P., and Canham, P. B. 1991. Demonstration of quantitative fabric analysis of tendon collagen using two-dimensional polarized light microscopy. *Matrix* 11(1):56–62.
106. Yeh, A. T., Choi, B., Nelson, J. S., and Tromberg, B. J. 2003. Reversible dissociation of collagen in tissues. *The Journal of Investigative Dermatology* 121(6):1332–1335.
107. Viidik, A. 1973. Functional properties of collagenous tissues. *International Review of Connective Tissues Research* 6, 127–215.
108. Thomopoulos, S., Williams, G. R., Gimbel, J. A., Favata, M., and Soslowsky, L. J. 2003. Variation of biomechanical, structural, and compositional properties along the tendon to bone insertion site. *Journal of Orthopaedic Research* 21(3):413–419.
109. Lake, S. P., Miller, K. S., Elliott, D. M., and Soslowsky, L. J. 2009. Effect of fiber distribution and realignment on the nonlinear and inhomogeneous mechanical properties of human supraspinatus tendon under longitudinal tensile loading. *Journal of Orthopaedic Research* 27(12):1596–1602.
110. Glazer, A. M., Lewis, J. G., and Kaminsky, W. 1996. An automatic optical imaging system for birefringent media. *Proceedings: Mathematical, Physical and Engineering Sciences* 452(1955):2751–2765.
111. Sander, E., Stylianopoulos, T., Tranquillo, R., and Barocas, V. 2009. Image-based biomechanics of collagen-based tissue equivalents. *IEEE Engineering in Medicine and Biology Magazine* 28(3):10–18.
112. Geday, M. A., Kaminsky, W., Lewis, J. G., and Glazer, A. M. 2000. Images of absolute retardance L.Deltan, using the rotating polariser method. *Journal of Microscopy* 198 (Pt 1):1–9.
113. Sander, E. A., Stylianopoulos, T., Tranquillo, R. T., and Barocas, V. H. 2009. Image-based multiscale modeling predicts tissue-level and network-level fiber reorganization in stretched cell-compacted collagen gels. *Proceedings of the National Academy of Sciences of the United States of America* 106(42):17675–17680.

114. Snedeker, J. G., Pelled, G., Zilberman, Y., Ben Arav, A., Huber, E., Muller, R., and Gazit, D. 2009. An analytical model for elucidating tendon tissue structure and biomechanical function from in vivo cellular confocal microscopy images. *Cells, Tissues, Organs* 190(2):111–119.
115. Snedeker, J. G., Pelled, G., Zilberman, Y., Gerhard, F., Muller, R., and Gazit, D. 2006. Endoscopic cellular microscopy for in vivo biomechanical assessment of tendon function. *Journal of Biomedical Optics* 11(6):064010.
116. Belkoff, S. M., and Haut, R. C. 1991. A structural model used to evaluate the changing microstructure of maturing rat skin. *Journal of Biomechanics* 24(8):711–720.
117. Sander, E. A., and Barocas, V. H. 2009. Comparison of 2D fiber network orientation measurement methods. *Journal of Biomedical Materials Research Part A* 88(2):322–331.
118. Paige, M. F., Rainey, J. K., and Goh, M. C. 1998. Fibrous long spacing collagen ultrastructure elucidated by atomic force microscopy. *Biophysical Journal* 74(6):3211–3216.
119. Ayres, C., Bowlin, G. L., Henderson, S. C., Taylor, L., Shultz, J., Alexander, J., Telemeco, T. A., and Simpson, D. G. 2006. Modulation of anisotropy in electrospun tissue-engineering scaffolds: Analysis of fiber alignment by the fast Fourier transform. *Biomaterials* 27(32):5524–5534.
120. Sivaguru, M., Durgam, S., Ambekar, R., Luedtke, D., Fried, G., Stewart, A., and Toussaint, K. C., Jr. 2010. Quantitative analysis of collagen fiber organization in injured tendons using Fourier transform-second harmonic generation imaging. *Optics Express* 18(24):24983–24993.
121. Fung, D. T., Sereysky, J. B., Basta-Pljakic, J., Laudier, D. M., Huq, R., Jepsen, K. J., Schaffler, M. B., and Flatow, E. L. 2010. Second harmonic generation imaging and Fourier transform spectral analysis reveal damage in fatigue-loaded tendons. *Annals of Biomedical Engineering* 38(5):1741–1751.
122. Russ, J. C. 1998. *The Image Processing Handbook*. Boca Raton, FL: CRC Press.
123. Zhou, Y., and Zheng, Y. P. 2008. Estimation of muscle fiber orientation in ultrasound images using revoting hough transform (RVHT). *Ultrasound in Medicine & Biology* 34(9):1474–1481.
124. Guglielmi, G., Grimston, S. K., Fischer, K. C., and Pacifici, R. 1994. Osteoporosis: Diagnosis with lateral and posteroanterior dual x-ray absorptiometry compared with quantitative CT. *Radiology* 192(3):845–850.
125. Dalstra, M., Huiskes, R., Odgaard, A., and van Erning, L. 1993. Mechanical and textural properties of pelvic trabecular bone. *Journal of Biomechanics* 26(4–5):523–535.
126. Link, T. M., Majumdar, S., Augat, P., Lin, J. C., Newitt, D., Lu, Y., Lane, N. E., and Genant, H. K. 1998. In vivo high resolution MRI of the calcaneus: Differences in trabecular structure in osteoporosis patients. *Journal of Bone and Mineral Research* 13(7):1175–1182.
127. Levitt, J. M., Hunter, M., Mujat, C., McLaughlin-Drubin, M., Munger, K., and Georgakoudi, I. 2007. Diagnostic cellular organization features extracted from autofluorescence images. *Optics Letters* 32(22):3305–3307.
128. Gregory, J. S., Stewart, A., Undrill, P. E., Reid, D. M., and Aspden, R. M. 2004. Identification of hip fracture patients from radiographs using Fourier analysis of the trabecular structure: a cross-sectional study. *BMC Medical Imaging* 4(1):4.
129. Mayer-Kuckuk, P., and Boskey, A. L. 2006. Molecular imaging promotes progress in orthopedic research. *Bone* 39(5):965–977.
130. Carlsen, H., Moskaug, J. O., Fromm, S. H., and Blomhoff, R. 2002. In vivo imaging of NF-kappa B activity. *The Journal of Immunology* 168(3):1441–1446.
131. Levitt, J. M., Baldwin, A., Papadakis, A., Puri, S., Xylas, J., Munger, K., and Georgakoudi, I. 2006. Intrinsic fluorescence and redox changes associated with apoptosis of primary human epithelial cells. *Journal of Biomedical Optics* 11(6):064012.
132. Zipfel, W. R., Williams, R. M., Christie, R., Nikitin, A. Y., Hyman, B. T., and Webb, W. W. 2003. Live tissue intrinsic emission microscopy using multiphoton-excited native fluorescence and second harmonic generation. *Proceedings of the National Academy of Sciences of the United States of America* 100(12):7075–7080.
133. Corazza, S., Mundermann, L., Chaudhari, A. M., Demattio, T., Cobelli, C., and Andriacchi, T. P. 2006. A markerless motion capture system to study musculoskeletal biomechanics: Visual hull and simulated annealing approach. *Annals of Biomedical Engineering* 34(6):1019–1029.

134. Leardini, A., Benedetti, M. G., Berti, L., Bettinelli, D., Nativo, R., and Giannini, S. 2007. Rear-foot, mid-foot and fore-foot motion during the stance phase of gait. *Gait & Posture* 25(3):453–462.
135. Pearson, A. M., Ivancic, P. C., Ito, S., and Panjabi, M. M. 2004. Facet joint kinematics and injury mechanisms during simulated whiplash. *Spine* 29(4):390–397.
136. Yoganandan, N., Pintar, F. A., and Klienberger, M. 1998. Cervical spine vertebral and facet joint kinematics under whiplash. *Journal of Biomechanical Engineering* 120(2):305–307.
137. Ono, K., Kaneoka, K., Wittek, A., and Kajzer, J. 1997. Cervical injury mechanism based on the analysis of human cervical vertebral motion and head–neck–torso kinematics during low speed rear impacts. *Stapp Car Crash Journal* 41, 339–356.
138. Bey, M. J., Zauel, R., Brock, S. K., and Tashman, S. 2006. Validation of a new model-based tracking technique for measuring three-dimensional, in vivo glenohumeral joint kinematics. *Journal of Biomechanical Engineering* 128(4):604–609.
139. Tashman, S., and Anderst, W. 2003. In-vivo measurement of dynamic joint motion using high speed biplane radiography and CT: Application to canine ACL deficiency. *Journal of Biomechanical Engineering* 125(2):238–245.
140. Papannagari, R., Gill, T. J., Defrate, L. E., Moses, J. M., Petruska, A. J., and Li, G. 2006. In vivo kinematics of the knee after anterior cruciate ligament reconstruction: A clinical and functional evaluation. *American Journal of Sports Medicine* 34(12):2006–2012.
141. Luan, F., Yang, K. H., Deng, B., Begeman, P. C., Tashman, S., and King, A. I. 2000. Qualitative analysis of neck kinematics during low-speed rear-end impact. *Clinical Biomechanics (Bristol, Avon)* 15(9):649–657.
142. Sundararajan, S., Prasad, P., Demetropoulos, C. K., Tashman, S., Begeman, P. C., Yang, K. H., and King, A. I. 2004. Effect of head–neck position on cervical facet stretch of post mortem human subjects during low speed rear end impacts. *Stapp Car Crash Journal* 48, 331–372.
143. Bain, A. C., Shreiber, D. I., and Meaney, D. F. 2003. Modeling of microstructural kinematics during simple elongation of central nervous system tissue. *Journal of Biomechanical Engineering* 125(6):798–804.
144. Hurschler, C., Loitz-Ramage, B., and Vanderby, R., Jr. 1997. A structurally based stress–stretch relationship for tendon and ligament. *Journal of Biomechanical Engineering* 119(4):392–399.
145. Lanir, Y. 1983. Constitutive equations for fibrous connective tissues. *Journal of Biomechanics* 16(1):1–12.
146. Quinn, K. P., Bauman, J. A., Crosby, N. D., and Winkelstein, B. A. 2010. Anomalous fiber realignment during tensile loading of the rat facet capsular ligament identifies mechanically induced damage and physiological dysfunction. *Journal of Biomechanics* 43(10):1870–1875.
147. Hanson, B., Klink, K., Matsuura, K., Robeson, S. M., and Willmott, C. J. 1992. Vector correlation: Review, exposition, and geographic application. *Annals of the Association of American Geographers* 82(1):103–116.
148. Quinn, K. P., and Winkelstein, B. A. 2010. Full field strain measurements of collagenous tissue by tracking fiber alignment through vector correlation. *Journal of Biomechanics* 43(13):2637–2640.
149. Quinn, K. P., and Winkelstein, B. A. Preconditioning is correlated with altered collagen fiber alignment in ligament. *Journal of Biomechanical Engineering* 133(6):064506.
150. Quinn, K. P., and Winkelstein, B. A. 2011. Detection of altered collagen fiber alignment in the cervical facet capsule after whiplash-like joint retraction. *Annals of Biomedical Engineering* 39(8):2163–2173.
151. Spalazzi, J. P., Gallina, J., Fung-Kee-Fung, S. D., Konofagou, E. E., and Lu, H. H. 2006. Elastographic imaging of strain distribution in the anterior cruciate ligament and at the ligament-bone insertions. *Journal of Orthopaedic Research* 24(10):2001–2010.
152. Wu, C. H., Chang, K. V., Mio, S., Chen, W. S., and Wang, T. G. 2011. Sonoelastography of the plantar fascia. *Radiology* 259(2):502–507.
153. Jenkyn, T. R., Ehman, R. L., and An, K. N. 2003. Noninvasive muscle tension measurement using the novel technique of magnetic resonance elastography (MRE). *Journal of Biomechanics* 36(12):1917–1921.

154. Ko, H. J., Tan, W., Stack, R., and Boppart, S. A. 2006. Optical coherence elastography of engineered and developing tissue. *Tissue Engineering* 12(1):63–73.
155. Flusberg, B. A., Jung, J. C., Cocker, E. D., Anderson, E. P., and Schnitzer, M. J. 2005. In vivo brain imaging using a portable 3.9 gram two-photon fluorescence microendoscope. *Optics Letters* 30(17):2272–2274.
156. Levene, M. J., Dombeck, D. A., Kasischke, K. A., Molloy, R. P., and Webb, W. W. 2004. In vivo multiphoton microscopy of deep brain tissue. *Journal of Neurophysiology* 91(4):1908–1912.
157. Ku, G., and Wang, L. V. 2005. Deeply penetrating photoacoustic tomography in biological tissues enhanced with an optical contrast agent. *Optics Letters* 30(5):507–509.
158. Li, C., and Wang, L. V. 2009. Photoacoustic tomography and sensing in biomedicine. *Physics in Medicine and Biology* 54(19):R59–97.

19

Mechanical Stimulation for Functional Orthopaedic Tissue Engineering

Siddarth D. Subramony, Margaret K. Boushell, Danielle R. Bogdanowicz, and Helen H. Lu

CONTENTS

19.1 Introduction

Orthopaedic tissue engineering provides an exciting strategy for musculoskeletal tissue regeneration and has significant promise for clinical repair. Using a combination of cells, growth factors, and biomaterials, as well as biochemical or physical stimulation, the principles of tissue engineering[1] have been readily applied to the formation of a variety of

connective tissues such as bone, cartilage, fibrocartilage, ligament, or tendon *in vitro* and *in vivo*. The majority of early studies in the field have centered on validating and optimizing methods and technologies for the *ex vivo* regeneration of musculoskeletal tissues. Building upon these initial successes, the emphasis in the field of orthopaedic tissue engineering in the past decade has shifted from tissue formation to tissue function,[2] concentrating on imparting biomimetic functionality to orthopaedic grafts and enabling their translation to the clinical setting.

This chapter focuses on a critical component of orthopaedic functional tissue engineering, namely, the controlled application of physiologic or optimized mechanical stimulation for the regeneration of musculoskeletal tissues. Specifically, the role of mechanical stimulation in the tissue engineering of several major musculoskeletal tissues such as bone, cartilage, ligaments, and tendons, as well as fibrocartilage, will be reviewed. For each type of tissue, the native mechanical environment will be described, and current efforts in the application of physical stimulation for its regeneration will be highlighted. The chapter will then conclude with a summary and recommendations for future directions.

19.2 Bone

19.2.1 Native Mechanical Environment

Bone serves as the primary structural support of the body, and it is the most commonly replaced organ, with more than 1 million bone grafting procedures reported annually.[1] It is composed of approximately 25% extracellular matrix (ECM), 50% mineral, and 25% water,[3] and is populated primarily by three cell types: osteoblasts, osteocytes, and osteoclasts.[4] Osteoblasts are cells derived from mesenchymal stem cells found within the bone marrow and are necessary for bone formation, through the secretion of the collagenous matrix, that is later mineralized.[5] Osteoclasts, on the other hand, are responsible for bone resorption during tissue remodeling and are derived from hematopoietic stem cells found in the blood and marrow. Finally, the most common cells in bone are osteocytes, making up about 95% of the bone's cell population.[5] These cells are located within the canaliculi of the bone matrix and extend their processes to other canaliculi to establish connections with surrounding cells via gap junctions.[5–7] Osteocytes are the mechanosensors of bone and are able to transduce mechanical loading signals into chemical signals that can be sent throughout the interconnected cell network quickly and efficiently.

Within the bone matrix, osteocytes, osteoblasts, and osteoclasts are linked together through gap junctions between cells to form a number of basic multicellular units. These small groupings of cells are interconnected through the growth of cellular processes and allow for cell–cell interactions. Under normal physiological conditions, in which the bone is consistently cyclically loaded, bone formation and resorption take place throughout life in response to daily loading. Mechanical loading of bone leads to fluid flow within the canaliculi. It is postulated that this fluid flow over osteocytes imposes cellular deformation by shear stresses ranging from 0.08 to 3.00 Pa[8] and is primarily responsible for mediating cell activity and promoting the release of signaling molecules to activate nearby osteoblasts and osteoclasts.[5,8–10] More specifically, depending on the location of the bone in the body, bone is subjected to different types of loading, including tension, compression, and bending.[11] Although osteocytes respond to local strains as a result of loading and release signals

indicating local microdamage within the bone, osteoclasts begin to resorb this minimally damaged bone. At the same time, due to a coupling signal, osteoblasts migrate and deposit nonmineralized collagen-based bone matrix at the site of bone resorption, which will later undergo calcification.[12] The matrix deposition that occurs during the remodeling process leads to new tissue formation organized along the dominant loading direction. This suggests that bone formation is regulated by the nature of mechanical stimuli, and subsequent localized fluid flow within canaliculi, that act on cells within bone.

Defects within bone tissue can develop for a number of reasons, ranging from high impact trauma to congenital deformities, as well as age- and disease-related changes in the skeleton. Considering that the size and shape, as well as the function and location, of the damaged bone can vary in each case, it can be difficult to engineer replacement tissue that adequately matches the defect. The current gold standard for large bone defects is the use of an autologous bone graft.[13] With autografts, there is no concern for immune rejection, and in most situations, these grafts can be cut to fit the defect size and shape. However, because of the limited supply of autologous bone, as well as issues associated with donor site morbidity post harvesting, there remains a significant interest in tissue-engineered bone grafts.[14] In bone tissue engineering, as for all musculoskeletal regeneration, there are a few major components that must be considered to optimize tissue-engineered options. These include the choice of scaffold, cells, and culture system. This section will review the current use of mechanical stimulation to enhance the performance and mechanical properties of tissue-engineered bone grafts, focusing on the effects of perfusion, shear, and compression/bending on bone regeneration.

Current efforts in the application of mechanical loading in bone formation and regeneration focus on mimicking the native loading environment, as well as the associated lacuno-canicular fluid flow experienced by mechanosensory osteocytes. These efforts often involve the engineering of bioreactor systems that are able to provide mechanical stimulation acting on cell-seeded scaffolds during three-dimensional (3D) culture *in vitro*. The following sections briefly review studies that have developed bioreactors based on perfusion or shear flow in order to mimic the lacuno-canicular fluid flow, as well as systems that impose mechanical loads on scaffolds, including both tension and bending.

19.2.2 Mechanical Stimulation for Bone Tissue Engineering

19.2.2.1 Turbulent Flow

One of the earliest bioreactors used in bone tissue engineering was the spinner flask, a stirring system that effectively mixes the medium surrounding the engineered construct to form a turbulent flow field on the surface. This system was initially developed to overcome the shortcomings of static monolayer culture, in which cell survival and matrix deposition were limited due to lack of accessibility to nutrients for cells located within the center of 3D constructs. By establishing a fluid flow system, nutrients and other molecules are able to diffuse more quickly toward the center of the scaffold, significantly enhancing cell survival and proliferation. Sikavitsas et al.[15] examined the effects of this fluid mixing and its associated shear stresses by seeding rat bone marrow stromal cells on poly-(lactide-*co*-glycolide) (PLGA) scaffolds and culturing the cell/scaffold constructs in a spinner flask. By day 14, both alkaline phosphatase (ALP) activity and osteocalcin secretion were significantly greater than for static controls. Additionally, by day 21, calcium deposition was up to 6.6 times higher than that noted for the static culture. However, because of the limited enhancement in nutrient diffusion within a spinner flask, mineral deposition was

confined to the outer surface of the scaffold. Therefore, alternative loading systems are still needed for bone tissue engineering.

19.2.2.2 Low Shear, Nonturbulent Flow

Another type of bioreactor developed to enhance nutrient delivery is the rotating wall vessel (RWV), originally designed by NASA. This bioreactor consists of a hollow cylindrical growth chamber, oriented horizontally, with an inner co-rotating gas exchange membrane. This rotating system allows for increased gas exchange and nutrient diffusion levels, with minimal damage-promoting fluid turbulence and shear stresses. Schwarz et al.[16] proved the efficacy of this device by filling an RWV with BHK-21 cells, along with hollow Cytodex microcarriers and culture medium, and allowing the system to rotate under microgravity conditions. After 90 h in culture, the cells formed 3D aggregates with incorporated microcarriers and secreted an organized ECM. Additionally, cell density within the vessel increased by 10-fold within the first 250 h of culture. Since the initial success of the RWV in culturing neoplastic cells, other groups have cultured cells on 3D scaffolds within an RWV and albeit with mixed results.

In the same study mentioned previously for turbulent flow stimulation, Sikavitsas et al.[15] cultured rat marrow stromal cells on porous PLGA scaffolds within an RWV and compared results with both a spinner flask and static culture. They determined an increase in ALP activity at 2 weeks when compared with static culture, but an overall lower ALP expression and mineral deposition when compared with the spinner flask. Similar results have been reported when culturing osteoblastic cells under nonturbulent flow conditions. Utilizing a multi-high aspect ratio vessel rotating unit, Botchwey et al.[17] examined the effects of nonturbulent flow on the ability of human osteoblast-like cells (SaOS-2) to maintain their osteoblastic phenotype when cultured on hollow, lighter-than-water PLGA microspheres. In this case, after 7 days in culture, this study showed an increased ALP expression and alizarin red staining for loaded scaffolds compared with static controls, highlighting an enhanced expression of the osteoblastic phenotype.

Similarly, in a comparison between the effects of fluid flow systems and rotary systems as used in the RWV, Goldstein et al.[18] seeded rat osteoblastic marrow stromal cells on PLGA foams in a rotary vessel. Although the rotating culture performed better than static culture in terms of osteoblastic marker expression and the ability of the system to establish a uniform cell distribution throughout the scaffold, the rotating vessel resulted in a lower ALP activity and osteocalcin expression than cells grown in a spinner flask and flow perfusion bioreactor after 14 days in culture. The lack of consistent successes with this device in culturing osteogenic cells highlights the potential need for other modes of mechanical stimulation to promote cell differentiation and expression of osteoblastic phenotype.

To this end, RWVs can also be used to introduce high-rate oscillatory flow instead of nonturbulent flow, in order to impose a shear stress on scaffolds similar to that experienced by osteocytes in the canaliculi during physiological loading. Work done by Yu et al.[19] showed that, by using a high-aspect-ratio rotational device to culture both heavier-than-water and lighter-than-water PLGA foam microspheres seeded with rat primary calvarial cells, the osteoblastic phenotype of cells can be enhanced. Based on their study, it was determined that the shear stresses induced by this bioreactor led to a twofold increase in matrix mineralization on scaffolds, as well as a significant increase in ALP activity and osteocalcin expression at both 4 and 7 days when compared with static culture. A summary of studies incorporating the application of turbulent and low shear, nonturbulent flow is provided in Table 19.1.

TABLE 19.1

Summary of Studies Using Application of Turbulent and Low Shear, Nonturbulent Flow

Study	Cell Type	Scaffold Material	Mechanical Stimulation	Observations
Botchwey et al.[17]	Human sarcoma osteogenic cells	Hollow, lighter-than-water PLGA microcarriers	Scaffolds cultured in a multi-high aspect ratio vessel unit rotating at 25 rpm	Increased ALP expression and alizarin red staining on rotated scaffolds compared with controls; retention of osteoblastic phenotype.
Marolt et al.[41]	Human bone marrow stromal cells	Porous silk scaffolds	Scaffolds cultured in slow turning bioreactor at 16–32 rpm	Homogeneous mineralized matrix deposition, bone tissue formation volume fraction similar to native trabecular bone after 5 weeks.
Qiu et al.[161]	Rat bone marrow stromal cells; osteosarcoma cells	Hollow hydroxyapatite-coated ceramic microspheres	Scaffolds cultured in high aspect rotating wall vessel (HARV) at 18 rpm	Increased cell density and matrix deposition in rotated culture for both cell types. Visualization of nodules indicated early matrix mineralization.
Rucci et al.[162]	Rat osteoblast-like cells	Conventional tissue culture dishes	Scaffolds cultured in RWV at 16 rpm (low shear, nonturbulent flow = 0.008 *g*)	Increased ALP expression and osteopontin and osteonectin levels, approximately twofold increase in BMP-4 expression after 48 h.
Schwarz et al.[16]	BHK-21 cells	Cytodex microcarriers	Scaffolds cultured in RWV at 12–14 rpm initial rotation speed (increased speed with increasing aggregate size)	Increased cell density and aggregate formation over 250 h in culture.
Sikavitsas et al.[15]	Rat marrow stromal cells	3D porous 75:25 PLGA scaffolds	Scaffolds cultured in RWV at 30 rpm or within a spinner flask with magnetic stirrer spinning at 30 rpm	Increased alkaline phosphate secretions and osteocalcin expression at day 14, compared with static controls. Increased calcium deposition in spinner flask compared with static culture. No changes for RWV, decreased calcium deposition in RWV.
Song et al.[163]	Rabbit osteoblasts	Bioderived bone scaffolds	Scaffolds cultured in RWV bioreactor	Fivefold increase in cell number compared with static culture; increased ALP expression after 1 week.
Song et al.[90]	Rat calvarial osteoblasts	Human bioderived bone scaffolds	Scaffolds cultured in spinner flask (20 rpm for first 6 h, then increased to 25 rpm) or in RWV bioreactor at speed necessary to minimize mechanical stresses	Calcium salt granules and mineralized nodules present in rotated samples; no calcification visible in spun/static cultures. Significantly increased cell proliferation in rotated samples compared with spinner flask.

19.2.2.3 Perfusion

A third type of bioreactor used for bone tissue engineering is the perfusion flow system (Table 19.2). This setup aims to enhance nutrient diffusion and increase fluid flow through scaffold pores, as evident in the case of the spinner flask and RWV. This device is, however, unique in that it is also able to provide additional mechanical stimulation to the culture system in the form of applied shear forces. Using this system, Bancroft et al.[20] first examined the effects of fluid flow on mineralized matrix deposition for bone tissue engineering after culturing rat bone marrow stromal cells on 3D titanium fiber

TABLE 19.2

Summary of Studies Using Application of Perfusion

Study	Cell Type	Scaffold Material	Mechanical Stimulation	Observations
Bancroft et al.[20]	Rat marrow stromal cells differentiated to osteoblasts	3D titanium fiber nonwoven meshes	Scaffolds cultured within a flow perfusion system at 0.3, 1, and 3 mL/min flow rates	Increased flow rates result in increased calcium deposition. Increased ALP activity and osteopontin expression in all groups compared with static culture.
Cartmell et al.[164]	Mouse osteoblastic cells	Hydrated trabecular bone scaffolds	Scaffolds cultured in a steel perfusion block at flow rates of 0.01, 0.1, 0.2, and 1.0 mL/min	Increased cell proliferation on 0.1 mL/min scaffolds and increased osteocalcin, ALP, and Runx2 activity in 0.2 mL/min. Medium flow perfusion enhances cell proliferation/differentiation.
Frohlich et al.[165]	Human adipose-derived stem cells	Decellularized trabecular bone scaffolds	Scaffolds cultured under medium perfusion (~0.01 Pa shear)	More uniform cell distribution in perfused samples. Medium flow perfusion unable to promote osteogenic differentiation without the aid of osteogenic supplements.
Glowacki et al.[166]	Mouse bone marrow stromal cells	Porous type I collagen sponges	Scaffolds cultured in glass column with medium flow perfusion at flow rate of 1.3 mL/min	Increased cell viability in perfused scaffolds over static controls.
Goldstein et al.[18]	Rat osteoblastic marrow stromal cells	Porous 75:25 PLGA 3D foam disks	Scaffolds cultured within a rotary vessel at 20 rpm, spinner flask, and constant-flow system with 0.03 mL/s flow rate	Increased ALP activity after 7 and 14 days in culture for flow system compared with convection system and static culture. Both flow and convection led to uniform cell distribution throughout foams versus parabolic distribution under static conditions.

(*continued*)

TABLE 19.2 Continued

Summary of Studies Using Application of Perfusion

Study	Cell Type	Scaffold Material	Mechanical Stimulation	Observations
Gomes et al.[167]	Rat bone marrow stromal cells	Cornstarch-PCL blend nanofiber scaffolds	Scaffolds cultured in perfusion system with peristaltic pump at flow rates of 0.3 and 1 mL/min	Immunohistochemical evidence of increased expression of growth factors (BMP-2, FGF-2, VEGF, and TGF-β1) in samples under increased flow rate.
Grayson et al.[168]	Human MSCs	Mineralized, decellularized bone	Scaffolds cultured in two different medium perfusion rate systems at flow rates of 100 and 400 μm/s	Twofold increase in cell number in higher flow rate group when compared with lower flow rate groups. Comparable ALP activity and protein expression in both flow rate groups.
Grayson et al.[169]	Bone marrow–derived human MSCs	Decellularized trabecular bone plugs	Scaffolds cultured in perfusion bioreactors at varying velocities (80, 400, 800, 1200, and 1800 μm/s)	Increased DNA content/scaffold at all time points compared with day 1 for all flow rates, increased osteopontin expression in 80 μm/s group between weeks 1 and 5, remained constant for 400 μm/s, and decreased for all other groups. Increased osteocalcin expression for all groups compared with day 1, significantly greater osteocalcin expression in 80 and 400 μm/s groups compared with others.
Holtorf et al.[170]	Rat bone marrow stromal cells	Titanium 3D nanofiber meshes	Scaffolds cultured in flow perfusion bioreactor at flow rate of 1 mL/min with and without osteogenic supplements (dexamethasone)	Greatest cellularity in perfused scaffolds without dexamethasone. Increased ALP activity/cell in perfused groups over static at both 8 and 16 days. Greatest ALP activity/cell in perfused scaffolds without dexamethasone after 16 days.
Holtorf et al.[171]	Primary rat bone marrow stromal cells	β-Tricalcium phosphate-hydroxyapatite porous ceramic scaffolds	Scaffolds cultured within PMMA perfusion block at a flow rate of 1 mL/min	Increased ALP activity in perfused scaffolds at days 8 and 16, compared with static culture. Significantly greater osteopontin expression at all time points in perfused samples.
Janssen et al.[172]	Goat bone marrow stromal cells	Macroporous biphasic calcium phosphate scaffolds	Scaffolds cultured in perfusion bioreactor system at flow rate of 4 mL/min, subcutaneous implantation postculture	Increased cell proliferation, matrix deposition, and calcium phosphate nodule formation after 19 days in culture, interconnectivity visible between scaffolds; identifiable mineralized bone and osteoid formation *in vivo*.

(*continued*)

TABLE 19.2 Continued

Summary of Studies Using Application of Perfusion

Study	Cell Type	Scaffold Material	Mechanical Stimulation	Observations
Meinel et al.[173]	Human bone marrow–derived MSCs	Porous collagen I foam discs	Scaffolds cultured in static dish, spinner flask with magnetic stirrer spinning at 50 rpm, and perfusion cartridge at a flow rate of 0.2 mL/min	Increased mineralization in scaffolds cultured in both spinner flask and perfusion cartridge when compared with static culture on collagen films, greater total calcium content within scaffolds in spinner flasks compared with perfused cartridge.
Sikavitsas et al.[174]	Rat bone marrow stromal cells	3D porous titanium fiber meshes	Scaffolds cultured in flow perfusion bioreactor at 0.3 mL/min with media containing 0, 3, or 6% dextran (to alter fluid viscosity/shear)	Doubling medium viscosity increases calcium deposition by fourfold; sevenfold increase in mineral deposition for triple viscosity. Thicker, well-distributed matrix on surface of perfused samples. Greater ALP activity on samples under perfusion at day 8.
Sikavitsas et al.[175]	Rat marrow stromal cells	PLLA nonwoven scaffolds	Scaffolds cultured in flow perfusion bioreactor at flow rate of 0.6 mL/min	Cellularity of perfused scaffolds 2.8-fold higher than static culture at 8 days. Significantly increased calcium deposition in perfused scaffolds at 16 days.
Terai et al.[176]	Neonatal rat mesenchymal stromal cell–derived osteoblasts	3D 85:15 PLGA foam sheets	Scaffolds cultured in rotational oxygen-permeable bioreactor	Mineralization observed within 2 weeks; increased density of ECM; cells maintain osteocytic differentiation.
Vance et al.[21]	Mouse osteoblastic cells	Porous tricalcium phosphate-hydroxyapatite scaffolds	Scaffolds cultured in perfusion bioreactor at flow rate of 0.025 mL/min with bouts of oscillatory fluid flow at rate of 40 mL/min for 30 min, performed once daily	At 24 h, scaffolds under perfusion flow alone and perfusion flow with mechanical stimulation increased prostaglandin-2 release (2.5-fold and 4.5-fold increase, respectively).
Wang et al.[177]	Bone marrow–derived osteoblasts	β-Tricalcium phosphate porous scaffolds	Scaffolds cultured in perfusion culture with fresh medium delivered at 2 mL/h by peristaltic pump, subcutaneous implantation in rats postculture	ALP activity and osteocalcin expression significantly higher than control; increased osteoblast activity and bone formation *in vivo* after perfused culture.
Yu et al.[19]	Rat primary calvarial cells	Heavier-than-water (HTW) and lighter-than-water (LTW) PLGA foam microspheres	Microspheres cultured (60:40 HTW:LTW) in high aspect ratio vessel bioreactor at 36 rpm	Twofold increase in matrix mineralization when compared with static culture; significant increase in ALP activity and osteocalcin levels at both 4 and 7 days.

meshes and subjecting them to various fluid flow rates. With that approach, as flow rates increased up to 3 mL/min, calcium deposition also increased in culture. Additionally, all cultures under fluid flow showed an increased ALP activity and osteopontin expression when compared with static culture. Based on the success of that study, other groups have built upon this system to incorporate flow into their 3D bioreactor systems. In a more complex system, Vance et al.[21] seeded MC3T3 osteoblastic cells onto porous tricalcium phosphate–hydroxyapatite scaffolds and cultured the cell/scaffold constructs within a perfusion bioreactor with either low-rate perfusion flow alone or low-rate perfusion paired with high-rate oscillatory flow. After 24 h in culture, both perfusion-only scaffolds and perfusion–oscillation scaffolds increased the release of prostaglandin-2, a molecule important to bone cell mechanotransduction,[22,23] by 2.5-fold and 4.5-fold, respectively, when compared with static controls.

19.2.2.4 Tensile, Compressive, and Bending

A more recently explored means of mechanical stimulation, tested for future bone tissue engineering applications, comes via bioreactors that are able to generate tensile, compressive, and bending loads (Table 19.3). These loading systems are able to impose stresses on scaffolds that are similar to those experienced by bone cells under physiological conditions, such as tension and bending. In work done by Ignatius et al.,[24] human fetal osteoblastic cells were seeded on 3D collagen I gels and were stretched daily under uniaxial tensile loading for 30 min at 1% strain. Results show that uniaxial tensile loading

TABLE 19.3

Summary of Studies Using Application of Tension, Compression, and Bending

Study	Cell Type	Scaffold Material	Mechanical Stimulation	Observations
Ignatius et al.[178]	Human fetal osteoblastic cells	3D collagen I gels	Scaffolds stretched daily for 30 min at 1% strain	Increased cell proliferation compared with static culture at all time points up to 21 days. Increased ALP expression in stretched gels on days 7 and 17 compared with static gels. Increased osteocalcin levels on day 21 compared with static.
Mauney et al.[26]	Human bone marrow stromal cells	Partially demineralized bone scaffolds	Scaffolds subjected to four-point bending in triangular waveform of 5 mm/min with maximum external displacement of 0.2 mm for 250 cycles daily	Osteogenic differentiation of BMSCs: increased ALP activity and osteocalcin and osteopontin expression. Increased mineralized matrix production compared with unloaded controls.
Sumanasinghe et al.[25]	Human MSCs	Linear 3D collagen I matrices	Scaffolds subjected to uniaxial cyclic tensile strain (0%, 10%, or 12%) for 4 h/day	Significant increase in BMP-2 expression at all time points for 10% strain, at 14 days for 12% strain.

increased cell proliferation at all time points, when compared with static culture, as well as increased ALP expression at early time points and increased osteocalcin levels by day 21. Sumanasinghe et al.[25] further proved the osteogenic capacity of uniaxial tension by seeding human mesenchymal stem cells (MSCs) on linear 3D collagen I matrices subjected to uniaxial cyclic loading at a number of different strain levels for 4 h/day. After 14 days in culture, it was determined that a significant increase in the expression of bone morphogenetic protein-2 (BMP-2), a common bone marker and morphogen, could be noted at all time points. Each of these studies offers insight into the possibility of applying uniaxial tension to bone tissue engineering to enhance osteogenesis in precursor cells.

Another example of a loading system that encourages osteogenic differentiation of precursor cells is seen in the work done by Mauney et al.[26] In their study, human bone marrow stromal cells were seeded onto partially demineralized bone scaffolds and subjected to four-point bending loads for 16 days. After that period, results show that cells subjected to four-point bending underwent osteogenic differentiation, noted by an increase in ALP activity and both osteocalcin and osteopontin expression. Additionally, cells produced an increased amount of mineralized matrix when compared with unloaded controls. Each of these studies indicates that mechanical loading that mimics the forces experienced by bone *in vivo* enhances osteogenesis and subsequent bone formation *in vitro*.

19.3 Articular Cartilage

19.3.1 Native Mechanical Environment

Articular cartilage lines the surfaces of the joints and enables near-frictionless motion and load bearing. Composed of both liquid and solid phases, cartilage is a highly specialized tissue with complex structure–function relationships.[27] The *in vivo* loading environment of cartilage has been extensively studied using both theoretical models and experimental approaches. It has been determined that cartilage experiences average stresses of 0.5 to 7.7 MPa and average compression amplitudes of approximately 13% during activities such as walking.[28–31] During more aggressive movement, the joints have been estimated to experience loading of up to 18 MPa.[32] Physiologic frequencies for compressive loading are between 0.1 and 2 Hz,[33] and the cyclic nature of the loading has been shown to result in an increase in interstitial fluid pressure that can support up to 90% of the applied stress.[34] Additionally, the equilibrium shear modulus has been measured to be approximately 2.6 MPa in human articular cartilage. Similarly, the vertical shift of cartilage due to shear forces has been found to range from 9° to 15°.[27,35–37]

Age- and disease-related degeneration of cartilage often leads to osteoarthritis that can result in severe pain and loss of joint function. Cartilage is largely avascular and aneural, and consequently, has a limited ability for self-repair.[38] Clinical treatments of osteoarthritis include joint lavage, periosteal grafts, subchondral drilling, and microfracture. However, poor long-term outcomes are associated with many of these techniques due to unwanted fibrocartilage formation and inadequate graft-to-bone integration.[39–41] Therefore, there is significant interest in tissue-engineered grafts for cartilage regeneration, which includes degradable polymer and hydrogel-based cartilage grafts that have been investigated for cartilage repair with promising results.[42–49] As such, the primary

challenge in functional tissue engineering of cartilage resides in how to design cartilage grafts that can withstand the physiologic frictional and mechanical demands of the native environment.

To this end, mechanical stimulation has been investigated extensively for cartilage tissue engineering, including the use of compression, hydrostatic pressure, and shear. Optimization of these loading regimens in terms of the type, magnitude, and duration of loading, as well as the effect of loading on diverse cell types and scaffold materials have been reported. The studies reviewed in the following sections are organized by load type, with a focus on compression, shear, and hydrostatic pressure.

19.3.2 Mechanical Stimulation for Cartilage Tissue Engineering

19.3.2.1 Compression

Compressive loading is the most commonly employed type of loading in cartilage tissue engineering (Table 19.4). In 1995, Buschmann et al.[50] showed that the biochemical properties of agarose-chondrocyte constructs could be significantly improved with 10 h of dynamic unconfined compressive loading and, conversely, that static loading results in the inhibition of chondrocyte biosynthesis. This landmark study revealed that the ECM plays a role in mechanotransduction because loading that was employed after ECM elaboration resulted in less change in cell shape with respect to loading applied before ECM deposition. Subsequent studies have confirmed that static loading leads to a suppression of proteoglycan and protein production, whereas dynamic loading leads to an enhancement in matrix synthesis.[51–53] These observations collectively suggest that the physiologic nature of the loading stress is paramount to enhancing the properties of tissue-engineered constructs.

Mauck et al.[54] investigated the effect of extended mechanical loading on bovine chondrocytes cultured in hydrogels. That work was highly significant because it was the first to examine long-term loading on tissue-engineered constructs. Mauck et al. constructed a novel bioreactor that permitted loading without removal from the culture environment. Using that system, the constructs were loaded for 1 month using a loading regimen of 5 days/week with three cycles per day of 1 h on/1 h off. The effect of the scaffold material was evaluated because experiments were performed with both agarose and alginate constructs; agarose constructs were found to result in higher mechanical properties than alginate constructs. Additionally, dynamically loaded constructs had more glycosaminoglycan (GAG) and collagen than the unloaded controls by day 28 and, most importantly, exhibited a 21-fold increase in aggregate modulus.

In an effort to study loading in an environment that more closely mimics the *in vivo* setting, Hunter et al.[51] applied short-term loading in a hybrid culture system in which agarose-chondrocyte constructs were grown within the annuli of middle zone cartilage explants. It was found that constructs cultured within the annuli were more negatively impacted by static compression, and were more positively affected by dynamic compression, than those constructs cultured in isolation. This study introduced a physiologically relevant culture model and suggested that fluid pressurization, which occurred due to the annular ring, could affect chondrocyte response within the gels. More recently, Seidel et al.[55] constructed a novel bioreactor that was designed to use long-term mechanical loading together with perfusion. In that study, polyglycolic acid (PGA)–chondrocyte constructs were cultured for a total of 67 days with the loading applied during the final 37 days of

TABLE 19.4

Summary of Studies Using Application of Compressive Loading to Chondrocytes

Study	Cell Type	Scaffold Material	Mechanical Stimulation	Observations
Appelman et al.[58]	Bovine chondrocytes	PEG with fibrinogen, albumin, or proteoglycan	15%, 1 Hz	Matrix bioactivity enhances chondrocyte mechanotransduction.
Appelman et al.[179]	Bovine chondrocytes	PEG with proteoglycans, fibrinogen or albumin	15%, 1 Hz	Permissive scaffolds show a larger increase in GAG and type II collagen when loaded compared with instructive scaffolds.
Bian et al.[67]	Adult canine chondrocytes	Agarose	Dynamic (10%, 1 Hz) or sliding contact loading (10%, 0.5 Hz, 10%)	Continuous growth factor supplementation is ideal for adult canine chondrocytes. Sliding simulates aspects of joint articulation and promoted engineered tissue development.
Bryant et al.[59]	Bovine chondrocytes	PEG with RGD	5–20%, 0.3 Hz	Dynamic loading enhances anabolic activities; continuous loading inhibits catabolic activity; intermittent loading stimulates catabolic activity. Biomechanical cues are regulated through manipulations in the gel structure.
Bryant et al.[180]	Bovine chondrocytes	10% and 20% PEGDM hydrogel	15%, 1 Hz	Dynamic loading does not affect GAG synthesis in loosely cross-linked gels but decreases GAG deposition in highly cross-linked gels.
Buschmann et al.[50]	Bovine chondrocytes	Agarose	Static (0.7 mm) and dynamic (3% or 30 μm displacement strain amplitude, 0.01–1.0 Hz)	Static compression inhibits biosynthesis; dynamic compression enhances biosynthesis; intensity of response is modulated by culture time.
Cassino et al.[181]	Equine chondrocytes	Alginate	Static (15%) and dynamic (15% strain, 1 Hz, triangle waveform)	Static compression results in higher collagen II mRNA expression than dynamic loading.
Chowdhury et al.[182]	Bovine chondrocytes	Agarose	15%, 1 Hz, 10 duty cycles	2 h of intermittent compression results in the most GAG.
Chowdhury et al.[183]	Human chondrocytes	Agarose	15%, 1 Hz	TGF-β3 modulates chondrocyte response to dynamic loading.

(*continued*)

TABLE 19.4 Continued

Summary of Studies Using Application of Compressive Loading to Chondrocytes

Study	Cell Type	Scaffold Material	Mechanical Stimulation	Observations
Demarteau et al.[184]	Adult human chondrocytes	Poly(ethylene glycol terephthalate) and poly(butylene terephthalate) foams	5 ± 5%, 0.1 Hz, 6 × (2 h on, 10 h off)	Changes in GAG synthesized, accumulated, and released are positively correlated to the GAG content of the constructs before loading.
El-Ayoubi et al.[185]	Adult canine chondrocytes	PLA	10%, 1 Hz	Dynamic loading increases chondrocyte viability.
Fehrenbacher et al.[186]	Porcine chondrocytes	Chitosan	5–15%, 0.1 Hz, 45 min on, 315 min off	Dynamic loading results in enhanced mRNA for aggrecan and increased GAG and collagen type II.
Hunter et al.[51]	Bovine chondrocytes	Agarose inside a 4 mm defect formed in middle-zone cartilage	Static (10%) and dynamic (10 ± 4% at 0.1 Hz or 1 Hz)	Static compression has a more negative effect on gels in hybrid model than free swelling gels; dynamic compression enhances matrix production in hybrid model faster than in free swelling.
Hunter et al.[57]	Bovine chondrocytes	Fibrin gels	Static (10%) and dynamic (10 ± 4% at 0.1 Hz or 1 Hz)	Dynamic loading results in softer gels and inhibits GAG and hydroxyproline synthesis.
Kelly et al.[187]	Bovine chondrocytes ± chondrons	Agarose	10%, 1 Hz, 3 h/day, 5 days/week	ECM that exists before loading modulates effect of loading with 60 million cells/mL.
Kelly et al.[188]	Bovine chondrocytes	Agarose	2 ± 10%, 1 Hz, 3 h/day, 5 days/week	Dynamic loading does not alter the spatial distribution of GAG and collagen but may improve collagen organization.
Kisiday et al.[189]	Bovine chondrocytes	Self-assembling peptide hydrogel	2.5%, 1 Hz, 30 min-1 h on, 30 min-7 h off	Alternate day loading stimulates enhanced GAG production with increased mechanical properties.
Kisiday et al.[190]	Bovine chondrocytes	Self-assembling peptide hydrogel	5 ± 2.5%, 0.3 Hz, 6 × (45 min on, 5 h and 15 min off) every other day	Partially mature cartilage tissue engineering constructs may be susceptible to catabolic degradation during loading due to increased MMPs and ADAMTS proteases.
Knight et al.[191]	Bovine chondrocytes	Agarose	Static (20%)	Matrix elaboration modulates cell deformation in response to loading.

(*continued*)

TABLE 19.4 Continued

Summary of Studies Using Application of Compressive Loading to Chondrocytes

Study	Cell Type	Scaffold Material	Mechanical Stimulation	Observations
Knight et al.[192]	Bovine chondrocytes	Agarose	Static and dynamic (0–15%, 0.3 Hz)	Static compression results in constant cell deformation; dynamic compression results in reduced cell deformation over time.
Kock et al.[193]	Porcine chondrocytes	Agarose	15%, 0.33 and 1 Hz, in the presence or absence of GRGDSP	RGD-dependent integrins are mechanotransducers with a role in the regulation of both ECM gene expression and matrix biosynthesis for chondrocytes in this model.
Lee et al.[194]	Bovine chondrocytes	Polyurethane fibrin composite	0–10%, 0.1 Hz, 1 h on, twice/day	Dynamic loading doubled the rate of GAG release to the media.
Lee et al.[52]	Adult canine chondrocytes	Type II collagen	Static (0–50%) and dynamic (10 ± 3%, 0.1 Hz)	Static compression decreases matrix production in a dose and time dependent manner; dynamic loading increases biosynthesis.
Lee et al.[65]	Zonal bovine chondrocytes	Agarose	Static (5–20%)	Loading causes cell shape changes; matrix elaboration modulates shape change and leads to increased recovery time.
Lee et al.[195]	Bovine chondrocytes	Agarose	Static and dynamic (15%, 0.3, 1, or 3 Hz)	Static strain inhibits cell proliferation and GAG synthesis; dynamic compression enhances cell proliferation and GAG synthesis.
Lee et al.[196]	Zonal bovine chondrocytes	Agarose	Static and dynamic (15%, 0.3, 1, or 3 Hz)	Loading response is dependent on the chondrocyte zone; mechanotransduction-induced regulation of GAG synthesis and proliferation are uncoupled.
Lima et al.[197]	Bovine chondrocytes	Agarose	10% unconfined deformation initially and tapering to 2% peak-to-peak deformation by day 42, 1 Hz, 3 h/day	Dynamic loading after TGF-β3 supplementation increases biosynthesis while loading during treatment decreases biosynthesis.
Mauck et al.[63]	Bovine chondrocytes	Agarose	10%, 1 Hz, 3 × (1 h on, 1 h off)/day, 5 days/week	Dynamic loading increases matrix and mechanical properties for 20 M cells/mL group but there was no increase for 60 M cells/mL.

(*continued*)

TABLE 19.4 Continued

Summary of Studies Using Application of Compressive Loading to Chondrocytes

Study	Cell Type	Scaffold Material	Mechanical Stimulation	Observations
Mauck et al.[64]	Bovine chondrocytes	Agarose	10%, 1 Hz, 3 × (1 h on, 1 h off)/day, 5 days/week	Dynamic loading does not enhance matrix with 60 M cells/mL but there is an increase in mechanical properties.
Mauck et al.[198]	Bovine chondrocytes	Agarose	10%, 1 Hz, 3 × (1 h on, 1 h off)/day, 5 days/week	TGF-β1 or IGF-1 acts synergistically with loading to increase matrix production and mechanical properties.
Mauck et al.[54]	Bovine chondrocytes	Agarose or alginate	10%, 1 Hz, 3 × (1 h on, 1 h off)/day, 5 days/week	Dynamic loading enhances GAG and collagen and results in a 21-fold increase in aggregate modulus.
Ng et al.[199]	Bovine chondrocytes	Agarose (2% layered with 3% agarose)	10%, 1 Hz, 3 h/day, 5 days/week	Dynamic loading results in preferential matrix deposition in 2% agarose layer causing the 2% agarose layer to be stiffer after loading than the 3% agarose layer.
Ng et al.[200]	Bovine chondrocytes	Agarose	10%, 1 Hz, 1 h on/1 h off for a total of 3 h loading/day, or 3 h continuous/day, or 6 h continuous/day; 5 days/week	Dynamic loading for 3 and 6 h increases dynamic modulus, cartilage oligomeric matrix protein, and collagen types II and IX. Type II and IX collagen deposition increases with loading duration.
Ragan et al.[53]	Bovine chondrocytes	Alginate	Static (60–100%) and dynamic (20 ± 4% at 0.5 Hz)	Static compression decreases aggrecan synthesis and increases the amount of aggrecan in the media; dynamic compression increases aggrecan production.
Roberts et al.[201]	Bovine chondrocytes	PEG with hyaluronan and link-N fragment	15%, 0.3 Hz, 8 × (30 min on, 90 min off)/day	Incorporation of ECM analogs aides in the retention of cell-secreted GAGs under loading conditions.
Schmidt et al.[60]	Bovine chondrocytes	PEG-fibrinogen	15%, 1 Hz	Dynamic loading results in increased GAG. There was no difference between PEG and PEG-fibrinogen.
Seidel et al.[55]	Bovine chondrocytes	PGA	Static (10%) and dynamic (2 ± 5%, 1 h on, 23 h off/day, 0.3 Hz)	Mechanical loading had the most effect on peripheral rings, top and bottom surfaces of scaffold.

(*continued*)

TABLE 19.4 Continued

Summary of Studies Using Application of Compressive Loading to Chondrocytes

Study	Cell Type	Scaffold Material	Mechanical Stimulation	Observations
Stojkovska et al.[202]	Bovine chondrocytes	Alginate	10%, 0.42 Hz, 1 h on, 1 h off	Dynamic loading results in cell proliferation.
Villanueva et al.[61]	Bovine chondrocytes	PEG with chondroitin sulfate	15%, 0.3 Hz	Dynamic loading inhibits cell proliferation for 20% and 40% ChS. Proteoglycan synthesis is stimulated for 20% and 40% ChS, but collagen deposition is only stimulated with 20% ChS.
Waldman et al.[62]	Bovine chondrocytes	Porous calcium phosphate	5%, 1 Hz, 400 cycles every other day	Mechanical loading increases ECM deposition and improves mechanical properties.
Waldman et al.[203]	Bovine chondrocytes	Porous calcium phosphate	1 g amplitude for 30 min, 1 Hz	Dynamic loading results in the largest chondrocytes response when applied early in culture; a single load can improve properties.
Wang et al.[204]	Rabbit chondrocytes	Polyurethane scaffolds with collagen gel encapsulation	20% or 30%, 0.1 Hz, for 4, 8, 12, or 24 h	Dynamic compression stimulates aggrecan gene; collagen gel encapsulation enhances collagen type I expression and prolongs aggrecan expression during postcompression period.
Wernike et al.[205]	Bovine chondrocytes	Porous polyurethane	10–20%, 0.5 Hz, 1 h/day, ceramic ball oscillated over the construct surface (±25°; 0.5 Hz)	Mechanical stimulation combined with low oxygen tension modulates the chondrocyte phenotype.
Wiseman et al.[66]	Bovine chondrocytes	Agarose	15%, 1 Hz	Passage 3 and 4 chondrocytes are less responsive to mechanical loading than earlier passages.
Xie et al.[206]	Rabbit chondrocytes	Poly(L-lactide-*co*-epsilon-caprolactone)	10%, varies loading protocols	Dynamic loading effects are modulated by loading cycle.

Note: PEG, poly(ethylene) glycol; RGD, amino acid: arginine-glycine-aspartic acid; GRGDSP, amino acid: glycine-arginine-glycine-aspartic acid-serine-proline; IGF-1, insulin growth factor-1.

culture. It was found that although loading had little effect on the core of the scaffolds, it noticeably impacted the peripheral ring of the scaffolds as well as the top and bottom surfaces. This study was the first introduction of a bioreactor for cartilage tissue engineering that incorporated both loading and media perfusion.

While many groups have developed ways to control the macroscopic culture environment, Bryant et al.[56] investigated the effect of controlling the immediate microscopic

environment in a loaded system by varying hydrogel cross-linking density of the cell-seeded constructs. Polyethylene glycol dimethacrylate gels, with controlled cross-linking density, were loaded for 48 h after a 24 h preculture period. It was determined that loading inhibited cell proliferation and GAG synthesis in highly cross-linked gels, whereas loading had no effect on proliferation or GAG synthesis in loosely cross-linked gels. This study demonstrated the importance of rational scaffold design for optimizing mechanical loading response. Similarly, Hunter[57] showed that dynamic loading in fibrin gels produced softer gels and inhibited matrix synthesis, suggesting that scaffold properties play a role in generating beneficial cell responses to loading. More recently, groups have designed scaffold systems that allow for controlled incorporation of molecules into polyethylene glycol hydrogels that can be used to study the effects of scaffold material on loading response. For example, fibrinogen, arginine–glycine–aspartic acid sequences, albumin, proteoglycans, and chondroitin sulfate have been incorporated into scaffold- loaded culture systems to investigate the effects of these molecules on mechanotransduction, cell proliferation, and GAG retention.[58–61] A positive response to mechanical loading has also been shown on nonhydrogel scaffolds. Waldman et al.[62] demonstrated that bovine chondrocytes exhibit increased biosynthesis, as measured by collagen and proteoglycan production, as well as higher mechanical properties when seeded atop porous calcium phosphate substrates and subjected to long-term dynamic loading (4 weeks). These studies collectively confirm that the local environment in which cells experience mechanical loading is vitally important to the enhancement, maintenance, and success of engineered constructs.

Although nearly all the published studies have used bovine chondrocytes, Lee et al.[52] extended loading studies to a more clinically relevant model using adult canine chondrocytes. These cells were seeded in type II collagen scaffolds for up to 24 h after about 30 days of preculture. It was reported that, just as with immature bovine chondrocytes in agarose, static compression promoted biosynthesis, and select dynamic loading regimens promoted biosynthesis. Importantly, these results demonstrated that adult cells respond to mechanical loading in a beneficial manner. In addition to cell age and species, the effects of chondrocyte density[63,64] and passage number[65,66] have been investigated. Interestingly, Bian et al.[67] later demonstrated the specificity of the optimization of the cell environment and loading in a study that determined that a loading regimen optimized for immature bovine chondrocyte culture could be further improved for adult canine chondrocytes. Preliminary data have shown that the canine agarose-chondrocyte constructs are not rejected after a 3-month period when allogenic canine chondrocytes are used. The extension of agarose scaffolds for use with a mature chondrocyte source is a significant step toward clinical translation.

Along this same line, several groups have evaluated the response of MSCs to compressive loading (Table 19.5). Similar to chondrocytes, mechanical loading results in increased proteoglycan deposition by MSCs both with transforming growth factor-β (TGF-β) treatment[68–77] and without it.[76,78,79] Spatial variations in the deposited matrix have been reported between the core and periphery of the constructs, which is thought to be due to differences in oxygen tension for the core and periphery regions.[68,77,80] In addition to chondrogenic matrix enhancement, upregulation of collagen II and aggrecan gene expression have also been reported.[68,72,75,81,82] Despite the focus on the use of growth factor supplementation with mechanical loading, there is little consensus on the optimal combination of growth factor supplementation and loading, although many of these studies indicate that the time of supplementation is a critical parameter for optimization.

TABLE 19.5

Summary of Studies Using Application of Compressive Loading to Stem Cells

Study	Cell Type	Scaffold Material	Mechanical Stimulation	Observations
Angele et al.[68]	Human MSCs	Hyaluronan–gelatin	40%, 0.33 Hz, 4 h/day	Cyclic compression enhances expression of collagen type II and aggrecan in mesenchymal progenitor cells resulting in an increased cartilaginous ECM formation.
Bian et al.[207]	Human MSCs	Hyaluronic acid	10%, 1 Hz, 5% tare strain, 4 h/day, 5 days/week	Dynamic loading increases the mechanical properties, as well as the GAG and collagen content.
Haugh et al.[80]	Porcine MSCs	Agarose	10%, 1 Hz, 1 h, on day 0, 7, 14, or 21	Construct core is more favorable for chondrogenesis than the periphery; cell response to mechanical stimulus varies with the spatial region and the temporal application of loading.
Huang et al.[69]	Bovine MSCs	Agarose	10%, 1 Hz, varying duty cycles	Dynamic loading in combination with a sufficient period of chondroinduction and sustained TGF-β exposure enhances matrix distribution and mechanical properties.
Huang et al.[208]	Rabbit MSCs	Agarose	15%, 1 Hz, 4 h/day	Dynamic loading promotes gene expression of Sox9, c-*Jun*, and both TGF-β receptors; TGF-β signal transduction and activities of AP-1 and Sox9 are involved in BM-MSC chondrogenesis promoted by dynamic compressive loading.
Huang et al.[78]	Rabbit MSCs	Agarose	10%, 1 Hz, 4 h/day	Dynamic loading alone induces chondrogenic differentiation of rabbit BM-MSCs as effectively as TGF-β or TGF-β plus loading treatment.
Jung et al.[71]	Rabbit MSCs	PLCL-fibrin composite	5%, 1 Hz, continuous	Mechanical loading enhances ECM deposition.
Kisiday et al.[79]	Equine MSCs	Agarose	2.5% with 7.5% static offset, 0.3 Hz, varying duty cycles	Dynamic loading for 12 h/day results in higher PG synthesis, even in the absence of growth factors.
Li et al.[72]	Human MSCs	Polyurethane fibrin composite	Compression (15%, 20%, or 30%, 0.1 or 1 Hz) and shear (ball oscillation of ±25° at 0.1 or 1 Hz)	Dynamic loading and surface shear enhance chondrogenesis of hMSCs; higher load frequency and higher compression amplitude induce higher GAG synthesis, chondrocytic gene expression, and TGF-β1 and TGF-β3 gene expression.
Mauck et al.[209]	Bovine chondrocytes and MSCs	Agarose	10%, 0.33, 1.0, or 3 Hz	Increased loading duration increases aggrecan and decreases type II collagen promoter activity for chondrocytes; loading increases GAG deposition by MSCs.

(*continued*)

TABLE 19.5 Continued

Summary of Studies Using Application of Compressive Loading to Stem Cells

Study	Cell Type	Scaffold Material	Mechanical Stimulation	Observations
McMahon et al.[74]	Rat MSCs	Type I collagen-GAG composite	10%, 1 Hz, continuous	Dynamic loading increases the rate of GAG synthesis.
Meyer et al.[210]	Porcine MSCs	Agarose	10%, 1 Hz, 1 h/day, 5 days/week	Continuous exposure to low oxygen tension is a more potent pro-chondrogenic stimulus than 1 h/day of dynamic compression.
Mouw et al.[75]	Bovine MSCs	Agarose	10 ± 3%, 1 Hz	Response to mechanical stimulation is dependent on growth factors, samples treated with TGF-β1 and dexamethasone being the most responsive. Collagen type I and II gene expressions were more responsive to loading than aggrecan expression.
Pelaez et al.[211]	Human MSCs	Fibrin gel	10%, 0.1, 0.5, or 1 Hz	Significant chondrogenic response achieved by hMSC in fibrin constructs after 8 h of compression spread out over 2 days.
Schatti et al.[81]	Human MSCs	Polyurethane fibrin composite	Compression (10–20%, 1 Hz) and/or shear (ball oscillation of ±25° at 1 Hz, with a 0.4 mm static offset)	Shear, superimposed on dynamic compression, leads to significant increases in chondrogenic gene expression.
Terraciano et al.[82]	Human MSCs and human embryoid body-derived cells	PEGDA	10%, 1 Hz, varying times	Mechanical stimulation increases ECM elaboration and expression of Sox-9, type II collagen, and aggrecan even in the absence of TGF-β1 for MSCs; inhibits differentiation of hEBd cells in the absence of TGF-β1 but increased differentiation in the presence of TGF-β1.
Thorpe et al.[77]	Porcine MSCs	Agarose	10%, 1 Hz, 1 h/day	Early (day 0) dynamic loading can inhibit chondrogenesis; inhibition does not occur if dynamic loading is started at day 21.

Note: PLCL, poly (L-lactide-co-ε-caprolactone); PEGDA, poly(ethylene) glycol diacrylate.

19.3.2.2 Hydrostatic Pressure

Hydrostatic pressure has been investigated for stimulating the cell response in several culture systems (Table 19.6), with the majority of the early studies performed using monolayer culture.[83–88] In 1991, Hall et al.[89] first demonstrated that matrix production could be enhanced in bovine cartilage slices by applying physiologic pressure (5–15 MPa), whereas supraphysiologic pressure (20–50 MPa) did not result in enhanced matrix production. The effects of hydrostatic pressure have been comprehensively reviewed by Elder and

TABLE 19.6

Summary of Studies Using the Application of Hydrostatic Loading to Chondrocytes

Study	Cell Type	Scaffold Material	Mechanical Stimulation	Observations
Carver and Heath[92]	Equine chondrocytes	PGA	500 psi, 5 s on, 15 s off for 20 min every 4 h	Hydrostatic loading increases GAG production.
Carver and Heath[91]	Equine chondrocytes	PGA	3.44 and 6.87 MPa, 20 min/4 h	6.87 MPa of loading increases both GAG and collagen.
De Maria et al.[93]	Adult bovine chondrocytes	3D PGA	1 Hz, h = 200 mm, approach and retraction velocities of 0.0116 m/s and 0.002 m/s, respectively	Loading increases GAG production after 24 and 48 h of stimulation.
Elder and Athanasiou[95]	Bovine chondrocytes	Scaffold-free (3D)	1, 5, or 10 MPa, 0, 0.1, or 1 Hz, 1 h/day	10 MPa combined with TGF-β1 increases GAG, collagen and mechanical properties.
Elder and Athanasiou[94]	Bovine chondrocytes	Scaffold-free	10 MPa, applied at varying time points	Application of hydrostatic loading from days 10 to 14 results in the highest aggregate modulus.
Hu and Athanasiou[96]	Bovine chondrocytes	Scaffold-free (3D)	10 MPa, 1 Hz, 4 h/day	Hydrostatic pressure increases collagen production.
Kunitomo et al.[97]	Rabbit chondrocytes	Alginate	10 or 50 MPa, continuous for 12 h	Nonphysiological hydrostatic loading on chondrocytes with the ECM in poor condition reduces matrix gene expression and increases expression of apoptosis and catabolic genes.
Mizuno and Ogawa[98]	Zonal bovine chondrocytes	Collagen gels inside polyvinylidene difluoride pouches	0–0.5 MPa, 0.5 Hz (accompanied by osmotic loading)	Hydrostatic loading results in mRNA of anabolic and catabolic molecules in surface-, middle-, and deep-zone cells, in descending order of magnitude.

Athanasiou,[90] and this chapter will focus on the studies that apply hydrostatic pressure in combination with 3D culture because the latter is critical for maintaining chondrocyte phenotype and cartilage formation. For chondrocytes, hydrostatic pressure has been shown to increase both GAG and collagen synthesis in PGA scaffolds.[91–93] Similarly, the application of hydrostatic pressure to cell-based 3D constructs results in increased proteoglycan and collagen deposition as well as an increase in aggregate modulus (Tables 19.6 and 19.7).[94–96] Conversely, hydrostatic pressure applied to chondrocytes with immature or freshly deposited ECM has been shown to reduce gene expression of proteoglycan core protein and collagen II and upregulate the expression of apoptotic and catabolic genes such as IL-6, IL-8, and ADAMTS-5.[97] Mizuno and Ogawa[98] similarly reported the modulation of anabolic and catabolic molecules produced by immature zonal bovine chondrocytes in the presence of hydrostatic pressure.

TABLE 19.7

Summary of Studies Using Application of Hydrostatic Loading to Stem Cells

Study	Cell Type	Scaffold Material	Mechanical Stimulation	Observations
Angele et al.[101]	Human MSCs	Scaffold-free	0.55–5.03 MPa, 1 Hz, 4 h/day	Hydrostatic pressure enhances GAG and collagen deposition.
Finger et al.[104]	Human MSCs	Agarose	Steady (7.5 MPa) or ramped (1–7.5 MPa over a 14-day period, 1 Hz) 4 h/day	Ramped and steady hydrostatic pressure enhances Sox9 expression but not collagen II and aggrecan mRNA.
Luo et al.[100]	Ovine MSCs	Polyester	0.1 MPa, 0.25 Hz, 30 min/day	Light, low-frequency pulsatile hydrostatic pressure results in increased proliferation, GAG and collagen.
Meyer et al.[99]	Porcine MSCs	Agarose	10 MPa, 1 Hz, 1 h/day, 5 days/week, starting at day 0 or day 21	Hydrostatic pressure results in enhanced collagen and GAG content, however response is donor-dependent.
Miyanishi et al.[105]	Human MSCs	Pellet culture	0.1, 1, or 10 MPa, 1 Hz, 4 h/day	Different levels of intermittent hydrostatic pressure differentially modulate hMSC chondrogenesis in the presence of TGF-β3.
Miyanishi et al.[106]	Human MSCs	Pellet culture	10 MPa, 1 Hz, 4 h/day	Hydrostatic pressure increases chondrogenic mRNA levels in both the presence and absence of TGF-β3.
Ogawa et al.[102]	Human adipose-derived stem cells	Collagen	Cyclic hydrostatic pressure at 0–0.5 MPa, 0.5 Hz	Chondrogenic-specific gene expression of type II and X collagen, aggrecan, and SRY-box9 and rate of ECM accumulation are increased in the hydrostatic pressure group.
Wagner et al.[103]	Human MSCs	Type I collagen sponge	1 MPa, 1 Hz, 4 h/day	Hydrostatic pressure increases proteoglycan staining and mRNA expression of aggrecan, type II collagen, and Sox9; also increases expression of type I collagen, but not Runx2 or TGF-β1 mRNA.

Hydrostatic pressure has also been used to stimulate MSC differentiation into chondrocytes (Table 19.7). Specifically, it has been reported to increase GAG and collagen deposition by porcine,[99] ovine,[100] and human adult stem cells.[101–103] Similarly, hydrostatic pressure has been shown to result in the upregulation of chondrogenic markers such as collagen II and aggrecan.[102–106] Chondrogenic differentiation of human MSCs in pellet culture via hydrostatic pressure has been demonstrated both with and without TGF-β3 supplementation.[106]

19.3.2.3 Shear and Complex Loading

The effect of shear loading on tissue engineering constructs has also been investigated, both in isolation and in combination with compression (Table 19.8). Waldman et al.[107] compared shear and compressive loading for chondrocytes seeded on calcium phosphate substrates and determined that shear loading produced the highest mechanical properties. It has since been demonstrated that flow frequency and duration modulate collagen II synthesis, GAG production, and mechanical properties of tissue-engineered constructs.[108] Additionally, the combined stimulation of compression and shear can result

TABLE 19.8

Summary of Studies Using the Application of Shear and Complex Loading

Study	Cell Type	Scaffold Material	Mechanical Stimulation	Observations
Cooper et al.[212]	Bovine chondrocytes	PEG	0.5 Hz (15 mL/min) and 1.5 Hz (17 mL/min)	Flow increases collagen type II gene expression.
Gemmiti et al.[213]	Bovine chondrocytes	Scaffold-free	0.001 Pa (0.1 mL/min) and 0.1 Pa (3.0 mL/min); continuous	Flow increases type I and type II collagen expression within 24 h of exposure and increasing shear results in increased mechanical properties.
Gemmiti et al.[214]	Bovine chondrocytes	Scaffold-free	1 dyne/cm^2	Fluid shear increases collagen and collagen II production and results in enhanced mechanical properties.
Grad et al.[215]	Bovine chondrocytes	Polyurethane	5%, 10%, or 20%, 0.1 Hz, with aluminum ball oscillation at 0.6 Hz with an amplitude of ±60°; 1 h on, twice/day	Surface motion upregulates surface zone protein and hyaluronan production.
Stoddart et al.[112]	Bovine chondrocytes	Scaffold-free	0.5 N, 0.276 Hz, intermittent and continuous loading via roller mechanism	Continuous cyclic loading leads to a decrease in GAG production and intermittent loading leads to an increase in GAG production.
Waldman et al.[107]	Bovine chondrocytes	Calcium polyphosphate substrates	6 min every other day of compression (5%, 1 Hz) or shear (2%, 1 Hz)	Shear loading results in the highest GAG, collagen, and mechanical properties.
Waldman et al.[109]	Bovine chondrocytes	Calcium polyphosphate substrates	Combined compression–shear (2–5%, 0.5 Hz, 400 cycles/day)	Dynamic combined compression and shear increases GAG and collagen production.
Wimmer et al.[111]	Bovine chondrocytes	Polyurethane	5%, 10%, or 20%, 0.1 Hz, with aluminum ball oscillation at 0.6 Hz with an amplitude of ±60°; 1 h on, twice/day	Surface motion stimulation increases cartilage oligomeric matrix protein mRNA compared with simply loaded constructs.

in enhanced ECM deposition and, subsequently, higher compressive and shear moduli of the constructs.[109]

To systematically study the effects of complex loading, advanced bioreactors have been designed that are capable of applying mechanical stimuli that more closely mimic the physiologic stimulation that cartilage experiences in its native environment. For example, Wimmer et al.[110,111] introduced a novel bioreactor, with contiguous cell-seeding capabilities, in which multiaxial loading delivers cyclic axial compression in tandem with surface motion. Using this system, the effects of complex loading on surface zone protein and

hyaluronan production/expression were investigated. Another novel bioreactor, introduced by Stoddart et al.,[112] applies load through a roller mechanism and can stimulate up to 20 constructs with four different loading patterns simultaneously. Schultz et al.[113] reported on a bioreactor that is capable of mechanical loading and tissue perfusion with a special focus on ensuring system sterility, which is in line with the current efforts to upgrade laboratory procedures to ensure the product safety of potentially translatable constructs.

19.4 Tendon and Ligament

19.4.1 Native Mechanical Environment

The lack of a robust healing response in tendons and ligaments, due to the limited vasculature and innervation present within these tissues, necessitates surgical intervention upon injury.[114] Because grafts are typically required to replace the damaged tissue, such as in the case of an anterior cruciate ligament (ACL) rupture,[115] tissue engineering is gaining increased attention due to its potential to eliminate shortcomings associated with graft healing and also result in superior healing. Conventional attempts to engineer ligaments and tendons have focused on the use of fibrous scaffolds, fabricated from both natural[116] and synthetic[117] polymers, to mimic the collagenous ultrastructure of native tissue. As the field has developed, research has focused on supplementing scaffolds and cells, the two primary components of tissue engineering approaches, with exogenous factors such as chemical and mechanical stimuli to further direct cell response and tissue formation.

Tendons and ligaments, much like other musculoskeletal tissues, are routinely exposed to mechanical challenges in their native environment because their major function is to maintain joint alignment and guide joint motion.[118] The primary modes of loading experienced by both tendons and ligaments are tensile and torsional loading.[2,118,119] The magnitude of these loads has been shown to depend on the tissue of interest and also varies between individuals, as may be expected due to differences in muscle strength.[120] Relative to failure capacity, tendons develop much larger forces than ligaments, reaching 30% to 40% of ultimate strength, whereas those of ligaments rarely exceed 10% to 12% of failure force.[2] Many studies have similarly established that the magnitude of strain varies between tendons and ligaments.[121,122] As a result, it is necessary for tissue engineering approaches to replicate the mechanical characteristics of the *specific* tissue of interest. Biomechanical considerations must also account for the fact that injuries to these tissues can cause joint instability, altering the load distribution and manifesting in abnormal knee kinematics and damage to other tissues surrounding the joint,[123] thereby underscoring the necessity of recapitulating the mechanical characteristics of native tissue.

Early research in this area focused on elucidating the importance of mechanical stimuli on tissue development and remodeling at the cellular level, specifically as it relates to the tendon and ligament cell response. Although it was initially shown that cyclic stretch affects the human fibroblast response,[124] more extensive studies evaluating the cell response to cyclic mechanical load were performed by Banes et al.[125,126] using avian tenocytes. Applying 5% strain at 1 Hz for 8 h/day to cells cultured on flexible silicone substrates, it was shown that mechanical strain, in conjunction with various growth factors,

can modulate tenocyte DNA synthesis.[126] Further studies revealed that mechanical load stimulated the expression of type I collagen and calmodulin.[125] It has since become well established that cyclic stretching of tendon and ligament cells *in vitro* enhances collagen synthesis and results in a variety of intracellular changes, including an enhancement of matrix protein and metabolite gene expression.[127,128] In addition, it has been widely reported that mechanical stimulation has similarly beneficial effects on explanted tendon and ligament tissues when applied *in vitro*.[129] Based on these findings, mechanical stimulation has been incorporated into ligament and tendon tissue engineering strategies.[2] The following sections will provide a summary review of the studies that have focused on the application of static/dynamic tensile, shear, and torsional loading for ligament and tendon regeneration.

19.4.2 Mechanical Stimulation for Ligament/Tendon Tissue Engineering

19.4.2.1 Static Tensile Loading

The simplest approach to mechanical stimulation of tissue-engineered constructs has been the application of static loads to guide cell orientation and matrix formation[130,131] of primary tendon and ligament cells (Table 19.9). For example, Cao et al.[130] cultured avian tenocytes on PGA fibrous scaffolds subjected to static tensile strain using a spring wire system. Their findings showed that the application of constant strain enhanced tissue maturation and increased mechanical properties of engineered tissue. However, the resulting collagenous matrix was more compacted than native tendon, indicating that static loading systems may not be optimal for tissue formation. Deng et al. extended this work and compared the response of human tenocytes and dermal fibroblasts on PGA fibers to static tension. It was reported that neo-tendon tissue formed using dermal fibroblasts was indistinguishable from that formed by tenocytes, indicating that dermal fibroblasts may be a suitable cell source for tissue engineering applications. Similar approaches have also been devised to study MSC response to static loads. van Eijk et al.[131] tested the effect of varying the temporal application of static load and found that static loading applied during the seeding process to MSCs, which were subsequently cultured on PLGA scaffolds, resulted in the greatest number of cells being present after 5 days of culture.

TABLE 19.9

Summary of Studies Using the Application of Static Tension

Study	Cell Type	Scaffold Material	Mechanical Stimulation	Observations
Cao et al.[130]	Avian tenocytes	PGA fibers	Static tension	Static strain increases the mechanical properties of constructs
Deng et al.[216]	Human tenocytes, Human dermal fibroblasts	PGA fibers	Static tension	Neo-tendon tissue formed using dermal fibroblasts on scaffolds subjected to static tension is indistinguishable from that formed by tenocytes using the same system
van Eijk et al.[131]	Goat bone marrow stem cells	Braided PLGA scaffold	Static tension applied by spring wire	Loading during seeding results in the greatest number of cells on scaffolds after 5 days although no differences in cell number or differentiation results after 23 days

19.4.2.2 Dynamic Tensile Loading

Extensive work has been performed using more physiologically relevant *dynamic* tensile stimulation regimens to guide cell response (Table 19.10). In early work performed with differentiated cells, Garvin et al.[132] reported on the application of 1% tensile strain at 1 Hz to avian flexor tendon cells cultured in collagen gels. It was demonstrated that cells align in the direction of the strain, and mechanical stimulation results in a threefold increase in construct ultimate tensile strength. In two separate reports, Webb et al.[133] seeded porous polyurethane scaffolds with human fibroblasts and evaluated cell response. In the first study, it was shown that tensile strain combined with ascorbic acid supplementation (0 versus 1 mM) can increase construct modulus, whereas tensile strain alone can enhance fibroblast proliferation. Mechanical strengthening of constructs was also accompanied by the expression of several matrix proteins, including type I collagen, TGF-β1, and connective tissue growth factor. Subsequently, in studies evaluating the impact of varying loading parameters, it was shown that fewer cycles per day, corresponding to the low to subphysiologic range of parameters, resulted in the greatest increases in construct elastic modulus.[134] Lee et al. investigated the effects of substrate morphology and mechanical stimulation on human ligament fibroblasts using unaligned and aligned polyurethane nanofiber scaffolds. Both total collagen and collagen per cell were enhanced with mechanical stimulation on the aligned nanofiber substrate as compared with the randomly oriented unaligned scaffold. Studies have also demonstrated that the response of differentiated cells can be enhanced with loading when using natural scaffolds, such as decellularized tendon tissue.[135,136]

Extending to stem cells, Butler et al. conducted a range of studies to investigate the impact of tensile stimulation on MSCs using a collagen sponge system for both ligament and tendon applications. Initial work, aimed at using tissue-engineered constructs for rabbit patellar tendon repair, evaluated type I collagen sponges seeded with rabbit MSC. After stimulating constructs for 2 weeks, once every 5 min for 8 h/day to a peak strain of 4%, it was observed that mechanically stimulated constructs had 2.5 times the linear stiffness of nonstimulated constructs. Furthermore, upon implantation *in vivo* into a rabbit patellar tendon defect model, increased mechanical properties were measured for stimulated constructs indicating that *in vitro* stimulation can improve tendon repair biomechanics.[137] Extending upon this work, MSC response to mechanical stimulation was further evaluated using gene expression analyses. It was observed that the application of similar mechanical stimulation regimen resulted in the upregulation of collagen type I and type III expression.[138] To further investigate the effect of mechanical stimulation, studies were conducted comparing the effect of loading on MSCs seeded in collagen sponges versus collagen gels. After subjecting both constructs to an identical loading regimen (2.4% strain every 5 min for 8 h/day) over a period of 14 days, it was observed that mechanical loading increased the linear stiffness of cell–sponge constructs but did not produce any such improvement in cell–gel properties, suggesting that the application of mechanical stimulation may need to be optimized based on the scaffold conformation.[139] Using the collagen sponge system, the loading regimen was optimized with an iterative approach in which peak strain (0.6%–4.8%), cycle number (10–10,000/day), and cycle repetition (1–50) were varied while maintaining frequency (1 Hz). Based on this analysis, it was determined that constructs stimulated with 2.4% strain for 3000 cycles/day and one cycle repetition produced the stiffest constructs.[140] To further investigate the effect of mechanical stimulation and scaffold stiffening, an alternative method was also evaluated to enhance construct stiffness. Specifically, type I collagen sponges were strengthened using additional dehydrothermal

TABLE 19.10

Summary of Studies Using Application of Dynamic Tension

Study	Cell Type	Scaffold Material	Mechanical Stimulation	Observations
Abousleiman et al.[144]	Rat MSCs	Human umbilical veins with cell-seeded collagen gels	2% strain at 0.0167 Hz for 1 h/day	Mechanical stimulation results in a significant increase in cell number and greater construct strength after 2 weeks.
Angelidis et al.[143]	Adipose-derived stem cells	Decellularized rabbit hind paw flexor tendons	1.25 N uniaxial stretch force, 1 cycle/min in alternating 1 h periods of mechanical loading and rest	Seeded constructs subjected to tensile strain reach an elastic modulus and ultimate tensile strength comparable to those of fresh tendons.
Barber et al.[217]	Human MSCs	Braided nanofibrous scaffold	10% strain at 1 Hz for 2 h/day	Tenogenic growth factors combined with cyclic strain result in differentiation toward a tenogenic lineage with significant upregulation of scleraxis.
Chokalingam et al.[218]	Murine MSCs	Collagen sponge	2.4% peak strain for 20 s at 1 Hz followed by 0% strain for 100 s, 5 h/day	Tensile stimulation increases type I collagen gene expression and linear stiffness.
Doroski et al.[219]	Human marrow stromal cells	PEG hydrogel	10% strain, 1 Hz, 2 h of strain followed by 3 h rest	Cyclic strain significantly upregulates all tendon/ligament fibroblastic genes.
Farng et al.[220]	Murine bone marrow stromal cells	Porous PCL scaffold	10% strain at 0.33 Hz	Mechanical and chemical stimulation (GDF-5) enhances mRNA production of collagen type I, II, and scleraxis.
Garvin et al.[132]	Avian flexor tendon cells	Collagen gel	1% strain at 1 Hz for 1 h/day	Cells align in the direction of strain, mechanical loading resulted in a threefold increase in ultimate tensile strength.
Issa et al.[145]	Rat MSCs	Human umbilical veins with cell-seeded collagen gels	2% strain at 0.0167 Hz for 1 h/day	The lowest seeding density (3 million cells/mL) results in the greatest construct tensile strength after 1 week of bioreactor culture.
Joshi et al.[134]	Human dermal fibroblasts	Porous polyurethane	2.5–10% strain amplitude, 5–50%/s strain rate, 0.1–1 Hz frequency, 1400–43,200 cycles/day for 1–24 h	Low to intermediate values of experimental variables (2.5% strain, 25%/s strain rate, 0.1–0.5 Hz frequency and 7200–28,800 cycles/day) result in highest construct elastic modulus.
Juncosa-Melvin et al.[137]	Rabbit MSCs	Collagen sponge	4% strain, once every 5 min for 8 h/day	Mechanical stimulation results in constructs with 2.5 times greater linear stiffness.

(*continued*)

TABLE 19.10 Continued

Summary of Studies Using Application of Dynamic Tension

Study	Cell Type	Scaffold Material	Mechanical Stimulation	Observations
Juncosa-Melvin et al.[221]	Rabbit MSCs	Collagen sponge	2.4% strain, once every 5 min for 8 h/day	Mechanical stimulation significantly increases the expression of type I collagen and type III collagen.
Kuo et al.[45]	Human MSCs	Type I collagen gel	Static tension; dynamic tension of 1% strain at 1 Hz for 30 min/day	Cyclic strain maintains scleraxis expression and regulates Wnt gene expression.
Lee et al.[222]	Human ligament fibroblasts	Polyurethane nanofibers	5% uniaxial strain at 12 cycles/min for 24 h	Tensile stimulation of fibroblasts on aligned nanofiber scaffolds increases collagen production.
Nirmalandhan et al.[141]	Rabbit MSCs	Collagen sponge	2.4% strain, 3000 cycles/day and one cycle repetition	Additional dehydrothermal cross-linking to stiffen scaffolds before mechanical stimulation results in decreased repair stiffness *in vivo*.
Nirmalandhan et al.[139]	Rabbit MSCs	Type I collagen gel; type I collagen sponge	2.4% strain, once every 5 min for 8 h/day	Mechanical stimulus improves linear stiffness and modulus of sponge constructs but not gel constructs.
Nirmalandhan et al.[223]	Rabbit MSCs	Type I collagen gel; type I collagen sponge	2.4% strain, once every 5 min for 8 h/day	Sponge constructs of greater length result in the highest *in vitro* linear stiffness.
Nirmalandhan et al.[140]	Rabbit MSCs	Collagen sponge	Varied peak strain, cycle number, and cycle repetition while controlling cycle frequency (1 Hz), rise and fall times (25% and 17% of the period, respectively), hours of stimulation/day (8 h/day), and total time of stimulation (12 days)	Ideal loading regimen consists of 2.4% strain, 3000 cycles/day and one cycle repetition.
Noth et al.[224]	Human MSCs	Type I collagen gel	3 mm stretch at 1 Hz continuously for 8 h/day	Cyclic strain results in the formation of a ligament-like matrix and an increase in the expression of collagen types I and II, fibronectin and elastin.
Petrigliano et al.[225]	Rat bone marrow stromal cells	Porous PCL scaffold	6% uniaxial strain at 0.125 Hz for 23 h/day	Stimulatory effects of bFGF are dose-sensitive and influenced by the addition of mechanical strain.

(*continued*)

TABLE 19.10 Continued

Summary of Studies Using Application of Dynamic Tension

Study	Cell Type	Scaffold Material	Mechanical Stimulation	Observations
Raif et al.[226]	Bovine synovial cells	Woven polyester scaffold	Varied applied strain from 0.5% to 4.7% at 0.35%/s	Application of strain results in collagen fibrils aligned in the direction of load and cell proliferation and ECM synthesis depends on magnitude of load.
Saber et al.[135]	Rabbit tenocytes	Decellularized rabbit hindpaw flexor digitorum equivalents	1.25 N uniaxial stretch force, 1 cycle/min in alternating 1 h periods of mechanical loading and rest	Bioreactor loading significantly increases the ultimate tensile strength and elastic modulus of seeded constructs.
Shearn et al.[227]	Rabbit MSCs	Collagen gel	2.4% strain, once every 5 min for 8 h/day	Preculturing with mechanical stimulation *in vitro* significantly increases structure and material properties of repaired *in vivo* tissue.
Subramony et al.[142]	Human MSCs	Aligned and unaligned PLGA nanofibers	1% strain for 90 min twice/day at 1 Hz	Fibroblastic differentiation only induced on aligned nanofibers when coupled with tensile loading.
Webb et al.[133]	Human fibroblasts	Porous polyurethane	10% strain at 0.25 Hz for 8 h/day	Tension increases construct modulus after 1 week in conjunction with ascorbic acid, strain alone significantly increases fibroblast proliferation. Strengthening was accompanied by increased expression of type I collagen, TGF-β1 and connective tissue growth factor.
Woon et al.[136]	Human adult dermal fibroblasts	Cadaveric human flexor and extensor tendons	Varied duty cycle, conditioning duration and load magnitude	Ultimate tensile strength of human allograft constructs is enhanced by reseeding and dynamic loading.

Note: GDF-5, growth/differentiation factor-5; bFGF, basic fibroblast growth factor.

cross-linking (ADHT), seeded with cells, and then subsequently mechanically stimulated. After implantation in a rabbit patellar tendon defect model for 12 weeks, it was demonstrated that increasing construct stiffness via ADHT decreased repair biomechanical properties.[141] These findings indicate that although cross-linking combined with mechanical stimulation may increase initial stiffness *in vitro*, these differences may not translate to improved *in vivo* outcomes. Studies performed by Subramony et al.[142] investigated the impact of nanofiber scaffold alignment and dynamic tensile strain on the fibroblastic differentiation of MSCs. It was shown that applying 1% tensile strain for 90 min twice daily at

a frequency of 1 Hz to MSCs cultured on aligned PLGA nanofibers resulted in the production type III collagen and the upregulation of several fibroblastic genes (type III collagen, fibronectin, and tenascin-C). Interestingly, it was shown that the same applied loading regimen did not result in fibroblastic differentiation of cells cultured on unaligned nanofibers, thereby indicating that biomimetic scaffold alignment and tensile stimulation are both critical for inducing fibroblastic differentiation of MSCs.

The response of stem cells to tensile stimulation has been further studied using extracellular matrix-based scaffolds. Angelidis et al.[143] reported that dynamic tensile strain of adipose-derived stem cell–seeded, decellularized rabbit flexor tendons can increase construct elastic modulus and ultimate tensile strength. Sikavitsas et al.[144] studied the response of rat MSCs seeded in human umbilical veins to dynamic strain; mechanical stimulation was shown to result in a significant increase in cell number and greater construct strength after 2 weeks of culture. In addition, lower cell seeding densities were shown to be optimal for long-term tissue formation.[145]

19.4.2.3 Dynamic Tensile and Torsional Loading

For more complex loading regimens, bioreactors have been designed to apply torsional strain, as well as sequential tensile and torsional strain, to tissue-engineered constructs for ligament or tendon tissue engineering (Table 19.11). Scaglione et al.[146] applied torsion to mouse 3T3 fibroblasts seeded in porous polycaprolactone (PCL) scaffolds and demonstrated

TABLE 19.11

Summary of Studies Using Application of Dynamic Torsion

Study	Cell Type	Scaffold Material	Mechanical Stimulation	Observations
Altman et al.[148]	Human MSCs, bovine MSCs	Type I collagen gel	10% stretch, 25% rotational strain concurrently at 0.0167 Hz	Application of mechanical stress upregulates ligament fibroblast markers and results in cell alignment in the direction of applied load.
Chen et al.[149]	Human bone marrow stromal cells	Silk fiber matrix	45° rotation at 1.39e-4 Hz	Cell response depends on the temporal application of mechanical stimulation.
Moreau et al.[150]	Human bone marrow stromal cells	Silk fiber matrix	Static tension; 45° rotation at a rate of 1 cycle/h; 45° rotation at a rate of 0.5 cycles/h	Rotation at 0.5 cycles/h is optimal when combined with bFGF stimulation.
Sawaguchi et al.[147]	Rabbit patellar tendon fibroblasts	Chitosan and hyaluronan scaffold	Stretch: 5% strain at 0.5 Hz for 18 h followed by 6 h rest, Rotation: 90° rotation at 0.5 Hz for 18 h followed by 6 h rest	Dynamic stretch combined with rotation results in greater cell number and increase expression of types I and III collagen and fibromodulin.
Scaglione et al.[146]	Mouse fibroblasts (3T3)	Porous polycaprolactone	Torsion of 100° at 600°/min	Collagen types I and III, tenascin-C gene expression are upregulated with the application of torsion.

that types I and III collagen and tenascin-C expression were upregulated. Similar findings were also reported by Sawaguchi et al.,[147] who applied a combination of tension and torsion to rabbit patellar tendon fibroblasts seeded in a chitosan and hyaluronan scaffold. It was shown that the dynamic loading regimen resulted in greater cell number and an upregulation of fibromodulin and types I and III collagen.

Altman et al.[148] evaluated the effect of tensile and torsional stimulation on MSCs. Initial studies were performed by seeding type I collagen gels with human MSCs and subjecting them to 10% stretch and 25% rotational strain concurrently at a frequency of 0.0167 Hz. It was reported that the application of mechanical stress upregulated the expression of ligament fibroblast markers, resulted in the production of type III collagen, and guided cell alignment in the direction of the applied load. Extending those findings, studies were conducted using a silk fiber–based ligament construct to optimize cell response.[116] In an effort to evaluate the effect of temporal variation in the application of mechanical stimulation, metabolic assays were conducted on MSC-seeded silk fiber ligament constructs. A loading regimen consisting of 45° of rotation at a frequency of 1.39×10^{-4} Hz was applied 1, 3, 6, or 9 days after cell seeding. The greatest enhancement of cell metabolic activity was found to occur when loading was applied 9 days after seeding.[149] Most recently, the effect of combined chemical and mechanical stimulation was evaluated using the silk fiber system. After optimizing the loading regimen in growth factor–free medium, cells were primed with medium containing basic fibroblast growth factor and epidermal growth factor, and then subjected to the optimal mechanical regimen (45° of rotation at 0.5 cycle/h for 12 h). Sequential chemical and mechanical stimulation was shown to enhance matrix production and ingrowth, and to direct cells toward fibroblastic differentiation.[150] These studies collectively demonstrate the multitude of parameters that can be varied to apply mechanical stimulation and direct tissue formation.

19.5 Fibrocartilage

19.5.1 Native Mechanical Environment

Fibrocartilaginous tissues, such as the meniscus, intervertebral disc (IVD), and the ligament and tendon-to-bone interfaces are of great interest for tissue engineering applications due to the high injury rates associated with these tissues and the myriad of subsequent pathological issues associated with such injuries. These tissues typically reside in mechanically complex environments, further increasing the difficulty of engineering suitable replacements and also complicating the process of recapitulating the native environment for mechanical stimulation purposes. The meniscus, which resides within the knee and acts as a shock absorber and joint stabilizer, is subjected to tension, compression, and shear as it supports the femoral condyles and guides joint motion. The IVD is composed of two distinct structures, the annulus fibrosus and the nucleus pulposus, which together serve to dampen the loads placed on the spine and enable spinal motion. The annulus fibrosus, which comprises the outer ring of the IVD, is characterized by a lamellar fibrocartilaginous structure that undergoes tension and compression as it maintains spinal stability. Lastly, the fibrocartilaginous insertion sites of ligaments, such as the ACL, and tendons, including the rotator cuff tendons, undergo a distinct transition from fibrous ligament/tendon tissue, to nonmineralized fibrocartilage, to mineralized fibrocartilage, and subsequently

to bone. During physiological loading, these structures experience both tension and compression and are instrumental in minimizing the formation of stress concentrations and in mediating load transfer.[151]

19.5.2 Mechanical Stimulation for Fibrocartilage Tissue Engineering

Based on the wide variety of locations that fibrocartilage is found within the body, as well as the diverse types of loading it is exposed to, a number of bioreactors have been developed to expose tissue-engineered scaffolds to mimic *in vivo* loading (Table 19.12). The earliest research in this relatively new field focused on engineering fibrocartilage found within the intervertebral disc. Specifically concerned with the development of the annulus fibrosus, Neidlinger-Wilke et al.[152] examined the effects of applying cyclic stretching and hydrostatic pressure to human annulus fibrosus cells seeded within collagen I gels. Based on these studies, it was shown that under cyclic stretching, annulus fibrosus cells increase collagen II and aggrecan expression, with a marked decrease in the expression of a destructive matrix metalloproteinase (MMP), that is, MMP-2. As for the effects of intermittent hydrostatic pressure on these same cells, cells within this collagen matrix show an increase in the expression of both collagen I and aggrecan, while decreasing the expression of the destructive MMPs, including MMP-2 and MMP-3.

Reza and Nicoll[153] built upon these promising findings regarding hydrostatic pressure by examining the effects of pressurized loading on annulus fibrosus cells seeded in a more physiologically relevant, fibrous matrix material. In their study, both bovine outer and inner annulus fibrosus cells were seeded onto fibrous PLGA scaffolds and pressurized for 4 h daily. This hydrostatic pressurization resulted in increased collagen II production and enhanced matrix organization when compared with unloaded controls. More recently, other forms of loading have also been applied to cells of the intervertebral disc to enhance fibrocartilage formation. In a study done by Chang et al.,[154] bovine annulus fibrosus cells were seeded on porous silk scaffolds and cultured under dynamic flow in spinner flasks with magnetic stir bars rotating at 60, 90, and 120 rpm. The results of their study showed that dynamic flow increases cell proliferation, collagen deposition, and proteoglycan accumulation when compared with static cultures.

Through elastographic imaging of neonatal bovine tibiofemoral joints, Spalazzi et al.[155] examined the strain profiles present along the length of the ACL and ACL-to-bone insertion site. According to these studies, both compressive and tensile loading are evident at the native ligament-to-bone interface. In accordance with these findings, research involving mechanical stimulation for ligament-to-bone and tendon-to-bone tissue engineering focuses on the application of dynamic loading to enhance the formation of fibrocartilaginous insertion tissue. To incorporate a compressive load profile during tendon-to-bone healing, Spalazzi et al. developed a mechanoactive collar, composed of aligned PLGA nanofibers and sintered PLGA-bioglass microspheres, which was first wrapped around the bovine patellar tendon and then allowed to contract the native tissue over time. Under these conditions, by day 1, loaded tendon tissue showed an increased matrix density and cellularity, as well as increased proteoglycan production. After 14 days in culture, the tissue maintained its dense, cellular appearance, as well as an increased expression of fibrocartilage markers, including collagen II, aggrecan, and TGF-β3.[156] In addition, Thomopoulos et al.[157] have recently examined the effects of both compression and tension in the form of cyclic loading on rat mesenchymal stromal cells for application toward the development of the tendon-to-bone interface. Cells were seeded into a collagen I gel matrix and exposed to a tensile hydrostatic stress field, subjecting separate regions of scaffolds

TABLE 19.12

Summary of Studies Using Application of Mechanical Stimulation for Fibrocartilage Tissue Engineering

Study	Target Tissue	Cell Type	Scaffold Material	Mechanical Stimulation	Observations
Aufderheide and Athanasiou[158]	Meniscus	Rabbit meniscus fibrochondrocytes	Agarose gels, PGA nonwoven meshes	Shear: scaffolds cultured in a rotating wall bioreactor rotating at a speed adjusted to maintain constructs in a settling regimen.	More intense Safranin O and Picrosirius Red staining for PGA scaffolds than agarose. Decreased GAG concentration for rotated scaffolds compared with static controls.
Baker et al.[160]	Meniscus	MSCs	Aligned PCL nanofiber scaffolds	Tension: scaffolds precultured for 6 weeks, then loaded at 6% strain at 1 Hz for 3 h/day.	Increased collagen deposition, gene expression (fibronectin, lysyl oxidase), and 16% increase in modulus and stiffness over unloaded controls.
Chang et al.[154]	Intervertebral disc	Annulus fibrosus cells from bovine caudal discs	Porous silk scaffolds	Perfusion: scaffolds cultured under dynamic flow in spinner flasks with magnetic stirring at 60, 90, and 120 rpm.	Dynamic flow increases tissue formation and matrix deposition compared with static culture; increased cell proliferation, collagen deposition/cell, and proteoglycan accumulation (90 rpm). No effect on cell distribution.
Connelly et al.[228]	Meniscus	Bovine calf bone marrow stromal cells	Fibrin gel constructs	Tension: scaffolds subjected to sinusoidal displacement of 10% at 1 Hz for 1 h, followed by 3 h of rest (six times daily).	Stimulatory effect on protein synthesis but not proteoglycan synthesis over first 12 days, increased collagen II, decreased collagen I and increased aggrecan.
Fox et al.[229]	Meniscus	Equine fibroblast-like synoviocytes	PLGA nonwoven scaffolds	Laminar fluid flow: scaffolds cultured in slow turning lateral vessel bioreactor at 22.5 rpm (with or without bFGF, TGF-β1, or IGF-1).	In combination with other appropriate stimuli (i.e., growth factors), synoviocytes have potential for fibrochondrogenesis in rotating system.

(*continued*)

TABLE 19.12 Continued

Summary of Studies Using Application of Mechanical Stimulation for Fibrocartilage Tissue Engineering

Study	Target Tissue	Cell Type	Scaffold Material	Mechanical Stimulation	Observations
Marsano et al.[159]	Meniscus	Primary human and bovine articular chondrocytes	Esterified hyaluronan nonwoven meshes	Shear: scaffolds cultured in a rotary culture bioreactor spinning from 16 rpm (at start) up to 50 rpm (at end) with a flow rate of 0.6 mL/min.	Bizonal cartilage formation with outgrowing fibrous capsule and inner GAG region for both cell types.
Neidlinger-Wilke et al.[152]	IVD: Annulus fibrosus	Human annulus fibrosus cells	Collagen I gels	Cyclic and static stretching: scaffolds subjected to cyclic stretching at 1%, 2%, 4%, and 8% strain at 1 Hz for 24 h or 0.25 MPa of intermittent hydrostatic pressure (IHP) at 0.1 Hz for 30 min daily.	Increased cell proliferation throughout 4-week period in IHP group, increased collagen I and aggrecan expression with decreased MMP-2 and MMP-3 expression in IHP group. Increased aggrecan, collagen II/ decreased MMP-3 expression in cyclic strain group.
Reza and Nicoll[153]	IVD: Annulus fibrosus	Bovine outer and inner annulus fibrosus cells	PLGA scaffolds	Hydrostatic pressure: scaffolds pressurized 4 h/day.	Significant increase in collagen II production in constructs at day 14 compared with unloaded constructs. Enhanced ECM organization.
Spalazzi et al.[151]	Tendon-to-bone interface	Bovine patellar tendon cells within a bovine patellar tendon graft	PLGA nanofibers and PLGA-bioglass microsphere graft collar	Scaffold-induced compression of tendon graft: over 15% graft compression after 14 days.	Increased tissue density and cellularity at both days 1 and 14. Increased expression of collagen II, aggrecan, and TGF-β3 at day 14 compared with uncompressed control. Greater proteoglycan content after day 1 in compressed grafts.

(*continued*)

TABLE 19.12 Continued

Summary of Studies Using Application of Mechanical Stimulation for Fibrocartilage Tissue Engineering

Study	Target Tissue	Cell Type	Scaffold Material	Mechanical Stimulation	Observations
Thomopoulos et al.[157]	Tendon-to-bone interface	Rat mesenchymal stromal cells	Collagen I gel	Cyclic versus static compression and tension: 1.5 mm amplitude and 1 Hz to apply cyclic tensile and compressive forces, as compared with static compressive and tensile loaded groups.	Increased scleraxis, aggrecan, and collagen I expression for cyclically loaded samples. Greater aggrecan and scleraxis expression in tensile region of cyclically loaded groups. On addition of chondrogenic TGF-β3, decreased Sox9 and increased aggrecan under cyclic loading.

to either compression or tension; cells that undergo cyclic loading in this environment express high levels of scleraxis, collagen I, and aggrecan as compared to static samples. More specifically, during cyclic loading, regions under cyclic tensile stresses show greater aggrecan and scleraxis mRNA expression when compared with cyclically compressed regions.

Work regarding the development of the fibrocartilage region of the meniscus has also been examined. In 2005, Aufderheide and Athanasiou[158] studied rabbit fibrochondrocytes under shear by seeding cells onto both agarose gels and PGA nonwoven meshes. In this study, scaffolds were cultured within a rotating wall bioreactor, which rotated at a speed adjusted to maintain constructs in a settling regimen. After 7 weeks, histology showed a more intense Safranin O and Picrosirius Red staining for PGA scaffolds cultured within this bioreactor system than seen in agarose gels. Additionally, a higher density stain can be seen surrounding the cells and nodules of PGA samples cultured within the rotating wall bioreactor, as compared with a lighter, but more uniform stain seen in static samples.

Similarly, Marsano et al.[159] examined the effects of shearing on both human and bovine articular chondrocytes in a rotary culture for application to meniscus tissue engineering. In this study, cells were seeded onto esterified hyaluronan nonwoven meshes and cultured in a rotary cell culture system at a rotational speed between 16 and 50 rpm, adjusted to maintain simulation of a continual free fall, and a flow rate of 0.6 mL/min. Based on gross analysis of scaffolds, a bilayer tissue was formed, with an outer layer of fibrous tissue resembling a fibrocartilage-like capsule, containing elongated cells within a collagenous matrix, and an inner GAG region. This distribution was shown to be consistent for both cell types, highlighting the potential for rotational culture in forming a bizonal cartilage tissue similar to that found within the native meniscus.

Also, toward the development of tissue-engineered menisci, Baker et al.[160] evaluated the ability of dynamic tensile loading to stimulate fibrous gene expression in nanofiber scaffolds seeded with MSCs. In this study, MSCs were seeded onto aligned PCL nanofibers and loaded at 6% strain at a frequency of 1 Hz for 3 h daily. Culturing under dynamic

tension resulted in higher collagen I deposition, as well as fibrous gene expression, including fibronectin, a cell-binding molecule and collagen deposition precursor,[102] and lysyl oxidase, an enzyme responsible for collagen cross-linking, when compared with unloaded controls. Tensile loading also resulted in an increased tensile modulus and matrix stiffness for loaded scaffolds.

19.6 Summary

The field of functional tissue engineering has advanced significantly in elucidating the role of mechanical loading in stimulating the regeneration of orthopaedic tissues. This chapter focuses on studies that have applied these understandings to the formation of bone, cartilage, tendon, ligament, and fibrocartilage, with substantial progress in all areas but many opportunities for future advances.

The studies highlighted in this chapter, as well as in others, demonstrate the importance of mechanical stimulation for the development of functional tissue-engineered scaffolds. The bioreactors developed thus far are able to minimize mass transport limitations associated with static culture, as well as use loading paradigms that are similar to those observed *in vivo* to promote new tissue formation. Current design in bioreactors must continue to be optimized and innovated for orthopaedic tissue engineering. Specifically, the design of bioreactors that facilitate temporal growth factor addition, biomimetic loading regimens, and long-term sterility is needed.

A range of studies have demonstrated that dynamic stimulation techniques can guide cell orientation, proliferation, and matrix deposition to enhance the functional properties of tissue-engineered constructs. As the field has advanced, a shift toward more clinically obtainable stem cells has developed, with many groups focusing on using dynamic stimulation to differentiate these cells toward a desired musculoskeletal phenotype. However, the optimal scaffold and mechanical stimulation parameters for this purpose have yet to be determined and require further investigation to advance the field and enable the clinical implementation of stem cell–based tissue-engineered grafts.

In closing, physiological loading is an essential component of the functional tissue engineering of orthopaedic grafts. Significant advances in this effort will be guided by continued understanding of the mechanism of mechanotransduction, as well as innovations in bioreactor design that will enable the integrative culture and stimulation of musculoskeletal tissue grafts. It is anticipated that such developments will enable the formation of functional tissues for clinical implementation and subsequent tissue regeneration.

References

1. Langer, R. and J. P. Vacanti. 1993. Tissue engineering. *Science* 260, 5110:920–926.
2. Butler, D. L., S. A. Goldstein, and F. Guilak. 2000. Functional tissue engineering: The role of biomechanics. *Journal of Biomechanical Engineering* 122, 6:570–575.
3. Schifferle, R. E. 2009. Periodontal disease and nutrition: separating the evidence from current fads. *Periodontology 2000* 50:78–89.

4. Holtorf, H. L., J. A. Jansen, and A. G. Mikos. 2006. Modulation of cell differentiation in bone tissue engineering constructs cultured in a bioreactor. *Advances in Experimental Medicine and Biology* 585:225–241.
5. Burger, E. H. and J. Klein-Nulend. 1999. Mechanotransduction in bone—role of the lacuno-canalicular network. *FASEB Journal* 13 Suppl:S101–S112.
6. Doty, S. B. 1981. Morphological evidence of gap junctions between bone cells. *Calcified Tissue International* 33, 5:509–512.
7. Shapiro, F. 1997. Variable conformation of GAP junctions linking bone cells: A transmission electron microscopic study of linear, stacked linear, curvilinear, oval, and annular junctions. *Calcified Tissue International* 61, 4:285–293.
8. Weinbaum, S., S. C. Cowin, and Y. Zeng. 1994. A model for the excitation of osteocytes by mechanical loading-induced bone fluid shear stresses. *Journal of Biomechanics* 27, 3:339–360.
9. Cowin, S. C., L. Moss-Salentijn, and M. L. Moss. 1991. Candidates for the mechanosensory system in bone. *Journal of Biomechanical Engineering* 113, 2:191–197.
10. Cowin, S. C., S. Weinbaum, and Y. Zeng. 1995. A case for bone canaliculi as the anatomical site of strain generated potentials. *Journal of Biomechanics* 28, 11:1281–1297.
11. Kleinnulend, J., R. Bacabac, and M. Mullender. 2005. Mechanobiology of bone tissue. *Pathologie Biologie* 53(10).
12. Mullender, M., A. J. El Haj, Y. Yang, M. A. van Duin, E. H. Burger, and J. Klein-Nulend. 2004. Mechanotransduction of bone cells in vitro: Mechanobiology of bone tissue. *Medical & Biological Engineering & Computing* 42, 1:14–21.
13. Yaszemski, M. J., R. G. Payne, W. C. Hayes, R. Langer, and A. G. Mikos. 1996. Evolution of bone transplantation: molecular, cellular and tissue strategies to engineer human bone. *Biomaterials* 17, 2:175–185.
14. Vaccaro, A. R., K. Chiba, J. G. Heller, T. C. Patel, J. S. Thalgott, E. Truumees, J. S. Fischgrund et al. 2002. Bone grafting alternatives in spinal surgery. *The Spine Journal.* 2, 3:206–215.
15. Sikavitsas, V. I., G. N. Bancroft, and A. G. Mikos. 2002. Formation of three-dimensional cell/polymer constructs for bone tissue engineering in a spinner flask and a rotating wall vessel bioreactor. *Journal of Biomedical Materials Research* 62, 1:136–148.
16. Schwarz, R. P., T. J. Goodwin, and D. A. Wolf. 1992. Cell culture for three-dimensional modeling in rotating-wall vessels: An application of simulated microgravity. *Journal of Tissue Culture Methods* 14, 2:51–57.
17. Botchwey, E. A., S. R. Pollack, E. M. Levine, and C. T. Laurencin. 2001. Bone tissue engineering in a rotating bioreactor using a microcarrier matrix system. *Journal of Biomedical Materials Research* 55, 2:242–253.
18. Goldstein, A. S., T. M. Juarez, C. D. Helmke, M. C. Gustin, and A. G. Mikos. 2001. Effect of convection on osteoblastic cell growth and function in biodegradable polymer foam scaffolds. *Biomaterials* 22, 11:1279–1288.
19. Yu, X., E. A. Botchwey, E. M. Levine, S. R. Pollack, and C. T. Laurencin. 2004. Bioreactor-based bone tissue engineering: The influence of dynamic flow on osteoblast phenotypic expression and matrix mineralization. *Proceedings of the National Academy of Sciences of the United States of America* 101, 31:11203–11208.
20. Bancroft, G. N., V. I. Sikavitsas, J. Van den Dolder, T. L. Sheffield, C. G. Ambrose, J. A. Jansen, and A. G. Mikos. 2002. Fluid flow increases mineralized matrix deposition in 3D perfusion culture of marrow stromal osteoblasts in a dose-dependent manner. *Proceedings of the National Academy of Sciences of the United States of America* 99, 20:12600–12605.
21. Vance, J., S. Galley, D. F. Liu, and S. W. Donahue. 2005. Mechanical stimulation of MC3T3 osteoblastic cells in a bone tissue-engineering bioreactor enhances prostaglandin E2 release. *Tissue Engineering* 11, 11–12:1832–1839.
22. Bakker, A. D., M. Joldersma, J. Klein-Nulend, and E. H. Burger. 2003. Interactive effects of PTH and mechanical stress on nitric oxide and PGE2 production by primary mouse osteoblastic cells. *American Journal of Physiology. Endocrinology and Metabolism* 285, 3:E608–E613.

23. Smalt, R., F. T. Mitchell, R. L. Howard, and T. J. Chambers. 1997. Induction of NO and prostaglandin E2 in osteoblasts by wall-shear stress but not mechanical strain. *American Journal of Physiology* 273, 4 Pt 1:E751–E758.
24. Ignatius, A., H. Blessing, A. Liedert, C. Schmidt, C. Neidlingerwilke, D. Kaspar, B. Friemert, and L. Claes. 2005. Tissue engineering of bone: Effects of mechanical strain on osteoblastic cells in type I collagen matrices. *Biomaterials* 26(3).
25. Sumanasinghe, R. D., S. H. Bernacki, and E. G. Loboa. 2006. Osteogenic differentiation of human mesenchymal stem cells in collagen matrices: Effect of uniaxial cyclic tensile strain on bone morphogenetic protein (BMP-2) mRNA expression. *Tissue Engineering* 12, 12:3459–3465.
26. Mauney, J. R., S. Sjostorm, J. Blumberg, R. Horan, J. P. O'Leary, G. Vunjak-Novakovic, V. Volloch, and D. L. Kaplan. 2004. Mechanical stimulation promotes osteogenic differentiation of human bone marrow stromal cells on 3-D partially demineralized bone scaffolds in vitro. *Calcified Tissue International* 74(5).
27. Zhu, W., V. C. Mow, T. J. Koob, and D. R. Eyre. 1993. Viscoelastic shear properties of articular cartilage and the effects of glycosidase treatments. *Journal of Orthopaedic Research* 11, 6: 771–781.
28. Afoke, N. Y., P. D. Byers, and W. C. Hutton. 1987. Contact pressures in the human hip joint. *The Journal of Bone and Joint Surgery. British Volume* 69, 4:536–541.
29. Armstrong, C. G., A. S. Bahrani, and D. L. Gardner. 1979. In vitro measurement of articular cartilage deformations in the intact human hip joint under load. *The Journal of Bone and Joint Surgery. American Volume* 61, 5:744–755.
30. Mow, V. C. and C. C. Wang. 1999. Some bioengineering considerations for tissue engineering of articular cartilage. *Clinical Orthopaedics and Related Research*, 367 Suppl:S204–S223.
31. von Eisenhart R., C. Adam, M. Steinlechner, M. Muller-Gerbl, and F. Eckstein. 1999. Quantitative determination of joint incongruity and pressure distribution during simulated gait and cartilage thickness in the human hip joint. *Journal of Orthopaedic Research* 17, 4:532–539.
32. Hodge, W. A., R. S. Fijan, K. L. Carlson, R. G. Burgess, W. H. Harris, and R. W. Mann. 1986. Contact pressures in the human hip joint measured in vivo. *Proceedings of the National Academy of Sciences of the United States of America* 83, 9:2879–2883.
33. Park, S., S. B. Nicoll, R. L. Mauck, and G. A. Ateshian. 2008. Cartilage mechanical response under dynamic compression at physiological stress levels following collagenase digestion. *Annals of Biomedical Engineering* 36, 3:425–434.
34. Ateshian, G. A. and H. Wang. 1995. A theoretical solution for the frictionless rolling contact of cylindrical biphasic articular cartilage layers. *Journal of Biomechanics* 28, 11:1341–1355.
35. Hayes, W. C. and L. F. Mockros. 1971. Viscoelastic properties of human articular cartilage. *Journal of Applied Physiology* 31, 4:562–568.
36. Simon, W. H., A. Mak, and A. Spirt. 1990. The effect of shear fatigue on bovine articular cartilage. *Journal of Orthopaedic Research* 8, 1:86–93.
37. Spirt, A. A., A. F. Mak, and R. P. Wassell. 1989. Nonlinear viscoelastic properties of articular-cartilage in shear. *Journal of Orthopaedic Research* 7, 1:43–49.
38. Hunziker, E. B. 1999. Biologic repair of articular cartilage. Defect models in experimental animals and matrix requirements. *Clinical Orthopaedics and Related Research*, 367 Suppl:S135–S146.
39. Bedi, A., B. T. Feeley, and R. J. Williams, III. 2010. Management of articular cartilage defects of the knee. *The Journal of Bone and Joint Surgery. American Volume* 92, 4:994–1009.
40. Hunziker, E. B. 2002. Articular cartilage repair: Basic science and clinical progress. A review of the current status and prospects. *Osteoarthritis Cartilage* 10, 6:432–463.
41. Marolt, D., A. Augst, L. E. Freed, C. Vepari, R. Fajardo, N. Patel, M. Gray et al. 2006. Bone and cartilage tissue constructs grown using human bone marrow stromal cells, silk scaffolds and rotating bioreactors. *Biomaterials* 27, 36:6138–6149.
42. Chao, P. H., S. Yodmuang, X. Wang, L. Sun, D. L. Kaplan, and G. Vunjak–Novakovic. 2010. Silk hydrogel for cartilage tissue engineering. *Journal of Biomedical Materials Research. Part B Applied Biomaterials* 95, 1:84–90.

43. Chikatsu, N., Y. Takeuchi, Y. Tamura, S. Fukumoto, K. Yano, E. Tsuda, E. Ogata, and T. Fujita. 2000. Interactions between cancer and bone marrow cells induce osteoclast differentiation factor expression and osteoclast-like cell formation in vitro. *Biochemical and Biophysical Research Communications* 267, 2:632–637.
44. Docheva, D., E. B. Hunziker, R. Fassler, and O. Brandau. 2005. Tenomodulin is necessary for tenocyte proliferation and tendon maturation. *Molecular and Cellular Biology* 25, 2:699–705.
45. Kuo, C. K. and R. S. Tuan. 2008. Mechanoactive tenogenic differentiation of human mesenchymal stem cells. *Tissue Engineering Part A.* 14, 10:1615–1627.
46. Mikos, A. G., G. Sarakinos, S. M. Leite, J. P. Vacanti, and R. Langer. 1993. Laminated three-dimensional biodegradable foams for use in tissue engineering. *Biomaterials* 14:323–330.
47. Murphy, W. L. and P. B. Messersmith. 2000. Compartmental control of mineral formation: Adaptation of a biomineralization strategy for biomedical use. *Polyhedron* 19, 3:357–363.
48. Roberts, J. J., G. D. Nicodemus, E. C. Greenwald, and S. J. Bryant. 2011. Degradation improves tissue formation in (un)loaded chondrocyte-laden hydrogels. *Clinical Orthopaedics and Related Research* 469, 10:2725–2734.
49. Schweitzer, R., J. H. Chyung, L. C. Murtaugh, A. E. Brent, V. Rosen, E. N. Olson, A. Lassar, and C. J. Tabin. 2001. Analysis of the tendon cell fate using Scleraxis, a specific marker for tendons and ligaments. *Development* 128, 19:3855–3866.
50. Buschmann, M. D., Y. A. Gluzband, A. J. Grodzinsky, and E. B. Hunziker. 1995. Mechanical compression modulates matrix biosynthesis in chondrocyte/agarose culture. *Journal of Cell Science* 108 (Pt 4):1497–1508.
51. Hunter, C. J. and M. E. Levenston. 2002. The influence of repair tissue maturation on the response to oscillatory compression in a cartilage defect repair model. *Biorheology* 39, 1–2:79–88.
52. Lee, C. R., A. J. Grodzinsky, and M. Spector. 2003. Biosynthetic response of passaged chondrocytes in a type II collagen scaffold to mechanical compression. *Journal of Biomedical Materials Research. Part A* 64, 3:560–569.
53. Ragan, P. M., V. I. Chin, H. H. Hung, K. Masuda, E. J. Thonar, E. C. Arner, A. J. Grodzinsky, and J. D. Sandy. 2000. Chondrocyte extracellular matrix synthesis and turnover are influenced by static compression in a new alginate disk culture system. *Archives of Biochemistry and Biophysics* 383, 2:256–264.
54. Mauck, R. L., M. A. Soltz, C. C. Wang, D. D. Wong, P. H. Chao, W. B. Valhmu, C. T. Hung, and G. A. Ateshian. 2000. Functional tissue engineering of articular cartilage through dynamic loading of chondrocyte-seeded agarose gels. *Journal of Biomechanical Engineering* 122, 3:252–260.
55. Seidel, J. O., M. Pei, M. L. Gray, R. Langer, L. E. Freed, and G. Vunjak-Novakovic. 2004. Long-term culture of tissue engineered cartilage in a perfused chamber with mechanical stimulation. *Biorheology* 41, 3–4:445–458.
56. Bryant, S. J., T. T. Chowdhury, D. A. Lee, D. L. Bader, and K. S. Anseth. 2004. Crosslinking density influences chondrocyte metabolism in dynamically loaded photocrosslinked poly(ethylene glycol) hydrogels. *Annals of Biomedical Engineering* 32, 3:407–417.
57. Hunter, C. 2004. Dynamic compression of chondrocyte-seeded fibrin gels: Effects on matrix accumulation and mechanical stiffness. *Osteoarthritis and Cartilage* 12(2).
58. Appelman, T. P., J. Mizrahi, J. H. Elisseeff, and D. Seliktar. 2009. The differential effect of scaffold composition and architecture on chondrocyte response to mechanical stimulation. *Biomaterials* 30(4).
59. Bryant, S. J., G. D. Nicodemus, and I. Villanueva. 2008. Designing 3D photopolymer hydrogels to regulate biomechanical cues and tissue growth for cartilage tissue engineering. *Pharmaceutical Research* 25(10).
60. Schmidt, O., J. Mizrahi, J. Elisseeff, and D. Seliktar. 2006. Immobilized fibrinogen in PEG hydrogels does not improve chondrocyte-mediated matrix deposition in response to mechanical stimulation. *Biotechnology and Bioengineering* 95, 6:1061–1069.
61. Villanueva, I., S. K. Gladem, J. Kessler, and S. J. Bryant. 2010. Dynamic loading stimulates chondrocyte biosynthesis when encapsulated in charged hydrogels prepared from poly(ethylene glycol) and chondroitin sulfate. *Matrix Biology* 29(1).

62. Waldman, S. D., C. G. Spiteri, M. D. Grynpas, R. M. Pilliar, and R. A. Kandel. 2004. Long-term intermittent compressive stimulation improves the composition and mechanical properties of tissue-engineered cartilage. *Tissue Engineering* 10, 9–10:1323–1331.
63. Mauck, R. L., S. L. Seyhan, G. A. Ateshian, and C. T. Hung. 2002. Influence of seeding density and dynamic deformational loading on the developing structure/function relationships of chondrocyte-seeded agarose hydrogels. *Annals of Biomedical Engineering* 30, 8:1046–1056.
64. Mauck, R. L., C. C. Wang, E. S. Oswald, G. A. Ateshian, and C. T. Hung. 2003. The role of cell seeding density and nutrient supply for articular cartilage tissue engineering with deformational loading. *Osteoarthritis and Cartilage* 11, 12:879–890.
65. Lee, D. A. and D. L. Bader. 1995. The development and characterization of an in vitro system to study strain-induced cell deformation in isolated chondrocytes. *In vitro Cellular & Developmental Biology. Animal* 31, 11:828–835.
66. Wiseman, M., D. L. Bader, T. Reisler, and D. A. Lee. 2004. Passage in monolayer influences the response of chondrocytes to dynamic compression. *Biorheology* 41, 3–4:283–298.
67. Bian, L., J. V. Fong, E. G. Lima, A. M. Stoker, G. A. Ateshian, J. L. Cook, and C. T. Hung. 2010. Dynamic mechanical loading enhances functional properties of tissue-engineered cartilage using mature canine chondrocytes. *Tissue Engineering Part A* 16, 5:1781–1790.
68. Angele, P., D. Schumann, M. Angele, B. Kinner, C. Englert, R. Hente, B. Fuchtmeier et al. 2004. Cyclic, mechanical compression enhances chondrogenesis of mesenchymal progenitor cells in tissue engineering scaffolds. *Biorheology* 41, 3–4:335–346.
69. Huang, A. H., M. J. Farrell, M. Kim, and R. L. Mauck. 2010. Long-term dynamic loading improves the mechanical properties of chondrogenic mesenchymal stem cell-laden hydrogel. *European Cells & Materials* 19:72–85.
70. Jung, Y., S. H. Kim, Y. H. Kim, and S. H. Kim. 2009. The effects of dynamic and three-dimensional environments on chondrogenic differentiation of bone marrow stromal cells. *Biomedical Materials* 4, 5:055009.
71. Jung, Y., S. H. Kim, Y. H. Kim, and S. H. Kim. 2009. The effects of dynamic and three-dimensional environments on chondrogenic differentiation of bone marrow stromal cells. *Biomedical Materials* 4, 5:055009.
72. Li, Z., S. J. Yao, M. Alini, and M. J. Stoddart. 2010. Chondrogenesis of human bone marrow mesenchymal stem cells in fibrin-polyurethane composites is modulated by frequency and amplitude of dynamic compression and shear stress. *Tissue Engineering Part A* 16, 2:575–584.
73. Mauck, R. L., B. A. Byers, X. Yuan, and R. S. Tuan. 2007. Regulation of cartilaginous ECM gene transcription by chondrocytes and MSCs in 3D culture in response to dynamic loading. *Biomechanics and Modeling in Mechanobiology* 6, 1–2:113–125.
74. McMahon, L. A., A. J. Reid, V. A. Campbell, and P. J. Prendergast. 2008. Regulatory effects of mechanical strain on the chondrogenic differentiation of MSCs in a collagen-GAG scaffold: Experimental and computational analysis. *Annals of Biomedical Engineering* 36, 2:185–194.
75. Mouw, J. K., J. T. Connelly, C. G. Wilson, K. E. Michael, and M. E. Levenston. 2007. Dynamic compression regulates the expression and synthesis of chondrocyte-specific matrix molecules in bone marrow stromal cells. *Stem Cells* 25, 3:655–663.
76. Terraciano, V., N. Hwang, L. Moroni, H. B. Park, Z. Zhang, J. Mizrahi, D. Seliktar, and J. Elisseeff. 2007. Differential response of adult and embryonic mesenchymal progenitor cells to mechanical compression in hydrogels. *Stem Cells* 25, 11:2730–2738.
77. Thorpe, S. D., C. T. Buckley, T. Vinardell, F. J. O'Brien, V. A. Campbell, and D. J. Kelly. 2010. The response of bone marrow–derived mesenchymal stem cells to dynamic compression following TGF-beta3 induced chondrogenic differentiation. *Annals of Biomedical Engineering* 38, 9:2896–2909.
78. Huang, C. Y., K. L. Hagar, L. E. Frost, Y. Sun, and H. S. Cheung. 2004. Effects of cyclic compressive loading on chondrogenesis of rabbit bone-marrow derived mesenchymal stem cells. *Stem Cells* 22, 3:313–323.
79. Kisiday, J. D., D. D. Frisbie, C. W. McIlwraith, and A. J. Grodzinsky. 2009. Dynamic compression stimulates proteoglycan synthesis by mesenchymal stem cells in the absence of chondrogenic cytokines. *Tissue Engineering Part A* 15, 10:2817–2824.

80. Haugh, M. G., E. G. Meyer, S. D. Thorpe, T. Vinardell, G. P. Duffy, and D. J. Kelly. 2011. Temporal and spatial changes in cartilage-matrix-specific gene expression in mesenchymal stem cells in response to dynamic compression. *Tissue Engineering Part A* 17, 23–24:3085–3093.
81. Schatti, O., S. Grad, J. Goldhahn, G. Salzmann, Z. Li, M. Alini, and M. J. Stoddart. 2011. A combination of shear and dynamic compression leads to mechanically induced chondrogenesis of human mesenchymal stem cells. *European Cells & Materials* 22:214–225.
82. Terraciano, V., N. Hwang, L. Moroni, H. B. Park, Z. Zhang, J. Mizrahi, D. Seliktar, and J. Elisseeff. 2007. Differential response of adult and embryonic mesenchymal progenitor cells to mechanical compression in hydrogels. *Stem Cells* 25, 11:2730–2738.
83. Ikenoue, T., M. C. Trindade, M. S. Lee, E. Y. Lin, D. J. Schurman, S. B. Goodman, and R. L. Smith. 2003. Mechanoregulation of human articular chondrocyte aggrecan and type II collagen expression by intermittent hydrostatic pressure in vitro. *Journal of Orthopaedic Research* 21, 1:110–116.
84. Jortikka, M. O., J. J. Parkkinen, R. I. Inkinen, J. Karner, H. T. Jarvelainen, L. O. Nelimarkka, M. I. Tammi, and M. J. Lammi. 2000. The role of microtubules in the regulation of proteoglycan synthesis in chondrocytes under hydrostatic pressure. *Archives of Biochemistry and Biophysics* 374, 2:172–180.
85. Smith, R. L., J. Lin, M. C. Trindade, J. Shida, G. Kajiyama, T. Vu, A. R. Hoffman et al. 2000. Time-dependent effects of intermittent hydrostatic pressure on articular chondrocyte type II collagen and aggrecan mRNA expression. *Journal of Rehabilitation Research and Development* 37, 2:153–161.
86. Smith, R. L., S. F. Rusk, B. E. Ellison, P. Wessells, K. Tsuchiya, D. R. Carter, W. E. Caler, L. J. Sandell, and D. J. Schurman. 1996. In vitro stimulation of articular chondrocyte mRNA and extracellular matrix synthesis by hydrostatic pressure. *Journal of Orthopaedic Research* 14, 1:53–60.
87. Suh, J. K., G. H. Baek, A. Aroen, C. M. Malin, C. Niyibizi, C. H. Evans, and A. Westerhausen-Larson. 1999. Intermittent sub-ambient interstitial hydrostatic pressure as a potential mechanical stimulator for chondrocyte metabolism. *Osteoarthritis and Cartilage* 7, 1:71–80.
88. Takahashi, K., T. Kubo, K. Kobayashi, J. Imanishi, M. Takigawa, Y. Arai, and Y. Hirasawa. 1997. Hydrostatic pressure influences mRNA expression of transforming growth factor-beta 1 and heat shock protein 70 in chondrocyte-like cell line. *Journal of Orthopaedic Research* 15, 1:150–158.
89. Hall, A. C., J. P. Urban, and K. A. Gehl. 1991. The effects of hydrostatic pressure on matrix synthesis in articular cartilage. *Journal of Orthopaedic Research* 9, 1:1–10.
90. Song, K., T. Liu, Z. Cui, X. Li, and X. Ma. 2008. Three-dimensional fabrication of engineered bone with human bio-derived bone scaffolds in a rotating wall vessel bioreactor. *Journal of Biomedical Materials Research. Part A* 86, 2:323–332.
91. Carver, S. E. and C. A. Heath. 1999. Increasing extracellular matrix production in regenerating cartilage with intermittent physiological pressure. *Biotechnology and Bioengineering* 62, 2:166–174.
92. Carver, S. E. and C. A. Heath. 1999. Semi-continuous perfusion system for delivering intermittent physiological pressure to regenerating cartilage. *Tissue Engineering* 5, 1:1–11.
93. De Maria, C., S. Giusti, D. Mazzei, A. Crawford, and A. Ahluwalia. 2011. Squeeze pressure bioreactor: A hydrodynamic bioreactor for noncontact stimulation of cartilage constructs. *Tissue Engineering. Part C, Methods* 17, 7:757–764.
94. Elder, B. D. and K. A. Athanasiou. 2009. Effects of temporal hydrostatic pressure on tissue-engineered bovine articular cartilage constructs. *Tissue Engineering Part A* 15, 5:1151–1158.
95. Elder, B. D. and K. A. Athanasiou. 2008. Synergistic and additive effects of hydrostatic pressure and growth factors on tissue formation. *PLoS One* 3, 6:e2341.
96. Hu, J. C. and K. A. Athanasiou. 2006. The effects of intermittent hydrostatic pressure on self-assembled articular cartilage constructs. *Tissue Engineering* 12, 5:1337–1344.
97. Kunitomo, T., K. A. Takahashi, Y. Arai, K. Sakao, K. Honjo, M. Saito, A. Inoue et al. 2009. Influence of extracellular matrix on the expression of inflammatory cytokines, proteases, and apoptosis-related genes induced by hydrostatic pressure in three-dimensionally cultured chondrocytes. *Journal of Orthopaedic Science* 14, 6:776–783.

98. Mizuno, S. and R. Ogawa. 2011. Using changes in hydrostatic and osmotic pressure to manipulate metabolic function in chondrocytes. *American Journal of Physiology. Cell Physiology* 300, 6:C1234–C1245.
99. Meyer, E. G., C. T. Buckley, A. J. Steward, and D. J. Kelly. 2011. The effect of cyclic hydrostatic pressure on the functional development of cartilaginous tissues engineered using bone marrow derived mesenchymal stem cells. *Journal of the Mechanical Behavior of Biomedical Materials* 4, 7:1257–1265.
100. Luo, Z. J. and B. B. Seedhom. 2007. Light and low-frequency pulsatile hydrostatic pressure enhances extracellular matrix formation by bone marrow mesenchymal cells: an in-vitro study with special reference to cartilage repair. *Proceedings of the Institution of Mechanical Engineers. Part H* 221, 5:499–507.
101. Angele, P., J. U. Yoo, C. Smith, J. Mansour, K. J. Jepsen, M. Nerlich, and B. Johnstone. 2003. Cyclic hydrostatic pressure enhances the chondrogenic phenotype of human mesenchymal progenitor cells differentiated in vitro. *Journal of Orthopaedic Research* 21, 3:451–457.
102. Ogawa, R., S. Mizuno, G. F. Murphy, and D. P. Orgill. 2009. The effect of hydrostatic pressure on three-dimensional chondroinduction of human adipose-derived stem cells. *Tissue Engineering Part A* 15, 10:2937–2945.
103. Wagner, D. R., D. P. Lindsey, K. W. Li, P. Tummala, S. E. Chandran, R. L. Smith, M. T. Longaker, D. R. Carter, and G. S. Beaupre. 2008. Hydrostatic pressure enhances chondrogenic differentiation of human bone marrow stromal cells in osteochondrogenic medium. *Annals of Biomedical Engineering* 36, 5:813–820.
104. Finger, A. R., C. Y. Sargent, K. O. Dulaney, S. H. Bernacki, and E. G. Loboa. 2007. Differential effects on messenger ribonucleic acid expression by bone marrow–derived human mesenchymal stem cells seeded in agarose constructs due to ramped and steady applications of cyclic hydrostatic pressure. *Tissue Engineering* 13, 6:1151–1158.
105. Miyanishi, K., M. C. Trindade, D. P. Lindsey, G. S. Beaupre, D. R. Carter, S. B. Goodman, D. J. Schurman, and R. L. Smith. 2006. Dose- and time-dependent effects of cyclic hydrostatic pressure on transforming growth factor-beta3–induced chondrogenesis by adult human mesenchymal stem cells in vitro. *Tissue Engineering* 12, 8:2253–2262.
106. Miyanishi, K., M. C. Trindade, D. P. Lindsey, G. S. Beaupre, D. R. Carter, S. B. Goodman, D. J. Schurman, and R. L. Smith. 2006. Effects of hydrostatic pressure and transforming growth factor-beta 3 on adult human mesenchymal stem cell chondrogenesis in vitro. *Tissue Engineering* 12, 6:1419–1428.
107. Waldman, S. D., C. G. Spiteri, M. D. Grynpas, R. M. Pilliar, and R. A. Kandel. 2003. Long-term intermittent shear deformation improves the quality of cartilaginous tissue formed in vitro. *Journal of Orthopaedic Research* 21, 4:590–596.
108. Gemmiti, C. V. and R. E. Guldberg. 2009. Shear stress magnitude and duration modulates matrix composition and tensile mechanical properties in engineered cartilaginous tissue. *Biotechnology and Bioengineering* 104, 4:809–820.
109. Waldman, S. D., D. C. Couto, M. D. Grynpas, R. M. Pilliar, and R. A. Kandel. 2007. Multiaxial mechanical stimulation of tissue engineered cartilage: Review. *European Cells & Materials* 13:66–73.
110. Grad, S., C. R. Lee, K. Gorna, S. Gogolewski, M. A. Wimmer, and M. Alini. 2005. Surface motion upregulates superficial zone protein and hyaluronan production in chondrocyte-seeded three-dimensional scaffolds. *Tissue Engineering* 11, 1–2:249–256.
111. Wimmer, M. A., S. Grad, T. Kaup, M. Hanni, E. Schneider, S. Gogolewski, and M. Alini. 2004. Tribology approach to the engineering and study of articular cartilage. *Tissue Engineering* 10, 9–10:1436–1445.
112. Stoddart, M. J., L. Ettinger, and H. J. Häuselmann. 2006. Enhanced matrix synthesis in de novo, scaffold free cartilage-like tissue subjected to compression and shear. *Biotechnology and Bioengineering* 95(6).
113. Schulz, R. M., and A. Bader. 2007. Cartilage tissue engineering and bioreactor systems for the cultivation and stimulation of chondrocytes. *European Biophysics Journal* 36(4–5).

114. Woo, S., K. An, and C. B. Frank. 2000. Anatomy, biology, and biomechanics of tendon and ligament. In *Orthopaedic Basic Science*, edited by Buckwalter, J. A., Einhorn T. A., and Simon S. R., 581–616. Rosemont, IL: American Academy of Orthopaedic Surgery.
115. Gotlin, R. S. and G. Huie. 2000. Anterior cruciate ligament injuries. Operative and rehabilitative options. *Physical Medicine and Rehabilitation Clinics of North America* 11, 4:895–928.
116. Altman, G. H., R. L. Horan, H. H. Lu, J. Moreau, I. Martin, J. C. Richmond, and D. L. Kaplan. 2002. Silk matrix for tissue engineered anterior cruciate ligaments. *Biomaterials* 23, 20:4131–4141.
117. Moffat, K. L., A. S. Kwei, J. P. Spalazzi, S. B. Doty, W. N. Levine, and H. H. Lu. 2009. Novel nanofiber-based scaffold for rotator cuff repair and augmentation. *Tissue Engineering Part A* 15, 1:115–126.
118. Wang, J. H. 2006. Mechanobiology of tendon. *Journal of Biomechanics.* 39, 9:1563–1582.
119. Vunjak-Novakovic, G., G. Altman, R. Horan, and D. L. Kaplan. 2004. Tissue engineering of ligaments. *Annual Review of Biomedical Engineering* 6:131–156.
120. Komi, P. V., S. Fukashiro, and M. Jarvinen. 1992. Biomechanical loading of Achilles tendon during normal locomotion. *Clinics in Sports Medicine* 11, 3:521–531.
121. Korvick, D. L., J. F. Cummings, E. S. Grood, J. P. Holden, S. M. Feder, and D. L. Butler. 1996. The use of an implantable force transducer to measure patellar tendon forces in goats. *Journal of Biomechanics* 29, 4:557–561.
122. Sakane, M., R. J. Fox, S. L. Woo, G. A. Livesay, G. Li, and F. H. Fu. 1997. In situ forces in the anterior cruciate ligament and its bundles in response to anterior tibial loads. *Journal of Orthopaedic Research* 15, 2:285–293.
123. Andriacchi, T. P. and A. Mündermann. 2006. The role of ambulatory mechanics in the initiation and progression of knee osteoarthritis. *Current Opinion in Rheumatology* 18, 5.
124. Almekinders, L. C., A. J. Banes, and C. A. Ballenger. 1993. Effects of repetitive motion on human fibroblasts. *Medicine and Science in Sports and Exercise* 25, 5:603–607.
125. Banes, A. J., G. Horesovsky, C. Larson, M. Tsuzaki, S. Judex, J. Archambault, R. Zernicke et al. 1999. Mechanical load stimulates expression of novel genes in vivo and in vitro in avian flexor tendon cells. *Osteoarthritis and Cartilage* 7, 1:141–153.
126. Banes, A. J., M. Tsuzaki, P. Hu, B. Brigman, T. Brown, L. Almekinders, W. T. Lawrence, and T. Fischer. 1995. PDGF-BB, IGF-I and mechanical load stimulate DNA synthesis in avian tendon fibroblasts in vitro. *Journal of Biomechanics* 28, 12:1505–1513.
127. Hsieh, A. H., C. M. Tsai, Q. J. Ma, T. Lin, A. J. Banes, F. J. Villarreal, W. H. Akeson, and K. L. Sung. 2000. Time-dependent increases in type-III collagen gene expression in medical collateral ligament fibroblasts under cyclic strains. *Journal of Orthopaedic Research* 18, 2:220–227.
128. Lee, D. A., S. P. Frean, P. Lees, and D. L. Bader. 1998. Dynamic mechanical compression influences nitric oxide production by articular chondrocytes seeded in agarose. *Biochemical and Biophysical Research Communications* 251, 2:580–585.
129. Hannafin, J. A., S. P. Arnoczky, A. Hoonjan, and P. A. Torzilli. 1995. Effect of stress deprivation and cyclic tensile loading on the material and morphologic properties of canine flexor digitorum profundus tendon: An in vitro study. *Journal of Orthopaedic Research* 13, 6:907–914.
130. Cao, D., W. Liu, X. Wei, F. Xu, L. Cui, and Y. Cao. 2006. In vitro tendon engineering with avian tenocytes and polyglycolic acids: A preliminary report. *Tissue Engineering* 12, 5:1369–1377.
131. van Eijk, F., D. B. F. Saris, L. B. Creemers, J. Riesle, W. Jaap Willems, C. A. van Blitterswijk, A. J. Verbout, and W. J. A. Dhert. 2008. The effect of timing of mechanical stimulation on proliferation and differentiation of goat bone marrow stem cells cultured on braided PLGA scaffolds. *Tissue Engineering Part A* 14(8).
132. Garvin, J., J. Qi, M. Maloney, and A. J. Banes. 2003. Novel system for engineering bioartificial tendons and application of mechanical load. *Tissue Engineering* 9, 5:967–979.
133. Webb, K., R. W. Hitchcock, R. M. Smeal, W. Li, S. D. Gray, and P. A. Tresco. 2006. Cyclic strain increases fibroblast proliferation, matrix accumulation, and elastic modulus of fibroblast-seeded polyurethane constructs. *Journal of Biomechanics* 39(6).
134. Joshi, S. D. and K. Webb. 2008. Variation of cyclic strain parameters regulates development of elastic modulus in fibroblast/substrate constructs. *Journal of Orthopaedic Research* 26(8).

135. Saber, S., A. Y. Zhang, S. H. Ki, D. P. Lindsey, R. L. Smith, J. Riboh, H. Pham, and J. Chang. 2010. Flexor tendon tissue engineering: Bioreactor cyclic strain increases construct strength. *Tissue Engineering Part A* 16, 6:2085–2090.
136. Woon, C. Y. L., A. Kraus, S. S. Raghavan, B. C. Pridgen, K. Megerle, H. Pham, and J. Chang. 2011. Three-dimensional-construct bioreactor conditioning in human tendon tissue engineering. *Tissue Engineering. Part A* 17(19–20).
137. Juncosa-Melvin, N., J. T. Shearn, G. P. Boivin, C. Gooch, M. T. Galloway, J. R. West, V. S. Nirmalanandhan, G. Bradica, and D. L. Butler. 2006. Effects of mechanical stimulation on the biomechanics and histology of stem cell–collagen sponge constructs for rabbit patellar tendon repair. *Tissue Engineering* 12, 8:2291–2300.
138. Juncosa-Melvin, N., K. S. Matlin, R. W. Holdcraft, V. S. Nirmalanandhan, and D. L. Butler. 2007. Mechanical stimulation increases collagen type I and collagen type III gene expression of stem cell–collagen sponge constructs for patellar tendon repair. *Tissue Engineering* 13, 6:1219–1226.
139. Nirmalanandhan, V. S., M. R. Dressler, J. T. Shearn, N. Juncosa-Melvin, M. Rao, C. Gooch, G. Bradica, and D. L. Butler. 2007. Mechanical stimulation of tissue engineered tendon constructs: Effect of scaffold materials. *Journal of Biomechanical Engineering* 129(6).
140. Nirmalanandhan, V. S., J. T. Shearn, N. Juncosa-Melvin, M. Rao, C. Gooch, A. Jain, G. Bradica, and D. L. Butler. 2008. Improving linear stiffness of the cell-seeded collagen sponge constructs by varying the components of the mechanical stimulus. *Tissue Engineering Part A* 14(11).
141. Nirmalanandhan, V. S., N. Juncosa-Melvin, J. T. Shearn, G. P. Boivin, M. T. Galloway, C. Gooch, G. Bradica, and D. L. Butler. 2009. Combined effects of scaffold stiffening and mechanical preconditioning cycles on construct biomechanics, gene expression, and tendon repair biomechanics. *Tissue Engineering Part A* 15, 8:2103–2111.
142. Subramony, S. D., B. R. Dargis, M. Castillo, E. U. Azeloglu, M. S. Tracey, A. Su, and H. H. Lu. 2012. Effect of Nanofiber Alignment and Mechanical Loading on hMSC Differentiation. Paper presented at *International Symposium on Ligaments & Tendons XII*, 3 2012, at San Francisco, CA.
143. Angelidis, I. K., J. Thorfinn, I. D. Connolly, D. Lindsey, H. M. Pham, and J. Chang. 2010. Tissue engineering of flexor tendons: The effect of a tissue bioreactor on adipoderived stem cell–seeded and fibroblast-seeded tendon constructs. *The Journal of Hand Surgery* 35(9).
144. Abousleiman, R. I., Y. Reyes, P. McFetridge, and V. Sikavitsas. 2009. Tendon tissue engineering using cell-seeded umbilical veins cultured in a mechanical stimulator. *Tissue Engineering Part A* 15, 4:787–795.
145. Issa, R. I., B. Engebretson, L. Rustom, P. S. McFetridge, and V. I. Sikavitsas. 2011. The effect of cell seeding density on the cellular and mechanical properties of a mechanostimulated tissue-engineered tendon. *Tissue Engineering Part A* 17(11–12).
146. Scaglione, S., B. Zerega, R. Badano, U. Benatti, M. Fato, and R. Quarto. 2010. A three-dimensional traction/torsion bioreactor system for tissue engineering. *The International Journal of Artificial Organs* 33, 6:362–369.
147. Sawaguchi, N., T. Majima, T. Funakoshi, K. Shimode, K. Harada, A. Minami, and S.-I. Nishimura. 2010. Effect of cyclic three-dimensional strain on cell proliferation and collagen synthesis of fibroblast-seeded chitosan-hyaluronan hybrid polymer fiber. *Journal of Orthopaedic Science* 15(4).
148. Altman, G. H., R. L. Horan, I. Martin, J. Farhadi, P. R. Stark, V. Volloch, J. C. Richmond, G. Vunjak-Novakovic, and D. L. Kaplan. 2002. Cell differentiation by mechanical stress. *FASEB Journal* 16, 2:270–272.
149. Chen, J., R. L. Horan, D. Bramono, J. E. Moreau, Y. Wang, L. R. Geuss, A. L. Collette, V. Volloch, and G. H. Altman. 2006. Monitoring mesenchymal stromal cell developmental stage to apply on-time mechanical stimulation for ligament tissue engineering. *Tissue Engineering* 12, 11:3085–3095.
150. Moreau, J. E., D. S. Bramono, R. L. Horan, D. L. Kaplan, and G. H. Altman. 2008. Sequential biochemical and mechanical stimulation in the development of tissue-engineered ligaments. *Tissue Engineering Part A.* 14, 7:1161–1172.
151. Spalazzi, J. P., M. C. Vyner, M. T. Jacobs, K. L. Moffat, and H. H. Lu. 2008. Mechanoactive scaffold induces tendon remodeling and expression of fibrocartilage markers. *Clinical Orthopaedics and Related Research* 466, 8:1938–1948.

152. Neidlinger-Wilke, C., K. Wurtz, A. Liedert, C. Schmidt, W. Borm, A. Ignatius, H. J. Wilke, and L. Claes. 2005. A three-dimensional collagen matrix as a suitable culture system for the comparison of cyclic strain and hydrostatic pressure effects on intervertebral disc cells. *Journal of Neurosurgery. Spine* 2, 4:457–465.
153. Reza, A. T. and S. B. Nicoll. 2007. Hydrostatic pressure differentially regulates outer and inner annulus fibrosus cell matrix production in 3D scaffolds. *Annals of Biomedical Engineering* 36(2).
154. Chang, G., H. J. Kim, G. Vunjak-Novakovic, D. L. Kaplan, and R. Kandel. 2010. Enhancing annulus fibrosus tissue formation in porous silk scaffolds. *Journal of Biomedical Materials Research. Part A* 92, 1:43–51.
155. Spalazzi, J. P., J. Gallina, S. D. Fung-Kee-Fung, E. E. Konofagou, H. H. Lu. 2006. Elastographic imaging of strain distribution in the anterior cruciate ligament and at the ligament-bone insertions. *Journal of Orthopaedic Research* 24, 10:2001–2010.
156. Zhang, X., D. Bogdanowicz, C. Erisken, N. M. Lee, and H. H. Lu. 2012. Biomimetic scaffold design for functional and integrative tendon repair. *Journal of Shoulder and Elbow Surgery* 21, 2:266–277.
157. Thomopoulos, S., R. Das, V. Birman, L. Smith, K. Ku, E. L. Elson, K. M. Pryse, J. P. Marquez, and G. M. Genin. 2011. Fibrocartilage tissue engineering: The role of the stress environment on cell morphology and matrix expression. *Tissue Engineering Part A* 17, 7–8:1039–1053.
158. Aufderheide, A. C. and K. A. Athanasiou. 2005. Comparison of scaffolds and culture conditions for tissue engineering of the knee meniscus. *Tissue Engineering* 11, 7–8:1095–1104.
159. Marsano, A., D. Wendt, T. M. Quinn, T. J. Sims, J. Farhadi, M. Jakob, M. Heberer, and I. Martin. 2006. Bi-zonal cartilaginous tissues engineered in a rotary cell culture system. *Biorheology* 43, 3–4:553–560.
160. Baker, B. M., R. P. Shah, A. H. Huang, and R. L. Mauck. 2011. Dynamic tensile loading improves the functional properties of mesenchymal stem cell–laden nanofiber-based fibrocartilage. *Tissue Engineering Part A* 17, 9–10:1445–1455.
161. Qiu, Q. Q., P. Ducheyne, and P. S. Ayyaswamy. 1999. Fabrication, characterization and evaluation of bioceramic hollow microspheres used as microcarriers for 3-D bone tissue formation in rotating bioreactors. *Biomaterials* 20, 11:989–1001.
162. Rucci, N., S. Migliaccio, B. M. Zani, A. Taranta, and A. Teti. 2002. Characterization of the osteoblast-like cell phenotype under microgravity conditions in the NASA-approved rotating wall vessel bioreactor (RWV). *Journal of Cellular Biochemistry* 85, 1:167–179.
163. Song, K., Z. Yang, T. Liu, W. Zhi, X. Li, L. Deng, Z. Cui, and X. Ma. 2006. Fabrication and detection of tissue-engineered bones with bio-derived scaffolds in a rotating bioreactor. *Biotechnology and Applied Biochemistry* 45, Pt 2:65–74.
164. Cartmell, S. H., B. D. Porter, A. J. Garcia, and R. E. Guldberg. 2003. Effects of medium perfusion rate on cell-seeded three-dimensional bone constructs in vitro. *Tissue Engineering* 9, 6:1197–1203.
165. Frohlich, M., W. L. Grayson, D. Marolt, J. M. Gimble, N. Kregar-Velikonja, and G. Vunjak-Novakovic. 2010. Bone grafts engineered from human adipose-derived stem cells in perfusion bioreactor culture. *Tissue Engineering Part A* 16, 1:179–189.
166. Glowacki, J., S. Mizuno, and J. S. Greenberger. 1998. Perfusion enhances functions of bone marrow stromal cells in three-dimensional culture. *Cell Transplantation* 7, 3:319–326.
167. Gomes, M. E., C. M. Bossano, C. M. Johnston, R. L. Reis, and A. G. Mikos. 2006. In vitro localization of bone growth factors in constructs of biodegradable scaffolds seeded with marrow stromal cells and cultured in a flow perfusion bioreactor. *Tissue Engineering* 12, 1:177–188.
168. Grayson, W. L., S. Bhumiratana, C. Cannizzaro, P. H. Chao, D. P. Lennon, A. I. Caplan, G. Vunjak-Novakovic. 2008. Effects of initial seeding density and fluid perfusion rate on formation of tissue-engineered bone. *Tissue Engineering Part A* 14, 11:1809–1820.
169. Grayson, W. L., D. Marolt, S. Bhumiratana, M. Frohlich, X. E. Guo, and G. Vunjak-Novakovic. 2011. Optimizing the medium perfusion rate in bone tissue engineering bioreactors. *Biotechnology and Bioengineering* 108, 5:1159–1170.

170. Holtorf, H. L., J. A. Jansen, and A. G. Mikos. 2005. Flow perfusion culture induces the osteoblastic differentiation of marrow stroma cell–scaffold constructs in the absence of dexamethasone. *Journal of Biomedical Materials Research. Part A* 72, 3:326–334.
171. Holtorf, H. L., T. L. Sheffield, C. G. Ambrose, J. A. Jansen, and A. G. Mikos. 2005. Flow perfusion culture of marrow stromal cells seeded on porous biphasic calcium phosphate ceramics. *Annals of Biomedical Engineering* 33, 9:1238–1248.
172. Janssen, F. W., J. Oostra, A. Oorschot, and C. A. van Blitterswijk. 2006. A perfusion bioreactor system capable of producing clinically relevant volumes of tissue-engineered bone: In vivo bone formation showing proof of concept. *Biomaterials* 27, 3:315–323.
173. Meinel, L., V. Karageorgiou, R. Fajardo, B. Snyder, V. Shinde-Patil, L. Zichner, D. Kaplan, R. Langer, and G. Vunjak-Novakovic. 2004. Bone tissue engineering using human mesenchymal stem cells: Effects of scaffold material and medium flow. *Annals of Biomedical Engineering* 32, 1:112–122.
174. Sikavitsas, V. I., G. N. Bancroft, H. L. Holtorf, J. A. Jansen, and A. G. Mikos. 2003. Mineralized matrix deposition by marrow stromal osteoblasts in 3D perfusion culture increases with increasing fluid shear forces. *Proceedings of the National Academy of Sciences of the United States of America* 100, 25:14683–14688.
175. Sikavitsas, V. I., G. N. Bancroft, J. J. Lemoine, M. A. Liebschner, M. Dauner, and A. G. Mikos. 2005. Flow perfusion enhances the calcified matrix deposition of marrow stromal cells in biodegradable nonwoven fiber mesh scaffolds. *Annals of Biomedical Engineering* 33, 1:63–70.
176. Terai, H., D. Hannouche, E. Ochoa, Y. Yamano, and J. P. Vacanti. 2002. In vitro engineering of bone using a rotational oxygen-permeable bioreactor system. *Materials Science Engineering* 20:3–8.
177. Wang, Y., T. Uemura, J. Dong, H. Kojima, J. Tanaka, and T. Tateishi. 2003. Application of perfusion culture system improves in vitro and in vivo osteogenesis of bone marrow-derived osteoblastic cells in porous ceramic materials. *Tissue Engineering* 9, 6:1205–1214.
178. Ignatius, A., H. Blessing, A. Liedert, C. Schmidt, C. Neidlinger-Wilke, D. Kaspar, B. Friemert, and L. Claes. 2005. Tissue engineering of bone: effects of mechanical strain on osteoblastic cells in type I collagen matrices. *Biomaterials* 26, 3:311–318.
179. Appelman, T. P., J. Mizrahi, J. H. Elisseeff, and D. Seliktar. 2011. The influence of biological motifs and dynamic mechanical stimulation in hydrogel scaffold systems on the phenotype of chondrocytes. *Biomaterials* 32(6).
180. Bryant, S. J., K. S. Anseth, D. A. Lee, and D. L. Bader. 2004. Crosslinking density influences the morphology of chondrocytes photoencapsulated in PEG hydrogels during the application of compressive strain. *Journal of Orthopaedic Research* 22, 5:1143–1149.
181. Cassino, T. R., R. Anderson, B. J. Love, W. R. Huckle, D. K. Seamans, and K. Forsten-Williams. 2007. Design and application of an oscillatory compression device for cell constructs. *Biotechnology and Bioengineering* 98(1).
182. Chowdhury, T. 2003. Temporal regulation of chondrocyte metabolism in agarose constructs subjected to dynamic compression. *Archives of Biochemistry and Biophysics* 417(1).
183. Chowdhury, T. T., D. M. Salter, D. L. Bader, and D. A. Lee. 2004. Integrin-mediated mechanotransduction processes in TGFβ-stimulated monolayer-expanded chondrocytes. *Biochemical and Biophysical Research Communications* 318(4).
184. Demarteau, O., D. Wendt, A. Braccini, M. Jakob, D. Schafer, M. Heberer, and I. Martin. 2003. Dynamic compression of cartilage constructs engineered from expanded human articular chondrocytes. *Biochemical and Biophysical Research Communications* 310, 2:580–588.
185. El-Ayoubi, R., C. DeGrandpre, R. DiRaddo, A. M. Yousefi, and P. Lavigne. 2009. Design and dynamic culture of 3D-scaffolds for cartilage tissue engineering. *Journal of Biomaterials Applications* 25(5).
186. Fehrenbacher, A., E. Steck, W. Roth, A. Pahmeier, and W. Richter. 2006. Long-term mechanical loading of chondrocyte-chitosan biocomposites in vitro enhanced their proteoglycan and collagen content. *Biorheology* 43, 6:709–720.
187. Kelly, T. A., C. C. Wang, R. L. Mauck, G. A. Ateshian, and C. T. Hung. 2004. Role of cell-associated matrix in the development of free-swelling and dynamically loaded chondrocyte-seeded agarose gels. *Biorheology* 41, 3–4:223–237.

188. Kelly, T-A. N., K. W. Ng, C. C. B. Wang, G. A. Ateshian, and C. T. Hung. 2006. Spatial and temporal development of chondrocyte-seeded agarose constructs in free-swelling and dynamically loaded cultures. *Journal of Biomechanics* 39(8).
189. Kisiday, J. D., M. Jin, M. A. DiMicco, B. Kurz, and A. J. Grodzinsky. 2004. Effects of dynamic compressive loading on chondrocyte biosynthesis in self-assembling peptide scaffolds. *Journal of Biomechanics* 37(5).
190. Kisiday, J. D., J. H. Lee, P. N. Siparsky, D. D. Frisbie, C. R. Flannery, J. D. Sandy, and A. J. Grodzinsky. 2009. Catabolic responses of chondrocyte-seeded peptide hydrogel to dynamic compression. *Annals of Biomedical Engineering* 37(7).
191. Knight, M. M., D. A. Lee, and D. L. Bader. 1998. The influence of elaborated pericellular matrix on the deformation of isolated articular chondrocytes cultured in agarose. *Biochimica et Biophysica Acta* 1405, 1–3:67–77.
192. Knight, M. M., S. A. Ghori, D. A. Lee, and D. L. Bader. 1998. Measurement of the deformation of isolated chondrocytes in agarose subjected to cyclic compression. *Medical Engineering & Physics* 20, 9:684–688.
193. Kock, L. M., R. M. Schulz, C. C. van Donkelaar, C. B. Thümmler, A. Bader, and K. Ito. 2009. RGD-dependent integrins are mechanotransducers in dynamically compressed tissue-engineered cartilage constructs. *Journal of Biomechanics* 42(13).
194. Lee, C. R., S. Grad, K. Gorna, S. Gogolewski, A. Goessl, and M. Alini. 2005. Fibrin-polyurethane composites for articular cartilage tissue engineering: A preliminary analysis. *Tissue Engineering* 11, 9–10:1562–1573.
195. Lee, D. A. and D. L. Bader. 1997. Compressive strains at physiological frequencies influence the metabolism of chondrocytes seeded in agarose. *Journal of Orthopaedic Research* 15, 2:181–188.
196. Lee, D. A., T. Noguchi, M. M. Knight, L. O'Donnell, G. Bentley, and D. L. Bader. 1998. Response of chondrocyte subpopulations cultured within unloaded and loaded agarose. *Journal of Orthopaedic Research* 16, 6:726–733.
197. Lima, E. G., L. Bian, K. W. Ng, R. L. Mauck, B. A. Byers, R. S. Tuan, G. A. Ateshian, and C. T. Hung. 2007. The beneficial effect of delayed compressive loading on tissue-engineered cartilage constructs cultured with TGF-beta3. *Osteoarthritis Cartilage* 15, 9:1025–1033.
198. Mauck, R. L., S. B. Nicoll, S. L. Seyhan, G. A. Ateshian, and C. T. Hung. 2003. Synergistic action of growth factors and dynamic loading for articular cartilage tissue engineering. *Tissue Engineering* 9, 4:597–611.
199. Ng, K. W., R. L. Mauck, L. Y. Statman, E. Y. Lin, G. A. Ateshian, and C. T. Hung. 2006. Dynamic deformational loading results in selective application of mechanical stimulation in a layered, tissue-engineered cartilage construct. *Biorheology* 43, 3–4:497–507.
200. Ng, K. W., R. L. Mauck, C. C. B. Wang, T.-A. N. Kelly, M. M. Y. Ho, F. H. Chen, G. A. Ateshian, and C. T. Hung. 2009. Duty cycle of deformational loading influences the growth of engineered articular cartilage. *Cellular and Molecular Bioengineering* 2(3).
201. Roberts, J. J., G. D. Nicodemus, S. Giunta, and S. J. Bryant. 2011. Incorporation of biomimetic matrix molecules in PEG hydrogels enhances matrix deposition and reduces load-induced loss of chondrocyte-secreted matrix. *Journal of Biomedical Materials Research. Part A* 97A(3).
202. Stojkovska, J., B. Bugarski, and B. Obradovic. 2010. Evaluation of alginate hydrogels under in vivo–like bioreactor conditions for cartilage tissue engineering. *Journal of Materials Science: Materials in Medicine* 21(10).
203. Waldman, S., D. Couto, M. Grynpas, R. Pilliar, and R. Kandel. 2006. A single application of cyclic loading can accelerate matrix deposition and enhance the properties of tissue-engineered cartilage. *Osteoarthritis and Cartilage* 14(4).
204. Wang, P. Y., H. H. Chow, W. B. Tsai, and H. W. Fang. 2009. Modulation of gene expression of rabbit chondrocytes by dynamic compression in polyurethane scaffolds with collagen gel encapsulation. *Journal of Biomaterials Applications* 23, 4:347–366.
205. Wernike, E., Z. Li, M. Alini, and S. Grad. 2007. Effect of reduced oxygen tension and long-term mechanical stimulation on chondrocyte–polymer constructs. *Cell and Tissue Research* 331(2).

206. Xie, J., Z. Han, S. H. Kim, Y. H. Kim, and T. Matsuda. 2007. Mechanical loading-dependence of mRNA expressions of extracellular matrices of chondrocytes inoculated into elastomeric microporous poly(L-lactide-*co*-e-caprolactone) scaffold. *Tissue Engineering* 13(1).
207. Bian, L., D. Y. Zhai, E. C. Zhang, R. L. Mauck, and J. A. Burdick. 2012. Dynamic compressive loading enhances cartilage matrix synthesis and distribution and suppresses hypertrophy in hMSC-laden hyaluronic acid hydrogels. *Tissue Engineering Part A* 18, 7–8:715–724.
208. Huang, C. Y., P. M. Reuben, and H. S. Cheung. 2005. Temporal expression patterns and corresponding protein inductions of early responsive genes in rabbit bone marrow–derived mesenchymal stem cells under cyclic compressive loading. *Stem Cells* 23, 8:1113–1121.
209. Mauck, R. L., B. A. Byers, X. Yuan, and R. S. Tuan. 2007. Regulation of cartilaginous ECM gene transcription by chondrocytes and MSCs in 3D culture in response to dynamic loading. *Biomechanics and Modeling in Mechanobiology* 6, 1–2:113–125.
210. Meyer, E. G., C. T. Buckley, S. D. Thorpe, and D. J. Kelly. 2010. Low oxygen tension is a more potent promoter of chondrogenic differentiation than dynamic compression. *Journal of Biomechanics* 43, 13:2516–2523.
211. Pelaez, D., C. Y. Huang, and H. S. Cheung. 2009. Cyclic compression maintains viability and induces chondrogenesis of human mesenchymal stem cells in fibrin gel scaffolds. *Stem Cells and Development* 18, 1:93–102.
212. Cooper, J. A., W.-J. Li, L. A. O. Bailey, S. D. Hudson, S.-L. Gibson, K. S. Anseth, R. S. Tuan, and N. R. Washburn. 2007. Encapsulated chondrocyte response in a pulsatile flow bioreactor. *Acta Biomaterialia* 3(1).
213. Gemmiti, C. V. and R. E. Guldberg. 2009. Shear stress magnitude and duration modulates matrix composition and tensile mechanical properties in engineered cartilaginous tissue. *Biotechnology and Bioengineering* 104, 4:809–820.
214. Gemmiti, C. V. and R. E. Guldberg. 2006. Fluid flow increases type II collagen deposition and tensile mechanical properties in bioreactor-grown tissue-engineered cartilage. *Tissue Engineering* 12, 3:469–479.
215. Leininger, R. I., and D. M. Bigg. 1998. Polymers. In *Handbook of Biomaterials Evaluation: Scientific, Technical, and Clinical Testing of Implant Materials*, edited by Von Recum, A. F., 24–37. New York: Macmillan Publishing Company.
216. Deng, D., W. Liu, F. Xu, Y. Yang, G. Zhou, W. J. Zhang, L. Cui, and Y. Cao. 2009. Engineering human neo-tendon tissue in vitro with human dermal fibroblasts under static mechanical strain. *Biomaterials* 30(35).
217. Barber, J. G., A. M. Handorf, T. J. Allee, and W. J. Li. 2011. Braided nanofibrous scaffold for tendon and ligament tissue engineering. *Tissue Engineering Part A*.
218. Chokalingam, K., N. Juncosa-Melvin, S. A. Hunter, C. Gooch, C. Frede, J. Florert, G. Bradica, R. Wenstrup, and D. L. Butler. 2009. Tensile stimulation of murine stem cell-collagen sponge constructs increases collagen type I gene expression and linear stiffness. *Tissue Engineering Part A* 15, 9:2561–2570.
219. Doroski, D. M., M. E. Levenston, and J. S. Temenoff. 2010. Cyclic tensile culture promotes fibroblastic differentiation of marrow stromal cells encapsulated in poly(ethylene glycol)-based hydrogels. *Tissue Engineering. Part A* 16(11).
220. Farng, E., A. R. Urdaneta, D. Barba, S. Esmende, and D. R. McAllister. 2008. The effects of GDF-5 and uniaxial strain on mesenchymal stem cells in 3-D culture. *Clinical Orthopaedics and Related Research* 466(8).
221. Juncosa-Melvin, N., K. S. Matlin, R. W. Holdcraft, V. S. Nirmalanandhan, and D. L. Butler. 2007. Mechanical stimulation increases collagen type I and collagen type III gene expression of stem cell–collagen sponge constructs for patellar tendon repair. *Tissue Engineering* 13(6).
222. Lee, C. H., H. J. Shin, I. H. Cho, Y. M. Kang, I. A. Kim, K. D. Park, and J. W. Shin. 2005. Nanofiber alignment and direction of mechanical strain affect the ECM production of human ACL fibroblast. *Biomaterials* 26, 11:1261–1270.
223. Nirmalanandhan, V. S., M. Rao, J. T. Shearn, N. Juncosa-Melvin, C. Gooch, and D. L. Butler. 2008. Effect of scaffold material, construct length and mechanical stimulation on the in vitro stiffness of the engineered tendon construct. *Journal of Biomechanics* 41(4).

224. Noth, U., K. Schupp, A. Heymer, S. Kall, F. Jakob, N. Schutze, B. Baumann et al. 2005. Anterior cruciate ligament constructs fabricated from human mesenchymal stem cells in a collagen type I hydrogel. *Cytotherapy* 7, 5:447–455.
225. Petrigliano, F. A., C. S. English, D. Barba, S. Esmende, B. M. Wu, and D. R. McAllister. 2007. The effects of local bFGF release and uniaxial strain on cellular adaptation and gene expression in a 3D environment: Implications for ligament tissue engineering. *Tissue Engineering* 13(11).
226. Raïf, E. M., B. B. Seedhom, M. J. Pullan, and T. Toyoda. 2007. Cyclic straining of cell-seeded synthetic ligament scaffolds: Development of apparatus and methodology. *Tissue Engineering* 13(3).
227. Shearn, J. T., N. Juncosa-Melvin, G. P. Boivin, M. T. Galloway, W. Goodwin, C. Gooch, M. G. Dunn, and D. L. Butler. 2007. Mechanical stimulation of tendon tissue engineered constructs: Effects on construct stiffness, repair biomechanics, and their correlation. *Journal of Biomechanical Engineerin*g 129(6).
228. Connelly, J. T., E. J. Vanderploeg, J. K. Mouw, C. G. Wilson, and M. E. Levenston. 2010. Tensile loading modulates bone marrow stromal cell differentiation and the development of engineered fibrocartilage constructs. *Tissue Engineering Part A* 16, 6:1913–1923.
229. Fox, D. B., J. J. Warnock, A. M. Stoker, J. K. Luther, and M. Cockrell. 2010. Effects of growth factors on equine synovial fibroblasts seeded on synthetic scaffolds for avascular meniscal tissue engineering. *Research in Veterinary Science* 88, 2:326–332.

20

Advances in Biomaterials for Clinical Orthopaedic Applications

Michele A. Marcolongo and David Jamison, IV

CONTENTS

20.1 Introduction

The study, analysis, and development of biomaterials are of key importance in the field of clinically relevant orthopaedic devices. The main considerations are the biocompatibility and functional performance (e.g., mechanical, electrical, chemical) of the materials and systems involved. This chapter focuses on current, clinically available materials and emerging solutions for bone, cartilage, ligaments and tendons, and tissues of the spine.

20.2 Bone

Although bone has been studied as a tissue for many years, it is only within the past few decades that its mechanical and material properties have been given careful consideration.[1] Bone is composed of water (15%), mineral ions (39%), and organic extracellular matrix (42%).[2] Type I collagen is the major matrix protein in bone, forming 70% to 90% of the nonmineralized content of the bone. The mineral content of bone is made of calcium phosphates, most importantly hydroxyapatite (HA), which has a calcium deficiency of between 5% and 10%.[3]

The long bone, the most common type of bone in the body, is made up of cortical bone and trabecular bone. Cortical bone makes up the outer layer of the tissue and is very dense, with spaces only for blood vessels and bone cells or osteocytes. However, trabecular bone, the inner portion of the tissue, consists of a network of voids or trabeculae that are interconnected and occupied by bone marrow.

Bone is an anisotropic material, with its highest strength being in compression along the long axis of the bone. Cortical bone is very stiff, with only about a 2% failure strain. However, it is very strong, with an ultimate strength of approximately 200 MPa in compression.[4] Failure of bone can occur in a variety of ways because the material can undergo many different modes of loading. Traumatic failure can occur due to compression, bending, or torsion, although usually it is some combination of the three. Likewise, fatigue failure can occur in bone after many millions of cycles. In bone, this fatigue failure is due to a propagation of microscopic cracks in the tissue.[5,6]

20.2.1 Fracture Fixation

For the fixation of bone defects and fractures, patients usually require the use of pins, rods, screws, and plates, and possibly augmentation by the injection of cement for fixation.[3, 7–10] However, these fixation devices usually require secondary procedures to remove them once bone healing is complete.

The first absorbable sutures, developed in the 1960s, were made from synthetic polymers and were designed to be absorbed after serving their typical wound-closing function.[7,11] This eliminated the need for a follow-up procedure to remove a suture after the wound healing occurs. The use of synthetic, absorbable sutures has been the inspiration for the incorporation of other absorbable polymers that are now used to correct bone defects and for fracture fixation. Implants manufactured from bioabsorbable polymers have several advantages over nonabsorbable orthopaedic implant devices. They eliminate the need for a subsequent surgery to remove the construct after it has served its function, and allow natural bone to grow onto the polymer as it is being absorbed. The latter advantage results in the bone having superior structural integrity as it is regrowing and being able to support load earlier than with nonabsorbable materials. Additionally, absorbable implants may contain bioactive molecules that enhance growth and accelerate fracture healing.[12,13] The significant advantages of absorbable polymer implants have led to a large growth of research in this field.

Middleton and Tipton[11] identified four main criteria to assess the applicability of an absorbable polymer for use in fracture fixation devices:

1. The polymer absorption rate should match that of the rate of bone growth onto the polymer.
2. The polymer should ideally aid bone growth or at least not prevent it.

3. The polymer and its degradation products should be biocompatible to prevent an adverse reaction in the body.
4. The mechanical properties of the polymer must be appropriate to the specific application and be maintained throughout the life of the polymer.

The mechanism of polymer degradation is an important design consideration for absorbable materials in orthopaedic applications (Figure 20.1). Bulk degradation is the process invoked for most traditional absorbable polymers. In this process, water enters the bulk polymer *in vivo* and degrades it via hydrolysis. The products of the breakdown, carboxylic acids, progressively build up within the hollowed portion of the polymer, which, in turn, causes a further drop in the pH of the polymer. This continues until the polymer finally breaks apart, releasing the acid groups in a process called "acid bursting." This can result in inflammation in the tissue and a decrease in mechanical properties in the earlier stages of degradation.[11,14] Polylactic acid (PLA) is a polyester that is often used clinically for orthopaedic pins and screws. As it is an absorbable polyester, it holds clear advantages over nonabsorbable polymers. Although absorbable polymers such as PLA are generally preferred over their nonabsorbable counterparts, PLA has one major disadvantage in that it follows a bulk degradation pattern.[15,16]

In contrast to bulk degradation, surface erosion (Figure 20.1) results in the gradual thinning of the material while still maintaining the integrity of the bulk polymer. Absorbable polymers that typically undergo surface erosion are hydrophobic, so water is far less likely to enter the material, thus preventing bulk degradation from within. Significant research efforts are currently focusing on these emerging polymers, including tyrosine-derived polycarbonates, poly(ortho esters) (POEs), and polyimides.

Tyrosine-derived polycarbonates have amide, ester, and carbonate groups that can be hydrolyzed. These polycarbonates have demonstrated sufficient mechanical properties for bone fixation[9,17] and are biocompatible *in vivo*.[9] Tunable degradation times can be achieved with POEs by the addition of lactide or glycolide segments (or both) to the polymer.[18] Polyimides have been reported to degrade via surface erosion[16,19] and have been shown to be biocompatible *in vitro*.[16] Variable degradation times (from 1 to 63 days) can also be achieved with polyimides.[20]

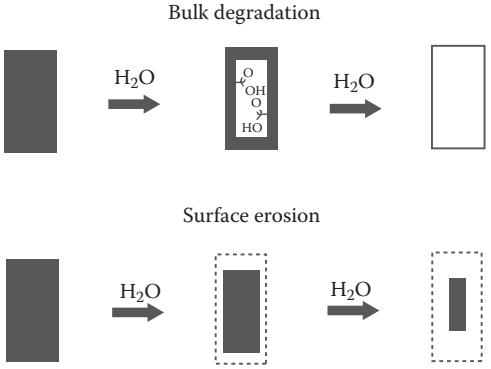

FIGURE 20.1
Schematic of polymer degradation mechanisms.

20.2.2 Total Joint Replacement

Devices for total joint replacement (TJR) incorporate low-friction–bearing surfaces to replace the function of cartilage. They are also needed in cases in which the bones in articulating joints are severely fractured or have worn away due to osteoporosis and no longer have full functionality. TJR systems are considered some of the most successful surgical procedures; they have a 90% survival rate at 10 years but decline precipitously after that.[21] Today, with an increasingly older population, and many younger patients needing joint replacement surgeries, it would be beneficial to improve the success rate for even longer durations.

One major problem affecting the success rate of TJR surgeries is implant loosening. It is a phenomenon originally thought to be caused by the use of bone cement for fixation of TJR implants. This loosening is associated with the presence of a fibrous tissue membrane that grows between the cement and cancellous bone, and can be seen clearly in autopsies or on radiographs as a large radiolucent gap.[22,23] Progression and widening of the fibrous membrane gap is termed "cement disease" and is seen as a physiological reaction to cement as a fixation technique.[24,25] Indeed, bone cement, typically made of polymethylmethacrylate (PMMA), does have clear disadvantages. PMMA polymerizes *in situ* through an exothermic reaction, which can reach temperatures as high as 90°C, potentially causing necrosis at the bone-cement interface.[26,27]

An alternative is cementless TJR designs for younger patients with normal bone quality. The designs began with simple impaction of the implant into the medullary canal[28,29] or a threaded system.[30] However, even these cementless designs are still affected by implant loosening and the infiltration of fibrous tissue layers between the bone and the implant.[31–33]

A fibrous response to implants is caused, in part, by the natural, chronic inflammatory response in the body known as the "foreign body reaction".[34] This reaction is also made worse by the presence of wear debris from ultrahigh molecular weight polyethylene (UHMWPE), metal alloys, and PMMA, which are typically used as the lining on the articulating surface of an implant. These foreign body reactions not only can prevent active bone regrowth but also can cause bone resorption, which is termed osteolysis.[35] This limits the structural integrity of bone and may accelerate the loosening of the device.

Osseointegration is the structural and functional connection between the living bone tissue and the implant.[36] In other words, osseointegration is the direct opposite of aseptic loosening, and also its solution. Significant research has been undertaken to develop methods to induce osseointegration in TJR implants. For bone to properly and securely anchor onto an implant, five factors must be controlled:[37]

1. Biocompatibility of the material
2. Form and macroscopic texture of the implant
3. Surface conditions (microtexture) of the implant
4. Surgical technique
5. Postimplantation loading conditions

For osseointegration of orthopaedics implants, care must also be taken to minimize both foreign body reactions and stress shielding to ensure long-term implant stability and fixation to bone. Stress shielding occurs when one material of greater stiffness and strength prevents the transfer of load to a second material. If an implant prevents the loads from being transmitted appropriately to bone, it can actually inhibit new bone ingrowth.

Titanium (Ti) has proven to be a good candidate for intramedullary stems in TJR implants due to its excellent biocompatibility, which permits tissue integration.[38–40] However, the amount of bone contact with the implant has been shown to be lower with smooth implant surfaces compared with that of rough implant surfaces.[41] For this reason, since the 1980s, many researchers have focused on developing new surface textures to improve initial implant stability and bone integration. Popular implant surface modifications currently include plasma-sprayed HA and Ti coatings [titanium plasma-sprayed (TPS)] on implants.[42]

HA makes up approximately 67% of bone and, as such, is a natural choice for use in implant surface treatment because of its osteoconductive nature. Additionally, increased roughness on TPS implants prohibits bone ingrowth on the porous structure, serving as an alternative to osteoconductive materials such as HA. Desired coating thicknesses are approximately 50 to 100 μm. With a continually aging population, damage to, and failure of, bone tissue—from injury or aging and osteoarthritis—will become an increasingly pervasive problem. The development and design of new materials for fracture fixation and total joint replacement will ensure that bone healing is as effective and complete as possible. As the use of resorbable polymers in this field continues to advance, the number of successful clinical procedures may increase and would reduce the need for costly revision surgeries.

20.3 Articular Cartilage

Cartilage is a soft tissue composed of the macromolecule collagen and proteoglycans. There are three types of cartilage: elastic cartilage, fibrocartilage, and articular cartilage. Articular cartilage, a prevalent type of cartilage in the body, is the subject of significant past and current research and will be the focus of this section. This type of cartilage is located on the articulating surfaces of all joints, and its main functions are to provide low-friction movement of the bones within the joint, while preventing contact stresses in the joint from reaching levels higher than the critical stress of bone. Along with synovial fluid, articular cartilage provides for a low-friction and wear-resistant surface. In fact, articular cartilage and synovial fluid lubricant combine to produce a coefficient of friction (0.005) that is lower than any man-made engineered system.[43]

20.3.1 Structure, Composition, and Function

Articular cartilage is composed of a high percentage of water (60%–80%), as well as collagen and proteoglycans. Additionally, there are chondrocytes, which are the cells responsible for the synthesis and maintenance of the cartilage extracellular matrix. Chondrocytes account for only 1% to 10% of the total volume of the tissue.[44]

Collagen is the largest nonaqueous component of cartilage. The building blocks of collagen are the tropocollagen molecule, which is composed of three polypeptide chains in a helical structure. Tropocollagen is 300 nm long and 1.5 nm wide, with a molecular weight of approximately 300 kDa. Articular cartilage largely contains type II collagen, although other collagen types are reported to be present in far lower amounts, including types V, VI, IX, X, and XI.[45] Collagen's molecular design makes it ideal for supporting tensile loads; however, its specific role in any soft tissue composite depends on the tissue in question

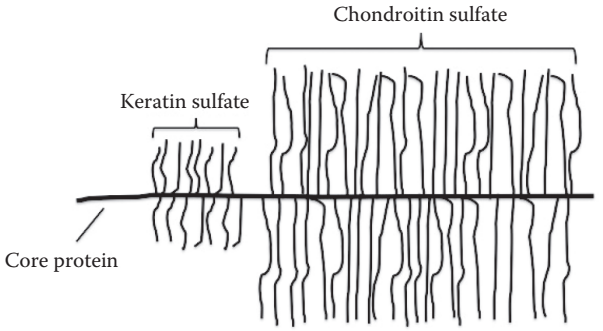

FIGURE 20.2
Schematic of an aggrecan molecule.

and the nature of the loading. In articular cartilage, the collagen fibers are closely associated with macromolecular gels, and their interaction provides for excellent compressive loading support. The diameter and spatial orientation of the fibers vary with depth below the articular surface.[46] Superficially (near the articulating surface), collagen is aligned in sheets, parallel to the surface,[47] whereas in the deep zone of the cartilage, the fibers are oriented more perpendicularly to the cartilage–bone interface.[48]

Proteoglycans are biomolecules that are composed of a protein core and at least one glycosaminoglycan (GAG) chain covalently attached. Several GAGs exist in cartilage, namely, chondroitin sulfate (CS), keratin sulfate (KS), and hyaluronan. The most abundant proteoglycan in cartilage is aggrecan (Figure 20.2). Aggrecan is a polyanion due to the negatively charged sulfate and carboxyl groups associated with KS and CS. This feature is important as it controls the ability of aggrecan to bind water osmotically. Only a small amount of water in cartilage is intracellular; most of it is imbibed due to the proteoglycan's hydrophilic nature. The highest water content is found near the articulating surface and decreases progressively moving toward the subchondral bone.[49] Movement of interstitial water in articular cartilage is important for joint lubrication and chondrocyte nutrition and viability.

20.3.2 Mechanical Properties

The function of articular cartilage is to provide low-friction, wear-resistant support for the joints while withstanding significant physiologic loads over the course of a lifetime. The physical and chemical interactions of the various components of cartilage are responsible for the mechanical properties of the tissue. In articular cartilage, there is a relationship between the osmotic swelling pressure—related with the concentration of charged GAGs—and the hydrostatic pressure. That relationship is caused by the tensile stresses on the collagen fiber network; that is, they balance one another. Fluid flow within cartilage is a function of the pressure differential (Δp), and its rate is related to any externally applied pressure (P_{applied}), the hydrostatic pressure (P_{elastic}), and swelling pressure (P_{swelling}) by the following relationship:

$$\Delta p = P_{\text{applied}} + P_{\text{elastic}} - P_{\text{swelling}}. \tag{20.1}$$

The time-dependent "creep" behavior is characteristic of all viscoelastic soft tissues. These tissues are traditionally modeled as biphasic materials, with a solid phase and a fluid phase. In compression, the primary loading mode of articular cartilage, several studies have shown an initial elastic behavior followed by a time-dependent creep in response to a rapidly applied force.[50,51] *In vivo* compression tests of cartilage are usually done via indentation tests and confined/unconfined uniaxial tests. The compressive aggregate modulus, H_A, of articular cartilage ranges from 0.08 to 2 MPa.[52–56]

Shear stresses are also an important factor in the analysis of the mechanical behavior of articular cartilage, as the tissue undergoes shear during normal rotational and translational movements of the joint. The shear modulus at equilibrium—that is, when there is no fluid flow in to or out of the cartilage—has been found to range between 0.05 and 0.25 MPa.[57] Understanding the biomechanics of articular cartilage is important, as knowledge of the tissue's mechanical behavior can provide insight into injury and degeneration pathways.

20.3.3 Mechanisms of Injury and Loss of Function

Cartilage will lose its functional properties in two ways: aging and injury. Because of a lack of vasculature that leads to a lack of adequate nutrient delivery, continued degeneration of the material is a major issue in articular cartilage, as the healing response is often insufficient.

Several changes occur to articular cartilage during the aging process. There is a decrease in thickness of cartilage at the articulating surfaces of adult versus immature cartilage.[58–60] Likewise, the number of chondrocytes decreases with age.[61] This is due to lower metabolic activity, increased apoptosis, and a subdued response to growth factors.[62–64] Collagen cross-linking has been observed to increase with age,[61] whereas proteoglycan content decreases,[65] resulting in a stiffer collagen. All these aging processes also make articular cartilage more prone to injury.

Cartilage injuries are classified as microfractures, chondral defects, and osteochondral defects. These can all be caused by repeated (although nondestructive) loading, torsional loading, impact loading, and joint malalignment. Damage to the cartilage network first leads to a loss of superficial GAGs.[66] Microfractures can trigger a change in the load distribution of the matrix, resulting in stress concentrations that can lead to further damage and also thickening of the subchondral bone.[67] As mentioned previously, articular cartilage is avascular, so repeated loading on the defects in the tissue often does not lead to pain (at least in the case of microfractures and chondral defects), which then also leads to further degeneration. Osteochondral defects do lead to bleeding, as the defect reaches the bone, and thus releases growth factor and progenitor cells unlike microfractures and chondral fissures. However, the repair tissue that is formed is a mixture of fibrocartilage and articular cartilage, which has impaired functionality.[68] This will lead to an eventual degeneration into osteoarthritis.

20.3.4 Current Clinical Treatment Methodologies

There are several clinical treatments that have traditionally been used to alleviate the pain due to osteoarthritis or to restore the functionality of articular cartilage. Chondral defects can be treated with a process called debridement, in which the defect is smoothed and reshaped. Removal of burrs, diseased tissue, delaminated tissue, and flaps can improve the low-friction gliding motion and provide relief to the joint. Cartilage debridement has

been performed in the knee, elbow, ankle, and shoulder with a relatively high rate of success and patient satisfaction.[69–74]

Microfracture can also serve as a surgical technique. In response to the low healing response of avascular cartilage, growth factors from an intentional microfracture process have been widely used for chondral defects of the knee, shoulder, and ankle.[75–78] The drawbacks to this method are obvious, since the healing response has been described previously, and the fibrocartilage has inferior material properties for the application needed. Also, the fibrocartilage replacement can leave a layer that is thinner than the rest of the tissue, resulting in abnormal load distribution that can lead to degeneration. To improve upon these issues, the microfracture technique has been used with a combination of coverings such as a periosteal flap or natural or synthetic materials.[76, 78–81] A recent study has shown that microfracture procedures are effective within the first 24 months in improving knee function, but their effectiveness subsequently wears off, particularly in older patients.[82,83]

Tissue grafting is also a common clinical solution. The three biological grafting procedures are autografts, allografts, and xenografts. These grafts, although they may be less stiff, contain live cells to potentially allow for tissue remodeling. Autografts present the lowest immunological response risk of the three because the donor material comes directly from the host. In this case, grafts are typically taken from non-load-bearing areas. Autografts have shown efficacy for up to 10 years.[84] Problems encountered with this method are an increased number in invasive surgeries (two are needed, one to remove the graft and one to place it in the defect), scarcity of source material, and donor site morbidity. Allografts solve the problem of donor tissue scarcity, but the risk of an immune response increases,[85] as well as the risk of disease transmission. Xenografts further heighten the immunological response risk.[86] Additionally, all methods have potential problems with creating a graft that adequately fits the defect.

20.3.5 Emerging Biomaterial Solutions

The lack of adequate, long-term success with current surgical techniques has led to an exploration of cell-based repair systems. Tissue engineered constructs *in vitro* must have a viable source of cells. These can come from native chondrocytes, although there are often too few in the body to be reasonably harvested for patient therapies.[87] Another possible cell source is autologous progenitor/stem cells. These cells are an attractive choice because they can be expanded *in vitro* to the required number of cells and then differentiated into their desired cell type. Also, stem cells are more plentiful because they can be found in many parts of the body. Recent focus has been on mesenchymal stem cells, adipose-derived stem cells,[88] embryonic stem cells (ESCs), and other sources. Much of the work to date supporting the use of ESCs for cartilage tissue engineering has come from mice.[89] Mouse ESC differentiation into chondrocytes has been demonstrated *in vitro* using bone morphogenetic proteins (BMP-2 and BMP-4).[90]

For *in vitro* engineered tissue constructs, one key design component is ensuring that the implant can support normal joint forces immediately after implantation. For this reason, cell-seeded systems are typically contained within a scaffold with inherent mechanical integrity. These scaffolds are typically resorbable. The success of the construct depends on the cells' ability to fabricate a substantive matrix at a rate comparable to the resorption rate of the scaffold.[86]

Although chondrocytes occupy a small percentage of articular cartilage tissue volume, they are indispensable in the synthesis and maintenance of the extracellular matrix. This is why the choice of cell types to use is crucial. Additionally, it is known that the loading profile

of a tissue determines its growth and response. To properly create a tissue-engineered cartilage construct, the mechanotransduction pathways must be better understood. Investigating these pathways *in vitro* is a key challenge. Analysis of the engineered tissue's response in compression, tension, sheer, and fatigue, as well as friction coefficients, must be performed in the laboratory.

Implantation of cartilage scaffolds *in vivo* is an emerging trend. This method allows for regeneration to occur with minimal additional manipulation. Physiological loads are applied naturally, and the biochemical and biomechanical cues needed for tissue growth are inherently present. One recent study is focused on repairing defect sites by inserting autologous or allogenic cells or tissue into the defect site and then covering it with a periosteal flap.[91] Other proposed solution methods include a functional insert that can restore mechanical function but does not regenerate tissue,[92,93] and using synthesized polymers, such as hydrogels, that can transition from a fluid to a fixed gel *in vivo*.[94,95]

20.4 Ligaments and Tendons

Ligaments connect two or more bones, whereas tendons connect muscle tissue to bone. Ligaments are primarily for the stabilization of joints, whereas tendons are important for muscle-directed movement. Both ligaments and tendons fall under the category of soft connective tissues. As most connective tissues have a similar composition, and therefore similar mechanical properties and functions, both tissues will be reviewed together in this section.

20.4.1 Structure and Composition

Connective tissues such as tendons and ligaments are primarily composed of collagen.[96] In fact, collagen is the most abundant protein in the mammalian body. Specifically, type I collagen is the primary collagen type in these tissues (nearly 80% of dry weight), providing the main load-bearing component. Collagen is particularly suited to resist large loads in tension. It is fibrous in nature, providing ligaments and tendons with an overall fibrous tissue structure. These tissues have a regular fiber orientation in the direction of the commonly applied load.

Tendons and ligaments consist of fascicles of collagen fibers, which largely run parallel to one another. The fibers are assembled from fibrils, which are 0.02 to 0.20 μm in diameter. Fibrils are broken down into the smaller subcomponents, subfibrils and microfibrils, and the individual tropocollagen molecule. Single fascicles and groups of fascicles are surrounded by sheaths, the former being the endotenon and the latter called the peritenon. Collagen bundles are subsequently cross-linked to each other, allowing for increased mechanical integrity. As with cartilage, cell density is low.[97] These fibroblasts are attached to individual collagen bundles and are responsible for the synthesis and propagation of the collagen.

20.4.2 Mechanical Properties

Both tendons and ligaments must withstand very large loads under regular physiologic applications. Tendons act to transmit muscular pulls to the skeletal structure. Experiments have shown that the tendon stresses can range from 42 to 110 MPa.[98,99] Due to muscle tone, a small amount of tension is always present in the tendon, ensuring that it is constantly taut even when the muscles are relaxed. Ultimate tensile strength in ligaments is

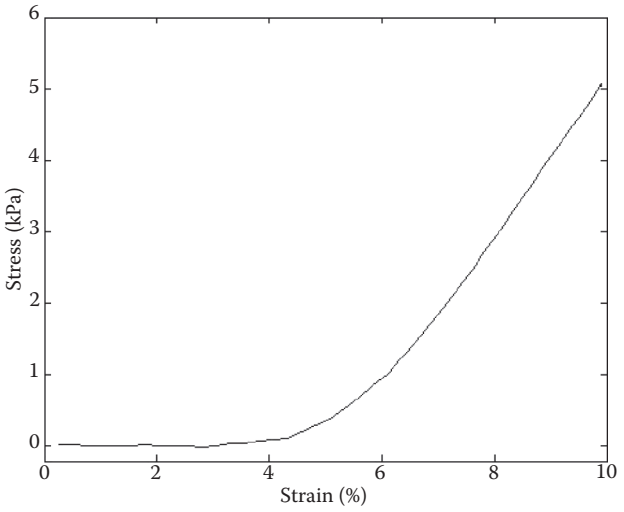

FIGURE 20.3
Typical stress–strain behavior of a tendon, subjected to uniaxial tension at 0.01%/s.

approximately 38 MPa, whereas maximum tensile load is approximately 1700 N.[100] Both ligaments and tendons must be able to withstand significant amounts of cyclic loading. The average healthy individual gets nearly 1.5 million strides per year.[101]

Ligaments and tendons exhibit viscoelastic behavior and are subjected to the same creep and relaxation responses as other viscoelastic tissues. However, this behavior is not as pronounced as in cartilage due to less fluid movement through the tissue during loading. Figure 20.3 shows a typical stress–strain response of a ligament or tendon. During the initial "toe" phase, minimal stresses are produced from relatively high strains, as crimped collagen fibers are elongated and straightened. During the "knee" phase, the fibers begin to be "recruited" and support the applied load. In the "linear" phase of the response, collagen fibers are fully recruited and bearing the applied load. This phase has the greatest increase in stress per unit strain (Figure 20.3).

20.4.3 Damage/Degeneration Mechanisms

The most common tissue injuries to ligaments and tendons are lacerations (partial thickness tears), ruptures (full thickness tears), and inflammation. These may be caused by a singular macrotrauma or progressive microtrauma, which itself is due to overuse.[102] The number of overuse injuries in the United States is estimated to be approximately 30% to 50% of all sports-related injuries.[103] Overuse injuries are a result of repetitive microtrauma caused by repeated exposure to forces whose magnitudes would not lead to failure in an isolated incident.[102]

As with most biological tissues, changes due to aging increase the likelihood of injury and reduce the effectiveness of normal biological healing mechanisms. Collagen content decreases as an individual ages.[1] With this reduction in collagen comes an associated decrease in mechanical strength of the tissue. This, combined with an already high incidence of ligament/tendon injuries (e.g., there are between an estimated 60,000 and 150,000 anterior cruciate ligament (ACL) reconstruction surgeries performed each year in the United States, amounting to more than $2 billion in medical expenses),[104] represents a significant problem for clinicians and engineers.

20.4.4 Current Clinical Solutions

A number of clinical remedies exist for the treatment of damaged ligaments or tendons. As mentioned previously, these tissues have low vascularization and so also have a limited capacity to heal.[105,106] For this reason, a simple suture procedure can often be ineffective. The other traditional surgical route is the use of grafts, either autogenic or allogenic.[108] Like cartilage, these grafts are advantageous in that they inherently possess the desired mechanical properties and promote cell proliferation. However, both approaches present some key disadvantages as well, including donor site morbidity and an added surgical site for autografts and an increased risk of disease transmission and immune response for allografts.

20.4.5 Emerging Technologies

As is the trend with most biomaterials, current research is investigating if the shortcomings of present solution methods can be overcome by biodegradable or absorbable polymers. These polymer grafts must be comparable to the natural tissue. Namely, they must be biocompatible, have a similar fatigue life cycle to that of natural tendon/ligament, and be resistant to creep behavior. Additionally, these materials should ideally degrade at the rate of natural tissue ingrowth to eliminate the problem of stress shielding and must promote tissue integration.[108]

Commonly chosen synthetic polymers for this application are PLA and polycaprolactone (PCL). PLA has been widely used in ACL devices as it degrades completely into lactic acid within ten months to four years depending on crystallinity, molecular weight, shape, and implantation site.[109] PCL has an even slower degradation rate and is often combined with PLA to reduce its brittle nature in slow-degrading devices. Silk, a natural polymer, has also been proposed for ligament and tendon repair due to its biocompatibility, slow degradation, and high tensile strength. Silk fibers lose the majority of their tensile strength only after one year *in vivo*.[110]

Braiding and twisting of fibers are the most common techniques for synthetic graft production. Their design allows them to be conformable and also shear-resistant. The composite architecture should be designed to accurately mimic the biomechanical profile and mechanical properties of the tissue.[111,112] Another consideration for the tissue-engineered scaffold is pore size. A minimum pore diameter of 150 μm is suggested for bone ingrowth and 200 to 250 μm for soft tissue ingrowth.[113] These pores increase the overall surface area for cell attachment, which, in turn, can enhance the regenerative properties of the implant by allowing tissue ingrowth into the interior of the matrix.[111] Overall, fabrication parameters, such as braiding and twisting angles, fiber diameter, and material selection, can greatly affect both the architecture of the graft, in terms of pore size and surface area, and mechanical properties under tensile load.

20.5 Spine and Intervertebral Disc

The spine is responsible for transferring loads from the head and trunk, along with any externally applied loads, to the pelvis. It is also important for the movement and flexibility of the upper body and is critical in the protection of the spinal cord from injury due

to trauma and excessive motion.[114] Injury, disease, and aging can affect the spine's ability to perform these essential functions. Often, this results in back pain, which represents a major problem in the health industry. More than 60% of the population experience back pain throughout their lifetime,[115] and this alone accounts for 2% of all physician visits.[116] There is a large research community investigating the spine, attempting to gain further knowledge.

20.5.1 Anatomy and Biomechanics

The interface between each vertebral body and its adjacent intervertebral disc (IVD) is called the endplate. Because the IVD is the largest avascular tissue in the body, all nutrient flow is achieved through diffusion and fluid flow,[114] for which the primary vehicle is the endplate. The endplate is partly cartilaginous and partly bony.

The disc has two distinct regions: the nucleus pulposus (NP) and the annulus fibrosus (AF). The composition of these two regions is important for the mechanical behavior of the disc and the spine in general. The cellular content of the disc is low; it comprises only 0.25% of tissue volume.[117] The extracellular matrix plays a large role in determining disc mechanical properties. The nucleus is a gelatinous structure made mostly of water (nearly 77% of wet weight). Proteoglycans are the next largest component of the NP, comprising 14% of disc wet weight. Randomly organized collagen fibers are also present in this area. The collagen provides tensile strength, whereas the proteoglycans create a large osmotic potential and draw water into the tissue. The annulus serves to contain the nucleus and is made up of the same constituents, although collagen represents a much larger portion of its dry weight (50%–70%).[118] The AF is organized in concentric layers called lamellae. These lamellae are made up of type I collagen and are arranged in alternating 30° angles.

The primary loading mode of the spine is compression, with torsion and bending being secondary. Most natural movements of the body result in the spine being loaded in some combination of these three modes. The vertebral bodies in the anterior column of the spine carry most of the applied compressive load. The IVD dissipates much of the energy that is transmitted to it. During loading, the NP builds a hydrostatic pressure and expands outward, putting the annulus fibers into radial tension.[119]

The IVD exhibits viscoelastic tissue properties due to the presence of hydrophilic proteoglycans. During a period of sustained creep loading, the spine can lose 1 to 2 mm of height because of the expulsion of water from the discs.[120] It is believed that postural effects on pain perception and spine mechanics are exaggerated during this period.

20.5.2 Damage and Degeneration

Damage to either the vertebral bodies or the IVD affects the entire spine. In the bony portion of the vertebral column, a traumatic event can result in vertebral body fractures. In addition to decreased stability, these fractures can result in increased load transfer to the adjoining vertebral bodies.

Within the disc, annular fissures may result from large loads on the spine. Significant fissures can lead to disc herniation, in which the gelatinous nucleus material can be expelled through the annular layers and even from the disc itself. The NP travels through the tears that have propagated through the thickness of the annulus. If the herniation is directed posteriorly, it will often cause spinal cord impingement, which can be a source of great pain.

Aging and associated degenerative changes also pose problems for spinal function. The vertebral bodies are subject to osteoporosis, which increases the risk of injuries due to trauma or even general use. In elderly patients, overloading can result in a "wedge fracture," in which the anterior portion of the vertebra collapses.[121] In an attempt to compensate, the posterior elements will often stress shield the anterior portion where the fracture is located. However, this increased load capacity can lead to an increased risk of injury in the neural arch and bony processes. Additionally, the stress shielding at the site of the wedge fracture can lead to bone loss at this location, increasing the chance of injury during spinal flexion.[122]

Increased bone loss directly affects the IVD in two ways. First, a loss of bone will limit the nutrient transport to the disc via the endplates. Because the IVD is avascular, this mode of attaining nutrients is vitally important for the tissue. Second, osteoporosis will lead to increased stresses being transferred to the disc, increasing the risk of catastrophic damage to that region.[123]

Disc degeneration is a major clinical issue. Although the pathways of disc degeneration are not fully understood, investigators point to a decreased uptake of nutrients through the endplate in combination with cumulative mechanical damage over time as the primary factors. A degenerated IVD has less collagen and proteoglycan content than a healthy one, particularly in the NP. This has an effect on the load-bearing behavior of the disc, reducing its water content and making the NP less gel-like and more fibrous.[124] As a result, the disc is less capable of dissipating the energy transferred to it and often behaves stiffer. This can impact the vertebrae, as they retain more of the applied load. Progressive disc degeneration can also lead to changes in stress concentrations in the AF and endplate (Figure 20.4).[123]

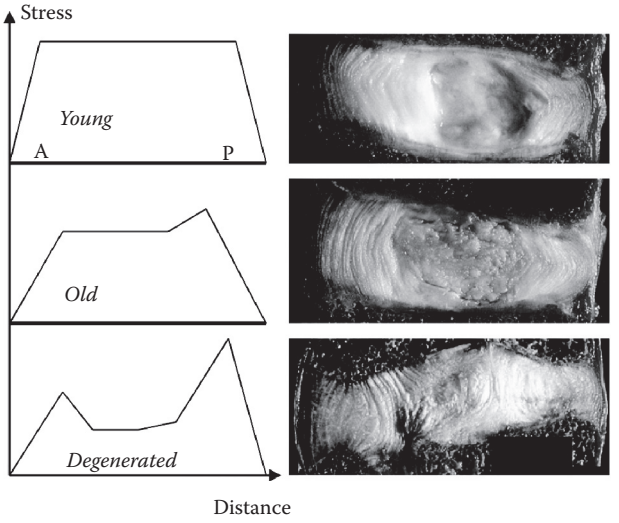

FIGURE 20.4
(See color insert.) Representative stress profiles for a young adult disc (top), old disc (middle), and degenerated disc (bottom). Stress concentrations increase with age and become large with degeneration. P, posterior; A, anterior. Photographs show midsagittal sections of corresponding similar discs. (Reprinted from Adams, M.A. et al., Copyright 2009, with permission from Elsevier.[138])

20.5.3 Current Solutions

Common surgical interventions for the spine and IVD are spinal fusion and total disc arthroplasty (TDA). For patients suffering from discogenic pain, herniations, or vertebral body fractures, a spinal fusion technique is often the proposed solution. Interbody fusion is used when the IVD is the cause of pain and discomfort. The procedure involves the disc in question being completely removed and having a bone graft placed in between the vertebrae in the now-unoccupied space. Spinal fusion surgery uses several devices including vertebral cages, in which the bone graft is inserted, and screws and wires to provide stability.[125]

Selection of materials for this application is as varied as it is paramount. The vertebral cage structure is of particular importance, as it will bear a significant amount of load and must not allow for stress shielding in the inferior or superior sections of the spine. Metals are typically used as the material for vertebral cages. Pure titanium and Ti alloys, as well as cobalt chrome, have been used in some devices. These designs are typically threaded and have a UHMWPE cap at each end. The UHMWPE caps are designed to contain the bone grafts within the hollow metal cage and prohibit adhesion to surrounding nerves and blood vessels. Titanium has the mechanical strength to satisfy the load-bearing requirement of the device, whereas its threaded structure provides stability to the implant. These constructs, however, are subject to fatigue failure if the bone graft does not fuse to the vertebrae and the metal's high modulus can still lead to stress shielding in adjacent sections of the spine.[125] Cobalt chrome has also been implemented as a porous metal in spinal surgery.[126] However, these designs have experienced problems with metal ion release, which can increase pain and also cause implant loosening and local bone resorption at the implant site.[127]

More recently, composite materials have been used in spinal cages to address the drawbacks of their metal counterparts. Polyaryletherketones (PAEKs) are in a family of high-temperature thermoplastic polymers that have been widely used in spinal fusion cage applications since their introduction in the 1990s.[128] The chemical structure of PAEKs allows for customization of the material and mechanical properties with the use of reinforcing agents such as glass and carbon fibers. Devices that use PAEKs are able to modulate the material to specifically mimic the properties of bone to adequately support physiologic loads in the spine without stress shielding.

The induced rigidity and abnormal curvature that can result from spinal fusion surgeries have spurred the need for the development of a fusion system whose rigidity decreases with time. Bioresorbable materials can provide the desired effect. Resorbable cages have stiffnesses comparable to those of bone, are radiolucent, and resorb over time, leaving the scaffold and allowing bone ingrowth.[129] These cages provide the additional benefit of eliminating the need for an additional surgery for implant removal. The most commonly used biodegradable materials are PLA and poly(glycolic acid) along with their isomers and copolymers. Because the chemical backbones of these polymers are hydrolytically unstable, their chains degrade when placed in the aqueous environment of the human body. Resorbable PLA cages have performed well in comparison with Ti cages in clinical studies. One such study showed that the PLA cages maintained 90% of their initial strength after six months, decreasing slowly to 70% after nine months, and then continue to be absorbed after two years.[130] Gradual resorption of the cage material allows for the fusion to gradually assume the role of structural support and potentially improve the success rate of fusion surgeries.

Nevertheless, spinal fusion has its limitations, which include morbidity of the harvested bone graft, accelerated degeneration of adjacent level discs, and long postoperative

recuperation times.[131] The use of TDA for the treatment of isolated degenerative discs and associated spinal problems has increased in popularity in recent years. The procedure eliminates the problematic disc while attempting to preserve the range of motion.[133] Stainless steel, cobalt-chromium alloys, and titanium alloys are the most common materials for the TDA prosthesis endplate. The prosthetic endplate interfaces with the bone via screws, fins, or serrations. Secure attachment is facilitated by producing a rough surface on the metal to facilitate bony ingrowth, as well as the use of titanium spray, calcium sulfate, or HA coatings.[132]

The choice of material for the bearing surface of the TDA device must be carefully considered. The material is expected to last for at least 85 million cycles without significant degeneration,[133] have high wear resistance, and have a low immunologic response to its wear particles. For this application, UHMWPE is often the material of choice. The polymer is often formed in a convex shape and articulates with a concave metal surface.

20.5.4 Emerging Solutions and Future Directions

The current trend in spinal surgical treatments is toward less invasive and destructive procedures. Additionally, it is desired to be able to intervene earlier in the disc degenerative cascade so that spinal fusion and TDA are unnecessary. Toward this end, researchers are investigating the usage of hydrogels for NP replacement.[134–137] These hydrogels could be implanted or simply injected into the disc and would help restore the tissue to its normal, healthy properties. This field of research is very new, and many different materials are being explored and analyzed. Examples include biodegradable gelatin, poly(ethylene glycol), and even CS-based hydrogels. CS-based hydrogels are of particular interest because they allow for the creation of a biomimetic material and because the NP is naturally made up of proteoglycans containing CS. This biomimetic polymer, which could be designed to be enzymatically resistant, would solve the issue of the breakdown and subsequent loss of aggrecan and CS within the disc.

Although the development and use of biocompatible materials for clinical applications have been occurring for decades, this is still very much an emerging field. There is still a great deal to be investigated and understood regarding the use of absorbable polymers to aid with tissue regeneration or the creation of polymers that can replace damaged tissue and restore normal function. The latter issue is of particular importance because device lifetimes of 10 to 20 years may no longer be suitable for the growing size of the aging population. The advancement of the field of biomaterials can also have a great effect on reducing the invasiveness of surgical procedures and the frequency with which such procedures need to be performed. Of particular importance is the desire to reduce the number of secondary or revision surgeries. Addressing these challenges is the overall goal for the future activities of researchers in clinical biomaterials.

References

1. Elices, M. 2000. *Structural Biological Materials: Design and Structure–Property Relationships*. Kidlington, Oxford, UK: Elsevier Science Ltd.
2. Blitz, R. M., and E. D. Pellegrino. 1969. The chemical anatomy of bone. *Journal of Bone and Joint Surgery* 51-A(3):456–466.

3. Posner, A. 1987. Bone mineral and the mineralization process. *Bone and Mineral Research* 5.
4. McElhaney, J. H., and E. F. Byars. 1965. Dynamic Response of Biological Materials. ASME paper: 1–8.
5. Bonfield, W. et al. 1978. Crack velocity and the fracture of bone. *Journal of Biomechanics* 11(10–12):473–479.
6. Melvin, J., and F. Evans. 1973. Crack propagation in bone, ASME Biomechanics Symposium.
7. Gilding, D., and A. Reed. 1979. Biodegradable polymers for use in surgery—polyglycolic/poly(actic acid) homo-and copolymers: 1. *Polymer* 20(12):1459–1464.
8. Muggli, D. S. et al. 1999. Crosslinked polyanhydrides for use in orthopedic applications: Degradation behavior and mechanics. *Materials Research* 46:271–278.
9. Tangpasuthadol, V. et al. 2000. Hydrolytic degradation of tyrosine-derived polycarbonates, a class of new biomaterials. Part II: 3-yr study of polymeric devices. *Biomaterials* 21(23): 2379–2387.
10. Bergsma, J. et al. 1995. Late degradation tissue response to poly(-lactide) bone plates and screws. *Biomaterials* 16(1):25–31.
11. Middleton, J. C., and A. J. Tipton. 2000. Synthetic biodegradable polymers as orthopedic devices. *Biomaterials* 21(23):2335–2346.
12. Burg, K. J. L. et al. 2000. Biomaterial developments for bone tissue engineering. *Biomaterials* 21(23):2347–2359.
13. Lu, L. et al. 2000. Controlled release of transforming growth factor 1 from biodegradable polymer microparticles. *Journal of Biomedical Materials Research* 50(3):440–451.
14. Gopferich, A. 1996. Mechanisms of polymer degradation and erosion. *Biomaterials* 17(2):103–114.
15. Andriano, K. et al. 1999. In vitro and in vivo comparison of bulk and surface hydrolysis in absorbable polymer scaffolds for tissue engineering. *Journal of Biomedical Materials Research* 48(5):602–612.
16. Attawia, M. A. et al. 1999. Proliferation, morphology, and protein expression by osteoblasts cultured on poly(anhydride co-imides). *Journal of Biomedical Materials Research* 48(3):322–327.
17. Pulapura, S., and J. Kohn. 1992. Tyrosine derived polycarbonates: Backbone modified 'pseudo' poly (amino acids) designed for biomedical applications. *Biopolymers* 32(4):411–417.
18. Ng, S. et al. 1997. Synthesis and erosion studies of self-catalyzed poly(ortho ester)s. *Macromolecules* 30(4):770–772.
19. Seidel, J. et al. 1996. Erosion of poly(anhydride co imides): A preliminary mechanistic study. *Journal of Applied Polymer Science* 62(8):1277–1283.
20. Uhrich, K. et al. 1997. In vitro degradation characteristics of poly(anhydride imides) containing trimellitylimidoglycine. *Journal of Applied Polymer Science* 63(11):1401–1411.
21. Malchau, H. et al. 2000. Prognosis of total hip replacement: 67th Annual Meeting of the American Academy of Orthopaedic Surgeons, Orlando, Florida.
22. Insall, J. N. et al. 1976. A comparison of four models of total knee-replacement prostheses. *The Journal of Bone and Joint Surgery. American Volume* 58(6):754.
23. Skolnick, M. D. et al. 1976. Geometric total knee arthroplasty. A two-year follow-up study. *The Journal of Bone and Joint Surgery. American Volume* 58(6):749.
24. Jones, L. C., and D. S. Hungerford. 1987. Cement disease. *Clinical Orthopaedics and Related Research* 225:192.
25. Wilson, J., and J. T. Scales. 1970. Loosening of total hip replacements with cement fixation: Clinical findings and laboratory studies. *Clinical Orthopaedics and Related Research* 72:145.
26. Mjoberg, B. et al. 1986. Mechanical loosening of total hip prostheses. A radiographic and roentgen stereophotogrammetric study. *Journal of Bone and Joint Surgery-British Volume* 68(5):770.
27. Sturup, J. et al. 1994. Effects of polymerization heat and monomers from acrylic cement on canine bone. *Acta Orthopaedica Scandinavica* 65(1):20–23.
28. Moore, A. T. 1957. The self-locking metal hip prosthesis. *The Journal of Bone and Joint Surgery. American Volume* 39(4):811.
29. Moore, A. T., and H. Bohlman. 1943. Metal hip joint. *The Journal of Bone and Joint Surgery* 25:688–692.

30. Ring, P. 1968. Complete replacement arthroplasty of the hip by the Ring prosthesis. *Journal of Bone and Joint Surgery-British Volume* 50(4):720.
31. Lennox, D. W. et al. 1987. A histologic comparison of aseptic loosening of cemented, press-fit, and biologic ingrowth prostheses. *Clinical Orthopaedics and Related Research* 225:171.
32. Maloney, W. et al. 1993. Severe osteolysis of the pelvic in association with acetabular replacement without cement. *The Journal of Bone and Joint Surgery. American Volume* 75(11):1627.
33. Maloney, W. J. et al. 1990. Endosteal erosion in association with stable uncemented femoral components. *Journal of Bone and Joint Surgery. American Volume* 72(7):1025–1034.
34. Coleman, D. et al. 1974. The foreign body reaction: a chronic inflammatory response. *Journal of Biomedical Materials Research* 8(5):199–211.
35. Charnley, J. 1963. Tissue reactions to polytetrafluoroethylene (letter). *Lancet* 2:1379.
36. Branemark, P. 1985. Introduction to osseointegration. In *Tissue-Integrated Prostheses: Osseointegration in Clinical Dentistry* 11–76. Chicago: Quintessence.
37. Albrektsson, T. et al. 1987. Present clinical applications of osseointegrated percutaneous implants. *Plastic and Reconstructive Surgery* 79(5):721.
38. Albrektsson, T. 1987. Bone–metal interface in osseointegration. *The Journal of Prosthetic Dentistry* 57:597–607.
39. Branemark, P. I. et al. 1969. Intra-osseous anchorage of dental prostheses: I. Experimental studies. *Scandinavian Journal of Plastic and Reconstructive Surgery and Hand Surgery* 3(2):81–100.
40. Williams, D. 1981. Titanium and titanium alloys. In *Biocompatibility of Clinical Implant Materials* 1:9–44. Boca Raton, FL: CRC Press.
41. Martinez, H. et al. 2001. Optimal implant stabilization in low density bone. *Clinical Oral Implants Research* 12(5):423–432.
42. Yaszemski, M. J. 2004. *Biomaterials in Orthopedics*. Informa HealthCare.
43. Mow, V. C., and G. Ateshian. 1997. Lubrication and wear of diarthrodial joints. *Basic Orthopedic Biomechanics* 275–315.
44. Maroudas, A. et al. 1975. Factors involved in the nutrition of the human lumbar intervertebral disc: Cellularity and diffusion of glucose in vitro. *Journal of Anatomy* 120(Pt 1):113.
45. Mayne, R. 1989. Cartilage collagens. What is their function, and are they involved in articular disease? *Arthritis & Rheumatism* 32(3):241–246.
46. Hunziker, E. B. et al. 1997. Ultrastructure of adult human articular cartilage matrix after cryotechnical processing. *Microscopy Research and Technique* 37(4):271–284.
47. Meachim, G., and S. Sheffield. 1969. Surface ultrastructure of mature adult human articular cartilage. *The Journal of Bone and Joint Surgery. British Volume* 51(3):529.
48. Muir, H., et al. 1970. The distribution of collagen in human articular cartilage with some of its physiological implications. *Journal of Bone and Joint Surgery-British Volume* 52(3):554.
49. Maroudas, A. 1979. Physicochemical properties of articular cartilage. *Adult Articular Cartilage* 2:215–290.
50. Armstrong, C., and V. Mow. 1982. Variations in the intrinsic mechanical properties of human articular cartilage with age, degeneration, and water content. *The Journal of Bone and Joint Surgery. American Volume* 64(1):88.
51. Kempson, G., and M. Freeman. 1979. *Adult Articular Cartilage*, 333–414. London: Pitman Medical.
52. Athanasiou, K. et al. 1994. Comparative study of the intrinsic mechanical properties of the human acetabular and femoral head cartilage. *Journal of Orthopaedic Research* 12(3):340–349.
53. Athanasiou, K. et al. 1998. Biomechanical topography of human articular cartilage in the first metatarsophalangeal joint. *Clinical Orthopaedics and Related Research* 348:269.
54. Athanasiou, K. et al. 1995. Biomechanical topography of human ankle cartilage. *Annals of Biomedical Engineering* 3(5):697–704.
55. Athanasiou, K. et al. 1991. Interspecies comparisons of in situ intrinsic mechanical properties of distal femoral cartilage. *Journal of Orthopaedic Research* 9(3):330–340.
56. Schinagl, R. M. et al. 1997. Depth dependent confined compression modulus of full thickness bovine articular cartilage. *Journal of Orthopaedic Research* 15(4):499–506.

57. Abbott, A. et al. 2003. Biomechanics of articular cartilage and menisci of the adult knee. *The Adult Knee* 1:81.
58. Armstrong, C., and D. Gardner. 1977. Thickness and distribution of human femoral head articular cartilage. Changes with age. *Annals of the Rheumatic Diseases* 36(5):407.
59. Meachim, G. 1971. Effect of age on the thickness of adult articular cartilage at the shoulder joint. *Annals of the Rheumatic Diseases* 30(1):43.
60. Meachim, G. et al. 1977. Effect of age on thickness of adult patellar articular cartilage. *Annals of the Rheumatic Diseases* 36(6):563.
61. Vignon, E. et al. 1977. The cellularity of fibrillated articular cartilage. A comparative study of age-related and osteoarthrotic cartilage lesions from the human femoral head]. *Pathologie-Biologie* 25(1):29.
62. Adams, C. S., and W. E. Horton, Jr. 1998. Chondrocyte apoptosis increases with age in the articular cartilage of adult animals. *The Anatomical Record* 250(4):418–425.
63. Barbero, A. et al. 2004. Age related changes in human articular chondrocyte yield, proliferation and post-expansion chondrogenic capacity. *Osteoarthritis and Cartilage* 12(6):476–484.
64. Martin, J. A. et al. 1997. Age related decline in chondrocyte response to insulin like growth factor I: The role of growth factor binding proteins. *Journal of Orthopaedic Research* 15(4): 491–498.
65. Axelsson, I., and A. Bjelle. 1979. Proteoglycan structure of bovine articular cartilage: Variation with age and in osteoarthrosis. *Scandinavian Journal of Rheumatology* 8(4):217–221.
66. Dekel, S., and S. Weissman. 1978. Joint changes after overuse and peak overloading of rabbit knees in vivo. *Acta Orthopaedica* 49(6):519–528.
67. Mankin, H. et al. 1994. Form and function of articular cartilage. *Orthopaedic Basic Science*, 1–44. Rosemont, IL: American Academy of Orthopaedic Surgeons.
68. Furukawa, T. et al. 1980. Biochemical studies on repair cartilage resurfacing experimental defects in the rabbit knee. *Journal of Bone and Joint Surgery* 62:79–89.
69. Chiu, F. Y., and C. M. Chen. 2007. Surgical debridement and parenteral antibiotics in infected revision total knee arthroplasty. *Clinical Orthopaedics and Related Research* 461:130.
70. Cuff, D. et al. 2008. The treatment of deep shoulder infection and glenohumeral instability with debridement, reverse shoulder arthroplasty and postoperative antibiotics. *Journal of Bone and Joint Surgery-British Volume* 90(3):336.
71. Federico, D. J., and B. Reider. 1997. Results of isolated patellar debridement for patellofemoral pain in patients with normal patellar alignment. *The American Journal of Sports Medicine* 25(5):663.
72. Gould, N., and A. Flick. 1985. Post-fracture, late debridement resection arthroplasty of the ankle. *Foot & Ankle* 6(2):70.
73. Jackson, R. 1997. Point–counterpoint: Arthroscopic debridement versus arthroplasty in the osteoarthritic knee. *The Journal of Arthroplastay* 12(4):465–470.
74. Vingerhoeads, B. et al. 2004. Debridement arthroplasty for osteoarthritis of the elbow (Outerbridge–Kashiwagi procedure). *Acta Orthopaedica Belgica* 70:306–310.
75. Bae, D. K. et al. 2006. Cartilage healing after microfracture in osteoarthritic knees. *Arthroscopy: The Journal of Arthroscopic & Related Surgery* 22(4):367–374.
76. Becher, C., and H. Thermann. 2005. Results of microfracture in the treatment of articular cartilage defects of the talus. *Foot & Ankle International/American Orthopaedic Foot and Ankle Society [and] Swiss Foot and Ankle Society* 26(8):583.
77. Kai, M. et al. 2006. Chondral resurfacing of articular cartilage defects in the knee with the microfracture techniquesurgical technique. *The Journal of Bone and Joint Surgery. American Volume* 88(1 Suppl 2):294–304.
78. Siebold, R. et al. 2003. Combination of microfracture and periostal-flap for the treatment of focal full thickness articular cartilage lesions of the shoulder: a prospective study. *Knee Surgery, Sports Traumatology, Arthroscopy* 11(3):183–189.
79. Dorotka, R. et al. 2005. Repair of articular cartilage defects treated by microfracture and a three-dimensional collagen matrix. *Biomaterials* 26(17):3617–3629.

80. Erggelet, C. et al. 2009. Formation of cartilage repair tissue in articular cartilage defects pretreated with microfracture and covered with cell free polymer based implants. *Journal of Orthopaedic Research* 27(10):1353–1360.
81. Hoemann, C. D. et al. 2005. Chitosan-glycerol phosphate/blood implants improve hyaline cartilage repair in ovine microfracture defects. *Journal of Bone and Joint Surgery. American Volume* 87(12):2671–2686.
82. Kreuz, P. C. et al. 2006. Is microfracture of chondral defects in the knee associated with different results in patients aged 40 years or younger? *Arthroscopy: The Journal of Arthroscopic & Related Surgery* 22(11):1180–1186.
83. Mithoefer, K. et al. 2009. Clinical efficacy of the microfracture technique for articular cartilage repair in the knee. *The American Journal of Sports Medicine* 37(10):2053.
84. Marcacci, M. et al. 1999. *Use of autologous grafts for reconstruction of osteochondral defects of the knee. Orthopedics* 22(6):595.
85. Langer, F., and A. Gross. 1974. Immunogenicity of allograft articular cartilage. *Plastic and Reconstructive Surgery* 54(4):507.
86. Athanasiou, K. A. et al. 2009. Articular cartilage tissue engineering. Synthesis Lectures on Tissue Engineering 1(1):1–182, San Rafael, CA: Morgan & Claypool Publishers.
87. Heng, B. C. et al. 2004. Directing stem cell differentiation into the chondrogenic lineage in vitro. *Stem Cells* 22(7):1152–1167.
88. Betre, H. et al. 2006. Chondrocytic differentiation of human adipose-derived adult stem cells in elastin-like polypeptide. *Biomaterials* 27(1):91–99.
89. Kramer, J. et al. 2003. In vitro differentiation of mouse ES cells: Bone and cartilage. *Methods in Enzymology* 365:251–268.
90. Kramer, J. et al. 2000. *Embryonic stem cell–derived chondrogenic differentiation in vitro: activation by BMP-2 and BMP-4*. *Mechanisms of Development* 92(2):193–205.
91. Brittberg, M. et al. 1994. Treatment of deep cartilage defects in the knee with autologous chondrocyte transplantation. *New England Journal of Medicine* 331(14):889–895.
92. Falez, F., and F. Sciarretta. 2005. Treatment of osteochondral symptomatic defects of the knee with SaluCartilage. *Journal of Bone and Joint Surgery - British Volume* 87(Supp II):202.
93. McNickle, A. G. et al. 2008. Overview of existing cartilage repair technology. *Sports Medicine and Arthroscopy Review* 16(4):196.
94. Elisseeff, J. et al. 1999. Transdermal photopolymerization for minimally invasive implantation. *Proceedings of the National Academy of Sciences of the United States of America* 96(6):3104.
95. Elisseeff, J. et al. 2000. Photoencapsulation of chondrocytes in poly (ethylene oxide)-based semi-interpenetrating networks. *Journal of Biomedical Materials Research* 51(2):164–171.
96. Comper, W. D., *Extracellular Matrix*, vol. 2. 1996: Boca Raton, FL: CRC Press.
97. Danylchuk, K. et al. 1978. Microstructural organization of human and bovine cruciate ligaments. *Clinical Orthopaedics* 131:294–298.
98. Komi, P. et al. 1992. Biomechanical loading of Achilles tendon during normal locomotion. *Clinics in Sports Medicine* 11(3):521.
99. Wahrenberg, H. et al. 1978. Knee muscular moment, tendon tension force and EMG during a vigorous movement in man. *Scandinavian Journal of Rehabilitation Medicine* 10(2):99.
100. Noyes, F. R., and E. S. Grood. 1976. The strength of the anterior cruciate ligament in humans and rhesus monkeys. *The Journal of Bone and Joint Surgery. American Volume* 58(8):1074.
101. Wallbridge, N., and D. Dowson. 1982. The walking activity of patients with artificial hip joints. *ARCHIVE: Engineering in Medicine 1971–1988* (vols 1–17), 11(2):95–96.
102. Micheli, L. J. 1986. Lower extremity overuse injuries. *Acta Medica Scandinavica* 220(S711):171–177.
103. Jarvinen, M. 1992. Epidemiology of tendon injuries in sports. *Clinics in Sports Medicine* 11(3):493.
104. Lyman, S. et al. 2009. Epidemiology of anterior cruciate ligament reconstruction: trends, readmissions, and subsequent knee surgery. *The Journal of Bone and Joint Surgery. American Volume* 91(10):2321–2328.
105. Khatod, M., and D. Amiel. 2003. Ligament biochemistry and physiology. *Daniel's Knee Injuries: Ligament and Cartilage Structure, Function, Injury, and Repair* 31.

106. Louie, L. et al. 1998. Tissue engineered tendon. *Frontiers in Tissue Engineering* 413–442. New York: Elsevier Science, Ltd.
107. Amiel, D. et al. 1990. Collagenase activity in anterior cruciate ligament: protective role of the synovial sheath. *Journal of Applied Physiology* 69(3):902.
108. Vieira, A. C. et al. 2009. Development of ligament tissue biodegradable devices: A review. *Journal of Biomechanics* 42(15):2421–2430.
109. Chen, C. C. et al. 2003. Preparation and characterization of biodegradable PLA polymeric blends. *Biomaterials* 24(7):1167–1173.
110. Altman, G. H. et al. 2002. Silk matrix for tissue engineered anterior cruciate ligaments. *Biomaterials* 23(20):4131–4141.
111. Freeman, J. W. et al. 2007. Tissue engineering of the anterior cruciate ligament using a braid-twist scaffold design. *Journal of Biomechanics* 40(9):2029–2036.
112. Horan, R. L. et al. 2006. Yarn design for functional tissue engineering. *Journal of Biomechanics* 39(12):2232–2240.
113. Konikoff, J. et al. 1974. Development of a single stage active tendon prosthesis. I. Distal end attachment. *Journal of Bone and Joint Surgery. American Volume* 56:848.
114. White, A. A., and M. M. Panjabi. 1990. *Clinical Biomechanics of the Spine*, vol. 446. Philadelphia, PA: Lippincott.
115. Atlas, S. J., and R. A. Deyo. 2001. Evaluating and managing acute low back pain in the primary care setting. *Journal of General Internal Medicine* 16(2):120–131.
116. Martin, B. I. et al. 2008. Expenditures and health status among adults with back and neck problems. *JAMA: the Journal of the American Medical Association* 299(6):656.
117. Errington, R. et al. 1998. Characterisation of cytoplasm filled processes in cells of the intervertebral disc. *Journal of Anatomy* 192(3):369–378.
118. Bron, J. L. et al. 2009. Repair, regenerative and supportive therapies of the annulus fibrosus: Achievements and challenges. *European Spine Journal* 18(3):301–313.
119. Adams, M. A., and P. J. Roughley. 2006. What is intervertebral disc degeneration, and what causes it? *Spine* 31(18):2151.
120. McMillan, D. et al. 1996. Effect of sustained loading on the water content of intervertebral discs: Implications for disc metabolism. *Annals of the Rheumatic Diseases* 55(12):880.
121. Hedlund, L. et al. 1989. Change in vertebral shape in spinal osteoporosis. *Calcified Tissue International* 44(3):168–172.
122. Pollintine, P. et al. 2004. Intervertebral disc degeneration can lead to "stress-shielding" of the anterior vertebral body: A cause of osteoporotic vertebral fracture? *Spine* 29(7):774.
123. Raj, P. P. 2008. Intervertebral disc: Anatomy physiology pathophysiology treatment. *Pain Practice* 8(1):18–44.
124. Buckwalter, J. A. 1995. Aging and degeneration of the human intervertebral disc. *Spine* 20(11):1307.
125. Martz, E. O. et al. 1997. Materials and design of spinal implants: A review. *Journal of Biomedical Materials Research* 38(3):267–288.
126. Waisbrod, H. 1988. Treatment of metastatic disease of the spine with anterior resection and stabilization by means of a new cancellous metal construct. *Archives of Orthopaedic and Trauma Surgery* 107(4):222–225.
127. Merritt, K., and S. A. Brown. 1996. Distribution of cobalt chromium wear and corrosion products and biologic reactions. *Clinical Orthopaedics and Related Research* 329:S233.
128. Kurtz, S. M., and J. N. Devine. 2007. PEEK biomaterials in trauma, orthopedic, and spinal implants. *Biomaterials* 28(32):4845–4869.
129. Wuisman, P. I. J. M., and T. Smit. 2006. Bioresorbable polymers: Heading for a new generation of spinal cages. *European Spine Journal* 15(2):133–148.
130. Nabhan, A. et al. 2009. Comparison of bioresorbable and titanium plates in cervical spinal fusion: Early radiologic and clinical results. *Journal of Spinal Disorders & Techniques* 22(3):155.
131. Cho, D. Y. et al. 2004. Treatment of multilevel cervical fusion with cages. *Surgical Neurology* 62(5):378–385.

132. White, A. P. et al. 2007. Intervertebral disc arthroplasty as an alternative to spinal fusion: rationale and biomechanical and design considerations. In *Spinal Reconstruction: Clinical Examples of Applied Basic Science, Biomechanics and Engineering*. 263–278. New York, NY: Informa Healthcare.
133. Hedman, T. P. et al. 1991. Design of an intervertebral disc prosthesis. *Spine* 16(6S):S256.
134. Cloyd, J. M. et al. 2007. Material properties in unconfined compression of human nucleus pulposus, injectable hyaluronic acid–based hydrogels and tissue engineering scaffolds. *European Spine Journal* 16(11):1892–1898.
135. Joshi, A. et al. 2006. Functional compressive mechanics of a PVA/PVP nucleus pulposus replacement. *Biomaterials* 27(2):176–184.
136. Vernengo, J. et al. 2008. Evaluation of novel injectable hydrogels for nucleus pulposus replacement. *Journal of Biomedical Materials Research Part B: Applied Biomaterials* 84(1):64–69.
137. Boelen, E. J. H. et al. 2007. Towards a functional radiopaque hydrogel for nucleus pulposus replacement. *Journal of Biomedical Materials Research Part B: Applied Biomaterials* 83(2):440–450
138. Adams, M. A. et al. 2009. The internal mechanical functioning of intervertebral discs and articular cartilage, and its relevance to matrix biology. *Matrix Biology* 28(7):384–389.

21

Prosthetics and Orthotics

Aaron K. L. Leung and Winson C. C. Lee

CONTENTS

21.1 Prosthetics and Orthotics

Prostheses and orthoses are used by people with physical disabilities to substitute for or assist with the functions of their affected limb or trunk segments. For the design of prosthetic and orthotic devices, the transmission of forces between the anatomical segment and the device, the distribution of pressure between the human–device interface, as well as the structure and material properties of the device need to be carefully considered.

This chapter starts with an introduction describing the relationships among prosthetic socket design, socket–limb interface pressure, and comfort in prosthetics intervention. It then proceeds to review residual limb pain, the effects of mechanical stress, and prosthetic socket design. Experimental measurement and prediction of interface pressure and

prosthetic shank flexibility using a finite-element (FE) modeling method are also discussed. Then, the biomechanical consideration for the use of advanced osseointegrated prosthetics is addressed. After that foundation, the second part of the chapter focuses on orthotics. This starts with a general description on the classification, requirements, and objectives of orthotic intervention. Following a regional approach, the biomechanical functions, including the strength and flexibility of various designs of orthotic interventions (from foot to hip levels for common pathological conditions), are discussed.

21.2 Prosthetics

There have been significant advancements in prosthetic components in the last two decades. By incorporating appropriate composite materials of carefully designed geometries, prosthetic feet can now store energy at heel strike and release the energy at terminal stance in an attempt to compensate for the loss of the active ankle joint motions. Some prosthetic designs use electric sensors to monitor the movements of the amputees and give signals to the prosthetic knee and ankle for appropriate motions. However, the most advanced prosthetic feet and knee do not ensure a successful prosthetic fit. A prosthesis cannot function if the interface between the prosthesis and the body limb segment is not well considered. A prosthetic socket is part of the prosthesis that contacts with human skin. Its design determines whether discomfort and pain are produced. This section introduces the state-of-the-art research in prosthetic biomechanics, with a focus on the lower limb. It looks into the mechanics at the socket–limb interface and residual limb pain, which can result from the unreasonably high stress applied at the interface.

21.2.1 Prosthetics, Prosthetic Socket, Interface Stress, and Comfort

There are millions of people globally who have had amputations. Most involve the lower limb at the transtibial level.[1,2] Amputation can happen at any age. Traumatic accidents, tumor, and infection are the major causes of amputations. Diabetes mellitus can lead to vascular disease, which is also one of the main causes of lower-limb amputation; there is a decreasing trend in the mean age of people suffering from diabetes mellitus. In addition, some babies are born with the absence of parts of the limbs as a congenital deficiency. Prosthetic replacement is one of the most significant rehabilitation programs for those who have lost their limbs.

The major function of an upper-limb prosthesis is to perform grasping. A mechanical upper-limb prosthesis requires body power (e.g., shoulder flexion) through harnessing to produce the desired controls and motions (e.g., prosthetic hand opening and closing). More advanced prostheses use electric signals (such as electromyographic signals) to control different components of the tasks. The main function of a lower-limb prosthesis is to restore walking. The prosthesis should be able to support the entire bodyweight, requiring that attention be paid to the distribution of mechanical stresses between the prosthesis and the residual limb.

A prosthesis should be comfortable to ensure that the amputee does not give up on the use of the prosthesis easily. To provide comfort, there should be an efficient transfer of mechanical stresses to the residual limb through the prosthetic socket. The socket of a lower-limb prosthesis is designed to support the bodyweight of an amputee by applying a

reasonable amount of stress to the residual limb. The shape of a prosthetic socket is not an exact replica of the residual limb but is modified so that the mechanical stresses are transferred to the residual limb efficiently. In doing so, the nonuniform thickness of the soft tissue and the difference in pain tolerance among different regions of the residual limb are managed. The following sections discuss the relationships among prosthetic design, mechanical stresses developed at the socket–limb interface, and pain. The focus will be on prostheses for amputations at the transtibial level due to the large percentage of amputees at this level.

21.2.2 Phantom and Residual Limb Pain

Pain is an unpleasant sensory experience associated with actual or potential tissue damage. It is common that individuals with acquired amputation experience pain. The locations of pain in amputees are commonly described as the phantom limb and the residual limb. Phantom limb pain is a painful sensation perceived in the region of the missing limb. Commonly, pain in the amputated portion of the limb is similar to the pain perceived in the limb before amputation,[3–5] and the pain site is primarily localized to the distal part of the missing limb.[6] This kind of pain is not related to mechanical stresses. It has been suggested that phantom pain is caused by the central nervous system misinterpreting impulses generated from the residual limb as originating from the missing limb.[7] Psychological factors and the degree of blood flow to the residual limb may also play a role.

Residual limb pain is different from phantom limb pain in that the pain site is at the residual limb as opposed to the phantom limb, which is perceived in the *missing* portion of the limb. Although residual limb pain is less frequent, those who have this pain experience it for longer periods, at a greater level of intensity, and with a greater amount of interference in their daily lifestyles than amputees who were experiencing phantom limb pain.[8] Residual limb pain can usually be explained biomechanically. Improper prosthetic fitting is one of the major causes of limb pain.[9,10] This occurs when the prosthesis applies intolerable pressure to the residual limb.

21.2.3 Residual Limb Pain and Mechanical Stresses

Pain tolerance in the context of prosthetics refers to the maximum average pressure the residual limb can tolerate without excessive effort. Pain tolerance can be measured by using a simple indentation method (Figure 21.1). In such measurements, force is applied to the test regions perpendicular to the skin surface through a flat-ended indenting material connected to a mechanical force transducer until it cannot be tolerated, and it is stopped when directed by the recipient.

Different regions of the residual limbs can be tested for pain. A study of eight transtibial amputees revealed that the areas of the midpatellar tendon (MPT) and medial tibial flare tolerated the highest amounts of pressure, whereas the distal end of the fibula tolerated the least amount of pressure.[11] This quantitative finding is consistent with the qualitative description of Radcliff and Foort.[12] Therefore, a patellar tendon–bearing (PTB) socket (detailed later in Section 21.2.4) is designed to have undercuts at the MPT and medial tibial flare regions, which relieves pressure at the distal end (Figure 21.2).

As far as other test regions are concerned, the soft-tissue regions, including the medial and lateral regions' tibial muscles, the midshank of the fibula, and the popliteal muscles, have lower pain tolerances than the thin-skin regions, including the tibial tuberosity, the fibular head, the medial tibial flare, and the midtibial crest (Table 21.1). This is in line with

FIGURE 21.1
(See color insert.) Mechanical force transducer used to measure the force applied to the residual limb in the indentation test.

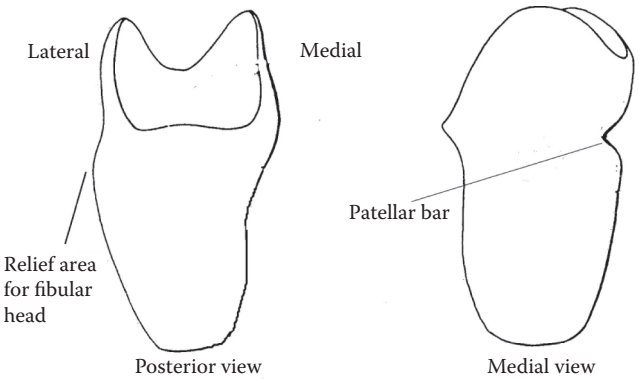

FIGURE 21.2
Typical patellar tendon–bearing (PTB) socket.

TABLE 21.1

Pain Tolerances of Different Regions of the Residual Limb

"Thin-Skin" Regions	Pain Tolerance (MPa)	"Soft Tissue" Regions	Pain Tolerance (MPa)
Tibial tuberosity	0.75 ± 0.24	Anteromedial tibia	0.60 ± 0.14
Fibular head	0.67 ± 0.23	Midshaft of fibula	0.54 ± 0.18
Medial tibial flare	0.67 ± 0.20	Popliteal muscle	0.51 ± 0.19
Midtibial crest	0.63 ± 0.20	Anterolateral tibia	0.48 ± 0.13

the design of the PTB socket. Undercuts and reliefs of the PTB socket are described in terms of displacements instead of force and pressure; for example, about 5 mm of relief is usually suggested for the socket at the fibular head region. Because the mechanical properties of the bony regions with the thin layer of soft tissue are much stiffer than the fleshy regions covered with the thicker soft tissue, for a given magnitude of undercut displacement, the stress produced in the thin-skin regions would be greater than that in the fleshy regions. Although the fleshy regions have a lower pain tolerance, they can tolerate displacement better than thin-skinned regions without pressure significantly shooting up. It is the basic principle of the PTB socket to allow more deformation to be applied at regions with more soft tissue and less deformation at regions with a thin layer of soft tissue.

With the same indentation method and the eight transtibial amputees,[11] each region was tested with two different indenters—Pelite and polypropylene. Pelite is a relatively soft material that is often used as a liner at the socket–residual limb interface, and polypropylene is a thermoplastic material commonly used for the fabrication of prosthetic sockets and orthoses. It was found that each region tolerated significantly higher loads with the softer indenting material (Pelite) than the harder material (polypropylene). This explains why the use of a Pelite prosthetic liner can improve comfort; the softer Pelite indenting material has the ability to deform when loading is applied. The deformation can reduce the peak tissue stress by increasing the contact area with the tissue. The effects of the sharp edge of the indenting material could also be attenuated by the deformability of the Pelite. The relatively stiff polypropylene indenter, however, deforms very little. The stress in the soft tissue at the edge of the stiff polypropylene indenter could be several times greater than that at the center of the indenter.

Another study of six transtibial amputees showed that the pain tolerance increases after walking.[13] Amputee subjects were asked to walk at self-selected comfortable walking speeds on a treadmill. At each trial, they walked for an assigned number of walking steps: 500, 1000, 1500, and 2000 steps. The order of the trials was randomized, and an at least 30-minute rest period was given to the subjects between trials. Immediately after each walking trial, pain tolerance of the residual limbs was measured. It was found that the pain tolerance increased as the number of walking steps increased. The pain tolerance at 2000 steps was 13.4% significantly higher than that recorded before the walking trials. The increase in pain tolerance can be explained by the massage-like effect when the prosthetic socket repeatedly applies pressure onto the residual limb during walking. Some other studies showed that massage aids venous return, relaxes musculature, and relieves tension throughout the body, which helps relieve pain.[14] Noting the potential pain-relief ability, gentle tapping to the distal end and massage over the residual limb have been the therapeutic interventions for amputees with residual limb pain. Some studies also suggest that exercise causes the secretion of endorphins, which may reduce pain.[15]

21.2.4 Prosthetic Design and Mechanical Stress

21.2.4.1 Basic Socket Design

A PTB transtibial socket (Figure 21.2) deforms areas that are deformation-tolerant and provides relief to some pressure-sensitive areas.[12] The transtibial residual limb has several areas that are covered by a thin layer of soft tissues. These areas include the patella, tibial crest, fibular head, and tibial and fibular distal ends. If these thin-skin areas are compressed, high stresses are produced. To reduce the chance of pain and skin breakdown, a PTB socket is designed to provide relief to these areas. Reliefs are also made at the hamstring tendons

and the peroneal nerve that passes the neck of the fibula. Both areas cannot tolerate high pressure. Stress reduction to these areas has to be achieved by redistributing the stress to other areas that have to bear higher stresses. A PTB socket has some undercuts at the areas of the patellar ligament and medial tibial flare, which are the major weight-bearing areas. Undercuts are also created at the areas of the posterior calf muscles, medial shaft of the tibia, and lateral shaft of the fibula, which are covered by a thicker layer of soft tissues.

21.2.4.2 Experimental Measurement of Prosthetic Socket–Residual Limb Interface Stresses

Pressure sensors can be used to directly measure the socket–limb interface stresses. Two measurement techniques have been used: (1) thin sensors are placed between the skin surface and the socket, and (2) holes are drilled at the socket and sensors are positioned through the socket. Previous studies have documented the changes in the socket–limb interface pressure due to fluctuations of the limb volume and under different alignments, cadence, walking tasks, and distal prosthetic components. The accuracy of the measurement depends on the size and type of the sensors, calibration methods, and the consideration of the viscoelastic properties of the soft tissue, as well as the sensors. The maximum pressure applied from a PTB socket during walking is usually less than 220 kPa. Very low pressure is recorded at the bony prominence, hamstring tendons, and the distal end of the residual limb where there is little physical contact with the socket.

21.2.4.3 Computational Finite-Element Modeling

FE analysis divides large and complex structures into small elements of simple shapes. Classic mechanics equations are used to describe the force and displacement of each element. The behavior of the entire structure can then be calculated by combining the equations. Some commercial software packages are available that enable users to build a model in a computer environment and compute the mechanical stress upon application of loads using FE analysis.

In lower-limb prosthetics, FE modeling has been used to study the effects of the shapes and the material properties of the socket,[16–18] the materials of the liners,[18,19] prosthetic alignment,[17,20] residual limb geometry,[18] and frictional properties at the interface[21] on the stress distribution over the residual limb. Attempts have also been made to use FE models to perform real-time stress analyses of the soft tissues and to evaluate the fit of a prosthetic socket by comparing the socket–limb interface pressure with the pressure tolerance of different regions of the limb.

FE analysis has advantages over experimental tests in that pressure, shear stress, and motions can be analyzed over the entire structure, and parametric analysis can be performed efficiently. However, the accuracy of model predictions depends on the geometrical representation of the residual limb and the socket, mechanical properties, and load assignments, as well as the simulation techniques used for the contact between the limb and the socket.

21.2.4.4 Processes of Creating an Finite-Element Model to Study Socket–Limb Interface Stresses

Three steps are required in establishing the FE models: (1) Geometries of the residual limb and the prosthetic socket must be obtained. Computed tomography and magnetic resonance imaging (MRI) can be used to obtain the geometry of the internal bones and the residual limb surfaces of an individual amputee. In earlier days, a less expensive method

using biplanar X-ray to obtain the bones and a digitized loose-wrap cast to obtain the residual limb surface were employed. Anthropometric data from the literature have also been used.[22,23] Geometries of the prosthetic socket can be created by using appropriate computer-aided design (CAD) software; (2) Material properties must be assigned. Bones and prosthetic sockets are usually assigned by a Young's modulus and a Poisson ratio based on previous measurements or values in the literature. They are sometimes assumed to be rigid and fixed bodies. Regarding soft tissues, many previous models assumed it to be elastic, isotropic, homogeneous materials to reduce the complexity of the model; and (3) Loading profiles and contact characteristics are assigned. Loading has been either applied to the proximal end of the femur with the socket fixed or applied to the distal end of the socket with all of the bones and upper end of the soft tissue fixed. The force data are based on those obtained from force platforms, strain-gauge instrumented pylons, or approximated from the bodyweight of the subject. Some earlier models assumed that the residual limb and the prosthetic socket were tied together, where slip and separation at the socket–residual limb interface were not allowed.[17,20] This is unrealistic but saves computational time for a model simulation. More recent models separated the two structures. They allow sliding between the prosthetic socket and the residual limb[24,25]; the coefficient of friction at the interface between the socket and the limb was defined. If the shear force exceeds the frictional force, sliding occurs.

21.2.4.5 Using an Finite-Element Model to Investigate Effects of Shank Flexibility on Socket–Limb Interface Stress

Conventionally, a transtibial prosthesis is composed of a prosthetic socket and a prosthetic foot that is attached rigidly by means of a metal pylon and some adaptors (Figure 21.3). This is the most common approach that has been in use for more than 50 years. Another approach is to fabricate the socket together with the shank out of one piece of a high-temperature thermoplastic material (Figure 21.3). The thermoplastic prosthesis is called a "monolimb." It is far less commonly used due to concerns about durability. In addition, the

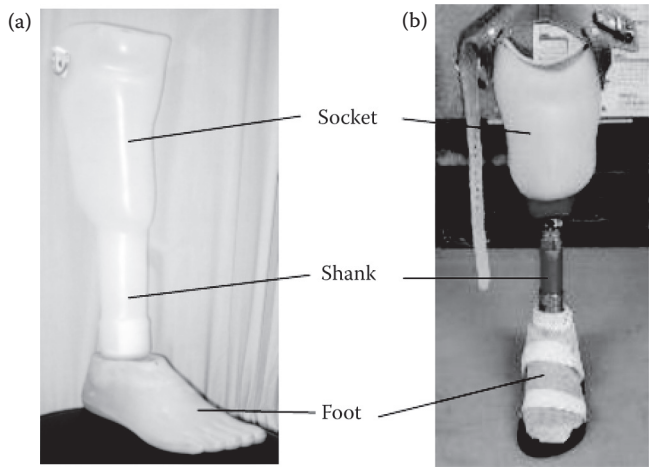

FIGURE 21.3
(See color insert.) A monolimb in which the socket and the shank are formed by one piece of thermoplastic (a), and a conventional transtibial prosthesis in which the shank and the foot are connected by a metal shank (b).

exchange of prosthetic components is not allowed. However, the flexibility of the shank can be tailored. Reducing the material thickness and the cross-sectional area of the shank would increase its flexibility. This could potentially compensate for the lost ankle motions. The shank flexibility might also reduce the mechanical stress applied to the residual limb because the shank deformation can absorb some energy.

An FE model was created to study the effect of shank flexibility on the prosthetic socket–residual limb interface stress. In this FE model,[24,25] the geometries of the bones and soft tissues were obtained by MRI of a transtibial amputee. The geometry of the prosthesis was prepared from CAD software; a PTB socket was used. Different geometries of shanks were created (Figure 21.4), giving different degrees of shank flexibility. A commercial software package for FE analysis was used. An FE mesh with three-dimensional (3D) tetrahedral elements was assigned. The number of elements assigned varied among different monolimb designs ranging from 37,836 to 38,565. Appropriate material properties were assigned, with the Young's modulus of 200 kPa for soft tissues and 1500 MPa for the monolimb structure, as well as a Poisson ratio of 0.45 for soft tissues and 0.3 for the monolimb. The prosthetic foot was partitioned into a keel region and a surrounding rubber foam and was assigned Young's moduli of 700 and 5 MPa, respectively.

The four bones were given fixed boundaries. External loading was applied at the plantar surface of the prosthetic foot according to gait analysis data of the same amputee to simulate heel strike of the gait.[24,25] A coefficient of friction (μ) of 0.5 was assigned for the socket–limb interface. Sliding was allowed only when the shear stress at the interface exceeded the critical shear stress value $\tau > \tau_{crit} = \mu p$, where p is the value of normal stress. The analysis was performed with different shank designs of the monolimb as shown in Figure 21.4.

Shank flexibilities were altered by changing the cross-sectional geometry of the shank. For the monolimb design A (Figure 21.4), the prosthetic foot dorsiflexed to 4.2° at heel off. Reducing the anteroposterior dimension of the shank at the distal end (design B; Figure 21.4) led to increases in the flexibility of the shank. The foot dorsiflexed to 16.3° at heel off in the monolimb design B.

As expected, high pressures fell on the MPT, anterolateral tibia, anteromedial tibia, and popliteal depression regions, where socket undercuts were made. The peak stress values at those four critical regions were different when different shank designs were used. Increases in shank flexibility tended to lead to general decreases in the peak stresses applied to the residual limb. For example, the pressure applied at the patellar tendon areas

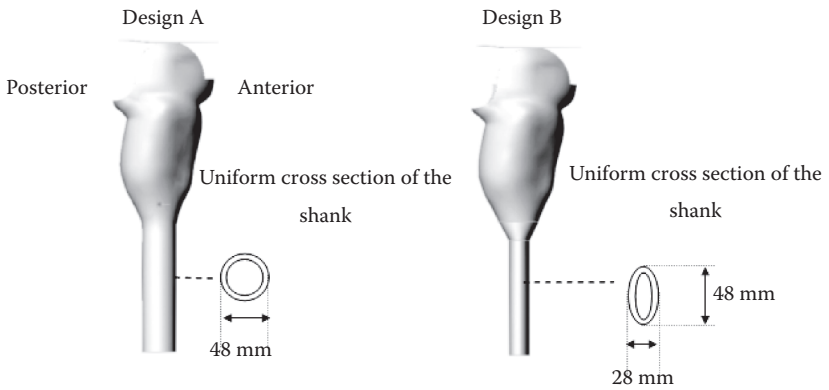

FIGURE 21.4
Two different shank designs analyzed using FE model.

was reduced from 350 to 230 kPa when switching from design A to design B. The trend could be explained when considering energy. Deformation of the prosthesis absorbs some energy, causing the reduction of the energy to actually be transferred to the residual limb. The magnitude of the stresses applied onto the skin surface of the residual limb is related to the comfort perceived by the amputees. A subsequent gait analysis[26] revealed that subjects perceived greater comfort when using a prosthesis with a more flexible shank.

21.2.5 Advancement of Lower-Limb Prostheses—Osseointegration

Researchers are developing a surgical technique that allows a prosthesis to be directly anchored to the bone. The technique is called "osseointegration." The anchorage relies on a fixation system that includes a titanium implant and an abutment.[27] The proximal end of the abutment is directly attached to the implant, and it protrudes through the soft tissue that allows the attachment of the external prosthesis. The absence of a prosthetic socket can alleviate residual limb pain.[28] Amputees using transfemoral osseointegrated prostheses exhibit a greater range of hip motion and report better sitting comfort.[29] They also have improved sensory feedback.[27] There are over 90 transfemoral amputees in the world that are fitted with osseointegrated fixation developed by Dr. R. Branemark. They have had complications in using a socket-type prosthesis due to short residual limbs and soft tissue problems.[27]

Those who use osseointegrated prostheses have to complete a long rehabilitation process so that the bone can tolerate the load during walking. Mechanical failures of the abutment sometimes occur after extended use or accidental application of high magnitude of load.[28] Loosening of the implants after long-term usage also may be an issue due to stress shielding that triggers bone resorption, but the very strong bonding between the titanium implant and the bone may also prevent this from happening. The above-mentioned factors are mechanically related. Biomechanists have measured the 3D loads applied at the abutment during various activities, including walking upstairs, downstairs, up and down an incline, and around a circle.[30,31] Attempts have also been made to use these measured data, together with computational FE modeling, to analyze the stresses transferred to the bone.[32]

21.3 Orthotics

Orthoses are classified by the International Organization for Standardization according to the body parts to which the orthoses are applied. Related orthotic components or parts can be generally divided into interface materials, connectors, structural components, and exterior materials.[33]

Orthoses are classified as follows:

1. Lower-limb orthoses include foot orthosis (FO), ankle–foot orthosis (AFO), knee orthosis (KO), knee–ankle–foot orthosis (KAFO), hip orthosis, and hip–knee–ankle–foot orthosis (HKAFO).
2. Upper limb orthoses include hand orthosis, wrist–hand orthosis, elbow orthosis, elbow–wrist–hand orthosis, shoulder orthosis, and shoulder–elbow–wrist–hand orthosis.

3. Spinal orthoses include cervical orthosis, cervicothoracic orthosis, cervicothoracolumbosacral orthosis, thoracolumbosarcal orthosis, and lumbosacral orthosis.

The functional requirements of these orthoses include the following:[34]

1. To prevent, reduce, or stabilize a deformity
2. To modify the range of motion (ROM) of a joint
3. To add to the length, or alter the shape, of a segment
4. To compensate for weak muscle activity or to control muscle hyperactivity
5. To reduce or redistribute the load on tissues

An orthosis, through one or more of the functions listed above, achieves the following objectives:[34]

1. Relieve pain
2. Manage deformities
3. Prevent an excessive range of joint motions
4. Increase the range of joint motions
5. Compensate for abnormalities of segment length or shape
6. Manage abnormal neuromuscular functions
7. Protect tissues
8. Promote healing
9. Promote other effects such as placebo, provide warmth, and offer positional feedback

Because lower-limb orthoses are most commonly used, this discussion will focus on information related to lower-limb orthotics.

Orthoses apply a three-point pressure control system or a ground reaction force (GRF) control system to maintain anatomical joints in a correct position. In a three-point pressure control system, an orthosis stops or resists the rotation of two body segments about their shared point of rotation. Two forces are applied at the free end of a limb segment, and both are opposed by a third force applied at the point of rotation. A variation of the three-point pressure control, which is more often used in orthotic practice, is the four-point pressure system[35] in which the central force is separated into two forces. The four-point pressure system also produces the required bending moment but without inducing an undesired shearing stress.

When the foot or the orthosis/shoe combination comes in contact with the ground, a GRF is applied to the lower extremity by the ground. This produces moments about the anatomical joints. The resulting motion at the anatomical joints depends on the position of the line of action of the GRF and the movement available at the anatomical joints. If the line of action of the GRF goes through the anatomical joint, then no moment or rotational motion will be created about that joint. If the line of action of the GRF is aligned to one side of the anatomical joint, then a moment is created about the joint. In that case, the GRF rotates the segment about the joint unless it is restricted by counteracting moments from the muscles, ligaments, bony blocks, or other structures. During the swing phase of walking, the foot and orthosis do not touch the ground and no GRF is generated.

21.3.1 Foot Orthoses

An FO is a mechanical device that applies force or pressure through soft tissue to the bony structure to treat various foot and foot-related problems, such as flatfoot, clubfoot, hallux valgus, plantar fasciitis, callus formation, and foot ulcers. The functions of FOs include the following: (1) redirection of forces passing through the foot structure, (2) increase of total contact area, and (3) redistribution of the interface pressure between the foot and the orthoses. FOs can be divided into two basic categories: corrective and accommodative. They can be used to relieve pain, increase heel cushion, correct flexible deformity, increase foot stability, and prevent skin breakdowns such as ulcerations.

The triplanar axis of the subtalar joint forms an angle with all three cardinal planes.[36] The triplanar motions that occur at the subtalar joint are called pronation and supination. Wright et al.[37] defined the neutral position of the subtalar joints as the relaxed standing foot posture (RSFP) when the subject was standing relaxed with the knees fully extended, the arms at the sides, feet 6 in. apart, and with a comfortable amount of toeing-out. Root et al.[38] defined the subtalar joint neutral position (SJNP) as neither pronated nor supinated. McPoil and Cornwall redefined the "neutral" position of the subtalar joint during a walking cycle as the RSFP, which had an average value of 3.64° in eversion, rather than the SJNP.[39] The average time to maximum pronation occurred at 37.9% of the gait cycle. The mean path of subtalar joint motion during the first 60% of the walking cycle occurred between the static angles measured at the RSFP and single leg standing.[40] The SJNP should not be the aim of orthotic intervention because the neutral position of the subtalar joint occurred at 66% and 74% of the gait cycle and was supinated.[41]

"Posted orthosis" refers to the use of wedges added or posted under the forefoot or the hindfoot to prevent abnormal pronation of the subtalar joint. This is de-emphasized, and total contact approach FO is an effective way to control pronation.[42] The medial surface contour of the orthosis must stabilize the medial apical bony structure of the arch.[43] The orthosis should also transmit load through the lateral support structures of the foot, locking the calcaneocuboid joint and decreasing strain in the plantar aponeurosis.[44] A nonposted orthosis reduces maximum pronation as does a posted orthosis.[45] The thermally formed foam plastic total plantar contact FO is one of the most commonly used orthoses for patients with structural foot deformities and neuropathic foot problems such as plantar fasciitis, hallux valgus, and diabetic feet. The orthosis is usually applied to redistribute and reduce plantar pressure under the heel and the metatarsal regions.[46,47] FOs are made with materials of different densities. However, the custom-molded shape rather than the material stiffness of the insoles is more important in reducing peak pressure.[48] An atypical amount or pattern of loading may reflect systemic or localized lower extremity pathology and may serve as an indicator or a predictor of further pathology or worsening of the existing pathology.[49]

Three types of foot shape collection methods are used for the provision of a custom-made FO. These include (1) the digitizing or scanning approach of computer-aided design and computer-aided manufacturing (CAD-CAM) methods, (2) partial weight-bearing foam impression, and (3) nonweight-bearing impression or casting. Although the second and third approaches are still commonly used, the CAD-CAM method is increasingly gaining popularity.

The effects of nonweight-bearing plaster casting, partial weight-bearing foam impression, nonweight-bearing laser scanning, and partial weight-bearing laser scanning methods on shape and plantar pressure have been compared.[50] However, there is no literature to support that the CAD-CAM methods offer better function to patients as compared with the traditional means.

21.3.2 Ankle–Foot Orthoses

AFOs are commonly prescribed to improve the gait of patients with neuromuscular diseases, such as stroke, cerebral palsy, or brain injury. A patient with a spastic ankle joint may require an AFO to prevent foot drop, whereas a patient with ankle instability may need it for better stability. An understanding of the mechanical properties inherent in the design of an AFO, such as flexibility, distribution of force, pressure, and strain, is important because it is key in preventing underprescription or overprescription and in providing an optimal orthosis for a patient. New generations of AFOs with torsional spring dampers,[51] artificial pneumatic muscles,[52] or oil dampers[53] have been designed with articulated joints to adjust the flexibility. With increased rigidity and depending on various angulations at the ankle section of the AFOs, external moments induced by the GRFs influence more proximal joints such as the knee and the hip to improve gait and posture. The amount of passive ankle joint stiffness and ankle ROM in subjects with various pathologies are commonly evaluated manually in the clinical setting. In addition, previous methodologies have involved the use of various devices in evaluating ankle stiffness and ROM.[35,54,55] These parameters are particularly important for orthotists to assess to enable them to determine the mechanical properties required in an AFO design. The mechanical characteristics of an AFO and the physiological characteristics of an anatomical ankle joint need to be matched to maximize the benefit from an orthotic intervention.[56]

Both neural and passive changes contribute to an incremental alteration in ankle joint stiffness.[57] The neural change may be caused by increased motor neuron excitability, whereas the passive change may be due to alterations in the passive mechanical properties of the muscle. The neural component of ankle joint stiffness is controlled by the central nervous system (CNS) independently from the passive component.[58] This control by the CNS deteriorates in the affected ankle joint in patients with stroke. If the change in the passive component of ankle joint stiffness is related to gait in patients with stroke, then the reduction of its stiffness by stretching therapies will result in change in their gait. Therefore, it could be hypothesized that an alteration (reduction) in the ankle joint stiffness would result in a demonstrable change (improvement) of certain gait parameters in patients with stroke. This may also be equated to a less asymmetric gait pattern between the affected and unaffected side. However, comparison of gait velocity between prestatic and poststatic stretching or after cyclic stretching treatment has not revealed significant differences within or between conditions.[59] This may be due to the fact that any improvements in ankle joint stiffness produced by stretching protocols, when measured during static non- or semi-weight-bearing conditions, may not be replicated in dynamic ankle motion.

AFOs improve gait velocity and balance in patients with stroke.[60–62] The use of AFOs results in a functional limb–orthosis combination with increased stiffness depending on the material used and the trim lines chosen. It is likely that improvement in gait and balance functions in patients with stroke may be attributed to a more typical sagittal plane inclination of the shank during midstance when compared with healthy age-matched controls.[63,64]

Functional analyses of AFO[65] have been conducted using either strain gauges to measure forces acting on an orthosis, gait analysis systems to measure plantar and dorsiflexion angles as a parameter of flexibility, experimental AFO to measure the moment generated, or in-shoe pressure measurement systems to measure pressure distribution. The advantage of functional analyses is that they capture the combined effect of an AFO and a lower limb and incorporate the influence of the interface frictional forces and the viscoelastic

properties of a limb on an AFO. However, multiple parameters that originate from human factors, such as the type of disease presented or the degree of gait deficiency, would make it difficult to synthesize the results to obtain a minimum of predictability in designing new AFOs.

Bench analyses have been conducted to investigate the torque–angle or torque–deflection relationships using a tensiometer, strain gauge, load cell, dial gauge, force plate, or muscle training machine.[65] Methods used to apply force to an AFO in previous bench studies have been generally grouped into two types, either direct application of force to a specific area of an orthosis or indirect application of force via a surrogate shank. The advantage of conducting bench analyses is that it is easier to control the experimental parameters in comparison to functional investigations. However, bench conditions do not completely represent the mechanical behavior of an AFO when it is worn during walking because the applied force cannot completely mimic the force acting on an AFO during ambulation. The flexibility of an AFO has been conventionally computed as torque (Nm) versus angle (degrees) or stiffness (Nm per degree). Measurement of flexibility in bench analyses has mainly been conducted in the sagittal plane, but measurements in other planes have also been attempted.

21.3.3 Knee Orthoses

The knee is the largest and most complex synovial joint, and its principal motions are flexion and extension. The rolling and sliding action of the femoral condyles on the tibial plateau present a continually changing center of rotation. As the bone geometry of the joint is incapable of providing stability to the joint, the major stabilizing elements are the fibrous tissues surrounding the joint. The joint capsule and ligaments provide the most stabilization. On the other hand, injury to the joint capsule or ligaments will produce instability. Orthotic devices are generally designed to control or prevent undesirable movement and promote a stabilized joint.

The bony articulation surfaces offer token stability. The fibrous structures around the joint, with its inherent ligamentous thickenings and the menisci, offer a greater but modest degree of stability. A number of the muscles that cross the knee joint offer some stability depending on their origin and insertion. The principal stabilizing structures are the two collateral and two cruciate ligaments. Knee braces are designed to transfer load. Depending on the designs of the leverage systems, they can be applied to prevent instability; for example, the designs can prevent abnormal forward translation of the tibia under the femur in anterior cruciate ligament injury or valgus deformity due to medial collateral ligament deficiency. Polycentric orthotic knee joints are preferred to match with normal knee motions to avoid complications such as chronic laxity of the prestressing ligaments.

Prophylactic knee braces aim to limit the strain on the medial cruciate ligament and the anterior cruciate ligament by shifting a lateral impact force away from the joint line to a more distal or proximal point.[66] However, this increases energy expenditure and restricts motion. Inferior migration of the brace also limits brace efficacy.[67] Rehabilitative knee braces are used to manage anterior cruciate ligament, posterior cruciate ligament, and medial cruciate ligament injuries with or without surgery. This aims to protect the damaged or reconstructed ligaments and allows early immobilization.[68] The proprioceptive ability of a knee joint is affected after an anterior cruciate ligament reconstruction. With the use of a knee brace, proprioception and muscle coordination are enhanced.[69] Functional knee braces are mainly designed for patients with anterior cruciate ligament deficiency or a reconstructed knee to participate in sports activities. Although there are

some subjective benefits, knee braces cannot control the translation and axial rotation at the physiological loads during vigorous exercise.[70] The valgus-inducing knee brace has been prescribed for osteoarthritis of the knee to reduce pain. The orthosis reduces the need for the muscles and ligaments to counteract pathological forces and also reduces internal joint forces within the medial compartment.[71]

21.3.4 Knee–Ankle–Foot Orthoses

A KAFO is required to augment the functions of the foot, ankle, and knee. Conceptually, a KAFO is a combination of a KO and an AFO. Sometimes, a distal section is added to a KO to prevent distal migration, thereby turning a KO into a KAFO. In other words, KAFOs are used in situations in which the forces required to accomplish an established condition are too great to be provided by a KO, or where the suspension of a KO may be too difficult to achieve. They are also indicated when both ankle and knee stability or weakness is present. Most KAFOs consist of proximal and distal arrangements joined by some kind of orthotic knee joint and are mainly divided into conventional and cosmetic (thermoformed) orthoses. A conventional KAFO can have single or double uprights (otherwise known as side members), which may be used to provide control of flexion and extension and lateral stability to the knee. The main biomechanical functions controlling motion, namely, free and limited motion or a locking action, may be applied to both the knee or the ankle in any combination. Double upright KAFOs are still sometimes called long leg calipers. As the name implies, cosmetic KAFOs are made of thermoplastic foot and ankle sections and thigh arrangements and are usually jointed by steel or duralumin uprights incorporating the desired type of orthotic knee joint. They are, for the most part, lighter in weight but are more difficult to adjust.

KAFOs are generally prescribed to control or prevent undesirable movement of the knee joint. The majority of patients who are prescribed a KAFO have difficulty in maintaining an upright position during the stance phase of gait. This may be due to an inability to prevent knee flexion because of muscle weakness or to the presence of a combined knee and ankle flexion deformity. The deformity may present itself in the coronal plane as genu valgum (bow leg) or genu varum (knock knee), or in the sagittal plane as genu recurvatum (knee hyperextension). KAFOs may be used to perform a number of biomechanical functions to influence the stability ROM of the knee and ankle joint. The way in which a KAFO can affect the function of the knee joint depends on the type of proximal arrangement, the materials used, and the type of orthotic knee joint chosen. Various types of orthotic knee joints may be used to achieve the required biomechanical function.

The most common orthotic application is to provide lateral stability to an unstable knee joint, in which restriction of movement in the sagittal plane is not desired. Genu varum and genu valgum are two conditions in which using the long lever arm of a KAFO can be effective in reducing the corrective forces to a minimum. If the deformity is severe enough to consider a weight-relieving design, then a setback type of free knee joint, which uses axial loading to lock itself into extension, should be used. In cases in which there is minimal axial load to be transmitted by the KAFO, it may be possible to use a single upright orthosis to control the deformity. A KAFO with stop function is required when there is a need to limit the range of joint motion. When the knee is required to be held in both flexion and extension, it may be achieved by straight uprights without knee joints or by using orthotic knee joints that lock and unlock but still provide a hold function when locked.

A number of stance-control KAFOs, both mechanical and electronic, have been developed for patients with quadriceps weakness. These designs prevent knee flexion in the

stance phase to provide stability, while also allowing knee flexion in the swing phase. This enables the patient to walk with a more normal gait pattern. Gait biomechanics and energy efficiency are improved compared with a locked knee device.[72,73]

21.3.5 Hip–Knee–Ankle–Foot Orthoses

The hip joint is a ball-and-socket articulation between the femoral head and the acetabulum, formed from the ilium, ischium, and pubis of the hip bone. The acetabular labrum and the transverse acetabular ligament increase stability by deepening the articulation. The head of the femur is completely positioned in the acetabulum when the hip is in flexion, abduction, and internal rotation. HKAFOs have a wide diversity of use and vary considerably in their design. They may be used for reciprocal walking, to control range of joint motion, and as support of the lower limb. The general orthotic objective at the hip level is to permit standing and ambulating where possible. Control of ROM of the hips can be provided by attaching an orthotic hip joint and a supporting band to the lateral upright of a KAFO, thus converting it into an HKAFO.

Perthes disease is an osteochondritis of the capital epiphysis of the femur. Some authorities advocate the use of an ischial weight-bearing KAFO to reduce axial forces transmitted through the hip during the remodeling period. These are made intentionally longer than the lower limb to force the leg into an unweighted abducted position, which orients the head of the femur into the acetabulum in a position that favors spherical remodeling as it heals. This maximum containment or close-packed position is deemed to be at 40° of abduction and 40° of flexion with induced internal rotation of the hip. The abducted position also reduces the forces generated by the hip abductors as the individual walks. The lateral uprights of the orthosis transmit body weight from the ischial tuberosity to the distal weight-supporting end. When weight-bearing relief is not part of the accepted treatment regime, various orthoses may be used to allow hip and knee flexion for sitting while giving the required degree of abduction. It has the disadvantage of not inducing internal rotation and indeed usually produces external hip rotation.

In the past, a paraplegic patient was usually fitted with conventional KAFOs or HKAFOs. In most instances, the wheelchair became the primary means of mobility because of the high energy consumption required to use the orthoses.[74] To improve the physiological and psychological well-being of such patients, they are encouraged to resume their ability to stand or walk in some way.[75] Physiologically, standing and walking can prevent the loss of bone mass and improve balance and hemodynamic response. These activities can also prevent joint contractures, improve urinary and bowel function, reduce spasticity, and decrease the incidence of pressure sores.[76] Likewise, patients can generally improve psychologically. Despite the fact that orthotic ambulation is not, for the most part, a functional replacement of wheelchair mobility, regular walking exercise is encouraged among patients with paraplegia.

A reciprocating gait orthosis allows one leg to be placed ahead of the other during walking to simulate a reciprocal walking gait. It is more often prescribed for patients with higher lesions. The trunk muscles of these patients are severely impaired. They require the trunk section of the reciprocating orthosis to support and stabilize their trunk during walking. The reciprocal walking gait pattern requires less effort to ambulate compared with the swing-through gait, which is facilitated by the conventional orthosis. The orthosis allows the transfer of energy from one leg to the other during the weight-shifting process.[77] Flexion of one hip causes a reciprocal hip extension of the opposite limb. With proper bracing of the trunk and hips, and the application of additional stiffness of the lateral uprights,

a reciprocating gait orthosis can provide a firm support to patients so that they can stand without the use of crutches or walkers. Their hands then become free to perform other activities while standing.[78] However, a pair of elbow crutches is normally required for walking. The gait performance of various orthoses, including reciprocating gait orthoses, among patients with paraplegia has been studied. Compared with other orthotic devices, the reciprocating gait orthosis is more energy efficient.[79] Powered walking devices or rehabilitation robotics have been developed and tested for some years. The mobility of people with paraplegia will be enhanced with the new development.

21.4 Summary

This chapter has focused on lower-limb prostheses and lower-limb orthoses because they are the most commonly used prosthetic and orthotic devices. In these external devices, biomechanics plays an important role because both types of devices modify the force systems applied to the body segments in an attempt to achieve some specific treatment goal(s). A lower-limb prosthesis allows amputees to regain locomotion by replacing the missing portion of the limb and transferring the ground reaction to the residual limb. To avoid soft tissue breakdown and pain at the residual limb, special attention has to be paid to the design of the prosthetic socket, as well as to the load tolerant capability of the different regions of the residual limb. A lower-limb orthosis can relieve musculoskeletal problems by applying a three-point force control system directly to the limbs, or by altering the way that the GRF is applied to the anatomical joints. Such force systems can stabilize the joints, modify ROM, and compensate/control for the weak/hyperactive muscles.

Future investigations should focus on how these modifications of the overall force system can affect the architecture of the soft tissue and bone. This would help elucidate the underlying mechanism of the prosthetic and orthotic treatments. This approach would also help identify if side effects, such as bone resorption after usage of prostheses and joint stiffness after immobilization, can be produced. In improving the prosthetic and orthotic designs, the choices of materials, shapes of the devices, functions of movable components, production cost, and time should be considered. Future designs should incorporate more electronic and intelligent components to control the movable parts of prosthetic and orthotic devices.

References

1. Murdoch, G., and W. A. Bennett. 1996. *Amputation: Surgical Practice and Patient Management*. Boston: Butterworth-Heinemann.
2. Wilson, A. B. 1989. *Limb Prosthetics*. New York: Demos Medical Pub.
3. Herta, F. 2000. Phantom-limb pain: Characteristics, cause, and treatment. *Lancet Neurology* 1(3):182–189.
4. Jensen, T. S., B. Krebs, J. Nielsen et al. 1985. Immediate and long-term phantom limb pain in amputees: Incidence, clinical characteristics and relationship to pre-amputation pain. *Pain* 21(3):267–278.

5. Katz, J., and R. Melzack. 1990. Pain "memories" in phantom limbs: Review and clinical observations. *Pain* 43(3):319–336.
6. Hill, A. 1999. Phantom limb pain: A review of the literature on attributes and potential mechanisms. *Journal of Pain and Symptom Management* 17(2):125–142.
7. Finnoff, J. 2001. Differentiation and treatment of phantom sensation, phantom pain, and residual-limb pain. *Journal of the American Podiatric Medical Association* 91(1):23–33.
8. Gallagher, P., D. Allen, and M. L. MacLachlan. 2001. Phantom limb pain and residual limb pain following lower limb amputation: A descriptive analysis. *Disability and Rehabilitation* 23(12):522–530.
9. Davis, R. W. 1993. Phantom sensation, phantom pain, and stump pain. *Archives of Physical Medicine and Rehabilitation* 74(1):79–91.
10. Golbranson, F. L., and R. W. Wirta. 1988. Volume changes occurring in post-operative below knee residual limbs. *Journal of Rehabilitation Research and Development* 25(2):11–18.
11. Lee, W. C. C., M. Zhang, and A. F. T. Mak. 2005. Regional differences in pain threshold and tolerance of trans-tibial residual limb: Including the effects of age and interface material. *Archives of Physical Medicine and Rehabilitation* 86(4):641–649.
12. Radcliff, C. W., and J. Foort. 1961. *The Patellar-Tendon-Bearing Below-Knee Prosthesis* Berkeley, CA: Biomechanics Laboratory, University of California.
13. Zhang, M., and W. C. C. Lee. 2006. Quantifying regional load bearing ability of trans-tibial stumps. *Prosthetics and Orthotics International* 30(1):25–34.
14. Kingdon, R. T., J. K. Stanley, and R. J. Kizior. *Pain Management* Philadelphia, PA: W. B. Saunders Company.
15. Koseoglu, E., A. Akboyraz, A. Soyuer et al. 2003. Aerobic exercise and plasma beta endorphin levels in patient with migrainous headache without aura. *Cephalalgia* 23:972–976.
16. Quesada, P., and H. B. Skinner. 1991. Analysis of a below-knee patellar tendon-bearing prosthesis: A finite element study. *Journal of Rehabilitation Research and Development* 28(3):1–12.
17. Reynolds, D. P., and M. Lord. 1992. Interface load analysis for computer-aided design of below-knee prosthetic sockets. *Medical & Biological Engineering & Computing* 30(4):419–426.
18. Zhang, M. 1995. Biomechanics of the Residual Limb and Prosthetic Socket Interface in Below-Knee Amputees. PhD diss., University of London.
19. Simpson, G., C. Fisher, and D. K. Wright. 2001. Modeling the interactions between a prosthetic socket, polyurethane liners and the residual limb in trans-tibial amputees using non-linear finite element analysis. *Biomedical Sciences Instrumentation* 37:343–347.
20. Sanders, J. E., and C. H. Daly. 1993. Normal and shear stresses on a residual limb in a prosthetic socket during ambulation: Comparison of finite element results with experimental measurements. *Journal of Rehabilitation Research and Development* 30(2):191–204.
21. Zhang, M., M. Lord, A. R. Turnersmith et al. 1995. Development of a non-linear finite element modeling of the below-knee prosthetic socket interface. *Medical Engineering & Physics* 17(8):559–566.
22. Silver-Thorn, M. B., and D. S. Childress. 1996. Parametric analysis using the finite element method to investigate prosthetic interface stresses for persons with trans-tibial amputation. *Journal of Rehabilitation Research and Development* 33(3):227–238.
23. Silver-Thorn, M. B., and D. S. Childress. 1997. Generic, geometric finite element analysis of the transtibial residual limb and prosthetic socket. *Journal of Rehabilitation Research and Development* 34(2):171–186.
24. Lee, W. C. C., M. Zhang, and D. A. Boone. 2004. Finite element analysis to determine the effect of monolimb flexibility on structural strength and interaction between residual limb and prosthetic socket. *Journal of Rehabilitation Research and Development* 41(6A):775–786.
25. Lee, W. C. C., M. Zhang, X. Jia, and J. T. M. Cheung. 2004. Finite element modeling of contact interface between trans-tibial residual limb and prosthetic socket. *Medical Engineering & Physics* 26(8):655–662.
26. Lee, W. C. C., and M. Zhang. 2006. Gait analysis of low-cost flexible-shank trans-tibial prostheses. *IEEE Transactions on Neural Systems and Rehabilitation Engineering* 14(3):370–377.

27. Brånemark, R., P. I. Brånemark, B. Rydevik et al. 2001. Osseointegration in skeletal reconstruction and rehabilitation: A review. *Journal of Rehabilitation Research and Development* 38(2):175–181.
28. Sullivan, J., M. Uden, K. Robinson et al. 2003. Rehabilitation of the trans-femoral amputee with an osseointegrated prosthesis: The United Kingdom experience. *Prosthetics and Orthotics International* 27(2):114–120.
29. Hagberg, K., E. Haggstrom, M. Uden et al. 2005. Socket versus bone-anchored trans-femoral prostheses: Hip range of motion and sitting comfort. *Prosthetics and Orthotics International* 29(2):153–163.
30. Lee, W. C. C., L. Frossard, K. Hagberg et al. 2007. Kinetics analysis of transfemoral amputees fitted with osseointegrated fixation performing various activities of daily living. *Clinical Biomechanics (Bristol, Avon)* 22(6):665–673.
31. Lee, W. C. C., L. Frossard, K. Hagberg et al. 2008. Magnitude and variability of loading on the osseointegrated fixation of transfemoral amputees during walking. *Medical Engineering & Physics* 30(7):825–833.
32. Lee, W. C. C., J. M. Doocey, L. Frossard et al. 2008. FE stress analysis of the interface between the bone and an osseointegrated implant for amputees—implications to refine the rehabilitation program. *Clinical Biomechanics (Bristol, Avon)* 23(10):1243–1250.
33. International Operation for Standardization. *ISO 13404:2005 Prosthetics and Orthotics. Classification and Description of Orthoses and Orthotic Components.* Geneva, Switzerland.
34. International Operation for Standardization. *ISO 8551:2003 Prosthetics and Orthotics. Functional Deficiencies. Description of the Person to Treated with an Orthosis, Clinical Objectives of Treatment, and Functional Requirements of the Orthosis*. Geneva, Switzerland.
35. Assal, M., J. B. Shofer, E. S. Rohr et al. 2003. Assessment of an electronic goniometer designed to measure equines contracture. *Journal of Rehabilitation Research and Development* 40(3):235–239.
36. Manter, J. T. 1941. Movements of the subtalar and transverse tarsal joints. *The Anatomical Record* 80:397–410.
37. Wright, D. G., S. M. Desai, and W. H. Henderson. 1964. Action of the subtalar and ankle–joint complex during the stance phase of walking. *Journal of Bone and Joint Surgery. American Volume* 46:361–382.
38. Root, M. L., W. P. Orien, and J. H. Weed. 1971. *Biomechanical Examination of the Foot Vol. 1.* Los Angeles: Clinical Biomechanics Corp.
39. McPoil, T. G., and M. W. Cornwall. 1994. Relationship between neutral subtalar joint position and pattern of rearfoot motion during walking. *Foot and Ankle International* 15(3):141–145.
40. McPoil, T. G., and M. W. Cornwall. 1996. Relationship between three static angles of the rearfoot and the pattern of rearfoot motion during walking. *The Journal of Orthopaedic and Sports Physical Therapy* 23(6):309–314.
41. Pierrynowski, M. R., and S. B. Smith. 1996. Rear foot inversion/eversion during gait relative to the subtalar joint neutral position. *Foot and Ankle International* 17(7):406–412.
42. Mueller, M. J., and M. J. Strube. 1994. Effects of three different posting methods on controlling abnormal subtalar pronation. Invited Commentary. *Physical Therapy* 74:65–66.
43. Kogler, G. F., S. E. Solomonidis, and J. P. Paul. 1996. Biomechanics of longitudinal arch support mechanisms in foot orthoses and their effect on plantar aponeurosis strain. *Clinical Biomechanics (Bristol, Avon)* 11(5):243–252.
44. Kogler, G. F., S. E. Solomonidis, and J. P. Paul. 1999. The influence of medial and lateral placement of orthotic wedges on loading of the plantar aponeurosis. *Journal of Bone and Joint Surgery. American Volume* 81(10):1403–1413.
45. Johanson, M. A., R. Donatell, M. J. Wooden et al. 1994. Effects of three different posting methods on controlling abnormal subtalar pronation. *Physical Therapy* 74(2):56–65.
46. Brown, M., S. Rudicel, and A. Esquenazi. 1996. Measurement of dynamic pressures at the shoe-foot interface during normal walking with various foot orthoses using the FSCAN system. *Foot and Ankle International* 17(3):152–156.
47. McPoil, T. G., and M. W. Cornwall. 1992. Effect of insole material on force and plantar pressures during walking. *Journal of the American Podiatric Medical Association* 82(8):412–416.

48. Cheung, T. M., and M. Zhang. 2005. A 3-dimensional finite element model of the human foot and ankle for insole design. *Archives of Physical Medicine and Rehabilitation* 86(2):353–358.
49. Orlin, M. N., and T. G. McPoil. 2000. Plantar pressure assessment. *Physical Therapy* 80(4):399–409.
50. Laughton, C., I. M. Davis, and D. S. Williams. 2002. A comparison of four methods of obtaining a negative impression of the foot. *Journal of the American Podiatric Medical Association* 92(5):261–268.
51. Blaya, J. A., and H. A. Herr. 2004. Adaptive control of a variable-impedance ankle–foot orthosis to assist drop-foot gait. *IEEE Transactions on Neural Systems and Rehabilitation Engineering* 12(1):24–31.
52. Ferris, D. P., J. M. Czerniecki, and B. Hannaford. 2005. An ankle–foot orthosis powered by artificial pneumatic muscles. *Journal of Applied Biomechanics* 21(2):189–197.
53. Yamamoto, S., A. Hagiwara, T. Mizobe et al. 2005. Development of an ankle–foot orthosis with an oil damper. *Prosthetics and Orthotics International* 29(3):209–219.
54. Harvey, L., A. Byak, M. Ostrovskaya et al. 2003. Reliability of a device designed to measure ankle mobility. *Spinal Cord* 41(10):539–562.
55. Orendurff, M. S., E. S. Rohr, B. J. Sangeorzan et al. 2006. An equinus deformity of the ankle accounts for only a small amount of the increased forefoot plantar pressure in patients with diabetes. *The Journal of Bone and Joint Surgery. British Volume* 88(1):65–68.
56. Bregman, D. J., V. De Groot, P. Van Diggele et al. 2010. Polypropylene ankle foot orthoses to overcome drop-foot gait in central neurological patients: a mechanical and functional evaluation. *Prosthetics and Orthotics International* 34(3):293–304.
57. Kobayashi, T., A. K. L. Leung, Y. Akazawa et al. 2011. Evaluating the contribution of a neural component of ankle joint resistive torque in patients with stroke using a manual device. *Brain Injury* 25(3):307–314.
58. Sasagawa, S., J. Ushiyama, K. Masani et al. 2009. Balance control under different passive contributions of the ankle extensors: quiet standing on inclined surfaces. *Experimental Brain Research* 196(4):537–544.
59. Bressel, E., and P. J. McNair. 2002. The effect of prolonged static and cyclic stretching on ankle joint stiffness, torque relaxation, and gait in people with stroke. *Physical Therapy* 82(9):880–887.
60. Cakar, E., O. Durmus, L. Tekin et al. 2010. The ankle–foot orthosis improves balance and reduces fall risk of chronic spastic hemiparetic patients. *European Journal of Physical and Rehabilitation Medicine* 46(3):363–368.
61. Fatone, S., E. Sorci, and A. Hansen. 2009. Effects of clinically prescribed ankle foot orthoses on ankle-foot roll-over shapes: A case series. *Journal of Prosthetics and Orthotics* 21(4):196–203.
62. Ramstrand, N., and S. Ramstrand. 2010. American Academy of Orthotists and Prosthetists: State-of-the science evidence report: The effect of ankle-foot orthoses on balance—a systematic review. *Journal of Prosthetics and Orthotics* 22(4):4–23.
63. Jagadamma, K. C., E. Owen, F. J. Coutts et al. 2010. The effects of tuning an ankle–foot orthosis footwear combination on kinematics and kinetics of the knee joint of an adult with hemiplegia. *Prosthetics and Orthotics International* 34(3):270–276.
64. Owen, E. 2010. The importance of being earnest about shank and thigh kinematics especially when using ankle–foot orthoses. *Prosthetics and Orthotics International* 34(3):254–269.
65. Kobayashi, T., A. K. L. Leung, and S. Hutchins. 2011. Techniques to measure rigidity of ankle-foot orthosis: A review. *Journal of Rehabilitation Research and Development* 48(5):565–576.
66. Erickson, A. R., K. Yasuda, B. Beynnon et al. 1993. An vitro dynamic evaluation of prophylactic knee braces during lateral impact loading. *American Journal of Sports Medicine* 21(1):26–35.
67. Greene, D. L., K. R. Hamson, C. Bay et al. 2000. Effects of protective knee bracing on speed and agility. *American Journal of Sports Medicine* 28(4):453–459.
68. Beynnon, B. D., M. H. Pope, C. M. Wertheimer et al. 1992. The effect of functional knee-braces on anterior cruciate ligament strain in vivo. *Journal of Bone and Joint Surgery. American Volume* 74(9):1298–1312.
69. Kuster, M. S., K. Grob, M. Kuster et al. 1999. The benefits of wearing a compression sleeve after ACL reconstruction. *Medicine and Science in Sports and Exercise* 31(3):368–371.

70. Beynnon, B. D., R. J. Johnson, B. C. Fleming et al. 1997. The effect of functional knee bracing on the anterior cruciate ligament in the weight-bearing and non–weight-bearing knee. *American Journal of Sports Medicine* 25(3):353–359.
71. Bulter, D. L., F. R. Noyes, and E. S. Grood. 1980. Ligamentous restraints to anterior–posterior drawer in the human knee. A biomechanical study. *Journal of Bone and Joint Surgery. American Volume* 62(2):259–270.
72. Hebert, J. S., and A. B. Liggins. 2005. Gait evaluation of an automatic stance-control knee orthosis in a patient with postpoliomyelitis. *Archives of Physical Medicine and Rehabilitation* 86(8):1676–1680.
73. Zissimopoulos, A., S. Fatone, and S. A. Gard. 2007. Biomechanical and energetic effects of a stance-control orthotic knee joint. *Journal of Rehabilitation Research and Development* 44(4):503–514.
74. Blackmer, J. 1997. Orthostatic hypotension in spinal cord injured patients. *The Journal of Spinal Cord Medicine* 20(2):212–217.
75. Jacobs, P. L., K. J. Klose, R. Guest et al. 1997. Relationship of oxygen uptake, heart rate, and rating of perceived exertion in persons with paraplegia during functional neuromuscular stimulation assisted ambulation. *Spinal Cord* 35(5):292–298.
76. Walter, J. A., P. G. Sola, J. Sacks et al. 1999. Indications for a home standing program for individuals with spinal cord injury. *The Journal of Spinal Cord Medicine* 22(3):152–158.
77. Winchester, P. K., J. J. Carollo, R. N. Parekh et al. 1993. A comparison of paraplegic gait performance using two types of reciprocating gait orthoses. *Prosthetics and Orthotics International* 17(2):101–106.
78. Harvey, L. A., M. B. Smith, G. M. Davis et al. 1997. Functional outcomes attained by T9–12 paraplegic patients with the walkabout and the Isocentric Reciprocal Gait Orthoses. *Archives of Physical Medicine and Rehabilitation* 78(7):706–711.
79. Harvey, L. A., G. M. Davis, M. B. Smith et al. 1998. Energy expenditure during gait using the walkabout and Isocentric Reciprocal Gait Orthoses in persons with paraplegic. *Archives of Physical Medicine and Rehabilitation* 79(8):945–949.

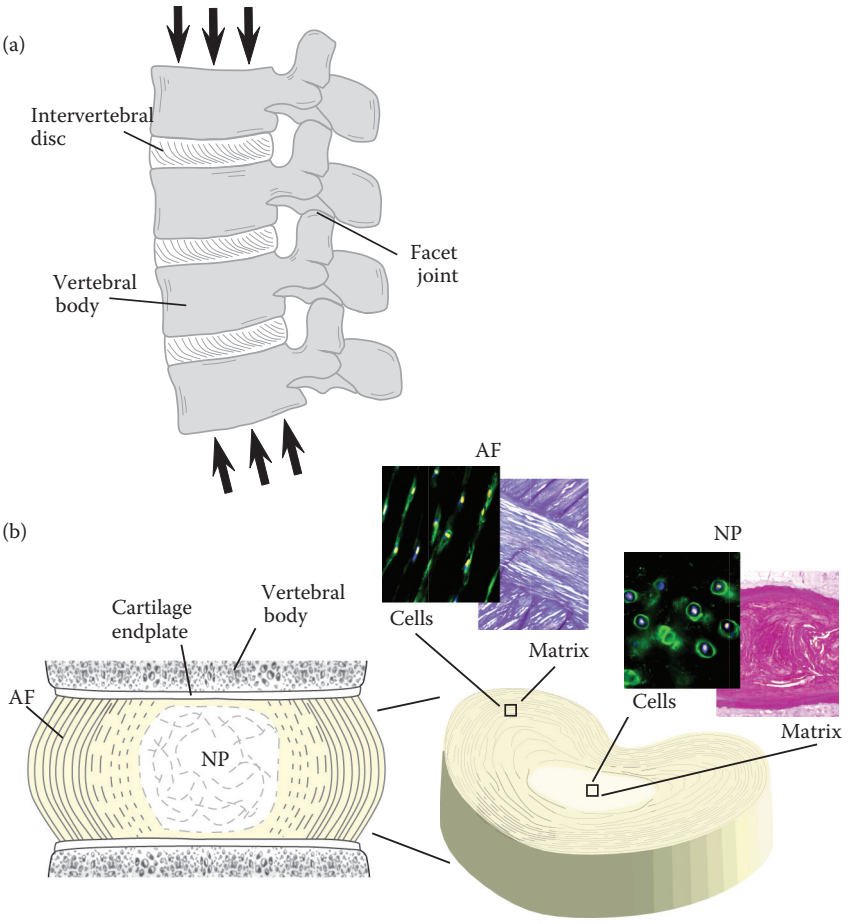

FIGURE 3.1
(a) Intervertebral disc (IVD) is situated between the vertebral bodies in the spinal column and supports loads, provides flexibility, and dissipates energy in the spine. (b) Disc is composed of distinct anatomic zones: the AF, NP, and cartilage endplates. The AF consists of concentric lamella of highly aligned collagen fibers, with cells typically aligned along the fiber direction. The NP is a gelatinous, highly hydrated tissue, with cells typically exhibiting rounded, unaligned morphologies.

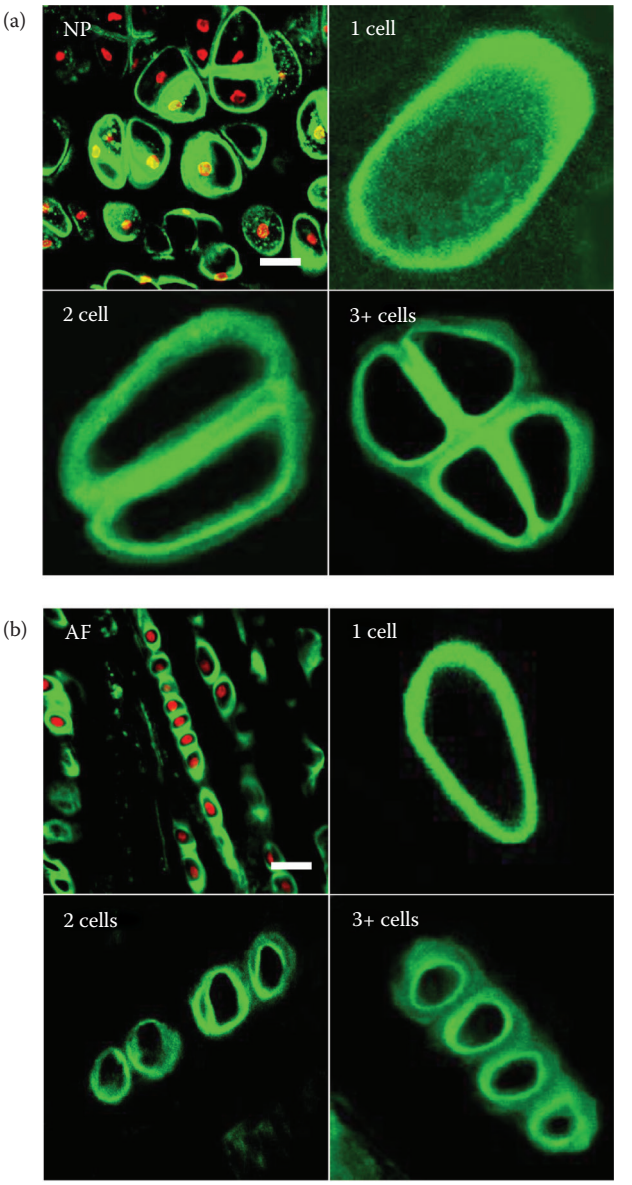

FIGURE 3.2
(a) NP cell–PCM morphology. In rat IVD tissues, nearly all NP cells are associated with a PCM region that is rich in type VI collagen (green). A majority of cells (>80%) reside in a PCM containing two or more cells in the NP. Scale bar = 20 μm, red = cell nuclei. (b) AF cell–PCM morphology. In rat NP tissues, AF cells are also associated with a PCM region rich in type VI collagen (green). A majority of AF cells are found in the PCM containing one or two cells (>90%) in the inner AF region, whereas more than half of the cells resided in the PCM containing three or more cells in the outer AF region. Scale bar = 20 μm, red = cell nuclei.

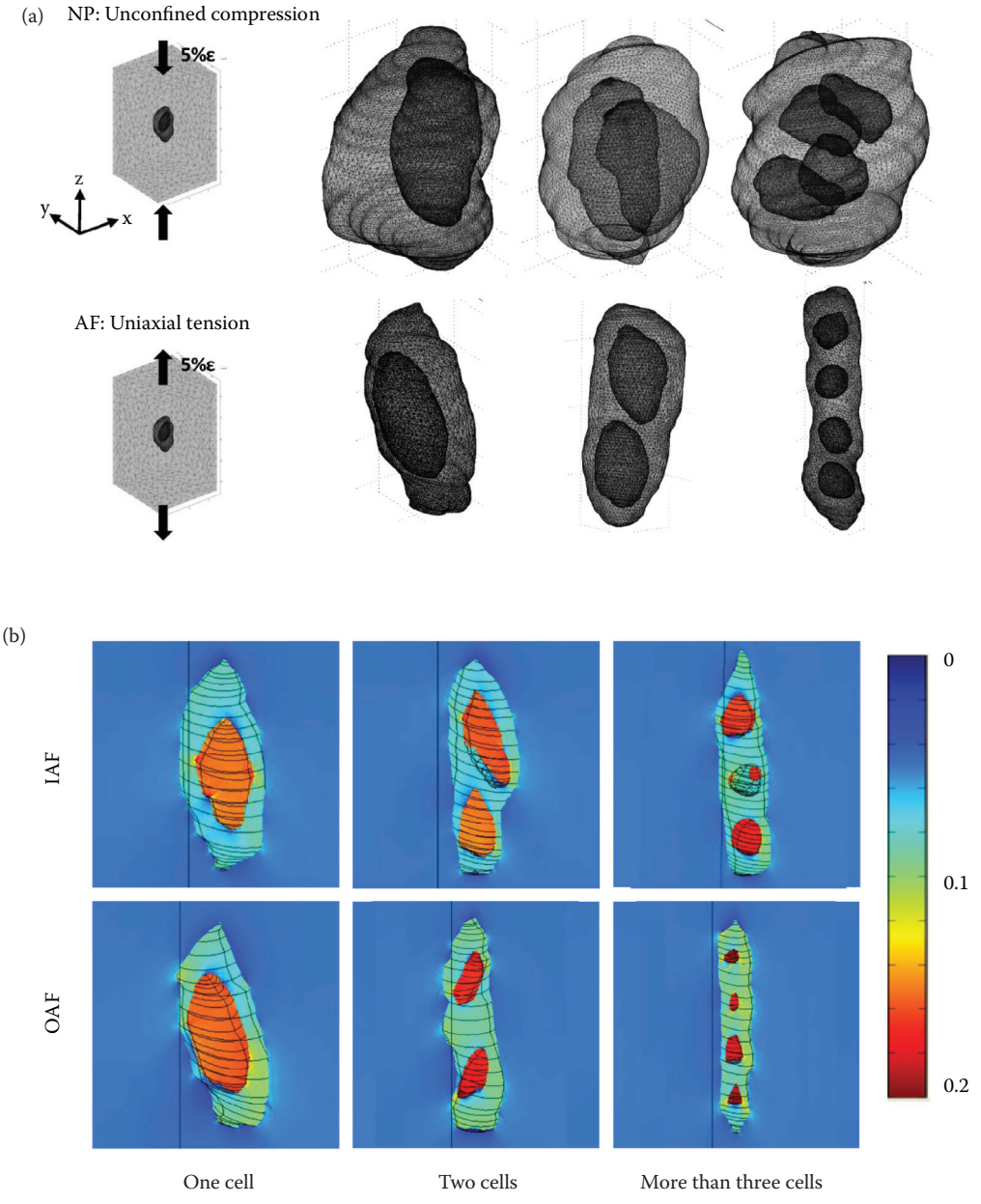

FIGURE 3.8
(a) Three-dimensional FEM of NP and AF cells in representative CMUs. FEM geometry models of CMUs in tetrahedron element meshes. For clarity, only meshes of the PCM and cell surfaces are shown above (not to scale). CMUs in the NP were subjected to an unconfined compression with 5% compressive strain along the principal axis of the CMU. CMUs in the AF were subjected to a uniaxial tension with 5% tensile strain along the principal axis of the CMU. All surfaces of the ECM are assumed to be free-draining. (b) Model predictions of volumetric strain in the AF cell and surrounding PCM after application of a tensile load. Volumetric strain for AF cells in the inner (IAF) and outer (OAF) regions at equilibrium under uniaxial tension. Strain amplification was seen from the extracellular to the pericellular and cellular scales. The strain amplification ratio was the highest in the CMUs with three or more cells and lowest in the CMUs with just one cell.

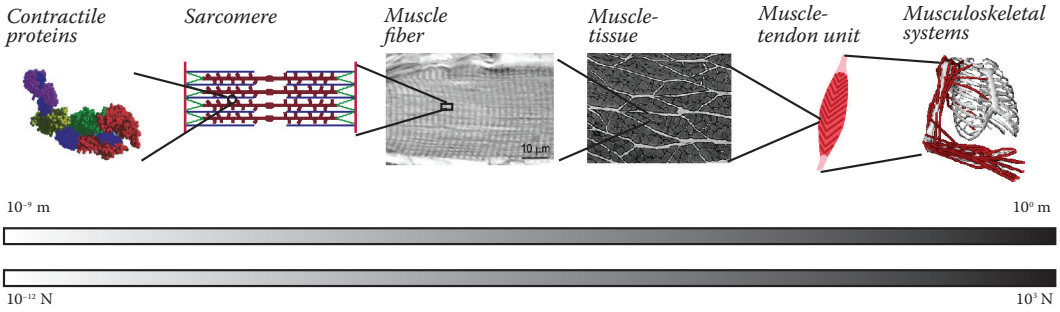

Structural characteristics

Myosin molecular structure Actin molecular structure Titin molecular structure	Desmin Optimal sarcomere length	Fiber type Optimal fiber length Specific tension Muscle spindles	Extracellular matrix Motor unit arrangement Cross-sectional geometry Intrafascicular fiber termination	Pennation angle Aponeurosis properties External tendon properties Golgi tendon organs Physiologic cross-sectional area	Moment arms Muscle attachments Joint kinematics Intermuscular connective tissue Inertial properties Coordination

Example clinical problems

Myosin-related myopathies Titinopathies	Muscular dystrophies Desminopothies	Fiber type transformation Spasticity	Fibrosis Fatty infiltration Scarring	Atrophy Hypertrophy Contractures Tendon injury	CNS impairment Joint impairment Bone deformity

FIGURE 4.1
Structure and function of muscle across several length scales. Muscle has a unique hierarchical structure that allows the actions of molecular motors that each generate pico-Newtons of force to be coordinated to generate up to 10^3 N of force in a whole muscle. Structural variations at each level of this hierarchy allow muscles to be tuned to their specific shape, size, and function. Similarly, muscle pathologies could arise at any level of this hierarchy and result in muscle dysfunction. ("Contractile proteins" image from Rayment, I., Rypniewski, W. R., Schmidt-Base, K., Smith, R., Tomchick, D. R., Benning, M. M. et al. 1993. Three-dimensional structure of myosin subfragment-1: A molecular motor. *Science* 261(5117):50–58. Reprinted with permission of AAAS. "Muscle tissue" image reprinted from *J. Biomech.*, 43, 16, Sharafi, B. and Blemker, S. S., A micromechanical model of skeletal muscle to explore the effects of fiber and fascicle geometry, 3207–3213, Copyright 2010, with permission from Elsevier. "Musculoskeletal system" image reprinted with kind permission from Springer Science+Business Media: *Ann. Biomed. Eng.*, A model of the upper extremity for simulating musculoskeletal surgery and analyzing neuromuscular control, 33, 6, 2005, 829–840, Holzbaur, K. R., Murray, W. M., Delp, S. L.)

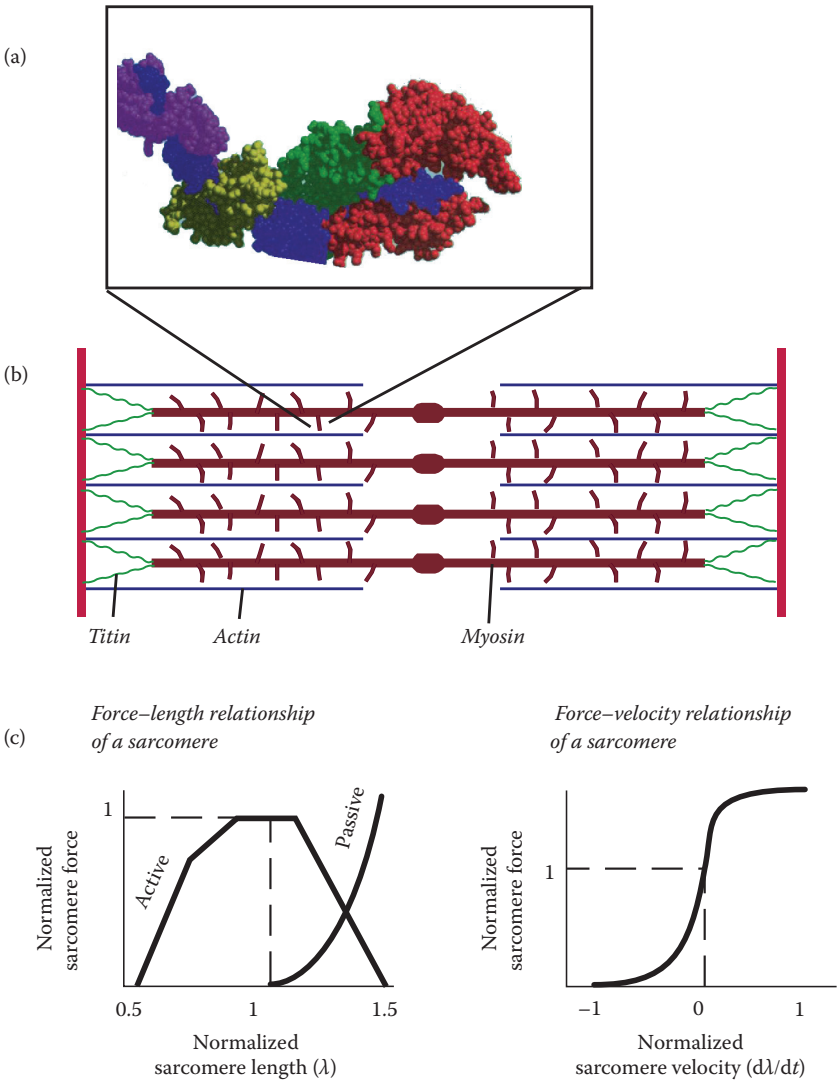

FIGURE 4.2
Molecular motors and the sarcomere. The action of myosin (a) provides force production within a muscle, and the sarcomere (b) is the fundamental structural unit of a muscle cell. Sarcomeres exhibit a force–length behavior (c) that is a result of changes in overlap between actin and myosin as the proteins slide past each other. Sarcomeres exhibit a force–velocity behavior (c) that is a result of the speed at which myosin motors can attach and reattach to actin. (Part (a) reprinted from Rayment, I., Rypniewski, W. R., Schmidt-Base, K., Smith, R., Tomchick, D. R., Benning, M. M. et al. 1993. Three-dimensional structure of myosin subfragment-1: A molecular motor. *Science* 261(5117):50–58. Reprinted with permission of AAAS.)

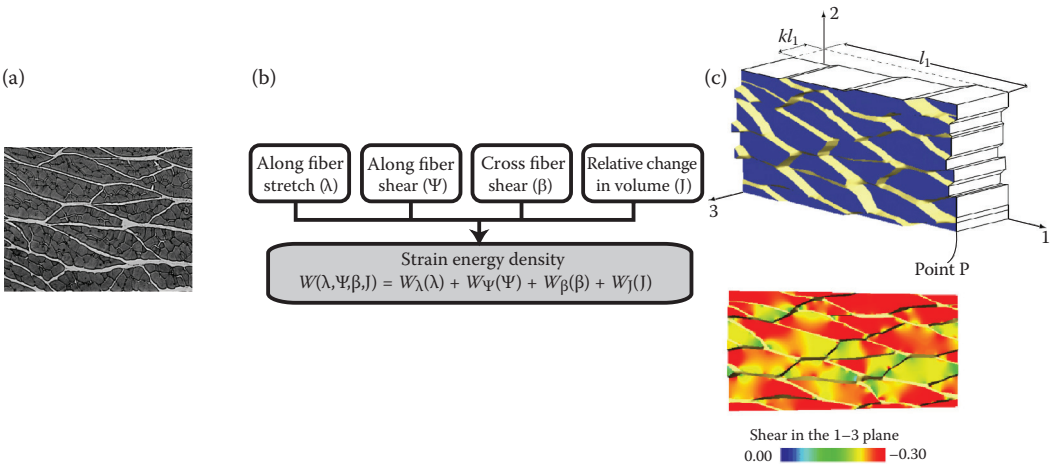

FIGURE 4.3
Muscle tissue structure. Muscle fibers are arranged within fascicles and surrounded by intramuscular connective tissue (a). Recent advances in micromechanical modeling (b, c) have allowed the exploration of how the morphological properties of fibers and connective tissues affect tissue-level mechanics of muscle. (Parts (a) and (c) reprinted from *J. Biomech.*, 43, 16, Sharafi, B. and Blemker, S. S., A micromechanical model of skeletal muscle to explore the effects of fiber and fascicle geometry, 3207–3213, Copyright 2010, with permission from Elsevier.)

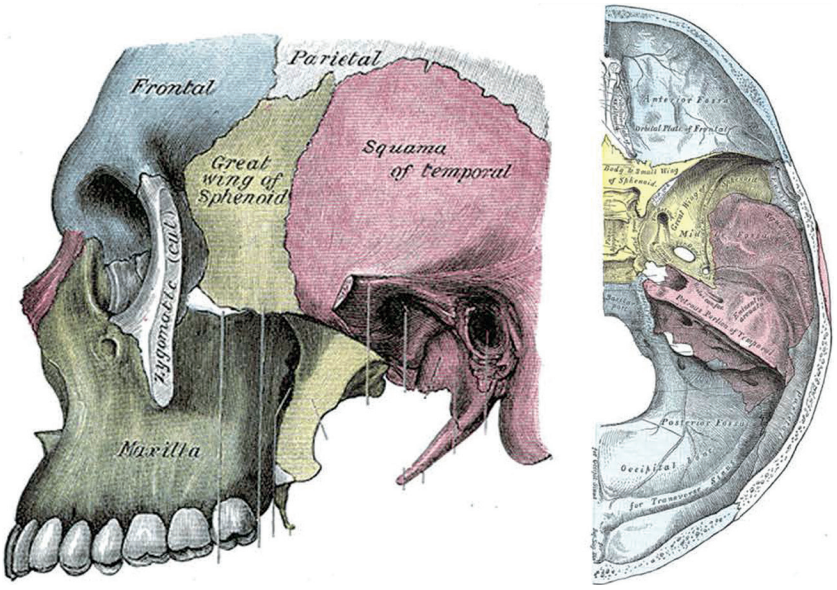

FIGURE 5.2
Diagram of the skull showing the location of temporal (red) and sphenoid (yellow) bones. Sphenoid and temporal bone form portions of the base of skull (right) and lateral walls (left) of the cranial cap. (From *Gray's Anatomy*, courtesy of Wikimedia Commons.)

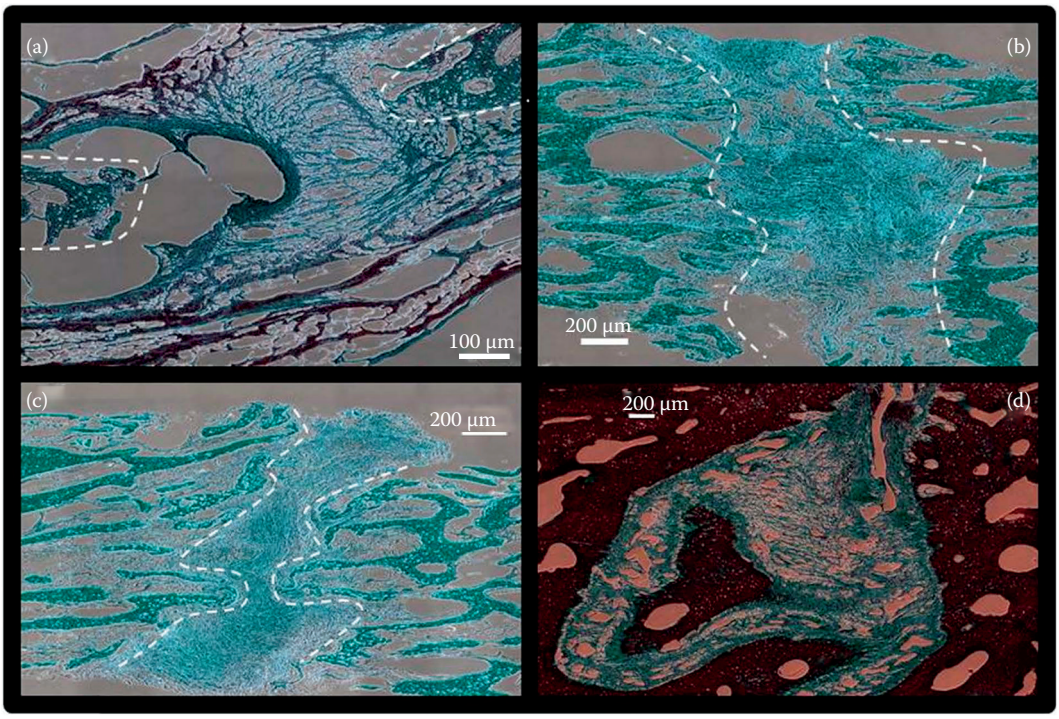

FIGURE 5.6
Suture samples (Masson's trichrome under transmitted light microscopy). Bone edges are outlined with dashed lines. (a) Neonate, showing the net-like arrangement of fibers in the mesenchyme. (b) The 9-month-old, displaying an increase in arranged fibers although still lacking order at the bone interface. (c) The 11-month-old, similar to the 9-month-old, showing increase in arranged fibers specifically in the bottom portion of the suture. (d) The 18-month-old, suture space narrows and is more clearly defined by bone edge and fibers are more aligned with the bone faces.

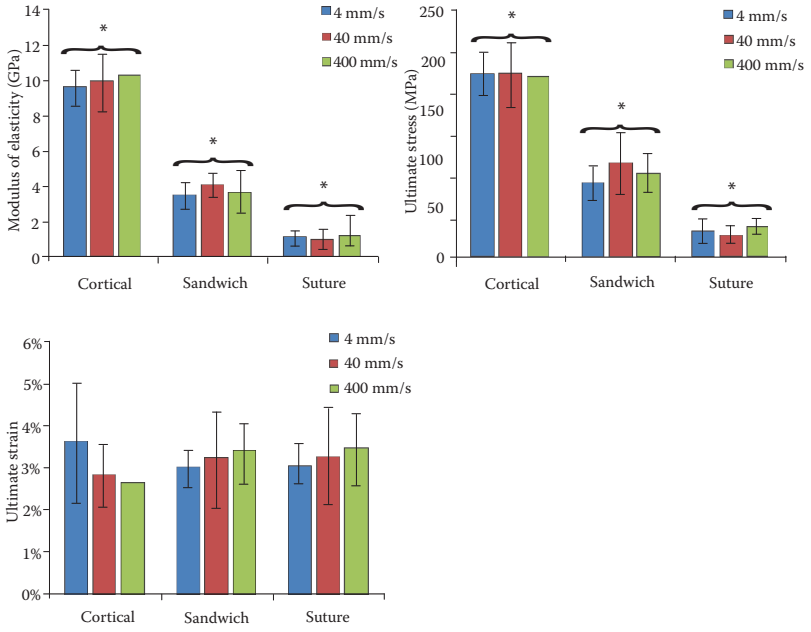

FIGURE 5.8
Both the modulus of elasticity and ultimate stress differ significantly between cortical, sandwich, and suture skull structures, but the same pattern is not observed for ultimate strain. Varying loading rate from 4 to 400 mm/s has no effect on any of the mechanical properties.

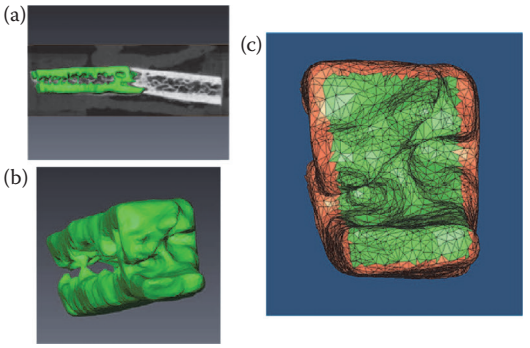

FIGURE 5.11
Pediatric skull bone images used to measure surface area interdigitation index. (a) Using Avizo 6.0 imaging software, a three-dimensional mesh was created from micro-CT scans of bone–suture–bone strips. (b) Two bones outlining the suture were separated to observe the suture interface. (c) Using LS-DYNA, the surface area was measured from both bone segments and excluded the top, bottom, and sides of the bone strip.

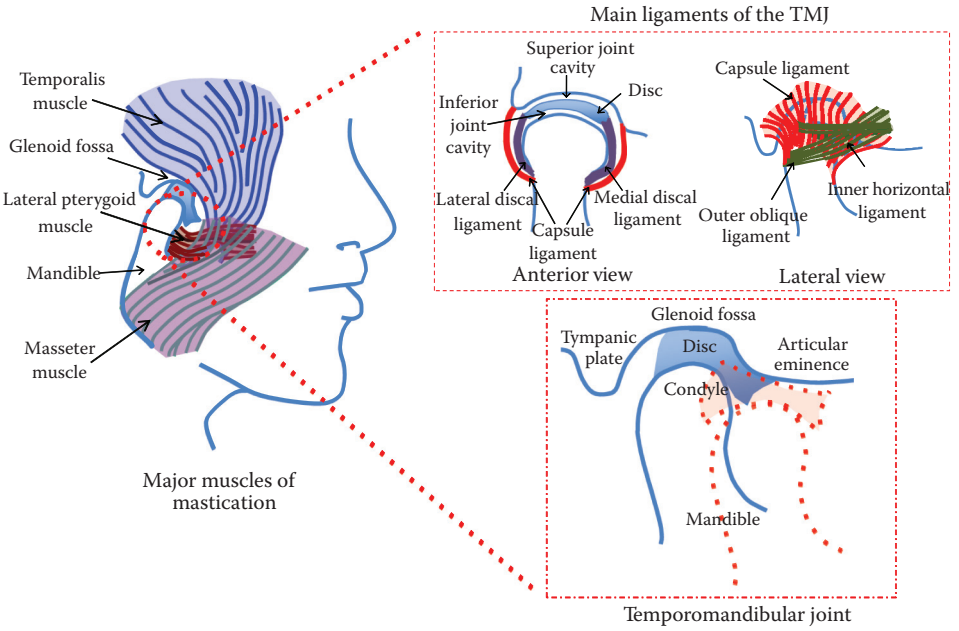

FIGURE 6.1
Overall anatomy of the TMJ, including the major muscles of mastication, the main ligaments, as well as an enlargement of the joint itself, highlighting its major components. The closed mouth position of the TMJ is shown in solid blue; the open mouth position is shown in dashed red.

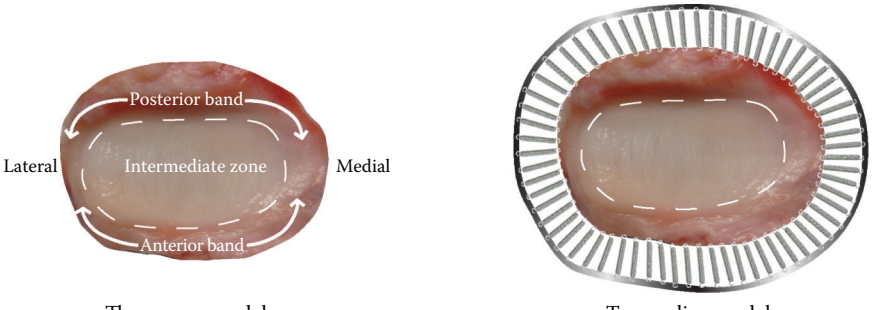

FIGURE 6.2
Superior view of the three-zone model and the trampoline model representations of the TMJ disc. In the trampoline model, trampoline springs represent the tension-generating function of the ligaments.

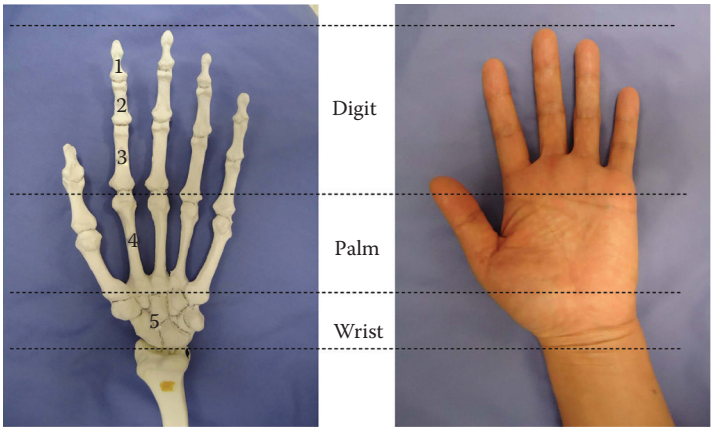

FIGURE 9.1
Human hand bony structure and functional components including wrist, palm, and digits. 1, distal phalanx; 2, middle phalanx; 3, proximal phalanx; 4, metacarpal bone; 5, carpal bones.

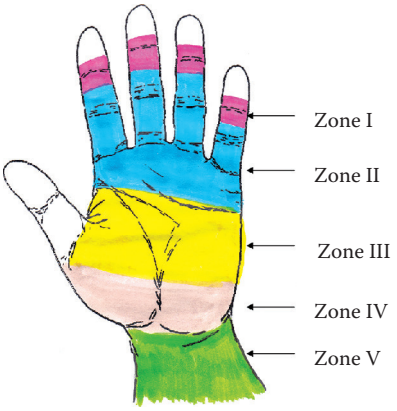

FIGURE 9.2
Flexor tendons are divided into five zones in the hand, wrist, and forearm. Zone I is the most distal portion. Zone II is the tendon portion that is located within the flexor sheath. Zone II is the critical zone in which two of the flexor tendons (FDP and FDS) are frequently injured. Zone III is the tendon portion from the proximal flexor sheath to the distal carpal tunnel. Zone IV is the tendon within the carpal tunnel area. Zone V is the most proximal portion of the tendon from the muscle origin to the proximal wrist.

FIGURE 9.14
Passive DIP and PIP joint motion result in buckling of the FDP tendon when the wrist is placed in flexion position, in which the force applied to the tendon was diminished. (Adapted from *J. Hand Surg. Am.*, 17, Horii, E. et al., Comparative flexor tendon excursion after passive mobilization: An in vitro study, 559–566, Copyright 1992, with permission from Elsevier.)

FIGURE 10.7
Neutrally aligned foot in eight positions.[17] From top left to bottom right: from maximal plantar flexion, inversion, and internal rotation to maximal dorsiflexion, eversion, and external rotation. Neutral position is the bottom left position. (Reprinted with permission from the American Society of Mechanical Engineers.)

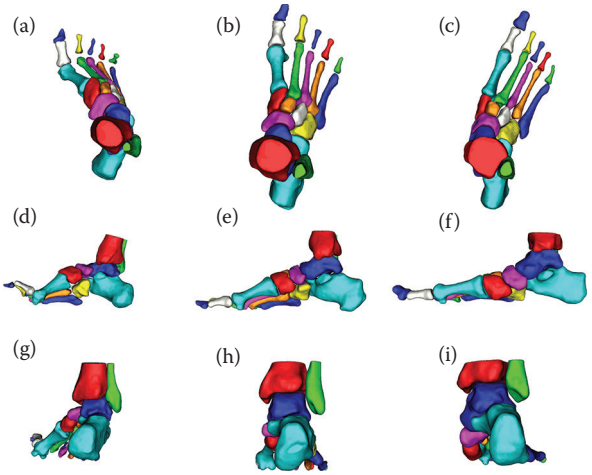

FIGURE 10.8
Pes cavus (a, d, and g), neutrally aligned (b, e, and h), and pes planus (c, f, and i) foot types. Right foot, transverse plane superior view (a, b, and c), sagittal plane medial view (d, e, and f), and coronal plane posterior view (g, h, and i).

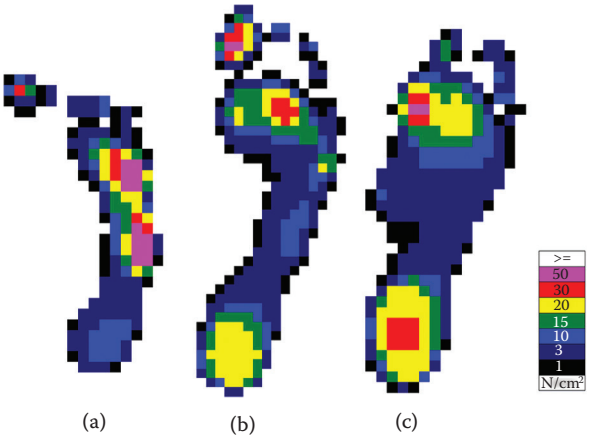

FIGURE 10.9
Distribution of plantar pressure for pes cavus (a), neutrally aligned (b), and pes planus (c) subjects. The cavus subject bears load on the lateral side of the foot, specifically on the base and head of the fifth metatarsal. The neutrally aligned subject bears load through the second metatarsal and the great toe. The planus subject bears load through the first metatarsal head.

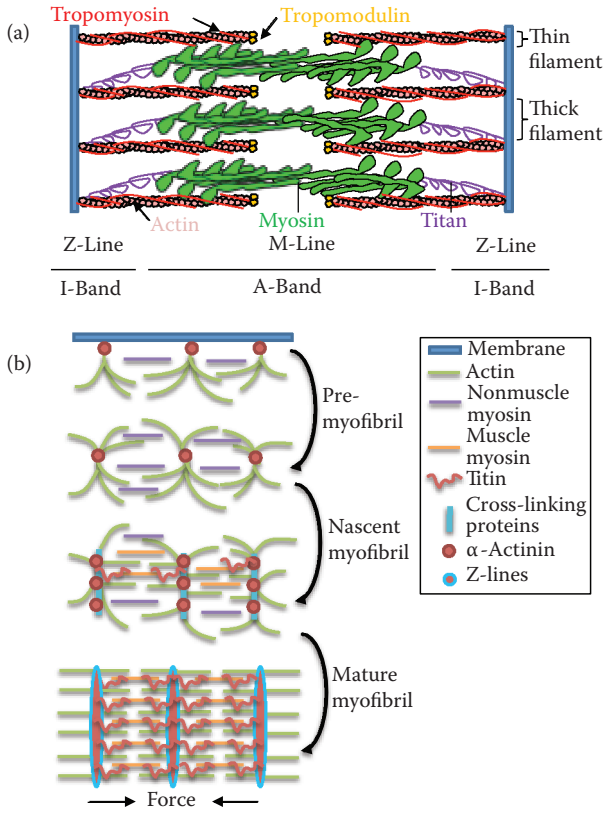

FIGURE 11.5
Sarcomere: the contractile "force" behind muscle. (a) Sarcomere is complex structure composed of repeating units of actin- and myosin-containing filaments (thin and thick, respectively) that are bound by Z-lines. Actin and myosin slide against one another to generate contractions. (b) Sarcomere assembly model.

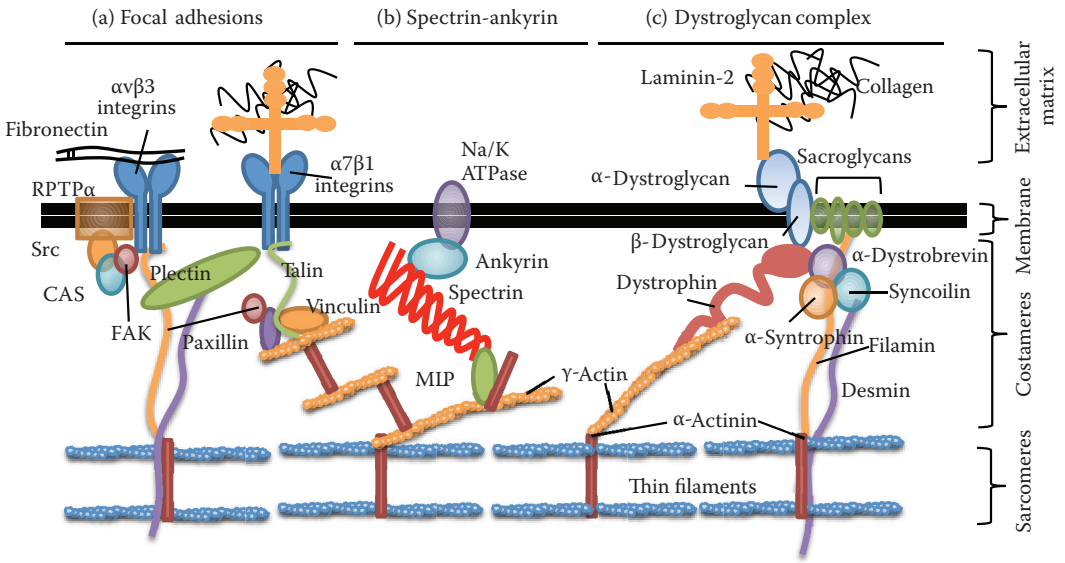

FIGURE 11.6
Schematic of three costameric connective structures: (a) focal adhesions, (b) spectrin-ankyrin, and (c) DGC between sarcomeres and the ECM as indicated. Although vastly incomplete and omitting all of the biochemical signaling pathways, the sheer complexity of the diagram and multiple transductive pathways for force is apparent.

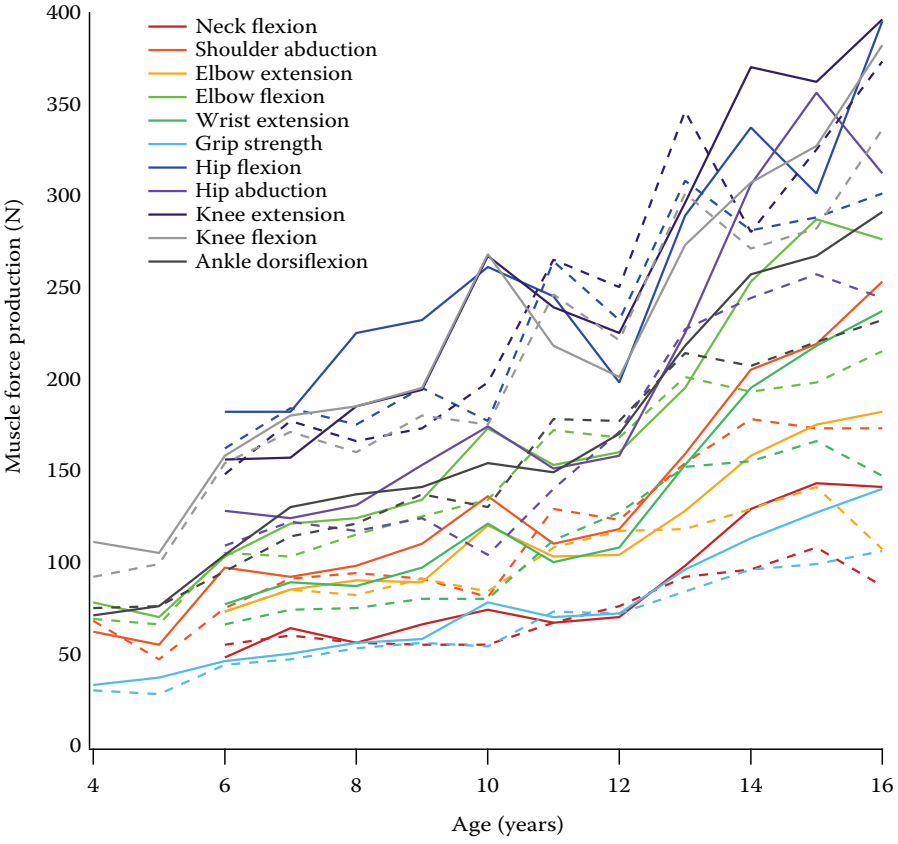

FIGURE 12.6
Maximum isometric muscle force production for different muscle groups throughout growth and development. Although each curve advances with subject age, the shape and slope of the curves are muscle group-dependent. These functional data reveal up to a 4-fold increase in muscle force production from 4 to 16 years of age. (Data from *Neuromuscul. Disord.*, 11(5), Beenakker, E. A. et al., Reference values of maximum isometric muscle force obtained in 270 children aged 4–16 years by hand-held dynamometry, 441–446, Copyright 2001.)

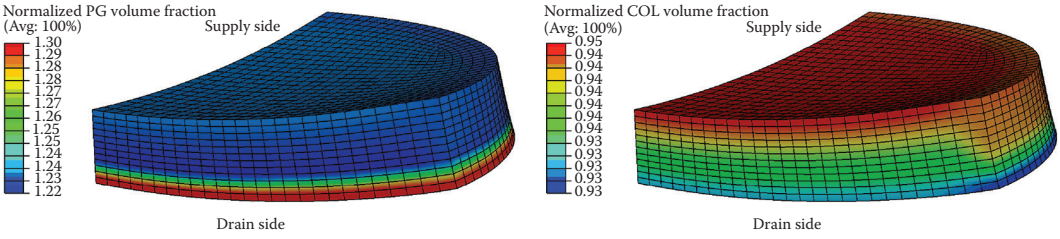

FIGURE 14.8
FEA specimens released from a permeation chamber after growth: contours of the final proteoglycan (PG) and collagen (COL) volume fractions for a shear growth trigger normalized. This configuration corresponds to release from the permeation chamber. The average dimension of the elements are 25.33 × 63.85 μm. The curvature deformation is scaled by a factor of 5 to highlight the nonuniform geometry that results from growth.

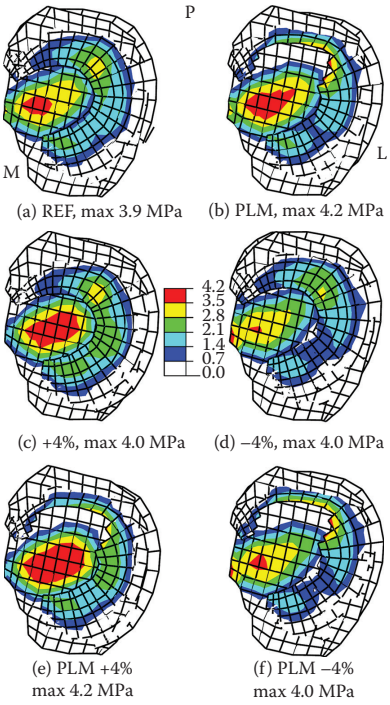

FIGURE 14.10
Contact stress distribution on the lateral tibial plateau under 200 N drawer and 1500 N compression preload. (a) REF, reference intact; (b) PLM, partial lateral meniscectomy; (c) +4%, plus 4% strain in ACL pre-strain; (d)–4%, minus 4% strain in ACL pre-strain; (e) PLM +4%, combined PLM with 4% strain increase in ACL pre-strain; (f) PLM –4%: combined PLM with 4% decrease in ACL pre-strain. Note that the maximum pressure is given for each case with a common legend for ease in comparisons. L, M, and P label the lateral, medial, and posterior directions, respectively. (From Shirazi, R., and Shirazi-Adl, A., *Clin. Biomech. (Bristol, Avon)*, 24 (9), 755–761, 2009. With permission.)

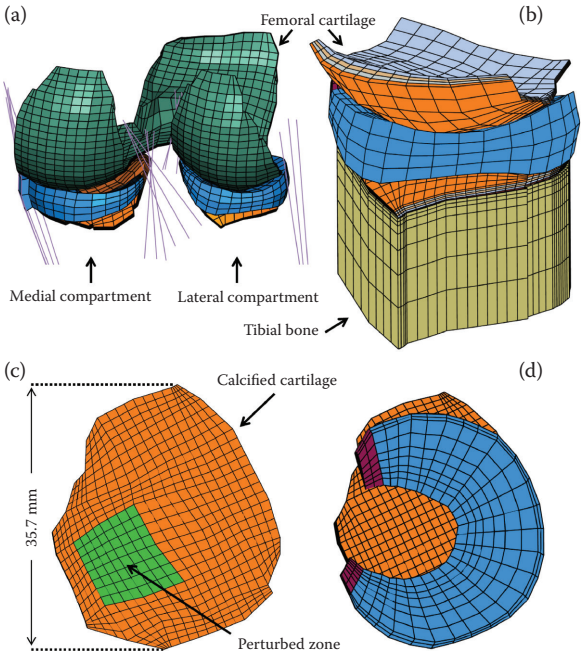

FIGURE 14.11
Finite-element model. (a) Posterior view of the tibiofemoral joint (also used to extract the lateral compartment to study the effect of bone injuries on overlying AC and knee joint biomechanics). (b) Lateral compartment of the joint with the calcified cartilage and tibial bony elements (subchondral, cancellous, and cortical) incorporated. (c) Top view of the tibial lateral cartilage at the calcified region depicting the localized area for various osteochondral defect models used in this study. (d) Top view of menisci (horns in blue) and tibial AC. (From Shirazi, R. and Shirazi-Adl, A., *J. Biomech.*, 42 (15), 2458–2465, 2009. With permission.)

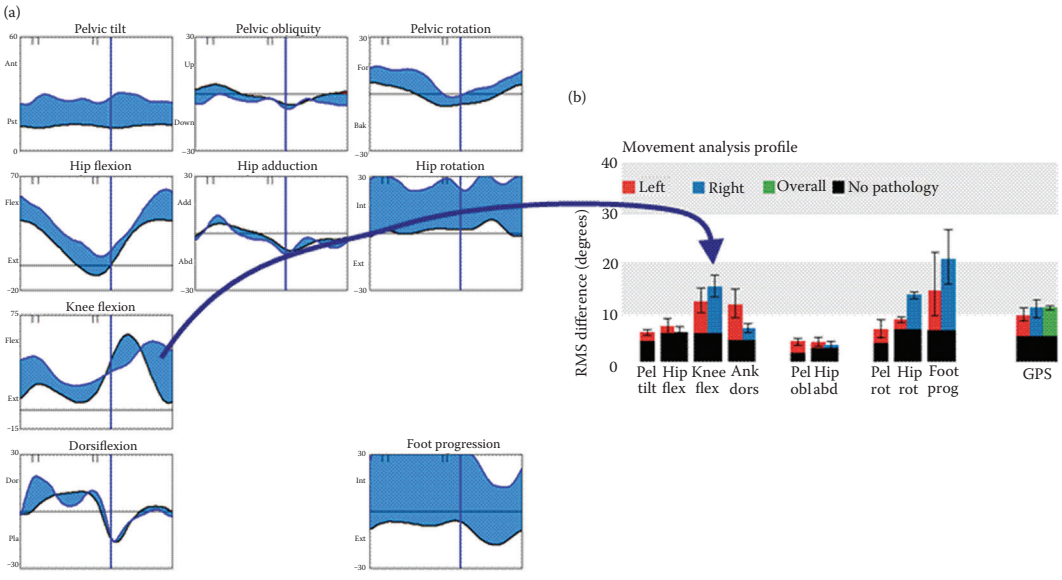

FIGURE 15.6
Movement analysis profile (MAP). (a) Data from the person being assessed and the average values for healthy adults plotted on the same graphs with the area between these traces shaded. This is a good visual representation of the root mean square difference between the traces that are the values plotted in the MAP histogram on (b). Values for (a) are in red and the right side in blue. The gait profile score (GPS) is the root mean square average of the values for all the data and can be taken as an overall score of gait abnormality. It can be defined for (a) (red), (b) (blue), or both (green). (Reprinted from *Gait Posture*, 30, 3, Baker, R. et al., 265–269, Copyright 2009, with permission from Elsevier.)

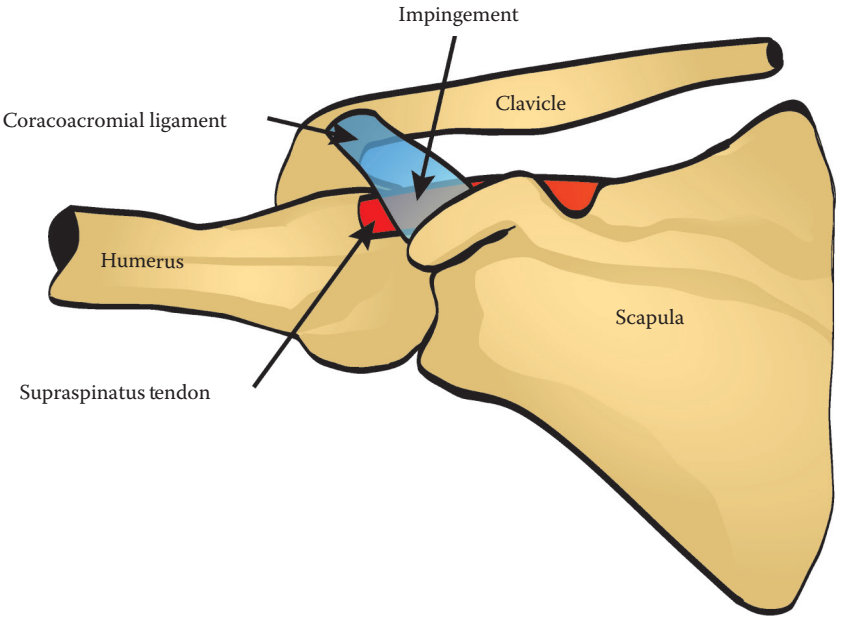

FIGURE 17.5
Impingement of the supraspinatus occurs whenever the arm is positioned above the horizontal plane. The coracoacromial ligament (blue) compresses the bursa and supraspinatus tendon (red) against the humerus.

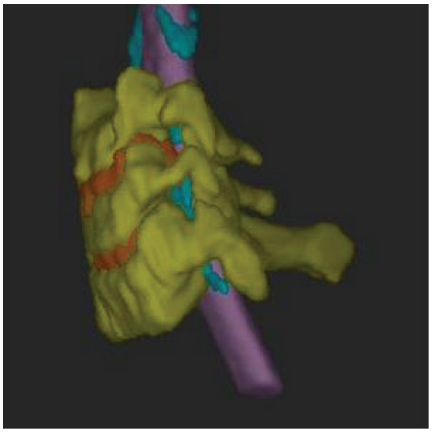

FIGURE 18.1
3D reconstruction of three cervical vertebrae (yellow) and their intervertebral discs (orange), as well as the spinal cord (purple) and nerve roots (cyan). The architectures of these musculoskeletal and neural tissues were produced using segmentation of sagittal (bone) and axial (neural) MR images.

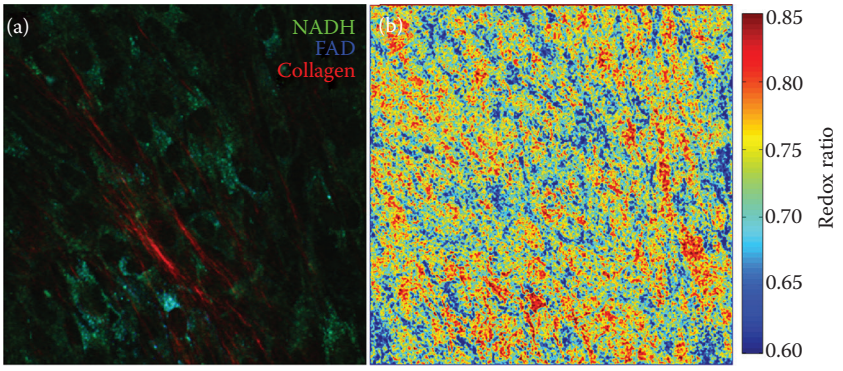

FIGURE 18.3
Nonlinear optical image of a mesenchymal stem cell culture undergoing osteoblastic differentiation. (a) False-color image highlights nicotinamide adenine dinucleotide (NADH; green) and flavin adenine dinucleotide (FAD; blue) fluorescence in cell mitochondria detected through TPEF imaging and collagen deposition (red) detected through SHG imaging. (b) Map of the cellular redox ratio FAD/(NADH+FAD) can be determined from the TPEF images, indicating higher redox ratios to be in regions with collagen fiber deposition.

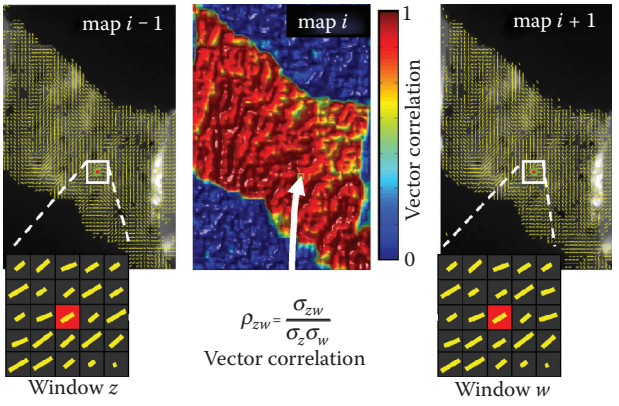

FIGURE 18.4
Schematic of a pixelwise vector correlation calculation to assess changes in collagen fiber alignment. The vector correlation for each pixel in a given map (i) is calculated from the alignment surrounding the pixel in the maps immediately preceding (i − 1) and following (i + 1) it. Normal realignment patterns throughout the ligament tissue are demonstrated by correlation values near 1.

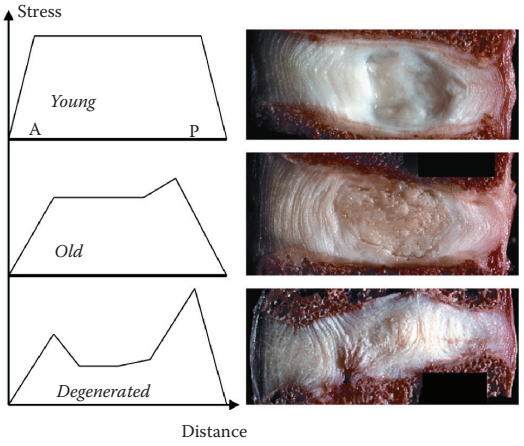

FIGURE 20.4
Representative stress profiles for a young adult disc (top), old disc (middle), and degenerated disc (bottom). Stress concentrations increase with age and become large with degeneration. P, posterior; A, anterior. Photographs show midsagittal sections of corresponding similar discs. (Reprinted from Adams, M. A. et al., Copyright 2009, with permission from Elsevier.)

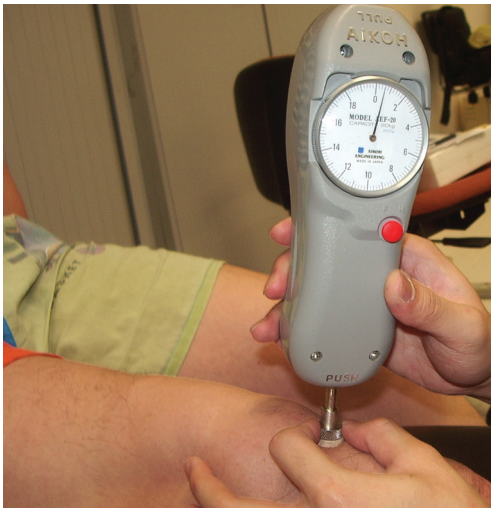

FIGURE 21.1
Mechanical force transducer used to measure the force applied to the residual limb in the indentation test.

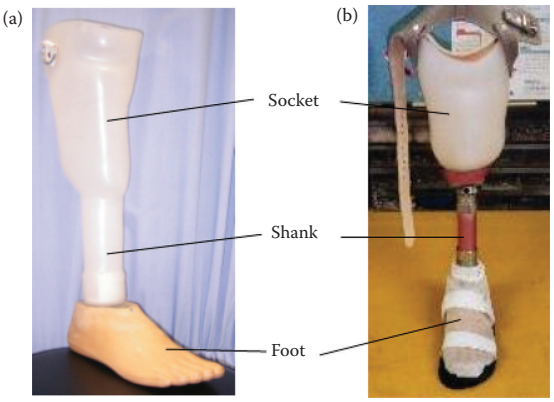

FIGURE 21.3
A monolimb in which the socket and the shank are formed by one piece of thermoplastic (a), and a conventional transtibial prosthesis in which the shank and the foot are connected by a metal shank (b).

Biomedical Engineering

ORTHOPAEDIC BIOMECHANICS

Given the strong current attention of orthopaedic, biomechanical, and biomedical engineering research on translational capabilities for the diagnosis, prevention, and treatment of clinical disease states, the need for reviews of the state-of-the-art and current needs in orthopaedics is very timely. ***Orthopaedic Biomechanics*** provides an in-depth review of the current knowledge of orthopaedic biomechanics across all tissues in the musculoskeletal system, at all size scales, and with direct relevance to engineering and clinical applications.

Discussing the relationship between mechanical loading, function, and biological performance, it first reviews basic structure–function relationships for most major orthopedic tissue types followed by the most-relevant structures of the body. It then addresses multiscale modeling and biologic considerations. It concludes with a look at applications of biomechanics, focusing on recent advances in theory, technology, and applied engineering approaches.

FEATURES

- Presents state-of-the-art findings and techniques of orthopedic biomechanics
- Integrates basic biomechanics and clinical-relevant applications
- Covers the entire body, addressing issues across several tissues and anatomic structures
- Includes applications of biomechanics
- Addresses current issues and opportunities facing the orthopaedic biomechanics community today
- Provides quantitative perspectives on cellular biomechanics, growth and development, the influence of aging and gender, and computational modeling of these and other factors
- Focuses on trauma and injury as well as diagnostic techniques such as gait analysis and imaging biomarkers

With contributions from leaders in the field, the book presents state-of-the-art findings, techniques, and perspectives. Much of orthopaedic, biomechanical, and biomedical engineering research is directed at the translational capabilities for the "real world." Addressing this from the perspective of diagnostics, prevention, and treatment in orthopaedic biomechanics, the book supplies novel perspectives for the interdisciplinary approaches required to translate orthopaedic biomechanics to today's real world.

K12804

ISBN: 978-1-4398-6093-9

90000

9 781439 860939

www.crcpress.com

CRC Press
Taylor & Francis Group
an informa business

6000 Broken Sound Parkway, NW
Suite 300, Boca Raton, FL 33487
711 Third Avenue
New York, NY 10017
2 Park Square, Milton Park
Abingdon, Oxon OX14 4RN, UK